Transformations of White Phosphorus Mediated by Low Valent Cobalt Complexes

Dissertation

Zur Erlangung des Doktorgrades der Naturwissenschaften

Dr. rer. nat.

an der Fakultät Chemie und Pharmazie der Universität Regensburg

vorgelegt von:

Sebastian Hauer

aus Deuerling

Regensburg, Mai 2024

Der experimentelle Teil der vorliegenden Arbeit wurde in der Zeit zwischen Dezember 2019 und März 2024 unter Anleitung von Prof. Dr. Robert Wolf am Institut für Anorganische Chemie der Universität Regensburg angefertigt.

Die Arbeit wurde angeleitet von:		Prof. Dr. Robert Wolf
Promotionsgesuch eingereicht am:		03.05.2024
Tag der mündlichen Prüfung:		17.06.2024
Promotionsausschuss:	Vorsitz:	Prof. Dr. Marcel Schorpp
	Erstgutachter	Prof. Dr. Robert Wolf
	Zweitgutachter	Prof. Dr. Jan J. Weigand
	Dritter Prüfer	Prof. Dr. Frank-Michael Matysik

Prologue

This thesis primarily reports on the synthesis, reactivity, and characterization of low-valent cobalt complexes and their application for white phosphorus transformation. Chapter 1 provides a categorized review of the transition-metal-mediated functionalization of P_4 with emphasis on recent research results. Chapter 2 addresses the [3+1] fragmentation of acylated tetraphosphidoligands, which provides access to acylcyanophosphanides and phosphines. Chapter 3 reports on the functionalization of anionic and neutral tetraphosphido complexes with electrophilic heterocycles. Chapters 4-5 describe the reactivity of tri- and tetraphosphido complexes with phosphorus-containing electrophiles to form polyphosphido complexes (Chapter 4) and functionalization with group 14 ambiphiles (Chapter 5), respectively. Chapter 6 covers a distinct project and describes the synthesis of new phosphorus-containing heterocycles by reaction of *tert*-butylphosphaalkyne or white phosphorus with diazoalkenes. Finally, Chapter 7 gives a summary of the results described in this thesis and provides a short outlook.

Prolog

Diese Dissertation behandelt hauptsächlich die Synthese, Reaktivität und Charakterisierung von niedervalenten Cobaltkomplexen und deren Anwendung für die Transformation von weißem Phosphor. Kapitel 1 gibt einen gruppierten Überblick über die übergangsmetallvermittelte P_4 Funktionalisierung mit Schwerpunkt auf aktuellen Forschungsergebnissen. Kapitel 2 beschreibt die [3+1] Fragmentierung von acylierten Tetraphosphidoliganden, wodurch Acylcyanophosphanide und -phosphine zugänglich werden. In Kapitel 3 wird die Funktionalisierung von anionischen und neutralen Tetraphosphidokomplexen mit elektrophilen Heterocumulenen behandelt. Kapitel 4-5 beschreiben die Reaktivität von Tri- und Tetraphosphido Komplexen mit phosphorhaltigen Elektrophilen zum Aufbau von Polyphosphidokomplexen (Kapitel 4), bzw. der Funktionalisierung mit Ambiphilen der Gruppe 14 (Kapitel 5). Kapitel 6 beschreibt ein thematisch unabhängiges Projekt zur Synthese neuer phosphorhaltiger Heterocyclen durch Umsetzung von *tert*-Butylphosphaalkin oder weißem Phosphor mit Diazoalkenen. Das letzte Kapitel 7 fasst die Ergebnisse dieser Arbeit zusammen und gibt einen kurzen Ausblick.

Table of Contents

1 Functionalization of Polyphosphido Ligands Derived from White Phosphorus[a]

Abstract: A myriad of useful organophosphorus compounds are accessible from white phosphorus (P_4), which are crucial for our modern society. However, current industrial routes used to transform P_4 into these products are indirect, wasteful, and highly hazardous. Transition-metal (TM)-mediated processes have emerged as promising and atom-efficient alternatives, leading to the development of a plethora of early and late transition metal polyphosphido complexes through the coordination of P_4. While this first step, often referred to as "activation", has become well established, the subsequent functionalization of these complexes remains a challenging goal in this field.

This chapter provides an overview of successful P_4-derived functionalization reactions of polyphosphido ligands in transition metal complexes, with a particular emphasis on recent developments not covered in previous review articles.

[a] The chapter was written by S. Hauer.

1.1 Introduction

Phosphorus, atomic number 15 in the periodic table, is one of the six biogenic elements essential for life on earth and was discovered by Hennig Brand in 1669.[1–4] Today, synthetic (organo-)phosphorus compounds (OPC) are ubiquitous in everyday life, e.g. in flame retardants, agrochemicals and pharmaceuticals, among many others.[5–7] The single most important feedstock material for the industrial synthesis of these compounds is white phosphorus (P_4) – the most reactive elemental allotrope – which is produced annually on a megaton scale from phosphate ore (apatite) *via* electric arc furnace reduction (Wöhler process). While the majority of this P_4 is then reoxidized to generate high-purity phosphoric acid (thermal H_3PO_4), the remaining fraction (ca. 18%) is used to prepare the numerous organophosphorus compounds relevant to industry and commerce.[5,8]

The established industrial route involves the conversion of P_4 into phosphorus trichloride (PCl_3) using hazardous chlorine gas (Cl_2, Scheme 1). PCl_3 is a highly corrosive liquid that must be stored under inert conditions and can be further oxidized using Cl_2 or O_2 to produce PCl_5 or $POCl_3$, respectively. Nucleophilic functionalization of these phosphorus chlorides then furnishes the desired organophosphorus products, alongside inorganic salt waste. This process is illustrated by the commercial preparation of industrially valuable triphenylphosphine (PPh_3), where chlorobenzene is treated with PCl_3 in the presence of molten sodium.[9] Alternatively, P_4 can be broken down into toxic and flammable phosphine gas (PH_3) *via* acid- or base-mediated disproportionation with concomitant loss of phosphorus due to oxidation.[5,6,8] PH_3 is then employed in hydrophosphination reactions of alkenes and ketones to yield the desired phosphorus compounds.

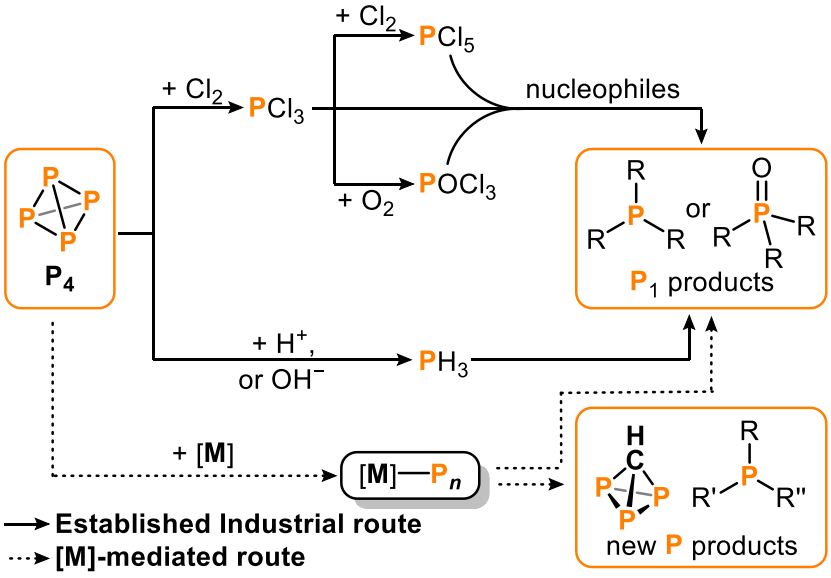

Scheme 1. Current industrial route toward monophosphorus compounds and metal mediated alternative.

Thus, these established routes are energy intensive, require highly hazardous reagents, proceed *via* harmful intermediates, and generate superstoichiometric amounts of chemical waste. As a result, contemporary research endeavors to develop alternative approaches for the functionalization of P_4, circumventing environmentally detrimental processes.

The incorporation of P_4 into the coordination sphere of a transition metal to generate a reactive polyphosphido complex [M]–P_n (= activation) has been widely examined over the past several decades and reviewed.[10–15] Through degradation into smaller P_1-P_3 fragments and aggregation into larger P_n (n ≥ 5) frameworks a plethora of fascinating polyphosphido complexes has become accessible, with examples of some common structural motifs illustrated in Figure 1. While strides have been made in functionalization to derive OPCs from P_4 in recent years, such as other P-atom sources, reactions of P_4 with main group elements, electrochemical and photochemical processes, the field of obtaining P_1 products directly from P_4 is still in its infancy and relies on processes hampered by poor selectivity or efficiency hence their transition to an industrial scale appears unlikely.[10,16–20] Thus, more traditional transition-metal-mediated routes are still highly desirable. Through activation of P_4, the transformation of the P_n moieties with suitable reagents (= functionalization) is facilitated. Studying these reactions could ultimately pave the way to an effective and environmentally friendly route toward organophosphorus derivatives derived from P_4. Additionally, such processes could provide access to polyphosphorus frameworks, phosphide materials and further unique and intriguing P-containing compounds, inaccessible by other synthetic pathways.

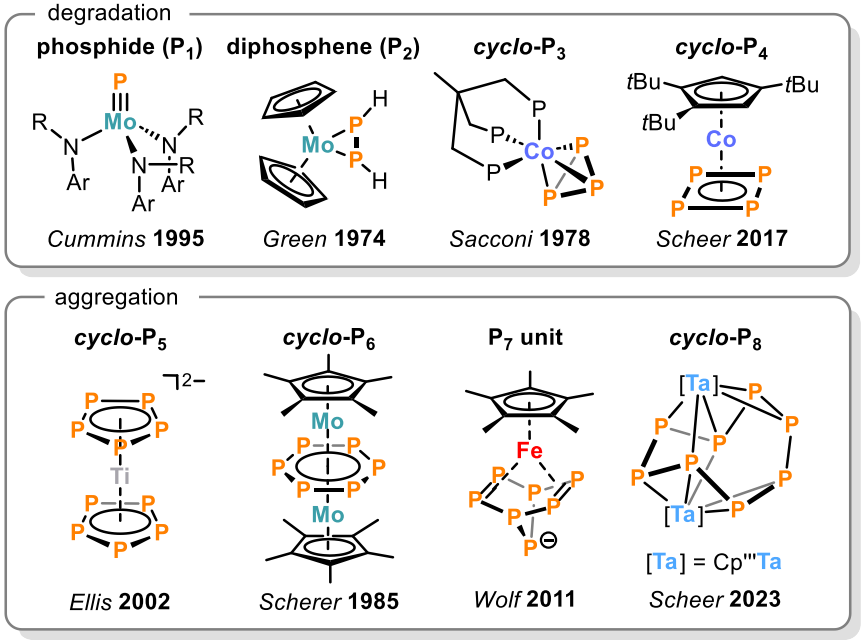

Figure 1. Transition metal polyphosphido complexes accessible through degradation and aggregation of P_4; R = *i*Pr, $C(CD_3)_2Me$, Ar = 3,5-$Me_2C_6H_3$, Cp''' = $C_5H_2tBu_3$.

Previous review articles have extensively covered various aspects of P_4 chemistry, including complexes with early/late transition metals, and two recent publications from our group focus on the functionalization and coordination chemistry of P_4.[10–15] Thus, this introduction will focus only on the most relevant previous contributions to this area, as well as recent work not covered in the aforementioned review articles. To assist the reader navigate this introduction, it is organized according to the degree of degradation or aggregation at the metal center. Therefore, one-step activation and functionalization will be discussed first, followed by functionalization of P_n units from lowest to highest nuclearity in the following sections.

1.2 One-Step Activation and Functionalization of P_4

A landmark example of a metal complex inducing simultaneous activation and functionalization of P_4 was reported in 1998, by Peruzzini and co-workers, when they demonstrated the direct hydrogenation of P_4 to yield PH_3 and primary organophosphines, RPH_2 (Scheme 2a).[21] When working in a closed system, the late transition metal hydrides of rhodium(III) (**1a**) and iridium(III) (**1b**) [(triphos)MH_3] (M = Rh, Ir; triphos = $MeC(CH_2PPh_2)_3$) were shown to simultaneously activate and functionalize P_4 in a single step [3+1] fragmentation reaction. Products of these reactions were the very stable *cyclo*-P_3 complexes **2** and P_1 product PH_3. Mechanistic insight into the hydrogenation was provided by the reaction of dihydridoethyl iridium complex **1c** with P_4 in an open system (Scheme 2b).

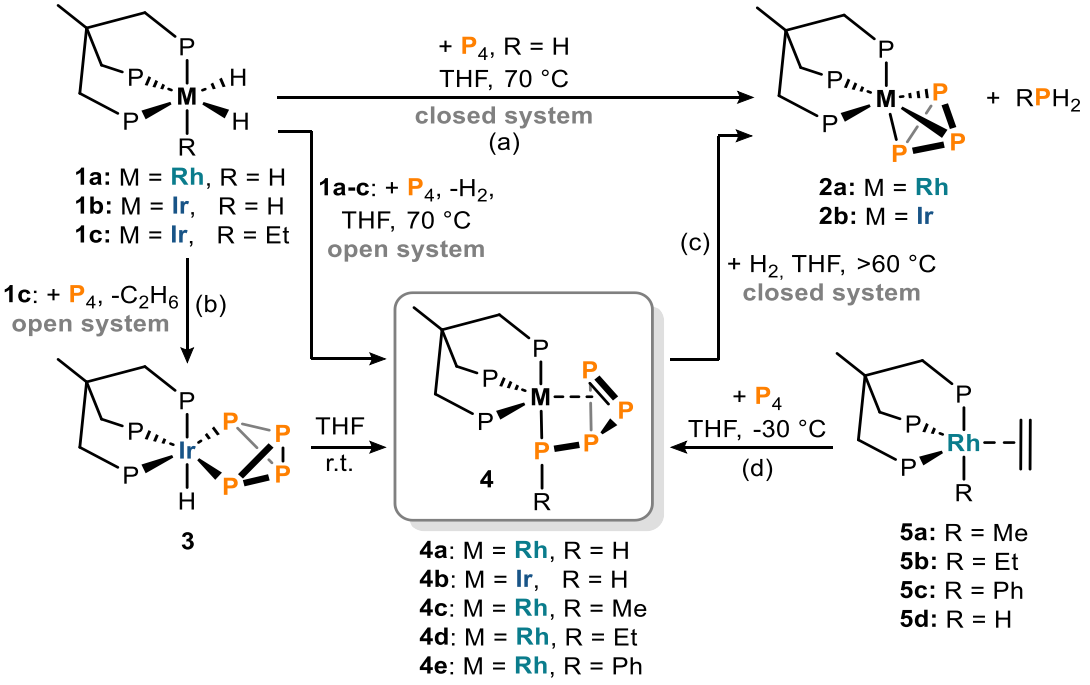

Scheme 2. Rhodium and iridium mediated [3+1] fragmentation of P_4 by stoichiometric hydrogenation; triphos = $MeC(CH_2PPh_2)_3$.

In this case, the formation of butterfly compound [(triphos)IrH(η^1:η^1-P_4)] (**3**) and evolution of ethane gas was initially observed. Compound **3**, formed by oxidative addition of P_4 to the iridium center, likely represents an initial intermediate *en route* to **2b**. Compound **3** slowly isomerizes to **4b** at room temperature, which subsequently reacts with H_2 above 60°C to give **2b** and PH_3 (Scheme 2c). One year later, Peruzzini and co-workers demonstrated that **4c-e** is also accessible by the reaction of rhodium ethylene complexes **5** with P_4 (Scheme 2d).[22] Upon release of the labile ethylene ligand from **5**, a transient, coordinatively unsaturated, 16-electron species [(triphos)RhR] was formed, which reacts with P_4 to give complexes analogous to **3**. Migration of the alkyl or aryl groups to the P_4 ligand resulted in **4c-e**, representing the first example of TM-mediated P−C bond formation, derived from P_4. Notably, the reaction of hydrido-ethylene derivative **5d** did not yield expected product **4a**, but the tetraphosphidoethyl derivative **4d** through loss of H_2, resulting from insertion of the ethylene ligand.[23] Subjecting **4c-e** to an atmosphere of H_2 and heating the solution to 60 °C led to fragmentation and the release of **2a** as well as primary phosphine $EtPH_2$ directly derived from P_4. These [3+1] fragmentations demonstrate the potential of a transition-metal-mediated approach for the transformation of P_4 into functionalized derivatives. However, so far only stoichiometric hydrogenation reactions have been reported. Even in the presence of up to 30 atm of H_2 and 10 equiv. of P_4, only stoichiometric hydrogenation was observed, which was attributed to the high stability of complexes **2**.[21] Thus the direct hydrogenation of P_4 still suffers from poor atom efficiency.

Nearly two decades later, Zhang and co-workers reported a further example for a one-pot [3+1] fragmentation and functionalization reaction of white phosphorus (Scheme 3).[24] Rare-earth metallacyclopentadienes **6** reacted with half an equivalent of P_4 and display dual dinucleophile/diene character. Thus, inducing fragmentation into P_3 and P_1 moieties, which were isolated as *cyclo*-P_3 complexes **7** and the lithium phospholide **8**. DFT calculations provided insight into the mechanism and revealed a dual role for **6**, explaining the required 2:1 stoichiometry. Following fragmentation, the released P_3 moiety was captured by a cycloaddition reaction with **6**, which yielded stereoselectively *exo*-bicyclo[4,1,0]triphosphaheptanide complexes **7**. Second, the P_1 fragment was captured by double nucleophilic attack of **6**, yielding **8**. The lithium P_1 species **8** had already been reported a year earlier by the same group, through the related [3+1] fragmentation of P_4 by 1,4-dilithium-1,3-butadienes.[25] This thereby represents a rare example for one-step activation and functionalization of P_4 mediated by rare earth metals,

with concomitant trapping of both fragments.[24,26–28] The chemically distinct phosphorus atoms in **7a** gave rise to two signals in the $^{31}P\{^{1}H\}$ NMR spectrum at $\delta = -198$ ppm (2P) and $\delta = -91$ ppm (1P), contrasting much more common and symmetrical late TM *cyclo*-P_3 complexes, which usually exhibit a singlet in the range of $\delta = -160$ to -210 ppm.[15,29]

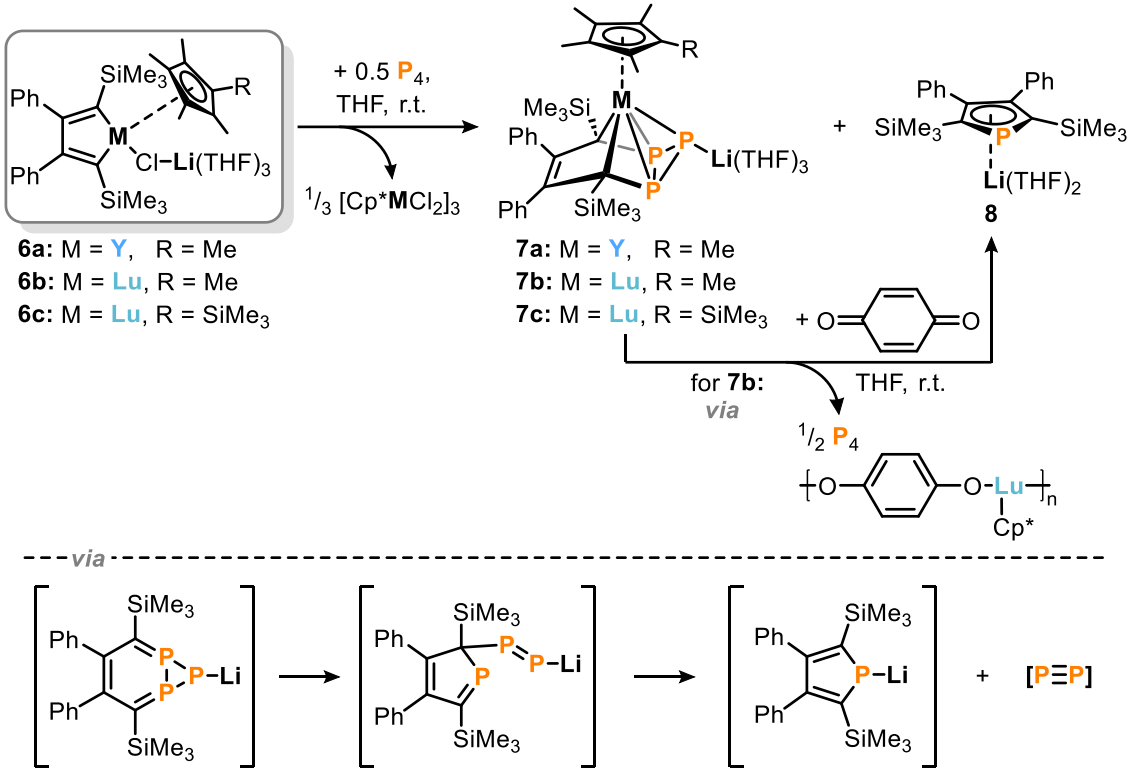

Scheme 3. Simultaneous activation and functionalization of P_4 by a rare-earth mediated [3+1] fragmentation; Cp* = η^5-C_5Me_5.

Additional equivalents of **8** could be generated by ring contraction of the *cyclo*-P_3 ligand in **7b** (R = Lu; R = Me) upon oxidation with *p*-benzoquinone. Addition of the oxidant led to [2+1] fragmentation with release of **8** and concomitant regeneration of P_4 in a ratio of 2:1. Monitoring *via* $^{31}P\{^{1}H\}$ NMR spectroscopy revealed a series of signals, which were assigned to proposed intermediates. A possible reaction sequence for the extrusion of the P_2 synthon was thereby proposed (Scheme 3 bottom).

Another example for yttrium mediated one-step activation and functionalization of P_4 was reported by Zhang, Zhou and co-workers.[30] Addition of half an equivalent of P_4 to the yttrium alkyl complex **9** in the presence of DMAP (4-dimethylaminopyridine) led to **10** (Scheme 4a). Complex **10** features a distorted *cyclo*-$P_4R_2^{2-}$ ligand bridging the two yttrium centers, derived from the insertion of P_4 into the yttrium-carbon bonds. Addition of HMPA ($[(CH_3)_2N]_3PO$), a selective cation solvate, promoted migration of the benzylic residues to a single phosphorus atom, releasing tribenzylphosphine **11** and forming the Zintl-type P_7^{3-} complex **12** (Scheme 4b).[31] In addition, heating of **10** led to a selective

1,2-benzyl shift to afford an R_2P-substituted *cyclo*-P_3 bridging ligand in **14** (Scheme 4c).[30] Extrusion of this *exo*-PR_2 moiety was achieved by addition of benzyl potassium to **13**, yielding the trinuclear Y_2K *cyclo*-P_3 complex **14** by elimination of **11**. Complex **14** is also accessible directly from **10** by addition of K−R, suggesting a benzylic migration induced by the strong nucleophile, followed by elimination of **11** (Scheme 4d). Thus, this procedure demonstrates an elegant two-step [3+1] fragmentation process of P_4 in which a phosphorus atom is derivatized to form an organophosphine.

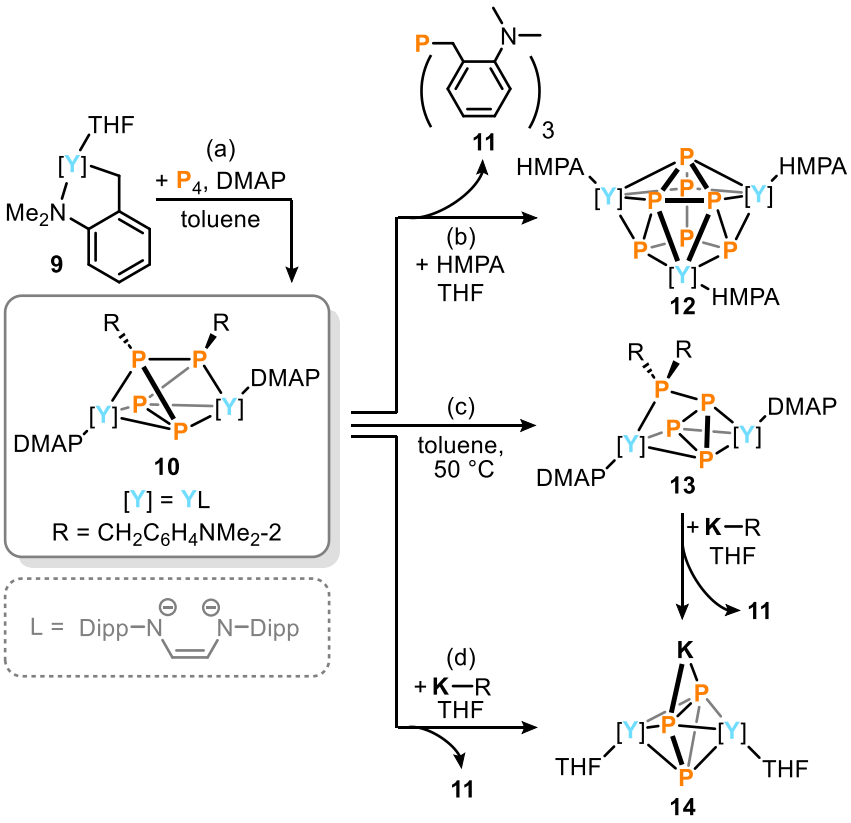

Scheme 4. Yttrium mediated synthesis of tribenzylphosphine *via* two-step [3+1] fragmentation of P_4, L = *N,N′*-di(2,6-diisopropylphenyl)-1,4-diazabutadiene, DMAP = 4-dimethylpyridine, HMPA = $[(CH_3)_2N]_3PO$.

In 2024 the same group of authors reported a direct construction of functionalized diphosphine ligands from P_4 mediated by silyl-bridged amido/methylene yttrium complex **15** (Scheme 5a).[32] Further derivatization of the diphosphanato yttrium complex **16** was reported using CS_2, which afforded the highly reorganized an dianionic 3,4-dithiolate ligand, bridging two yttrium atoms in a non-symmetric fashion in **17** (Scheme 5b). The reaction with an excess of CO gas (1 atm.) afforded the P–P and Y–P bond insertion product **18**. DFT provided insight into the unusual insertion, revealing that the first step of the reaction is the insertion of CO into a Y–P bond followed by the migration of another P atom to the resulting acyl carbon, thus proceeding *via* **19**. The preferential addition of the Y–P bond over the P–P bond was confirmed by treatment of **16** with electrophilic

heterocumulenes (Scheme 5d). From the reaction with azobenzene (PhN=NPh) compound **20** was isolated, bearing a functionalized diphosphine ligand. Moreover, the reactions with PhNCE (E = S, O) afforded the addition products **21**. Specifically, when **21a** was recrystallized from a THF/hexane mixture loss of the coordinating THF was observed, which led to rearrangement of the P_2 ligand and formation of **22**. Treatment of **16** with sulfur or selenium led to chalcogenylation of the diphosphine ligand and formation of the corresponding di-sulfides/selenides in **23** and **24**, respectively (Scheme 5e). The formation of **23** and **24** was explained by insertion of sulfur/selenium into each Y–P bond of **16**.

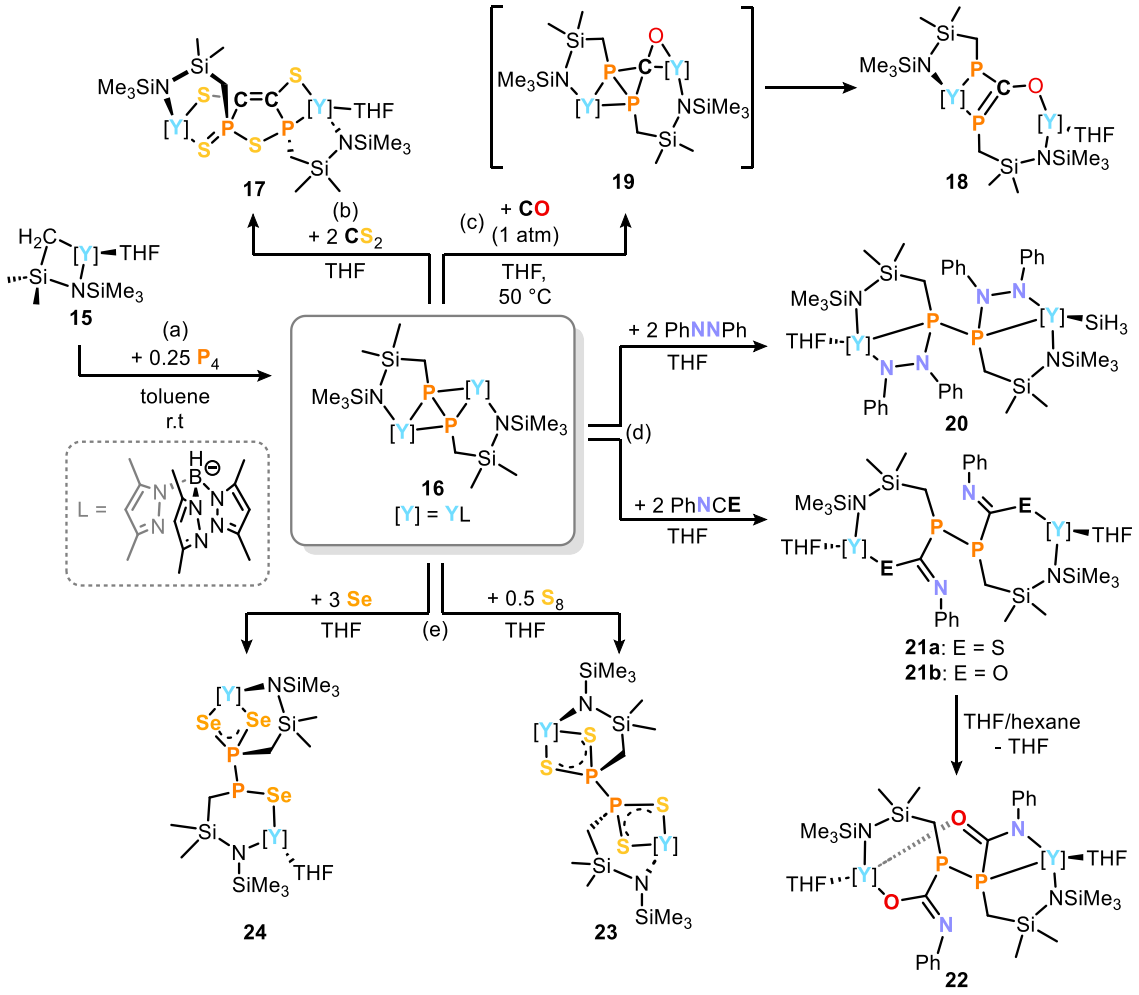

Scheme 5. Yttrium mediated one-step activation and functionalization of P_4 with further derivatization of the resulting P_2 ligand.

Building on these results, Zhan, Zhou, Li, and co-workers also reported a related direct functionalization of P_4 mediated by rare-earth metal dialkyl complexes **25** (Scheme 6).[32] Treatment of **25** with white phosphorus afforded the two rare-earth polyphosphorus complexes **26** and **27**, bearing norbornene-$(PhCH_2)P_7^{4-}$ or chain-$(PhCH_2)_4P_6^{4-}$ ligands, respectively, through release of tribenzylphosphine $P(CH_2Ph)_3$ **28**. The stoichiometry

used is of crucial importance for this reaction, and by changing the molar ratios, complexes **26** and **27** were synthesized in a targeted manner. Specifically, the lutetium complex **26b** was further functionalized using Me_3SiCl, affording the heptaphosphido cluster **29** and the lutetium dichloride **30**, which was recovered and subsequently used for regeneration of the starting material **25b** employing KCH_2Ph, thus making a fully closed synthetic cycle.

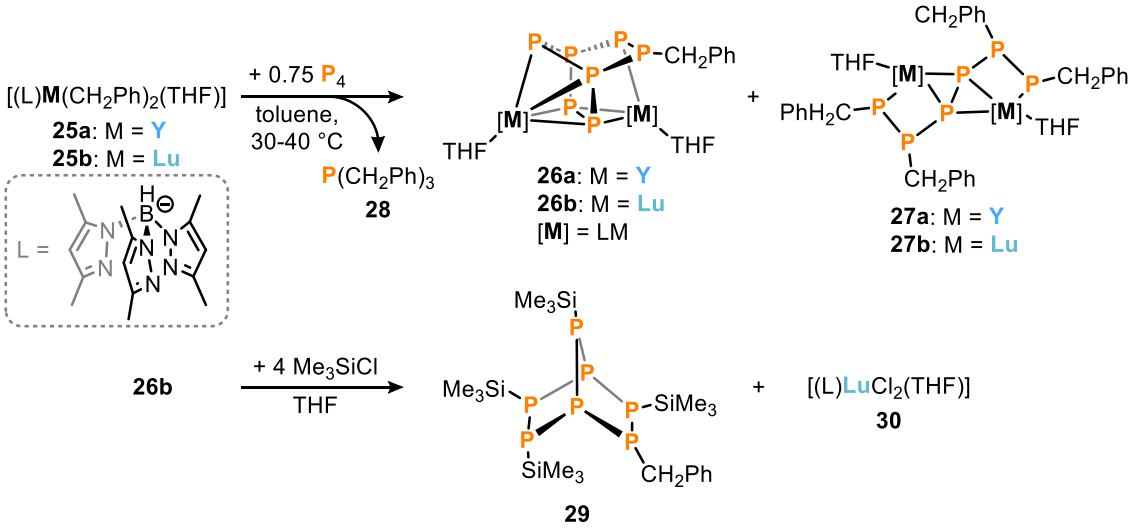

Scheme 6. Rare-earth-mediated synthesis and functionalization of P_7 and P_6 complexes starting from P_4.

In contrast to aforementioned examples of [3+1] fragmentation reactions, one-step transformation of P_4 can also lead to *cyclo*-P_3 ligands without concomitant generation of a P_1 moieties. Wolf, Hey-Hawkins and co-workers recently reported such an unusual [3+1] fragmentation reaction in which both the generated P_3 and P_1 units remain coordinated to the metal center, as illustrated in Scheme 7a.[33] Upon treatment with white phosphorus, the electron-rich bis(phosphanido) moiety in anionic $[Co\{1,2(PMes)_2C_2B_{10}H_{10}\}(cod)]^-$ (**31**, Mes = 2,4,6-$Me_3C_6H_2$ cod = 1,5-cyclooctadiene) abstracted a single phosphorus atom from P_4, generating a P_3 chain. The remaining three phosphorus atoms derived from P_4 formed the η^3-coordinating *cyclo*-P_3 ligand in **32**.

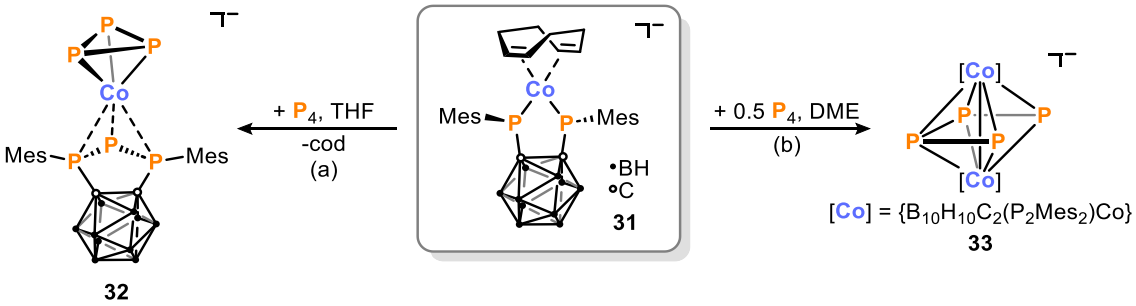

Scheme 7. Cobaltate mediated [3+1] fragmentation of P_4 and synthesis of homodinuclear complex; Mes = 2,4,6-$Me_3C_6H_2$, DME = dimethoxyethane.

Only few related examples that incorporate both the resulting P_3 and P_1 fragment in the same product have been reported in the literature.[27,28,34,35] Additionally, in the reaction a small amount of the binuclear complex $[\{B_{10}H_{10}C_2(P_2Mes_2)Co\}_2(\mu\text{-}\eta^4\text{:}\eta^4\text{-}P_4)]^-$ (**33**) was formed, featuring a P_4 chain in its molecular structure, as shown in Scheme 7b. By applying different conditions, **33** was cleanly synthesized in a targeted approach.

1.3 Functionalization of P_1 Ligands

Separating the P_4 activation step from subsequent functionalization allows for more versatile and targeted transformations.[11–17,36] Thus, the upcoming sections will focus on the functionalization of P_1 to P_4 ligands derived from P_4.

Cummins and co-workers demonstrated the impressive synthetic potential of niobium phosphide **33**, accessible by reduction of the bridging P_4-derived diphosphide precursor **34** with Na/Hg (Scheme 8a).[37,38] The latter complex **34** was obtained from activation of P_4 using the hydride **35**. Remarkably, monophosphide **33** was capable of further solvent-dependent P_4 activation (Scheme 8b).[39] When performing the reaction in a coordinating solvent (THF), addition of the entire tetrahedron occurred, accompanied by the migration of one amide ligand from the niobium center onto a phosphorus atom, resulting in the functionalized *cyclo*-P_5 anion **36**. Conversely, when the reaction was performed in a non-coordinating solvent (Et_2O), white phosphorus served as a source of P_2, which reacted with the phosphide moiety to give a *cyclo*-P_3 ligand in the niobium complex **37**. Reactions of **33** with phosphorus-containing electrophiles also provided formation of higher nuclearity oligophosphorus units through salt metathesis (Scheme 8c, d). Treatment of anion **33** with chlorophosphines at low temperatures yielded η^2-phosphanylphosphinidene complexes **38**,[38] while reaction of the chloroiminophosphine ClP=NMes* (Mes* = 2,4,6-*t*$Bu_3C_6H_2$) resulted in **39**.[40] Compound **39** features the diphosphorus analogue of an organic azide ligand (P=P=N−Mes*), coordinating through the P=P unit in an η^2-fashion. Remarkably, heating of **39** led to thermal release of a formal [P≡P] unit, which was trapped with 1,3-cyclohexadiene (1,3-CHD) to form the corresponding double cycloaddition adduct **40** and the niobium imide complex **41** (Scheme 8d).

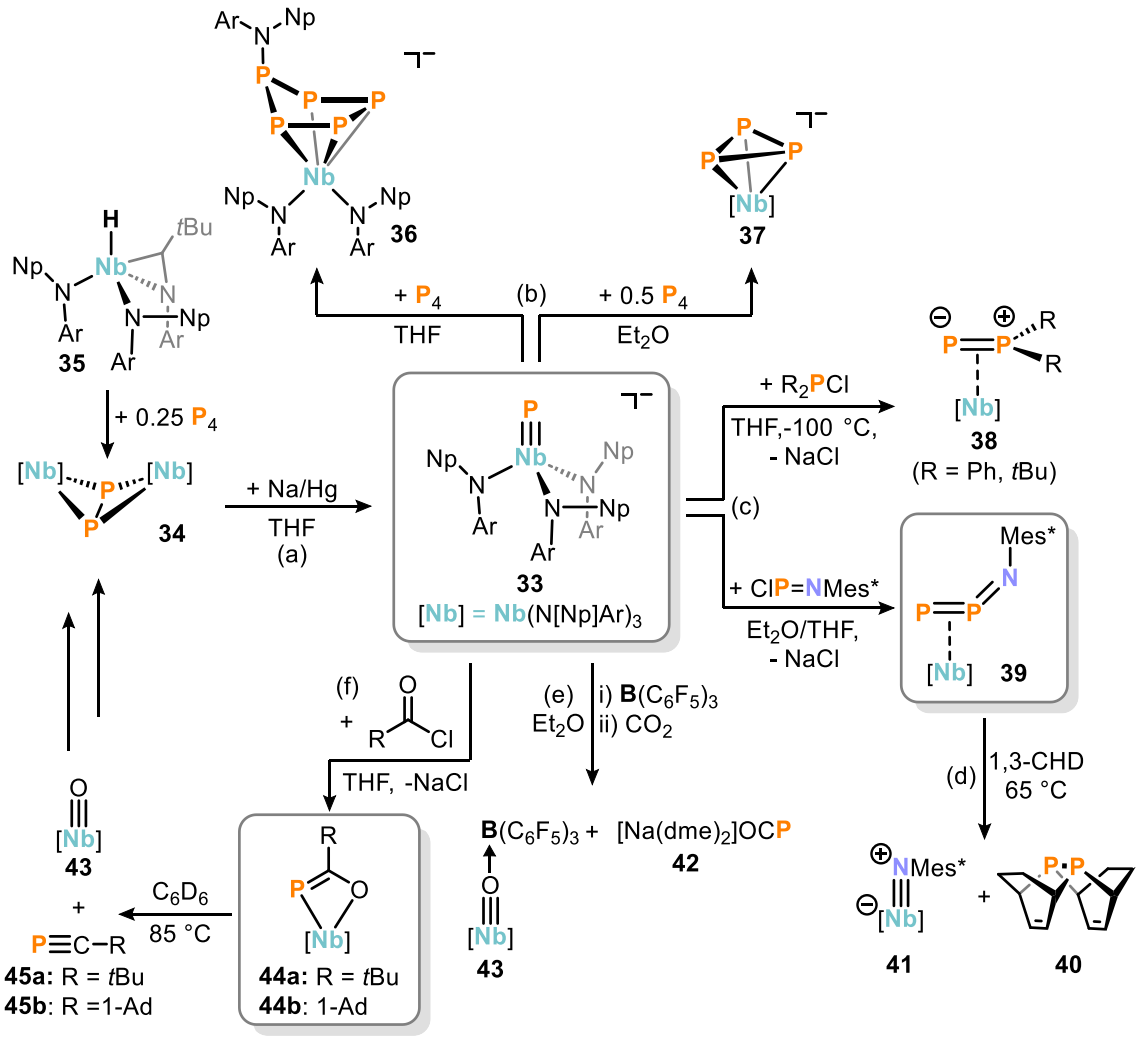

Scheme 8. Niobium phosphide mediated functionalization of P_4; Np = CH_2tBu, Ar = 3,5-$Me_2C_6H_3$, Mes* = 2,4,6-$tBu_3C_6H_2$, 1,3-CHD = 1,3-cyclohexadiene

The phosphide ligand in **33** can also act as a P_1^- transfer reagent in the synthesis of known organophosphorus reagents (Scheme 8e, f).[41] Treatment of the Lewis acid adduct **33**-$B(C_6F_5)_3$ with a stoichiometric amount of CO_2 led to a formal multiple bond metathesis, affording the sodium salt of the phosphaethynolate anion OCP^-, **42**, and oxo-niobium adduct **43**-$B(C_6F_5)_3$, featuring a strong Nb≡O triple bond. The driving force of this reaction is the oxophilicity of niobium, which induces [2+2] fragmentation of the cyclic Nb−P−C(O)−O intermediate.[42] Applying a similar strategy, Cummins and colleagues reported the transformation of acyl chlorides into the corresponding phosphaalkynes (Scheme 8f).[43] Treatment of **33** with RC(O)Cl yielded niobacycles **44**, which undergo thermolysis to yield phosphaalkynes **45** and the niobium(V)-oxo product **43**. This process was reported to form a closed synthetic cycle by stepwise deoxygenation of **43**, activation of P_4 to give **33**, and regeneration of **43** by reduction *via* **35**.

1.4 Functionalization of P_2 Ligands

The functionalization of P_2 ligands derived from P_4 is generally less common than that of P_1, P_3 and P_4 ligands.[12–15] The early examples for transformations of multinuclear P_2 complexes were reported by Scherer and co-workers as early as the 1990s and included oxidation of the phosphorus moieties using sulfur, or selenium.[44–46] In 2000, Scheer and co-workers reported the functionalization of a Cr_2P_2 complex with ECl_3 (E = P, As, Sb) and PCl_5.[47] More recently, Ruiz and co-workers reported the activation of P_4 with anionic dimolybdenum and ditungsten complexes (Scheme 9a).[48,49] The triple-bonded complexes **46** incorporate half an equivalent of P_4 under mild conditions, yielding tetrahedral and diphosphorus-bridged anions **47**.

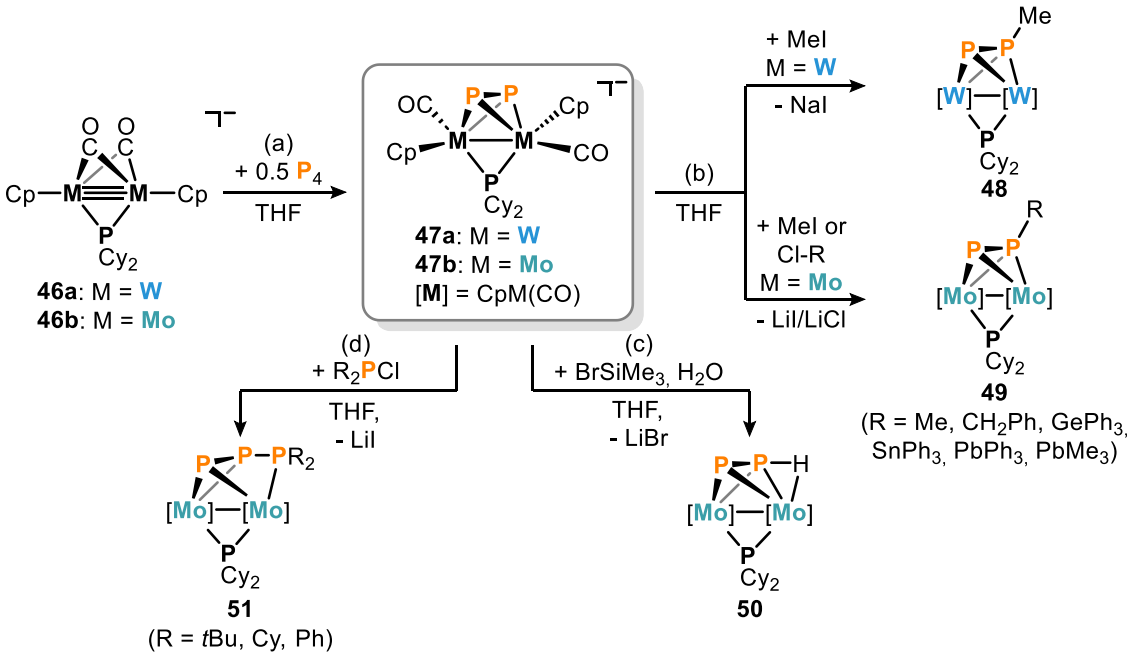

Scheme 9. Functionalization of dinuclear group 6 P_2-complexes with group 14 electrophiles and chlorophosphines; Cp = η^5-C_5H_5

The tungsten derivative **47a**, generated *in situ*, shows high reactivity toward electrophiles such as MeI, due to retention of its anionic character. Thus, the further functionalized and more stable methyldiphosphenyl complex **48** was isolated, bearing a methyl group at the P atom (Scheme 9b).[49] The reactivity of the molybdenum congener **47b** was more thoroughly explored by reactions with various group 14 electrophiles (C, Ge, Sn Pb), all giving rise to isostructural complexes **49**, bearing a functionalized P_2 moiety.[50] Conversely, the reaction of **47b** with $BrSiMe_3$ did not lead to the expected silyl diphosphenyl derivative, but instead gave the agostic diphosphenyl complex **50**. The authors suggested that the undetected silyldiphosphenyl species reacts rapidly with trace amounts of water, thus hydrolyzing the newly formed P−Si bond to give the final product

50 and a siloxane byproduct. Additionally, reactions of **47b** with chlorophosphines R_2PCl (R = *t*Bu, Cy, Me) selectively gave the corresponding phosphinodiphosphenyl complexes **51**.[51] For R = *t*Bu, **51** is in an equilibrium with an isomer in which the pendant P*t*Bu_2 group is non-coordinating to the molybdenum center.

1.5 Functionalization of P_3 Ligands

In contrast to P_2 ligands, the functionalization of P_3 ligands derived from P_4 has been subject to much more investigation. In fact, the first examples of transition-metal-mediated functionalization of P_3 ligands with carbon-based electrophiles were reported by Peruzzini and Stoppioni as early as 1986.[52,53] Treatment of previously discussed **2a-c** (*vide supra*, Scheme 2) with highly electrophilic alkylating agents yielded η^3-coordinating methyl- and ethyltriphosphirene ligands in cations **52** (Scheme 10a).[54] The cobalt complex **2c** was also protonated by treatment with triflic acid, yielding **53** (Scheme 10b).[55] Unlike the alkyl groups in **52**, the H^+ in **53** interacted with both the *cyclo*-P_3 ligand and the cobalt center, as indicated by spectroscopic and crystallographic studies, and was thus most likely located between the two.

Three decades later, Scheer and co-workers investigated the reactivity of nickel *cyclo*-P_3 species **54**, as an isolobal analogue to P_4, toward main group nucleophiles (Scheme 10c).[56,57] The reaction of $LiNMe_2$ with **54** yielded anionic η^2-triphosphirene complex **55** as an isolable product, bearing a newly formed P−N bond. In comparison, while the reaction of sandwich compound **54** with $LiPPh_2$ initially formed an analogous triphosphirene species **55**, according to variable temperature ^{31}P NMR studies, this complex rapidly reacted with another equivalent of **54** at room temperature to irreversible form the heptaphosphine complex **56**. While **56** was not readily purified due to high sensitivity, upon protonation with HBF_4 the product was structurally characterized. For Nu = NMe^- compound **56** was observed only in minor amounts.

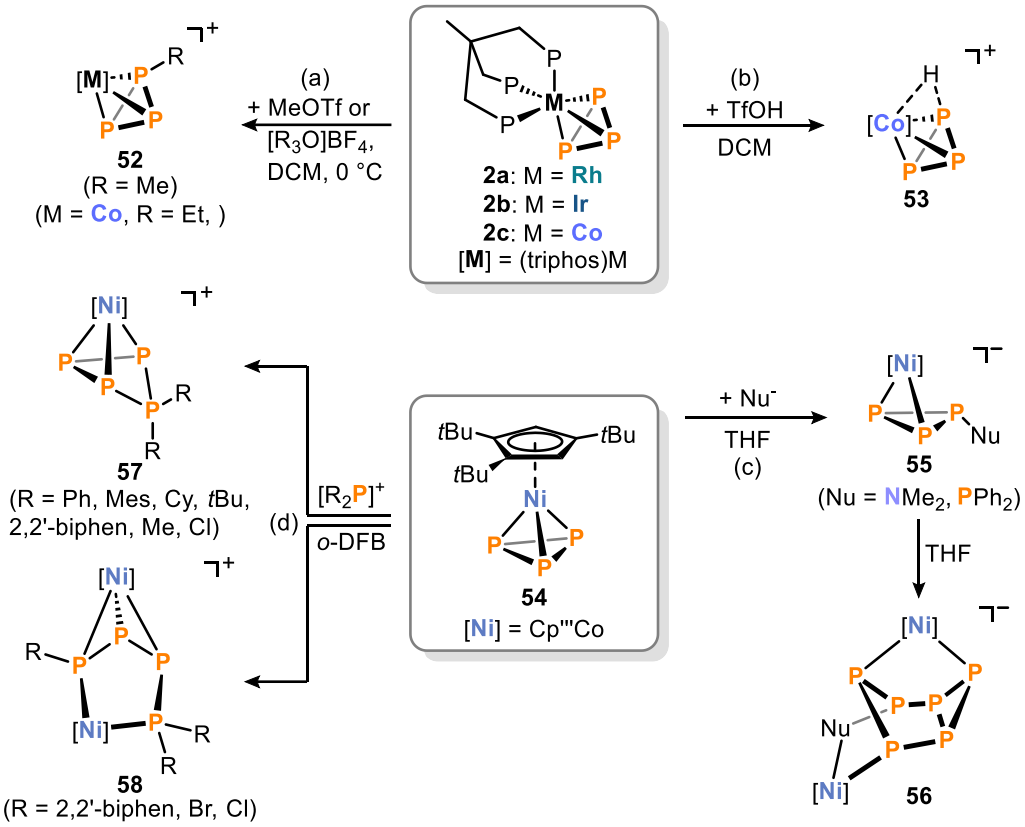

Scheme 10. Reactivity of neutral *cyclo*-P_3 complexes toward electrophiles and nucleophiles; TfOH = CF_3SO_3H, *o*-DFB = 1,2-$F_2C_6H_4$.

More recently, Scheer and co-workers reported the related reactivity of neutral **54** toward phosphenium cations $[RP_2]^+$ (Scheme 10d).[58] The cations were generated *in situ* from R_2PCl and a halide-abstracting agent (Tl[OTf], $Tl[GaCl_4]$; $[OTf]^- = CF_3SO_3^-$) and inserted into the triphosphirene ligand in **54**, yielding mononuclear cations **57**, bearing a η^3-coordinating *cyclo*-P_4R_2 ligand. However, the formation of binuclear complexes **58** was observed when cations $[Br_2P]^+$ and $[(2,2'\text{-biphen})P]^+$ were employed.

Related neutral complexes bearing η^2-triphosphirene ligands were reported in 2008 by Cummins and co-workers, through reaction of di- and trinuclear *cyclo*-P_3 complex anions **59a,b** with various electrophiles.[59] Oligonuclear anions **59** became initially accessible by transfer of $[(P_2)W(CO)_5]$ fragments to the $W(CO)_5$ adduct of niobium phosphide $Nb{\equiv}P^-$ **33**, with an improved and aforementioned synthesis reported three years later (*vide supra*, Scheme 8b).[39] Similar to the terminal niobium phosphide **33**, the triphosphirene ligand was functionalized upon treatment of **59** with ClP=NMes*, yielding NbP_4 complex **60** through concomitant loss of one $[W(CO)_5]$ fragment and migration of the second $[W(CO)_5]$ moiety to the iminophosphine (Scheme 11a). As indicated by $^{31}P\{^1H\}$ NMR spectroscopy, the exocyclic Mes*NP$[W(CO)_5]^+$ group circumambulated around the *cyclo*-P_3 ligand at room temperature, a dynamic process which was slowed upon cooling

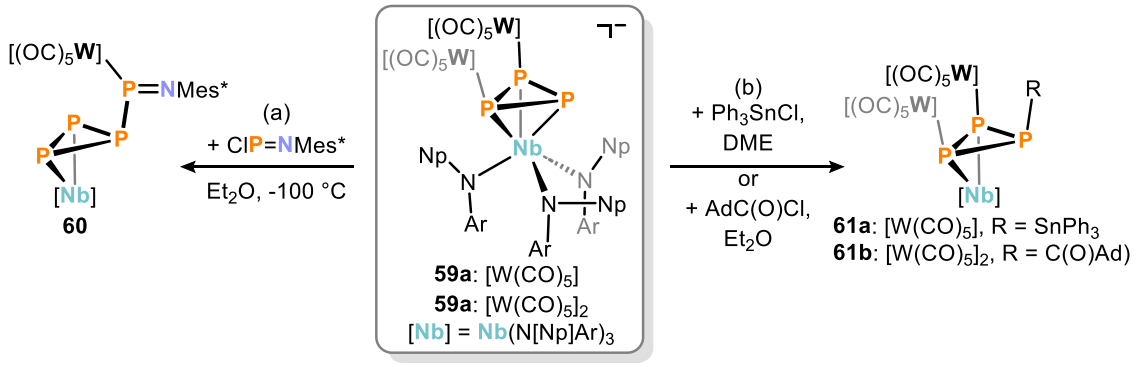

Scheme 11. Electrophilic functionalization of oligonuclear niobium *cyclo*-P_3 anions; Ar = 3,5-$Me_2C_6H_3$, Np = CH_2tBu, Mes* = 2,4,6-$tBu_3C_6H_2$.

the solution to −70 °C. Reactions of **59** with Ph_3SnCl and 1-adamantoyl chloride yielded the dinuclear P-stannylated and trinuclear P-acyclated species **61a** and **61b**, respectively (Scheme 11b).[59] However, the acylated derivative is thermally unstable and decomposes above temperatures of −20 °C, in contrast to acylated niobium P_1-species **44** (*vide supra*, Scheme 8).[43]

In 2009, Cummins and co-workers reported an anionic niobium *cyclo*-P_3 complex similar to **59**, bearing phenolato ligands instead of anilido ligands, and its use as a P-transfer reagent.[60] The reported synthesis involves reduction of niobium chloride **62** in the presence of white phosphorus affording the P_3-synthon **63** (Scheme 12a).[61] Upon treatment of **63** with the molybdenum(IV) iodide complex **64**, one phosphorus atom was abstracted to give the terminal molybdenum phosphide complex **65**, with elimination of NaI and concomitant formation of a transient niobium P_2-containing species, **66** (Scheme 12b).[62] **66** rapidly underwent dimerization, quantitively yielding the dinuclear *cyclo*-P_4 cluster **67** in a an overall 2 × (3−1) process. However, trapping **66** by conducting the reaction in neat 1,3-CHD afforded the corresponding cycloaddition product **68**, present in an equilibrium. Subsequent addition of the oxidant pyridine-*N*-oxide elicited liberation of the diphosphine ligand, and the formation of the aforementioned double cycloaddition adduct **40** (*cf.* Scheme 8) with concomitant release of the niobium oxo species **69**.[40]

Complex **63** also allowed access to higher polyphosphorus compounds, when used as a source of P_3^{3-} (Scheme 12c).[61] This was achieved by treatment of **63** with the electrophile Ph_3SnCl, yielding η^2-stannyltriphosphirene complex **70**. The resulting Ph_3Sn^+ moiety circumambulated around the *cyclo*-P_3 ring in solution and no locking out of this movement was observed on the NMR timescale at temperatures down to −90 °C (*cf.* complex **60**). Similar to the release of **40** from **68** (*cf.* Scheme 12b), the addition of pyridine-*N*-oxide liberated the triphosphirene moiety P_3SnPh_3.[62]

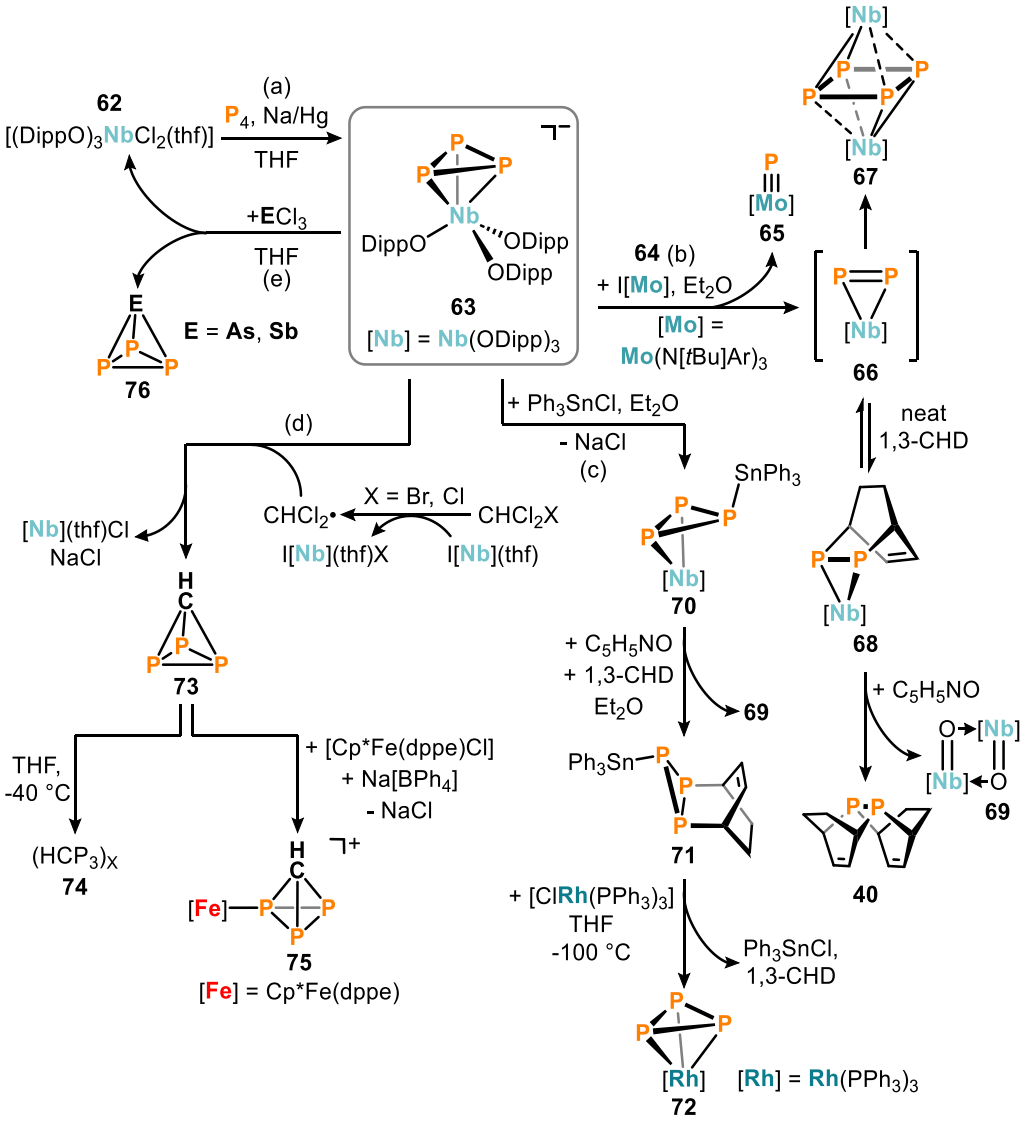

Scheme 12. Phosphorus transfer reactions promoted by anionic niobium *cyclo*-P_3 complex; 1,3-CHD= 1,3-cyclohexadiene, Ar = 3,5-$Me_2C_6H_3$, dppe = $Ph_2PCH_2CH_2PPh_2$.

This was trapped with excess 1,3-CHD to exclusively afford the *endo*-cycloaddition adduct **71**, along the niobium oxo dimer **69**. This liberation of phosphorus-containing molecules has been elucidated by DFT and proceeds through a redox-neutral Bayer-Villiger oxygen insertion into the Nb−P bond.[63] More specifically, the formation of the strong Nb≡O bond provided the driving force for the release of the Ph_3SnP_3 fragment and the P_2 adduct **40**. Owing to the reactive P−Sn bond and the 1,3-cyclohexadiene protecting group, **71** serves as a further P_3-transfer reagent.[61] Thus, transfer of the *cyclo*-P_3 unit onto Wilkinson's catalyst [$ClRh(PPh_3)_3$] was achieved through a [4+2] retrocycloaddition with concomitant loss of Ph_3SnCl and 1,3-CHD, resulting in octahedral rhodium complex **72** (*c.f.* complexes **2a-c**).[21,52,53] The Ph_3Sn-moiety in **71** can be replaced by other group 14 units, including Ph_3C-, Ph_3Si-, and Me_3Si-, allowing the assembly of a library of P_3^- transfer reagents exhibiting varied reactivity properties.

Recently, Cummins and co-workers reported that the role of **63** as a P_3 transfer reagent allows it to serve as a platform for the exceptional synthesis of mixed tetrahedranes.[64] Treatment of **63** with the carbon-centered radical $CHCl_2$•, generated *in situ* by halogen abstraction from bromodichloromethane or chloroform by the Nb(IV) complex [$(DippO)_3NbI(thf)$], generated triphosphatetrahedrane (**73**), and the side products [$(DippO)_3Nb(thf)Cl$] and NaCl (Scheme 12d). Upon concentrating a solution of **73** in THF, a black precipitate was formed and polymerization to $(HCP_3)_X$(**74**) was observed. This is in sharp contrast to the mono- and diphosphatetrahedrane, which can be isolated neat.[65,66] In addition, [Cp*Fe(dppe)Cl] (dppe = $Ph_2PCH_2CH_2PPh_2$), which has been shown to form stable adducts with P_4, reacted readily with tetrahedrane **73** under reductive conditions, yielding complex **75**.[67] In compound **75**, the tetrahedrane **73** is coordinating η^1- *via* a single phosphorus vertex, resulting in distortion in the tetrahedrane, as corroborated by $^{31}P\{^1H\}$ NMR spectroscopy, where the three phosphorus atoms give rise to two distinct resonances.[64] The authors also previously reported the facile synthesis of the binary interpnictogen tetrahedrane species EP_3 (**76**) *via* salt metathesis reactions of **63** with ECl_3 (E=As, Sb, Scheme 12e).[60] The byproduct of this reaction was the niobium(V) chloride complex **62**, which can be recycled to the *cyclo*-P_3 precursor (Scheme 12a), thereby closing the synthetic cycle.

1.6 Functionalization of P_4 Ligands

Considering that the generation of P_4 ligands is most commonly observed in transition-metal-mediated P_4 activation, the focus of research on phosphorus functionalization has unsurprisingly centered predominantly around these complexes. Various methods for the functionalization of tetrahedral P_4 ligands, "butterfly-P_4" (= [1.1.0]bicyclotetraphosphane-1,4-diyl) ligands, *cyclo*-P_4 units, and *catena*-P_4 species using transition metals have been reported and are detailed in two recent review articles.[14,15] However, the functionalization of *cyclo*-P_4 ligands is less common than that of tetrahedral or butterfly-P_4 ligands and significant advancements have been made in this field since the publication of these reviews. Thus, the following section gives an overview of these works, which are highly relevant to this thesis.

A two-step functionalization and fragmentation process mediated by low-valent cobalt complexes was reported by our group in 2019.[68] The *cyclo*-P_4 cobaltate **77** reacted quantitatively with R_2PCl (R = Cy, *t*Bu, Ph, Mes, $N(iPr)_2$), affording the neutral *cyclo*-P_5R_2 complexes **78** (Scheme 13a). The synthesis of isostructural products was also reported from the reaction of a heterodinuclear CoP_4Ga complex with

chlorophosphines,[69] and is detailed in recent review articles.[14,15] Upon treatment of **78** with cyanide salts distinct reaction outcomes were observed depending on the substituent R (Scheme 13b).[68] For R = Cy, *t*Bu, Ph, or N(*i*Pr)$_2$, the reaction with two equivalents of CN^- induced a [3+2] fragmentation, yielding anionic cyclotriphosphido cobalt complex **79** and 1-cyanodiphosphan-1-ide anions **80**. Conversely, the reaction of one equivalent of CN^- with **78**, where R = Mes, afforded CoP_5 complex **81**, featuring a rearranged P_5Mes_2 ligand. Complexes similar in structure to **81**, with partially displaced P_5R_2 ligands, may serve as key intermediates in the [3+2] fragmentations leading to **79** and **80**. However, the bulky mesityl substituent in **81** hindered such further reactivity.

Reactions of cobaltate **77** with the diphosphorus reagent **82** also allowed access to higher nuclearity phosphorus ligands (Scheme 13c).[70] VT-NMR spectroscopy showed the initial product of this reaction to be the hexaphosphido complex **83**, featuring a *cyclo*-P_5 ligand and an exocyclic ($^{Cl}Im^{Dipp}$)P moiety. However, **83** is thermally unstable and underwent disproportionation at room temperature into more stable CoP_7 (**84**) and CoP_5 (**85**) complexes.

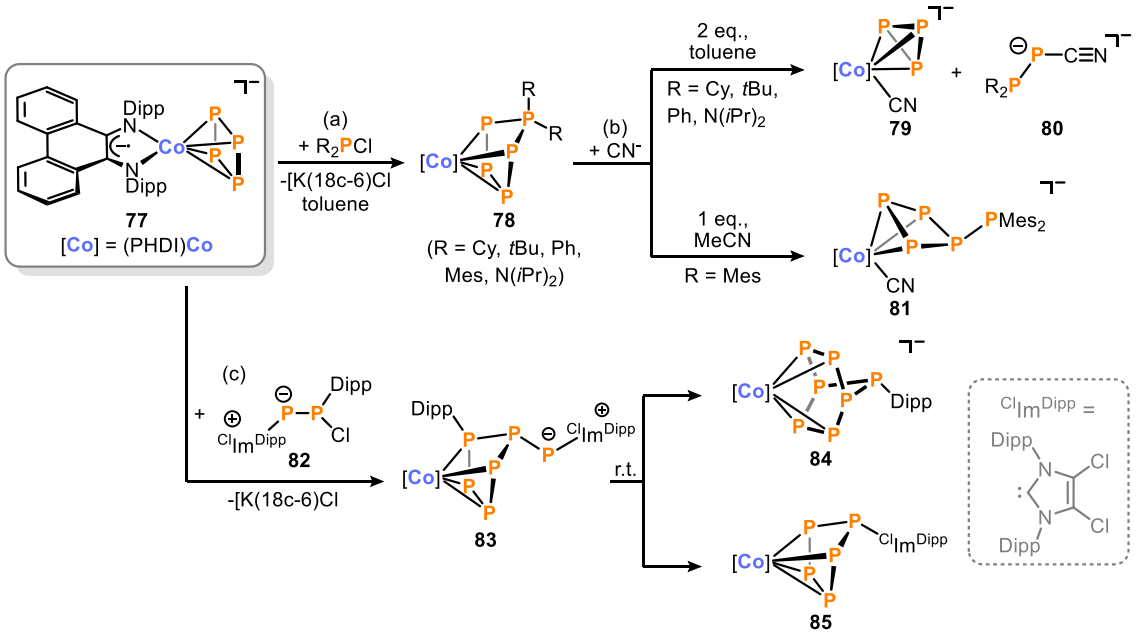

Scheme 13. Synthesis of *cyclo*-P_5R_2 complexes with subsequent [3+2] fragmentation and [4+2] condensation reaction of a *cyclo*-P_4 ligand with diphosphene; PHDI = bis(2,6-diisopropylphenyl)phenanthrene-9,10-diimine.

Scheer and co-workers also reported a series of functionalization reactions of end-deck *cyclo*-P_4 cobalt sandwich complex **86**, accessible by addition of P_4 to triple-decker complex **87** (Scheme 14).[71] Similar to the previously discussed reactivity of structurally related nickel *cyclo*-P_3 complex **54** (*cf.* Scheme 10), the *cyclo*-P_n ligand in compound **86** was functionalized upon treatment with nucleophiles (Scheme 14a).[72] At low

temperatures, reactions with organolithium reagents RLi (R = *t*Bu, CH_2SiMe_3) in the presence of chelating agents allowed isolation of the axial-substituted *cyclo*-P_4 complexes **88** as kinetic products. For R = CH_2SiMe_3 the equatorial isomer **88'** was also observed spectroscopically. Without complexation, **88** and **88'** form a mixture of products including bicyclo[3.3.0]octaphosphane **89**, 1,2--diorgano-substituted *cyclo*-P_5 anion **90** and the *cyclo*-P_3 cobaltate **91**. This reactivity resembles those of nickel η^2-triphosphirene species **55** illustrated in Scheme 10.[56]

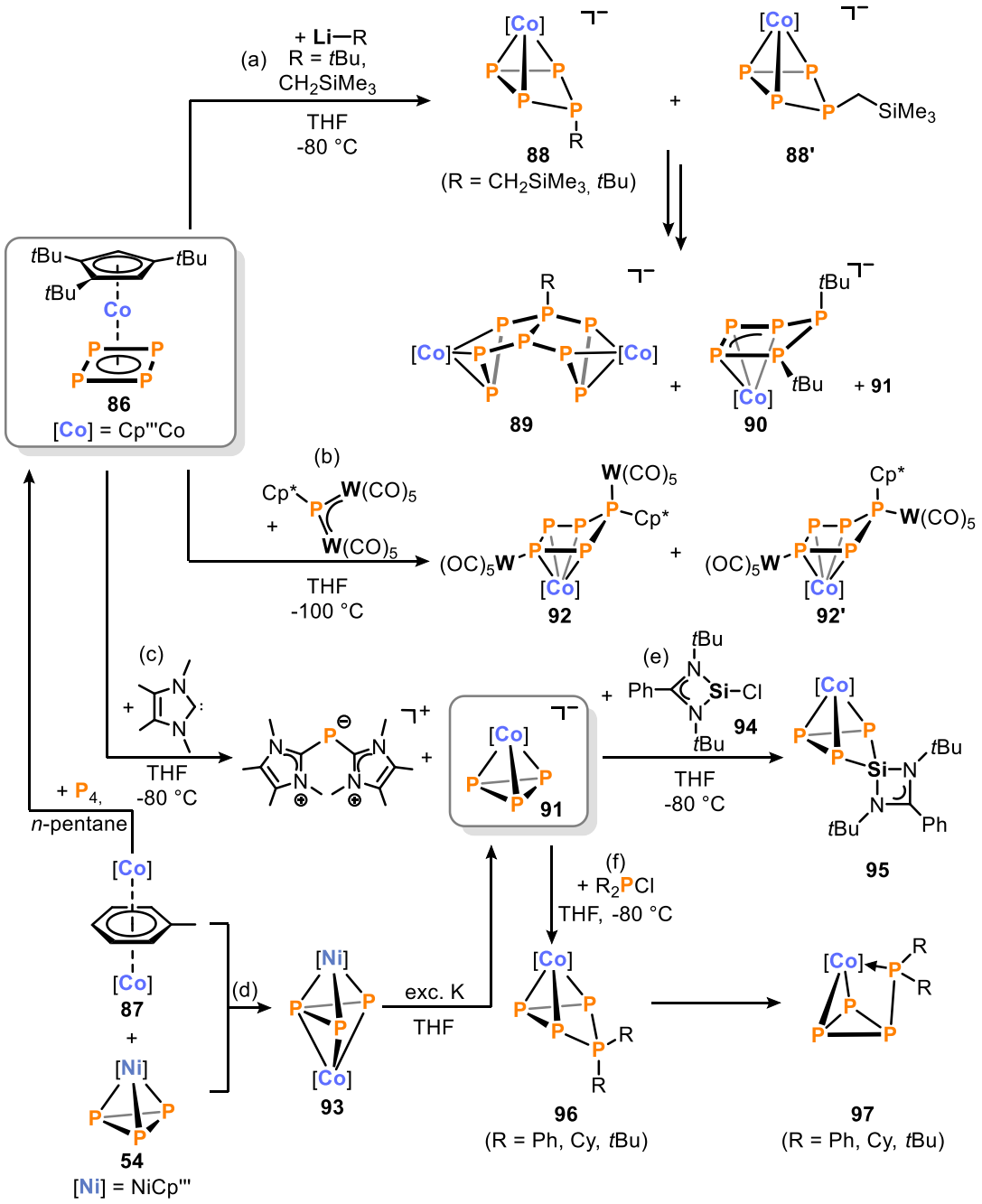

Scheme 14. Functionalization of P_4 mediated by end-deck *cyclo*-P_4 cobalt sandwich complex $Cp'''Co(\eta^4\text{-}P_4)$; $Cp''' = C_5H_2tBu_3$.

Treatment of complex **86** with the electrophilic phosphinidene complex [Cp*P{W(CO)$_5$}$_2$] resulted in the isomeric ring expansion products **92** and **92'**, through insertion into the *cyclo*-P$_4$ ligand with concomitant shift of a [W(CO)$_5$] fragment (Scheme 14b).[73] The authors found that the phosphinidene [Cp*P{W(CO)$_5$}$_2$] also induces ring expansion in the *cyclo*-P$_3$ niobate **63** (*vide supra*, Scheme 12), and additionally examined analogous reactions of **86** with the corresponding arsinidene.[60,73]

Complex **86** can also undergo ring contraction, induced by *N*-heterocyclic carbenes (NHC, Scheme 14c).[74] Treatment of **86** with two equivalents of NHC selectively abstracted one phosphorus atom and formed the cation [(NHC)$_2$P]$^+$, with *cyclo*-P$_3$ cobaltate **91** as the counteranion. Subsequently, Scheer and co-workers reported an improved synthesis for anion **91** *via* the triple-decker complex **93**, synthesized by reaction between the nickel sandwich complex **54** and cobalt toluene complex **87** (Scheme 14c).[75] Reduction of **93** with excess potassium yielded K[**91**], with concomitant loss of nickel as black precipitate. Due to the favorable salt elimination of KCl over (NHC)$_2$PCl the reactivity of K[**91**] with main group element chlorides was examined.[75] Salt metathesis with the chlorosilylene **94** led to insertion into the *cyclo*-P$_3$ moiety and the formation of an η^3-coordinating four membered ring P$_3$SiL (L = (*t*BuN)$_2$CPh) in **95** (Scheme 14e). Similarly K[**91**] was functionalized by chlorophosphines to afford **96**, featuring η^3-coordinating *cyclo*-P$_4$R$_2$ ligands. These complexes are isostructural to the previously described cations Cp'''Ni(η^3-P$_4$R$_2$)$^+$ (**57**, Scheme 10, *vide supra*). During the reaction a second complex **97** was also formed, bearing a η^2-*cyclo*-P$_3$ ligand with an exocyclic PR$_2$ unit engaging in η^1-coordination. According to ^{31}P{^{1}H} NMR spectroscopy, **97** was only formed in appreciable amounts when R = Ph.

1.7 Functionalization of P$_n$ Ligands ($n \geq 5$)

The formation of phosphorus-derived P$_n$ ligands with $n \geq 5$ through aggregation at the metal center is less common than the formation of ligands with $n \leq 4$ *via* degradation.[15] Thus, the functionalization of these ligands has been scarcely explored and most of these examples have been covered in a recent review article.[14] However, a series of transformations of the oligophosphorus-containing ferrocene analogue Cp*FeP$_5$ (**98**), derived from P$_4$ and first reported by Scherer in 1987,[76] have been reported since.

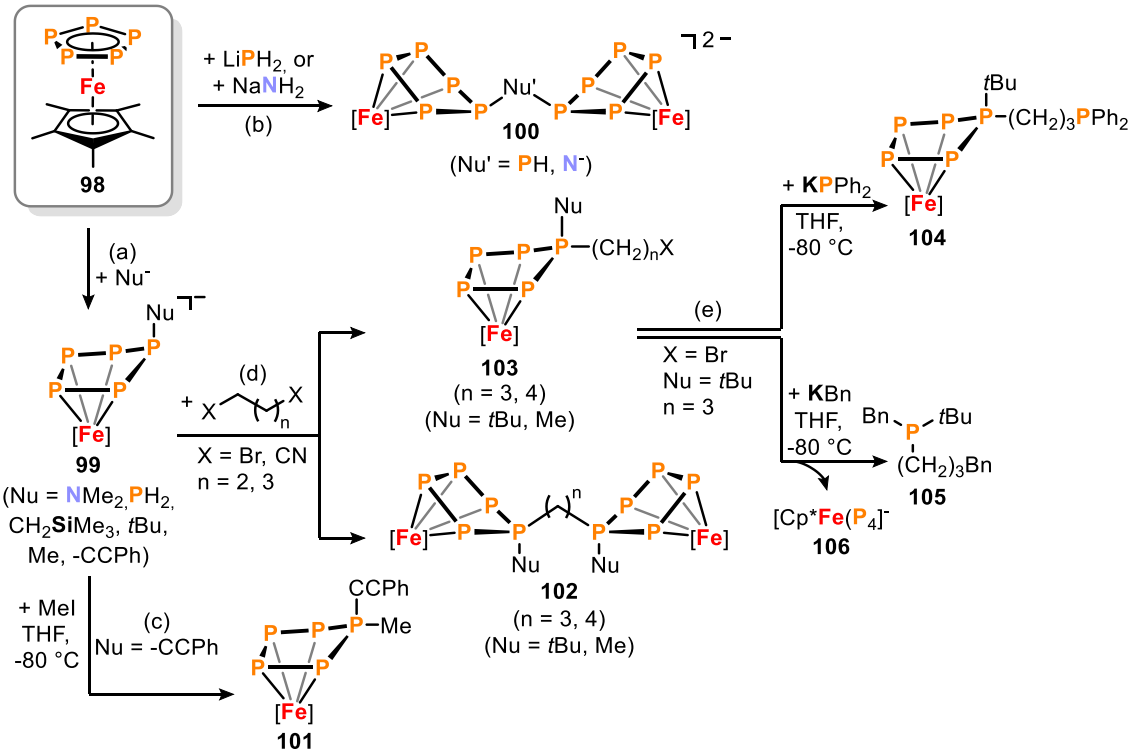

Scheme 15. Functionalization of the *cyclo*-P_5 ligand in pentamethylpentaphosphaferrocene to give monophosphorus compounds; Bn = $CH_2C_6H_5$

In 2014, Scheer and co-workers reported the functionalization of **98** with different main group nucleophiles (Nu = -NMe_2, -PH_2, -CH_2SiMe_3), yielding η^4-P_5Nu ferrate complexes **99** in an envelope conformation (Scheme 15a; *cf.* reactivity of NiP_3 **54**, Scheme 10).[77] Distinctively, for the nucleophiles $LiPH_2$ and $NaNH_2$, the formation of dinuclear complexes **100** was also observed (Scheme 15b). In 2023, an extended scope of reactivity toward nucleophiles (Nu = *t*Bu, Me, C≡CPh), and onward reactivity of **99** with carbon-centred electrophiles, was reported.[78] Introduction of a second alkyl group to **99** (Nu = C≡CPh) with methyl iodide afforded complex **101**, bearing a η^4-P_5(CCPh)(Me) ligand (Scheme 15c). Conversely, treatment of **99** with dihaloalkanes formed a mixture of di- and mononuclear complexes **102** and **103**, which were separated by column chromatography (Scheme 15d). Other isomers were formed as side products in these reactions, by migration of the alkyl residues. The reaction was reported to tolerate pseudoalkanes (nitriles) instead of halides and various alkyl chain lengths, affording a range of functionalized η^4-P_5R_2 ligands. Moreover, the bromide group in **103** (Nu = *t*Bu, n = 3) is accessible for further reactivity (Scheme 15e). Thus, salt metathesis with KPH_2 selectively yielded compound **104**, featuring a terminal PH_2 unit. In comparison, consecutive treatment of **103** with two equivalents of benzyl potassium (KBn) gave the asymmetrically substituted phosphine **105**. The first equivalent of KBn substituted the

bromide, while the second equivalent formed **105** with concomitant formation of $[Cp^*Fe(\eta^4\text{-}P_4)]^-$ (**106**).

In the same year, Scheer and co-workers reported a related approach based on the pentaphosphaferrocene dianion **107**, synthesized by reduction of **98** with excess potassium (Scheme 16a).[79,80] Treatment of **107** with dihaloalkanes of different chain lengths gave complexes **108** and **109** (*cf.* reactivity of monoanion **99** toward di-(pseudo-)haloalkanes, see Scheme 15d). Compound **108** features an $\eta^4\text{-}P_5(C_3H_6Br)_2$ ligand as a result of functionalization with two equivalents of electrophile. In contrast, compound **109** bears a spiro-cyclic ligand with a functional group similar to a phosphetane. The formation of **109** occurs by the initial formation of a monoanion **110**, followed by an intramolecular salt metathesis reaction. The doubly substituted phosphorus atom was released from the Cp*Fe fragment by successive treatment with LiAlH, or KBn to yield the corresponding secondary and tertiary cyclic phosphines, respectively (**111**, **112**, Scheme 16c). Overall, this procedure demonstrates an elegant route to P_4-derived organophosphines, which are good ligands in coordination chemistry, as exemplified by the reaction of **111** with $[Pt(PhCN)_2Cl_2]$, affording complex **113**.

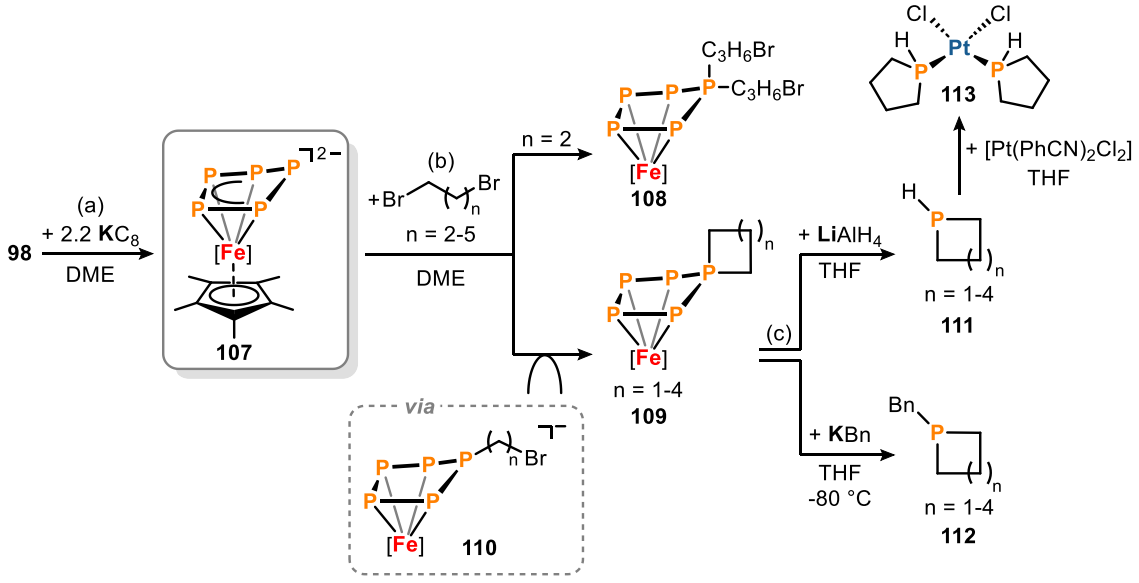

Scheme 16. Reactivity of **107** toward dihaloalkanes and subsequent release of cyclic phosphines, KBn = benzyl potassium.

Scheer and co-workers also reported a major breakthrough in transition-metal-mediated functionalized of P_4 – a closed synthetic cycle for the synthesis of asymmetric, monophosphorus compounds (Scheme 17).[81] Building on the nucleophilic functionalization of **98** to give the anionic species **99** (*vide supra*, Scheme 15a), treatment of these anions with alkyl halides selectively yielded 1,1-diorgano-substituted complexes **114** (Scheme 17a and b, R' = Me, *i*Pr).[77,81] Treatment with a second nucleophile (KBn,

n-Buli, MeLi) facilitated installation of a third substituent and release of the corresponding tertiary phosphine (Scheme 17c; R" = Bn, *n*-Bu, Me).[78,81] The resulting phosphines were conveniently separated from the crude mixture by distillation. Remarkably, the FeP_4^- byproduct **106** could be recycled to the starting material **98** by addition of P_4 and heating to 275 °C, thereby closing the synthetic cycle (Scheme 17d). Moreover, the entire synthetic cycle could be performed as a "one-pot" reaction, by sequential addition of the relevant reagents in up to three cycles without significant loss of yield. A limitation of this synthesis is the formation of KP_5 as a byproduct in the regeneration of **98** from **106**, hindering the atom-economy of the reaction.

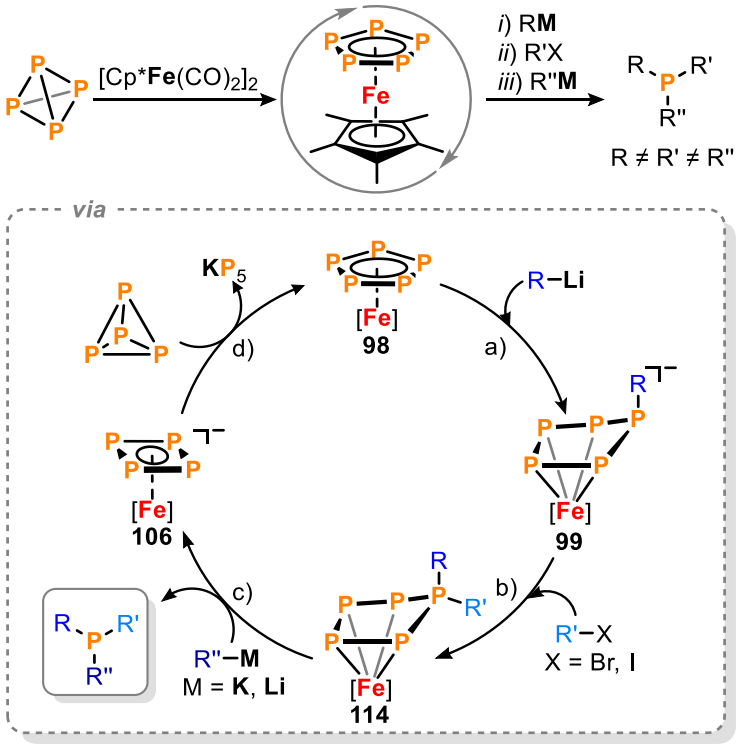

Scheme 17. Synthesis of asymmetric phosphines from P_4; R ≠ R' ≠ R"; R = NMe_2, CH_2SiMe_3, Me, *t*Bu, Ph; R' = Me, *i*Pr; R" = Bn, *n*-Bu, Me

In 2023, the same group reported the activation and functionalization of P_4 using the tantalum carbonyl complex Cp'''$Ta(CO)_4$ (**114**).[82] Distinct reactivity was observed depending on the cyclopentadienyl ligand and the reaction conditions (Scheme 18a). Photolysis of a solution of **114** and P_4 in toluene at room temperature afforded mononuclear *cyclo*-P_4 complex **115**, the Cp" analogue of which was first reported by Scherer in 1993.[83] Conversely, heating a solution of **114** and P_4 in 1,3-diisopropylbenzene at 203 °C afforded the Ta_2P_8 complex **116**, the first example of a *cyclo*-P_8 complex.[82] The *cyclo*-P_4 moiety in **115** was further functionalized with *in situ* generated pnictogenium ions from chlorophosphines and Tl[TEF] ([TEF]$^-$ =$[Al\{OC(CF_3)_3\}_4]^-$ (Scheme 18b).[84] For $[Ph_2P]^+$, insertion of the cation was observed,

resembling reactivity of **54** and **86** (*cf.* Scheme 10 and Scheme 14).[58,73] In contrast, when the electrophile was exchanged for the heavier arsenium $[Cy_2As]^+$, or stilbenium ion $[Cp'''SbI]^+$, the pnictogen coordinated to the *cyclo*-P_4 moiety in **117**[TEF] in the solid state.[84] However, in the case of Cy_2As, $^{31}P\{^1H\}$ NMR studies suggested the presence of an *cyclo*-P_4As ring, indicating insertion in solution. The arsenium cation $[Cy_2As]^+$ also coordinated to the *cyclo*-P_8 ring in **116**, giving rise to **118**[$BArF_{24}$] ($[BArF_{24}]^-$ =[B{3,5-$(CF_3)_2C_6H_3$}$_4$]$^-$), featuring an exocyclic $AsCy_2$ moiety (Scheme 18c).[82] The Lewis acid $[W(CO)_5(thf)]$ also served to coordinate **116** (Scheme 18d). The major product of this reaction was the tetranuclear complex **119**, accompanied by the formation of unstable and trinuclear **120**, hampering isolation of **119** in good yield. However, thermolysis led to selective cleavage of one $[W(CO)_5]$ fragment from the P_8-moiety and the formation of a single new species **121**, bearing the substituent at the same phosphorus atom as cation **118**. This phosphorus atom has a high contribution to the HOMO, explaining the observed reactivity.

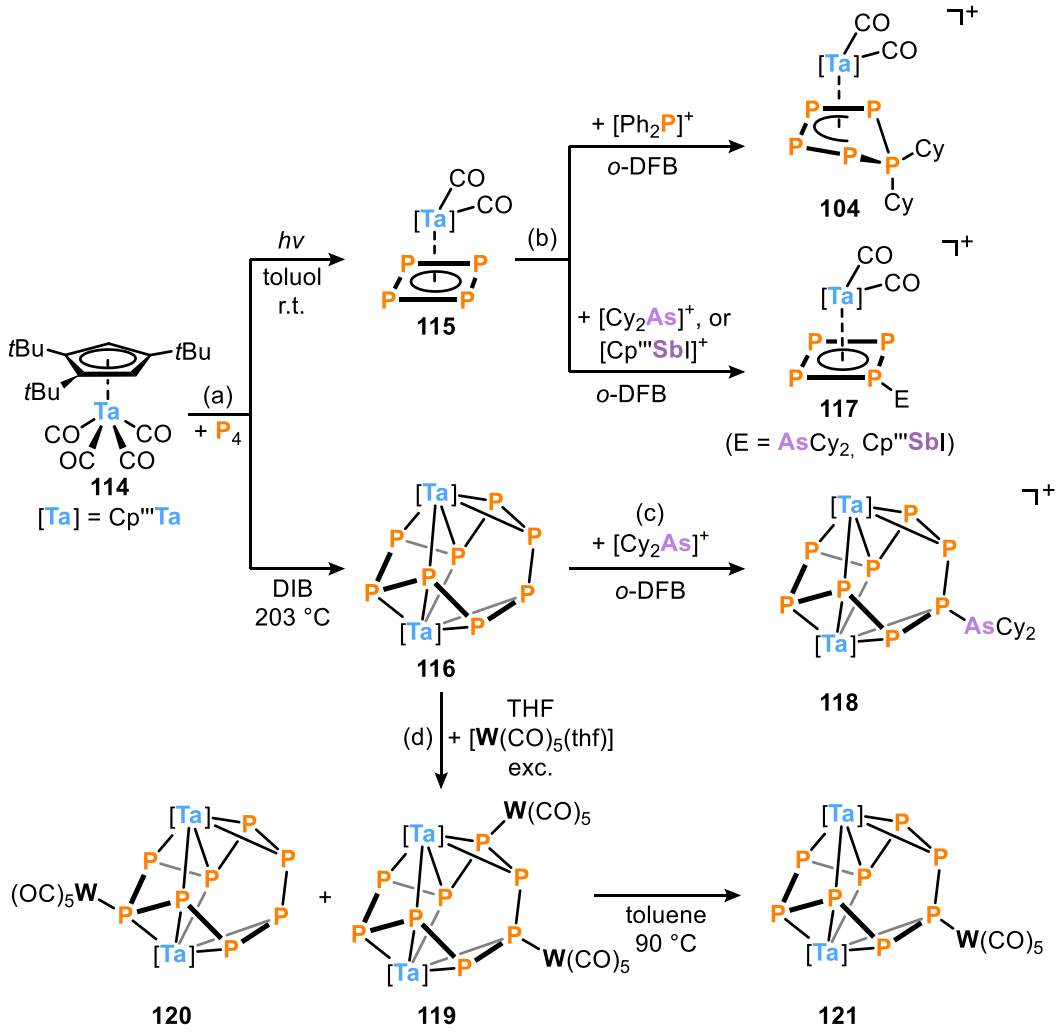

Scheme 18. Activation of P_4 by Cp'''Ta$(CO)_4$ and subsequent functionalization with pnictogenium ions; DIB = 1,3-diisopropyl-benzene, *o*-DFB = 1,2-difluorbenzene.

Complex **116** is susceptible to redox reactions, resulting in dimerization to give higher nuclearity species (Scheme 19). Oxidation using [Thia][TEF] yielded the dicationic P_{16} compound **122**$[TEF]_2$, *via* formation of a single new P–P bond between the *cyclo*-P_8 ligands of two molecules of **116**, resulting in a remarkable polyphosphorus ligand containing two linked *cyclo*-P_8 units. In contrast, the dimerization induced by reduction using KC_8 leads to simultaneous P–P bond cleavage and P–P bond formation, ultimately affording dianion $[K([2.2.2]crypt)]_2$**123**, in which the *cyclo*-P_8 rings of two molecules of **116** have both been broken to afford an uninterrupted, linear P_{16} chain, coordinated to four tantalum centers.

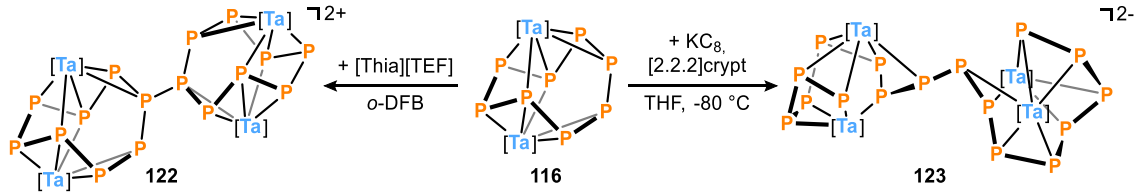

Scheme 19. Redox mediated dimerization reaction of tantalum *cyclo*-P_8 complex; $Thia^+ = C_{12}H_8S_2^+$, $TEF^- = [Al\{OC(CF_3)_3\}_4]^-$, [2.2.2]crypt = [2.2.2]Cryptand.

1.8 Conclusion and Outlook

In 1974, the first transition-metal-mediated functionalization of white phosphorus was reported by Green and co-workers.[85] Since then, there has been significant progress in the functionalization of P_4-derived TM-P_n complexes, which has been summarized in a series of review articles. While these results demonstrate the synthetic capabilities of transition metal complexes bearing P_n ligands to generate a multitude of varied and unprecedented polyphosphido ligands, the release of desirable (mono-)phosphorus compounds from the metal center has generally proven difficult.

Recently, however, important progress has been made in this field, as illustrated by the examples discussed in this chapter, employing both neutral and anionic transition metal complexes (Sections 1.2-1.7). Various approaches have given rise to remarkable (poly-)phosphorus species, such as mixed tetrahedrane compounds (AsP_3, HCP_3), and asymmetrically substituted phosphines. In particular, anionic complexes have emerged as promising platforms for P_4 functionalization, due to the fact that most transformations are carried out using electrophiles. In contrast to nucleophilic functionalization, a significant driving force for the reaction is provided by the concomitant and metathetical halide abstraction. Besides transition metal fragments bearing "classical" cyclopentadienyl and phosphine ligands, recent advancements highlight the potential of complexes featuring

redox-active ligands as attractive precursors for the synthesis of new phosphorus compounds. Moreover, while the coordination chemistry of P_4 has been studied extensively, the liberation of these P-rich species from the metal centers remains challenging and thus far has only been exemplary achieved, despite the potential use of these molecules as building blocks in the synthesis of new phosphorus compounds. Complexes such as **77** (see Scheme 13), which are already under investigation in the Wolf group, can be used for further functionalization. Through variation of the ligand system, distinct reactivity can be achieved, opening up avenues for new phosphorus-containing compounds directly derived from P_4.

References

[1] D. C. B. Whittet, I. E. Chiar, *Astron. Astrophys. Rev.* **1993**, *5*, 1–35.
[2] J. Emsley, *The 13th Element: The Sordid Tale of Murder, Fire, and Phosphorus*, WILEY, New York, **2002**.
[3] K. Ashley, D. Cordell, D. Mavinic, *Chemosphere* **2011**, *84*, 737–746.
[4] A. F. Holleman, E. Wiberg, N. Wiberg, *Lehrbuch der anorganischen Chemie*, De Gruyter, Berlin, **2017**.
[5] D. E. C. Corbridge, *Phosphorus 2000. Chemistry, Biochemistry & Technology*, Elsevier, Amsterdam, **2002**.
[6] G. Bettermann, W. Krause, G. Riess, T. Hofmann, in *Ullmanns Encycl. Ind. Chem.*, John Wiley & Sons, Ltd, Weinheim, **2000**, pp. 1–18.
[7] J. Svara, N. Weferling, T. Hofmann, in *Ullmanns Encycl. Ind. Chem.*, John Wiley & Sons, Ltd, Weinheim, **2006**, pp. 1–48.
[8] W. Gleason, *JOM* **2007**, *59*, 17–19.
[9] D. E. C. Corbridge, *Phosphorus: An Outline of Its Chemistry, Biochemistry and Technology*, Elsevier, New York, **1994**.
[10] M. Scheer, G. Balázs, A. Seitz, *Chem. Rev.* **2010**, *110*, 4236–4256.
[11] M. Peruzzini, L. Gonsalvi, A. Romerosa, *Chem. Soc. Rev.* **2005**, *34*, 1038–1047.
[12] B. M. Cossairt, N. A. Piro, C. C. Cummins, *Chem. Rev.* **2010**, *110*, 4164–4177.
[13] M. Caporali, L. Gonsalvi, A. Rossin, M. Peruzzini, *Chem. Rev.* **2010**, *110*, 4178–4235.
[14] C. M. Hoidn, D. J. Scott, R. Wolf, *Chem. Eur. J.* **2020**, *27*, 1886–1902.
[15] L. Giusti, V. R. Landaeta, M. Vanni, J. A. Kelly, R. Wolf, M. Caporali, *Coord. Chem. Rev.* **2021**, *441*, 213927.
[16] M. Caporali, M. Serrano-Ruiz, M. Peruzzini, in *Chem. Chlorine* (Eds.: P. Tundo, L.-N. He, E. Lokteva, C. Mota), Springer, Cham, **2016**, pp. 97–136.
[17] J. E. Borger, A. W. Ehlers, J. C. Slootweg, K. Lammertsma, *Chem. – Eur. J.* **2017**, *23*, 11738–11746.
[18] D. Scheschkewitz, *Nat. Chem.* **2020**, *12*, 785–787.
[19] N. A. Giffin, J. D. Masuda, *Coord. Chem. Rev.* **2011**, *255*, 1342–1359.
[20] T. Xin, C. C. Cummins, *ACS Cent. Sci.* **2023**, *9*, 1575–1580.
[21] M. Peruzzini, J. A. Ramirez, F. Vizza, *Angew. Chem. Int. Ed.* **1998**, *37*, 2255–2257.
[22] P. Barbaro, M. Peruzzini, J. A. Ramirez, F. Vizza, *Organometallics* **1999**, *18*, 4237–4240.
[23] P. Barbaro, A. Ienco, C. Mealli, M. Peruzzini, O. J. Scherer, G. Schmitt, F. Vizza, G. Wolmershäuser, *Chem. – Eur. J.* **2003**, *9*, 5195–5210.
[24] S. Du, J. Yin, Y. Chi, L. Xu, W.-X. Zhang, *Angew. Chem. Int. Ed.* **2017**, *56*, 15886–15890.
[25] L. Xu, Y. Chi, S. Du, W.-X. Zhang, Z. Xi, *Angew. Chem. Int. Ed.* **2016**, *55*, 9187–9190.
[26] M. Scheer, U. Becker, M. H. Chisholm, J. C. Huffman, F. Lemoigno, O. Eisenstein, *Inorg. Chem.* **1995**, *34*, 3117–3119.
[27] M. Scheer, U. Becker, *Chem. Ber.* **1996**, *129*, 1307–1310.
[28] M. Scheer, U. Becker, J. Magull, *Polyhedron* **1998**, *17*, 1983–1989.
[29] M. Di Vaira, L. Sacconi, P. Stoppioni, *J. Organomet. Chem.* **1983**, *250*, 183–195.
[30] F. Zhang, J. Zhang, Z. Chen, L. Weng, X. Zhou, *Inorg. Chem.* **2019**, *58*, 8451–8459.
[31] R. R. Dykstra, in *Encycl. Reag. Org. Synth. EROS*, John Wiley & Sons, Ltd, **2001**.
[32] F. Zhang, I. del Rosal, K. Han, J. Zhang, L. Maron, X. Zhou, *Inorg. Chem. Front.* **2024**, *11*, 1742–1753.

[33] P. Coburger, J. Leitl, D. J. Scott, G. Hierlmeier, I. G. Shenderovich, E. Hey-Hawkins, R. Wolf, *Chem. Sci.* **2021**, *12*, 11225–11235.
[34] M. Scheer, K. Schuster, U. Becker, *Phosphorus Sulfur Silicon Relat. Elem.* **1996**, *109*, 141–144.
[35] R. Grünbauer, G. Balázs, M. Scheer, *Chem. – Eur. J.* **2020**, *26*, 11722–11726.
[36] F. Scalambra, M. Peruzzini, A. Romerosa, in *Adv. Organomet. Chem.* (Ed.: P.J. Pérez), Academic Press, **2019**, pp. 173–222.
[37] J. S. Figueroa, C. C. Cummins, *J. Am. Chem. Soc.* **2003**, *125*, 4020–4021.
[38] J. S. Figueroa, C. C. Cummins, *Angew. Chem. Int. Ed.* **2004**, *43*, 984–988.
[39] D. Tofan, B. M. Cossairt, C. C. Cummins, *Inorg. Chem.* **2011**, *50*, 12349–12358.
[40] N. A. Piro, J. S. Figueroa, J. T. McKellar, C. C. Cummins, *Science* **2006**, *313*, 1276–1279.
[41] I. Krummenacher, C. C. Cummins, *Polyhedron* **2012**, *32*, 10–13.
[42] G. Ménard, D. W. Stephan, *J. Am. Chem. Soc.* **2010**, *132*, 1796–1797.
[43] J. S. Figueroa, C. C. Cummins, *J. Am. Chem. Soc.* **2004**, *126*, 13916–13917.
[44] O. J. Scherer, J. Braun, P. Walther, C. Heckmann, G. Wolmershäuser, *Angew. Chem. Int. Ed. Engl.* **1991**, *30*, 852–854.
[45] O. J. Scherer, G. Berg, G. Wolmershäuser, *Chem. Ber.* **1995**, *128*, 635–639.
[46] O. J. Scherer, C. Vondung, G. Wolmershäuser, *Angew. Chem. Int. Ed. Engl.* **1997**, *36*, 1303–1305.
[47] S. Umbarkar, P. Sekar, M. Scheer, *J. Chem. Soc. Dalton Trans.* **2000**, 1135–1137.
[48] M. A. Alvarez, M. E. García, D. García-Vivó, A. Ramos, M. A. Ruiz, *Inorg. Chem.* **2011**, *50*, 2064–2066.
[49] M. A. Alvarez, M. E. García, D. García-Vivó, M. A. Ruiz, M. F. Vega, *Organometallics* **2015**, *34*, 870–878.
[50] M. A. Alvarez, M. E. García, D. García-Vivó, A. Ramos, M. A. Ruiz, *Inorg. Chem.* **2012**, *51*, 11061–11075.
[51] M. A. Alvarez, M. E. García, D. García-Vivó, R. Lozano, A. Ramos, M. A. Ruiz, *Inorg. Chem.* **2013**, *52*, 9005–9018.
[52] M. D. Vaira, L. Sacconi, *Angew. Chem. Int. Ed. Engl.* **1982**, *21*, 330–342.
[53] G. Capozzi, L. Chiti, M. Di Vaira, M. Peruzzini, P. Stoppioni, *J. Chem. Soc., Chem. Commun.* **1986**, 1799–1800.
[54] A. Barth, G. Huttner, M. Fritz, L. Zsolnai, *Angew. Chem. Int. Ed. Engl.* **1990**, *29*, 929–931.
[55] M. Di Vaira, P. Stoppioni, S. Midollini, F. Laschi, P. Zanello, *Polyhedron* **1991**, *10*, 2123–2129.
[56] E. Mädl, G. Balázs, E. V. Peresypkina, M. Scheer, *Angew. Chem. Int. Ed.* **2016**, *55*, 7702–7707.
[57] F. Meurer, F. Kleemiss, C. Riesinger, G. Balázs, V. Vuković, I. G. Shenderovich, C. Jelsch, M. Bodensteiner, *Chem. – Eur. J.* **2024**, e202303762.
[58] M. Scheer, C. Riesinger, L. Duetsch, G. Balazs, M. Bodensteiner, *Chem. – Eur. J.* **2020**, 10.1002/chem.202003291.
[59] N. A. Piro, C. C. Cummins, *J. Am. Chem. Soc.* **2008**, *130*, 9524–9535.
[60] B. M. Cossairt, M.-C. Diawara, C. C. Cummins, *Science* **2009**, *323*, 602–602.
[61] B. M. Cossairt, C. C. Cummins, *Angew. Chem. Int. Ed.* **2010**, *49*, 1595–1598.
[62] A. Velian, C. C. Cummins, *Chem. Sci.* **2012**, *3*, 1003–1006.
[63] G. R. Morello, T. R. Cundari, *Organometallics* **2016**, *35*, 3624–3634.
[64] M.-L. Y. Riu, M. Ye, C. C. Cummins, *J. Am. Chem. Soc.* **2021**, *143*, 16354–16357.
[65] G. Hierlmeier, P. Coburger, M. Bodensteiner, R. Wolf, *Angew. Chem. Int. Ed.* **2019**, *58*, 16918–16922.

[66] M.-L. Y. Riu, R. L. Jones, W. J. Transue, P. Müller, C. C. Cummins, *Sci. Adv.* **2020**, *6*, eaaz3168.
[67] I. de los Rios, J.-R. Hamon, P. Hamon, C. Lapinte, L. Toupet, A. Romerosa, M. Peruzzini, *Angew. Chem. Int. Ed.* **2001**, *40*, 3910–3912.
[68] C. M. Hoidn, T. M. Maier, K. Trabitsch, J. J. Weigand, R. Wolf, *Angew. Chem. Int. Ed.* **2019**, *58*, 18931–18936.
[69] C. G. P. Ziegler, T. M. Maier, S. Pelties, C. Taube, F. Hennersdorf, A. W. Ehlers, J. J. Weigand, R. Wolf, *Chem. Sci.* **2019**, *10*, 1302–1308.
[70] C. M. Hoidn, K. Trabitsch, K. Schwedtmann, C. Taube, J. J. Weigand, R. Wolf, *Chem. – Eur. J.* **2023**, e202301930.
[71] F. Dielmann, A. Timoshkin, M. Piesch, G. Balázs, M. Scheer, *Angew. Chem. Int. Ed.* **2017**, *56*, 1671–1675.
[72] M. Piesch, M. Seidl, M. Scheer, *Chem. Sci.* **2020**, *11*, 6745–6751.
[73] M. Piesch, M. Seidl, M. Stubenhofer, M. Scheer, *Chem. – Eur. J.* **2019**, *25*, 6311–6316.
[74] M. Piesch, S. Reichl, M. Seidl, G. Balázs, M. Scheer, *Angew. Chem. Int. Ed.* **2019**, *58*, 16563–16568.
[75] M. Piesch, S. Reichl, M. Seidl, G. Balázs, M. Scheer, *Angew. Chem. Int. Ed.* **2021**, *60*, 15101–15108.
[76] O. J. Scherer, T. Brück, *Angew. Chem. Int. Ed. Engl.* **1987**, *26*, 59–59.
[77] E. Mädl, M. V. Butovskii, G. Balázs, E. V. Peresypkina, A. V. Virovets, M. Seidl, M. Scheer, *Angew. Chem. Int. Ed.* **2014**, *53*, 7643–7646.
[78] S. Reichl, F. Riedlberger, M. Piesch, G. Balázs, M. Seidl, M. Scheer, *Chem. Sci.* **2023**, *14*, 7285–7290.
[79] M. V. Butovskiy, G. Balázs, M. Bodensteiner, E. V. Peresypkina, A. V. Virovets, J. Sutter, M. Scheer, *Angew. Chem. Int. Ed.* **2013**, *52*, 2972–2976.
[80] S. Reichl, G. Balázs, M. Scheer, *Chem. Sci.* **2023**, *14*, 3834–3838.
[81] S. Reichl, E. Mädl, F. Riedlberger, M. Piesch, G. Balázs, M. Seidl, M. Scheer, *Nat. Commun.* **2021**, *12*, 5774.
[82] C. Riesinger, F. Dielmann, R. Szlosek, A. V. Virovets, M. Scheer, *Angew. Chem. Int. Ed.* **2023**, *62*, e202218828.
[83] O. J. Scherer, R. Winter, G. Wolmershäuser, *Z. Für Anorg. Allg. Chem.* **1993**, *619*, 827–835.
[84] C. Riesinger, A. Erhard, M. Scheer, *Chem. Commun.* **2023**, *59*, 10117–10120.
[85] J. C. Green, M. L. H. Green, G. E. Morris, *J. Chem. Soc. Chem. Commun.* **1974**, 212–213.

2 Cobalt-Mediated [3+1] Fragmentation of White Phosphorus: Access to Acylcyanophosphanides[a,b]

Abstract: Despite the accessibility of numerous transition metal polyphosphido complexes through transition-metal-mediated activation of white phosphorus, the targeted functionalization of P_n ligands to obtain functional monophosphorus species remains challenging. In this study, we introduce a new [3+1] fragmentation procedure for *cyclo*-P_4 ligands, leading to the discovery of acylcyanophosphanides and -phosphines. Treatment of the complex [K(18c-6)][(Ar*BIAN)Co(η^4-P_4)] ([K(18c-6)]**3**, 18c-6 = [18]crown-6, Ar* = 2,6-dibenzhydryl-4-isopropylphenyl, BIAN = 1,2-bis(arylimino)acenaphthene diimine) with acyl chlorides results in the formation of acylated tetraphosphido complexes [(Ar*BIAN)Co(η^4-P_4C(O)R)] (R = *t*Bu, Cy, 1-Ad, Ph; **4a-d**). Subsequent reactions of **4a-d** with cyanide salts yield acylated cyanophosphanides [RC(O)PCN]$^-$ (**9a-d**$^-$) and the *cyclo*-P_3 cobaltate anion [(Ar*BIAN)Co(η^3-P_3)(CN)]$^-$ (**8**$^-$). Further reactions of **4a-d** with trimethylsilyl cyanide (Me_3SiCN) and isocyanides provide insight into a plausible mechanism of this [3+1] fragmentation reaction, as these reagents partially displace the P_4C(O)R ligand from the cobalt center. Several potential intermediates of the [3+1] fragmentation were characterized. Additionally, the introduction of a second acyl substituent was achieved by treating [K(18c-6)]**9b** with CyC(O)Cl, resulting in the first bis(acyl)monocyanophosphine $(CyC(O))_2PCN$ (**10**).

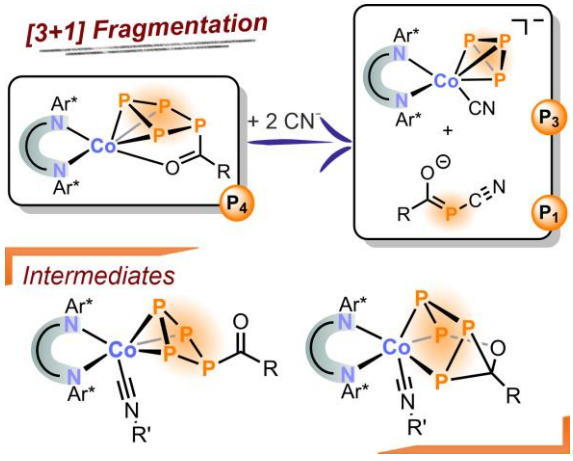

[a] Reproduced from S. Hauer, T. M. Horsley Downie, G. Balázs, K. Schwedtmann, J. J. Weigand, R. Wolf, *Angew. Chem. Int. Ed.* **2023**, e202317170.

[b] The synthetic investigations and the characterization of the reported compounds was performed by S. Hauer. G. Balázs calculated the $^{31}P\{^1H\}$ chemical shifts. S. Hauer wrote the manuscript draft. T. M. Horsley Downie, R. Wolf and J. J. Weigand reviewed and edited the manuscript. R. Wolf and J. J. Weigand supervised the project.

2.1 Introduction

Transition-metal-mediated processes offer promising and atom-efficient synthetic routes to organophosphorus compounds derived from white phosphorus (P_4), but represent a challenging goal in this field.[1] Research over several decades has led to the development of a plethora of early and late transition metal polyphosphido complexes through the activation of P_4.[2] While coordination chemistry approaches have demonstrated the potential for P_4 functionalization, achieving the release of desirable (mono-)phosphorus compounds from the metal center has generally proven difficult. Seminal studies by Peruzzini and co-workers have explored the hydrogenation of P_4 using rhodium and iridium hydride complexes.[3] More recently, Scheer and co-workers utilized the pentaphosphaferrocene [Cp*Fe(η^5-P_5)] (Cp* = η^5-C_5Me_5) to prepare asymmetrically substituted phosphines from P_4.[4] Despite these notable achievements, the successful generation of organophosphorus compounds through transition-metal-mediated P_4 functionalization remains limited.

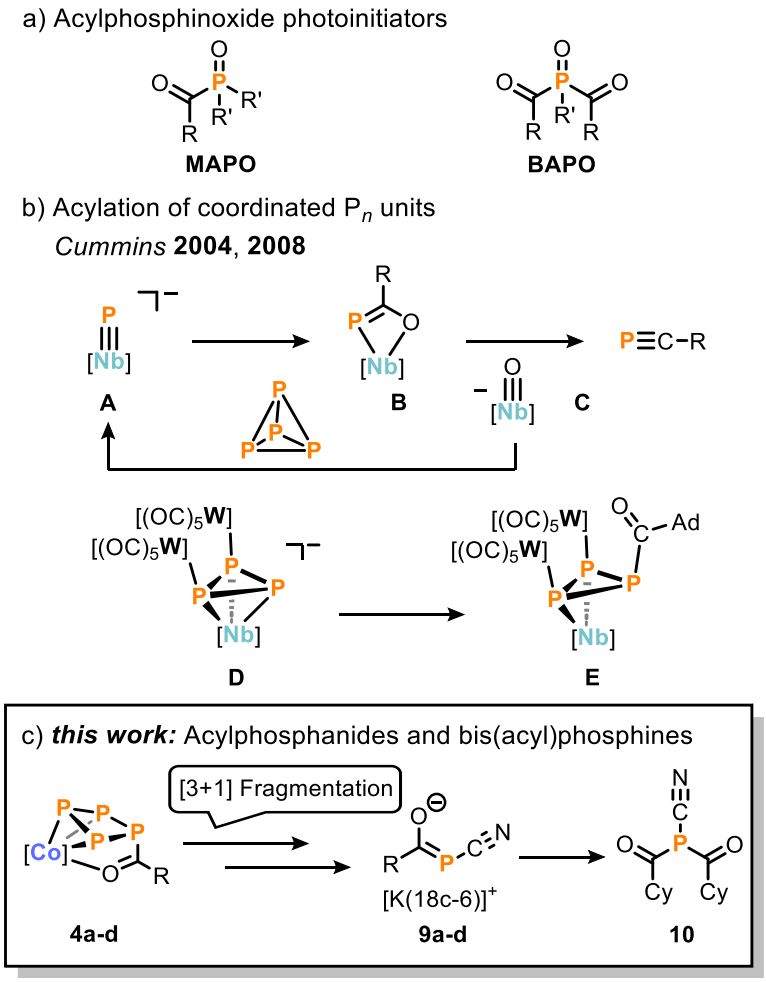

Figure 1. a) Selected industrially applied mono- and bis(acyl)phosphineoxides (MAPOs and BAPOs); R, R' = alkyl or aryl. b) acylation of coordinated P_n-ligands. c) synthesis of acylated mono- and bis(acyl)phosphines starting from P_4 by [3+1] fragmentation of acylated tetraphosphido ligands; R = *t*Bu, Cy, 1-Ad, Ph.

Another highly desirable class of organophosphorus compounds is represented by mono- and bis(acyl)phosphine oxides (MAPOs and BAPOs, Figure 1a). These compounds exhibit intriguing photoactivity, allowing the generation of phosphinoyl and acyl radicals even under weak, visible-light irradiation.[5] Recent studies have reported various methods for the synthesis of mono-, bis-, and tris(acyl)phosphines. These methods include reactions of alkali metal phosphanides MPH_2 (M = Li, Na, K),[6] or phosphaethynolates MPCO[7] with electrophiles, as well as the formal insertion of *tert*-butyl phosphinidene (*t*Bu−P)[8] into the C−Cl bond of acyl chlorides. More recently, a one-pot reaction of P_4, dilithio reagents, and acyl chlorides has also been explored.[9] However, it is important to note that the scope of these methods is often limited, and the resulting products remain bound to the metal center.[10] Cummins and co-workers reported the reaction of the terminal phosphide complex $[P{\equiv}Nb(N[Np]Ar)_3]^-$ (**A**, Np = neopentyl, Ar = 3,5-$Me_2C_6H_3$) with acyl chlorides to give niobacycles of the form **B** (Figure 1b).[11] Subsequent development of this chemistry has seen the release of a P_1 moiety through thermolysis, which induces a [2+2] fragmentation, yielding the phosphaalkynes R−C≡P (R = *t*Bu, 1-Ad) and the niobium(V)-oxo product **C**. This process was reported to form a closed synthetic cycle, as compound **A** was regenerated through stepwise deoxygenation of **C**, P_4 activation, and reduction. In a separate investigation, the reaction of the trinuclear *cyclo*-P_3 complex anion **D** with 1-adamantoyl chloride was studied, which yielded the corresponding P_3-acylated species **E**.[12] However, **E** exhibits thermal instability and decomposes above temperatures of −20 °C, limiting further investigation into the reactivity of acyl-substituted P_n ligands. These pioneering works have demonstrated the suitability of P-acylated ligands as precursors for the synthesis of certain monophosphorus compounds. However, to date, only the P_1-niobacyle **B** has been extensively studied in this regard.

Our previous investigation into the reactivity of transition metalate anions with P_4 has indicated that anionic polyphosphorus complexes hold potential as versatile tools for the synthesis of unique phosphorus compounds.[13] Recently, we reported on the [3+2] fragmentation of pentaphosphido ligands within the coordination sphere of cobalt, leading to new P_2 anions $[R_2PPCN]^-$ (R = Cy, *t*Bu, Ph, N(*i*Pr)$_2$).[14] However, compounds containing a PCN unit remain underreported, with a particular scarcity of anionic species, the notable exception being the dicyanophosphide anion $[P(CN)_2]^-$.[15]

Advancing on this strategy, we have synthesized the first acylated cyanophosphanides $[RC(O)PCN]^-$ (**9a-d**$^-$) through the intermediacy of tetraphosphido complexes

[(Ar*BIAN)Co(η^4-P_4)]$^-$ (**3**$^-$) and [(Ar*BIAN)Co(η^3:η^1-P_4C(O)R] (**4a-d**). The anionic *cyclo*-P_4 complex **3**$^-$ can initiate P−C bond formation and subsequently undergo [3+1] fragmentation, liberating the acylated P_1 unit. Furthermore, the reaction of P_1-species [K(18c-6)]**9b** with acyl chloride yielded bis(acyl)monocyanophosphine $(CyC(O))_2PCN$ (**10**), which possesses the crucial motif found in industrial photoinitiators.[5]

2.2 Results and Discussion

Our study commenced with the preparation of the sterically demanding α-diimine Ar*BIAN (**1**),[16] which was employed as a ligand in our target complexes. Our aim was to suppress the previously reported formation of dinuclear cobalt-P_4 complexes by introducing a bulky substituent Ar* on the BIAN ligand, thus facilitating the accessibility of the P_4^{2-} synthon for functionalization.[17] Previous synthetic methods for sterically encumbered BIAN ligands required significant synthetic effort and typically resulted in poor yields.[16,18] However, by templating with $ZnCl_2$, the α-diimine **1** was successfully obtained in a good yield (70%).[19] Subsequently, ligand **1** was treated with the cobaltate $[K(thf)_{0.2}][Co(cod)_2]$ (cod = 1,5-cyclooctadiene) and 18c-6 in THF to afford [K(18c-6)][(Ar*BIAN)Co(cod)] ([K(18c-6)]**2**). The complex was isolated as dark brown crystals in good yield (77%) from a THF/*n*-hexane mixture. The ^{1}H NMR spectrum of [K(18c-6)]**2** (see Figure S3, Supporting Information (SI)) exhibits signals corresponding to Ar*, as well as the characteristic signals of the BIAN backbone at δ = 4.21 – 6.30 ppm.[17b,20]

Monitoring *via* $^{31}P\{^1H\}$ NMR spectroscopy shows that complex [K(18c-6)]**2** reacts quantitatively with white phosphorus to afford the desired mononuclear *cyclo*-P_4 complex [K(18c-6)][(Ar*BIAN)Co(η^4-P_4)] ([K(18c-6)]**3**; Scheme 1a). This compound crystallizes as dark purple needles from a toluene/*n*-hexane mixture. The reaction can be conducted on a multigram scale (> 2.7 g), furnishing [K(18c-6)]**3** in a good isolated yield of 63%. This provides an accessible precursor for the subsequent functionalization of the P_4^{2-} ligand. Single-crystal X-ray diffraction (XRD) analysis (Figure S83, SI) of compound [K(18c-6)]**3** revealed a nearly planar *cyclo*-P_4 unit with P−P bond lengths ranging from 2.1539(9) to 2.1772(1) Å (mean: 2.17 Å). These bond lengths lie between typical P−P single and P=P double bond lengths ($\sum r_{PP}$ 2.22 Å vs. 2.04 Å),[21] indicating the presence of a P_4^{2-} ligand.[13c,14,17a,22] Additionally, the C−C (1.426(3) Å) and C−N (1.335(3) Å and 1.330(3) Å) bond lengths in the ligand backbone of **3** indicate the presence of a radical anionic Ar*BIAN$^{\bullet-}$ ligand.[23]

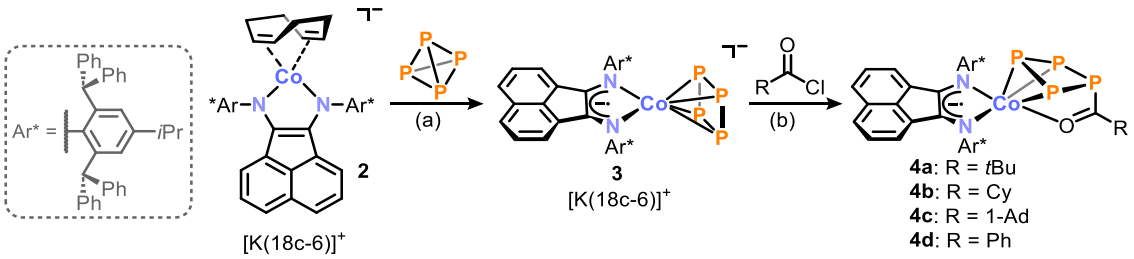

Scheme 1. Activation of P_4 by [K(18c-6)]**2** and subsequent functionalization of the *cyclo*-P_4 unit in [K(18c-6)]**3** with acyl chlorides (18c-6 = [18]-crown-6, Ar* = 2,6-dibenzhydryl-4-isopropylphenyl); reagents/by-products and conditions: a) +P_4/−1,5 cyclooctadiene (1,5-cod); THF, r.t., 1 d; b) +RC(O)Cl/−[K(18c-6)]Cl; toluene, r.t., 1 d; yields: [K(18c-6)]**2**: 77%, [K(18c-6)]**3**: 63%, **4a**: 58%, **4b**: 54%, **4c**: 66%, **4d**: 67%.

The $^{31}P\{^1H\}$ NMR spectrum of [K(18c-6)]**3** in C_6D_6 exhibits a sharp singlet at δ = 113.0 ppm, which compares well with the value calculated by DFT (δ = 137 ppm at the PBE0/def2-TZVP/aug-pcSseg-2 (P) level, see Table S14, SI). In comparison, two other previously reported mononuclear cobalt *cyclo*-P_4 complexes, anionic $[(^{Dipp}PHDI)Co(\eta^4\text{-}P_4)]^-$ (^{Dipp}PHDI = bis(2,6-diisopropylphenyl)phenanthrene-9,10-diimine) and neutral $[Cp'''Co(\eta^4\text{-}P_4)]$ (Cp''' = $C_5H_2tBu_3$), exhibit $^{31}P\{^1H\}$ NMR resonances at δ = 136.5 ppm and δ = 175.2 ppm, respectively.[14,22b]

To explore the underreported chemistry of acylated polyphosphido ligands, introducing the P-acyl group as a functional group at the tetraphosphido ligand in [K(18c-6)]**3** was of particular interest. Treatment of [K(18c-6)]**3** with acyl chlorides RC(O)Cl (R = *t*Bu, Cy, 1-Ad, Ph; see Scheme 1b) in toluene elicits a color change from purple to magenta.

Crystallization from the reaction mixtures yielded magenta-colored crystals of the acylated tetraphosphido complexes $[(Ar^*BIAN)Co(\eta^3{:}\eta^1\text{-}P_4C(O)R]$ (**4a-d**) in good yields (54% to 67%). Crystallographic studies conducted on three of the complexes, **4a-c**, revealed the presence of an acylated *cyclo*-P_4 ring in a puckered conformation. The *cyclo*-P_4 ring coordinates to Co *via* three P atoms in an η^3 fashion and additionally *via* the oxygen atom through η^1-coordination. Complexes **4a-c** are essentially isostructural. Specifically, in the case of **4a** (see Figure 2a), the P1−P2 (2.2459(9) Å) and P1−P4 (2.2515(6) Å) bond lengths involving the acyl-substituted P atom P1 are slightly longer than expected for typical P−P single bonds ($\sum r_{PP}$ 2.22 Å).[21] In contrast, the P2−P3 (2.1610(7) Å) and the P3−P4 (2.1547(9) Å) bond lengths are slightly shorter, indicating partial double bond character. The C3−O1 (1.242(3) Å) double bond length falls within the expected range for carbonyl groups ($\sum r_{CO}$ 1.24 Å), while the Co1−O1 (2.0741(1) Å) bond length exceeds the sum of the covalent radii for a Co−O single bond ($\sum r_{CoO}$ 1.74 Å).[21]

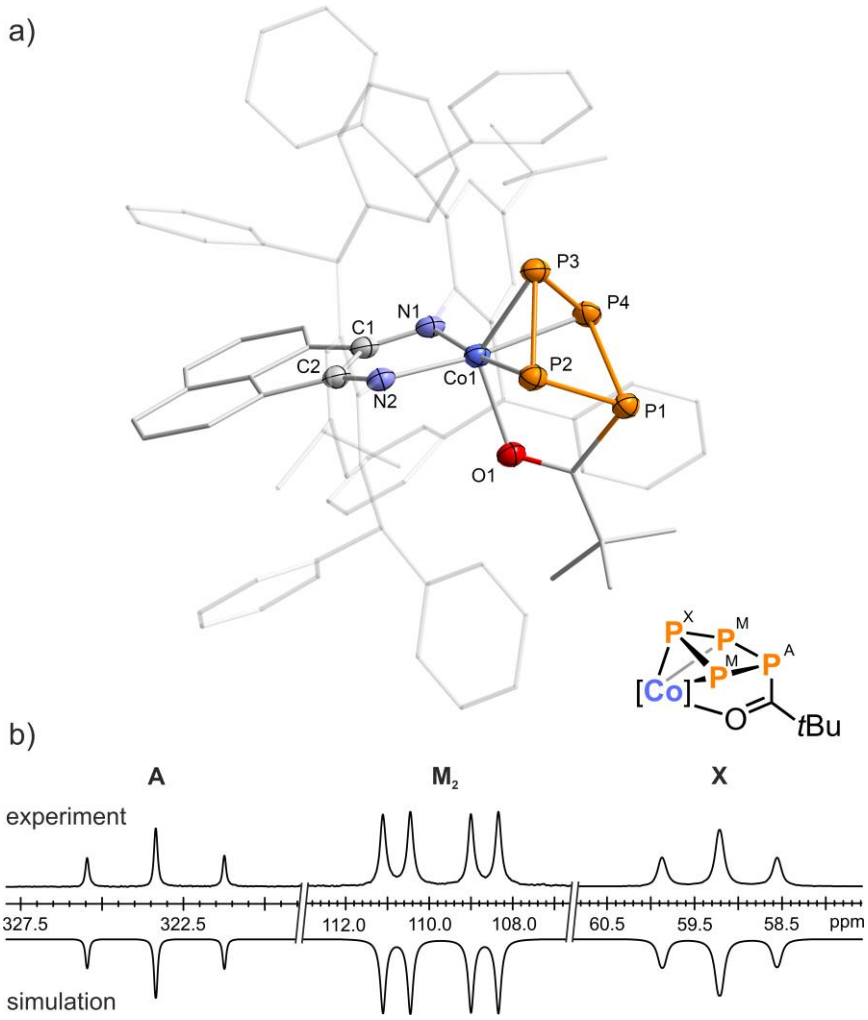

Figure 2. a) Solid-state molecular structure of [(Ar*BIAN)Co(η^3:η^1-P_4C(O)*t*Bu)] (**4a**);[45] thermal ellipsoids are shown at the 50% probability level; hydrogen atoms and disorder are omitted for clarity. Selected bond lengths [Å] and angles [°]: P1−P2 2.2459(9), P2−P3 2.1610(7), P3−P4 2.1547(9), P1−P4 2.2515(6), Co1−P2 2.2974(6), Co1−P3 2.2930(7), Co1−P4 2.2936(8), Co1−O1 2.0741(1), P1−C3 1.889(2), C3−O1 1.242(3), P1−P2−P3 89.83(3), P2-P3-P4 87.25(3), P4-P1-P2 82.92(2); b) experimental (upward) and simulated (downward) $^{31}P\{^1H\}$ NMR spectra of **4a**, with nuclei assigned to an AM_2X spin system: $\delta(P_A)$ = 323.3 ppm, $\delta(P_M)$ = 109.7 ppm, $\delta(P_X)$ = 59.2 ppm, $^1J_{AM}$ = −342 Hz, $^1J_{MX}$ = −106 Hz, $^2J_{AX}$ = 7 Hz. The spectra of the related compounds **4b-d** are very similar (see SI); [Co] = (Ar*BIAN)Co.

Each of the complexes **4a-d** features an AM_2X spin system in the $^{31}P\{^1H\}$ NMR spectra (see Figure 2b for **4a**; see SI for similar spectra of **4b-d**). The resonances of **4a** (δ = 323.3 (P_A), 109.7 (P_M), 59.2 (P_X) ppm; *c.f.* the DFT-calculated chemical shifts of 315 (P_A), 99 (P_M) and 67 ppm (P_X)) – especially P_A, the coordinating phosphorus nucleus – are deshielded in comparison to related neutral cobalt complexes and niobacycles **B**.[11,24] Quantum chemical calculations performed at the BP86/def2-TZVP level of theory predict the C=O stretching vibration for **4a** at $\tilde{\nu}_{CO}$ =1462 cm^{-1} (see Figure S92, SI), which is between the regions characteristic of a C=O double and single bond (1700 cm^{-1} vs. 1100 cm^{-1}).[25] However, in the ATR-IR spectrum, the C=O vibration overlaps with BIAN C−N vibrations in the fingerprint region, making unambiguous identification challenging. Similar behavior was reported for niobacycles **B**.[11]

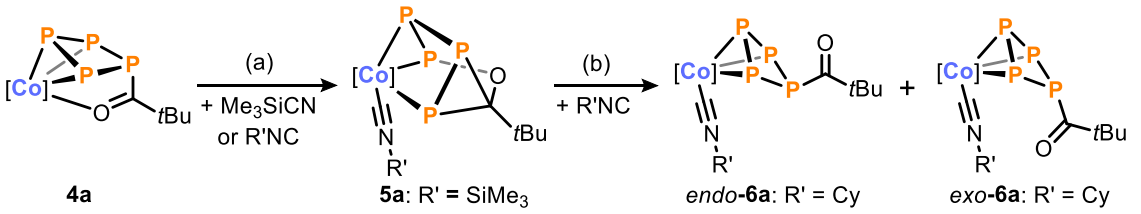

Scheme 2. Rearrangement and partial release of phosphoracylic ligands in **4a** is induced by trimethylsilyl cyanide (Me_3SiCN) or isocyanides R'NC (R' = Cy, *t*Bu, Mes, Ph); reagents and conditions: a) +1.3 eq. Me_3SiCN; toluene, r.t., 14 h; b) +10.0 eq. CyNC; toluene, r.t., 2 h; yields: **5a**: 77%, **6a**: 57%; [Co] = (Ar*BIAN)Co; for further combinations see also Table S8 and Figures S46-52 in the SI.

Having demonstrated that the P_4^{2-} ligand of anion $\mathbf{3}^-$ was readily functionalized to give **4a-d**, our focus shifted toward isolating new organophosphorus compounds by displacing the phosphorus moiety from the coordination sphere of the cobalt center. To achieve this, **4a-d** were reacted with neutral cyanide Me_3SiCN (Scheme 2a). Specifically, the addition of one equivalent of substrate to a solution of **4a** (R = *t*Bu) resulted in a color change from magenta to dark green. Analysis of the $^{31}P\{^1H\}$ NMR spectrum of the reaction mixture revealed the complete consumption of **4a**, with the formation of a new species **5a**, exhibiting four distinct resonances in a 1:1:1:1 ratio (*vide infra*). Equivalent reactions of **4b-d** toward Me_3SiCN gave very similar $^{31}P\{^1H\}$ NMR spectra, indicating the formation of compounds analogous to **5a** (Figure S47, SI).

Compound **5a** was isolated as a green crystalline solid in 75% yield after crystallization from toluene/*n*-hexane at low temperature (−35 °C).[26] Analysis of **5a** by XRD revealed an edge-bridged trigonal prismane derivative resulting from the insertion of the acyl group into one of the P−P bonds of **4a** (Figure 3a).[27] The prismane core consists of two triangular planes – one formed by cobalt and two phosphorus atoms, and the other by the carbonyl carbon and two phosphorus atoms. The P4−C4 edge is bridged by the carbonyl oxygen atom. Thus, the isocyanide substrate has displaced the coordination of the carbonyl to the cobalt center in **4a**, leading to rearrangement of the $P_4C(O)R$ ligand. While related compounds containing prismatic units based on *catena*-E_4 (E = P, As) moieties are typically stabilized by two metal fragments, **5a** represents an unusual example where the P_4 core is supported by only one metal fragment and substituted with an organic residue.[28] The Co1-P3-P4 plane is nearly parallel to the P1-P2-C4 plane, with a twist angle of 14.2°. The P1−P2 and P2−P3 bond lengths (2.1961(1) and 2.207(1) Å, respectively) fall within the range of P−P single bonds ($\sum r_{PP}$ 2.22 Å), while the shorter P3–P4 bond (2.1355(1) Å) implies the retention of significant double bond character.[21] Similar discrepancies between P–P bond lengths have been observed in previous prismane-derived complexes.[28b,d,e] This suggests that

bonding of the polyphosphorus ligand in **5a** is best described as a localized Co1−P1 σ-bond, with the P3−P4 unit engaging in π-coordination to the cobalt center. While the cyanide Me_3SiCN was used as the reactant, the crystal structure for **5a** reveals the coordination of the corresponding isocyanide, Me_3SiNC. It is known that an equilibrium exists between the cyanide and isocyanide isomers of Me_3SiCN.[29] Thus, the coordination of Me_3SiCN to the cobalt center induces a quantitative isomerization, favoring the coordination of a silyl isocyanide (−C≡NSiMe$_3$) ligand over the cyanide (−N≡CSiMe$_3$) ligand due to energetic considerations. This is supported by a sharp vibration mode at $\tilde{\nu}_{CN}$ = 2012 cm^{-1} in the infrared spectrum and a broadening of the **C**≡N $^{13}C\{^1H\}$ NMR resonance at δ = 195.0 ppm ($\Delta\nu_{1/2}$ = 25 Hz), corroborating the coordination of the carbon to the cobalt center in **5a**.[25]

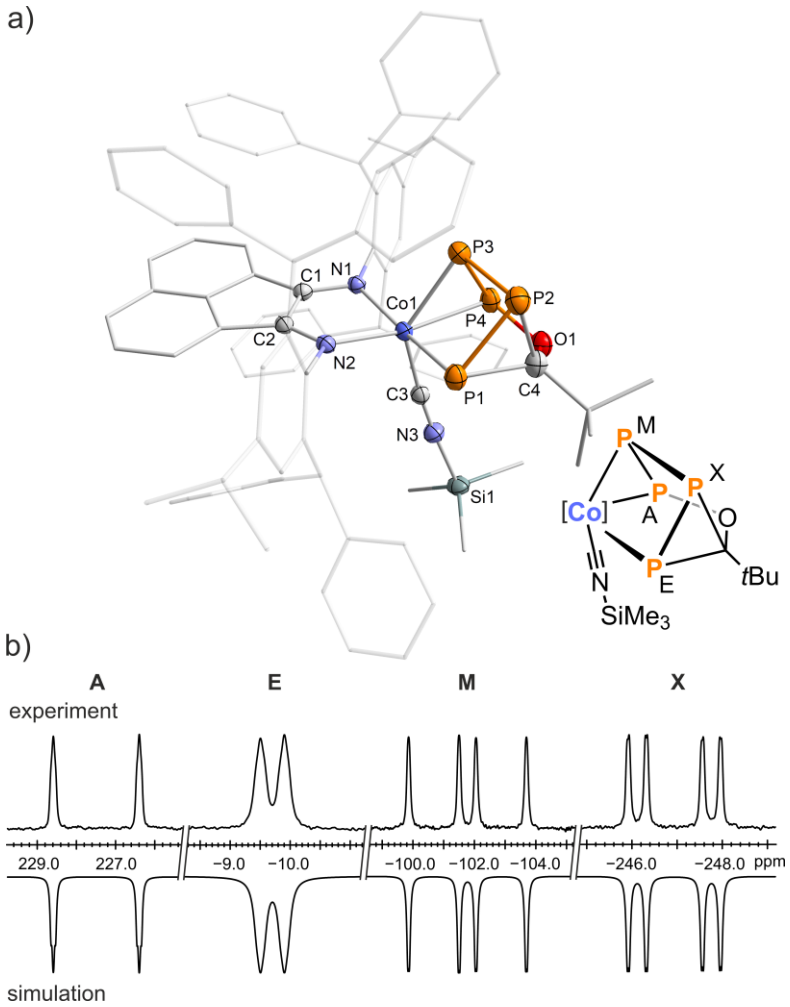

Figure 3. a) Solid-state molecular structure of [(Ar*BIAN)Co(Me$_3$SiNC)(η^2:η^1-P$_4$CO*t*Bu)] (**5a**);[45] thermal ellipsoids are shown at the 50% probability level; hydrogen atoms and disorder are omitted for clarity. Selected bond lengths [Å] and angles [°]: P1−P2 2.1961(1), P2−P3 2.207(1), P3−P4 2.1355(1), Co1−P1 2.2895(7), Co1−P3 2.3330(8), Co1−P4 2.2987(8), C4−O1 1.432(3), P4−O1 1.6722(2), Co1−C3 1.851(2), Co1-C3-N3 174.3(2), C3-N3-Si1 176.14(2); b) experimental (upward) and simulated (downward) $^{31}P\{^1H\}$ NMR spectra of **5a** with nuclei assigned to an AEMX spin system: δ(P$_A$) = 228.1 ppm, δ(P$_E$) = −10.7 ppm, δ(P$_M$) = −102.4 ppm, δ(P$_X$) = −245.1 ppm, $^1J_{AM}$ = −355 Hz, $^1J_{MX}$ = −267 Hz, $^1J_{EX}$ = −64 Hz, $^2J_{AX}$ = 8 Hz, $^2J_{ME}$ = 9 Hz, $^3J_{AE}$ = −11 Hz. The spectra of the related compounds **5b-r** are very similar (see SI, Figures S47-S52); [Co] = (Ar*BIAN)Co.

The $^{31}P\{^1H\}$ NMR spectrum of **5a** in C_6D_6 exhibits four resonances corresponding to an AEMX spin system. These appear as two doublets (δ = 228.2 (P_A) ppm and δ = −10.7 (P_E) ppm) and two doublets of doublets (δ = −102.5 (P_M) ppm and δ = −245.2 (P_X) ppm) (Figure 3b), characteristic of an asymmetric *catena*-P_4 unit.[13d,30] The $^{31}P\{^1H\}$ NMR spectrum was successfully simulated by an iterative fitting procedure (Figure S29, SI), which identified small $^2J_{PP}$ and $^3J_{PP}$ couplings. The $^1J_{PP}$ coupling constants vary widely from −355 to −64 Hz. The resonance attributed to P1 at δ = −10.7 ppm is significantly broadened ($\Delta\nu_{1/2}$ = 99 Hz; $^1J_{PP}$ = −64 Hz), likely due to interactions with the quadrupolar ^{59}Co nucleus, which is consistent with the Co−P1 bond constituting the major cobalt-phosphorus interaction.[31]

Considering the observed isomerization to the isocyanide for neutral cyanide,[29] we proceeded to react compounds **4a-d** with alkyl and aryl isocyanides R'NC (R' = Cy, *t*Bu, Mes, Ph) (Scheme 2b). Initially, the formation of analogues of the previously described complex, **5a** were also observed in these reactions (Figure S48, SI). Continuous addition of up to 10 equivalents of isocyanide leads to a clean reaction and full conversion to two isomeric η^3-*cyclo*-P_4 complexes *endo*-**6** and *exo*-**6**. These stereoisomers only differ by the position of the acyl substituent. A similar mixture of isomers was observed in reactions with related CoP_n complexes.[30c,32] The transformation of **5** to **6** could also be induced by heat, albeit with concomitant decomposition of **5**.

A wide range of reactions of **4a-d** toward different isocyanides and isoelectronic carbon monoxide have been explored, which gave very similar results. Further details of the reactions and the resulting complexes **6b-p**, observed by $^{31}P\{^1H\}$ NMR spectroscopy, can be found in the SI (Table S8, Figures S46-52).

Specifically, in the reaction of **4a** (R = *t*Bu) toward cyclohexyl isocyanide both *exo*- and *endo*-isomers of **6a** are formed at low temperature, as evidenced by a variable temperature (VT) NMR monitoring experiment (Figure S60, SI). Additional DFT calculations revealed that *endo*-**6a** and *exo*-**6a** are isoenergetic (see the SI for details).

Both stereoisomers of **6a** co-crystallize from a saturated *n*-hexane solution in 57% overall yield as dark green crystals, which were analyzed by XRD. The molecular structures of **6a** are analogous to **4a**, with the $P_4C(O)R$ ligand coordinated to the cobalt center in an η^3 fashion (Figure 4), while the carbonyl moieties have been displaced from coordination to the cobalt by one molecule of isocyanide. The bond lengths of the η^3-$P_4C(O)R$ ligand in the solid-state molecular structures of **6a** closely agree with those of the η^3:η^1-$P_4C(O)R$ ligand in **4a-c**.

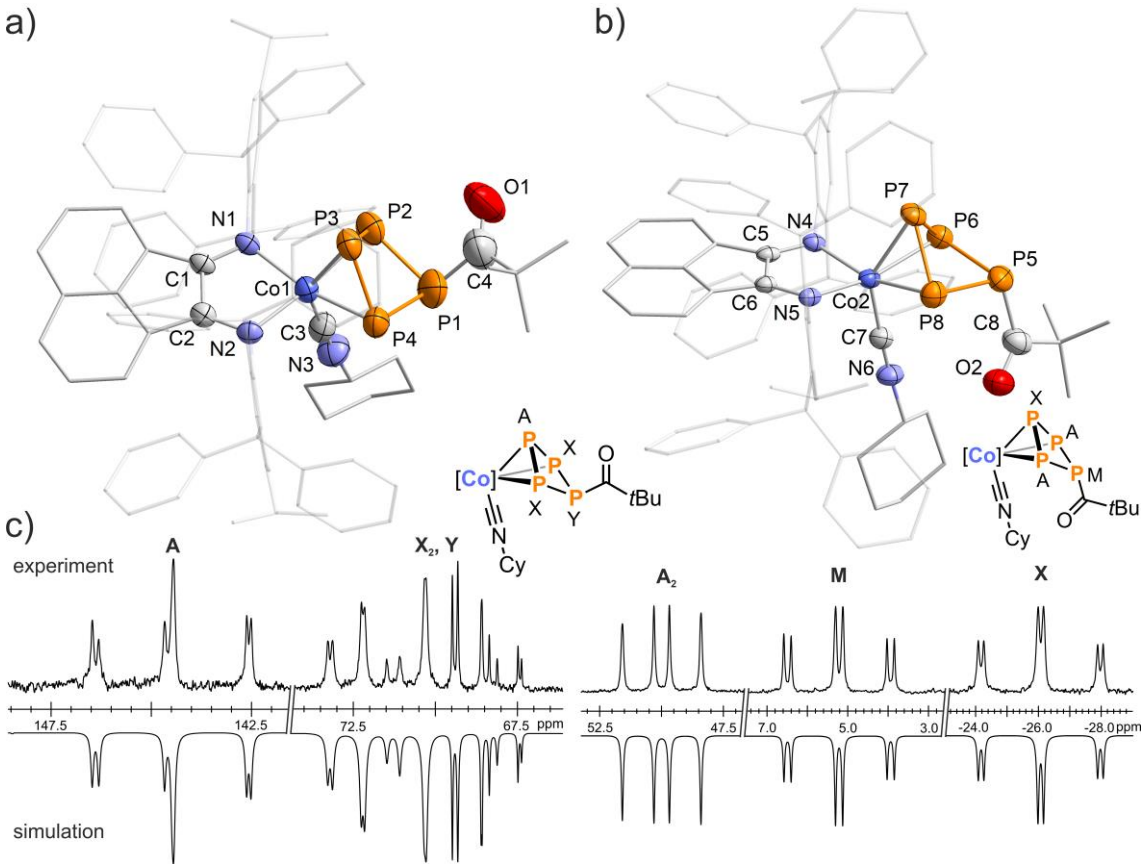

Figure 4. Solid-state structures of a) *endo*-[(Ar*BIAN)Co(CyNC)(η^3-P_4C(O)*t*Bu)] (*endo*-**6a**) and b) *exo*-[(Ar*BIAN)Co(CyNC)(η^3-P_4C(O)*t*Bu)] (*exo*-**6a**) in the co-crystal;[45] thermal ellipsoids are shown at the 50% probability level; hydrogen atoms, disorder and non-coordinating solvent molecules are omitted for clarity. Selected bond lengths [Å] and angles [°] of *endo*-**6a**: P1−P2 2.218(3), P1−P4 2.232(3), P2−P3 2.191(2), P3−P4 2.165(3), Co1−P2 2.3000(2), Co1−P3 2.2983(2), Co1−P4 2.3027(2), Co1−C3−N3 178.4(5); c) experimental (upward) and simulated (downward) $^{31}P\{^1H\}$ NMR spectra of *endo*-**6a** with nuclei assigned to an AX_2Y spin system: $\delta(P_A)$ = 144.5 ppm, $\delta(P_x)$ = 71.7 ppm, $\delta(P_Y)$ = 68.6 ppm, $^1J_{AX}$ = −318 Hz, $^1J_{XY}$ = −165 Hz, $^2J_{AY}$ = −5 Hz; exo-6a: $\delta(P_A)$ = 50.0 ppm, $\delta(P_M)$ = 5.2 ppm, $\delta(P_Y)$ = −26.1 ppm, $^1J_{AX}$ = −308 Hz, $^1J_{AM}$ = −207 Hz, $^2J_{MX}$ = 29 Hz.

In contrast, the $^{31}P\{^1H\}$ NMR signals of *endo*-**6a** and *exo*-**6a** differ markedly from each other and from those of **4a-d** (Figure 4c). *Endo*-**6a** features an AX_2Y spin system in C_6D_6, in which the signal for the coordinating phosphorus atom P3 is shifted significantly upfield in comparison to **4a** (δ = 143.3 ppm for *endo*-**6a** versus δ = 323.3 ppm for **4a**). In comparison to *endo*-**6a**, the resonances constituting the A_2MX spin system observed for *exo*-**6a** are shifted further upfield. The considerable differences in the chemical shifts of the *endo*- and *exo*-isomers of **6a** are nicely reproduced by our DFT calculations and correlate well with the experimental values (Table S13, SI). The different orientations of the −C(O)R substituents in solution, leading to reduced orbital overlap of the phosphorus atoms, are also evident in the $^{31}P\{^1H\}$ NMR spectra, with greater $^1J_{PP}$ coupling constants observed for the *exo*-isomer in **6a** (*exo*-**6a**: $^1J_{AM}$ = −207 Hz vs. *endo*-**6a**: $^1J_{XY}$ = −165 Hz). The full set of parameters, including simulation by an iterative fitting procedure, can be

found in the SI (Figures S35-36). In the ATR-IR spectrum of **6a**, the bands at $\tilde{\nu}_{CO}$ = 1599 and 1640 cm^{-1}, respectively, can be attributed to the C=O stretching vibration.[25]

Additional single-crystal XRD data was obtained for *endo*-**6a**, where only one isomer was observed in solid-state, as well as further combinations of R and R' in *exo*-**6d** (R = Ph, R' = Cy) and *endo*-**6e** (R = *t*Bu, R' = *t*Bu; Figures S86-88, SI). During XRD analysis of **6a**, crystals of a minor side product, [(Ar*BIAN)Co(CyNC)$_2$(η^1-P_4CO*t*Bu)] (**7**), were also discovered. Structural analysis of these revealed a cobalt complex bearing two isocyanide ligands. This saturation of the coordination sphere is facilitated by the severance of most of the cobalt-phosphorus interactions, resulting in an η^1-coordinated [1.1.0]bicyclotetraphosphane-1,4-diyl ("P_4 butterfly") ligand.[33] A more detailed discussion of **7** can be found in the Supporting Information (Figure S89).

To gain further insight into the distribution of isomers, a VT NMR spectroscopic analysis of the isolated crystalline material of **6a** was conducted. The crystals were dissolved in toluene-d_8 at −80 °C and the temperature was gradually increased while monitoring by $^{31}P\{^1H\}$ NMR spectroscopy (Figure S94-95, SI). The spectra at low temperature show predominantly the signals assigned to *exo*-**6a**. An increase in temperature leads to an increase in signal intensity for *endo*-**6a**. This observation was attributed to crystal packing effects, which likely influence the solid-state structures and lead to a preference for the crystallization of one isomer over the other. Once the isomerization has occurred and an equilibrium established, cooling the solution back down to low temperature did not reassert a single isomer as a significantly major species in the mixture.

To investigate whether the stronger cyanide anion, CN^-, of certain cyanide salts would completely cleave an organophosphorus fragment from the complexes, **4a-d** were reacted with two equivalents of [M]CN ([M] = nBu$_4$N$^+$, Et$_4$N$^+$, K(18c-6)$^+$).[14,34] This resulted in the selective formation of *cyclo*-P_3 cobalt complex [(Ar*BIAN)Co(CN)(η^3-P_3)]$^-$ (**8**$^-$) and the acylated cyanophosphanides [RC(O)PCN]$^-$ (**9a-d**$^-$) (Scheme 3). This was initially indicated by the $^{31}P\{^1H\}$ NMR spectra, in which two singlets were observed in a 3:1 integral ratio (Figures S53-56, SI). The observed chemical shift of δ = −218.7 ppm for [K(18-6)]**8** is close to the reported values for [(^{Dipp}PHDI)Co(η^3-P_3)(CN)]$^-$ (δ = −193.2 ppm), [{$B_{10}H_{10}C_2$(P_3Mes$_2$)}Co(η^3-P_3)]$^-$ (δ = −250.9 ppm, Mes = 2,4,6-$Me_3C_6H_2$), and other related *cyclo*-P_3 complexes.[14,24,35]

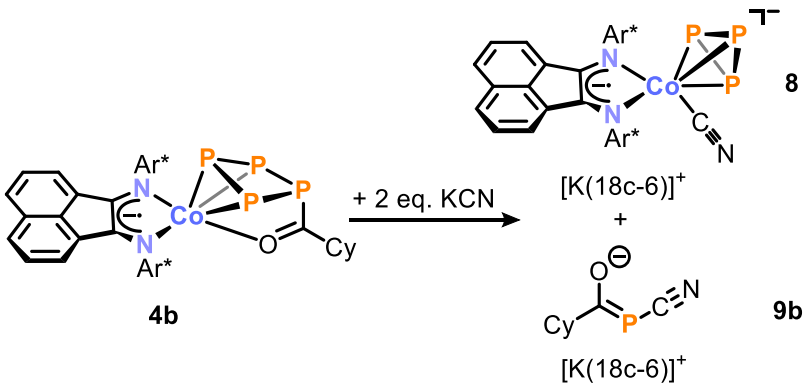

Scheme 3. Cyanide induced [3+1] fragmentation of **4b**; reagents/by-products and conditions: +2.2 eq. KCN/+2.2 eq. 18c-6; THF, r.t., 3 d; yields: [K(18c-6)]**8**: 60%, [K(18c-6)]**9b**: 31%.

Acylcyanophosphanides, to our knowledge, have not been reported previously.[36] The $^{31}P\{^1H\}$ NMR signals of **9a-d**$^-$ (**9a**$^-$: δ = −44.0 ppm, **9b**$^-$: δ = −45.2 ppm, **9c**$^-$: δ = −45.5 ppm, **9d**$^-$: δ = −30.1 ppm) are noticeably shifted upfield compared to the $^{31}P\{^1H\}$ NMR resonance of the related anion [PhPCN]$^-$ (δ = 70.3 ppm).[37] The reaction of **4a-d** with the CN^- anion represents a remarkable [3+1] fragmentation of a tetraphosphido ligand to yield a *cyclo*-P_3^- species and an organic monophosphorus compound. While a few transition-metal-mediated [3+1] fragmentations of P_4 are known in which the generated P_3 and P_1 moieties remain coordinated to a transition metal atom,[28b,35b,38] the release of P_1 species from polyphosphorus ligands has rarely been observed.[3,4,33f,35a,39]

In the case of R = Cy, the products [K(18c-6)]**8** and [K(18c-6)]**9b** are easily separated by fractional crystallization. [K(18c-6)]**8** crystallizes from the concentrated toluene reaction mixture at room temperature, affording purple crystals in 60% yield. XRD analysis confirmed the coordination of the *cyclo*-P_3 and cyanide ligand to the cobalt center (Figure 5a). The Co−C (1.931(9) Å) and C−N (1.158(4) Å) bond lengths, as well as the CN stretching vibration ($\tilde{\nu}_{CN}$ = 2069 cm^{-1}), fall within the typical range for cobalt cyanide complexes.[25,40,41] The *cyclo*-P_3 ring coordinates to the metal center in a η^3 fashion, with average P−P (2.143(7) Å) and Co−P (2.302(9) Å) distances comparable to reported anionic cobalt *cyclo*-P_3 complexes.[14,24,35] Colorless crystals of [K(18c-6)]**9b** were isolated in 31% yield from the mother liquor at −35 °C. Due to similar solubility, further fractions of isolated crystalline material of [K(18c-6)]**9b** contained also small amounts of [K(18c-6)]**8**. Figure 5b displays the solid-state molecular structure of [K(18c-6)]**9b**, which features a P_1 anion with acyl- and cyanide substituents. Both the oxygen and the nitrogen atoms coordinate to the potassium counterion. Additional single-crystal XRD data was obtained for isostructural [K(18c-6)]**9a** and [K(18c-6)]**9d** and is given in the Supporting Information (Figures S90-91).

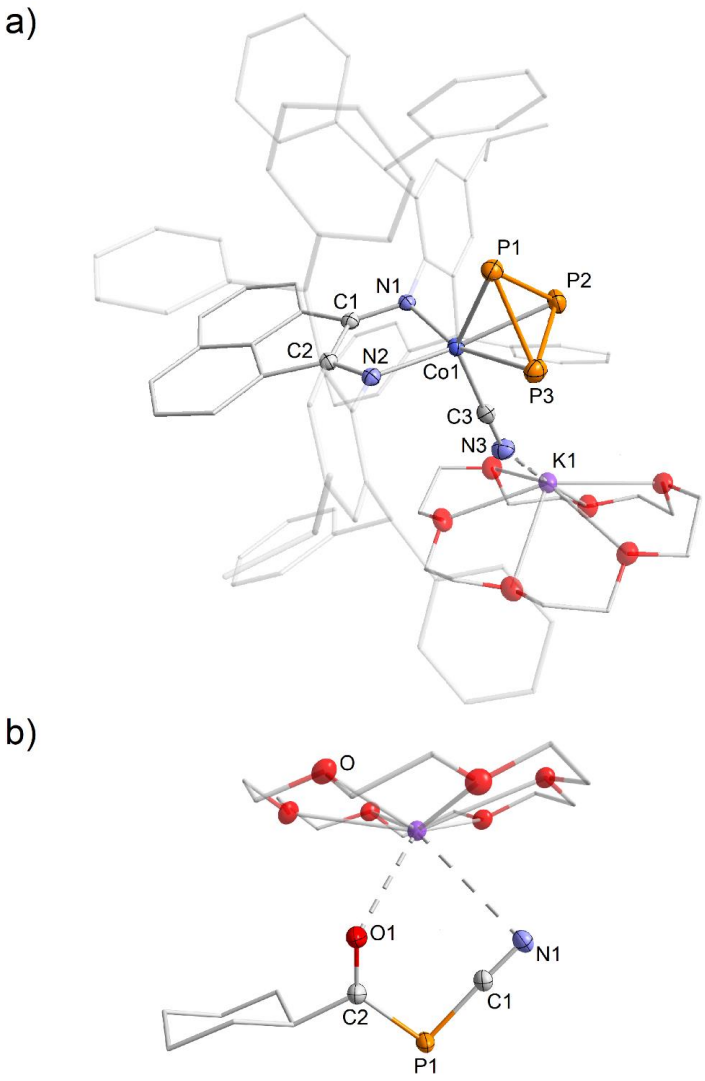

Figure 5. Solid-state molecular structures of a) [K(18c-6)][(Ar*BIAN)Co(CN)(η^3-P_3)] ([K(18c-6)]**8**) and b) K(18c-6)][CyC(O)PCN] ([K(18c-6)]**9b**);[45] thermal ellipsoids are shown at the 50% probability level; hydrogen atoms and disorder are omitted for clarity. Selected bond lengths [Å] and angles [°] of [K(18c-6)]**8**: P1−P2 2.1318(5), P1−P3 2.1306(5), P2−P3 2.1682(4), Co1−P1 2.3070(4), Co1−P2 2.3001(4), Co1−P3 2.3014(3), Co1−C3 1.9323(1), C1−N1 1.3211(2), C3−N3 1.1583(2), C1−C2 1.4486(2), K1−N3 2.9111(1), P1-P2-P3 59.396(2), P1-P3-P2 59.452(2), P2-P1-P3 61.152(2), Co1-C3-N3 177.83(1); [K(18c-6)]**9b**: P1−C1 1.7789(1), P1−C2 1.7960(1), C1−N1 1.1519(2), C2−O1 1.2397(1), P1-C1-N1 176.77(9), C1-P1-C2 95.08(5).

Specifically in the case of **9b**$^-$, the similar P1−C1 (1.7789(1) Å) and P1−C2 (1.7960(1) Å) bond lengths lie between those expected for a P=C double and a P−C single bond ($\sum r_{PC}$ 1.69 Å vs. 1.86 Å), indicating partial delocalization.[21] Furthermore, the C1−N1 (1.1519(2) Å) bond length of the nearly linear PCN group (P1-C1-N1 176.8(8)°) is comparable to that of the cyanophosphanide [Na(18c-6)][P(SiPh$_3$)(CN)] (C−N 1.161 Å, P−C 1.761 Å) reported by Grützmacher and co-workers.[42] On the other hand, the C−N (1.248(5) Å) bond length of 1-aza-phospha-allenide [*i*Pr=N=C=P]$^-$ is noticeably longer than that of **9b**$^-$, and the P−C (1.603(3) Å) bond length is shorter.

These observations suggest several contributing resonance structures analogous to those proposed for $[P(SiPh_3)(CN)]^-$.[42,43] A natural resonance theory analysis conducted at the TPSS/def2-TZVP level of theory revealed that the phosphaenolate resonance form **I** (37.4%) is the primary contributor to the electronic ground state, contrasting with the contributions of 1-aza-3-phosphaallenide **II** and phosphide **III** (Scheme 4). In comparison, calculations for the related compound $[P(SiPh_3)(CN)]^-$ showed a significantly higher contribution to the phosphide form (76.4%).[43] The IR spectrum of **9b** exhibits two characteristic stretching vibrations at $\tilde{\nu}_{CN}$ = 2101 cm^{-1} and $\tilde{\nu}_{CO}$ = 1544 cm^{-1}, which are in good agreement with the calculated values ($\tilde{\nu}_{CN}$ = 2099 cm^{-1} and $\tilde{\nu}_{CO}$ = 1565 cm^{-1}), as well as with those of other alkyl cyanophosphanides $[RP(CN)]^-$ (R = Me, Et, Ph; $\tilde{\nu}_{CN}$ = 2080 to 2160 cm^{-1}).[37] These values are higher than that reported for cyanodiphosphanide $[tBu_2PPCN]^-$ ($\tilde{\nu}_{CN}$ = 2049 cm^{-1}).[14] In contrast, the CO stretching frequency is lower than expected for typical organic compounds (≈ 1700 cm^{-1}), indicating the relatively high contribution of Lewis type formula **I** (Scheme 4).[25]

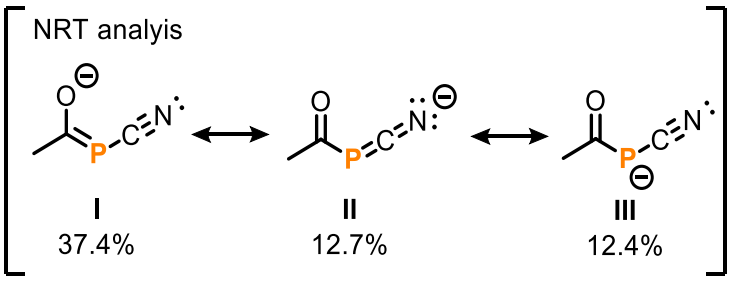

Scheme 4. Natural resonance theory (NRT) weights for the dominant Lewis structures of the model cyanophosphanide **9-Me**$^-$ (R = Me) (TPSS/def2-TZVP) are provided. Comparable ratios for **9b**$^-$ can be found in the SI.[44]

The [3+1] fragmentation reaction mechanism of **4a-d** by M[CN] is proposed to involve an initial attack of a cyanide anion at the cobalt center, displacing the coordination of the carbonyl and forming an anionic species analogous in structure to neutral **6** (*vide supra*, also see the SI, Scheme S1). Subsequent nucleophilic attack by a second cyanide anion at the acyl-substituted P atom leads to the release of **9a-d**$^-$ and the formation of the *cyclo*-P_3 species **8**$^-$. The reaction rate is influenced by the steric demands of the substituents in **4a-d** and even more by the solubility of the cyanide source [M]CN. Monitoring the reaction between **4d** (R = Ph) with $[Et_4N]CN$ over a 14-hour period using ^{31}P NMR spectroscopy revealed several intermediate sets of signals that closely resemble an AX_2Y and an A_2MX spin system, exhibiting similar chemical shifts as observed for *endo*- and *exo*-**6a** (Figure S57, SI). Unfortunately, the formation of these intermediates in only minor quantities has impeded the successful isolation and characterization of them so far. Nevertheless, the $^{31}P\{^1H\}$ NMR spectroscopic data indicate that analogues of the

previously described complex, **6**, featuring *exo*- and *endo*-η^3-$P_4C(O)R$ ligands may serve as potential intermediates in the reaction.

A second acyl substituent can be introduced to **9b**$^-$ to generate a bis(acyl)monocyanophosphine (Scheme 5). Therefore, performing salt metathesis of [K(18c-6)]**9b** with CyC(O)Cl yields $(CyC(O))_2PCN$ (**10**), which was isolated as a colorless oil in 81% yield. The $^{31}P\{^1H\}$ NMR spectrum of **10** exhibits a sharp singlet at $\delta = -8.2$ ppm, which is shifted slightly upfield compared to the alkyl-substituted bis(acyl)phosphine P(C(O)Ad)(C(O)Ph)*t*Bu (δ = 37 ppm).[8] In the $^{13}C\{^1H\}$ NMR spectrum, two characteristic doublet resonances can be assigned to the acyl (δ = 211.2 ppm; $^1J_{PC}$ = 52 Hz) and cyano carbon atoms (δ = 117.1 ppm; $^1J_{PC}$ =62 Hz). In comparison, the resonances for [K(18c-6)]**9b** were observed at $\delta = 238.1$ ppm for the acyl and $\delta = 136.7$ ppm for the cyano carbon atoms.

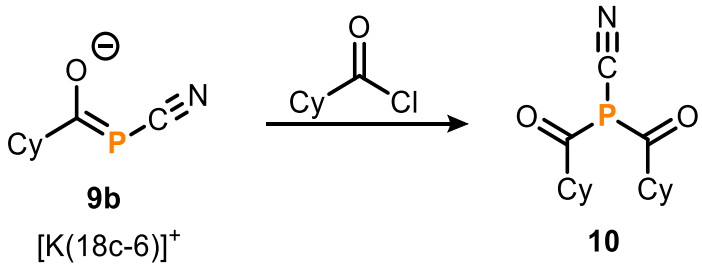

Scheme 5. Functionalization of [K(18c-6)]**9b** with cyclohexanecarboxylic acid chloride to **10**; reagents/by-products and conditions: + CyC(O)Cl/−[K(18c-6)]Cl; C_6D_6, r.t., 1 h; isolated yield: 81%.

Additionally, the IR spectrum of **10** displays CO stretching frequencies at $\tilde{\nu}_{CO}$ = 1715 and 1681 cm^{-1}, which agree well with the calculated values ($\tilde{\nu}_{CO}$ = 1709 and 1693 cm^{-1}), confirming the constitution of the bis(acyl)cyanophosphine $(CyC(O))_2PCN$.

2.3 Conclusion

In this study, we have synthesized the acylated tetraphosphido complexes [(Ar*BIAN)Co(η^3:η^1-P_4COR)] (**4a-d**) with various alkyl and aryl substituents using a two-step process involving P_4, [K(18c-6)]**2** and RC(O)Cl. These ligands provide a platform for the study of P-acylated ligands. Treatment of the $P_4C(O)R$ complexes with trimethylsilyl cyanide and isocyanides resulted in P−Co bond cleavage, leading to the formation of pnictogen derivatives, including prismane in **5**, as well as *endo*- and *exo*-isomers of η^3-coordinating tetraphosphido ligands (**6**). Additionally, treatment of **4a-d** with two equivalents of the cyanide anion facilitated the release of acylcyanophosphanides $RC(O)PCN^-$ **9a-d**$^-$ through a remarkable [3+1] fragmentation process, resulting in the formation of a cyclotriphosphido cobalt complex **8**$^-$. Monitoring of the [3+1] fragmentation reaction provided insight into the involvement of

intermediates similar to **6,** which have rearranged polyphosphorus ligands and are considered key intermediates *en route* to the anions $\mathbf{8}^-$ and ($\mathbf{9a\text{-}d}^-$). Additionally, we have synthesized the bis(acyl)cyanophosphine $(CyC(O))_2PCN$ (**10**), highlighting the useful reactivity of these anions. Overall, our findings demonstrate the potential of metalate activation and functionalization of P_4 in accessing new (poly-)phosphorus species. We anticipate that this approach will open up avenues for the synthesis of unique phosphorus compounds in future research endeavors. Ongoing investigations are focused on further exploring these possibilities.

2.4 Experimental Details

General Synthetic Methods

All reactions and product manipulations were carried out in flame-dried glassware under an inert atmosphere of argon using standard Schlenk-line or glovebox techniques (maintained at <0.1 ppm H_2O and <0.1 ppm O_2). The starting materials 2,6-bis(diphenylmethyl)-4-isopropylaniline[46], $[K(thf)_{0.2}][Co(1,5\text{-cod})_2]$[47] and MesNC[48] were prepared according to previously reported procedures. All other chemicals were purchased from commercial suppliers and used without further purification.

Solvents were dried and degassed with a MBraun SPS800 solvent purification system. All dry solvents except *n*-hexane and *n*-pentane were stored under argon over activated 3 Å molecular sieves in gas-tight ampules. *n*-Hexane and *n*-pentane were instead stored over potassium mirrors.

General Analytical Techniques

NMR spectra were recorded on Bruker Avance 400 spectrometers at 300 K and were internally referenced to residual solvent resonances (^{1}H NMR: C_6D_6: 7.15 ppm; $^{13}C\{^1H\}$ C_6D_6: 128.06 ppm). $^{31}P\{^1H\}$ spectra were referenced externally to 85% $H_3PO_{4(aq.)}$. Chemical shifts, δ, are given in ppm referring to external standards of tetramethylsilane (^{1}H, $^{13}C\{^1H\}$). ^{1}H, ^{13}C and ^{31}P NMR signals were assigned based on 2D NMR spectra (COSY, HSQC, HMBC, NOESY and ROESY). Melting points were measured on samples in sealed capillaries on a Stuart SMP10 melting point apparatus. UV/Vis spectra were recorded on an Ocean Optics Flame Spectrometer with a DH-2000-BAL light source. Mass spectra of compound **10** was recorded on an Agilent Q-TOF 6540 UHD device by the by the Central Analytical Department at the University of Regensburg Regensburg and compound [K(18c-6)]**3** on a Finnigan MAT 95 device. Elemental analysis were performed by the Central Analytical Department of the University of Regensburg using a Vario micro cube. IR spectra were recorded with a Bruker ALPHA spectrometer equipped with a diamond ATR unit.

NMR Simulations

For compounds which give rise to a higher order spin system in the $^{31}P\{^1H\}$ NMR spectrum, the resolution enhanced $^{31}P\{^1H\}$ NMR spectrum was transferred to the software gNMR, version 5.0.6, by Cherwell Scientific.[49] The full line shape iteration procedure of gNMR was applied to obtain the best match of the fitted to the experimental

spectrum. $^1J(^{31}P^{31}P)$ coupling constants were set to negative values and all other signs of the coupling constants were obtained accordingly.[50]

2.4.1 Synthesis of Compounds

Ar*BIAN (1):

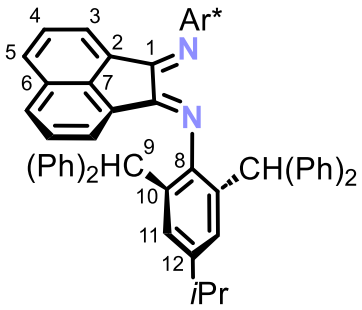

All preparative steps were performed under atmospheric air. To a 100 mL round bottom flask was added $ZnCl_2$ (1.50 g, 11.0 mmol, 1.1 equiv.), acenaphthenequinone (1.76 g, 9.7 mmol, 1.0 equiv.), 2,6-bis(diphenylmethyl)-4-isopropylaniline (10.28 g, 22.0 mmol, 2.3 equiv.) and acetic acid (30 mL). The yellow suspension was refluxed for 5 h at 118 °C. After cooling to r.t. the reaction mixture was filtered over a P3 glass frit, and the yellow solid was washed with acetic acid (3 × 25 mL) and subsequently with Et_2O (7 × 25 mL). The crude product was dissolved in DCM (150 mL). To this, a solution of potassium oxalate (4.00 g, 24.1 mmol, 2.5 equiv.) in H_2O (22 mL) was added and stirred for 1 h. The organic phase was separated and washed with H_2O (3 × 75 mL) and subsequently dried over $MgSO_4$. After removing the solvent, the orange solid was recrystallized from a mixture of *n*-heptane/DCM 1:1 (100 mL) at −19 °C. The product was separated by filtration, washed with cold *n*-pentane (20 mL) and dried *in vacuo* to give microcrystalline orange powder. Slow diffusion of *n*-hexane into a saturated toluene solution of **1** yielded crystals suitable for single-crystal X-ray diffraction.

Yield: 7.32 g (70%).

M.p.: 234 °C

^{1}H NMR (400.30 MHz, 300 K, C_6D_6): δ/ppm = 1.06 (d, $^3J_{HH}$ = 6.9 Hz, 12H, −CH(C*H*$_3$)$_2$ of *i*Pr), 2.62 (sept, $^3J_{HH}$ = 6.9 Hz, 2H, −C*H*(CH$_3$)$_2$ of *i*Pr), 6.03 (s, 4H, −C^9*H*(Ph)$_2$), 6.50-6.54 (m, 2H, C^4−*H* of BIAN), 6.58-6.62 (m, 6H, C^2−*H* of BIAN overlapping with C−*H*$_{Ar}$ of Ph), 6.70-6.73 (m, 8H, C−*H*$_{Ar}$ of Ph), 6.93-6.97 (m, 4H, C−*H*$_{Ar}$ of Ph), 6.99-7.03 (m, 8H, C−*H*$_{Ar}$ of Ph), 7.09 (d, $^3J_{HH}$ = 8.1 Hz, 2H, C^5−*H* of BIAN), 7.16-7.18 (m, 8H, C−*H*$_{Ar}$ of Ph overlapping with C_6D_6 solvent signal), 7.25-7.28 (m, 12H, C^{11}−*H* overlapping with C−*H*$_{Ar}$ of Ph).

^{13}C{^{1}H} NMR (100.66 MHz, 300 K, C_6D_6): δ /ppm = 23.9 (s, −CH(*C*H$_3$)$_2$ of *i*Pr), 33.5 (s, −*C*H(CH$_3$)$_2$ of *i*Pr), 52.1 (s, −*C*^{9}H(Ph)$_2$), 123.7 (s, *C*^{3}−H of BIAN), 125.7 (s, *C*$_{Ar}$−H of Ph), 126.1 (s, *C*$_{Ar}$−H of Ph) 126.6 (s, *C*^{4}−H of BIAN), 126.7 (s, *C*^{11}−H), 127.6 (s, *C*^{5}−H of BIAN overlapping with C_6D_6 solvent signal), 127.9 (s, *C*$_{Ar}$−H of Ph), 128.1 (s, *C*$_{Ar}$−H of Ph), 129.1 (s, *C*^{2} of BIAN), 129.5 (s, *C*$_{Ar}$−H of Ph), 129.6 (s, *C*^{6} of BIAN), 130.0 (s,

C_{Ar}–H of Ph), 131.4 (s, C^{10}), 140.0 (s, C^7 of BIAN), 143.3 (s, C_{Ar} of Ph), 143.6 (s, C^{12}), 144.1 (C_{Ar} of Ph), 147.5 (s, C^8–N), 162.4 (s, C^1=N of BIAN). The ^{1}H and ^{13}C{^{1}H} NMR signals compare well with those reported for **1** in CD_2Cl_2.[51]

UV/Vis (THF, λ_{max} / nm, ε_{max} / L·mol^{-1}·cm^{-1}): 260sh (35000), 280 (31000), 310 (16000), 330sh (11000), 360 (4000).

Elemental analysis calcd. for $C_{82}H_{68}N_2$ (Mw = 1081.46 g·mol^{-1}):
C 91.07, H 6.34, N 2.59; found C 90.72, H 6.17, N 2.46.

[K(18c-6)][(Ar*BIAN)Co(η^4-1-5-cod)] ([K(18c-6)]2):

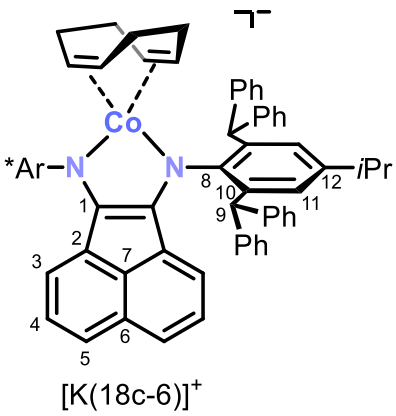

To a deep yellowish green solution of [K(thf)$_{0.2}$][Co(η^4-1,5-cod)$_2$] (0.40 g, 1.22 mmol, 1.05 equiv.) and [18]crown-6 (18c-6, 0.32 g, 1.22 mmol, 1.05 equiv.) in THF (30 mL), an orange solution of **1** (1.25 g, 1.16 mmol, 1.00 equiv.) in THF (30 mL) was added slowly at −30 °C. The resulting deep brown solution was stirred for one day while warming to r.t.. The solvent was removed under vacuum and the resulting dark solid was dissolved in THF (15 mL). Subsequently the suspension was filtered through a P3 glass frit. The filtrate was layered with *n*-hexane (30 mL). After one week, dark brown crystals suitable for single-crystal X-ray diffraction were obtained and isolated by filtration, washed with *n*-hexane (3 × 4 mL) and dried *in vacuo*.

Yield: 1.39 g (77 %).

^{1}H NMR (400.30 MHz, 300 K, THF-d_8): δ/ppm = 0.24-0.26 (m, 4H, CH_2 of COD), 1.19 (br s, 4H, CH_2 of COD), 1.33 (d, $^3J_{HH}$ = 6.9 Hz, 12H, −CH(CH_3)$_2$ of *i*Pr), 2.73 (br s, 4H, C*H* of COD), 2.94 (sept, $^3J_{HH}$ = 6.9 Hz, 2H, −C*H*(CH$_3$)$_2$ of *i*Pr), 3.66 (s, 24H, 18c-6), 4.22 (d, $^3J_{HH}$ = 6.9 Hz, 2H, C^3–*H* of BIAN), 5.80-5.84 (m, 2H, C^4–*H* of BIAN), 6.29 (d, $^3J_{HH}$ = 8.1 Hz, 2H, C^5–*H* of BIAN), 6.68-6.73 (m, 12H, C–H_{Ar} of Ph), 7.08-7.12 (m, 4H, C–H_{Ar} of Ph), 7.22-7.28 (m, 14H, C–H_{Ar} of Ph), 7.37 (s, 4H, C^{11}–*H*), 7.39 (s, 4H, −C^9*H*(Ph)$_2$), 7.66-7.68 (m, 8H, C–H_{Ar} of Ph).

^{13}C{^{1}H} NMR (100.66 MHz, 300 K, THF-d_8): δ/ppm = 25.5 (s, −CH(*C*H$_3$)$_2$ of *i*Pr overlapping with THF-d_8 solvent signal), 31.6 (s, *C*H$_2$ of COD), 35.5 (s, −*C*H(CH$_3$)$_2$ of *i*Pr), 52.8 (s, −*C*^{9}H(Ph)$_2$), 67.1 (s, *C*H of COD), 71.8 (s, 18c-6), 116.8 (s, C^3–H of BIAN), 119.2 (s, C^5–H of BIAN), 125.5 (s, C_{Ar}–H of Ph), 125.9 (s, C_{Ar}–H of Ph), 127.3 (s, C^4–H of BIAN), 127.6 (s, C^{11}–H), 128.1 (s, C_{Ar}–H of Ph), 128.6 (s, C_{Ar}–H of Ph), 131.6 (s,

C_{Ar}–H of Ph), 132.4 (s, C_{Ar}–H of Ph), 133.7 (s, C^7 of BIAN), 138.2 (s, C^6 of BIAN), 141.8 (s, C^{10}), 141.9 (s, C^{12}), 142.6 (s, C^1=N of BIAN), 148.0 (s, C_{Ar} of Ph), 149.0 (s, C_{Ar} of Ph), 155.0 (s, C^8–N).

UV/Vis (THF, λ_{max} / nm, ε_{max} / L·mol^{-1}·cm^{-1}): 250 (57000), 280sh (28000), 440 (14000).

Elemental analysis calcd. for $C_{102}H_{104}CoKN_2O_6$ (Mw = 1551.99 g·mol^{-1}):
C 78.94, H 6.75, N 1.81; found C 78.80, H 6.68, N 1.71.

[K(18c-6)][(Ar*BIAN)Co(η^4-P$_4$)] ([K(18c-6)]3):

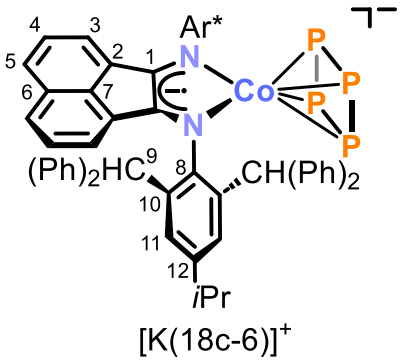

A 250 mL Schlenk flask was charged with P_4 (339 mg, 2.73 mmol, 1.0 equiv.), [K(18c-6)]**2**] (4.241 g, 2.73 mmol, 1.0 equiv.) and THF (170 mL). The resulting deep brown mixture was stirred for one day, over which time the color changed to dark purple. The solvent was removed, and the dark residue extracted into toluene (100 mL). The resulting solution was filtered through a P4 glass frit, concentrated to 70 mL, and layered with *n*-hexane (150 mL). After ten days shimmering purple crystals, of sufficient quality for analysis by XRD, were isolated by decantation of the supernatant. The crystals were washed with *n*-pentane (3 × 12 mL) and dried *in vacuo*.

Yield: 2.70 g (63 %).

^{1}H NMR (400.13 MHz, 300 K, C_6D_6): δ/ppm = 1.03 (d, $^3J_{HH}$ = 6.9 Hz, 12H, −CH(C*H*$_3$)$_2$ of *i*Pr), 2.62 (sept, $^3J_{HH}$ = 6.9 Hz, 2H, −C*H*(CH$_3$)$_2$ of *i*Pr), 3.24 (s, 24H, 18c-6), 5.84 (d, $^3J_{HH}$ = 7.0 Hz, 2H, C^3–*H* of BIAN), 6.48-6.51 (m, 2H, C^4–*H* of BIAN), 6.71-6.75 (m, 4H, C–H_{Ar} of Ph), 6.79-6.83 (m, 8H, C–H_{Ar} of Ph), 7.03-7.04 (m, 12H, C–H_{Ar} of Ph), 7.27 (d, $^3J_{HH}$ = 8.2 Hz, 2H, C^5–*H* of BIAN), 7.31-7.33 (m, 8H, C–H_{Ar} of Ph), 7.35 (s, 4H, C^{11}–*H*), 7.45-7.47 (m, 8H, C–H_{Ar} of Ph), 7.67 (s, 4H, −C^9*H*(Ph)$_2$).

^{13}C{^{1}H} NMR (100.61 MHz, 300 K, C_6D_6): δ/ppm = 24.6 (s, −CH(*C*H$_3$)$_2$ of *i*Pr), 34.3 (s, −*C*H(CH$_3$)$_2$ of *i*Pr), 52.5 (s, −*C*^{9}H(Ph)$_2$), 70.9 (s, 18c-6), 120.3 (*C*^{3}–H of BIAN), 122.8 (s, *C*^{5}–H of BIAN), 125.5 (s, C_{Ar}–H of Ph), 126.4 (s, C_{Ar}–H of Ph), 127.5 (s, *C*^{11}–H), 128.2 (s, C_{Ar}–H of Ph overlapping with C_6D_6 solvent signal), 128.2 (s, *C*^{4}–H of BIAN overlapping with C_6D_6 solvent signal), 128.5 (s, C_{Ar}–H of Ph overlapping with C_6D_6 solvent signal), 130.9 (s, *C*^{6} of BIAN), 131.3 (s, C_{Ar}–H of Ph), 131.6 (s, C_{Ar}–H of Ph), 134.4 (s, *C*^{2} of BIAN), 136.6 (s, *C*^{10}), 136.8 (*C*^{7} of BIAN), 144.5 (s, *C*^{12}), 145.1 (s, C_{Ar} of Ph), 148.2 (s, C_{Ar} of Ph), 156.3 (s, *C*^{1}=N of BIAN), 158.4 (s, *C*^{8}–N).

$^{31}P\{^1H\}$ NMR (162.04 MHz, 300 K, C_6D_6): δ/ppm = 113.0 (s, *cyclo*-P_4).

UV/Vis (toluene, λ_{max} / nm, ε_{max} / $L \cdot mol^{-1} \cdot cm^{-1}$): 310sh (49000), 570 (78000).

IR (solid state): ν/ cm^{-1} = 3055w (C−H), 3023w (C−H), 2953w (C−H), 2884w (C−H), 1598w, 1492m (C−N), 1449m, 1417w, 1530w, 1248w, 1104s, 1031w, 961w, 837w, 814w, 763m, 736m, 695vs, 605m.

Elemental analysis calcd. for $C_{94}H_{92}CoKN_2O_6P_4$ (Mw = 1567.70 $g \cdot mol^{-1}$):
C 72.02, H 5.92, N 1.79; found C 73.32, H 6.13, N 1.41.

TOF-MS (ESI, THF): m/z(%) calculated for $C_{82}H_{68}CoN_2P_4^-$ [M^-]: 1263.3665;
found: 1263.3157.

[(Ar*BIAN)Co(η³:η¹-P₄C(O)*t*Bu)] (4a):

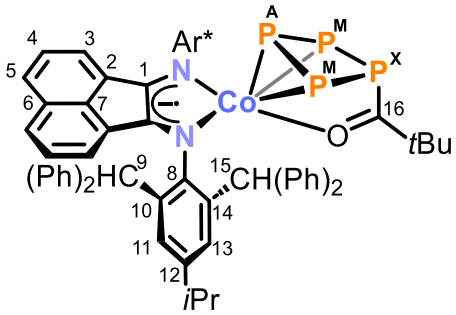

Neat pivaloyl chloride (15.4 mg, 15.6 µL, 0.128 mmol, 1.0 equiv.) was added to a deep purple solution of [K(18c-6)]**3** (200 mg, 0.128 mmol, 1.0 equiv.) in toluene (2 mL). The reaction mixture was stirred overnight. A magenta suspension was formed. The solid was removed by filtration over a pad of silica (2 × 1 cm) and the residue was washed with toluene (3 mL). The combined filtrates were evacuated to dryness, and the deep purple residue was extracted into Et_2O (25 mL). The magenta extract was concentrated until incipient crystallization at one fifth of the original volume. Storage at −19 °C for one day gave shimmering deep magenta crystals, which were isolated by decantation of the mother liquor and dried *in vacuo*. Slow diffusion of *n*-hexane into a saturated toluene solution of **4a** yielded crystals suitable for single-crystal X-ray diffraction.

Yield: 100 mg (58%).

^1H NMR (400.13 MHz, 300 K, C_6D_6): δ/ppm = 0.22 (s, 9H, −C(C*H*$_3$)$_3$ of *t*Bu), 1.04-1.07 (m, 12H, −CH(C*H*$_3$)$_2$ of *i*Pr), 2.61 (sept, $^3J_{HH}$ = 6.9 Hz, 2H, −C*H*(CH$_3$)$_2$ of *i*Pr), 4.83 (s, 2H, −C^9*H*(Ph)$_2$), 6.04 (d, $^3J_{HH}$ = 7.1 Hz, 2H, C^3−*H* of BIAN), 6.21-6.25(m, 2H, C^4−*H* of BIAN), 6.63-6.64 (m, 6H, C−*H*$_{Ar}$ of Ph), 6.73-6.80 (m, 6H, C−*H*$_{Ar}$ of Ph), 6.91-6.98 (m, 14H, C−*H*$_{Ar}$ of Ph), 7.05-7.11 (m, 6H, C−*H*$_{Ar}$ of Ph), 7.15-7.16 (m, 2H, C^{11}−*H* overlapping with C_6D_6 solvent signal), 7.39-7.41 (m, 4H, −C^9*H*(Ph)$_2$ overlapping with C^5−*H* of BIAN), 7.46-7.47 (m, 2H, C^{13}−*H*), 7.72-7.73 (m, 4H, C−*H*$_{Ar}$ of Ph), 7.86-7.88 (m, 4H, C−*H*$_{Ar}$ of Ph).

$^{13}C\{^1H\}$ NMR (100.61 MHz, 300 K, C_6D_6): δ/ppm = 24.4 (s, −CH(CH_3)$_2$ of *i*Pr), 24.6 (s, −CH(CH_3)$_2$ of *i*Pr), 25.8 (d, $^3J_{CP}$ = 3.2 Hz, −C(CH_3)$_3$ of *t*Bu), 34.4 (s, −CH(CH$_3$)$_2$ of *i*Pr), 51.0 (d, $^2J_{CP}$ = 14.6 Hz, −C(CH$_3$)$_3$ of *t*Bu), 51.2 (s, −C^9H(Ph)$_2$), 52.5 (s, −C^{15}H(Ph)$_2$), 122.1 (s, C^3–H of BIAN), 125.2 (s, C^5–H of BIAN), 126.7 (s, C_{Ar}–H of Ph), 127.0 (s, C_{Ar}–H of Ph), 127.3 (s, C_{Ar}–H of Ph), 128.3 (s, C^{13}–H overlapping with C_6D_6 solvent signal), 128.4 (s, C_{Ar}–H of Ph overlapping with C_6D_6 solvent signal), 128.8 (s, C^{11}–H overlapping with C_6D_6 solvent signal), 128.9 (s, C_{Ar}–H of Ph overlapping with C_6D_6 solvent signal), 129.1 (s, C_{Ar}–H of Ph), 129.2 (s, C_{Ar}–H of Ph), 129.5 (s, C^4–H of BIAN), 130.1 (s, C_{Ar}–H of Ph), 130.9 (s, C_{Ar}–H of Ph), 130.9 (s, C_{Ar}–H of Ph), 131.4 (s, C_{Ar}–H of Ph), 132.5 (s, C^6 of BIAN), 134.8 (s, C^{10}), 135.2 (s, C^2 of BIAN), 135.9 (s, C^7 of BIAN), 137.4 (s, C^{14}), 143.9 (s, C_{Ar} of Ph), 144.8 (s, C_{Ar} of Ph), 145.5 (s, C_{Ar} of Ph), 146.5 (s, C^{12}), 147.6 (s, C_{Ar} of Ph), 151.6 (s, C^8–N), 166.8 (s, C^1=N of BIAN), 256.9 (d, $^1J_{CP}$ = 93.2 Hz, C^{16}=O).

$^{31}P\{^1H\}$ NMR (162.04 MHz, 300 K, C_6D_6): (AM_2X) spin system δ/ppm = 59.2 (t, 1P, P_X), 109.7 (dd, 2P, P_M), 323.3 (t, 1P, P_A), for parameters obtained by simulation, see Figure S12 and Table S1.

UV/Vis (toluene, λ_{max} / nm, ε_{max} / L·mol^{-1}·cm^{-1}): 530 (8500), 750 (13000).

IR (solid state): ν/ cm^{-1} = 3023w (C−H), 2960w (C−H), 2865w (C−H), 1599m, 1516m, 1491s (C−N), 1452m-sh (C=O), 1417m, 1362w, 1336w, 1294m, 1256m, 1192m, 1149w, 1119w, 1076w, 1031m, 967w, 943m, 893m, 820w, 761s, 736vs, 696vs, 657m, 634m, 605s, 578m, 540m, 511w, 467m, 406w.

Elemental analysis calcd. for $C_{87}H_{77}CoN_2OP_4$ (Mw = 1349.41 g·mol^{-1}):
C 77.44, H 5.75, N 2.08; found C 77.69, H 5.95, N 1.83.

[(Ar*BIAN)Co(η^3:η^1-P_4C(O)Cy)] (4b):

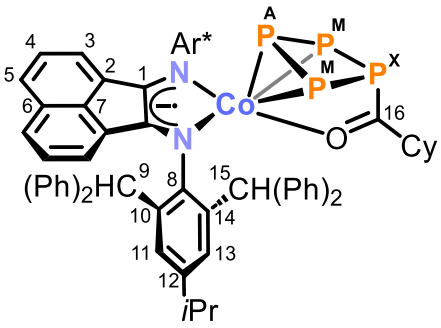

Neat cyclohexanecarboxylic acid chloride (37.4 mg, 34.6 µL, 0.255 mmol, 1.0 equiv.) was added to a deep purple solution of [K(18c-6)]**3** (400 mg, 0.255 mmol, 1.0 equiv.) in toluene (12 mL). The reaction mixture was stirred overnight. A magenta suspension was formed. The solid was removed by filtration over a pad of silica (1.5 × 2 cm) and the residue was washed with toluene (2 x 3.5 mL). The combined filtrates were evacuated to dryness, and the deep magenta residue was extracted into a mixture of Et_2O (100 mL) and MTBE (8 mL). The extract

was filtered and concentrated until incipient crystallization at one seventh of the original volume. Storage at −19 °C gave shimmering deep magenta crystals, which were isolated by decantation of the mother liquor and dried *in vacuo*. The crystalline solid contains 0.9 molecules of Et_2O per molecule of compound after drying as indicated by the $^{1}H/^{13}C\{^{1}H\}$ NMR spectra and elemental analysis. Slow diffusion of *n*-hexane into a saturated toluene solution of **4b** yielded crystals suitable for single-crystal X-ray diffraction.

Yield: 189 mg (54%).

^{1}H NMR (400.30 MHz, 300 K, C_6D_6): δ/ppm = 0.05-0.14 (m, 2H, CH_2 of Cy), 0.25-0.48 (m, 3H, CH_2 of Cy), 0.62-0.68 (m, 1H, C−*H* of Cy), 1.04-1.07 (m, 15H, −CH(CH_3)$_2$ of *i*Pr overlapping with CH_2 of Cy overlapping with Et_2O solvent signal), 1.28-1.31 (m, 2H, CH_2 of Cy), 2.61 (sept, $^{3}J_{HH}$ = 6.9 Hz, 2H, −C*H*(CH$_3$)$_2$ of *i*Pr), 4.96 (s, 2H, −C^{9}*H*(Ph)$_2$), 6.09 (d, $^{3}J_{HH}$ = 7.1 Hz, C^{3}−*H* of BIAN), 6.19-6.23 (m, 2H, C^{4}−*H* of BIAN), 6.60-6.67 (m, 6H, C−H_{Ar} of Ph), 6.76-6.84 (m, 6H, C−H_{Ar} of Ph), 6.88-7.03 (m, 18H, C−H_{Ar} of Ph), 7.06-7.12 (m, 2H, C−H_{Ar} of Ph), 7.20-7.21 (m, 2H, C^{11}−*H*), 7.36 (s, 2H, −C^{15}*H*(Ph)$_2$), 7.40 (d, $^{3}J_{HH}$ = 8.2 Hz, C^{5}−*H* of BIAN), 7.47-7.49 (m, 2H, C^{13}−*H*), 7.69-7.71 (m, 4H, C−H_{Ar} of Ph), 7.78-7.80 (m, 4H, C−H_{Ar} of Ph).

^{13}C{^{1}H} NMR (100.61 MHz, 300 K, C_6D_6): δ/ppm = 24.5 (s, −CH(*C*H$_3$)$_2$ of *i*Pr), 24.6 (s, −*C*H(CH$_3$)$_2$ of *i*Pr), 25.7 (s, *C*H$_2$ of Cy), 26.3 (s, *C*H$_2$ of Cy), 28.5 (d, $^{3}J_{CP}$ = 5.1 Hz, *C*H$_2$ of Cy), 34.5 (s, −*C*H(CH$_3$)$_2$ of *i*Pr), 51.4 (s, −*C*^{9}H(Ph)$_2$), 52.6 (s, −*C*^{15}H(Ph)$_2$), 57.4 (d, $^{2}J_{CP}$ = 16.7 Hz, *C*−H of Cy), 122.3 (s, *C*^{3}−H of BIAN), 125.2 (s, *C*^{5}−H of BIAN), 126.7 (s, *C*$_{Ar}$−H of Ph), 126.7 (s, *C*$_{Ar}$−H of Ph), 127.0 (s, *C*$_{Ar}$−H of Ph), 127.3 (s, *C*$_{Ar}$−H of Ph), 128.0 (s, *C*^{13}−H), 128.5 (s, *C*$_{Ar}$−H of Ph overlapping with C_6D_6 solvent signal), 128.5 (s, *C*^{11}−H overlapping with C_6D_6 solvent signal), 128.9 (s, *C*$_{Ar}$−H of Ph overlapping with C_6D_6 solvent signal), 129.0 (s, *C*$_{Ar}$−H of Ph overlapping with C_6D_6 solvent signal), 129.2 (s, *C*$_{Ar}$−H of Ph), 129.4 (s, *C*^{4}−H of BIAN), 130.1 (s, *C*$_{Ar}$−H of Ph), 130.6 (s, *C*$_{Ar}$−H of Ph), 130.9 (s, *C*$_{Ar}$−H of Ph), 131.5 (s, *C*$_{Ar}$−H of Ph), 132.4 (s, *C*^{6} of BIAN), 134.5 (s, *C*^{10}), 135.0 (s, *C*^{2} of BIAN), 136.3 (s, *C*^{7} of BIAN), 137.3 (s, *C*^{14}), 143.9 (s, *C*$_{Ar}$ of Ph), 144.9 (s, *C*$_{Ar}$ of Ph), 145.4 (s, *C*$_{Ar}$ of Ph), 146.6 (s, *C*^{12}), 147.6 (s, *C*$_{Ar}$ of Ph), 151.8 (s, *C*^{8}–N), 166.7 (s, *C*^{1}=N of BIAN), 254.1 (d low intens., $^{1}J_{CP}$ = 86.2 Hz, *C*^{16}=O).

^{31}P{^{1}H} NMR (162.04 MHz, 300 K, C_6D_6): (AM_2X) spin system δ/ppm = 54.2 (t, 1P, P_X), 114.2 (dd, 2P, P_M), 307.9 (t, 1P, P_A), for parameters obtained by simulation, see Figure S16 and Table S2.

UV/Vis (toluene, λ_{max} / nm, ε_{max} / L·mol^{-1}·cm^{-1}): 375sh (6500), 530 (7500), 740 (11000).

IR (solid state): v/ cm^{-1}: 3056w (C−H), 3023w (C−H), 2955m (C−H), 2923m (C−H), 2849w (C−H), 1599m, 1526s, 1492vs (C−N), 1418s, 1381m, 1301m, 1261m, 1194m, 1149m, 1114m, 1076m, 1031m, 973m, 896w, 842w, 818w, 766s, 736vs, 695vs, 635m, 606s, 578m, 542s, 513m, 465s, 408m.

Elemental analysis calcd. for $(C_{89}H_{79}CoN_2OP_4)\cdot(Et_2O)_{0.9}$ (Mw = 1376.46 g·mol^{-1}): C 77.12, H 6.15, N 1.94; found C 77.39, H 6.22, N 1.88.

[(Ar*BIAN)Co(η³:η¹-P₄C(O)Ad)] (4c):

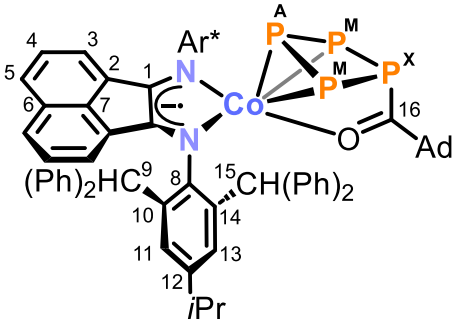

Neat 1-adamantanecarboxylic acid chloride (31.7 mg, 0.159 mmol, 1.0 equiv.) was added to a deep purple solution of [K(18c-6)]**3** (250 mg, 0.159 mmol, 1.0 equiv.) in toluene (6 mL). The reaction mixture was stirred overnight, and a magenta suspension was formed. The solid was removed by filtration over a pad of silica (2 x 2 cm). After washing the silica with toluene (3 x 4 mL) the solvent of the combined filtrates was removed. Subsequently the residue was extracted into toluene (10 mL). The magenta extract was filtered and layered with *n*-hexane (40 mL). After two days dark shimmering magenta crystals suitable for XRD formed, which were isolated by filtration of the mother liquor, washed with *n*-hexane (2 × 4 mL), and dried *in vacuo*. The crystalline solid contains 0.3 molecules of toluene and 0.5 molecules of *n*-hexane per molecule of compound after drying as indicated by the $^{1}H/^{13}C\{^{1}H\}$ NMR spectra and elemental analysis.

Yield: 150 mg (66%).

^{1}H NMR (400.13 MHz, 300 K, C_6D_6): δ/ppm = 0.83 (br s, 6H, $C_{sek}H_2$ of Ad), 0.94-0.97 (m, 3H, $C_{sek}H_2$ of Ad), 1.04−1.07 (m, 12H, −CH(CH_3)$_2$ of *i*Pr), 1.12−1.18 (m, 3H, $C_{sek}H_2$ of Ad), 1.32 (br s, 3H, $C_{tert}H$ of Ad), 2.60 (sept, $^{3}J_{HH}$ = 6.8 Hz, 2H, −C*H*(CH_3)$_2$ of *i*Pr), 4.84 (s, 2H, −$C^{9}H$(Ph)$_2$), 6.03 (d, $^{3}J_{HH}$ = 7.1 Hz, 2H, C^{3}−*H* of BIAN), 6.20-6.24 (m, 2H, C^{4}−*H* of BIAN), 6.63-6.64 (m, 6H, C−H_{Ar} of Ph), 6.73-6.81 (m, 6H, C−H_{Ar} of Ph), 6.90-7.12 (m, 20H, C−H_{Ar} of Ph), 7.14-7.15 (m, 2H, C^{11}−*H* overlapping with C_6D_6 solvent signal), 7.38-7.41 (m, 4H, −$C^{15}H$(Ph)$_2$ overlapping with C^{5}−*H* of BIAN), 7.47-7.48 (m, 2H, C^{13}−*H*), 7.61-7.82 (br m, 4H, C−H_{Ar} of Ph), 7.82-8.10 (br m, 4H, C−H_{Ar} of Ph).

^{13}C{^{1}H} NMR (100.61 MHz, 300 K, C_6D_6): δ /ppm = 24.4 (s, −CH(CH_3)$_2$ of *i*Pr), 24.6 (s, −CH(CH_3)$_2$ of *i*Pr), 28.1 (s, C_{tert}−H of Ad), 34.4 (s, −CH(CH_3)$_2$ of *i*Pr), 36.2 (s, $C_{sek}H_2$

of Ad), 37.3 (s, $C_{sek}H_2$ of Ad), 51.2 (s, $-C^9H(Ph)_2$), 52.5 (s, $-C^{15}H(Ph)_2$), 53.8 (s, d, $^2J_{CP}$ = 13.6 Hz, C_{quart} of Ad), 122.0 (s, C^3–H of BIAN), 125.1 (s, C^5–H of BIAN), 126.6 (s, C_{Ar}–H of Ph), 126.7 (s, C_{Ar}–H of Ph), 127.0 (s, C_{Ar}–H of Ph), 127.2 (s, C_{Ar}–H of Ph), 128.2 (s, C^{13}–H overlapping with C_6D_6 solvent signal), 128.4 (s, C_{Ar}–H of Ph overlapping with C_6D_6 solvent signal), 128.9 (s, C^{11}–H overlapping with C_6D_6 solvent signal), 128.9 (s, C_{Ar}–H of Ph overlapping with C_6D_6 solvent signal), 129.0 (s, C_{Ar}–H of Ph overlapping with C_6D_6 solvent signal), 129.1 (s, C_{Ar}–H of Ph), 129.4 (s, C^4–H of BIAN), 130.1 (s, C_{Ar}–H of Ph), 130.9 (s, C_{Ar}–H of Ph), 131.0 (br s, C_{Ar}–H of Ph), 131.4 (br s, C_{Ar}–H of Ph), 132.5 (s, C^6 of BIAN), 134.8 (s, C^{10}), 135.2 (s, C^2 of BIAN), 135.9 (s, C^7 of BIAN), 137.6 (s, C^{14}), 143.9 (s, C_{Ar} of Ph), 144.8 (s, C_{Ar} of Ph), 145.5 (s, C_{Ar} of Ph), 146.4 (s, C^{12}), 147.8 (s, C_{Ar} of Ph), 151.7 (s, C^8–N), 166.8 (s, C^1=N of BIAN), 255.8 (d, $^1J_{CP}$ = 88.0 Hz, C^{16}=O, very low intensity).

^{1}P{^{1}H} NMR (162.04 MHz, 300 K, C_6D_6): (AM_2X) spin system δ/ppm = 57.4 (t, 1P, P_X), 111.2 (dd, 2P, P_M), 322.6 (t, 1P, P_A), for parameters obtained by simulation, see Figure S20 and Table S3.

UV/Vis (toluene, λ_{max} / nm, ε_{max} / L·mol^{-1}·cm^{-1}): 520 (7000), 750 (10000).

IR (solid state): ν/ cm^{-1} = 3055w (C–H), 3023w (C–H), 2954m (C–H), 2905m (C–H), 2852m (C–H), 1599m, 1523s, 1492vs (C–N), 1451s, 1419s, 1382w, 1342w, 1301m, 1256w, 1194s, 1149m, 1070w, 1031m, 990m, 949w, 919s, 818s, 761s, 737vs, 695vs, 633m, 605s, 577m, 541s, 497m, 465s, 408w.

Elemental analysis calcd. for $(C_{93}H_{83}CoN_2OP_4)\cdot(toluene)_{0.3}\cdot(n\text{-hexane})_{0.5}$ (Mw = 1427.53 g·mol^{-1}): C 78.64, H 6.22, N 1.87; found C 78.82, H 6.16, N 1.78.

[(Ar*BIAN)Co(η^3:η^1-P$_4$C(O)Ph)] (4d):

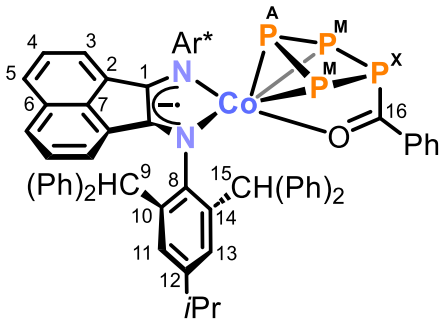

Neat benzoyl chloride (22.4 mg, 18.5 µL, 0.159 mmol, 1.0 equiv.) was added to a deep purple solution of [K(18c-6)]**3** (250 mg, 0.159 mmol, 1.0 equiv.) in toluene (5 mL). The reaction mixture was stirred overnight. A magenta suspension was formed. The solid was removed by filtration over a pad of silica (1.5 × 2 cm) and the residue was washed with toluene (3 × 5 mL). The combined filtrates were concentrated to approximately 10 mL and layered with *n*-hexane (35 mL). Storage for one day at room temperature and another two days at −19 °C gave shimmering deep magenta crystals, which were isolated by filtration, washed with cold

n-hexane (1 × 3 mL) and dried *in vacuo*. The crystalline solid contains 0.3 molecules of toluene and 0.1 molecules of *n*-hexane per molecule of compound after drying as indicated by the $^{1}H/^{13}C\{^{1}H\}$ NMR spectra and elemental analysis.

Yield: 145 mg (67%).

^{1}H NMR (400.13 MHz, 300 K, C_6D_6): δ/ppm = 1.04-1.06 (m, 12H, −CH(CH_3)$_2$ of *i*Pr), 2.62 (sept, $^{3}J_{HH}$ = 6.9 Hz, 2H, −C*H*(CH$_3$)$_2$ of *i*Pr), 5.16 (s, 2H, −C^{9}*H*(Ph)$_2$), 6.20 (d, $^{3}J_{HH}$ = 6.8 Hz, 2H, C^{3}–*H* of BIAN), 6.23-6.27 (m, 4H, C^{4}–*H* of BIAN overlapping with C−H_{ortho} of −C(O)Ph), 6.42-6.45 (m, 2H, C−H_{Ar} of Ph), 6.57-6.70 (m, 11H, C−H_{Ar} of Ph overlapping with C−H_{meta} of −C(O)Ph), 6.79-6.83 (m, 2H, C−H_{Ar} of Ph), 6.86-6.88 (m, 4H, C−H_{Ar} of Ph), 6.94-7.13 (m, 16H, C−H_{Ar} of Ph overlapping with C−H$_{*para*}$ of −C(O)Ph and C_6D_6 solvent signal), 7.27 (m, 2H, C^{11}–*H*), 7.44 (d, $^{3}J_{HH}$ = 8.0 Hz, 2H, C^{5}–*H* of BIAN), 7.47-7.49 (m, 6H, C^{13}–*H* overlapping with C−H_{Ar} of Ph), 7.54 (s, 2H, −C^{15}*H*(Ph)$_2$), 7.72-7.74 (m, 4H, C−H_{Ar} of Ph).

^{13}C{^{1}H} NMR (100.66 MHz, 300 K, C_6D_6): δ/ppm = 24.4 (s, −CH(*C*H$_3$)$_2$ of *i*Pr), 24.6 (s, −CH(*C*H$_3$)$_2$ of *i*Pr), 34.5 (s, −*C*H(CH$_3$)$_2$ of *i*Pr), 51.6 (s, −*C*^{9}H(Ph)$_2$), 52.6 (s, −*C*^{15}H(Ph)$_2$), 122.7 (s, *C*^{3}–H of BIAN), 125.4 (s, *C*^{5}–H of BIAN), 126.3 (s, C_{Ar}–H of Ph), 126.7 (s, C_{Ar}–H of Ph), 127.0 (s, C_{Ar}–H of Ph), 127.3 (s, s, C$_{*ortho*}$–H of −C(O)Ph), 128.0 (s, *C*^{13}–H), 128.2 (s, C_{Ar}–H of Ph overlapping with C_6D_6 solvent signal), 128.3 (s, *C*^{13}–H overlapping with C_6D_6 solvent signal), 128.5 (s, C_{Ar}–H of Ph overlapping with C_6D_6 solvent signal), 128.5 (C$_{*para*}$–H of −C(O)Ph overlapping with C_6D_6 solvent signal), 128.9 (s, C_{Ar}–H of Ph overlapping with C_6D_6 solvent signal), 129.0 (s, C_{Ar}–H of Ph overlapping with C_6D_6 solvent signal), 129.2 (s, C_{Ar}–H of Ph), 129.4 (s, *C*^{4}–H of BIAN), 130.1 (s, C_{Ar}–H of Ph), 130.3 (s, C_{Ar}–H of Ph), 130.9 (s, C_{Ar}–H of Ph), 131.5 (s, C_{Ar}–H of Ph), 132.3 (s, *C*^{6} of BIAN), 133.3 (s, C_{meta}–H of −C(O)Ph), 134.5 (s, *C*^{10}), 134.7 (s, *C*^{2} of BIAN), 136.6 (s, *C*^{7} of BIAN), 137.1 (s, *C*^{14}), 140.4 (d, $^{2}J_{CP}$ = 19.5 Hz, C_{Ar} of −C(O)Ph), 144.7 (s, C_{Ar} of Ph), 144.9 (s, C_{Ar} of Ph), 145.4 (s, C_{Ar} of Ph), 146.2 (s, C_{Ar} of Ph), 146.7 (s, *C*^{12}), 151.5 (s, *C*^{8}–N), 166.1 (s, *C*^{1}=N of BIAN), 233.4 (d, *C*^{16}=O, detected *via* $^{1}H/^{13}C$ HMBC NMR spectroscopy).

^{31}P{^{1}H} NMR (162.04 MHz, 300 K, C_6D_6): (AM_2X) spin system δ/ppm = 50.1 (t, 1P, P_X), 119.4 (dd, 2P, P_M), 295.0 (t, 1P, P_A), for parameters obtained by simulation, see Figure S25 and Table S4.

UV/Vis (toluene, λ_{max} / nm, ε_{max} / L·mol^{-1}·cm^{-1}): 310sh (30000), 410sh (7000), 530 (12000), 740 (14000).

IR (solid state): ν/ cm^{-1} = 3057w (C−H), 3023w (C−H), 2956w (C−H), 1599m, 1530m, 1492s (C−N), 1445m, 1417m, 1362w, 1300m, 1216m, 1194m, 1172m, 1076w, 1031m, 1000w, 966w, 910s, 820m, 762s, 737s, 696vs, 627m, 605s, 578m, 542m, 512m, 466m. **Elemental analysis** calcd. for $(C_{89}H_{73}CoN_2OP_4)\cdot(\text{toluene})_{0.3}\cdot(n\text{-hexane})_{0.1}$ (Mw = 1369.40 g·mol^{-1}): C 78.32, H 5.44, N 2.01; found C 78.22, H 5.50, N 1.92.

[(Ar*BIAN)Co((CH₃)₃SiNC)(η²:η¹-P₄CO*t*Bu)] (5a):

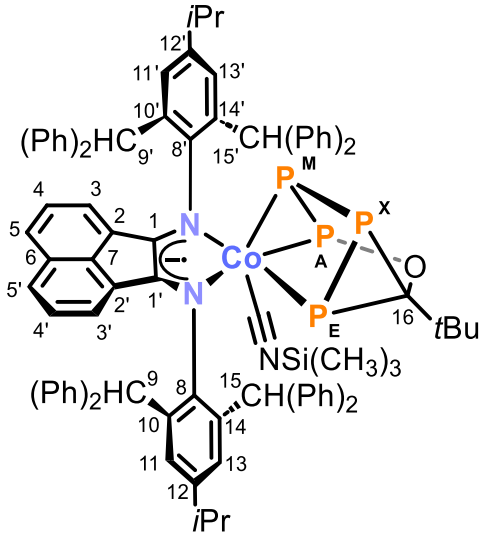

Neat trimethylsilyl cyanide (7.1 mg, 8.9 µL, 0.071 mmol, 1.3 equiv.) was added to a magenta solution of **4a** (74 mg, 0.055 mmol, 1.0 equiv.) in toluene (3 mL). The reaction mixture was stirred for 14 hours. The dark green reaction mixture was filtered and layered with *n*-hexane (20 mL). Shimmering dark green crystals suitable for single-crystal X-ray diffraction were formed after five days at −35 °C. The crystalline solid was isolated by decantation of the mother liquor, washed with *n*-hexane (2 × 2 mL) and dried *in vacuo*. The crystalline solid contains 0.2 molecules of toluene and 0.7 molecules of *n*-hexane per molecule of compound after drying as indicated by the $^{1}H/^{13}C\{^{1}H\}$ NMR spectra and elemental analysis. Compound **5a** decomposes in solution at ambient temperature over several days. The ^{1}H NMR spectrum of the decomposition solution after three weeks shows predominantly uncoordinated Ar*BIAN (**1**) ligand. The compound can be stored as a solid at ambient temperature without any decomposition observable by spectroscopy.

Yield: 59 mg (77%)

^{1}H NMR (400.13 MHz, 288 K, C_6D_6): δ/ppm = −0.39 (s, 9H, −Si(C*H*₃)₃), 1.00-1.03 (m, 12H, −CH(C*H*₃)₂ of *i*Pr), 1.26 (s, 9H, −C(C*H*₃)₃ of *t*Bu overlapping with *n*-hexane solvent signal), 2.52 (sept, $^{3}J_{HH}$ = 6.9 Hz, 1H, −CH(C*H*₃)₂ of *i*Pr), 2.61 (sept, $^{3}J_{HH}$ = 6.9 Hz, 1H, −CH(C*H*₃)₂ of *i*Pr), 4.99 (d, $^{3}J_{HH}$ = 7.1 Hz, 1H, $C^{3/3'}$−*H* of BIAN), 5.59-5.60 (d, J_{PH} = 4.1 Hz through space, 1H, −C^{9}*H*(Ph)₂), 5.94-5.98 (m, 1H, $C^{4/4'}$−*H* of BIAN), 6.19 (d, $^{3}J_{HH}$ = 7.1 Hz, $C^{3/3'}$−*H* of BIAN), 6.41-6.59 (m, 8H, $C^{4/4'}$−H of BIAN overlapping with −$C^{9'}$*H*(Ph)₂ overlapping with C−H_{Ar} of Ph), 6.71-6.84 (m, 6H, C−H_{Ar} of Ph), 6.90-7.13 (m, 13H, $C^{5/5'}$−*H* of BIAN overlapping with C−H_{Ar} of Ph overlapping with C_6D_6 solvent signal), 7.17-7.24 (m, 8H, −$C^{15/15'}$*H*(Ph)₂ overlapping with $C^{5/5'}$−*H* of BIAN overlapping

with C−H_{Ar} of Ph), 7.27-7.28 (m, 2H, C−H_{Ar} of Ph), 7.31-7.32 (m, 1H, $C^{11/11'}$–*H*), 7.39-7.40 (m, 1H, $C^{11/11'}$–*H*), 7.47-7.48 (m, 1H, $C^{13/13'}$–*H*), 7.55-7.56 (m, 1H, $C^{13/13'}$–*H*), 7.57-7.61 (m, 3H, −$C^{15/15'}$*H*$(Ph)_2$ overlapping with C−H_{Ar} of Ph), 7.64-7.66 (m, 2H, C−H_{Ar} of Ph), 7.83-7.85 (m, 2H, C−H_{Ar} of Ph), 8.03 (s br, 2H, C−H_{Ar} of Ph).

^{13}C{^{1}H} NMR (100.61 MHz, 288 K, C_6D_6): δ/ppm = −0.1 (s, −Si(*C*$H_3)_3$), 23.9 (s, −CH(*C*$H_3)_2$ of *i*Pr), 24.4 (s, −CH(*C*$H_3)_2$ of *i*Pr), 24.5 (s, −CH(*C*$H_3)_2$ of *i*Pr), 24.8 (s, −CH(*C*$H_3)_2$ of *i*Pr), 31.6 (s, −C(*C*$H_3)_3$ of *t*Bu), 34.1 (s, −*C*H$(CH_3)_2$ of *i*Pr), 34.3 (s, −*C*H$(CH_3)_2$ of *i*Pr), 37.7 (m, −*C*$(CH_3)_3$ of *t*Bu), 52.1 (s, −$C^{9'}$H$(Ph)_2$), 52.2 (s, −$C^{15/15'}$H$(Ph)_2$), 52.3 (s, −$C^{15/15'}$H$(Ph)_2$), 53.3 (d, J_{PC} = 15.0 Hz through space, −C^9H$(Ph)_2$), 119.5-119.7 (m, C^{16}), 123.0 (s, $C^{3/3'}$–*H* of BIAN), 123.9 (s, $C^{3/3'}$–H of BIAN), 125.6 (s, $C^{5/5'}$–*H* of BIAN), 126.2 (s, $C^{5/5'}$–H of BIAN), 126.5 (s, C_{Ar}–H of Ph), 126.7 (s, C_{Ar}–H of Ph), 126.9 (s, C_{Ar}–H of Ph), 127.0 (s, C_{Ar}–H of Ph), 127.0 (s, C_{Ar}–H of Ph), 127.1 (s, C_{Ar}–H of Ph), 127.4 (s, C_{Ar}–H of Ph), 127.9 (s, C_{Ar}–H of Ph), 128.0 (s, $C^{4/4'}$–H of BIAN), 128.3 (s, $C^{11/11'}$–H overlapping with C_6D_6 solvent signal), 128.3 (s, C_{Ar}–H of Ph overlapping with C_6D_6 solvent signal), 128.5 (s, $C^{4/4'}$–H of BIAN overlapping with C_6D_6 solvent signal), 128.6 (s, C_{Ar}–H of Ph overlapping with C_6D_6 solvent signal), 128.7 (s, C_{Ar}–H of Ph overlapping with C_6D_6 solvent signal), 128.8 (s, C_{Ar}–H of Ph overlapping with C_6D_6 solvent signal), 128.9 (s, C_{Ar}–H of Ph overlapping with C_6D_6 solvent signal), 129.0 *(s,* $C^{11/11'}$–H overlapping with C_6D_6 solvent signal), 129.1 (s, C_{Ar}–H of Ph), 129.1 (s, C_{Ar}–H of Ph), 129.2 (s, $C^{13/13'}$–H), 130.1 (s, C_{Ar}–H of Ph), 130.3 (s, C^6 of BIAN), 130.8 (s, C_{Ar}–H of Ph), 131.0 (s, $C^{13/13'}$–H), 131.1 (s, $C^{2/2'}$ of BIAN), 131.2 (s, C_{Ar}–H of Ph), 131.2 (s, C_{Ar}–H of Ph), 131.4 (s, $C^{2/2'}$ of BIAN), 131.6 (s, C_{Ar}–H of Ph), 131.7 (s, C_{Ar}–H of Ph), 131.7 (s, C_{Ar}–H of Ph), 131.9 (s, C_{Ar}–H of Ph), 131.9 (s, C_{Ar}–H of Ph), 135.5 (s, $C^{10/10'}$), 135.9 (s, $C^{10/10'}$), 138.1 (s, C^7 of BIAN), 138.7 (s, $C^{14/14'}$), 139.2 (s, $C^{14/14'}$), 142.8 (s, C_{Ar} of Ph), 143.1 (s, C_{Ar} of Ph), 143.7 (s, C_{Ar} of Ph), 144.0 (s, C_{Ar} of Ph), 146.3 (s, $C^{12/12'}$), 146.4 (s, $C^{12/12'}$), 146.6 (s, C_{Ar} of Ph), 147.0 (s, C_{Ar} of Ph), 147.4 (s, $C^{8/8'}$–N), 147.5 (s, C_{Ar} of Ph), 147.6 (s, C_{Ar} of Ph), 152.5 (s, $C^{8/8'}$–N), 162.2 (s, $C^{1/1'}$=N of BIAN), 163.6 (s, $C^{1/1'}$=N of BIAN), 190.5 (s, *C*≡NSi$(CH_3)_3$).

^{31}P{^{1}H} NMR (161.98 MHz, 288 K, C_6D_6): (AEMX) spin system δ/ppm = −245.2 (dd, 1P, P_X), −102.5 (dd, 1P, P_M), −10.7 (br d, 1P, Δν½ = 99 Hz, P_E), 228.2 (d, 1P, P_A), for parameters obtained by simulation, see Figure S29 and Table S5. Spin system was assigned based on the coupling constants and shift in the $P_{E/X}C$ three-ring as reported for similar P_3 motifs.[24]

^{29}Si {^{1}H} NMR (79.49 MHz, 288 K, C_6D_6): δ/ppm = 4.5 (s, −*Si*$(CH_3)_3$).

UV/Vis (toluene, λ_{max} / nm, ε_{max} / $L \cdot mol^{-1} \cdot cm^{-1}$): 310sh (26000), 440 (9000), 600 (10000), 830 (10500).

IR (solid state): v/ cm^{-1} = 3055w (C−H), 3026w (C−H), 2955w (C−H), 2859w (C−H), 2012vs (C≡N), 1600w, 1541w, 1493m (C−N), 1451m, 1417m, 1384w, 1359w, 1296m, 1255m, 1194w, 1152w, 1077w, 1032w, 1044w, 949w, 846s, 760s, 737m, 696vs, 656m, 605m.

Elemental analysis calcd. for $(C_{91}H_{86}CoN_3OP_4Si)\cdot(toluene)_{0.2}\cdot(n\text{-hexane})_{0.7}$ (Mw = 1448.62 $g \cdot mol^{-1}$): C 75.96, H 6.43, N 2.75; found C 75.65, H 6.42, N 2.71.

***endo*- and *exo*-[(Ar*BIAN)Co(CyNC)(η^3-P_4C(O)*t*Bu)] (*endo*-/*exo*-6a):**

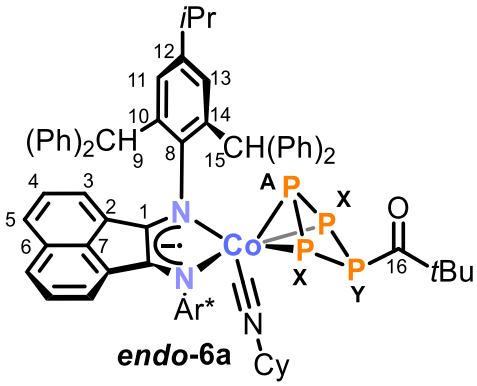

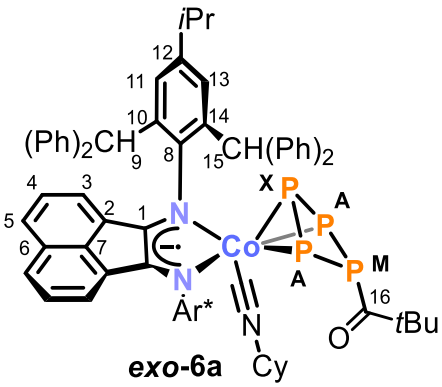

Neat cyclohexyl isocyanide (48.6 mg, 55.3 µL, 0.44 mmol, 10.0 equiv.) was added to a magenta solution of **4a** (60 mg, 0.044 mmol, 1.0 equiv.) in toluene (2.0 mL). The reaction mixture changed to a dark green while stirring for two hours. After removing the solvent, the resulting dark residue was taken up in *n*-hexane (3 × 3 mL) and the resulting extracts were filtered. After storage for one day at room temperature, shimmering green crystals suitable for single-crystal X-ray diffraction had formed. The crystals were isolated by decantation of the supernatant, washed with *n*-hexane (3 × 0.5 mL), and dried *in vacuo*. The crystalline solid contains 0.5 molecules of *n*-hexane per molecule of **6a** after drying as indicated by the $^1H/^{13}C\{^1H\}$ NMR spectra and elemental analysis.

Yield: 38 mg (57%).

^{1}H NMR (400.13 MHz, 300 K, C_6D_6): δ/ppm = 0.46-0.74 (m, 10H, C*H*$_2$ of Cy overlapping from *endo*-**6a** and *exo*-**6a**), 0.95-1.16 (m, 39H, −CH(C*H*$_3$)$_2$ of *i*Pr from *endo*-**6a** and *exo*-**6a** overlapping with −C(C*H*$_3$)$_3$ of *t*Bu from *exo*-**6a** overlapping with C*H*$_2$ of Cy from *endo*-**6a** and *exo*-**6a**), 1.43 (s, 9H, −C(C*H*$_3$)$_3$ of *t*Bu from *endo*-**6a**), 1.64-1.70 (m, 4H, C*H*$_2$ of Cy overlapping from *endo*-**6a** and *exo*-**6a**), 2.09-2.14 (m, 1H, C−*H* of Cy from *endo*-**6a**), 2.48-2.58 (m, 4H, −C*H*(CH$_3$)$_2$ of *i*Pr overlapping from *endo*-**6a** and *exo*-**6a**), 2.79-2.85 (m, 1H, C−*H* of Cy from *exo*-**6a**), 5.63 (d, $^3J_{HH}$ = 7.1 Hz,

2H, C^3–*H* of BIAN from *exo*-**6a**), 5.75-5.76 (m, 4H, C^3–*H* of BIAN from *endo*-**6a** overlapping with –C^9*H*$(Ph)_2$ from *endo*-**6a**), 5.85 (s, 2H, –C^9*H*$(Ph)_2$ from *exo*-**6a**), 6.14-6.17 (m, 2H, C^4–*H* of BIAN from *exo*-**6a**), 6.19-6.23 (m, 2H, C^4–*H* of BIAN from *endo*-**6a**), 6.57-6.75 (m, 16H, C–H_{Ar} of Ph overlapping from *endo*-**6a** and *exo*-**6a**), 6.82-6.88 (m, 17H, C–H_{Ar} of Ph overlapping from *endo*-**6a** and *exo*-**6a**), 6.96-6.99 (m, 3H, C–H_{Ar} of Ph from *endo*-**6a** or *exo*-**6a**), 7.05-7.14 (m, 24H, C–H_{Ar} of Ph overlapping from *endo*-**6a** and *exo*-**6a** overlapping with C^5–*H* of BIAN from *endo*-**6a** and *exo*-**6a** overlapping with C_6D_6 solvent signal), 7.27-7.30 (m, 6H, C^{11}–*H* from *endo*-**6a** overlapping with C–H_{Ar} of Ph from *endo*-**6a**), 7.36-7.41 (m, 10H, C^{13}–*H* of *endo*-**6a** overlapping with C^{11}–*H* of *exo*-**6a** overlapping with C^{13}–*H* of *exo*-**6a** overlapping with C–H_{Ar} of Ph from *endo*-**6a** or *exo*-**6a**), 7.59-7.62 (m, 8H, C–H_{Ar} of Ph overlapping from *endo*-**6a** and *exo*-**6a**), 7.67 (s, 2H, –C^{15}*H*$(Ph)_2$ from *exo*-**6a**), 7.74-7.76 (m, 4H, C–H_{Ar} of Ph from *endo*-**6a**), 7.91-7.94 (m, 6H, –C^{15}*H*$(Ph)_2$ of *endo*-**6a** overlapping with C–H_{Ar} of Ph from *exo*-**6a**).

$^{13}C\{^1H\}$ NMR (100.61 MHz, C_6D_6, 300 K): δ/ppm = 24.1 (s, –CH(*C*$H_3)_2$ of *i*Pr from *endo*-**6a**), 24.2 (s, –CH(*C*$H_3)_2$ of *i*Pr from *exo*-**6a**), 24.5 (s, –CH(*C*$H_3)_2$ of *i*Pr from *exo*-**6a**), 24.5 (s, –CH(*C*$H_3)_2$ of *i*Pr from *endo*-**6a**), 25.0 (s, *C*H_2 of Cy from *endo*-**6a**), 25.1 (s, *C*H_2 of Cy from *exo*-**6a**), 25.3 (s, *C*H_2 of Cy from *exo*-**6a**), 25.3 (s, *C*H_2 of Cy from *endo*-**6a**), 28.0 (d, $^3J_{CP}$ = 3.6 Hz, –C(*C*$H_3)_3$ of *t*Bu from *exo*-**6a**), 28.5 (s, –C(*C*$H_3)_3$ of *t*Bu from *endo*-**6a**), 32.3 (s, *C*H_2 of Cy from *endo*-**6a** or *exo*-**6a**), 32.3 (s, *C*H_2 of Cy from *endo*-**6a** or *exo*-**6a**), 34.2 (s, –*C*H$(CH_3)_2$ of *i*Pr from *endo*-**6a**), 34.3 (s, –*C*H$(CH_3)_2$ of *i*Pr from *exo*-**6a**), 49.0 (d, $^2J_{CP}$ = 18.5 Hz, –*C*$(CH_3)_3$ of *t*Bu from *exo*-**6a**), 49.8 (d, $^2J_{CP}$ = 20.4 Hz, –*C*$(CH_3)_3$ of *t*Bu from *endo*-**6a**), 51.8 (d, J_{PC} = 5.3 Hz (through space), –*C*^{9}H$(Ph)_2$ from *endo*-**6a**), 52.1 (s, d, J_{PC} = 57.1 Hz (through space), –*C*^{9}H$(Ph)_2$ from *exo*-**6a**), 52.6 (s, –*C*^{15}H$(Ph)_2$ from *endo*-**6a**), 52.7 (s, –*C*^{15}H$(Ph)_2$ from *exo*-**6a**), 56.6 (s, *C*–H of Cy from *endo*-**6a**), 57.4 (*C*–H of Cy from *exo*-**6a**), 123.1 (s, *C*^{3}–H of BIAN from *exo*-**6a**), 123.4 (s, *C*^{3}–H of BIAN from *endo*-**6a**), 126.2 (s, *C*^{5}–H of BIAN from *exo*-**6a**), 126.5 (s, *C*^{5}–H of BIAN from *endo*-**6a**), 126.6 (s, C_{Ar}–H of Ph from *endo*-**6a** or *exo*-**6a**), 126.6 (s, C_{Ar}–H of Ph from *endo*-**6a** or *exo*-**6a**), 126.8 (s, C_{Ar}–H of Ph from *endo*-**6a** or *exo*-**6a**), 127.0 (s, C_{Ar}–H of Ph from *endo*-**6a** or *exo*-**6a**), 127.1 (s, C_{Ar}–H of Ph from *endo*-**6a** or *exo*-**6a**), 127.2 (s, C_{Ar}–H of Ph from *endo*-**6a** or *exo*-**6a**), 127.4 (s, C_{Ar}–H of Ph from *endo*-**6a** or *exo*-**6a**), 127.4 (s, C_{Ar}–H of Ph from *endo*-**6a** or *exo*-**6a**), 128.1 (s, *C*^{4}–H of BIAN from *endo*-**6a**), 128.3 (s, C^4–*H* of BIAN from *exo*-**6a**), 128.4 (s, C_{Ar}–H of Ph from *endo*-**6a** or *exo*-**6a** overlapping with C_6D_6 solvent signal), 128.6 (s, C_{Ar}–H of

Ph from *endo*-**6a** or *exo*-**6a** overlapping with C_6D_6 solvent signal), 128.8 (s, C_{Ar}–H of Ph from *endo*-**6a** or *exo*-**6a** overlapping with C_6D_6 solvent signal), 128.9 (s, C_{Ar}–H of Ph from *endo*-**6a** or *exo*-**6a** overlapping with C_6D_6 solvent signal), 128.9 (s, C_{Ar}–H of Ph from *endo*-**6a** or *exo*-**6a** overlapping with C_6D_6 solvent signal), 129.0 (s, C^{11}–H from *endo*-**6a**), 129.1 (s, C^{11}–H from *exo*-**6a**), 129.2 (s, C^{13}–H from *exo*-**6a**), 129.3 (s, C^{13}–H from *endo*-**6a**), 130.6 (s, C^2 of BIAN from *exo*-**6a**), 130.6 (s, C^6 of BIAN from *endo*-**6a**), 130.7 (s, C^2 of BIAN from *exo*-**6a**), 130.8 (s, C^2 of BIAN from *endo*-**6a**), 130.8 (s, C_{Ar}–H of Ph from *endo*-**6a** or *exo*-**6a**), 131.2 (s, C_{Ar}–H of Ph from *endo*-**6a** or *exo*-**6a**), 131.2 (s, C_{Ar}–H of Ph from *endo*-**6a** or *exo*-**6a**), 131.3 (s, C_{Ar}–H of Ph from *endo*-**6a** or *exo*-**6a**), 131.4 (s, C_{Ar}–H of Ph from *endo*-**6a** or *exo*-**6a**), 131.5 (s, C_{Ar}–H of Ph from *endo*-**6a** or *exo*-**6a**), 135.4 (s, C^{10} from *exo*-**6a**), 135.5 (s, C^{10} from *endo*-**6a**), 137.4 (s, C^7 of BIAN from *exo*-**6a**), 138.0 (s, C^7 of BIAN from *endo*-**6a**), 138.7 (s, C^{14} from *endo*-**6a**), 139.3 (s, C^{14} from *exo*-**6a**), 143.1 (s, C_{Ar} of Ph from *endo*-**6a** or *exo*-**6a**), 143.2 (s, C_{Ar} of Ph from *endo*-**6a** or *exo*-**6a**), 145.1 (s, C_{Ar} of Ph from *endo*-**6a** or *exo*-**6a**), 145.3 (s, C^8–N from *endo*-**6a**), 145.4 (s, C_{Ar} of Ph from *endo*-**6a** or *exo*-**6a**), 145.5 (s, C^8–N from *exo*-**6a**), 146.3 (s, C_{Ar} of Ph from *endo*-**6a** or *exo*-**6a**), 146.5 (s, C^{12} from *exo*-**6a**), 146.8 (s, C^{12} from *endo*-**6a**), 147.2 (s, C_{Ar} of Ph from *endo*-**6a** or *exo*-**6a**), 147.8 (s, C_{Ar} of Ph from *endo*-**6a** or *exo*-**6a**), 147.9 (s, C_{Ar} of Ph from *endo*-**6a** or *exo*-**6a**), 166.2 (s, C^1=N of BIAN from *exo*-**6a**), 167.6 (s, C^1=N of BIAN from *endo*-**6a**), 235.1 (s, C^{16}=O of *endo*-**6a**, detected by $^1H/^{13}C$ HMBC-spectroscopy), 235.6 (s, C^{16}=O of *exo*-**6a**, detected by $^1H/^{13}C$ HMBC-spectroscopy), the signal for *C*≡N of coordinating isocyanides could not be detected.

$^{31}P\{^1H\}$ NMR (161.98 MHz, 300 K, C_6D_6): (AX_2Y) spin system for *endo*-**6a** and (A_2MX) spin system for *exo*-**6a** δ/ppm = −26.5 (dt, 1P, P_X of *exo*-**6a**), 5.0 (dt, 1P, P_M of *exo*-**6a**), 50.5 (dd, 2P, P_A of *exo*-**6a**), 67.3-73.2 (m, 3P, P_{XY} of *endo*-**6a**), 142.5-146.5 (m, 1P, P_A of *endo*-**6a**), for parameters obtained by simulation, see Figure S35 and Table S6 for *endo*-**6a** and Figure S36 and Table S7 for *exo*-**6a**.

UV/Vis (toluene, λ_{max} / nm, ε_{max} / $L \cdot mol^{-1} \cdot cm^{-1}$): 310sh (12000), 430sh (3500), 500 (5000), 700 (8000).

IR (solid state): ν/ cm^{-1} = 3058w (C−H), 3025w (C−H), 2956w (C−H), 2931w (C−H), 2858w (C−H), 2163w (C≡N), 2115m (C≡N), 1640m (C=O), 1599m (C=O), 1561w, 1493m (C−N), 1446m, 1419w, 1384w, 1362w, 1295m, 1254w, 1191m, 1077w, 1031m, 947w, 915m, 823m, 762m, 738m, 697vs, 655m, 604s.

Elemental analysis calcd. for $(C_{94}H_{88}CoN_3OP_4)\cdot(n\text{-hexane})_{0.4}$ (Mw = 1458.58 g·mol^{-1}): C 77.58, H 6.38, N 2.80; found C 77.62, H 6.15, N 2.87.

[K(18c-6)][(Ar*BIAN)Co(CN)(η^3-P$_3$)] ([K(18c-6)]8) and [K(18c-6)][CyC(O)PCN] ([K(18c-6)]9b):

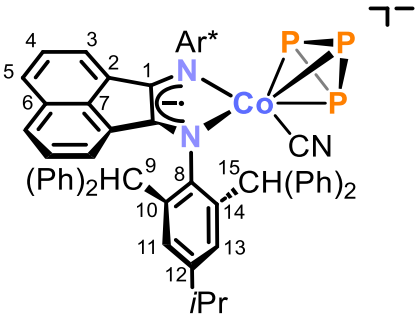

KCN (17.5 mg, 0.268 mmol, 2.2 equiv.), 18c-6 (70.8 mg, 0.268 mmol, 2.2 equiv.) and **4b** (168 mg, 0.122 mmol, 1.0 equiv.) were suspended in THF (7 mL). The magenta mixture was stirred for three days over which time the color changed to a deep purple. The solvent was removed *in vacuo* and the resulting dark solid taken up in toluene (6 mL). The solution was filtered and concentrated to one quarter of the original volume. After one day, shimmering purple crystals of ([K(18c-6)]**8**) suitable for single-crystal X-ray diffraction were formed. The crystals were isolated by decantation of the mother liquor, washed with *n*-hexane (3 × 1 mL) and dried *in vacuo*. The crystalline solid of ([K(18c-6)]**8**) contains 0.8 molecules of toluene and 0.2 molecules of *n*-hexane per molecule of compound after drying as indicated by the ^{1}H/^{13}C{^{1}H} NMR spectra and elemental analysis. The mother liquor was stored at −35 °C. After one day, colorless crystals of ([K(18c-6)]**9b**) suitable for single-crystal X-ray diffraction were formed. The crystals were isolated by decantation of the mother liquor, washed with *n*-hexane (3 × 0.5 mL) and dried *in vacuo*. Further [K(18c-6)]**9b** can be isolated by concentrating the mother liquor and storing it at −35 °C. These fractions contain minor amounts of [K(18c-6)]**8** as impurity.

([K(18c-6)]**8**): **Yield**: 120 mg (60%)

^{1}H NMR (400.13 MHz, 300 K, C_6D_6): δ/ppm = 1.06-1.09 (m, 12H, −CH(C*H*$_3$)$_2$ of *i*Pr), 2.64 (sept, $^3J_{HH}$ = 6.9 Hz, 2H, −C*H*(CH$_3$)$_2$ of *i*Pr), 2.91 (s, 24H, 18c-6), 5.73 (s, 2H, −C^9*H*(Ph)$_2$), 5.93 (d, $^3J_{HH}$ = 7.1 Hz, 2H, C^3−*H* of BIAN), 6.32-6.36 (m, 2H, C^4−*H* of BIAN), 6.68-6.75 (m, 8H, C−*H*$_{Ar}$ of Ph), 6.88-6.92 (m, 4H, C−*H*$_{Ar}$ of Ph), 6.97-7.03 (m, 12H, C−*H*$_{Ar}$ of Ph), 7.15-7.19 (m, 4H, C^5−*H* of BIAN overlapping with C^{11}−*H* and C_6D_6 solvent signal), 7.21-7.25 (m, 6H, C^{13}−*H* overlapping with C−*H*$_{Ar}$ of Ph), 7.39-7.41 (m, 4H, C−*H*$_{Ar}$ of Ph), 7.95-7.97 (m, 4H, C−*H*$_{Ar}$ of Ph), 8.03-8.05 (m, 4H, C−*H*$_{Ar}$ of Ph), 8.83 (s, 2H, −C^{15}*H*(Ph)$_2$).

$^{13}C\{^1H\}$ NMR (100.61 MHz, 300 K, C_6D_6): δ/ppm = 24.5 (s, −CH(CH_3)$_2$ of *i*Pr), 24.7 (s, −CH(CH_3)$_2$ of *i*Pr), 34.2 (s, −CH(CH_3)$_2$ of *i*Pr), 50.9 (s, −C^9H(Ph)$_2$), 51.9 (s, −C^{15}H(Ph)$_2$), 69.9 (s, 18c-6), 120.9 (s, C^3–H of BIAN), 123.9 (s, C^5–H of BIAN), 125.8 (s, C_{Ar}–H of Ph), 126.3 (s, C_{Ar}–H of Ph), 126.3 (s, C_{Ar}–H of Ph), 126.7 (s, C_{Ar}–H of Ph), 128.3 (s, C_{Ar}–H of Ph overlapping with C_6D_6 solvent signal), 128.3 (s, C^4–H of BIAN overlapping with C_6D_6 solvent signal), 128.4 (s, C_{Ar}–H of Ph overlapping with C_6D_6 solvent signal), 128.5 (s, C_{Ar}–H of Ph overlapping with C_6D_6 solvent signal), 128.6 (s, C^{11}–H overlapping with C_6D_6 solvent signal), 128.9 (s, C_{Ar}–H of Ph overlapping with C_6D_6 solvent signal), 129.0 (s, C^{13}–H overlapping with C_6D_6 solvent signal), 131.5 (s, C_{Ar}–H of Ph), 131.5 (s, C^2 of BIAN), 131.9 (s, C_{Ar}–H of Ph), 131.9 (s, C_{Ar}–H of Ph), 132.0 (s, C_{Ar}–H of Ph), 133.7 (s, C^6 of BIAN), 134.5 (s, C^{10}), 134.5 (s, C^7 of BIAN), 138.5 (s, C^{14}), 143.8 (s, C_{Ar} of Ph), 144.8 (s, C^{12}), 145.6 (s, C_{Ar} of Ph), 146.8 (s, C_{Ar} of Ph), 150.2 (s, C_{Ar} of Ph), 153.4 (s, C^8–N), 165.8(s, C^1=N of BIAN); *C*≡N of coordinated cyanide not detected.

$^{31}P\{^1H\}$ NMR (162.04 MHz, 300 K, C_6D_6): δ/ppm = −218.7 (s, *cyclo*-P_3).

UV/Vis (toluene, λ_{max} / nm, ε_{max} / L·mol^{-1}·cm^{-1}): 330sh (16000), 390sh (4000), 550 (16000), 690sh (7500).

IR (solid state): ν/ cm^{-1} = 3056w (C−H), 3024w (C−H), 2954m (C−H), 2885m (C−H), 2069m (C≡N), 1599m, 1493s (C−N), 1449m, 1351m, 1296m, 1249m, 1193w, 1162w, 1105vs, 1031m, 960m, 829w, 763m, 737m, 698vs, 605s.

Elemental analysis calcd. for ($C_{101}H_{92}CoKN_3O_6P_3$)·(toluene)$_{0.8}$·(*n*-hexane)$_{0.2}$ (Mw = 1634.81 g·mol^{-1}): C 75.03, H 5.91, N 2.43; found C 74.74, H 6.25, N 2.29.

([K(18c-6)]**9b**): **Yield**: 18 mg (31%).

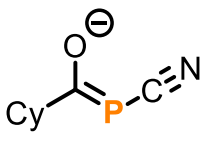

^1H NMR (400.30 MHz, 300 K, C_6D_6): δ/ppm = 1.16-1.37 (m, 3H, CH_2 of Cy), 1.59-1.67 (m, 1H, CH_2 of Cy), 1.68-1.82 (m, 4H, CH_2 of Cy), 2.11-2.21 (m, 2H, CH_2 of Cy), 2.70−2.87 (m, 1H, C−*H* of Cy), 3.24 (s, 24H, 18c-6).

$^{13}C\{^1H\}$ NMR (100.61 MHz, 300 K, C_6D_6): δ/ppm = 27.5 (s, *C*H$_2$ of Cy), 27.6 (s, *C*H$_2$ of Cy), 32.4 (s, *C*H$_2$ of Cy), 32.5 (s, *C*H$_2$ of Cy), 54.8 (d, $^2J_{CP}$ = 66.3 Hz, *C*−H of Cy), 70.7 (s, 18c-6), 136.7 (d, $^1J_{CP}$ = 104.4 Hz, *C*≡N), 238.1 (d, $^1J_{CP}$ = 75.0 Hz, *C*=O).

$^{31}P\{^1H\}$ NMR (162.04 MHz, 300 K, C_6D_6): δ/ppm = −45.2 (s).

IR (solid state): ν/ cm^{-1} = 2885m (C−H), 2852m (C−H), 2101s (C≡N), 1544s (C=O), 1472m, 1450m, 1350s, 1284w, 1249w, 1103vs, 1038w, 961vs, 884w, 838m, 801w, 779w, 621w.

Elemental analysis calcd. for $C_{20}H_{35}KNO_7P$ (Mw = 471.57 g·mol^{-1}):
C 50.94, H 7.48, N 2.97; found C 50.93, H 7.32, N 2.84.

(CyC(O))$_2$PCN (10):

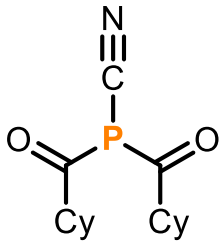

Neat Cyclohexanecarboxylic acid chloride (7.7 mg, 7.2 µL, 0.053 mmol, 1.0 equiv.) was added to a colorless solution of [K(18c-6)]**9-Cy** (25 mg, 0.053 mmol, 1.0 equiv.) in C_6D_6 (1 mL). The solid was removed by filtration over a pad of silica (1.0 × 0.5 cm) and the residue was washed with benzene (3 × 0.5 mL). The solvent was removed from the combined filtrates *in vacuo*, yielding the product as a clear colorless oil.

Yield: 12 mg (81%).

^{1}H NMR (400.30 MHz, 300 K, C_6D_6): δ/ppm = 0.82-1.43 (m, 20H, C*H*$_2$ of Cy), 1.64-1.77 (m, 4H, C*H*$_2$ of Cy), 2.89-2.96 (m, 2H, C−*H* of Cy).

^{13}C{^{1}H} NMR (100.61 MHz, 300 K, C_6D_6): δ/ppm = 25.1 (d, $^3J_{CP}$ = 8.8 Hz *C*H$_2$ of Cy), 25.6 (s, *C*H$_2$ of Cy), 28.2 (s, *C*H$_2$ of Cy), 28.6 (s, *C*H$_2$ of Cy), 54.1 (d, $^2J_{CP}$ = 66.3 Hz, *C*−H of Cy), 116.5 (d, $^1J_{CP}$ = 62.0 Hz, *C*≡N), 210.6 (d, $^1J_{CP}$ = 51.6 Hz, *C*=O).

^{31}P{^{1}H} NMR (162.04 MHz, 300 K, C_6D_6): δ/ppm = −8.1 (s).

IR (solution in cyclohexane; 1 cm cuvette) ν/cm^{-1} = 2689w, 2658s, 1815w, 1751w, 1715m (C=O), 1681s (C=O), 1257vs, 1136w, 951m, 904m, 864m, 741w.

LC-QTOF (APCI, MeCN): m/z(%) calcd. for $C_{15}H_{22}NO_2P^+$+NH_4^+: 297.17;
found: 297.17.

2.4.2 NMR Spectra

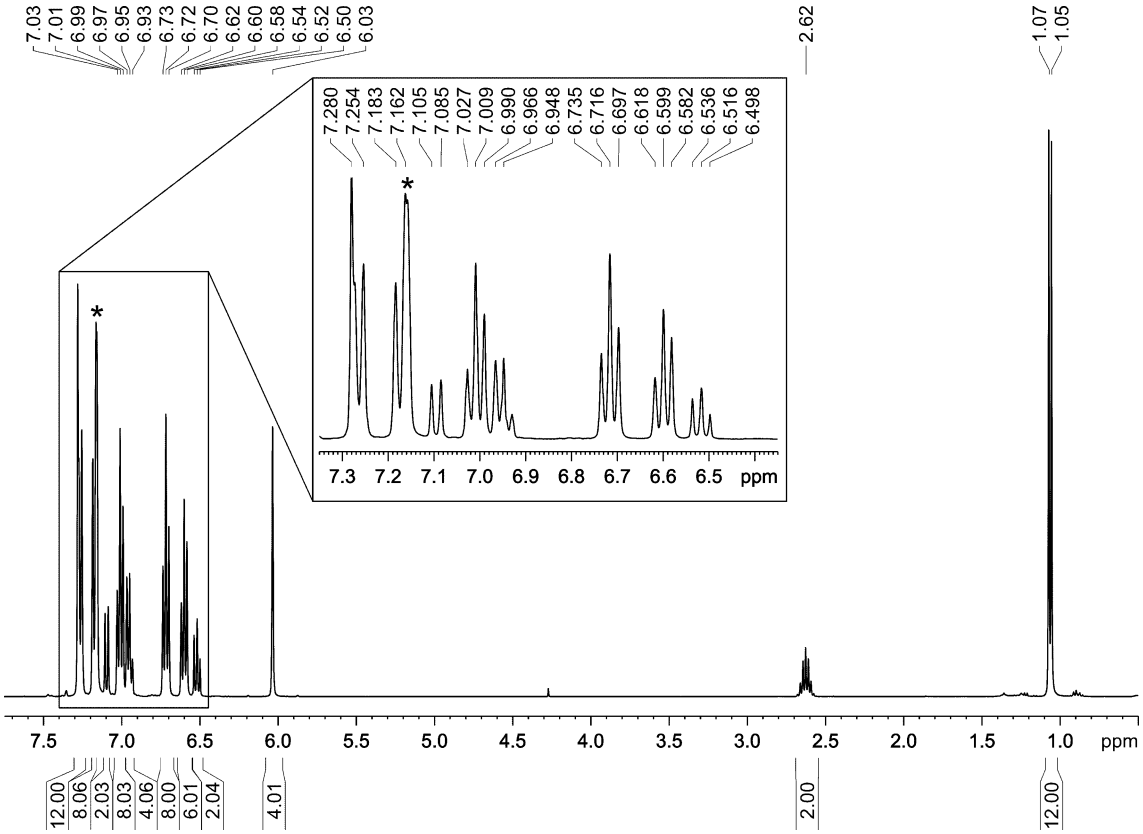

Figure S1. ^{1}H NMR spectrum (400.30 MHz, 300 K, C_6D_6) of Ar*BIAN (**1**); * C_6D_6.

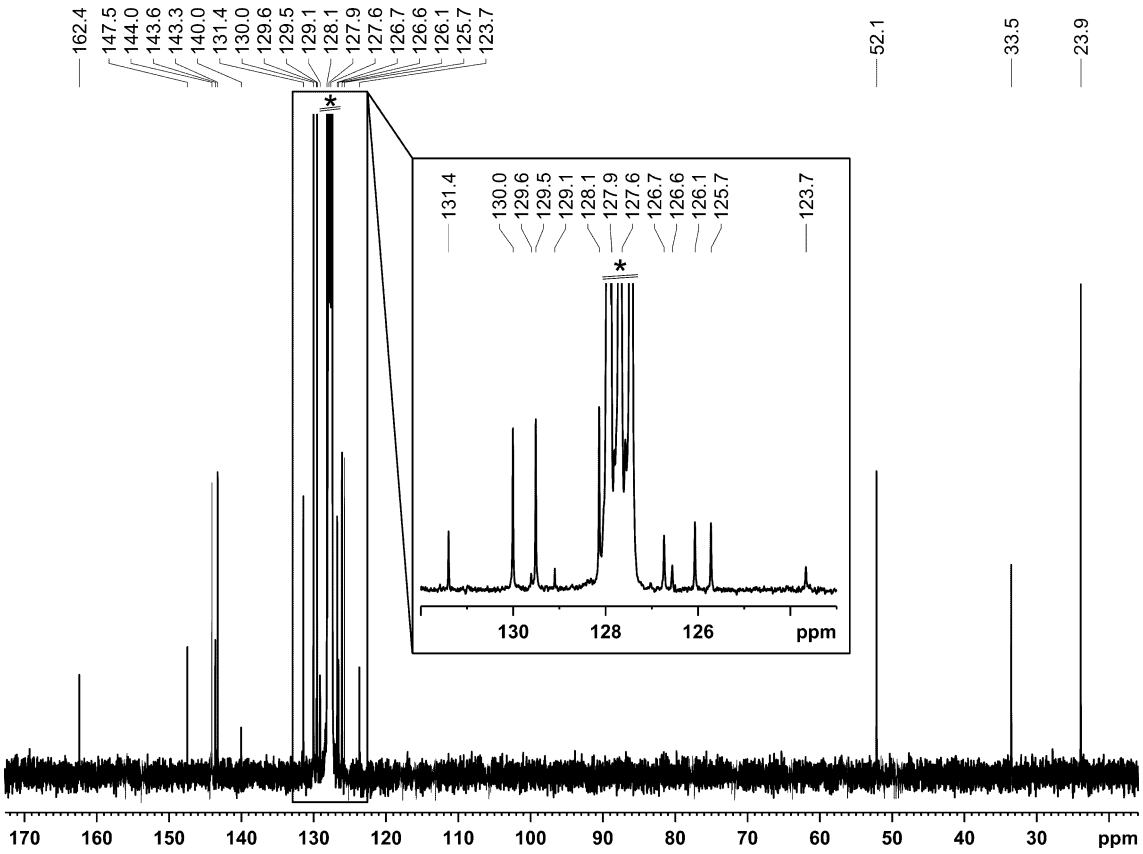

Figure S2. $^{13}C\{^{1}H\}$ NMR spectrum (100.66 MHz, 300 K, C_6D_6) of Ar*BIAN (**1**); * C_6D_6.

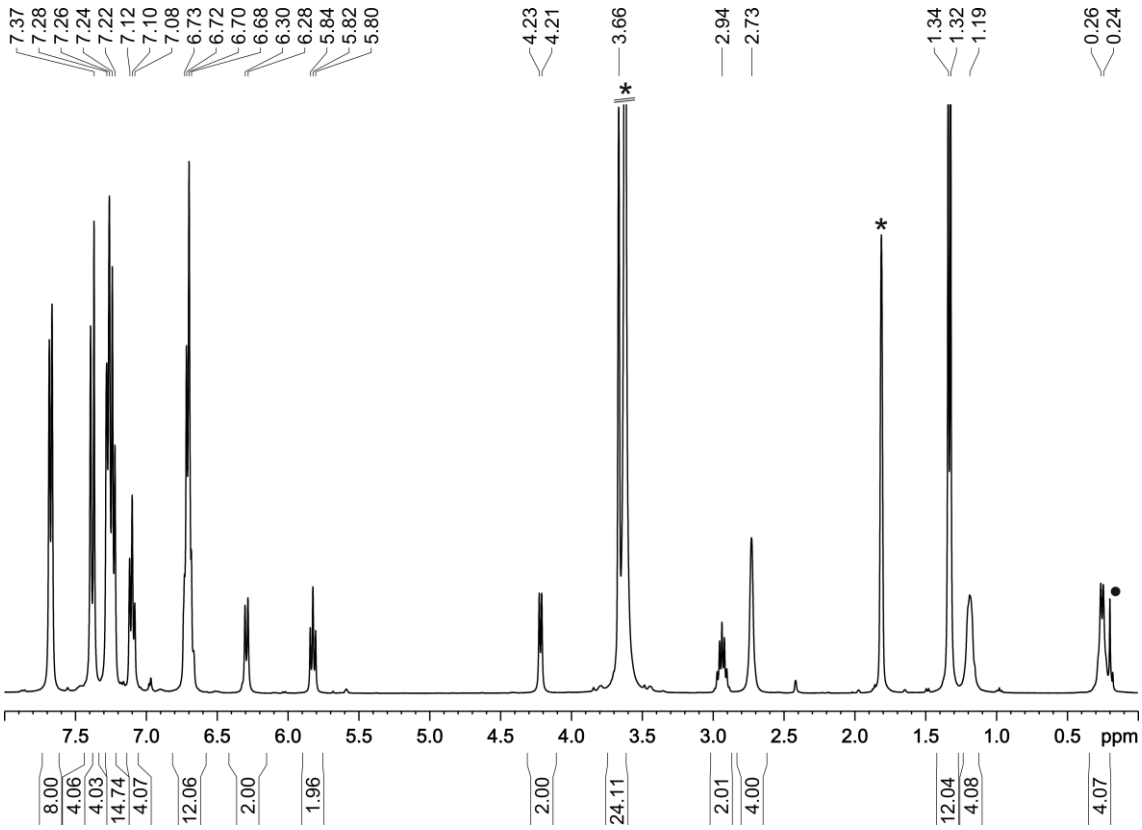

Figure S3. ^{1}H NMR spectrum (400.30 MHz, 300 K, THF-d_8) of [K(18c-6)][(Ar*BIAN)Co(η^4-1-5-cod)] ([K(18c-6)]**2**); • unknown impurity, * THF-d_8.

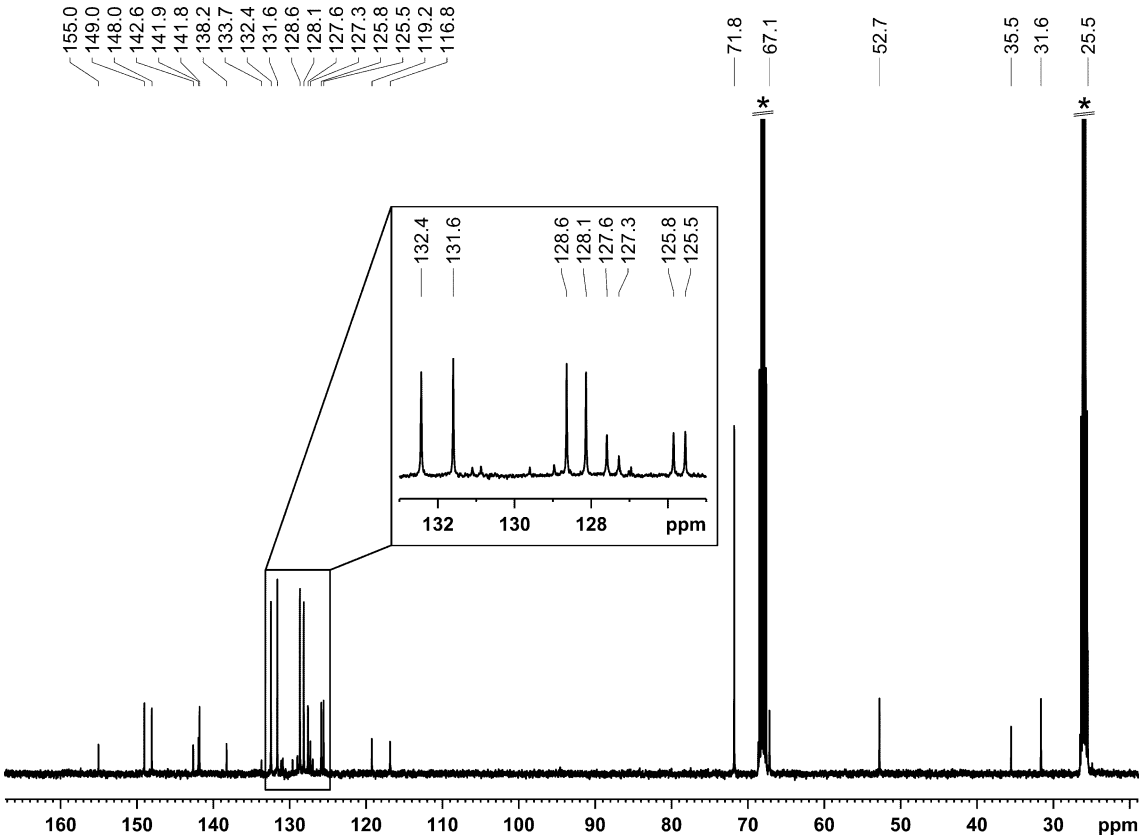

Figure S4. ^{13}C{^{1}H} NMR spectrum (100.66 MHz, 300 K, THF-d_8) of [K(18c-6)][(Ar*BIAN)Co(η^4-1-5-cod)] ([K(18c-6)]**2**); * THF-d_8

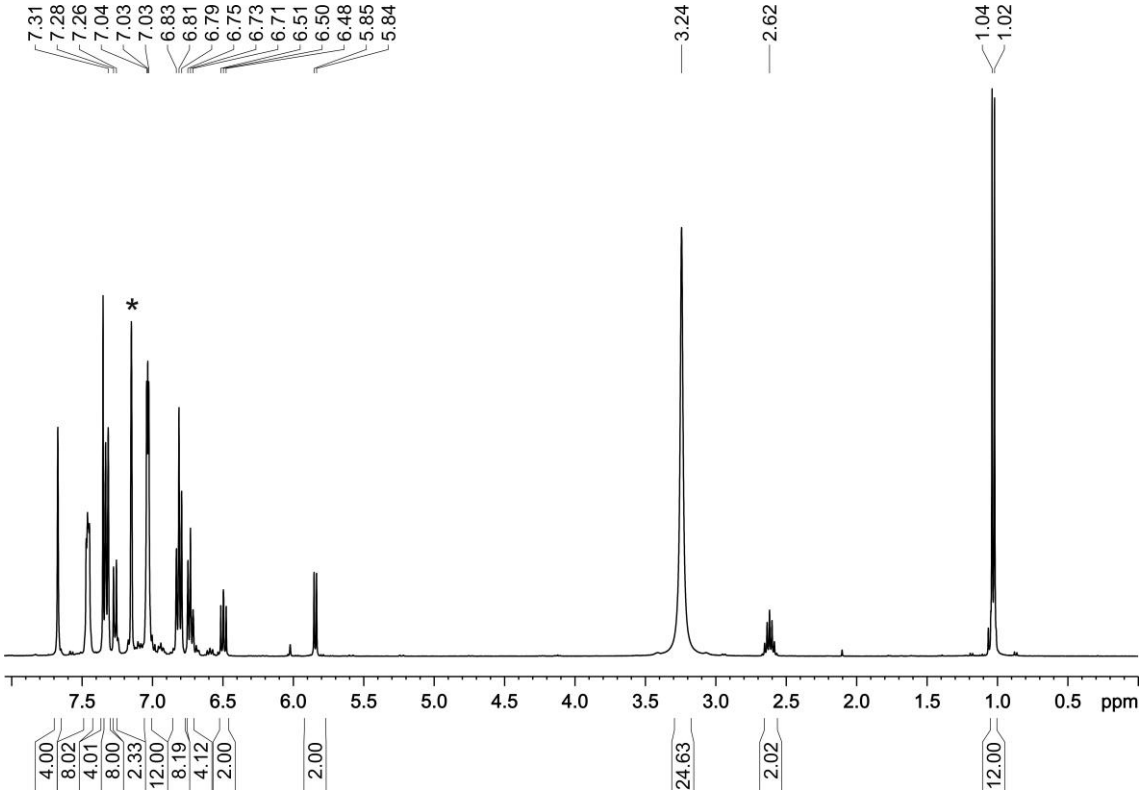

Figure S5. ^{1}H NMR spectrum (400.13 MHz, 300 K, C_6D_6) of [K(18c-6)][(Ar*BIAN)Co(η^4-P_4)] ([K(18c-6)]**3**); * C_6D_6.

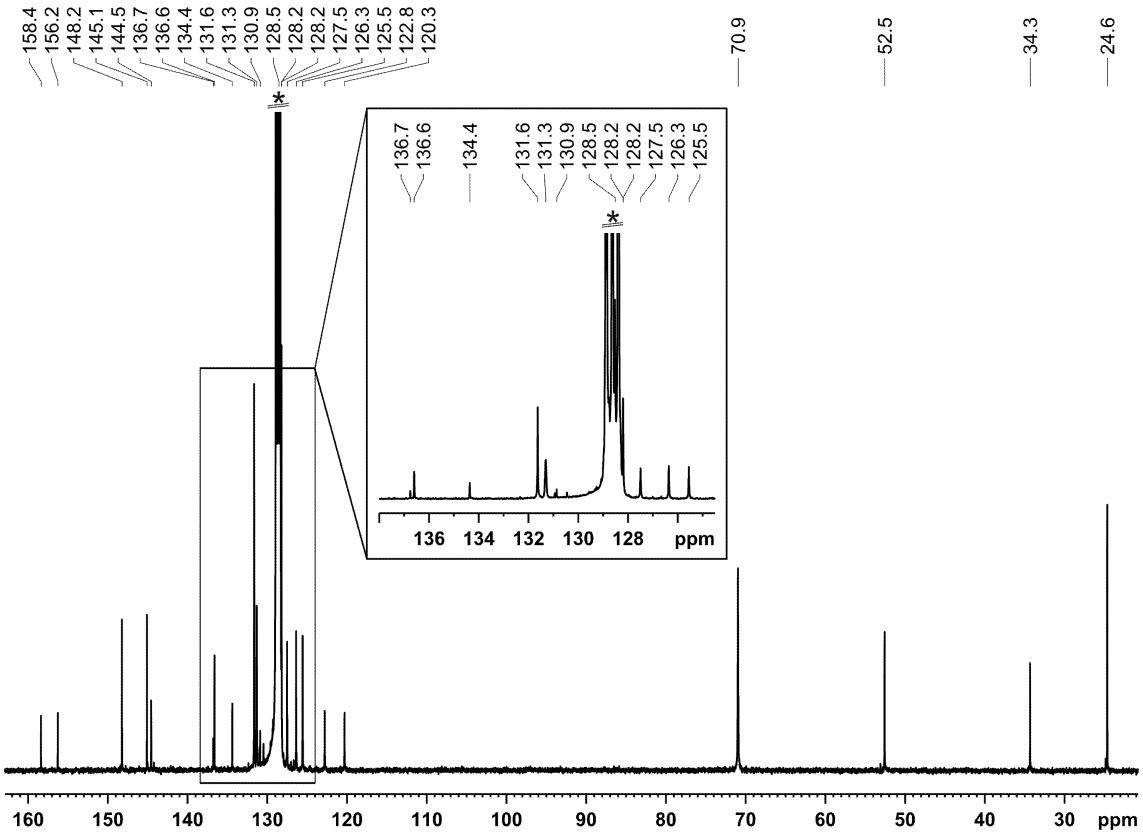

Figure S6. $^{13}C\{^{1}H\}$ NMR spectrum (100.61 MHz, 300 K, C_6D_6) of [K(18c-6)][(Ar*BIAN)Co(η^4-P_4)] ([K(18c-6)]**3**); * C_6D_6.

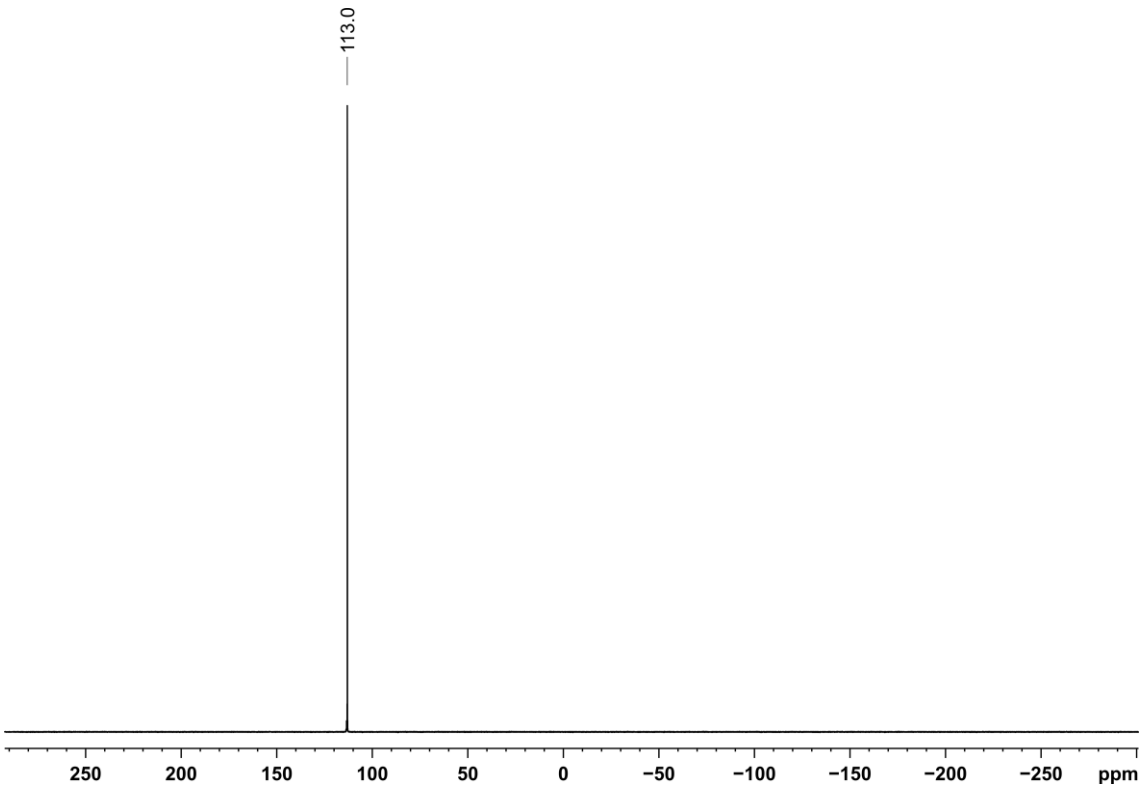

Figure S7. $^{31}P\{^{1}H\}$ NMR spectrum (162.04 MHz, 300 K, C_6D_6) of [K(18c-6)][(Ar*BIAN)Co(η^4-P_4)] ([K(18c-6)]**3**).

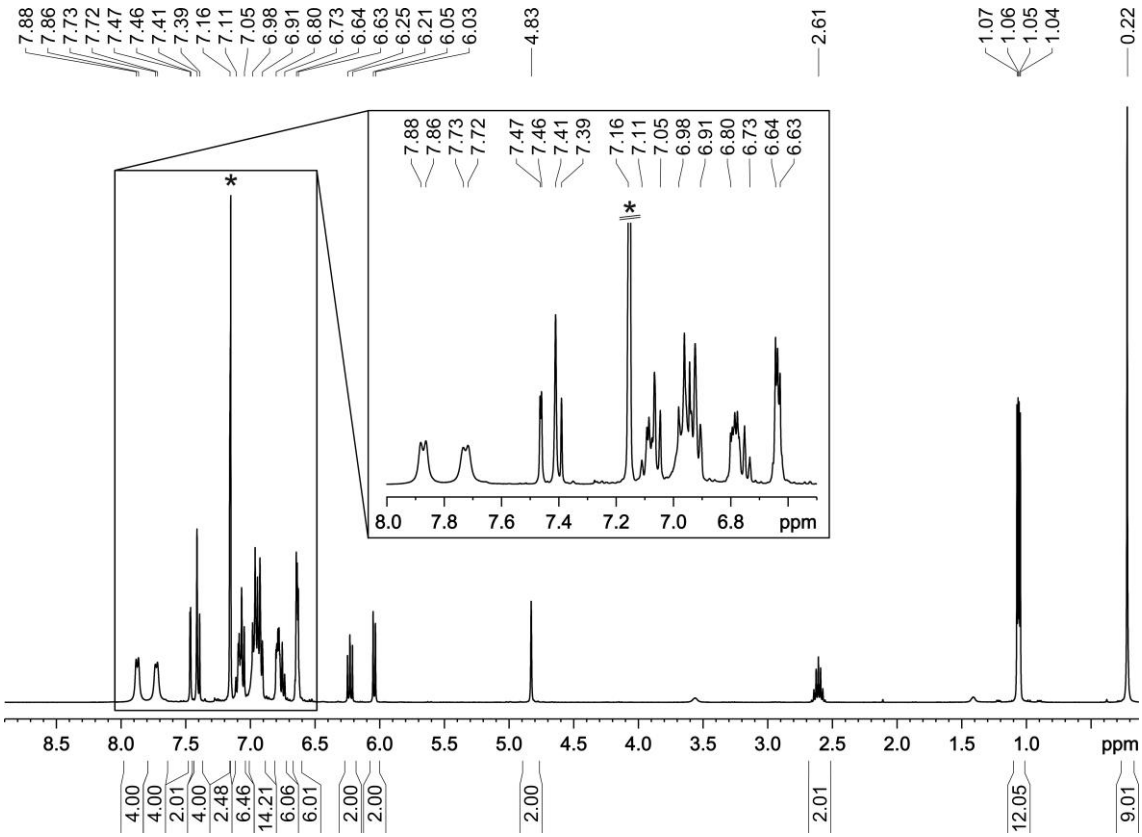

Figure S8. ^{1}H NMR spectrum (400.13 MHz, 300 K, C_6D_6) of [(Ar*BIAN)Co(η^3:η^1-P_4C(O)*t*Bu)] (**4a**); * C_6D_6.

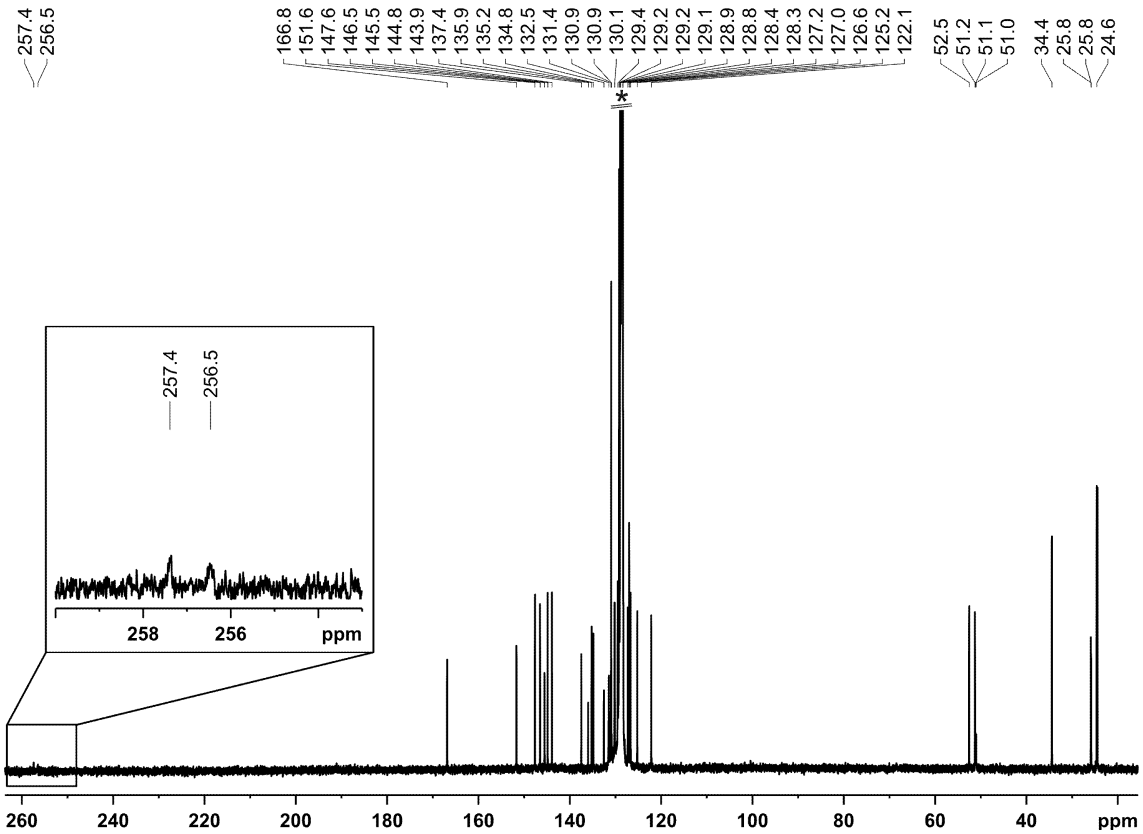

Figure S9. $^{13}C\{^1H\}$ NMR spectrum (100.61 MHz, 300 K, C_6D_6) of [(Ar*BIAN)Co(η^3:η^1-$P_4C(O)tBu$)] (**4a**); * C_6D_6.

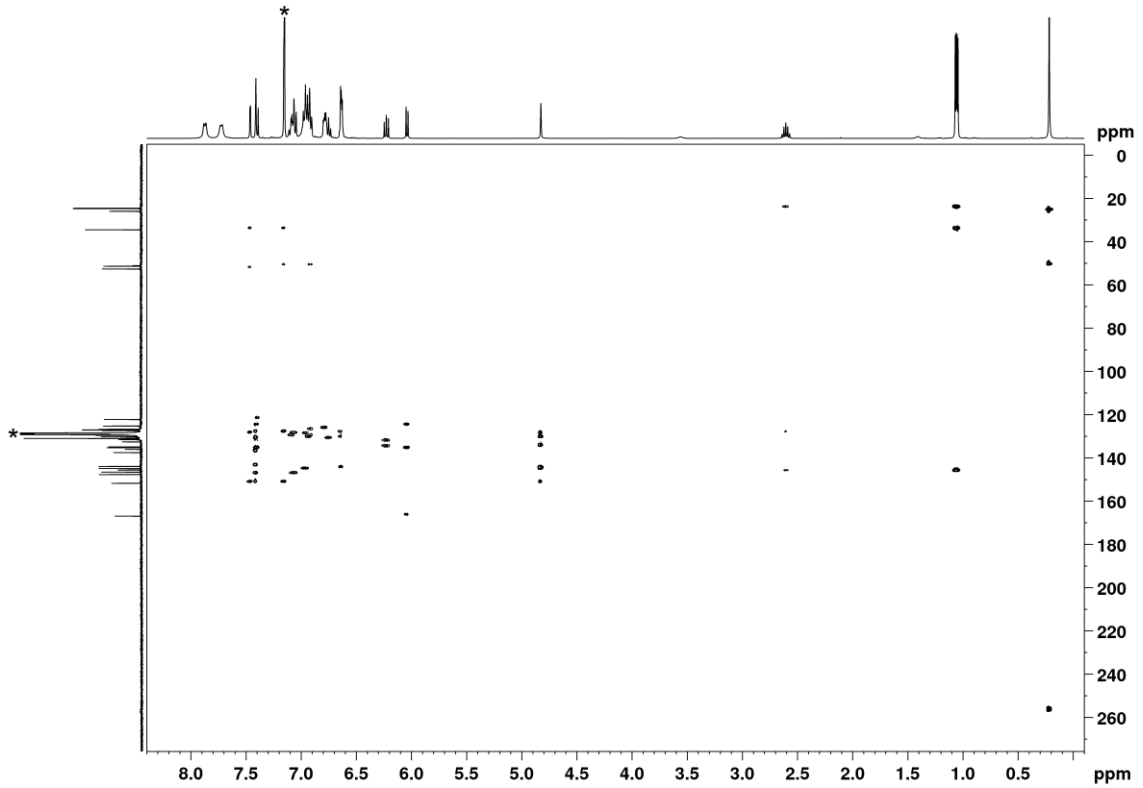

Figure S10. $^1H/^{13}C$ HMBC NMR spectrum (400.13/100.61 MHz, 300 K, C_6D_6) of [(Ar*BIAN)Co(η^3:η^1-$P_4C(O)tBu$)] (**4a**); * C_6D_6.

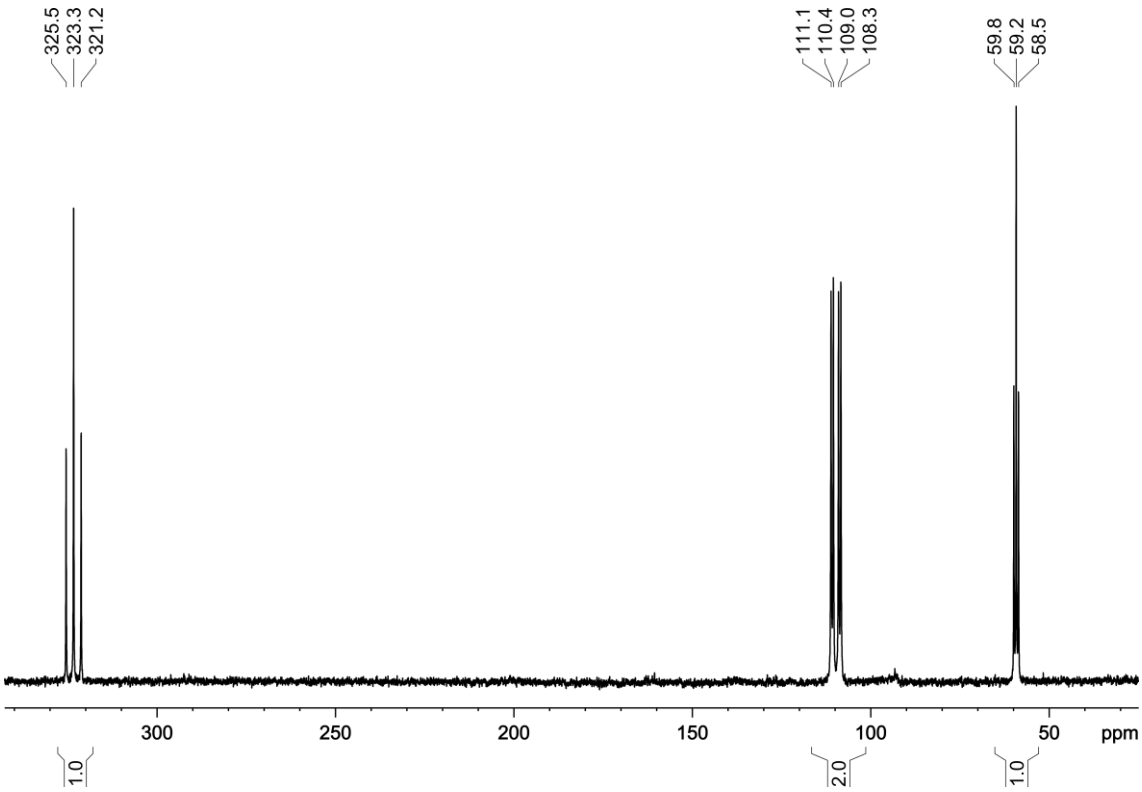

Figure S11. $^{31}P\{^{1}H\}$ NMR spectrum (162.04 MHz, 300 K, C_6D_6) of [(Ar*BIAN)Co(η^3:η^1-$P_4C(O)tBu$)] (**4a**).

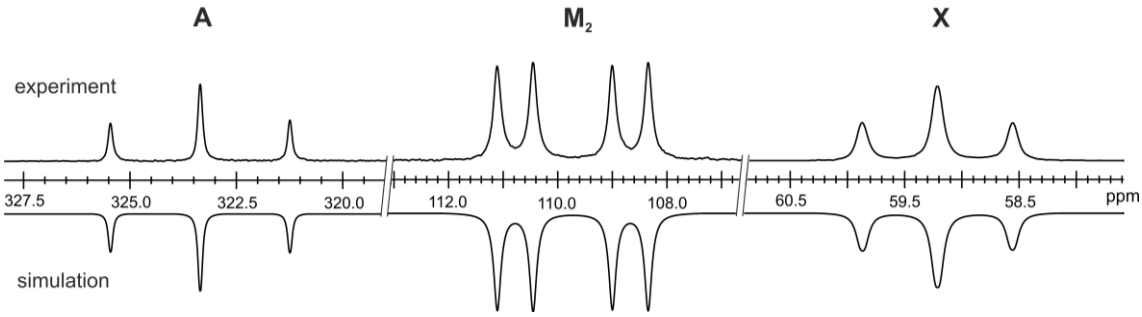

Figure S12. Section of the $^{31}P\{^{1}H\}$ NMR (162.04 MHz, 300 K, C_6D_6) of [(Ar*BIAN)Co(η^3:η^1-$P_4C(O)tBu$)] (**4a**); experimental (upwards) and simulation (downwards).

Table S1. Chemical shifts and coupling constants from the iterative fit of the AM_2X spin system and schematic representation of the $CoP_4C(O)tBu$ core of [(Ar*BIAN)Co(η^3:η^1-$P_4C(O)tBu$)] (**4a**).

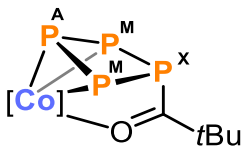	$\delta(A) = 323.3$ ppm	$^{1}J_{AM} = -341.6$ Hz
	$\delta(M) = 109.7$ ppm	$^{1}J_{MX} = -106.2$ Hz
	$\delta(X) = 59.2$ ppm	$^{2}J_{AX} = 7.2$ Hz

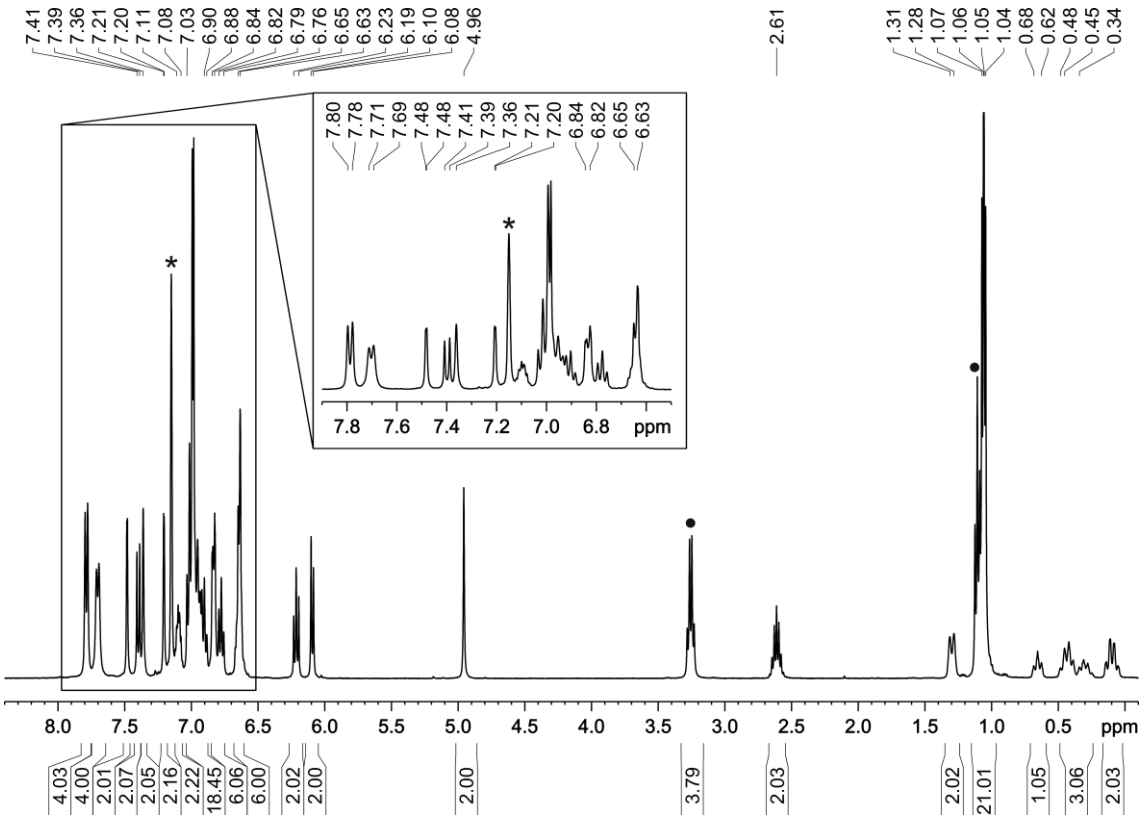

Figure S13. ^{1}H NMR spectrum (400.13 MHz, 300 K, C_6D_6) of [(Ar*BIAN)Co(η^3:η^1-$P_4C(O)Cy$] (**4b**); • Et_2O, * C_6D_6.

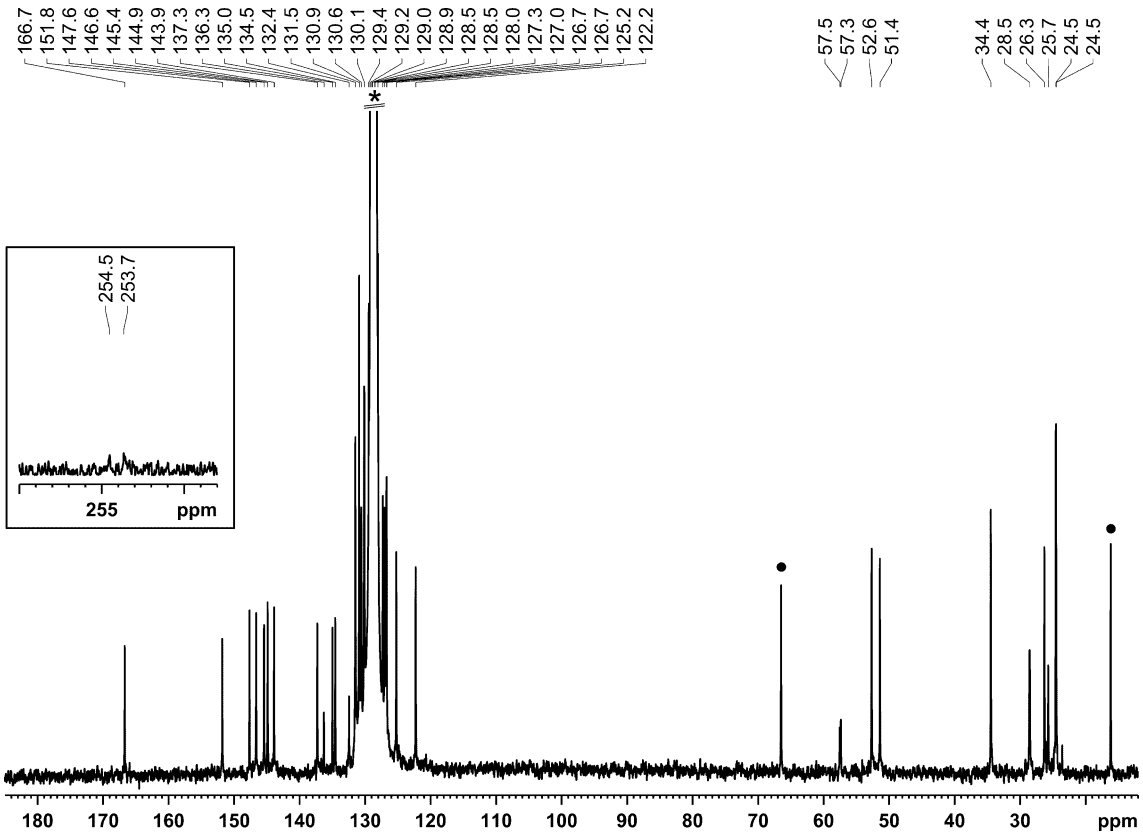

Figure S14. $^{13}C\{^{1}H\}$ NMR spectrum (100.61 MHz, 300 K, C_6D_6) of [(Ar*BIAN)Co(η^3:η^1-$P_4C(O)Cy$] (**4b**); • Et_2O, * C_6D_6.

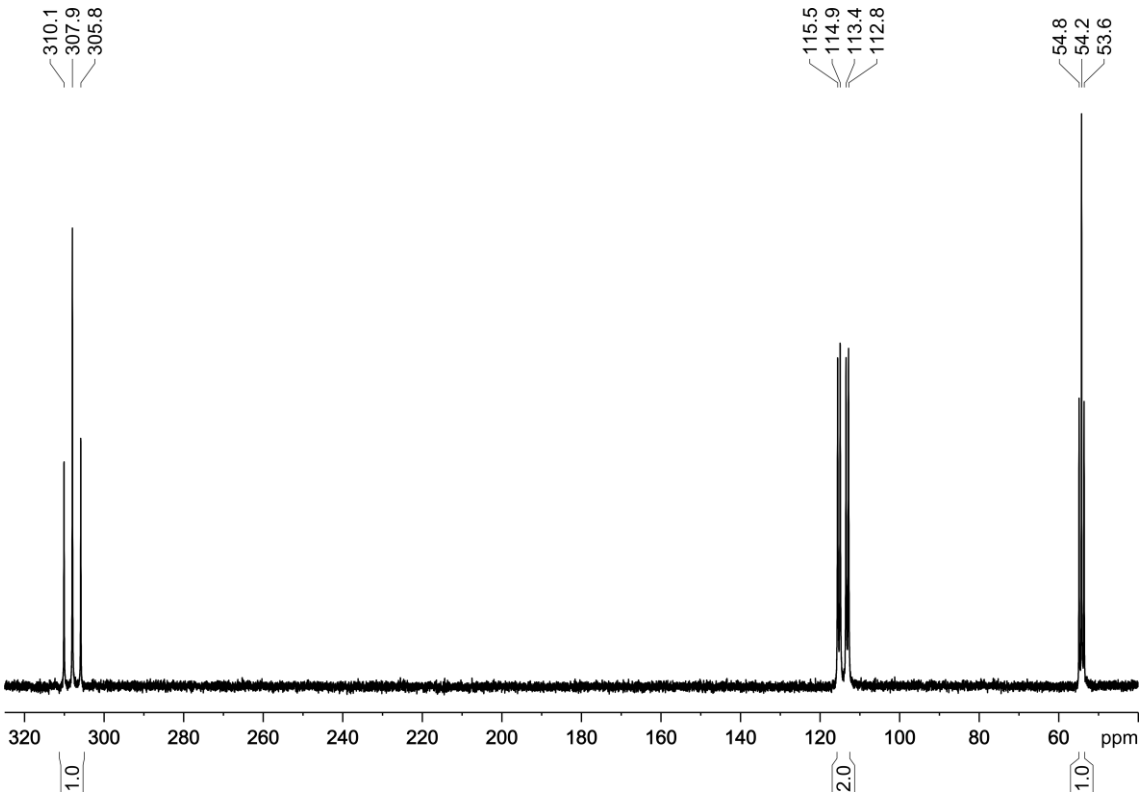

Figure S15. $^{31}P\{^{1}H\}$ NMR spectrum (162.04 MHz, 300 K, C_6D_6) of [(Ar*BIAN)Co(η^3:η^1-$P_4C(O)Cy$] (**4b**).

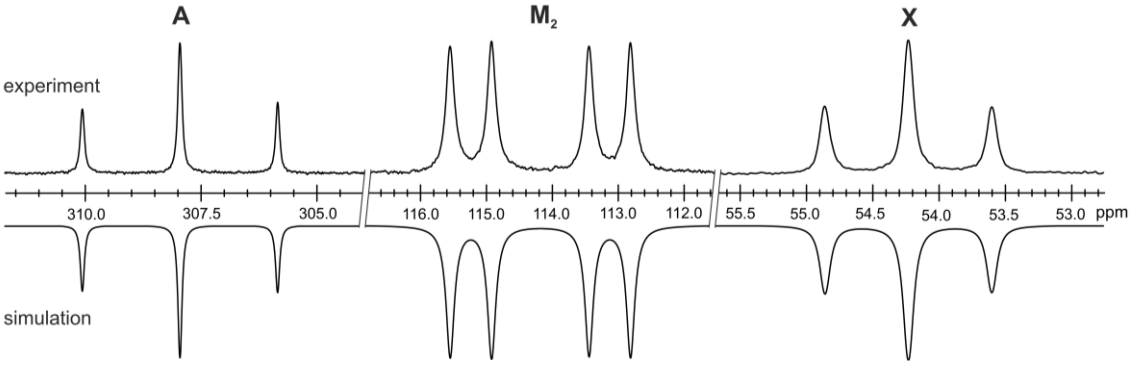

Figure S16. Section of the $^{31}P\{^{1}H\}$ NMR (162.04 MHz, 300 K, C_6D_6) of [(Ar*BIAN)Co(η^3:η^1-$P_4C(O)Cy$] (**4b**); experimental (upwards) and simulation (downwards).

Table S2. Chemical shifts and coupling constants from the iterative fit of the AM_2X spin system and schematic representation of the $CoP_4C(O)Cy$ core of [(Ar*BIAN)Co(η^3:η^1-$P_4C(O)Cy$] (**4b**).

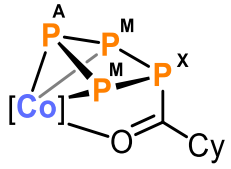	$\delta(A) = 307.9$ ppm	$^{1}J_{AM} = -314.5$ Hz
	$\delta(M) = 114.2$ ppm	$^{1}J_{MX} = -101.9$ Hz
	$\delta(X) = 54.2$ ppm	$^{2}J_{AX} = 4.0$ Hz

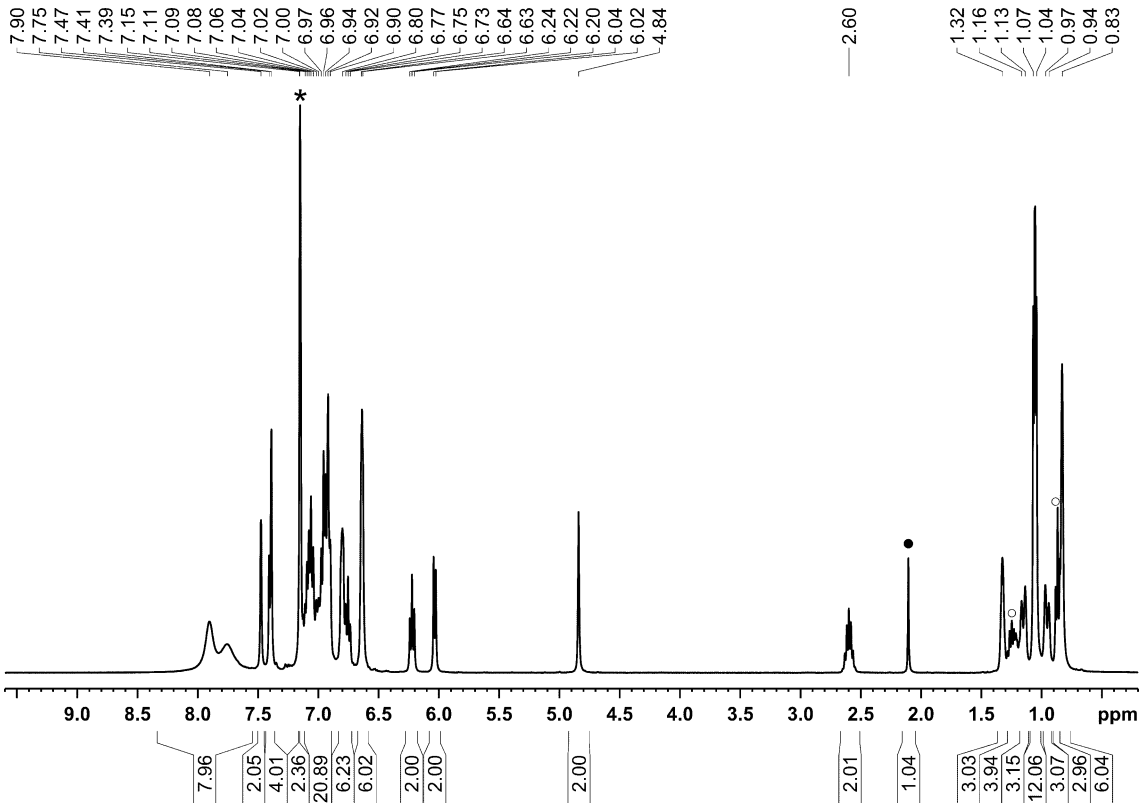

Figure S17. ^{1}H NMR spectrum (400.13 MHz, 300 K, C_6D_6) of [(Ar*BIAN)Co(η^3:η^1-$P_4C(O)Ad$)] (**4c**); ○ *n*-hexane, • toluene, * C_6D_6.

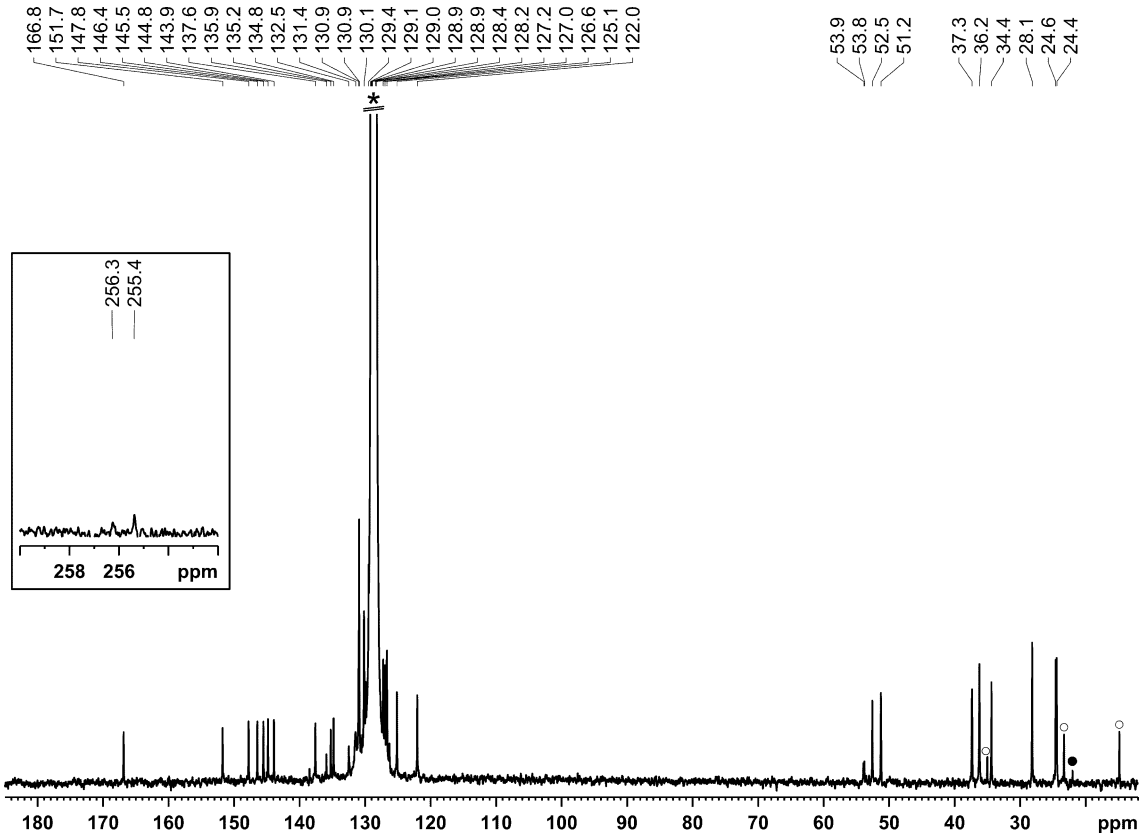

Figure S18. $^{13}C\{^{1}H\}$ NMR spectrum (100.61 MHz, 300 K, C_6D_6) of [(Ar*BIAN)Co(η^3:η^1-$P_4C(O)Ad$)] (**4c**); ○ *n*-hexane, • toluene, * C_6D_6.

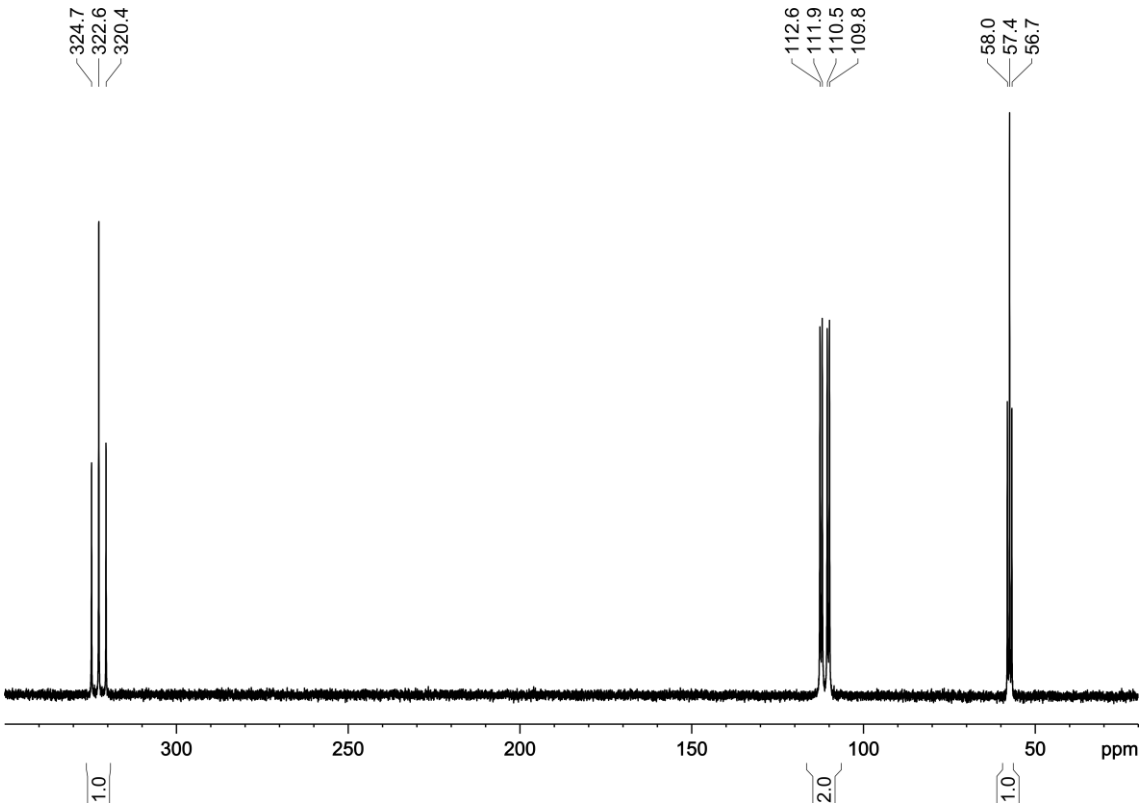

Figure S19. $^{31}P\{^{1}H\}$ NMR spectrum (162.04 MHz, 300 K, C_6D_6) of [(Ar*BIAN)Co(η^3:η^1-$P_4C(O)Ad$)] (**4c**).

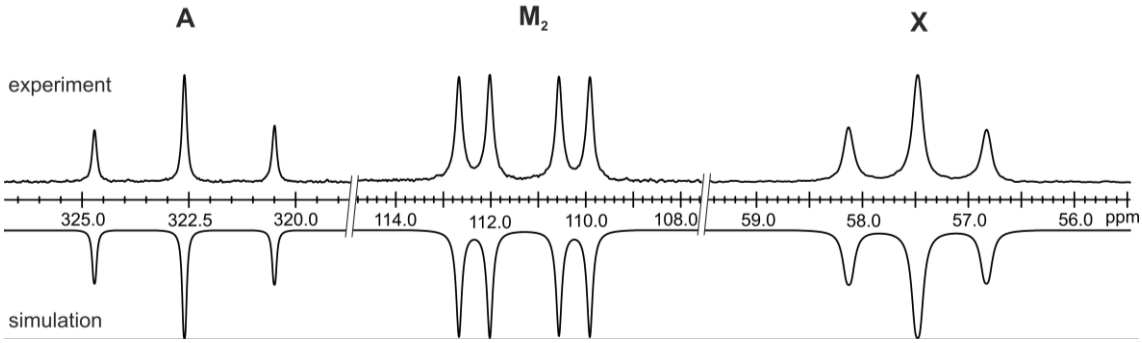

Figure S20. Section of the $^{31}P\{^{1}H\}$ NMR (162.04 MHz, 300 K, C_6D_6) of [(Ar*BIAN)Co(η^3:η^1-$P_4C(O)Ad$)] (**4c**); experimental (upwards) and simulation (downwards).

Table S3. Chemical shifts and coupling constants from the iterative fit of the AM_2X spin system and schematic representation of the $CoP_4C(O)Ad$ core of [(Ar*BIAN)Co(η^3:η^1-$P_4C(O)Ad$)] (**4c**).

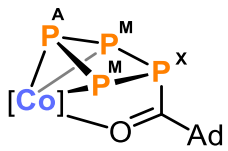	$\delta(A) = 322.6$ ppm	$^{1}J_{AM} = -341.3$ Hz
	$\delta(M) = 111.3$ ppm	$^{1}J_{MX} = -105.3$ Hz
	$\delta(X) = 57.5$ ppm	$^{2}J_{AX} = 6.9$ Hz

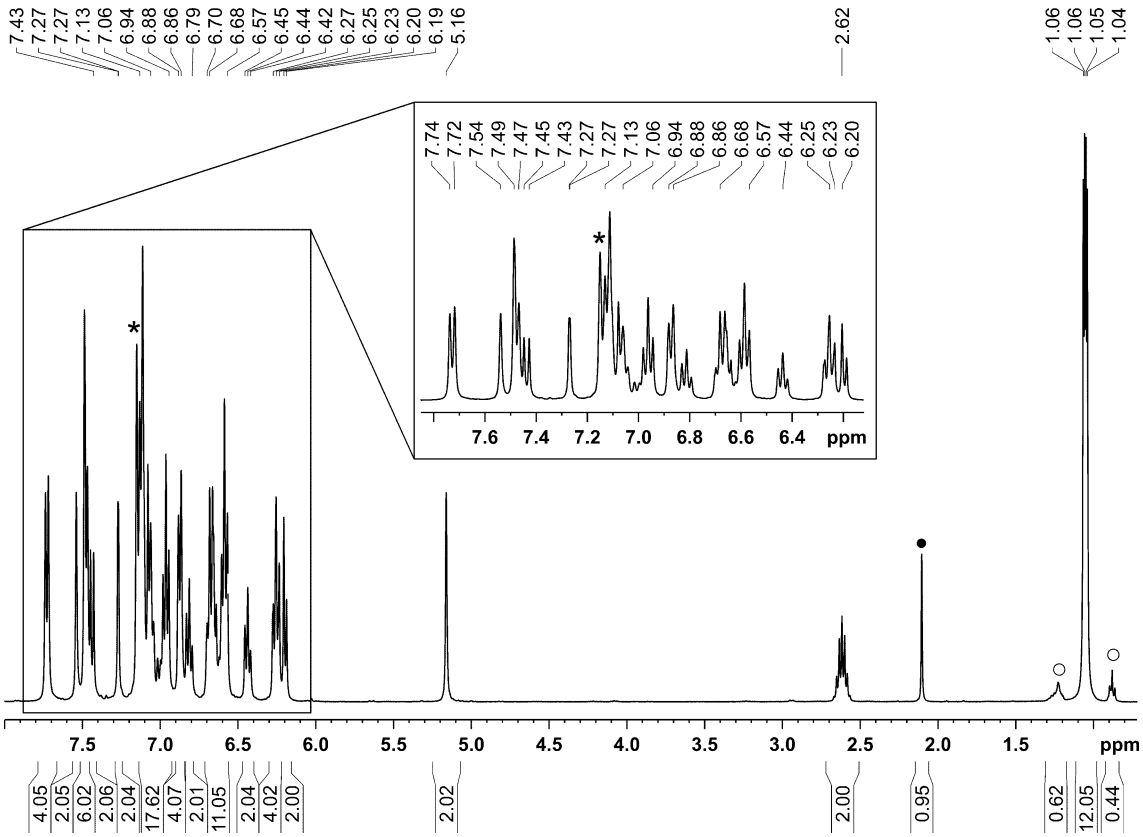

Figure S21. ^{1}H NMR spectrum (400.13 MHz, 300 K, C_6D_6) of [(Ar*BIAN)Co(η^3:η^1-$P_4C(O)Ph$)] (**4d**); • toluene, ○ *n*-hexane, * C_6D_6.

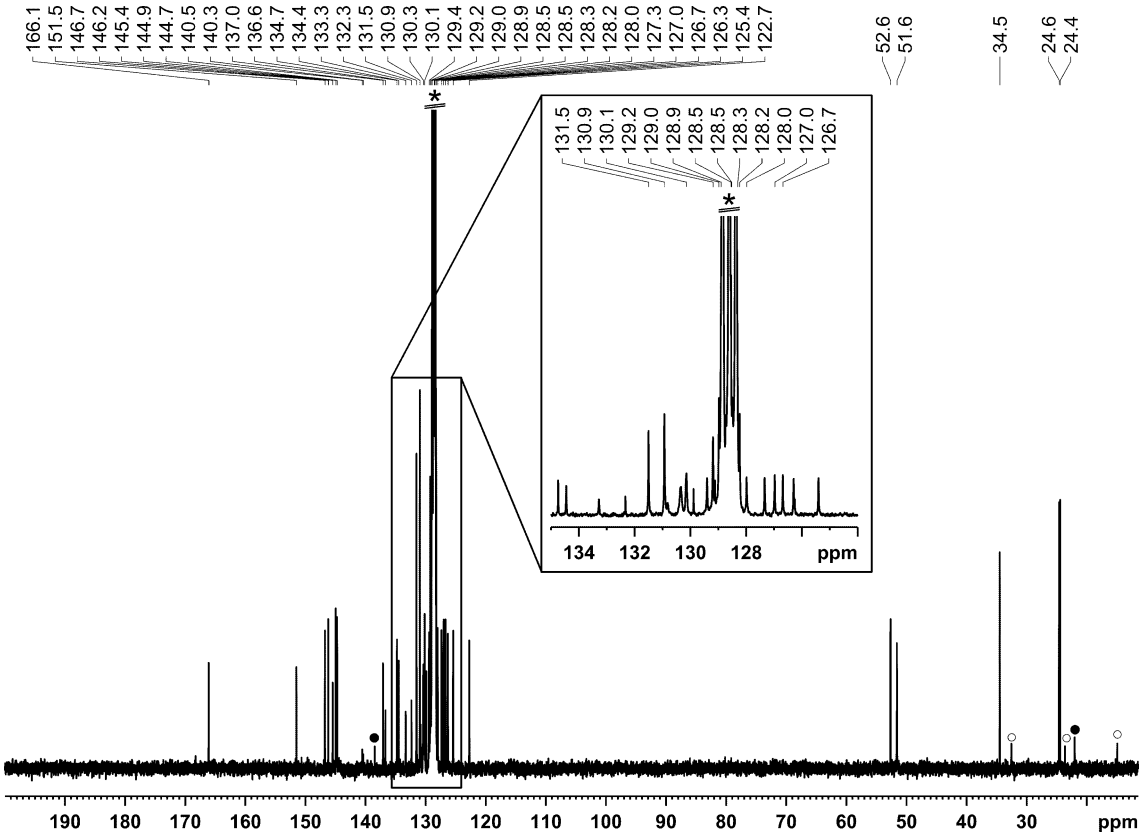

Figure S22. $^{13}C\{^{1}H\}$ NMR spectrum (100.66 MHz, 300 K, C_6D_6) of [(Ar*BIAN)Co(η^3:η^1-$P_4C(O)Ph$)] (**4d**); ○ *n*-hexane, • toluene, * C_6D_6.

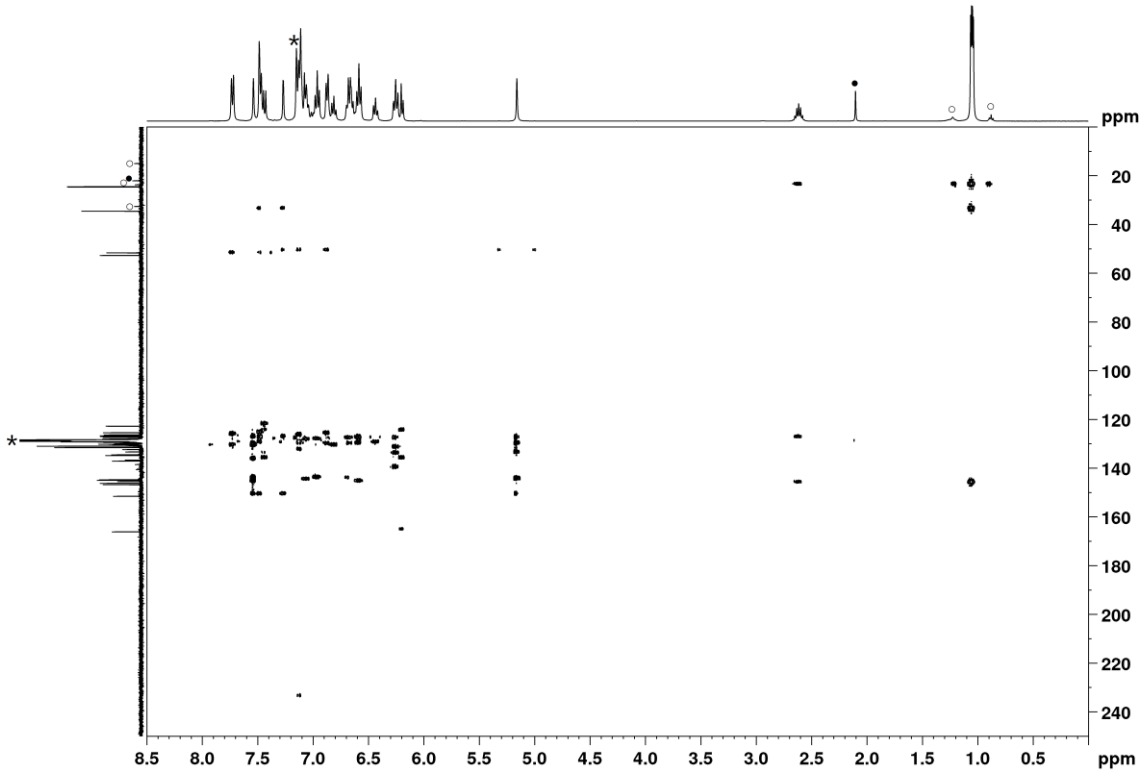

Figure S23. . $^{1}H/^{13}C$ HMBC NMR spectrum (400.13/100.66 MHz, 300 K, C_6D_6) of [(Ar*BIAN)Co(η^3:η^1-$P_4C(O)Ph$)] (**4d**); * C_6D_6.

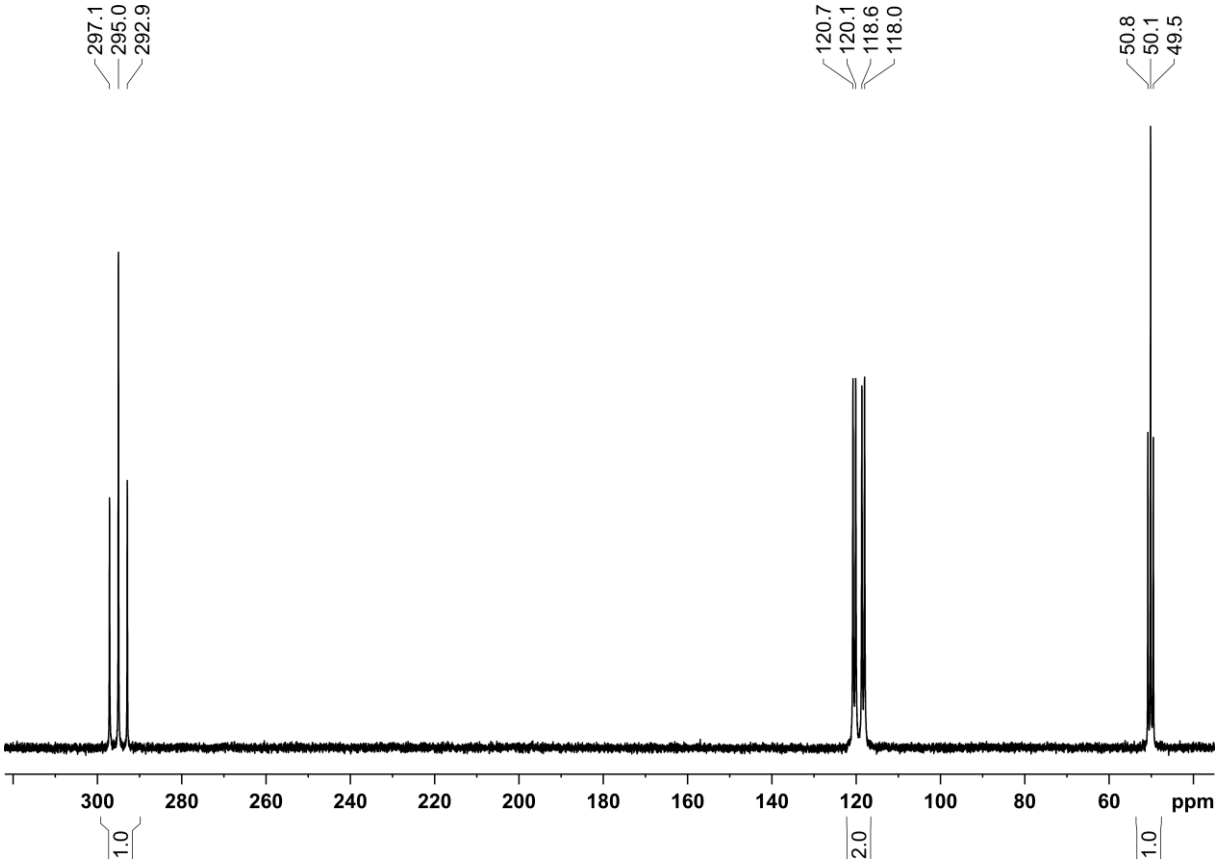

Figure S24. $^{31}P\{^{1}H\}$ NMR spectrum (162.04 MHz, 300 K, C_6D_6) of [(Ar*BIAN)Co(η^3:η^1-$P_4C(O)Ph$)] (**4d**).

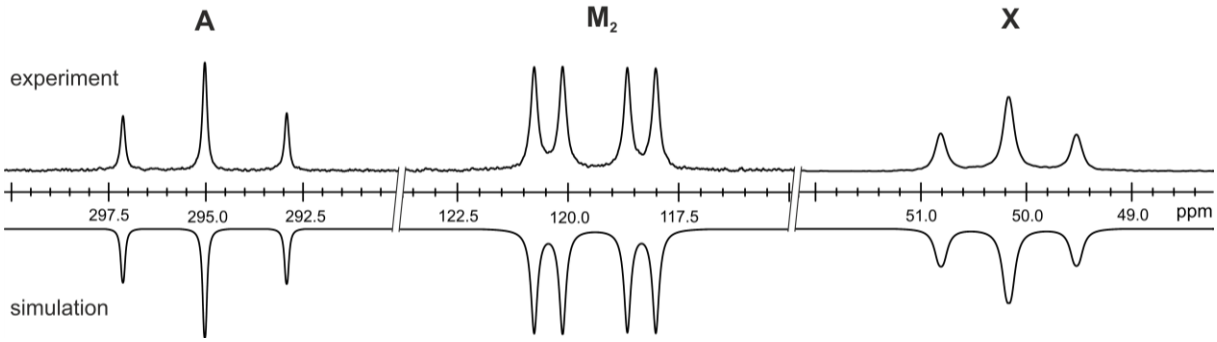

Figure S25. Section of the $^{31}P\{^1H\}$ NMR (162.04 MHz, 300 K, C_6D_6) of [(Ar*BIAN)Co(η^3:η^1-$P_4C(O)Ph$)] (**4d**); experimental (upwards) and simulation (downwards).

Table S4. Chemical shifts and coupling constants from the iterative fit of the AM_2X spin system and schematic representation of the $CoP_4C(O)Ph$ core of [(Ar*BIAN)Co(η^3:η^1-$P_4C(O)Ph$)] (**4d**).

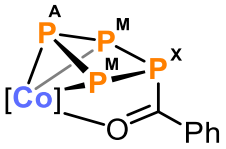	$\delta(A) = 295.0$ ppm	$^1J_{AM} = -341.2$ Hz
	$\delta(M) = 119.4$ ppm	$^1J_{MX} = -104.2$ Hz
	$\delta(X) = 50.2$ ppm	$^2J_{AX} = 7.8$ Hz

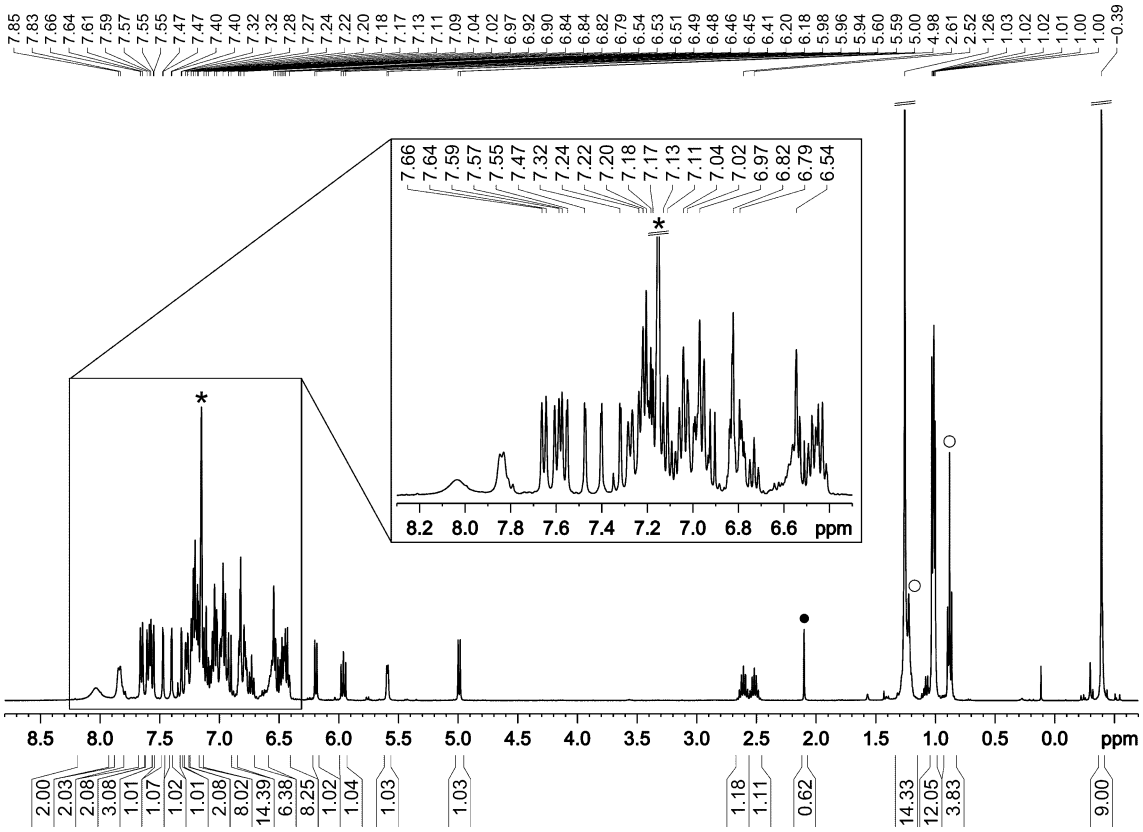

Figure S26. ^1H NMR spectrum (400.13 MHz, 288 K, C_6D_6) of [(Ar*BIAN)Co($(CH_3)_3SiNC$)(η^2:η^1-P_4CO*t*Bu)] (**5a**); ○ *n*-hexane, • toluene, * C_6D_6.

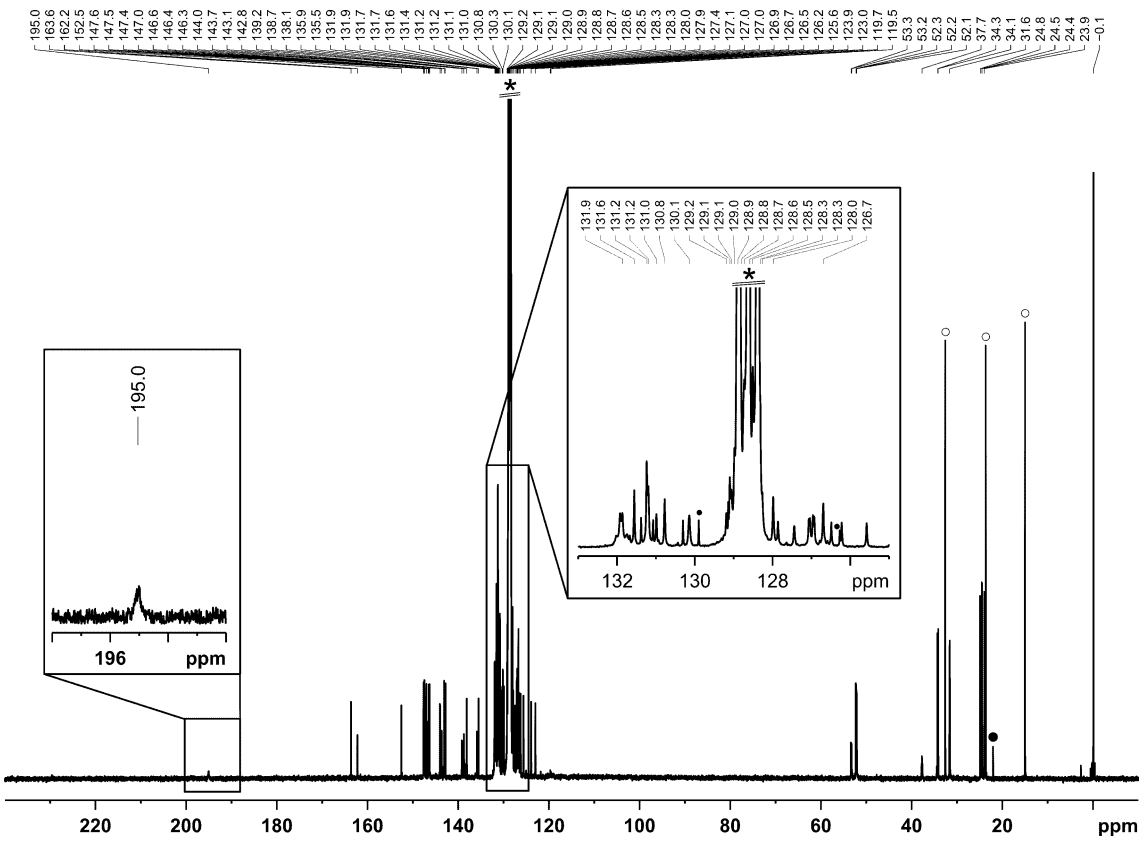

Figure S27. $^{13}C\{^1H\}$ NMR spectrum (100.61 MHz, 288 K, C_6D_6) of [(Ar*BIAN)Co((CH$_3$)$_3$SiNC)(η^2:η^1-P_4CO*t*Bu)] (**5a**); ○ *n*-hexane, • toluene, * C_6D_6.

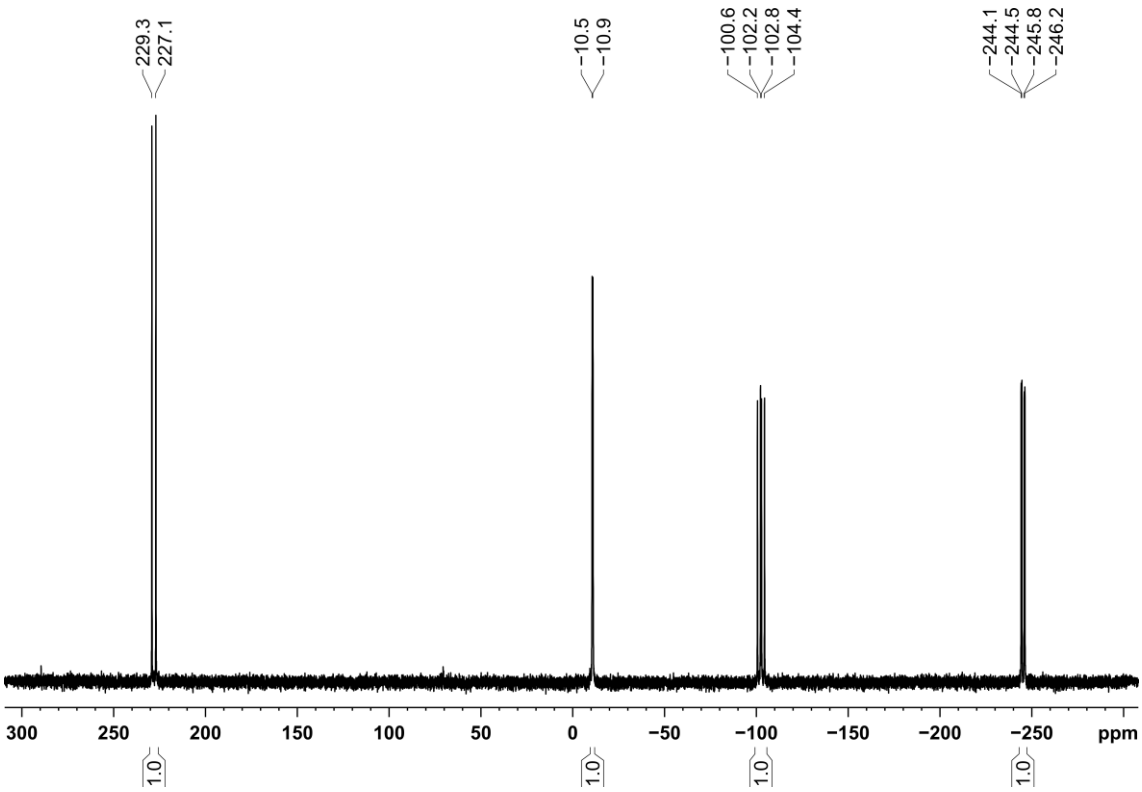

Figure S28. $^{31}P\{^1H\}$ NMR spectrum (161.98 MHz, 288 K, C_6D_6) of [(Ar*BIAN)Co((CH$_3$)$_3$SiNC)(η^2:η^1-P_4CO*t*Bu)] (**5a**).

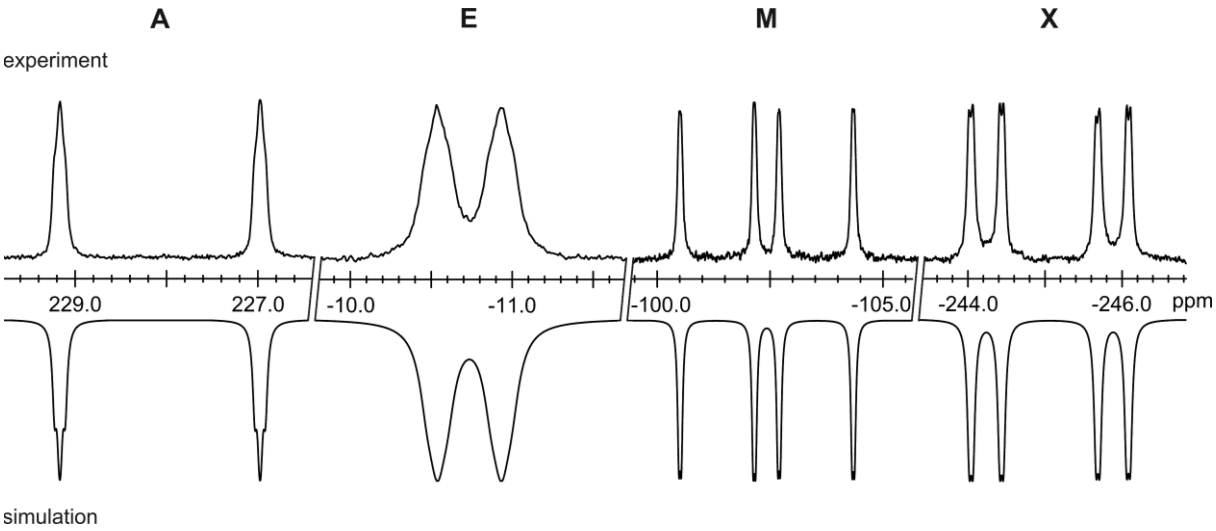

Figure S29. Section of the $^{31}P\{^1H\}$ NMR (161.98 MHz, 288 K, C_6D_6) of [(Ar*BIAN)Co((CH$_3$)$_3$SiNC)(η^2:η^1-P$_4$CO*t*Bu)] (**5a**); experimental (upwards) and simulation (downwards).

Table S5. Chemical shifts and coupling constants from the iterative fit of the AEMX spin system and schematic representation of the CoP$_4$CO*t*Bu core of [(Ar*BIAN)Co((CH$_3$)$_3$SiNC)(η^2:η^1-P$_4$CO*t*Bu)] (**5a**).

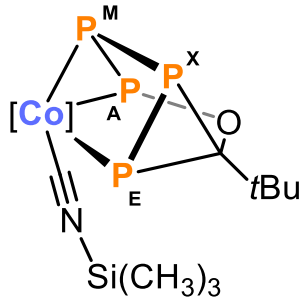

δ(A) = 228.1 ppm	$^1J_{AM}$ = −355.0 Hz
δ(E) = −10.7 ppm	$^1J_{MX}$ = −266.5 Hz
δ(M) = −102.4 ppm	$^1J_{EX}$ = −64.1 Hz
δ(X) = −245.1 ppm	$^2J_{EM}$ = 9.0 Hz
	$^2J_{AX}$ = 7.9 Hz
	$^3J_{AE}$ = −11.1 Hz

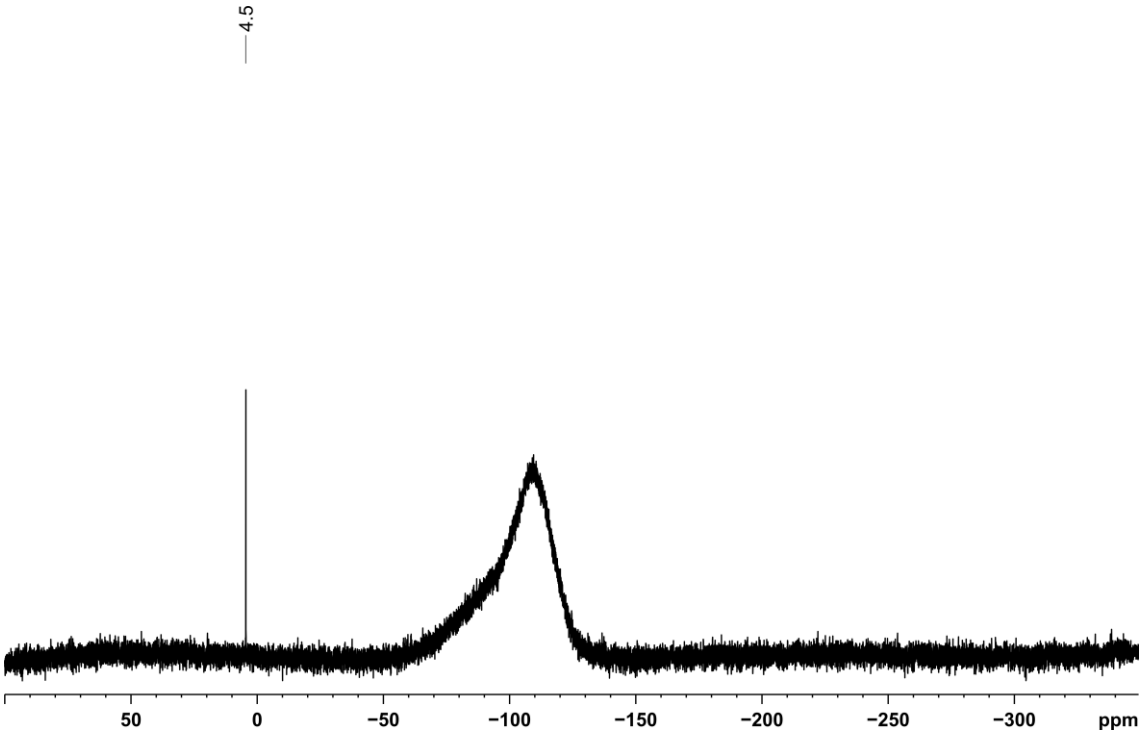

Figure S30. $^{29}Si\{^1H\}$ NMR spectrum (79.49 MHz, 288 K, C_6D_6) of [(Ar*BIAN)Co((CH$_3$)$_3$SiNC)(η^2:η^1-P_4CO*t*Bu)] (**5a**).

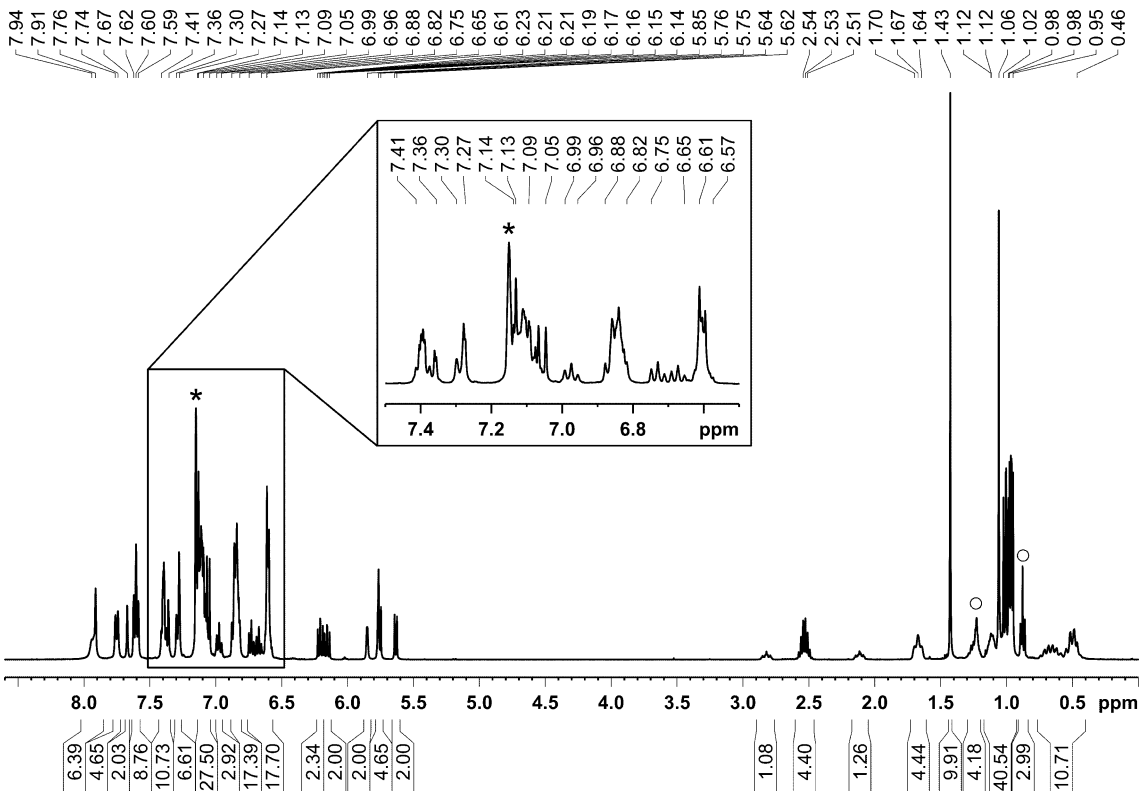

Figure S31. ^1H NMR spectrum (400.13 MHz, 300 K, C_6D_6) of *exo*-/*endo*-[(Ar*BIAN)Co(CyNC)(η^3-P_4C(O)*t*Bu)] (**6a**); ○ *n*-hexane, * C_6D_6.

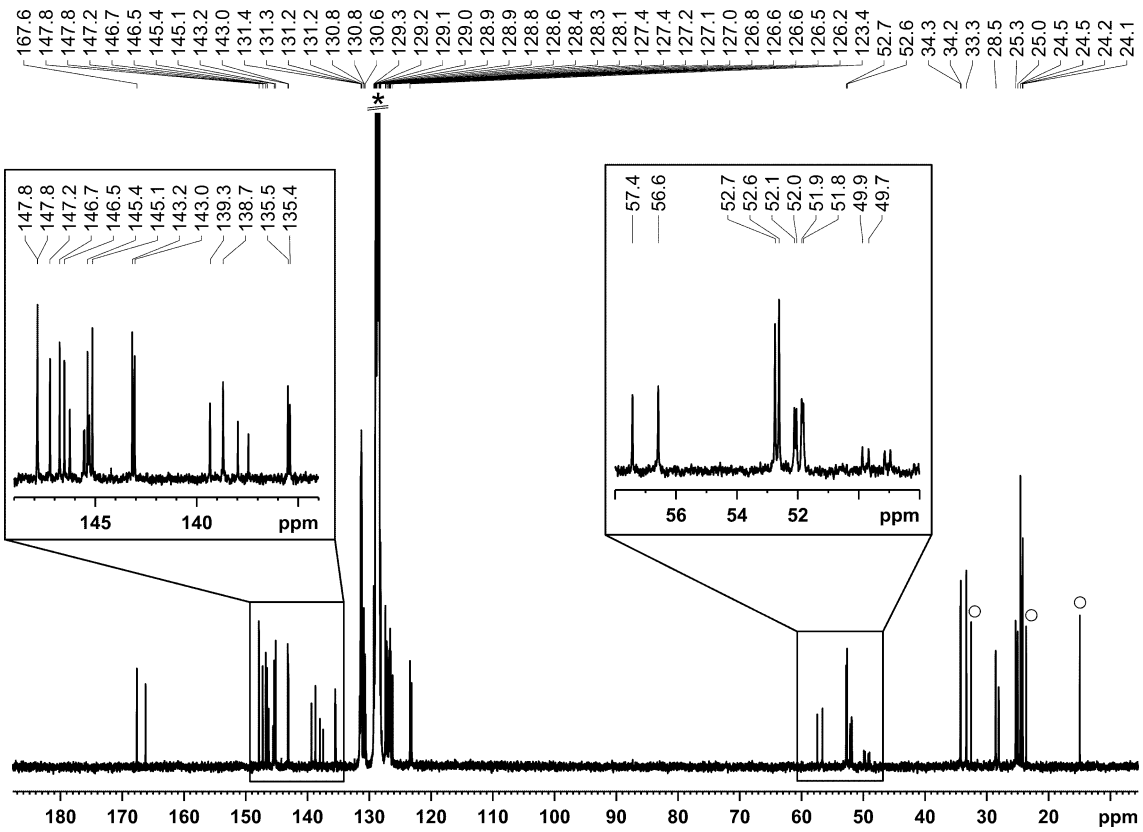

Figure S32. $^{13}C\{^1H\}$ NMR spectrum (100.61 MHz, 300 K, C_6D_6) of *exo*-/*endo*-[(Ar*BIAN)Co(CyNC)(η^3-$P_4C(O)tBu$)] (**6a**); ○ *n*-hexane, * C_6D_6.

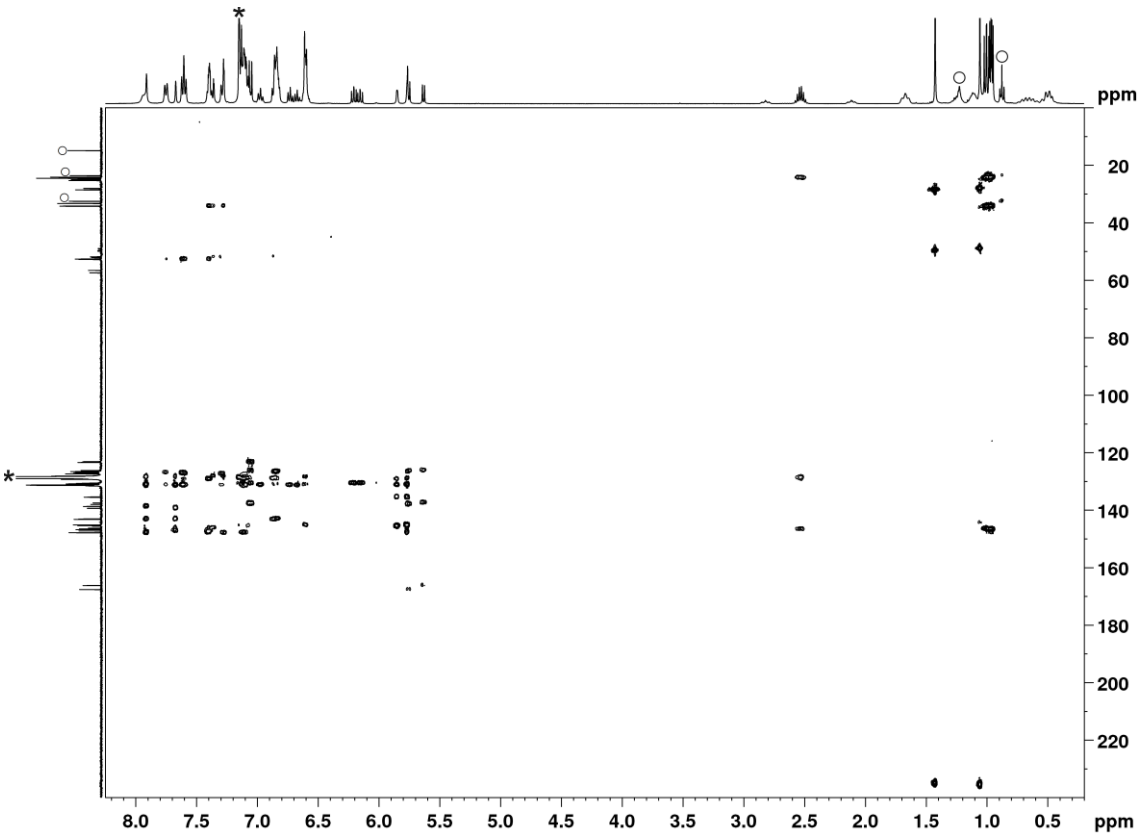

Figure S33. $^1H/^{13}C$ HMBC NMR spectrum (400.13/100.61 MHz, 300 K, C_6D_6) of *exo*-/*endo*-[(Ar*BIAN)Co(CyNC)(η^3-$P_4C(O)tBu$)] (**6a**); ○ *n*-hexane, * C_6D_6.

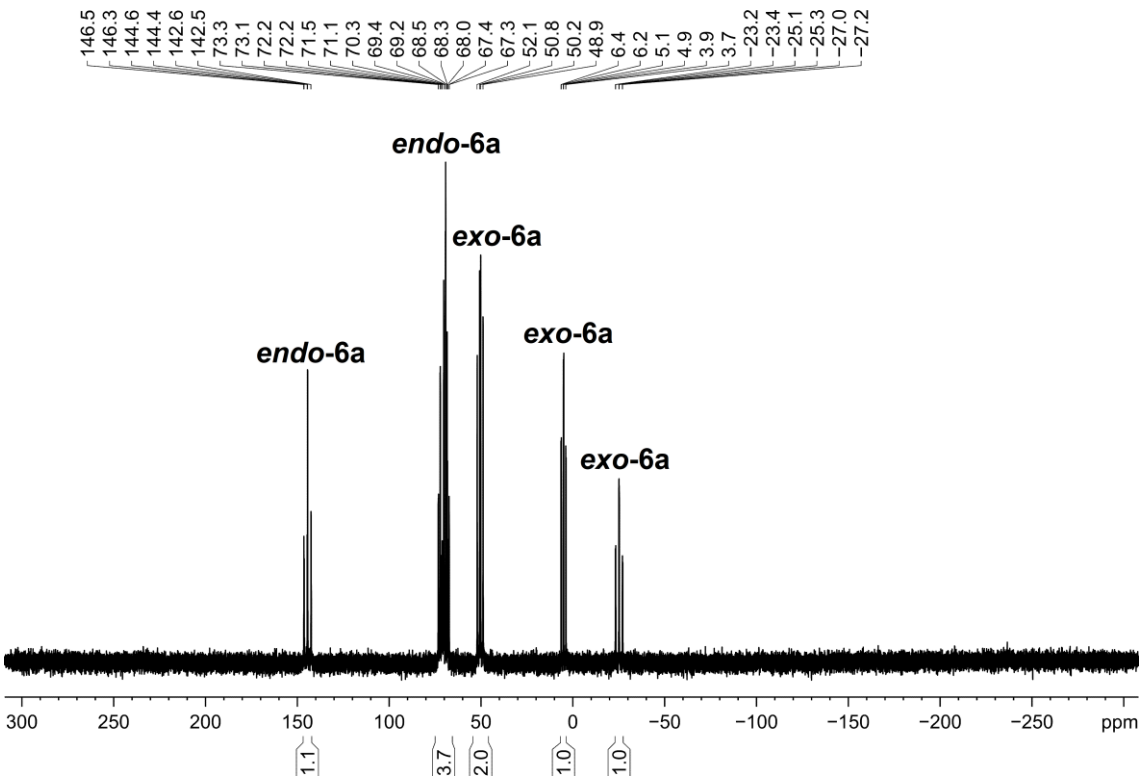

Figure S34. $^{31}P\{^{1}H\}$ NMR spectrum (161.98 MHz, 300 K, C_6D_6) of *exo*-/*endo*-[(Ar*BIAN)Co(CyNC)(η^3-$P_4C(O)t$Bu)] (**6a**).

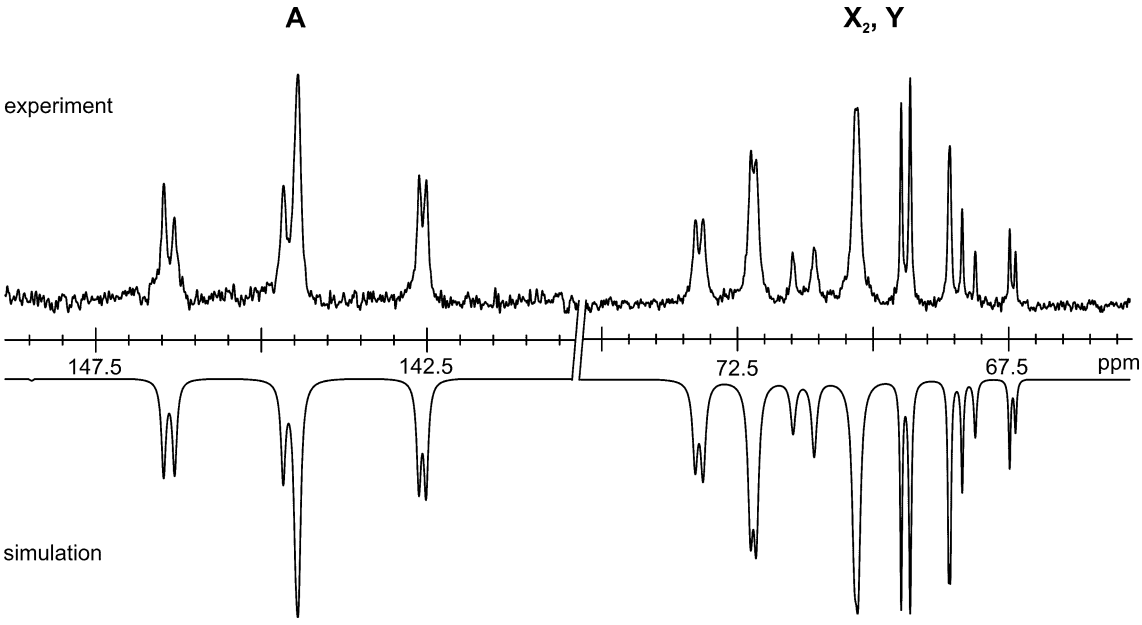

Figure S35. Section of the $^{31}P\{^{1}H\}$ NMR (161.98 MHz, 300 K, C_6D_6) of *endo*-[(Ar*BIAN)Co(CyNC)(η^3-$P_4C(O)t$Bu)] (*endo*-**6a**); experimental (upwards) and simulation (downwards).

Table S6. Chemical shifts and coupling constants from the iterative fit of the AX_2Y spin system and schematic representation of the *endo*-Co(CyNC)P_4C(O)*t*Bu core of *endo*-[(Ar*BIAN)Co(CyNC)(η^3-P_4C(O)*t*Bu)] (*endo*-**6a**).

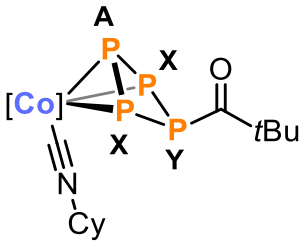

δ(A) = 144.5 ppm	$^1J_{AX}$ = −318.2 Hz
δ(X) = 71.7 ppm	$^1J_{XY}$ = −164.5 Hz
δ(Y) = 68.6 ppm	$^2J_{AY}$ = −5.4 Hz

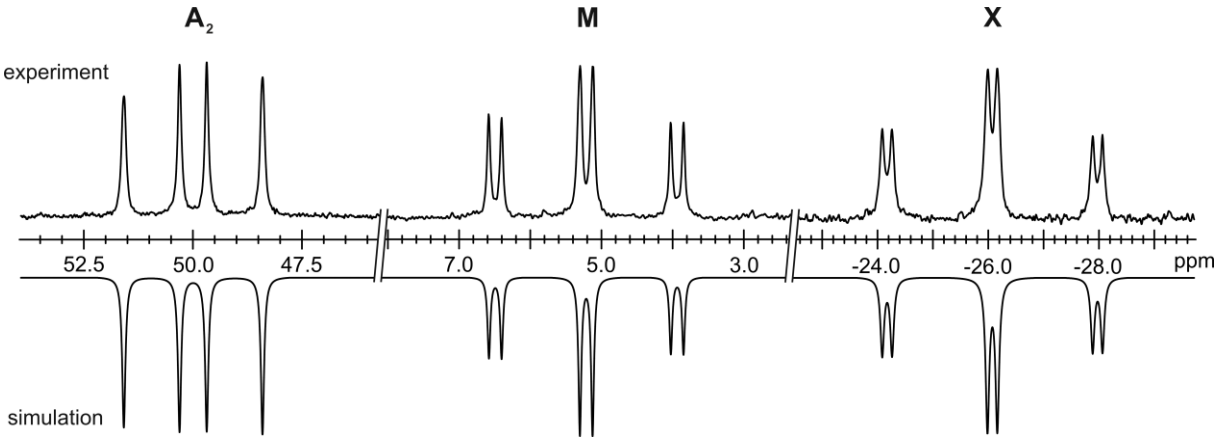

Figure S36. Section of the $^{31}P\{^1H\}$ NMR (161.98 MHz, 300 K, C_6D_6) *exo*-[(Ar*BIAN)Co(CyNC)(η^3-P_4C(O)*t*Bu)] (*exo*-**6a**); experimental (upwards) and simulation (downwards).

Table S7. Chemical shifts and coupling constants from the iterative fit of the A_2MX spin system and schematic representation of the *exo*-Co(CyNC)P_4C(O)*t*Bu core of *exo*-[(Ar*BIAN)Co(CyNC)(η^3-P_4C(O)*t*Bu)] (*exo*-**6a**).

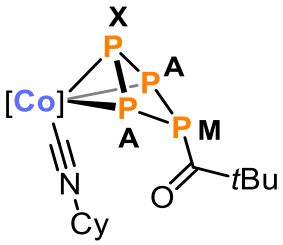

δ(A) = 50.0 ppm	$^1J_{AX}$ = −308.0 Hz
δ(M) = 5.2 ppm	$^1J_{AM}$ = −207.0 Hz
δ(X) = −26.1 ppm	$^2J_{MX}$ = 28.8 Hz

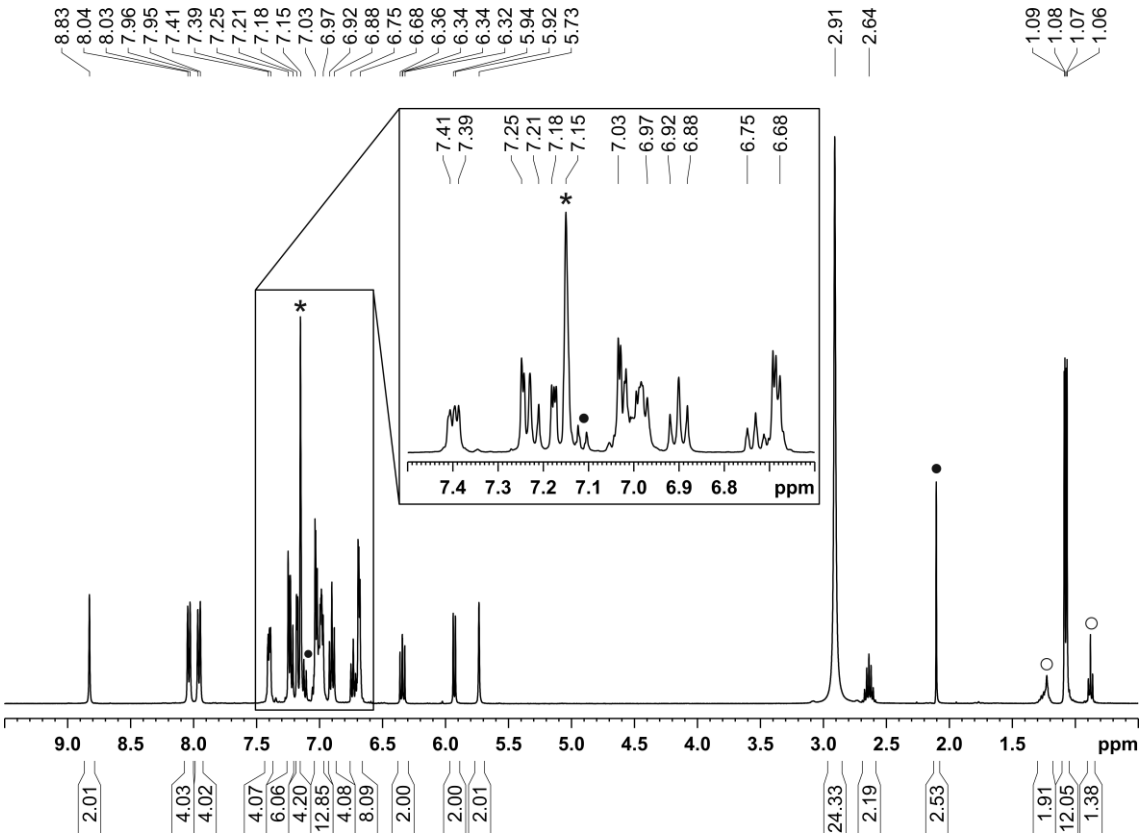

Figure S37. ^{1}H NMR spectrum (400.13 MHz, 300 K, C_6D_6) of [K(18c-6)][(Ar*BIAN)Co(CN)(η^3-P_3)] ([K(18c-6)]**8**); • toluene, ○ *n*-hexane, * C_6D_6.

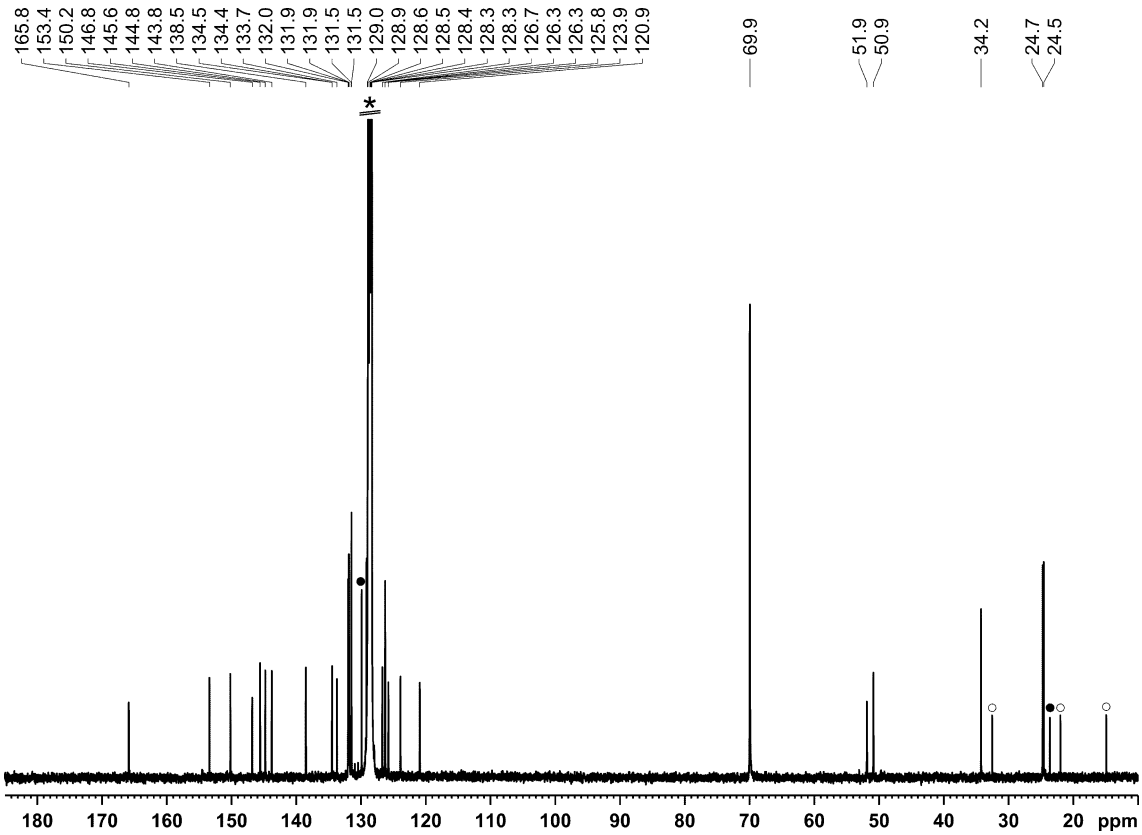

Figure S38. ^{13}C{^{1}H} NMR spectrum (100.61 MHz, 300 K, C_6D_6) of [K(18c-6)][(Ar*BIAN)Co(η^3-P_3)(CN)] ([K(18c-6)]**8**); • toluene, ○ *n*-hexane, * C_6D_6.

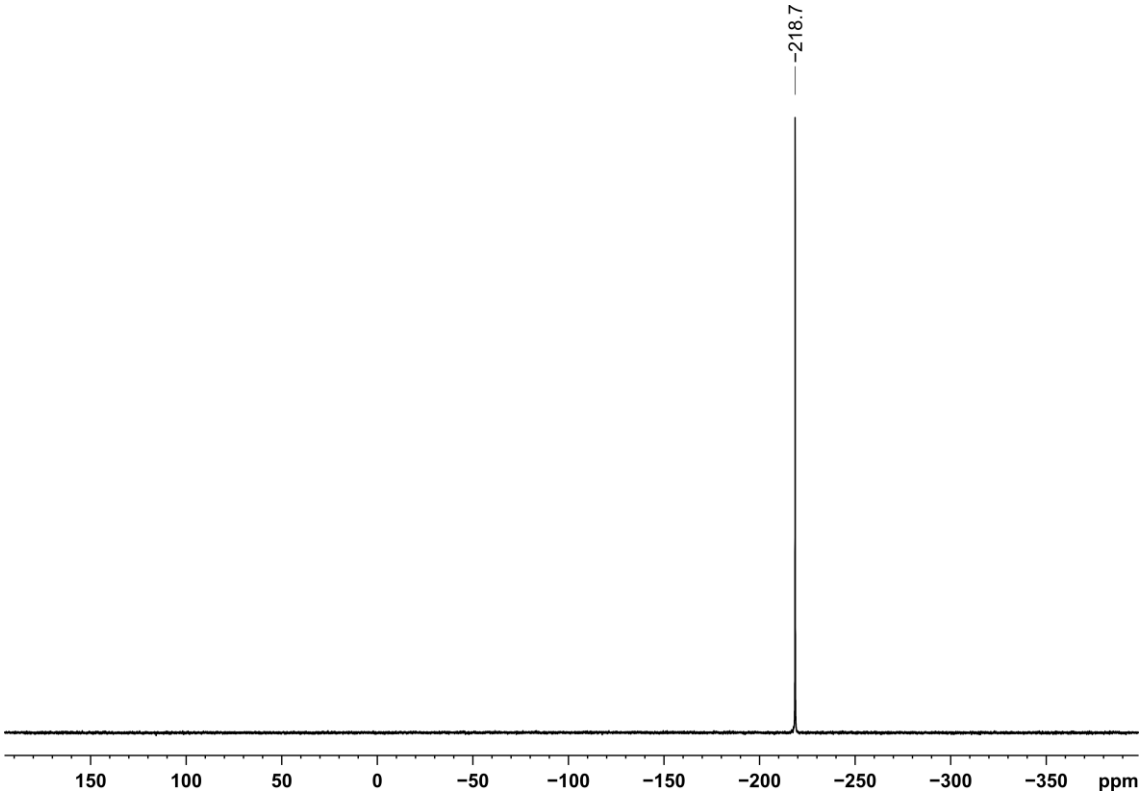

Figure S39. $^{31}P\{^{1}H\}$ NMR spectrum (162.04 MHz, 300 K, C_6D_6) of [K(18c-6)][(Ar*BIAN)Co(CN)(η^3-P_3)] ([K(18c-6)]**8**).

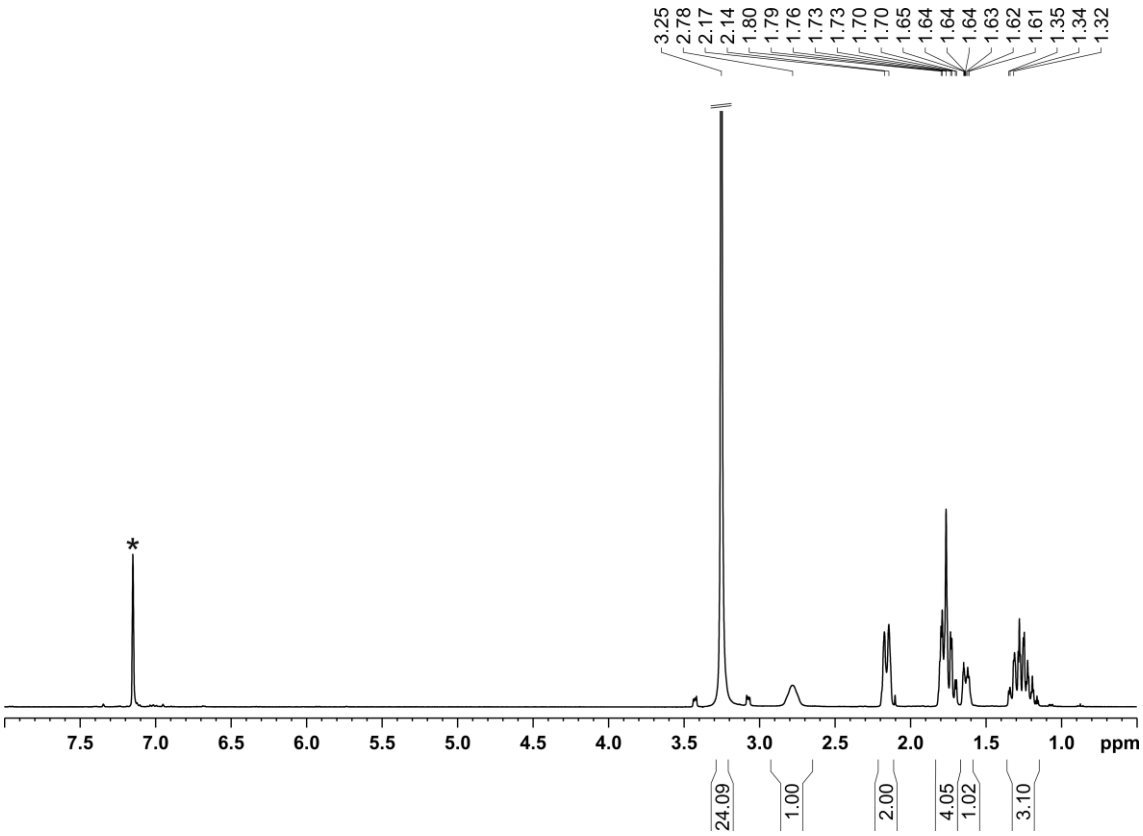

Figure S40. ^{1}H NMR spectrum (400.30 MHz, 300 K, C_6D_6) of [K(18c-6)][CyC(O)PCN] ([K(18c-6)]**9b**); * C_6D_6.

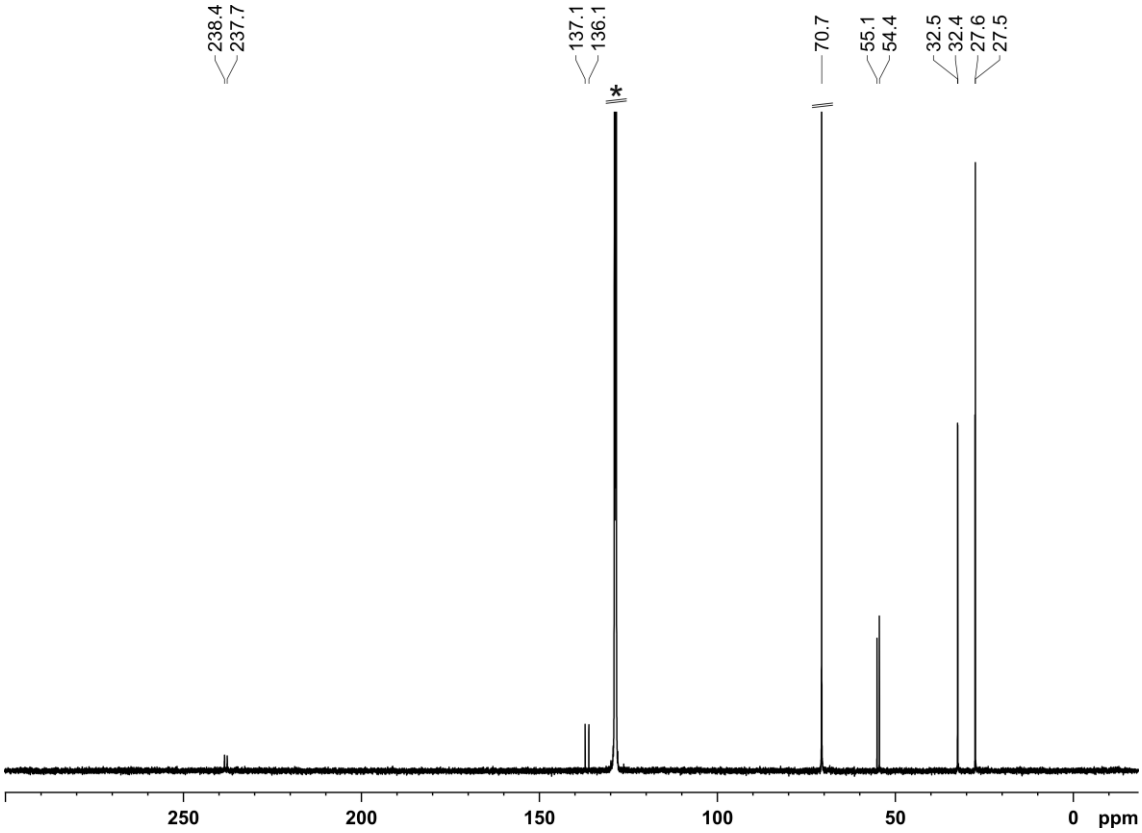

Figure S41. $^{13}C\{^{1}H\}$ NMR spectrum (100.61 MHz, 300 K, C_6D_6) of [K(18c-6)][CyC(O)PCN] ([K(18c-6)]**9b**); * C_6D_6.

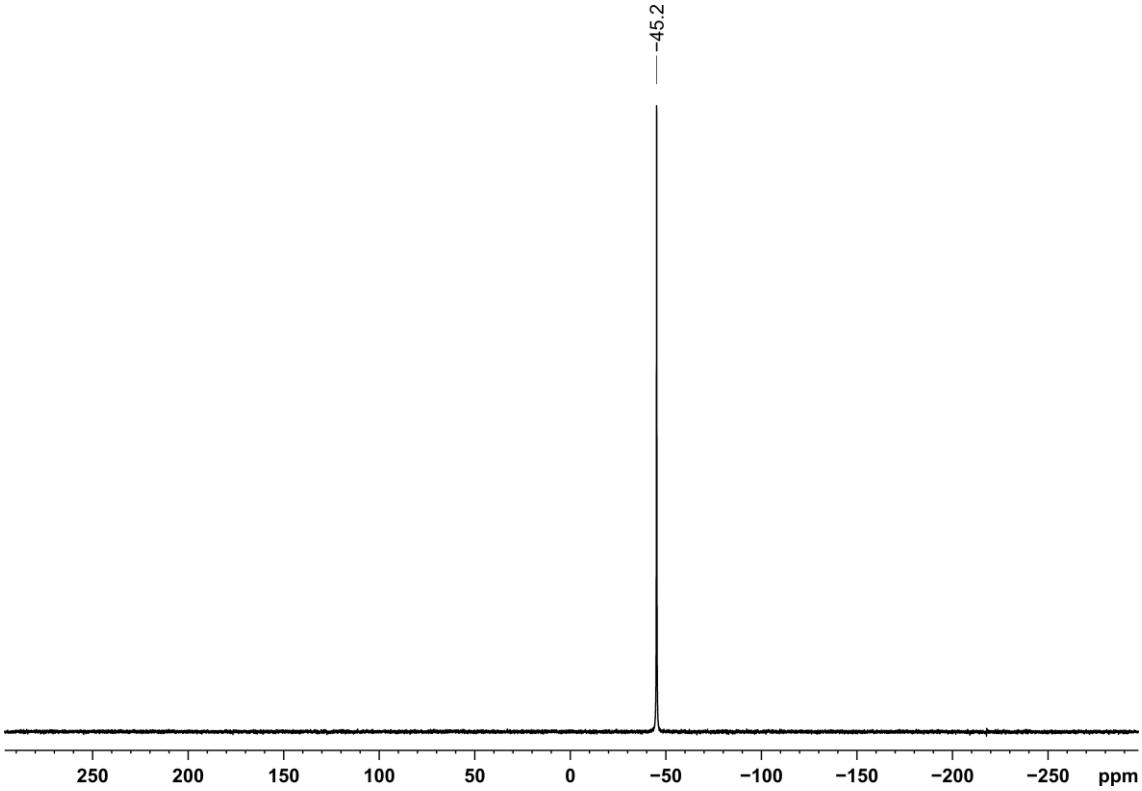

Figure S42. $^{31}P\{^{1}H\}$ NMR spectrum (162.04 MHz, 300 K, C_6D_6) of [K(18c-6)][CyCOPCN] ([K(18c-6)]**9b**).

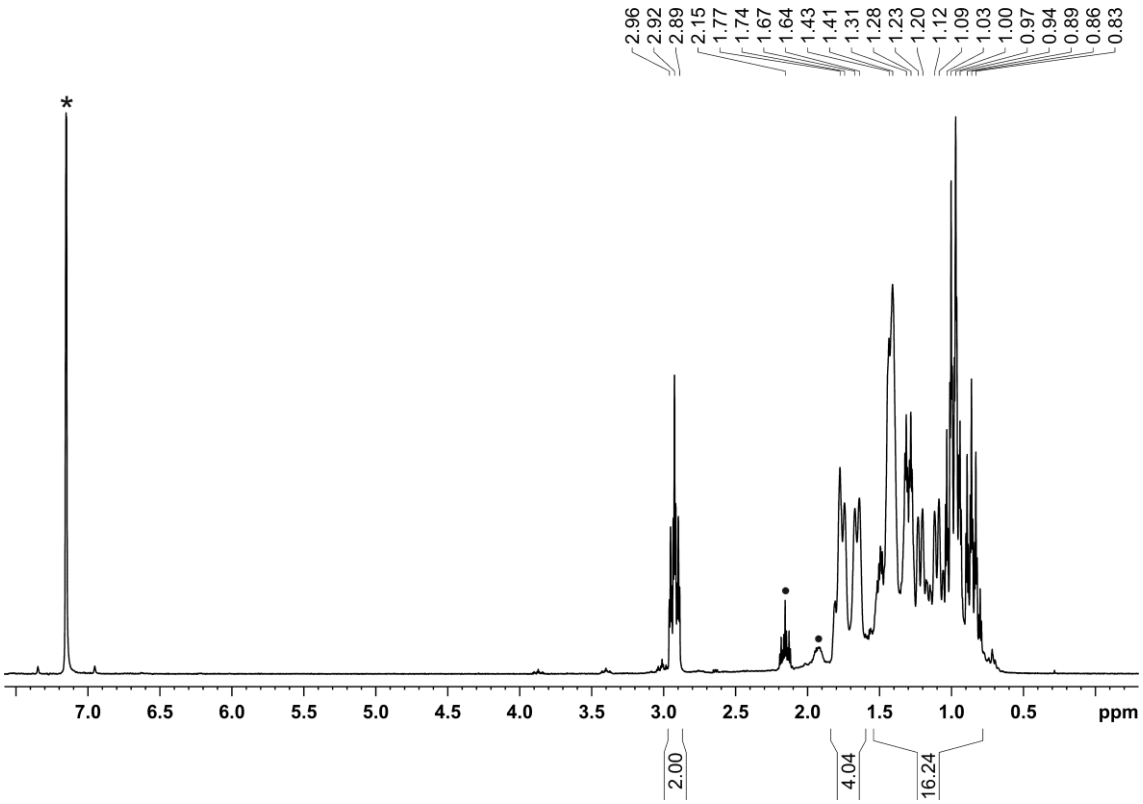

Figure S43. ^{1}H NMR spectrum (400.30 MHz, 300 K, C_6D_6) of $(CyC(O))_2PCN$ (**10**); • unknown impurity, * C_6D_6.

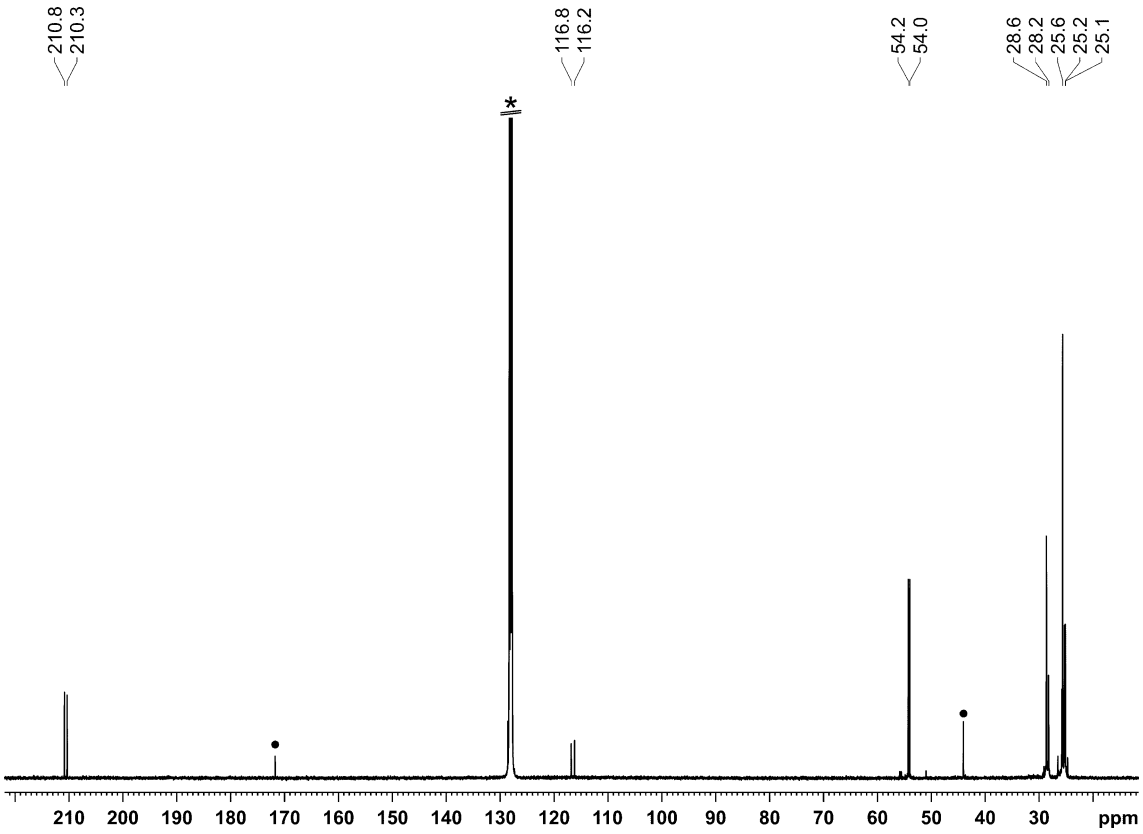

Figure S44. $^{13}C\{^{1}H\}$ NMR spectrum (100.61 MHz, 300 K, C_6D_6) of $(CyC(O))_2PCN$ (**10**); • unknown impurity, * C_6D_6.

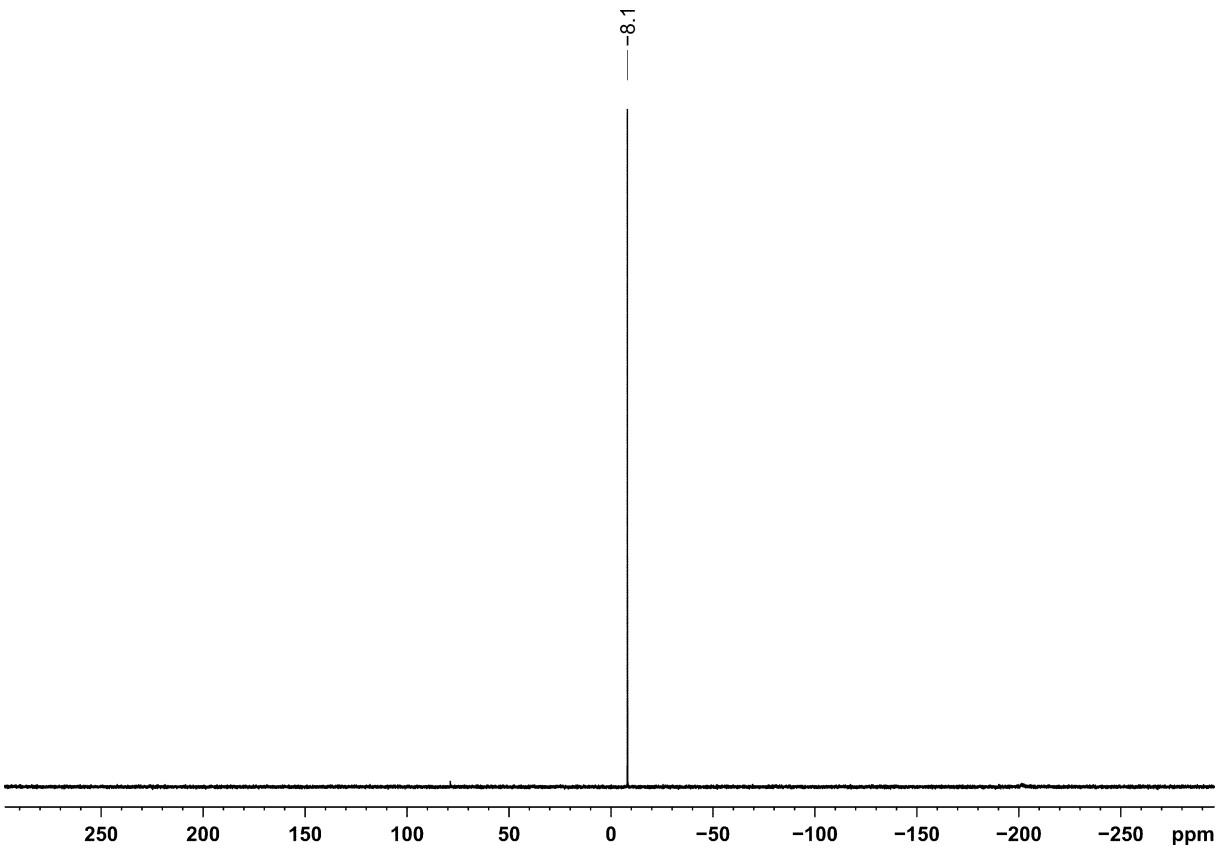

Figure S45. $^{31}P\{^{1}H\}$ NMR spectrum (162.04 MHz, 300 K, C_6D_6) of $(CyC(O))_2PCN$ (**10**).

2.4.3 Additional Experiments

5a was isolated in 75% yield and **6a** in 57% yield (*vide supra*). A series of reactions was performed according to the general procedure given below to further analyze the reactivity of **4a-d** toward Me_3SiCN and isocyanides R'NC (R' = Cy, *t*Bu, Mes, Ph). **5b**-**r** and **6b**-**6p** (see Table S8 for the substitutions of these derivatives) were not isolated, but were identified by $^{31}P\{^1H\}$ NMR spectroscopy (Figures S47-S52) and, for selected examples, by XRD (Figures S87-88). Crystals suitable for XRD analysis for *endo*-**6a**, co-crystals of *endo*-/*exo*-**6a** and **7** were obtained from a concentrated *n*-hexane solution after work-up according to the synthesis procedure for **6a** (*vide supra*). Crystals suitable for XRD analysis for *exo*-**6d and** *endo*-**6e** were obtained from a concentrated *n*-hexane solution after synthesis according to the general procedure given below.

General Procedure: **4a-d** (0.011 mmol) was dissolved in C_6D_6 (0.6 mL) in a J. Young valve NMR tube. The corresponding cyanide/Me_3SiCN was added neat. The NMR tube was sealed and the reaction mixture was analyzed by multinuclear NMR spectroscopy.

The ratio of **5** and **6** formed, and the ratio of *endo*- and *exo*- isomers of **6**, was found to vary depending on the substituents R and R', and the stoichiometry of **4** and R'NC. For example, reactions with **4d** generally favored the formation of *exo*-**6** over the *endo*-isomer. In a similar vein, reactions with MesCN favored the formation of *endo*-**6** (Figure S51), whereas reactions with PhCN favored the formation of *exo*-**6** (Figure S52).

Table S8. Residues of compounds **5a-r** and **6a-p**; **5a** was isolated in 75% yield and **6a** in 57%; remaining compounds were not isolated and identified by NMR spectroscopy and partially XRD; ratio of *endo*- and *exo*- isomers of **6a** may vary, depending on the substituents R and R'.

	R =	**R'=**	*endo-/exo-*	**R =**	**R'=**
5a	*t*Bu	$SiMe_3$	**6a**	*t*Bu	Cy
5b	Cy	$SiMe_3$	**6b**	Cy	Cy
5c	1-Ad	$SiMe_3$	**6c**	1-Ad	Cy
5d	Ph	$SiMe_3$	**6d**	Ph	Cy
5e	*t*Bu	Cy	**6e**	*t*Bu	*t*Bu
5f	Cy	Cy	**6f**	Cy	*t*Bu
5g	1-Ad	Cy	**6g**	1-Ad	*t*Bu
5h	Ph	Cy	**6h**	Ph	*t*Bu
5i	*t*Bu	*t*Bu	**6i**	*t*Bu	Mes
5j	Cy	*t*Bu	**6j**	Cy	Mes
5k	1-Ad	*t*Bu	**6k**	1-Ad	Mes
5l	Ph	*t*Bu	**6l**	Ph	Mes
5m	*t*Bu	Mes	**6m**	*t*Bu	Ph
5n	Cy	Mes	**6n**	Ph	Ph
5o	1-Ad	Mes			
5p	Ph	Mes			
5q	*t*Bu	Ph			
5r	Ph	Ph			

Reaction of [(Ar*BIAN)Co(η^3:η^1-P_4C(O)Ad)] (4c) toward CO gas

[(Ar*BIAN)Co(η^3:η^1-P_4C(O)Ad)] (**4c**) (16 mg, 0.011 mmol, 1.0 equiv.) was dissolved in C_6D_6 (0.6 mL) in a J. Young valve NMR tube. The purple solution was frozen using a cooling bath. The inert gas was exchanged for 1 atm CO, by evacuating the NMR tube and slowly thawing the solution until gas evolution from the solution ceased and repressurized it with CO. This process was repeated twice and the color changed to a dark blue. The J. Young valve NMR tube was closed and analyzed by $^{31}P\{^1H\}$ NMR spectroscopy (see Figure S46).

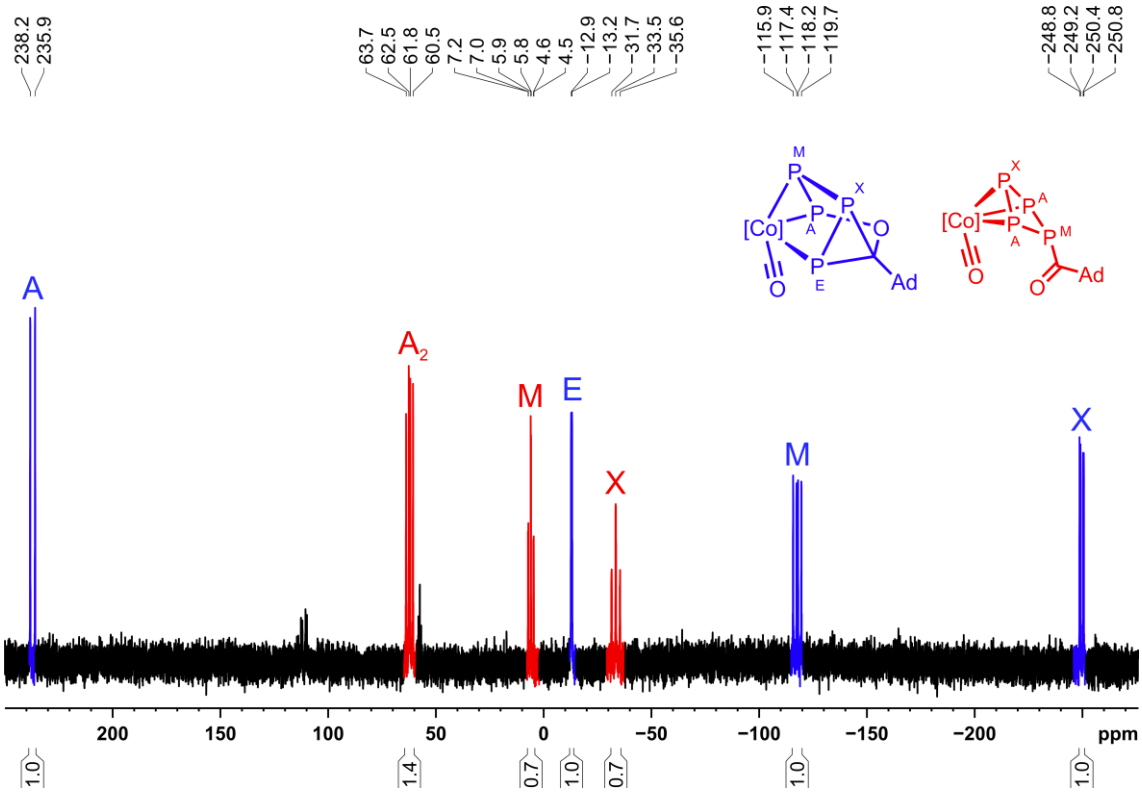

Figure S46. $^{31}P\{^1H\}$ NMR spectrum (162.04 MHz, 300 K, C_6D_6) of the reaction between [(Ar*BIAN)Co(η^3:η^1-P_4C(O)Ad)] (**4c**) toward CO gas exhibiting two sets of signals attributed to two proposed compounds; *blue*: δ/ppm = −249.8 (dd, 1P, P_X), −117.8 (dd, 1P, P_M), −13.1 (d, 1P, P_E), 237.9 (d, 1P, P_A). *red*: δ/ppm = −33.5 (dt, 1P, P_X), 5.8 (dt, 1P, P_M), 62.2 (dd, 2P, P_A); [Co] = (Ar*BIAN)Co.

Reactions of [(Ar*BIAN)Co(η^3:η^1-$P_4C(O)R$)] (4b: R = Cy, 4c: R = 1-Ad, 4d: R = Ph) with Me_3SiCN

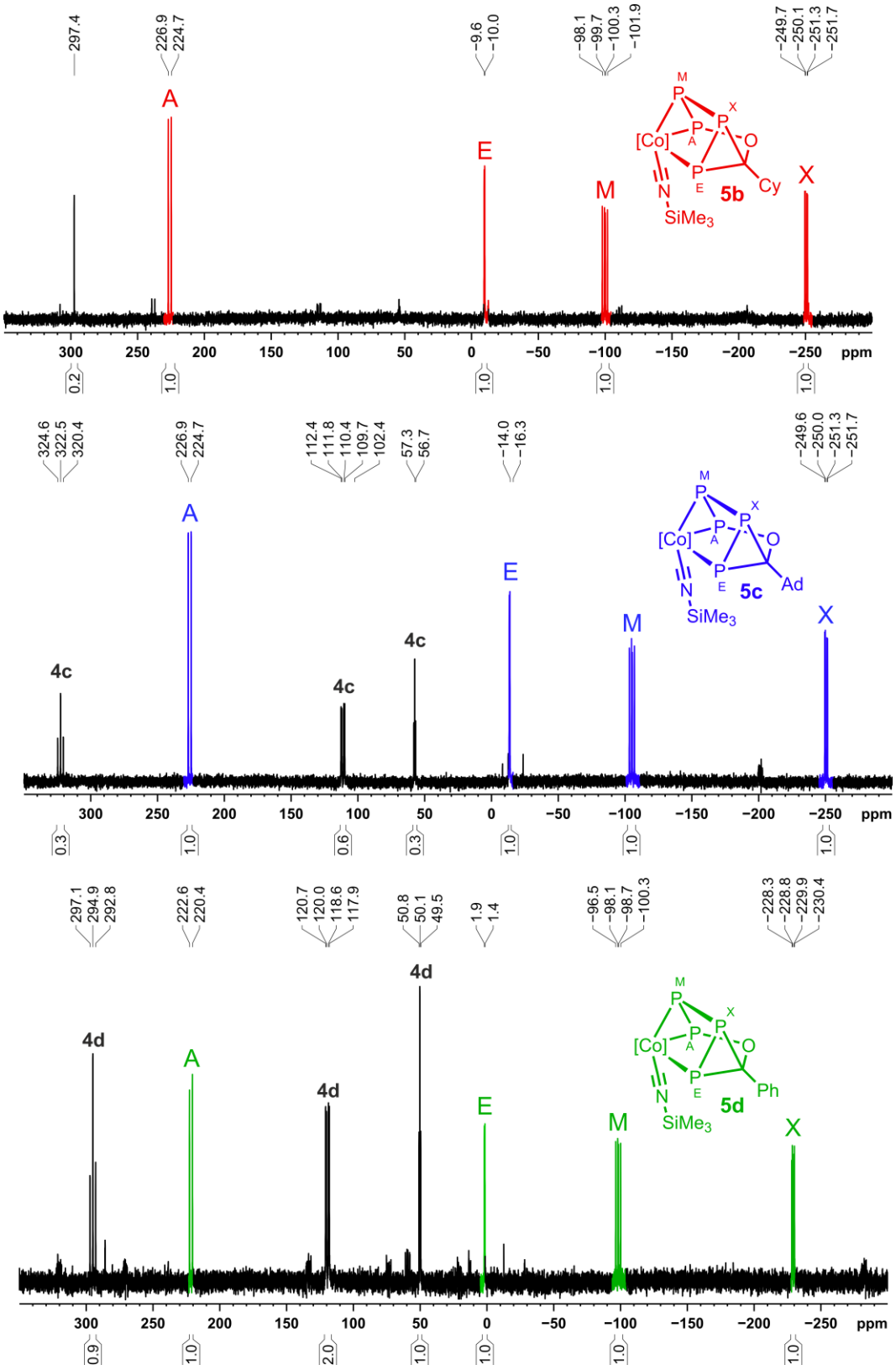

Figure S47. $^{31}P\{^1H\}$ NMR spectra (162.04 MHz, 300 K, C_6D_6) of the reaction of [(Ar*BIAN)Co(η^3:η^1-$P_4C(O)R$)] (**4b-d**) with Me_3SiCN exhibiting an AEMX spin system attributed to proposed compounds **5b-d**; *red* (**5b**): δ/ppm = −250.7 (dd, 1P, P_X), −100.0 (dd, 1P, P_M), −9.8 (br d, 1P, P_E), 225.7 (d, 1P, P_A); *blue* (**5c**): δ/ppm = −250.7 (dd, 1P, P_X), −105.2 (dd, 1P, P_M), −13.7 (br d, 1P, P_E), 225.9 (d, 1P, P_A); *green* (**5d**): δ/ppm = −229.4 (dd, 1P, P_X), −98.4 (dd, 1P, P_M), 1.6 (br d, 1P, P_E), 221.5 (d, 1P, P_A); [Co] = (Ar*BIAN)Co.

Reactions of [(Ar*BIAN)Co(η^3:η^1-$P_4C(O)tBu$)] (4a) with isocyanide CyNC

[(Ar*BIAN)Co(η^3:η^1-$P_4C(O)tBu$)] (**4a**) was dissolved in C_6D_6 (0.6 mL) in a J. Young valve NMR tube and various equivalents of cyclohexyl isocyanide were added in each case (*vide infra*). The purple solution changed color to a dark green. The J. Young valve NMR tube was closed and analyzed by $^{31}P\{^1H\}$ NMR spectroscopy (see Figure S48).

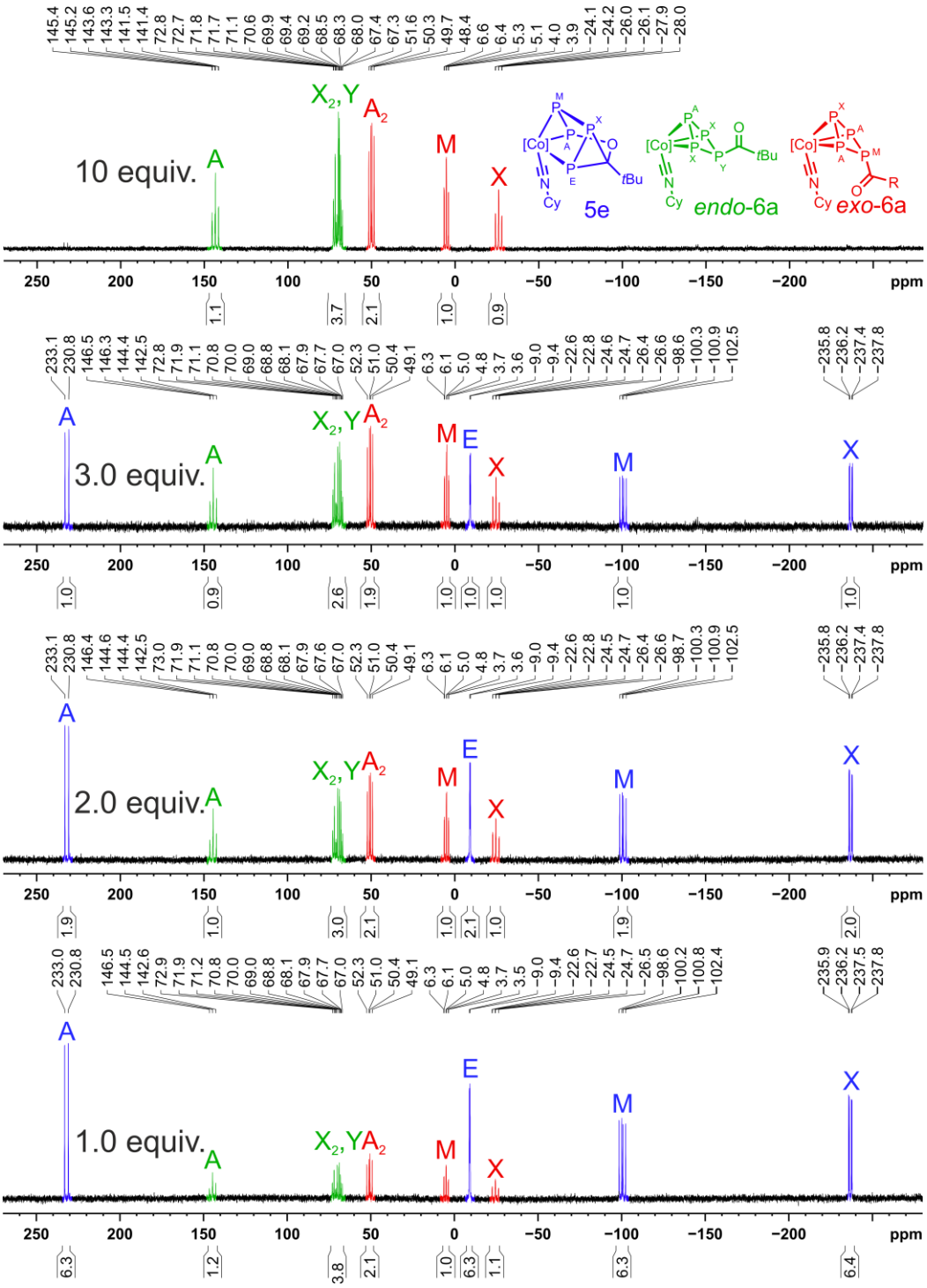

Figure S48. $^{31}P\{^1H\}$ NMR spectra (162.04 MHz, 300 K, C_6D_6) of the reaction of [(Ar*BIAN)Co(η^3:η^1-$P_4C(O)tBu$)] (**4a**) with different equivalents of CyNC showing three spin spin systems attributed to *blue* (**5e**): δ/ppm = −236.9 (dd, 1P, P_X), −100.5 (dd, 1P, P_M), −9.1 (br d, 1P, P_E), 231.9 (d, 1P, P_A); *green* (*endo*-**6a**): δ/ppm = 67.0-73.0 (m, 3P, P_{XY}), 142.5-146.4 (m, 1P, P_A); *red* (*exo*-**6a**): δ/ppm = −24.5 (dt, 1P, P_X), 5.0 (dt, 1P, P_M), 50.5 (dd, 2P, P_A**)**; [Co] = (Ar*BIAN)Co.

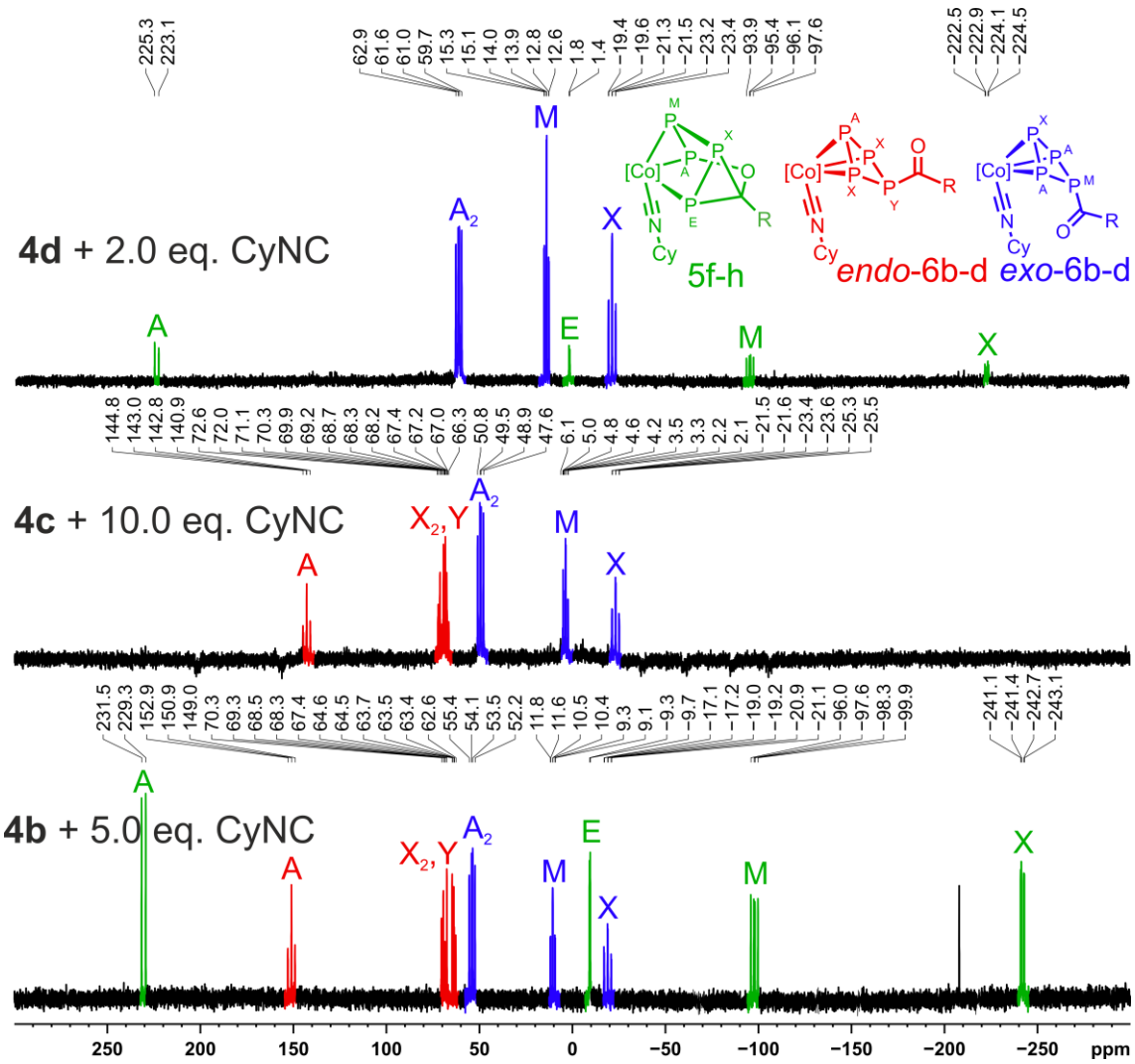

Figure S49. $^{31}P\{^{1}H\}$ NMR spectra (162 MHz, 300 K, C_6D_6) of the reactions of [(Ar*BIAN)Co(η^3:η^1-$P_4C(O)R$)] (**4b-d**) with different equivalents of CyNC showing three spin systems attributed to different structures shown in *green* (**5f-h**), *red* (*endo*-**6b-d**) and *blue* (*exo*-**6b-d**); [Co] = (Ar*BIAN)Co.

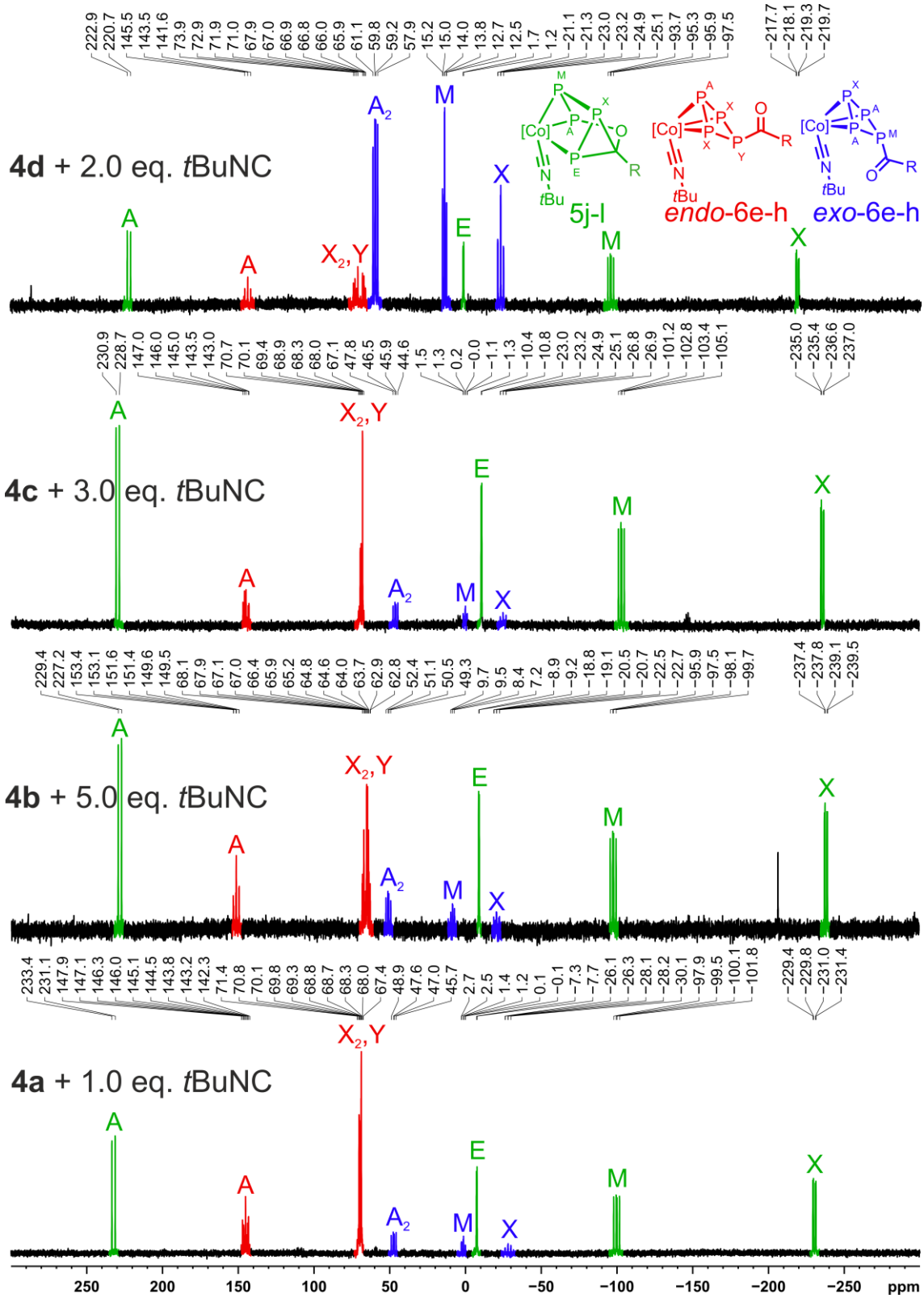

Figure S50. $^{31}P\{^{1}H\}$ NMR spectra (162 MHz, 300 K, C_6D_6) of the reactions of [(Ar*BIAN)Co(η^3:η^1-$P_4C(O)R$)] (**4a-d**) with different equivalents of *t*BuNC showing three spin systems attributed to different structures shown in *green* (**5j-l**), *red* (*endo*-**6e-h**) and *blue* (*exo*-**6e-h**); [Co] = (Ar*BIAN)Co.

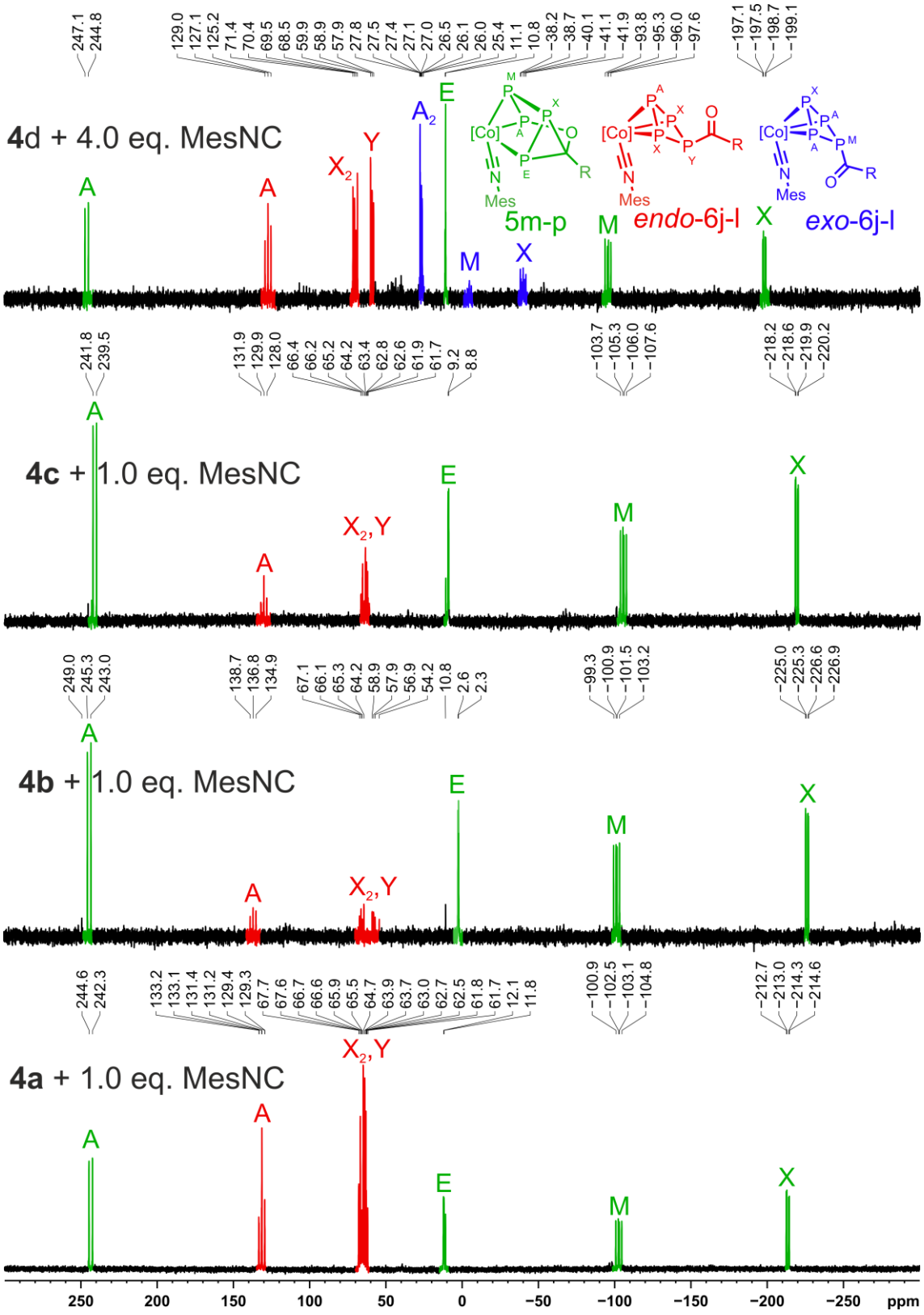

Figure S51. $^{31}P\{^{1}H\}$ NMR spectra (162 MHz, 300 K, C_6D_6) of the reactions of [(Ar*BIAN)Co(η^3:η^1-$P_4C(O)R$)] (**4a-d**) with different equivalents of MesNC showing three spin systems attributed to different structures shown in *green* (**5m-p**), *red* (*endo*-**6j-l**) and *blue* (*exo*-**6j-l**); Mes = 2,4,6-$Me_3C_6H_2$, [Co] = (Ar*BIAN)Co.

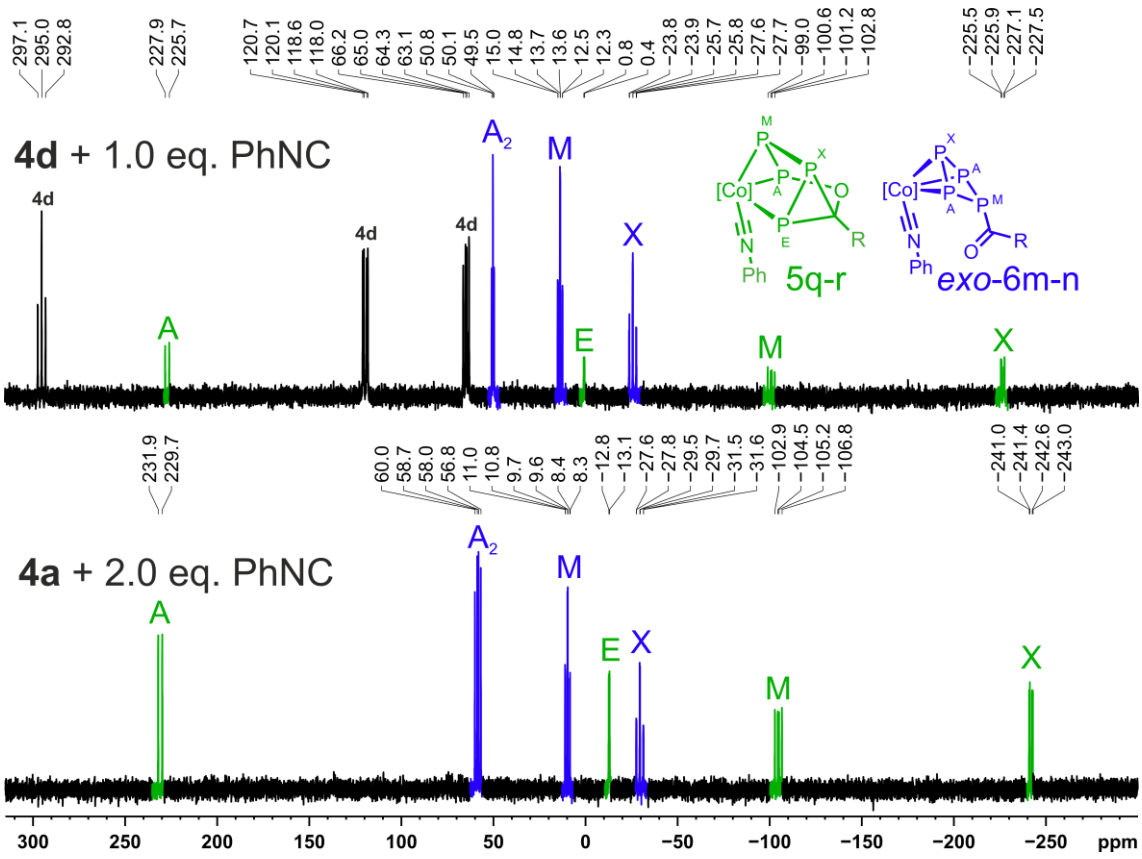

Figure S52. $^{31}P\{^1H\}$ NMR spectra (162 MHz, 300 K, C_6D_6) of the reactions of [(Ar*BIAN)Co(η^3:η^1-$P_4C(O)R$)] (**4a** and **4d**) with different equivalents of PhNC showing two spin systems attributed to different structures shown in *green* (**5q-r**) and *blue* (*exo*-**6m-n**); [Co] = (Ar*BIAN)Co.

[K(18c-6)]**9b** was isolated in 31% yield (*vide supra*). A series of reactions was performed according to the general procedure given below to further analyze the reactivity of **4a-d** toward KCN. **9a-d**$^-$ were not isolated, but were identified by $^{31}P\{^1H\}$ NMR spectroscopy (Figures S53-S56) and, for selected examples, by XRD (Figures S86-S87, R = *t*Bu, Cy, Ph). Crystals of [K(18c-6)])**9a** and [K(18c-6)])**9d** were grown from saturated toluene solutions.

General Procedure: In a glovebox, **4a-d** (0.02 mmol), KCN (2.2 equiv.) and 18c-6 (2.2 equiv.) were suspended in THF (2.0 mL). The magenta mixture was stirred for three days over which time the color changed to a deep purple. 0.6 mL of this reaction mixture was transferred to a J. Young valve NMR tube with a C_6D_6-capillary and the reaction mixture was analyzed by $^{31}P\{^1H\}$ NMR spectroscopy.

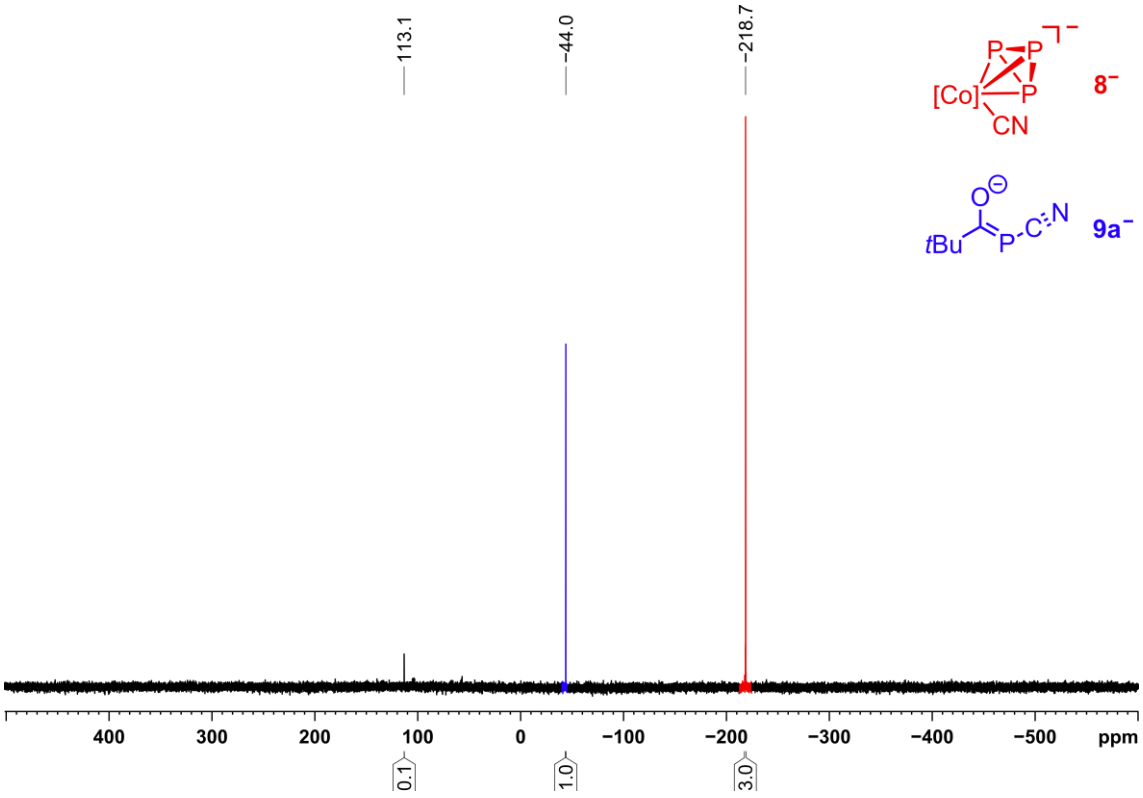

Figure S53. $^{31}P\{^1H\}$ NMR spectrum (162 MHz, 300 K, C_6D_6-capillary) of the reaction between [(Ar*BIAN)Co(η^3:η^1-P_4C(O)*t*Bu)] (**4a**) toward KCN/18c-6 exhibiting two singlets in a 1:3 ratio; [Co] = (Ar*BIAN)Co.

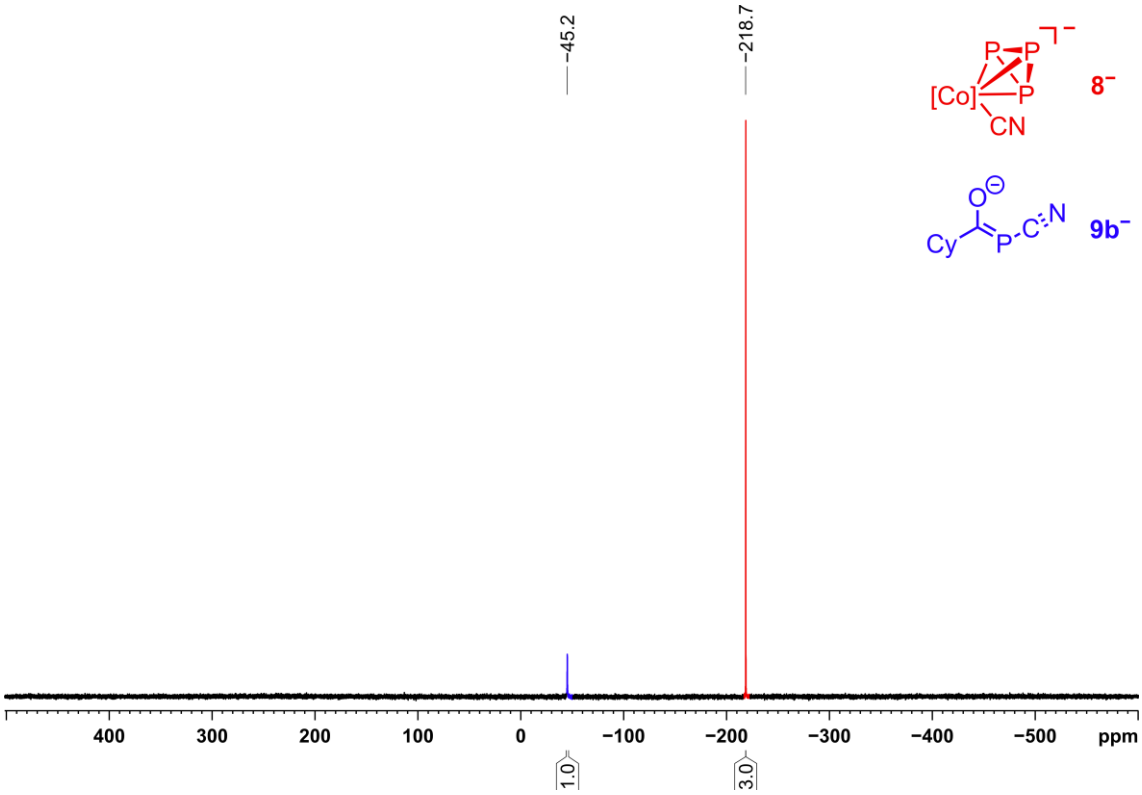

Figure S54. $^{31}P\{^{1}H\}$ NMR spectrum (162 MHz, 300 K, C_6D_6-capillary) of the reaction between [(Ar*BIAN)Co(η^3:η^1-$P_4C(O)Cy$)] (**4b**) toward KCN/18c-6 exhibiting two singlets in a 1:3 ratio; [Co] = (Ar*BIAN)Co.

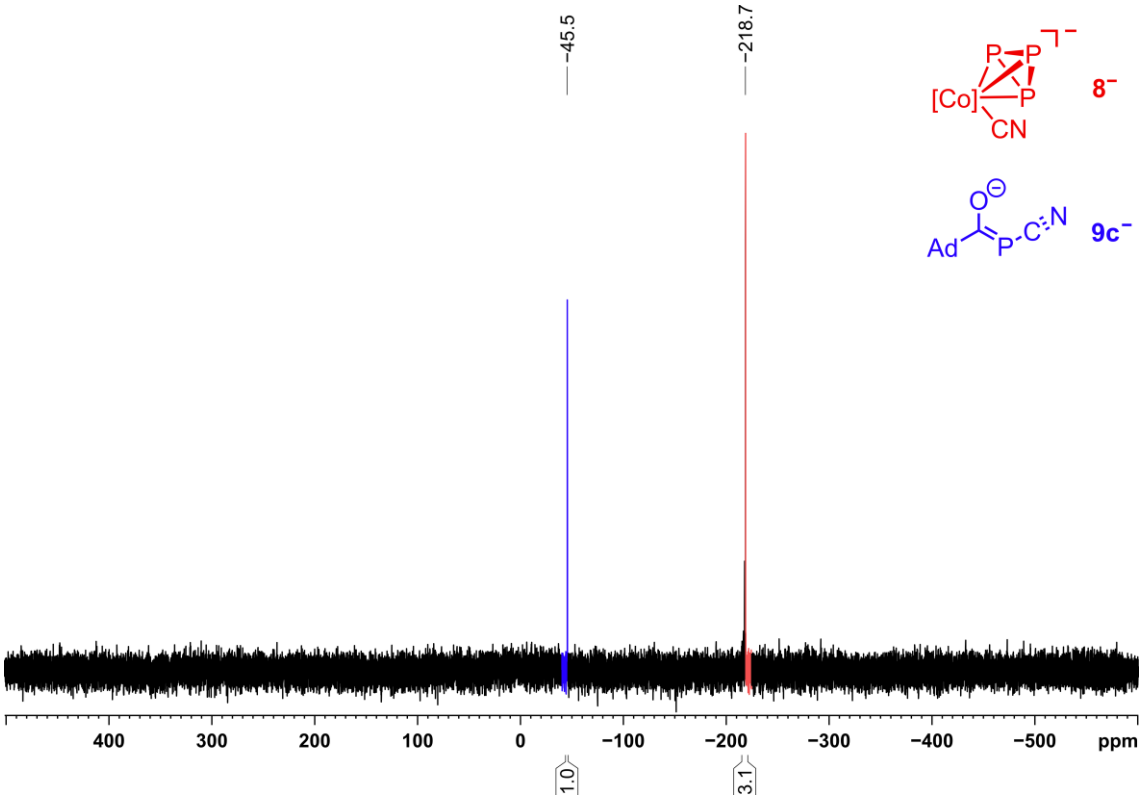

Figure S55. $^{31}P\{^{1}H\}$ NMR spectrum (162 MHz, 300 K, C_6D_6-capillary) of the reaction between [(Ar*BIAN)Co(η^3:η^1-$P_4C(O)Ad$)] (**4c**) toward KCN/18c-6 exhibiting two singlets in a 1:3 ratio; [Co] = (Ar*BIAN)Co.

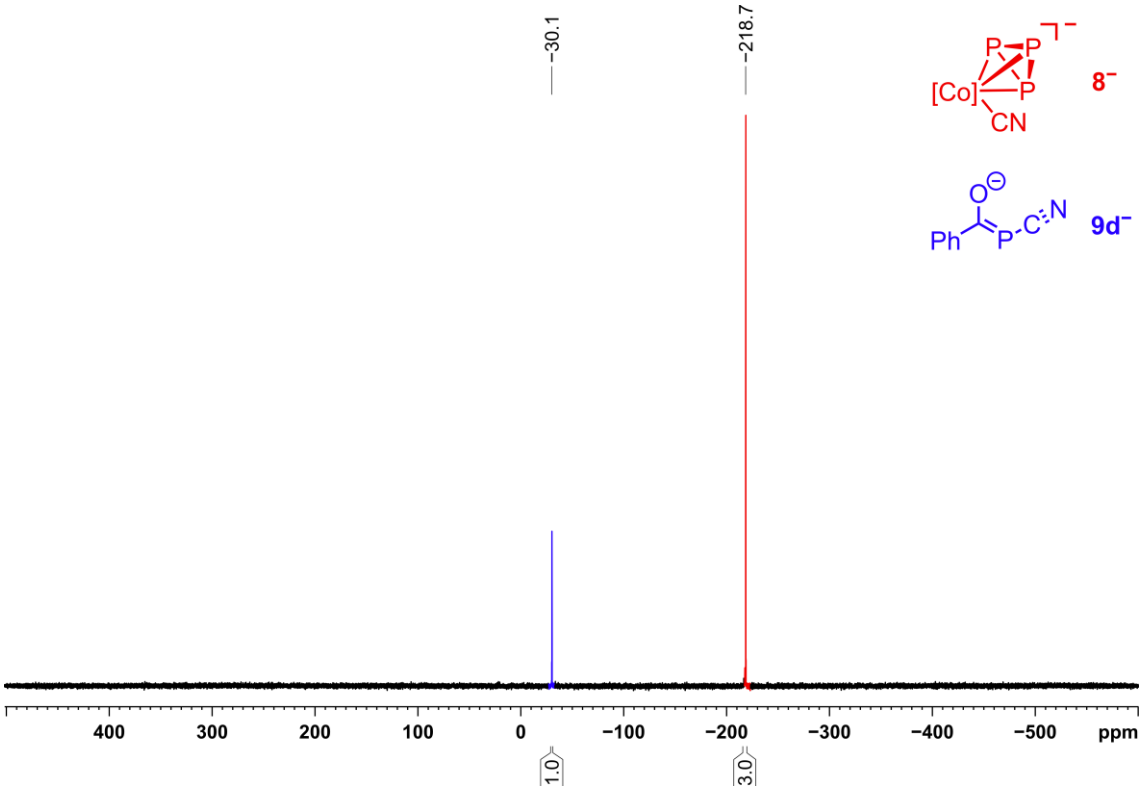

Figure S56. $^{31}P\{^{1}H\}$ NMR spectrum (162.04 MHz, 300 K, C_6D_6-capillary) of the reaction between [(Ar*BIAN)Co(η^3:η^1-P_4C(O)Cy)] (**4b**) toward KCN/18c-6 exhibiting two singlets in a 1:3 ratio; [Co] = (Ar*BIAN)Co.

2.4.4 Reaction monitoring

In a glovebox $[Et_4N]CN$ (3.8 mg, 0.024 mmol, 2.2 equiv.) was added to a thawing solution of [(Ar*BIAN)Co(η^3:η^1-$P_4C(O)Ph$)] (**4d**) (15.0 mg, 0.011 mmol, 1.0 equiv) in 0.6 mL of THF-d_8 in a J. Young valve NMR tube. The first NMR measurements started 15 minutes later. ^1H and $^{31}P\{^1H\}$ NMR measurements were performed at a temperature of 298 K. After 3.5 h, $^{31}P\{^1H\}$ and ^1H NMR measurements were performed every 25 min until a total reaction time of 14 hours. Figure S57 (*vide infra*) shows the sum over 35 of 35 $^{31}P\{^1H\}$ NMR spectra recorded during this time.

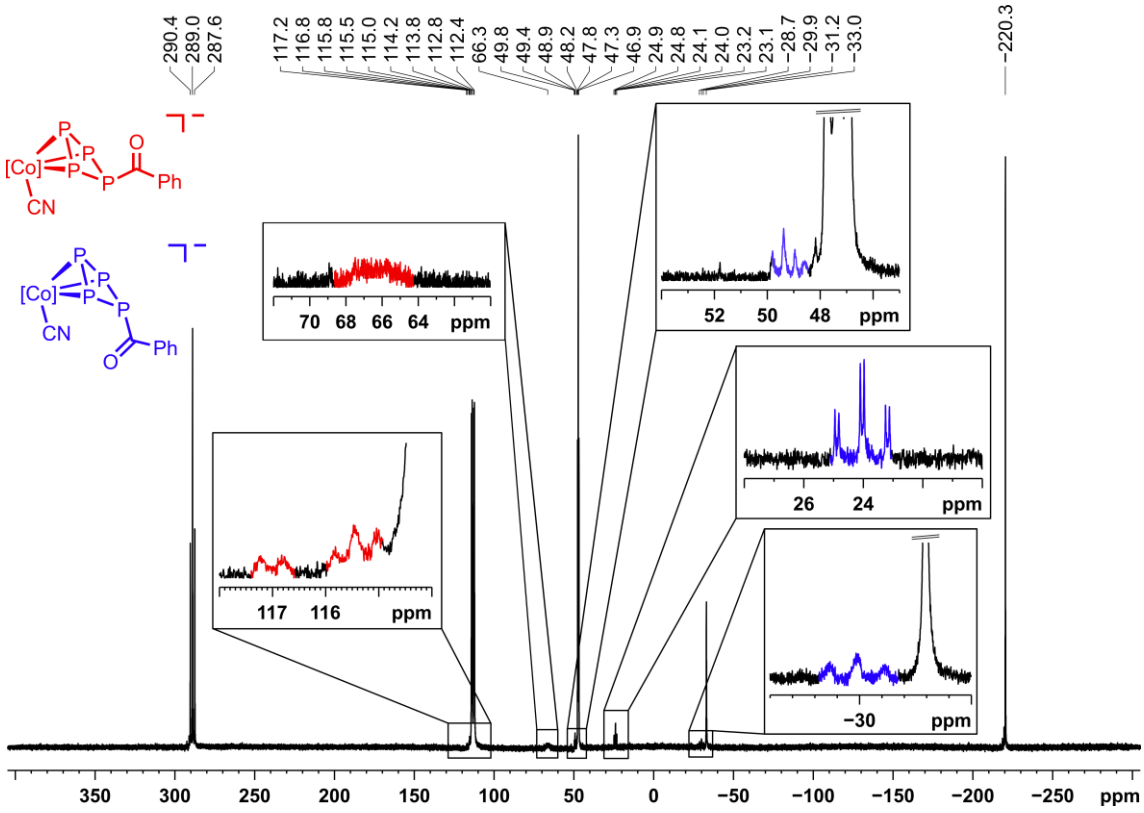

Figure S57. Sum over 35 $^{31}P\{^1H\}$ NMR spectra (242.90 MHz, 298 K, THF-d_8) of the reaction between [(Ar*BIAN)Co(η^3:η^1-$P_4C(O)Ph$)] (**4d**) and $[Et_4N]CN$ recorded every 25 min from 3.5 h to 14 h of total reaction time. The spectrum shows two sets of intermediate signals marked in *red* and *blue* attributed to two proposed structures.

In a J. Young valve NMR tube solid **6a** (15 mg, 0.010 mmol) was dissolved in toluene-d_8 (0.6 mL), which was precooled to −80 °C. The dark green mixture was kept at this temperature and the first NMR measurements started 10 minutes later. $^{31}P\{^1H\}$ NMR measurements were performed and the temperature stepwise increased (*vide infra*; Figure S58 and Figure S59).

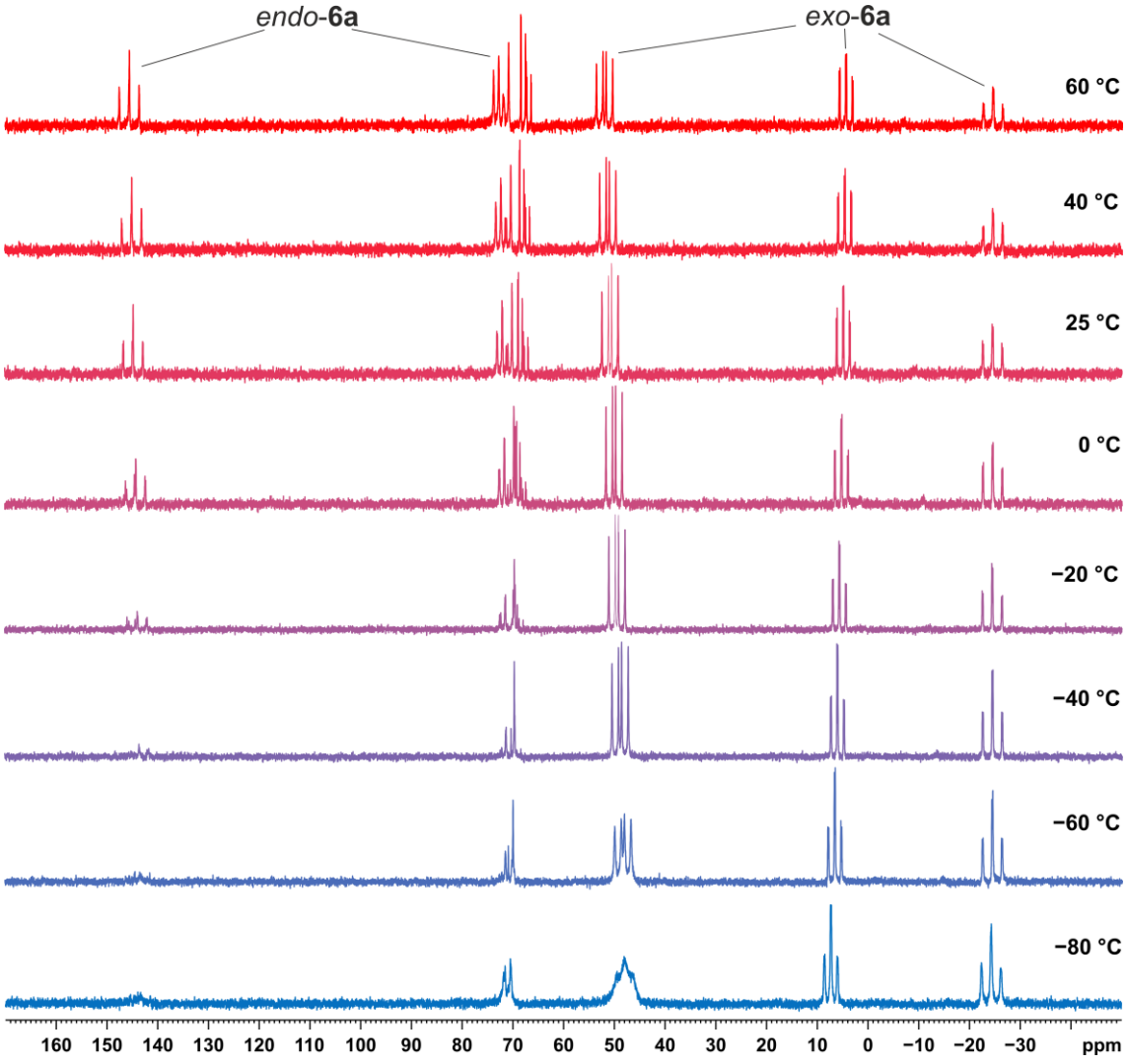

Figure S58. $^{31}P\{^1H\}$ NMR monitoring (161.98 MHz, toluene-d_8) of *endo*-/*exo*[(Ar*BIAN)Co(CyNC)(η^3-P_4C(O)*t*Bu)] (**6a**).

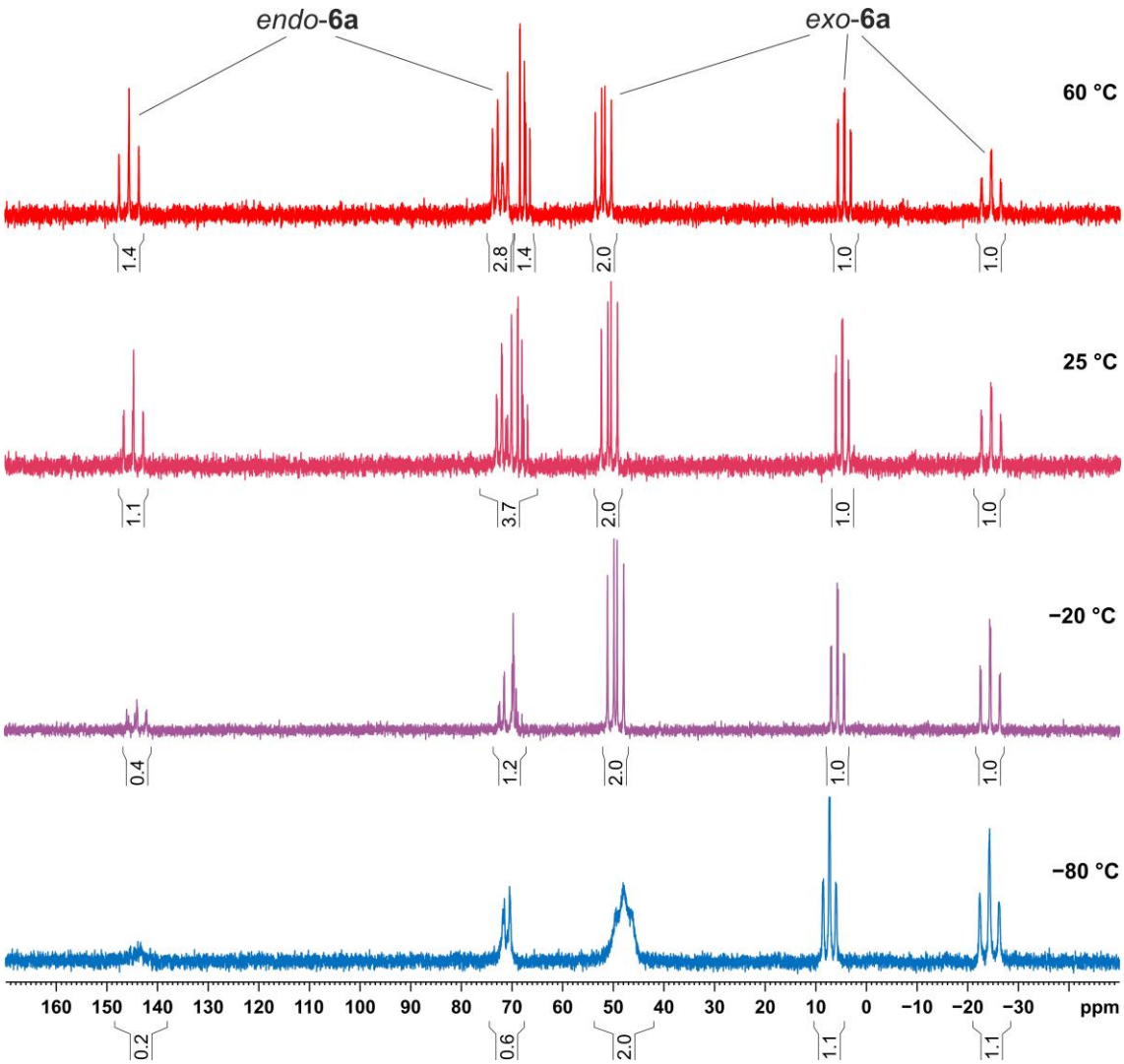

Figure S59. Selected spectra of the $^{31}P\{^{1}H\}$ NMR monitoring (161.98 MHz, toluene-d_8) of [(Ar*BIAN)Co(CyNC)(η^3-$P_4C(O)tBu$)] (**6a**) with integrals shown.

To solid **4a** (15 mg, 0.010 mmol, 1.0 equiv.) in a J. Young valve NMR tube a precooled (−80 °C) solution of cyclohexyl isocyanide (3.6 mg, 4.1 µL, 0.033 mmol, 3.0 equiv.) in toluene-d_8 (0.6 mL), was added at −80 °C. The magenta mixture was kept at this temperature and the first NMR measurements started 10 minutes later. $^{31}P\{^1H\}$ NMR measurements were performed and the temperature stepwise increased (*vide infra*; Figure S60). Spectra below −20 °C were not plotted, as no reaction was observed and only signals for **4a** were detected.

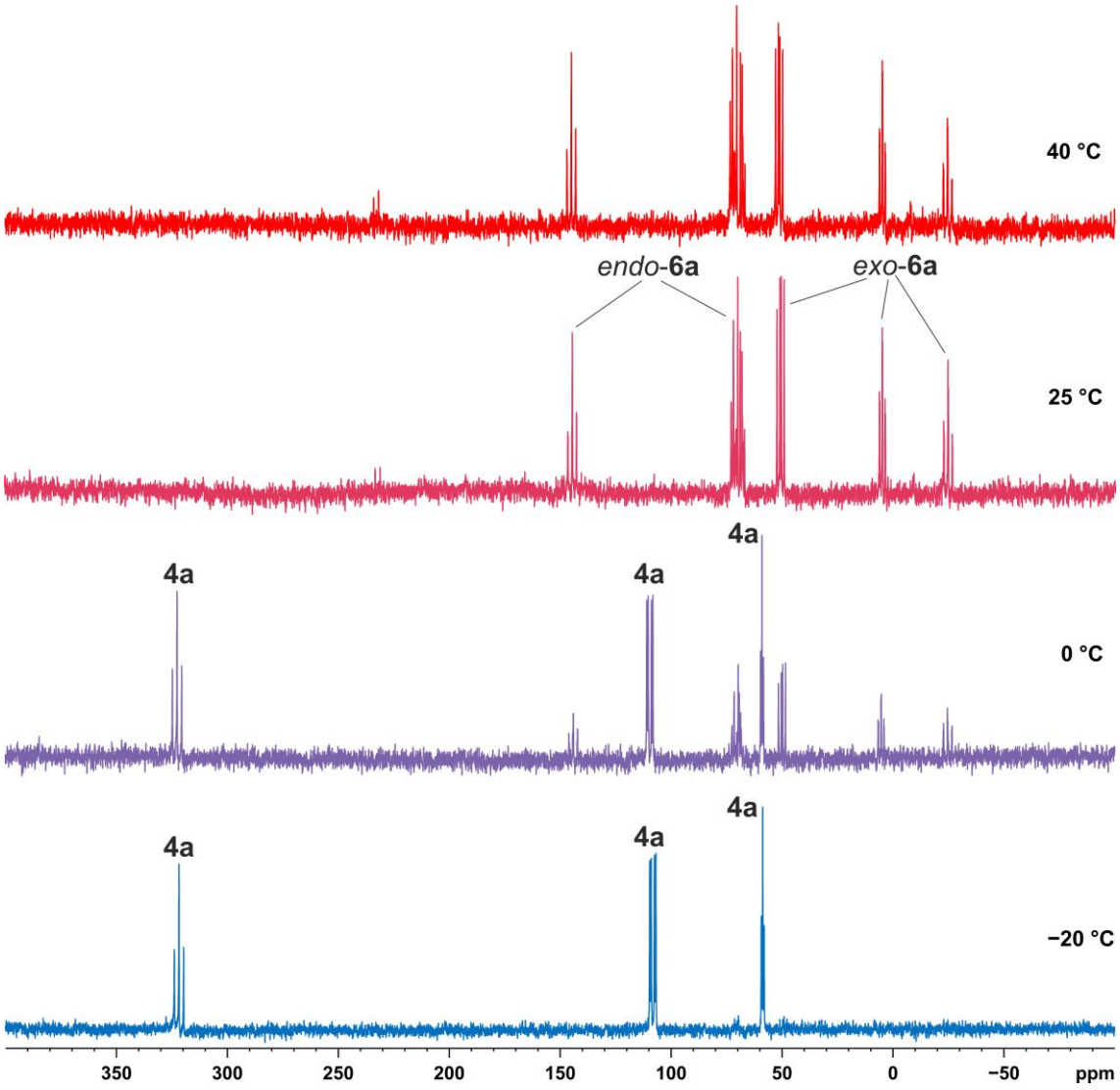

Figure S60. $^{31}P\{^1H\}$ NMR monitoring (161.98 MHz, toluene-d_8) of of the reaction between [(Ar*BIAN)Co(η^3:η^1-P_4C(O)*t*Bu)] (**4a**) toward 3.0 eq. CyNC affording *endo*-/*exo*-[(Ar*BIAN)Co(CyNC)(η^3-P_4C(O)*t*Bu)] (**6a**).

2.4.5 Proposed Reaction Mechanism

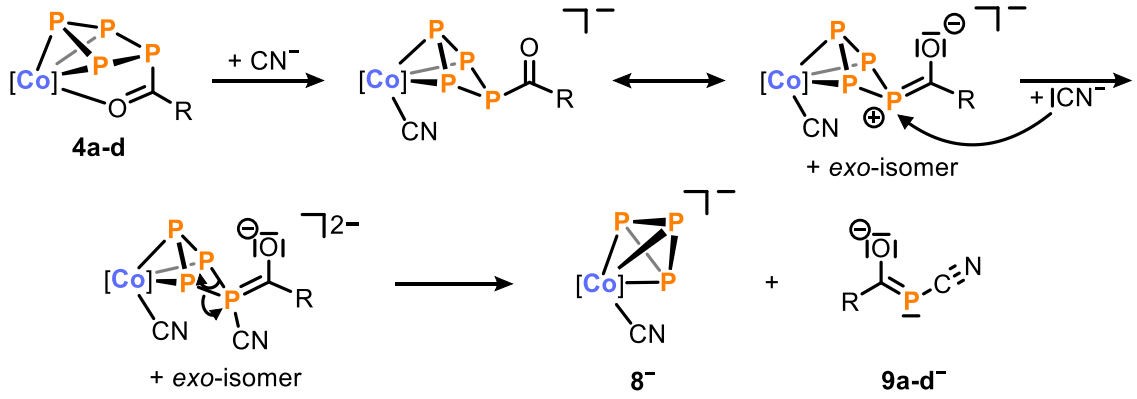

Scheme S1. Proposed reaction mechanism for cyanide induced [3+1] fragmentation reactions of **4a-d** to **8**$^{-}$ and **9a-d**$^{-}$.

2.4.6 UV/Vis Spectra

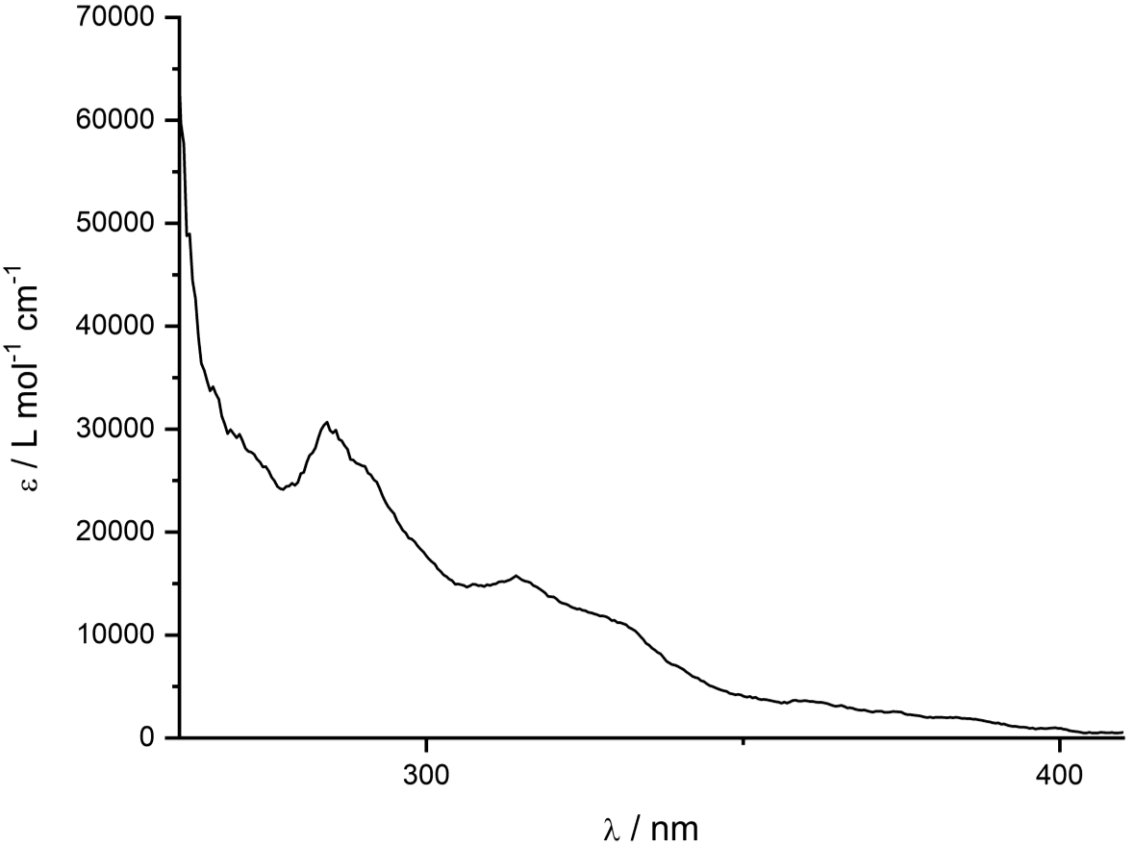

Figure S61. UV/Vis spectrum of Ar*BIAN (**1**) recorded in THF.

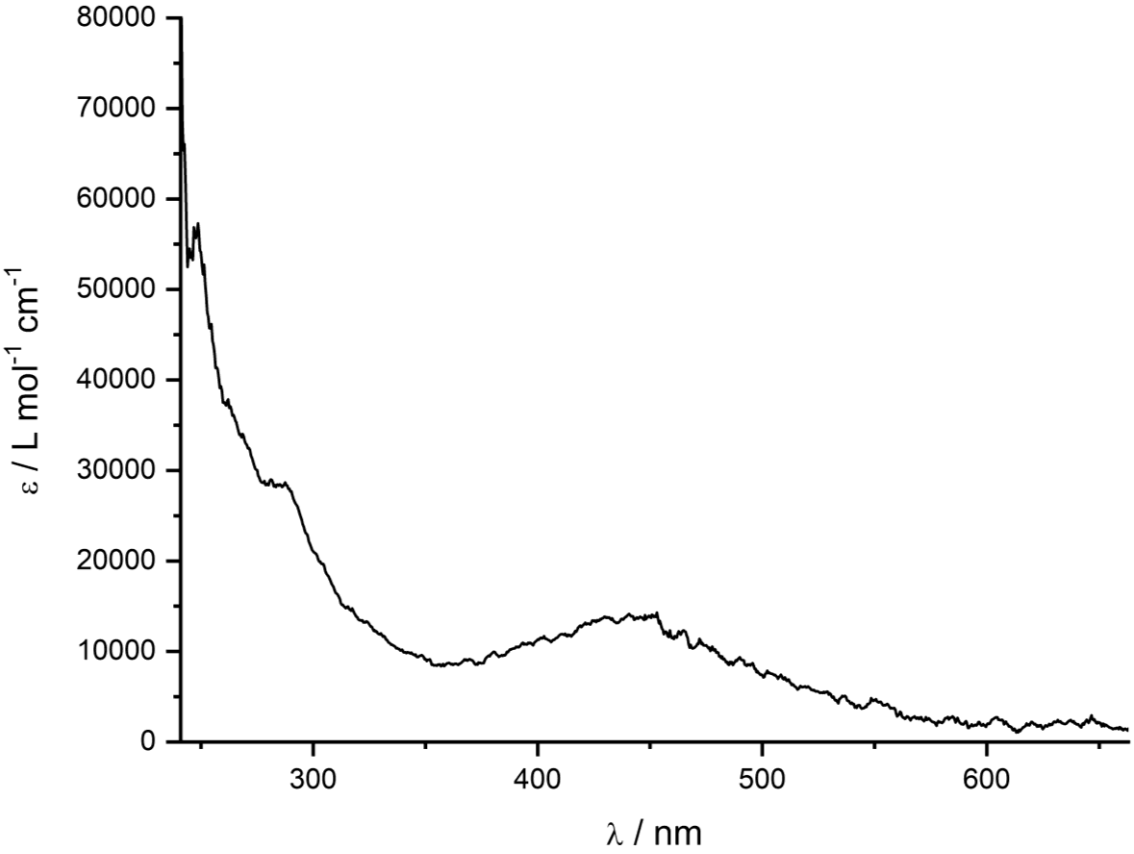

Figure S62 UV/Vis spectrum of [K(18c-6)][(Ar*BIAN)Co(η^4-1-5-cod)] ([K(18c-6)]**2**) recorded in THF.

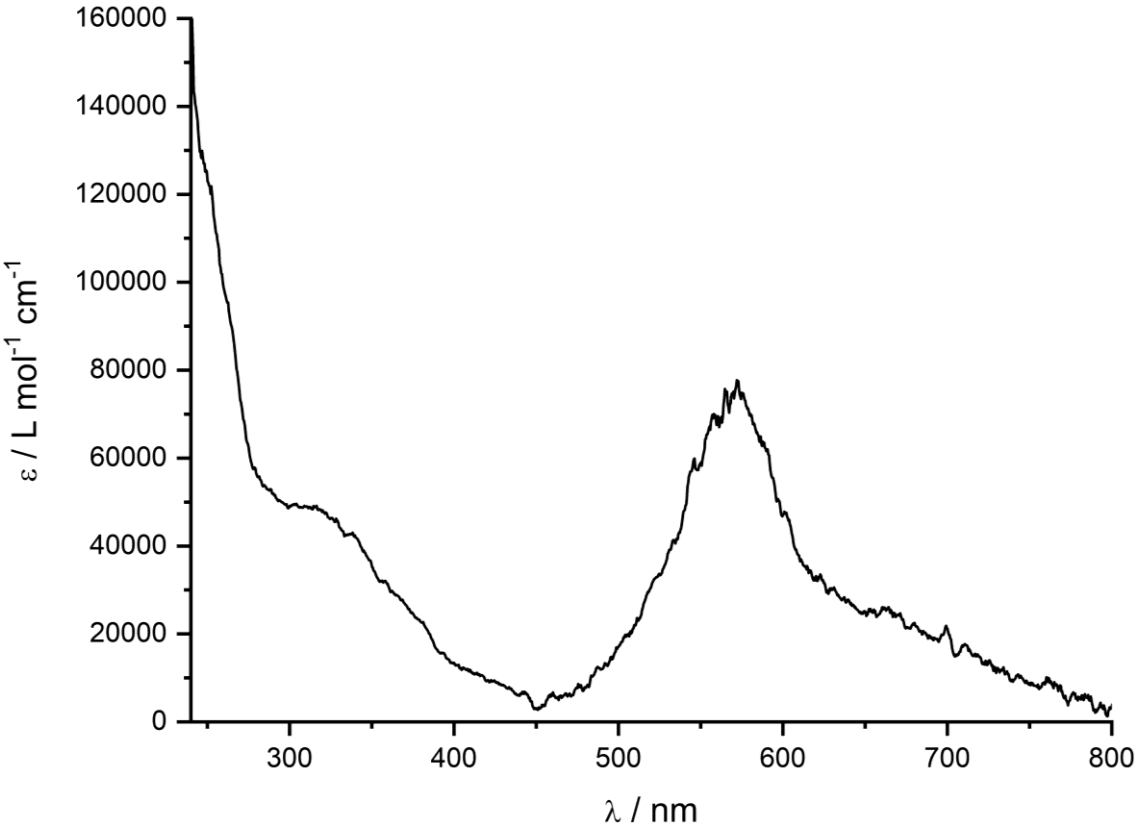

Figure S63. UV/Vis spectrum of [K(18c-6)][(Ar*BIAN)Co(η^4-P_4)] ([K(18c-6)]**3**) recorded in toluene.

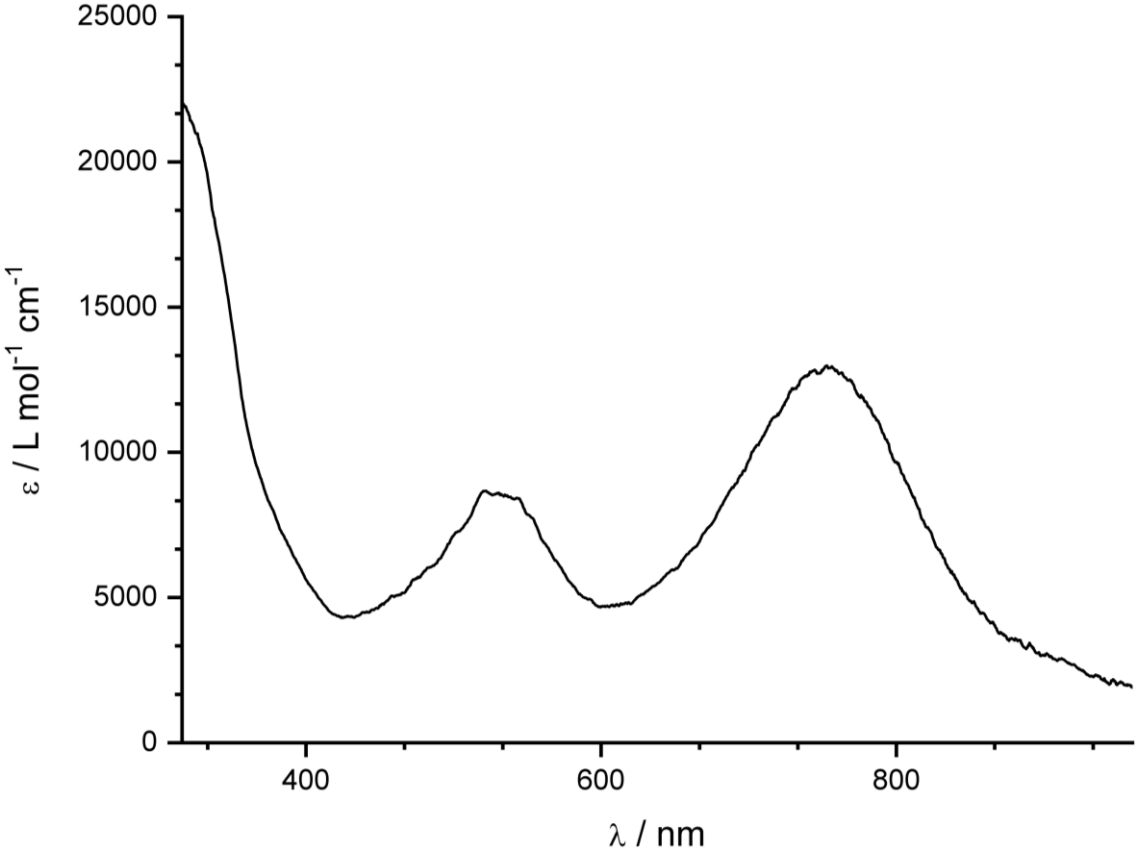

Figure S64. UV/Vis spectrum of [(Ar*BIAN)Co(η^3:η^1-P_4C(O)*t*Bu)] (**4a**) recorded in toluene.

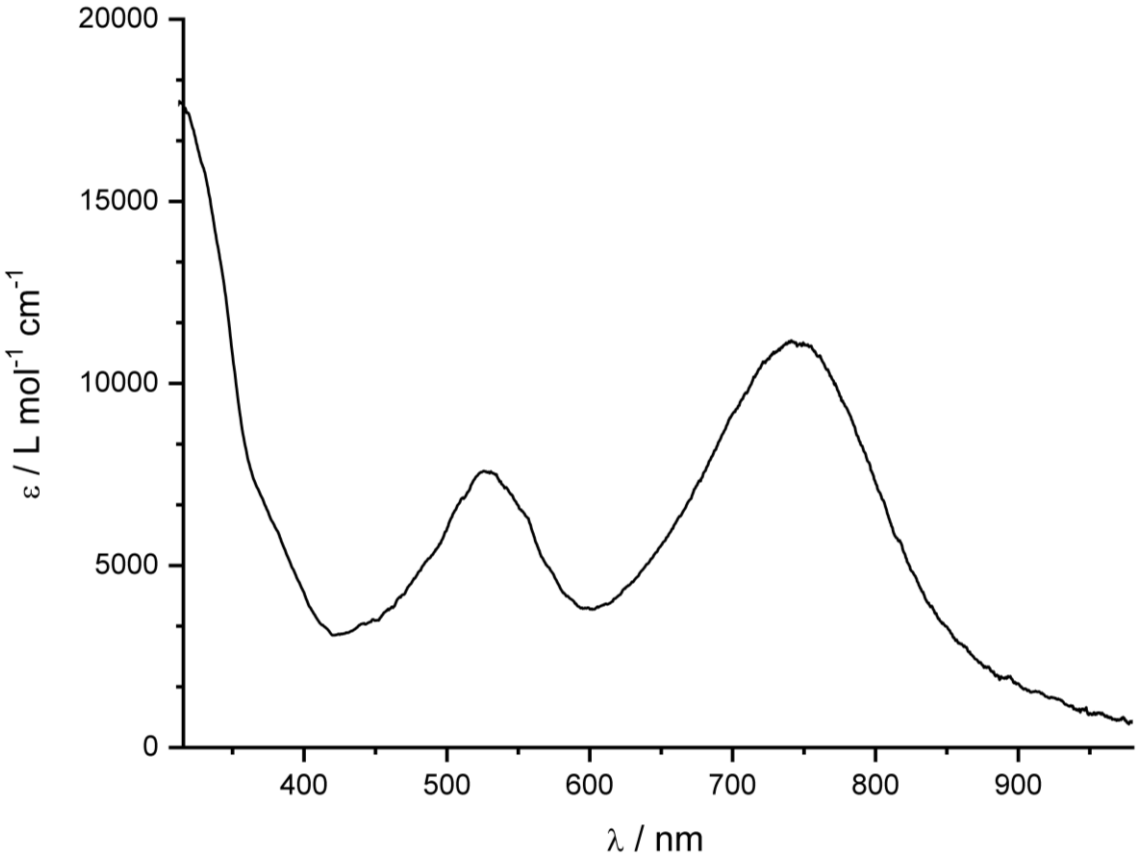

Figure S65. UV/Vis spectrum of [(Ar*BIAN)Co(η^3:η^1-P_4C(O)Cy)] (**4b**) recorded in toluene.

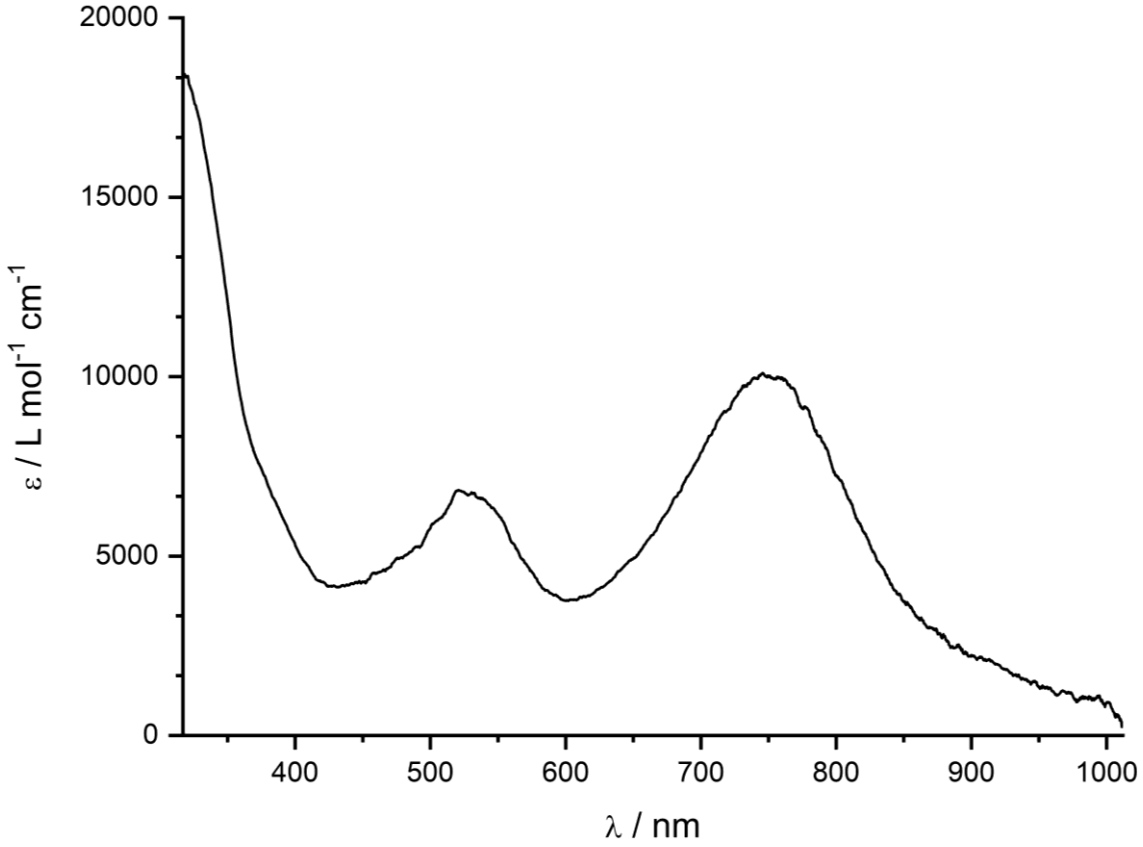

Figure S66. UV/Vis spectrum of [(Ar*BIAN)Co(η^3:η^1-P_4C(O)Ad)] (**4c**) recorded in toluene.

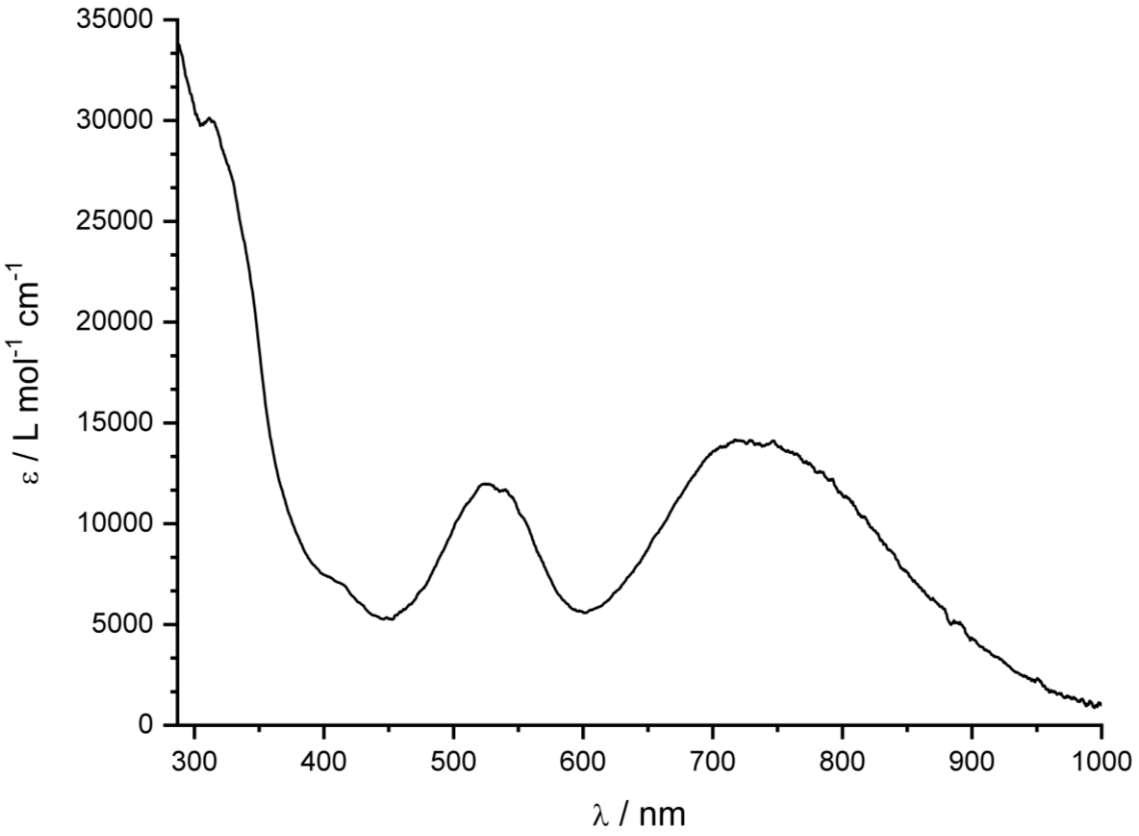

Figure S67. UV/Vis spectrum of [(Ar*BIAN)Co(η^3:η^1-P_4C(O)Ph)] (**4d**) recorded in toluene.

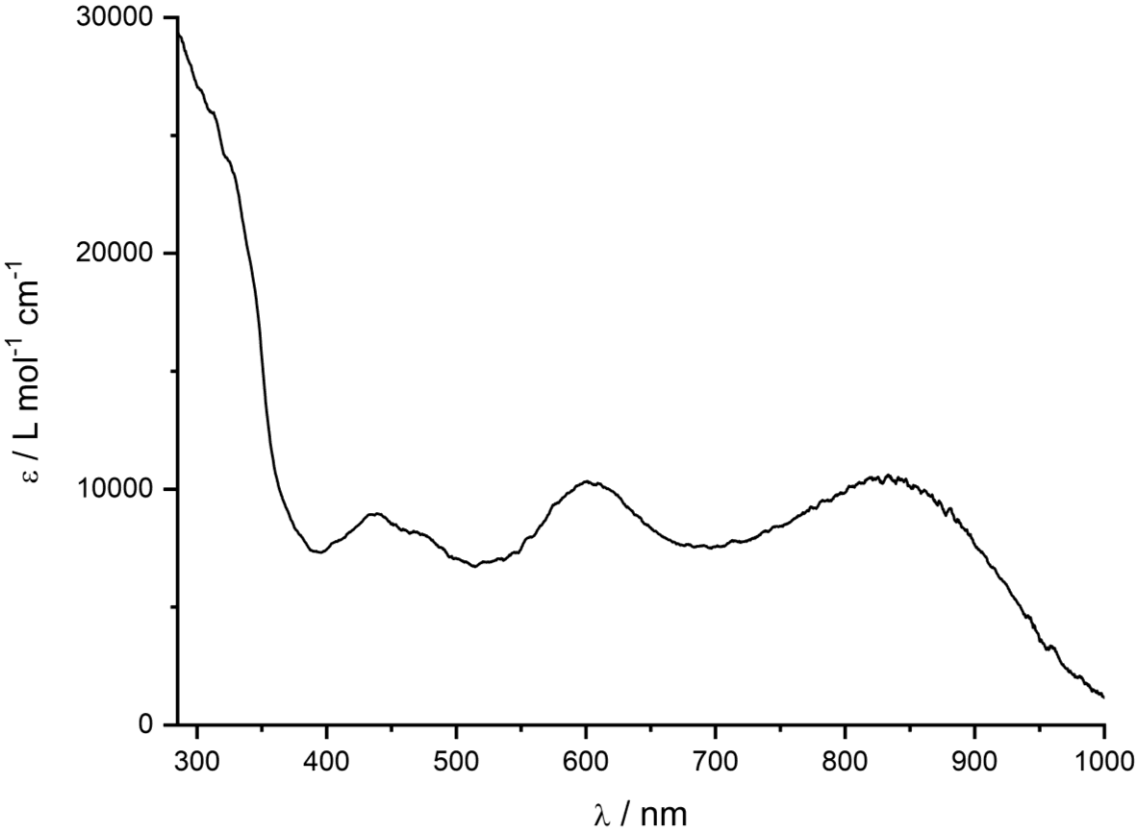

Figure S68. UV/Vis spectrum of [(Ar*BIAN)Co($(CH_3)_3$SiNC)(η^2:η^1-P_4CO*t*Bu)] (**5a**) recorded in toluene.

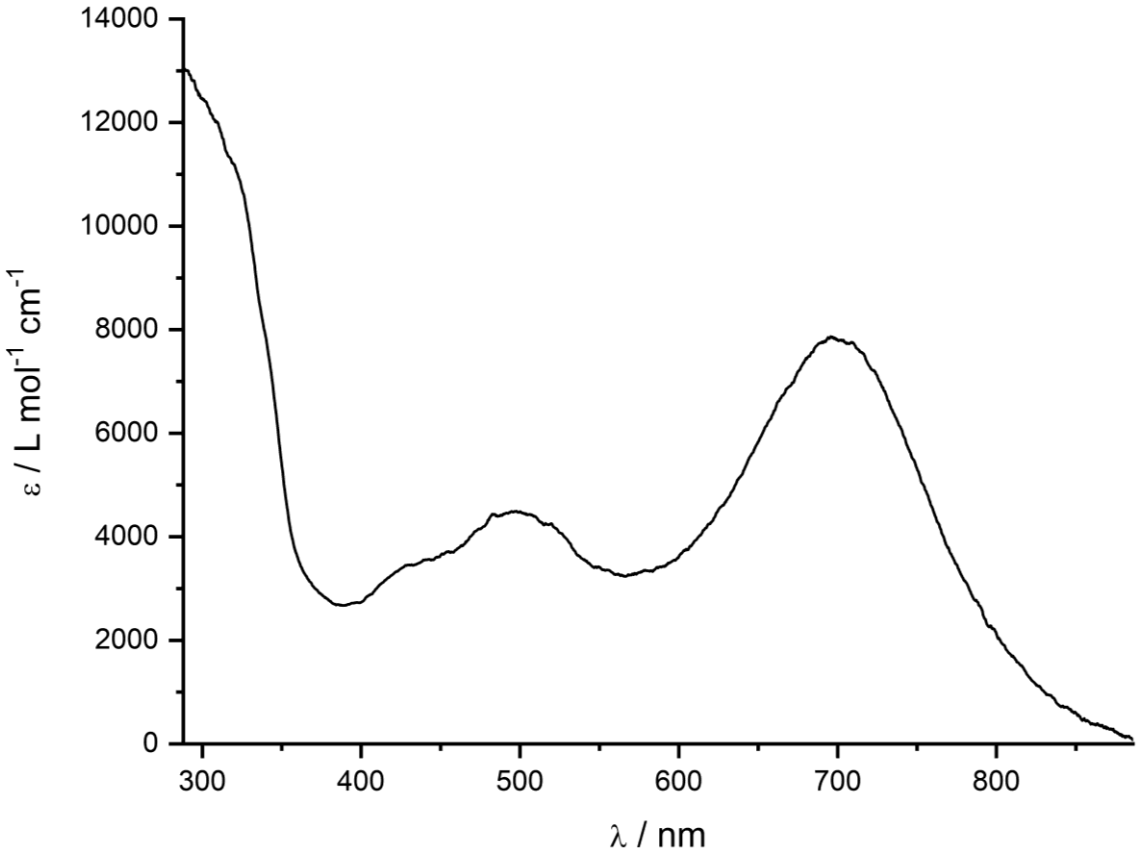

Figure S69. UV/Vis spectrum of *exo*-/*endo*-[(Ar*BIAN)Co(CyNC)(η^3-P_4C(O)*t*Bu)] (**6a**) recorded in toluene.

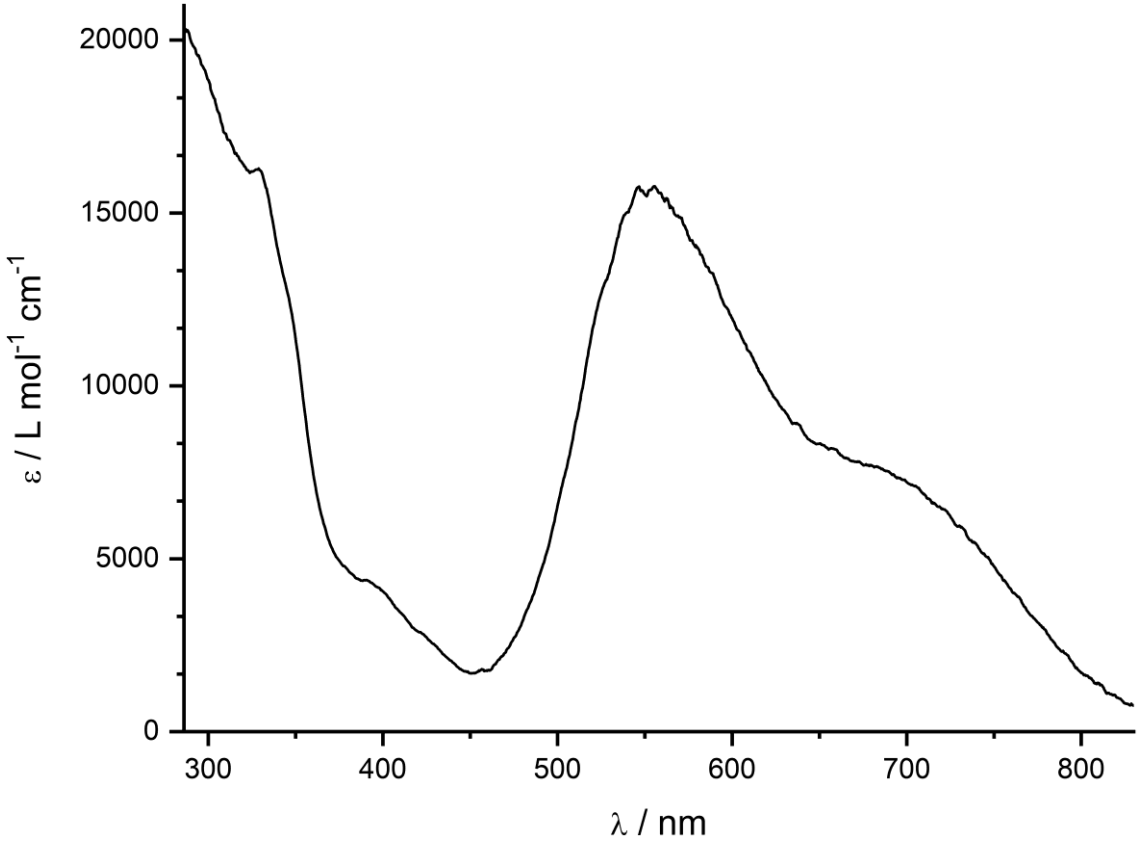

Figure S70. UV/Vis spectrum of [K(18c-6)][(Ar*BIAN)Co(CN)(η^3-P_3)] ([K(18c-6)]**8**) recorded in toluene.

2.4.7 IR Spectra

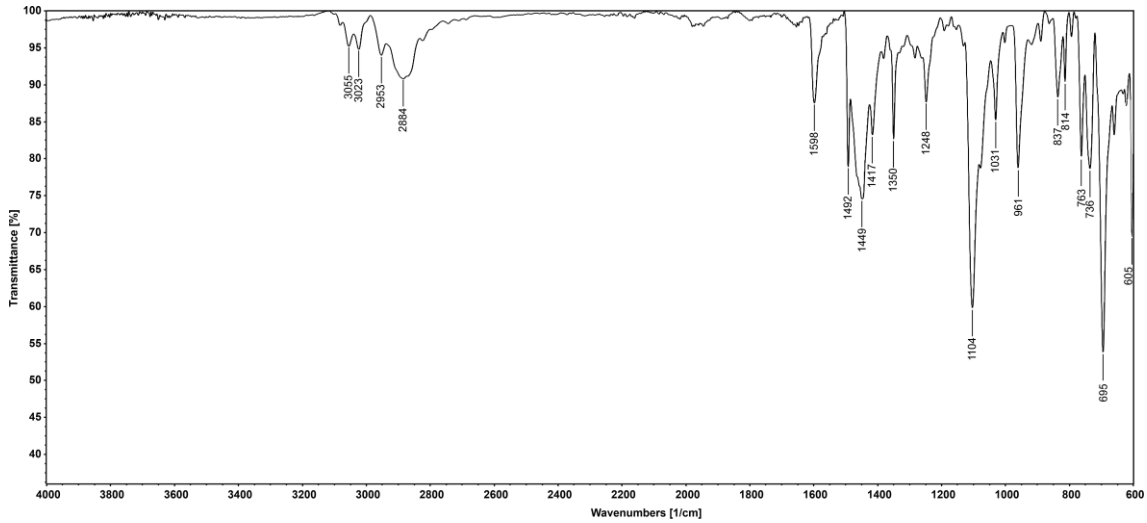

Figure S71. Solid state ATR-IR spectrum of [K(18c-6)][(Ar*BIAN)Co(η^4-P_4)] ([K(18c-6)]**3**).

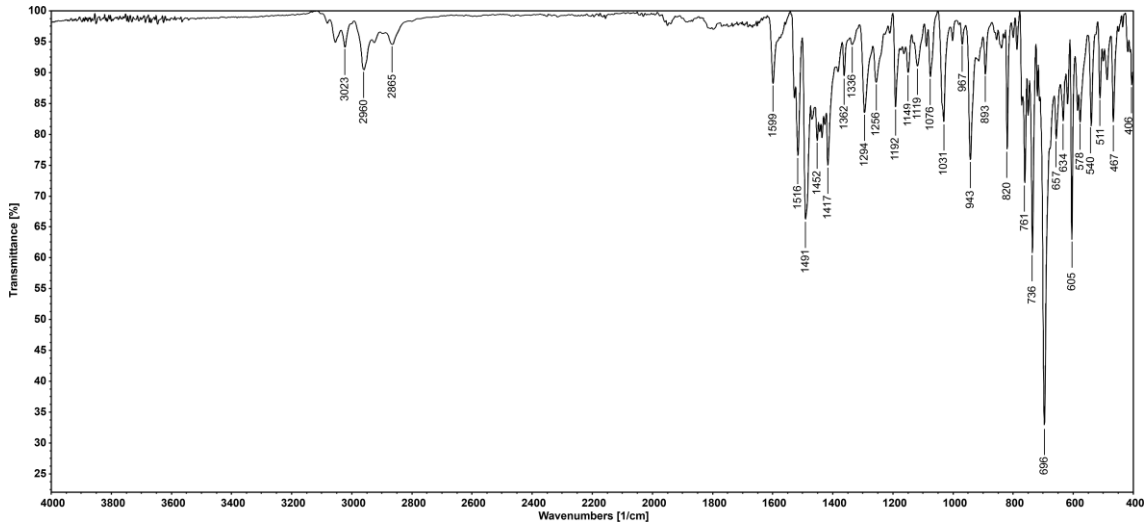

Figure S72. Solid state ATR-IR spectrum of [(Ar*BIAN)Co(η^3:η^1-P_4C(O)*t*Bu)] (**4a**).

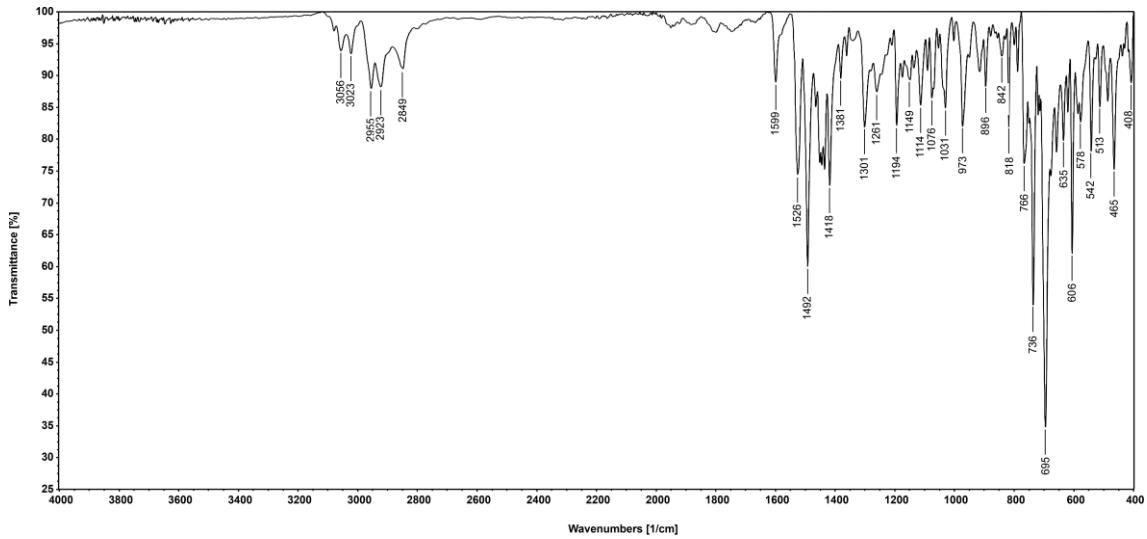

Figure S73. Solid state ATR-IR spectrum of [(Ar*BIAN)Co(η^3:η^1-P_4C(O)Cy)] (**4b**).

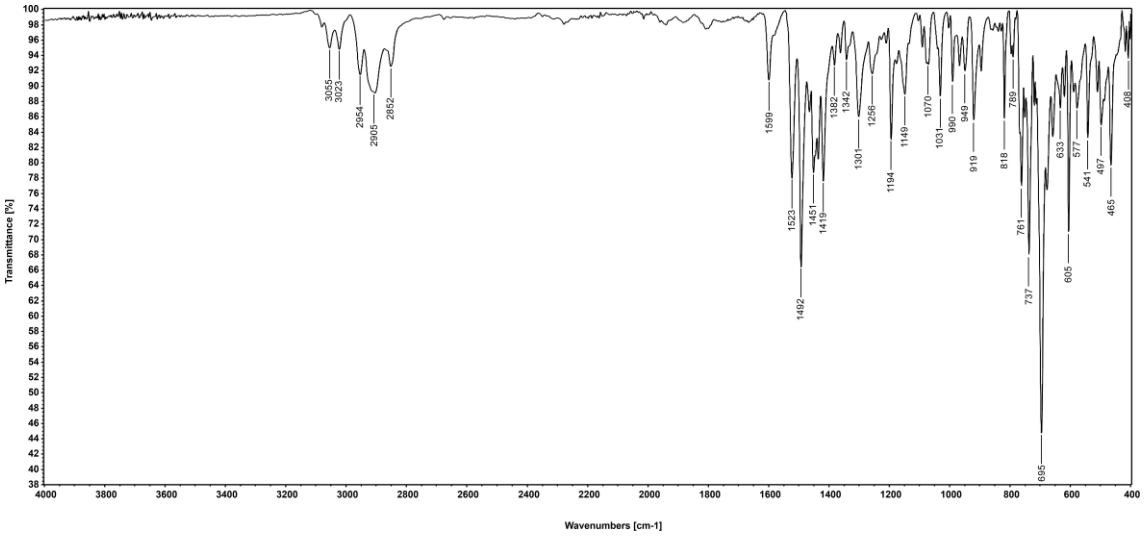

Figure S74. Solid state ATR-IR spectrum of [(Ar*BIAN)Co(η^3:η^1-P_4C(O)Ad)] (**4c**).

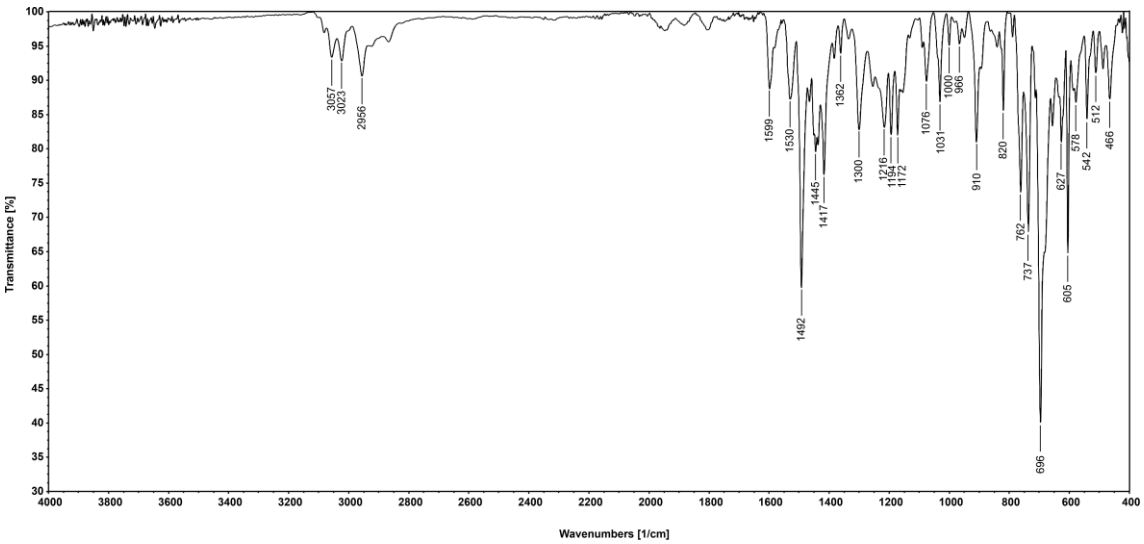

Figure S75. Solid state ATR-IR spectrum of [(Ar*BIAN)Co(η^3:η^1-P_4C(O)Ph)] (**4d**).

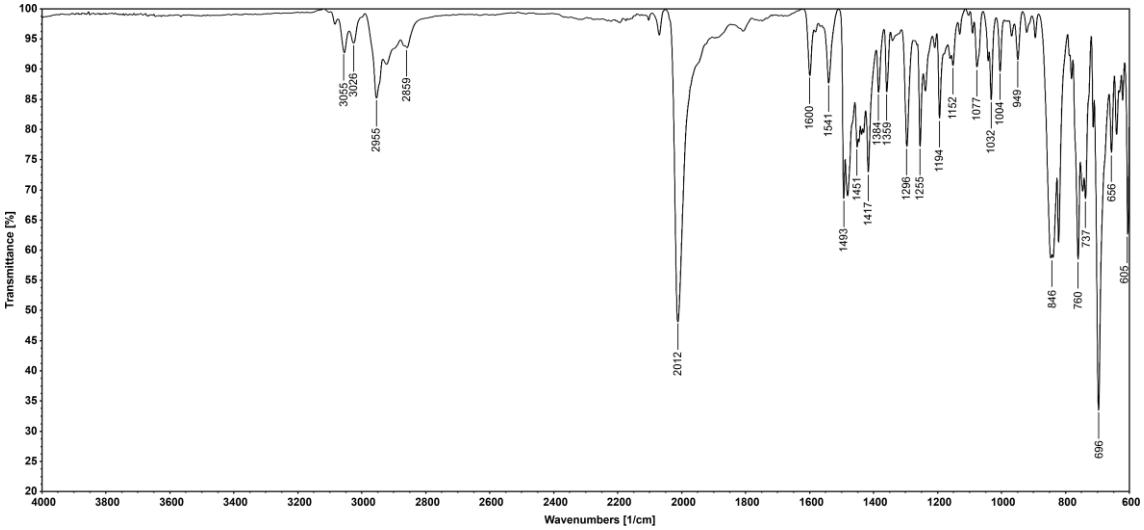

Figure S76. Solid state ATR-IR spectrum of [(Ar*BIAN)Co($(CH_3)_3$SiNC)(η^2:η^1-P_4CO*t*Bu)] (**5a**).

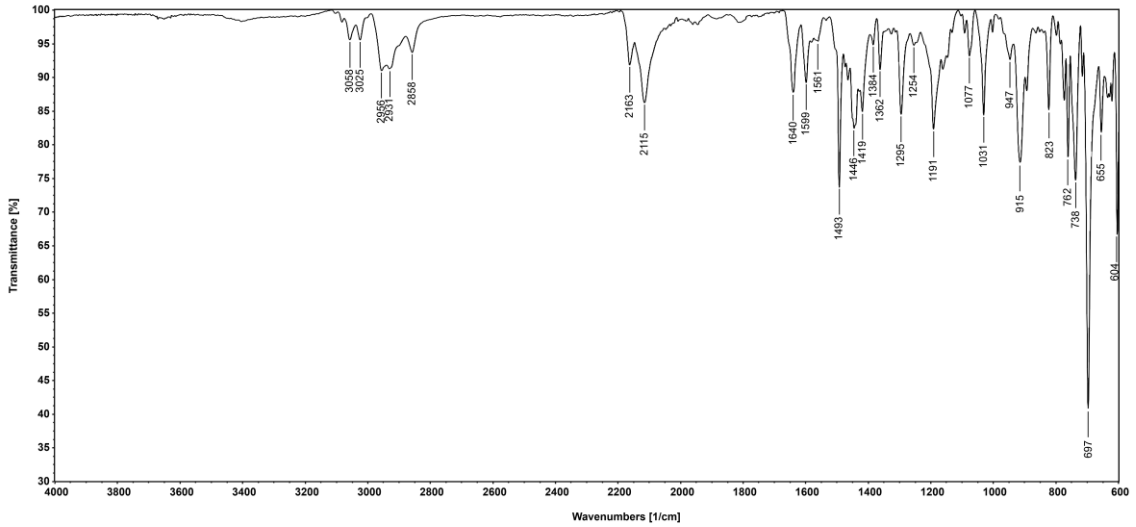

Figure S77. Solid state ATR-IR spectrum of *exo*-/*endo*-[(Ar*BIAN)Co(CyNC)(η^3-P_4C(O)*t*Bu)] (**6a**).

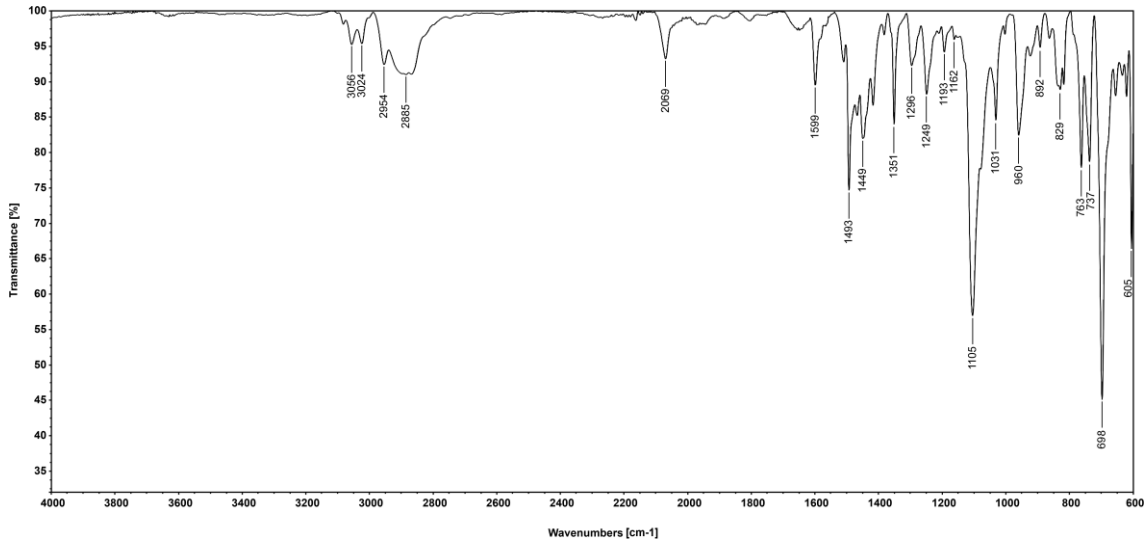

Figure S78. Solid state ATR-IR spectrum of [K(18c-6)][(Ar*BIAN)Co(CN)(η^3-P_3)] ([K(18c-6)]**8**).

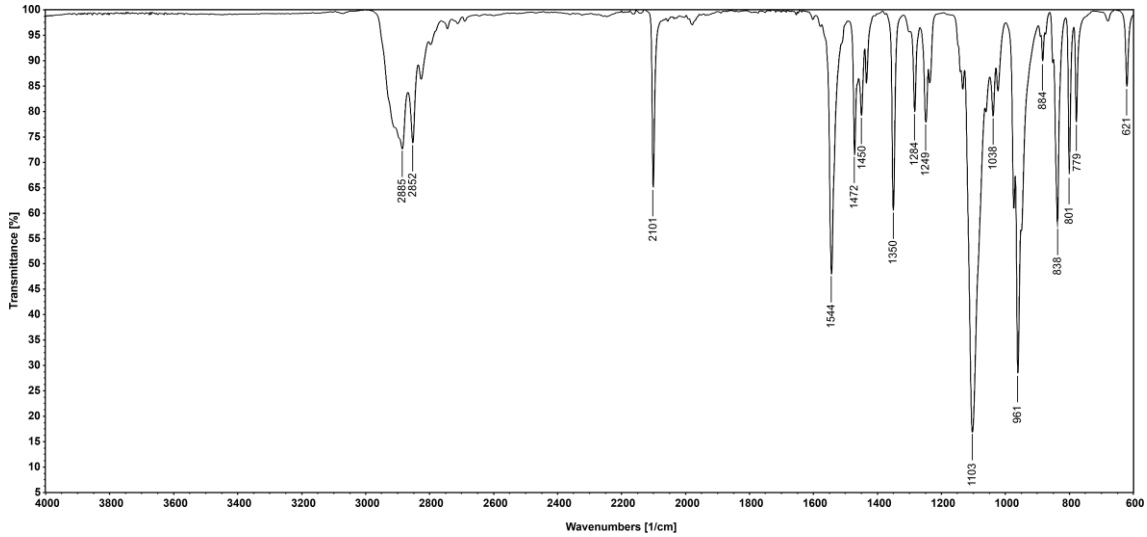

Figure S79. Solid state ATR-IR spectrum of [K(18c-6)][CyC(O)PCN] ([K(18c-6)]**9b**).

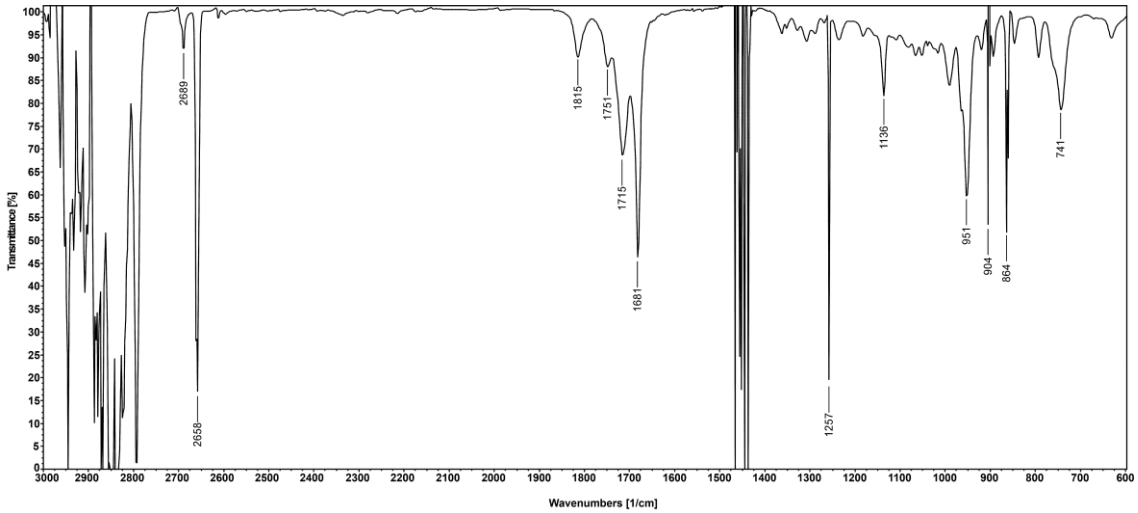

Figure S80. IR spectrum of $(CyC(O))_2PCN$ (**10**) recorded in cyclohexane.

2.4.8 Single Crystal X-Ray Diffraction Data

Single-crystal X-ray diffraction data were recorded on Rigaku GV1000 TitanS2, SuperNova Atlas and XtaLAB Synergy R DW system HyPix-Arc 150 diffractometers with Cu-Kα radiation (λ = 1.54184 Å). Crystals were selected under mineral oil, mounted on micromount loops and quench-cooled using an Oxford Cryosystems open flow N_2 cooling device. Either semi-empirical multi-scan absorption corrections[52] or analytical ones[53] were applied to the data. The structures were solved with SHELXT[54] solution program using dual methods and by using Olex2 as the graphical interface.[55] The models were refined with ShelXL[56] using full matrix least squares minimization on F^2.[57] The hydrogen atoms were located in idealized positions and refined isotropically with a riding model.

Ar*BIAN (1): The crystal of 1 contained one severely disordered toluene molecule and a solvent mask was calculated, which found 364 electrons in a volume of 2244 $Å^3$ in one void per unit cell. This is consistent with the presence of 1 toluene per Formula Unit which account for 400 electrons per unit cell. As **1** was crystallized by slow diffusion of *n*-hexane into a saturated toluene solution of **1** this serves as evidence for the presence of toluene in this position.

[K(18c-6)]2: The crystal of [K(18c-6)]**2** contained two severely disordered THF molecules per asymmetric unit. One of them was modeled, while the other one was refined by using the solvent mask command: A solvent mask was calculated, and 108 electrons were found in a volume of 360 $Å^3$ in one void per unit cell. This is consistent with the presence of 0.5 THF per Formula Unit which account for 80 electrons per unit cell. As [K(18c-6)]**2** was crystallized by slow diffusion of *n*-hexane into a saturated THF solution of [K(18c-6)]**2** this serves as evidence for the presence of THF in this position.

[K(18c-6)]3: The crystal of [K(18c-6)]**3** contained two severely disordered toluene molecules per asymmetric unit. One of them was modeled, while the other one was refined by using the solvent mask command: A solvent mask was calculated, and 51 electrons were found in a volume of 295 $Å^3$ in one void per unit cell. This is consistent with the presence of 0.5 toluene per Formula Unit which account for 50 electrons per unit cell. As [K(18c-6)]**3** was crystallized by slow diffusion of *n*-hexane into a saturated toluene solution of [K(18c-6)]**3** this serves as evidence for the presence of toluene in this position.

endo-/*exo*-**6a:** The cocrystal of *endo*-/*exo*-**6a** contained five *n*-hexane molecules per asymmetric unit. One of them was modeled, while the other severely disordered ones

were refined by using the solvent mask command: A solvent mask was calculated and 818 electrons were found in a volume of 2418 $Å^3$ in one void per unit cell. This is consistent with the presence of *n*-hexane per formula unit which account for 800 electrons per unit cell.

[(Ar*BIAN)Co(CyNC)$_2$(η^1-P_4CO*t*Bu)] (**7**): Structural analysis of **7** revealed that two molecules of the isocyanide are coordinated to the cobalt center. This saturation of the coordination sphere is facilitated by the severance of most of the cobalt-phosphorus interactions, resulting in an η^1-coordinated [1.1.0]bicyclotetraphosphane-1,4-diyl ("P_4 butterfly") ligand (Figure S89).[33] In complex **7**, the transannular P−P bond (2.1852(2) Å) is shorter compared to the peripheral P−P bonds (mean: 2.216 Å), which is a common feature of P_4 butterfly complexes. Additionally, **7** features a formal radical anionic BIAN ligand (mean of Ar*BIAN C−N bond lengths: 1.330 Å and C1−C2: 1.455(3) Å).[23] Moreover, the average Co−C (1.853(9) Å) and C≡N (**7a**: 1.152(6) Å) bond lengths of the isocyanide ligands are typical for neutral cobalt isocyanide complexes.[58]

The following section provides figures of the molecular structures with selected bond lengths and angles, which were not given in section 2.2 itself.

Table S9. Crystallographic data and structure refinement for compounds **1**-**4a**.

Compound	**1**	[K(18c-6)]**2**	[K(18c-6)]**3**	**4a**
CCDC	2269452	2269840	2269251	2269454
Empirical formula	$C_{82}H_{68}N_2$	$C_{110}H_{120}CoKN_2O_8$	$C_{101}H_{100}CoKN_2O_6P_4$	$C_{87}H_{77}CoN_2OP_4$
Formula weight	1081.38	1696.10	1659.73	1349.31
Temperature/K	123(1)	123(2)	123(1)	100(1)
Crystal system	orthorhombic	monoclinic	triclinic	monoclinic
Space group	*Pbca*	*C*2/*c*	*P*-1	*C*2/*c*
a/Å	22.6338(2)	19.1104(2)	14.2821(4)	23.0284(4)
b/Å	19.97100(10)	19.07250(1)	14.3155(5)	15.2934(2)
c/Å	29.2836(2)	27.3545(2)	25.0529(7)	42.0740(6)
α/°	90	90	103.851(3)	90
β/°	90	105.1750(1)	92.984(2)	110.503(2)
γ/°	90	90	113.699(3)	90
Volume/Å^3	13236.76(16)	9622.60(14)	4490.1(3)	13879.1(4)
Z	8	4	2	8
ρ_{calc}g/cm^3	1.085	1.171	1.228	1.291
μ/mm^{-1}	0.469	2.226	3.013	3.196
F(000)	4592.0	3616.0	1748.0	5664.0
Crystal size/mm^3	0.276 × 0.172 × 0.11	0.23 × 0.152 × 0.112	0.429 × 0.161 × 0.12	0.243 × 0.091 × 0.06
Diffractometer	XtaLAB Synergy R, DW system, HyPix-Arc 150	XtaLAB Synergy R, DW system, HyPix-Arc 150	GV1000, TitanS2	XtaLAB Synergy R, DW system, HyPix-Arc 150
Radiation	Cu Kα (λ = 1.54184)	Cu Kα (λ = 1.54184)	Cu Kα (λ = 1.54184)	Cu Kα (λ = 1.54184)
2Θ range for data collection/°	6.036 to 149.84	6.666 to 148.046	6.856 to 147.642	4.484 to 146.538
Index ranges	−28 ≤ h ≤ 27, −12 ≤ k ≤ 23, –35 ≤ l ≤ 36	−23 ≤ h ≤ 21, −22 ≤ k ≤ 22, −33 ≤ l ≤ 33	−17 ≤ h ≤ 17, −17 ≤ k ≤ 15, −31 ≤ l ≤ 31	−27 ≤ h ≤ 27, −18 ≤ k ≤ 18, −51 ≤ l ≤ 42
Reflections collected	95022	69479	48248	39994
Independent reflections	13366 [R_{int} = 0.0214, R_{sigma} = 0.0145]	9487 [R_{int} = 0.0218, R_{sigma} = 0.0139]	17336 [R_{int} = 0.0356, R_{sigma} = 0.0325]	13214 [R_{int} = 0.0312, R_{sigma} = 0.0323]
Data/restraints/ parameters	13366/0/837	9487/863/884	17336/196/1258	13214/36/895
Goodness-of-fit on F^2	1.033	1.048	1.032	1.054
Final R indexes [I>=2σ (I)]	R_1 = 0.0468, wR_2 = 0.1293	R_1 = 0.0630, wR_2 = 0.1828	R_1 = 0.0576, wR_2 = 0.1533	R_1 = 0.0446, wR_2 = 0.1140
Final R indexes [all data]	R_1 = 0.0528, wR_2 = 0.1341	R_1 = 0.0683, wR_2 = 0.1880	R_1 = 0.0619, wR_2 = 0.1578	R_1 = 0.0580, wR_2 = 0.1201
Largest diff. peak/hole / e Å^{-3}	0.27/−0.24	0.69/−0.47	0.83/−0.47	0.48/−0.30
Flack parameter	/	/	/	/

Table S10. Crystallographic data and structure refinement for compounds **1**-**6a**.

Compound	**4b**	**4c**	**5a**	*endo*-/*exo*-**6a**
CCDC	2269458	2269460	2269469	2269469
Empirical formula	$C_{95}H_{93}CoN_2OP_4$	$C_{99}H_{97}CoN_2OP_4$	$C_{97}H_{100}CoN_3OP_4Si$	$C_{218}H_{246}Co_2N_6O_2P_8$
Formula weight	1461.52	1513.59	1534.69	3347.81
Temperature/K	123(1)	123(1)	123(1)	123(1)
Crystal system	monoclinic	monoclinic	monoclinic	monoclinic
Space group	$P2_1/c$	$P2_1/c$	$P2_1/n$	$P2_1/c$
a/Å	21.8483(2)	21.7682(2)	13.62636(7)	14.29290(10)
b/Å	14.50900(10)	14.82840(10)	27.46562(15)	22.4741(2)
c/Å	26.5786(2)	26.4891(3)	22.79365(10)	59.8256(7)
α/°	90	90	90	90
β/°	111.2460(10)	109.7670(10)	104.4385(5)	92.9650(10)
γ/°	90	90	90	90
Volume/Å^3	7852.69(12)	8046.53(14)	8261.23(7)	19191.5(3)
Z	4	4	4	4
ρ_{calc}g/cm^3	1.236	1.249	1.234	1.159
μ/mm^{-1}	2.862	2.811	2.881	2.402
F(000)	3088.0	3200.0	3248.0	7144.0
Crystal size/mm^3	0.284 × 0.14 × 0.054	0.647 × 0.072 × 0.065	0.2 × 0.09 × 0.06	0.179 × 0.081 × 0.035
Diffractometer	XtaLAB Synergy R, DW system, HyPix-Arc 150	Agilent Technologies SuperNova, Atlas	XtaLAB Synergy R, DW system, HyPix-Arc 150	XtaLAB Synergy R, DW system, HyPix-Arc 150
Radiation	Cu Kα (λ = 1.54184)	Cu Kα (λ = 1.54184)	Cu Kα (λ = 1.54184)	Cu Kα (λ = 1.54184)
2Θ range for data collection/°	4.34 to 149.176	6.936 to 132.082	5.136 to 148.872	4.92 to 134.154
Index ranges	−27 ≤ h ≤ 27, −17 ≤ k ≤ 14, −33 ≤ l ≤ 33	−25 ≤ h ≤ 24, −15 ≤ k ≤ 17, −29 ≤ l ≤ 30	−16 ≤ h ≤ 16, −33 ≤ k ≤ 34, −28 ≤ l ≤ 23	−16 ≤ h ≤ 17, −26 ≤ k ≤ 26, −71 ≤ l ≤ 71
Reflections collected	218480	28281	126409	279595
Independent reflections	15830 [R_{int} = 0.0351, R_{sigma} = 0.0176]	13479 [R_{int} = 0.0203, R_{sigma} = 0.0253]	16592 [R_{int} = 0.0255, R_{sigma} = 0.0195]	34264 [R_{int} = 0.0968, R_{sigma} = 0.0531]
Data/restraints/ parameters	15830/0/934	13479/18/969	16592/18/987	34264/310/1993
Goodness-of-fit on F^2	1.059	1.033	1.033	1.019
Final R indexes [I>=2σ (I)]	R_1 = 0.0568, wR_2 = 0.1582	R_1 = 0.0404, wR_2 = 0.1092	R_1 = 0.0499, wR_2 = 0.1458	R_1 = 0.0887, wR_2 = 0.2394
Final R indexes [all data]	R_1 = 0.0627, wR_2 = 0.1629	R_1 = 0.0431, wR_2 = 0.1116	R_1 = 0.0554, wR_2 = 0.1503	R_1 = 0.1110, wR_2 = 0.2542
Largest diff. peak/hole / e Å^{-3}	0.98/−0.57	1.17/−0.53	0.69/−0.78	0.81/−0.74
Flack parameter	/	/	/	/

Table S11. Crystallographic data and structure refinement for compounds **6a**-**7**.

Compound	*endo*-**6a**	*exo*-**6d**	*endo*-**6e**	**7**
CCDC	2269471	2269474	2269477	2269521
Empirical formula	$C_{94}H_{88}CoN_3OP_4$	$C_{210}H_{208}Co_2N_6O_2P_8$	$C_{92}H_{86}CoN_3OP_4$	$C_{107}H_{113}CoN_4OP_4$
Formula weight	1458.48	3213.43	1432.44	1653.82
Temperature/K	123(1)	123(1)	123(1)	123(1)
Crystal system	monoclinic	monoclinic	monoclinic	triclinic
Space group	$P2_1/n$	$P2_1/n$	$P2_1/n$	P-1
a/Å	12.8517(2)	28.4861(4)	12.1922(2)	13.7757(3)
b/Å	31.8675(5)	23.2938(3)	47.9684(7)	14.8043(4)
c/Å	19.0864(3)	29.4384(4)	13.3409(2)	25.6965(5)
α/°	90	90	90	78.281(2)
β/°	94.863(2)	115.943(2)	106.388(2)	89.374(2)
γ/°	90	90	90	62.721(2)
Volume/Å^3	7788.7(2)	17565.4(5)	7485.3(2)	4540.3(2)
Z	4	4	4	2
ρ_{calc}g/cm^3	1.244	1.215	1.271	1.210
μ/mm^{-1}	2.889	2.607	2.997	2.538
F(000)	3072.0	6800.0	3016.0	1756.0
Crystal size/mm^3	0.401 × 0.222 × 0.16	0.332 × 0.238 × 0.175	0.18 × 0.16 × 0.04	0.21 × 0.15 × 0.07
Diffractometer	XtaLAB Synergy R, DW system, HyPix-Arc 150	Agilent Technologies SuperNova, Titan S2	XtaLAB Synergy R, DW system, HyPix-Arc 150	Agilent Technologies SuperNova, Titan S2
Radiation	Cu Kα (λ = 1.54184)	Cu Kα (λ = 1.54184	Cu Kα (λ = 1.54184)	Cu Kα (λ = 1.54184)
2Θ range for data collection/°	5.412 to 147.812	6.894 to 134.492	3.684 to 148.432	7.252 to 134.094
Index ranges	$-15 \le h \le 14$, $-39 \le k \le 39$, $-23 \le l \le 23$	$-22 \le h \le 33$, $-27 \le k \le 27$, $-35 \le l \le 35$	$-14 \le h \le 15$, $-58 \le k \le 59$, $-15 \le l \le 8$	$-16 \le h \le 16$, $-17 \le k \le 16$, $-30 \le l \le 30$
Reflections collected	50788	102262	125529	66404
Independent reflections	15042 [R_{int} = 0.0435, R_{sigma} = 0.0305]	30952 [R_{int} = 0.0528, R_{sigma} = 0.0498]	14717 [R_{int} = 0.0317, R_{sigma} = 0.0198]	15564 [R_{int} = 0.0487, R_{sigma} = 0.0370]
Data/restraints/ parameters	15042/0/935	30952/92/2118	14717/84/1276	15564/66/1119
Goodness-of-fit on F^2	1.132	1.022	1.044	1.078
Final R indexes [I>=2σ (I)]	R_1 = 0.0492, wR_2 = 0.1463	R_1 = 0.0678, wR_2 = 0.1720	R_1 = 0.0549, wR_2 = 0.1581	R_1 = 0.0793, wR_2 = 0.2142
Final R indexes [all data]	R_1 = 0.0519, wR_2 = 0.1477	R_1 = 0.0848, wR_2 = 0.1875	R_1 = 0.0603, wR_2 = 0.1629	R_1 = 0.0893, wR_2 = 0.2242
Largest diff. peak/hole / e Å^{-3}	0.76/−0.57	1.30/−0.74	1.25/−0.86	1.84/−0.73
Flack parameter	/	/	/	/

Table S12. Crystallographic data and structure refinement for compounds **8**-**9d**.

Compound	[K(18c-6)]**8**	[K(18c-6)]**9a**	[K(18c-6)]**9b**	[K(18c-6)]**9d**
CCDC	2269484	2269513	2269494	2269504
Empirical formula	$C_{109}H_{108}CoKN_3O_6P_3$	$C_{18}H_{33}KNO_7P$	$C_{20}H_{35}KNO_7P$	$C_{20}H_{29}KNO_7P$
Formula weight	1746.92	445.52	471.56	464.51
Temperature/K	123(1)	123(1)	100(1)	123(1)
Crystal system	triclinic	monoclinic	monoclinic	orthorhombic
Space group	*P*-1	$P2_1/n$	$P2_1/c$	$P2_12_12_1$
a/Å	14.20621(7)	10.0106(2)	9.79050(10)	9.87640(10)
b/Å	17.37333(7)	14.0801(3)	14.09650(10)	14.78170(10)
c/Å	19.84846(12)	16.5959(4)	18.92820(10)	16.2197(2)
α/°	82.8786(4)	90	90	90
β/°	70.7499(5)	94.147(2)	104.6820(10)	90
γ/°	86.3030(4)	90	90	90
Volume/Å^3	4587.75(4)	2333.07(9)	2527.02(4)	2367.91(4)
Z	2	4	4	4
ρ_{calc}g/cm^3	1.265	1.268	1.239	1.306
μ/mm^{-1}	2.818	2.952	2.755	2.939
F(000)	1844.0	952.0	1008.0	984.0
Crystal size/mm^3	0.404 × 0.129 × 0.123	0.2 × 0.13 × 0.06	0.28 × 0.23 × 0.09	0.338 × 0.22 × 0.18
Diffractometer	XtaLAB Synergy R, DW system, HyPix-Arc 150	Agilent Technologies SuperNova, Titan S2	XtaLAB Synergy R, DW system, HyPix-Arc 150	XtaLAB Synergy R, DW system, HyPix-Arc 150
Radiation	Cu Kα (λ = 1.54184)	Cu Kα (λ = 1.54184)	Cu Kα (λ = 1.54184)	Cu Kα (λ = 1.54184)
2Θ range for data collection/°	4.744 to 148.778	8.244 to 133.732	7.916 to 146.304	8.092 to 148.648
Index ranges	$-17 \le h \le 17$, $-15 \le k \le 20$, $-24 \le l \le 24$	$-11 \le h \le 11$, $-16 \le k \le 16$, $-19 \le l \le 19$	$-12 \le h \le 10$, $-17 \le k \le 17$, $-22 \le l \le 23$	$-10 \le h \le 12$, $-18 \le k \le 18$, $-20 \le l \le 16$
Reflections collected	117206	36868	28205	17999
Independent reflections	18323 [R_{int} = 0.0166, R_{sigma} = 0.0097]	4126 [R_{int} = 0.0796, R_{sigma} = 0.0265]	4935 [R_{int} = 0.0188, R_{sigma} = 0.0105]	4623 [R_{int} = 0.0208, R_{sigma} = 0.0169]
Data/restraints/ parameters	18323/15/1179	4126/0/385	4935/0/411	4623/0/281
Goodness-of-fit on F^2	1.080	1.045	1.044	1.020
Final R indexes [I>=2σ (I)]	R_1 = 0.0277, wR_2 = 0.0757	R_1 = 0.0456, wR_2 = 0.1204	R_1 = 0.0237, wR_2 = 0.0655	R_1 = 0.0446, wR_2 = 0.1240
Final R indexes [all data]	R_1 = 0.0283, wR_2 = 0.0760	R_1 = 0.0485, wR_2 = 0.1238	R_1 = 0.0244, wR_2 = 0.0660	R_1 = 0.0454, wR_2 = 0.1250
Largest diff. peak/hole / e Å^{-3}	0.35/−0.34	0.97/−0.37	0.31/−0.22	0.75/−0.30
Flack parameter	/	/	/	-0.002(4)

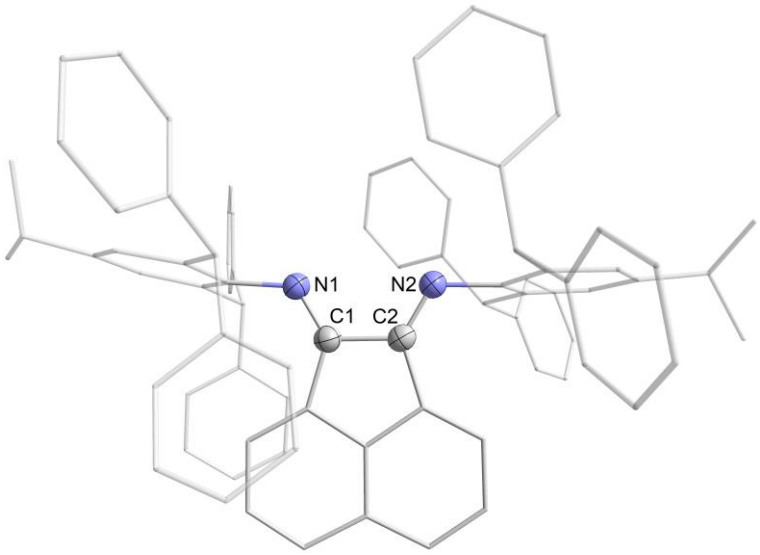

Figure S81. Solid-state molecular structure of Ar*BIAN (**1**) shown at the 50% probability level with hydrogen atoms and disorder in one of the *i*Pr groups, as well as a phenyl group omitted for clarity. Selected bond lengths [Å] and angles [°]: N1−C1 1.2748(2), N2−C2 1.2746(2), C1−C2 1.5294(2), N1−C1−C2 120.00(1), N2−C2−C1 121.02(1).

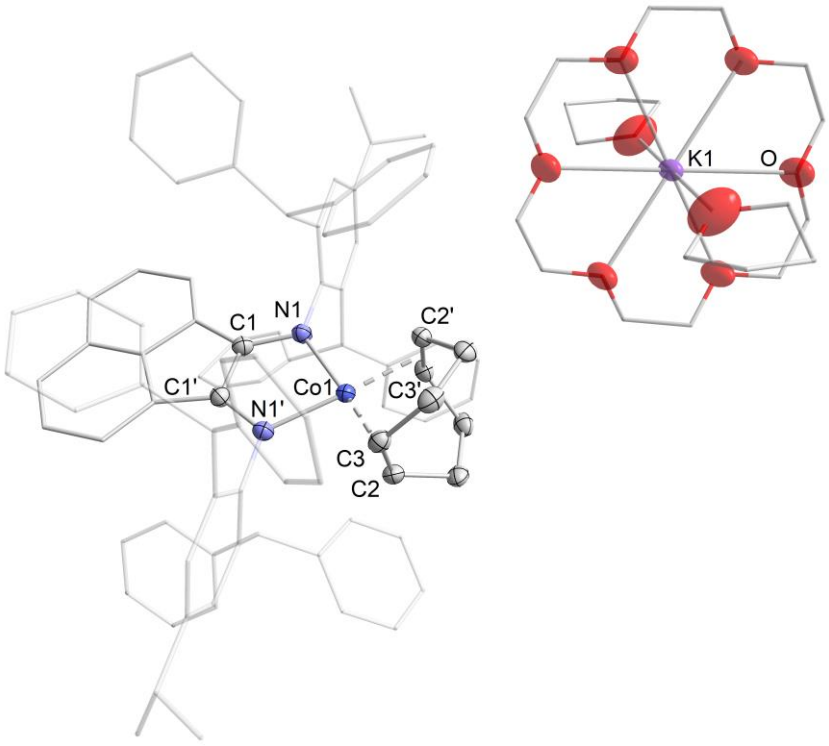

Figure S82. Solid-state molecular structure of [K(18c-6)][(Ar*BIAN)Co(η^4-1-5-cod)] ([K(18c-6)]**2)** shown at the 50% probability level. Hydrogen atoms, non coordinating solvent molecules and disorder in Ar*BIAN and 18c-6 omitted for clarity. The asymmetric unit contains only half of the molecule. Selected bond lengths [Å] and angles [°]: Co1−C2 2.036(2), Co1−C3 2.022(2), Co1−N1 1.9265(2), C2−C3 1.402(3), N1−C1 1.374(3), C1−C1' 1.382(4), N1−Co1−N1' 83.13(1).

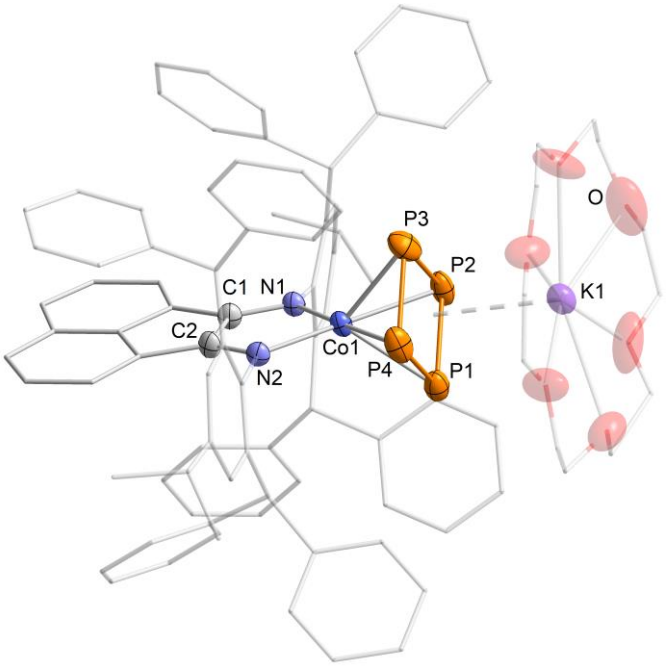

Figure S83. Solid-state molecular structure of [K(18c-6)][(Ar*BIAN)Co(η^4-P_4)] ([K(18c-6)]**3**) shown at the 50% probability level. Hydrogen atoms, non coordinating solvent molecules and disorder in the Ar*BIAN ligand and in 18c-6 omitted for clarity. Selected bond lengths [Å] and angles [°]: P1−P2 2.1539(9), P1−P4 2.1626 (1), P3−P2 2.1763(1), P3−P4 2.1772(1), Co1−P1 2.3193(7), Co1−P2 2.3068(7), Co1−P3 2.3261(8), Co1−P4 2.2943(7), K1−P_4^{centr} 3.1726(6), Co1−N1 1.9077(2), Co1−N2 1.9231(2), N1−C1 1.335(3), N2−C2 1.330(3), C1−C2 1.426(3), P2−P1−P4 89.41(4), P1−P4−P3 90.95(4), P4−P3−P2 88.44(4), P3−P2−P1 91.20(4), N1−Co1−N2 84.69(8).

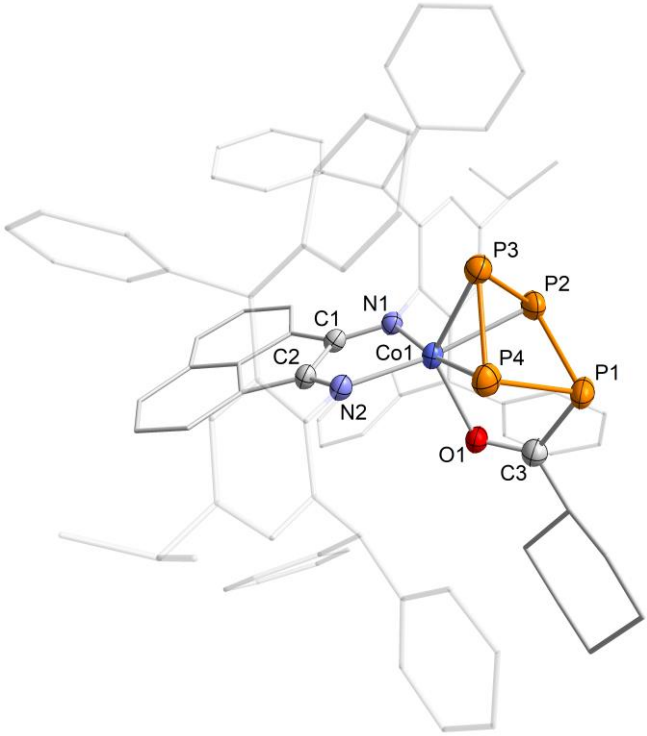

Figure S84. Solid-state molecular structure of [(Ar*BIAN)Co(η^3:η^1-P_4C(O) Cy)] (**4b**) shown at the 50% probability level. Hydrogen atoms and non coordinating solvent molecules omitted for clarity. Selected bond lengths [Å] and angles [°]: P1−P2 2.2371(1), P1−P4 2.2570(1), P2−P3 2.1593(1), P3−P4 2.1559(1), Co1−P2 2.3019(8), Co1−P3 2.2844(9), Co1−P4 2.2934(7), Co1−O1 2.0933(2), P1−C3 1.876(3), C3−O1 1.239(3), Co1−N1 1.9578(2), Co1−N2 1.960(2), C1−C2 1.448(3), P2−P1−P4 82.79(4), P1−P4−P3 89.96(4), P4−P3−P2 87.05(4), P3−P2−P1 90.41(4), Co1−O1−C3 116.73(2), O1−C3−P1 117.7(2), N1−Co1−N2 82.88(8).

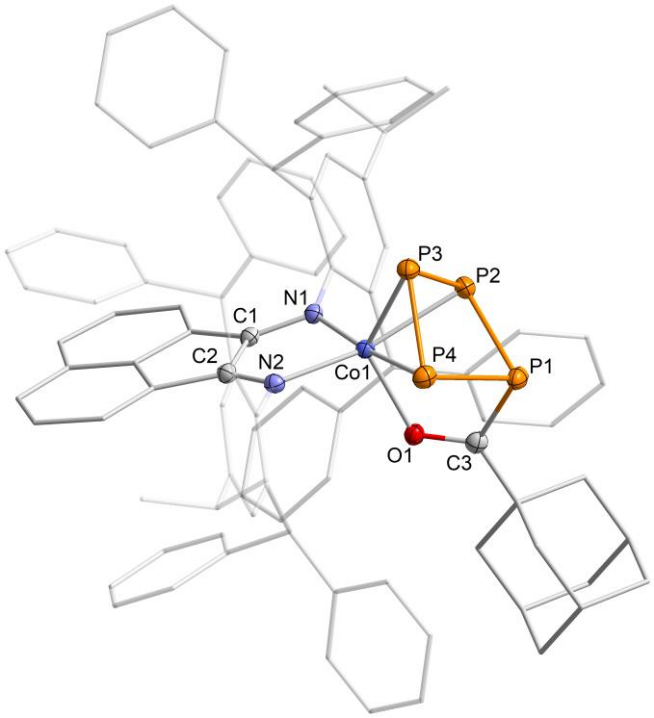

Figure S85. Solid-state molecular structure of [(Ar*BIAN)Co(η^3:η^1-P_4C(O)Ad)] (**4c**) shown at the 50% probability level. Hydrogen atoms and non coordinating solvent molecules omitted for clarity. Selected bond lengths [Å] and angles [°]: P1−P2 2.244(7), P1−P4 2.2450(8), P2−P3 2.1562(7), P3−P4 2.1626(8), Co1−P2 2.2957(5), Co1−P3 2.2793(6), Co1−P4 2.2998(5), Co1−O1 2.0925(1), P1−C3 1.879(2), C3−O1 1.245(2), Co1−N1 1.9570(2), Co1−N2 1.9624(2), C1−C2 1.446(3), P2−P1−P4 83.05(2), P1−P4−P3 89.88(3), P4−P3−P2 87.14(3), P3−P2−P1 90.05(3), Co1−O1−C3 116.54(1), O1−C3−P1 117.63(1), N1−Co1−N2 83.25(6).

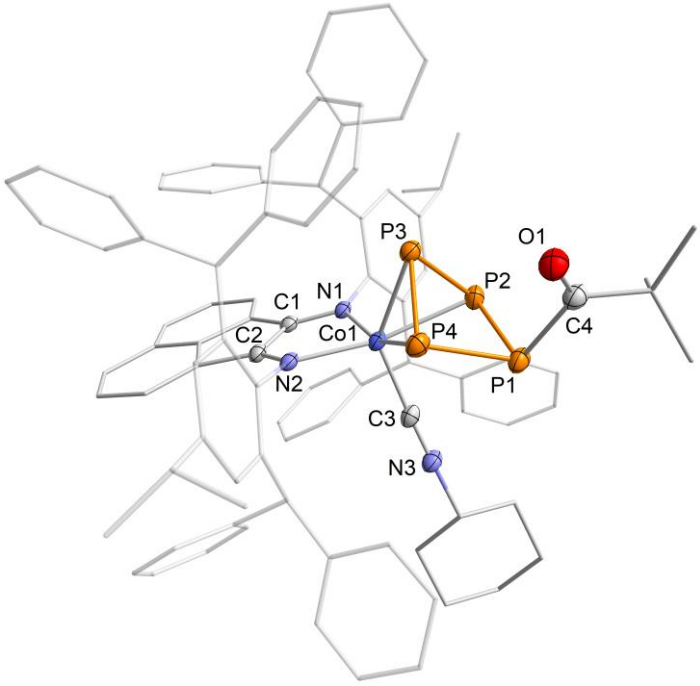

Figure S86. Solid-state molecular structure of *endo*-[(Ar*BIAN)Co(CyNC)(η^3-P_4C(O)*t*Bu)] (*endo*-**6a**) shown at the 50% probability level. Hydrogen atoms are omitted for clarity. Selected bond lengths [Å] and angles [°]: P1−P2 2.2438(8), P1−P4 2.2199(9), P2−P3 2.1686(9), P3−P4 2.1643(8), Co1−P2 2.3205(6), Co1−P3 2.2939, Co1−P4 2.3143(6), P1−C4 1.905(2), C4−O1 1.203(3), Co1−C3 1.862(2), C3−N3 1.160(3), Co1−N1 1.9775(2), Co1−N2 1.9775(2), C1−C2 1.455(3), P2−P1−P4 80.51(3), P1−P4−P3 91.51(3), P4−P3−P2 83.47(3), P3−P2−P1 90.76(3), Co1−C3−N3 177.38(2), P1−C4−O1 121.46(2), N1−Co1−N2 81.99(6).

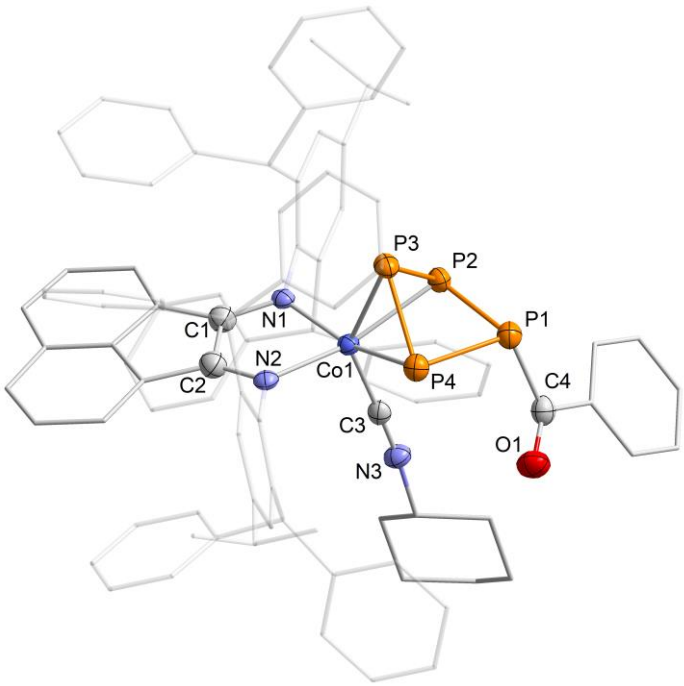

Figure S87. Solid-state molecular structure of *exo*-[(Ar*BIAN)Co(CyNC)(η^3-P_4C(O)Ph)] (*exo*-**6d**) shown at the 50% probability level. Hydrogen atoms are omitted for clarity. The asymmetric unit contained a second crystallographically independent molecule and four molecules of *n*-hexane, which are not shown. Selected bond lengths [Å] and angles [°]: P1−P2 2.2299(1), P1−P4 2.2107(1), P2−P3 2.1802(1), P3−P4 2.1863(1), Co1−P2 2.3039(9), Co1−P3 2.2862(9), Co1−P4 2.307(1), P1−C4 1.872(4), C4−O1 1.224(4), Co1−C3 1.857(3), C3−N3 1.168(4), Co1−N1 1.998(3), Co1−N2 1.995(3), C1−C2 1.460(4), P2−P1−P4 81.26(4), P1−P4−P3 83.51(4), P4−P3−P2 82.94(4), P3−P2−P1 83.20(5), Co1−C3−N3 178.2(3), P1−C4−O1 119.3(3), N1−Co1−N2 81.16(1).

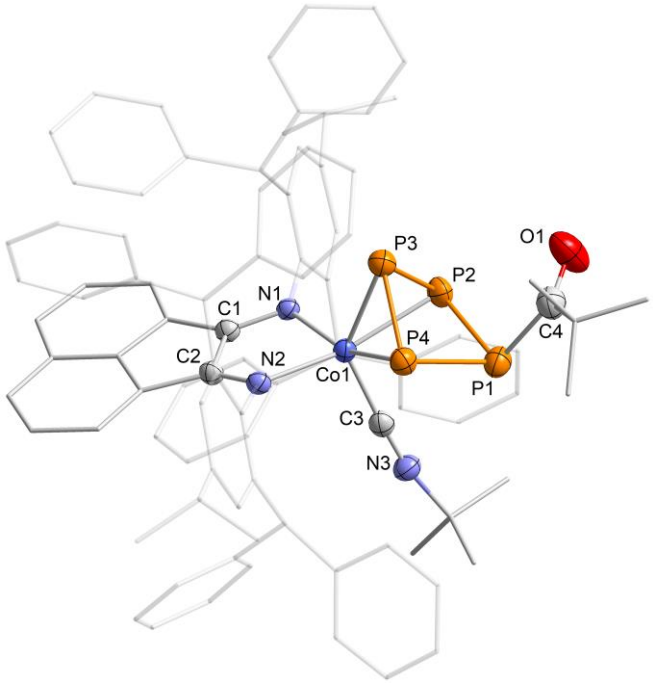

Figure S88. Solid-state molecular structure of *endo*-[(Ar*BIAN)Co(*t*BuNC)(η^3-P_4C(O)*t*Bu)] (*endo*-**6e**) shown at the 50% probability level. Hydrogen atoms are omitted for clarity. Selected bond lengths [Å] and angles [°]: P1−P2 2.2388(1), P1−P4 2.2332(1), P2−P3 2.1684(1), P3−P4 2.1514(8), Co1−P2 2.3164(8), Co1−P3 2.2996(8), Co1−P4 2.2876(7), P1−C4 1.874(3), C4−O1 1.216(4), Co1−C3 1.868(3), C3−N3 1.161(4), Co1−N1 1.984(2), Co1−N2 1.993(2), C1−C2 1.459(3), P2−P1−P4 80.56(4), P1−P4−P3 90.77(4), P4−P3−P2 84.03(4), P3−P2−P1 90.18(4), Co1−C3−N3 176.9(2), P1−C4−O1 119.8(3), N1−Co1−N2 82.29(8).

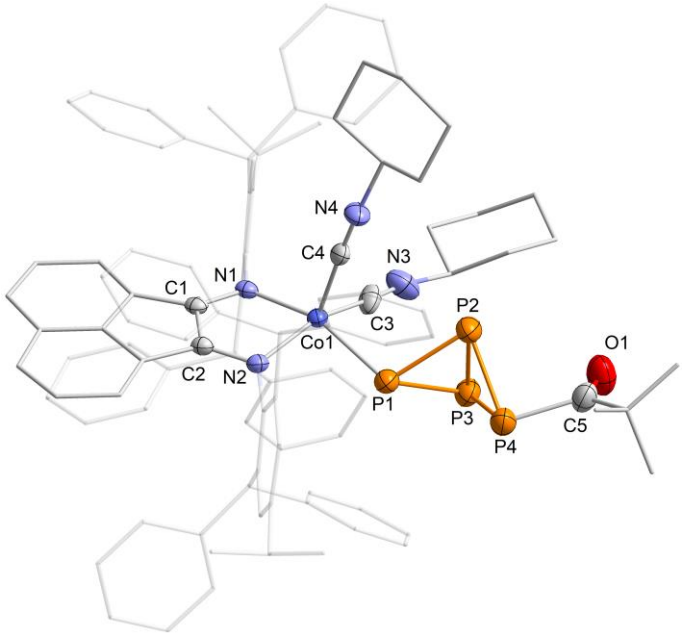

Figure S89. Solid-state molecular structure of [(Ar*BIAN)Co(CyNC)$_2$(η^1-P_4CO*t*Bu)] (**7**) shown at the 50% probability level. Hydrogen atoms and non coordinating solvent molecules omitted for clarity. Selected bond lengths [Å] and angles [°]: P1−P2 2.2095(2), P1−P3 2.2298(2), P2−P3 2.2167(2), P2−P4 2.2167(2), P3−P4 2.2083(2), Co1−P1 2.2708(1), P4−C5 1.916(5), C5−O1 1.203(6), Co1−C3 1.838(5), Co1−C4 1.869(4), C3−N3 1.087(6), C4−N4 1.163(5), Co1−N1 1.968(3), Co1−N2 1.950(3), N1−C1 1.323(5), N2−C2 1.335(5), C1−C2 1.428(5), P1−P2−P4 80.00(6), P1−P3−P4 79.75(6), P2−P1−P3 58.97(5), P2−P4−P3 59.19(6), Co1−C3−N3 174.4(4), Co1−C4−N4 176.4(4), P4−C5−O1 122.0(4), N1−Co1−N2 82.32(1).

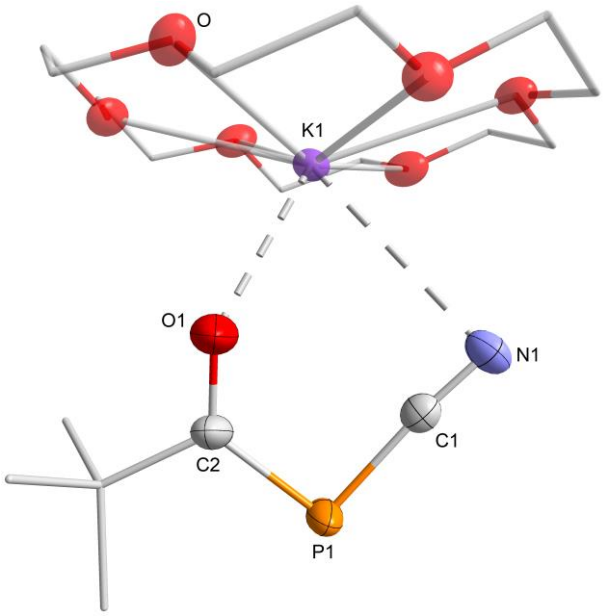

Figure S90. Solid-state molecular structure of [K(18c-6)][*t*BuC(O)PCN] ([K(18c-6)]**9a**) shown at the 50% probability level. Hydrogen atoms are omitted for clarity. Selected bond lengths [Å] and angles [°]: P1−C1 1.777(2), P1−C2 1.782(2), C1−N1 1.152(3), K1−N1 3.323(2), K1−O1 2.653(2), C2−O1 1.247(3), P1−C1−N1 174.6(2), C1−P1−C2 95.41(2).

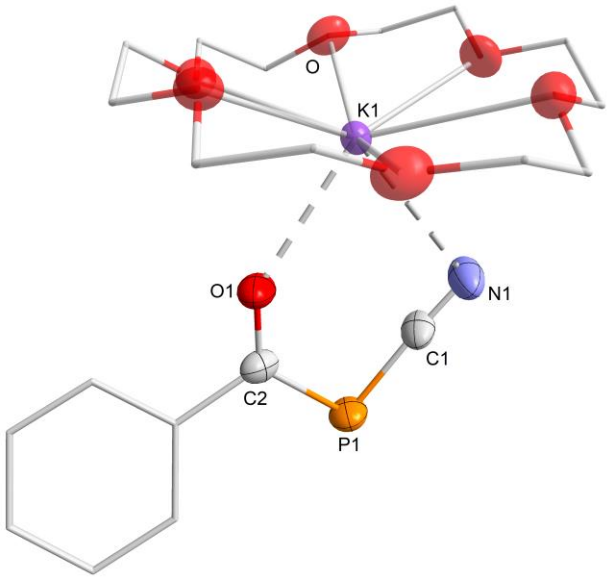

Figure S91. Solid-state molecular structure of [K(18c-6)][PhC(O)PCN] ([K(18c-6)]**9d**) shown at the 50% probability level. Hydrogen atoms are omitted for clarity. Selected bond lengths [Å] and angles [°]: P1−C1 1.769(4), P1−C2 1.796(4), C1−N1 1.149(6), K1−N1 3.035(4), K1−O1 2.741(3), C2−O1 1.231(5), P1−C1−N1 175.5(4), C1−P1−C2 96.06(2).

2.4.9 Quantum Chemical Calculations

General Methods

Geometry optimization and frequency analysis were carried out with the ORCA program package.[59] All calculations were conducted in the gas phase. Geometry optimization for [(Ar*BIAN)Co(η^3:η^1-P_4C(O)*t*Bu)] (**4a**), [(Ar*BIAN)Co(η^3:η^1-P_4C(O)Cy)] (**4b**), [(Ar*BIAN)Co(η^3:η^1-P_4C(O)Ad)] (**4c**), [CyC(O)PCN]$^-$ (**9b**), and (CyC(O))$_2$PCN (**10**) have been carried out at the BP86/def2-TZVP level of theory.[60] H_3CC(O)PCN$^-$ (**9-Me**) was optimized on the TPSS/def2-TZVP level of theory. Calculated IR Spectra were rendered using the software Avogadro.[61]

Calculation of the ^{31}P NMR chemical shifts

All calculations have been performed with the ORCA program package.[59] The geometry of the molecules has been optimized using the BP86,[62] PBE[63] and TPSS[64] functionals together with the def2-SVP basis set for C and H and def2-TZVP for all other atoms, using tight convergence criteria. The dispersion correction has been incorporated *via* the D3BJ[60] scheme and the solvent effects by using the CPCM model[65] with the dielectric constant of benzene. The ^{31}P chemical shifts has been calculated using the GIAO[66] formalism as single point calculations using the aug-pcSseg-2 basis set[67] (taken from the Basis Set Exchange library[68]) for phosphorus and the def2-TZVP basis set for all other atoms. In case of the hybrid functionals the RIJCOSX approximation has been used.[69] The single point calculation with the PBE0[70] functional has been performed on the PBE optimized geometry, while the single point calculations with the TPSSh[71] and TPSS0 (a 25% exchange version of TPSSh) functionals the TPSS optimized geometry has been used. The calculated absolute shifts has been referenced to the absolute shift of 85% H_3PO_4 using PH_3 as a secondary standard (d_{PH3} in C_6D_6 = −240 ppm) by using the equation: $d_{calc,X} = s_{calc,PH3} - s_{calc,X} - 240$ ppm. The PBE0 functional reproduced best the experimental chemical shifts.

Table S13. Calculated (at the D3BJ-PBE0/def2-TZVP/aug-pcSseg-2 @P/CPCM level of theory) and experimental ^{31}P NMR chemical shifts.

	4a		*endo*-**6a**		*exo*-**6a**		*exo*-**6d**		*endo*-**6d**	
	calcd.	exp.	calcd.	exp.	calcd.	exp.	calcd.	exp.	calcd.	exp.
P1	95	109.7	174	144.5	−3	−26.1	89	61.3	64	-
P2	104	109.7	61	71.7	61	50	8	−21.4	167	-
P3	67	59.2	82	71.7	83	50	67	61.3	130	-
P4	315	323.3	88	68.6	10	5.2	23	13.9	71	-
	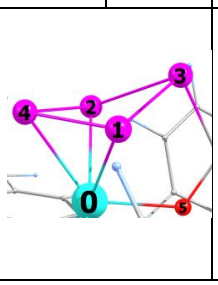		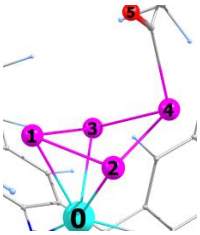				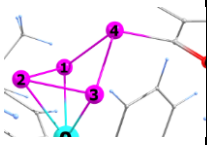		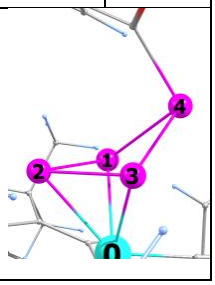	

Table S14. Calculated (at the D3BJ-PBE0/def2-TZVP/aug-pcSseg-2 @P/CPCM level of theory) and experimental ^{31}P NMR chemical shifts.

	exo-**7a**	*endo*-**7a**	**3**$^{-}$	
	calcd.	calcd.	calcd.	exp.
P1	−10	149	137	113.0
P2	−321	−219		
P3	−276	−229		
P4	−105	39		
	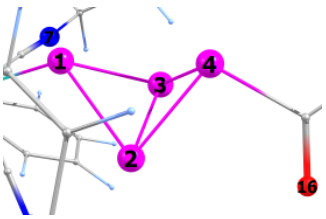	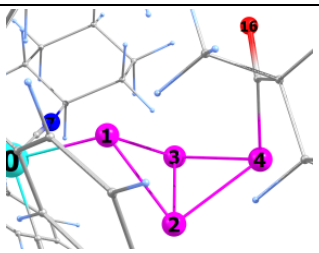	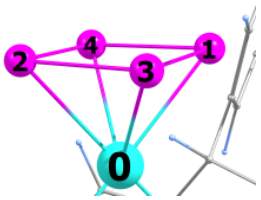	

Table S15. Calculated ^{31}P NMR chemical shifts using different functionals together with the D3BJ dispersion corrections, def2-TZVP/aug-pcSseg-2 @P basis sets and CPCM model.

		BP86	TPSS	PBE	PBE0	TPSSh	TPSS0
PH_3	P	561	581	568	576	583	585
4a	**P1**	181	128	180	95	103	53
	P2	194	134	190	104	108	58
	P3	139	99	143	67	74	39
	P4	371	312	368	315	299	266
endo-**6a**	**P1**	252	194	231	174	180	147
	P2	116	72	112	61	56	27
	P3	144	100	150	82	78	39
	P4	151	114	145	88	94	68
exo-**6a**	**P1**	66	27	47	−3	14	−17
	P2	111	58	92	61	49	31
	P3	125	85	129	83	70	42
	P4	59	33	56	10	18	−3
endo-**6d**	**P1**	138	94	138	89	77	49
	P2	84	36	59	8	23	−8
	P3	101	65	103	67	54	34
	P4	73	45	71	23	29	8
exo-**6d**	**P1**	120	82	121	64	63	32
	P2	254	194	230	167	177	141
	P3	183	133	183	130	116	87
	P4	127	89	120	71	72	51
exo-**7a**	**P1**	58	16	55	−10	-9	-43
	P2	−274	−304	−288	−321	−315	−332
	P3	−239	−256	−234	−276	−271	−291
	P4	−89	−106	-90	−105	−110	−117
endo-**7a**	**P1**	201	159	202	149	139	112
	P2	−176	−206	−179	−219	−220	−239
	P3	−188	−217	−203	−229	−226	−239
	P4	24	17	31	39	21	28
3$^-$	**P1**	157	119	152	114	109	96
	P2	162	124	157	118	113	99
	P3	170	146	169	161	146	147
	P4	172	140	164	157	140	142
	average	165	132	160	137	127	121

Frequency analysis

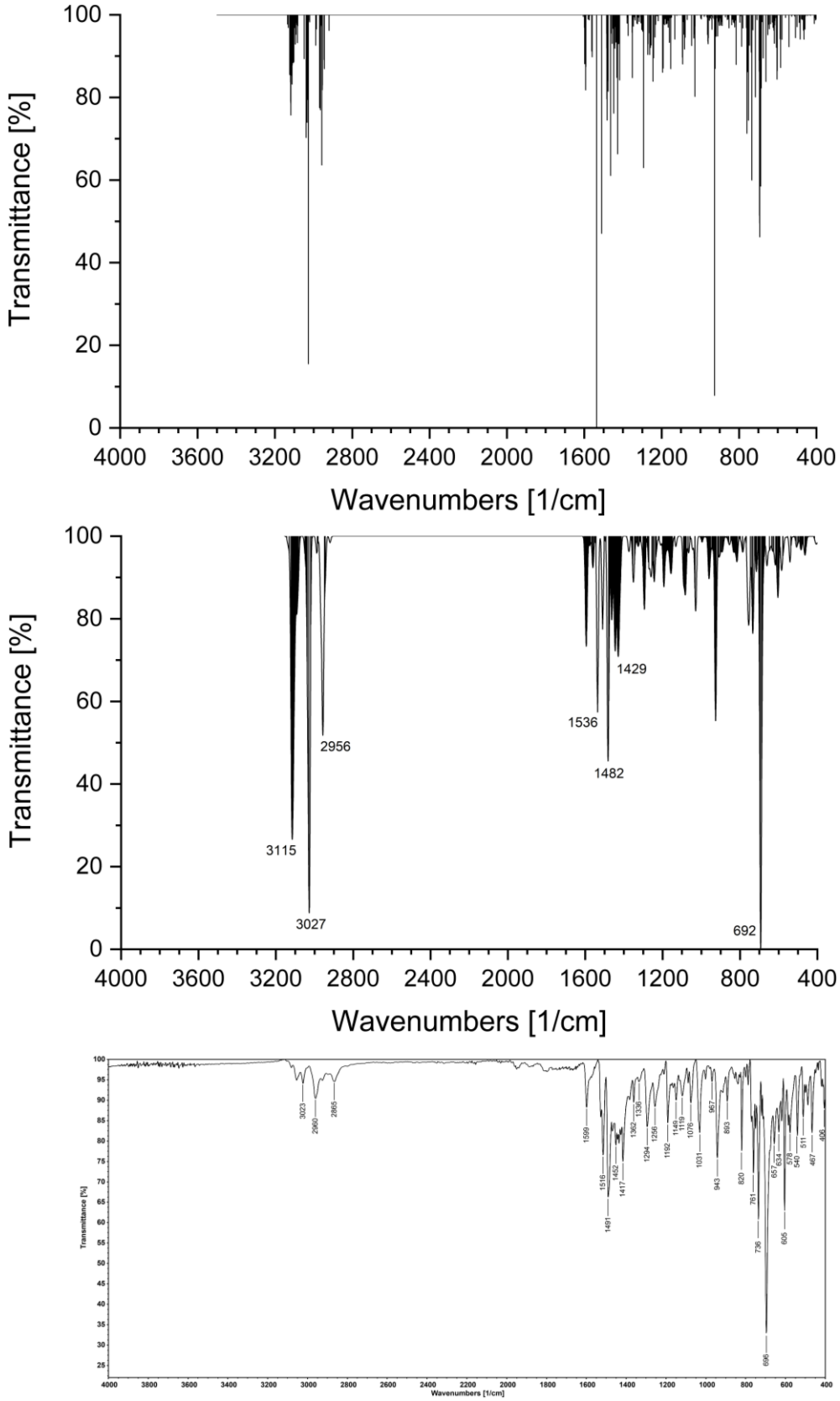

Figure S92. Comparison of DFT calculated (BP86/def2-TZVP, top/middle) and experimental (bottom) IR spectra of compound [(Ar*BIAN)Co(η^3:η^1-P_4C(O)*t*Bu)] (**4a**). DFT calculated IR spectra without peak broadening (top): scaling type: linear, line shape: gaussian, scale factor: 1.00, peak width: 0.0, points per peak 10. DFT calculated IR spectra settings (middle): scaling type: linear, line shape: gaussian, scale factor: 1.00, peak width: 10.0, points per peak 10.

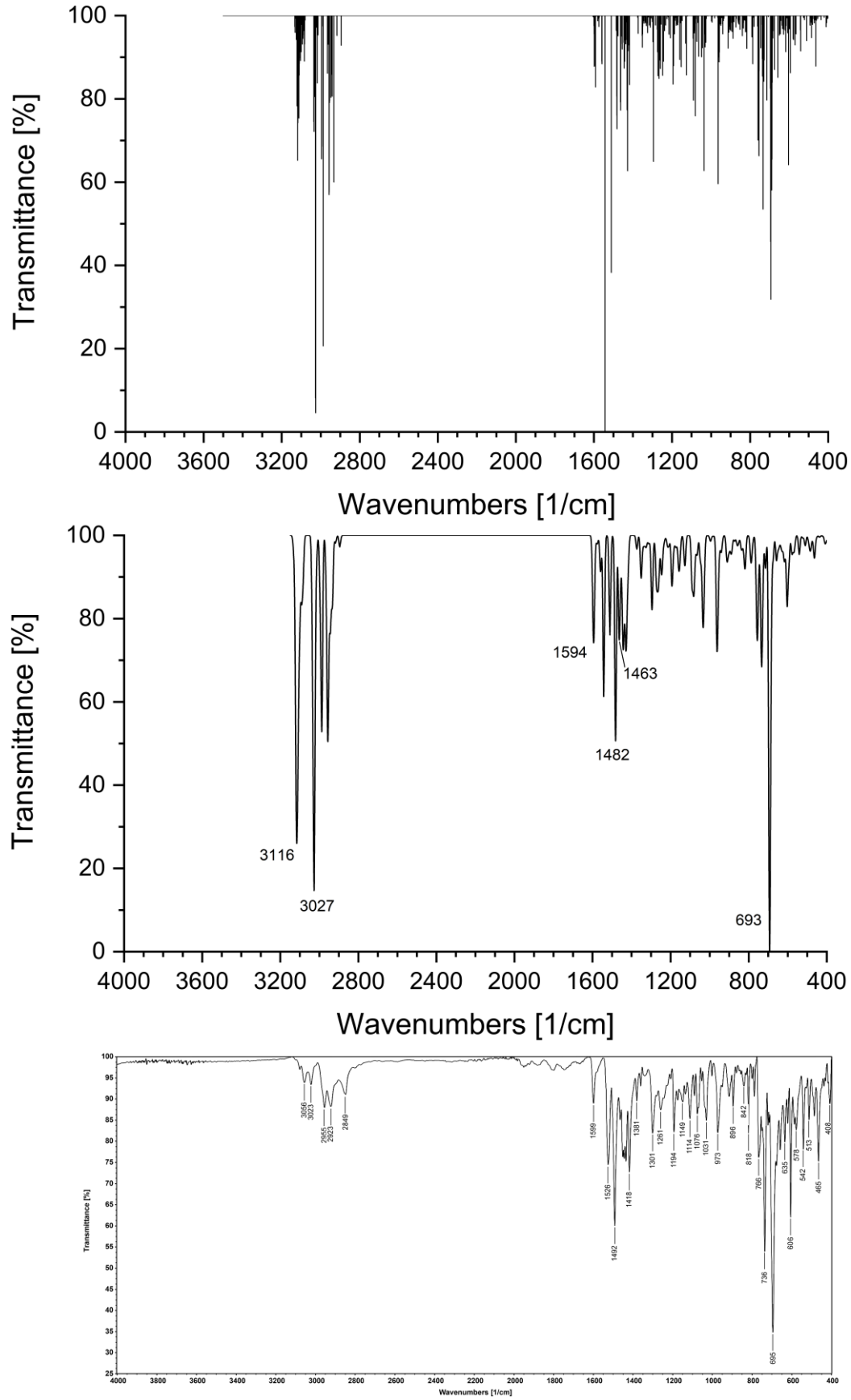

Figure S93. Comparison of DFT calculated (BP86/def2-TZVP, top/middle) and experimental (bottom) IR spectra of compound [(Ar*BIAN)Co(η^3:η^1-P_4C(O)Cy)] (**4b**). DFT calculated IR spectra without peak broadening (top): scaling type: linear, line shape: gaussian, scale factor: 1.00, peak width: 0.0, points per peak 10. DFT calculated IR spectra settings (middle): scaling type: linear, line shape: gaussian, scale factor: 1.00, peak width: 10.0, points per peak 10.

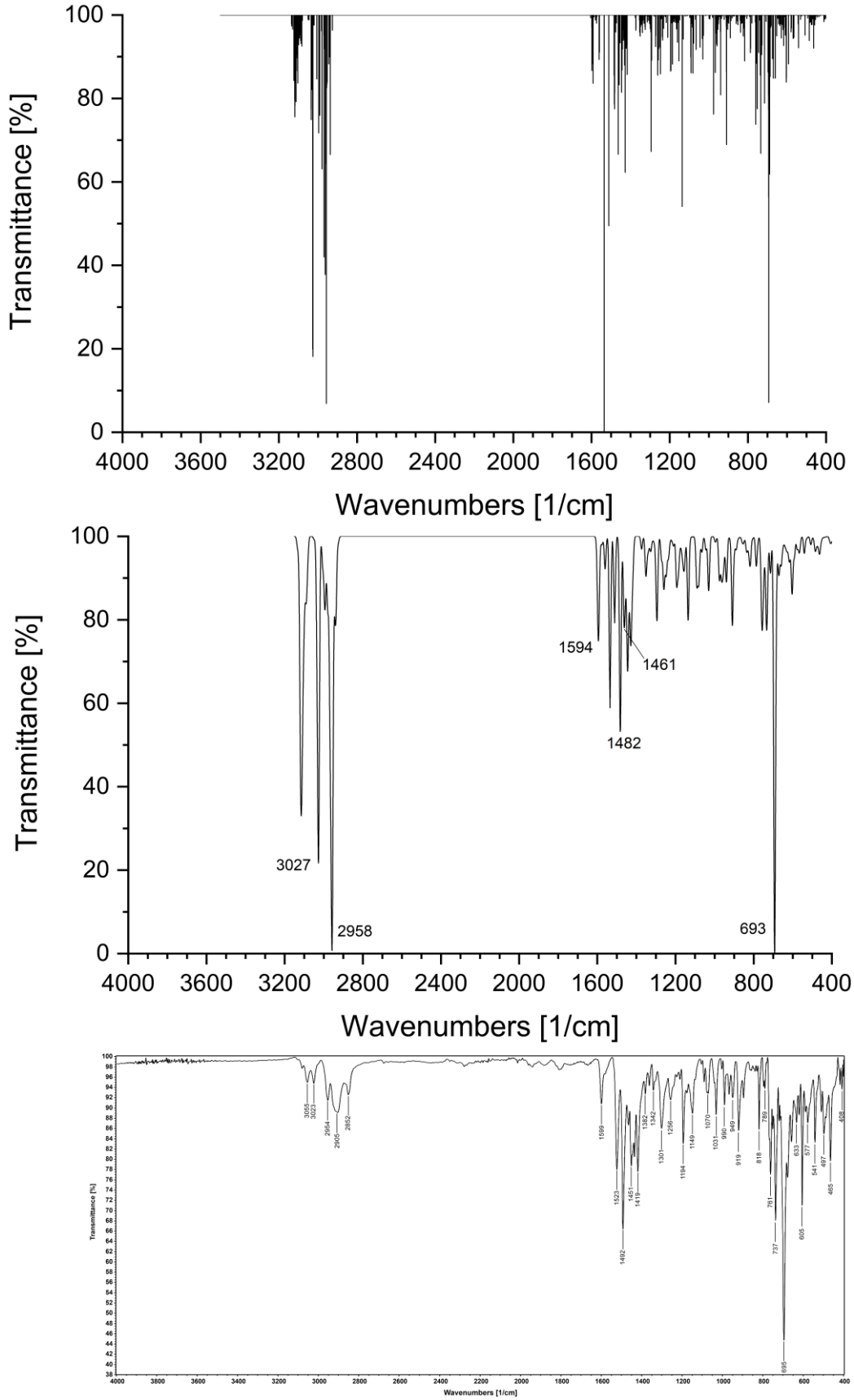

Figure S94. Comparison of DFT calculated (BP86/def2-TZVP, top/middle) and experimental (bottom) IR spectra of compound [(Ar*BIAN)Co(η^3:η^1-P_4C(O)Ad)] (**4c**). DFT calculated IR spectra without peak broadening (top): scaling type: linear, line shape: gaussian, scale factor: 1.00, peak width: 0.0, points per peak 10. DFT calculated IR spectra settings (middle): scaling type: linear, line shape: gaussian, scale factor: 1.00, peak width: 10.0, points per peak 10.

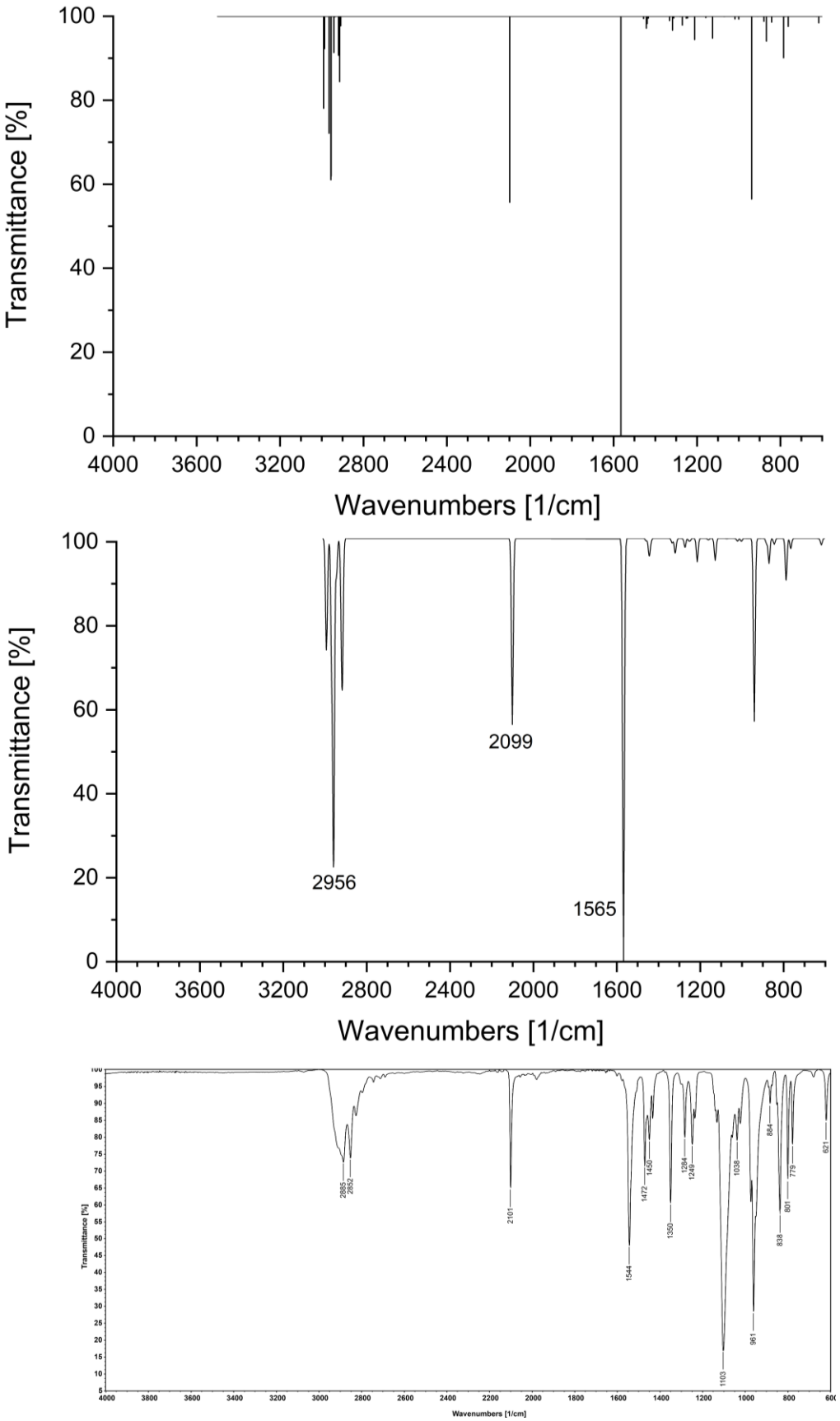

Figure S95. Comparison of DFT calculated (BP86/def2-TZVP, top/middle: $[CyC(O)PCN]^-$ (**9b**)) and experimental (bottom: [K(18c-6]**9b**]) IR spectra. DFT calculated IR spectra without peak broadening (top): scaling type: linear, line shape: gaussian, scale factor: 1.00, peak width: 0.0, points per peak 10. DFT calculated IR spectra settings (middle): scaling type: linear, line shape: gaussian, scale factor: 1.00, peak width: 10.0, points per peak 10.

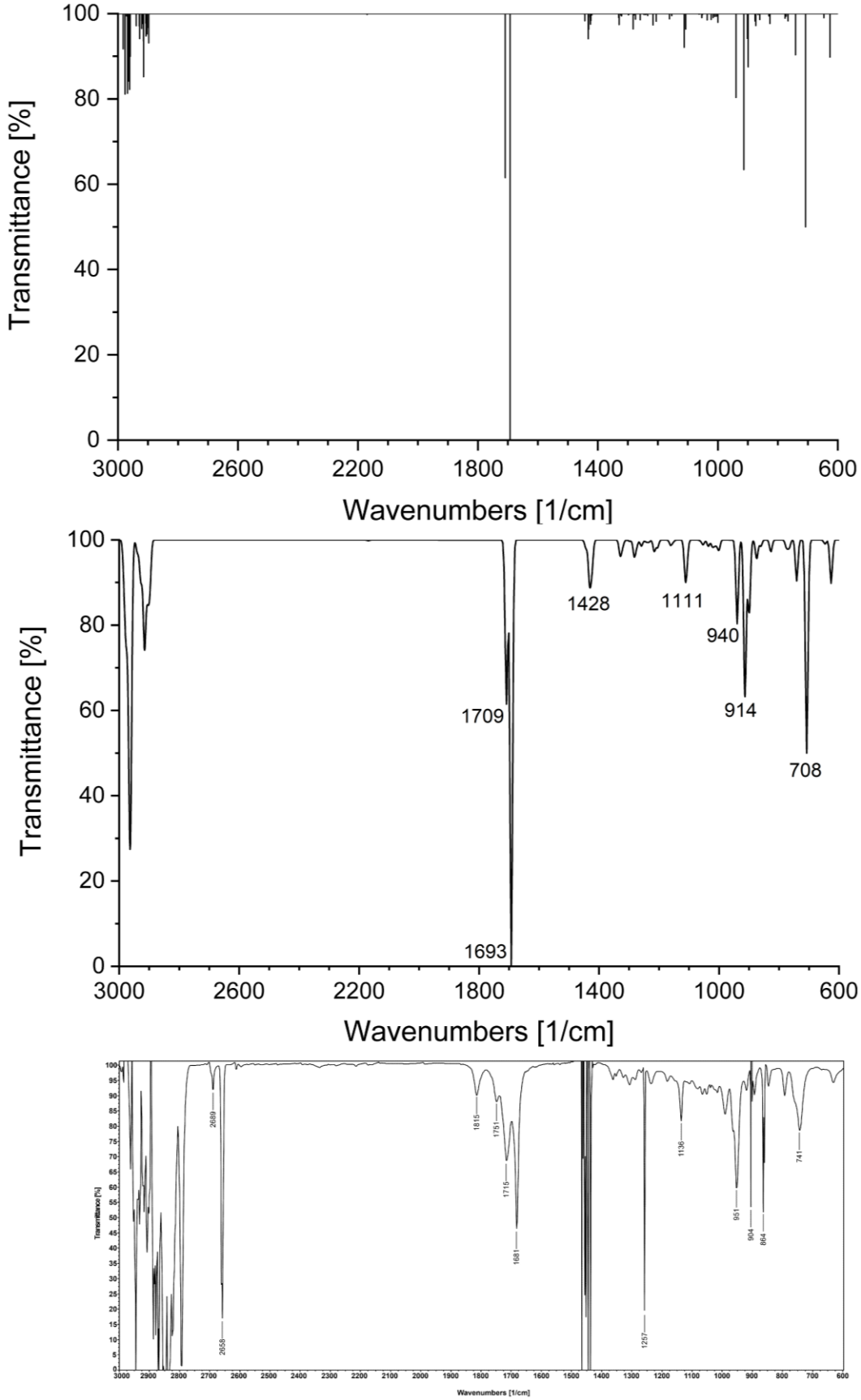

Figure S96. Comparison of DFT calculated (BP86/def2-TZVP, top/middle) and experimental (bottom) IR spectra of compound $(CyC(O))_2PCN$ (**10**). DFT calculated IR spectra without peak broadening (top): scaling type: linear, line shape: gaussian, scale factor: 0.99, peak width: 0.0, points per peak 10. DFT calculated IR spectra settings (middle): scaling type: linear, line shape: gaussian, scale factor: 0.99, peak width: 10.0, points per peak 10.

Natural theory analysis

$[CyC(O)PCN]^-$ (**9b**):

TOPO matrix for the leading resonance structure:

PCN unit: 1P 4C 3N

Atom	1	2	3	4	5	6	7	8	9	10	11	12	13	14	15	16	17
1. P	1	0	0	1	2	0	0	0	0	0	0	0	0	0	0	0	0
2. O	0	3	0	0	1	0	0	0	0	0	0	0	0	0	0	0	0
3. N	0	0	1	3	0	0	0	0	0	0	0	0	0	0	0	0	0
4. C	1	0	3	0	0	0	0	0	0	0	0	0	0	0	0	0	0
5. C	2	1	0	0	0	1	0	0	0	0	0	0	0	0	0	0	0
6. C	0	0	0	0	1	0	1	1	0	0	0	1	0	0	0	0	0
7. C	0	0	0	0	0	1	0	0	1	0	0	0	0	1	0	1	0
8. C	0	0	0	0	0	1	0	0	0	0	1	0	1	0	0	0	0
9. C	0	0	0	0	0	0	1	0	0	1	0	0	0	0	0	0	1
10. C	0	0	0	0	0	0	0	0	1	0	1	0	0	0	1	0	0
11. C	0	0	0	0	0	0	0	1	0	1	0	0	0	0	0	0	0
12. H	0	0	0	0	0	1	0	0	0	0	0	0	0	0	0	0	0
13. H	0	0	0	0	0	0	0	1	0	0	0	0	0	0	0	0	0
14. H	0	0	0	0	0	0	1	0	0	0	0	0	0	0	0	0	0
15. H	0	0	0	0	0	0	0	0	0	1	0	0	0	0	0	0	0
16. H	0	0	0	0	0	0	1	0	0	0	0	0	0	0	0	0	0
17. H	0	0	0	0	0	0	0	0	1	0	0	0	0	0	0	0	0
18. H	0	0	0	0	0	0	0	0	0	1	0	0	0	0	0	0	0
19. H	0	0	0	0	0	0	0	1	0	0	0	0	0	0	0	0	0
20. H	0	0	0	0	0	0	0	0	1	0	0	0	0	0	0	0	0
21. H	0	0	0	0	0	0	0	0	0	0	1	0	0	0	0	0	0
22. H	0	0	0	0	0	0	0	0	0	0	1	0	0	0	0	0	0

RS	Resonance Weight(%)	Added(Removed)
1	5.18	
2	4.29	P 1- O 2, (P 1- C 5), (O 2), C 5
3	4.22	P 1- N 3, (P 1- C 5), O 2- C 5, (N 3- C 4), (O 2), C 4
4	4.06	(P 1- C 5), O 2- C 5, P 1, (O 2)
5	3.42	P 1- C 4, (P 1- C 5), O 2- C 5, (N 3- C 4), (O 2), N 3
6	3.04	P 1- O 2, P 1- N 3, (P 1- C 5), (P 1- C 5), O 2- C 5, (N 3- C 4), (O 2), (O 2), C 4,C 5
7	2.31	P 1- O 2, P 1- C 4, (P 1- C 5), (P 1- C 5), O 2- C 5, (N 3- C 4), (O 2), (O 2), N 3, C 5
8	2.17	(P 1- C 5), O 2- C 5, O 2- C 5, (C 5- C 6), C 6- C 8, (C 8- C 11), P 1, (O 2), (O 2), C 11
9	2.17	(P 1- C 5), O 2- C 5, O 2- C 5, (C 5- C 6), C 6- C 7, (C 7- C 9), P 1, (O 2), (O 2), C 9
10	1.94	P 1- C 4, P 1- C 4, (P 1- C 5), (P 1- C 5), O 2- C 5, (N 3- C 4), (N 3- C 4), N 3- C5, (O 2), N 3
11	1.57	P 1- O 2, (P 1- C 5), C 5- C 6, (C 6- C 7), (C 6- C 8), C 7- C 9, (C 9- H 20), (O 2), C 8, H 20
12	1.55	P 1- C 4, (P 1- C 5), O 2- C 5, O 2- C 5, (N 3- C 4), (C 5- C 6), C 6- C 8, (C 8- C 11), (O 2), (O 2), N 3, C 11
13	1.54	P 1- O 2, P 1- C 4, (P 1- C 5), (P 1- C 5), O 2- C 5, (N 3- C 4), (N 3- C 4), N 3- C 5, (O 2), (O 2), N 3, C 4
14	1.54	P 1- C 4, (P 1- C 5), O 2- C 5, O 2- C 5, (N 3- C 4), (C 5- C 6), C 6- C 7, (C 7- C 9), (O 2), (O 2), N 3, C 9
15	1.54	P 1- O 2, P 1- C 4, (P 1- C 5), (N 3- C 4), C 5- C 6, (C 6- C 7), (C 6- C 8), C 8- C 11, (C 11- H 22), (P 1), (O 2), N 3, C 7, H 22
16	1.53	P 1- N 3, (N 3- C 4), (P 1), C 4
17	1.40	P 1- O 2, (O 2- C 5), (P 1), C 5
18	1.30	C 7- C 9, (C 7- H 14), (C 9- H 17), H 17
19	1.30	C 8- C 11, (C 8- H 13), (C 11- H 21), H 21
20	1.29	C 7- C 9, (C 7- H 16), (C 9- C 10), C 10
21	1.29	C 8- C 11, (C 8- H 19), (C 10- C 11), C 10
22	1.23	C 9- C 10, (C 9- H 20), (C 10- C 11), C 11
23	1.23	(C 9- C 10), C 10- C 11, (C 11- H 22), C 9
24	1.21	C 9- C 10, (C 9- H 17), (C 10- H 15), H 15
25	1.21	C 10- C 11, (C 10- H 15), (C 11- H 21), H 15
26	1.19	P 1- C 4, P 1- C 4, (P 1- C 5), (P 1- C 5), O 2- C 5, O 2- C 5, (N 3- C 4), (N 3- C 4), (O 2), (O 2), N 3, N 3
27	1.15	(C 8- C 11), C 10- C 11, (C 10- H 18), C 8
28	1.15	(C 7- C 9), C 9- C 10, (C 10- H 18), C 7
29	1.13	P 1- O 2, (P 1- C 4), (P 1- C 5), (P 1- C 5), O 2- C 5, N 3- C 4, P 1, P 1, (O 2), (O 2), (N 3), C 5
30	1.11	C 10- C 11, (C 10- H 15), (C 11- H 21), H 21
31	1.11	C 9- C 10, (C 9- H 17), (C 10- H 15), H 17
32	1.07	P 1- O 2, (P 1- C 4), (P 1- C 5), (P 1- C 5), P 1- H 12, O 2- C 5, N 3- C 4, (C 6- H 12), P 1, (O 2), (O 2), (N 3), C 5, C 6
33	1.01	P 1- O 2, P 1- C 4, (P 1- C 5), (N 3- C 4), C 5- C 6, (C 6- C 7), (C 6- C 8), C 8- C 11, (C 11- H 22), (P 1), (O 2), N 3, C 6, C 7

34 1.01 P 1- O 2, (P 1- C 5), C 5- C 6, (C 6- C 7), (C 6- C 8), C 7- C 9, (C 9- H 20), (O 2), C 6, C 8
35 1.00 P 1- N 3, (P 1- C 4), (P 1- C 5), O 2- C 5, (C 5- C 6), P 1, (O 2), (O 2), (N 3), C 4, C 5, C 6
36 0.99 P 1- O 2, (P 1- C 5), (P 1- C 5), O 2- C 5, P 1, (O 2), (O 2), C 5
37 0.97 C 8- C 11, (C 8- H 13), (C 11- H 21), H 13
38 0.97 C 7- C 9, (C 7- H 14), (C 9- H 17), H 14
39 0.90 (P 1- C 5), O 2- C 5, O 2- C 5, (C 5- C 6), C 6- C 7, (C 6- H 12), (C 7- H 14), P 1, (O 2), (O 2), C 6, H 14
40 0.88 (P 1- C 5), O 2- C 5, O 2- C 5, (C 5- C 6), C 6- C 8, (C 6- H 12), (C 8- H 13), P 1, (O 2), (O 2), C 6, H 13
41 0.86 (P 1- C 4), (P 1- C 5), (P 1- C 5), P 1- H 12, O 2- C 5, O 2- C 5, N 3- C 4, (C 6- H 12), P 1, P 1, (O 2), (O 2), (N 3), C 6
42 0.84 (P 1- C 4), (P 1- C 5), (P 1- C 5), O 2- C 5,O 2- C 5, N 3- C 4, P 1, P 1, P 1, (O 2), (O 2), (N 3)
43 0.82 C 6- C 8, (C 6- H 12), (C 8- H 13), H 13
44 0.81 P 1- O 2, P 1- N 3, (P 1- C 4), (P 1- C 5), (O 2), (N 3), C 4, C 5
45 0.81 P 1- C 4, P 1- C 4, P 1- C 4, (P 1- C 5), (P 1- C 5), O 2- C 5, O 2- C 5, (N 3- C 4), (N 3- C 4), (N 3- C 4), (P 1), (O 2), (O 2), N 3, N 3, N 3
46 0.80 C 6- C 7, (C 6- H 12), (C 7- H 14), H 14
47 0.80 C 8- C 11, (C 8- H 19), (C 10- C 11), H 19
48 0.79 C 7- C 9, (C 7- H 16), (C 9- C 10), H 16
49 0.78 P 1- C 4, (N 3- C 4), (P 1), N 3
50 0.76 P 1- O 2, (P 1- C 5), (N 3- C 4), (O 2), (O 2), N 3, C 4, C 5
51 0.74 (P 1- C 4), N 3- C 4, P 1, (N 3)
52 0.71 P 1- N 3, (P 1- C 4), (P 1- C 5), O 2- C 5, P 1, (O 2), (N 3), C 4
53 0.70 (C 7- C 9), C 9- C 10, (C 10- H 18), H 18
54 0.70 (C 8- C 11), C 10- C 11, (C 10- H 18), H 18
55 0.69 (P 1- C 5), O 2- C 5, O 2- C 5, (C 5- C 6), C 6- C 8, (C 8- H 13), P 1, (O 2), (O 2), H 13
56 0.69 (P 1- C 5), O 2- C 5, O 2- C 5, (C 5- C 6), C 6- C 7, (C 7- H 14), P 1, (O 2), (O 2), H 14
57 0.66 P 1- O 2, (P 1- C 5), C 5- C 6, (C 6- C 8), C 8- C 11, (C 11- H 22), (O 2), H 22
58 0.66 P 1- C 4, (P 1- C 5), (N 3- C 4), C 5
59 0.63 P 1- O 2, P 1- C 4, (P 1- C 5), (N 3- C 4), C 5- C 6, (C 6- C 7), C 7- C 9, (C 9- H 20), (P 1), (O 2), N 3, H 20
60 0.61 P 1- C 4, P 1- C 4, (P 1- C 5), (N 3- C 4), (N 3- C 4), (P 1), N 3, C 5
61 0.55 P 1- O 2, P 1- C 4, P 1- C 4, (P 1- C 5), (P 1- C 5), O 2- C 5, (N 3- C 4), (N 3- C 4), (N 3- C 4), N 3- C 5, (P 1), (O 2), (O 2), N 3, N 3, C 4
62 0.52 (P 1- C 5), O 2- C 5, O 2- C 5, (C 5- C 6), C 6- C 7, (C 6- H 12), (C 7- H 14), P 1, (O 2), (O 2), C 6, H 12
63 0.51 (P 1- C 5), O 2- C 5, O 2- C 5, (C 5- C 6), C 6- C 8, (C 6- H 12), (C 8- H 13), P 1, (O 2), (O 2), C 6, H 12
64 0.45 C 6- C 8, (C 6- H 12), (C 8- H 13), H 12
65 0.44 P 1- O 2, (P 1- C 4), (P 1- C 5), (P 1- C 5), P 1- C 6, O 2- C 5, N 3- C 4, (C 6- H 12), P 1, (O 2), (O 2), (N 3), C 5, H 12
66 0.43 C 6- C 7, (C 6- H 12), (C 7- H 14), H 12
67 0.40 P 1- O 2, (P 1- C 5), C 7- C 9, (C 7- H 14), (C 9- H 17), (O 2), C 5, H 17
68 0.40 P 1- O 2, (P 1- C 5), C 8- C 11, (C 8- H 13), (C 11- H 21), (O 2), C 5, H 21
69 0.39 P 1- O 2, (P 1- C 5), C 7- C 9, (C 7- H 16), (C 9- C 10), (O 2), C 5, C 10
70 0.39 P 1- C 4, P 1- C 4, (P 1- C 5), (P 1- C 5), O 2- C 5, O 2- C 5, (N 3- C 4), (N 3- C 4), (C 6- C 7), C 6- C 8, (C 8- H 19), (O 2), (O 2), N 3, N 3, H 19
71 0.39 P 1- O 2, (P 1- C 5), C 8- C 11, (C 8- H 19), (C 10- C 11), (O 2), C 5, C 10
72 0.36 P 1- O 2, (P 1- C 4), (P 1- C 5), (P 1- C 5), O 2- C 5, N 3- C 4, C 6- C 7, (C 6- C 8), (C 7- H 16), P 1, P 1, (O 2), (O 2), (N 3), C 5, H 16
73 0.34 P 1- N 3, (P 1- C 5), O 2- C 5, (N 3- C 4), C 7- C 9, (C 7- H 14), (C 9- H 17), (O 2), C 4, H 17
74 0.34 P 1- N 3, (P 1- C 5), O 2- C 5, (N 3- C 4), C 8- C 11, (C 8- H 13), (C 11- H 21), (O 2), C 4, H 21
75 0.33 P 1- O 2, (P 1- C 5), C 9- C 10, (C 9- H 20), (C 10- C 11), (O 2), C 5, C 11
76 0.33 P 1- O 2, (P 1- C 5), (C 9- C 10), C 10- C 11,(C 11- H 22), (O 2), C 5, C 9
77 0.33 P 1- N 3, (P 1- C 5), O 2- C 5, (N 3- C 4), C 7- C 9, (C 7- H 16), (C 9- C 10), (O 2), C 4, C 10
78 0.33 P 1- N 3, (P 1- C 5), O 2- C 5, (N 3- C 4), C 8- C 11, (C 8- H 19), (C 10- C 11), (O 2),C 4, C 10
79 0.32 P 1- C 4, P 1- C 4, (P 1- C 5), (P 1- C 5), O 2- C 5, O 2- C 5, (N 3- C 4), (N 3- C 4), C 6- C 7, (C 6- C 8), (C 7- H 16), (O 2), (O 2), N 3, N 3, H 16
80 0.31 P 1- O 2, (P 1- C 5), (P 1- C 5), O 2- C 5, (N 3- C 4), N 3- C 5, P 1, (O 2), (O 2), C 4
81 0.31 P 1- O 2, (P 1- C 5), C 9- C 10, (C 9- H 17),(C 10- H 15), (O 2), C 5, H 15
82 0.31 P 1- O 2, (P 1- C 5), C 10- C 11, (C 10- H 15), (C 11- H 21), (O 2), C 5, H 15
83 0.30 P 1- N 3, (N 3- C 4), (P 1), C 4
84 0.28 P 1- O 2, P 1- N 3, (P 1- C 5), (N 3- C 4), (P 1), (O 2), C 4, C 5
85 0.27 P 1- C 4, (P 1- C 5), O 2- C 5, O 2- C 5, (N 3- C 4), (C 5- C 6), C 6- C 7, (C 6- H 12),(C 7- H 14), (O 2), (O 2), N 3, C 6, H 14
86 0.27 (P 1- C 4), (P 1- C 5), (P 1- C 5), P 1- C 6,O 2- C 5, O 2- C 5, N 3- C 4, (C 6- H 12),P 1, P 1, (O 2), (O 2), (N 3), H 12
87 0.26 P 1- N 3, (P 1- C 5), O 2- C 5, (N 3- C 4), C 9- C 10, (C 9- H 20), (C 10- C 11), (O 2), C 4, C 11
88 0.26 P 1- N 3, (P 1- C 5), O 2- C 5, (N 3- C 4), (C 9- C 10), C 10- C 11, (C 11- H 22), (O 2), C 4, C 9

89 0.26 P 1- C 4, (P 1- C 5), O 2- C 5, O 2- C 5, (N 3- C 4), (C 5- C 6), C 6- C 8, (C 6- H 12), (C 8- H 13), (O 2), (O 2), N 3, C 6, H 13
90 0.25 P 1- O 2, (P 1- C 5), (C 8- C 11), C 10- C 11, (C 10- H 18), (O 2), C 5, C 8
91 0.25 P 1- O 2, (P 1- C 5), (C 7- C 9), C 9- C 10, (C 10- H 18), (O 2), C 5, C 7
92 0.25 P 1- C 4, P 1- C 4, (P 1- C 5), (P 1- C 5), O 2- C 5, O 2- C 5, (N 3- C 4), (N 3- C 4), (C 6- C 7), C 6- C 8, (C 8- H 19), (O 2), (O 2), N 3, N 3, C 7
93 0.24 P 1- N 3, (P 1- C 5), O 2- C 5, (N 3- C 4), C 9- C 10, (C 9- H 17), (C 10- H 15), (O 2), C 4, H 15
94 0.24 P 1- N 3, (P 1- C 5), O 2- C 5, (N 3- C 4), C 10- C 11, (C 10- H 15), (C 11- H 21), (O 2), C 4, H 15
95 0.24 P 1- O 2, (P 1- C 4), (P 1- C 5), (P 1- C 5), O 2- C 5, N 3- C 4, (C 6- C 7), C 6- C 8, (C 8- H 19), P 1, P 1, (O 2), (O 2), (N 3), C 5, H 19
96 0.22 P 1- O 2, (P 1- C 5), C 10- C 11, (C 10- H 15), (C 11- H 21), (O 2), C 5, H 21
97 0.22 P 1- O 2, (P 1- C 5), C 9- C 10, (C 9- H 17), (C 10- H 15), (O 2), C 5, H 17
98 0.19 P 1- O 2, (P 1- C 4), (P 1- C 5), (P 1- C 5), O 2- C 5, N 3- C 4, C 6- C 7, (C 6- C 8),(C 7- H 16), P 1, P 1, (O 2), (O 2), (N 3), C 5, C 8
99 0.19 (P 1- C 5), O 2- C 5, O 2- C 5, (C 5- C 6),C 6- C 7, (C 6- C 8), (C 7- H 16), P 1, (O 2), (O 2), C 6, H 16
100 0.19 (P 1- C 5), O 2- C 5, O 2- C 5, (C 5- C 6), (C 6- C 7), C 6- C 8, (C 8- H 19), P 1, (O 2), (O 2), C 6, H 19
101 0.19 P 1- N 3, (P 1- C 5), O 2- C 5, (N 3- C 4), (C 8- C 11), C 10- C 11, (C 10- H 18), (O 2), C 4, C 8
102 0.19 P 1- N 3, (P 1- C 5), O 2- C 5, (N 3- C 4), (C 7- C 9), C 9- C 10, (C 10- H 18), (O 2), C 4, C 7
103 0.18 (P 1- C 5), O 2- C 5, C 7- C 9, (C 7- H 14), (C 9- H 17), P 1, (O 2), H 17
104 0.18 (P 1- C 5), O 2- C 5, C 8- C 11, (C 8- H 13), (C 11- H 21), P 1, (O 2), H 21
105 0.17 (P 1- C 5), O 2- C 5, C 7- C 9, (C 7- H 16),(C 9- C 10), P 1, (O 2), C 10
106 0.17 (P 1- C 5), O 2- C 5, C 8- C 11, (C 8- H 19), (C 10- C 11), P 1, (O 2), C 10
107 0.16 (P 1- C 5), O 2- C 5, O 2- C 5, (C 5- C 6), C 6- C 9, (C 9- H 20), P 1, (O 2), (O 2), H 20
108 0.16 (P 1- C 5), O 2- C 5, O 2- C 5, (C 5- C 6), C 6- C 11, (C 11- H 22), P 1, (O 2), (O 2),H 22
109 0.15 (P 1- C 4), (P 1- C 5), (P 1- C 5), P 1- C 8, O 2- C 5, O 2- C 5, N 3- C 4, (C 6- C 8), P 1, P 1, (O 2), (O 2), (N 3), C 6
110 0.15 P 1- N 3, (P 1- C 5), O 2- C 5, (N 3- C 4), C 10- C 11, (C 10- H 15), (C 11- H 21), (O 2), C 4, H 21
111 0.15 P 1- C 4, P 1- C 4, (P 1- C 5), (P 1- C 5), O 2- C 5, O 2- C 5, (N 3- C 4), (N 3- C 4), C 6- C 7, (C 6- C 8), (C 7- H 16), (O 2), (O 2), N 3, N 3, C 8
112 0.15 P 1- N 3, (P 1- C 5), O 2- C 5, (N 3- C 4), C 9- C 10, (C 9- H 17), (C 10- H 15), (O 2), C 4, H 17
113 0.15 (P 1- C 4), (P 1- C 5), (P 1- C 5), P 1- C 7, O 2- C 5, O 2- C 5, N 3- C 4, (C 6- C 7), P 1, P 1, (O 2), (O 2), (N 3), C 6
114 0.11 (P 1- C 5), O 2- C 5, C 9- C 10, (C 9- H 20), (C 10- C 11), P 1, (O 2), C 11
115 0.11 (P 1- C 5), O 2- C 5, (C 9- C 10), C 10- C 11, (C 11- H 22), P 1, (O 2), C 9
others 0.73

100.00 * Total *

Summary of Natural Population Analysis:

	Natural	Natural Population			
Atom No	Charge	Core	Valence	Rydberg	Total
P 1	0.02284	9.99994	4.94720	0.03002	14.97716
O 2	-0.62042	1.99999	6.59325	0.02718	8.62042
N 3	-0.44161	1.99999	5.40927	0.03235	7.44161
C 4	-0.04142	1.99998	3.99147	0.04997	6.04142
C 5	0.20750	1.99998	3.74688	0.04564	5.79250
C 6	-0.31314	1.99998	4.29121	0.02194	6.31314
C 7	-0.40977	1.99998	4.39801	0.01178	6.40977
C 8	-0.40964	1.99998	4.39792	0.01174	6.40964
C 9	-0.40261	1.99998	4.39325	0.00937	6.40261
C 10	-0.40456	1.99998	4.39493	0.00965	6.40456
C 11	-0.40258	1.99998	4.39322	0.00938	6.40258
H 12	0.20452	0.00000	0.79299	0.00249	0.79548
H 13	0.21192	0.00000	0.78465	0.00343	0.78808
H 14	0.21215	0.00000	0.78442	0.00344	0.78785
H 15	0.19381	0.00000	0.80381	0.00238	0.80619
H 16	0.21326	0.00000	0.78481	0.00194	0.78674
H 17	0.18891	0.00000	0.80875	0.00234	0.81109
H 18	0.19426	0.00000	0.80400	0.00174	0.80574
H 19	0.21347	0.00000	0.78459	0.00194	0.78653
H 20	0.19709	0.00000	0.80103	0.00189	0.80291
H 21	0.18894	0.00000	0.80872	0.00234	0.81106
H 22	0.19710	0.00000	0.80101	0.00189	0.80290
* Total *	-1.00000	29.99979	59.71539	0.28482	90.00000

$[H_3CC(O)PCN]^-$ (**9-Me**):

TOPO matrix for the leading resonance structure:
PCN unit: 1P 4C 3N

Atom	1	2	3	4	5	6	7	8	9
1. P	1	0	0	1	2	0	0	0	0
2. O	0	3	0	0	1	0	0	0	0
3. N	0	0	1	3	0	0	0	0	0
4. C	1	0	3	0	0	0	0	0	0
5. C	2	1	0	0	0	1	0	0	0
6. C	0	0	0	0	1	0	1	1	1
7. H	0	0	0	0	0	1	0	0	0
8. H	0	0	0	0	0	1	0	0	0
9. H	0	0	0	0	0	1	0	0	0

RS	Resonance Weight(%)	Added(Removed)
1	37.40	
2	12.72	P 1- C 4, (P 1- C 5), O 2- C 5, (N 3- C 4), (O 2), N 3
3	12.14	(P 1- C 5), O 2- C 5, P 1, (O 2)
4	7.98	P 1- C 4, (P 1- C 5), (P 1- C 5), O 2- C 5, O 2- C 5, (N 3- C 4), P 1, (O 2), (O 2), N 3
5	5.60	P 1- C 4, (P 1- C 5), O 2- C 5, O 2- C 5, (N 3- C 4), (C 5- C 6), (O 2), (O 2), N 3, C 6
6	5.02	(P 1- C 5), O 2- C 5, O 2- C 5, (C 5- C 6), P 1, (O 2), (O 2), C 6
7	4.53	(P 1- C 4), (P 1- C 5), O 2- C 5, N 3- C 4, P 1, P 1, (O 2), (N 3)
8	3.53	(P 1- C 5), C 5- C 6, (C 6- H 8), H 8
9	3.17	(P 1- C 5), (P 1- C 5), O 2- C 5, O 2- C 5, P 1, P 1, (O 2), (O 2)
10	2.58	P 1- C 4, (P 1- C 5), (N 3- C 4), C 5
11	1.69	P 1- C 4, (P 1- C 5), (P 1- C 5), O 2- C 5, O 2- C 5, (N 3- C 4), P 1, (O 2), (O 2), N 3
12	1.44	P 1- C 4, (P 1- C 5), (N 3- C 4), C 5
13	1.12	P 1- C 4, P 1- C 4, (P 1- C 5), (P 1- C 5), O 2- C 5, (N 3- C 4), (N 3- C 4), (O 2), N 3, C 5
14	0.55	P 1- C 4, (P 1- C 5), (P 1- C 5), O 2- C 5, (N 3- C 4), P 1, (O 2), C 5
15	0.54	(P 1- C 4), N 3- C 4, P 1, (N 3)
others	0.00	
	100.00	* Total *

Summary of Natural Population Analysis:

Atom	No	Natural Charge	Natural Population: Core	Valence	Rydberg	Total
P	1	-0.02209	9.99996	4.99272	0.02942	15.02209
O	2	-0.60613	2.00000	6.57985	0.02628	8.60613
N	3	-0.45586	1.99999	5.42394	0.03193	7.45586
C	4	-0.03942	1.99999	3.99176	0.04767	6.03942
C	5	0.21277	1.99999	3.74449	0.04274	5.78723
C	6	-0.68615	1.99999	4.67273	0.01343	6.68615
H	7	0.20062	0.00000	0.79798	0.00140	0.79938
H	8	0.19565	0.00000	0.80090	0.00345	0.80435
H	9	0.20060	0.00000	0.79800	0.00140	0.79940
* Total *		-1.00000	19.99992	31.80237	0.19770	52.00000

Cartesian Coordinates of optimized structures

[(Ar*BIAN)Co(η^3:η^1-P_4C(O)*t*Bu)] (**4a**):

Co	-0.23791442339567	17.10780778630257	18.82665834535711
P	1.05371653722313	17.43797982415091	16.98043814260479
P	-0.34973437857771	19.00619482287993	17.52825446364170
P	1.95498822274092	17.75454102825701	18.93016354724532
O	-0.59774045798695	18.31520471632586	20.42354520734231
N	-0.08694762606174	15.42323020862935	19.81382988167105
N	-2.00253297339348	16.41053201540457	18.37416597531651
P	1.11438072067582	19.88873347826631	19.04457966289441
C	-0.04731356720664	19.44758636362659	20.45870414116053
C	1.07646287386509	14.81797753986962	20.38136757685911
C	-1.25107071753523	14.80096967657001	19.90347022763536
C	-2.31436468272720	15.33018810214740	19.06598640306961
C	-2.91644905435905	16.94197826217013	17.41697580338694
C	-0.37405800036221	20.40703533382257	21.57326290982164
C	1.75349548866575	13.83077658529404	19.62967098952934
C	1.57123507686204	15.21677773362480	21.63568658361240
C	-1.76130842869823	13.62557009245580	20.60567665606347
C	-3.48619994032585	14.46757816976897	19.20647344464238
C	-2.91026683441970	16.43054852741347	16.10330340382767
C	-3.76020001663094	18.01472429932841	17.76713878002937
C	0.93153771210847	20.88069341996508	22.26753010400154
C	-1.30062232236001	19.76201424870951	22.62328169627748
C	-1.08918535419141	21.64823681978421	20.96125694622807
C	1.27553767772404	13.42941477986338	18.24151411689443
C	2.90299956920214	13.24716586442449	20.16475407634974
C	2.75011100497993	14.62793615230441	22.11260570159945
C	0.80853491670584	16.22312069971905	22.48316145660290
C	-3.10592508301084	13.47017535961609	20.15261141875418
C	-1.25957279094015	12.72750779141412	21.53434316363093
C	-4.76018848939128	14.43058802406687	18.67190069865611
C	-3.77595857874331	16.99746139016188	15.16342323680320
C	-2.01353876476070	15.25543382477512	15.72864647932268
C	-4.64158934708316	18.51571267923015	16.80390284767358
C	-3.71994106778780	18.56178485796529	19.18945175284854
H	1.44941358435023	20.01370593121884	22.69652125109465
H	1.60711995738220	21.33290771858788	21.52308166050644
C	0.59425291134554	21.89582559451433	23.37446898161143
H	-0.79560665029291	18.88413294215871	23.05427384616901
H	-2.22360701992578	19.40840277300610	22.13603192689552
C	-1.62976137189779	20.77791738417278	23.73169999853917
C	-1.41618714883830	22.65855141256850	22.07617015129594
H	-0.44397664901637	22.11315026835787	20.19781875765910
H	-2.01170085707083	21.32776265459865	20.46065699035632
C	1.26180086197285	11.90961491900130	18.08605667479537
H	0.23188499642690	13.76625060609822	18.15894253795661
C	2.01991267361108	14.12939958479258	17.10759795576390
C	3.42880705596358	13.63733251994910	21.40108723928845
H	3.40427431049306	12.47278542268420	19.58053434252042
H	3.15258818406362	14.96815084181599	23.06961272616665
C	-0.15243167594134	15.52935108858323	23.44690099865783
H	0.18433082034398	16.81401471152438	21.79363224759258
C	1.73443114018836	17.22360164674030	23.18138571230637
C	-3.96124711009629	12.44401434374988	20.58943469614039
H	-0.23749470470636	12.80585571660441	21.90124596058483
C	-2.11190584143784	11.69156889488749	21.99748802362229
H	-5.08876602643947	15.17034127140719	17.94375426846211
C	-5.63714730267681	13.39780357480511	19.09576999374042
H	-3.73163652097026	16.63066287763577	14.13604265840563
C	-4.66603782011511	18.02345312736083	15.49590177546497
C	-1.40055716701214	15.39819432174373	14.33649597012419
H	-1.16119233785958	15.26616035090962	16.43220833892741
C	-2.75668355044958	13.93817679159308	15.94393986760474
H	-5.30144521263966	19.34269404547270	17.07498250823608
C	-4.03549282212535	20.04955075680198	19.29771668361703
H	-2.67504358733043	18.45550811242079	19.52450283232146
C	-4.54766953921722	17.66458418288418	20.09988027065772
C	-0.11465962894021	23.11777476063929	22.75982034280426
H	1.53468016317790	22.20878698570220	23.85677415543498
C	-0.32564178828478	21.23037789895483	24.41534310411013
H	-2.28999622179237	20.29665126440057	24.47157147038297
C	-2.34076924861032	21.99628718126491	23.11456440817521

H	-1.93011250965900	23.51936348990575	21.61815386197025
C	0.23556286312337	11.16848057470815	18.69055224357745
C	2.26389474331931	11.22213718714491	17.38953551709218
C	3.21722720110129	14.83073609954743	17.29008621981200
C	1.47684724725200	14.05300700592884	15.81411196118765
C	4.70537137734058	13.01643254361048	21.94015017044984
C	0.21384981260592	14.38507646700712	24.17005188719818
C	-1.42713577316471	16.06851908062874	23.66253175800452
C	1.51412075683521	17.65531690058278	24.49588279774245
C	2.82367005998144	17.76564002624519	22.47697695573245
C	-3.41816161697914	11.54000280675877	21.54754067294373
C	-5.26887387664953	12.43349849852503	20.02277802399440
H	-1.72010837154105	10.98984524181746	22.73514743617195
H	-6.64139847271078	13.36721047777076	18.67119895109731
C	-5.60147094287378	18.61193546826439	14.45404972735981
C	-0.82227859302879	16.62251444314920	13.96308413764666
C	-1.32941133854449	14.32602639067528	13.43920798809854
C	-2.17682119187835	12.91321955629942	16.69860128378553
C	-4.03888912091002	13.72534756696507	15.41591479450741
C	-3.47402582429856	20.95124613233458	18.37575704107198
C	-4.79041881422216	20.56840759426157	20.35750407142885
C	-5.91736591862248	17.46622050345463	19.87356075262077
C	-3.92717171055883	16.95528656644078	21.13331483572071
H	0.54592050602396	23.60998596487343	22.02659234990960
H	-0.34074392048292	23.85896775931351	23.54442308400963
H	-0.55146386938117	21.94042226344653	25.22853438440979
H	0.18671044145956	20.36483825597707	24.86499964349790
H	-3.27887191568108	21.68333337914193	22.63030503799833
H	-2.60203736731000	22.72216427252865	23.90282639877739
H	-0.54908680747594	11.69105436931716	19.23953208436522
C	0.21020644065838	9.77641138215792	18.60413740055947
H	3.05858123803954	11.78729629908312	16.89983804899035
C	2.24421193414245	9.82640318141480	17.30489465146043
H	3.64983681028057	14.91580387869404	18.28710559023671
C	3.85361453512091	15.44442665918368	16.20386955308190
H	0.54646884343366	13.50558680698046	15.65127958139530
C	2.10459205149228	14.66545676877258	14.73269645446127
H	4.89684572146250	13.47187039018686	22.92675101436554
C	5.90547818409072	13.33963152818571	21.03213984121580
C	4.55507394398847	11.49847571165446	22.14123757852648
H	1.19707344891260	13.94071545190124	24.01298037124321
C	-0.66983648620618	13.79343146590480	25.07458097446077
H	-1.72695889226366	16.96079881077855	23.11257269885524
C	-2.30818521876750	15.49204574109162	24.58142734528559
H	0.67447714824756	17.25157100173187	25.06260426282581
C	2.36163773820852	18.59499532718540	25.09364389247171
C	3.67253784480297	18.69861353277337	23.07258865553718
H	3.00668077185349	17.44630459462081	21.44893467594118
H	-4.03562252312498	10.72496653297327	21.93090993100770
H	-5.98012157300302	11.65998099405339	20.31914640490080
H	-6.22718220198393	19.36274416560275	14.96606188529638
C	-6.53725945941040	17.54394169918614	13.86194538922284
C	-4.81165283137145	19.33246761884320	13.34646869253585
H	-0.87393645339152	17.46984931791889	14.64899586899265
C	-0.19263383842862	16.77117876492811	12.72847106719398
H	-1.76703131421617	13.36546655765556	13.71363626210779
C	-0.70000948310081	14.47222022510654	12.19750289332913
H	-1.18369185685339	13.05623292955321	17.12184184917981
C	-2.85618684678608	11.71855405296550	16.94662234685023
H	-4.51851560222623	14.51056323161895	14.83076749629475
C	-4.72217619742478	12.53193906386313	15.65327322576187
H	-2.86533743232132	20.56494501338425	17.55664647783079
C	-3.66499560158204	22.32637354415861	18.50984569466021
H	-5.22625954578212	19.88762822201758	21.08968828329203
C	-4.98154278656912	21.94772071944302	20.49460347283163
H	-6.40835419459298	18.00635753146620	19.06175946768541
C	-6.64582395906137	16.57112113129237	20.65778590159997
H	-2.85507878962711	17.08717166861186	21.29081821637048
C	-4.64624054288336	16.03572127285712	21.90236388136158
H	-0.60040704771053	9.22082412185040	19.07943198371408
C	1.21764437093497	9.09789087667196	17.91049547344227
H	3.03306037648229	9.30785060285230	16.75710981676272
H	4.77724589940065	16.00146321567232	16.36879038568363
C	3.30105680182197	15.36444368110867	14.92523031151034
H	1.64429742823511	14.61538970299390	13.74529538244202
H	5.77073836220504	12.89836807703631	20.03298817591466
H	6.83665777376660	12.93470039376520	21.45585647701810

H	6.02491043589925	14.42505095326543	20.90650858585316
H	3.71049422876802	11.26835155406930	22.80631532143008
H	5.46876104191269	11.07151664415493	22.58102250700028
H	4.37429154542525	10.98901631807756	21.18289187722278
H	-0.36619721322467	12.89685857897705	25.61789880844286
C	-1.93582914000107	14.34576302347342	25.28664636005745
H	-3.28787509668747	15.94329568906748	24.74559184083797
C	3.44663619955641	19.11781362630096	24.38794698297699
H	2.17045417844584	18.91546808199189	26.11919817373128
H	4.50770260289360	19.10718989841457	22.50140256506577
H	-7.10836666212672	17.03498949516717	14.65160054109452
H	-5.96626777889188	16.77960169769674	13.31320955801959
H	-7.24953003345839	17.99698923998637	13.15636000324358
H	-4.16934487891628	18.62538075583074	12.80001041292654
H	-4.16454223165040	20.11422749755555	13.76838391036352
H	-5.49368588263572	19.79973254250043	12.62032074815026
C	-0.13038730758195	15.69478902788700	11.83642755796338
H	0.25615997807308	17.72996815669383	12.46417564342493
H	-0.65460616111644	13.62310356247398	11.51335889570739
H	-2.37841817748494	10.94721641160203	17.55147140724420
C	-4.13705816757255	11.52567738325670	16.42808313792126
H	-5.72347807538639	12.39249334437608	15.24185068822538
H	-3.21031173899972	23.00616997737559	17.78737338486198
C	-4.41974472052557	22.83288769281539	19.57317518479703
H	-5.56940985093953	22.32928099160112	21.33114331025591
H	-7.70940168827759	16.42135030576994	20.46405895971152
C	-6.00804411273008	15.84237269978907	21.66745176710371
H	-4.12817565712274	15.44346332907256	22.65587439621445
H	1.19931258701815	8.00928617449143	17.83868427843247
H	3.78944786224143	15.85711305635133	14.08326679910628
H	-2.62593516977976	13.88703925274404	25.99622058256032
H	4.10812906086385	19.84851683166463	24.85553123090474
H	0.36171247854497	15.80901763358270	10.86928580370431
H	-4.67955717790642	10.60126294779885	16.63067742802849
H	-4.56650388978318	23.90846453445966	19.68219322078091
H	-6.56663918524128	15.11092778336351	22.25280657939208

[(Ar*BIAN)Co(η^3:η^1-P_4C(O)Cy)] (**4b**):

Co	-0.77223824912580	5.02304271680318	18.63471930306901
P	0.60414494961996	4.65313496954498	16.85022380963121
P	1.35107227215012	4.18229846008975	18.83309619593093
P	-0.95137516575728	3.19650662192121	17.25439744786162
O	-1.31211997194016	3.82656424057116	20.16441559642739
N	-0.52152914029469	6.69398604210486	19.61601996773186
N	-2.52121877570629	5.78727176314776	18.25728248553376
P	0.30952953292303	2.12506879350639	18.83457457802747
C	-0.85255015834969	2.65506518156620	20.21305468737115
C	0.67808251206861	7.22434935536510	20.18068430965033
C	-1.65213023713603	7.37098213756275	19.74254741273635
C	-2.77413344986754	6.86906509227516	18.96683132114361
C	-3.46546086986556	5.23137559568703	17.34942944241893
C	-1.23889311738539	1.75761798324124	21.35654990685025
C	1.39566211728599	8.20507484695669	19.46311949960267
C	1.15438303009660	6.75271466296101	21.41838278065241
C	-2.08589058433106	8.57467779405517	20.44907022346817
C	-3.91077946802432	7.76626797861678	19.15929847920177
C	-4.33767069869237	4.20647510103760	17.75892158085583
C	-3.40405006442472	5.63625000151785	15.99900782693822
H	-1.85738719919095	0.95840082391222	20.89754881811247
C	-2.07614842151418	2.47815456049612	22.42225116903222
C	-0.00265883137712	1.08044977311545	21.99283945970690
C	2.56353184647006	8.72453550334579	20.02597366439430
C	0.93699056950607	8.65167680983308	18.08194652237101
C	2.34444785342193	7.28274846653161	21.92881345908960
C	0.31854662961241	5.75325865390744	22.20381527260699
C	-3.44984077709742	8.76306153238034	20.06893878814604
C	-1.50706848679375	9.47483750434210	21.32820271381388
C	-5.20971046685042	7.83459521405490	18.69002848043761
C	-4.41006745534908	3.80968221567128	19.22884828984696
C	-5.14199726086500	3.59251306984412	16.79104747497068
C	-4.23056478768983	4.99755734253710	15.07338398041619
C	-2.48414238013712	6.78450509897372	15.59758124484111
H	-2.95815528617147	2.94045753672167	21.95745879893836
H	-1.46972660200432	3.29399416868515	22.84906729629804
C	-2.49502721138776	1.51492385815319	23.53728719523471
H	0.65473577701999	1.86340666789008	22.40258922506612

H	0.57446952436910	0.54591422890516	21.22272547217298
C	-0.42393001801746	0.12315580919501	23.11475885785796
H	3.10056519280994	9.49742798080010	19.47247057297387
C	3.06106604760457	8.27524141001577	21.25477314525214
C	1.64104880056188	7.92390635806862	16.93919326006558
C	0.99780844257713	10.16938006835903	17.93338443014056
H	-0.12238972684828	8.36992666289422	18.00033166976113
H	2.72251353515686	6.89979433209516	22.87966109967736
C	1.13101141911201	4.74403033392326	23.00842980855027
C	-0.74004361216094	6.49157399535191	23.01256494843871
H	-0.23212676980452	5.16083452132719	21.45779575319940
C	-4.25039813370068	9.82086913295854	20.53391622089057
H	-0.46907302747399	9.37146803348124	21.64102693009513
C	-2.30263058796987	10.54429473641415	21.81751198211795
H	-5.60075398125370	7.08963518464162	17.99836136502292
C	-6.03304243450552	8.89614181966711	19.14548188056646
H	-3.47588453650278	4.16741095260395	19.69277975373418
C	-4.41482534514572	2.30355452138061	19.48102056735496
C	-5.54632648802973	4.56214627865786	19.91620986959641
C	-5.10506952488953	3.96927288718655	15.44660111568444
H	-5.78815460888395	2.76524294035901	17.09337635619863
H	-4.15936276698592	5.29613175275262	14.02563661497167
C	-1.88676057932789	6.63182587910535	14.20174138042947
H	-1.62297420567226	6.75397328471124	16.29076810149107
C	-3.19314965502489	8.11651111910965	15.83008901832707
H	-3.07418994541798	2.05887879080080	24.29988141656827
H	-3.16822366722173	0.74918693899746	23.11380082414534
C	-1.27575414514734	0.83491934188054	24.17326998179292
H	-1.00161670858072	-0.71210568661888	22.68017058330952
H	0.47408431187886	-0.31590393637141	23.57692907469752
C	4.35089570609368	8.83720803489090	21.82677728516371
C	2.82583246693932	7.19734823777577	17.10423171043384
C	1.07252237400690	7.99962211419067	15.65673423923856
C	2.06541904259314	10.81148178954124	17.29254931946999
C	-0.02792074202856	10.95449243113361	18.47980980720080
C	2.23208596059302	4.10763298497483	22.40947536355058
C	0.76565057446213	4.35996802985618	24.30526908591555
C	-0.40013836858289	7.51557740874998	23.90799042879980
C	-2.08995064675321	6.16371273706944	22.84895182763122
C	-3.62765854451417	10.72586789894131	21.44231662888107
C	-5.58623114007481	9.86068314813407	20.03892707957766
H	-1.84893745391390	11.24785161070863	22.51694487298966
H	-7.05888540308747	8.94790028067504	18.77902576648075
C	-3.67481442461920	1.44134801782961	18.65554205260156
C	-5.04914609078572	1.76038266146386	20.60774832232405
C	-6.88205182302369	4.40105407732395	19.51867588375939
C	-5.26340980672594	5.47197636989531	20.94053521363990
C	-5.96140976211224	3.26226530797923	14.41062826225133
C	-1.82204881711121	7.69811131681754	13.29702526731780
C	-1.30731204339617	5.40614835179689	13.83365606871664
C	-2.56600931530822	9.14047140613724	16.54831115487464
C	-4.49346605454993	8.34083945867805	15.35433021625487
H	-1.59385879622665	0.12213149603082	24.95050592940326
H	-0.65572836927186	1.59950727371672	24.67169553988927
H	4.51796408002307	8.34270866043992	22.79887120724979
C	5.55044293403717	8.50830321425776	20.92004702571307
C	4.24553487311752	10.35137435925434	22.07884760825924
H	3.27425557245476	7.10872929241553	18.09417584149992
C	3.42835843626367	6.56330334043042	16.01057556572061
H	0.14969198502516	8.56359387236759	15.50749771583573
C	1.66349473639938	7.36194990512961	14.56887945467902
H	2.85789321234935	10.21051026725707	16.84307609736724
C	2.11213864570986	12.20640393935476	17.21020312121516
H	-0.86324005760865	10.46632623254115	18.98392331338238
C	0.01284057413666	12.34663036777114	18.39497595954931
H	2.52259133754369	4.38967662128388	21.39551955387807
C	2.94644557185077	3.12033893793521	23.08859813344465
H	-0.08990399771176	4.83597692040816	24.78582672124746
C	1.48087318278010	3.37011843578455	24.98799862494469
H	0.64872493557296	7.78766782851039	24.03730406540117
C	-1.38878485568678	8.20082250752663	24.61541769495457
H	-2.35184332767794	5.37060299688381	22.14636204910469
C	-3.08308123956870	6.84453901113352	23.55761559659723
H	-4.19837774396329	11.56557379444530	21.84427287658412
H	-6.25870502077087	10.65717446468649	20.36387679977559
H	-3.17463311183948	1.84547386050955	17.77334845811832
C	-3.56141088869231	0.08190711397435	18.95239011531135

H	-5.62803381382046	2.41217847385387	21.26361206635064
C	-4.93802086389935	0.39973957496377	20.90749288927669
H	-7.12632210399032	3.69483723711395	18.72457330302877
C	-7.90094745382749	5.14064748733026	20.12047218535438
H	-4.22593477322772	5.62701714197466	21.23576878214747
C	-6.27784782087818	6.22083901284175	21.54238285145842
H	-6.57476618104808	2.51900972097864	14.94815231666664
C	-6.91776885035240	4.23765103841368	13.70271003289049
C	-5.08750442314957	2.50596772148199	13.39385381757086
H	-2.26018133211267	8.65962102238529	13.56737558814873
C	-1.19626237414963	7.54555956929519	12.05420424127369
H	-1.35568192931799	4.56211589910256	14.52437397188829
C	-0.68188700313836	5.25110342268785	12.59777050939923
H	-1.55870058818515	8.98457065919586	16.93313979400243
C	-3.21684083459287	10.34833156073076	16.80892899676180
H	-5.00610187687919	7.55247975605044	14.80118178094874
C	-5.14838917975854	9.54751493726364	15.60513612954327
H	5.44126642466868	8.98903518865726	19.93609773267626
H	5.63714361907608	7.42478859019932	20.75668890718218
H	6.48906080992406	8.86799006465787	21.36753054538079
H	5.16763749894412	10.73445966464952	22.54096296689277
H	3.40204506219676	10.58451174286735	22.74422203404277
H	4.08986210588380	10.89858029096649	21.13701831642618
H	4.34452187766625	5.98994799089526	16.16081967535217
C	2.85045180967064	6.64228832299098	14.74296282924033
H	1.18207084537304	7.40951023177377	13.59131143190763
H	2.95114497822800	12.68987897091172	16.70665281186006
C	1.08660973443604	12.97951321817086	17.76052142902601
H	-0.79813158819096	12.93785578442474	18.82438731751254
H	3.79254353076338	2.63502989243461	22.59928697479961
C	2.57358419643036	2.74580394625941	24.38401439198685
H	1.17805678062512	3.08674174676318	25.99749130873796
H	-1.10814903163615	9.00259743365692	25.30061086266431
C	-2.73613675391484	7.87000110262363	24.43896846222212
H	-4.12943800600844	6.57097480945260	23.42191858939846
C	-4.19030059737169	-0.44624935371874	20.08392343960605
H	-2.97146396289549	-0.56321704977224	18.29919237679738
H	-5.43783884973010	0.00099170655455	21.79184217113846
H	-8.93351902033176	5.00407461407922	19.79429621865356
C	-7.60154273931137	6.05927372226323	21.13259502291740
H	-6.02853251234384	6.95632493637681	22.30846619543020
H	-7.54997949335546	4.76986235568899	14.42782628034765
H	-7.57247176247280	3.70104023891791	12.99994339435674
H	-6.35780208132465	4.99037491504936	13.12732268250948
H	-4.45748898745587	3.20425577307021	12.82238615867331
H	-5.71220293022470	1.95152511808248	12.67753099700337
H	-4.42143601465466	1.79291928497905	13.89958421215540
H	-1.15501278115249	8.39045936252388	11.36459559153279
C	-0.62460491136477	6.32229644306772	11.69902550026849
H	-0.23196003889667	4.29160967692967	12.33798469776261
H	-2.70485265663201	11.12014500411892	17.38461733569944
C	-4.51543374396523	10.55411729957316	16.34123174507682
H	-6.16453553908351	9.69746131839761	15.23605002307119
H	3.31092022186005	6.13181084052453	13.89590480079246
H	1.12011781011141	14.06783387540557	17.68981361398883
H	3.12964147133450	1.97225178521343	24.91566117192295
H	-3.51064172683892	8.41214859108123	24.98314856554769
H	-4.10096056718895	-1.50763611437965	20.32016473791339
H	-8.39570799694061	6.64949615459951	21.59207965596205
H	-0.13475655341997	6.20341581815548	10.73130765785388
H	-5.03552366285453	11.48865425500175	16.55552821927652

[(Ar*BIAN)Co(η^3:η^1-P_4C(O)Ad)] (**4c**):

Co	-0.23791442339567	17.10780778630257	18.82665834535711
P	1.05371653722313	17.43797982415091	16.98043814260479
P	-0.34973437857771	19.00619482287993	17.52825446364170
P	1.95498822274092	17.75454102825701	18.93016354724532
O	-0.59774045798695	18.31520471632586	20.42354520734231
N	-0.08694762606174	15.42323020862935	19.81382988167105
N	-2.00253297339348	16.41053201540457	18.37416597531651
P	1.11438072067582	19.88873347826631	19.04457966289441
C	-0.04731356720664	19.44758636362659	20.45870414116053
C	1.07646287386509	14.81797753986962	20.38136757685911
C	-1.25107071753523	14.80096967657001	19.90347022763536
C	-2.31436468272720	15.33018810214740	19.06598640306961

C	-2.91644905435905	16.94197826217013	17.41697580338694
C	-0.37405800036221	20.40703533382257	21.57326290982164
C	1.75349548866575	13.83077658529404	19.62967098952934
C	1.57123507686204	15.21677773362480	21.63568658361240
C	-1.76130842869823	13.62557009245580	20.60567665606347
C	-3.48619994032585	14.46757816976897	19.20647344464238
C	-2.91026683441970	16.43054852741347	16.10330340382767
C	-3.76020001663094	18.01472429932841	17.76713878002937
C	0.93153771210847	20.88069341996508	22.26753010400154
C	-1.30062232236001	19.76201424870951	22.62328169627748
C	-1.08918535419141	21.64823681978421	20.96125694622807
C	1.27553767772404	13.42941477986338	18.24151411689443
C	2.90299956920214	13.24716586442449	20.16475407634974
C	2.75011100497993	14.62793615230441	22.11260570159945
C	0.80853491670584	16.22312069971905	22.48316145660290
C	-3.10592508301084	13.47017535961609	20.15261141875418
C	-1.25957279094015	12.72750779141412	21.53434316363093
C	-4.76018848939128	14.43058802406687	18.67190069865611
C	-3.77595857874331	16.99746139016188	15.16342323680320
C	-2.01353876476070	15.25543382477512	15.72864647932268
C	-4.64158934708316	18.51571267923015	16.80390284767358
C	-3.71994106778780	18.56178485796529	19.18945175284854
H	1.44941358435023	20.01370593121884	22.69652125109465
H	1.60711995738220	21.33290771858788	21.52308166050644
C	0.59425291134554	21.89582559451433	23.37446898161143
H	-0.79560665029291	18.88413294215871	23.05427384616901
H	-2.22360701992578	19.40840277300610	22.13603192689552
C	-1.62976137189779	20.77791738417278	23.73169999853917
C	-1.41618714883830	22.65855141256850	22.07617015129594
H	-0.44397664901637	22.11315026835787	20.19781875765910
H	-2.01170085707083	21.32776265459865	20.46065699035632
C	1.26180086197285	11.90961491900130	18.08605667479537
H	0.23188499642690	13.76625060609822	18.15894253795661
C	2.01991267361108	14.12939958479258	17.10759795576390
C	3.42880705596358	13.63733251994910	21.40108723928845
H	3.40427431049306	12.47278542268420	19.58053434252042
H	3.15258818406362	14.96815084181599	23.06961272616665
C	-0.15243167594134	15.52935108858323	23.44690099865783
H	0.18433082034398	16.81401471152438	21.79363224759258
C	1.73443114018836	17.22360164674030	23.18138571230637
C	-3.96124711009629	12.44401434374988	20.58943469614039
H	-0.23749470470636	12.80585571660441	21.90124596058483
C	-2.11190584143784	11.69156889488749	21.99748802362229
H	-5.08876602643947	15.17034127140719	17.94375426846211
C	-5.63714730267681	13.39780357480511	19.09576999374042
H	-3.73163652097026	16.63066287763577	14.13604265840563
C	-4.66603782011511	18.02345312736083	15.49590177546497
C	-1.40055716701214	15.39819432174373	14.33649597012419
H	-1.16119233785958	15.26616035090962	16.43220833892741
C	-2.75668355044958	13.93817679159308	15.94393986760474
H	-5.30144521263966	19.34269404547270	17.07498250823608
C	-4.03549282212535	20.04955075680198	19.29771668361703
H	-2.67504358733043	18.45550811242079	19.52450283232146
C	-4.54766953921722	17.66458418288418	20.09988027065772
C	-0.11465962894021	23.11777476063929	22.75982034280426
H	1.53468016317790	22.20878698570220	23.85677415543498
C	-0.32564178828478	21.23037789895483	24.41534310411013
H	-2.28999622179237	20.29665126440057	24.47157147038297
C	-2.34076924861032	21.99628718126491	23.11456440817521
H	-1.93011250965900	23.51936348990575	21.61815386197025
C	0.23556286312337	11.16848057470815	18.69055224357745
C	2.26389474331931	11.22213718714491	17.38953551709218
C	3.21722720110129	14.83073609954743	17.29008621981200
C	1.47684724725200	14.05300700592884	15.81411196118765
C	4.70537137734058	13.01643254361048	21.94015017044984
C	0.21384981260592	14.38507646700712	24.17005188719818
C	-1.42713577316471	16.06851908062874	23.66253175800452
C	1.51412075683521	17.65531690058278	24.49588279774245
C	2.82367005998144	17.76564002624519	22.47697695573245
C	-3.41816161697914	11.54000280675877	21.54754067294373
C	-5.26887387664953	12.43349849852503	20.02277802399440
H	-1.72010837154105	10.98984524181746	22.73514743617195
H	-6.64139847271078	13.36721047777076	18.67119895109731
C	-5.60147094287378	18.61193546826439	14.45404972735981
C	-0.82227859302879	16.62251444314920	13.96308413764666
C	-1.32941133854449	14.32602639067528	13.43920798809854
C	-2.17682119187835	12.91321955629942	16.69860128378553

C	-4.03888912091002	13.72534756696507	15.41591479450741
C	-3.47402582429856	20.95124613233458	18.37575704107198
C	-4.79041881422216	20.56840759426157	20.35750407142885
C	-5.91736591862248	17.46622050345463	19.87356075262077
C	-3.92717171055883	16.95528656644078	21.13331483572071
H	0.54592050602396	23.60998596487343	22.02659234990960
H	-0.34074392048292	23.85896775931351	23.54442308400963
H	-0.55146386938117	21.94042226344653	25.22853438440979
H	0.18671044145956	20.36483825597707	24.86499964349790
H	-3.27887191568108	21.68333337914193	22.63030503799833
H	-2.60203736731000	22.72216427252865	23.90282639877739
H	-0.54908680747594	11.69105436931716	19.23953208436522
C	0.21020644065838	9.77641138215792	18.60413740055947
H	3.05858123803954	11.78729629908312	16.89983804899035
C	2.24421193414245	9.82640318141480	17.30489465146043
H	3.64983681028057	14.91580387869404	18.28710559023671
C	3.85361453512091	15.44442665918368	16.20386955308190
H	0.54646884343366	13.50558680698046	15.65127958139530
C	2.10459205149228	14.66545676877258	14.73269645446127
H	4.89684572146250	13.47187039018686	22.92675101436554
C	5.90547818409072	13.33963152818571	21.03213984121580
C	4.55507394398847	11.49847571165446	22.14123757852648
H	1.19707344891260	13.94071545190124	24.01298037124321
C	-0.66983648620618	13.79343146590480	25.07458097446077
H	-1.72695889226366	16.96079881077855	23.11257269885524
C	-2.30818521876750	15.49204574109162	24.58142734528559
H	0.67447714824756	17.25157100173187	25.06260426282581
C	2.36163773820852	18.59499532718540	25.09364389247171
C	3.67253784480297	18.69861353277337	23.07258865553718
H	3.00668077185349	17.44630459462081	21.44893467594118
H	-4.03562252312498	10.72496653297327	21.93090993100770
H	-5.98012157300302	11.65998099405339	20.31914640490080
H	-6.22718220198393	19.36274416560275	14.96606188529638
C	-6.53725945941040	17.54394169918614	13.86194538922284
C	-4.81165283137145	19.33246761884320	13.34646869253585
H	-0.87393645339152	17.46984931791889	14.64899586899265
C	-0.19263383842862	16.77117876492811	12.72847106719398
H	-1.76703131421617	13.36546655765556	13.71363626210779
C	-0.70000948310081	14.47222022510654	12.19750289332913
H	-1.18369185685339	13.05623292955321	17.12184184917981
C	-2.85618684678608	11.71855405296550	16.94662234685023
H	-4.51851560222623	14.51056323161895	14.83076749629475
C	-4.72217619742478	12.53193906386313	15.65327322576187
H	-2.86533743232132	20.56494501338425	17.55664647783079
C	-3.66499560158204	22.32637354415861	18.50984569466021
H	-5.22625954578212	19.88762822201758	21.08968828329203
C	-4.98154278656912	21.94772071944302	20.49460347283163
H	-6.40835419459298	18.00635753146620	19.06175946768541
C	-6.64582395906137	16.57112113129237	20.65778590159997
H	-2.85507878962711	17.08717166861186	21.29081821637048
C	-4.64624054288336	16.03572127285712	21.90236388136158
H	-0.60040704771053	9.22082412185040	19.07943198371408
C	1.21764437093497	9.09789087667196	17.91049547344227
H	3.03306037648229	9.30785060285230	16.75710981676272
H	4.77724589940065	16.00146321567232	16.36879038568363
C	3.30105680182197	15.36444368110867	14.92523031151034
H	1.64429742823511	14.61538970299390	13.74529538244202
H	5.77073836220504	12.89836807703631	20.03298817591466
H	6.83665777376660	12.93470039376520	21.45585647701810
H	6.02491043589925	14.42505095326543	20.90650858585316
H	3.71049422876802	11.26835155406930	22.80631532143008
H	5.46876104191269	11.07151664415493	22.58102250700028
H	4.37429154542525	10.98901631807756	21.18289187722278
H	-0.36619721322467	12.89685857897705	25.61789880844286
C	-1.93582914000107	14.34576302347342	25.28664636005745
H	-3.28787509668747	15.94329568906748	24.74559184083797
C	3.44663619955641	19.11781362630096	24.38794698297699
H	2.17045417844584	18.91546808199189	26.11919817373128
H	4.50770260289360	19.10718989841457	22.50140256506577
H	-7.10836666212672	17.03498949516717	14.65160054109452
H	-5.96626777889188	16.77960169769674	13.31320955801959
H	-7.24953003345839	17.99698923998637	13.15636000324358
H	-4.16934487891628	18.62538075583074	12.80001041292654
H	-4.16454223165040	20.11422749755555	13.76838391036352
H	-5.49368588263572	19.79973254250043	12.62032074815026
C	-0.13038730758195	15.69478902788700	11.83642755796338
H	0.25615997807308	17.72996815669383	12.46417564342493

H	-0.65460616111644	13.62310356247398	11.51335889570739
H	-2.37841817748494	10.94721641160203	17.55147140724420
C	-4.13705816757255	11.52567738325670	16.42808313792126
H	-5.72347807538639	12.39249334437608	15.24185068822538
H	-3.21031173899972	23.00616997737559	17.78737338486198
C	-4.41974472052557	22.83288769281539	19.57317518479703
H	-5.56940985093953	22.32928099160112	21.33114331025591
H	-7.70940168827759	16.42135030576994	20.46405895971152
C	-6.00804411273008	15.84237269978907	21.66745176710371
H	-4.12817565712274	15.44346332907256	22.65587439621445
H	1.19931258701815	8.00928617449143	17.83868427843247
H	3.78944786224143	15.85711305635133	14.08326679910628
H	-2.62593516977976	13.88703925274404	25.99622058256032
H	4.10812906086385	19.84851683166463	24.85553123090474
H	0.36171247854497	15.80901763358270	10.86928580370431
H	-4.67955717790642	10.60126294779885	16.63067742802849
H	-4.56650388978318	23.90846453445966	19.68219322078091
H	-6.56663918524128	15.11092778336351	22.25280657939208

$[CyC(O)PCN]^-$ (**9b**):

O	0.18555743948105	3.24463881502523	11.59947762093877
C	1.00854395399100	3.45792858564996	10.69388945608590
P	2.81206136648738	3.61207530023323	10.73948888884219
C	0.47281383472175	3.63415339008194	9.24731476870133
C	3.10534798114151	3.37335885495585	12.47243745453704
C	-0.25734901171295	2.35670818214954	8.79807450000557
C	-0.47283207306619	4.84607277526959	9.18255367115064
H	1.32899183484303	3.81305980115539	8.56892555391658
N	3.42700312360801	3.23562179810640	13.59579388119928
C	-0.90388698968286	2.51293436260107	7.41526512878192
H	-1.02887907933871	2.13160485169430	9.55438758400118
H	0.45017374941145	1.51201267089605	8.80405759230764
C	-1.12010693267677	5.00507595237032	7.80035620590337
H	-1.25147457071389	4.70153496254547	9.95117566221330
H	0.08286703101453	5.75641149912940	9.45915003751034
C	-1.84859821714549	3.72262056240381	7.37332769351212
H	-0.11226102493422	2.65054490964404	6.65535493908965
H	-1.44771380400147	1.59316144683833	7.13788301102703
H	-0.33717447984541	5.23716588792007	7.05457834481115
H	-1.81850008458328	5.86004121293342	7.79770713892543
H	-2.69186569151542	3.54264266154613	8.06472822494128
H	-2.28339835548305	3.84054151685037	6.36565264159814

$[H_3CC(O)PCN]^-$ (**9-Me**):

P	2.82210438582387	3.61888508995228	10.75980268906573
O	0.19635772691127	3.24157861924754	11.59534027817413
N	3.40841608248689	3.23351538529857	13.61227777333043
C	3.09144915982999	3.37650772950377	12.49100058960958
C	1.01339838305646	3.45886217909980	10.69049855011384
C	0.47800819139630	3.63190533599939	9.24538204756455
H	0.90428488745784	2.87517875645300	8.57566190610907
H	-0.61148838655483	3.52958333921713	9.26488183411588
H	0.74562256959221	4.61631556522850	8.84265733191674

$(CyC(O))_2PCN$ (**10**):

O	0.22709231889085	1.83858576430081	10.65933419973752
C	0.97427138806159	1.46731690323529	9.78418553815327
C	0.50162723579965	0.88716087289605	8.46038279505726
C	3.00836360983912	2.51710109942375	11.44222132638720
C	-0.59861101784957	-0.16972894113403	8.65543808357745
C	-0.00272942407097	2.05024770824315	7.56990179091697
H	1.36208479592963	0.42880296579191	7.94210888613393
N	3.11824709133838	3.11326481168564	12.43916086722088
C	-1.08900041259200	-0.69766703406437	7.30183380552396
H	-1.42904954073290	0.29219257257126	9.21197117101721
H	-0.22377353451329	-0.99566008481654	9.28109128128811
C	-0.49732466159760	1.51596854321384	6.21945082719011
H	-0.82185842239141	2.55918888990431	8.10368582542993
H	0.79972990681240	2.79045017520364	7.42560865991900
C	-1.57931942733673	0.44290134786151	6.39982809715745
H	-0.26205629499883	-1.23122785581659	6.79879259509431
H	-1.88913282318864	-1.43738784774417	7.45735763701187
H	0.35567823621491	1.08674692289874	5.66467076870363

H	-0.87899275586193	2.35047265951168	5.61124544584613
H	-2.47336433383939	0.90361086331666	6.85497650862677
H	-1.89160539787676	0.04866202730775	5.42066831863052
O	4.23320966733138	-0.13371415237281	11.35926924485404
C	3.50645255936111	-0.03276617766285	10.40113226787750
P	2.88052127203014	1.72945714687753	9.86539831470816
C	3.10814099725886	-1.18420185168983	9.49416021228673
C	3.73675262647751	-1.02741962971545	8.08889176848104
C	3.46302788684272	-2.54906570334375	10.10006165158543
H	2.01067370073530	-1.12892902683790	9.37512998308968
C	3.26249710827344	-2.15817189197116	7.16688514488024
H	4.83451919575617	-1.05846774621276	8.19268784166549
H	3.49215783010418	-0.04572648821223	7.65356638255399
C	2.99360297472097	-3.68104644418171	9.17605537914213
H	4.55381991444802	-2.60161563349863	10.24469523987419
H	3.01310392569980	-2.64246001941826	11.09915098003054
C	3.57670733115946	-3.53666430668131	7.76371641987767
H	2.17161934917085	-2.06243447162268	7.01683762741715
H	3.72832312464739	-2.04993960531941	6.17547666400563
H	1.89046090768477	-3.66864490671070	9.11737901052049
H	3.27150646472451	-4.65454747259340	9.60767857951696
H	4.67210139945890	-3.66695017646284	7.80930336365505
H	3.19239522807797	-4.33178380616013	7.10658949535409

Cartesian coordinates of the optimized geometry of [(Ar*BIAN)Co(η^3:η^1-P_4C(O)*t*Bu)] (**4a**) at the D3BJ-PBE/def2-TZVP/def2-SVP@C,H/CPCM(C_6H_6) level:

Co	3.31457423456193	6.12899167623824	15.90108813348184
P	3.44062694386576	7.86107261551146	17.37906622434346
P	5.42929552022738	5.76988757801808	16.66538743821758
P	4.59543354229073	6.40745388543398	18.68789920372136
P	4.94632867373035	7.71238180817774	15.82054433654526
O	2.65349946371380	4.99157510819918	17.46993818051366
N	3.34894031147856	4.80919741364497	14.44660307213436
N	1.60396376056645	6.63612307115839	15.08588396275031
C	2.18804578007213	4.74393466831244	13.81287667681369
C	3.21867877009092	5.13579742800565	18.58601303586127
C	1.20973239512804	5.76901979606329	14.16956123815733
C	-0.04812948173463	7.88065890075728	16.45355375075235
C	4.41629416109805	3.95432272794371	14.02199664486956
C	0.30659503028659	4.43773493543624	12.51981584717356
C	1.07029028263068	8.96103743931108	14.54905767396383
C	4.68225262313801	2.74514284879135	14.70966284734874
C	1.61462569127871	3.90355624549958	12.75657524267147
C	3.77288219389419	2.29797885490253	15.84923365460065
H	3.36324337975384	3.22062592370293	16.30915344408270
C	0.84468989976818	7.81567882438962	15.35484563096687
C	2.79516295402935	4.29934618177613	19.78643577471354
C	0.01739664255989	5.57789880453390	13.33792547061978
C	4.99937300226234	5.65613317197063	12.18322713605493
H	3.97139104098972	5.99207056123841	12.42160197919576
C	5.21136838084299	4.33144958926051	12.90686220130621
C	-0.49688086624808	7.00015814358355	18.80105587182581
C	-0.31514317833960	6.65515384728374	17.31631529073574
H	0.59063657573213	6.01520792017481	17.25938573963709
C	-0.72470990122146	9.08562391341778	16.70481438402104
H	-1.41008920498950	9.12828562793027	17.56464885360361
C	2.57962842723081	1.54301797387340	15.26776103595290
C	1.99460799903269	8.90181121559429	13.33710019044860
H	2.71897306255171	8.07827839209605	13.52026996403933
C	-1.47080974599955	5.82291966627307	16.76190800354864
C	5.73320948759529	1.92500894791499	14.25984158985098
H	5.94572939975322	0.98888887806581	14.79952346167609
C	5.92438741983969	6.77238895825033	12.66746701036169
C	0.21153651982829	8.27922854466381	20.76780013330942
H	0.87227636848385	9.03894419096149	21.21315966180621
C	-1.38021508273511	4.41778220030993	16.74775522205572
H	-0.45897492649877	3.93717011517010	17.11018016962450
C	1.27992038719831	2.06385497755951	15.39952309773677
H	1.13632552283583	3.00130999973346	15.95656863175310
C	2.84297093778260	10.16622026308352	13.18276706763934
C	-2.66283956855854	6.42102889960084	16.30591408834161
H	-2.75522187063750	7.51720445265127	16.30338912427852
C	1.20604934048494	8.52860042051204	12.08123901677150
C	-0.59652944943587	3.90553493778572	11.57193331034864
C	-3.73059716459942	5.63755237199900	15.84282224982693

H	-4.64929821965328	6.12643660651791	15.48343153477568
C	3.50551810457320	10.69455434487527	14.31223750865814
H	3.35659231141465	10.22188700003276	15.29565982588455
C	3.95277929392743	4.94489456127472	9.97931457527456
H	3.04050169869402	4.69760849622308	10.54146078990202
C	0.33466453314651	7.96931104580577	19.40599054099449
H	1.09280324791246	8.48357598979641	18.79539279366844
C	7.05416574816760	6.54454715374456	13.47467400916860
H	7.29081349307015	5.52412681316019	13.80912401346076
C	-0.74126816043325	7.61781710471895	21.56146164803293
H	-0.83906897865647	7.85956733642081	22.63082249526504
C	1.66002696683912	7.49857562749512	11.23752936808043
H	2.58753758892321	6.96682848620721	11.49158409392851
C	-0.52187778090582	10.23690550820251	15.92456395809740
C	4.50429797611378	1.55515140875728	16.96626880446751
C	5.06558699439084	5.47303098700128	10.66539954941420
C	2.03079258745838	2.79586365550683	12.02056857530553
H	3.02274957202403	2.34808977477130	12.16846154155328
C	-1.44539803118227	6.34179954093232	19.60839361209334
H	-2.10469226110942	5.58334802849092	19.16220995452010
C	0.38745797972062	10.15170032318039	14.85973366179452
H	0.59120498530261	11.05013424937640	14.25601238321192
C	-3.62981197628725	4.23688521283803	15.83597410405618
H	-4.46698634152240	3.62059498301122	15.47450883919076
C	2.33730090304385	5.26282460542796	20.90496628792154
H	3.14110801101509	5.97725400646718	21.17571043256193
H	2.08173826880099	4.67307269811578	21.80870836598773
H	1.44573865845713	5.84223654927854	20.60126623891120
C	6.24172709819515	3.47335866860693	12.49140216954413
H	6.84169851784077	3.76989823045180	11.61756958965671
C	6.52446994133775	2.26510485646146	13.15185110244993
C	-0.14165397113385	2.76659869488398	10.83577286063438
H	-0.80282094521383	2.30523314387546	10.08581621911461
C	-1.56427236337504	6.64431561394142	20.97614698911712
H	-2.31367258533997	6.11546386781298	21.58512949225162
C	4.03382927657319	3.50942006930047	20.26878005764844
H	4.39725007027105	2.81275673276438	19.49127280671001
H	3.76070133316823	2.91936802706144	21.16724751522372
H	4.86461566119325	4.19037231547724	20.54479502888623
C	1.65862837397005	3.33745896295520	19.41156421431280
H	0.76065413063240	3.89235162575001	19.07751296462484
H	1.37899872260616	2.72988142507107	20.29507245365862
H	1.96309113222956	2.64844103430320	18.59971641341198
C	3.04290438564167	10.79131580681653	11.93788047519903
H	2.53878449274776	10.39407509398234	11.04462820316238
C	-2.45167781036267	3.62932024212831	16.29754355485723
H	-2.36739776684747	2.53216816387647	16.31456138480796
C	4.33927723676128	11.81494176772750	14.20145687704740
H	4.84737042322116	12.20546460502342	15.09653789632175
C	5.64026221933643	8.09412847263001	12.26058088050413
H	4.76043838897270	8.28834863470749	11.62775428371361
C	0.00909641474578	9.19011534237881	11.73809358532841
H	-0.37366918372194	9.99448394478597	12.38300571875619
C	5.77775972595354	1.99413172487488	17.39226093702404
H	6.24922335896061	2.85080840427181	16.88663636112987
C	-1.21116285945490	6.21375689133213	13.19074388501948
H	-1.46922568254171	7.10204258141840	13.78185506385317
C	1.13140764420983	2.24088357185302	11.06485278655186
H	1.45846893426632	1.36150416188912	10.48971198848244
C	7.58826555889796	8.92260173487882	13.45270635803423
H	8.23113127479227	9.75939790891302	13.76570490785656
C	3.99696646406663	4.72263032513843	8.59527490874815
H	3.11335500916285	4.31206385423743	8.08209869848738
C	4.52889803872699	12.43407220081882	12.95353232465854
H	5.18195921610871	13.31569464641115	12.86438478451577
C	2.75557392892178	0.34833642279266	14.53885366710724
H	3.76578954592918	-0.07197669320290	14.42025569700609
C	7.88070023510506	7.61441220303067	13.86409027822746
H	8.75506122394680	7.41811432786869	14.50343022640203
C	3.87876243794363	11.91647452047574	11.82311298821162
H	4.01904404713415	12.39048626392646	10.83931678048082
C	6.46052486649816	9.16042495254038	12.64733692449559
H	6.20441302488946	10.18342811024184	12.33326161594370
C	0.18198155068943	1.42297783170091	14.80256451783204
H	-0.81963538456576	1.86820043068344	14.88803484738188
C	0.93878605697683	7.12175040662809	10.09411353844919
H	1.31535040678794	6.30464067379000	9.46064477247862

C	6.44307085656366	1.35956708063761	18.45136770577339
H	7.43560483664667	1.71978242877373	18.76296090908608
C	5.16176607676445	5.02337458762814	7.86936966537888
H	5.19905947543632	4.85186698312123	6.78271075338128
C	-0.25583597413018	7.78113844626077	9.76981294846496
H	-0.83050359271598	7.48303597636362	8.87968805076194
C	-1.85764089388819	4.57089358584601	11.45730422294790
H	-2.60446069040900	4.19984976565640	10.73836109560312
C	-2.13864395840302	5.68785125053982	12.24492737814364
H	-3.11227206567764	6.18886506881166	12.13510560218393
C	3.90904849728818	0.47598195096642	17.64921579225891
H	2.91413907413478	0.12274210829444	17.34054734763659
C	-0.71420051517764	8.82226329480797	10.59411144388027
H	-1.65033624786198	9.34769999031127	10.34935778560213
C	7.66102580607139	1.36746036958226	12.68811976711075
H	7.64909085263158	0.46788750195770	13.34145790327728
C	6.22701309354666	5.77532758696361	9.92741600332895
H	7.10097729866436	6.19877180636602	10.44494640590485
C	9.02282168142976	2.06050457796774	12.86908206223487
H	9.09268551000982	2.97023204250655	12.23691393925442
H	9.85293051373834	1.38404153211059	12.57882946021344
H	9.17971815905694	2.36902037953166	13.92233103095521
C	1.66032403048941	-0.30336077957600	13.95456928714266
H	1.81730877050596	-1.23440897377250	13.38814996562379
C	0.36852003454723	0.23736037823400	14.07751972911742
H	-0.48911588429740	-0.26119357515434	13.60081723986440
C	5.84274188980322	0.27810312564514	19.11812340824930
H	6.36357339678772	-0.22070763288052	19.94964428517755
C	6.27638904775964	5.54914630080680	8.54173545948534
H	7.19399476551770	5.79104658708528	7.98343224239717
C	4.57012860355170	-0.15551592674019	18.71651929161620
H	4.08427854510146	-0.99659789302689	19.23489966711610
C	7.45795889347428	0.89890464500065	11.23740300931786
H	6.48768549522624	0.37653102605309	11.11516169156012
H	8.26649915043927	0.20366746021180	10.93149761770049
H	7.46930977433209	1.75647261242884	10.53271036896236
C	-1.24555078355433	11.53608422170752	16.24294767661776
H	-0.92341928037576	12.27879615419422	15.48098717469252
C	-2.77098116317422	11.37675630119437	16.12740231965145
H	-3.28366695655598	12.34500898042950	16.30188180736471
H	-3.15692270704657	10.65512651788689	16.87768622230641
H	-3.06228632211372	11.00810200134816	15.12304776751928
C	-0.83933931167020	12.07446922980917	17.62579880944550
H	0.25706130747960	12.22451981737975	17.69094100896612
H	-1.13021048282130	11.36741121903606	18.43076244433843
H	-1.33514328283965	13.04491007400187	17.83417116080592

Cartesian coordinates of the optimized geometry of *endo*-[(Ar*BIAN)Co(CyNC)(η^3-P_4C(O)*t*Bu)] (***endo*-6a**) at the D3BJ-PBE/def2-TZVP/def2-SVP@C,H/CPCM(C_6H_6) level (Total Energy: -6619,22324940716 a.u.):

Co	0.06759365009705	-0.07934735940167	-0.01388424198693
P	-2.09856408385219	-0.69626360639027	-0.46551892524205
P	-1.73233775690348	0.54921498066403	1.28909702252991
P	-1.26663942184504	1.02595740169519	-1.52264250071416
P	-2.03094494573090	2.41463826274560	0.07516992623888
O	-4.61346827797852	1.61840986050765	0.47204749302320
N	1.17992601098463	-1.01550488400905	-1.33393802984771
N	0.89929219080685	-1.37244072500707	1.21974078136489
N	1.47239098550814	2.48342706580620	0.64604460239913
C	1.89668450364526	-2.03093267386776	0.66026195534216
C	0.54379047231451	-1.59248330562325	2.58659037815628
C	3.66644069826536	-3.31275431691605	-0.06880816038468
C	1.09533075020023	-0.87164884058791	-2.75076668359348
C	2.03857640627395	-1.84963790090371	-0.78370796224974
C	2.93821140702968	-2.95903752788239	1.11325575784783
C	0.53460883823088	-4.18397256573669	-2.78477541056460
C	3.15284642847719	-2.68344779457487	-1.24795624195823
C	4.00614048345428	0.60626522469735	-2.43638280112508
C	-1.78561410618232	-3.25675053878793	-3.33397195798817
C	0.54932579937569	-0.87444972359989	4.90829846783065
H	0.89572069053993	-0.16375340718123	5.67464960188216
C	-0.35456826596717	-2.64220874550607	2.91295871438063
C	-0.76841974293238	-2.77579790755727	4.25129957187361
H	-1.45009465086002	-3.60033678461539	4.51170788053917
C	0.29184167687226	-1.78036244551120	-3.48671677982948
C	2.59768440779951	1.16889194398526	-2.58146250099026
H	2.16191476206880	1.16743623979008	-1.56246952088053

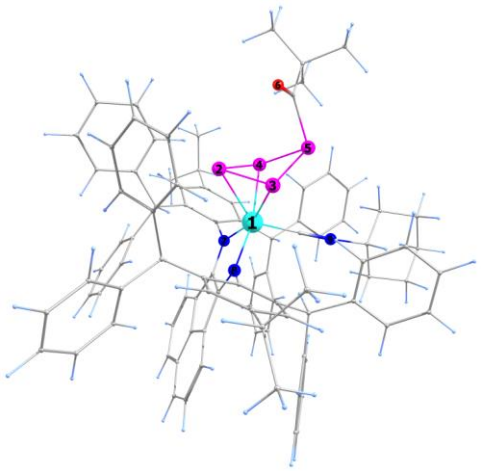

C	4.51621252265685	0.31761650242515	-1.15735870368171
H	3.88816517679947	0.52682243738267	-0.27817209373474
C	-0.86816293209196	-3.62147628500937	1.86008504734776
H	-0.24188603221939	-3.47081243528782	0.95968276122357
C	-2.31052774031617	-3.38546709252935	1.40991803694729
C	-0.38257177524759	-2.96316763676919	-2.79907164391249
H	-0.53702940450256	-2.67031169057738	-1.73638622863805
C	3.33613063384225	-3.49632471842676	2.33558365908921
H	2.80703805273532	-3.25508374362776	3.26713546972015
C	1.73206700616143	0.21651917124383	-3.39570477935570
C	-0.64587779518444	-5.06893493087367	2.30640554578508
C	4.88630441318771	-3.82164396556376	-2.49104892907082
H	5.37176111423966	-4.02414869775406	-3.45757093570205
C	2.11364463904211	0.29598233129838	3.28870051340035
H	2.09279424983355	0.45191292853114	2.19167490827880
C	3.76350010732153	-2.94432307277457	-2.46922775610551
H	3.40228394002841	-2.48294125947061	-3.39810637507537
C	3.50928115197352	-0.24357633881753	3.60346804773333
C	-0.35421809849850	-1.89261823834198	5.26029584694867
C	-2.24510660193613	-4.57030193864628	-3.54626120247069
H	-1.55945499046717	-5.41609459997549	-3.39096078216761
C	1.83623919805274	1.67444250030958	3.89224027486452
C	1.03033983782772	-0.72545251169131	3.59802250936423
C	4.77933273758401	-4.18480807679037	-0.06932987484933
C	0.15952533801792	-1.58378248706356	-4.87150204048053
H	-0.49213125502064	-2.27143271163133	-5.43220984192008
C	0.93691307801995	1.46545753694957	0.37996837991640
C	0.76164022487436	-4.87994288539676	-1.58344794033200
H	0.27447798875970	-4.52923348042869	-0.66217505897496
C	2.52823823271156	2.62202895412522	-3.04361856996409
C	1.58079713944460	0.35990288253647	-4.78549657347980
H	2.06572551551817	1.21223240634192	-5.28722261274916
C	0.79986207050958	-0.52791679830892	-5.54442525415151
C	0.52811941818309	2.20376140055212	3.82873420086181
H	-0.28106757276391	1.58882383333897	3.40225441120040
C	5.78708982316282	-0.25613638829445	-0.99715375011073
H	6.15386174483099	-0.49994561314303	0.01082151308913
C	1.17211455708137	-4.64438094606654	-3.95432684832446
H	1.01440923044925	-4.11351877261879	-4.90504274234049
C	-2.76607354421280	-4.07332077850219	0.26220652968301
H	-2.08280326963014	-4.75540170833998	-0.26747457408739
C	-4.46008126345399	-3.74709524183020	-4.14089223080554
H	-5.49850492137495	-3.93783086759271	-4.45228295365871
C	5.39053140507782	-4.42736948595487	-1.33967989632433
H	6.26243910305982	-5.09662275329521	-1.40381212673847
C	-2.68924332010115	-2.19048972165948	-3.53695745084516
H	-2.34857580005688	-1.15475028741105	-3.38428129396228
C	4.45880205777182	-4.37336766821688	2.35600830925506
H	4.77826656167251	-4.79046184666201	3.32292422979262
C	-3.88796076340793	2.30585673289410	-0.24008386255861
C	1.26821364150096	3.19824327141414	-3.32100244177342
H	0.36492948958648	2.57053421742452	-3.25330311464601
C	4.80559576395165	0.31708344571030	-3.56076103772865
H	4.41803988510888	0.52541865489340	-4.56982761054484
C	4.56491229588272	0.01269079781176	2.70572538674219
H	4.35880410478214	0.58664185846170	1.78956378428262
C	-4.01199029772240	-2.43109111360980	-3.93321023476291
H	-4.69893192231123	-1.58254112767010	-4.07587907791642
C	5.16565766887596	-4.71595058716584	1.20111160004106
H	6.02816477665299	-5.39749497712087	1.26458382488270
C	-0.86991203690580	-2.02648363864218	6.68485144881658
H	-1.51476857612763	-2.93162493469909	6.70951671846782
C	-3.20218737960787	-2.52361604231165	2.07334662019082
H	-2.86800570317669	-1.97083058609949	2.96251535424319
C	5.86549321501299	-0.44918327936759	2.96054886530990
H	6.67405961983504	-0.23063211813609	2.24605421820362
C	3.79440331871181	-0.97840059925900	4.77142547316560
H	2.98964588747301	-1.20466087340657	5.48591716871138
C	6.13352897960493	-1.18916514872971	4.12280574681035
H	7.14977117649423	-1.56181374782459	4.32213088726552
C	3.66888613652317	3.44481528921795	-3.11406015930337
H	4.65909772939955	3.01783949387403	-2.89684906923855
C	5.09168938575350	-1.44957778978497	5.02755068100239
H	5.28812098621483	-2.02898860483729	5.94294351820239
C	-4.51011367749099	-2.33587013868862	1.58950889650790
H	-5.18350459746643	-1.63663990016864	2.10796369563227
C	1.61253073958051	-5.99491757451944	-1.53795083329661

H	1.77947988316691	-6.51270593649443	-0.58126141379014
C	0.60461950693063	-5.68398768517892	2.09460129666904
H	1.40100693298610	-5.12329812489215	1.58476669103997
C	-3.57022274082099	-4.81447820307246	-3.94794047030724
H	-3.90658611336748	-5.85051350286636	-4.10848210986604
C	2.85848455718724	2.47883892421057	4.43158249036520
H	3.88407872363577	2.08616092102835	4.49199741688669
C	-1.65553969785063	-5.80787271923814	2.95500315868122
H	-2.64663939837830	-5.35287130482332	3.10504666186929
C	6.08105494232798	-0.24598069904256	-3.40611665228408
H	6.69101272644404	-0.46872415132748	-4.29526578218340
C	2.03019974908123	3.74707387194226	0.97939022723995
H	1.75081241608046	3.94307856997547	2.03855100975050
C	-4.94346912051554	-3.01010829455256	0.43982041611533
H	-5.96080552055576	-2.84795577792520	0.05241538685200
C	6.57449701413581	-0.53987694190024	-2.12300769553809
H	7.56773512430533	-0.99842305392384	-2.00284474978959
C	2.02024013066382	-5.76106539857838	-3.91719004408444
H	2.51456994962290	-6.10077642775078	-4.84052445361229
C	-4.06484097899089	-3.88640792710388	-0.22295251331365
H	-4.38271041045237	-4.40720038321767	-1.13896477058201
C	2.24955366283434	-6.43729394659335	-2.70714706567894
H	2.92592729262125	-7.30501765718648	-2.67607016342234
C	0.27445542550277	-2.23768811067065	7.69021325454271
H	0.88843192658640	-3.12132151863640	7.42265097194028
H	-0.12402808935268	-2.39107507590341	8.71404789793784
H	0.94739447516974	-1.35540626492756	7.72396494792082
C	0.25304770788919	3.50120404474984	4.28231973114663
H	-0.77311766743207	3.89382242003751	4.21334798684027
C	1.15391797355676	4.55261347609566	-3.66322311447752
H	0.15941564740711	4.97864469554951	-3.86817655540024
C	-4.47851467345968	3.24146334724617	-1.32491197944933
C	0.60836435777691	-0.32294824534514	-7.03965953364566
H	1.28650366781335	0.50519775767036	-7.34026441816900
C	-0.83425976566625	0.11631371256778	-7.34872420695832
H	-1.55940954489635	-0.67196830955268	-7.05681999484166
H	-0.96532793463846	0.31303041168109	-8.43281016311204
H	-1.10016177216059	1.03854537799791	-6.79406760020955
C	-1.74100517464204	-0.81797334274104	7.07029192412506
H	-1.14908267982274	0.12107081847877	7.05431135011190
H	-2.15494196621775	-0.93885308165003	8.09254052720738
H	-2.58789998333177	-0.69277685282387	6.36608483149019
C	0.84686112970411	-6.99671391961656	2.52659402438908
H	1.83179372061275	-7.45503747087985	2.34616826956882
C	1.42488365409359	4.84982591355521	0.09256301043469
H	0.32205148361395	4.84626436436403	0.21137903058083
H	1.63903335405908	4.60192806964590	-0.96768436184948
C	3.56588371304399	3.71489590506938	0.87901101076082
H	3.84556266425080	3.43871807782308	-0.16064499611300
H	3.96113563177814	2.92822731445619	1.55327263030541
C	1.28290366336862	4.29874691011614	4.81345903724495
H	1.06903267952029	5.31851965821727	5.16823447179601
C	-1.41516460306830	-7.12009892086007	3.39318762580899
H	-2.21686104622112	-7.68058552245423	3.89853978865546
C	2.58504864577821	3.78063523153664	4.88783880349157
H	3.39990367645432	4.39222663214997	5.30518292107942
C	3.55659602435607	6.19655805065710	0.35966256110976
H	3.85660743528312	6.02533092071050	-0.69825283280777
H	3.97231430661018	7.18310862396725	0.65287221861935
C	-0.16316623615371	-7.72027231045243	3.18181395336253
H	0.02216088481552	-8.75119299250486	3.52026290613185
C	-3.46567133027304	3.54027603931082	-2.44200607272907
H	-2.53745504153829	4.00110655604735	-2.04351544223554
H	-3.90736882734941	4.25129234062792	-3.16993584515643
H	-3.18108400750304	2.61996208905951	-2.99078069181301
C	3.55608126292761	4.80490939625910	-3.45380909089182
H	4.46158955738210	5.42940279464285	-3.50132923969543
C	2.29975244346034	5.36488140018008	-3.73111544450371
H	2.21211624634752	6.42945925053533	-3.99664606927961
C	2.02480278021033	6.21478719553751	0.44733386237770
H	1.60450804667709	6.98894284281614	-0.22761783812337
H	1.71867807147932	6.49570849388591	1.48007358882092
C	4.15073310905063	5.08607721272523	1.23635375843423
H	3.93463484538795	5.30262130916695	2.30669990581918
H	5.25554522571750	5.05665936490784	1.13730308373533
C	-5.74343752143750	2.59480196827349	-1.91270605189457
H	-5.49781249270168	1.64455760872805	-2.42934898673615

H	-6.21077918286542	3.27954342016182	-2.64921054403473
H	-6.48244272868098	2.37066648992167	-1.12013718259612
C	-4.84084689613508	4.55297837436039	-0.58826892183117
H	-5.56702725794436	4.36293724445853	0.22697359037148
H	-5.29614916249287	5.26981750743288	-1.30292314238914
H	-3.94014940891556	5.02822351412884	-0.14915162912157
C	0.99996770333481	-1.56928798305103	-7.84960167860141
H	2.04208029580664	-1.88054943693717	-7.63385704889708
H	0.91660413484596	-1.37258455914621	-8.93811011599081
H	0.33487808235989	-2.42683049642844	-7.61613556687365

Cartesian coordinates of the optimized geometry of *exo*-[(Ar*BIAN)Co(CyNC)(η^3-P_4C(O)*t*Bu)] (***exo*-6a**) at the D3BJ-PBE/def2-TZVP/def2-SVP@C,H/CPCM(C_6H_6) level (Total Energy: -6619,22319541952 a.u.):

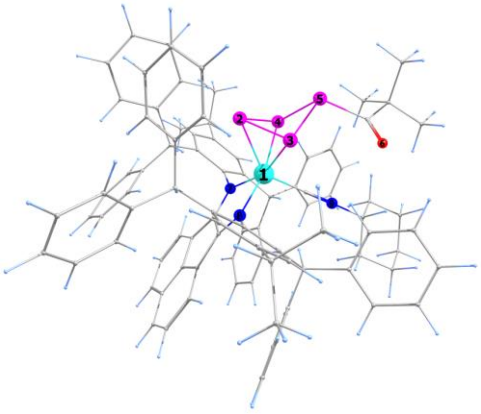

Co	0.11116053453340	0.01261097090254	0.00415011575000
P	-2.00929247628637	-0.71655466849947	-0.43897322700745
P	-1.68119863158105	0.52042336172885	1.34506387408016
P	-1.29255499387046	1.09432538224969	-1.44956251210415
P	-2.55985400517661	2.12679115392436	0.08394982831302
O	-1.30105856763041	3.74365048236790	1.86723815611290
N	1.20893964964215	-0.94979263204670	-1.34911679503647
N	0.96741409584694	-1.30767800779133	1.22176319378515
N	1.54574781945170	2.58064769839354	0.56436118744070
C	1.93690399509644	-1.98321991331782	0.63915078009946
C	0.60447634165002	-1.55460219007915	2.58269790625401
C	3.64991172057967	-3.31997766703759	-0.12989668888439
C	1.09145850525051	-0.83691959197776	-2.76705614876172
C	2.06008614804387	-1.79628221696542	-0.80944365351157
C	2.95033396027095	-2.95528600704772	1.06498112512452
C	0.52929623619334	-4.16552920107701	-2.79526292456524
C	3.13897188877965	-2.66493514772431	-1.29562686843687
C	4.02388124930758	0.55364373902682	-2.51546385324081
C	-1.79801480166440	-3.24042982073947	-3.28292989128089
C	0.60250112936824	-0.87137730577709	4.91799519642959
H	0.96035155420016	-0.17942158104661	5.69606156924250
C	-0.30691893761770	-2.60071772803620	2.89137242792815
C	-0.72726048365590	-2.74916170238585	4.22721984204241
H	-1.41414545370408	-3.57346873051994	4.47347567958968
C	0.27104188199426	-1.75621949119988	-3.47448397922428
C	2.64249987870456	1.17521546016833	-2.68294396528042
H	2.21528153694112	1.25059944263044	-1.66261063668272
C	4.55031746680330	0.34614403452923	-1.22743419151805
H	3.95266800409730	0.64757532673216	-0.35309531979577
C	-0.82762699194189	-3.57370101477377	1.83435362883802
H	-0.22080164356832	-3.40854306928032	0.92305627565310
C	-2.28430564891213	-3.36171574880042	1.41660567053416
C	-0.38513352600229	-2.94190854375224	-2.77359962092354
H	-0.51201660924395	-2.65705061533372	-1.70533313684521
C	3.33585657314695	-3.53127890299274	2.27319717227446
H	2.82039631923209	-3.29160188647668	3.21210706201557
C	1.72858801914921	0.22817443485902	-3.45011216759582
C	-0.58878376555589	-5.02509749440993	2.26593201987561
C	4.79936145970829	-3.86809910331941	-2.57714721870489
H	5.25540716516330	-4.08703648952058	-3.55433548047065
C	2.21874798118130	0.28008865228478	3.34663508571898
H	2.17123039844039	0.54356942188495	2.27095793237851
C	3.71275471378468	-2.94761337551147	-2.52990151374675
H	3.34711523650040	-2.47572513786412	-3.45129946378216
C	3.58622197858310	-0.36307849989046	3.57287854720197
C	-0.31307778282133	-1.88489503214825	5.25100852392224
C	-2.25720336393804	-4.55776511740338	-3.47484364756843
H	-1.56921466592869	-5.40055874125081	-3.31464410214875
C	2.03964956768309	1.59411171060651	4.10996656556709
C	1.09381165125704	-0.71043134967173	3.61382936163040
C	4.72417594793341	-4.23935055744811	-0.15622764247933
C	0.11523394173695	-1.58332068612585	-4.86026192828718
H	-0.54988072937434	-2.27750903710764	-5.39627689157614
C	0.98055268871875	1.56418099529693	0.35587993754307
C	0.79018551736967	-4.86961415531758	-1.60607685631252
H	0.33892535632914	-4.51831203441164	-0.66719142650484
C	2.64976238155292	2.59716780831932	-3.23698318829594
C	1.55630061465707	0.34400662316901	-4.84016796346509
H	2.04867422464546	1.17538684151526	-5.36869497260349
C	0.75264825570768	-0.54924312269384	-5.56718777697772
C	0.86498566615436	2.34640125630778	3.89340020580236
H	0.08527693141252	1.96354024307062	3.21680846957751
C	5.80376313194925	-0.26078469469609	-1.04945949994315

H	6.18726645096700	-0.43544619736529	-0.03385819901225
C	1.12107837882620	-4.62742842040635	-3.98806110273163
H	0.93744255604711	-4.09102999745655	-4.93081555260212
C	-2.74083554151582	-4.02700269485904	0.25616737368432
H	-2.04470419602298	-4.66041652781630	-0.31548675301954
C	-4.47697827942986	-3.74759849884720	-4.06797566542574
H	-5.51632166166865	-3.94437811364685	-4.37251266569917
C	5.30160714414438	-4.49854701790896	-1.43856608191126
H	6.14260630893983	-5.20414959532231	-1.52283718708470
C	-2.70590707911470	-2.17936149066950	-3.49315503023327
H	-2.36776445402757	-1.14097071810043	-3.35566925051100
C	4.42254730718837	-4.45197252136314	2.26896283670491
H	4.73265932638094	-4.89808974705882	3.22583468061827
C	-1.78587245662229	3.72327249227307	0.73662594120484
C	1.41640815654076	3.24842831976775	-3.46207516657021
H	0.47835003775093	2.69763073005912	-3.28534130591024
C	4.78596765238228	0.14457597752647	-3.62865016703645
H	4.38157653662715	0.28686060451659	-4.64264198136996
C	4.63363312396345	-0.10745175696336	2.66667092799510
H	4.44274471033547	0.53850396528107	1.79650826442680
C	-4.03046628119455	-2.42850230814798	-3.87878309547083
H	-4.71956894619418	-1.58336787163779	-4.02973820983226
C	5.10339304686872	-4.80398907264143	1.10150215618884
H	5.93730950562280	-5.52178772910762	1.14452003971755
C	-0.83724389033077	-2.03430810993949	6.67061983530386
H	-1.48472987018945	-2.93793660837332	6.68131489242430
C	-3.19375659210312	-2.56065336813607	2.13028477507633
H	-2.86029652973520	-2.02386856927935	3.02921149790137
C	5.90917957405239	-0.66064161042052	2.85955412104588
H	6.71486666955007	-0.44436690372893	2.14116584979795
C	3.85359371137869	-1.18498102660676	4.68641940663888
H	3.05163229130749	-1.40631539005221	5.40634780827721
C	6.16030614432794	-1.48561623672637	3.96688666715551
H	7.15766750127879	-1.92647287908349	4.11602511164651
C	3.83788001476953	3.32043279371383	-3.45565479250020
H	4.80915355952768	2.83563448746042	-3.28019367603260
C	5.12682761232527	-1.74167249561189	4.88226812169687
H	5.31075422960382	-2.38531544853056	5.75644366184183
C	-4.52073499947405	-2.41447710871755	1.68641393537275
H	-5.21198539828191	-1.77040432101800	2.25129719369227
C	1.62935720222982	-5.99424040879502	-1.59480932919991
H	1.82440209604461	-6.51751326042221	-0.64649770344006
C	0.65314670084321	-5.64147016656132	2.01388562371530
H	1.43517795919511	-5.08092766830373	1.48387235379336
C	-3.58385231265789	-4.81039411236319	-3.86534206355207
H	-3.91822693898234	-5.84932236087419	-4.01058561009700
C	3.02014316136892	2.11216795643967	4.97783441221986
H	3.94421698483972	1.54317717390682	5.15631343263851
C	-1.57982698051177	-5.76884588232208	2.93836332042928
H	-2.56712943291665	-5.31659486925793	3.11832631703348
C	6.04385693447524	-0.45118449555001	-3.45628432015719
H	6.62451288300066	-0.76613895323987	-4.33710261540526
C	2.22368337303752	3.78460185445743	0.90523234769024
H	1.61657990442109	4.26559680254729	1.70610956491949
C	-4.95555085531041	-3.06566297797920	0.52382432446588
H	-5.98976339072255	-2.93777527402464	0.16937868807658
C	6.55560997785767	-0.66063287579562	-2.16424386877941
H	7.53463605842997	-1.14420535939653	-2.02715775635623
C	1.95548525285883	-5.75489185889139	-3.98563508743146
H	2.41255404796327	-6.09629815189668	-4.92736839486315
C	-4.05774099496822	-3.87813711961040	-0.19194905399329
H	-4.37580228070844	-4.38017594112161	-1.11813846387615
C	2.21849699273736	-6.43979315350480	-2.78744464525734
H	2.88475634635364	-7.31583051125885	-2.78353941038852
C	0.30094386913235	-2.25896104006446	7.68014350913370
H	0.91511584313835	-3.14052085138911	7.40603995289200
H	-0.10372326196556	-2.42320817371917	8.69985554959075
H	0.97473328370105	-1.37806932473261	7.72732173762279
C	0.68449043343838	3.58996721625693	4.51383253955242
H	-0.23234062070104	4.16234521883305	4.30924944655624
C	1.37434944220189	4.58078455365880	-3.89357880963295
H	0.40130679047553	5.06871607269916	-4.05788479395369
C	-2.02002994117527	5.01612298999312	-0.07702038391844
C	0.54437074413200	-0.38096187815302	-7.06464801494244
H	1.21866446990136	0.43965443023575	-7.39328021018841
C	-0.90163358481112	0.04870741259774	-7.37057135272491
H	-1.62334866692755	-0.73307122106384	-7.05360594046584

H	-1.04283795426194	0.21920679815304	-8.45780324408945
H	-1.16351854250348	0.98364028068488	-6.83575450766239
C	-1.70672623426365	-0.82707813478920	7.06390104783971
H	-1.11125745612593	0.10978392465513	7.06069288655524
H	-2.12708422652512	-0.95729820996194	8.08240521157987
H	-2.54882307703392	-0.69139438694769	6.35588696626746
C	0.90733961700262	-6.95672008936640	2.43159036180806
H	1.88684965368624	-7.41325675945032	2.21967259581982
C	2.31392982499785	4.73069150299529	-0.30377529181227
H	1.29927722193883	4.93495843024305	-0.69521378617872
H	2.86616162141829	4.21353690730143	-1.11453779757544
C	3.62617970875906	3.48347879689538	1.46735252188046
H	4.20064934855885	2.93372558859116	0.68984255712091
H	3.53655381220829	2.82208014136071	2.34959661197924
C	1.67259731283956	4.10243641802338	5.37350079010402
H	1.53252081053830	5.08005182075382	5.85995384436228
C	-1.32794931194496	-7.08342046791453	3.36221687910659
H	-2.11573529968058	-7.64607877756422	3.88665984337673
C	2.83780756638541	3.35686524912547	5.60646761856275
H	3.61799494158683	3.74477920148654	6.27966759768506
C	4.42705009472056	5.74905587729693	0.64958969177889
H	5.06223362760653	5.29773191065056	-0.14548637807000
H	4.92085760915274	6.69630525947553	0.95082696899488
C	-0.08297691175272	-7.68349913792480	3.11216048998800
H	0.11130578907961	-8.71624363881958	3.43982307360713
C	-3.52852048485532	5.34780615812444	0.03148923291546
H	-4.15324417632283	4.54707342927646	-0.41134132299545
H	-3.73876218107037	6.29349224784171	-0.51022889417758
H	-3.83262946534949	5.48035637191328	1.08933782868598
C	3.79750939039083	4.65955147917711	-3.88327764804277
H	4.73920578922872	5.20712405551033	-4.04325933846669
C	2.56692373904199	5.29567830247163	-4.10352503802792
H	2.53478357914669	6.34371281182323	-4.43852769368357
C	3.03345583684865	6.02942451010646	0.07251399843548
H	3.10348069096249	6.68185621325139	-0.82238452074109
H	2.42690496451129	6.58546709379683	0.82257653893329
C	4.34857662059712	4.78338254062305	1.83904636062120
H	3.80335717236125	5.27083366996992	2.67802581669996
H	5.36246234494605	4.54591650875646	2.22235171094076
C	-1.19985094464527	6.16919835405723	0.51954700711138
H	-1.48407853341110	6.35649314374776	1.57275099091398
H	-1.37307658078896	7.09711644856443	-0.06210281516829
H	-0.11541792145378	5.94750766204670	0.50146338608471
C	-1.64946292688859	4.77625134112703	-1.55164206469232
H	-0.58389586694302	4.49548232993517	-1.66334345013710
H	-1.82887155133673	5.69736115267869	-2.14337059580603
H	-2.26027705870920	3.96546104514807	-1.99936318041553
C	0.92938747928104	-1.64808429400091	-7.84536915848416
H	1.97604168952048	-1.94882237255440	-7.63669424073450
H	0.82855141985899	-1.48319479039706	-8.93767327627026
H	0.27198000519043	-2.50112454283438	-7.57633596985567

Cartesian coordinates of the optimized geometry of *exo*-[(Ar*BIAN)Co(CyNC)(η^3-P_4C(O)Ph)] (***exo*-6d**) at the D3BJ-PBE/def2-TZVP/def2-SVP@C,H/CPCM(C_6H_6) level:

Co	-0.01451841218233	0.01099817456756	-0.01948309017288
P	1.53151926975108	-1.43016895440028	0.86024910892057
P	2.21223576756554	0.13574432126923	-0.51730280518018
P	1.41984267772202	1.45172879138093	1.05022950983932
P	2.34806781885155	-0.04895546994329	2.41431472220683
N	-0.79768513998581	-1.24460119557731	-1.33416280632781
O	0.66327175641310	0.85644463864629	4.35284272779612
N	-0.93378662226302	1.34289494403959	-1.17797148309571
N	-1.82077181894194	-0.16743285078562	2.36373217161060
C	-1.10639812389231	-3.56669302361935	-0.57103848311297
C	-1.72156958531192	0.78506343351622	-2.07365213691052
C	-1.09834962412701	-0.09508681408584	1.43346438107037
C	-1.63795671510363	-0.67371706648365	-2.17095386749993
C	-2.69825825351516	1.25985743992613	-3.06039001183037
C	-2.26732687128505	-3.12241950356928	0.30888528997070
H	-2.09090616705754	-2.05047285945070	0.52830975366017
C	0.27351579629309	4.82982173313175	-1.75317093037450
H	0.97619170244114	5.35912792787495	-2.41409739261270
C	-3.17814851843235	0.07838116653967	-3.71127132929947
C	-2.72667524131005	2.79258238939130	0.59799531500815
H	-2.51065493963344	1.70587633187312	0.56859575840551
C	0.34614963550258	-5.33978169752929	-1.45691470511034

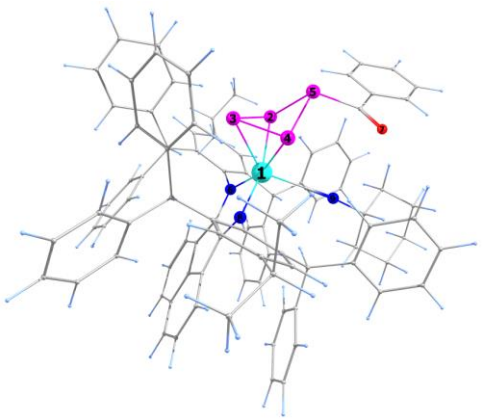

C	-1.35424176005760	4.85663755916756	0.01714712058679
H	-1.91877784293780	5.40173864084094	0.79020843741943
C	-2.31337356626173	-3.81695262393233	1.66871823848393
C	-0.68670057336094	-4.90517827999392	-0.60633199132605
H	-1.17302057398563	-5.62036373240449	0.07469949918630
C	-3.57959374851376	-3.18746248971822	-0.46536574846871
C	-2.35452631310063	-4.97774620015523	4.25554196415957
H	-2.36912613938295	-5.42594367309484	5.26076257908626
C	1.38535271754563	-1.38049919553473	4.79701834363817
C	-0.81604339716950	2.76390762550472	-1.09575194699697
C	-3.51494572118795	-4.29670659510874	2.22526246779453
H	-4.44852168235636	-4.21833508663767	1.64930124505162
C	0.11599666542468	3.44466634147818	-1.92691157167002
C	-3.53712097193202	-4.87054428207498	3.50879427791200
H	-4.48909408113807	-5.23639083805301	3.92372017634018
C	0.95828616642560	-4.38839708306012	-2.28950113770009
H	1.78525334227289	-4.70346684454125	-2.94550026225508
C	-0.46975837485231	-2.62919037026376	-1.42226813432529
C	-2.79974357082497	3.15751584396860	2.08007376523741
C	-1.58907009819752	3.48015701207341	-0.14774753603191
C	-4.04535710411954	2.97515173323028	-0.15324757380439
C	-1.15007950412834	-4.49779206390425	3.71223399586194
H	-0.21893158712198	-4.55328813152524	4.29453321488187
C	1.22633374854236	-2.03383829363428	-3.24351182807981
H	1.15738618048606	-1.03764058480894	-2.75121905124478
C	-2.92143195989936	-2.33701677165156	-3.78505601309315
H	-2.46635042541488	-3.27798385407333	-3.44955350472334
C	-1.13128307525702	-3.91920335293644	2.43564579983710
H	-0.18539125842422	-3.53108934316080	2.02452018693514
C	2.04651825633486	-2.53803907499884	4.33133447584045
H	2.49149935444405	-2.54817984276308	3.32418700354612
C	2.72467688499277	-2.26188545704416	-3.46000708139304
C	-4.16445799328951	0.09208304405777	-4.72503438293544
C	-0.42488623197125	5.55319168515114	-0.77082352744685
C	-3.99339818141494	-4.36140387040811	-1.12667556209299
H	-3.35641692984875	-5.25826009710309	-1.09081371783865
C	0.73875808637937	3.41609734559439	-4.36738925215479
C	0.82562751851307	-6.78311374987116	-1.43441874253555
H	1.54147184119095	-6.89735289647094	-2.27736321591290
C	-1.65280018776408	3.40930615736937	4.22764982949331
H	-0.71388176176007	3.40352784957022	4.80062393143818
C	0.57560188171986	-3.03413685057450	-2.29277804331210
C	-4.02764847190417	3.35983351899128	2.74030758734035
H	-4.96418061418001	3.33128877468777	2.16423426492416
C	3.32186041021914	-2.13284120123936	-4.72893745848749
H	2.69134320375270	-1.93382136610519	-5.60758827960261
C	-2.55514945538140	-1.11739646884267	-3.22772209301303
C	0.43901666921324	-1.92926004363239	-4.54726877766321
C	0.91786778048514	2.72591344246887	-3.01122710790110
H	0.48434898132066	1.71176428228904	-3.11094255891182
C	-4.40394159840496	-2.05023475433953	-0.53906475035034
H	-4.07988662730794	-1.13018594466535	-0.03110571595756
C	-1.61276114970588	3.18977185286781	2.84355609774221
H	-0.64450980182396	3.01408706752564	2.34906633344787
C	-2.77539831131762	-0.11618487726880	3.41963022244635
H	-2.70223624028907	0.90501698678544	3.85446521771997
C	0.09391013582464	-0.66718592450717	-5.06446160322366
H	0.39045864803489	0.23621630906303	-4.51183393643638
C	2.39893225448779	2.51401114366916	-2.69366272374924
C	0.05071707400490	-3.07602293584651	-5.26796898054214
H	0.30614027955952	-4.07336440401658	-4.87969663847166
C	-4.54816693461735	4.25188296805832	-0.47784918280753
H	-3.98769535707587	5.15018746839471	-0.18105633655438
C	-2.88380574900129	3.60902227694802	4.87703877252592
H	-2.91674255954450	3.77916738090840	5.96405357570851
C	2.13797528242208	-3.67864608421011	5.14149030351330
H	2.65621431660304	-4.57476884810467	4.76828171421937
C	5.53501851278361	-2.49175896091140	-3.77552878483190
H	6.62551951151401	-2.57914460739785	-3.89759689200389
C	-5.20020461164958	-4.39295507567643	-1.84145141128287
H	-5.50588775689561	-5.31730178273854	-2.35561592472789
C	-0.35706936121239	3.08269431967044	-5.18765370144564
H	-1.06105571838611	2.30583693488737	-4.85887317816093
C	-6.47893204124835	3.25675274600571	-1.58014743764063
H	-7.41984410516843	3.36739013413993	-2.14037838106069
C	-4.68049664622942	1.37580178598723	-5.08617176006467
H	-5.45239342011963	1.44947446925705	-5.86800821730275

C	-5.75168762279093	4.39249862152172	-1.18461422050139
H	-6.12388495237851	5.39895648925189	-1.43099762651793
C	0.81964189744101	-1.38707574949696	6.09160163740817
H	0.32231083529847	-0.47360834578612	6.45088761859687
C	1.58840490557688	-7.07625865198442	-0.12941336410085
H	2.44006461773437	-6.37877530636276	0.00063524855733
H	1.98388094048381	-8.11297643737256	-0.12469370659948
H	0.92219818196408	-6.96167215626932	0.75132879594587
C	-3.91710683968452	-2.34497343183496	-4.80445460920372
H	-4.21110841233078	-3.31242885201969	-5.23844554385094
C	-4.21363193164824	2.53041883580568	-4.45366872230825
H	-4.62976945085106	3.50639833520572	-4.74501274716218
C	4.71416319454649	-2.24689272324240	-4.88660622379767
H	5.15689571516985	-2.14127640755321	-5.88915136853984
C	1.28704295824430	-0.13705824512341	3.96031961843429
C	3.56157689858989	-2.51243337734796	-2.35032308841969
H	3.11628670183105	-2.61926142719858	-1.34908034620259
C	4.95017477466177	-2.62484579660674	-2.50442334401807
H	5.58065321803889	-2.81356004980129	-1.62185854174253
C	-0.18199661828604	7.04208158765749	-0.57702515206146
H	-0.86941293390578	7.37857081621079	0.22933068567732
C	-4.78500655052427	1.84704573427937	-0.55549598174460
H	-4.39188939633822	0.84511715514969	-0.33112715820767
C	-6.01257144404108	-3.24812510917331	-1.91077990527379
H	-6.95398752463444	-3.26992696865329	-2.48041361601005
C	-4.07020794333872	3.58532023106172	4.12718810380112
H	-5.04120700202104	3.73973126934807	4.62278353392917
C	-4.52902739396183	-1.17999624513424	-5.26801588300569
H	-5.29465539607185	-1.23414482635586	-6.05740810051819
C	-0.63178855503037	-0.54477444918674	-6.25928815527482
H	-0.89512786110034	0.45540436723909	-6.63553154311935
C	3.07970097066609	3.17624674247815	-1.65649130483449
H	2.54036794760259	3.88174878255808	-1.00869671890846
C	-4.19825118973073	-0.31881735980085	2.86658269425818
H	-4.24114669612876	-1.31090279612774	2.36825593602086
H	-4.40957583553695	0.45006887186734	2.09674425405121
C	1.63451561818426	4.40754019571865	-4.81684053989513
H	2.51583064347768	4.65783973799189	-4.20651367417787
C	-1.01996774029829	-1.69447723319911	-6.96362969416638
H	-1.59703115031347	-1.60455647111639	-7.89648849232360
C	-5.61123622657227	-2.07502652241411	-1.25400313116478
H	-6.23691841466094	-1.17124836124360	-1.30416194966781
C	0.90401157862909	-2.52859169545137	6.89788951128889
H	0.45985640086574	-2.52448693699282	7.90507246294601
C	3.11965520972330	1.60134502512745	-3.49699477826196
H	2.60251696266212	1.06936120517849	-4.31092479413398
C	1.56487695462213	-3.67678494528048	6.42491937429539
H	1.63525896395038	-4.57304603139241	7.06018215013913
C	-5.99148348440940	1.98131183708555	-1.26006325528225
H	-6.54404618072337	1.08328119062109	-1.57520830978003
C	-0.67016371863718	-2.96091320442078	-6.46582680093089
H	-0.96956410162357	-3.86928689771032	-7.01127632867886
C	-0.51932466892591	7.84010916486551	-1.84782482329218
H	-0.38449947128014	8.92795292017247	-1.67741075770284
H	-1.56708485634174	7.66673700846213	-2.16612904975957
H	0.14102549365744	7.54836186776333	-2.69105115275847
C	-5.22947871830374	-0.25426358979564	3.99897958089567
H	-5.23342918576741	0.77452224984648	4.42318398196791
H	-6.24445911442618	-0.42886991118495	3.58540527175694
C	-2.45314888523879	-1.14498280602540	4.51327321375111
H	-1.43297163252231	-0.96329185723679	4.89842846238496
H	-2.45507663593243	-2.15623955087066	4.05937541517006
C	-0.56642125057600	3.73139135951912	-6.41423805639012
H	-1.43167683382845	3.45210018027418	-7.03565928238850
C	-4.91289909307096	-1.26568785480157	5.10845324910506
H	-5.65150987201935	-1.17787527249149	5.93239769574396
H	-5.00903038155842	-2.29706961095419	4.70107583762174
C	-0.32013248120712	-7.78414861573114	-1.65042010789527
H	-1.05281213964733	-7.74494161711453	-0.81754525897472
H	0.06937694356789	-8.82161252168446	-1.69836649389527
H	-0.86676491586251	-7.57701083987541	-2.59269361219270
C	1.42597539818390	5.06236062169921	-6.04127065351516
H	2.13715033562214	5.83453377839623	-6.37322431768734
C	0.32318114202325	4.72899392547298	-6.84476360192877
H	0.16322709193523	5.23941389767751	-7.80680852219297
C	-3.48750405319579	-1.07225054584700	5.64129781530772
H	-3.24853622647241	-1.83727158234210	6.40901639718549

H	-3.41238097442021	-0.08265930604440	6.14556183764718
C	1.25853285855379	7.31312581700876	-0.10966721365928
H	1.99296804218899	6.99734485724414	-0.88003164671611
H	1.49006064674906	6.76000207290984	0.82272417007772
H	1.41544487287324	8.39475919469517	0.08092388806095
C	4.47273661489266	1.33889156955719	-3.25671232202102
H	5.00014263329956	0.59583122895637	-3.87418652686762
C	4.44228841335358	2.91999436799790	-1.41711596999125
H	4.95254913571220	3.43729521794165	-0.59022861652725
C	5.14103179391939	1.99872392508700	-2.20941301874372
H	6.20260922402903	1.78740057826439	-2.00973637827871
C	-3.21892313507015	2.49633972354342	-3.43539670532899
H	-2.88211258614159	3.42809418662147	-2.96120431467298

Cartesian coordinates of the optimized geometry of *endo*-[(Ar*BIAN)Co(CyNC)(η^3-P_4C(O)Ph)] (***endo*-6d**) at the D3BJ-PBE/def2-TZVP/def2-SVP@C,H/CPCM(C_6H_6) level:

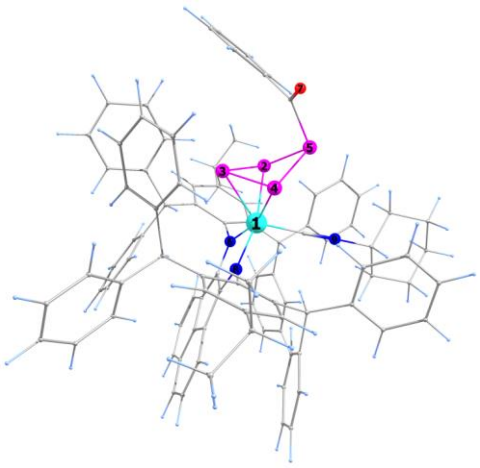

Co	-0.11009358776894	0.06482392141395	0.08629658466317
P	1.34474360319089	-1.36370123023954	1.14484677370286
P	2.15891031504041	0.13237674578594	-0.22538724590998
P	1.25555702575301	1.51474785608534	1.20585371297254
P	1.65627668203809	0.04805603897943	2.87826499386648
N	-0.82197142653359	-1.22348987503923	-1.22367343584362
O	3.90296322939435	1.49242089484252	3.20390570389359
N	-0.92519782609468	1.36695237796505	-1.14903328196138
N	-1.93129773447920	-0.01212350276632	2.46111688298634
C	-1.17569713400860	-3.52824674100133	-0.41342216735574
C	-1.66846052958078	0.79464819806527	-2.07515547768249
C	-1.23552418554292	0.00598624327519	1.50784271492890
C	-1.60673407401125	-0.66634960846831	-2.12284336553561
C	-2.58556226656924	1.25695748847117	-3.12224063091718
C	-2.38215031454939	-3.07542017820445	0.39665302547615
H	-2.23860342748998	-1.99107085935899	0.58248484102096
C	0.27190646669004	4.85238315296704	-1.75655615016339
H	1.00443313601824	5.37181022662735	-2.39274903486466
C	-3.05717930220031	0.06452513482917	-3.75880841060404
C	-2.76629946524034	2.80937296242493	0.54427207751325
H	-2.48035953982507	1.73958249990495	0.57727085021662
C	0.34674700267160	-5.31329048473016	-1.14818113476470
C	-1.45169092195158	4.90580775161622	-0.07718229032637
H	-2.06803095558533	5.46450763737678	0.64509842235003
C	-2.45438937684451	-3.72299145312278	1.78043930034535
C	-0.74110251827534	-4.86284063334442	-0.37909196307054
H	-1.25991170483802	-5.56107976740289	0.29535947921324
C	-3.67492070587612	-3.20204893454378	-0.40425711655118
C	-2.53613329274812	-4.80100670662766	4.40233584467508
H	-2.56804575328792	-5.21891630064922	5.42011431869606
C	4.46640769491990	-0.69684278097543	2.43985138973127
C	-0.81451292155043	2.79013955448884	-1.08898777898661
C	-3.64477908455789	-4.26747724879980	2.29910588791969
H	-4.55376537119740	-4.27465158233185	1.68006673620112
C	0.15105162925195	3.45906879813133	-1.88834051946447
C	-3.68677064003160	-4.79961170356481	3.60015148253996
H	-4.62921845612236	-5.21858316038160	3.98536537434737
C	1.00072557574834	-4.38192513497967	-1.97134725762730
H	1.87137060265496	-4.70772874429769	-2.56224450316911
C	-0.49535214614600	-2.61126227992901	-1.25201442319451
C	-2.91032926659162	3.22415011684832	2.00606711106587
C	-1.64044516641736	3.51804354228635	-0.19675657788845
C	-4.06020109510046	2.86582583096283	-0.26373630858989
C	-1.34112037575354	-4.26192621571711	3.89324318746316
H	-0.43144133702475	-4.24997329395891	4.51323443349079
C	1.31416261616802	-2.05388929318746	-2.97160140032556
H	1.22328578279152	-1.04916009187419	-2.49900575335824
C	-2.84799596898877	-2.35633213826084	-3.74218363369109
H	-2.42536399131181	-3.29410599175997	-3.35927810446048
C	-1.30286791078381	-3.72588364606618	2.59866592057826
H	-0.36533385379469	-3.29601348287513	2.20868208438102
C	4.18510369310891	-2.06499849374923	2.64084720954459
H	3.25299251468950	-2.36254322061932	3.14531909369764
C	2.82118474456706	-2.28925500315963	-3.09291737994096
C	-3.99629449498393	0.06373284534887	-4.81598968877994
C	-0.50023265127585	5.59531963701531	-0.84583668807289
C	-3.96277078006063	-4.33898951161299	-1.18498994398070
H	-3.23010137718947	-5.15793823959293	-1.24324352536567
C	0.98618071370014	3.35961909751016	-4.26193883003492
C	0.84559843889409	-6.74646076503538	-1.04396252057402

H	1.59339083461362	-6.88588903679363	-1.85478591493814
C	-1.85259327009352	3.64229558972288	4.17393134616501
H	-0.93628712605345	3.75264431633260	4.77393538919803
C	0.60687340459977	-3.03341889564414	-2.04058617893028
C	-4.16989571485406	3.33939320007582	2.62619106892858
H	-5.08290433661843	3.21456989278816	2.02538625274534
C	3.49247364942445	-2.20751182636295	-4.32807457116554
H	2.91511148169542	-2.04447841006858	-5.24981004466153
C	-2.48195513559086	-1.12634506155306	-3.20784360356019
C	0.60095092329890	-1.97334753140974	-4.31832778724645
C	1.04145876100536	2.70980182693298	-2.87729973908812
H	0.61443633897383	1.69326609542820	-2.98383089500508
C	-4.62895363081813	-2.16786761501851	-0.35147132621845
H	-4.42346426989401	-1.28455663636867	0.27167316699890
C	-1.75245183973218	3.38287665403983	2.79962000972374
H	-0.76016537721610	3.28137911589483	2.33148116170555
C	-2.77461258587365	0.04491968354630	3.60360141688457
H	-2.87265462312647	1.11999267643379	3.87046683408091
C	0.30997554012312	-0.72138144091593	-4.89112949602253
H	0.60067350101177	0.19310536925136	-4.35369645095684
C	2.48271895932061	2.49811550798529	-2.40973777814864
C	0.22271003629305	-3.13417108002469	-5.02189120046713
H	0.43415027083675	-4.12373581621795	-4.58967213924417
C	-4.62947615139830	4.08702156324368	-0.67787153043233
H	-4.14826369288240	5.03571053179817	-0.39735661609622
C	-3.11532801131203	3.75140992459866	4.78390808804681
H	-3.19485924876459	3.95259628824088	5.86312926482232
C	5.10010374799405	-3.04207872528534	2.22389948953336
H	4.88173252113455	-4.10678756652479	2.39664960791133
C	5.64526634040860	-2.52120909931527	-3.23076184973838
H	6.74144138492513	-2.60771548156726	-3.28396917259654
C	-5.16529293378327	-4.43159253866147	-1.90282017163613
H	-5.36797845993053	-5.32531859229520	-2.51311880334251
C	-0.05848470734017	3.03166473344086	-5.14909730775444
H	-0.80741206957707	2.28578295774106	-4.84750432707038
C	-6.41269157688624	2.90317554675828	-1.84084478342165
H	-7.31916063917703	2.91888039108503	-2.46488528750982
C	-4.47223797121379	1.34409502000796	-5.23878975448639
H	-5.20777259440764	1.40643445899697	-6.05583802728070
C	-5.79609923629106	4.10649363725855	-1.45696902501029
H	-6.22337199662312	5.07034574449245	-1.77427678504112
C	5.66956004887360	-0.31985571936710	1.80483339581178
H	5.87101334489161	0.75007088379697	1.64616491182789
C	1.56599676575611	-6.96603199479971	0.29933554193332
H	2.40087456041228	-6.24783326323184	0.42745131620051
H	1.97822072083136	-7.99412332963139	0.36589871002945
H	0.86619589143567	-6.82365330866004	1.14944865897385
C	-3.79792542986590	-2.37919788705292	-4.80480224942719
H	-4.09255813864268	-3.35478429549564	-5.21991815837648
C	-4.01350606024618	2.50931428924973	-4.62023704590850
H	-4.39941004982455	3.48253326354215	-4.95878878894178
C	4.89204544133515	-2.32275398174869	-4.39772534578785
H	5.39403864443502	-2.25451943655893	-5.37533437580251
C	3.51344324403412	0.37181554575899	2.86669761847459
C	3.59089277644188	-2.49563563025347	-1.92649227990517
H	3.08871747401495	-2.57003998972311	-0.94920636231174
C	4.98620663833418	-2.60850023369010	-1.99242189859601
H	5.55846435763088	-2.75528100335355	-1.06415110298301
C	-0.30710135315276	7.09723881556192	-0.70332595002481
H	-1.03500462389297	7.44482169557283	0.06174841424167
C	-4.69463897242274	1.66873841652045	-0.64558583384758
H	-4.25050615940143	0.70946238629854	-0.34034317018073
C	-6.10393978907783	-3.38812320745984	-1.85089420107144
H	-7.04361727914840	-3.45753963159767	-2.41966084676979
C	-4.27254469696830	3.60125007559551	4.00364593597168
H	-5.26703073466053	3.68561268482807	4.46851127856720
C	-4.36333113181399	-1.21855302876470	-5.33330260804539
H	-5.09441192987523	-1.28399537831109	-6.15397868411256
C	-0.35473232641975	-0.62245129005162	-6.12303183960756
H	-0.57787878734525	0.37031903667128	-6.54247315344083
C	3.04743483566246	3.15000940262097	-1.29880003912344
H	2.44544572078043	3.86142086930072	-0.71607556896611
C	-4.17384226816938	-0.50222881762689	3.26821524706238
H	-4.06541482920995	-1.54814064441948	2.91020813494248
H	-4.60762154174078	0.09352113231014	2.43859004070510
C	1.94003366755770	4.31307683636748	-4.67143365622972
H	2.77891489803480	4.56000255563269	-4.00274470190431

C	-0.73402189362192	-1.78579004403958	-6.80979974683030
H	-1.26381112754803	-1.71377606599039	-7.77179929660636
C	-5.83383280264785	-2.25621114217785	-1.06565853238060
H	-6.56618287522631	-1.43677951748052	-1.00476133989546
C	6.57104239554864	-1.29836000744746	1.36747710270224
H	7.49816695931948	-1.00064782631527	0.85427583018022
C	3.28127037713257	1.58028654348053	-3.12981898306184
H	2.85449576496874	1.05950930197508	-4.00121985974863
C	6.29035050377011	-2.66022719351204	1.58101985785765
H	7.00205940758835	-3.42849976472991	1.24167472297512
C	-5.85839215590736	1.68173138144394	-1.43002781267050
H	-6.32010514276719	0.73159571198960	-1.73794581643565
C	-0.43632379238690	-3.04255093222816	-6.25688141281944
H	-0.72957308852469	-3.96146167227766	-6.78785743053919
C	-0.61857264036460	7.83245193353505	-2.01818862405248
H	-0.51757212014155	8.92971496967867	-1.88987332004851
H	-1.64959162258677	7.61791548986277	-2.36487105318128
H	0.07864021365043	7.52289087904642	-2.82457070315692
C	-5.07778195599686	-0.46104830315200	4.50558834594693
H	-5.25621018917119	0.60007418044717	4.79063588032725
H	-6.06928182261148	-0.89175969860113	4.25496025886284
C	-2.13177672350564	-0.69669172955404	4.78879263483110
H	-1.14366729998050	-0.24289665480673	5.00763903002141
H	-1.95041252206272	-1.74902853312886	4.48601608538554
C	-0.15826003722050	3.64633240285568	-6.40638375851677
H	-0.98352556037439	3.37183344211418	-7.08191021315387
C	-4.44514752225992	-1.20739519953450	5.68782899072899
H	-5.10429460891120	-1.14685960017709	6.57876225070242
H	-4.35245796080034	-2.28637393203625	5.42980633184155
C	-0.27476994056239	-7.77684068490376	-1.25320424189526
H	-1.03312219731100	-7.71849094688181	-0.44488099270471
H	0.13443853016561	-8.80773037093548	-1.24711193424106
H	-0.79561663778231	-7.61764830373173	-2.21910117145263
C	1.84049247402981	4.93415948266408	-5.92698883547305
H	2.59523597968965	5.67706363317707	-6.22808965134118
C	0.79039634300795	4.60462952043540	-6.79950704565793
H	0.71626136391883	5.08811930219594	-7.78559835732937
C	-3.05291474681658	-0.65053281925370	6.01317154053504
H	-2.58949659592723	-1.21744376318008	6.84686420547501
H	-3.14897783551012	0.40222608629270	6.36184228463482
C	1.10575673003966	7.43075715647043	-0.19408415791196
H	1.87834166823957	7.10707333488036	-0.92255590756634
H	1.31716547015050	6.92249418251270	0.76813433622013
H	1.22350599310482	8.52339771375715	-0.04231406978252
C	4.59367412288090	1.29954222791209	-2.73483473539034
H	5.18051935094638	0.55171767194805	-3.28980563392746
C	4.36805857717887	2.87114637809602	-0.89978056435973
H	4.78108137647265	3.37277488213175	-0.01121761709714
C	5.14149016726955	1.94232264502433	-1.60925982169745
H	6.16689528313051	1.70990803996882	-1.28322098389389
C	-3.06575504716080	2.49007854656926	-3.55750771491520
H	-2.73461741940533	3.43001709471891	-3.09552966096906

Cartesian coordinates of the optimized geometry of *exo/exo*-[(Ar*BIAN)Co(CyNC)$_2$(η^1-P_4CO*t*Bu)] (***exo/exo*-7**) at the D3BJ-PBE/def2-TZVP/def2-SVP@C,H/CPCM(C_6H_6) level:

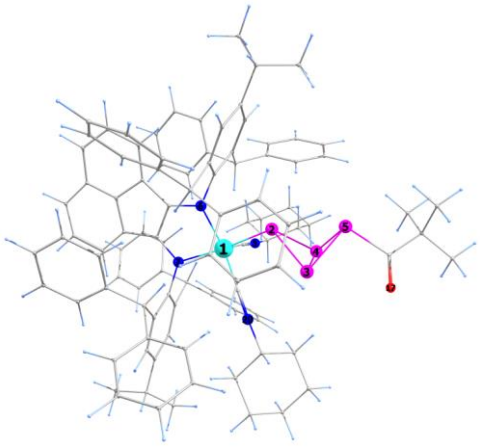

Co	-0.03082667691455	0.06922619916802	-0.01005177771540
P	-1.80993988349175	-1.07274266738333	-0.79781780383026
P	-2.18150645607041	-0.85659645640020	-3.00756623244490
P	-1.14724882852924	-2.64437488161893	-2.25435196431299
P	-3.35619730449219	-2.67168434255183	-2.52629934391688
N	-0.99655758097927	0.34440641444310	1.66244975936011
N	1.15015674009438	1.45483962331066	0.75142175303663
N	1.60016498790671	-2.44086713642075	0.11784938327556
C	-0.32973772577386	1.11576984100971	2.53157534794904
C	-0.50394412768904	1.50865713120817	3.93511546381026
C	0.86600129970735	1.73327678082815	2.02173306559445
C	0.62347759299444	2.34381255507140	4.23199013033420
C	0.47257142303985	4.86081363813365	0.84187522260575
C	-3.83429062429645	1.77617789633736	-0.20069712225660
C	-3.42211812778449	1.88052662342692	1.26801696822946
H	-2.37541277488326	2.24176194318783	1.26381781832077
O	-2.83814553405803	-2.93800137646449	-5.25334985633241
C	-2.23021391049728	-0.22328767763012	2.10891869228625
C	1.89844490886248	3.35417475240176	-0.60137537621426
N	0.68051889548174	0.68660480270630	-2.82862435592163
C	2.19353506581973	2.12647392714512	0.05301842280664

C	3.47830657876607	1.54576725059987	-0.08034101488686
C	1.48968548949433	2.50980288996674	3.10253201401220
C	-1.42073671831767	1.24831387001907	4.95155576238731
H	-2.29669062051707	0.60592686177806	4.78580712138441
C	4.43546056739083	2.18160144142397	-0.89276520086034
H	5.41492881537258	1.69478161576046	-1.01728845792507
C	-3.42213167659876	0.53379425980488	1.98307723574531
C	4.52360401435694	-0.75986992965924	-0.21731950951959
C	2.89518255399809	3.96336968937936	-1.38124935947448
H	2.65725292546461	4.90580561268373	-1.89993107971375
C	0.87212185504703	2.90927312279829	5.50108763051906
C	-0.69350164428520	4.86748583556962	1.63178774480916
H	-1.55160744425047	4.24540817520904	1.33678457548548
C	-4.23859440741639	2.92225635337779	2.03537529566321
C	3.83965264526265	0.27718943276213	0.67760930222230
H	2.87887665932926	-0.18620761204081	0.98372055578858
C	0.52949919202215	4.00786338827995	-0.42388455529256
H	-0.19362660908632	3.17671959143849	-0.28459264945591
C	-2.26780031348456	-1.52465068549738	2.66935449903731
C	-0.09381559674833	2.63070500245175	6.52067726371438
H	0.04436357277592	3.04722790548820	7.53055807384427
C	4.17086219051603	3.39514002858347	-1.54795313196819
C	-1.17166590477782	-3.81880950421577	2.52581308566411
C	-3.49604443184881	-2.03454707113682	3.12010935148636
H	-3.51823967630146	-3.05651857265999	3.52886133994060
C	0.95090091594998	-1.45420793585219	0.10154460735858
C	-4.62074738285209	-0.00201195531445	2.48729647746510
H	-5.53800836218966	0.60525422996558	2.42586614234342
C	2.64819208906432	3.26373156870083	3.25754177282208
H	3.34721376337783	3.41462274812121	2.42459383572929
C	-4.68398151492289	-1.28499038650125	3.05620807298035
C	-4.74667953251289	0.81440535993200	-0.67549987109232
H	-5.14576454257713	0.05509649816668	0.01174666149558
C	0.36077365077800	0.46387683346692	-1.71210570257135
C	0.09015706164394	4.76244499772401	-1.67883343335391
C	-1.19731200715285	1.82607892802882	6.23724864363790
H	-1.92481859816941	1.61516304949492	7.03595516689113
C	1.55518089622508	5.66907039981733	1.24154789488490
H	2.48219035573765	5.66557911133896	0.64853522760818
C	4.59790126507731	0.57039792076942	1.97239470460188
C	-3.31630024484630	2.71546874752964	-1.11661080458463
H	-2.60070801537185	3.47541737725886	-0.76607617394261
C	-0.98479554817223	-2.33384185127379	2.82806354568359
H	-0.28553354798074	-1.95602070470305	2.05491312729138
C	-0.77365417850420	5.64385991101340	2.79733522350762
H	-1.69247135694867	5.61722380305504	3.40228324401307
C	2.07296362847395	3.67826741280031	5.62796365511280
H	2.32413127104006	4.13816052000651	6.59647257527898
C	4.00138005232170	-1.00227327589014	-1.50773848431313
H	3.14541626980125	-0.40897519647010	-1.86169631827668
C	2.92424567556032	3.83684789688066	4.53454642113753
H	3.84656382629900	4.42560065090473	4.65429320277112
C	-0.58706473230865	-4.83096717642198	3.31087582712333
H	-0.01972648708939	-4.55795994187997	4.21280898201910
C	5.61449249470734	-1.53651330517987	0.21694155246563
H	6.03792015531956	-1.36447777268617	1.21731345377479
C	-0.33585093789519	-2.01611734706475	4.17038405105735
C	5.23250928174824	4.10609327155315	-2.37424484032423
H	4.70209642631193	4.86909980768378	-2.98498288917644
C	-6.00054360077867	-1.86015786755747	3.55590346813920
H	-6.76639233048193	-1.06323521079308	3.43616366575258
C	2.35997246334016	-3.63679329683404	0.22878558877786
H	3.22829649850812	-3.52831435439473	-0.45934528136536
C	1.47634107249735	6.45579994359339	2.40125069696473
H	2.33790269473949	7.07191948316169	2.70164494221635
C	0.31374227234312	6.44198214895049	3.18755013614498
H	0.25750883639827	7.04518108341666	4.10646572388457
C	-5.13736025900581	0.79778240097599	-2.02479109509266
H	-5.84359934421313	0.02974729913851	-2.37536743768803
C	-3.71734672170669	3.44079881831266	3.23992461364912
H	-2.73086381394334	3.10122584075024	3.59022726569387
C	-0.35617739676261	4.01908618447356	-2.79234817658280
H	-0.42064708090647	2.92486171489186	-2.71038501218608
C	-0.98070809776868	-2.29856482551597	5.39223211855783
H	-1.95860926238648	-2.80378943342124	5.38878878894054
C	-1.43497248049687	-6.55130248051736	1.80589827671158
H	-1.53718872007634	-7.61142886454113	1.52801668132870

C	5.58178972686052	1.57493828527585	2.06768073913157
H	5.80682983535010	2.20306733558712	1.19399703200883
C	5.63472167239281	-2.76743127222087	-1.88687463481356
H	6.06508259002660	-3.54713249992732	-2.53360140079880
C	-1.88796810253499	-4.19942602297050	1.36806652514225
H	-2.33799650932825	-3.41989953321774	0.73245558147363
C	-4.61838365926738	1.74139998033700	-2.92484562922122
H	-4.91766422356749	1.72171074695646	-3.98379163312931
C	-5.50205132175838	3.36823495571304	1.60379581079405
H	-5.92053409506335	2.98370155192813	0.66153292692816
C	-2.01972306205951	-5.54859448596703	1.01207127964436
H	-2.57760271508371	-5.81608974703383	0.10113121894228
C	-0.71848633560233	-6.18560478859459	2.95552375337426
H	-0.25514552846689	-6.95954963537489	3.58690403326684
C	4.54861916758242	-1.99305658117059	-2.33373134839025
H	4.11956870771006	-2.16624579599382	-3.33318991997175
C	6.21746267156939	4.84921690901786	-1.45221259245727
H	6.76896026321440	4.13013167566831	-0.81011748061538
H	5.68670928871711	5.55803014097497	-0.78514838974144
H	6.96405229057490	5.42072331753123	-2.04159781673243
C	-3.70253794194102	2.70217075856554	-2.46456861231503
H	-3.27616376369699	3.44317419754361	-3.15738823540888
C	6.16492550353203	-2.53304061551162	-0.60911343682910
H	7.01781050117596	-3.12778349452316	-0.24717410609703
C	-0.65309353470196	6.05535030380299	-4.09041407989861
H	-0.94092100715994	6.55846861802675	-5.02615735083182
C	-0.72115678584288	4.65496201140054	-3.98743000637208
H	-1.06801742151084	4.05217363466361	-4.84153829860283
C	0.14166831181458	6.16509340790524	-1.78871829962287
H	0.46956751180706	6.76478795187520	-0.92682322250504
C	-6.43546748079372	-3.06352560465411	2.70091493782508
H	-6.51613291095237	-2.78688820665123	1.63034509946005
H	-7.41956313149894	-3.45243627915419	3.03474546461117
H	-5.70038874269571	-3.89180048351979	2.77865657323504
C	2.89435517111015	-3.79977732453943	1.66384276962434
H	2.02931092653394	-3.81032121712120	2.36146059395984
H	3.51989723823905	-2.92097069904525	1.91888924252996
C	-4.43971855587186	4.37548049953105	3.99462706554717
H	-4.01130849565141	4.76553268493156	4.93123648656743
C	1.52226766056720	-4.85255148048723	-0.20650833901616
H	1.18198821149164	-4.70852824674942	-1.25226043835066
H	0.61197054191887	-4.89143155644454	0.42694592662239
C	-3.29158550629696	-3.50465199173469	-4.27089542827962
C	-0.22510236265165	6.80621276901627	-2.98497028773612
H	-0.17760125994701	7.90432428467925	-3.04942564612679
C	5.97556977541590	3.16764232180823	-3.33634970890719
H	6.67378344260330	3.74127019638610	-3.97933251922085
H	5.27179137705977	2.62022930992310	-3.99463077264289
H	6.57886002093566	2.41515879404433	-2.78757071074622
C	0.90511620824984	-1.35418616190561	4.20550862508940
H	1.40091949047954	-1.10426786632188	3.25535928653764
C	-5.70246499011279	4.81207228549837	3.55696224743428
H	-6.27108176878142	5.54758204323119	4.14638479992490
C	-0.39826979796500	-1.92678600462552	6.61274970669117
H	-0.91874430436442	-2.15198108367531	7.55653056879832
C	4.32680881607662	-0.20241177191112	3.11965616020476
H	3.56062109695944	-0.99034699824432	3.06642017243735
C	-3.89532376928096	-4.92425393080783	-4.32805400184793
C	-5.93498534449299	-2.22659475539548	5.04794419781796
H	-5.19437765441787	-3.03304236728874	5.23121494247686
H	-6.91924271872603	-2.59032876619370	5.40822555625576
H	-5.64250836311986	-1.35287056776864	5.66463231093821
C	2.86766730690763	-6.31683573087806	1.36832274309027
H	2.00955425703216	-6.43405691602499	2.06596999845729
H	3.47331686648146	-7.24373216451373	1.44592071184584
C	1.08801586927442	0.84421387759140	-4.17944311702671
H	0.23883802211229	1.32070800820364	-4.72262154276346
C	2.32657857512900	-6.14911769134674	-0.05752393493185
H	1.68616625878525	-7.01202470485070	-0.33471628335999
H	3.17635508023581	-6.14165415579579	-0.77669723780542
C	0.83491634188188	-1.25274485654690	6.63242257095001
H	1.28109562824059	-0.94069174060713	7.58892246567250
C	6.26490050273158	1.80507227922692	3.27233898216528
H	7.02196819897262	2.60287066152902	3.32346697863664
C	-5.40765022848126	-4.78888258586095	-4.03817109126676
H	-5.59479604159585	-4.35482745045329	-3.03497057725236
H	-5.88116995244606	-5.79168039883463	-4.06957930254361

H	-5.90527571104634	-4.14748084249117	-4.79315928130696
C	3.69709684402068	-5.09874578212183	1.79531281774899
H	4.60891063337936	-5.02840396100745	1.16042757196668
H	4.05073127692750	-5.21167653390310	2.84110512310339
C	-6.22922396077588	4.30428508473122	2.35977901700603
H	-7.21578815641311	4.64050450509074	2.00476788071468
C	1.48546305062483	-0.96618869170465	5.42331964005995
H	2.43812874442343	-0.41684980890985	5.42224983551691
C	1.83058490602798	-0.35348018595189	-6.27589167983938
H	0.99483574517827	0.06950776233761	-6.87672412123154
H	2.05742060694232	-1.34713870786287	-6.71432438832676
C	5.01251487018205	0.01779984888831	4.32435573935497
H	4.78320976136868	-0.60237712807334	5.20451201063113
C	3.04767243191173	0.57597826156557	-6.37553979107249
H	3.34455194809206	0.71071945529150	-7.43647331674753
H	3.91364798490296	0.09950782960904	-5.86271596619701
C	5.98293918837803	1.02876858145095	4.40758967064632
H	6.51528114199863	1.21162638163307	5.35338273282790
C	1.36669162163948	-0.52633166910284	-4.82502743256985
H	2.15478265580616	-1.03421339693013	-4.22761842712968
H	0.45469247033077	-1.15431097421658	-4.76115093224596
C	2.31044452737828	1.77484812804533	-4.26782901502747
H	3.12691541276123	1.33378376933805	-3.65608417353600
H	2.06362043290879	2.75205072939420	-3.80752338585351
C	2.76460705812740	1.93512449002862	-5.72199078912932
H	1.97146275812109	2.46431631428363	-6.29625957420324
H	3.66385342710178	2.58450396746937	-5.76215619032280
C	-3.67059073673070	-5.53263150608528	-5.71889413288018
H	-4.14317031431364	-4.91610872711824	-6.50787343816564
H	-4.10783488198439	-6.55060565495164	-5.75990080445722
H	-2.59009725953760	-5.60657096314686	-5.95205008922440
C	-3.23159759475021	-5.79819299993145	-3.24325278533881
H	-2.13914378727496	-5.88616170291456	-3.40987019455918
H	-3.67120058794473	-6.81640568960089	-3.26519235160189
H	-3.38984824163881	-5.38069907018703	-2.22775303308240

Cartesian coordinates of the optimized geometry of *exo/endo*-[(Ar*BIAN)Co(CyNC)$_2$(η^1-P_4CO*t*Bu)] (***exo,endo*-7**) at the D3BJ-PBE/def2-TZVP/def2-SVP@C,H/CPCM(C_6H_6) level:

Co	-0.08607990773448	-0.10926806420533	0.03180688599930
P	-1.80848086493792	-1.34390005839220	-0.77253847109711
P	-2.06919321650502	-1.13927906548501	-2.99950609274181
P	-0.98018189454829	-2.89565724747810	-2.17160205348566
P	-2.98299411377887	-3.13741345655193	-3.05810702328958
N	-1.05699466722538	0.22238494038289	1.70089989821765
N	1.05964888406978	1.34007593953030	0.73038854628998
N	1.64527126919928	-2.54217497736475	0.31073779870590
C	-0.40168555928079	1.03952588652941	2.53368176760106
C	-0.56948479367500	1.48761593450811	3.92194399577946
C	0.77142751372290	1.67142519655501	1.98517393333315
C	0.52660988791727	2.37979029250071	4.16388669491154
C	0.26686047086824	4.71068906849822	0.68182594763421
C	-4.25203011987706	1.78138916490603	0.06029293901170
C	-3.52488423385453	1.74657915932281	1.40447673919073
H	-2.46950903556311	2.00122444523692	1.17631033790684
O	-3.96404743179086	-4.21206753567920	-0.75822502531356
C	-2.27508424147023	-0.36855627680853	2.15778070249116
C	1.70568657060409	3.20224985117396	-0.71936186797882
N	0.69700133471893	0.43006531219675	-2.78504188127109
C	2.06695423949531	2.02548374270979	-0.00808535497537
C	3.37808452012893	1.50474475754155	-0.11918962414222
C	1.37049787969668	2.52942915666869	3.01624375447718
C	-1.44957496144877	1.22619510626666	4.96807574592191
H	-2.28409779868322	0.52253415568842	4.85101048819813
C	4.29873303521861	2.14906575472227	-0.96686219340941
H	5.30223661953779	1.70920991786009	-1.07278882642674
C	-3.49502562920240	0.34187365238174	2.00356389714117
C	4.54599189437774	-0.74721366777054	-0.13831157717201
C	2.66393875684767	3.82040182421561	-1.53838252676308
H	2.37414875724498	4.71979914112081	-2.10491832711960
C	0.76822860172076	3.01431655019555	5.40167720611203
C	-0.79764143295438	4.59480670520905	1.59344961559339
H	-1.58046789416049	3.84653168107083	1.40867471507074
C	-4.03056361849679	2.83610846462800	2.35651495663619
C	3.80137425062087	0.29483409328108	0.69997075302523
H	2.86395577332924	-0.20159756882456	1.02513368829820
C	0.31074741659332	3.79704522757286	-0.54104453966799

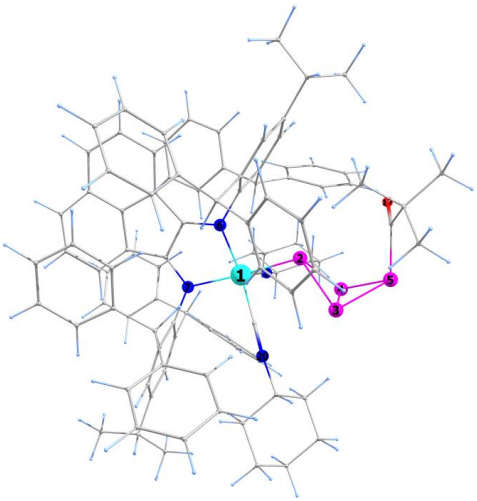

H	-0.36229140780395	2.94251159290608	-0.32022918992575
C	-2.26981129709151	-1.67064192631891	2.72111718254000
C	-0.16722901035347	2.73858605207707	6.44952649042558
H	-0.03336995930792	3.20730200388682	7.43685954910987
C	3.96689051464406	3.31016197196390	-1.68418537480924
C	-1.02344610194120	-3.90933055899451	2.71829260772692
C	-3.48859854988534	-2.24271670441865	3.12198212404509
H	-3.47310214719838	-3.25972484654202	3.54023548672771
C	0.94731956904643	-1.59295506260829	0.23320767562934
C	-4.68636232663002	-0.27762020019359	2.41715258627200
H	-5.63733654375745	0.26222448359188	2.28911972424838
C	2.49099766263581	3.34729428180579	3.11332497630356
H	3.16771352521703	3.49218004788386	2.26104001430759
C	-4.71137725840550	-1.56528043486355	2.97843753528198
C	-5.65550486274139	1.89123032092555	-0.02420140337389
H	-6.25109333511618	1.98389901123299	0.89687697070854
C	0.33833053723272	0.23482027221925	-1.67485796027176
C	-0.22174031878757	4.43944848767478	-1.82038099498903
C	-1.23343599304557	1.86837120172953	6.22318074539936
H	-1.93461930707445	1.65575462385741	7.04468814527720
C	1.27453120122964	5.66011635173852	0.94659954951855
H	2.13266972314430	5.75064608071566	0.26332580115587
C	4.53373302128832	0.68930636153101	1.98238560833492
C	-3.51031341709166	1.71402650041381	-1.13440991974819
H	-2.41331565433811	1.63464042662725	-1.07713487711902
C	-0.94933957780936	-2.40085171093081	2.94418557308864
H	-0.25705623660559	-2.01785128928741	2.16767479368224
C	-0.86049259325542	5.39272114964927	2.74505634725650
H	-1.69992394026250	5.26629506410228	3.44561758856574
C	1.93115231603079	3.84588982140499	5.47082147238010
H	2.17379911298478	4.36331655007683	6.41212534785238
C	4.05083763396539	-1.07881079831887	-1.41931412541412
H	3.17337610456456	-0.54151882783342	-1.80902074874107
C	2.75545105920886	3.99617947152404	4.35573097914223
H	3.64688142164384	4.63748684274145	4.43055527189675
C	-0.34496794675954	-4.82571504750009	3.54632792712039
H	0.20823766167175	-4.45778965976776	4.42279264520906
C	5.66747167595776	-1.44784586250948	0.34459165535567
H	6.07046453705239	-1.20549535651203	1.33878345181723
C	-0.34206515590788	-1.99596489626467	4.28280411021098
C	4.98648446516951	4.02756536861709	-2.55673228084659
H	4.41589465971688	4.73501914243532	-3.19760246707706
C	-6.02655968668866	-2.16837478921895	3.45119609292734
H	-6.83177179860600	-1.66687954523416	2.87005527853101
C	2.48961368327233	-3.67879752778022	0.43421343854715
H	3.31395678595282	-3.53958691418460	-0.30087987793867
C	1.21173511877600	6.47070261106405	2.09058777552797
H	2.01175279953624	7.20193021018649	2.28456798885611
C	0.14725123970449	6.33666159443405	2.99693504220709
H	0.11034485048123	6.95799290931241	3.90468146063659
C	-6.29922394252981	1.91053598316114	-1.27020657028056
H	-7.39611677389409	1.99357556982906	-1.31632959529343
C	-4.26555814883689	2.61405285228307	3.72632448417122
H	-4.14453876979302	1.60431053149861	4.13903828600522
C	-0.76145204669602	3.60159115833350	-2.81998091805383
H	-0.81073971852413	2.51861497516266	-2.63772403797466
C	-1.01244129875106	-2.23571241361659	5.49957832168665
H	-1.98680410706318	-2.74805373758222	5.49162516643750
C	-1.06676637960277	-6.68967429733155	2.15149260291807
H	-1.08530602075732	-7.76866003517276	1.93400216437073
C	5.48631792904388	1.72707388576808	2.02439172444622
H	5.70087358911315	2.30848880127663	1.11628017485840
C	5.77033194341923	-2.78052860827253	-1.69338513159466
H	6.24378658930992	-3.57079719001614	-2.29557815446015
C	-1.71810975271705	-4.41079309663345	1.59600756292400
H	-2.24982389698447	-3.71870920954395	0.92557626712652
C	-5.54884779512183	1.83610194611048	-2.45628794147183
H	-6.05384810573984	1.85894934819777	-3.43399786903801
C	-4.20765100025658	4.14587963487572	1.85647170065519
H	-4.03664239509704	4.34213342283874	0.78703035086671
C	-1.74423352255353	-5.78405032665942	1.31641058601572
H	-2.29832774129337	-6.13770952530144	0.43383606195127
C	-0.36545938026971	-6.20343941230146	3.26572765861665
H	0.17078173186147	-6.90021088975581	3.92865230932720
C	4.65415585194819	-2.08255017665191	-2.18887412259193
H	4.24561188575371	-2.32763469068639	-3.18182736483964
C	5.94577256999274	4.85956262985222	-1.68480453647143

H	6.53755693626803	4.19966499649275	-1.01569231067679
H	5.39038633740422	5.57530559934395	-1.04574307903787
H	6.65832808003422	5.43470844278329	-2.31155368872138
C	-4.15011722611604	1.74533071047234	-2.38403371304631
H	-3.54785575881807	1.70576128418590	-3.30460687424694
C	6.27403270230668	-2.45713938415249	-0.42439922429855
H	7.14932288449871	-2.99204810731293	-0.02466222711428
C	-1.17494400010652	5.51270374722411	-4.26609206044946
H	-1.54618396289185	5.93125871861821	-5.21403824282486
C	-1.23270756879544	4.12835195506618	-4.03076492647173
H	-1.65504461947824	3.45329870952321	-4.79166174770249
C	-0.18186862541305	5.82599896787929	-2.06187805874039
H	0.21320959374359	6.50104441679322	-1.28845178756478
C	-6.13152067903345	-3.67784033286885	3.19358921506870
H	-5.93000142838724	-3.92644437268742	2.13170296196956
H	-7.14605431878269	-4.04496934569430	3.44932556725564
H	-5.41093201394210	-4.24946226916398	3.81425909736724
C	3.10559155229723	-3.74839102733276	1.84366530127840
H	2.28091068703825	-3.80906113687209	2.58589475795061
H	3.66850943797972	-2.81451974021335	2.04224427616402
C	-4.64998957874408	3.66588792904498	4.57536716061014
H	-4.82057092205722	3.46389705770232	5.64417172111470
C	1.72323274407583	-4.96744194376894	0.08959881597678
H	1.30720672874193	-4.88572639398759	-0.93536515602269
H	0.86315004743094	-5.05901726438910	0.78388444439393
C	-4.22288559786065	-3.38894491238234	-1.62461192056250
C	-0.65080626231208	6.35776295873769	-3.27574601752724
H	-0.61019815628101	7.44510725599729	-3.44415192091665
C	5.76269520955002	3.07801439569210	-3.48144422214283
H	6.42954764277958	3.65072520520934	-4.15761116415899
H	5.07858694588407	2.46988826249670	-4.10633461279873
H	6.40275330874772	2.37910756140787	-2.90412151926603
C	0.89643515076708	-1.33027306286200	4.31963080654640
H	1.41462896916297	-1.11826623034048	3.37202990217123
C	-4.81185957785764	4.96324080178654	4.06764635731910
H	-5.11176070204775	5.78822888190974	4.73177244331671
C	-0.45648157625278	-1.81973376517114	6.71822785122476
H	-0.99553581351369	-2.01328470118253	7.65863105592316
C	4.27256727731619	-0.02049105677159	3.17154393986199
H	3.52991041542477	-0.83235274480558	3.15833056470194
C	-5.60599162686242	-2.70247150354478	-1.70435254797912
C	-6.25396983292895	-1.83885191957159	4.93872704053444
H	-5.46100822019080	-2.30104430130712	5.56373807918346
H	-7.23407245564063	-2.22374672766038	5.28928761174850
H	-6.22822400027711	-0.74464335897968	5.11627430011633
C	3.28113828997696	-6.26833378049331	1.61297686026582
H	2.48411437045269	-6.44683432282027	2.36844352945060
H	3.97291907206308	-7.13458427633031	1.66975914826014
C	1.06870790493656	0.55105471373456	-4.15042531899718
H	0.14255161284507	0.81391403256108	-4.71371489354261
C	2.64042132438127	-6.18906638513889	0.22085977348751
H	2.05876201104744	-7.10966952642422	0.00751344657152
H	3.44051299235222	-6.13352608719222	-0.55120155795689
C	0.77590160881826	-1.14407461117237	6.73968189001385
H	1.20245878354329	-0.79907069390939	7.69379167313999
C	6.15063090497082	2.04878417546062	3.21840822689250
H	6.88407794350740	2.86988813068699	3.22810218940354
C	-6.68669247764677	-3.78562686857096	-1.51174610007361
H	-6.67563754926662	-4.51591581860838	-2.34645699823667
H	-7.68828142260019	-3.31085978405691	-1.48089604944237
H	-6.52905173194180	-4.33709822918565	-0.56473302684865
C	4.02288808130300	-4.97098651003973	1.96167488410320
H	4.88662844864484	-4.83887283632647	1.27201378983250
H	4.44333076154668	-5.02312782352235	2.98729615592568
C	-4.59099601712598	5.19776619789544	2.69934450757159
H	-4.71300743483881	6.21020140627607	2.28461240458981
C	1.45107032709151	-0.89900541309237	5.53485459684275
H	2.40345630578565	-0.34911378079899	5.53498832865293
C	2.03127026513958	-0.66851608343479	-6.14689572917706
H	1.14053768418533	-0.45471719627097	-6.77906057362384
H	2.43654956944455	-1.63992163997908	-6.49814686471840
C	4.93961822123135	0.29179222096326	4.36635584753524
H	4.72068505850861	-0.28101384656908	5.28064368403062
C	3.06586112810951	0.44987102349795	-6.32992329923456
H	3.35127657125239	0.54218449192530	-7.39843505118342
H	3.99359963752583	0.18224578907275	-5.77528544555972
C	5.88020161663095	1.33336472861353	4.39587748125751

H	6.39849034029318	1.58743835745829	5.33297698360927
C	1.59415183279298	-0.79518702001948	-4.68338866511901
H	2.45849574289357	-1.10079917719851	-4.05580040694846
H	0.80948806903110	-1.56851759001220	-4.55489032729104
C	2.09647397149022	1.68009643388857	-4.33518679412747
H	2.96996982304958	1.46372683489781	-3.68408095701569
H	1.66241427202850	2.63342462001420	-3.97376234902799
C	2.53513992894866	1.78783881931799	-5.79912498877762
H	1.67005309560920	2.11501109737271	-6.41822132430744
H	3.30512089815906	2.58140133040666	-5.89571371883947
C	-5.64691267826010	-1.70219590454028	-0.53196162786993
H	-5.50881457130879	-2.22264880022230	0.43384029105394
H	-6.62455991319716	-1.17928796841993	-0.51888222672867
H	-4.85111923356942	-0.93734245841148	-0.61915788333595
C	-5.82655740187287	-1.96433121160895	-3.03276095290239
H	-5.09911751720672	-1.14067662441990	-3.16847161775178
H	-6.84002329712077	-1.51363102769849	-3.04024621969061
H	-5.75354532284343	-2.64744879552457	-3.90340947926198

Cartesian coordinates of the optimized geometry of *exo/endo*-[(Ar*BIAN)Co (η^4-P_4)] (**3**) at the D3BJ-PBE/def2-TZVP/def2-SVP@C,H/CPCM(C_6H_6) level:

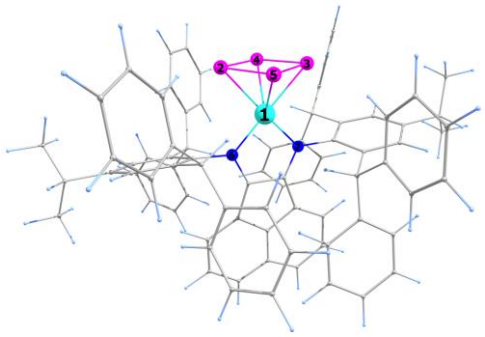

Co	0.13628919339096	0.12729354455756	0.29482010975562
P	1.75895756710467	-1.32612884529092	-0.50306330763690
P	1.01812206887727	1.50841750370778	-1.36471423282833
P	2.38359582459124	0.66440643166293	0.11960310235598
P	0.34390822519680	-0.47341168824218	-1.94247165739533
N	-0.65930794131445	-1.05527375525647	1.55287070673243
N	-1.06126333240632	1.41398480772524	1.02010660948917
C	-0.36428190743016	-2.41103246390137	1.87471541617576
C	-1.28726532484166	2.73641386520155	0.55035437251901
C	-2.32727807693829	2.97108339961448	-0.38243106791344
C	-0.44032599877544	3.79583308080325	0.96506958382690
C	-2.48313077487359	4.26807303972696	-0.90612076037222
H	-3.25133098411902	4.44327112436663	-1.67671015201621
C	-0.82766588652729	-3.46186625639895	1.03929701675251
C	0.66311494014400	3.51355607807133	1.97926180995487
H	1.02681085182244	2.48611723744969	1.75017786958696
C	-1.66554204510355	5.33730009593862	-0.50453133558899
C	-1.51243251993127	-3.15695539054486	-0.28926063863040
C	0.09831445399197	3.45513270053869	3.39228075378796
C	0.36371195318696	2.33684783301702	4.20355349412948
H	0.97855372725313	1.52262813960035	3.79185192449182
C	-0.15178566458343	2.24847101412014	5.50579788993296
H	0.06021484309017	1.35848206123179	6.11791102489962
C	-0.94490814907125	3.28810242575623	6.01823223504674
H	-1.36165179055756	3.21749715297558	7.03471236775516
C	-1.21515813857230	4.41114040442193	5.21893969370248
H	-1.84620463899013	5.22541081441411	5.60808213279390
C	-0.70096324894900	4.49133567309656	3.91545976015564
H	-0.93484739991072	5.36368201290006	3.28521794899194
C	-1.61459816369927	-0.45694257394264	2.29861917665175
C	0.35453045339332	-2.71236352956401	3.06589754434600
C	0.98349782060644	-1.60000699307441	3.90659428283255
H	0.39529049605845	-0.68205547940602	3.70930386471739
C	0.87412819142738	-1.87094335193976	5.40527607059160
C	-0.25467093420970	-1.42600262500765	6.12316500835365
H	-1.03392964588435	-0.85576960401587	5.59816458401874
C	-0.39602753589033	-1.70434894758686	7.49180743538949
H	-1.28750133119152	-1.34431954627637	8.02867494380404
C	0.59400976137271	-2.43372924835163	8.17031297160051
H	0.48574028288208	-2.65251613773484	9.24395402032999
C	1.72998229533494	-2.87191615840316	7.46933335290768
H	2.51843204450374	-3.43505758689745	7.99280205439821
C	1.86993643396334	-2.58769872279809	6.10153568883289
H	2.77278069322236	-2.91499147625772	5.56314931682779
C	0.53057148328535	-4.05662067040017	3.42901078423640
H	1.07017841908124	-4.27959739580036	4.36152494045402
C	-1.81925370304778	0.92867217728280	2.01734217877715
C	-0.65327644834892	5.07896664043734	0.44019435760126
H	0.01875659464574	5.89134164244984	0.75776735615700
C	0.03508555319639	-5.11483283319203	2.64684938946963
C	1.86815588046528	4.43529014975531	1.81817966694320
C	2.35264890189086	5.26255341778960	2.84829789393036
H	1.84350495643829	5.26887063781631	3.82316013008336
C	3.48169633694048	6.07752808223684	2.64790490881313
H	3.84223310760074	6.71667536967487	3.46922101169431

C	4.14690232320220	6.07623465793127	1.41347123167585
H	5.03146700837359	6.71294980933758	1.25688307075584
C	3.67542414370271	5.24872956723763	0.37808037544653
H	4.19081058646001	5.22974432853191	-0.59474162861386
C	2.55070828405913	4.43893570315708	0.58043868129728
H	2.18094095986019	3.79868832316359	-0.23774405766099
C	-2.53457051245593	-0.86565377294990	3.36273932716360
C	-3.00482086519874	-2.86883176289988	-0.20656824357852
C	-3.81851266324748	-3.33162259797685	0.84324740290950
H	-3.35880748355487	-3.86079047087445	1.69079384675408
C	-5.21041924823374	-3.13072377726882	0.81311714069746
H	-5.82998970658479	-3.49325508157684	1.64831589206978
C	-5.80676966170918	-2.47250896858276	-0.27291140820011
H	-6.89542181934748	-2.31181947545604	-0.29477354471410
C	-4.99981679789084	-1.99085606373780	-1.31893250993813
H	-5.45020367703533	-1.44314926799924	-2.16095199764189
C	-3.61233160044565	-2.17978865605821	-1.28004374059932
H	-2.98009997229598	-1.79360532794840	-2.09573729956173
C	-1.83642304624610	6.72529406861634	-1.10504744659128
H	-2.72765211226596	6.68191385364999	-1.76877811764171
C	2.42134467925338	-1.27899920334611	3.48806872865460
C	3.10429132018455	-1.99823516480402	2.49070068128136
H	2.60419020595468	-2.83674702015862	1.98694052967927
C	4.41244191776403	-1.64237944035207	2.11685359579333
H	4.91844366188917	-2.20866812921999	1.31992789449536
C	5.06236495952078	-0.56856256311919	2.74200952823592
H	6.08261584806862	-0.28502685265238	2.44153306075683
C	4.39487737862749	0.14819058402211	3.75002356953738
H	4.89017690073415	0.99650508645534	4.24730819388216
C	3.08993550256023	-0.20617659461022	4.11766742286830
H	2.57986483153517	0.35483402357395	4.91590150616587
C	-0.62273375483744	-4.79216914504260	1.44907814440836
H	-0.98626560308539	-5.60540697403745	0.80153954105095
C	-1.21410556170866	-4.23763115501916	-1.32993431500374
C	-2.15643905819788	-5.22295441449540	-1.68569826468080
H	-3.15789670497503	-5.20280122150837	-1.23002943316734
C	-1.83524393181420	-6.22422206029021	-2.61808567229952
H	-2.58744398773655	-6.98448443625648	-2.88124347901913
C	-0.56541144316132	-6.25411870809523	-3.21514319720851
H	-0.31475524329352	-7.03459183049738	-3.95030290566188
C	0.38167609147560	-5.27448461852961	-2.86958879898959
H	1.38020375411523	-5.28089450063448	-3.33368398858450
C	0.05926051607836	-4.27973439537776	-1.93588430023857
H	0.81059486544834	-3.52144053533470	-1.65824272018049
C	-2.85925043386362	-2.04705872862079	4.03307770353387
H	-2.34661036249515	-2.99276319787189	3.80839970359418
C	-2.84095360514642	1.45437219391761	2.92640445804356
C	0.22415008379194	-6.56217194999192	3.07681558325104
H	-0.26285385792801	-7.19399083968356	2.30215914132471
C	-3.24765763975849	1.82903663174757	-0.80357889564818
C	-3.47085816798780	1.77252163185149	-2.31397142926221
C	-2.34911756429897	1.84420921906989	-3.16950990852545
H	-1.35018736210721	2.00710129643701	-2.73147040474640
C	-2.49127355615860	1.71202722337162	-4.55718744536433
H	-1.59977233567783	1.76315116432934	-5.20128692250360
C	-3.76292048832090	1.50787847317993	-5.12186970336226
H	-3.87624648596472	1.40259777428650	-6.21200482111324
C	-4.88481057021712	1.43699955464020	-4.28247862613937
H	-5.88649235291822	1.27638424006202	-4.71141773513397
C	-4.73902954712779	1.56669919697917	-2.88962853440009
H	-5.62326188409944	1.50153837609663	-2.23860363439387
C	-3.24330399807327	0.33224935471381	3.72539716258850
C	-2.10454189711300	7.78889677871124	-0.02719095313517
H	-2.99364724914484	7.52947755711614	0.58257751125417
H	-2.27759929348325	8.78433659606267	-0.48646753095448
H	-1.23967760083821	7.88499066865856	0.66196498931334
C	-4.53174234595918	1.81530687527893	0.02174751694849
C	-5.36900989331816	2.94633404777550	0.11113454062525
H	-5.10156004984934	3.86680338902755	-0.42854157012230
C	-6.53361776993869	2.91890397849588	0.89312533789706
H	-7.17108807037987	3.81505988591450	0.95424846514209
C	-6.88104052954849	1.75739787516114	1.60373651442744
H	-7.78697195944305	1.73976730215912	2.22931188688670
C	-6.05750083922833	0.62516685994242	1.51889066340815
H	-6.30654474747599	-0.29087187764310	2.07549881459746
C	-4.89521428178578	0.65758354750686	0.73358957965319
H	-4.24548503813017	-0.22726632050302	0.68325579068350

C	-3.86157977276623	-2.00705728615812	5.04864600604961
H	-4.10439575479681	-2.94240721008102	5.57696363020826
C	-3.45853212331385	2.68130964772956	3.15254532888022
H	-3.19894469551884	3.56716767536734	2.55739545586782
C	-0.62337055232952	7.10400324193043	-1.97344688897935
H	0.30141491668780	7.15631061079382	-1.36139072443811
H	-0.76922812208078	8.09468231060199	-2.45270357997494
H	-0.45373890071481	6.35322573100113	-2.77109952324619
C	-4.23506412817030	0.39284597213394	4.72554177547418
C	1.71295583477724	-6.94603171956980	3.12597411924439
H	2.25358776767461	-6.34492735407194	3.88674282402666
H	2.20533289802326	-6.77145428695171	2.14814316251453
H	1.83870467103638	-8.01636134641156	3.39170128464498
C	-4.45660898004315	2.76735112995833	4.16803858555255
H	-4.94303430331082	3.74033867987707	4.33915025272630
C	-4.53308481259773	-0.83552569903713	5.40164679265309
H	-5.29741644095523	-0.85023779796424	6.19457501593060
C	-4.84356768687286	1.67235344728511	4.94015324897718
H	-5.62418149333486	1.78234718522201	5.70930749146564
C	-0.46951655193387	-6.84702278721113	4.42008169208607
H	-0.01920672125711	-6.24544507054950	5.23723901117013
H	-0.37266187223707	-7.91715803967915	4.69834589417649
H	-1.54890332587315	-6.59724428390573	4.37543050751113
H	-2.70374780005839	0.89039642014925	-0.56007983211418
H	-1.04757340938161	-2.21591104566192	-0.66265667879799

References

[1] Selected literature for the synthesis of phosphorus compounds: a) D. E. C. Corbridge, *Phosphorus 2000. Chemistry, Biochemistry & Technology*, Elsevier, Amsterdam, **2002**; b) G. Bettermann, W. Krause, G. Riess, T. Hofmann, in *Ullmann's Encyclopedia of Industrial Chemistry*, John Wiley & Sons, Ltd, Weinheim, **2000**, pp. 1–18; c) J. Svara, N. Weferling, T. Hofmann, in *Ullmann's Encyclopedia of Industrial Chemistry*, John Wiley & Sons, Ltd, Weinheim, **2006**, pp. 1–48; d) M. Caporali, M. Serrano-Ruiz, M. Peruzzini, in *Chemistry Beyond Chlorine*, Springer, Cham, **2016**, pp. 97–136; e) W. Gleason, *JOM* **2007**, *59*, 17–19; f) J. E. Borger, A. W. Ehlers, J. C. Slootweg, K. Lammertsma, *Chem. Eur. J.* **2017**, *23*, 11738–11746.

[2] Reviews on the coordination chemistry of phosphorus: a) M. Peruzzini, L. Gonsalvi, A. Romerosa, *Chem. Soc. Rev.* **2005**, *34*, 1038–1047; b) B. M. Cossairt, N. A. Piro, C. C. Cummins, *Chem. Rev.* **2010**, *110*, 4164–4177; c) M. Scheer, G. Balázs, A. Seitz, *Chem. Rev.* **2010**, *110*, 4236–4256; d) M. Caporali, L. Gonsalvi, A. Rossin, M. Peruzzini, *Chem. Rev.* **2010**, *110*, 4178–4235; e) C. M. Hoidn, D. J. Scott, R. Wolf, *Chem. Eur. J.* **2021**, 1886–1902; f) L. Giusti, V. R. Landaeta, M. Vanni, J. A. Kelly, R. Wolf, M. Caporali, *Coord. Chem. Rev.* **2021**, *441*, 213927.

[3] M. Peruzzini, J. A. Ramirez, F. Vizza, *Angew. Chem. Int. Ed.* **1998**, *37*, 2255–2257; *Angew. Chem.* **1998**, *110*, 2376–2378.

[4] S. Reichl, E. Mädl, F. Riedlberger, M. Piesch, G. Balázs, M. Seidl, M. Scheer, *Nat. Commun.* **2021**, *12*, 5774.

[5] Selected literature on MAPOs and BAPOs: a) W. Rutsch, K. Dietliker, D. Leppard, M. Köhler, L. Misev, U. Kolczak, G. Rist, *Prog. Org. Coat.* **1996**, *27*, 227–239; b) U. Kolczak, G. Rist, K. Dietliker, J. Wirz, *J. Am. Chem. Soc.* **1996**, *118*, 6477–6489; c) K. Dietliker, *A Compilation of Photoinitiators: Commercially Available for UV Today*, SITA Technology, London, **2002**; d) J. P. Fouassier, J. Lalev´ee, *Photoinitiators for Polymer Synthesis Scope, Reactivity and Efficiency*, Wiley-VCH, Weinheim, **2012**; e) K. Dietliker, T. Jung, J. Benkhoff, H. Kura, A. Matsumoto, H. Oka, D. Hristova, G. Gescheidt, G. Rist, *Macromol. Symp.* **2004**, *217*, 77–98; f) M. Griesser, D. Neshchadin, K. Dietliker, N. Moszner, R. Liska, G. Gescheidt, *Angew. Chem. Int. Ed.* **2009**, *48*, 9359–9361; *Angew. Chem.* **2009**,*121*, 9523 –9525; g) Recent work on coordination properties: A. Widera, R. Conti, E. Schrader, M. Aebli, M. Wörle, H. Grützmacher, *ChemPlusChem* **2023**, *88*, e202200451.

[6] a) C. L. Liotta, M. L. MeLaughlin, B. A. O'Brien, *Tetrahedron Lett.* **1984**, *25*, 1249–1252; b) G. Becker, W. Schwarz, N. Seidler, M. Westerhausen, *Z. Anorg. Allg. Chem.* **1992**, *612*, 72–82; c) A. Huber, A. Kuschel, T. Ott, G. Santiso-Quinones, D. Stein, J. Bräuer, R. Kissner, F. Krumeich, H. Schönberg, J. Levalois-Grützmacher, H. Grützmacher, *Angew. Chem. Int. Ed.* **2012**, *51*, 4648–4652; *Angew. Chem.* **2012**,124, 4726 –4730. d) J. Wang, G. Siqueira, G. Müller, D. Rentsch, A. Huch, P. Tingaut, J. Levalois-Grützmacher, H. Grützmacher, *Chem. Commun.* **2016**, *52*, 2823–2826; e) K. X. Bhattacharyya, S. Dreyfuss, N. Saffon-Merceron, N. Mézailles, *Chem. Commun.* **2016**, *52*, 5179–5182; f) A. Eibel, M. Schmallegger, M. Zalibera, A. Huber, Y. Bürkl, H. Grützmacher, G. Gescheidt, *Eur. J. Inorg. Chem.* **2017**, *2017*, 2469–2478.

[7] a) D. Heift, Z. Benkő, R. Suter, R. Verel, H. Grützmacher, *Chem. Sci.* **2016**, *7*, 6125–6131; b) J. M. Goicoechea, H. Grützmacher, *Angew. Chem. Int. Ed.* **2018**, *57*, 16968–16994; *Angew. Chem.* **2018**, *130*, 17214–17240.

[8] K. M. Szkop, M. B. Geeson, D. W. Stephan, C. C. Cummins, *Chem. Sci.* **2019**, *10*, 3627–3631.

[9] J. Hu, Z. Chai, W. Liu, J. Wei, Z.-J. Lv, W.-X. Zhang, *Green Synthesis and Catalysis* **2022**, accepted, DOI: 10.1016/j.gresc.2022.12.008.

[10] P. Kumar, U. Sharma, G. S. Ananthnag, *Appl. Organomet. Chem.* **2022**, *36*, e6672.
[11] J. S. Figueroa, C. C. Cummins, *J. Am. Chem. Soc.* **2004**, *126*, 13916–13917.
[12] N. A. Piro, C. C. Cummins, *J. Am. Chem. Soc.* **2008**, *130*, 9524–9535.
[13] Selected examples for the synthesis of unusual phosphorus compounds from our group: a) E.-M. Schnöckelborg, J. J. Weigand, R. Wolf, *Angew. Chem. Int. Ed.* **2011**, *50*, 6657–6660; *Angew. Chem.* **2011**, *123*, 6787–6790; b) S. Pelties, D. Herrmann, B. de Bruin, F. Hartl, R. Wolf, *Chem. Commun.* **2014**, *50*, 7014–7016; c) U. Chakraborty, J. Leitl, B. Mühldorf, M. Bodensteiner, S. Pelties, R. Wolf, *Dalton Trans.* **2018**, *47*, 3693–3697. d) C. M. Hoidn, C. Rödl, M. L. McCrea-Hendrick, T. Block, R. Pöttgen, A. W. Ehlers, P. P. Power, R. Wolf, *J. Am. Chem. Soc.* **2018**, *140*, 13195–13199; e) G. Hierlmeier, P. Coburger, N. P. van Leest, B. de Bruin, R. Wolf, *Angew. Chem. Int. Ed.* **2020**, *59*, 14148–14153; *Angew. Chem.* **2020**, *132*, 14252–14257; f) J. A. Kelly, V. Streitferdt, M. Dimitrova, F. F. Westermair, R. M. Gschwind, R. J. F. Berger, R. Wolf, *J. Am. Chem. Soc.* **2022**, *144*, 20434–20441.
[14] C. M. Hoidn, T. M. Maier, K. Trabitsch, J. J. Weigand, R. Wolf, *Angew. Chem. Int. Ed.* **2019**, *58*, 18931–18936; *Angew. Chem.* **2019**, *131*, 19107–1911.
[15] a) A. Schmidpeter, F. Zwaschka, *Angew. Chem. Int. Ed. Engl.* **1977**, *16*, 704–705; *Angew. Chem.* **1977**, *89*, 747–747; b) W. S. Sheldrick, J. Kroner, F. Zwaschka, A. Schmidpeter, *Angew. Chem. Int. Ed. Engl.* **1979**, *18*, 934–935; *Angew. Chem.* **1979**, *91*, 998–1000; c) Y. Mei, Z. Yan, L. L. Liu, *J. Am. Chem. Soc.* **2022**, *144*, 1517–1522.
[16] Y. Zeng, Q. Mahmood, Q. Zhang, T. Liang, W.-H. Sun, *Eur. Polym. J.* **2018**, *103*, 342–350.
[17] Dinuclear Cobalt P_4 complexes: a) S. Yao, N. Lindenmaier, Y. Xiong, S. Inoue, T. Szilvási, M. Adelhardt, J. Sutter, K. Meyer, M. Driess, *Angew. Chem. Int. Ed.* **2015**, *54*, 1250–1254; *Angew. Chem.* **2015**, *127*, 1266–1270; b) S. Pelties, T. Maier, D. Herrmann, B. de Bruin, C. Rebreyend, S. Gärtner, I. G. Shenderovich, R. Wolf, *Chem. Eur. J.* **2017**, *23*, 6094–6102; c) F. Spitzer, C. Graßl, G. Balázs, E. Mädl, M. Keilwerth, E. M. Zolnhofer, K. Meyer, M. Scheer, *Chem. Eur. J.* **2017**, *23*, 2716–2721.
[18] J. L. Rhinehart, N. E. Mitchell, B. K. Long, *ACS Catal.* **2014**, *4*, 2501–2504.
[19] L. Guo, W. Kong, Y. Xu, Y. Yang, R. Ma, L. Cong, S. Dai, Z. Liu, *J. Organomet. Chem.* **2018**, *859*, 58–67.
[20] C. G. P. Ziegler, T. M. Maier, S. Pelties, C. Taube, F. Hennersdorf, A. W. Ehlers, J. J. Weigand, R. Wolf, *Chem. Sci.* **2019**, *10*, 1302–1308.
[21] Calculated single- and double-bond lengths: a) P. Pyykkö, M. Atsumi, *Chem. Eur. J.* **2009**, *15*, 186–197; b) P. Pyykkö, M. Atsumi, *Chem. Eur. J.* **2009**, *15*, 12770–12779.
[22] Related *cyclo*-P_4 complexes: a) O. J. Scherer, J. Vondung, G. Wolmershäuser, *Angew. Chem. Int. Ed. Engl.* **1989**, *28*, 1355–1357; *Angew. Chem.* **1989**, *101*, 1395–1397; b) F. Dielmann, A. Timoshkin, M. Piesch, G. Balázs, M. Scheer, *Angew. Chem. Int. Ed.* **2017**, *56*, 1671–1675; *Angew. Chem.* **2017**, *129*, 1693–1698; c) A. Cavaillé, N. Saffon-Merceron, N. Nebra, M. Fustier-Boutignon, N. Mézailles, *Angew. Chem. Int. Ed.* **2018**, *57*, 1874–1878; *Angew. Chem.* **2018**, *130*, 1892–1896; d) K. A. Mandla, C. E. Moore, A. L. Rheingold, J. S. Figueroa, *Angew. Chem. Int. Ed.* **2019**, *58*, 1779–1783; *Angew. Chem.* **2019**, *131*,1793–1797; e) K. A. Mandla, M. L. Neville, C. E. Moore, A. L. Rheingold, J. S. Figueroa, *Angew. Chem. Int. Ed.* **2019**, *58*, 15329–15333; *Angew. Chem.* **2019**, *131*,15473–15477.
[23] For BIAN in different oxidation states see: M. M. Khusniyarov, K. Harms, O. Burghaus, J. Sundermeyer, *Eur. J. Inorg. Chem.* **2006**, 2985–2996; and references herein.

[24] M. Piesch, S. Reichl, M. Seidl, G. Balázs, M. Scheer, *Angew. Chem. Int. Ed.* **2021**, *60*, 15101–15108; *Angew. Chem.* **2021**, *133*, 15228–15236.

[25] G. Socrates, *Infrared and Raman Characteristic Group Frequencies: Tables and Charts*, Wiley, Chichester, **2004**.

[26] Note: Compound **5a** decomposes in solution at ambient temperature over several days. The ^{1}H NMR spectrum of the decomposition solution after three weeks shows predominantly uncoordinated Ar*BIAN (**1**) ligand.

[27] T. J. Katz, Nancy. Acton, *J. Am. Chem. Soc.* **1973**, *95*, 2738–2739.

[28] Related prismatic *catena*-E_4 (E = P, As) units: a) O. J. Scherer, J. Braun, P. Walther, G. Wolmershäuser, *Chem. Ber.* **1992**, *125*, 2661–2665; b) M. Scheer, U. Becker, *Chem. Ber.* **1996**, *129*, 1307–1310; c) S. Yao, Y. Xiong, C. Milsmann, E. Bill, S. Pfirrmann, C. Limberg, M. Driess, *Chem. Eur. J.* **2010**, *16*, 436–439; d) T. Li, N. Arleth, M. T. Gamer, R. Köppe, T. Augenstein, F. Dielmann, M. Scheer, S. N. Konchenko, P. W. Roesky, *Inorg. Chem.* **2013**, *52*, 14231–14236; e) V. Heinl, M. Schmidt, M. Eckhardt, M. Eberl, A. E. Seitz, G. Balázs, M. Seidl, M. Scheer, *Chem. Eur. J.* **2021**, *27*, 11649–11655.

[29] Isomerization of cyanide to isocyanide: a) T. A. Bither, W. H. Knoth, R. V. Lindsey, W. H. Sharkey, *J. Am. Chem. Soc.* **1958**, *80*, 4151–4153; b) D. Seyferth, N. Kahlen, *J. Am. Chem. Soc.* **1960**, *82*, 1080–1082; c) O. Dietz, V. M. Rayón, G. Frenking, *Inorg. Chem.* **2003**, *42*, 4977–4984; d) G. Ballmann, H. Elsen, S. Harder, *Angew. Chem. Int. Ed.* **2019**, *58*, 15736–15741; *Angew. Chem.* **2019**, *131*,15883–15888; e) Z.-J. Lv, Z. Chai, M. Zhu, J. Wei, W.-X. Zhang, *J. Am. Chem. Soc.* **2021**, *143*, 9151–9161.

[30] Related *catena*-P_4 units: a) O. J. Scherer, G. Berg, G. Wolmershäuser, *Chem. Ber.* **1995**, *128*, 635–639; b) P. Barbaro, M. Di Vaira, M. Peruzzini, S. Seniori Costantini, P. Stoppioni, *Inorg. Chem.* **2009**, *48*, 1091–1096; c) M. Piesch, M. Seidl, M. Stubenhofer, M. Scheer, *Chem. Eur. J.* **2019**, *25*, 6311–6316; d) J. Müller, G. Balázs, M. Scheer, *Chem. Commun.* **2021**, *57*, 2257–2260.

[31] a) K. Heinze, G. Huttner, L. Zsolnai, A. Jacobi, P. Schober, *Chem. Eur. J.* **1997**, *3*, 732–743; b) M. Di Vaira, M. P. Ehses, M. Peruzzini, P. Stoppioni, *Polyhedron* **1999**, *18*, 2331–2336.

[32] M. Piesch, M. Seidl, M. Scheer, *Chem. Sci.* **2020**, *11*, 6745–6751.

[33] Selected examples of [1.1.0]bicyclotetraphosphane-1,4-diyl (P_4 butterfly) compounds: a) O. J. Scherer, G. Schwarz, G. Wolmershäuser, *Z. Anorg. Allg. Chem.* **1996**, *622*, 951–957; b) O. J. Scherer, T. Hilt, G. Wolmershäuser, *Organometallics* **1998**, *17*, 4110–4112; c) C. Schwarzmaier, A. Y. Timoshkin, G. Balázs, M. Scheer, *Angew. Chem. Int. Ed.* **2014**, *53*, 9077–9081; *Angew. Chem.* **2014**, *126*, 9223–9227; d) S. Pelties, A. W. Ehlers, R. Wolf, *Chem. Commun.* **2016**, *52*, 6601–6604; e) J. E. Borger, A. W. Ehlers, M. Lutz, J. C. Slootweg, K. Lammertsma, *Angew. Chem. Int. Ed.* **2014**, *53*, 12836–12839; *Angew. Chem.* **2014**, *126*, 13050–13053; f) J. E. Borger, A. W. Ehlers, M. Lutz, J. C. Slootweg, K. Lammertsma, *Angew. Chem. Int. Ed.* **2017**, *56*, 285–290; *Angew. Chem.* **2017**, *129*, 291–296; g) J. Bresien, K. Faust, C. Hering-Junghans, J. Rothe, A. Schulz, A. Villinger, *Dalton Trans.* **2016**, *45*, 1998–2007; h) J. E. Borger, M. K. Jongkind, A. W. Ehlers, M. Lutz, J. C. Slootweg, K. Lammertsma, *ChemistryOpen* **2017**, *6*, 350–353.

[34] Application of cyanide to release polyphosphorus molecules from a copper(I)iodide matrix: A. Pfitzner, M. F. Bräu, J. Zweck, G. Brunklaus, H. Eckert, *Angew. Chem. Int. Ed.* **2004**, *43*, 4228–4231; *Angew. Chem.* **2004**, *116*, 4324–4327.

[35] Related *cyclo*-P_3 complexes: a) M. Piesch, S. Reichl, M. Seidl, G. Balázs, M. Scheer, *Angew. Chem. Int. Ed.* **2019**, *58*, 16563–16568; *Angew. Chem.* **2019**, *131*,

16716–16721; b) P. Coburger, J. Leitl, D. J. Scott, G. Hierlmeier, I. G. Shenderovich, E. Hey-Hawkins, R. Wolf, *Chem. Sci.* **2021**, *12*, 11225–11235.

[36] The conjugate acids have been studied computationally: A. C. Tsipis, *Organometallics* **2006**, *25*, 2774–2781.

[37] R. M. K. Deng, K. B. Dillon, *J. Chem. Soc., Chem. Commun.* **1981**, 1170.

[38] a) R. Grünbauer, G. Balázs, M. Scheer, *Chem. Eur. J.* **2020**, *26*, 11722–11726; b) M. Scheer, U. Becker, J. Magull, *Polyhedron* **1998**, *17*, 1983–1989; c) M. Scheer, K. Schuster, U. Becker, *Phosphorus Sulfur Silicon Relat. Elem.* **1996**, *109*, 141–144.

[39] a) L. Xu, Y. Chi, S. Du, W.-X. Zhang, Z. Xi, *Angew. Chem. Int. Ed.* **2016**, *55*, 9187–9190; *Angew. Chem.* **2016**, *128*, 9333–9336; b) S. Du, J. Yin, Y. Chi, L. Xu, W.-X. Zhang, *Angew. Chem. Int. Ed.* **2017**, *56*, 15886–15890; *Angew. Chem.* **2017**, *129*, 16102–16106; c) F. Zhang, J. Zhang, Z. Chen, L. Weng, X. Zhou, *Inorg. Chem.* **2019**, *58*, 8451–8459.

[40] P. Rigo, A. Turco, *Coord. Chem. Rev.* **1974**, *13*, 133–172.

[41] A search of the Cambridge Crystal Structure Database (CCSD), version 5.44, 04/2023, revealed 120 cobalt complexes bearing only one terminal cyanide ligand with a mean Co−C Distance of 1.899 Å (Median 1.888 Å) and a mean C≡N distance of 1.137 Å (median 1.144 Å).

[42] G. Le Corre, J. J. Gamboa-Carballo, Z. Li, H. Grützmacher, *Angew. Chem. Int. Ed.* **2021**, *60*, 24817–24822; *Angew. Chem.* **2021**,*133*, 25021 –25026.

[43] G. Becker, H. Brombach, S. T. Horner, E. Niecke, W. Schwarz, R. Streubel, E.-U. Würthwein, *Inorg. Chem.* **2005**, *44*, 3080–3086.

[44] Note: Natural Resonance Theory (NRT) analysis was performed on model compound **9-Me**$^-$ to avoid no bond resonance structures in the cyclohexyl residue.

[45] Deposition Numbers 2269452 (for **1**), 2269840 (for [K(18c-6)]**2**), 2269251 (for [K(18c-6)]**3)**, 2269454 (for **4a**), 2269458 (for **4b**), 2269460 (for **4c**), 2269469 (for **5a**), 2302117 (for endo-/exo-**6a**), 2269471 (for endo-**6a**), 2269474 (for exo-**6d**), 2269477 (for endo-**6e**), 2269521 (for **7**), 2269484 (for [K(18c-6)]**8**), 2269513 (for [K(18c-6)]**9a**), 2269494 (for [K(18c-6)]**9b**), and 2269504 (for [K(18c-6)]**9d**) contain the supplementary crystallographic data for this paper. These data are provided free of charge by the joint Cambridge Crystallographic Data Centre and Fachinformationszentrum Karlsruhe Access Structures service.

[46] T. Suzuki, Y. Kajita, H. Masuda, *Dalton Trans.* **2014**, *43*, 9732-9739.

[47] a) K. Jonas, R. Mynott, C. Krüger, J. C. Sekutowski, Y.-H. Tsay, *Angew. Chem. Int. Ed. Engl.* **1976**, 15, 767 –768; *Angew. Chem.* **1976**, 88, 808 –809; b) K. Jonas, USpatent 4169845, **1979**.

[48] Bardsley, Kathryn, K. Bardsley, M. Hagigeorgiou, I. Lengyel, V. Cesare, *Synth. Commun.* **2013**, *43*, 1727-1733.

[49] P. H. M. Budzelaar, in IvorySoft: gNMR for Windows, NMR Simulation Program, **2006**.

[50] a) E. G. Finer, R. K. Harris, *Mol. Phys.* **1967**, *13*, 65–75; b) S. Aime, R. K. Harris, E. M. McVicker, M. Fild, *J. Chem. Soc. Dalton Trans.* **1976**, 2144–2153; c) J. P. Albrand, H. Faucher, D. Gagnaire, J. B. Robert, *Chem. Phys. Lett.* **1976**, *38*, 521–523; d) H. C. E. McFarlane, W. McFarlane, J. A. Nash, *J. Chem. Soc. Dalton Trans.* **1980**, 240–244; e) M. A. M. Forgeron, M. Gee, R. E. Wasylishen, *J. Phys. Chem. A* **2004**, *108*, 4895–4908; f) J. E. Del Bene, J. Elguero, I. Alkorta, *J. Phys. Chem. A* **2004**, *108*, 3662–3667.

[51] Y. Zeng, Q. Mahmood, Q. Zhang, T. Liang, W. Sun, *Eur. Polym. J.* **2018**, *103*, 342-350.

[52] a) G. M. Sheldrick, SADABS, Bruker AXS, Madison, USA, **2007**; b) CrysAlisPro, Scale3 Abspack, Rigaku Oxford Diffraction, **2019**.

[53] R. C. Clark, J. S. Reid, *Acta Crystallogr. Sect. A* **1995**, *51*, 887–897.
[54] G. M. Sheldrick, *Acta Crystallogr. Sect. Found. Adv.* **2015**, *71*, 3–8.
[55] O. V. Dolomanov, L. J. Bourhis, R. J. Gildea, J. a. K. Howard, H. Puschmann, *J. Appl. Crystallogr.* **2009**, *42*, 339–341.
[56] G. M. Sheldrick, *Acta Crystallogr. Sect. C Struct. Chem.* **2015**, *71*, 3–8.
[57] G. M. Sheldrick, *Acta Crystallogr. A* **2008**, *64*, 112–122.
[58] A search of the Cambridge Crystal Structure Database (CCSD), version 5.44, 04/2023, revealed 67 cobalt complexes bearing only one terminal isocyanide ligand with a mean Co−C distance of 1.839 Å (median 1.833 Å) and a mean C≡N distance of 1.162 Å (median 1.164 Å).
[59] a) R. A. Kendall, H. A. Früchtl, *Theor. Chem. Acc.* **1997**, 97, 158–163. b) F. Neese, *WIREs Comput. Mol. Sci.* **2012**, *2*, 73–78. c) F. Neese, *WIREs Comput. Mol. Sci.* **2018**, *8*, 1327.
[60] a) S. Grimme, S. Ehrlich, L. Goerigk, J. Comput. Chem. 2011, 32, 1456–1465. b) S.Grimme, J.Antony, S.Ehrlich, H.Krieg, *J. Chem. Phys.*, 132, **2010**, 154104. c) F. Weigend, R. Ahlrichs, *Phys. Chem. Chem. Phys.* 7, **2005**, 3297-3305. (d) F. Weigend, Phys. *Chem. Chem. Phys.*, 8, **2006**, 1057-1065.
[61] M. . D. Hanwell, D. E. Curtis, D. C. Lonie, T. Vandermeersch, E. Zurek, G. R. Hutchison, *J. Cheminformatics* **2012**, 4, 17.
[62] A. D. Becke, *Phys. Rev. A* **1988**, *38*, 3098-3100; J. P. Perdew, *Phys. Rev. B* **1986**, *33*, 8822-8824. Erratum: *Phys. Rev. B* **1986**, *34*, 7406-7406.
[63] J. P. Perdew, K. Burke, M. Ernzerhof, *Phys. Rev. Lett.* **1996**, *77*, 3865-3868.
[64] J. Tao, J. P. Perdew, V. N. Staroverov, G. E. Scuseria, *Phys. Rev. Letters* **2003**, *91*, 146401.
[65] a) J. Tomasi, B. Mennucci, R. Cammi, *Chem. Rev.* **2005**, *105*, 2999-3094; b) V. Barone, M. Cossi, *J. Phys. Chem. A* **1998**, *102*, 1995-2001.
[66] a) J. R. Cheeseman, G. W. Trucks, T. A. Keith, M. J. Frisch, *J. Chem. Phys.* **1996**, *104*, 5497-5509; b) K. Wolinski, J. F. Hinton, P. Pulay, *J. Am. Chem. Soc.* **1990**, *112*, 8251-8260; c) R. Ditchfield, *Molec. Phys.* **1974**, *27*, 789-807; d) R. McWeeny, *Phys. Rev.* **1962**, *126*, 1028-1034; e) F. London, *J. Phys. Radium* **1937**, *8*, 397-409; g) G. L. Stoychev, A. A. Auer, R. Izsák, F. Neese, *J. Chem. Theory Comput.* **2018**, *14*, 619-637.
[67] F. Jensen, *J. Chem. Theory Comput.* **2015**, *11*, 132-138.
[68] B. P. Pritchard, D. Altarawy, B. Didier, T. D. Gibson, T. L. Windus, *J. Chem. Inf. Model.* **2019**, *59*, 4814-4820.
[69] F. Neese, F. Wennmohs, A. Hansen, U. Becker, *Chem. Phys.* **2009**, *356*, 98-109.
[70] J. P. Perdew, M. Ernzerhof, K. Burke, *J. Chem. Phys.* **1996**, *105*, 9982-9985.
[71] a) V. N. Staroverov, G. E. Scuseria, J. Tao, J. P. Perdew, *J. Chem. Phys.* **2003**, *119*, 12129-12137; b) V. N. Staroverov, G. E. Scuseria, J. Tao, J. P. Perdew, *J. Chem. Phys.* **2004**, *121*, 11507-11507

3 Functionalization of Tetraphosphido Ligands by Heterocumulenes[a,b]

Abstract: Although numerous polyphosphido complexes have been accessed through the transition-metal-mediated activation and functionalization of white phosphorus (P_4), the selective functionalization of the resulting polyphosphorus ligands in these compounds remains underdeveloped. In this study, the reactions between cyclotetraphosphido cobalt complexes and heterocumulenes are explored, leading to functionalized P_4 ligands. Specifically, the reaction of carbon disulfide (CS_2) with [K(18c-6)][(Ar*BIAN)Co(η^4-P_4)] ([K(18c-6)]**1**, 18c-6 = [18]crown-6) affords the adduct [K(18c-6)][(Ar*BIAN)Co(η^3:η^1-P_4CS_2)] ([K(18c-6)]**3**), in which CS_2 is attached to a single phosphorus atom (Ar* = 2,6-dibenzhydryl-4-isopropylphenyl, BIAN = 1,2-bis(arylimino)acenaphthene diimine). In contrast, the insertion of bis(trimethylsilyl)sulfur diimide $S(NSiMe_3)_2$ into a P–P bond of **1**$^-$ yields [K(18c-6)][(Ar*BIAN)Co(η^3:η^1-$P_4SN_2(SiMe_3)_2$)] (K(18c-6)]**4**). This salt further reacts with Me_3SiCl to form [(Ar*BIAN)Co(η^3:η^1-$P_4SN_2(SiMe_3)_3$)] (**5**), featuring a rare azatetraphosphole ligand. Moreover, treatment of the previously reported complex [(Ar*BIAN)Co(η^3:η^1-$P_4C(O)t$Bu)] (**2**) with isothiocyanates results in P–C bond insertion, yielding [(Ar*BIAN)Co(η^3:η^1-$P_4C(S)N(R)C(O)t$Bu)] (**6a-b**; R = Cy, Ph).

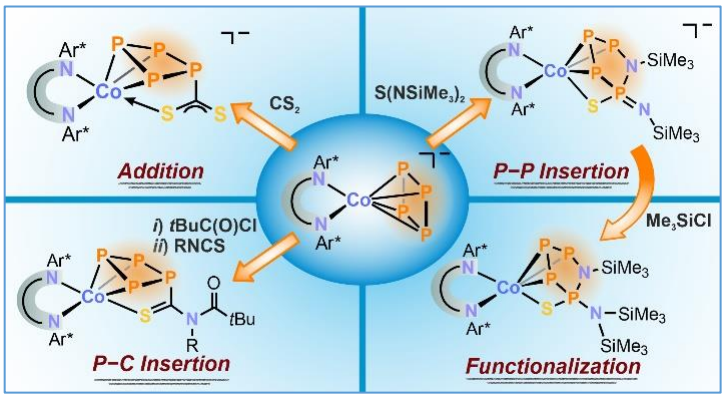

[a] Reproduced from S. Hauer, G. Balázs, F. Gliese, F. Meurer, T. M. Horsley Downie, C. Hennig, J. J. Weigand, and R. Wolf, *Inorg. Chem.* **2024**, 10.1021/acs.inorgchem.4c00808

[b] S. Hauer performed the synthetic investigations and characterization of the reported compounds. G. Balázs conducted the DFT calculations. F. Gliese performed synthetic investigations as part of his B.Sc. thesis. F. Meurer and C. Hennig collected SCXRD data of compounds [K(18c-6)]**4** and **5** and assisted in the structure solution and refinement. S. Hauer wrote the manuscript draft. T. M. Horsley Downie, R. Wolf and J. J. Weigand reviewed and edited the manuscript. R. Wolf and J. J. Weigand supervised the project.

3.1 Introduction

The reaction of white phosphorus with transition metal complexes represents a powerful strategy in the synthesis of distinctive phosphorus-based compounds.[1] Transition-metal-mediated P_4 functionalization processes typically involve two principal steps, which have been subject to considerable investigation: Initially, a transition metal complex facilitates the cleavage of one or more P–P bonds of the P_4 tetrahedron, yielding metal complexes that incorporate an activated polyphosphido ligand. Subsequently, these P_n units undergo functionalization through reactions with suitable nucleophiles or electrophiles. The first step – P_4 activation – has been widely investigated and can result in a wide variety of polyphosphorus structures, with ligands containing from one to eight P atoms.[1] In particular, P_4 ligands such as [1.1.0]bicyclotetraphosphane-1,4-diide (commonly referred to as "butterfly-P_4^{2-}") and cyclotetraphosphide (*cyclo*-P_4^{2-}) units, emerge as prevalent structural motifs (see Figure 1a).[2,3] The subsequent functionalization of the coordinated P_n units typically constitutes a separate step.[1] While the reactivity in this step can vary based on the electronic properties of the transition metal

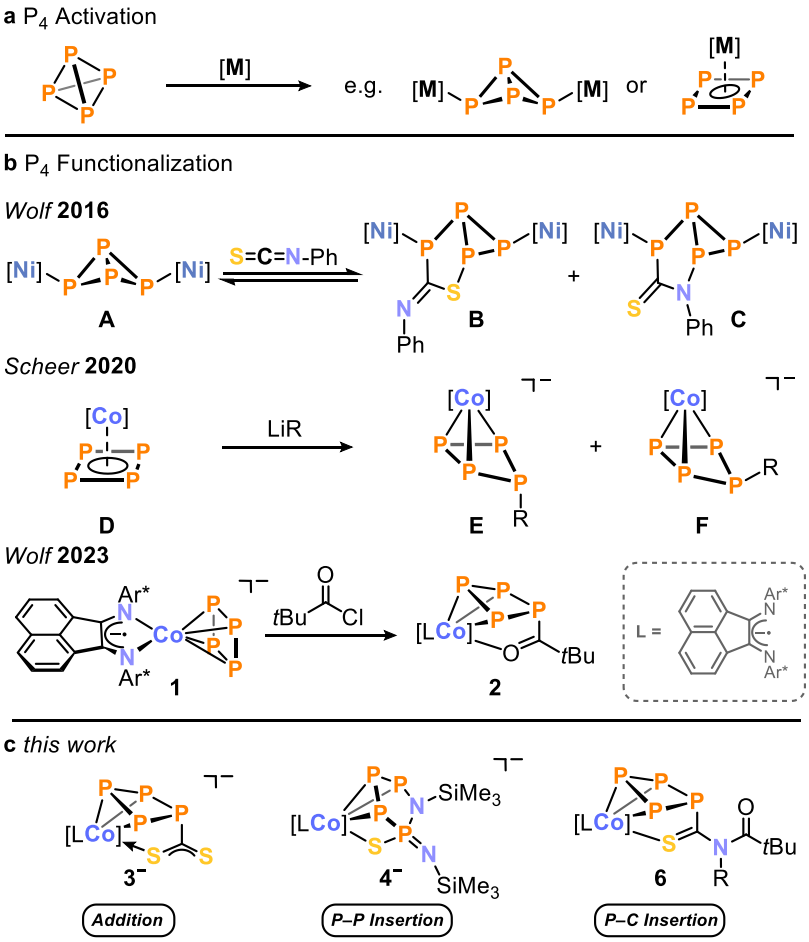

Figure 1. a) Activation and b) functionalization of white phosphorus; [Ni] = [CpNi(IMes)] (IMes = 1,3-bis(2,4,6-trimethylphenyl)imidazolin-2-ylidene); [Co] = [Cp'''Co(η^4-P_4)] (Cp''' = $C_5H_2tBu_3$), R = CH_2SiMe_3, *t*Bu; Ar* = 2,6-dibenzhydryl-4-isopropylphenyl; c) [LCo] = [(Ar*BIAN)Co], R = Cy, Ph.

fragment, it is generally acknowledged that functionalization of P_4 has not been as thoroughly explored as its activation. Several routes for the functionalization of butterfly-P_4 complexes have been reported, including reactions such as the addition and insertion of nucleophiles and electrophiles (including alkylation), fragmentation, and the transition metal coordination.[2,4] During our prior work, in which we reported the synthesis of the nickel butterfly-P_4 complex **A**, it was found that phenyl isothiocyanate (PhNCS) inserts into a P−P bond of the butterfly moiety. This reaction facilitated the formation of unusual bicyclo[3.1.0]heterohexane isomers **B** and **C** (Figure 1b).[2d,5]

While several *cyclo*-P_4 complexes have been reported, their reactivity has not been as extensively investigated as the butterfly-P_4 counterparts.[1,3] A study by Scheer and co-workers demonstrated that treatment of the *cyclo*-P_4 complex [Cp'''Co(η^4-P_4)] (**D**, Cp''' = $C_5H_2t Bu_3$) with carbon-centered nucleophiles leads to isomeric compounds **E** and **F** (Figure 1b).[6]

In a recent study, we reported the anionic *cyclo*-P_4 complex [(Ar*BIAN)Co(η^4-P_4)]$^-$ (**1**$^-$, Figure 1b) and its reaction with acyl chlorides, yielding the functionalized *cyclo*-P_4 complex [(Ar*BIAN)Co(η^3:η^1-$P_4C(O)t Bu$] (**2**).[7] When compound **2** was treated with nitriles or isocyanides, there was a partial displacement of the $P_4C(O)R$ ligand from the cobalt center. Moreover, reaction with two equivalents of KCN induced a [3+1] fragmentation process, releasing a monophosphorus species in the form of an acylcyanophosphide.

Our previous work has revealed that polyphosphido complexes exhibit promising reactivity toward electrophiles and nucleophiles, indicating that transition-metal-P_n complexes hold potential as precursors for the targeted synthesis of unique (poly-)phosphorus compounds (Figure 1).[5,8] Building upon these insights, we herein report the functionalization of the anionic complex **1**$^-$ and its acylated, neutral counterpart **2** with electrophilic heterocumulenes. In this study, we present the synthesis of anionic cobalt complexes **3**$^-$ and **4**$^-$, featuring $CoP_4CS_2^-$ and Co(η^3:η^1-$P_4SN_2(SiMe_3)_2)^-$ cores, respectively. We investigate their structural and electronic properties, as revealed by X-ray crystallography using synchrotron radiation and density functional theory (DFT). Additionally, the reactivity of complexes **3**$^-$ and **4**$^-$ toward electrophiles in salt metathesis is examined. We also demonstrate the feasibility of further functionalizing the polyphosphido ligand in $CoP_4C(O)t Bu$ with isothiocyanates, resulting in the formation of [Co(η^3:η^1-$P_4C(S)N(R)C(O)t Bu$)] complexes (**6**, R = Cy, Ph).

3.2 Results and Discussion

The addition of carbon disulfide to a purple solution of [K(18c-6)]**1** in THF resulted in a blue coloration within a few hours. $^{31}P\{^{1}H\}$ NMR spectroscopy confirmed the complete conversion of the anionic **1**$^{-}$ into a single new species, [K(18c-6)][(Ar*BIAN)Co(η^3:η^1-P_4CS_2)] ([K(18c-6)]**3**), exhibiting an AXY_2 spin system (*vide infra*). This new complex crystallized in 89% yield as dark blue blocks from a THF/*n*-hexane mixture (Scheme 1).

Single crystal X-ray diffraction (SCXRD) analysis elucidated the structure of the complex, revealing a puckered *cyclo*-P_4 ligand in a η^3-coordinating mode (Figure 2a). A CS_2 moiety is bound *via* the carbon atom to the non-coordinating phosphorus atom P4. Additionally, one sulfur atom from the CS_2 moiety exhibits η^1-coordination to the cobalt center. The similar C−S bond distances, 1.698(5) Å and 1.664(5) Å, are intermediate between those of typical C−S single and double bonds ($\sum r_{CS}$ 1.78 Å vs. 1.61 Å).[9] The Co−S1 bond length (2.2724(1) Å) is notably longer than the Co−S distance in the structurally related complex [(triphos)Co(η^2-CS_2)] (2.206(4) Å; triphos = $MeC(CH_2PPh_2)_3$) and exceeds the length of a typical Co−S single bond ($\sum r_{CoS}$ 2.14 Å).[10] These observations support the description of the P_4CS_2 ligand as featuring a delocalized exocyclic CS_2-moiety acting as a pendant donor ligand, as depicted in Scheme 1. The delocalization of the η^3-coordinated P1-P2-P3 moiety is apparent by shorter bond lengths among the coordinating phosphorus atoms (P1−P2 2.169(2) Å and P2−P3 2.169(7) Å) compared to those involving the non-coordinating ones (P1−P4 2.228(6) Å and P3−P4 2.222(7) Å). This structural motif is similar to the behavior observed in the related complex [(Ar*BIAN)Co(η^3:η^1-$P_4C(O)tBu$)] (**2**, *vide infra*) and in the series of complexes [Cp'''Co(η^3-P_4R_2)] (R = Ph, Cy, *t*Bu).[7,11]

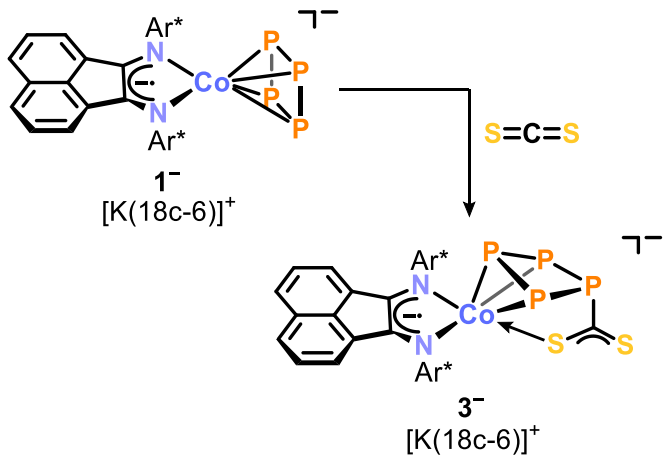

Scheme 1. Addition of CS_2 to the tetraphosphido ligand in [K(18c-6)]**1**; reagents and conditions: +1.2 equiv. CS_2; THF, r.t., 1 d; yield: [K(18c-6)]**3**: 89%.

The $^{31}P\{^{1}H\}$ NMR spectrum of [K(18c-6)]**3** features an AXY_2 spin system, corroborating the existence of a C_s symmetric tetraphosphido ligand (Figure 2b). The simulated P−P coupling constants are in agreement with those of [Cp'''Co(η^3-P_4R_2)] complexes, reported to exhibit AMM'X spin systems, and the previously reported complex **2**, which gives rise to an AM_2X spin system.[7,11] The resonance for the coordinating phosphorus atom P_x at δ = 99.6 ppm is shifted significantly upfield in comparison to **2** (δ = 323.3 ppm), but appears downfield shifted relative to the equivalent phosphorus atom of [Cp'''Co(η^3-P_4Ph_2)] (δ = −80.7 ppm).

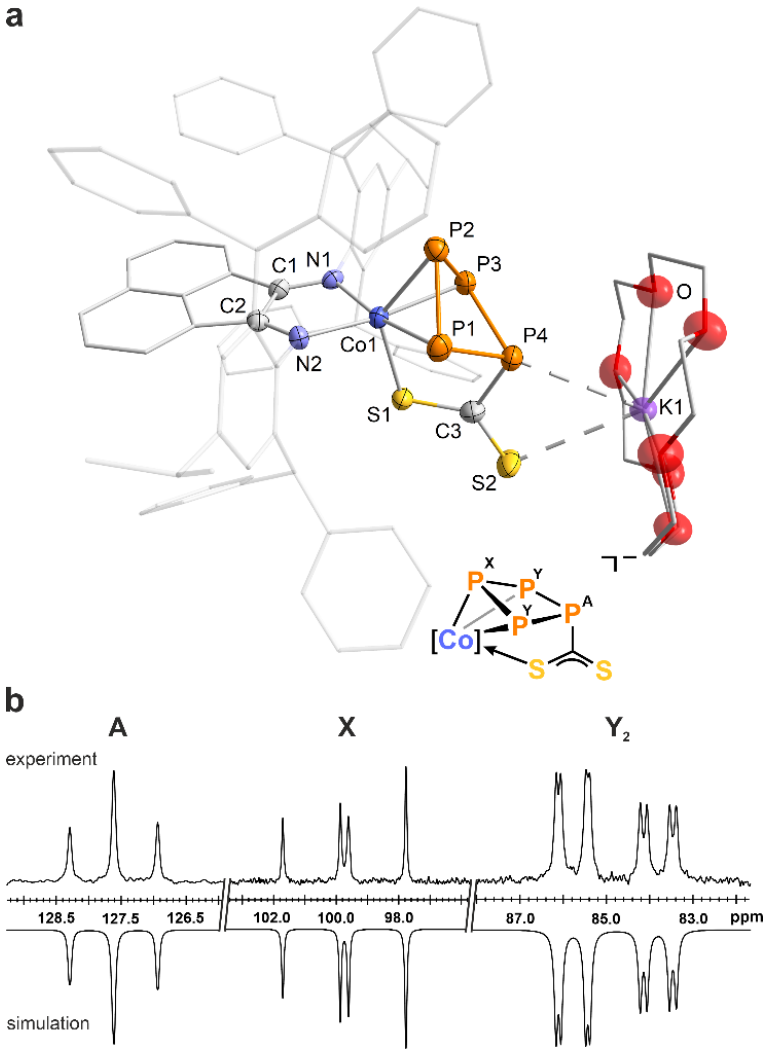

Figure 2. (a) Solid-state molecular structure of [K(18c-6)][(Ar*BIAN)Co(η^3:η^1-P_4CS_2)] ([K(18c-6)]**3**); thermal ellipsoids are shown at the 50% probability level; hydrogen atoms, solvent molecules and disorder are omitted for clarity. Selected bond lengths [Å] and angles [°]: P1−P2 2.169(2), P2−P3 2.1697(2), P3−P4 2.230(2), P1−P4 2.2286(2), Co1−P1 2.2936(1), Co1−P2 2.3031(2), Co1−P3 2.2815(2), Co1−S1 2.2725(1), Co1−N1 1.998(4), Co1−N2 1.976(4), P4−C3 1.850(6), C3−S1 1.698(5), C3−S2 1.664(5), P1-P2-P3 85.08(7), P2-P3-P4 88.93(7), P3-P4-P1 82.44(6), P4-P1-P2 88.81(8). b) experimental (upward) and simulated (downward) $^{31}P\{^{1}H\}$ NMR spectra of [K(18c-6)]**3** in THF-d_8 with nuclei assigned to an AXY_2 spin system: $\delta(P_A)$ = 127.6 ppm, $\delta(P_X)$ = 99.6 ppm, $\delta(P_Y)$ = 84.9 ppm, $^{1}J_{XY}$ = −320 Hz, $^{1}J_{AY}$ = −110 Hz, $^{2}J_{AX}$ = 5 Hz.

The anionic nature of $\mathbf{3}^-$ renders it a suitable precursor for further functionalization *via* salt metathesis with electrophiles. Addition of one equivalent of $[Ph_3C]OTf$ (OTf =

$CF_3SO_3^-$) to a [K(18c-6)]**3** solution in C_6D_6 induces an immediate color change from blue to magenta, accompanied by the precipitation of [K(18c-6)]OTf, as confirmed by X-ray diffraction (XRD) analysis. The $^{31}P\{^1H\}$ NMR spectrum features a single AXY_2 spin system, verifying the selective formation of a new phosphorus-containing species (see Figure S25 and Scheme S1 in the Supporting Information (SI)). Iterative simulation identified two large $^1J_{PP}$ coupling constants of −308 Hz and −287 Hz, alongside a $^2J_{PP}$ coupling constant of 27 Hz (Figure S26 and Table S5), indicating a structural similarity to **3**$^-$, likely with an alkylated CS_2 component. Despite repeated efforts to crystallize the product and its adducts with coordinating Lewis acids such as $W(CO)_5$, $Al(C_2H_5)_3$, and AuCl, single crystals suitable for analysis by XRD have remained elusive.

Inspired by the successful functionalization of the *cyclo*-P_4 ligand in **1**$^-$ with CS_2 (*vide supra*), we extended our investigation to include reactions with other heterocumulenes. While attempts to functionalize the P_n moieties with isocyanates and isothiocyanates led to complex mixtures of products that impeded characterization, the use of sulfur diimide $S(NSiMe_3)_2$ resulted in the selective formation of [K(18c-6)][(Ar*BIAN)Co(η^3:η^1-$P_4SN_2(SiMe_3)_2$)] ([K(18c-6)]**4**, Scheme 2a). $^{31}P\{^1H\}$ NMR spectroscopic monitoring revealed a quantitative reaction and complete conversion within six days at 35 °C, using a slight excess of the diimide (1.5 equiv.). Surprisingly, the diimide variant with alkyl substituents, $S(NtBu)_2$, did not undergo any reaction under similar conditions, or at further elevated temperature.

A SCXRD analysis, using synchrotron radiation at the Rossendorf Beamline BM20 (ESRF), conducted on crystals obtained from a toluene/*n*-hexane mixture, revealed the structure of anion **4**$^-$, featuring an η^3-coordinating azatetraphosphole ring (Figure 3a).[12] The structure bears an exocyclic $NSiMe_3$ group alongside a sulfur atom, both bound to the same phosphorus atom, indicating the insertion of a Me_3SiN moiety into a P−P bond. The azaphosphole ring adopts an envelope conformation with the nitrogen atom N3 positioned at the apex, at a distance of 0.700(6) Å above the plane formed by P1, P2, P3, and P4. This conformation resembles cyclic P_4N frameworks observed in oligophosphines such as *cyclo*-$[NP(PPh_2)_2]_2$, *cyclo*-$[(PMe)(PPh_2)N]_2$, and *cyclo*-$[(PPh)_4NR]$ (R = Me, Cy),[13c,h] as well as related compounds.[13] To our knowledge, [K(18c-6)]**4** is the first example of a transition metal complex bearing a *cyclo*-P_4N ligand framework. The P1−P2 and the P3−P4 bond lengths of 2.205(2) Å and 2.200(8) Å, respectively, agree with typical P−P single bonds ($\sum r_{PP}$ 2.22 Å), whereas the P2−P3 bond length at 2.047(2) Å suggests partial P=P double bond character.[9] This interpretation is

supported by calculated bond orders of 0.89, 1.05 and 1.13, despite the optimized P2−P3 distance in the theoretical models (2.155 Å) being slightly longer than the experimental value (*vide infra*).

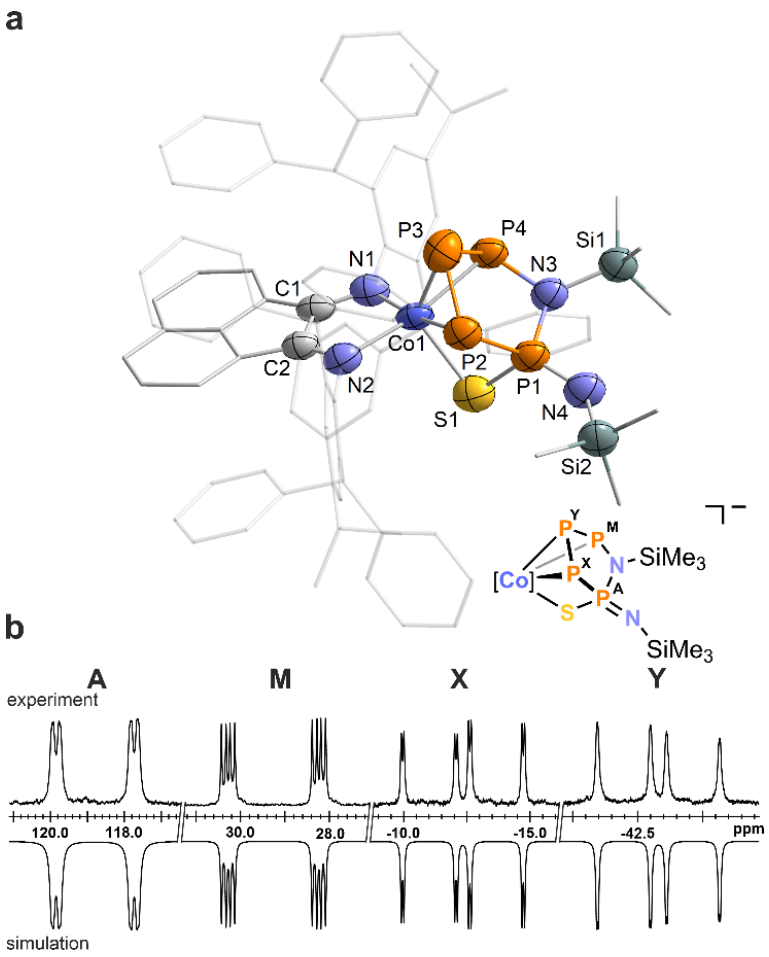

Figure 3. (a) Solid-state molecular structure of [K(18c-6)][(Ar*BIAN)Co(η^3:η^1-$P_4SN_2(SiMe_3)_2$)] ([K(18c-6)]**4**); thermal ellipsoids are shown at the 50% probability level; hydrogen atoms, solvent molecules, $[K(18c\text{-}6)]^+$ and disorder are omitted for clarity. Selected bond lengths [Å] and angles [°]: P1−P2 2.205(2), P2−P3 2.047(2), P3−P4 2.200(8), P1−N3 1.681(4), P4−N3 1.749(5), P1−S1 2.049(2), P1−N4 1.567(5), Co1−P2 2.336(2), Co1−P3 2.235(2), Co1−P4 2.327(2), Co1−S1 2.391(2), P1-P2-P3 103.00(7), P2-P3-P4 95.57(8), P3-P4-N3 104.75(2), P4-N3-P1 109.5(3), Co1-S1-P1 81.90(8), Si1-N3-P1 124.6(3), Si2-N4-P1 134.0(3). (b) experimental (upward) and simulated (downward) $^{31}P\{^1H\}$ NMR spectra of $\mathbf{4}^-$ with nuclei assigned to an AMXY spin system: $\delta(P_A)$ = 118.8 ppm, $\delta(P_M)$ = 29.2 ppm $\delta(P_X)$ = −12.4 ppm, $\delta(P_Y)$ = −43.2 ppm, $^1J_{XY}$ = −431 Hz, $^1J_{AX}$ = −343 Hz, $^1J_{MY}$ = −331 Hz, J_{MX} = 17 Hz, J_{AY} = 10 Hz, J_{AM} = −32 Hz.

To corroborate the molecular structure derived from SCXRD data, we carried out geometry optimization for anion $\mathbf{4}^-$ using the TPSS-D4/def2-TZVP CPCM level of theory. Subsequent intrinsic bond orbital analysis (IBO, see SI for details) identified single bonds within the cyclic P_4N moiety and a polarized P=N (P1−N4) double bond (see IBO 155 in Figure S43 in SI).[14] Additionally, a lone pair was observed on N4, residing in a p-type orbital with slight delocalization over the P_2N unit, which contributes to the stabilization of the planar geometry at N4. The Mayer Bond Order (MBO) analysis further supports the double bond character of the P1−N4 bond, with a calculated MBO of

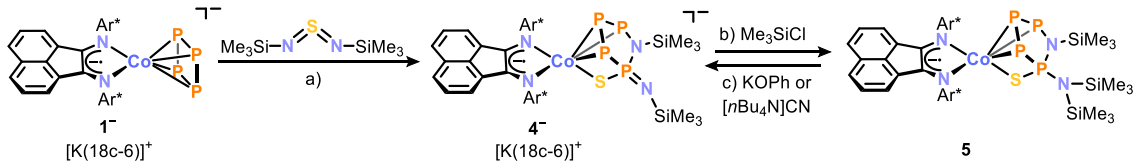

Scheme 2. Reaction of [K(18c-6)]**1** with sulfur diimide and subsequent functionalization with trimethylsilylchloride; reagents/by-products and conditions: a) +1.5 equiv. $S(NSiMe_3)_2$; THF, 35 °C, 6 d; b) +Me_3SiCl/−[K(18c-6)]Cl; toluene, r.t., 3 h; c) +1.0 equiv. [*n*Bu_4N]CN; C_6D_6, r.t., 3 h or +1.0 equiv. KOPh/+1.0 equiv. 18c-6; C_6D_6, r.t., 3 d; yields: [K(18c-6)]**4**: 63%, **5**: 63%.

1.57. These theoretical insights align well with the P1−N4 bond length of 1.567(5) Å, which falls in the expected range for a P=N double bond ($\sum r_{PN}$ 1.62 Å).[9] Conversely, the MBO value of the endocyclic P1−N3 and P4−N3 bonds are 1.05 and 0.95, respectively, indicative of single bonds.

The $^{31}P\{^1H\}$ NMR spectrum of [K(18c-6)]**4** in CD_3CN exhibits an AMXY spin system, distinguished by large $^1J_{PP}$ coupling constants ranging from −331 Hz to −431 Hz, with chemical shifts recorded at δ = 118.8 (P_A), 29.2 (P_E), −12.4 (P_M), and −43.2 (P_X) ppm (Figure 3b and Figure S7, SI). These findings are characteristic for an asymmetric *catena*-P_4 unit, consistent with previous observations for similar systems.[7,8b,15] The largest $^1J_{PP}$ coupling constant was observed between phosphorus atoms P2 and P3, further supporting partial P=P double bond character. In the $^{29}Si\{^1H\}$ NMR spectrum, two distinct doublets emerge: one at δ = −17.9 ppm corresponding to the imino- group, and one at δ = 3.6 ppm, assigned to the amino- group. These groups feature $^2J_{SiP}$ coupling constants of 16.6 Hz and 6.1 Hz, respectively. For comparison, the resonance of $S(NSiMe_3)_2$ appears at δ = 1.6 ppm in toluene-d_8.[16] The more pronounced $^2J_{SiP}$ coupling associated with the exocyclic $NSiMe_3$ group is likely a consequence of its involvement in the P1=N4 multiple bond.

Given the ionic nature of **4**$^-$ and the anticipated nucleophilicity of the phosphaimino nitrogen N4 (Mulliken charge −0.48), we hypothesized that it would readily undergo salt metathesis reaction with electrophiles. Our assumption was confirmed when the addition of Me_3SiCl to a solution of [K(18c-6)]**4** in toluene resulted in an immediate color change from blue to purple due to the formation of [(Ar*BIAN)Co(η^3:η^1-$P_4SN_2(SiMe_3)_3$)] (**5**, Scheme 2b), which was crystallized as purple needles from *n*-hexane at −35 °C in 63% isolated yield. Synchrotron SCXRD analysis of **5** revealed the silylation of the imino moiety, resulting in a bis(trimethylsilyl)amino group (Figure 4a).[12] The structural characteristics of **5** closely resemble those of its precursor **4**$^-$ (*vide supra*), including the presence of a central η^3-coordinating azatetraphosphole ring. However, the P1−N4 bond length (1.666(4) Å) is elongated due to its increased single bond character. The silylated

nitrogen atom N4 in **5** adopts an almost trigonal planar geometry (∑∢ 358°) positioned 0.144(4) Å above the plane defined by Si2, Si3, and the chiral phosphorus atom P1. The presence of the trimethylsilyl groups attached to N4 is reflected in the ^{1}H NMR spectrum by two distinct signals, which persist even when the sample is subjected to a variable temperature (VT) NMR experiment at up to 100 °C (Figure S11, SI). This phenomenon is attributed to restricted rotation around the P1−N4 bond, which frustrates chemical equivalence of the trimethylsilyl groups on the NMR timescale. In addition, the three inequivalent silicon atoms are discernible in the ^{29}Si{^{1}H} NMR spectrum, giving rise to two doublets at δ = 7.4 (Si3, $^{2}J_{SiP}$ = 11 Hz) and δ = 11.6 ppm (Si2, $^{2}J_{SiP}$ = 6 Hz), as well as a singlet at δ = 9.3 ppm for Si1. The assignment of the signals has been facilitated through both homo- and heteronuclear 2D NMR spectroscopy, further supported by the

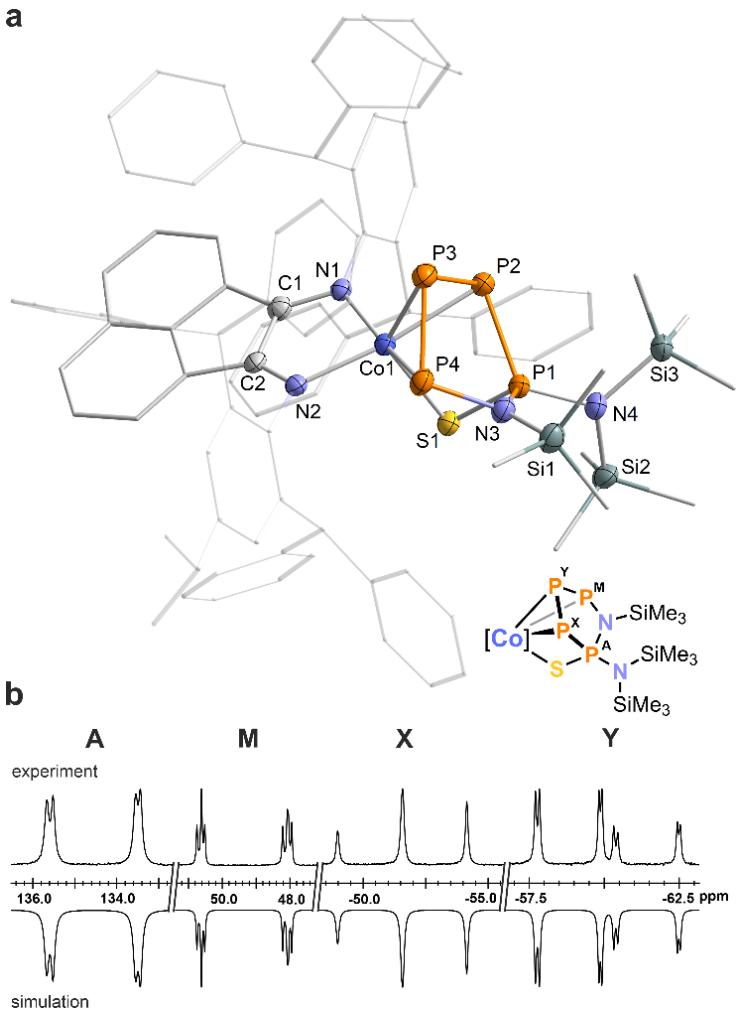

Figure 4. (a) Solid-state molecular structure of [(Ar*BIAN)Co(η^{3}:η^{1}-$P_4SN_2(SiMe_3)_3$)] (**5**); thermal ellipsoids are shown at the 50% probability level; hydrogen atoms, solvent molecules and disorder are omitted for clarity. Selected bond lengths [Å] and angles [°]: P1−P2 2.1966(2), P2−P3 2.1451(2), P3−P4 2.1789(2), Co1−P2 2.3297(1), Co1−P3 2.3210(1), Co1−P4 2.2935(1), Co1−S1 2.3416(1), Co1−N1 1.970(4), P1−N3 1.670(4), P4−N3 1.782(4), P1−N4 1.666(4), P1−S1 2.0261(2), P1-P2-P3 100.50(6), P2-P3-P4 94.04(6), P2-P1-N4 120.79(1), P1-N3-P4 106.3(2), P1-N4-Si3 120.1(2), Si3-N4-Si2 120.8(2). (b) experimental (upward) and simulated (downward) ^{31}P{^{1}H} NMR spectra of **5** with nuclei assigned to an AMXY spin system: $\delta(P_A)$ = 134.5 ppm, $\delta(P_M)$ = 49.3 ppm $\delta(P_X)$ = −51.8 ppm, $\delta(P_Y)$ = −59.9 ppm, $^{1}J_{XY}$ = −423 Hz, $^{1}J_{MY}$ = −425 Hz, $^{1}J_{AX}$ = −350 Hz, J_{MX} = 31 Hz, J_{AY} = 11 Hz, J_{AM} = −21 Hz.

observed $^{2}J_{SiP}$ coupling constants (*vide supra*). The P_4 in **5** unit gives rise to an AMXY spin system in the $^{31}P\{^{1}H\}$ NMR spectrum (Figure S4b), featuring chemical shifts and coupling constants akin to those of the precursor $\mathbf{4}^{-}$ and related asymmetric P_4-chains.[7,8b,15] In contrast, the symmetrical, uncoordinated, and cyclic azaphosphane [$(PPh)_4NMe$] exhibits two multiplet resonances at $\delta = 126.0$ ppm and $\delta = 13.2$ ppm, which are distinct from the resonances of compound **5**.[13h] In particular, the resonances of the middle phosphorus atoms in the chain of **5** are observed at higher field at $\delta = -51.8$ ppm and $\delta = -59.9$ ppm.

The addition of the $-SiMe_3$ group is a reversible process, as treatment of **5** with either cyanide or alkoxide salts regenerate anion $\mathbf{4}^{-}$. These feature either $[n\mathrm{Bu}_4\mathrm{N}]^{+}$ or $[\mathrm{K(18c\text{-}6)}]^{+}$ cations, depending on the salt used (Scheme 2c), resembling classic acid-base reactivity (Figure S27).

Shifting our focus from anionic *cyclo*-P_4 complex $\mathbf{1}^{-}$, we investigated the acylated and neutral [(Ar*BIAN)Co(η^3:η^1-$P_4C(O)t$Bu)] (**2**), anticipating it might exhibit similar reactivity toward electrophilic heterocumulenes. However, likely due to the reduced nucleophilicity of the acylated phosphorus atoms in **2**, no significant reactivity was observed with either CS_2 or $S(NR)_2$. Nonetheless, the addition of sulfur-containing isothiocyanates, specifically CyNCS or PhNCS, to a solution of **2** resulted in a notable color change from magenta to purple (Scheme 3). The reaction with PhNCS (1.1 equiv.) led to the complete conversion of **2** within three hours, according to $^{31}P\{^{1}H\}$ NMR spectroscopic monitoring. In contrast, the reaction with CyNCS (1.4 equiv.) proceeded at a markedly slower pace and achieved full conversion after three days. We propose a reaction mechanism for the isothiocyanate insertion that begins with the attack of the acylated phosphorus atom on the carbon atom of the heterocumulene. This is followed by attack of the nitrogen on the carbonyl carbon atom, and finally the coordination of the sulfur atom to the cobalt center (see the SI, Scheme S2). The resulting complexes [(Ar*BIAN)Co(η^3:η^1-$P_4C(S)N(R)C(O)t$Bu)] (R = Cy (**6a**); R = Ph (**6b**)) were isolated in 80% and 64% yield, respectively.

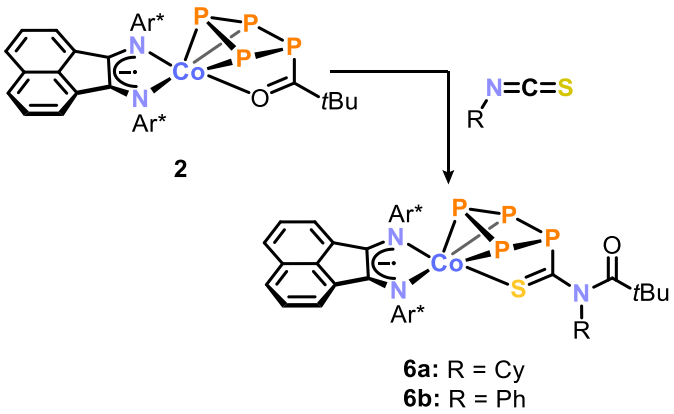

Scheme 3. Insertion of isothiocyanates into the P–C bond of **2**; reagents and conditions: +1.4 equiv. CyNCS; toluene, r.t., 3 d (**6a**); +1.1 equiv. PhNCS; toluene, r.t., 3 h (**6b**); yields: **6a**: 80% **6b**: 63%.

Single-crystal XRD analysis performed on large block-shaped crystals, grown from toluene, confirmed the insertion of the isothiocyanate into the P−C bond of **2**, forming **6a** (Figure 5). While there are documented instances of isothiocyanates undergoing insertion into P−P, P−Si, and P−H bonds, to our knowledge this marks the first example of a reaction involving a P−C bond.[5,17] In **6a**, the thioacyl group coordinates to the cobalt *via* the sulfur atom, rather than through the oxygen atom of the remote acyl group.[7] This coordination shift is reflected in the ATR-IR spectrum, where the C=O stretching vibration in **6a** was distinctly observed at $\tilde{\nu}_{CO}$ = 1727 cm^{-1}, a band typical for thioacyl groups.[18] This contrasts the C=O stretch in **2**, which was predicted to occur at $\tilde{\nu}_{CO}$ = 1462 cm^{-1}, thus overlapping with the BIAN C−N vibrations in the fingerprint region.[7] The puckered *cyclo*-P_4 moiety observed in complex **6a** closely resembles that in complexes **2**, **3**$^-$ and [Cp'''Co(η^3-P_4R_2)] (Cp''' = C_5H_2tBu$_3$; R = Ph, Cy, *t*Bu),[7,11] featuring elongated P1–P2 (2.2437(8) Å) and P1−P4 (2.2360(7) Å) bond lengths alongside shorter P2−P3 (2.1697(7) Å) and P3−P4 (2.1669(8) Å) bond lengths, indicative of some degree of multiple bond character. Furthermore, the bond lengths of S1−C3 (1.696(2) Å) and C3−N3 (1.343(3) Å) are elongated relative to those in free aryl isothiocyanate (S−C, 1.566 Å; C−N 1.152 Å), indicating increased single bond character in **6a**.[19] The coordination sphere of the cobalt center is completed by an Ar*BIAN$^{\bullet-}$ radical anion.[20] The phenyl-substituted derivative is essentially isostructural with **6b** (Figure S38, SI).

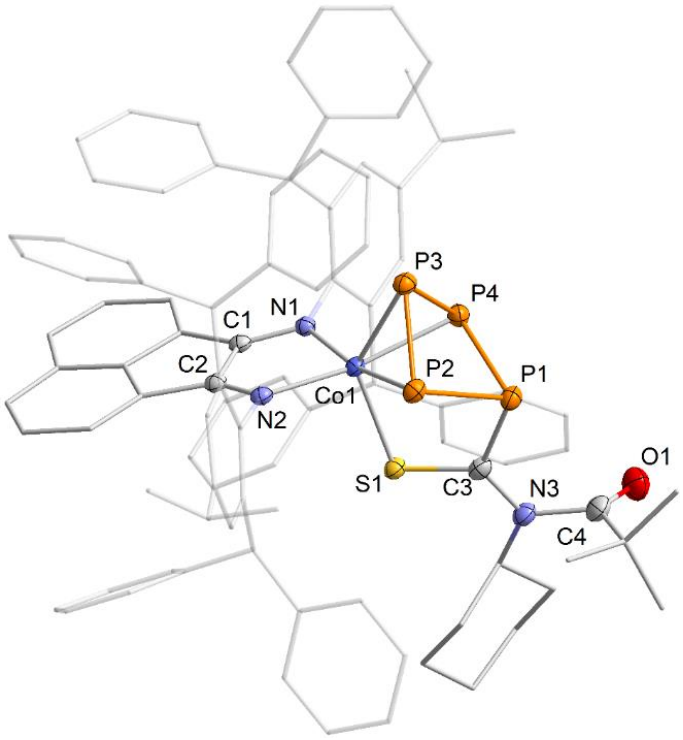

Figure 5. Solid-state molecular structure of [(Ar*BIAN)Co(η^3:η^1-P_4C(S)N(Cy)C(O)*t*Bu)] (**6a**); thermal ellipsoids are shown at the 50% probability level; hydrogen atoms and solvent molecules are omitted for clarity. Selected bond lengths [Å] and angles [°]: P1−P2 2.2437(8), P2−P3 2.1697(7), P3−P4 2.1669(8), P1−P4 2.2360(7), Co1−P2 2.2881(5), Co1−P3 2.2915(6), Co1−P4 2.2838(8), Co1−S1 2.2583(6), Co1−N1 1.9701(2), Co1−N2 1.9693(2), S1−C3 1.696(2), C3−N3 1.343(3), C4−N3 1.471(3), P1−C3 1.856(2), C4−O1 1.196(3), P1−P2−P3 88.80(3), P2-P3-P4 85.38(3), P3-P4-P1 89.07(3), P4-P1-P2 82.05(3).

The $^{31}P\{^1H\}$ NMR spectrum of **6a** in C_6D_6 features two triplets at δ = 86.3 (P_M) ppm and δ = 117.3 (P_A) ppm, as well as a significantly broadened signal ($\Delta\nu_{½}$ = 2500 Hz) at δ = 93.0 ($P_{E/X}$) ppm. This broadening suggests a dynamic process occurring in solution. Given the solid-state molecular structure of **6a**, two distinct signals are expected for the phosphorus atoms P2 and P4 if the rotation is restricted around the C4−N3 or the C3−N3 axis, with the latter axis exhibiting partial multiple bond character (1.343(3) Å vs. $\sum r_{CN}$ 1.46 Å for a single bond; labeling according to Figure 5). VT $^{31}P\{^1H\}$ NMR spectroscopy elucidated this phenomenon further, revealing that the broad resonance at ambient temperature separates into two distinct signals at 0 °C. These resolve below −40 °C into resonances, indicative of an AEMX spin system (Figure 6). In contrast, the $^{31}P\{^1H\}$ NMR spectrum of **6b**, which possesses nearly identical C3−N3 and C4−N3 bond lengths, displays well-resolved signals conforming to an AB_2X spin system with similar chemical shifts akin to those of **6a** (see Figure S23, SI). This distinct behavior in solution is probably due to hindered rotational motion resulting from the steric demand of the substituent.

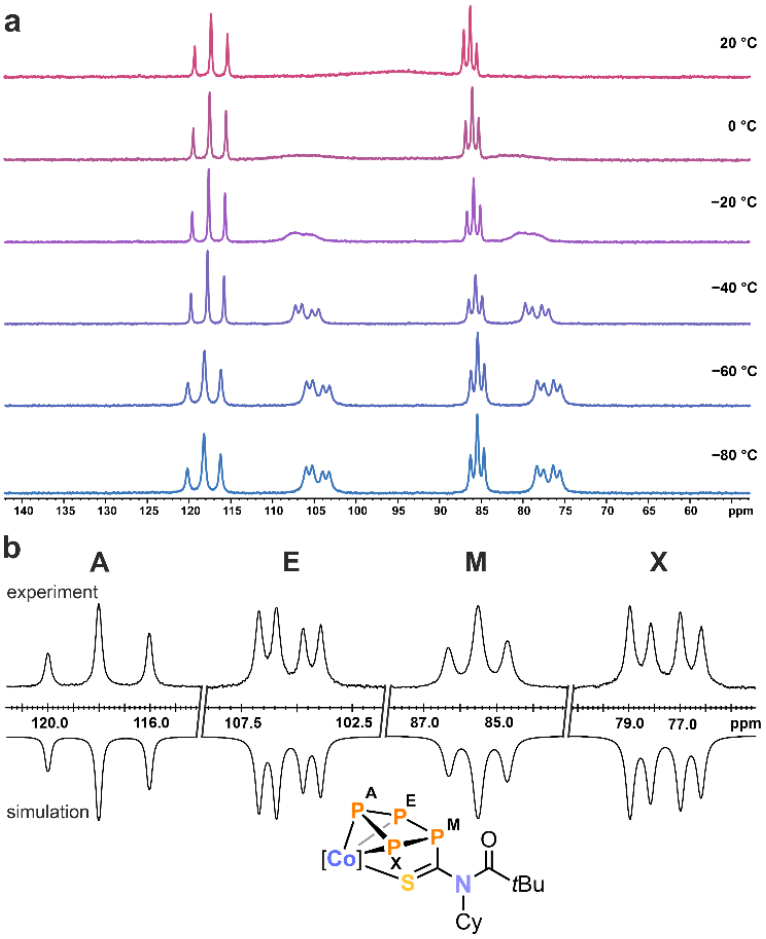

Figure 6. (a) Variable temperature $^{31}P\{^{1}H\}$ NMR spectra of **6a** in toluene-d_8. (b) experimental (upward) and simulated (downward) $^{31}P\{^{1}H\}$ NMR spectra of **6a** at −60 °C in toluene-d_8 with nuclei assigned to an AEMX spin system: $\delta(P_A)$ = 117.9 ppm, $\delta(P_E)$ = 105.4 ppm, $\delta(P_M)$ = 85.5 ppm, $\delta(P_X)$ = 77.6 ppm, $^{1}J_{AE}$ = −324 Hz, $^{1}J_{AX}$ = −321, $^{1}J_{EM}$ = −129 Hz, $^{1}J_{MX}$ = −133 Hz, $^{2}J_{AM}$ = 18 Hz, $^{2}J_{EX}$ = 20 Hz.

Complex **6a**, which incorporates the alkyl-substituted isothiocyanate CyNCS, demonstrates stability in solution even when heated to 50 °C for up to three weeks. In sharp contrast, the phenyl-substituted counterpart, **6b** undergoes chemical transformation within just a few hours at room temperature to more thermally-stable species. Although the specific products resulting from **6b**'s reactivity have not been successfully isolated for detailed characterization so far, continuous monitoring *via* $^{31}P\{^{1}H\}$ NMR spectroscopy has provided valuable insights. The $^{31}P\{^{1}H\}$ NMR spectra of the reaction mixture involving **6b** display the selective emergence of two distinct sets of signals. These were simulated and identified as ABMX and AEMX spin systems (Figure S28-30 and Table S6-7, SI), and bear strong resemblance to those observed in previously reported *cyclo*-P_4 and *catena*-P_4 complexes, suggesting that **6b**'s reactivity in solution might lead to similar structural motifs.[7,11,15]

3.3 Conclusion

The reaction of anionic *cyclo*-P_4 complex $\mathbf{1}^-$ with CS_2 leads to the electrophilic addition of the heterocumulene to the *cyclo*-P_4 ligand, resulting in the formation of $\mathbf{3}^-$, which features a puckered η^3:η^1-P_4CS_2 ligand. Initial reactivity studies of $\mathbf{3}^-$ toward electrophiles indicate a propensity for salt metathesis reactions, suggesting new pathways for subsequent functionalization. Upon employing the sulfur diimide $S(NSiMe_3)_2$ as the reactant, P−P bond insertion was facilitated for *cyclo*-P_4 complex $\mathbf{1}^-$, yielding complex $\mathbf{4}^-$, with a novel CoP_4N^- core. Compound $\mathbf{3}^-$ represents the first azatetraphosphole complex and undergoes further functionalization to yield **5** upon reaction with Me_3SiCl. These compounds, $\mathbf{4}^-$ and **5**, have been characterized with various analytical techniques, including single crystal X-ray structural analysis at synchrotron facilities and computational chemistry studies. The neutral complex **2** exhibits discrepant reactivity, undergoing insertion of isothiocyanates into the P−C bond of the acylated tetraphosphido ligand, yielding the highly derivatized complexes **6a** and **6b**. This new reaction type expands the repertoire of P−C bond insertion reactions available for the strategic functionalization of tetraphosphido ligands.

Overall, our findings highlight the versatility and potential of low-valent polyphosphido complexes for effecting targeted and diverse transformations of P_4. With increased availability of routes to various *cyclo*-P_4 complexes, particularly highlighted by recent advancements, this paves the way to unique phosphorus compounds. Ongoing research in this area is instrumental in deepening our understanding of reactivity patterns and mechanisms, laying the essential groundwork for the development of systems capable of facilitating the efficient transition-metal-mediated functionalization of P_4.

3.4 Experimental Details

General Synthetic Methods

All reactions and product manipulations were carried out in flame-dried glassware under an inert atmosphere of argon using standard Schlenk-line or glovebox techniques (maintained at <0.1 ppm H_2O and <0.1 ppm O_2). [K(18c-6)][(Ar*BIAN)Co(η^4-P_4)] ([K(18c-6)]**1**) and [(Ar*BIAN)Co(η^3:η^1-$P_4C(O)t$Bu)] (**2**) were prepared according to previously reported procedures.[7] $S(NSiMe_3)_2$ and CS_2 (c = 5.0 M in THF) were purchased from Sigma Aldrich; PhNCS, CyNCS from Alfa Aesar; and all were used as received. $S(NtBu)_2$ was provided by D. Stalke (University of Göttingen).

Solvents were dried and degassed with a MBraun SPS800 solvent purification system. All dry solvents except *n*-hexane was stored under argon over activated 3 Å molecular sieves in gas-tight ampules. *n*-Hexane was instead stored over potassium mirrors.

General Analytical Techniques

NMR spectra were recorded on Bruker Avance 400 spectrometers at 300 K and were internally referenced to residual solvent resonances (^{1}H NMR: C_6D_6: 7.15 ppm, THF-d_8: 1.72 ppm, MeCN-d_3: 1.96 ppm, toluene-d_8: 2.11 ppm; $^{13}C\{^1H\}$ C_6D_6: 128.06 ppm, THF-d_8: 25.31 ppm, MeCN-d_3: 1.79, toluene-d_8: 21.37 ppm). $^{31}P\{^1H\}$ spectra were referenced externally to 85% $H_3PO_{4(aq.)}$. Chemical shifts, δ, are given in ppm referring to external standards of tetramethylsilane (^{1}H, $^{13}C\{^1H\}$). ^{1}H, ^{13}C and ^{31}P NMR signals were assigned based on 2D NMR spectra (COSY, HSQC, HMBC, NOESY and ROESY).

UV/Vis spectra were recorded on an Ocean Optics Flame Spectrometer with a DH-2000-BAL light source. Elemental analysis were performed by the Central Analytics Department of the University of Regensburg using a Vario micro cube. Mass spectra of compound [K(18c-6)]**4** was recorded on a Finnigan MAT 95 spectrometer. IR spectra were recorded with a Bruker ALPHA spectrometer equipped with a diamond ATR unit.

NMR Simulations

For compounds which give rise to a higher order spin system in the $^{31}P\{^1H\}$ NMR spectrum, the resolution enhanced $^{31}P\{^1H\}$ NMR spectrum was transferred to the software gNMR, version 5.0.6, by Cherwell Scientific.[21] The full line shape iteration procedure of gNMR was applied to obtain the best match of the fitted to the experimental spectrum. $^1J(^{31}P^{31}P)$ coupling constants were set to negative values and all other signs of the coupling constants were obtained accordingly.[22]

3.4.1 Synthesis of Compounds

[K(18c-6)][(Ar*BIAN)Co(η³:η¹-P₄CS₂)] ([K(18c-6)]3):

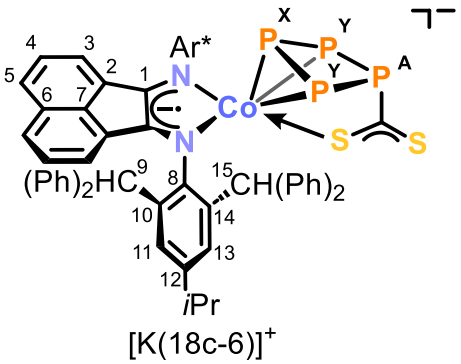

A stock solution of CS_2 (30.6 µL, c = 5.0 M in THF, 0.153 mmol, 1.2 equiv.) was added to a deep purple solution of [K(18c-6)][(Ar*BIAN)Co(η⁴-P_4)] (200 mg, 0.128 mmol, 1.0 equiv.) in THF (4 mL) at room temperature. The reaction mixture was stirred overnight, resulting in a blue solution which was filtered. The filtrate was layered with *n*-hexane (12 mL). After three days, blue shimmering crystals had formed, which were isolated by decantation of the mother liquor, washed with *n*-hexane (2 × 1 mL) and dried *in vacuo*. The solid contained 0.4 molecules of *n*-hexane and 0.7 molecules of THF after drying as indicated by $^{1}H/^{13}C\{^{1}H\}$ NMR spectra and elemental analysis. Slow diffusion of *n*-hexane into a saturated toluene solution of [K(18c-6)]**3** yielded crystals suitable for single-crystal X-ray diffraction.

Yield: 186 mg (0.115 mmol, 89%).

^{1}H NMR (400.13 MHz, 300 K, THF-d_8): δ/ppm = 1.11-1.16 (m, 12H, −CH(CH_3)$_2$ of *i*Pr), 2.78 (sept, $^{3}J_{HH}$ = 6.9 Hz, 2H, −C*H*(CH$_3$)$_2$ of *i*Pr), 3.45 (br s, 24H, 18c-6), 5.06 (s, 2H, −C^{9}*H*(Ph)$_2$), 5.50 (d, $^{3}J_{HH}$ = 7.1 Hz, 2H, C^{3}–*H* of BIAN), 6.22-6.26 (m, 2H, C^{4}–*H* of BIAN), 6.41-6.46 (m, 8H, C–H_{Ar} of Ph), 6.51-6.59 (m, 4H, C–H_{Ar} of Ph), 6.65-6.70 (m, 4H, C–H_{Ar} of Ph), 6.79-6.81 (m, 4H, C–H_{Ar} of Ph), 6.85-6.86 (m, 2H, C^{11}–*H*), 6.90-7.10 (m, 14H, C–H_{Ar} of Ph overlapping with C^{13}–*H*), 7.23 (d, $^{3}J_{HH}$ = 8.2 Hz, 2H, C^{5}–*H* of BIAN), 7.31-7.33 (m, 4H, C–H_{Ar} of Ph), 7.57-7.59 (m, 4H, C–H_{Ar} of Ph), 7.96 (s, 2H, −C^{15}*H*(Ph)$_2$).

^{13}C{^{1}H} NMR (100.66 MHz, 300 K, THF-d_8): δ /ppm = 23.9 (s, −CH(*C*H$_3$)$_2$ of *i*Pr), 24.3 (s, −CH(*C*H$_3$)$_2$ of *i*Pr), 34.2 (s, −*C*H(CH$_3$)$_2$ of *i*Pr), 51.1 (s, −*C*^{9}H(Ph)$_2$), 52.5 (s, −*C*^{15}H(Ph)$_2$), 71.1 (s, 18c-6), 120.7 (s, *C*^{3}–H of BIAN), 122.9 (s, *C*^{5}–H of BIAN), 125.3 (s, C_{Ar}–H of Ph), 125.6 (s, C_{Ar}–H of Ph), 125.7 (s, C_{Ar}–H of Ph), 125.9 (s, C_{Ar}–H of Ph), 127.4 (s, *C*^{11}–H), 127.5 (s, *C*^{13}–H), 127.6 (s, C_{Ar}–H of Ph), 127.7 (s, C_{Ar}–H of Ph), 127.7 (s, C_{Ar}–H of Ph), 128.0 (s, C_{Ar}–H of Ph), 128.2 (s, *C*^{4}–H of BIAN), 130.6 (s, C_{Ar}–H of Ph), 130.8 (s, C_{Ar}–H of Ph), 130.9 (s, *C*^{6} of BIAN), 131.2 (s, C_{Ar}–H of Ph), 131.5 (s, C_{Ar}–H of Ph), 134.0 (s, *C*^{2} of BIAN), 134.1 (s, *C*^{10}), 134.4 (s, *C*^{7} of BIAN), 138.8 (s, *C*^{14}), 143.6 (s, C_{Ar} of Ph), 143.9 (s, *C*^{12}), 145.0 (s, C_{Ar} of Ph), 146.6 (s, C_{Ar} of Ph), 147.6 (s, C_{Ar} of Ph), 150.9 (s, *C*^{8}–N), 159.8 (s, *C*^{1}=N of BIAN); *C*=S: not detected.

$^{31}P\{^{1}H\}$ NMR (162.04 MHz, 300 K, THF-d_8): (AXY_2) spin system δ/ppm = 83.3-86.1 (m, 2P, P_Y), 97.8-101.7 (m, 1P, P_X), 127.6 (t, 1P, P_A), for parameters obtained by simulation, see Figure S3 and Table S1.

UV/Vis (THF, λ_{max} / nm, ε_{max} / $L \cdot mol^{-1} \cdot cm^{-1}$): 330 (22000), 375sh (14000), 570 (15000), 725 (10500).

Elemental analysis calcd. for $(C_{95}H_{92}CoKN_2O_6P_4S_2) \cdot (n\text{-hexane})_{0.4}(THF)_{0.7}$ (M_w = 1643.84 $g \cdot mol^{-1}$): C 69.62, H 6.02, N 1.62, S 3.71; found C 69.25 , H 6.07, N 1.48, S 4.11.

[K(18c-6)][(Ar*BIAN)Co(η³:η¹-P₄SN₂(SiMe₃)₂)] [K(18c-6)]4):

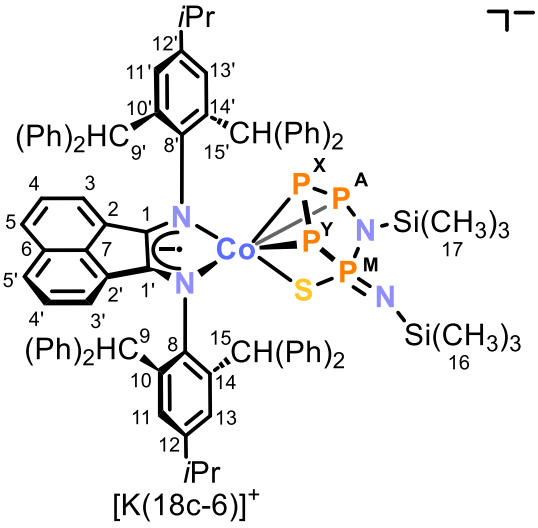

N,N-Bis(trimethylsilyl)sulfurdiimide (19.8 mg, 22.6 µL, 0.096 mmol, 1.5 equiv.) was added to a deep purple solution of [K(18c-6)][(Ar*BIAN)Co(η⁴-P₄)] (100 mg, 0.064 mmol, 1.0 equiv.) in THF (2 mL). The reaction mixture was stirred at 35 °C for six days, resulting in a blue solution which was filtered. *n*-Hexane (40 mL) was added while stirring, precipitating a purple solid, which was isolated by filtration, washed with *n*-hexane (3 × 2 mL) and dried *in vacuo*. Slow diffusion of *n*-hexane into a saturated toluene solution of [K(18c-6)]**4** yielded crystals suitable for single-crystal X-ray diffraction.

Yield: 71 mg (0.040 mmol, 63%).

^{1}H NMR (400.30 MHz, 300 K, MeCN-d_3): δ/ppm = −0.14 (s, 9H, −Si($C^{16}H_3$)$_3$), 0.06 (s, 9H, −Si($C^{17}H_3$)$_3$), 1.11-1.17 (m, 12H, −CH(CH_3)$_2$ of *i*Pr), 2.76-2.88 (m, 2H, −C*H*(CH_3)$_2$ of *i*Pr), 3.55 (s, 24H, 18c-6), 4.66 (s, 1H, −$C^{9/9'}$*H*(Ph)$_2$), 4.98 (d, $^3J_{HH}$ = 7.1 Hz, 1H, $C^{3/3'}$–*H* of BIAN), 5.19 (s, 1H, −$C^{9/9'}$*H*(Ph)$_2$), 5.71 (d, $^3J_{HH}$ = 7.1 Hz, 1H, $C^{3/3'}$–*H* of BIAN), 6.06-6.19 (m, 7H, $C^{4/4'}$–*H* of BIAN overlapping with C–H_{Ar} of Ph), 6.32-6.36 (m, 2H, C–H_{Ar} of Ph), 6.47-6.59 (m, 7H, $C^{4/4'}$–*H* of BIAN overlapping with C–H_{Ar} of Ph), 6.73-6.77 (m, 2H, C–H_{Ar} of Ph), 6.81-6.98 (m, 11H, $C^{11/11'}$–*H* overlapping with $C^{13/13'}$–*H* overlapping with C–H_{Ar} of Ph), 7.03-7.32 (m, 16H, $C^{5/5'}$–*H* of BIAN overlapping with C–H_{Ar} of Ph), 7.43-7.48 (m, 3H, $C^{5/5'}$–*H* of BIAN overlapping with C–H_{Ar} of Ph), 7.95 (s, 1H, −$C^{15/15'}$*H*(Ph)$_2$), 8.49 (s, 1H, −$C^{15/15'}$*H*(Ph)$_2$).

$^{13}C\{^1H\}$ NMR (100.61 MHz, 300 K, MeCN-d_3): δ/ppm = 1.5 (d, $^3J_{CP}$ = 3.9 Hz, −Si($C^{17}H_3$)$_3$ overlapping with MeCN-d_3 solvent signal), 4.7 (d, $^3J_{CP}$ = 3.1 Hz, −Si($C^{16}H_3$)$_3$), 24.2 (s, −CH(CH_3)$_2$ of *i*Pr), 24.4 (s, −CH(CH_3)$_2$ of *i*Pr), 24.4 (s, −CH(CH_3)$_2$ of *i*Pr), 24.6 (s, −CH(CH_3)$_2$ of *i*Pr), 34.3 (s, −CH(CH_3)$_2$ of *i*Pr), 34.4 (s, −CH(CH_3)$_2$ of *i*Pr), 50.9 (s, $-C^{9/9'}$H(Ph)$_2$), 51.3 (s, $-C^{15/15'}$H(Ph)$_2$), 51.6 (s, $-C^{9/9'}$H(Ph)$_2$), 52.0 (s, $-C^{15/15'}$H(Ph)$_2$), 71.0 (s, 18c-6), 120.5 (s, $C^{3/3'}$–H of BIAN), 120.7 (s, $C^{3/3'}$–H of BIAN), 123.0 (s, $C^{5/5'}$–H of BIAN), 123.3 (s, $C^{5/5'}$–H of BIAN), 125.5 (s, C_{Ar}–H of Ph), 126.0 (s, C_{Ar}–H of Ph), 126.1 (s, C_{Ar}–H of Ph), 126.1 (s, C_{Ar}–H of Ph), 126.2 (s, C_{Ar}–H of Ph), 126.2 (s, C_{Ar}–H of Ph), 126.6 (s, C_{Ar}–H of Ph), 127.5 (s, $C^{13/13'}$–H), 127.7 (s, $C^{13/13'}$–H), 127.9 (s, C_{Ar}–H of Ph), 128.1 (s, $C^{11/11'}$–H), 128.1 (s, C_{Ar}–H of Ph), 128.1 (s, $C^{11/11'}$–H), 128.2 (s, C_{Ar}–H of Ph), 128.3 (s, C_{Ar}–H of Ph), 128.4 (s, $C^{4/4'}$–H of BIAN), 128.7 (s, C_{Ar}–H of Ph), 128.7 (s, $C^{4/4'}$–H of Ph), 128.8 (s, C_{Ar}–H of Ph), 129.3 (s, C_{Ar}–H of Ph), 130.7 (s, C_{Ar}–H of Ph), 131.2 (s, C_{Ar}–H of Ph), 131.2 (s, C_{Ar}–H of Ph), 131.3 (s, C_{Ar}–H of Ph), 131.4 (s, C_{Ar}–H of Ph), 131.4 (s, C_{Ar}–H of Ph), 131.4 (s, C_{Ar}–H of Ph), 131.4 (s, C_{Ar}–H of Ph), 131.5 (s, C^6 of BIAN), 131.6 (s, C_{Ar}–H of Ph), 131.7 (s, C_{Ar}–H of Ph), 132.9 (s, $C^{10/10'}$), 134.2 (s, $C^{10/10'}$), 134.6 (s, C^7 of BIAN), 134.7 (s, $C^{2/2'}$ of BIAN), 134.9 (s, $C^{2/2'}$ of BIAN), 137.9 (s, $C^{14/14'}$), 139.3 (s, $C^{14/14'}$), 143.1 (s, C_{Ar} of Ph), 144.1 (s, C_{Ar} of Ph), 144.4 (s, $C^{12/12'}$), 144.5 (s, $C^{12/12'}$), 144.6 (s, C_{Ar} of Ph), 145.0 (s, C_{Ar} of Ph), 146.7 (s, C_{Ar} of Ph), 147.9 (s, C_{Ar} of Ph), 148.5 (s, C_{Ar} of Ph), 150.0 (s, C_{Ar} of Ph), 153.8 (s, $C^{8/8'}$–N), 155.4 (s, $C^{8/8'}$–N), 159.9 (s, $C^{1/1'}$=N of BIAN), 161.6 (s, $C^{1/1'}$=N of BIAN).

$^{31}P\{^1H\}$ NMR (161.98 MHz, 300 K, MeCN-d_3): (AMXY) spin system δ/ppm = −43.2 (dd, 1P, P_Y), −12.4 (ddd, 1P, P_X), 29.2 (ddd, 1P, P_M), 118.8 (dd, 1P, P_A), for parameters obtained by simulation, see Figure S7 and Table S2.

$^{29}Si\{^1H\}$ NMR (79.49 MHz, 300 K, MeCN-d_3): δ/ppm = −17.9 (d, $^2J_{SiP}$ = 16.6 Hz, −*Si*($C^{16}H_3$)$_3$), 3.6 (d, $^2J_{SiP}$ = 6.1 Hz, −*Si*($C^{17}H_3$)$_3$).

UV/Vis (THF, λ_{max} / nm, ε_{max} / L·mol^{-1}·cm^{-1}): 320sh (17000), 550 (10000), 710 (9000).

Elemental analysis calcd. for ($C_{100}H_{110}CoKN_4O_6P_4SSi_2$) (Mw = 1774.15 g·mol^{-1}):
C 67.70, H 6.25, N 3.16, S 1.81; found C 67.29, H 6.29, N 3.04, S 1.72.

TOF-MS (ESI, THF): m/z(%) calculated for ($C_{88}H_{86}CoN_4P_4SSi_2$)$^-$ [M$^-$]: 1470.4424; found 1470.4298.

[(Ar*BIAN)Co(η³:η¹-P₄SN₂(SiMe₃)₃)] (5):

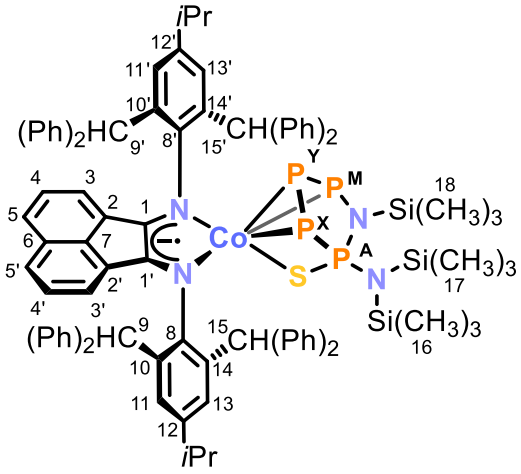

A stock solution of Me_3SiCl (53.5 µL, 1.58 M in toluene, 0.085 mmol, 1.0 equiv.) was added to a blue solution of [K(18c-6)][(Ar*BIAN)Co(η³:η¹-$P_4SN_2(SiMe_3)_2$] (150 mg, 0.085 mmol, 1.0 equiv.) in toluene (3.5 mL). The reaction mixture was stirred for 3 hours, over which the color changed to purple. The suspension was filtered through a pad of silica (0.5 × 1 cm) and washed with toluene (3 × 1 mL). The solvent was removed, and the purple residue extracted with *n*-hexane (8 mL). The filtrate was concentrated to half of the original volume. Storage for one day at room temperature and one day at −35 °C gave numerous shimmering purple crystals of sufficient quality for XRD, which were isolated by decantation of the mother liquor and dried *in vacuo*. The crystalline solid contained 0.1 equivalents of *n*-hexane and 0.1 equivalents of toluene after drying as indicated by $^1H/^{13}C\{^1H\}$ NMR spectra and elemental analysis.

Yield: 82 mg (0.053 mmol, 63%).

^{1}H NMR (400.13 MHz, 300 K, C_6D_6): δ/ppm = 0.05 (s, 9H, –Si(C$^{16}H_3$)$_3$), 0.20 (s, 9H, –Si(C$^{18}H_3$)$_3$), 0.38 (s, 9H, –Si(C$^{17}H_3$)$_3$), 1.09-1.14 (m, 12H, –CH(CH_3)$_2$ of *i*Pr), 2.58-2.71 (m, 2H, –CH(CH$_3$)$_2$ of *i*Pr), 5.40 (s, 1H, –C$^{9/9'}H$(Ph)$_2$), 5.43 (s, 1H, –C$^{9/9'}H$(Ph)$_2$), 5.55 (d, $^3J_{HH}$ = 7.1 Hz, 1H, C$^{3/3'}$–H of BIAN), 6.02 (d, $^3J_{HH}$ = 7.1 Hz, 1H, C$^{3/3'}$–H of BIAN), 6.17-6.21 (m, 1H, C$^{4/4'}$–H of BIAN), 6.29-6.33 (m, 1H, C$^{4/4'}$–H of BIAN), 6.49-6.56 (m, 4H, C–H_{Ar} of Ph), 6.62-6.76 (m, 10H, C–H_{Ar} of Ph), 6.92-6.94 (m, 2H, C–H_{Ar} of Ph), 7.03-7.21 (m, 10H, d ($^3J_{HH}$ = 8.1 Hz) of C$^{4/4'}$–H of BIAN overlapping with C–H_{Ar} of Ph overlapping with d ($^3J_{HH}$ = 8.2 Hz) of C$^{4/4'}$–H of BIAN overlapping with C_6D_6 solvent signal), 7.27-7.34 (m, 8H, C–H_{Ar} of Ph), 7.37-7.37 (m, 1H, C$^{11/11'}$–H), 7.41-7.44 (m, 7H, C$^{11/11'}$–H overlapping with $C^{13/13'}$–H overlapping with C–H_{Ar} of Ph), 7.46 (s, 1H, –C$^{15/15'}H$(Ph)$_2$), 7.51-7.53 (m, 2H, C–H_{Ar} of Ph), 7.72-7.74 (m, 2H, C–H_{Ar} of Ph), 7.97 (s, 1H, –C$^{15/15'}H$(Ph)$_2$).

^{13}C{^{1}H} NMR (100.61 MHz, 300 K, C_6D_6): δ/ppm = 2.8 (d, $^3J_{PC}$ = 8.1 Hz, –Si(C^{17}H$_3$)$_3$), 5.2 (dd, $^3J_{PC}$ = 5.9 Hz, 3.5 Hz, –Si(C^{18}H$_3$)$_3$), 5.7 (d, $^3J_{PC}$ = 1.8 Hz, –Si(C^{16}H$_3$)$_3$), 24.0 (s, –CH(CH$_3$)$_2$ of *i*Pr), 24.0 (s, –CH(CH$_3$)$_2$ of *i*Pr), 24.1 (s, –CH(CH$_3$)$_2$ of *i*Pr), 24.1 (s, –CH(CH$_3$)$_2$ of *i*Pr), 33.8 (s, –CH(CH$_3$)$_2$ of *i*Pr), 33.9 (s, –CH(CH$_3$)$_2$ of *i*Pr), 51.1 (s,

−$C^{9/9'}$H(Ph)$_2$), 51.7 (s, −$C^{9/9'}$H(Ph)$_2$), 52.0 (s, −$C^{15/15'}$H(Ph)$_2$), 52.4 (s, −C^{15}H(Ph)$_2$), 121.8 (s, $C^{3/3'}$–H of BIAN), 122.0 (s, $C^{3/3'}$–H of BIAN), 124.4 (s, $C^{5/5'}$–H of BIAN), 124.4 (s, $C^{5/5'}$–H of BIAN), 125.7 (s, C_{Ar}–H of Ph), 125.7 (s, C_{Ar}–H of Ph), 125.9 (s, C_{Ar}−H of Ph), 126.0 (s, C_{Ar}−H of Ph), 126.1 (s, C_{Ar}−H of Ph), 126.2 (s, C_{Ar}−H of Ph), 127.0 (s, C_{Ar}−H of Ph), 127.7 (s, $C^{4/4'}$−H of BIAN overlapping with C_6D_6 solvent signal), 127.7 (s, C_{Ar}−H of Ph overlapping with C_6D_6 solvent signal), 127.8 (s, C_{Ar}−H of Ph overlapping with C_6D_6 solvent signal), 127.9 (s, C_{Ar}−H of Ph overlapping with C_6D_6 solvent signal), 128.0 (s, $C^{4/4'}$−H of BIAN overlapping with C_6D_6 solvent signal), 128.0 (s, C_{Ar}−H of Ph overlapping with C_6D_6 solvent signal), 128.1 (s, C_{Ar}−H of Ph overlapping with C_6D_6 solvent signal), 128.1 (s, C_{Ar}−H of Ph overlapping with C_6D_6 solvent signal), 128.2 (s, C_{Ar}−H of Ph overlapping with C_6D_6 solvent signal), 128.3 (s, C_{Ar}−H of Ph overlapping with C_6D_6 solvent signal), 128.3 (s, $C^{13/13'}$−H overlapping with C_6D_6 solvent signal), 128.4 (s, $C^{13/13'}$−H overlapping with C_6D_6 solvent signal), 128.5 (s, $C^{11/11'}$−H), 128.6 (s, $C^{11/11'}$−H), 130.2 (s, C_{Ar}−H of Ph), 130.5 (s, C^6 of BIAN), 130.7 (s, C_{Ar}−H of Ph), 130.8 (s, C_{Ar}−H of Ph), 130.8 (s, C_{Ar}−H of Ph), 131.0 (s, C_{Ar}−H of Ph), 131.0 (s, C_{Ar}−H of Ph), 131.0 (s, C_{Ar}−H of Ph), 131.3 (s, C_{Ar}−H of Ph), 131.4 (s, C_{Ar}−H of Ph), 132.3 (s, $C^{2/2'}$ of BIAN), 132.4 (s, $C^{2/2'}$ of BIAN), 132.9 (s, $C^{10/10'}$), 135.2 (s, $C^{10/10'}$), 136.5 (s, C^7 of BIAN), 137.9 (s, $C^{14/14'}$), 138.8 (s, $C^{14/14'}$), 142.8 (s, C_{Ar} of Ph), 143.1 (s, C_{Ar} of Ph), 143.4 (s, C_{Ar} of Ph), 143.8 (s, C_{Ar} of Ph), 145.3 (s, $C^{12/12'}$), 145.5 (s, $C^{12/12'}$), 146.1 (s, C_{Ar} of Ph), 146.5 (s, C_{Ar} of Ph), 147.8 (s, C_{Ar} of Ph), 148.1 (s, C_{Ar} of Ph), 150.9 (s, $C^{8/8'}$–N), 152.2 (s, $C^{8/8'}$–N), 163.1 (s, $C^{1/1'}$=N of BIAN), 164.2 (s, $C^{1/1'}$=N of BIAN).

^{31}P{^{1}H} NMR (162.04 MHz, 300 K, C_6D_6): (AMXY) spin system δ/ppm = −60.1 (dd, 1P, P_Y), −54.2 - −49.0 (m, 1P, P_X), 47.9-50.8 (m, 1P, P_M), 133.4-135.7 (m, 1P, P_A), for parameters obtained by simulation, see Figure S13 and Table S3.

^{29}Si{^{1}H} NMR (79.49 MHz, 300 K, C_6D_6): δ/ppm = 7.4 (d, $^2J_{SiP}$ = 10.9 Hz, −*Si*($C^{17}H_3$)$_3$), 9.3 (s, −*Si*($C^{18}H_3$)$_3$), 11.6 (d, $^2J_{SiP}$ = 6.1 Hz, −*Si*($C^{16}H_3$)$_3$).

UV/Vis (THF, λ_{max} / nm, ε_{max} / L·mol^{-1}·cm^{-1}): 330sh (17000), 550 (11000), 700 (14000).

Elemental analysis calcd. for ($C_{91}H_{95}CoN_4P_4SSi_3$)·(toluene)$_{0.1}$·(*n*-hexane)$_{0.1}$ (M_w = 1543.93 g·mol^{-1}): C 70.98, H 6.27, N 3.59, S 2.05; found C 71.33, H 5.88, N 3.51, S 2.07.

[(Ar*BIAN)Co(η³:η¹-P₄C(S)N(Cy)C(O)*t*Bu)] (6a):

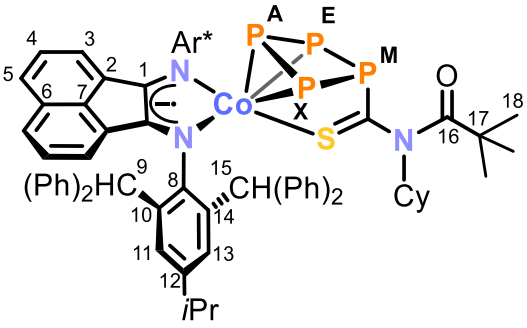

Neat cyclohexyl isothiocyanate (7.3 mg, 7.4 µL, 0.052 mmol, 1.4 equiv.) was added to a magenta-colored solution of [(Ar*BIAN)Co(η³:η¹-P₄C(O)*t*Bu)] (50 mg, 0.037 mmol, 1.0 equiv.) in toluene (1.5 mL). The reaction mixture was stirred for three days, giving a purple solution. The solvent was removed *in vacuo*. Subsequently, the resulting purple residue was washed with *n*-hexane (3 × 0.5 mL) and dried *in vacuo* yielding a deep purple powder. Crystals of suitable for XRD were grown by slow evaporation of a concentrated toluene solution containing **6a**.

Yield: 44 mg (0.030 mmol, 80%).

^{1}H NMR (400.13 MHz, 300 K, C_6D_6): δ/ppm = 0.60-0.65 (m, 5H, C*H*$_2$ of Cy), 0.92 (s, 9H,−C(C^{18}*H*$_3$)$_3$ of *t*Bu), 1.02-1.05 (m, 12H, −CH(C*H*$_3$)$_2$ of *i*Pr), 1.16-1.22 (m, 3H, C*H*$_2$ of Cy), 1.46-1.49 (m, 2H, C*H*$_2$ of Cy), 2.58 (sept, $^{3}J_{HH}$ = 6.9 Hz, 2H, −C*H*(CH$_3$)$_2$ of *i*Pr), 3.43-3.48 (m, 1H, C−*H* of Cy), 5.50 (s, 2H, −C^{9}*H*(Ph)$_2$), 5.89 (d, $^{3}J_{HH}$ = 7.1 Hz, 2H, C^{3}−*H* of BIAN), 6.22-6.26 (m, 2H, C^{4}−*H* of BIAN), 6.64-6.65 (m, 6H, C−*H*$_{Ar}$ of Ph), 6.71-6.75 (m, 2H, C−*H*$_{Ar}$ of Ph), 6.82-6.98 (m, 10H, C−*H*$_{Ar}$ of Ph), 7.06-7.15 (m, 14H, C−*H*$_{Ar}$ of Ph overlapping with C_6D_6 solvent signal), 7.19 (d, $^{3}J_{HH}$ = 8.2 Hz, 2H, C^{5}−*H* of BIAN), 7.29-7.29 (m, 2H, C^{11}−*H*), 7.36-7.37 (m, 2H, C^{13}−*H*), 7.64-7.65 (m, 8H, C−*H*$_{Ar}$ of Ph), 7.92 (s, 2H, −C^{15}*H*(Ph)$_2$).

^{13}C{^{1}H} NMR (100.66 MHz, 300 K, C_6D_6): δ/ppm = 24.4 (s, −CH(*C*H$_3$)$_2$ of *i*Pr), 24.5 (s, −CH(*C*H$_3$)$_2$ of *i*Pr), 26.1 (s, *C*H$_2$ of Cy), 26.6 (s, *C*H$_2$ of Cy), 29.0 (s, −C(*C*^{18}H$_3$)$_3$ of *t*Bu), 31.2 (s, *C*H$_2$ of Cy), 34.4 (s, −*C*H(CH$_3$)$_2$ of *i*Pr), 44.1 (s, −*C*^{17}(CH$_3$)$_3$ of *t*Bu), 51.7 (s, −*C*^{9}H(Ph)$_2$), 53.3 (s, −*C*^{15}H(Ph)$_2$), 67.1 (s, *C*H of Cy), 122.6 (s, *C*^{3}−H of BIAN), 125.4 (s, *C*^{5}−H of BIAN), 126.5 (s, *C*$_{Ar}$−H of Ph), 126.6 (s, *C*$_{Ar}$−H of Ph), 126.9 (s, *C*$_{Ar}$−H of Ph), 127.3 (s, *C*$_{Ar}$−H of Ph), 128.4 (s, *C*$_{Ar}$−H of Ph overlapping with C_6D_6 solvent signal), 128.5 (s, *C*^{13}−H overlapping with C_6D_6 solvent signal), 128.6 (s, *C*^{4}−H of BIAN overlapping with C_6D_6 solvent signal), 128.6 (s, *C*$_{Ar}$−H of Ph overlapping with C_6D_6 solvent signal), 128.8 (s, *C*^{11}−H overlapping with C_6D_6 solvent signal), 128.9 (s, *C*$_{Ar}$−H of Ph overlapping with C_6D_6 solvent signal), 129.2 (s, *C*$_{Ar}$−H of Ph), 130.6 (s, *C*$_{Ar}$−H of Ph), 130.9 (s, *C*$_{Ar}$−H of Ph), 131.1 (s, *C*^{6} of BIAN overlapping with *C*$_{Ar}$−H of Ph), 131.1 (s, *C*^{6} of BIAN overlapping with *C*$_{Ar}$−H of Ph), 131.4 (s, *C*$_{Ar}$−H of Ph), 132.6 (s, *C*^{2} of BIAN), 135.2 (s, *C*^{10}), 136.8 (s, *C*^{7} of BIAN), 139.0 (s, *C*^{14}), 143.5 (s, *C*$_{Ar}$ of Ph), 145.3

(s, C_{Ar} of Ph), 146.0 (s, C_{Ar} of Ph), 146.3 (s, C^{12}), 148.5 (s, C_{Ar} of Ph), 149.7 (s, C^{8}–N), 164.3 (s, C^{1}=N of BIAN), 183.1 (s, C^{16}(O)*t*Bu); *C*=S: not detected.

$^{31}P\{^{1}H\}$ NMR (162.04 MHz, 300 K, C_6D_6): δ/ppm = 86.3 (t, 1P), 93.0 (br s, $\Delta\nu_{½}$ = 2500 Hz, 2P), 117.3 (t, 1P); (161.98 MHz, toluene-d_8, 213 K): (AEMX) spin system δ/ppm = 77.6 (dd, 1P, $P_{E/X}$), 85.5 (t, 1P, P_M), 105.3 (dd, 1P, $P_{E/X}$), 118.0 (t, 1P, P_A), for parameters obtained by simulation, see Figure S19 and Table S4. Spin system was assigned based on DFT calculated values (*vide infra*).

UV/Vis (toluene, λ_{max} / nm, ε_{max} / L·mol^{-1}·cm^{-1}): 330 (12000), 430 (2500), 550 (5000), 720 (8000).

IR (solid state): ν/ cm^{-1} = 3058w, 3023w, 2953w, 2928w, 1944w, 1805w, 1727m (C=O), 1600w, 1533m, 1492s, 1446m, 1417m, 1369s, 1322m, 1297m, 1255w, 1193m, 1153w, 1101w, 1076w, 1035m, 1007m, 920w, 895w, 842w, 820m, 761m, 736s, 736m, 696s, 654m, 634m, 606s.

Elemental analysis calcd. for ($C_{94}H_{88}CoN_3OP_4S$) (M_w = 1490.65 g·mol^{-1}):
C 75.74, H 5.95, N 2.82, S 2.15; found: C 75.60, H 5.93, N 2.58, S 1.75.

[(Ar*BIAN)Co(η^3:η^1-P_4C(S)N(Ph)C(O)tBu)] (6b):

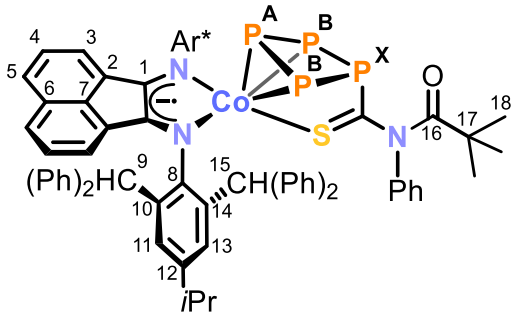

Neat PhNCS (11.0 mg, 9.7 µL, 0.081 mmol, 1.1 equiv.) was added to a magenta-colored solution of [(Ar*BIAN)Co(η^3:η^1-P_4C(O)*t*Bu)] (100 mg, 0.074 mmol, 1.0 equiv.) in toluene (2 mL). The reaction mixture was stirred for three hours, over which the color changed to purple. The solvent was removed *in vacuo*, and the purple residue extracted with *n*-hexane (30 mL). The mixture was filtered, and the filtrate concentrated until incipient crystallization. Purple crystals formed upon storage for two days at −35 °C. The crude product (84 mg) was isolated by decantation of the supernatant. Recrystallization from Et_2O (2 mL) at −35 °C gave shimmering deep purple crystals, which were isolated by decantation of the mother liquor and dried *in vacuo*. The compound decomposes to new species (identified by ABMX and AEMX spin systems in the $^{31}P\{^{1}H\}$ NMR spectrum) in solution at ambient temperature over the course of hours (see the SI for details). Crystals of sufficient quality of **6b** were grown by slow diffusion of *n*-hexane into a concentrated toluene solution containing **6b**.

Yield: 69 mg (0.046 mmol, 63%).

^{1}H NMR (400.13 MHz, 300 K, C_6D_6,): δ/ppm = 0.76 (s, 9H,−C(C$^{18}H_3$)$_3$ of *t*Bu), 1.00-1.03 (m, 12H, −CH(CH_3)$_2$ of *i*Pr), 2.55 (sept, $^{3}J_{HH}$ = 6.9 Hz, 2H, −CH(CH$_3$)$_2$ of *i*Pr), 5.45 (s, 2H, −C^{9}H(Ph)$_2$), 5.80-5.82 (m, 2H, C−H_{ortho} of PhNCS), 5.85 (d, $^{3}J_{HH}$ = 7.1 Hz, 2H, C^{3}–H of BIAN), 6.21-6.25 (m, 2H, C^{4}–H of BIAN), 6.57-6.82 (m, 17H, C−$H_{meta/para}$ of PhNCS overlapping with C−H_{Ar} of Ph), 7.01-7.16 (m, 16H, C^{5}–H of BIAN overlapping with C−H_{Ar} of Ph overlapping with C_6D_6 solvent signal), 7.25-7.29 (m, 6H, C^{11}–H overlapping with C−H_{Ar} of Ph), 7.31-7.34 (m, 6H, C^{13}–H overlapping with C−H_{Ar} of Ph), 7.57 (s, 2H, −C^{15}H(Ph)$_2$), 7.74-7.76 (br m, 4H, C−H_{Ar} of Ph).

^{13}C{^{1}H} NMR (100.61 MHz, 273 K, toluene-d_8): δ/ppm = 24.3 (s, −CH(CH_3)$_2$ of *i*Pr), 24.5 (s, −CH(CH_3)$_2$ of *i*Pr), 28.5 (s, −C(C^{18}H$_3$)$_3$ of *t*Bu), 34.3 (s, −CH(CH$_3$)$_2$ of *i*Pr), 43.3 (s, −C^{17}(CH$_3$)$_3$ of *t*Bu), 51.4 (s, −C^{9}H(Ph)$_2$), 52.9 (s, −C^{15}H(Ph)$_2$), 122.5 (s, C^{3}–H of BIAN), 125.5 (s, C^{5}–H of BIAN overlapping with toluene-d_8 solvent signal), 126.5 (s, C_{Ar}–H of Ph), 126.5 (s, C_{Ar}–H of PhNCS), 126.6 (s, C_{Ar}–H of Ph), 127.2 (s, C_{Ar}–H of Ph), 127.9 (s, C_{Ar}–H of Ph), 128.3 (s, C^{4}–H of BIAN overlapping with toluene-d_8 solvent signal), 128.3 (s, C_{ortho}–H of PhNCS overlapping with toluene-d_8 solvent signal), 128.4 (s, C_{Ar}–H of Ph overlapping with toluene-d_8 solvent signal), 128.5 (s, C^{11}–H overlapping with toluene-d_8 solvent signal), 128.6 (s, C_{Ar}–H of Ph overlapping with toluene-d_8 solvent signal), 128.8 (s, C^{13}–H overlapping with toluene-d_8 solvent signal), 128.7 (s, C_{Ar}–H of Ph overlapping with toluene-d_8 solvent signal), 128.9 (s, C_{Ar}–H of Ph overlapping with toluene-d_8 solvent signal), 130.1 (s, C_{Ar}–H of PhNCS), 130.2 (s, C_{Ar}–H of Ph), 130.7 (s, C^{6} of BIAN), 130.9 (s, C_{Ar}–H of Ph), 131.1 (s, C_{Ar}–H of Ph), 132.0 (s, C^{2} of BIAN), 135.2 (s, C^{10}), 136.6 (s, C^{7} of BIAN), 138.7 (s, C^{14}), 141.6 (s, C_{ipso} of PhNCS), 142.7 (s, C_{Ar} of Ph), 145.0 (s, C_{Ar} of Ph), 145.8 (s, C_{Ar} of Ph), 146.2 (s, C^{12}), 148.5 (s, C_{Ar} of Ph), 149.0 (s, C^{8}–N), 164.4 (s, C^{1}=N of BIAN), 182.2 (s, C^{16}=O of −C(O)*t*Bu); *C*=S: not detected.

^{31}P{^{1}H} NMR (162.04 MHz, 300 K, C_6D_6): (AB_2X) spin system δ/ppm = 95.5-98.8 (m, 1P, P_X), 103.8-109.5 (m, 3P, P_A/P_B), for parameters obtained by simulation, see Figure S23 and Table S5.

UV/Vis (toluene, λ_{max} / nm, ε_{max} / L·mol^{-1}·cm^{-1}): 325 (22500), 530 (9000), 710 (13000).

IR (solid state): ν/ cm^{-1} = 3056w, 3023w, 2956w, 2924w, 2160w, 2031w, 1735w (C=O), 1685w, 1598w, 1530w, 1492m, 1450m, 1471m, 1361w, 1296w, 1253w, 1192w, 1163w, 1075w, 1030w, 949w, 917w, 894w, 820m, 737m, 695s, 655m, 605m.

Elemental analysis calcd. for ($C_{94}H_{82}CoN_3OP_4S$) (M_w = 1484.60 g·mol^{-1}): C 76.05, H 5.57, N 2.83, S 2.16; found: C 76.34, H 5.69, N 2.82, S 1.97.

3.4.2 NMR Spectra

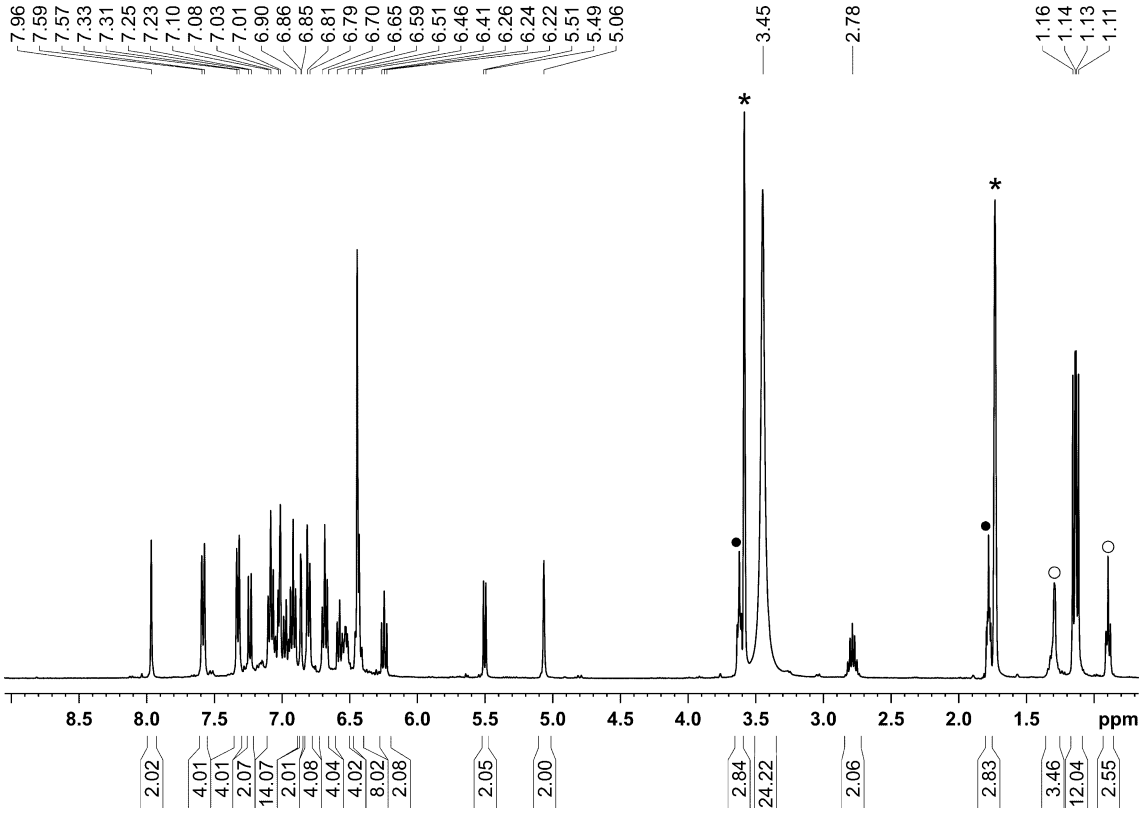

Figure S1. ^{1}H NMR spectrum (400.30 MHz, 300 K, THF-d_8) of [K(18c-6)][(Ar*BIAN)Co(η^3:η^1-P_4CS_2)] ([K(18c-6)]**3**); ○ *n*-hexane, • THF, * THF-d_8.

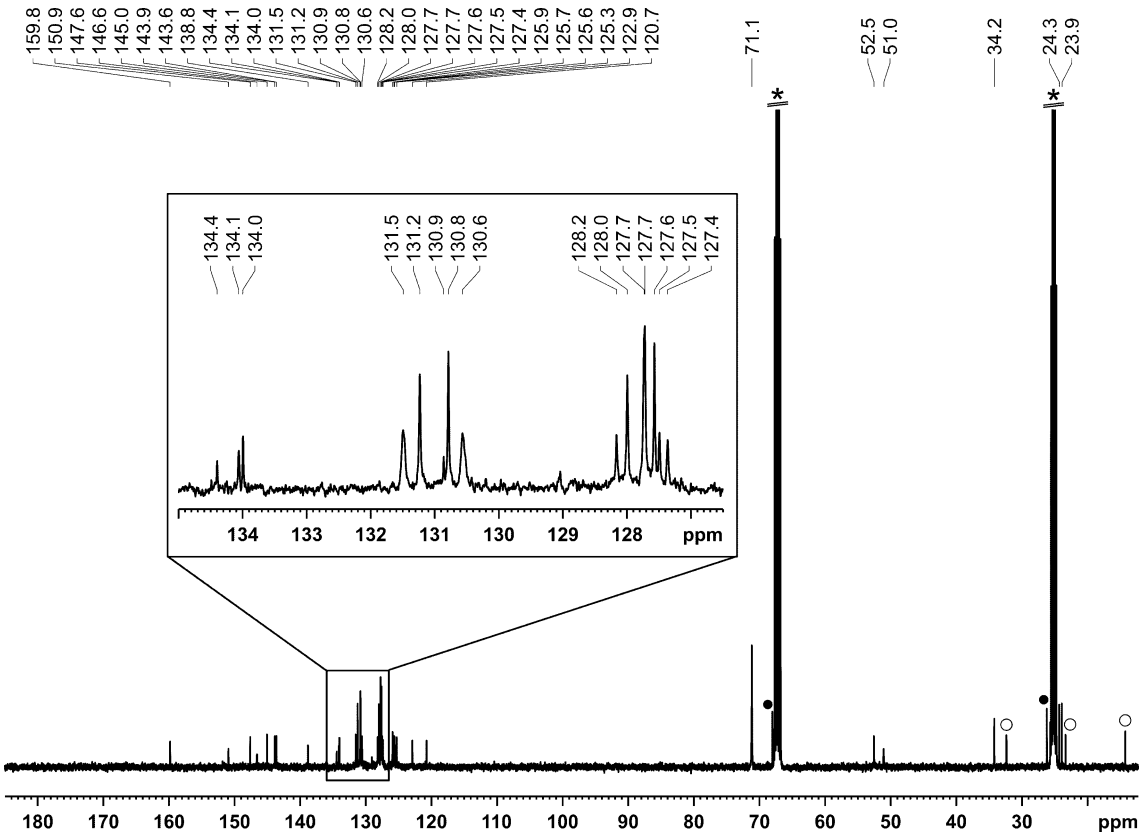

Figure S2. ^{13}C{^{1}H} NMR spectrum (100.66 MHz, 300 K, THF-d_8) of [K(18c-6)][(Ar*BIAN)Co(η^3:η^1-P_4CS_2)] ([K(18c-6)]**3**); ○ *n*-hexane, • THF, * THF-d_8.

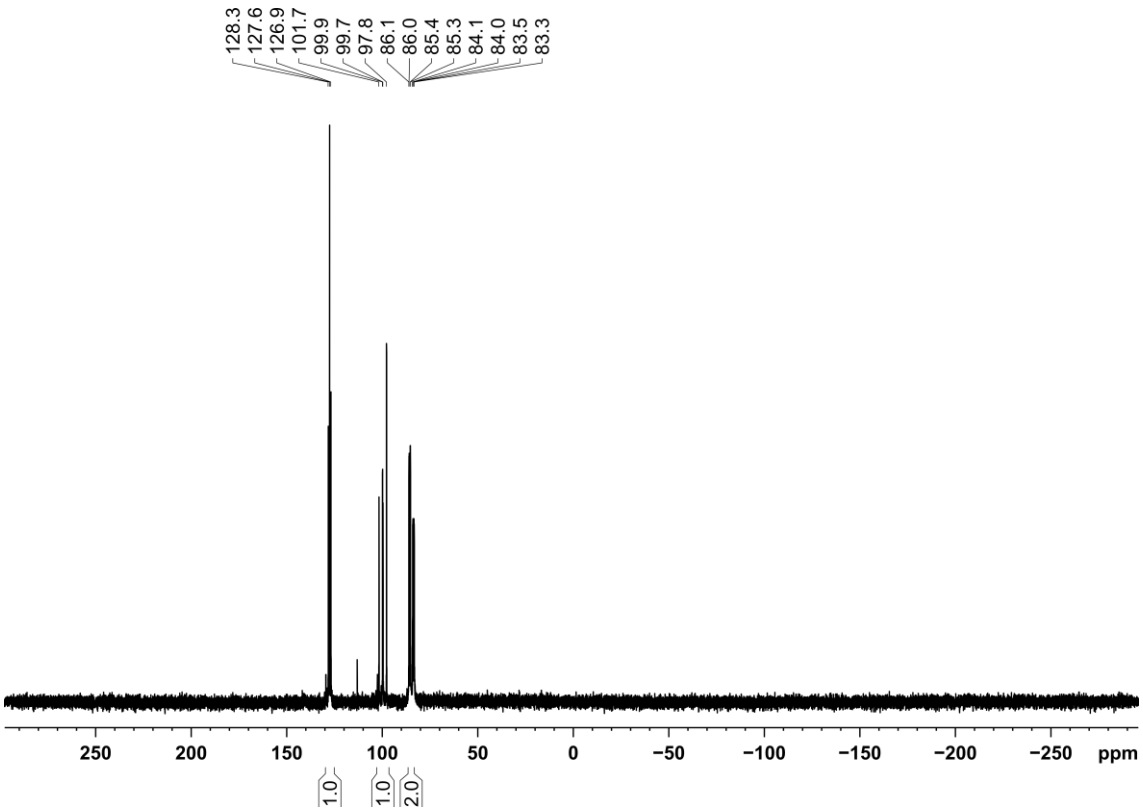

Figure S3. $^{31}P\{^{1}H\}$ NMR spectrum (162.04 MHz, 300 K, THF-d_8) of [K(18c-6)][(Ar*BIAN)Co(η^3:η^1-P_4CS_2)] ([K(18c-6)]**3**).

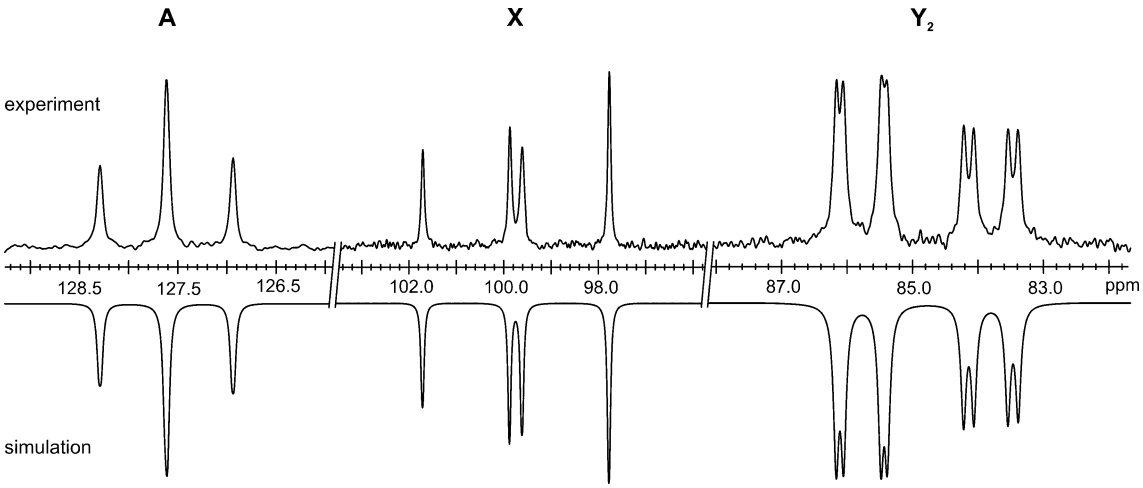

Figure S4. Section of the $^{31}P\{^{1}H\}$ NMR spectrum (162.04 MHz, 300 K, THF-d_8) of [K(18c-6)][(Ar*BIAN)Co(η^3:η^1-P_4CS_2)] ([K(18c-6)]**3**); experimental (upwards) and simulation (downwards).

Table S1. Chemical shifts and coupling constants from the iterative fit of the AXY_2 spin system and schematic representation of the CoP_4CS_2 core of [K(18c-6)][(Ar*BIAN)Co(η^3:η^1-P_4CS_2)] ([K(18c-6)]**3**).

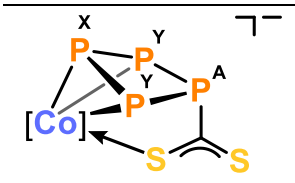	δ(A) = 127.6 ppm	$^{1}J_{XY}$ = –320.5 Hz
	δ(X) = 99.6 ppm	$^{1}J_{AY}$ = –110.1
	δ(Y) = 84.9 ppm	$^{2}J_{AX}$ = 5.4 Hz

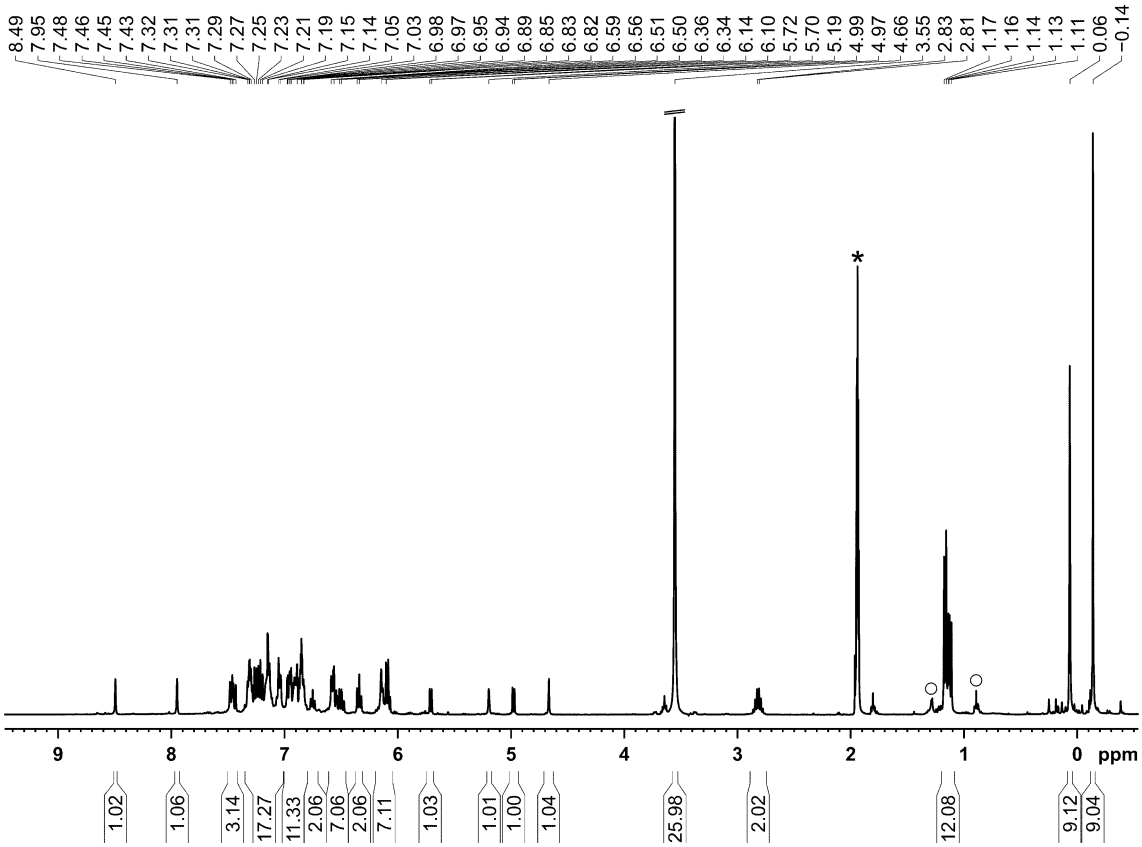

Figure S5. ^{1}H NMR spectrum (400.30 MHz, 300 K, MeCN-d_3) of [K(18c-6)][(Ar*BIAN)Co(η^3:η^1-$P_4SN_2(SiMe_3)_2$)] ([K(18c-6)]**4**); ○ *n*-hexane, * MeCN-d_3.

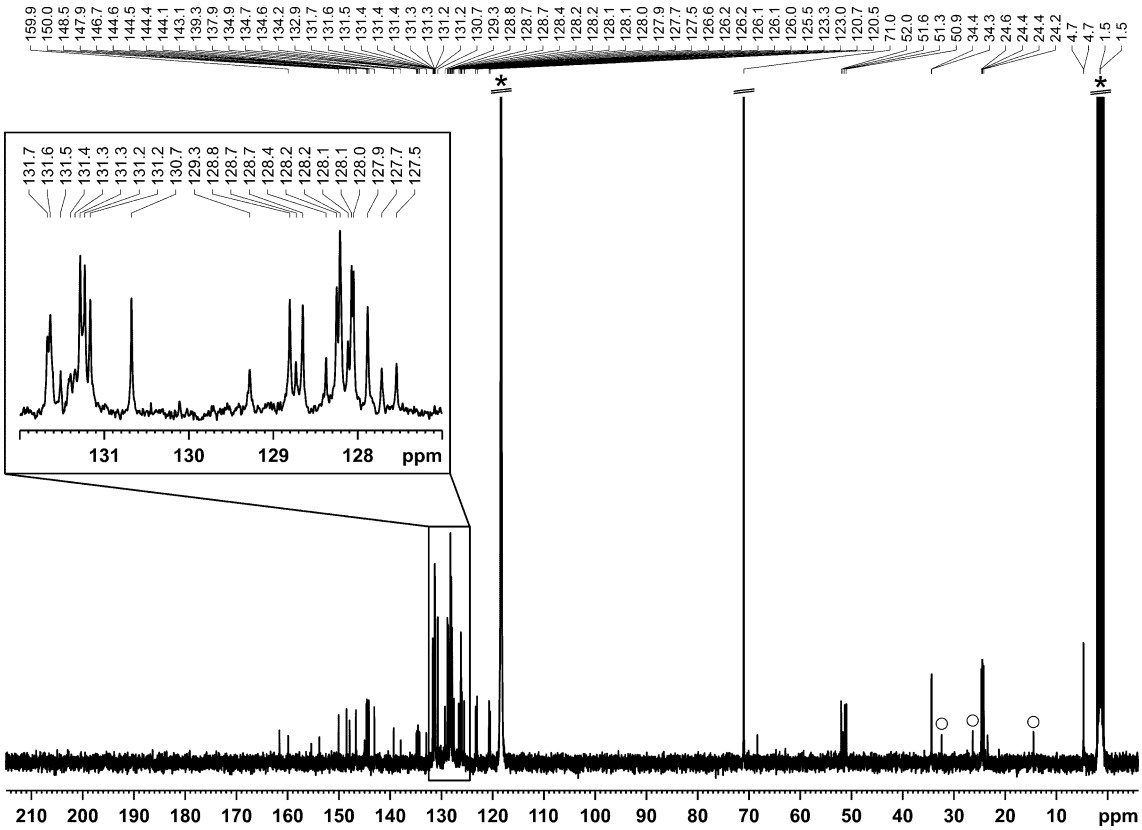

Figure S6. ^{13}C{^{1}H} NMR spectrum (100.66 MHz, 300 K, MeCN-d_3) of [K(18c-6)][(Ar*BIAN)Co(η^3:η^1-$P_4SN_2(SiMe_3)_2$)] ([K(18c-6)]**4**); ○ *n*-hexane, * MeCN-d_3.

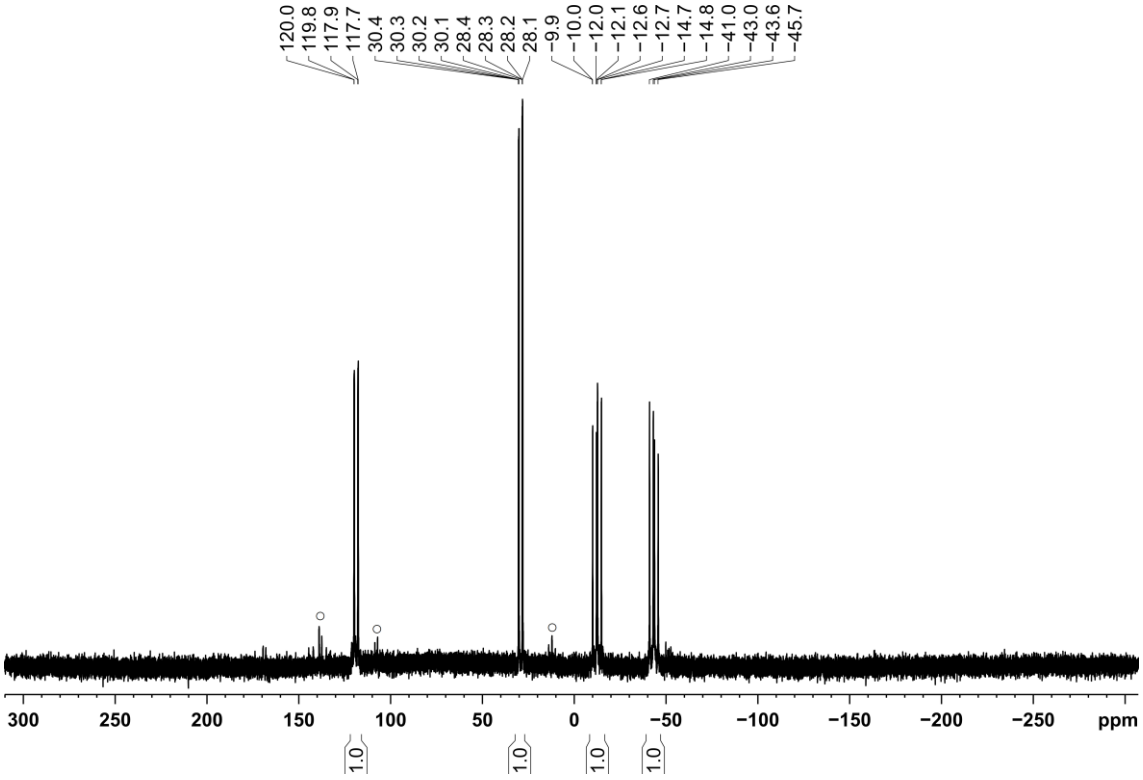

Figure S7. $^{31}P\{^{1}H\}$ NMR spectrum (161.98 MHz, 300 K, MeCN-d_3) of [K(18c-6)][(Ar*BIAN)Co(η^3:η^1-$P_4SN_2(SiMe_3)_2$)] ([K(18c-6)]**4**); ○ unknown impurity.

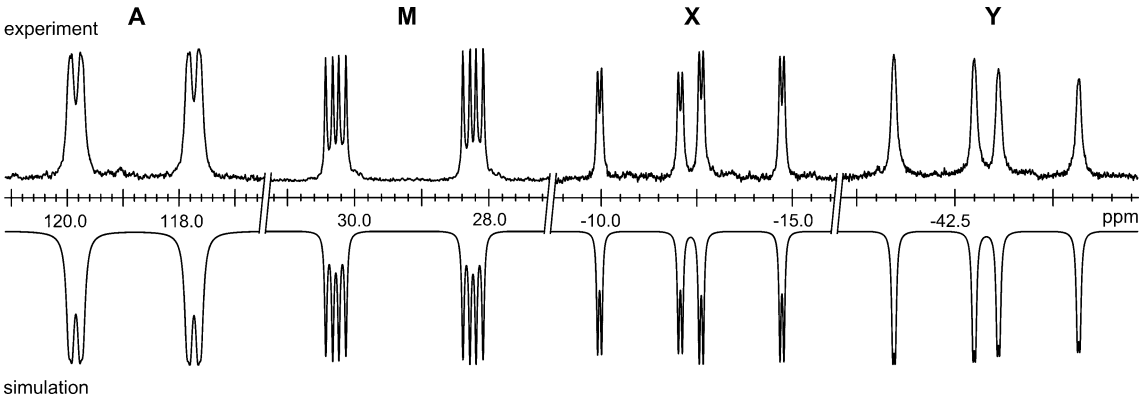

Figure S8. Section of the $^{31}P\{^{1}H\}$ NMR spectrum (161.98 MHz, 300 K, MeCN-d_3) of [K(18c-6)][(Ar*BIAN)Co(η^3:η^1-$P_4SN_2(SiMe_3)_2$)] ([K(18c-6)]**4**); experimental (upwards) and simulation (downwards).

Table S2. Chemical shifts and coupling constants from the iterative fit of the AMXY spin system and schematic representation of the $CoP_4SN_2(SiMe_3)_2$ core of [K(18c-6)][(Ar*BIAN)Co(η^4-$P_4SN_2(SiMe_3)_2$)] ([K(18c-6)]**4**).

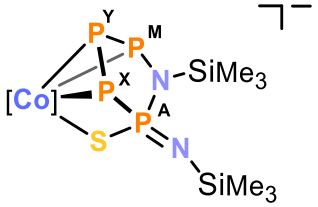

δ(A) = 118.8 ppm	$^{1}J_{XY}$ = −431.2 Hz
δ(M) = 29.2 ppm	$^{1}J_{AX}$ = −342.6 Hz
δ(X) = −12.4 ppm	$^{1}J_{MY}$ = −331.1 Hz
δ(Y) = −43.2 ppm	J_{MX} = 16.8 Hz
	J_{AY} = 10.4 Hz
	J_{AM} = −31.7 Hz

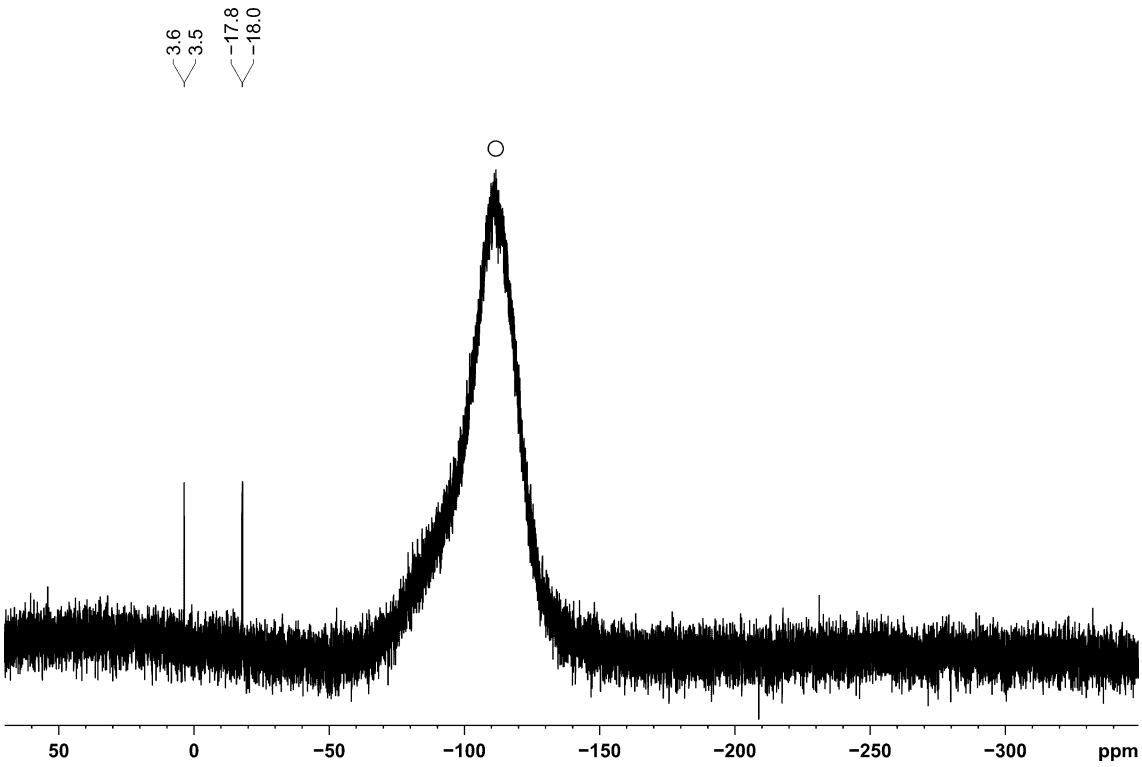

Figure S9. $^{29}Si\{^{1}H\}$ NMR spectrum (79.49 MHz, 300 K, MeCN-d_3) of [K(18c-6)][(Ar*BIAN)Co(η^3:η^1-$P_4SN_2(SiMe_3)_2$)] ([K(18c-6)]**4**); ○ background signal from glass tube.

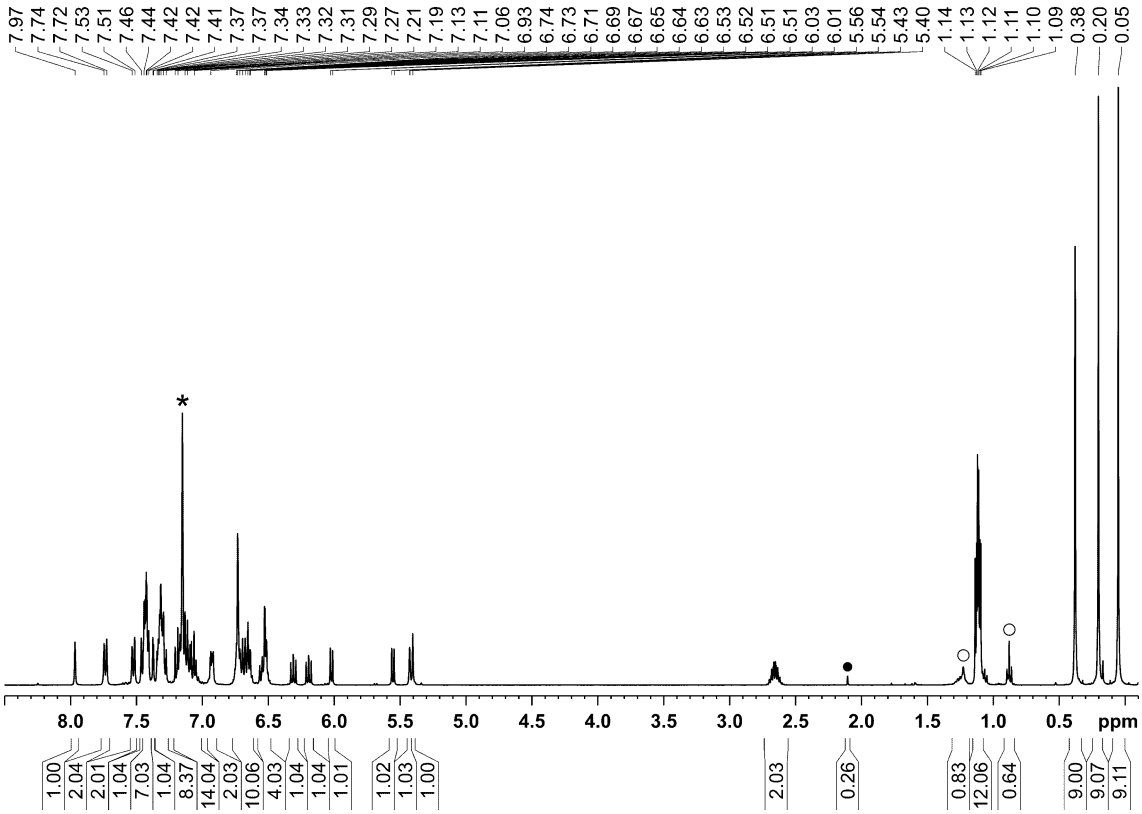

Figure S10. ^{1}H NMR spectrum (400.30 MHz, 300 K, C_6D_6) of [(Ar*BIAN)Co(η^3:η^1-$P_4SN_2(SiMe_3)_3$)] (**5**); ○ *n*-hexane, • toluene, * C_6D_6.

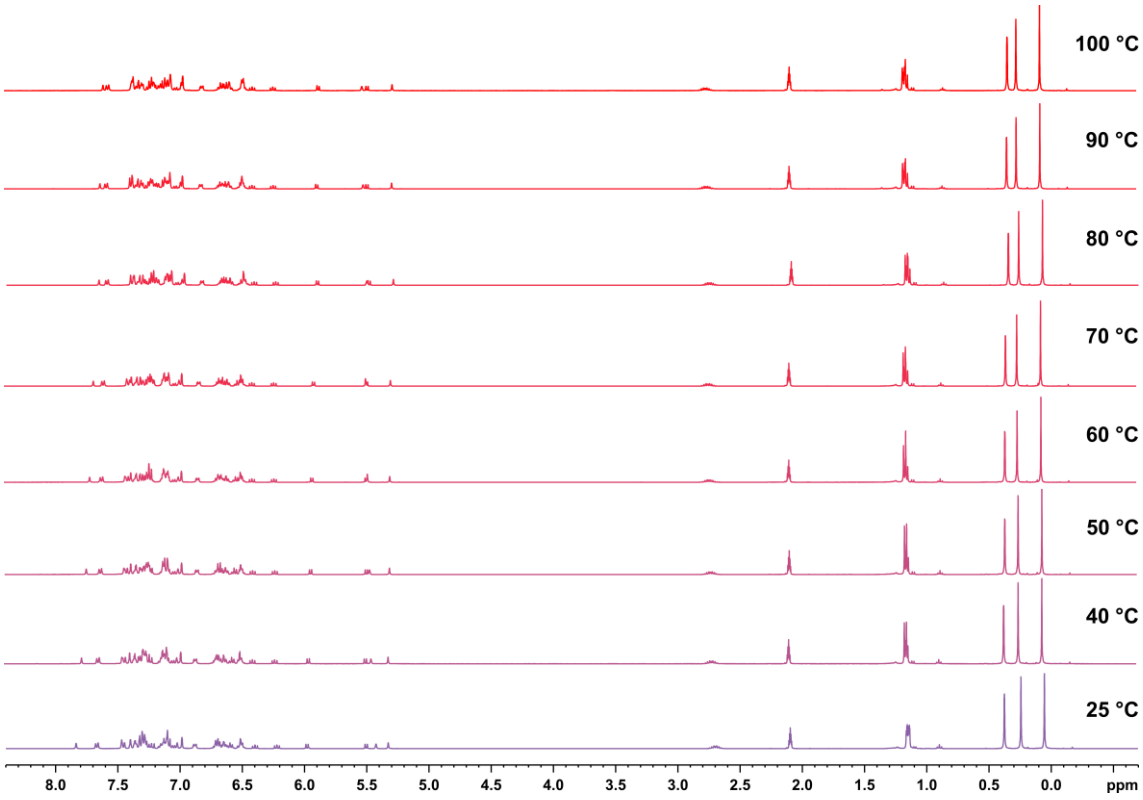

Figure S11. ^{1}H NMR monitoring (400.13 MHz, toluene-d_8) of [(Ar*BIAN)Co(η^3:η^1-$P_4SN_2(SiMe_3)_3$)] (**5**).

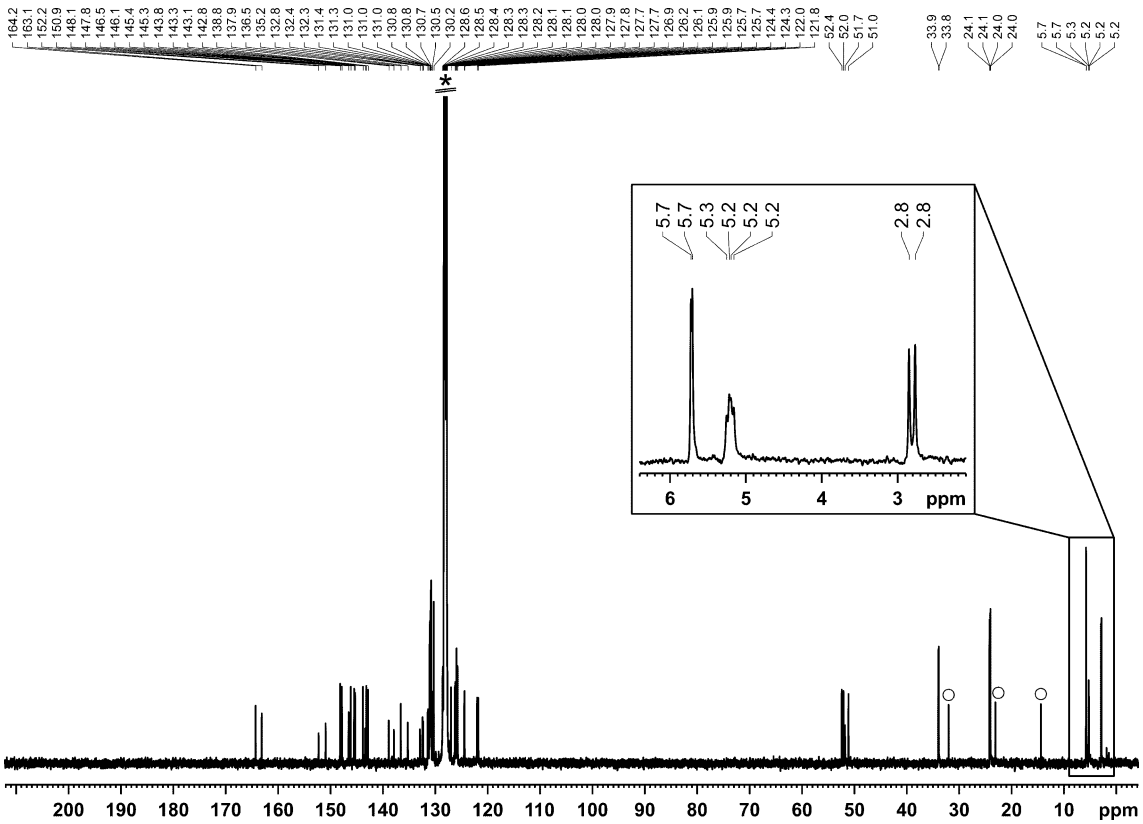

Figure S12. $^{13}C\{^{1}H\}$ NMR spectrum (100.60 MHz, 300 K, C_6D_6) of [(Ar*BIAN)Co(η^3:η^1-$P_4SN_2(SiMe_3)_3$)] (**5**); ○ *n*-hexane, * C_6D_6.

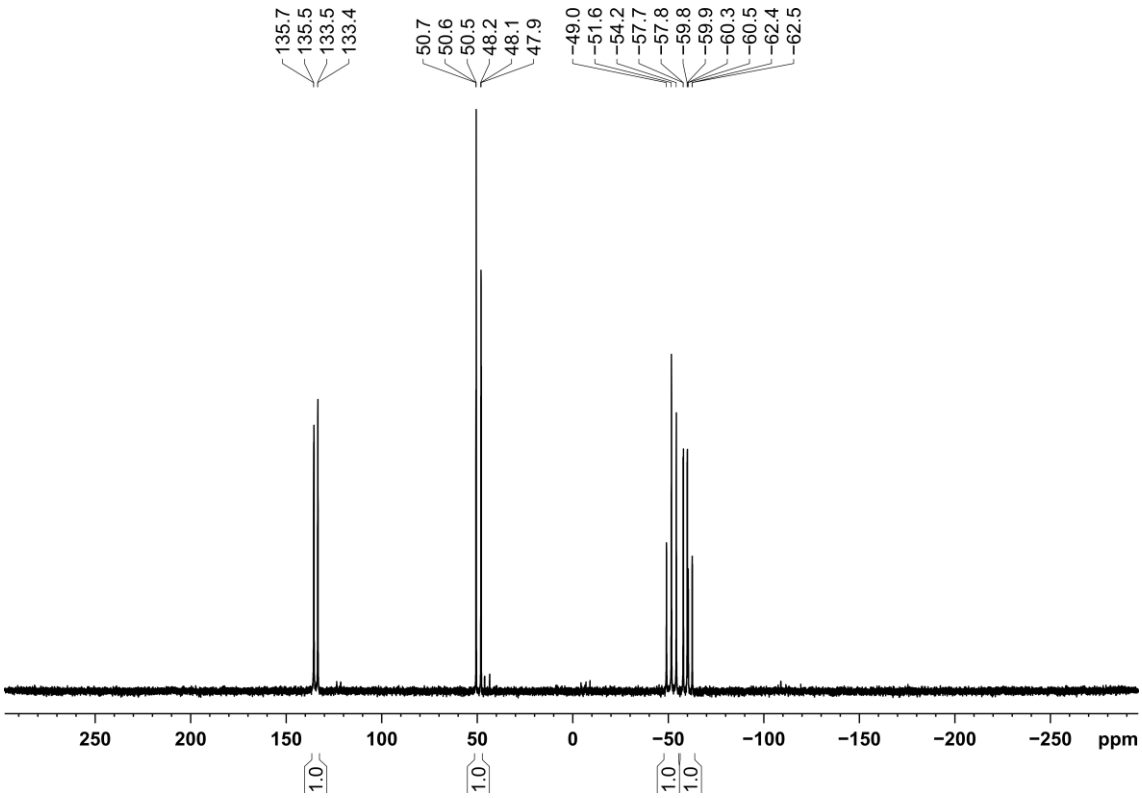

Figure S13. $^{31}P\{^{1}H\}$ NMR spectrum (162.04 MHz, 300 K, C_6D_6) of [(Ar*BIAN)Co(η^3:η^1-$P_4SN_2(SiMe_3)_3$)] (**5**).

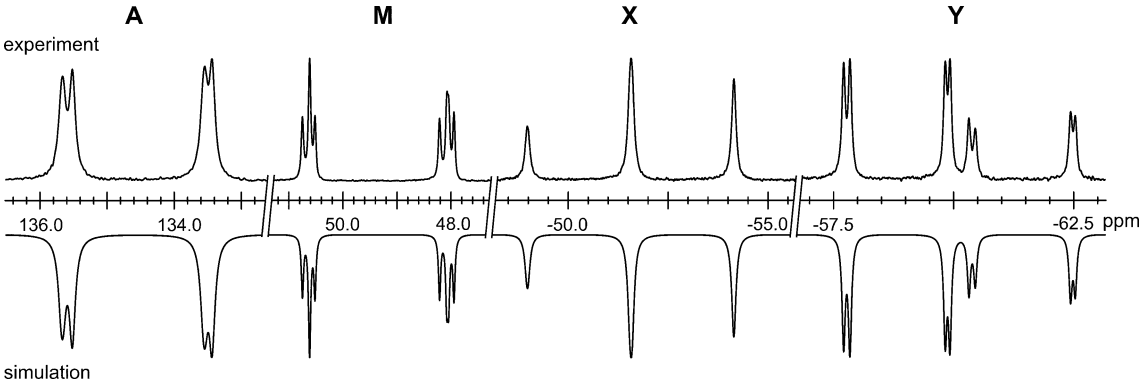

Figure S14. Section of the $^{31}P\{^{1}H\}$ NMR spectrum (162.04 MHz, 300 K, C_6D_6) of [(Ar*BIAN)Co(η^3:η^1-$P_4SN_2(SiMe_3)_3$)] (**5**); experimental (upwards) and simulation (downwards).

Table S3. Chemical shifts and coupling constants from the iterative fit of the AMXY spin system and schematic representation of the $CoP_4SN_2(SiMe_3)_3$ core of [(Ar*BIAN)Co(η^3:η^1-$P_4SN_2(SiMe_3)_3$)] (**5**).

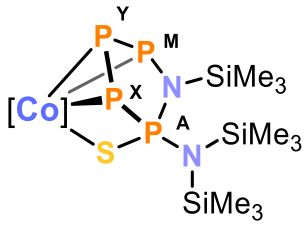	δ(A) = 134.5 ppm	$^{1}J_{XY}$ = −422.6 Hz
	δ(M) = 49.3 ppm	$^{1}J_{MY}$ = −425.4 Hz
	δ(X) = −51.8 ppm	$^{1}J_{AX}$ = −349.5 Hz
	δ(Y) = −59.9 ppm	J_{MX} = 30.6 Hz
		J_{AY} = 10.9 Hz
		J_{AM} = −21.3 Hz

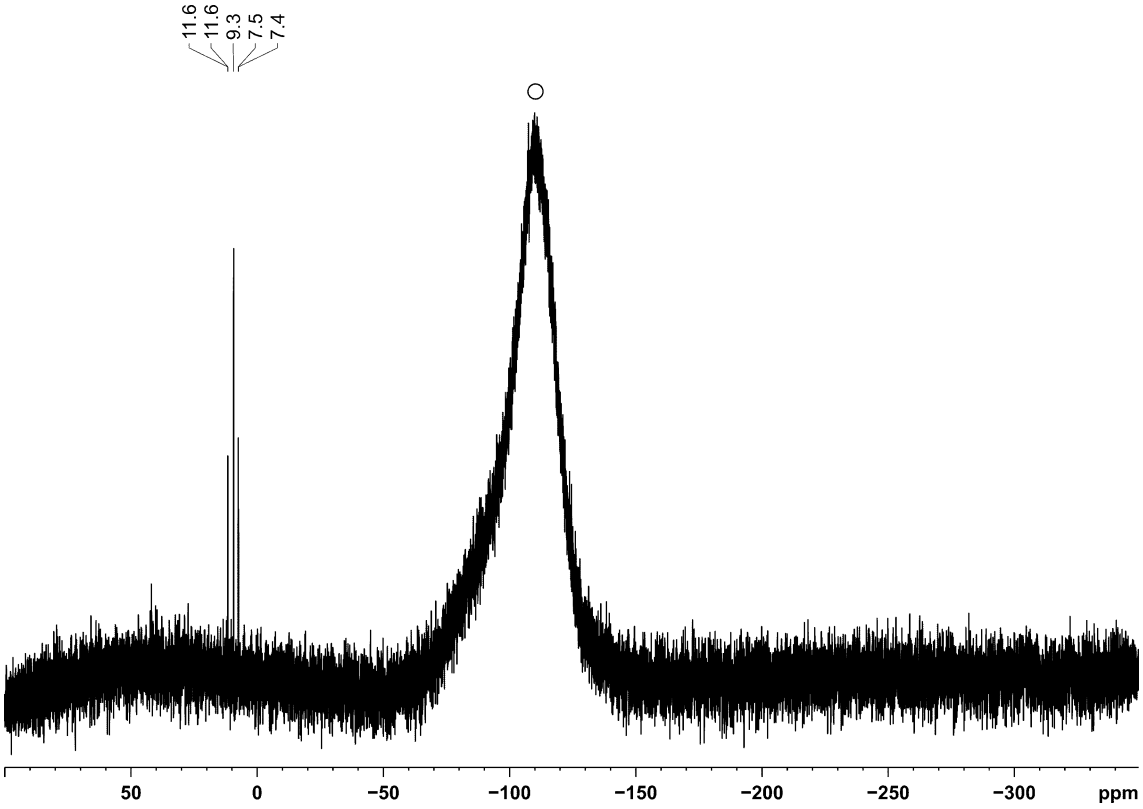

Figure S15. $^{29}Si\{^{1}H\}$ NMR spectrum (79.49 MHz, 300 K, C_6D_6) of [(Ar*BIAN)Co(η^3:η^1-$P_4SN_2(SiMe_3)_3$)] (**5**); ○ background signal from glass tube.

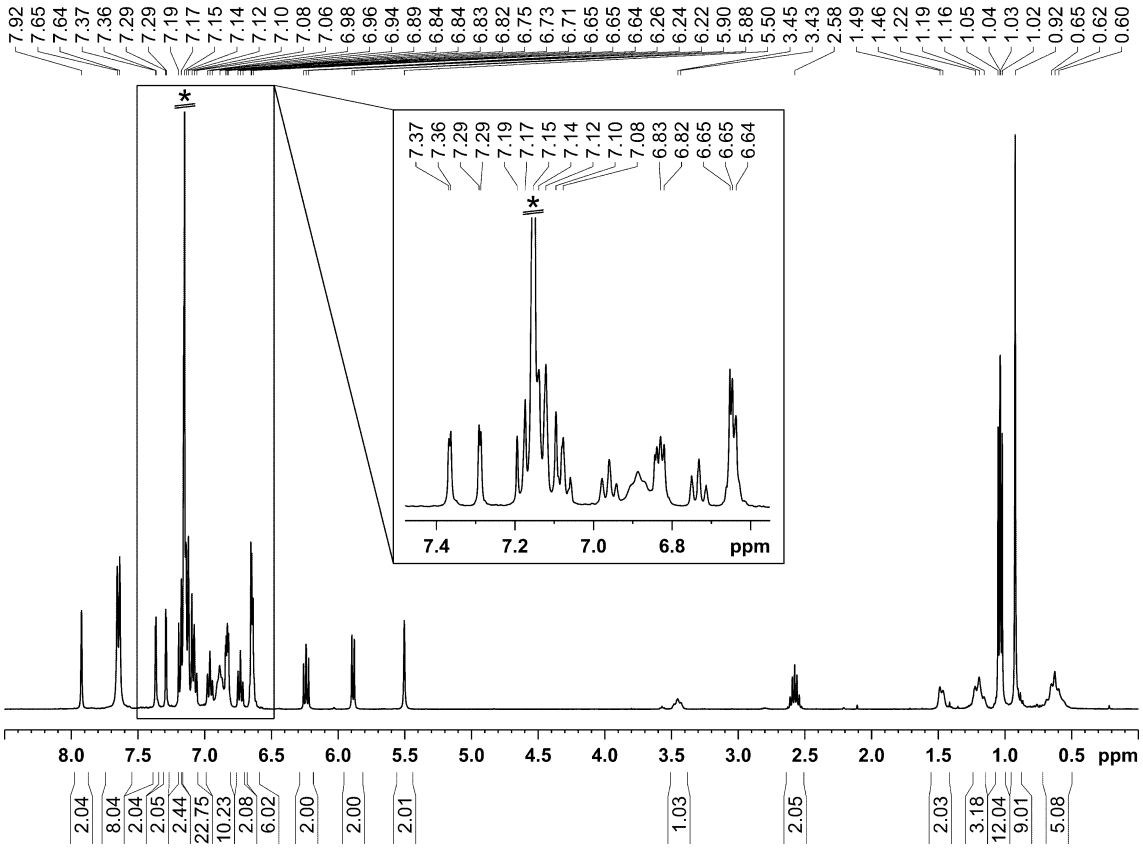

Figure S16. ^{1}H NMR spectrum (400.13 MHz, 300 K, C_6D_6,) of [(Ar*BIAN)Co(η^3:η^1-$P_4C(S)N(Cy)C(O)tBu$)] (**6a**); * C_6D_6.

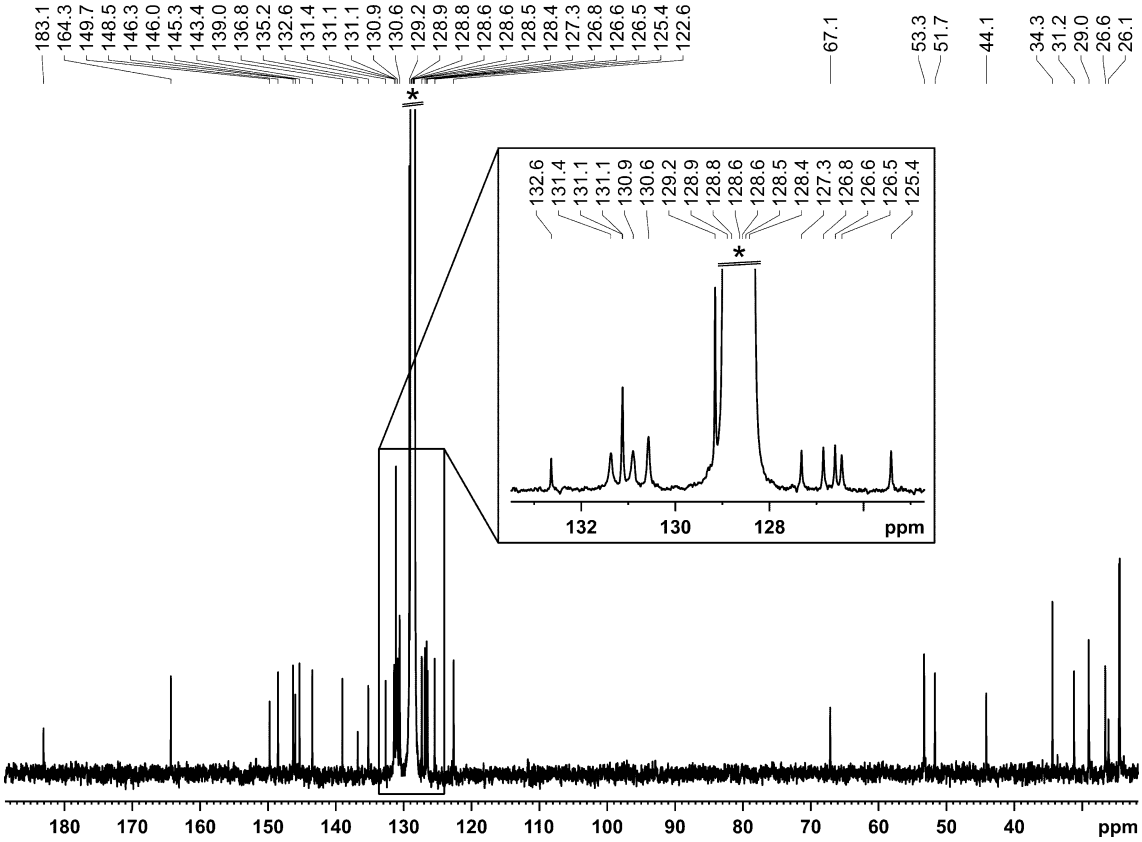

Figure S17. $^{13}C\{^{1}H\}$ NMR spectrum (100.66 MHz, 300 K, C_6D_6) of [(Ar*BIAN)Co(η^3:η^1-$P_4C(S)N(Cy)C(O)tBu$)] (**6a**); * C_6D_6.

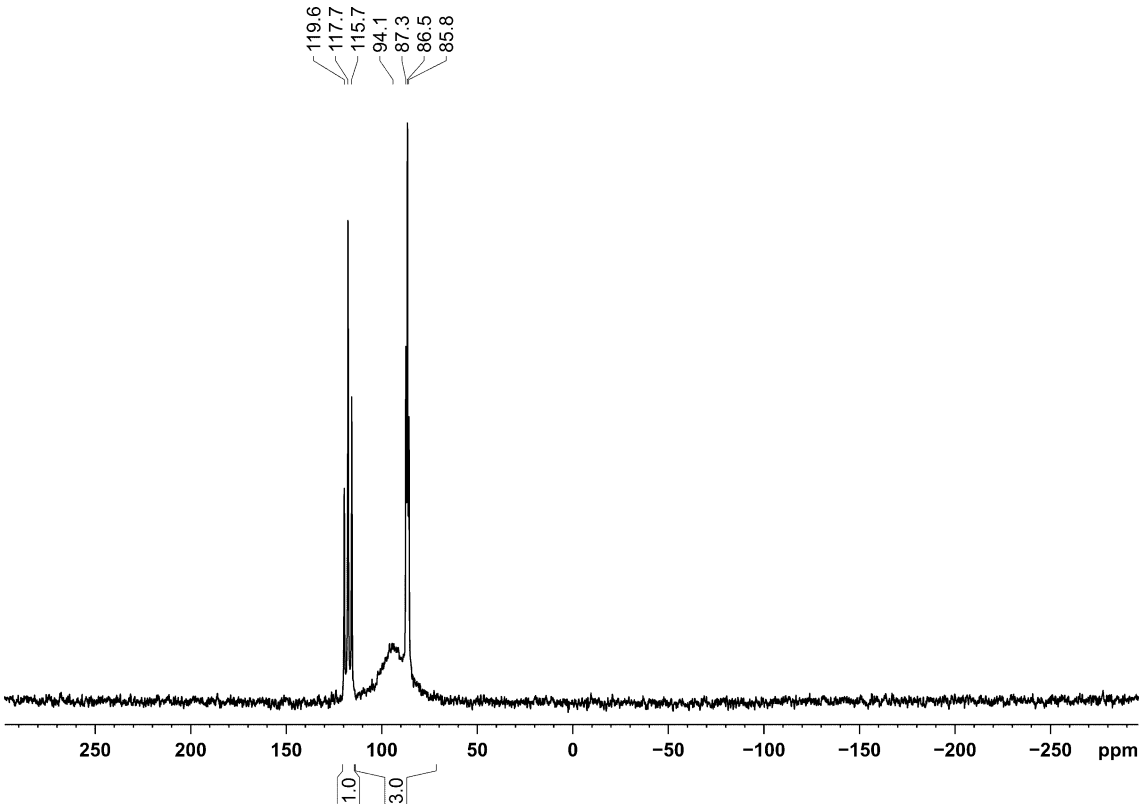

Figure S18. $^{31}P\{^{1}H\}$ NMR spectrum (162.04 MHz, 300 K, C_6D_6) of [(Ar*BIAN)Co(η^3:η^1-$P_4C(S)N(Cy)C(O)tBu$)] (**6a**).

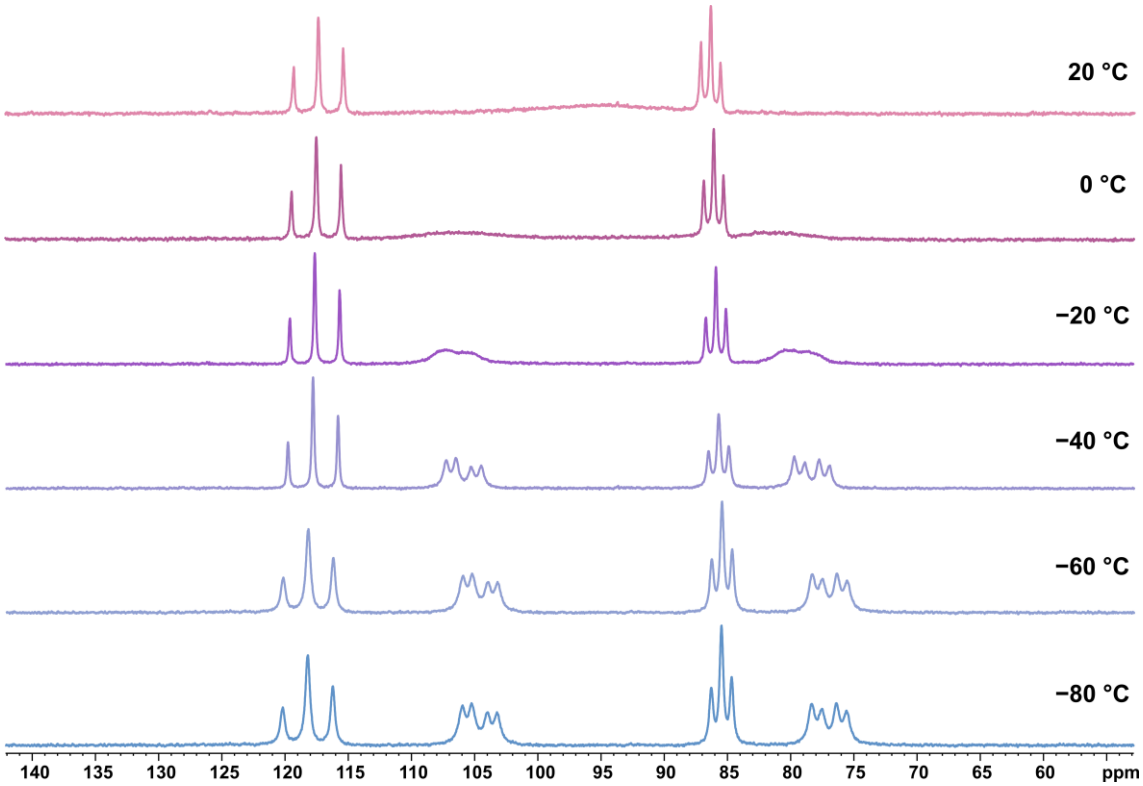

Figure S19. $^{31}P\{^{1}H\}$ NMR monitoring (161.98 MHz, toluene-d_8) of [(Ar*BIAN)Co(η^3:η^1-$P_4C(S)N(Cy)C(O)tBu$)] (**6a**).

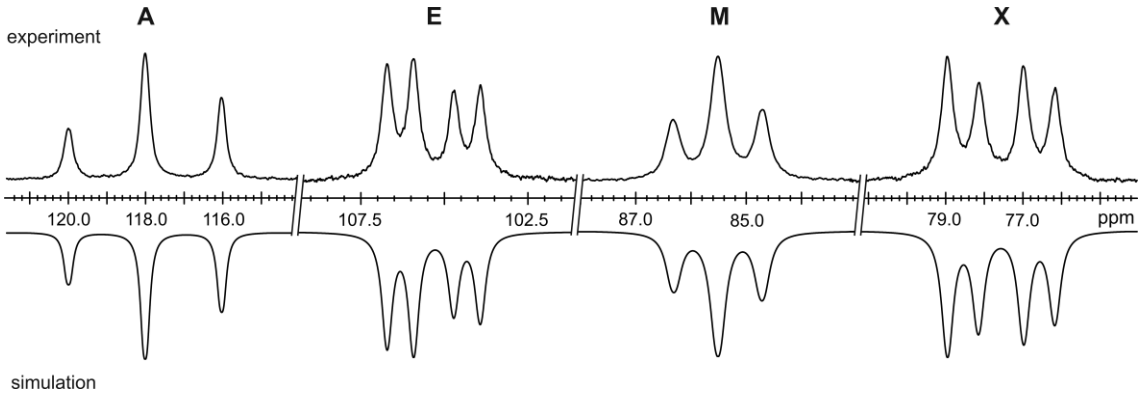

Figure S20. Section of the $^{31}P\{^{1}H\}$ NMR spectrum (161.98 MHz, 213 K, toluene-d_8) of [(Ar*BIAN)Co(η^3:η^1-$P_4C(S)N(Cy)C(O)tBu$)] (**6a**); experimental (upwards) and simulation (downwards).

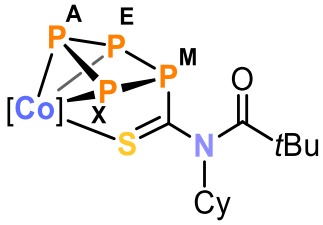

δ(A) = 117.9 ppm	$^{1}J_{AE}$ = −324.3 Hz
δ(E) = 105.4 ppm	$^{1}J_{AX}$ = −321.3 Hz
δ(M) = 85.5 ppm	$^{1}J_{EM}$ = −129.0 Hz
δ(X) = 77.6 ppm	$^{1}J_{MX}$ = −132.9 Hz
	$^{2}J_{AM}$ = 18.0 Hz
	$^{2}J_{EX}$ = 19.7 Hz

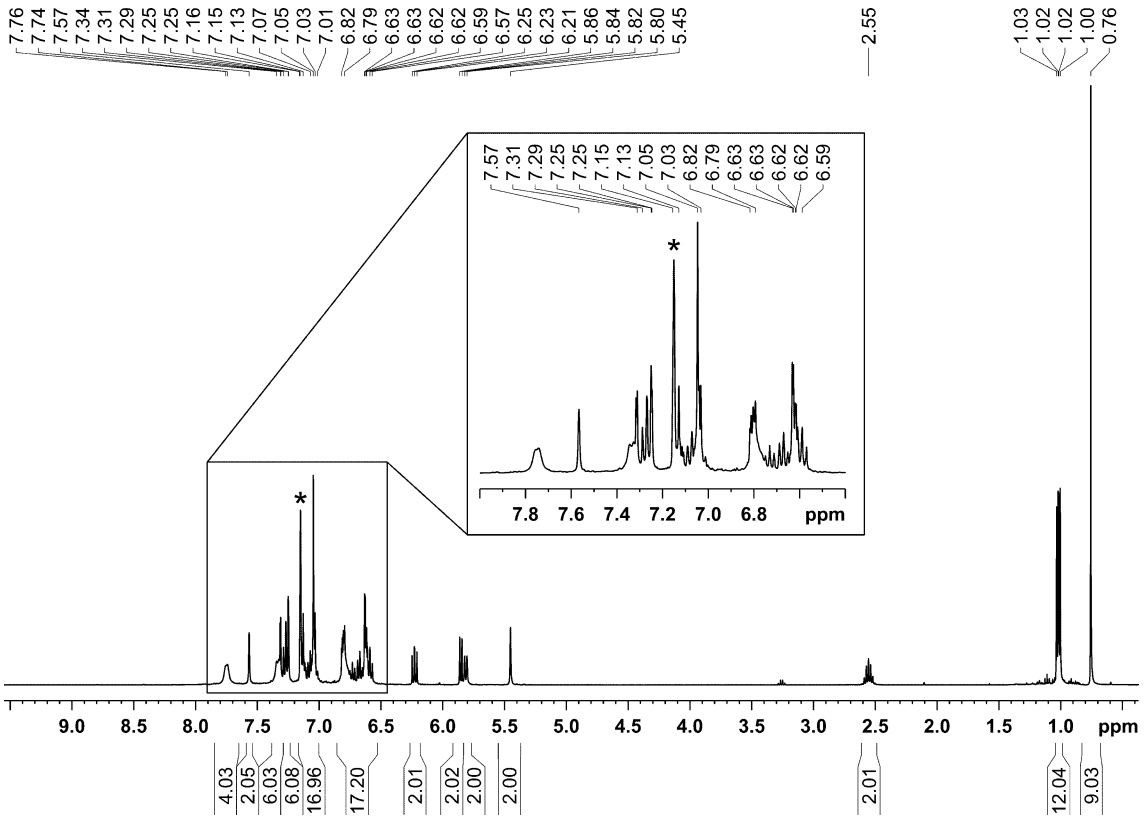

Figure S21. ^{1}H NMR spectrum (400.13 MHz, 300 K, C_6D_6) of [(Ar*BIAN)Co(η^3:η^1-$P_4C(S)N(Ph)C(O)t$Bu)] (**6b**); * C_6D_6.

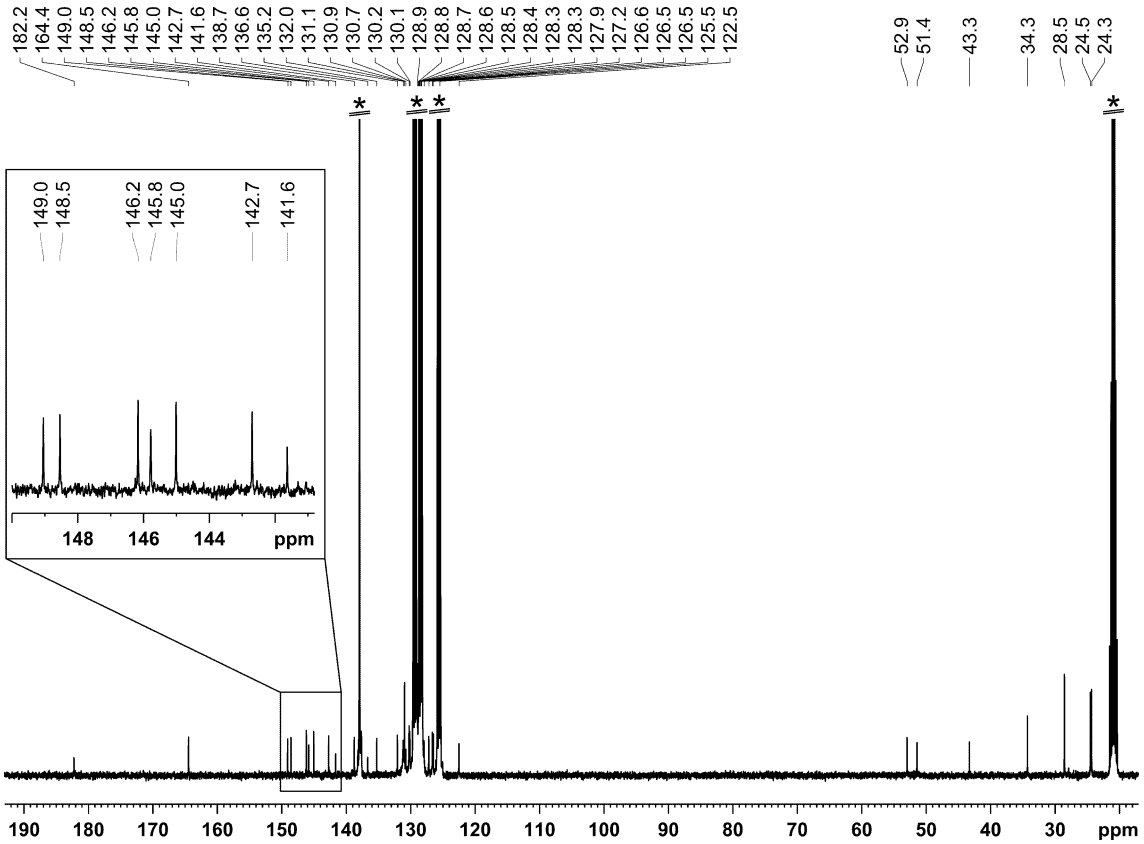

Figure S22. $^{13}C\{^{1}H\}$ NMR spectrum (100.61 MHz, 273 K, toluene-d_8) of [(Ar*BIAN)Co(η^3:η^1-$P_4C(S)N(Ph)C(O)t$Bu)] (**6b**); * toluene-d_8.

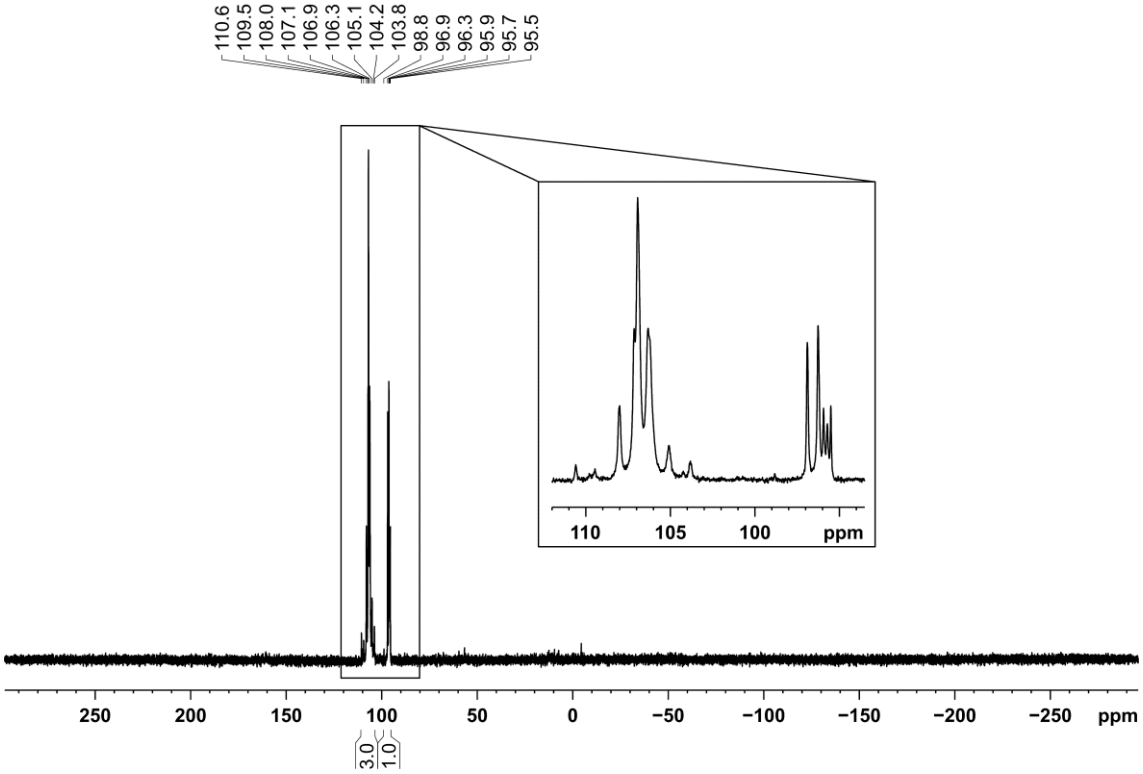

Figure S23. $^{31}P\{^{1}H\}$ NMR spectrum (162.04 MHz, 300 K, C_6D_6) of [(Ar*BIAN)Co(η^3:η^1-$P_4C(S)N(Ph)C(O)tBu$)] (**6b**).

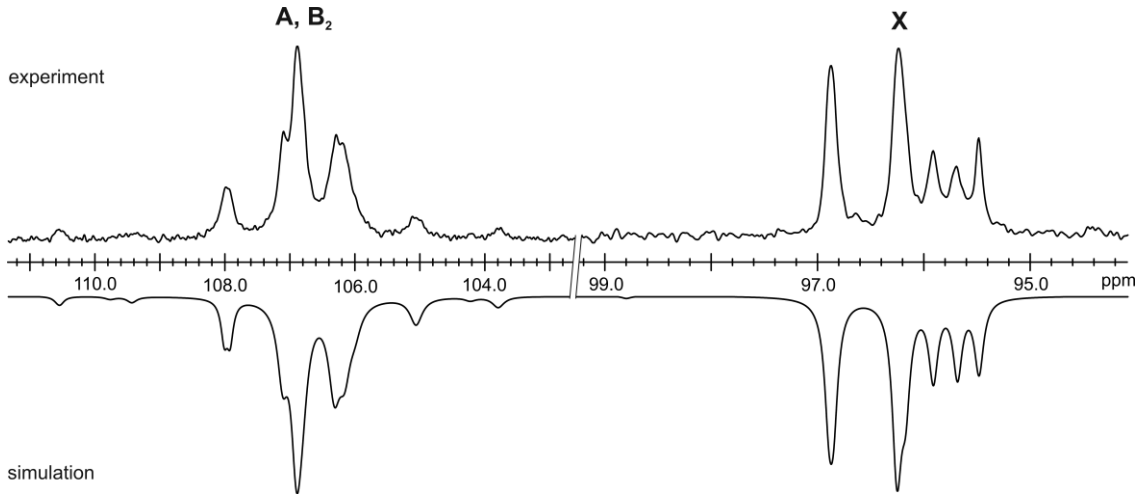

Figure S24. Section of the $^{31}P\{^{1}H\}$ NMR spectrum (162.04 MHz, 300 K, C_6D_6) of [(Ar*BIAN)Co(η^3:η^1-$P_4C(S)N(Ph)C(O)tBu$)] (**6b**); experimental (upwards) and simulation (downwards).

Table S4. Chemical shifts and coupling constants from the iterative fit of the AB_2X spin system and schematic representation of the $CoP_4C(S)N(Ph)C(O)tBu$ core of [(Ar*BIAN)Co(η^3:η^1-$P_4C(S)N(Ph)C(O)tBu$)] (**6b**).

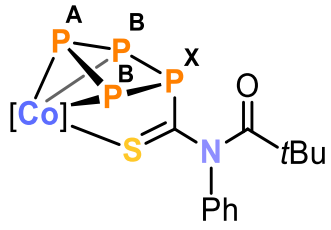	$\delta(A) = 108.0$ ppm	$^{1}J_{AB} = -325.4$ Hz
	$\delta(B) = 106.0$ ppm	$^{1}J_{BX} = -121.2$ Hz
	$\delta(X) = 96.2$ ppm	$^{2}J_{AX} = 14.5$ Hz

3.4.3 Additional Experiments

Reaction of [K(18c-6)][(Ar*BIAN)Co(η^3:η^1-P_4CS_2)] ([K(18c-6)]3) with [Ph_3C]OTf

In a J. valve NMR tube [K(18c-6)][(Ar*BIAN)Co(η^3:η^1-P_4CS_2)] ([K(18c-6)]**3**) (20 mg, 0.012 mmol, 1.0 equiv.) was dissolved in C_6D_6 (0.7 mL). To the resulting blue solution, solid [Ph_3C]OTf (5 mg, 0.012 mmol, 1.0 equiv.) was added inducing a color change to magenta within a few minutes. The NMR tube was closed and analyzed by $^{31}P\{^1H\}$ NMR spectroscopy (Figure S25). The resulting signal sets were successfully simulated as AXY_2 spin system (Figure S26 and Table S5).

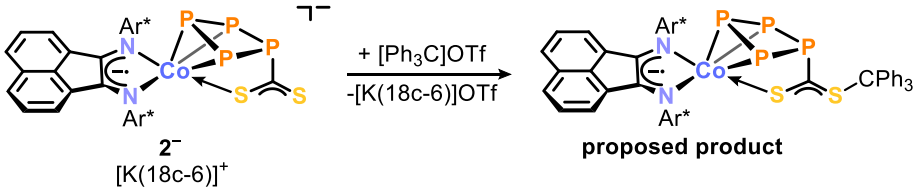

Scheme S1. Reaction of [K(18c-6)]**3** toward [Ph_3C]OTf with proposed reaction product; reagents and conditions: +1.0 eq. [Ph_3C]OTf; C_6D_6, r.t., 1 h.

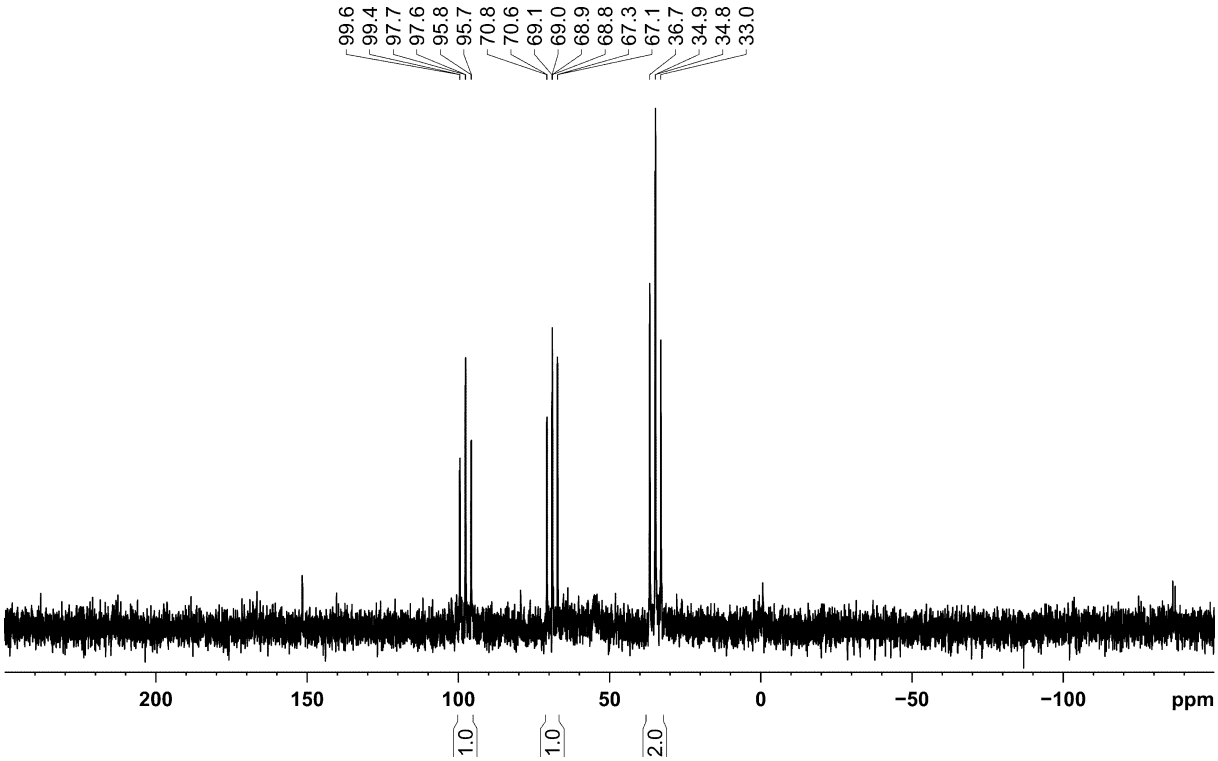

Figure S25. $^{31}P\{^1H\}$ NMR spectrum (162.04 MHz, 300 K, C_6D_6) of the reaction between [K(18c-6)][(Ar*BIAN)Co(η^3:η^1-P_4CS_2)] ([K(18c-6)]**3**) and [Ph_3C]OTf.

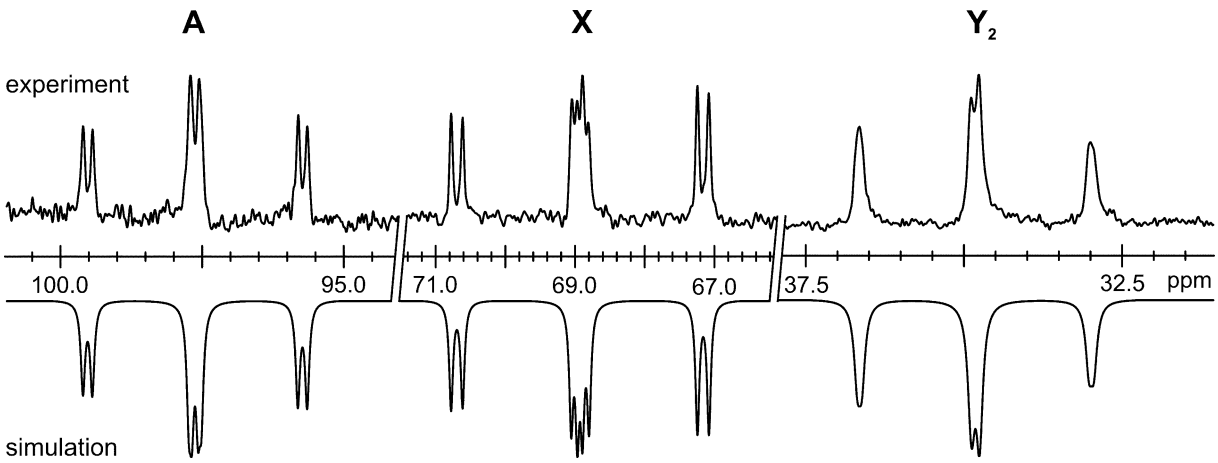

Figure S26. Section of the $^{31}P\{^{1}H\}$ NMR spectrum (162.04 MHz, 300 K, C_6D_6) of the reaction between ([K(18c-6)]**3**) and $[Ph_3C]OTf$; experimental (upwards) and simulation (downwards).

Table S5. Chemical shifts and coupling constants from the iterative fit of the AXY_2 spin of the reaction between ([K(18c-6)]**2**) and $[Ph_3C]OTf$.

δ(A) = 97.6 ppm	$^{1}J_{AY}$ = −307.5 Hz
δ(X) = 68.9 ppm	$^{1}J_{XY}$ = −286.9 Hz
δ(Y) = 34.9 ppm	$^{2}J_{AX}$ = 27.3 Hz

Reaction of [(Ar*BIAN)Co(η^3:η^1-$P_4SN_2(SiMe_3)_3$)] (5) with [*n*Bu_4N]CN

To a purple solution of [(Ar*BIAN)Co(η^3:η^1-$P_4SN_2(SiMe_3)_3$)] (**5**) (13 mg, 0.008 mmol, 1.0 equiv.) in C_6D_6 (0.7 mL), [*n*Bu_4N]CN (2.3 mg, 0.008 mmol, 1.0 equiv.) was added. The color changed immediately to blue and after 3 h the reaction mixture was transferred to a J. valve NMR tube and analyzed by $^{31}P\{^1H\}$ NMR spectroscopy (see Figure S27).

Reaction of [(Ar*BIAN)Co(η^3:η^1-$P_4SN_2(SiMe_3)_3$)] (5) with KOPh/18c-6

To a purple solution of [(Ar*BIAN)Co(η^3:η^1-$P_4SN_2(SiMe_3)_3$)] (**5**) (20 mg, 0.013 mmol, 1.0 equiv.) in C_6D_6 (0.7 mL) KOPh (1.7 mg, 0.013 mmol, 1.0 equiv.) and [18]crown-6 (18c-6, 3.3 mg, 0.013 mmol, 1.0 equiv.) was added. The color changed to blue and after 3 h the reaction mixture was transferred to a J. valve NMR tube and analyzed by $^{31}P\{^1H\}$ NMR spectroscopy (see Figure S27).

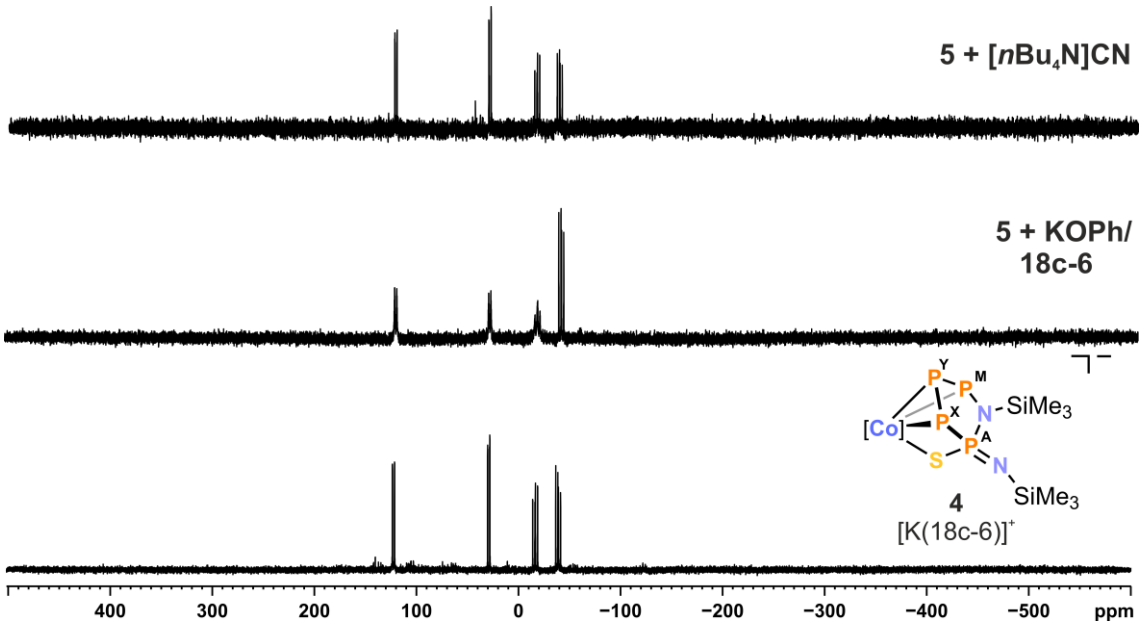

Figure S27. $^{31}P\{^1H\}$ NMR spectra (162.04 MHz, 300 K, C_6D_6) of the reactions between [(Ar*BIAN)Co(η^3:η^1-$P_4SN_2(SiMe_3)_3$)] (**5**) with [*n*Bu_4N]CN (*top*) and KOPh/18c-6 (*middle*); as well as [K(18c-6)][(Ar*BIAN)Co(η^3:η^1-$P_4SN_2(SiMe_3)_2$)] ([K(18c-6)]**4**) (*bottom*) for comparison.

Rearrangement of [(Ar*BIAN)Co(η^3:η^1-$P_4C(S)N(Ph)C(O)tBu$)] (6b)

A purple solution of [(Ar*BIAN)Co(η^3:η^1-$P_4C(S)N(Ph)C(O)tBu$)] (**6b**) (20 mg, 0.013 mmol, 1.0 equiv.) in C_6D_6 (0.7 mL) was heated to 45 °C for 1 d to complete the reaction. The reaction mixture was transferred to a J. Young valve NMR tube and analyzed by $^{31}P\{^1H\}$ NMR spectroscopy (see Figure S28).

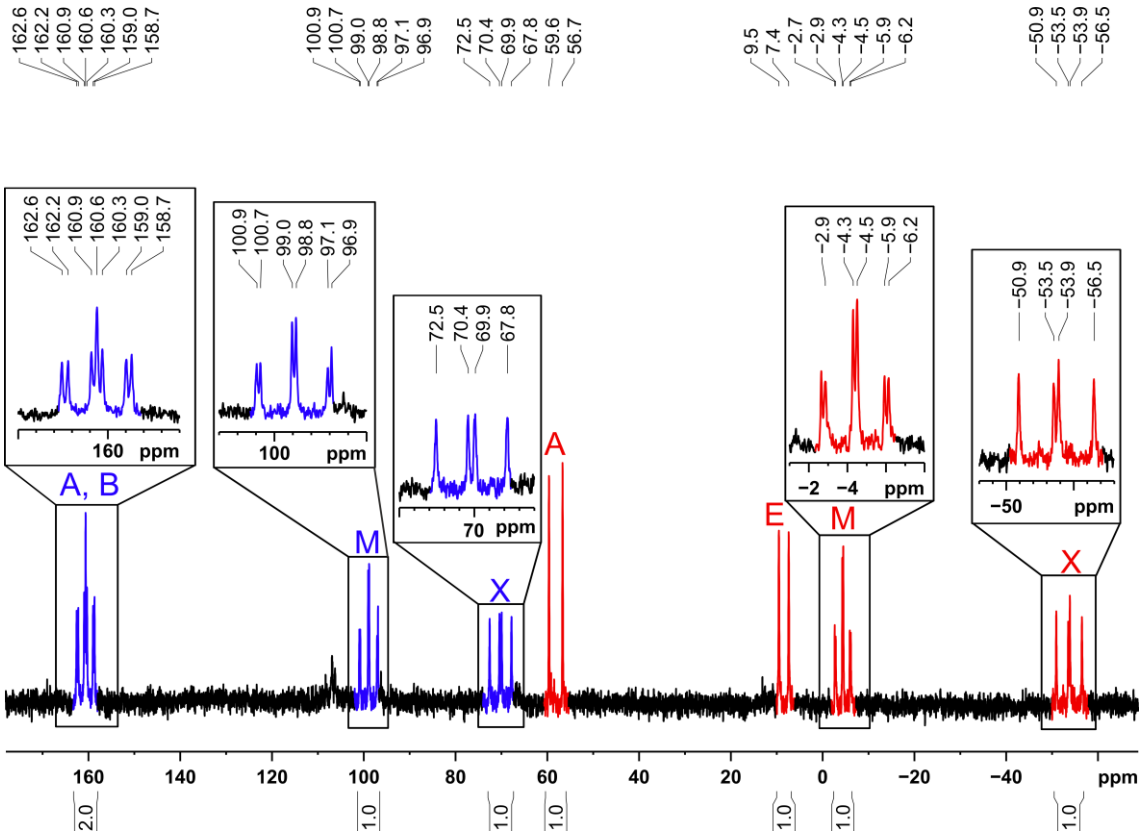

Figure S28. $^{31}P\{^1H\}$ NMR spectrum (162.04 MHz, 300 K, C_6D_6) after the thermally induced rearrangement of [(Ar*BIAN)Co(η^3:η^1-$P_4C(S)N(Ph)C(O)tBu$)] (**6b**) exhibiting two sets of signals attributed to two proposed spin systems marked in *blue* (ABMX) and *red* (AEMX).

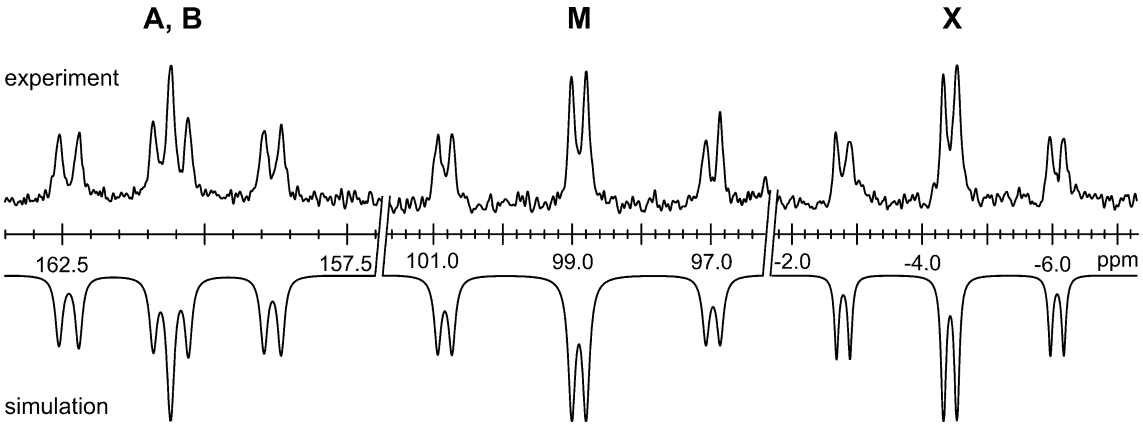

Figure S29. Section of the $^{31}P\{^1H\}$ NMR spectrum (162.04 MHz, 300 K, C_6D_6) of the thermally induced rearrangement of [(Ar*BIAN)Co(η^3:η^1-$P_4C(S)N(Ph)C(O)tBu$)] (6b); experimental (upwards) and simulation (downwards); simulations as AA'MX and A_2MX spin systems did not converge.

Table S6. Chemical shifts and coupling constants from the iterative fit of the ABMX spin of the thermally induced rearrangement of [(Ar*BIAN)Co(η^3:η^1-P_4C(S)N(Ph)C(O)*t*Bu)] (**6b**); simulations as AA'MX and A_2MX spin systems did not converge.

δ(A) = 160.4 ppm	$^1J_{AM}$ = −312.5 Hz
δ(B) = 160.7 ppm	$^1J_{BM}$ = −314.5 Hz
δ(M) = 98.9 ppm	$^1J_{AX}$ = −263.9 Hz
δ(X) = −4.4 ppm	$^1J_{BX}$ = −268.3 Hz
	$^2J_{MX}$ = 33.5 Hz
	$^2J_{AB}$ = 6.3 Hz

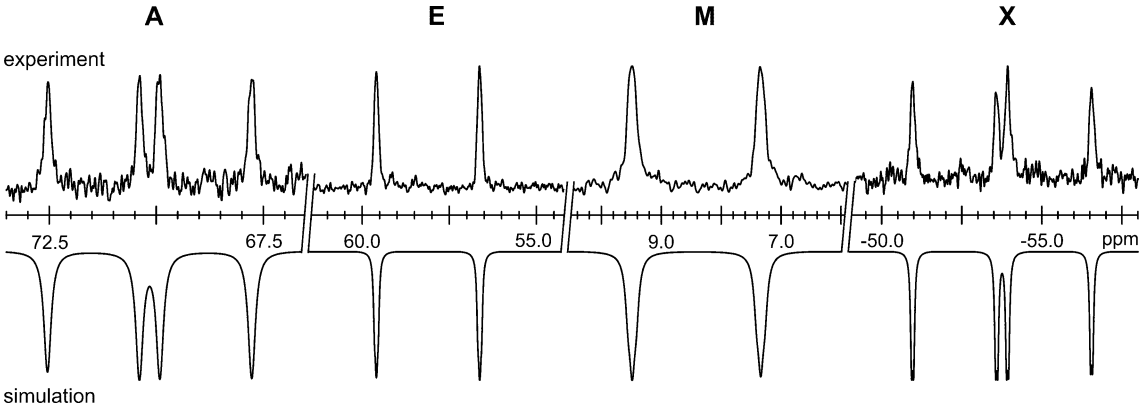

Figure S30. Section of the $^{31}P\{^1H\}$ NMR spectrum (162.04 MHz, 300 K, C_6D_6) of the thermally induced rearrangement of [(Ar*BIAN)Co(η^3:η^1-P_4C(S)N(Ph)C(O)*t*Bu)] (**6b**); experimental (upwards) and simulation (downwards).

Table S7. Chemical shifts and coupling constants from the iterative fit of the AEMX spin of the thermally induced rearrangement of [(Ar*BIAN)Co(η^3:η^1-P_4C(S)N(Ph)C(O)*t*Bu)] (**6b**).

δ(A) = 70.1 ppm	$^1J_{AX}$ = −425.3 Hz
δ(E) = 58.1 ppm	$^1J_{EX}$ = −480.5 Hz
δ(M) = 8.4 ppm	$^1J_{AM}$ = −347.8 Hz
δ(X) = −53.7 ppm	$^2J_{AE}$ = 6.8 Hz
	$^2J_{MX}$ = −10.7 Hz
	$^3J_{EM}$ = −11.2 Hz

3.4.4 Proposed Reaction Mechanism

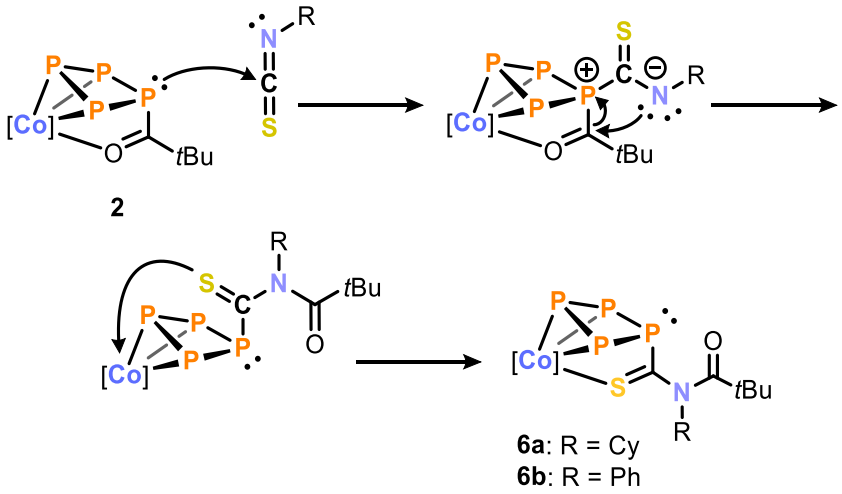

Scheme S2. Proposed reaction mechanism for insertion reaction of isothiocyanates RNCS (R = Cy, Ph) in P−C bonds of [(Ar*BIAN)Co(η^3:η^1-P_4C(O)*t*Bu)] (**2**) yielding **6a** and **6b**.

3.4.5 UV/Vis Spectra

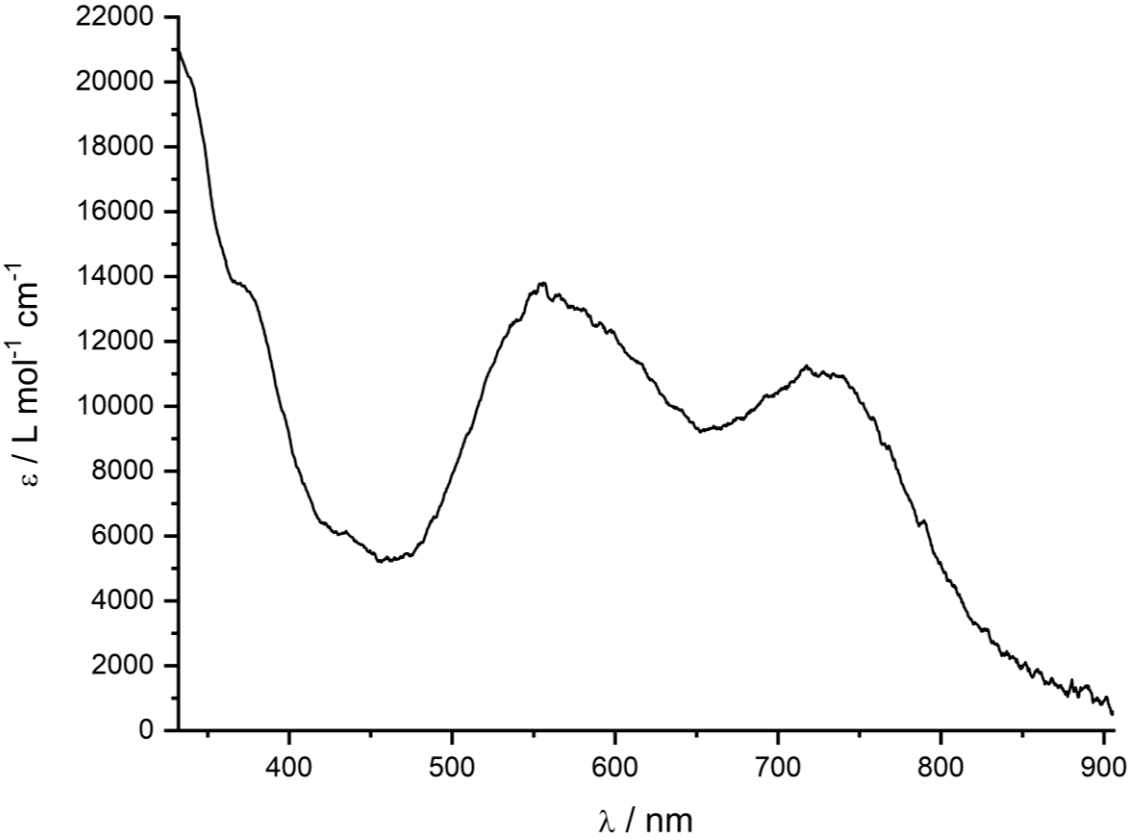

Figure S31. UV/Vis spectrum of [K(18c-6)][(Ar*BIAN)Co(η^3:η^1-P_4CS_2)] ([K(18c-6)]**3**) recorded in THF.

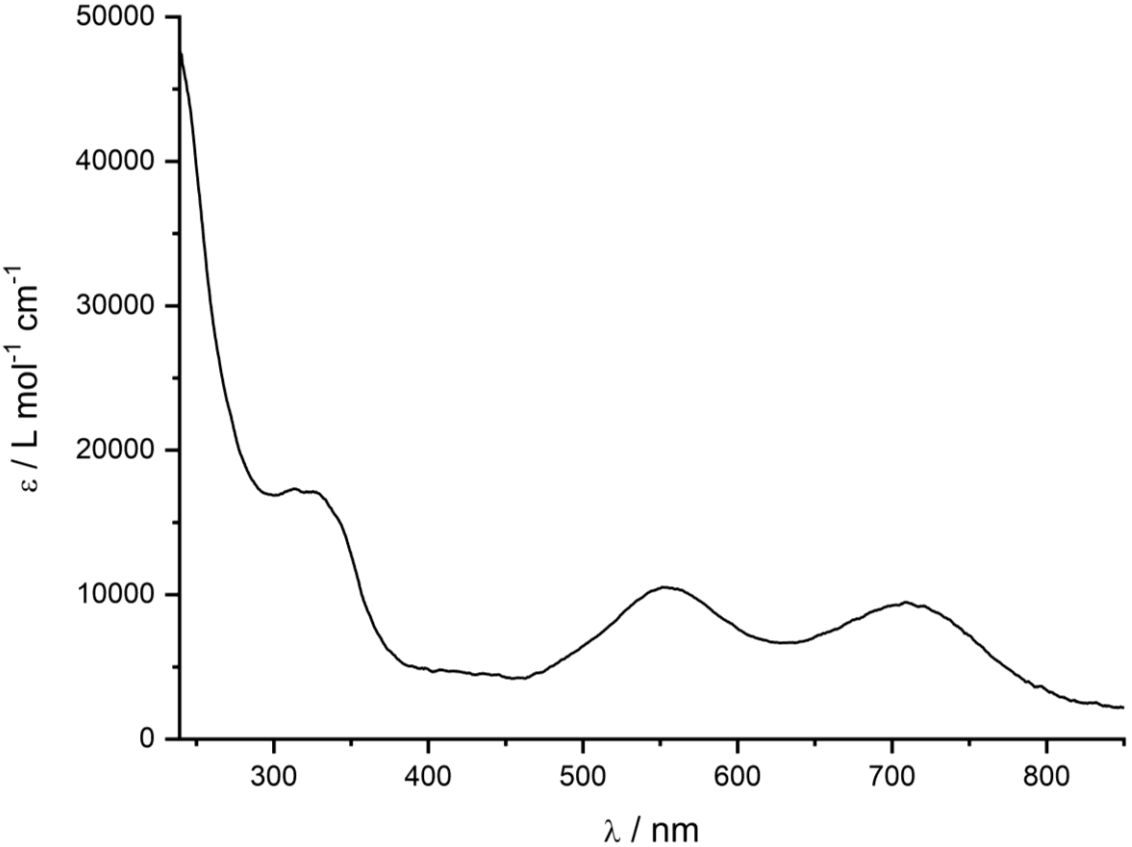

Figure S32 UV/Vis spectrum of [K(18c-6)][(Ar*BIAN)Co(η^3:η^1-$P_4SN_2(SiMe_3)_2$)] ([K(18c-6)]**4**) recorded in THF.

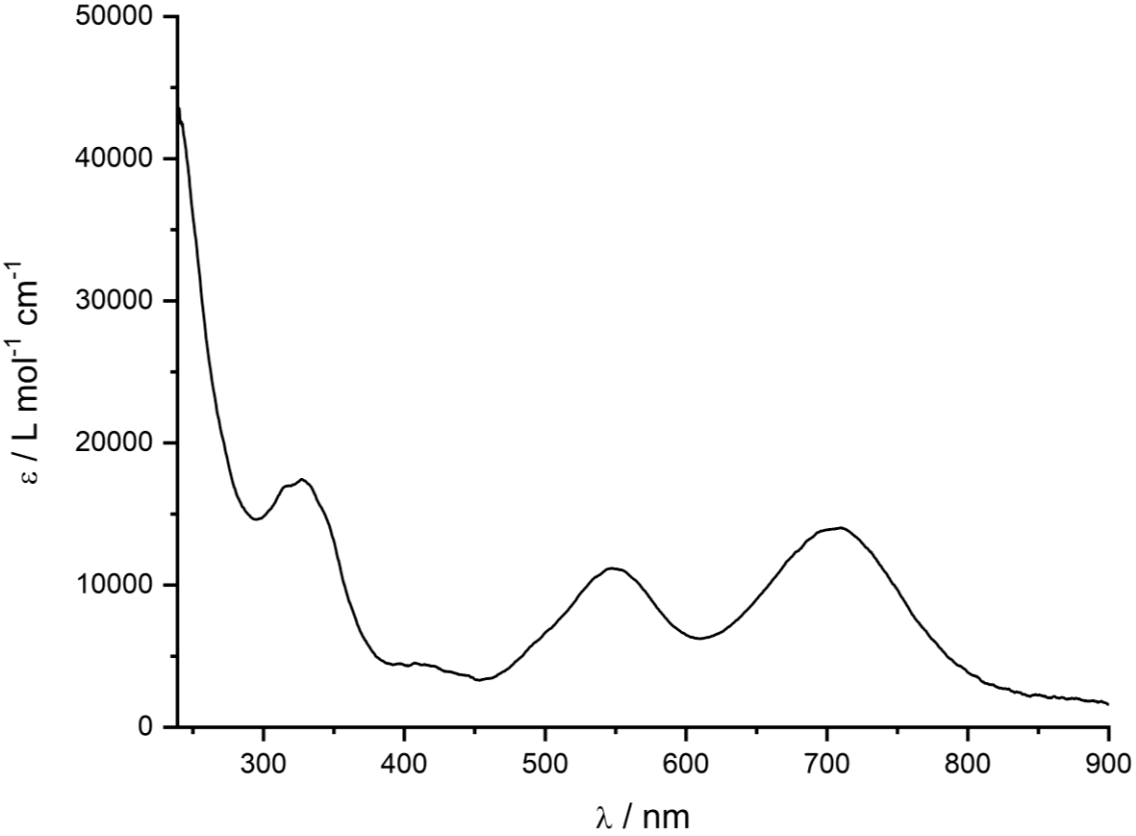

Figure S33. UV/Vis spectrum of [(Ar*BIAN)Co(η^3:η^1-$P_4SN_2(SiMe_3)_3$)] (**5**) recorded in THF.

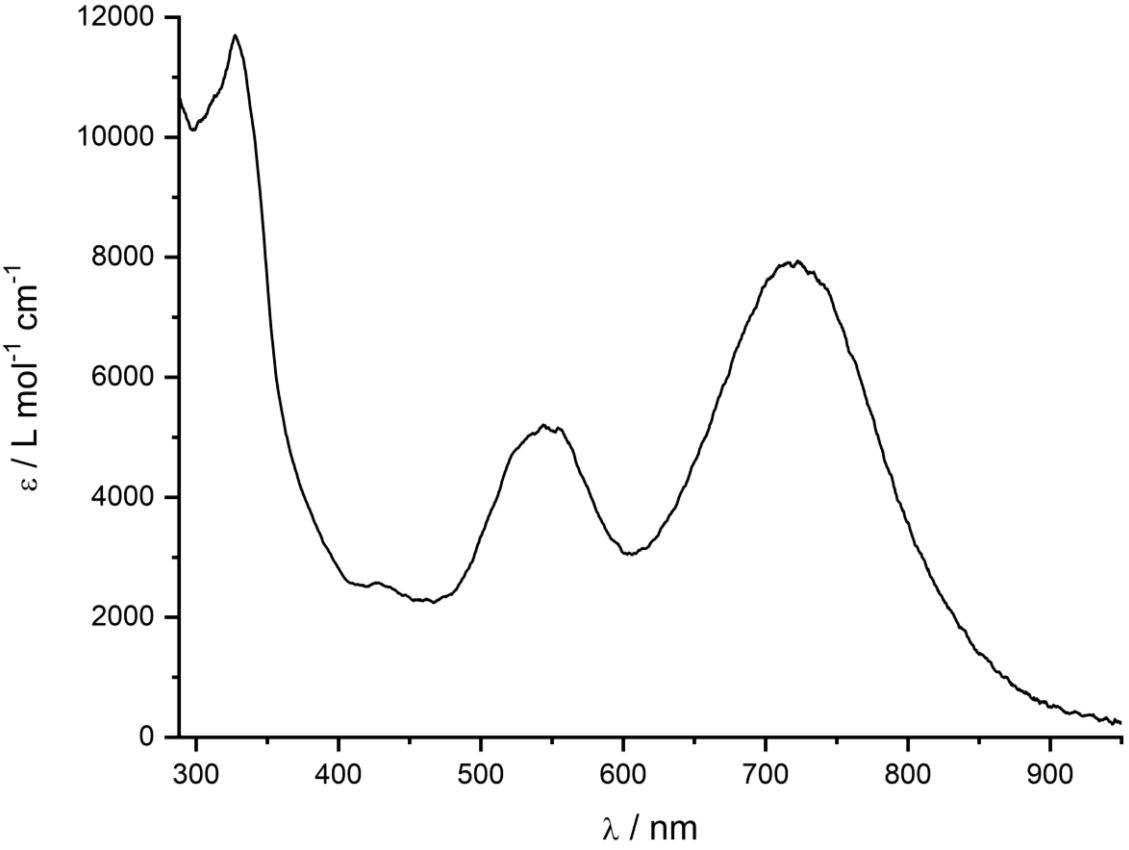

Figure S34. UV/Vis spectrum of [(Ar*BIAN)Co(η^3:η^1-$P_4C(S)N(Cy)C(O)t$Bu)] (**6a**) recorded in toluene.

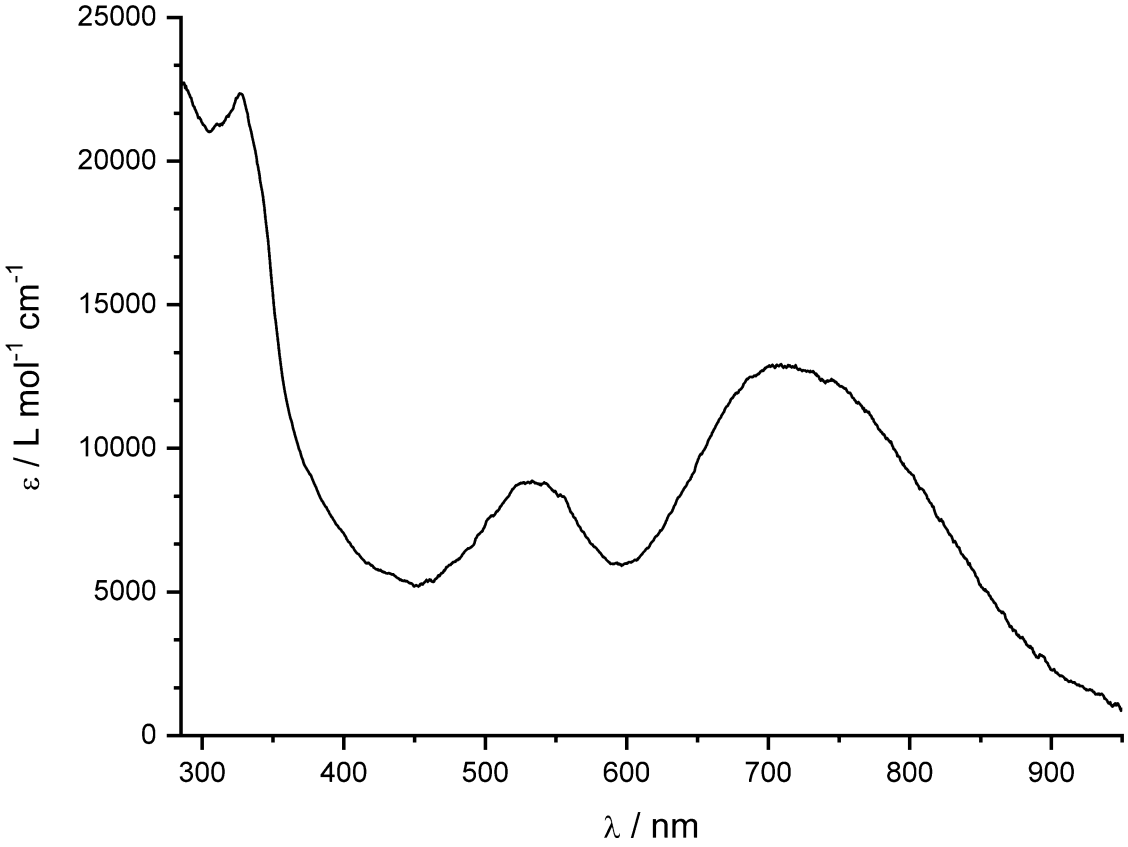

Figure S35. UV/Vis spectrum of [(Ar*BIAN)Co(η^3:η^1-P_4C(S)N(Ph)C(O)*t*Bu)] (**6b**) recorded in toluene.

3.4.6 IR Spectra

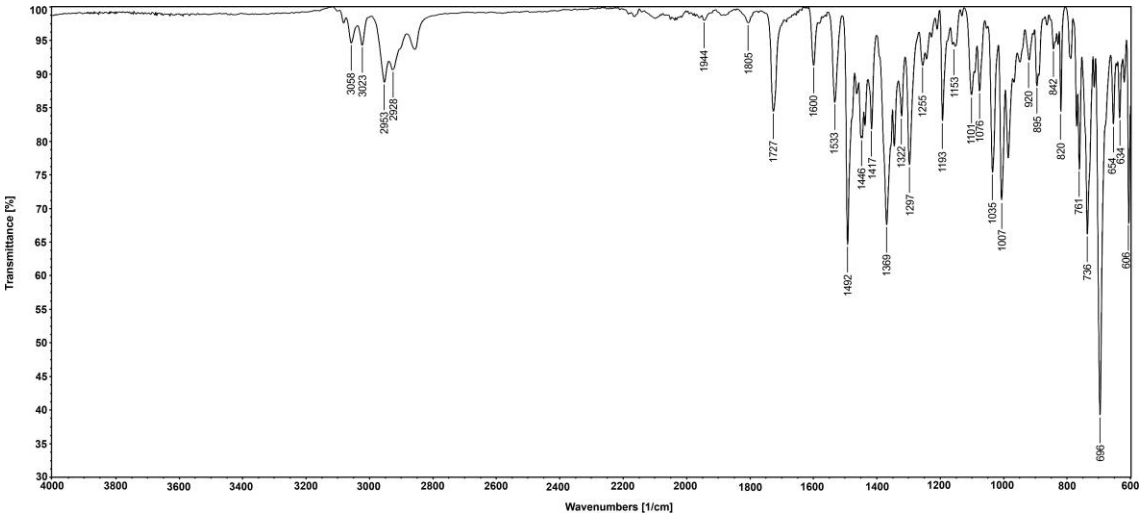

Figure S36. Solid state ATR-IR spectrum of [(Ar*BIAN)Co(η^3:η^1-P_4C(S)N(Cy)C(O)*t*Bu)] (**6a**).

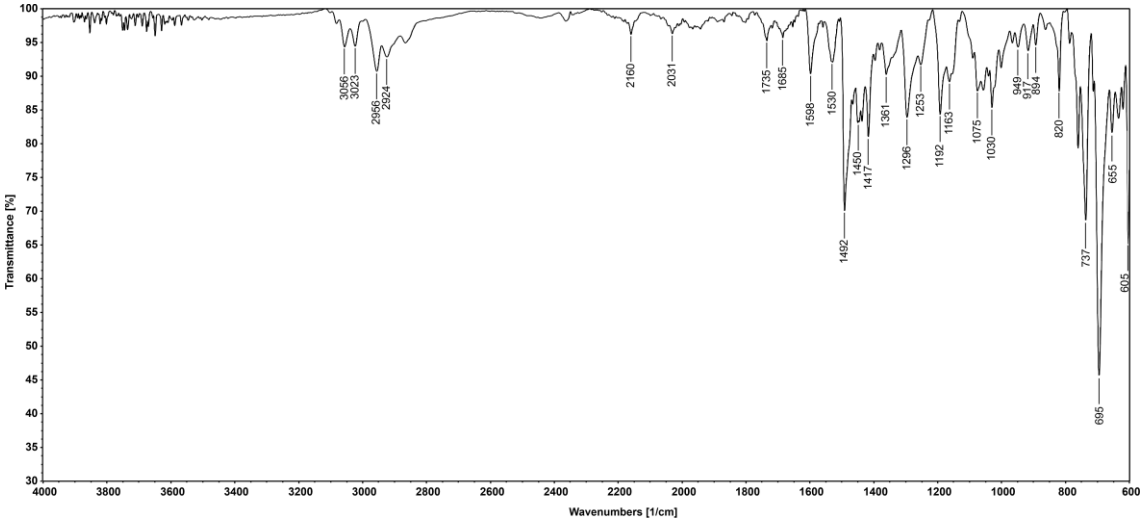

Figure S37. Solid state IR spectrum of [(Ar*BIAN)Co(η^3:η^1-P_4C(S)N(Ph)C(O)*t*Bu)] (**6b**).

3.4.7 Single Crystal X-Ray Diffraction Data

The single-crystal X-ray diffraction data were recorded on Rigaku Oxford Diffraction SuperNova Atlas (TitanS2) or XtaLAB Synergy DW (HyPix-Arc 150) diffractometers with Cu-Kα radiation (λ = 1.54184 Å). The solid state structures for [K(18c-6)]**4** and **5** were measured at the European Synchrotron BM20 (λ = 0.56385).[12] Crystals were selected under mineral oil, mounted on micromount loops and quench-cooled using an Oxford Cryosystems open flow N_2 cooling device.

Either semi-empirical multi-scan absorption corrections[23] or analytical ones[24] were applied to the data. The structures were solved with SHELXT[25] solution program using dual methods and by using Olex2 as the graphical interface.[26] The models were refined with ShelXL[27] using full matrix least squares minimization on F^2.[28] The hydrogen atoms were located in idealized positions and refined isotropically with a riding model.

[K(18c-6)]**4**: The crystal of [K(18c-6)]**4** contained two severely disordered toluene molecules per asymmetric unit. They were refined by using the solvent mask command: A solvent mask was calculated and 376 electrons were found in a volume of 1704 $Å^3$ in one void per unit cell. This is consistent with the presence of 2.0 toluene per Asymmetric Unit which account for 400 electrons per unit cell. As [K(18c-6)]**4** was crystallized by slow diffusion of *n*-hexane into a saturated toluene solution of [K(18c-6)]**4** this serves as evidence for the presence of toluene in this position. One molecule of toluene is clearly visible in vicinity of the crown ether but could not be properly modelled due to severe disorder.

5: The crystal of **5** contained 1.75 *n*-hexane molecules per in two voids per asymmetric unit. They were refined by using the solvent mask command: A solvent mask was calculated and 169 electrons were found in a volume of 924 $Å^3$ in two voids per unit cell. This is consistent with the presence of 0.75 *n*-hexane and 1.0 *n*-hexane per Formula Unit which account for 175 electrons per unit cell. As **5** was crystallized from *n*-hexane this serves as evidence for the presence of *n*-hexane in these positions, though they proved to be severely disordered.

6b: The crystal of **6b** contained 1.5 severely disordered toluene molecules and 1 severely disordered *n*-hexane molecules per asymmetric unit. They were refined by using the solvent mask command: A solvent mask was calculated, and 268 electrons were found in a volume of 1313 $Å^3$ in two voids per unit cell. This is consistent with the presence of 1.5 molecules toluene and 1.0 molecule of n-*h*exane per Formula Unit which account for 250 electrons per unit cell. As **6b** was crystallized from a mixture slow diffusion of *n*-hexane

and concentrated toluene solution of **6b** this serves as evidence for the presence of toluene and *n*-hexane in these positions, though they were severely disordered.

The following section provides figures of the molecular structures with selected bond lengths and angles, which were not given in section 3.2 itself.

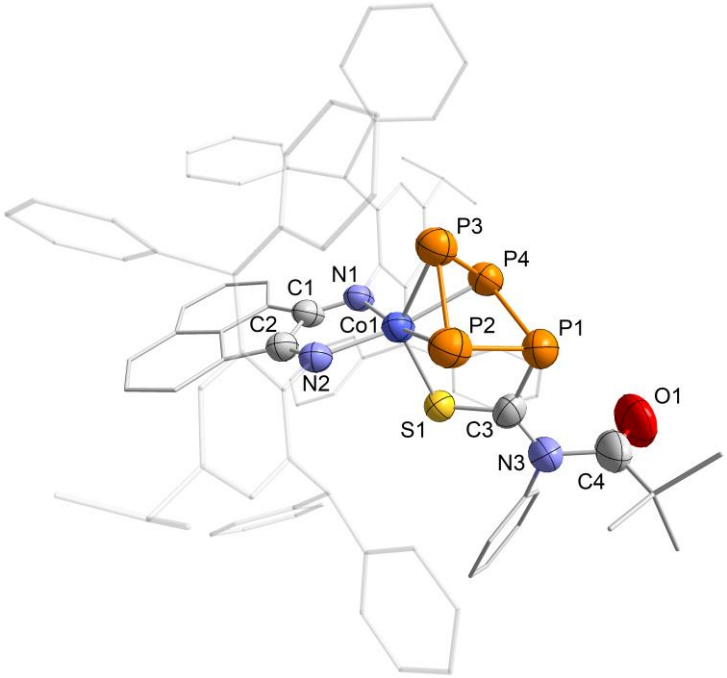

Figure S38. Solid-state molecular structure of [(Ar*BIAN)Co(η^3:η^1-P_4C(S)N(Ph)C(O)*t*Bu)] (**6b**) shown at the 50% probability level. Hydrogen atoms, and disorder in the *t*Bu-group omitted for clarity. The asymmetric unit contained a second crystallographically independent molecule which is not shown. Selected bond lengths [Å] and angles [°]: P1−P2 2.240(2), P2−P3 2.163(2), P3−P4 2.169(2), P1−P4 2.2339(2), Co1−P2 2.2818(2), Co1−P3 2.2994(2), Co1−P4 2.2851(2), Co1−S1 2.2597(1), Co1−N1 1.976(3), Co1−N2 1.984(4), C1−N1 1.295(6), C2−N2 1.325(5), C1−C2 1.446(6), P1−C3 1.861(6), C4−O1 1.211(8), C3−N3 1.343(7), C4−N3 1.462(7), P1−P2−P3 89.20(8), P2-P3-P4 84.96(8), P3-P4-P1 89.20(8), P4-P1-P2 81.68(7), Co1-S1-C3 104.8(2), C3-N3-C4 119.2(5).

Table S8. Crystallographic data and structure refinement for compounds **1-4a**.

Compound	**[K(18c-6)]3**	**[K(18c-6)]4**	**5**
CCDC	2279508	2325202	2279478
Empirical formula	$C_{102}H_{100}CoKN_2O_6P_4S_2$	$C_{114}H_{126}CoKN_4O_6P_4SSi_2$	$C_{91}H_{95}CoN_4P_4SSi_3$
Formula weight	1735.86	1958.33	1543.84
Temperature/K	123.0(1)	100.0(1)	100.0(1)
Crystal system	triclinic	monoclinic	triclinic
Space group	*P-1*	$P2_1/c$	*P-1*
a/Å	13.3668(6)	18.4952(7)	12.2911(3)
b/Å	14.1612(7)	21.7710(3)	13.8135(4)
c/Å	26.4289(10)	33.4049(12)	27.6744(6)
α/°	91.088(3)	90	88.140(2)
β/°	102.650(3)	128.156(6)	80.963(2)
γ/°	114.462(4)	90	83.427(2)
Volume/Å^3	4409.1(4)	10576.8(9)	4609.3(2)
Z	2	4	2
ρ_{calc}g/cm^3	1.308	1.230	1.112
μ/mm^{-1}	3.523	0.191	0.193
F(000)	1824.0	4144.0	1628.0
Crystal size/mm^3	0.307 × 0.202 × 0.08	0.2 × 0.1 × 0.1	0.4 × 0.1 × 0.05
Diffractometer	SuperNova, Atlas	Synchrotron BM20, Pilatus 2M	Synchrotron BM20, Pilatus 2M
Radiation	Cu Kα (λ = 1.54184)	Synchrotron (λ = 0.56356)	Synchrotron (λ = 0.56385)
2Θ range for data collection/°	7.436 to 147.114	2.872 to 39.346	3.09 to 39.366
Index ranges	−16 ≤ h ≤ 16, −17 ≤ k ≤ 13, −32 ≤ l ≤ 32	−22 ≤ h ≤ 22, −26 ≤ k ≤ 26, −39 ≤ l ≤ 39	−14 ≤ h ≤ 14, −16 ≤ k ≤ 16, −33 ≤ l ≤ 33
Reflections collected	30775	173474	80554
Independent reflections	17336 [R_{int} = 0.0751, R_{sigma} = 0.1100]	18869 [R_{int} = 0.0731, R_{sigma} = 0.0355]	16392 [R_{int} = 0.01258, R_{sigma} = 0.0945]
Data/restraints/ parameters	16938/3/1091	18869/2086/1357	16392/93/1005
Goodness-of-fit on F^2	1.023	1.064	1.079
Final R indexes [I>=2σ (I)]	R_1 = 0.0812, wR_2 = 0.2011	R_1 = 0.0741, wR_2 = 0.2131	R_1 = 0.0818, wR_2 = 0.1648
Final R indexes [all data]	R_1 = 0.1305, wR_2 = 0.2373	R_1 = 0.1047, wR_2 = 0.2366	R_1 = 0.1119, wR_2 = 0.1779
Largest diff. peak/hole / e Å^{-3}	0.8/−0.54	0.67/−0.55	1.27/−0.30
Flack parameter	/	/	/

Table S9. Crystallographic data and structure refinement for compounds **1**-**6a**.

Compound	**6a**	**6b**
CCDC	2279472	2279703
Empirical formula	$C_{216}H_{208}Co_2N_6O_2P_8S_2$	$C_{188}H_{164}Co_2N_6O_2P_8S_2$
Formula weight	3349.61	2968.98
Temperature/K	123.0(1)	294.0(3)
Crystal system	monoclinic	triclinic
Space group	*P2₁/c*	*P-1*
a/Å	30.2915(4)	13.8753(3)
b/Å	23.9570(2)	23.4656(6)
c/Å	27.2607(4)	27.8232(3)
α/°	90	86.0020(10)
β/°	116.0843(17)	86.5260(10)
γ/°	90	82.975(2)
Volume/Å^3	17768.0(4)	8956.7(3)
Z	4	2
ρ_{calc}g/cm^3	1.252	1.101
μ/mm^{-1}	2.814	2.734
F(000)	7072.0	3112.0
Crystal size/mm^3	0.279 × 0.147 × 0.12	0.24 × 0.2 × 0.12
Diffractometer	SuperNova, TitanS2	Synergy DW, HyPix-Arc 150
Radiation	Cu Kα (λ = 1.54184)	Cu Kα (λ = 1.54184)
2Θ range for data collection/°	6.946 to 133.7	3.802 to 134.16
Index ranges	$35 \le h \le 36$, $-28 \le k \le 27$, $-32 \le l \le 29$	$-16 \le h \le 16$, $-28 \le k \le 28$, $-20 \le l \le 33$
Reflections collected	161149	111416
Independent reflections	31309 [R_{int} = 0.0411, R_{sigma} = 0.0277]	31704 [R_{int} = 0.0765, R_{sigma} = 0.0785]
Data/restraints/ parameters	31309/66/2154	31704/209/1925
Goodness-of-fit on F^2	1.021	1.013
Final R indexes [I>=2σ (I)]	R1 = 0.0436, wR2 = 0.1105	R_1 = 0.0856, wR_2 = 0.2506
Final R indexes [all data]	R_1 = 0.0538, wR_2 = 0.1180	R_1 = 0.1331, wR_2 = 0.2816
Largest diff. peak/hole / e Å^{-3}	0.67/−0.59	1.11/−0.49
Flack parameter	/	/

3.4.8 Quantum Chemical Calculations

General Methods

All calculations were performed with the ORCA 5.0 program.[29] The geometry was optimized starting from the X-ray coordinates at the TPSS[30]/def2-TZVP[31] level. Dispersion correction was included *via* the Grimme's D4 model,[32] and the solvent effects by using the CPCM model.[33] The Intrinsic Bonding Orbitals[34] were calculated as implemented in ORCA and visualized using ChemCraft.[35]

Calculation of the ^{31}P NMR chemical shifts

The geometry of the molecules has been optimized using the PBE[36] functional together with the def2-SVP basis set for C and H and def2-TZVP for all other atoms, using tight convergence criteria. The dispersion correction has been incorporated *via* the D3BJ[37] scheme and the solvent effects by using the CPCM model with the dielectric constant of benzene. The ^{31}P chemical shifts has been calculated using the GIAO[38] formalism as single point calculations with the PBE0[39] functional using the aug-pcSseg-2 basis set[40] (taken from the Basis Set Exchange library[41]) for phosphorus and the def2-TZVP basis set for all other atoms. In case of the hybrid functional PBE0 the RIJCOSX approximation has been used.[42] The calculated absolute shifts has been referenced to the absolute shift of 85% H_3PO_4 using PH_3 as a secondary standard (d_{PH3} in C_6D_6 = −240 ppm) by using the equation: $d_{calc,X} = s_{calc,PH3} - s_{calc,X} - 240$ ppm.

Table S10. Calculated (at the D3BJ-PBE0/def2-TZVP/aug-pcSseg-2 @P/CPCM level of theory) and experimental ^{31}P NMR chemical shifts of [(Ar*BIAN)Co(η^3:η^1-$P_4C(S)N(Cy)C(O)t$Bu)] (**6a**).

	calcd.	exp. (at 213K)
P3	91	85.5
P4	123	105.4
P5	125	117.9
P6	110	77.6
	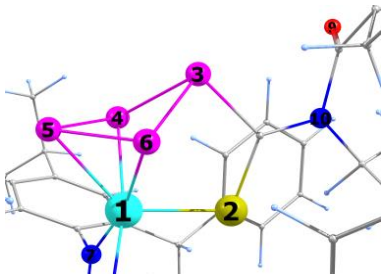	

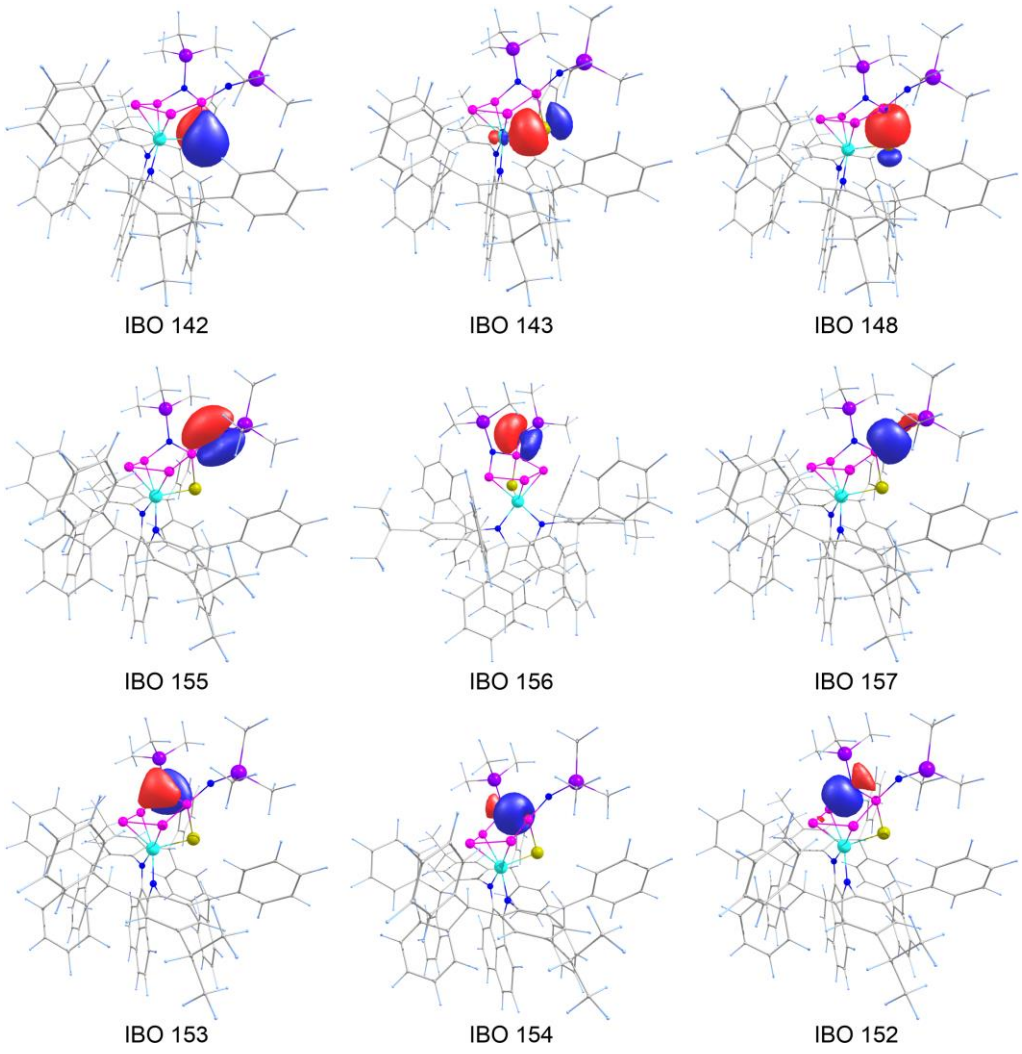

Figure S39. Selected Intrinsic Bonding Orbitals of [(Ar*BIAN)Co(η^3:η^1-$P_4SN_2(SiMe_3)_2$)]$^-$ (**4**$^-$) at the TPSS-D4/def2-TZVP CPCM(THF) level of theory.

Selected IBOs

MO 158: 10Si - 0.336766 and 8N - 0.668073
MO 157: 9N - 0.579533 and 5P - 0.422175
MO 156: 9N - 0.840853 and 5P - 0.079905
MO 155: 9N - 0.754930 and 5P - 0.142491
MO 154: 8N - 0.576713 and 5P - 0.404438
MO 153: 8N - 0.848485 and 5P - 0.050514
MO 152: 8N - 0.597646 and 2P - 0.363415
MO 151: 7N - 0.861723 and 0Co - 0.192947
MO 150: 6N - 0.883734 and 0Co - 0.186604
MO 149: 5P - 0.575444 and 4P - 0.471926
MO 148: 5P - 0.445004 and 1S - 0.576771
MO 147: 4P - 0.518845 and 3P - 0.490022
MO 146: 4P - 0.519738 and 0Co - 0.423037
MO 145: 3P - 0.526900 and 2P - 0.492273
MO 144: 2P - 0.555703 and 0Co - 0.424569
MO 143: 1S - 0.717700 and 0Co - 0.162893
MO 142: 1S - 0.920644 and 0Co - 0.012502

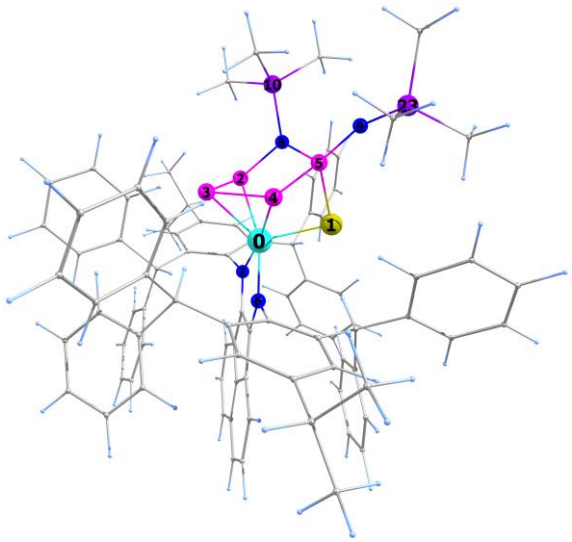

Figure S40. Optimized geometry of $[(Ar^*BIAN)Co(\eta^3{:}\eta^1\text{-}P_4SN_2(SiMe_3)_2)]^-$ (**4**$^-$) at the TPSS-D4/def2-TZVP CPC(THF) level of theory and atom labeling.

Cartesian coordinates of the optimized geometry of $[(Ar^*BIAN)Co(\eta^3{:}\eta^1\text{-}P_4SN_2(SiMe_3)_2)]^-$ (**4**$^-$) at the TPSS-D4/def2-TZVP CPC(THF) level of theory.

Co	0.12269356182392	0.03991539174372	-0.13889055865780
S	0.84479587300004	0.70002707086195	-2.22766303871057
P	-0.88606923754045	-1.78612115898880	-1.04896118972262
P	-2.01200657282663	-0.58398514621266	0.38497795984413
P	-1.75020275403189	1.22751560740456	-0.75261021887770
P	-1.15064602338650	0.45278294418441	-2.74203118573080
N	0.76167137813099	1.39614444767224	1.12139684371542
N	1.57856146334266	-1.00047295723704	0.60683032464767
N	-1.40224592359920	-1.22027605899079	-2.62204451323577
N	-1.68623245955753	0.97312815055237	-4.10823310259208
Si	-2.79769524983070	-1.97701436244346	-3.41777109865314
C	-4.37156968466898	-1.06472598032021	-2.94473019272394
H	-4.35455950920002	-0.03767999951167	-3.32398760488712
H	-4.48067425935328	-1.02444706530140	-1.85442876917244
H	-5.25402453115864	-1.56992503454872	-3.35783614294479
C	-2.58058706890929	-2.00498280959929	-5.28008717615475
H	-3.45890459787620	-2.46597012374279	-5.75066044890539
H	-1.69988756543358	-2.59041011171975	-5.56668721449442
H	-2.46384211210174	-0.99034383708004	-5.66919052558307
C	-2.88278220332523	-3.74943983058860	-2.79169498492441
H	-3.11431728032464	-3.80318300287393	-1.72239747966050
H	-1.93804645845318	-4.27973472427433	-2.96005840328807
H	-3.67221746904939	-4.28462779548853	-3.33646683683761
Si	-2.32086730726717	2.39413167600414	-4.79209156571552
C	-3.15877459076805	3.50492738230990	-3.51298610457000
H	-4.01497945348585	2.98852899852379	-3.06055719598702

H	-3.52624998988070	4.43492324411170	-3.96647300876870
H	-2.47157645134069	3.77017491623192	-2.70216194854255
C	-3.62447063118935	1.90969535421571	-6.07174676481380
H	-3.18986376138083	1.27680437611245	-6.85580759704197
H	-4.05803776108396	2.79418652133517	-6.55698216943308
H	-4.44291418257556	1.34663268709386	-5.60562079117012
C	-0.96987835387333	3.35973051405474	-5.69119957635060
H	-0.15443618085484	3.62675507417076	-5.01003010269327
H	-1.35516501190587	4.28677604527343	-6.13578152074413
H	-0.54582207453102	2.75022299857890	-6.49971084424867
C	1.86683098903642	1.02023755055618	1.74545919747685
C	0.28920153814980	2.71707281759608	1.40962902575579
C	2.32510278528900	-0.31516239797778	1.45616868313277
C	1.76676240236386	-2.41186846668885	0.48599541428637
C	2.76375767862345	1.61127201241576	2.73283542961024
C	-0.70859878313960	2.92808679496505	2.38011719483269
C	0.84936990952190	3.81023985193477	0.72208808867120
C	3.52640528177855	-0.57365674886553	2.23728542114721
C	2.38130900595660	-2.97628984125966	-0.64452111076726
C	1.20647290685159	-3.24188113611826	1.47844481156767
C	3.74784229877739	0.61549620982097	2.98352507185204
C	2.85323210328663	2.81393412938887	3.40596823837747
C	-1.46578099256443	1.77489950636365	3.02644423922870
C	-1.04142165184638	4.24424314432655	2.71442903322689
C	1.85395309989637	3.58984155961918	-0.40112372259290
C	0.47547637923227	5.10299255956962	1.08344777544474
C	4.39760717925930	-1.63263621158022	2.39823496947200
C	2.98116030887036	-2.08993158777164	-1.72299981876452
C	2.42984658278611	-4.36627313415159	-0.76004222220025
C	0.56576819959185	-2.66509750606615	2.73343999825173
C	1.25100531463408	-4.62513077961637	1.30048132232229
C	4.81036822924662	0.78052770538584	3.88261954811193
H	2.14323803398474	3.61557189175779	3.23665116120234
C	3.91331454070753	2.99595251205991	4.32960847279746
C	-0.88067857524053	1.24804317780954	4.32535359178882
H	-1.45016582437758	0.94414312747988	2.30678093047279
C	-2.93429311663525	2.15961515138685	3.23296754502115
H	-1.80867399503144	4.41332526015408	3.46585900655162
C	-0.44744377857210	5.34501196542718	2.10097131285011
C	1.63082958628788	4.57067534703751	-1.54606623804201
H	1.65302843692006	2.59081717238605	-0.80765504152135
C	3.27385115563451	3.57558791856956	0.13623112701944
H	0.90386548372579	5.93803038510995	0.53538025005485
C	5.48948317078924	-1.47908106367296	3.28721813165616
H	4.25389640146436	-2.56932216033692	1.87405705566447
H	2.37707462126012	-1.17447937467016	-1.74682862919598
C	4.41593554772173	-1.67973342430052	-1.43531904765400
C	2.85181700093516	-2.72394641208731	-3.10405179410171
H	2.89708968507164	-4.80141479791995	-1.64016804860977
C	1.86338707067757	-5.21112594917571	0.19382111786780
C	-0.74038558592536	-3.37200663353017	3.09366664490501
C	1.56324036510895	-2.64749132637428	3.88770860707343
H	0.29844682597628	-1.62273724903003	2.51769110687015
H	0.76588193268252	-5.25544132497862	2.04123632376745
C	4.86868052206779	2.02335626435291	4.57087111332140
C	5.70348961905808	-0.31795140413970	4.01257327649106
H	3.97981617688098	3.94381293252100	4.85705112462673
C	0.03152805694308	1.96945325591725	5.09552714499931
C	-1.37056738538857	0.03139435574132	4.82380526427359
C	-3.43804217022165	2.52631223387182	4.48611982187506
C	-3.80031739418711	2.18902659459452	2.13359294866922
C	-0.83887696757911	6.75882576397619	2.48482738825935
C	0.32644792015392	4.76839483783675	-2.02303443655970
C	2.67715709033526	5.25348082072312	-2.17169862214522
C	4.06557412834454	2.43880071733138	-0.03202853953927
C	3.80033307499746	4.66382216482837	0.84170376213445
H	6.17540704244034	-2.31274909834305	3.41065252484182
C	5.29788148198434	-2.48399767551616	-0.70925664729638
C	4.89603579644057	-0.48436882290841	-1.98523421196831
C	3.91461068823776	-3.38070104999715	-3.73281114200399
C	1.61406720304794	-2.66793743010540	-3.75691330063201
C	1.88226261339648	-6.71665465221698	0.01323379440595
C	-1.07371034584772	-3.68571988845618	4.41401998599152
C	-1.66829156317852	-3.66376812868338	2.08451907796643
C	2.27271641740629	-3.79702476315118	4.25565559196267
C	1.77971305021178	-1.47234420855757	4.60846841217971
H	5.66815342335762	2.20916602743064	5.28396566887296

H	6.54851241971582	-0.24873239557353	4.69316469991384
H	0.41599629632846	2.91338193489794	4.72444796852054
C	0.43668188407370	1.49872682832281	6.34757468227072
H	-2.07247170096419	-0.54442995332827	4.22558076750736
C	-0.98564466440678	-0.42971707583991	6.07860689675644
H	-2.78527798023388	2.50983557183605	5.35392287505689
C	-4.77170640580610	2.91273815964566	4.63675442373340
H	-3.42021619103197	1.91647741021113	1.15227833253070
C	-5.13377039279292	2.56701036444202	2.27965076617571
H	-1.54068265286402	6.68467637771642	3.32568329625067
C	0.38092728735601	7.57443013537040	2.94768997711809
C	-1.55982185194987	7.46601988368548	1.32247480823462
H	-0.49467652700542	4.23419625902011	-1.55270070528835
C	0.07220015328601	5.64408706717603	-3.07422434118352
H	3.69653131184715	5.10705930905692	-1.82746407225554
C	2.42702360435213	6.12892908819647	-3.23294934359819
H	3.66453760273329	1.58800008099345	-0.57607335421880
C	5.34330074761814	2.36871065054528	0.52447839324573
H	3.19527619883296	5.55490949589180	0.98524419448422
C	5.08417253364919	4.60866734845617	1.37874816598618
H	4.94161855028864	-3.41556374277222	-0.27862531131755
C	6.62947442846268	-2.10368560840868	-0.53115015756233
H	4.21804326483380	0.14477310157881	-2.55739488265452
C	6.22498637087979	-0.10239442019265	-1.81455373528953
H	4.88463234181096	-3.42259387067228	-3.24529732916891
C	3.74318671872602	-3.98240088935974	-4.98195288954532
H	0.78501502412840	-2.14805897187081	-3.28524936631279
C	1.44209414076247	-3.26312319825487	-5.00535007087598
H	2.42519920880457	-6.92468892171921	-0.91796164132218
C	2.62481333477282	-7.41484615731609	1.16612757828301
C	0.45345715283028	-7.27158216826606	-0.13241867882048
H	-0.36895652328684	-3.46870687802614	5.21025095670592
C	-2.30472770405136	-4.27070060827415	4.72217041869925
H	-1.41923655833107	-3.44042732932825	1.05000661688239
C	-2.89724759788866	-4.24529923720254	2.38662736980336
H	2.12605609313859	-4.72157559447949	3.70575744309949
C	3.17685817136680	-3.77008305054322	5.31566862348882
H	1.23937735295461	-0.57251428978942	4.33421623957755
C	2.68753539921455	-1.43777661379700	5.66664909434078
H	1.15268143227244	2.07155862674372	6.93146206442066
C	-0.08240217572150	0.30694365661504	6.84936571099277
H	-1.37845437752725	-1.37116184656779	6.45142875222190
C	-5.62668926711210	2.93333743001854	3.53443247111013
H	-5.14111874624063	3.19689245463918	5.61887747149086
H	-5.78887440946479	2.57464275880539	1.41207056818518
H	1.11235156881446	7.67049749582900	2.13682822002069
H	0.87714173221350	7.09237989317703	3.79701852260202
H	0.07669029364822	8.58289647755122	3.25066875958770
H	-1.88348413997936	8.46902278221502	1.62385670232907
H	-2.44014910609059	6.89749455238975	1.00460753477887
H	-0.89209116593386	7.56924566878940	0.45917125627653
C	1.12403378902685	6.33421822542652	-3.68335177639520
H	-0.94656258924720	5.78439991169517	-3.42370166420840
H	3.25557242157335	6.65287544854745	-3.70293508700843
H	5.92963293798837	1.46241440264212	0.40932867849542
C	5.85590657734131	3.45359294912839	1.23340450785922
H	5.47590325377920	5.45941512225486	1.93062052316315
H	7.29922478073047	-2.73945568639967	0.04222835117118
C	7.09861367369052	-0.91209665269843	-1.08353030617770
H	6.57767631221902	0.83148033814281	-2.24395197482249
H	4.57985234595423	-4.49155403823214	-5.45382423125569
C	2.50545871369069	-3.92685819887950	-5.62296652674816
H	0.47767045129051	-3.20504348019304	-5.50217655960381
H	3.65190107681446	-7.04417014019111	1.25328606479957
H	2.65995618222237	-8.49782349986586	1.00070089074107
H	2.11591260564059	-7.23420263402155	2.12013201485053
H	-0.12604884701413	-7.09029721782012	0.78033119949034
H	0.47718246140758	-8.35280933698761	-0.31107790230214
H	-0.06925519156918	-6.79228863346311	-0.96698373813244
C	-3.22246419898538	-4.55257891436466	3.71062030005028
H	-2.54344233731686	-4.50601068604078	5.75635473898498
H	-3.60201046543197	-4.45868658691952	1.58689410010987
H	3.72111463699498	-4.67249953362284	5.58290419294290
C	3.38959165268723	-2.58640902776572	6.02548968885352
H	2.84840427847618	-0.50783468536724	6.20320328474843
H	0.22598231469533	-0.05686573210703	7.82564047096066
H	-6.66621915450047	3.22792708022596	3.65138546515506

H	0.92767006962581	7.01904682590681	-4.50395219663733
H	6.84671519975256	3.39864876119587	1.67633300780840
H	8.13405001422095	-0.61314032264633	-0.94413182447121
H	2.37114150295188	-4.38972624427076	-6.59710497270153
H	-4.17973900112879	-5.00857577051287	3.94893584779469
H	4.10304825818226	-2.55997255854244	6.84502326123710

Selected Mayer bond orders

B(0-Co, 1-S) : 0.5380 B(0-Co, 2-P) : 0.7770 B(0-Co, 3-P) : 0.5890
B(0-Co, 4-P) : 0.6590 B(0-Co, 6-N) : 0.6346 B(0-Co, 7-N) : 0.6431
B(0-Co, 36-C) : 0.1026 B(0-Co, 38-C) : 0.1067 B(1-S , 5-P) : 1.0783
B(2-P , 3-P) : 1.0473 B(2-P , 8-N) : 0.9456 B(2-P , 39-C) : 0.1375
B(3-P , 4-P) : 1.1267 B(4-P , 5-P) : 0.8914 B(4-P , 37-C) : 0.1155
B(5-P , 8-N) : 1.0454 B(5-P , 9-N) : 1.5552 B(6-N , 36-C) : 1.3603
B(6-N , 37-C) : 0.5935 B(7-N , 38-C) : 1.4323 B(7-N , 39-C) : 0.5138
B(8-N , 10-Si) : 0.9672 B(9-N , 23-Si) : 1.2503 B(10-Si, 11-C) : 0.9915
B(10-Si, 15-C) : 0.9869 B(10-Si, 19-C) : 1.0217 B(11-C , 12-H) : 0.9573
B(11-C , 13-H) : 0.9434 B(11-C , 14-H) : 0.9355 B(15-C , 16-H) : 0.9345

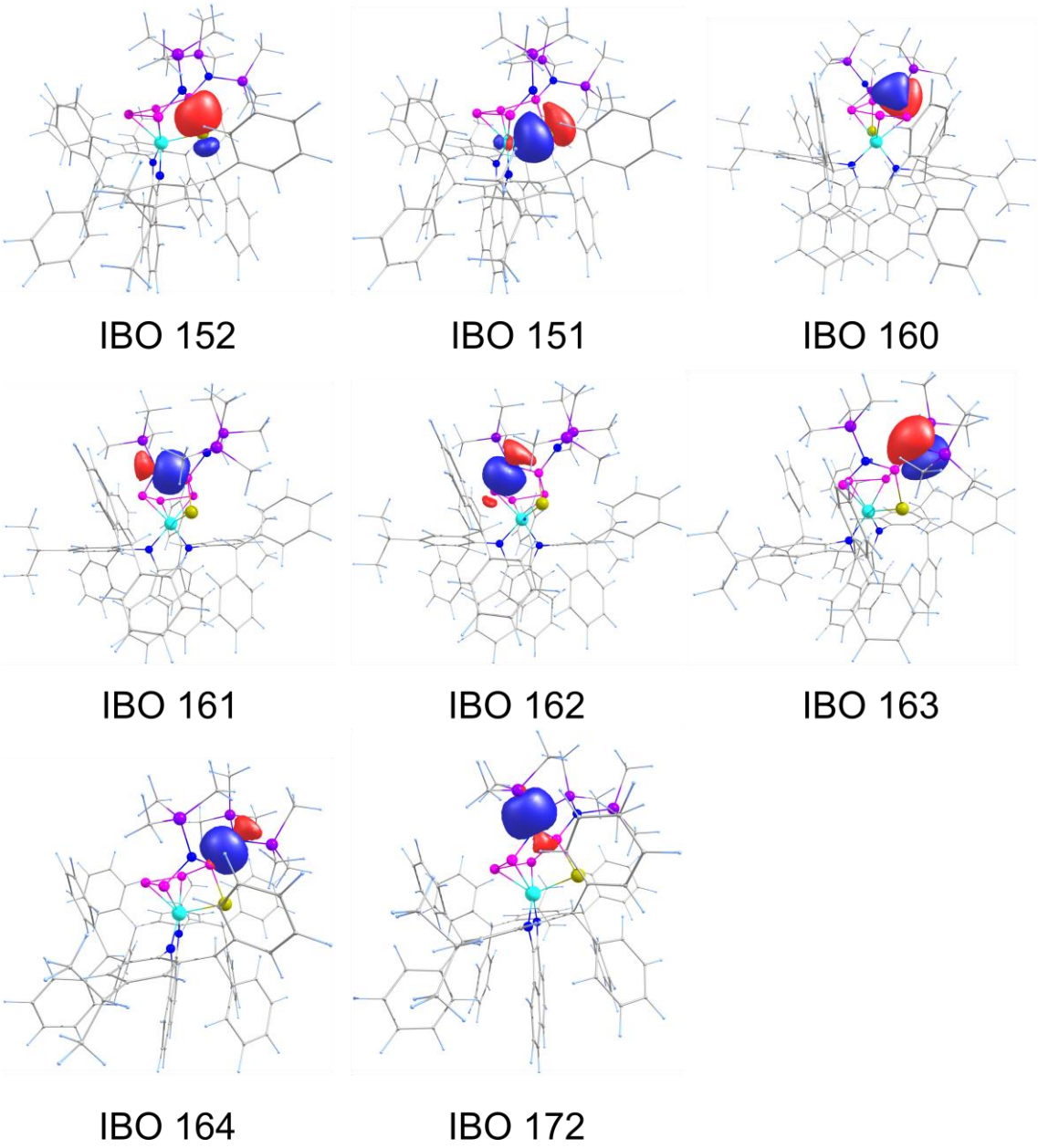

Figure S41. Selected Intrinsic Bonding Orbitals of [(Ar*BIAN)Co(η^3:η^1-$P_4SN_2(SiMe_3)_3$)] (**5**) at the TPSS-D4/def2-TZVP CPCM(THF) level.

Selected IBOs

MO 174: 16Si - 0.338160 and 9N - 0.663503
MO 173: 15Si - 0.343615 and 9N - 0.664794
MO 172: 14Si - 0.335445 and 8N - 0.672070
MO 164: 9N - 0.591659 and 2P - 0.393448
MO 163: 9N - 0.805886 and 2P - 0.080942
MO 162: 8N - 0.603899 and 5P - 0.342525
MO 161: 8N - 0.551419 and 2P - 0.426669
MO 160: 8N - 0.827895 and 2P - 0.059011
MO 159: 7N - 0.861832 and 0Co - 0.201273
MO 158: 6N - 0.874984 and 0Co - 0.188600
MO 157: 5P - 0.483267 and 4P - 0.524460
MO 156: 5P - 0.571919 and 0Co - 0.396117
MO 155: 4P - 0.464757 and 3P - 0.540127
MO 154: 3P - 0.411902 and 2P - 0.631653
MO 153: 3P - 0.550641 and 0Co - 0.373465
MO 152: 2P - 0.461122 and 1S - 0.553043
MO 151: 1S - 0.725958 and 0Co - 0.176304
MO 150: 1S - 0.922476 and 0Co - 0.011767

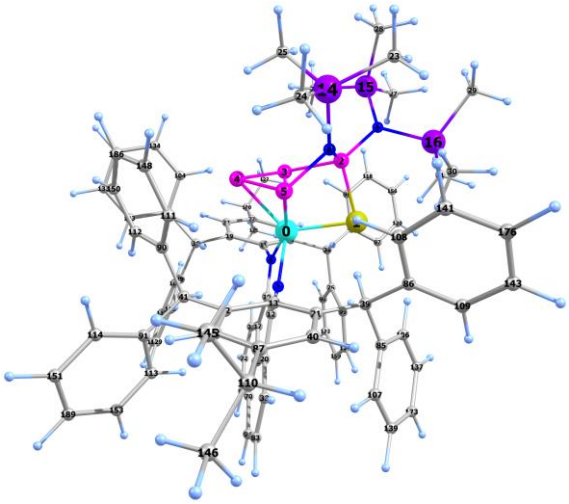

Figure S42. Optimized geometry of [(Ar*BIAN)Co(η^3:η^1-$P_4SN_2(SiMe_3)_3$)] (**5**) at the TPSS-D4/def2-TZVP CPC(THF) level and atom labeling.

Cartesian coordinates of the optimized geometry of [(Ar*BIAN)Co(η^3:η^1-$P_4SN_2(SiMe_3)_3$)] (**5**) at the TPSS-D4/def2-TZVP CPC(THF) level.

Co	-0.09491285559101	0.09500971359674	-0.06058070639845
S	-0.43758113871060	0.68105869098351	-2.26809467208034
P	1.06351249244783	-0.67327259434489	-2.52249480281810
P	2.10983498656390	0.01092835683576	-0.70917108808589
P	1.40998884037338	-1.43883335706982	0.71582167167789
P	-0.24156958314395	-2.09610730513094	-0.55371779030161
N	0.12090780909033	1.76813418781937	0.93077059467113
N	-1.84976104826616	0.09986326302084	0.77225026667929
N	0.42593744943622	-2.18805583308749	-2.19556710861261
N	1.76046545833374	-0.63470465725289	-4.03954690856217
C	-0.98770819879779	2.14410153247410	1.53285667461906
C	1.30687993094590	2.54298395393614	1.11972998887270
C	-2.09621934326781	1.22384646241014	1.42218089525790
C	-2.81767633773818	-0.95159183735568	0.89899111965175
Si	0.99699924430022	-3.80773792396743	-2.66929279885406
Si	3.52700064746981	-0.71903740663204	-4.34630417887549
Si	0.68162593518606	-0.21258686641089	-5.43237191666832
C	-1.39720322906195	3.26289456414438	2.37096328428113
C	1.66721821282111	3.51131308088877	0.16541723775578
C	2.12640449752048	2.29885581249682	2.23303416766509
C	-3.22502897601255	1.76868969691861	2.16264453328530
C	-3.71298790466434	-1.23970424881904	-0.14240726772966
C	-2.85349914727277	-1.70489561991058	2.09103687523521
C	0.90143367924085	-4.02753284215595	-4.52549343023048
C	-0.14532340563707	-5.06288772392562	-1.86641917157360
C	2.72887265121664	-4.07731673111963	-1.99906501707251
C	4.53741191234800	-0.58862876844361	-2.77282138457006

C	4.04238552557411	0.72526926331413	-5.42846652149554
C	4.00564813758730	-2.32616050262610	-5.19254765554989
C	1.34593867997946	-0.99167612294648	-7.01163838037692
C	-1.04264860391426	-0.91209712316507	-5.21713443021472
C	0.61017086404505	1.65113984705592	-5.62842126211666
C	-2.74980026323338	2.99252781547286	2.71257716386654
C	-0.79937084093615	4.40537590732842	2.86116353119793
C	0.75363726127796	3.76835567275620	-1.02189452060950
C	2.83282452700577	4.24791914000832	0.35947088884899
C	1.72032067113197	1.31935360860966	3.32435202495447
C	3.31714123924692	3.02334445926034	2.35417185828721
C	-4.52867061516229	1.38339977607343	2.41816079201224
C	-3.65633258727912	-0.47081848489300	-1.44793171939488
C	-4.66213211272211	-2.24755683095941	0.03998203903984
C	-1.84640837432442	-1.49607022648696	3.21373638646201
C	-3.81730581513418	-2.70292739169702	2.22490572478236
H	-0.14246920485397	-4.06664972003051	-4.85531501094617
H	1.37639755433068	-4.97810155645022	-4.79940422218061
H	1.40563711474536	-3.23063522089039	-5.07431107641804
H	-0.02279664781286	-5.10392850513013	-0.78004307749247
H	0.10043360633811	-6.05363797780107	-2.27295284488136
H	-1.19913338159458	-4.86258074281651	-2.08390730242953
H	3.45146128610677	-3.34689564273211	-2.37311888365932
H	3.09249022189348	-5.07760857487544	-2.26528700791428
H	2.71448545942078	-3.99891696596578	-0.90547331159672
H	4.45249369412681	0.39691850737967	-2.30546227709349
H	5.58562919923385	-0.73439815060345	-3.06870692661177
H	4.29657444433604	-1.34400900404364	-2.01937737621311
H	3.63240149138503	0.70446117480955	-6.44130315080324
H	5.13681997967403	0.70521199922134	-5.51448478035264
H	3.76046001700821	1.67540081840316	-4.96716138072246
H	3.84872083920769	-3.19825527773514	-4.55104322999613
H	5.07942865290987	-2.27141944307711	-5.41739128418877
H	3.47910358881924	-2.49822282138872	-6.13510925679230
H	2.36655968952239	-0.71387216236433	-7.28378921832273
H	0.68615517540953	-0.64643862812618	-7.81952246057873
H	1.28094522881415	-2.08424919465954	-6.98319483183409
H	-1.02828319427558	-1.95954084786758	-4.90781073080057
H	-1.53924487550017	-0.85874521035950	-6.19528093980904
H	-1.64552476523080	-0.35803359037548	-4.49553277900526
H	0.26937389952094	2.13155741782014	-4.70598398224016
H	-0.10063935511693	1.90254769668927	-6.42629806986016
H	1.58229427451973	2.07561462100576	-5.89572222131263
C	-3.52783949041979	3.83245555123357	3.52281733585113
H	0.23150593252918	4.64999219754059	2.63571947245276
C	-1.56769026322766	5.26464130502963	3.68461888154033
C	1.50668326083688	4.24240635984979	-2.25703652493812
H	0.30881662364054	2.80014922608394	-1.28381120874880
C	-0.38680069053735	4.67915238556125	-0.59885192380632
H	3.09831987074220	5.00308857869331	-0.37458083277982
C	3.68263809667392	4.00907816800999	1.44214021041736
H	0.98672573211041	0.62548285430477	2.89019518145972
C	1.02293212697755	2.06224241100110	4.46083344662404
C	2.89188774728991	0.46574992611694	3.80668882217948
H	3.98262164544400	2.80340596211421	3.18528268696379
H	-4.93538618047734	0.45489966098405	2.03560237367746
C	-5.33534093161819	2.22750573231996	3.22123950146552
H	-2.61609439145096	-0.14439337896649	-1.57122817121410
C	-4.50612889891065	0.78812711115849	-1.43678940271726
C	-3.95410789796794	-1.37829093980142	-2.63964835205681
C	-4.73848023031591	-2.98813650996685	1.21690499488977
H	-5.35188388189473	-2.46819990816986	-0.77111813232404
H	-1.41211304952992	-0.49990808338132	3.08639452503608
C	-0.68195270820391	-2.48229833652786	3.17561440949760
C	-2.53714780197576	-1.52227854270601	4.57669446559206
H	-3.84067738064536	-3.27374111416610	3.14899580346618
C	-2.88768414929912	5.00432676148603	4.01220702702540
C	-4.86447750929923	3.41234973704386	3.76626342562295
H	-1.09589513411945	6.16275040813511	4.07290045387857
C	2.69961920542503	3.60172984666935	-2.62407367084122
C	1.02922435750134	5.27261942043668	-3.07266702279556
C	-0.13753514260430	5.95168119760517	-0.07215126929078
C	-1.70721082169453	4.23531774183260	-0.68771620448893
C	4.96982284160767	4.79214907175091	1.61531676329236
C	-0.24240137355522	1.66028080890535	4.89033353094728
C	1.62447165715174	3.15335826005189	5.09876997748183
C	3.05363839327704	0.13040376051081	5.15414662484226

C	3.80163547401538	-0.05631047372578	2.87704803758043
H	-6.35920445468128	1.92453474213789	3.42214806443361
C	-4.09381629262127	1.88970278993861	-2.19646672876520
C	-5.71265607917484	0.87138198673536	-0.73693233122011
C	-3.22925861249765	-2.57149756438903	-2.76908397174936
C	-4.89959437512280	-1.06464012153411	-3.61886806968999
C	-5.76751039646457	-4.08856375717916	1.38413910849466
C	-0.68182553977004	-3.64029262415715	2.39618038582902
C	0.42485026405511	-2.22476509125071	3.99710577033891
C	-3.15987410622429	-0.36880567227280	5.06585215824446
C	-2.59816016684219	-2.69084377898211	5.34497844800891
H	-3.43749437508139	5.69363950710834	4.64788303953204
H	-5.51752530593575	4.02317920034943	4.38448270914462
H	3.07773103628207	2.78753105173712	-2.01184630362472
C	3.41746865979447	4.01489300101024	-3.74319766036023
H	0.10175436420180	5.77447951374621	-2.81376797424826
C	1.73403909199347	5.67177135488365	-4.21177649083814
H	0.88722022928434	6.30400456956044	0.01575393200506
C	-1.18745204742462	6.76265638068976	0.35279568878065
H	-1.90810078069768	3.24294334488222	-1.08212663984949
C	-2.76186568065352	5.03667667688237	-0.24713283851943
C	4.68180741227331	6.28458748151051	1.85864458673197
H	5.47345132026605	4.39229999251179	2.50481635955640
C	5.90646070077918	4.60486428318928	0.40857612746466
H	-0.72641206817703	0.82209235060224	4.40104387093999
C	-0.90353713059178	2.32959842219590	5.91994213399317
H	2.60724886863713	3.49021025617694	4.78426953028704
C	0.97208635941598	3.82566683952822	6.13036858519920
H	2.36073716714655	0.52260208370337	5.89241773044533
C	4.09456153173581	-0.70620319406259	5.56459244410350
C	4.83817370232240	-0.89482820499151	3.28070260677095
H	3.69764056895508	0.20176013312009	1.82731506892601
H	-3.16018281117445	1.82954662968064	-2.75071005009572
C	-4.86809865308369	3.04738569595326	-2.25652949555957
H	-6.05035913683841	0.02612863815246	-0.14442643128599
C	-6.48777683722827	2.03106765582147	-0.78713554884602
H	-2.49405654034521	-2.82616403016954	-2.00990463620288
C	-3.44290364099149	-3.42755751299057	-3.84445786704982
H	-5.47395874912760	-0.14656267326871	-3.53945847519257
C	-5.11625283638628	-1.92138207215480	-4.70282335756578
H	-6.38144438668375	-4.10035705984661	0.47432219140617
C	-5.08680751001872	-5.46311554131764	1.51849155781949
C	-6.69301703496333	-3.81701418975814	2.58333020378723
H	-1.52862430512711	-3.85990023916304	1.75534015271856
C	0.40622223533288	-4.51798924918649	2.42852755606463
H	0.43561019309409	-1.32942008648065	4.61237053694184
C	1.50803772900533	-3.09541873274547	4.03315722976128
C	-3.27922244167399	-2.71004775217477	6.56290383961449
H	-3.11708749219627	0.54716382965285	4.48687807379757
C	-3.83695445363218	-0.38153906575229	6.28459532943396
H	-2.10585438127053	-3.59169722662663	4.98947406459483
H	4.35846938076214	3.53096183130917	-3.98852198258847
C	2.93812449003395	5.05390155839923	-4.54501660783600
H	1.34318023772967	6.47570668559465	-4.83015616889594
H	-0.97797659802340	7.74725546733005	0.76288639052484
C	-2.50483522249708	6.30429580399400	0.27207183322348
H	-3.77963773284812	4.66282160936290	-0.30340281512859
H	4.17734616870393	6.72670278800037	0.99158802012509
H	5.61507303746653	6.83441979566018	2.02563556257813
H	4.03708690886505	6.42143421509587	2.73340702174870
H	6.13514631687242	3.54550177091885	0.25035579295193
H	6.84763140958032	5.14350076267794	0.56702180846072
H	5.44325507802381	4.99253438747438	-0.50622483658409
H	-1.89275940916610	2.00282432210726	6.22578416701989
C	-0.29756704994169	3.41779338659714	6.54434073539958
H	1.45458643183090	4.67393403802751	6.60914523347273
C	4.99067575266855	-1.22393505820707	4.62986841716475
H	4.20117407000027	-0.95335929020585	6.61768455169773
H	5.52890743175485	-1.29042660385886	2.54047154572984
C	-6.06912147419302	3.12334289183020	-1.54769645722279
H	-4.52962684918355	3.89288827229812	-2.84908655871625
H	-7.41938674504271	2.08070198115423	-0.22947835723830
C	-4.39121886042506	-3.10590435184678	-4.81998528898523
H	-2.86722919054414	-4.34577011035909	-3.92695438437161
H	-5.85772017676073	-1.65930222850668	-5.45322569595081
H	-4.44406579322890	-5.66812546182610	0.65572687529081
H	-5.83801462828138	-6.25801940296478	1.58833024185958

H	-4.46675574274802	-5.50093911070014	2.42179923650108
H	-6.12106720241090	-3.79418215717760	3.51815688060109
H	-7.45028838447253	-4.60458895741550	2.66839938838053
H	-7.20505921503299	-2.85500887852493	2.47379384991250
H	0.39330473461980	-5.40958644207438	1.80715050003459
C	1.50287681584319	-4.24951006098061	3.24379630860657
H	2.36202134020811	-2.86697432376454	4.66398171526828
H	-4.30972837858460	0.52770041876543	6.64687940313556
C	-3.90252660197352	-1.55507178675549	7.03815036659192
H	-3.31805775686919	-3.62843266068431	7.14283419181615
H	3.49790629798271	5.37557733867489	-5.41899387714135
H	-3.32255661121833	6.92748310521434	0.62364318420738
H	-0.81079198554926	3.94882841595559	7.34137224717146
H	5.80085893191382	-1.87466286138259	4.94767269677720
H	-6.67079624338290	4.02732577733406	-1.58619250625917
H	-4.56046457266618	-3.77237654425158	-5.66141319075986
H	2.35065964844377	-4.92911748050359	3.26313432165118
H	-4.42803417281821	-1.56786038485034	7.98909943662863

Selected Mayer bond orders

B(0-Co, 1-S) : 0.5148 B(0-Co, 2-P) : 0.1152 B(0-Co, 3-P) : 0.5962
B(0-Co, 4-P) : 0.6023 B(0-Co, 5-P) : 0.7655 B(0-Co, 6-N) : 0.6067
B(0-Co, 7-N) : 0.6431 B(0-Co, 10-C) : 0.1037 B(1-S , 2-P) : 1.1306
B(2-P , 3-P) : 0.9243 B(2-P , 5-P) : 0.1200 B(2-P , 8-N) : 1.1307
B(2-P , 9-N) : 1.0679 B(3-P , 4-P) : 1.1568 B(3-P , 11-C) : 0.1393
B(4-P , 5-P) : 0.9993 B(5-P , 8-N) : 0.8822 B(5-P , 13-C) : 0.1126
B(6-N , 10-C) : 1.4624 B(6-N , 11-C) : 0.5041 B(7-N , 12-C) : 1.4878
B(7-N , 13-C) : 0.5416 B(8-N , 14-Si) : 0.9525 B(9-N , 15-Si) : 0.9312
B(9-N , 16-Si) : 0.8669 B(10-C , 12-C) : 1.1445 B(10-C , 17-C) : 0.8632
B(11-C , 18-C) : 1.3677 B(11-C , 19-C) : 1.4178 B(12-C , 20-C) : 1.0060
B(13-C , 21-C) : 1.3306 B(13-C , 22-C) : 1.2937 B(14-Si, 23-C) : 1.0166
B(14-Si, 24-C) : 1.0322 B(14-Si, 25-C) : 1.0167 B(15-Si, 26-C) : 1.0334
B(15-Si, 27-C) : 1.0216 B(15-Si, 28-C) : 1.0080 B(16-Si, 29-C) : 1.0018

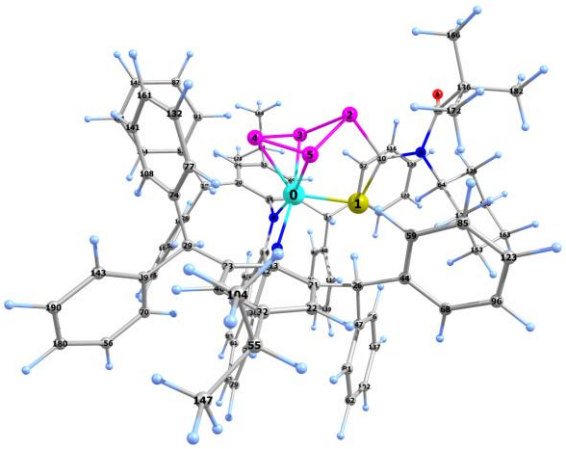

Figure S43. Optimized geometry of [(Ar*BIAN)Co(η^3:η^1-P_4C(S)N(Cy)C(O)*t*Bu)] (**6a**) at the D3BJ-PBE0/def2-SVP@C,H/def2-TZVP@Co,P,N,S CPC(Benzene) level and atom labeling.

Cartesian coordinates of the optimized geometry of [(Ar*BIAN)Co(η^3:η^1-P_4C(S)N(Cy)C(O)*t*Bu)] (**6a**) at the D3BJ-PBE0/def2-SVP@C,H/def2-TZVP@Co,P,N,S CPC(Benzene) level and atom labeling.

Co	0.06464451910644	0.05278912545616	0.03711093113424
S	2.24720515022026	-0.11091573874997	-0.40370262897884
P	1.91910580868605	-0.19273919980089	2.59981971230055
P	0.56823734319903	1.41612637869779	1.78502751683577
P	-1.12666571282865	0.06028989457554	1.99595867626874
P	0.34532747331950	-1.51382153237536	1.65859714135848
N	-0.49127094337635	1.48781009463051	-1.19125324096054
N	-0.72155464031940	-1.09912109041212	-1.37625290597672
O	5.36175273656963	0.89330833167595	2.99270877704679
N	4.35754282794314	-0.24133829223673	1.24027071759658
C	3.02111642492179	-0.21221745257880	1.11056690254058
C	-1.78632476300401	0.54027027562380	-4.42897670534360
C	-1.05327973262111	-0.40903040360409	-2.45802430112203
C	-1.01226482289554	-2.50131306923242	-1.35353747102305

C	-0.94032196201516	1.04168901692047	-2.34823577096379
C	-0.45149688254322	2.88350421250118	-0.89838314421950
C	-1.42170276804657	1.64466883236138	-3.59521835366330
C	0.72590161871987	3.63426968247363	-1.13200635844513
C	-2.87845234117937	2.69953093062278	-0.11700152663689
H	-2.59968295222906	1.62377120741675	-0.06518413221082
C	-1.57772750817770	3.48084919348291	-0.27369893364434
C	-0.00518508218900	-3.45695526669215	-1.63978642928847
C	-0.33566559242573	-4.82394853694098	-1.61322603847583
H	0.45510541992209	-5.56042550900314	-1.82641974358894
C	-1.92539962630095	-1.88697001068095	-4.48290920281175
H	-1.81564201960946	-2.87960183372674	-4.02762736967805
C	1.39699314821149	-3.01304136133722	-2.02950286383867
H	1.56709350814763	-2.04251091662281	-1.51748815315849
C	-3.74720650245982	2.86809941369730	-1.36381637907457
C	-3.44110389834174	-1.93528461570988	-0.69810038364818
H	-3.11246642796267	-0.94643943793275	-1.07167996257233
C	3.25887196015961	3.40369735762527	-1.29399603417648
C	-1.63271424545153	-5.27346812447967	-1.32083202663854
C	-2.33351740417611	-2.92841430501000	-1.04437455238772
C	1.90268766933263	3.01042938564346	-1.87380969098569
H	1.82807371973003	1.91580900708097	-1.70605205261889
C	-1.48869503785890	4.82375147331919	0.12860004056782
H	-2.35520780035583	5.27107039440637	0.63947801753627
C	-1.58854009189787	-0.72717926379055	-3.78790377897839
C	-4.74044011809553	-2.27217126408244	-1.43273975232206
C	-2.61250129833198	-4.30486851845593	-1.04227158212253
H	-3.64023369625065	-4.62659907263311	-0.81622671955384
C	-1.59077366393197	2.93729492301827	-4.07952110114249
H	-1.33196034296207	3.81368079290408	-3.47108531993650
C	2.48489452656857	-3.94379428238780	-1.49263408498939
C	1.60585211669312	4.48980918722018	-3.94974522036828
H	1.58577219555480	5.37627960352692	-3.29807654662941
C	1.53784019588471	-2.72623823715132	-3.51964173537533
C	1.76914155407367	3.21078921188892	-3.37992402500542
C	0.76369961323729	4.97574519145787	-0.71162559348180
H	1.69014203939903	5.55214941417659	-0.86398090023971
C	-0.32741951721320	5.59038171952140	-0.07567798838068
C	-3.62303403842291	2.98787798877821	1.18743337434178
C	-4.27439747650590	1.74066222003752	-2.01959628814883
H	-4.04976366028383	0.73966815807262	-1.62509313973727
C	-1.96256676109206	-6.75757265023512	-1.27789120122752
H	-1.05717384220563	-7.29885914741893	-1.62911091431232
C	3.46144257576344	3.28708690541398	0.09974336248259
H	2.62086581135908	2.97369147488902	0.73966524438758
C	2.49624198801862	-4.25775441924021	-0.11543840781370
H	1.70814046414802	-3.84556649202448	0.53562291458070
C	-2.30786355742483	0.68586232148330	-5.73511016569570
C	1.12068309714015	-3.26855757130901	-5.86662946668707
H	0.63705355397506	-3.91064988985017	-6.61890232208411
C	5.23213013199754	-0.15058400303664	0.04010923204884
H	4.68896908990535	0.54715715565524	-0.63808013099858
C	2.33181553260899	-1.63986564466810	-3.93957382267810
H	2.81563140578449	-1.00590001413470	-3.17925565683696
C	3.50549420761272	-4.46924296537826	-2.30791043326720
H	3.51647199727672	-4.23560949726898	-3.38234335708916
C	-4.93165212160315	-1.83231839632286	-2.75808751132802
H	-4.15500947994170	-1.22289011300627	-3.24133584236497
C	1.45248026896112	4.64266187263487	-5.33609519029639
H	1.32259621112861	5.64939782734800	-5.76275534396845
C	-3.67220987070028	-1.75887796369753	0.80349466873437
C	-5.06200176038462	1.87066769335149	-3.17384015369476
H	-5.45178679879209	0.96890927630480	-3.66965711889744
C	-3.12552649964982	-2.61741466977724	1.77459531032244
H	-2.48137758194322	-3.45240797789209	1.46344277235907
C	-2.44074399942132	-1.76170442754715	-5.80598989225975
H	-2.70177566032043	-2.67984002265815	-6.35390515208804
C	0.94119536685517	-3.54071493199040	-4.50114564206708
H	0.31891018858714	-4.39369163349724	-4.19099266227652
C	-2.63138274882234	-0.52507730484952	-6.42479545554414
H	-3.03675811606692	-0.47635234113349	-7.44745422521353
C	3.49327051378175	-5.08040902525112	0.42600120688433
H	3.47799853095663	-5.31825889071745	1.50046489243398
C	-3.57209343296258	3.22885099957300	3.62389737083388
H	-2.98978208511862	3.27557579024450	4.55699917561403
C	-2.10891593395294	3.10490335506634	-5.39543201716478
H	-2.23691864339066	4.12818804970492	-5.77916752832397

C	-2.90653981457738	3.05945177643705	2.40185960717567
H	-1.80778173693103	2.98589713235285	2.38825804320205
C	-0.24588014852003	7.03194535558370	0.40293722868467
H	0.73640258003687	7.42735688899970	0.06412384716440
C	4.93095252067490	-0.17320711768230	2.60635890881872
C	4.51333976155152	-5.28467001946021	-1.76372181888541
H	5.30287402048490	-5.68305594234185	-2.41971408894074
C	-2.45796662315145	2.02665656408048	-6.20984216363496
H	-2.85558058779224	2.20344689774225	-7.22122631607680
C	-4.03983099980179	4.14257846953815	-1.89060193179993
H	-3.63254446499109	5.04034944681183	-1.40230580073728
C	1.90779874828091	-2.17941826190446	-6.27377882255147
H	2.04540024051033	-1.96330418749728	-7.34426789780629
C	-2.24837375708915	-7.21178700902007	0.16472265542092
H	-3.14497079838536	-6.69866390219542	0.57141542075148
H	-1.39547929053188	-6.97992286404784	0.83383537986456
H	-2.43560926237665	-8.30459947993707	0.20724892533367
C	-4.48494910419969	-0.68575019742384	1.23254756034354
H	-4.91894897632430	-0.00118518791680	0.48711186005746
C	-5.34086605274007	3.14432110140435	-3.69117233187234
H	-5.95018608817157	3.25232566454398	-4.60138794563888
C	4.34433977239045	3.80094469843536	-2.09683113083476
H	4.21114214985406	3.88705980178714	-3.18533520774585
C	-4.83022750154259	4.28055082425246	-3.04118714990309
H	-5.04183219134192	5.28514294916944	-3.43910854277259
C	4.70839999598573	3.56449167261020	0.67441663599862
H	4.84579691107314	3.44097655335494	1.75906293713845
C	1.77651133396138	2.09219583177249	-4.23464344226815
H	1.88213734966448	1.08674236930554	-3.80052328904132
C	5.33530047484215	-1.51767221509882	-0.65860844449803
H	4.32699923691826	-1.94854392018084	-0.81362394499222
H	5.88756265404384	-2.21945540068160	0.00314614843270
C	4.51110042334980	-5.59569821778352	-0.39595189106690
H	5.29616729940766	-6.23959712646432	0.02928312169102
C	6.62213206920962	0.43478189635366	0.30124803723021
H	7.19686064144031	-0.23905696117501	0.97183341273069
H	6.53912137624671	1.41238957710492	0.81043511900956
C	1.45333305957914	3.51682410948314	-6.17718671021039
H	1.31780275893166	3.63620428487501	-7.26298003574236
C	5.78313998124896	3.97067176006328	-0.13666394432252
H	6.76442542273315	4.19014962322577	0.31140603108691
C	-3.38209067181891	-2.40650812096765	3.14185722829150
H	-2.93559944204320	-3.08275116551978	3.88692957559429
C	-5.02632067297605	3.09667515838129	1.23404238342535
H	-5.60443448973649	3.04061681318382	0.30011028219608
C	5.09619758052738	-1.48605629239665	3.39348450876679
C	2.51954857840529	-1.36822338163314	-5.30366680853086
H	3.14487889543886	-0.51504206646721	-5.60820406637193
C	1.61705269169676	2.23904950799355	-5.62121700454740
H	1.60171781092797	1.34609681424915	-6.26451285693964
C	-4.73795280707280	-0.47131759353035	2.59211742656424
H	-5.35048589703725	0.38933195815037	2.90094831106368
C	-5.75181131424793	-3.04818849700575	-0.83127711573494
H	-5.63004128787281	-3.37991225443704	0.21120242574199
C	-4.97319528534588	3.33462272545732	3.65817421937505
H	-5.49709342825302	3.46896419986766	4.61692518425212
C	-3.12294061809663	-7.11716050676048	-2.22003306552518
H	-3.30857660587944	-8.21076978328201	-2.21518239281399
H	-2.90655257167823	-6.80794993774290	-3.26252504241530
H	-4.06452962020989	-6.61795577196939	-1.90960349781251
C	-5.69658892550610	3.26903934681601	2.45760067336814
H	-6.79446969599799	3.35173825519251	2.46822850259666
C	6.07214343145211	-1.37328727958565	-1.99468582667651
H	5.46244018373456	-0.73682393847121	-2.67478322016191
H	6.15205495287013	-2.36611104391913	-2.48420866365225
C	-6.09403862366163	-2.16667369610068	-3.46917550991785
H	-6.22013267273440	-1.80955022995649	-4.50325409091953
C	7.36612116587783	0.58439125968495	-1.03502570730760
H	6.83237815637251	1.33807543540136	-1.65528936816910
H	8.37926367733545	0.99659065686805	-0.84788024601922
C	-4.18603703961649	-1.33497119678048	3.55505629698757
H	-4.37570021665516	-1.16369746662956	4.62560794387982
C	7.45659803355946	-0.74226897775262	-1.80079303540240
H	8.09988787116103	-1.44938592759958	-1.23008784344675
H	7.95383409273698	-0.58696688928931	-2.78105679865452
C	4.79075047375817	-1.19659409196078	4.87499742194516
H	3.72238833073653	-0.93184718582077	5.00332079830207

H	5.40659913827538	-0.35551371926017	5.24618841298801
H	5.01044554245477	-2.09569508549837	5.48415440027166
C	5.59630903751778	4.08597059156418	-1.52224152090859
H	6.43142779886180	4.39955658023314	-2.16770191502045
C	4.24271440344703	-2.64877195155828	2.87359292892042
H	4.48569865240818	-3.56451400749197	3.44870742499930
H	4.43215934183435	-2.86023320221887	1.80535429215844
H	3.15777212844397	-2.45699455762207	2.99937325570506
C	-1.34496617051310	7.90720279953986	-0.22169356112455
H	-1.31226751814251	7.86660010743709	-1.32928507693340
H	-1.22927968834433	8.96587344737740	0.08906676589976
H	-2.35450830826990	7.57536387107062	0.09940272691467
C	-7.09029768658438	-2.95052042098469	-2.86412587695213
H	-8.00400740582672	-3.21323484711833	-3.41890109170836
C	6.59695571433983	-1.85909755668123	3.24477315089174
H	7.24845530237685	-1.02552631832636	3.57165756310826
H	6.85251895037434	-2.12326870342901	2.19950389511558
H	6.80902195211055	-2.74374280672049	3.87791350999595
C	-0.27537967716099	7.10493641719621	1.93980708610451
H	-0.15676161400739	8.15158739537595	2.28853570199467
H	0.53694486356243	6.49637626206913	2.38527688511805
H	-1.23882538701565	6.72338405000703	2.33834991185842
C	-6.91428706581741	-3.38904900176191	-1.54168901944343
H	-7.69172076983169	-3.99723342929321	-1.05391711156402

Selected Mayer bond orders

B(0-Co, 1-S) : 0.6756 B(0-Co, 3-P) : 0.8753 B(0-Co, 4-P) : 0.6587
B(0-Co, 5-P) : 0.8884 B(0-Co, 6-N) : 0.6422 B(0-Co, 7-N) : 0.6420
B(0-Co, 12-C) : 0.1128 B(0-Co, 14-C) : 0.1231 B(1-S , 9-N) : 0.1308
B(1-S , 10-C) : 1.2942 B(2-P , 3-P) : 0.9688 B(2-P , 5-P) : 0.9674
B(2-P , 10-C) : 0.9788 B(3-P , 4-P) : 1.0906 B(4-P , 5-P) : 1.0799
B(6-N , 14-C) : 1.4179 B(6-N , 15-C) : 0.8827 B(7-N , 12-C) : 1.4100
B(7-N , 13-C) : 0.8900 B(8-O , 95-C) : 2.1220 B(9-N , 10-C) : 1.2811
B(9-N , 64-C) : 0.9179 B(9-N , 95-C) : 0.8634 B(11-C , 16-C) : 1.1890
B(11-C , 38-C) : 1.1992 B(11-C , 61-C) : 1.2639 B(12-C , 14-C) : 1.0896

References

[1] Reviews on the coordination chemistry of phosphorus: a) M. Peruzzini, L. Gonsalvi, A. Romerosa, *Chem. Soc. Rev.* **2005**, *34*, 1038–1047; b) M. Caporali, L. Gonsalvi, A. Rossin, M. Peruzzini, *Chem. Rev.* **2010**, *110*, 4178–4235; c) B. M. Cossairt, N. A. Piro, C. C. Cummins, *Chem. Rev.* **2010**, *110*, 4164–4177; d) M. Scheer, G. Balázs, A. Seitz, *Chem. Rev.* **2010**, *110*, 4236–4256; e) M. Caporali, M. Serrano-Ruiz, M. Peruzzini, in *Chemistry Beyond Chlorine* (Eds.: P. Tundo, L.-N. He, E. Lokteva, C. Mota), Springer, Cham, **2016**, pp. 97–136; f) J. E. Borger, A. W. Ehlers, J. C. Slootweg, K. Lammertsma, *Chem. Eur. J.* **2017**, *23*, 11738–11746; g) C. M. Hoidn, D. J. Scott, R. Wolf, *Chem. Eur. J.* **2021**, 1886–1902; h) L. Giusti, V. R. Landaeta, M. Vanni, J. A. Kelly, R. Wolf, M. Caporali, *Coord. Chem. Rev.* **2021**, *441*, 213927.

[2] Selected examples of [1.1.0]bicyclotetraphosphane-1,4-diyl (P_4 butterfly) compounds: a) P. Binger, B. Biedenbach, C. Krüger, M. Regitz, *Angew. Chem. Int. Ed. Engl.* **1987**, *26*, 764–765; b) O. J. Scherer, G. Schwarz, G. Wolmershäuser, *Z. Anorg. Allg. Chem.* **1996**, *622*, 951–957; c) O. J. Scherer, T. Hilt, G. Wolmershäuser, *Organometallics* **1998**, *17*, 4110–4112; d) C. Schwarzmaier, A. Y. Timoshkin, G. Balázs, M. Scheer, *Angew. Chem. Int. Ed.* **2014**, *53*, 9077–9081; e) S. Pelties, D. Herrmann, B. de Bruin, F. Hartl, R. Wolf, *Chem. Commun.* **2014**, *50*, 7014–7016; f) J. E. Borger, M. K. Jongkind, A. W. Ehlers, M. Lutz, J. C. Slootweg, K. Lammertsma, *ChemistryOpen* **2017**, *6*, 350–353.

[3] Selected examples for *cyclo*-P_4 complexes: a) O. J. Scherer, J. Vondung, G. Wolmershäuser, *Angew. Chem. Int. Ed. Engl.* **1989**, *28*, 1355–1357; b) S. Yao, N. Lindenmaier, Y. Xiong, S. Inoue, T. Szilvási, M. Adelhardt, J. Sutter, K. Meyer, M. Driess, *Angew. Chem. Int. Ed.* **2015**, *54*, 1250–1254; c) F. Dielmann, A. Timoshkin, M. Piesch, G. Balázs, M. Scheer, *Angew. Chem. Int. Ed.* **2017**, *56*, 1671–1675; d) A. Cavaillé, N. Saffon-Merceron, N. Nebra, M. Fustier-Boutignon, N. Mézailles, *Angew. Chem. Int. Ed.* **2018**, *57*, 1874–1878; e) K. A. Mandla, M. L. Neville, C. E. Moore, A. L. Rheingold, J. S. Figueroa, *Angew. Chem. Int. Ed.* **2019**, *58*, 15329–15333; f) K. A. Mandla, C. E. Moore, A. L. Rheingold, J. S. Figueroa, *Angew. Chem. Int. Ed.* **2019**, *58*, 1779–1783; g) C. M. Hoidn, T. M. Maier, K. Trabitsch, J. J. Weigand, R. Wolf, *Angew. Chem. Int. Ed.* **2019**, *58*, 18931–18936.

[4] a) O. J. Scherer, T. Hilt, G. Wolmershäuser, *Angew. Chem. Int. Ed.* **2000**, *39*, 1425–1427; b) M. Scheer, S. Deng, O. J. Scherer, M. Sierka, *Angew. Chem. Int. Ed.* **2005**, *44*, 3755–3758; c) C. Schwarzmaier, M. Bodensteiner, A. Y. Timoshkin, M. Scheer, *Angew. Chem. Int. Ed.* **2014**, *53*, 290–293; d) C. Schwarzmaier, S. Heinl, G. Balázs, M. Scheer, *Angew. Chem. Int. Ed.* **2015**, *54*, 13116–13121; e) A. E. Seitz, M. Eckhardt, A. Erlebach, E. V. Peresypkina, M. Sierka, M. Scheer, *J. Am. Chem. Soc.* **2016**, *138*, 10433–10436; f) J. E. Borger, A. W. Ehlers, M. Lutz, J. C. Slootweg, K. Lammertsma, *Angew. Chem. Int. Ed.* **2017**, *56*, 285–290; g) J. Müller, S. Heinl, C. Schwarzmaier, G. Balázs, M. Keilwerth, K. Meyer, M. Scheer, *Angew. Chem. Int. Ed.* **2017**, *56*, 7312–7317; h) J. E. Borger, M. K. Jongkind, A. W. Ehlers, M. Lutz, J. C. Slootweg, K. Lammertsma, *ChemistryOpen* **2017**, *6*, 350–353; i) R. Grünbauer, G. Balázs, M. Scheer, *Chem. Eur. J.* **2020**, *26*, 11722–11726; j) S. Reichl, R. Grünbauer, G. Balázs, M. Scheer, *Chem. Commun.* **2021**, *57*, 3383–3386; k) R. Grünbauer, C. Schwarzmaier, M. Eberl, G. Balázs, M. Scheer, *Inorganica Chim. Acta* **2021**, *518*, 120234; l) M. Weber, G. Balázs, A. V. Virovets, E. Peresypkina, M. Scheer, *Molecules* **2021**, *26*, 3920.

[5] S. Pelties, A. W. Ehlers, R. Wolf, *Chem. Commun.* **2016**, *52*, 6601–6604.

[6] M. Piesch, M. Seidl, M. Scheer, *Chem. Sci.* **2020**, *11*, 6745–6751.

[7] S. Hauer, T. M. H. Downie, G. Balázs, K. Schwedtmann, J. J. Weigand, R. Wolf, *Angew. Chem. Int. Ed.* **2023**, e202317170.

[8] a) U. Chakraborty, J. Leitl, B. Mühldorf, M. Bodensteiner, S. Pelties, R. Wolf, *Dalton Trans.* **2018**, *47*, 3693–3697; b) C. M. Hoidn, C. Rödl, M. L. McCrea-Hendrick, T. Block, R. Pöttgen, A. W. Ehlers, P. P. Power, R. Wolf, *J. Am. Chem. Soc.* **2018**, *140*, 13195–13199; c) C. G. P. Ziegler, T. M. Maier, S. Pelties, C. Taube, F. Hennersdorf, A. W. Ehlers, J. J. Weigand, R. Wolf, *Chem. Sci.* **2019**, *10*, 1302–1308; d) A. K. Adhikari, C. G. P. Ziegler, K. Schwedtmann, C. Taube, Jan. J. Weigand, R. Wolf, *Angew. Chem. Int. Ed.* **2019**, *58*, 18584–18590.

[9] Calculated single- and double-bond lengths: a) P. Pyykkö, M. Atsumi, *Chem. Eur. J.* **2009**, *15*, 186–197; b) P. Pyykkö, M. Atsumi, *Chem. Eur. J.* **2009**, *15*, 12770–12779.

[10] C. Bianchini, D. Masi, C. C. Mealli, A. Meli, *Inorg. Chem.* **1984**, *23*, 2838–2844.

[11] M. Piesch, S. Reichl, M. Seidl, G. Balázs, M. Scheer, *Angew. Chem. Int. Ed.* **2021**, *60*, 15101–15108.

[12] A. C. Scheinost, J. Claussner, J. Exner, M. Feig, S. Findeisen, C. Hennig, K. O. Kvashnina, D. Naudet, D. Prieur, A. Rossberg, M. Schmidt, C. Qiu, P. Colomp, C. Cohen, E. Dettona, V. Dyadkin, T. Stumpf, *J Synchrotron Rad* **2021**, *28*, 333–349.

[13] Related cyclic P_4N frameworks: a) K. Issleib, Ch. Rockstroh, I. Duchek, E. Fluck, *Z. Anorg. Allg. Chem.* **1968**, *360*, 77–87; b) M. Baudler, J. Vesper, P. Junkes, H. Sandmann, *Angew. Chem. Int. Ed. Engl.* **1971**, *10*, 940–940; c) M. Baudler, E. Tolls, E. Clef, B. Kloth, D. Koch, *ZAAC* **1977**, *435*, 21–32; d) M. Baudler, P. Lütkecosmann, *Z. Anorg. Allg. Chem.* **1981**, *472*, 38–44; e) A. Hinz, A. Schulz, A. Villinger, *Chem. Eur. J.* **2014**, *20*, 3913–3916; f) S. C. Kosnik, G. J. Farrar, E. L. Norton, B. F. T. Cooper, B. D. Ellis, C. L. B. Macdonald, *Inorg. Chem.* **2014**, *53*, 13061–13069; g) F. Dielmann, G. Bertrand, *Chemistry – A European Journal* **2015**, *21*, 191–198; h) M. Höhne, M. Joksch, K. Konieczny, B. H. Müller, A. Spannenberg, N. Peulecke, U. Rosenthal, *Chem. Eur. J.* **2017**, *23*, 4298–4309; i) J. Bresien, A. Hinz, A. Schulz, A. Villinger, *European Journal of Inorganic Chemistry* **2018**, *2018*, 1679–1682.

[14] a) F. Weigend, M. Häser, H. Patzelt, R. Ahlrichs, *Chem. Phys. Lett.* **1998**, *294*, 143–152; b) J. Tao, J. P. Perdew, V. N. Staroverov, G. E. Scuseria, *Phys. Rev. Lett.* **2003**, *91*, 146401; c) V. N. Staroverov, G. E. Scuseria, J. Tao, J. P. Perdew, *J. Chem. Phys.* **2003**, *119*, 12129–12137; d) V. N. Staroverov, G. E. Scuseria, J. Tao, J. P. Perdew, *J. Chem. Phys.* **2004**, *121*, 11507; e) F. Weigend, R. Ahlrichs, *Phys. Chem. Chem. Phys.* **2005**, *7*, 3297–3305; f) J. Tomasi, B. Mennucci, R. Cammi, *Chem. Rev.* **2005**, *105*, 2999–3094; g) F. Weigend, *Phys. Chem. Chem. Phys.* **2006**, *8*, 1057–1065; h) E. Caldeweyher, C. Bannwarth, S. Grimme, *J. Chem. Phys.* **2017**, *147*, 034112; i) E. Caldeweyher, S. Ehlert, A. Hansen, H. Neugebauer, S. Spicher, C. Bannwarth, S. Grimme, *J. Chem. Phys.* **2019**, *150*, 154122.

[15] Related *catena*-P_4 units: a) O. J. Scherer, G. Berg, G. Wolmershäuser, *Chem. Ber.* **1995**, *128*, 635–639; b) P. Barbaro, M. Di Vaira, M. Peruzzini, S. Seniori Costantini, P. Stoppioni, *Inorg. Chem.* **2009**, *48*, 1091–1096; c) M. Piesch, M. Seidl, M. Stubenhofer, M. Scheer, *Chem. Eur. J.* **2019**, *25*, 6311–6316; d) Müller, G. Balázs, M. Scheer, *Chem. Commun.* **2021**, *57*, 2257–2260.

[16] M. Herberhold, S. Gerstmann, B. Wrackmeyer, H. Borrmann, *J. Chem. Soc., Dalton Trans.* **1994**, 633–636.

[17] a) L. Weber, S. Uthmann, H. Bögge, A. Müller, H.-G. Stammler, B. Neumann, *Organometallics* **1998**, *17*, 3593–3598; b) J. Barluenga, E. Rubio, M. Tomás, in *Comprehensive Organic Functional Group Transformations II* (Eds.: A.R. Katritzky, R.J.K. Taylor), Elsevier, Oxford, **2005**, pp. 545–572.

[18] G. Socrates, *Infrared and Raman Characteristic Group Frequencies: Tables and Charts*, Wiley, Chichester, **2004**.

[19] D. Laliberté, T. Maris, J. D. Wuest, *Can. J. Chem.* **2004**, *82*, 386–398.

[20] M. M. Khusniyarov, K. Harms, O. Burghaus, J. Sundermeyer, *Eur. J. Inorg. Chem.* **2006**, *2006*, 2985–2996.
[21] P. H. M. Budzelaar, in IvorySoft: gNMR for Windows, NMR Simulation Program, **2006**.
[22] a) E. G. Finer, R. K. Harris, *Mol. Phys.* **1967**, *13*, 65–75; b) S. Aime, R. K. Harris, E. M. McVicker, M. Fild, *J. Chem. Soc. Dalton Trans.* **1976**, 2144–2153; c) J. P. Albrand, H. Faucher, D. Gagnaire, J. B. Robert, *Chem. Phys. Lett.* **1976**, *38*, 521–523; d) H. C. E. McFarlane, W. McFarlane, J. A. Nash, *J. Chem. Soc. Dalton Trans.* **1980**, 240–244; e) M. A. M. Forgeron, M. Gee, R. E. Wasylishen, *J. Phys. Chem. A* **2004**, *108*, 4895–4908; f) J. E. Del Bene, J. Elguero, I. Alkorta, *J. Phys. Chem. A* **2004**, *108*, 3662–3667.
[23] a) G. M. Sheldrick, SADABS, Bruker AXS, Madison, USA, **2007**; b) CrysAlisPro, Scale3 Abspack, Rigaku Oxford Diffraction, **2019**.
[24] R. C. Clark, J. S. Reid, *Acta Crystallogr. Sect. A* **1995**, *51*, 887–897.
[25] G. M. Sheldrick, *Acta Crystallogr. Sect. Found. Adv.* **2015**, *71*, 3–8.
[26] O. V. Dolomanov, L. J. Bourhis, R. J. Gildea, J. a. K. Howard, H. Puschmann, *J. Appl. Crystallogr.* **2009**, *42*, 339–341.
[27] G. M. Sheldrick, *Acta Crystallogr. Sect. C Struct. Chem.* **2015**, *71*, 3–8.
[28] G. M. Sheldrick, *Acta Crystallogr. A* **2008**, *64*, 112–122.
[29] a) F. Neese, *Wiley Interdiscip. Rev.-Comput. Mol. Sci.* **2012**, *2*, 73–78; b) F. Neese, *Comput. Mol. Sci.* **2018**, *8*, e1327.
[30] a) J. Tao, J. P. Perdew, V. N. Staroverov, G. E. Scuseria, *Phys. Rev. Lett.* **2003**, *91*, 146401; b) V. N. Staroverov, G. E. Scuseria, J. Tao, J. P. Perdew, *The Journal of Chemical Physics* **2004**, *121*, 11507.
[31] a) F. Weigend, *Phys. Chem. Chem. Phys.* **2006**, *8*, 1057–1065; b) F. Weigend, R. Ahlrichs, *Phys. Chem. Chem. Phys.* **2005**, *7*, 3297–3305; c) F. Weigend, M. Häser, H. Patzelt, R. Ahlrichs, *Chemical Physics Letters* **1998**, *294*, 143–152.
[32] a) E. Caldeweyher, S. Ehlert, A. Hansen, H. Neugebauer, S. Spicher, C. Bannwarth, S. Grimme, *J. Chem. Phys.* **2019**, *150*, 154122; b) E. Caldeweyher, S. Ehlert, A. Hansen, H. Neugebauer, S. Spicher, C. Bannwarth, S. Grimme, *J. Chem. Phys.* **2019**, *150*, 154122.
[33] a) J. Tomasi, B. Mennucci, R. Cammi, *Chem. Rev.* **2005**, *105*, 2999–3094; b) V. Barone, M. Cossi, *J. Phys. Chem. A* **1998**, *102*, 1995–2001.
[34] G. Knizia, *J. Chem. Theory Comput.* **2013**, *9*, 4834–4843.
[35] Chemcraft - graphical software for visualization of quantum chemistry computations. https://www.chemcraftprog.com
[36] J. P. Perdew, K. Burke, M. Ernzerhof, *Phys. Rev. Lett.* **1996**, *77*, 3865–3868.
[37] a) S. Grimme, S. Ehrlich, L. Goerigk, *J. Comput. Chem.* **2011**, *32*, 1456–1465; b) S. Grimme, J. Antony, S. Ehrlich, H. Krieg, *J. Chem. Phys.* **2010**, *132*, 154104.
[38] a) F. London, *J. Phys. Radium* **1937**, *8*, 397–409; b) R. McWeeny, *Phys. Rev.* **1962**, *126*, 1028–1034; c) R. Ditchfield, *Molec. Phys.* **1974**, *27*, 789–807; d) K. Wolinski, J. F. Hinton, P. Pulay, *J. Am. Chem. Soc.* **1990**, *112*, 8251–8260; e) J. R. Cheeseman, G. W. Trucks, T. A. Keith, M. J. Frisch, *J. Chem. Phys.* **1996**, *104*, 5497–5509; f) G. L. Stoychev, A. A. Auer, R. Izsák, F. Neese, *J. Chem. Theory Comput.* **2018**, *14*, 619–637.
[39] J. P. Perdew, M. Ernzerhof, K. Burke, *J. Chem. Phys.* **1996**, *105*, 9982-9985.
[40] F. Jensen, *J. Chem. Theory Comput.* **2015**, *11*, 132–138.
[41] B. P. Pritchard, D. Altarawy, B. Didier, T. D. Gibson, T. L. Windus, *J. Chem. Inf. Model.* **2019**, *59*, 4814–4820.
[42] F. Neese, F. Wennmohs, A. Hansen, U. Becker, *Chem. Phys.* **2009**, *356*, 98–109.

Synthesis of Polyphosphido Cobalt Complexes through P−P Bond Condensation[a,b]

Abstract:

Transition metal polyphosphido complexes are latent tools for the targeted synthesis of extended phosphorus frameworks by P−P condensation reactions. This chapter presents a reactivity study of the tri- and tetraphosphido cobalt complexes [K(18c-6)][(Ar*BIAN)Co(CN)(η^3-P_3)] (**1**) and [K(18c-6)][(Ar*BIAN)Co(η^4-P_4)] (**3**) toward diorganochlorophosphines and cationic phosphorus species (18c-6 = [18]-crown-6; Ar* = 2,6-dibenzhydryl-4-isopropylphenyl; BIAN = 1,2-bis(arylimino)acenaphthene diimine). Treatment of complexes **1** and **3** with R_2PCl leads to *cyclo*-P_4R_2 and *cyclo*-P_5R_2 frameworks in complexes **2** and **4**. Further reactions of **1** and **3** with tetracationic $[(L_CP)_4][OTf]_4$ (**N**$[OTf]_4$; L_C = 4,5-dimethyl-1,3-diisopropyl-imidazol-2-yl) afford expanded polyphosphorus frameworks, as evidenced by $^{31}P\{^1H\}$ NMR spectroscopy. From these reactions the heptaphosphido complex [(Ar*BIAN)Co(η^2:η^2-P_7L_C)] (**7**) was isolated in good yield and characterized by single crystal X-ray diffraction, and spectroscopic methods. The pentaphosphido complex [(Ar*BIAN)Co(η^4-P_5L_C)] (**8**) was identified by ^{31}P NMR spectroscopy alongside **7**. Complexes **7** and **8** likely result from the disproportionation of the intermediate complex [(Ar*BIAN)Co(η^4-P_5L_C(PL_C)]OTf (**9**).

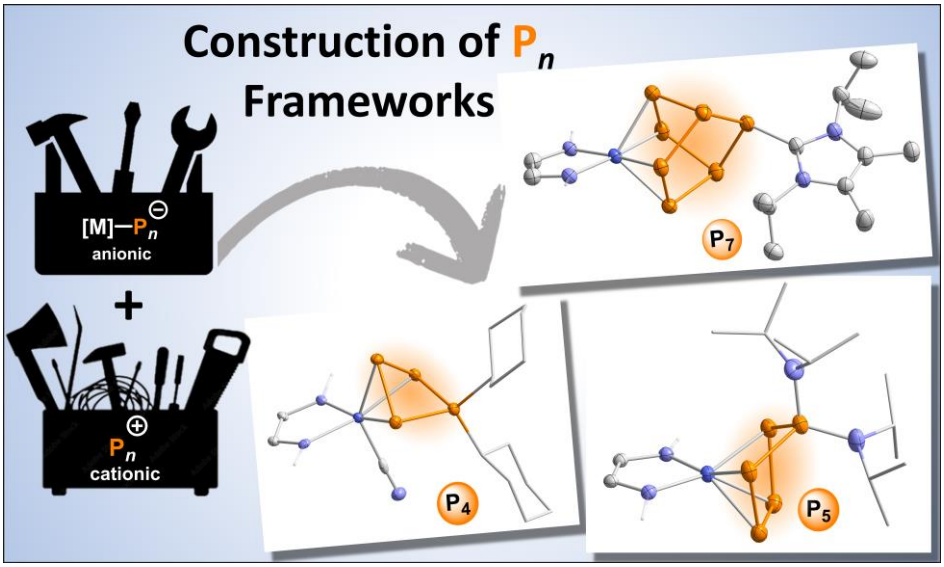

[a] S. Hauer, K. Trabitsch, R. Wolf, J. J. Weigand, unpublished results.

[b] S. Hauer performed the synthetic investigations and the characterization of the reported compounds. P. Royla synthesized the precursor compound **N**$[OTf]_4$. K. Trabitsch performed the reactions with the related PHDI cobalt complexes that are discussed for comparison. S. Hauer wrote the chapter. R. Wolf and J. J. Weigand supervised the project.

4.1 Introduction

Phosphorus possesses a pronounced tendency to form extended frameworks, which becomes evident in its various allotropes. This tendency is supported by the relative strength of the P−P single bond (200 kJ·mol^{-1}), as well as the phosphorus carbon diagonal relationship, since carbon is known to form extended homoatomic structures, e.g. in diamond.[1,2] Over the past several decades, early and late transition metal polyphosphido complexes have attracted considerable attention as latent tools for the synthesis of distinct (poly-)phosphorus compounds.[3–8] In principle, the phosphorus framework in such complexes can be expanded by P−P condensation reactions of suitable cationic and anionic building blocks. However, the targeted synthesis of extended polyphosphorus frameworks remains a challenging goal in this field.[9]

Studies in our group have shown that tetraphosphido complexes **A** and **B** can undergo salt metathesis reactions with monochlorophosphines, leading to insertion of R_2P- units and providing access to pentaphosphido ligands $[P_5R_2]^-$ in **C** and **D** (Scheme 1a).[10–12] The resulting isostructural *cyclo*-P_5R_2 ligands feature an envelope conformation and may be regarded as transition metal complexes of the corresponding $[P_5R_2]^+$ cage cations.[13-16] In subsequent work, Scheer and co-workers extended this concept of ring expansion reactions to the insertion of *in situ* generated $[R_2P]^+$ moieties.[17–20] The cations are generated from chlorophosphines and suitable halide abstractors, e.g. Tl(I) salts. Using this approach, the neutral *cyclo*-P_3 complex **E** can be transformed to cationic **G**, containing a *cyclo*-P_4R_2 scaffold (Scheme 1b).[17] Furthermore, R_2PCl also reacts with strained *cyclo*-P_3 ligands to afford the ring-expanded product, **H**.[21]

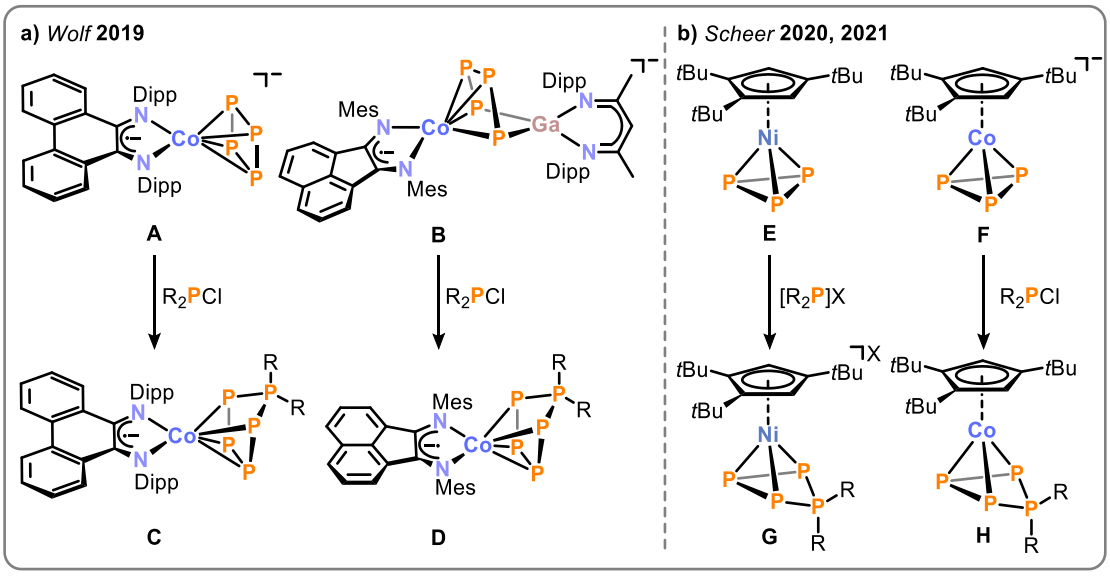

Scheme 1. Expansion reactions of a) tetra- to pentaphosphido ligands and b) tri- to tetraphosphido ligands with R_2PCl; R = alky, or aryl; Dipp = 2,6-*i*$Pr_2C_6H_3$; Mes = 2,4,6-$Me_3C_6H_2$; X = OTf^-, SbF_6^-, $GaCl_4^-$, BAr^{F-}, TEF^-; BAr^{F-} = $[B(C_6F_5)_4]^-$; TEF^- = $[Al(OC(CF_3)_3)_4]^-$.

The *cyclo*-P_3 unit found in the anion $[(PHDI)Co(CN)(\eta^3\text{-}P_3)]^-$ (PHDI = bis(2,6-diisopropylphenyl)phenanthrene-9,10-diimine), derived from the [3+2] fragmentation of CoP_5 complexes of type **C**, can also be functionalized in salt metathesis reactions involving R_2PCl.[22] Apart from the ring expansion reactions of *cyclo*-P_n complexes with chlorophosphines, or phosphenium cations (*vide supra*), the targeted expansion of P_n ligands with other electrophiles to attain extended frameworks remains highly challenging.[18,20] The use of phosphenium cations is complicated by their instability and the formation of $R_2ClP{-}PR_2^+$ type adducts that inhibit their reactivity.[23]

Recently, our group reported the reaction of **A** with the diphosphorus species $[(^{Cl}Im^{Dipp})P_2(Dipp)]Cl$ (**I**[Cl]) ($^{Cl}Im^{Dipp}$ = 4,5-dichloro-1,3-bis(2,6-diisopropylphenyl)-imidazol-2-yl) (Scheme 2).[9] Salt metathesis reactions of the corresponding chloride **I**[Cl], or triflate **I**[OTf] with the *cyclo*-P_4 complex **A** initially leads to hexaphosphido complex **J**, featuring a *cyclo*-P_5 ring and an exocyclic $(^{Cl}Im^{Dipp})P$ moiety. **J** is thermally unstable at ambient temperature and disproportionates into **K**, which contains a CoP_7 core, and the CoP_5 complex **L**.[9] The resulting products feature extended phosphorus frameworks and highlight the potential of (NHC)-stabilized polyphosphorus cations as suitable reagents for transition metal polyphosphido complexes.[24–27]

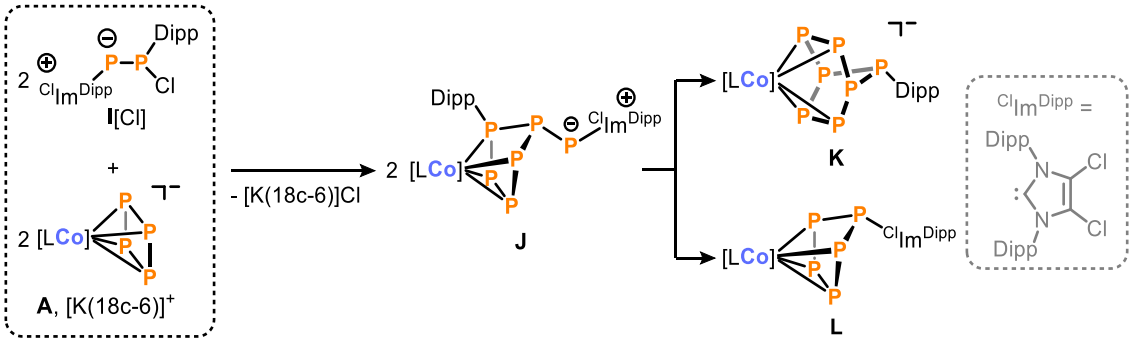

Scheme 2. Formation of **J**, **K** and **L** by P−P condensation of cyclotetraphosphido cobalt complex **A** with **I**[OTf] or **I**[Cl]; $^{Cl}Im^{Dipp}$ = 4,5-dichloro-1,3-bis(2,6-diisopropylphenyl)-imidazol-2-yl; [LCo] = (PHDI)Co.

The *cyclo*-tetraphosphane $[(L_C{-}P)_4]^{4+}$ ($\mathbf{N}^{4+}$) was reported in 2019. This tetracation is easily obtained as the triflate salt **N**$[OTf]_4$ (L_C = 4,5-dimethyl-1,3-diisopropyl-imidazol-2-yl). Recently, a more efficient synthetic route has been reported, allowing its synthesis on a scale exceeding 50 grams with 88% yield, providing easy access to a suitable cationic building block.[27,28] $\mathbf{N}^{4+}$ can be considered a formal tetramer of the cationic phosphinidene $[L_C{-}P]^+$. Computational studies suggest a high electrophilicity of the P_4 ring, due to the four imidazoliumyl substituents. Thus, the addition of $[M(PPh_3)_4]$ (M = Pd, Pt) induces transition metal mediated [2+2] fragmentation, resulting in the formation of group 10 complexes **O** (Scheme 3a).[27] These complexes feature an η^2-coordinating

$[L_CP{=}PL_C]^{2+}$ ligand. In contrast, treatment of **N**$[OTf]_4$ with an excess of AuCl(tht) leads to a reductive insertion of the gold atom into the P_4 ring and the formation of **P**, featuring a five-membered P_4Au core (Scheme 3b). Moreover, $\mathbf{N}^{4+}$ is readily cleaved *via* nucleophilic fragmentation with tertiary phosphines R_3P (R = Ph, Me, Et, Cy), affording the phosphonio–phosphanides **Q** (Scheme 3c).[28] The latter act as cationic phosphinidene transfer reagents in phospha-Wittig-type reactions toward various substrates, such as thioketones to yield cationic phosphaalkenes $[L_C{-}P{=}CR_2]^+$ (**R**, Scheme 3c). Strikingly, these phosphaalkenes proved to be excellent precursors for the preparation of very rare metallaphosphiranes $[\eta^2{-}(L_CP{=}CR_2)M]$ (M = Pd^0 and Pt^0 (**S**)) when treated with $[M(PPh_3)_4]$ (Scheme 3d). Additionally, reaction of **R** with one equivalent of $[Fe_2(CO)_9]$ yielded the κ^1-phosphaalkene complex **T** (Scheme 3e). Thus, **N**$[OTf]_4$ has proven to be an excellent precursor for the synthesis of various new phosphorus species, including (poly-)phosphorus transition metal complexes.[27,28]

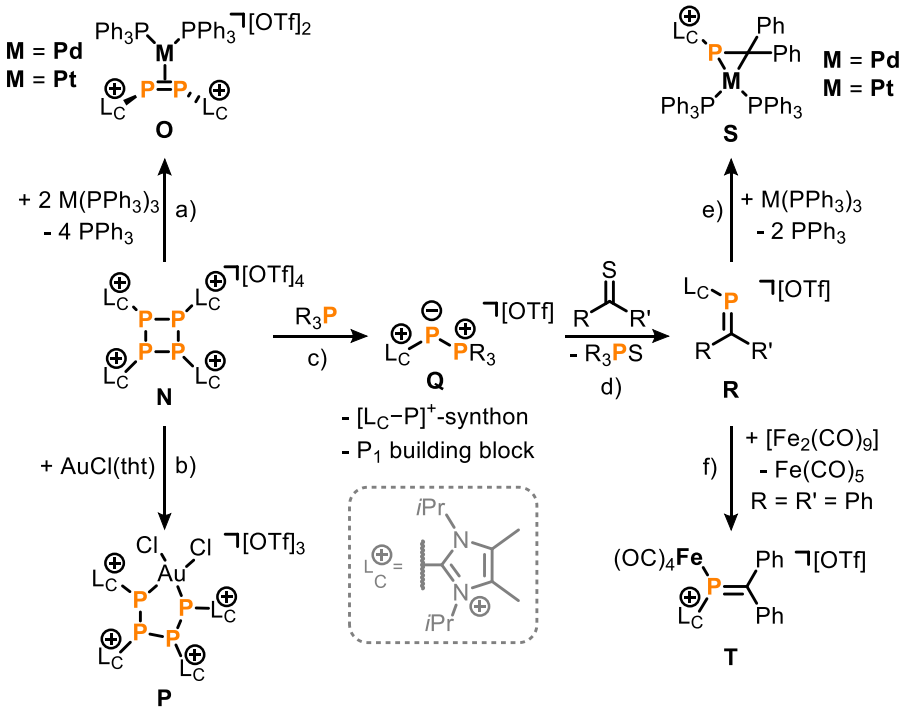

Scheme 3. a) Transition metal mediated [2+2] fragmentation, b) reductive insertion and c) nucleophilic fragmentation of tetraphosphetane **N**$[OTf]_4$. d) Conversion to phosphaalkenes and subsequent e) η^2- and f) κ^1-coordinating complexes; tht = tetrahydrothiophene; R = Aryl, Alkyl; R' = Aryl, Alkyl, OMe.

In this chapter, the synthesis and characterization of complexes with a *cyclo*-P_4R_2 ligand is presented, starting from the cyclotriphosphido complex $[(Ar^*BIAN)Co(CN)(\eta^3\text{-}P_3)]^-$ *via* insertion of R_2P- units. Moreover, the expansion of the *cyclo*-P_4 ring in $[(Ar^*BIAN)Co(\eta^4\text{-}P_4)]^-$ to a pentaphosphido ligand has been achieved, applying a similar synthetic strategy. In addition, rthe general applicability of these anionic polyphosphido complexes for P–P condensation reactions toward tetracationic tetraphosphane **N**$[OTf]_4$

is demonstrated. This is illustrated in the synthesis and characterization of bicyclo[2.2.1]heptaphosphide [(Ar*BIAN)Co(η^2:η^2-P_7L_C)].

4.2 Results and Discussion

This study started with the investigation of the reactivity of recently reported (see Chapter 2) cyclotriphosphido cobaltate [K(18c-6)][(Ar*BIAN)Co(CN)(η^3-P_3)] (**1**, 18c-6 = 18-crown-6; Ar* = 2,6-dibenzhydryl-4-isopropylphenyl; BIAN = 1,2-bis(arylimino)acenaphthene diimine) toward R_2PCl (R = *t*Bu, N(*i*Pr)$_2$, Cy).[29] No reaction was observed for R = *t*Bu in toluene. Neither prolonged stirring of the reaction mixture nor heating resulted in a reaction, according to $^{31}P\{^1H\}$ NMR spectroscopic monitoring. This lack of reactivity was attributed to the steric hindrance exhibited by both reaction partners. In contrast, a color change from purple to cyan was observed at 40 °C for R = N(*i*Pr)$_2$, Cy. According to $^{31}P\{^1H\}$ NMR spectroscopic analyses of the reaction solutions, the reaction is completed within one week and leads to the selective formation of complexes **2a** and **2b** (Scheme 4).

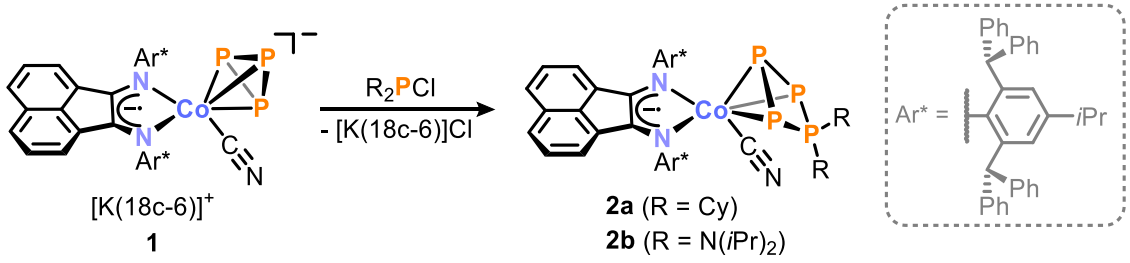

Scheme 4. Ring expansion of **1** with R_2PCl yielding the *cyclo*-P_4R_2 complexes **2**; reagents/by-products and conditions: +R_2PCl/−[K(18c-6)]Cl; toluene, 40 °C, 7 d; isolated yields: **2a**: 34%, **2b**: 11%.

Crystallization from a toluene/*n*-hexane solution yielded cyan colored crystals of **2a** [(Ar*BIAN)Co(CN)(η^3-P_4R_2)] in moderate yield (34%). The relatively low yield is due to the high solubility of **2a** in common organic solvents. X-ray diffraction (XRD) analysis conducted on single crystals of **2a** revealed the presence of a *cyclo*-P_4R_2 ligand in a puckered conformation coordinated η^3 to the cobalt center (Figure 1a). Additionally, a formally radical anionic Ar*BIAN$^{\bullet-}$ ligand (C1−N1 1.307(7), C2−N2 1.309(7), C1−C2 1.459(7) Å) and a cyanide ligand complete the coordination sphere.[30] The Co−C (1.900(6) Å) and C≡N (1.135(8) Å) bond lengths, as well as the CN stretching vibration ($\tilde{\nu}_{CN}$ = 2091 cm^{-1}), fall within the typical range for cobalt cyanide complexes.[31–33] Additionally, the P2−P3 (2.202(2) Å) and P3−P4 (2.2015(2) Å) bond lengths are in a common range for P−P single bonds ($\sum r_{PP}$ 2.22 Å).[34,35] In contrast, the bond lengths P1−P2 (2.1703(2) Å) and P1−P4 (2.176(2) Å), which involve the organo-substituted phosphorus atom P1, are slightly shorter than expected for typical P−P single bonds,

suggesting a delocalized system and a phosphonium-like character for P1. Furthermore, the bond lengths observed in **2a** align closely with those reported for NiP_4R_2 **G** (R = Ph, Mes, Cy, 2,2'-biphen, Me), CoP_4R_2 **H** (R = Ph, Cy, *t*Bu), and the [(PHDI)Co(CN)(η^3-P_4R_2)] analogue (R = Cy, Ph) (see Scheme 1).[17,21,22]

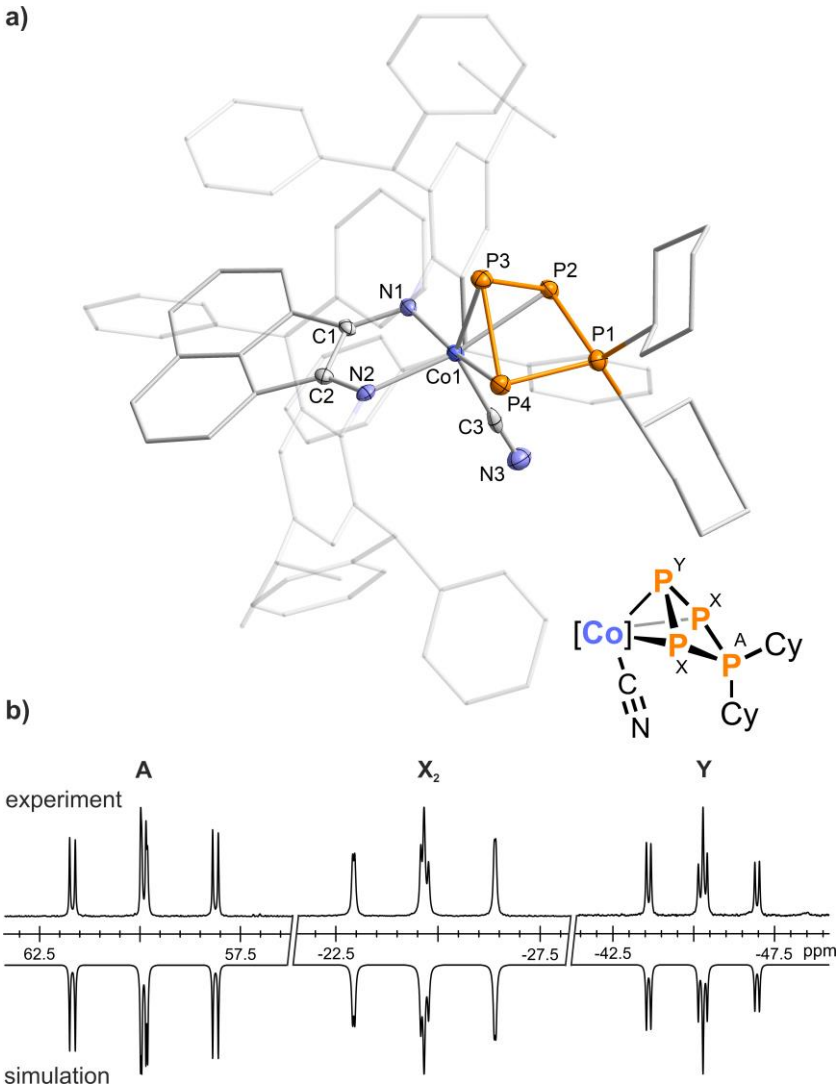

Figure 1. a) Solid-state molecular structure of [(Ar*BIAN)Co(CN)(η^3-P_4Cy_2)] (**2a**); thermal ellipsoids are shown at the 50% probability level; hydrogen atoms and non-coordinating solvent molecules omitted for clarity. Selected bond lengths [Å] and angles [°]: P1−P2 2.1703(2), P1−P4 2.176(2), P2−P3 2.202(2), P3−P4 2.2015(2), Co1−P2 2.2922(2), Co1−P3 2.2692(2), Co1−P4 2.2933(2), Co1−C3 1.901(6), C3−N3 1.135(8), Co1−N1 1.970(5), Co1−N2 2.002(4), N1−C1 1.307(7), N2−C2 1.309(7), C1−C2 1.459(7), P1-P2-P3 82.71(7), P2-P3-P4 86.36(7), P3-P4-P1 82.60(7), P4-P1-P2 87.79(7), Co1-C3-N3 177.8(5), N1-Co1-N2 82.26(2), N1-C1-C2 115.6(5); b) experimental (upward) and simulated (downward) $^{31}P\{^1H\}$ NMR spectra of **2a**, with nuclei assigned to an AX_2Y spin system: $\delta(P_A)$ = 59.9 ppm, $\delta(P_X)$ = −24.7 ppm, $\delta(P_Y)$ = −45.2 ppm, $^1J_{AX}$ = −289 Hz, $^1J_{XY}$ = −272 Hz, $^2J_{AY}$ = 24 Hz. The spectra of the related compound **2b** is very similar (see the SI for further details); [Co] = (Ar*BIAN)Co.

Both complexes **2a** and **2b** exhibit an AX_2Y spin system in the $^{31}P\{^1H\}$ NMR spectrum, consistent with the observed solid-state molecular structure and confirmed through an iterative fitting procedure (Figure 1b). Specifically, the resonances of **2a** (δ = 59.9 (P_A), −24.7 (P_X), −45.2 (P_Y) ppm) are shifted significantly upfield compared to

related acylated CoP_4 complexes [(Ar*BIAN)Co(η^1:$\eta^1$$P_4$C(O)R)] ($\delta$ = 323.3 (P_A), 109.7 (P_M), 59.2 (P_X) ppm for R = *t*Bu).[29] In addition, the observed coupling pattern is similar to that reported for Cp'''CoP_4R_2 **H** (R = Cy; AMM'X) and PDHI analogue [(PHDI)Co(CN)(η^3-P_4Cy_2)], featuring an AM_2X spin system.[21,22]

In order to probe if this type of ring expansion reaction can be extended to other P_n ligands, we investigated the reactivity of *cyclo*-P_4 complex [K(18c-6)][(Ar*BIAN)Co(η^4-P_4)] (**3**) toward R_2PCl. Gratifyingly, **3** also reacts selectively with one equivalent of R_2PCl (R = *t*Bu, N(*i*Pr)$_2$) in a salt metathesis reaction yielding **4** (Scheme 5). In contrast to triphosphido complex **1**, CoP_4 species **3** readily reacts with the sterically congested *t*Bu_2PCl and the reaction with (N(*i*Pr)$_2$)$_2$PCl is notably faster (1 d vs. 7 d), highlighting the increased nucleophilicity and thus reactivity of **3** toward electrophiles.

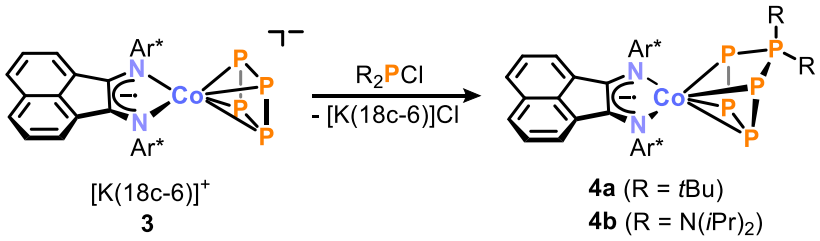

Scheme 5. Salt metathesis of **3** with R_2PCl affording the ring-expanded *cyclo*-P_5R_2 complexes **4**; reagents/by-products and conditions: +R_2PCl/−[K(18c-6)]Cl; **4a**: toluene, 32 °C, 4 weeks, **4b**: toluene, r.t., 1 d; isolated yields: **4a**: 79%, **4b**: 73%.

Complexes [(Ar*BIAN)Co(η^4-P_5R_2)] (**4a**: R = *t*Bu; **4b**: R = N(*i*Pr)$_2$) were obtained as turquoise needles in good isolated yields of 79% and 73% for **4a** and **4b**, respectively. Single crystal X-ray diffraction (SCXRD) analysis of these confirmed the insertion of the R_2P- moiety into one P−P bond of the *cyclo*-P_3 unit, leading to the formation of η^4-coordinating *cyclo*-P_5R_2 ligands in **4a** and **4b** (Figure 2a). These complexes exhibit structural characteristics akin to those observed in **C** and **D,** bearing cobalt ^{Mes}BIAN and PHDI backbones, respectively (*vide supra*).[10,11] In **4a**, the P−P bond lengths range from 2.133(1) to 2.163(3) Å. These bond lengths lie between typical P−P single and P=P double bond lengths ($\sum r_{PP}$ 2.22 Å vs. 2.04 Å), suggesting delocalization within the P_5R_2 ligand.[34,35]

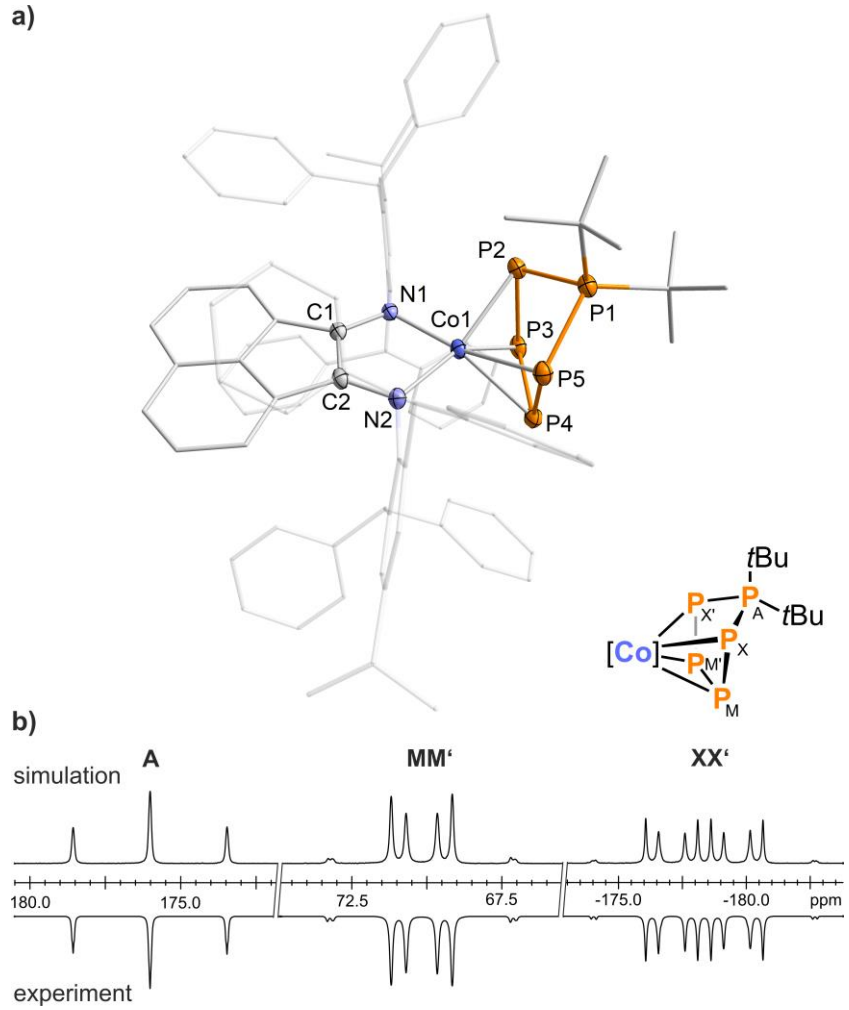

Figure 2. a) Solid-state molecular structure of [(Ar*BIAN)Co(η^4-P$_5$*t*Bu$_2$)] (**4a**); thermal ellipsoids are shown at the 50% probability level; The asymmetric unit cell contained a second crystallographically independent molecule with very similar structural parameters; only one of these molecules is shown. Hydrogen atoms, disorder in the *t*Bu group and non-coordinating solvent molecules are omitted for clarity. Selected bond lengths [Å] and angles [°]: P1−P2 2.158(1), P1−P5 2.1632(1), P2−P3 2.1633(1), P3−P4 2.1330(1), P4−P5 2.1544(1), Co1−P2 2.3407(8), Co1−P3 2.3193(8), Co1−P4 2.3169(9), Co1−P5 2.3510(8), Co1−N1 1.935(2), Co1−N2 1.945(2), N1−C1 1.331(3), N2−C2 1.341(3), C1−C2 1.424(4), P1-P2-P3 101.26(4), P1-P5-P4 102.45(4), P2-P3-P4 104.11(4), P3-P4-P5 103.29(4), N1-Co1-N2 83.90(9), N1-C1-C2 115.4(2), N2-C2-C1 116.5(2); b) experimental (upward) and simulated (downward) $^{31}P\{^1H\}$ NMR spectra of **4a**, with nuclei assigned to an AMM'XX' spin system: $\delta(P_A)$ = 176.0 ppm, $\delta(P_M)$ = 70.2 ppm, $\delta(P_X)$ = −178 ppm, $^1J_{AX} = {}^1J_{AX'}$ = −413 Hz, $^1J_{MX} = {}^1J_{M'X'}$ = −369 Hz, $^1J_{MM'}$ = −411 Hz, $^2J_{MX'} = {}^2J_{M'X}$ = 39 Hz, $^2J_{AM} = {}^2J_{AM'}$ = 6 Hz, $^2J_{XX'}$ = 19 Hz. The spectra of the related compound **4b** is very similar (see Figure S13); [Co] = (Ar*BIAN)Co.

The $^{31}P\{^1H\}$ NMR spectrum of **4a** revealed an AMM'XX' spin system, which was simulated by an iterative fitting procedure, identifying large $^1J_{PP}$ coupling constants ranging from −369 Hz to −413 Hz (Figure 2a). The chemical shifts and coupling pattern compare well with those reported for the PHDI analogue **C** (R = *t*Bu) and the ^{Mes}BIAN cobalt complex **D** (R = *t*Bu).[10,11]

Thus, the selective reactions to give **2** and **4** demonstrated that **1** and **3** are suitable precursors for ring expansion reactions and complexes containing extended oligophosphorus frameworks. To extend the scope of this type of reaction to other

electrophiles, the reactions of **1** and **3** with the phosphinidene $[L_C{-}P]^+$ transfer reagent **N**$[OTf]_4$ (see introduction Scheme 3) were investigated next. To this end, a deep purple solution of **1** in THF was treated with half an equivalent of **N**$[OTf]_4$, resulting in a rapid transition to blue color (Scheme 6).

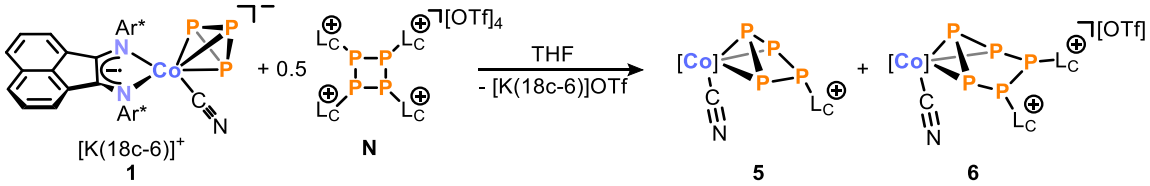

Scheme 6. Reaction of *cyclo*-P_3 complex **1** with **N**$[OTf]_4$ affording the polyphosphido complexes **5** and **6**; reagents/by-products and conditions: +0.5 eq. **N**$[OTf]_4$/−[K(18c-6)]OTf; THF, r.t. °C, 1 h.

The $^{31}P\{^1H\}$ NMR spectrum of the reaction mixture revealed the emergence of two distinct sets of signals (Figure 3). Despite efforts, single crystals of the resulting products and its adducts with $W(CO)_5$, $Al(C_2H_5)_3$, and AuCl suitable for SCXRD could not be obtained. Nevertheless, from the analogous reactions of $[(n\text{Bu})_4\text{N}][(\text{PHDI})\text{Co}(\text{CN})(\eta^3\text{-}P_3)]$ with **N**$[OTf]_4$, the resulting products $[(\text{PHDI})\text{Co}(\text{CN})(\eta^3\text{-}P_4L_C)]$ and $[(\text{PHDI})\text{Co}(\text{CN})(\eta^3\text{-}P_5L_{C2})]$OTf could be isolated in 36% and 14% yield, respectively, and structurally characterized.[36]

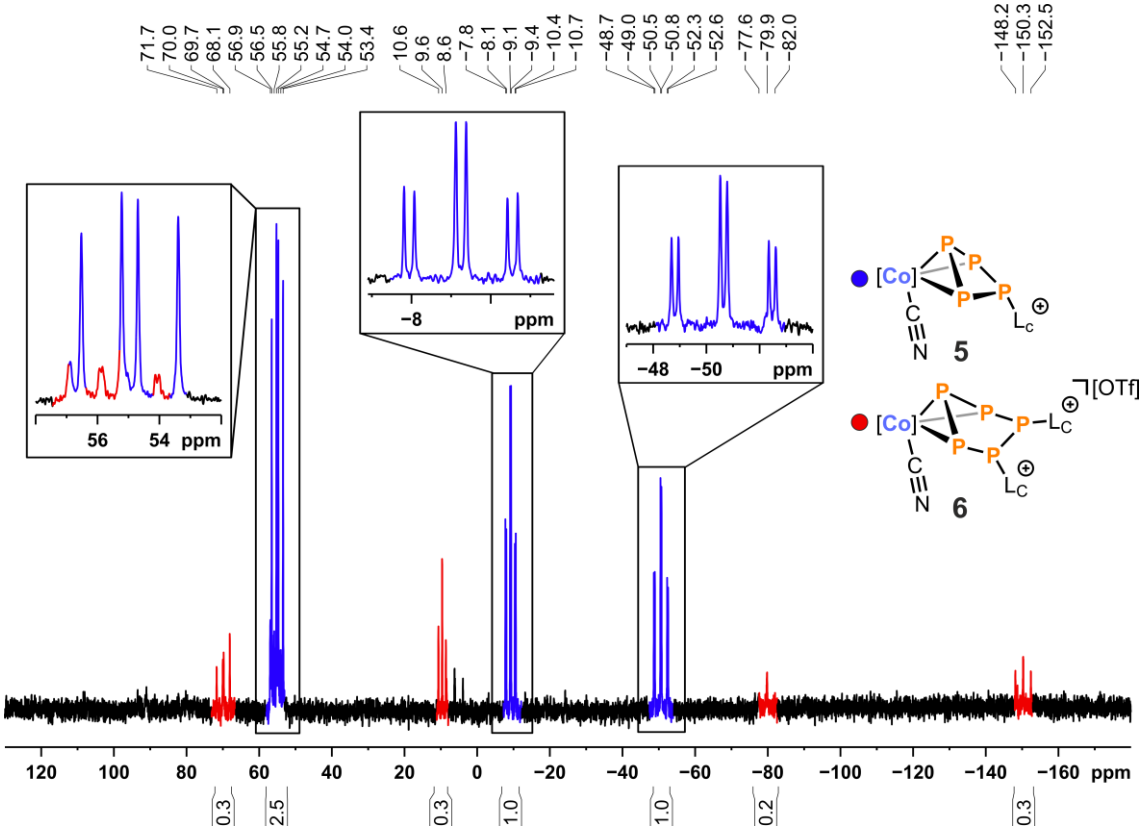

Figure 3. $^{31}P\{^1H\}$ NMR spectrum (162.04 MHz, 300 K, C_6D_6-capillary) of the reaction solution of **1** and 0.5 eq. **N**$[OTf]_4$ in THF exhibiting two sets of signals attributed to two proposed species; *blue*: A_2MX spin system assigned to **5**; *red*: ABCDE spin system assigned to **6**; [Co] = (Ar*BIAN)Co.

Both sets of signals could be assigned by comparison with the very similar ^{31}P NMR data of the related PHDI compounds,.[36] The signals with higher intensity (highlighted in *blue* in Figure 3) were assigned to the salt metathesis product [(Ar*BIAN)Co(CN)(η^3-P_4L_C)] (**5**) in the $^{31}P\{^1H\}$ NMR spectrum (*vide supra*). **5** constitutes the product resulting from the insertion of a $[L_C{-}P]^+$ unit into the *cyclo*-P_3 ring in **1**, with concomitant elimination of KOTf. On the other hand, the set of signals with lower intensity (marked in *red* in Figure 3) was assigned to the cationic *cyclo*-P_5 complex **6**. Complex **6** gives rise to an ABCDE spin system in the $^{31}P\{^1H\}$ NMR spectrum. This is presumably due to a hindered rotation of the imidazolium-2-yl caused by steric crowding. Similar observations have been made for the PHDI analogue.

The formation of **6** can be explained by the cleavage of $\mathbf{N}^{4+}$ into two P_2^{2+} units and the subsequent insertion of one $[L_C{-}P]_2^{2+}$ moiety into a P−P bond in **1**. Similar transition metal-induced [2+2] fragmentation of $\mathbf{N}^{4+}$ has been reported for the synthesis of dicationic diphosphene complexes **O** of Pd and Pt (*vide supra*, Scheme 3).[27] Whereas the Ar*BIAN system preferentially gives **5**, the reaction of the PHDI *cyclo*-P_3 complex toward **N**$[OTf]_4$ mainly affords the analogue of **6**, according to $^{31}P\{^1H\}$ NMR spectroscopic monitoring. This is possibly due to the lower steric hindrance offered by the PHDI ligand compared to the Ar*BIAN ligand, allowing the presence of two L_C substituents. A similar distribution of products was observed regardless of the reactions solvent (toluene, THF), contrasting the high solvent dependency exhibited by the PHDI system.[36]

Next, to explore whether this strategy is restricted to triphosphido complexes, the reactivity of the CoP_4 complex **3** toward **N**$[OTf]_4$ was investigated. Indeed, addition of half an equivalent of solid **N**$[OTf]_4$ to a solution of **3** in THF causes a rapid color change from purple to dark blue (Scheme 7).

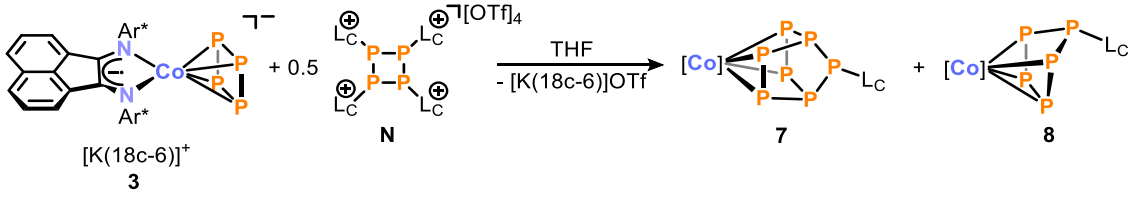

Scheme 7. Reaction of *cyclo*-P_4 complex **3** with **N**$[OTf]_4$ affording the polyphosphido complexes **7** and **8**; reagents/by-products and conditions: +0.5 eq. **N**$[OTf]_4$/−[K(18c-6)]OTf; THF, r.t. °C, 1 d; isolated yield **7**: 39%.

The $^{31}P\{^1H\}$ NMR spectrum of the reaction solution revealed two sets of signals (Figure 4). The set of signals marked in *blue* was assigned to an AMM'XX'YY' spin system, which is very similar to previously reported anionic P_7 cage compound

[(PHDI)Co(η^4-P_7Dipp)]$^-$ (**K**, Scheme 2).[9] Compared to **K**, the entire set of resonances (δ = 46.8 (P_A), −22.3 (P_M), −74.6 (P_X), −133.8 (P_Y) ppm) is shifted upfield (Figure S17, SI).[9]

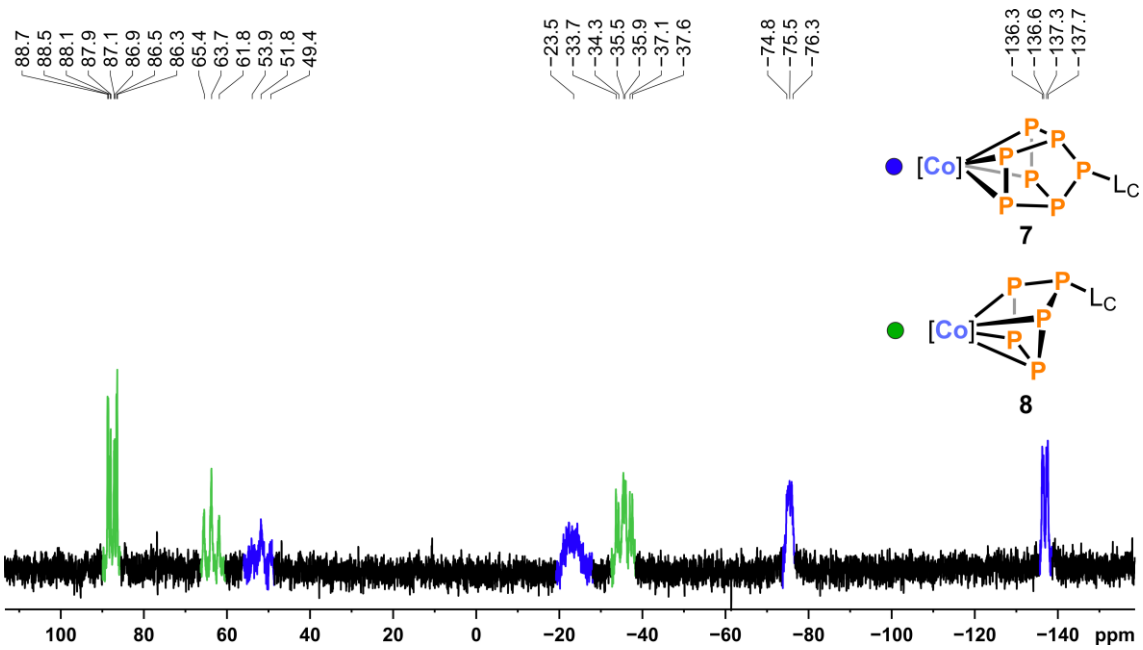

Figure 4. $^{31}P\{^1H\}$ NMR spectrum (162.04 MHz, 300 K, C_6D_6-capillary) of the reaction solution of **3** and **N**[OTf]$_4$ in THF exhibiting two sets of signals attributed to two proposed species; *blue*: AMM'XX'YY' spin system assigned to **7**; *green*: AA'MXX' spin system assigned to **8**; [Co] = (Ar*BIAN)Co.

After work-up, dark blue crystals of [(Ar*BIAN)Co(η^2:η^2-P_7L_C)] (**7**) were isolated in a 39% yield from a 1,4-dioxane/*n*-hexane mixture. SCXRD analysis of **7** confirmed the presence of a bicyclo[2.2.1]heptaphosphide framework coordinating η^2:η^2 to the cobalt atom (Figure 5). Several transition metal complexes featuring a norbornadiene-like P_7 framework have been previously reported, such as [Cp*Fe(η^4-P_7)]$^-$,[37] [Fe(HP_7)$_2$]$^{2-}$,[38] [P_7M(CO)$_3$]$^{3-}$ (M = Cr, Mo, W),[39] [P_7Ni(CO)]$^{3-}$,[40] and more recently in anionic **K** (*vide supra*).[9] These examples were synthesized by reacting P_4 with ferrate, or Zintl phase K_3P_7 with metal halides, or carbonyls. Thus, heptaphosphide **K** was afforded by a completely different "bottom up" approach. Building upon the synthetic pathway toward **K**, we have found that through use of different cationic organophosphorus reagents, such as **N**[OTf]$_4$, further phosphorus frameworks, in neutral **7**, are made accessible.

The second set of signals, marked in *green*, was assigned to an AA'MXX' spin system which strongly resembles those of the previously reported iron pentaphosphido complexes [Cp*Fe(η^4-P_5R)]$^-$[41] (Cp* = η^5-C_5Me_5; R = CH_2SiMe_3, NMe_2) and [Cp*Fe(η^4-P_5(NHC))][42] (NHC = IMes [1,3-bis(2,4,6-trimethylphenyl)imidazolin-2-ylidene], IPr [1,3-bis(2,6-diisopropylphenyl)imidazolin-2-ylidene]), [Cp^{Ar}Co(η^4-P_5R_2)][$GaCl_4$][12] ($C_5(C_6H_4$-4-Et$)_5$; R = *i*Pr, Cy) and

[Cp'''Ta(CO)$_2$(η^4-P$_5$Ph$_2$)].[20] Although no crystals suitable for SCXRD have been obtained for the corresponding complex [(Ar*BIAN)Co(η^4-P$_5$L$_C$)] (**8**) so far, the PHDI analogue has been isolated in 18% yield as the dinuclear W(CO)$_5$-adduct.[36] The structure is related to *cyclo*-P$_5$ complexes **C**,[11] **D**[10] and **4a-b**, resulting from an insertion of R$_2$P-units into *cyclo*-P$_4$ ligands (*vide supra*, Scheme 1).

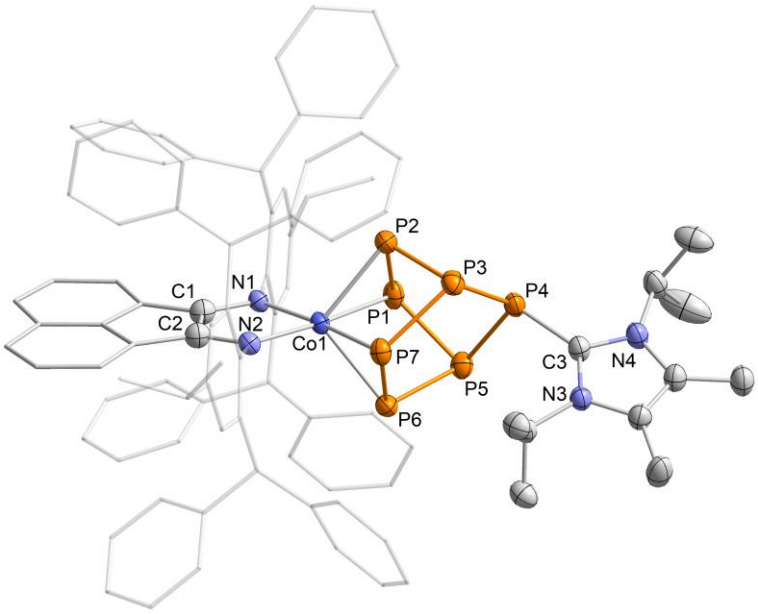

Figure 5. Solid-state molecular structure of [(Ar*BIAN)Co(η^2:η^2-P$_7$L$_C$)] (**7**); thermal ellipsoids are shown at the 50% probability level; hydrogen atoms, non coordinating solvent molecules and disorder in der Ar*BIAN ligand are omitted for clarity. Selected bond lengths [Å] and angles [°]: P1−P2 2.1627(8), P1−P5 2.1967(7), P2−P3 2.2235(7), P3−P4 2.1788(7), P3−P7 2.2138(6), P4−P5 2.1758(6), P5−P6 2.2249(6), P6−P7 2.1397(7), Co1−P1 2.3118(5), Co1−P2 2.3349(5), Co1−P6 2.3513(5), Co1−P7 2.3002(5), P4−C3 1.855(2), C3−N3 1.350(2), C3−N4 1.356(2), Co1−N1 1.9699(2), Co1−N2 19.481(1), N1−C1 1.332(2), N2−C2 1.345(2), C1−C2 1.421(2), P1-P2-P3 104.49(3), P2-P3-P4 92.46(3), P3-P4-P5 103.21(2), P4-P5-P6 110.36(3), P5-P6-P7 104.96(2), P2-P3-P7 79.61(2), N3-C3-N4 106.81(2), N1-Co1-N2 82.81(6).

In a similar, previously reported reaction, heptaphosphido complex **K** and pentaphosphido complex (PHDI)Co{η^4-*cyclo*-P$_5$(^{Cl}Im^{Dipp})} (**L**) are formed by disproportionation of two molecules of a hexaphosphido complex, [(PHDI)Co{η^4-*cyclo*-P$_5$Dipp(P(^{Cl}Im^{Dipp})}] (**J**). Thus, a similar reaction sequence could be operating in the reaction of **3** with **N**[OTf]$_4$ (Scheme 8). Thus far, no intermediates have been detected by ^{31}P{^{1}H} NMR spectroscopic monitoring of the reaction. Nevertheless, electrospray ionization mass spectrometry (ESI-MS) of the reaction solution detected a molecular ion peak at *m/z* = 1686.602, suggesting the presence of a hexaphosphido complex, [(Ar*BIAN)Co{η^4-*cyclo*-P$_5$L$_C$(PL$_C$)}]OTf (**9**), as an intermediate. Monocationic **9** arises from the formal insertion of a diphosphene cation [L$_C$−P]$_2^{2+}$ ("=$^1/_2$ **N**$^{4+}$") into the tetraphosphido ligand in **3**. Insertion of the [L$_C$−P]$_2^{2+}$ fragment into the *cyclo*-P$_4$ ring of **3** could yield two possible structural motifs for the phosphorus framework in **9**: a structure analogous to **6**, featuring a *cyclo*-P$_6$ ligand, or a *cyclo*-P$_5$ ligand with an exocyclic P−L$_C^+$

moiety. In our previous study such an η^4-coordinating hexaphosphido complex with an envelope structure could be isolated (**J**, Scheme 2). Structural analysis elucidated an exocyclic two-coordinate phosphorus atom at the apex in **J**. Thus, the second option as depicted in Scheme 8 is more likely, as [9] Subsequently, **9** quickly disproportionates to complexes **7** and **8**.

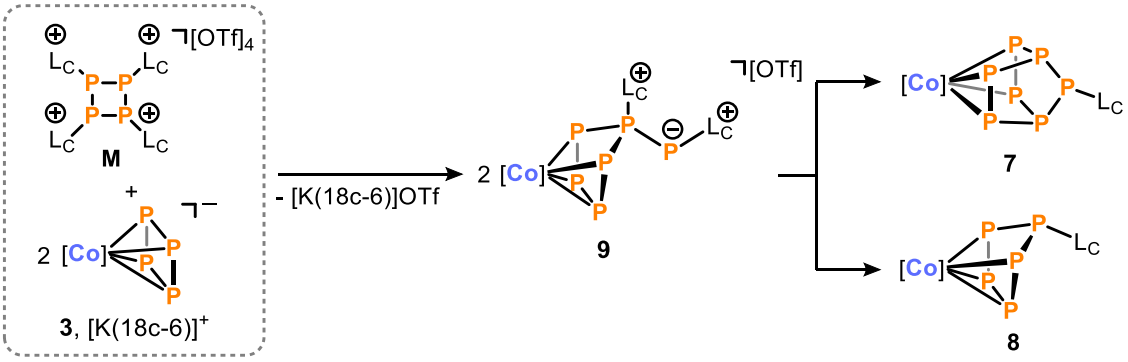

Scheme 8. Proposed reaction sequence for the P−P condensation reaction of [K(18c-6)][(Ar*BIAN)Co(η^4-P_4)] (**3**) with **N**[OTf]$_4$.

After work-up further by-products are apparent in the ^{1}H and ^{31}P{^{1}H} spectra of the reaction solutions. These include the free carbene, L_C, and Ar*BIAN, as well as minor amounts of white phosphorus and the dinuclear oxidation product, [(Ar*BIAN)$_2$Co$_2$(μ,η^4:η^4-P_4)], as evidenced by a singlet at δ = 216 ppm in the ^{31}P{^{1}H} spectrum.[43] These by-products are most likely formed during the disproportionation.[9] After the successful isolation of compound **7**, the ^{31}P{^{1}H} spectrum of the mother liquor clearly shows the presence of cobalt pentaphosphido complex **8** (Figure 6). Current research efforts are focused on crystallizing the pentaphosphido complex from this enriched mother liquor.

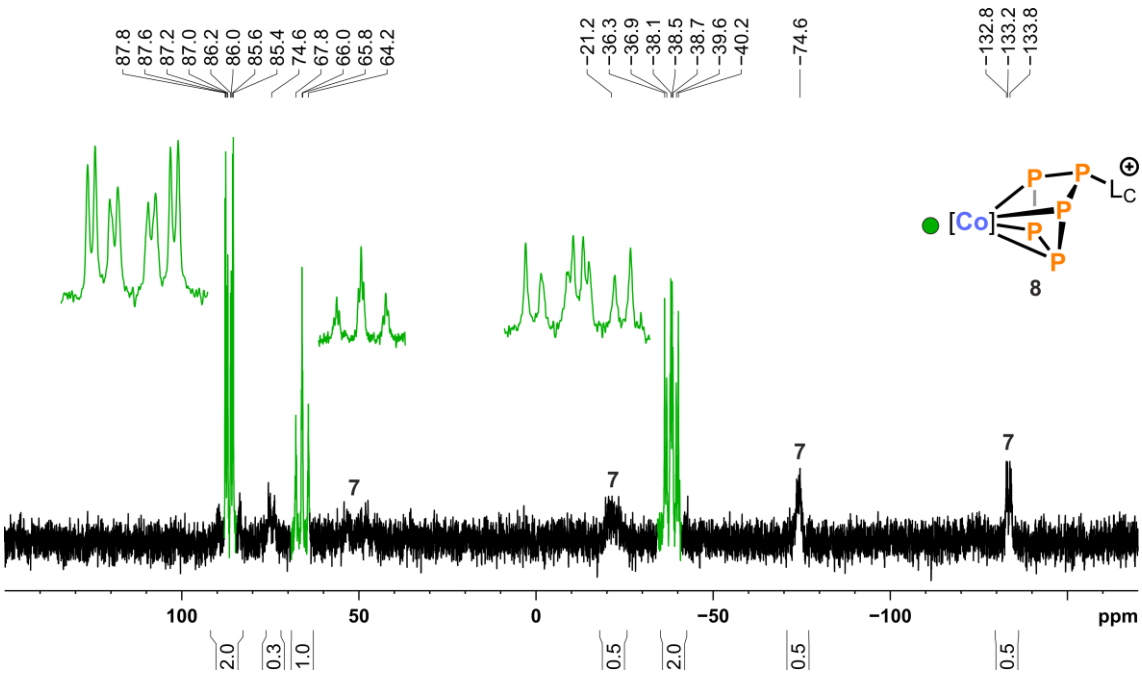

Figure 6. $^{31}P\{^{1}H\}$ NMR spectrum (162.04 MHz, 300 K, C_6D_6-capillary) of the mother liquor after isolation of **7** in toluene; *green*: AA'MXX' spin system assigned to **8**; signals of residual CoP_7 complex **7** is marked with **7**; traces of oxidation product at δ = 216 ppm are not depicted; [Co] = (Ar*BIAN)Co.

4.3 Conclusion

In this work, we have demonstrated that the tetraphosphido complexes **2a,b**, featuring a puckered *cyclo*-P_4R_2 ligand, are accessible through ring expansion reactions of triphosphido complex **1** with R_2PCl. The CoP_5 complexes **4** are similarly synthesized in high yield by insertion of R_2P- moieties into the *cyclo*-P_4 ligands in **3**. These reactions highlight the accessibility of *cyclo*-P_n ligands for the synthesis of extended phosphorus frameworks. Using this approach, reactions of the phosphinidene $[L_C{-}P]^+$ transfer reagent **N**$[OTf]_4$ with **1** and **3** were examined. $^{31}P\{^{1}H\}$ NMR spectroscopic monitoring of the reaction of $\mathbf{N}^{4+}$ with **1** revealed the formation of neutral cyclotetraphosphido complex **5** as the major product and cationic $CoP_5L_{C2}^+$ complex **6** as a side product. Despite the good selectivity observed in these insertion reactions, the resulting products have, thus far, eluded crystallization. Strikingly, ESI-MS spectra suggest that the reaction of CoP_4 complex **3** with **N**$[OTf]_4$ initially yields a CoP_6 intermediate, **9**, *via* 1,1-insertion of a $[L_C{-}P]_2^{2+}$ fragment into the *cyclo*-P_4 ring. Disproportionation of compound **9** gives rise to extended P_n-frameworks in both the CoP_7 complex **7** and the CoP_5 complex **8**. These results illustrate that the strategic combination of cationic P_n^+ and anionic transition metal polyphosphides TM-P_n^- represents a fruitful strategy for the synthesis of unique (poly-)phosphorus compounds.

4.4 Experimental Details

General Synthetic Methods

All reactions and product manipulations were carried out in oven-dried glassware under an inert atmosphere of argon using standard Schlenk line or glovebox techniques (maintained at <0.1 ppm H_2O and <0.1 ppm O_2). $[(L_C)_4P_4][OTf]_4$ (L_C = 4,5-dimethyl-1,3-diisopropylimidazol-2-yl)[27,28] was prepared and kindly provided by Philipp Royla (research group of Prof. Jan J. Weigand, TU Dresden), [K(18c-6)][(Ar*BIAN)Co(η^4-P_4)], as well as [K(18c-6)][(Ar*BIAN)Co(CN)(η^3-P_3)] were prepared according to procedures previously reported within this thesis (Chapter 2). All other chemicals were purchased from commercial suppliers and used without further purification.

Solvents were dried and degassed with an MBraun SPS800 solvent purification system. All dry solvents except *n*-hexane and *n*-pentane were stored under argon over activated 3 Å molecular sieves in gas-tight ampules. *n*-Hexane and *n*-pentane were instead stored over potassium mirrors.

General Analytical Techniques

NMR spectra were recorded on Bruker Avance 400 spectrometers at 300 K and were internally referenced to residual solvent resonances (^{1}H NMR: C_6D_6: 7.15 ppm; $^{13}C\{^1H\}$ C_6D_6: 128.06 ppm). Chemical shifts δ are given in ppm referring to external standards of tetramethylsilane (^{1}H, $^{13}C\{^1H\}$) or 85% H_3PO_4(aq.) ($^{31}P\{^1H\}$). ^{1}H, ^{13}C and ^{31}P NMR signals were assigned based on 2D NMR spectra (COSY, HSQC, HMBC, NOESY and ROESY).

UV/Vis spectra were recorded on an Ocean Optics Flame Spectrometer with a DH-2000-BAL light source. Mass spectra were recorded by the Central Analytical Department at the University of Regensburg using a Jeol AccuTOF GCX. Elemental analysis were performed by the Central Analytical Department of the University of Regensburg using a Vario micro cube. IR spectra were recorded with a Bruker ALPHA spectrometer equipped with a diamond ATR unit.

NMR Simulations

For compounds which give rise to a higher order spin system in the $^{31}P\{^1H\}$ NMR spectrum, the resolution enhanced $^{31}P\{^1H\}$ NMR spectrum was transferred to the software gNMR, version 5.0.6, by Cherwell Scientific.[44] The full line shape iteration procedure of gNMR was applied to obtain the best match of the fitted to the experimental

spectrum. $^{1}J(^{31}P^{31}P)$ coupling constants were set to negative values and all other signs of the coupling constants were obtained accordingly.[45–50]

4.4.1 Synthesis of Compounds

[(Ar*BIAN)Co(CN)(η³-P₄Cy₂)] (2a):

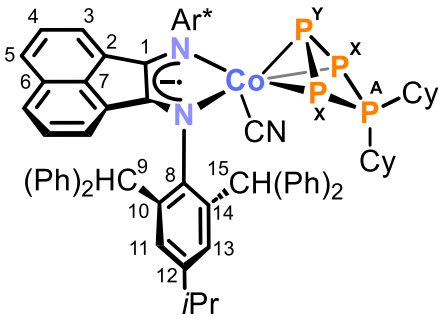

A stock solution of Cy_2PCl (273 µL, c = 0.112 M in *n*-hexane, 0.031 mmol, 1.1 equiv.) was added to a deep purple solution of [K(18c-6)][(Ar*BIAN)Co(CN)(η³-P₃)] (50 mg, 0.031 mmol, 1.0 equiv.) in toluene (1.5 mL). The reaction mixture was stirred for two weeks at 40 °C. The color slowly changed to cyan during that period. The solid was removed by filtration over a pad of silica (1 × 0.5 cm) and the residue was washed with toluene (2 × 0.5 mL). The combined filtrates were concentrated to approx. 1 mL and layered with *n*-hexane (3.5 mL). Storage of the solution at room temperature for five days and one day at −35 °C gave shimmering cyan crystals formed, which were isolated by decantation of the mother liquor, washed with *n*-hexane (2 × 1 mL) and dried *in vacuo*.

Yield: 15 mg (34%)

^{1}H NMR (400.13 MHz, 300 K, C_6D_6): δ/ppm = 0.79-0.91 (m, 4H, C*H*₂ of Cy), 0.97-1.01 (m, 12H, −CH(C*H*₃)₂ of *i*Pr), 1.05-1.35 (m, 6H, C*H*₂ of Cy), 1.48-1.63 (m, 6H, C*H*₂ of Cy), 1.71-1.78 (m, 5H, C*H* of Cy overlapping with C*H*₂ of Cy), 2.55 (sept, $^{3}J_{HH}$ = 6.9 Hz, 2H, −C*H*(CH₃)₂ of *i*Pr), 3.72-3.81 (m, 1H, C*H* of Cy), 5.71 (s, 2H, −C^{9}*H*(Ph)₂), 5.89 (d, $^{3}J_{HH}$ = 7.1 Hz, 2H, C^{3}−*H* of BIAN), 6.25-6.29 (m, 2H, C^{4}−*H* of BIAN), 6.60-6.66 (m, 8H, C−*H*$_{Ar}$ of Ph), 6.81-6.85 (m, 8H, C−*H*$_{Ar}$ of Ph), 7.02-7.23 (m, 14H, d ($^{3}J_{HH}$ = 8.2 Hz, 2H, C^{5}−*H* of BIAN) overlapping with C−*H*$_{Ar}$ of Ph overlapping with C_6D_6 solvent signal), 7.27 (m, 2H, C^{11}−*H*), 7.31-7.35 (m, 4H, C−*H*$_{Ar}$ of Ph), 7.55-7.56 (m, 2H, C^{13}−*H*), 7.93-7.97 (m, 8H, C−*H*$_{Ar}$ of Ph), 9.02 (s, 2H, −C^{15}*H*(Ph)₂).

^{13}C{^{1}H} NMR (100.61 MHz, 300 K, C_6D_6): δ/ppm = 23.7 (s, −CH(*C*H₃)₂ of *i*Pr), 23.9 (s, −CH(*C*H₃)₂ of *i*Pr), 25.4 (d, $^{2}J_{PC}$ = 3.5 Hz, *C*H₂ of Cy), 25.9 (s, *C*H₂ of Cy), 26.2 (s, *C*H₂ of Cy), 26.3 (s, *C*H₂ of Cy), 27.0 (d, $^{2}J_{PC}$ = 11.3 Hz, *C*H₂ of Cy), 30.8 (s, *C*H₂ of Cy), 33.6 (s, −*C*H(CH₃)₂ of *i*Pr), 37.6 (d, $^{1}J_{PC}$ = 13.4 Hz, *C*−H of Cy), 40.9 (d, $^{1}J_{PC}$ = 7.1 Hz, *C*−H of Cy), 51.0 (s, −*C*^{9}H(Ph)₂), 51.2 (d, J_{PC} = 4.7 Hz through space, −*C*^{15}H(Ph)₂), 123.3 (s, *C*^{3}−H of BIAN), 125.7 (s, *C*$_{Ar}$−H of Ph), 125.9 (s, *C*$_{Ar}$−H of Ph), 126.2 (s, *C*$_{Ar}$−H of Ph), 126.2 (s, *C*$_{Ar}$−H of Ph), 126.4 (s, *C*^{5}−H of BIAN), 127.4 (s, *C*^{4}−H of BIAN), 127.7 (s, *C*$_{Ar}$−H of Ph overlapping with C_6D_6 solvent signal), 127.9 (s, *C*$_{Ar}$−H of Ph overlapping

with C_6D_6 solvent signal), 127.9 (s, C^{11}–H overlapping with C_6D_6 solvent signal), 128.1 (s, C_{Ar}–H of Ph overlapping with C_6D_6 solvent signal), 128.2 (s, C_{Ar}–H of Ph), 128.3 (s, C_{Ar}–H of Ph), 128.8 (s, C^{13}–H), 129.4 (s, C^2 of BIAN), 129.8 (s, C^6 of BIAN), 130.4 (s, C_{Ar}–H of Ph), 130.6 (s, C_{Ar}–H of Ph), 131.1 (s, C_{Ar}–H of Ph), 134.4 (s, C^{10}), 138.1 (s, C^7 of BIAN), 139.8 (s, C^{14}), 143.3 (s, C_{Ar} of Ph), 144.4 (s, C_{Ar} of Ph), 145.1 (m, C_{Ar} of Ph), 146.2 (s, C^{12}), 146.6 (s, C^8–N), 147.2 (s, C_{Ar} of Ph), 168.6 (s, C^1=N of BIAN); C≡N of coordinated cyanide not detected.

^{31}P{^{1}H} NMR (162.04 MHz, 300 K, C_6D_6): AX_2Y spin system δ/ppm = −47.0 - −43.5 (m, 1P, P_Y), −26.4 - −22.9 (m, 2P, P_X), 58.1 – 61.8 (m, 1P, P_A) for parameters obtained by simulation, see Figure S4 and Table S1.

UV/Vis (THF, λ_{max} / nm, ε_{max} / L·mol^{-1}·cm^{-1}): 240 (60000), 310sh (15000), 390 (6000), 490 (6000), 680 (15000).

IR (solid state): v/ cm^{-1} = 3056w (C−H), 3023w (C−H), 2921m (C−H), 2848m (C−H), 2091m (C≡N), 1599w, 1565w, 1492s (C−N), 1439m, 1417m, 1296w, 1192w, 1030w, 695vs, 604s, 585s.

Elemental Analysis calcd. for ($C_{95}H_{90}CoN_3P_4$) (Mw = 1456.61 g·mol^{-1}):
C 78.34, H 6.23, N 2.88; found C 78.24, H 6.62, N 2.43.

[(Ar*BIAN)Co(CN(η^3-P$_4$(N(*i*Pr$_2$)$_2$)] (2b):

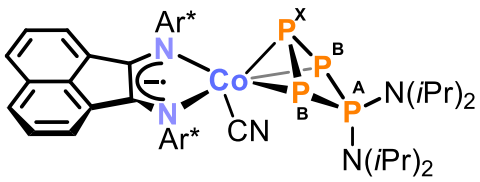

Neat (iPr$_2$N)$_2$PCl (8.2 mg, 0.031 mmol, 1.0 equiv.) was added to a deep purple solution of [K(18c-6)][(Ar*BIAN)Co(CN)(η^3-P$_3$)] (50 mg, 0.031 mmol, 1.0 equiv.) in toluene (2.0 mL). The reaction mixture was stirred for one week at 40 °C. The color slowly changed to cyan during that time. The solid was removed by filtration over a pad of silica (1.5 × 0.5 cm) and the residue washed with toluene (2 × 0.5 mL). Volatiles of the combined filtrates were removed *in vacuo* and the remaining residue taken up in *n*-hexane. -Storage of the solution at −35 °C for four days gave shimmering cyan crystals formed, which were isolated by decantation of the mother liquor, washed with *n*-hexane (1 × 0.5 mL) and dried *in vacuo*.

Yield: 5 mg (11%).

^{1}H NMR (400.30 MHz, 300 K, C_6D_6): δ/ppm = 0.95-0.99 (m, 12H, −N(CH(CH_3)$_2$)$_2$), 1.15-1.19 (m, 24H, −CH(CH_3)$_2$ of *i*Pr overlapping with −N(CH(CH_3)$_2$)$_2$), 2.54 (sept, $^3J_{HH}$ = 6.9 Hz, 2H, −CH(CH_3)$_2$ of *i*Pr), 3.87 (br sept, 2H, −N(CH(CH$_3$)$_2$)$_2$), 4.24 (br sept,

2H, −N(C*H*(CH$_3$)$_2$)$_2$), 5.76-5.78 (m, 4H, C−*H* of BIAN overlapping with −C*H*(Ph)$_2$), 6.26-6.30 (m, 2H, C−*H* of BIAN), 6.57-7.34 (m, 36H, C−*H*$_{Ar}$ of Ph overlapping with C$_6$D$_6$ solvent signal), 7.56 (s, 2H, C−*H*$_{Ar}$), 7.84-7.86 (m, 4H, C−*H*$_{Ar}$ of Ph), 8.00-8.01 (m, 4H, C−*H*$_{Ar}$ of Ph), 8.88 (s, 2H, −C*H*(Ph)$_2$).

^{31}P{^{1}H} NMR (162.04 MHz, 300 K, C$_6$D$_6$): AB$_2$X spin system δ/ppm = −118.9 - −115.6 (m, 1P, P$_X$), −63.3 - −65.6 (m, 3P, P$_{AB}$).

No further characterization has been carried out due to the low amount of sample and small scale of the reaction.

[(Ar*BIAN)Co(η^4-P$_5$*t*Bu$_2$)] (4a):

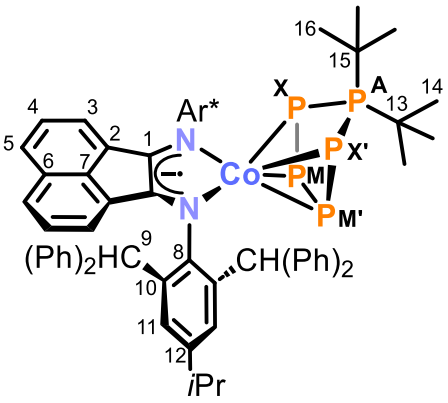

A stock solution of *t*Bu$_2$PCl (1.23 mL, c = 0.078 M in toluene, 0.096 mmol, 1.0 equiv.) was added dropwise to a deep purple solution of [K(18c-6)][(Ar*BIAN)Co(η^4-P$_4$)] (150 mg, 0.096 mmol, 1.0 equiv.) in toluene (25 mL). The reaction mixture was stirred for four weeks at 32 °C. The color slowly changed to dark turquoise during that time. The mixture was filtered over a pad of silica (1.5 × 1 cm) and washed with toluene (10 mL). The volume of the dark turquoise filtrate was reduced to one third and layered with *n*-pentane (12 mL). After twelve days shimmering dark turquoise crystals had formed, which were isolated by decantation of the mother liquor, washed with *n*-pentane (1 mL) and dried *in vacuo*. A second crop of crystals was obtained by further concentrating the mother liquor and storing the solution in the freezer at –35 °C. The second fraction was isolated and combined with the first fraction.

Yield: 107 mg (79%, combined yield of the first and second crop of crystals).

^{1}H NMR (400.13 MHz, 300 K, C$_6$D$_6$): δ/ppm = 0.23 (d, $^3J_{PH}$ = 13.9 Hz, 9H, −C(C^{14}*H*$_3$)$_3$), 0.92 (d, $^3J_{PH}$ = 12.9 Hz, 9H, −C(C^{16}*H*$_3$)$_3$), 1.17 (d, $^3J_{HH}$ = 6.9 Hz, 12H, −CH(C*H*$_3$)$_2$ of *i*Pr), 2.74 (sept, $^3J_{HH}$ = 6.9 Hz, 2H, −C*H*(CH$_3$)$_2$ of *i*Pr), 5.24 (d, $^3J_{HH}$ = 7.1 Hz, 2H, C^3−*H* of BIAN), 6.12-6.16 (m, 2H, C^4−*H* of BIAN), 6.54 (br. s, 4H, −C^9*H*(Ph)$_2$), 6.64-6.74 (m, 12H, C−*H*$_{Ar}$ of Ph), 7.10-7.21 (m, 22H, C^5−*H* of BIAN overlapping with C−*H*$_{Ar}$ of Ph overlapping with C$_6$D$_6$ solvent signal), 7.70 (s, 4H, C^{11}−*H*), 7.79-7.81 (m, 8H, C−*H*$_{Ar}$ of Ph).

$^{13}C\{^1H\}$ NMR (100.61 MHz, 300 K, C_6D_6): δ/ppm = 24.6 (s, −CH(CH_3)$_2$ of *i*Pr), 29.4 (s, −C($C^{14}H_3$)$_3$), 32.2 (s, −C($C^{16}H_3$)$_3$), 34.6 (s, −*C*H(CH_3)$_2$ of *i*Pr), 41.7 (m, −C^{15}(CH_3)$_3$), 43.6 (d, $^1J_{CP}$ = 5.5 Hz, −C^{13}(CH_3)$_3$), 53.1 (s, −C^9H(Ph)$_2$), 121.8 (s, C^3–H of BIAN), 124.1 (s, C^5–H of BIAN), 126.6 (s, C_{Ar}–H of Ph), 126.8 (s, C_{Ar}–H of Ph), 128.1 (s, C^4–H of BIAN), 128.5 (s, C_{Ar}–H of Ph overlapping with C_6D_6 solvent signal), 128.6 (s, C^{11}–H overlapping with C_6D_6 solvent signal), 130.4 (s, C^6 of BIAN), 131.3 (s, C_{Ar}–H of Ph), 132.3 (s, C_{Ar}–H of Ph), 133.6 (s, C^2 of BIAN), 137.6 (s, C^7 of BIAN), 138.4 (s, C^{10}), 145.2 (s, C_{Ar}–H of Ph), 146.0 (s, C^{12}), 146.6 (s, C_{Ar}–H of Ph), 150.7 (s, C^8–N), 156.7 (s, C^1=N of BIAN).

$^{31}P\{^1H\}$ NMR (162.04 MHz, 300 K, C_6D_6): AMM'XX' spin system δ/ppm = −182.7 - −174.0 (m, 2P, $P_{XX'}$), 67.1-73.3 (m, 2P, $P_{MM'}$), 176.0 (t, 1P, P_A), for parameters obtained by simulation, see Figure S10 and Table S2.

UV/Vis (toluene, λ_{max} / nm, ε_{max} / L·mol^{-1}·cm^{-1}): 400sh (4500), 580 (6000), 670 (6000).

Elemental Analysis calcd. for ($C_{90}H_{86}CoN_2P_5$) (Mw = 1409.49 g·mol^{-1}):
C 76.69, H 6.15, N 1.99; found C 76.91, H 6.19, N 1.90.

[(Ar*BIAN)Co(η^4-P_5(N(*i*Pr$_2$)$_2$)$_2$)] (4b):

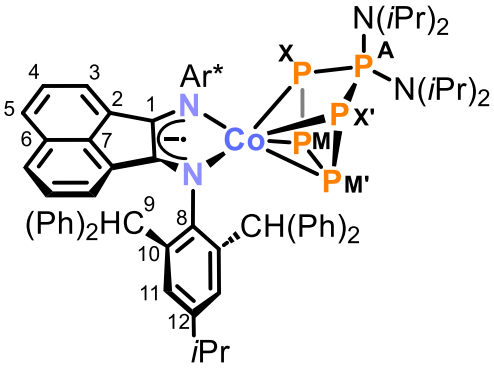

Toluene (11 ml) was added to neat (*i*Pr$_2$N)$_2$PCl (34 mg, 0.128 mmol, 1.0 equiv.) and [K(18c-6)][(Ar*BIAN)Co(η^4-P_4)] (200 mg, 0.128 mmol, 1.0 equiv.). The purple reaction mixture was stirred for one day. The color slowly changed to dark turquoise during that time. The mixture was filtered over a pad of silica (2 × 1.5 cm) and washed with toluene (3 × 10 mL). The volume of the dark turquoise filtrate was reduced to approximately 8 mL and layered with *n*-pentane (32 mL). Storage of the solution a room temperature gave shimmering dark turquoise crystals, which were isolated by decantation of the mother liquor, washed with *n*-pentane (1 × 3 mL) and dried *in vacuo*. The crystalline solid contains 0.5 molecules of toluene per molecule of compound after drying as indicated by the $^1H/^{13}C\{^1H\}$ NMR spectra and elemental analysis.

Yield: 139 mg (73%).

^{1}H NMR (400.13 MHz, 300 K, C_6D_6): δ/ppm = 0.64 (d, $^3J_{HH}$ = 6.8 Hz, 12H, −N(CH(CH_3)$_2$)$_2$), 0.79 (d, $^3J_{HH}$ = 6.9 Hz, 12H, −N(CH(CH_3)$_2$)$_2$), 1.12 (d, $^3J_{HH}$ =

6.9 Hz, 12H, −CH(CH_3)$_2$ of *i*Pr), 2.70 (sept, $^3J_{HH}$ = 6.9 Hz, 2H, −CH(CH_3)$_2$ of *i*Pr), 3.13 (sept, $^3J_{HH}$ = 6.7 Hz, 2H, −N(CH(CH$_3$)$_2$)$_2$), 3.58 (br sept, 2H, −N(CH(CH$_3$)$_2$)$_2$), 5.23 (d, $^3J_{HH}$ = 7.1 Hz, C^3−H of BIAN), 6.13-6.17 (m, 2H, C^4−H of BIAN), 6.57-6.70 (m, 16H, C−H_{Ar} of Ph overlapping with −C^9H(Ph)$_2$), 7.09-7.26 (m, 22H, C−H_{Ar} of Ph overlapping with d ($^3J_{HH}$ = 8.2 Hz of C^5−H of BIAN, 2H) overlapping with C_6D_6 solvent signal), 7.65 (s, 4H, C^{11}−H), 7.86-7.88 (m, 8H, C−H_{Ar} of Ph).

^{13}C{^{1}H} NMR (100.61 MHz, 300 K, C_6D_6): δ/ppm = 24.2 (s, −N(CH(*C*H$_3$)$_2$)$_2$), 24.6 (s, −CH(*C*H$_3$)$_2$ of *i*Pr), 24.8 (s, −N(CH(*C*H$_3$)$_2$)$_2$), 34.5 (s, −*C*H(CH$_3$)$_2$ of *i*Pr), 48.1 (s, −N(*C*H(CH$_3$)$_2$)$_2$), 52.4 (s, −N(*C*H(CH$_3$)$_2$)$_2$), 53.1 (s, −*C*^{9}H(Ph)$_2$), 121.6 (s, *C*^{3}−H of BIAN), 123.9 (s, *C*^{5}−H of BIAN), 126.6 (s, *C*$_{Ar}$−H of Ph), 126.9 (s, *C*$_{Ar}$−H of Ph), 128.1 (s, *C*^{4}−H of BIAN), 128.5 (s, *C*$_{Ar}$−H of Ph overlapping with C_6D_6 solvent signal), 128.5 (s, *C*$_{Ar}$−H of Ph overlapping with C_6D_6 solvent signal), 129.3 (s, *C*^{11}−H), 130.4 (s, *C*^{6} of BIAN), 131.3 (s, *C*$_{Ar}$−H of Ph), 132.4 (s, *C*$_{Ar}$−H of Ph), 133.6 (s, *C*^{2} of BIAN), 137.4 (s, *C*^{7} of BIAN), 138.6 (s, *C*^{10}), 145.0 (s, *C*$_{Ar}$ of Ph), 145.9 (s, *C*^{12}), 147.0 (s, *C*$_{Ar}$ of Ph), 151.2 (s, *C*^{8}−N), 156.9 (s, *C*^{1}=N of BIAN).

^{31}P{^{1}H} NMR (162.04 MHz, 300 K, C_6D_6): AMM'XX' spin system δ/ppm = −144.3 - −135.8(m, 2P, P$_{XX'}$), 39.4 − 45.4 (m, 2P, P$_{MM'}$), 135.4 (t, 1P, P$_A$), for parameters obtained by simulation, see Figure S14 and Table S3.

UV/Vis (toluene, λ_{max} / nm, ε_{max} / L·mol^{-1}·cm^{-1}): 425 (14500), 580 (23500), 675 (21000).

Elemental analysis calcd. for ($C_{94}H_{96}CoN_4P_5$)·(toluene)$_{0.5}$ (Mw = 1495.63 g·mol^{-1}): C 75.96, H 6.54, N 3.63; found C 76.31, H 6.47, N 3.52.

[(Ar*BIAN)Co(η^4-P$_7$L$_C$)] (7):

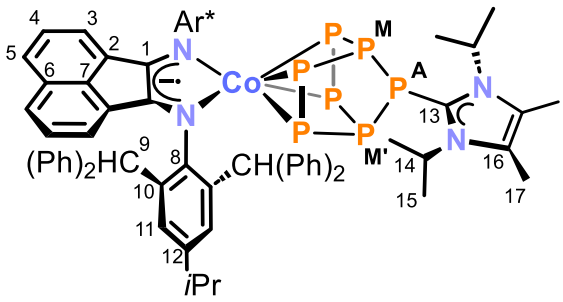

Tetracation **M**[OTf]$_4$ (69 mg, 0.048 mmol, 0.5 eq.) was added to a deep purple solution of [K(18c-6)][(Ar*BIAN)Co(η^4-P$_4$)] (150 mg, 0.096 mmol, 1.0 eq.) in THF (4 mL). After stirring at ambient temperature overnight, the color had changed to a deep blue. Subsequently, the solvent was evaporated to dryness. The remaining dark solid was extracted with 1,4-dioxane (5 × 1 mL). The extracts were filtered over a pad of silica (2 × 0.5 cm) and washed with 1,4-dioxane (2 × 1 mL). The dark blue filtrate was concentrated to approx. 5 mL and layered with *n*-hexane (20 mL). Storage of the solution for five days gave shimmering dark blue crystals, which were

isolated by decantation of the mother liquor, washed with *n*-hexane (4 × 1 mL) and dried *in vacuo*. To remove residual [K(18c-6)]OTf the solids were dissolved in toluene (4 mL). The resulting solution was filtered over a pad of silica (2 × 0.5 cm) and washed with 1,4-dioxane (2 × 1 mL). The solvent was evaporated, the residue washed with *n*-hexane (3 × 1 mL) and dried *in vacuo*.

Yield: 57 mg (39%).

^{1}H NMR (400.13 MHz, 300 K, C_6D_6): δ /ppm = 0.60 (d, $^{3}J_{HH}$ = 6.6 Hz, 12H, C^{15}–*H*), 1.01 (s, 6H, C^{17}–*H*), 1.18 (d, $^{3}J_{HH}$ = 6.9 Hz, 12H, −CH(C*H*$_3$)$_2$ of *i*Pr), 2.77 (sept, $^{3}J_{HH}$ = 6.9 Hz, 2H, −C*H*(CH$_3$)$_2$ of *i*Pr), 3.67 (br. s, 2H, C^{14}–*H*), 5.58 (d, $^{3}J_{HH}$ = 7.1 Hz, 2H, C^{3}–*H* of BIAN), 6.36 – 6.40 (m, 2H, C^{4}–*H* of BIAN), 6.65 – 6.68 (m, 4H, C−H_{Ar} of Ph), 6.73 – 6.79 (m, 12H, C−H_{Ar} of Ph overlapping with −C^{9}*H*(Ph)$_2$), 7.13 – 7.17 (m, 6H, C−H_{Ar} of Ph overlapping with C_6D_6 solvent signal), 7.23 – 7.27 (m, 10H, C−H_{Ar} overlapping with C^{5}–*H* of BIAN), 7.54 (s, 4H, C^{11}–*H*), 7.92 – 7.94 (m, 8H, C−H_{Ar} of Ph).

^{13}C{^{1}H} NMR (100.61 MHz, 300 K, C_6D_6): δ /ppm = 9.4 (s, C^{17}–H), 20.9 (s, C^{15}–H), 24.2 (s, −CH(*C*H$_3$)$_2$ of *i*Pr), 34.0 (s, −*C*H(CH$_3$)$_2$ of *i*Pr), 52.2 (s, −C^{9}H(Ph)$_2$), 52.4(br. s, C^{14}–H), 120.4 (s, C^{3}–H of BIAN), 122.7 (C^{5}–H of BIAN), 125.7 (s, C_{Ar}–H of Ph), 126.0 (s, C_{Ar}–H of Ph), 127.7 (s, C^{4}–H of BIAN overlapping with C_6D_6 solvent signal), 127.8 (s, C^{16} overlapping with C_6D_6 solvent signal), 127.9 (s, C_{Ar}–H of Ph overlapping with C_6D_6 solvent signal), 128.0 (s, C^{11}–H overlapping with C_6D_6 solvent signal), 128.1 (s, C_{Ar}–H of Ph overlapping with C_6D_6 solvent signal), 130.3 (s, C^{2} of BIAN), 130.8 (s, C_{Ar}–H of Ph), 131.6 (s, C_{Ar}–H of Ph), 134.1 (s, C^{6} of BIAN), 136.1 (s, C^{10}), 136.9 (s, C^{7} of BIAN), 144.7 (s, C^{12}), 145.0 (s, C_{Ar} of Ph), 146.5 (s, C_{Ar} of Ph), 152.6 (s, C^{1}=N of BIAN), 154.9 (s, C^{8}–N).

^{31}P{^{1}H} NMR (161.98 MHz, 300 K, C_6D_6): AMM'XX'YY' spin system δ/ppm = −136.1 - −131.5 (m, 2P, $P_{YY'}$), −76.1 - 72.1 (m, 2P, $P_{XX'}$), −25.8 - 19.9 (m, 2P, $P_{MM'}$), 46.8 (t, 1P, P_A).

UV/Vis (toluene, λ_{max} / nm, ε_{max} / L·mol^{-1}·cm^{-1}): 320sh (13000), 440 (6000), 560 (9000), 660 (14000).

Elemental analysis calcd. for ($C_{93}H_{88}CoN_4P_7$) (Mw = 1537.5 g·mol^{-1})

C 72.65, H 5.77, N 3.64; found C 73.06, H 6.24, N 3.48.

Reaction of [K(18c-6)][(Ar*BIAN)Co(CN)(η^3-P_3)] (1) with N[OTf]$_4$:

Tetracation **N**[OTf]$_4$ (6 mg, 0.004 mmol, 0.5 eq.) was added to a deep purple solution of [K(18c-6)][(Ar*BIAN)Co(CN)(η^3-P_3)] (14 mg, 0.008 mmol, 1.0 eq.) in THF (2 mL). After stirring at ambient temperature for one hour, the color had changed to a deep blue and a $^{31}P\{^1H\}$ spectrum of the reaction mixture was recorded using a C_6D_6-capillary (Figure 3). Subsequently, all volatiles were removed *in vacuo*. The dark solid was extracted with small portions of toluene, benzene, 1,4-dioxane and THF. No crystals have been obtained so far from these concentrated extracts, or by slow vapor diffusion of *n*-hexane into these. The ^{31}P NMR spectrum of the reaction mixture looks similar to the spectrum obtained when conducting the reaction in toluene (see Section 4.2 Figure 3). The salt metathesis product, showing signals marked in *blue*, is the major component of the reaction solution, while cationic insertion product (showing signals marked in *red*) is the minor component.

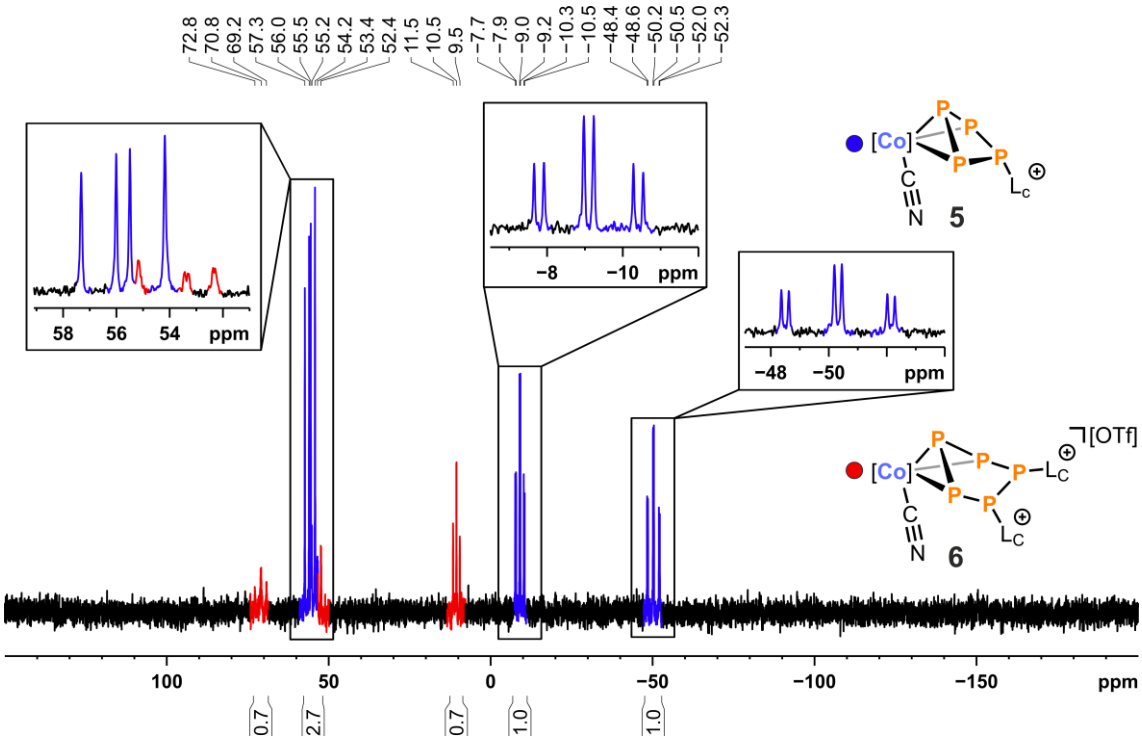

Figure S18. $^{31}P\{^1H\}$ NMR spectrum (162.04 MHz, 300 K, C_6D_6-capillary) of the reaction solution of **1** and 0.5 eq. **N**[OTf]$_4$ in toluene exhibiting two sets of signals attributed to two proposed species; *blue*: A_2MX spin system assigned to **5**; *red*: ABCDE spin system assigned to **6**; [Co] = (Ar*BIAN)Co.

4.4.2 NMR Spectra

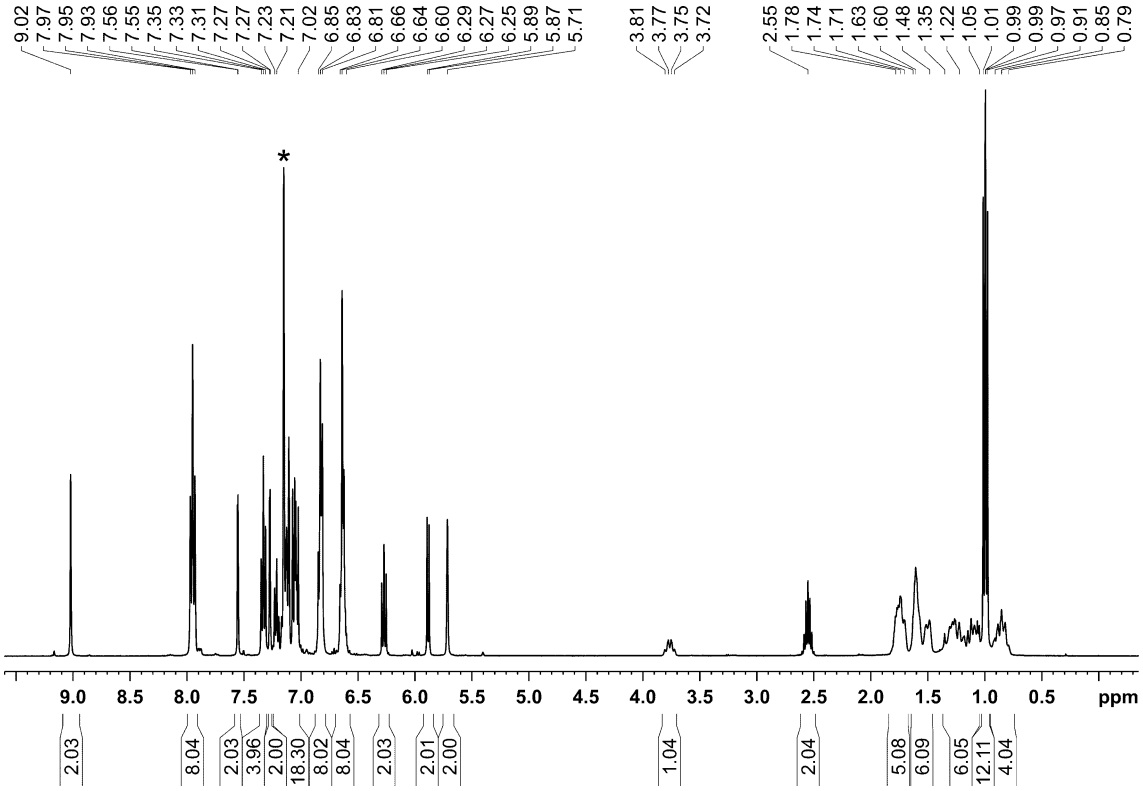

Figure S1. ^{1}H NMR spectrum (400.13 MHz, 300 K, C_6D_6,) of [(Ar*BIAN)Co(CN)(η^3-P_4Cy_2)] (**2a**); * C_6D_6.

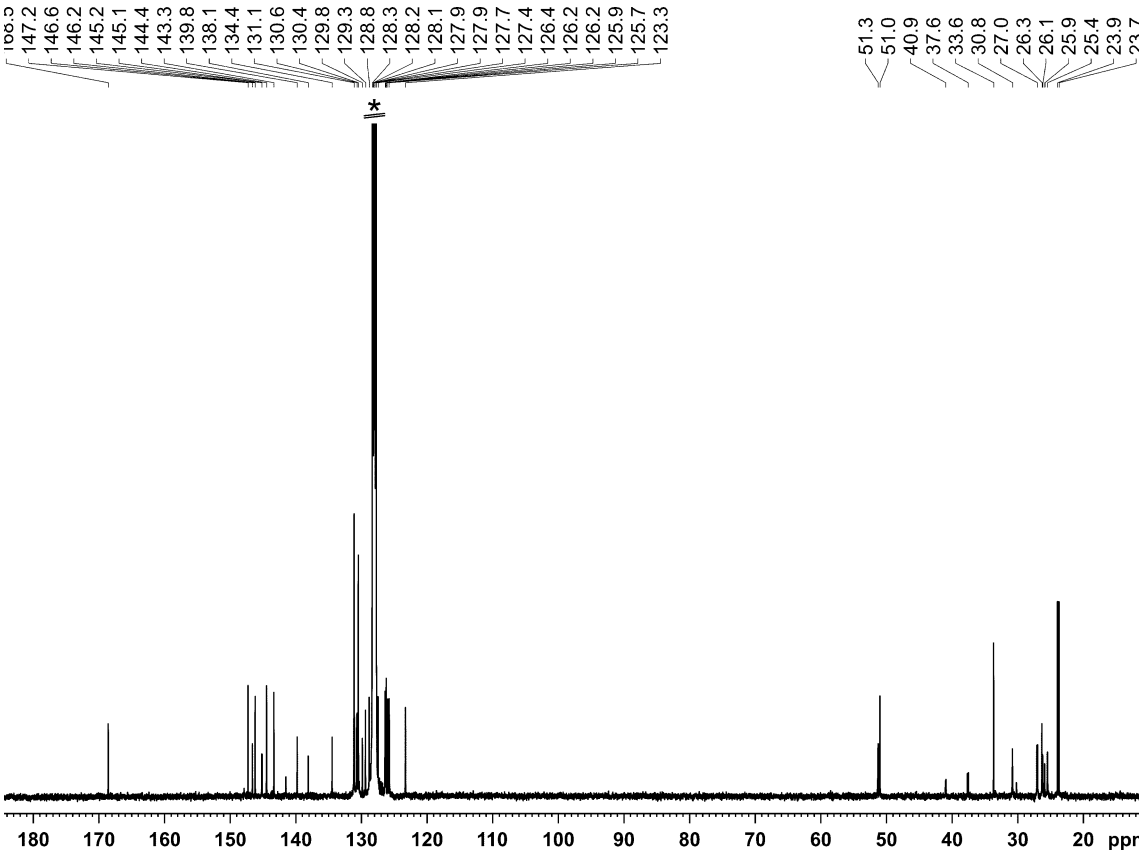

Figure S2. ^{13}C{^{1}H} NMR spectrum (100.61 MHz, 300 K, C_6D_6) of [(Ar*BIAN)Co(CN)(η^3-P_4Cy_2)] (**2a**); * C_6D_6.

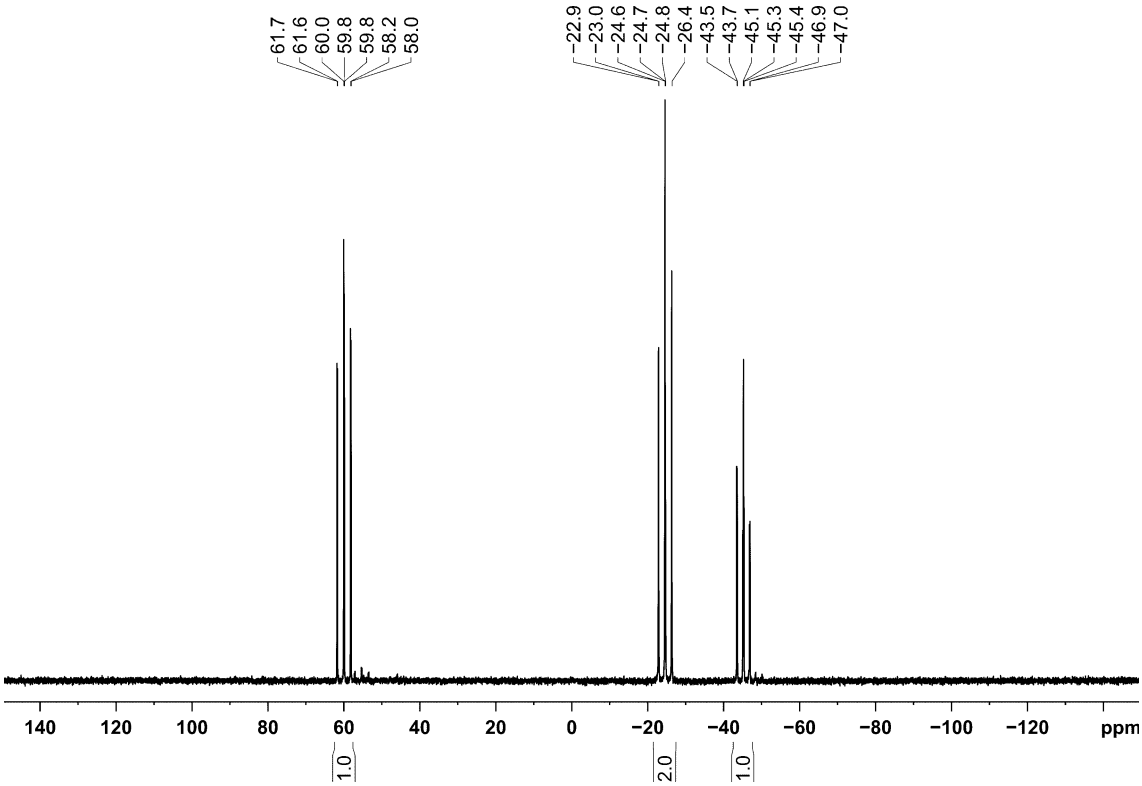

Figure S3. $^{31}P\{^{1}H\}$ NMR spectrum (162.04 MHz, 300 K, C_6D_6) of [(Ar*BIAN)Co(CN)(η^3-P_4Cy_2)] (**2a**).

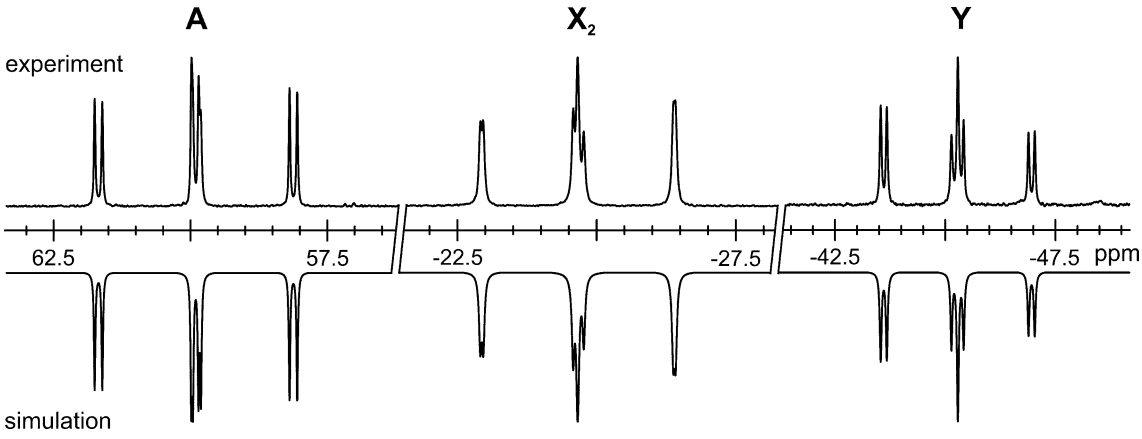

Figure S4. Section of the $^{31}P\{^{1}H\}$ NMR (162.04 MHz, 300 K, C_6D_6) spectra of [(Ar*BIAN)Co(CN)(η^3-P_4Cy_2)] (**2a**); experimental (upwards) and simulation (downwards).

Table S1. Chemical shifts and coupling constants from the iterative fit of the AX_2Y spin system and schematic representation of the CoP_4Cy_2 core of [(Ar*BIAN)Co(CN)(η^3-P_4Cy_2)] (**2a**).

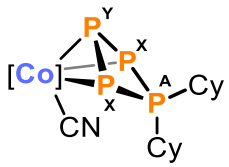	δ(A) = 59.9 ppm	$^{1}J_{AX}$ = −289.2 Hz
	δ(X) = −24.7 ppm	$^{1}J_{XY}$= −272.3 Hz
	δ(Y) = −45.2 ppm	$^{2}J_{AY}$ = 23.8 Hz

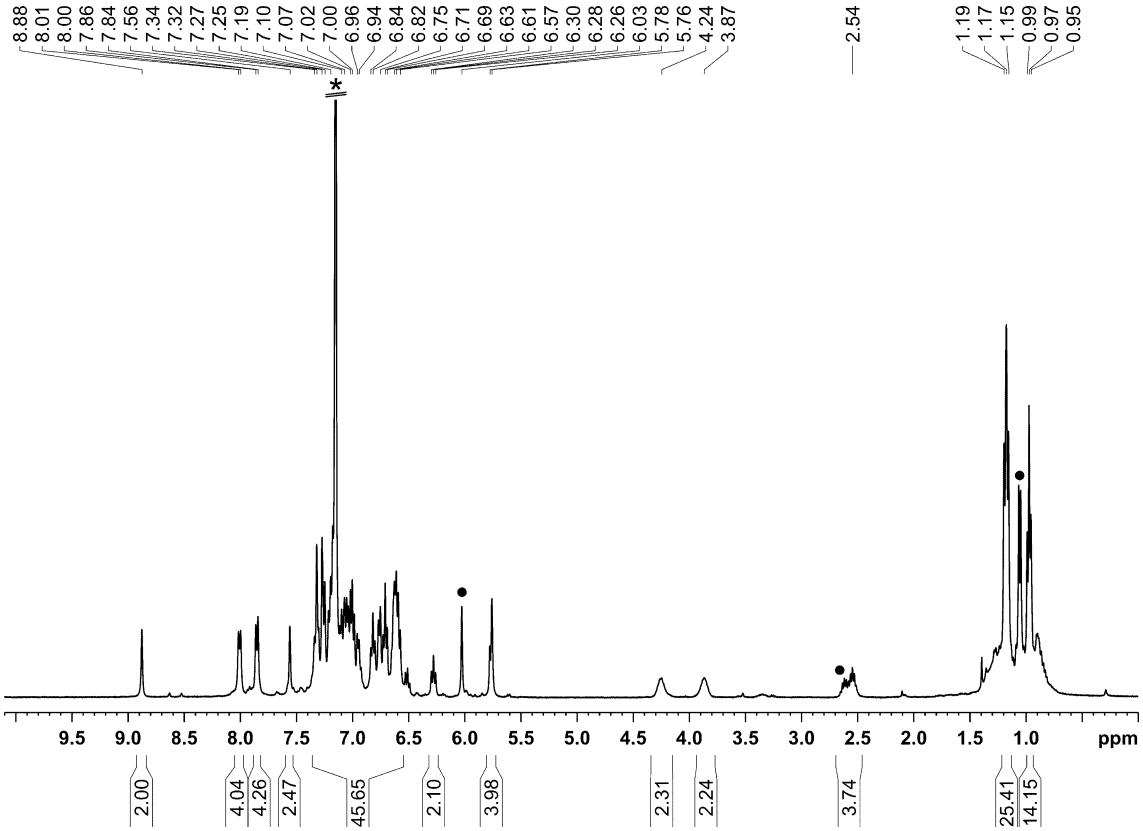

Figure S5. ^{1}H NMR spectrum (400.30 MHz, 300 K, C_6D_6,) of [(Ar*BIAN)Co(CN)(η^3-P_4(N(iPr$_2$)$_2$)] (**2b**); • free Ar*BIAN ligand; * C_6D_6.

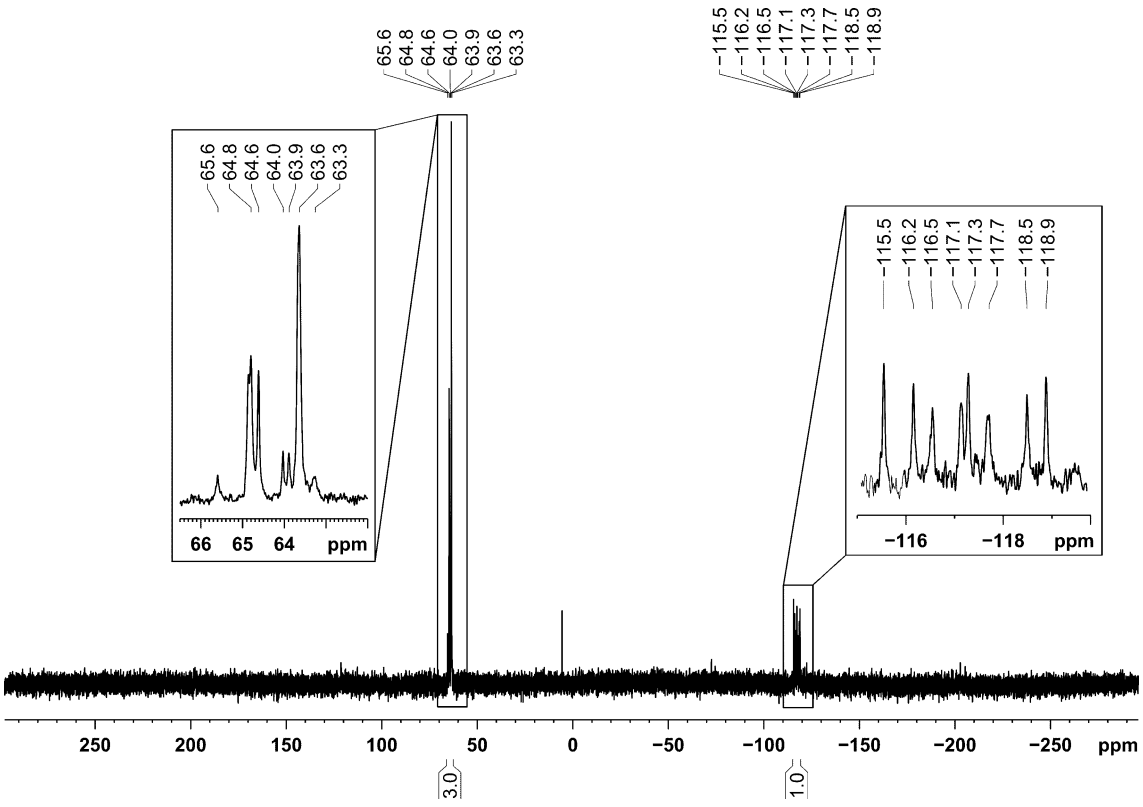

Figure S6. $^{31}P\{^{1}H\}$ NMR spectrum (162.04 MHz, 300 K, C_6D_6) of [(Ar*BIAN)Co(CN)(η^3-P_4(N(iPr$_2$)$_2$)] (**2b**).

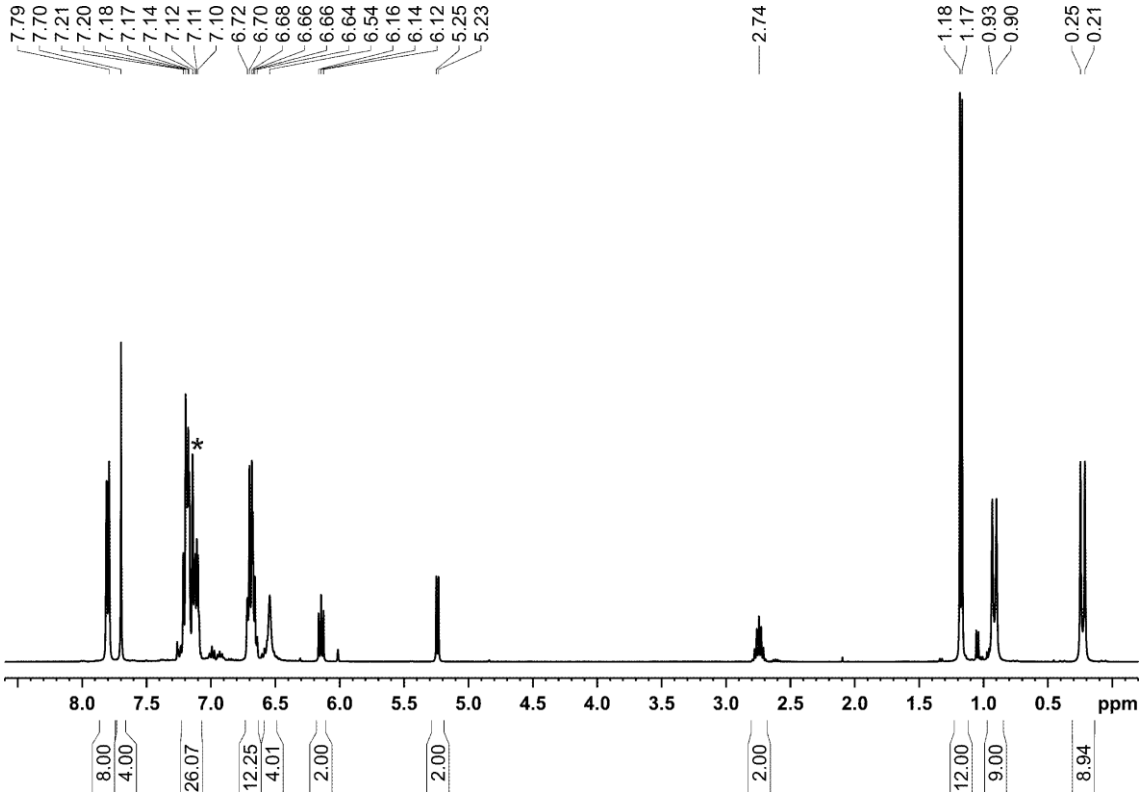

Figure S7. ^{1}H NMR spectrum (400.13 MHz, 300 K, C_6D_6,) of [(Ar*BIAN)Co(η^4-P_5tBu$_2$)] (**4a**); * C_6D_6.

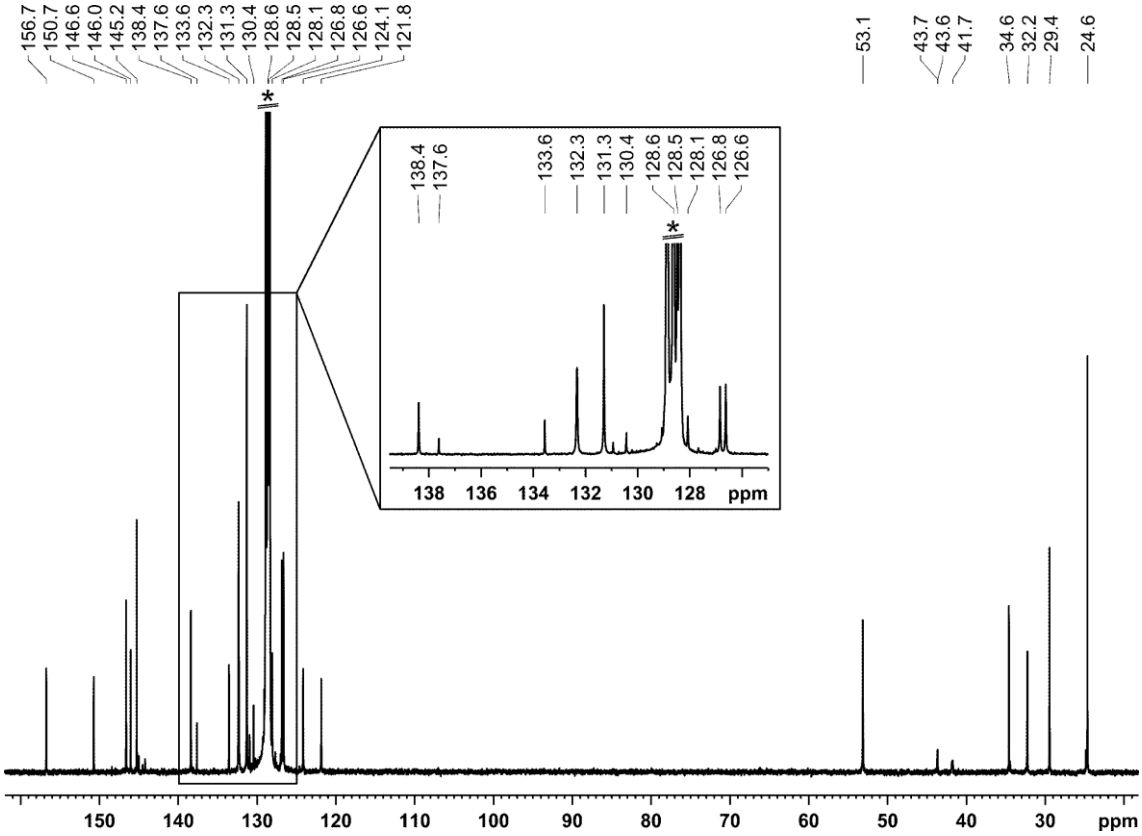

Figure S8. ^{13}C{^{1}H} NMR spectrum (100.61 MHz, 300 K, C_6D_6) of [(Ar*BIAN)Co(η^4-P_5tBu$_2$)] (**4a**); * C_6D_6.

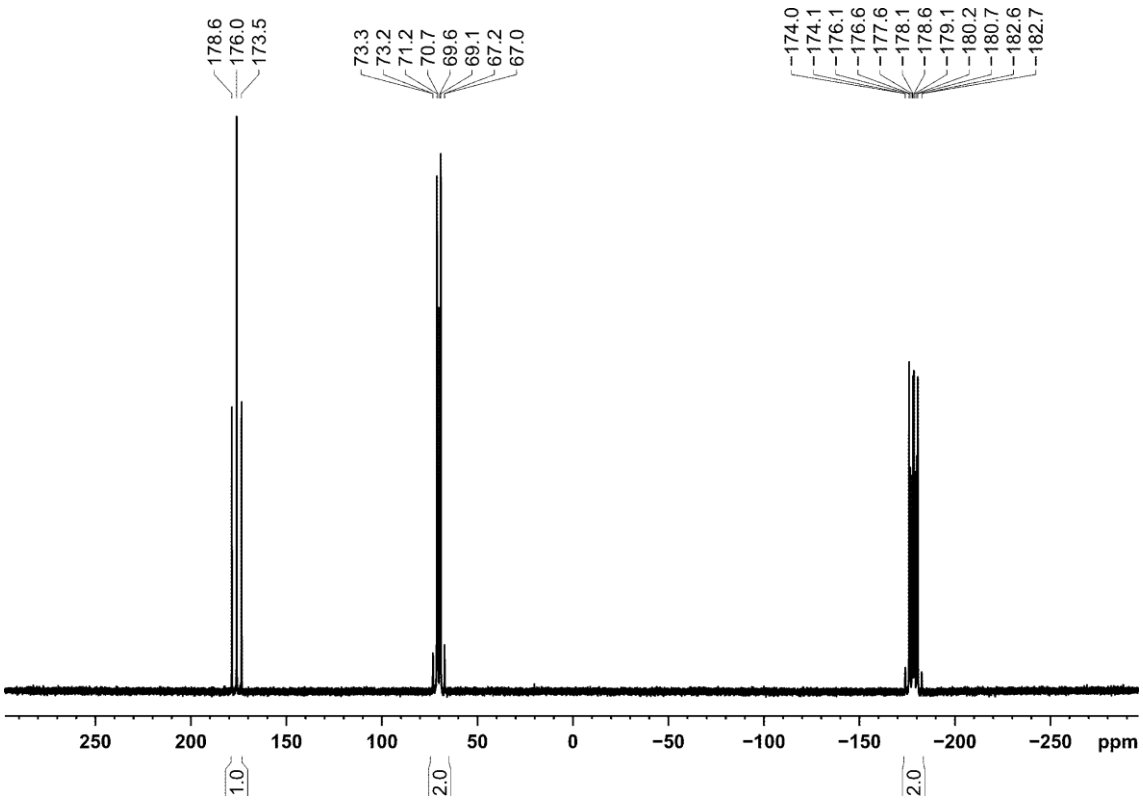

Figure S9. $^{31}P\{^{1}H\}$ NMR spectrum (162.04 MHz, 300 K, C_6D_6) of [(Ar*BIAN)Co(η^4-P_5tBu$_2$)] (**4a**).

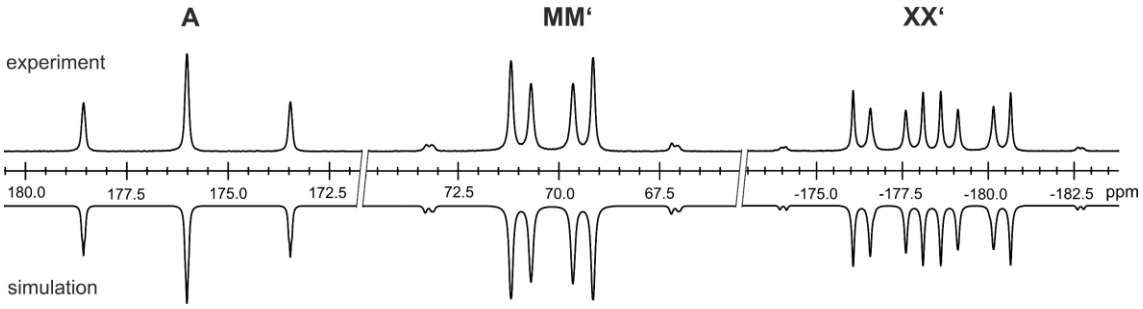

Figure S10. Section of the $^{31}P\{^{1}H\}$ NMR (162.04 MHz, 300 K, C_6D_6) spectra of [(Ar*BIAN)Co(η^4-P_5tBu$_2$)] (**4a**); experimental (upwards) and simulation (downwards).

Table S2. Coupling constants from the iterative fit of the AMM'XX' spin system and schematic representation of the $CoP_5(t\text{Bu})_2$ core of [(Ar*BIAN)Co(η^4-P_5tBu$_2$)] (**4a**).

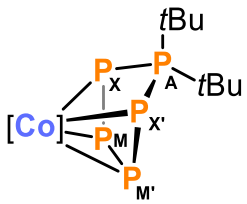	δ(A) = 176.0 ppm	$^{1}J_{AX} = {}^{1}J_{AX'} = -413.4$ Hz
	δ(M) = 70.2 ppm	$^{1}J_{MX} = {}^{1}J_{M'X'} = -368.8$ Hz
	δ(X) = −178.4 ppm	$^{1}J_{MM'} = -411.3$ Hz
		$^{2}J_{MX'} = {}^{2}J_{M'X} = 39.2$ Hz
		$^{2}J_{AM} = {}^{2}J_{AM'} = 6.4$ Hz
		$^{2}J_{XX'} = 18.5$ Hz

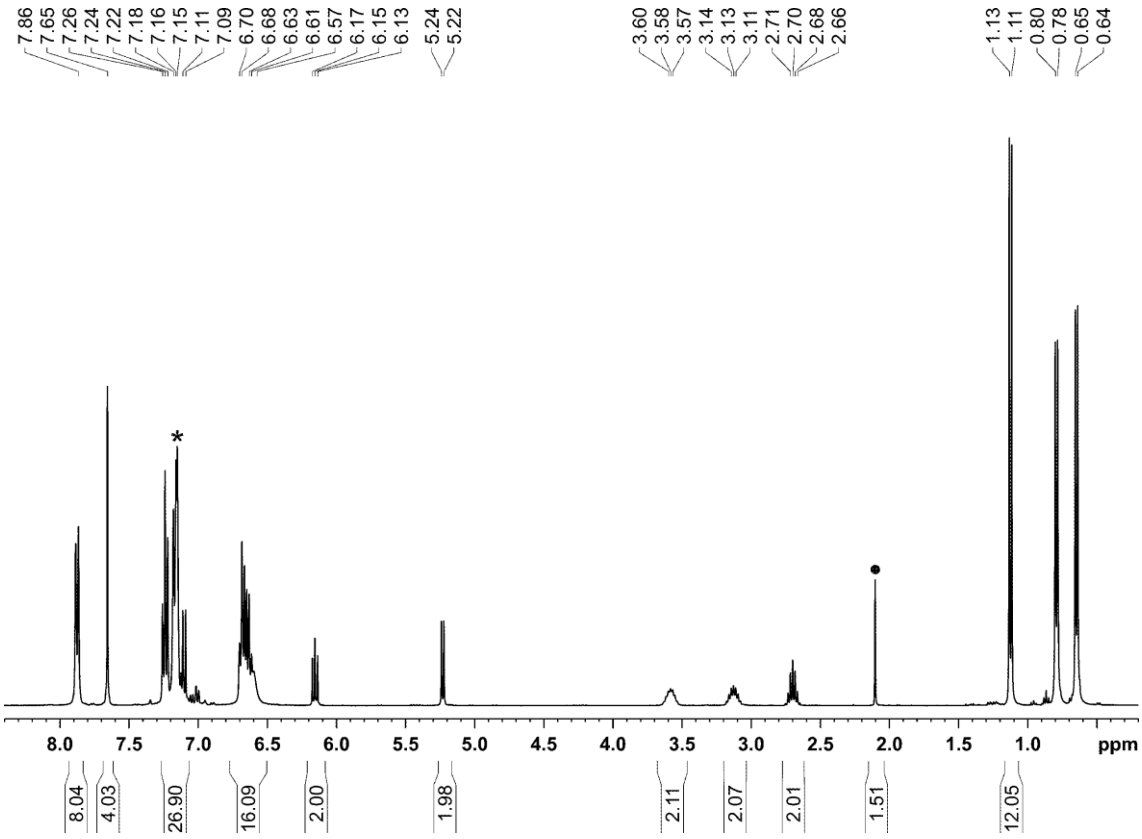

Figure S11. ^{1}H NMR spectrum (400.13 MHz, 300 K, C_6D_6,) of [(Ar*BIAN)Co(η^4-P_5(N(*i*Pr$_2$)$_2$)] (**4b**); • toluene, * C_6D_6.

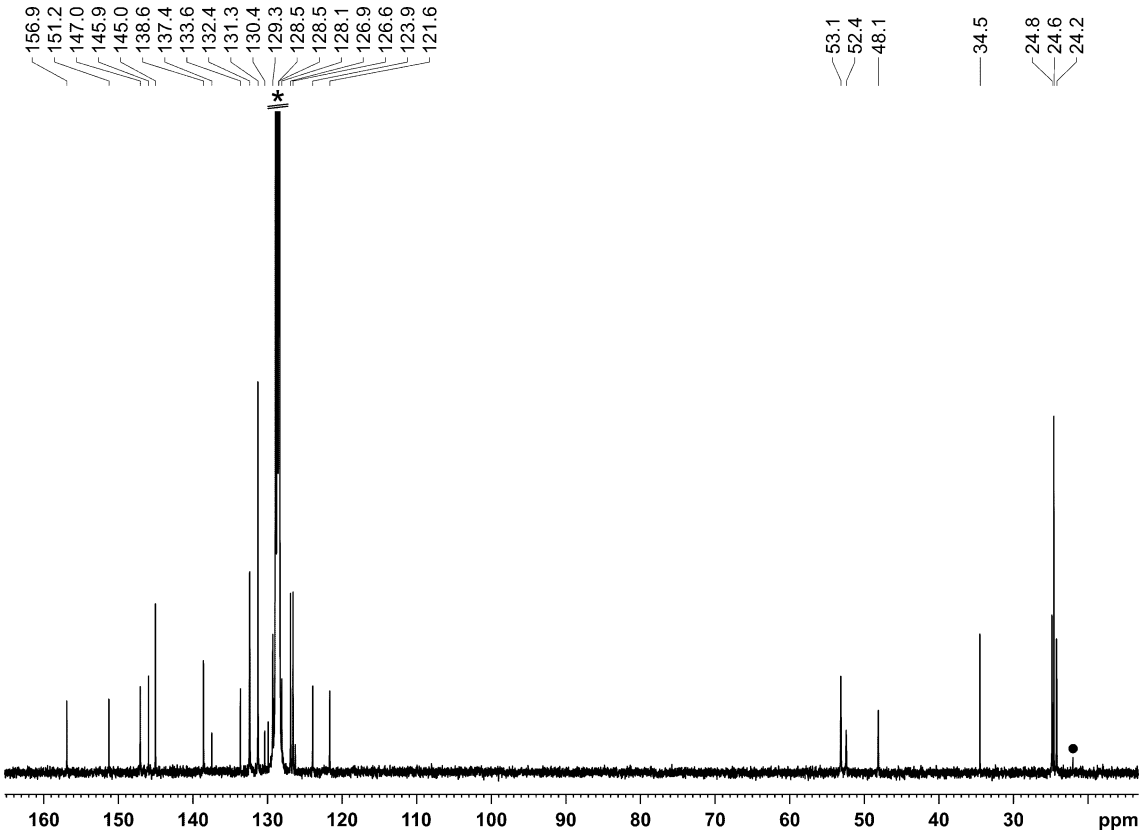

Figure S12. ^{13}C{^{1}H} NMR spectrum (100.61 MHz, 300 K, C_6D_6) of [(Ar*BIAN)Co(η^4-P_5(N(*i*Pr$_2$)$_2$)] (**4b**); • toluene, * C_6D_6.

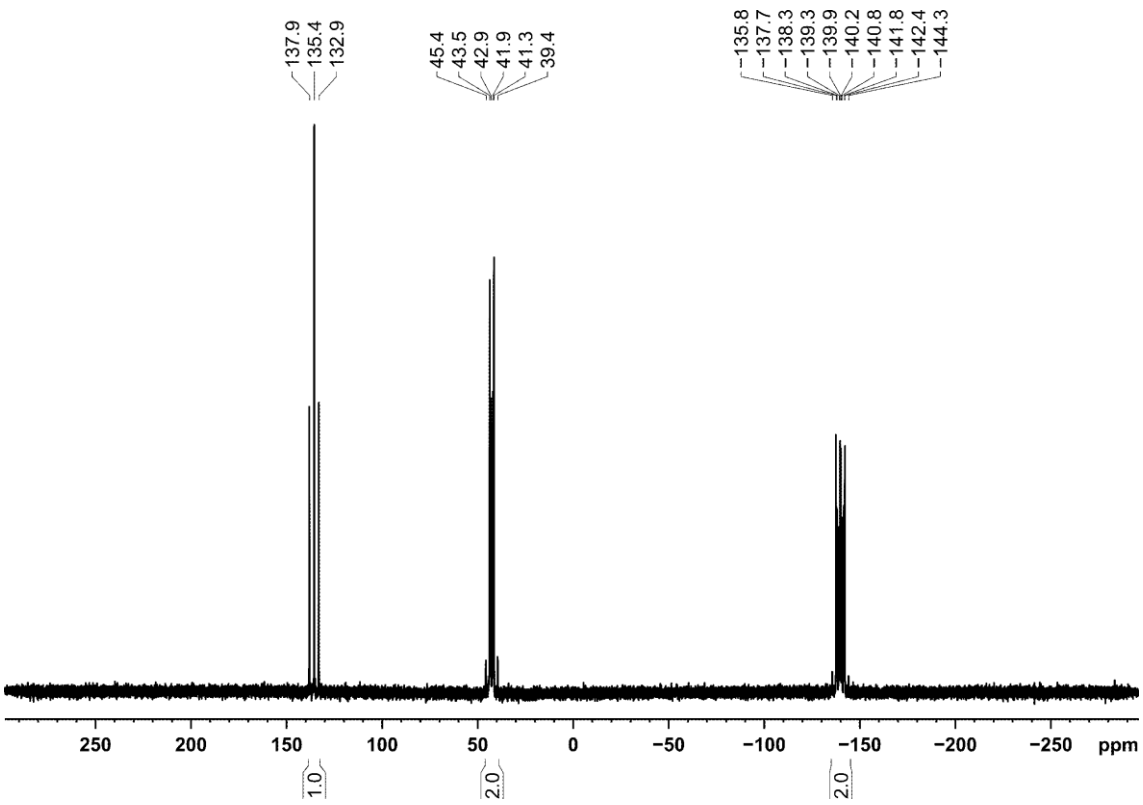

Figure S13. $^{31}P\{^{1}H\}$ NMR spectrum (162.04 MHz, 300 K, C_6D_6) of [(Ar*BIAN)Co(η^4-P_5(N(iPr$_2$)$_2$)] (**4b**).

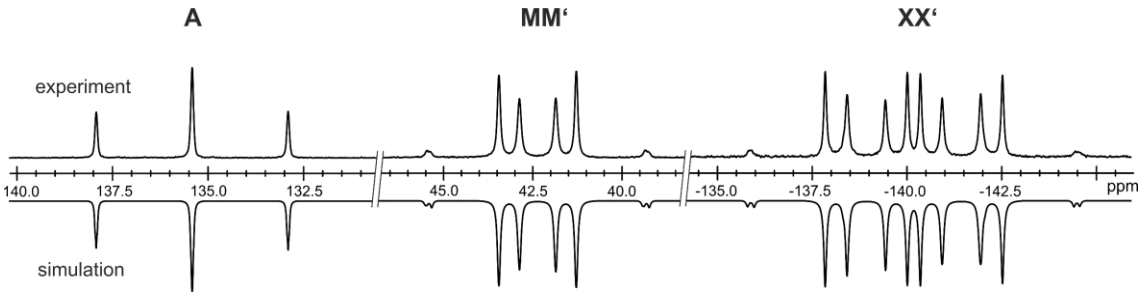

Figure S14. Section of the $^{31}P\{^{1}H\}$ NMR (162.04 MHz, 300 K, C_6D_6) spectra of [(Ar*BIAN)Co(η^4-P_5(N(iPr$_2$)$_2$)] (**4b**); experimental (upwards) and simulation (downwards).

Table S3. Coupling constants from the iterative fit of the AMM'XX' spin system and schematic representation of the $CoP_5(N(iPr)_2)_2$ core of [(Ar*BIAN)Co(η^4-P_5(N(iPr$_2$)$_2$)] (**4b**).

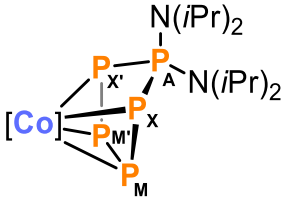	δ(A) = 135.4 ppm	$^1J_{AX} = {}^1J_{AX'} = -406.7$ Hz
	δ(M) = 42.4 ppm	$^1J_{MX} = {}^1J_{M'X'} = -377.1$ Hz
	δ(X) = −140.2 ppm	$^1J_{MM'} = -411.0$ Hz
		$^2J_{MX'} = {}^2J_{M'X} = 26.1$ Hz
		$^2J_{AM} = {}^2J_{AM'} = 4.9$ Hz
		$^2J_{XX'} = 15.6$ Hz

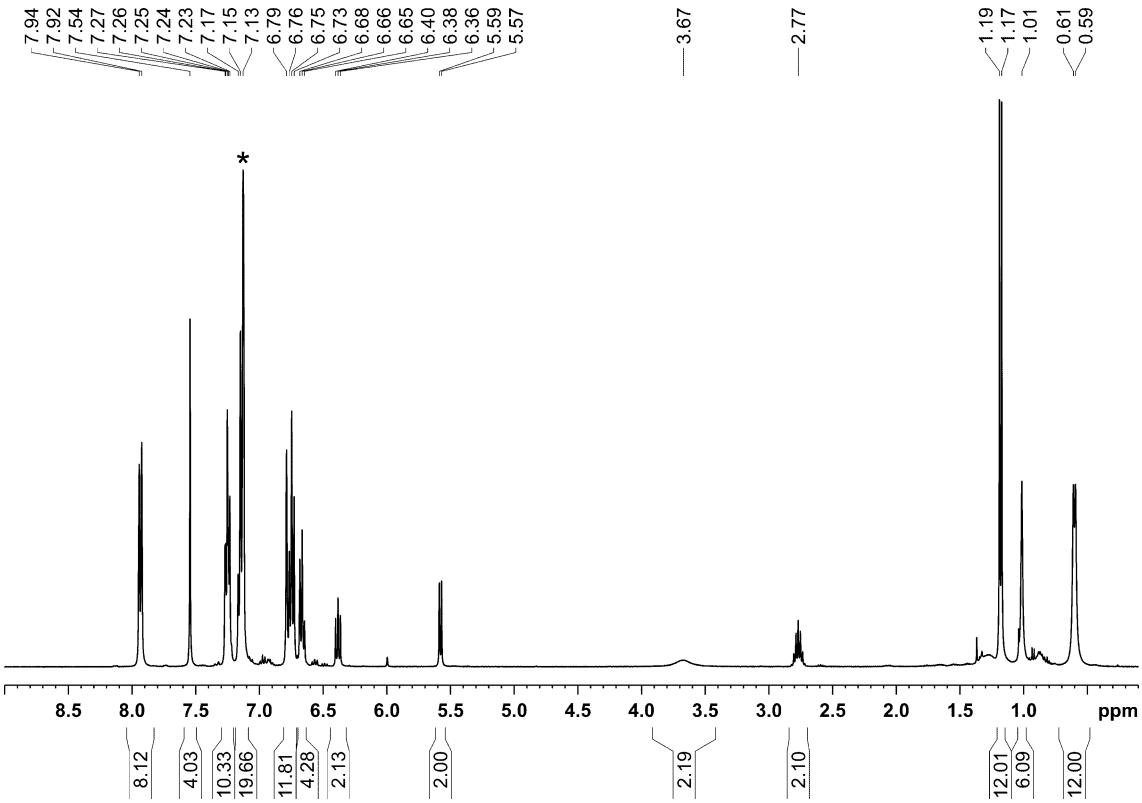

Figure S15. ^{1}H NMR spectrum (400.13 MHz, 300 K, C_6D_6,) of [(Ar*BIAN)Co(η^4-P_7L_C)] (**7**); * C_6D_6.

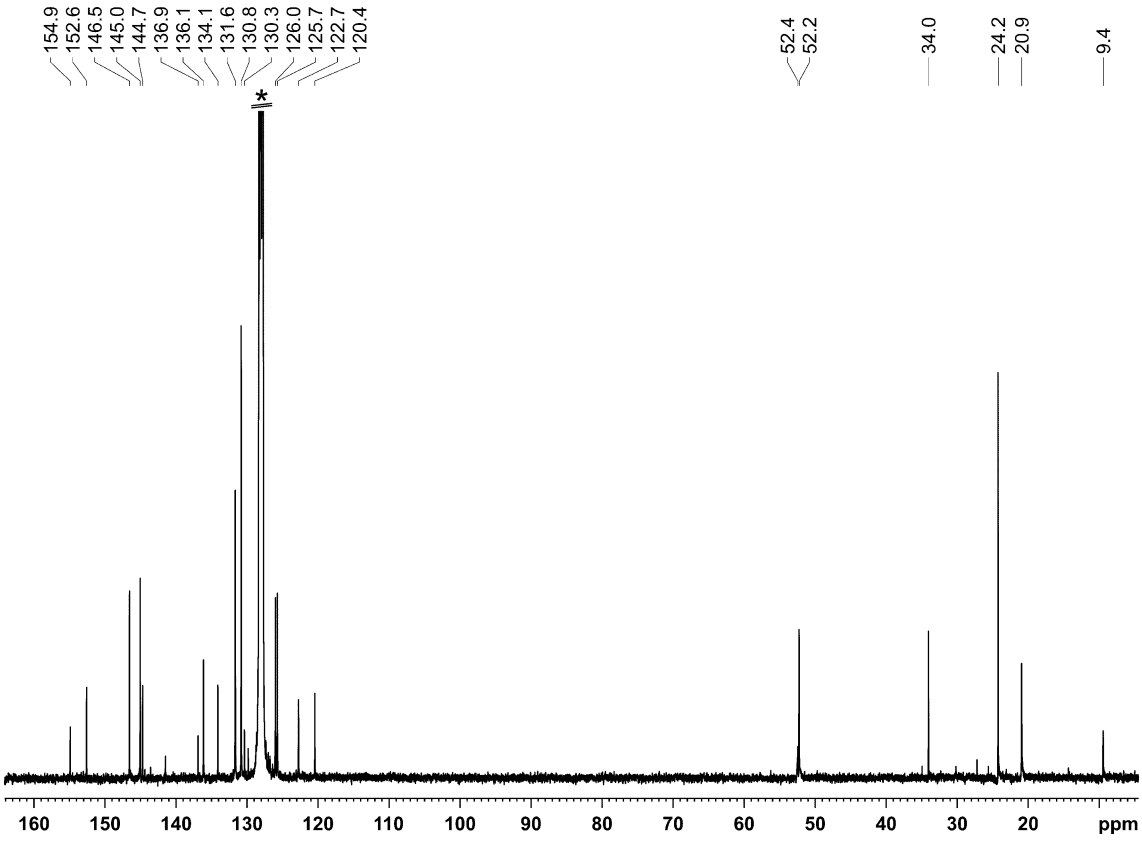

Figure S16. ^{13}C{^{1}H} NMR spectrum (100.61 MHz, 300 K, C_6D_6) of [(Ar*BIAN)Co(η^4-P_7L_C)] (**7**); * C_6D_6.

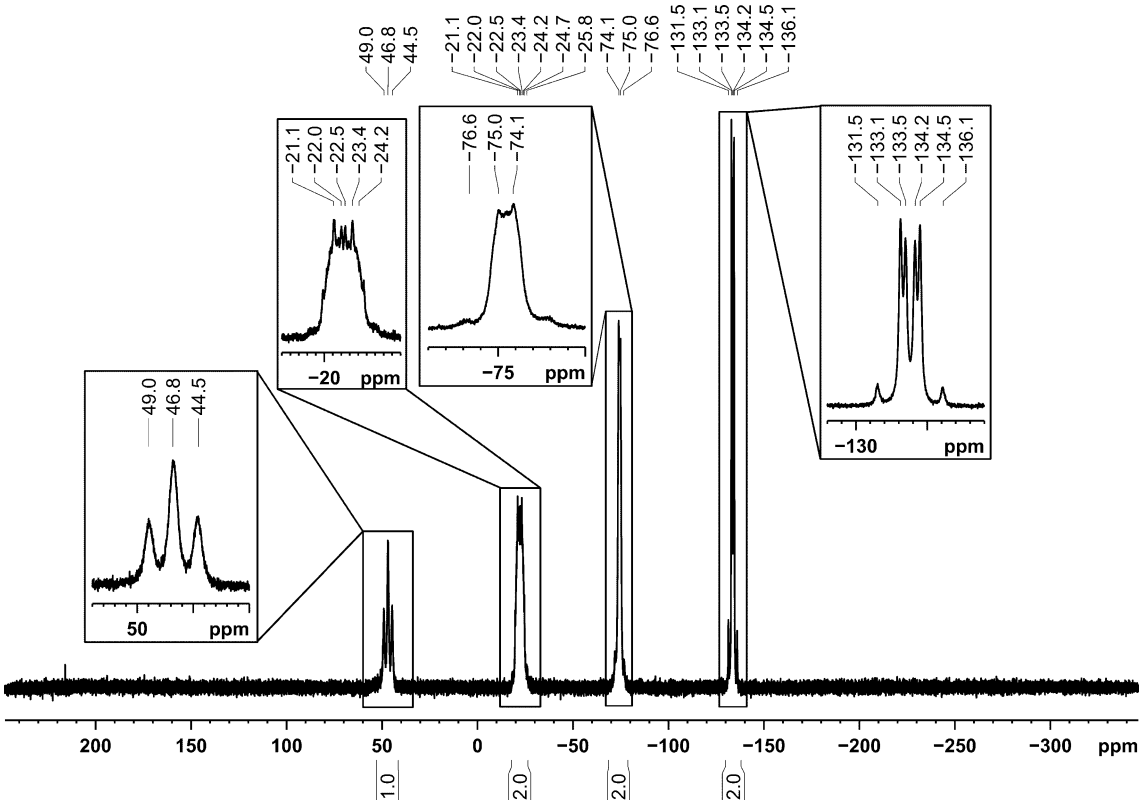

Figure S17. $^{31}P\{^{1}H\}$ NMR spectrum (162.04 MHz, 300 K, C_6D_6) of [(Ar*BIAN)Co(η^4-P_7L_C)] (**7**).

4.4.3 UV/Vis Spectra

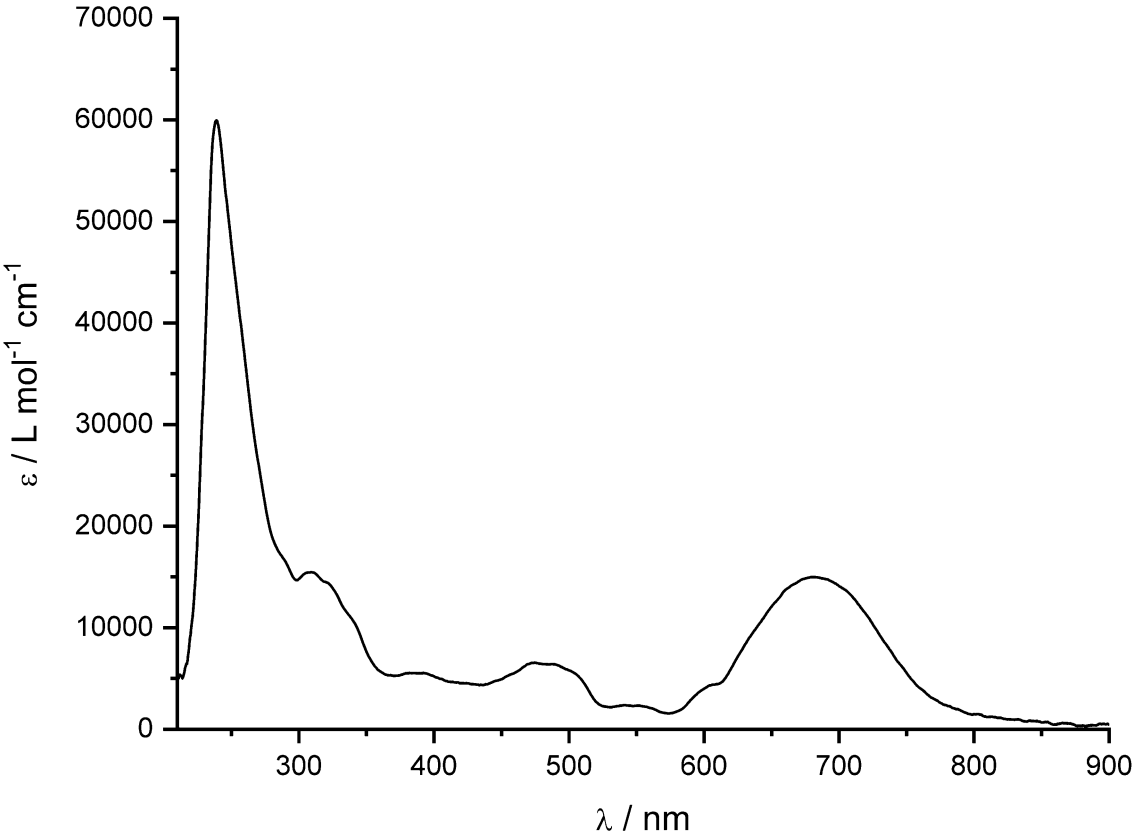

Figure S19. UV/Vis spectrum of [(Ar*BIAN)Co(CN)(η^3-P_4Cy_2)] (**2a**) recorded in THF.

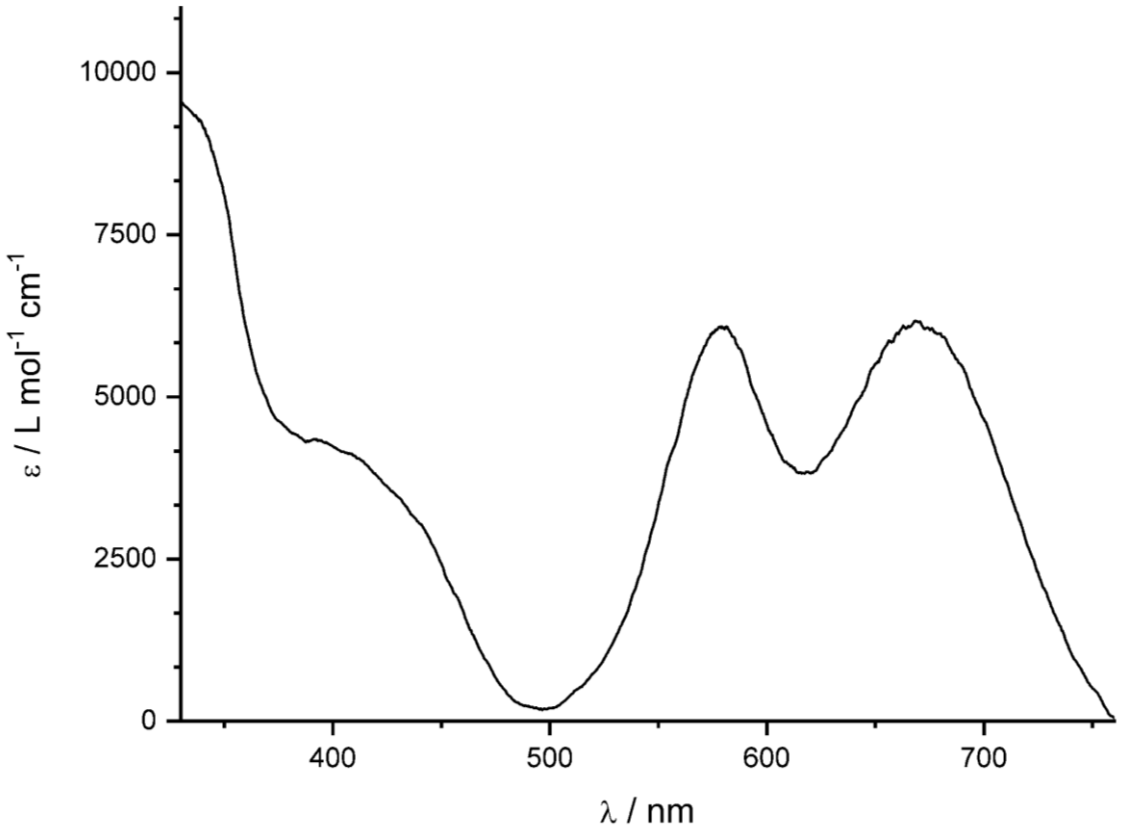

Figure S20. UV/Vis spectrum of [(Ar*BIAN)Co(η^4-P_5tBu_2)] (**4a**) recorded in toluene.

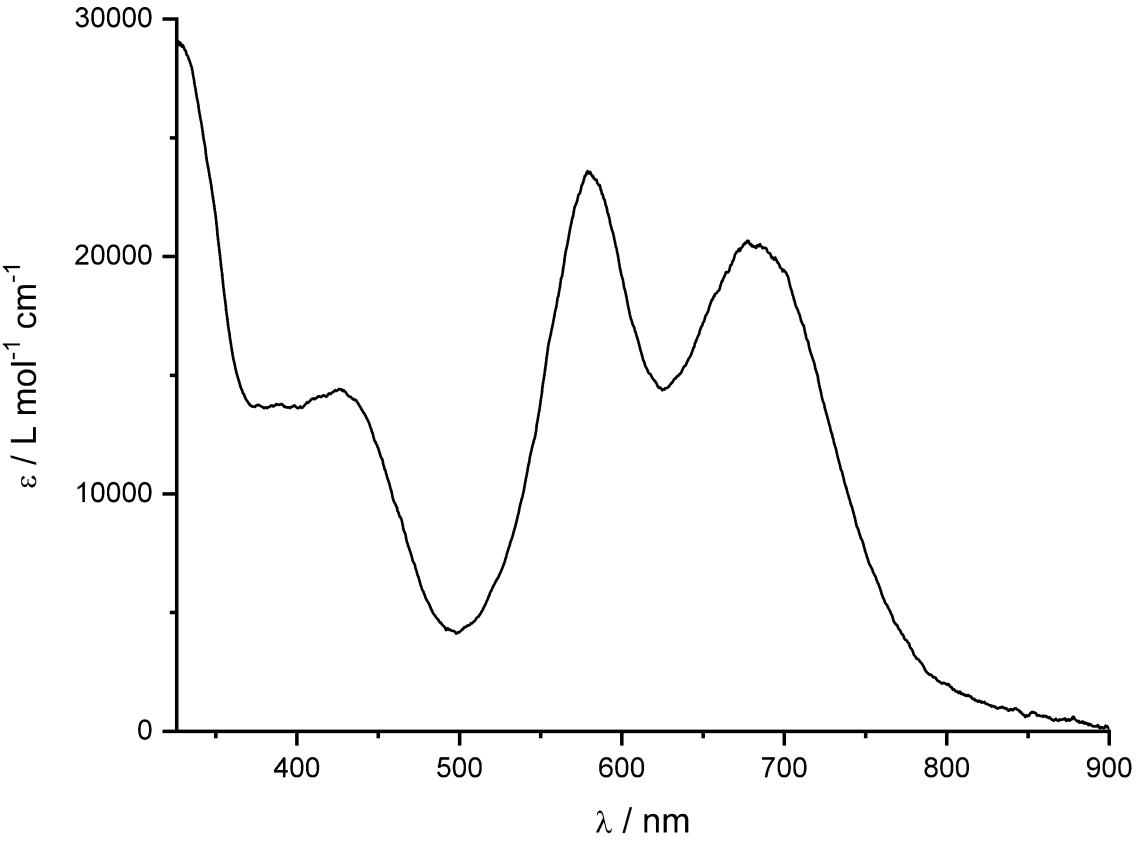

Figure S21. UV/Vis spectrum of [(Ar*BIAN)Co(η^4-P_5(N(*i*Pr_2)$_2$)] (**4b**) recorded in toluene.

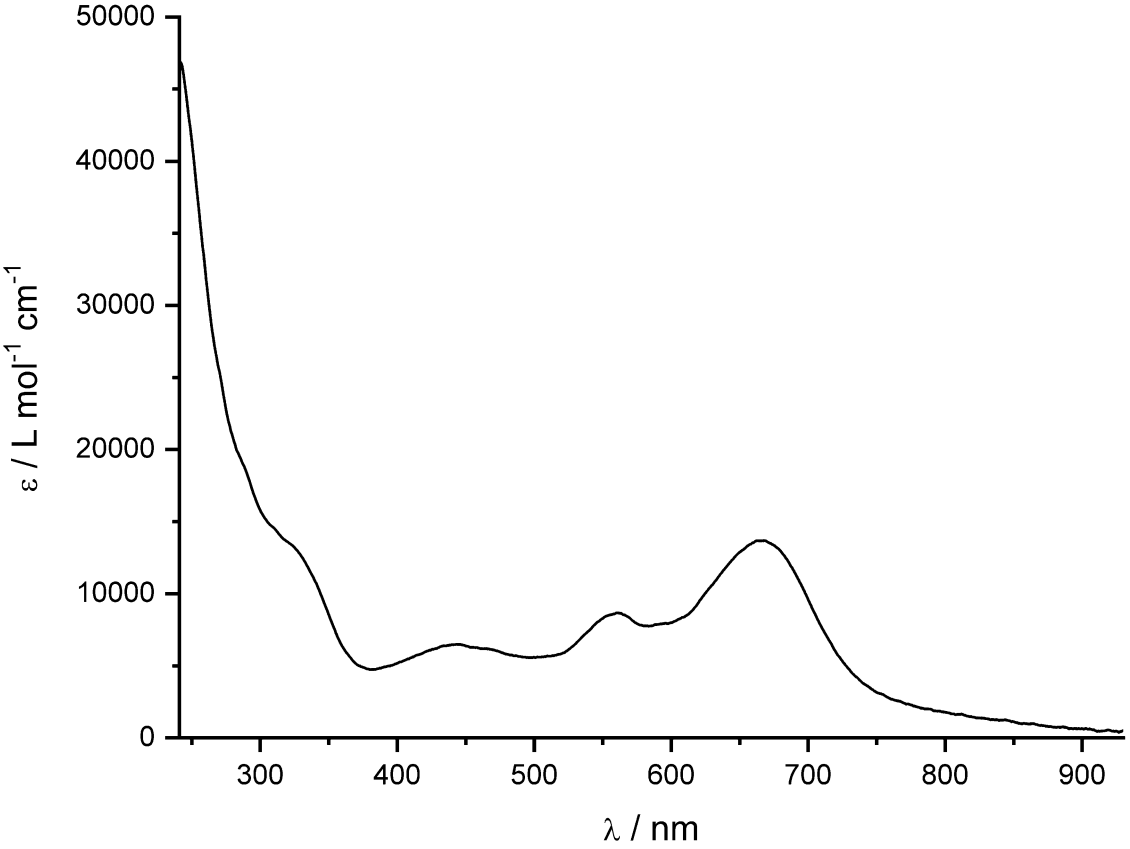

Figure S22. UV/Vis spectrum of [(Ar*BIAN)Co(η^4-P_7L_C)] (**7**) recorded in THF.

4.4.4 IR Spectra

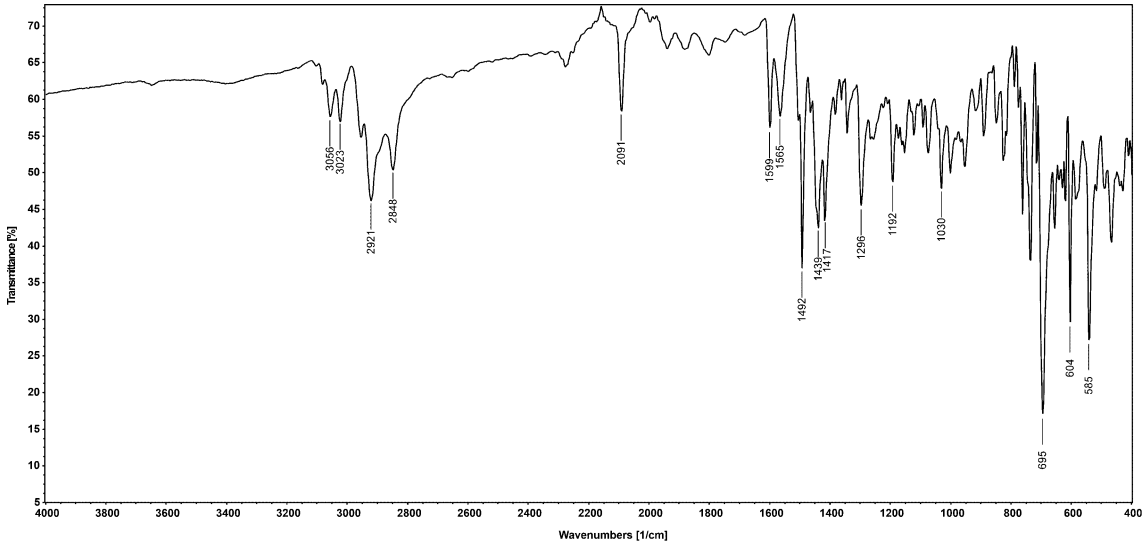

Figure S23. Solid state ATR-IR spectrum of [(Ar*BIAN)Co(CN)(η^3-P_4Cy_2)] (**2a**).

4.4.5 Single Crystal X-Ray Diffraction Data

Single crystal X-ray diffraction data were recorded on Rigaku Oxford Diffraction SuperNova Atlas or XtaLAB Synergy R (DW system, Hypix-Arc 150) devices with Cu-K_α radiation (λ= 1.54184 Å). Crystals were selected under mineral oil, mounted on micromount loops and quench-cooled using an Oxford Cryosystems open flow N_2 cooling device. Either semi-empirical multi-scan absorption corrections[51,52] or analytical ones[53] were applied to the data. The structures were solved with SHELXT[54] solution program using dual methods and by using Olex2 as the graphical interface.[55] The models were refined with ShelXL[56] using full matrix least squares minimization on F^2.[57] The hydrogen atoms were located in idealized positions and refined isotropically with a riding model.

[(Ar*BIAN)Co(CN)(η^3-P_4Cy_2)] (**2a**): Crystals were obtained by slow diffusion of *n*-hexane into a saturated toluene solution of **2a**. The crystal structure of **2a** contained two severely disordered *n*-hexane molecules per asymmetric unit. One molecule of *n*-hexane was modelled for disorder in a 55:45 ratio, while the other, which did not lend itself to effective modeling, was accounted for by use of a solvent mask. The solvent mask was calculated, and 102 electrons were found in a volume of 462 $Å^3$ in one void per unit cell. This is consistent with the presence of 1.0 *n*-hexane per formula unit which account for 100 electrons per unit cell.

[(Ar*BIAN)Co(η^4-P_5tBu_2)] (**4a**): Crystals were obtained by slow diffusion of *n*-pentane into a saturated toluene solution of **4a**. The crystal structure of **4a** contained two times half a molecule of *n*-pentane and two toluene molecules each per asymmetric unit. One toluene molecule was modeled without disorder and the other one was modelled for disorder in a 55:45 ratio. The *n*-pentane molecules were severely disordered and refined by using the solvent mask command: A solvent mask was calculated, and 93 electrons were found in a volume of 500 $Å^3$ in two voids per unit cell. This is consistent with the presence of 2 × 0.5 *n*-pentane per formula unit which account for 84 electrons per unit cell.

[(Ar*BIAN)Co(η^4-P_7L_C)] (**7**): Crystals were obtained by slow diffusion of *n*-hexane into a saturated toluene solution of **7**. The crystal structure of **7** contained one full and additional 0.75 severely disordered 1,4-dioxane molecules per asymmetric unit. A solvent mask was calculated which found 153 electrons in a volume of 697 $Å^3$ in one void per unit cell. This is consistent with the presence of 1.75 1,4-dioxanes per formula unit which account for 168 electrons per unit cell.

The following section provides figures of the molecular structures with selected bond lengths and angles, which were not given in section 4.2 itself.

Table S4. Crystallographic data and structure refinement for compounds **2-5**.

Compound	**2a**	**4a**	**4b**	**7**
Empirical formula	$C_{101}H_{104}CoN_3P_4$	$C_{194}H_{188}Co_2N_4P_{10}$	$C_{94}H_{96}CoN_4P_5$	$C_{93}H_{88}CoN_4P_7$
Formula weight	1628.85	3003.03	1495.52	1663.57
Temperature/K	123(1)	100(1)	123(1)	123(1)
Crystal system	monoclinic	triclinic	orthorhombic	triclinic
Space group	$P2_1$	P-1	$Pna2_1$	P-1
a/Å	15.2435(2)	13.60598(10)	30.9069(4)	14.31880(10)
b/Å	18.9554(2)	23.98531(15)	19.5965(3)	15.61740(10)
c/Å	15.8508(2)	26.39734(19)	13.02160(10)	21.9186(2)
α/°	90	98.3571(6)	90	90.5700(10)
β/°	102.2540(10)	104.1729(6)	90	108.1410(10)
γ/°	90	91.1376(6)	90	108.5180(10)
Volume/Å^3	4475.68(10)	8249.88(10)	7886.76(17)	4384.35(7)
Z	2	2	4	2
ρ_{calc}g/cm^3	1.209	1.209	1.260	1.260
μ/mm^{-1}	2.553	2.906	3.044	3.140
F(000)	1736.0	3168.0	3160.0	1752.0
Crystal size/mm^3	0.251 × 0.107 × 0.079	0.221 × 0.162 × 0.103	0.204 × 0.072 × 0.051	0.164 × 0.063 × 0.046
Diffractometer	SuperNova, Dualflex, TitanS2	XtaLAB Synergy R, DW system, HyPix-Arc 150	XtaLAB Synergy R, DW system, HyPix-Arc 150	XtaLAB Synergy R, DW system, HyPix-Arc 150
Radiation	CuKα (λ = 1.54184)	CuKα (λ = 1.54184)	Cu Kα (λ = 1.54184)	Cu Kα (λ = 1.54184)
2Θ range for data collection/°	7.37 to 133.918	3.73 to 148.554	5.34 to 146.13	6.012 to 151.58
Index ranges	−17 ≤ h ≤ 17, −22 ≤ k ≤ 20, −18 ≤ l ≤ 17	−16 ≤ h ≤ 16, −26 ≤ k ≤ 29, −32 ≤ l ≤ 32	−37 ≤ h ≤ 36, −22 ≤ k ≤ 23, −11 ≤ l ≤ 15	−17 ≤ h ≤ 17, −18 ≤ k ≤ 19, −27 ≤ l ≤ 26
Reflections collected	36708	127795	30252	86378
Independent reflections	13451 [R_{int} = 0.0733, R_{sigma} = 0.0601]	31983 [R_{int} = 0.0301, R_{sigma} = 0.0269]	11704 [R_{int} = 0.0248, R_{sigma} = 0.0307]	17859 [R_{int} = 0.0287, R_{sigma} = 0.0257]
Data/restraints/ parameters	13451/26/999	31983/269/2010	11704/1/1146	17859/96/1014
Goodness-of-fit on F^2	1.024	1.034	1.032	1.081
Final R indexes [I>=2σ (I)]	R_1 = 0.0599, wR_2 = 0.1525	R_1 = 0.0574, wR_2 = 0.1517	R_1 = 0.0422, wR_2 = 0.1114	R_1 = 0.0403, wR_2 = 0.1083
Final R indexes [all data]	R_1 = 0.0627, wR_2 = 0.1559	R_1 = 0.0626, wR_2 = 0.1550	R_1 = 0.0477, wR_2 = 0.1153	R_1 = 0.0474, wR_2 = 0.1120
Largest diff. peak/hole / e Å^{-3}	0.40/−0.74	1.09/−0.86	0.70/−0.34	0.50/-0.36
Flack parameter	−0.036(3)	/	−0.033(2)	/

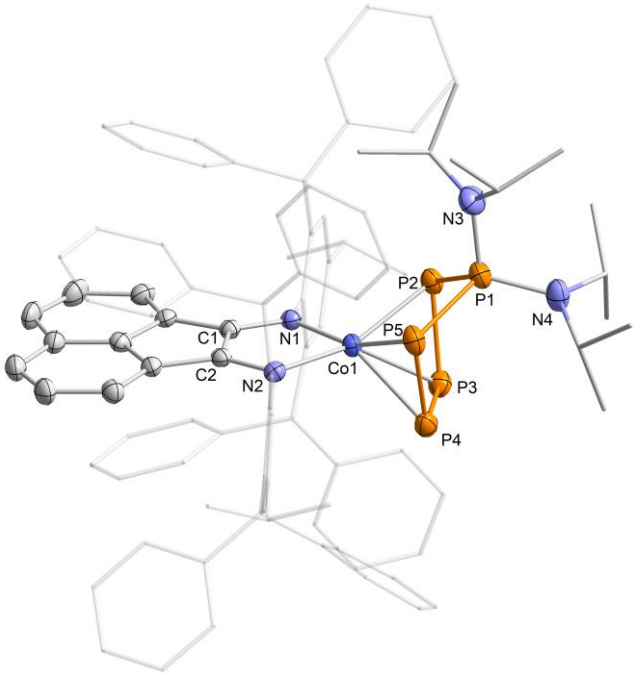

Figure S24. Solid-state molecular structure of [(Ar*BIAN)Co(η^4-P_5(N(*i*Pr_2)$_2$)] (**4b**) shown at the 50% probability level. Hydrogen atoms are omitted for clarity. Selected bond lengths [Å] and angles [°]: P1−P2 2.1613(1), P2−P3 2.1481(2), P3−P4 2.1404(2), P4−P5 2.1497(2), Co1−P2 2.3095(1), Co1−P3 2.3369(1), Co1−P4 2.3488(1), Co1−P5 2.3365(1), P1−N3 1.678(5), P1−N4 1.655(4), Co1−N1 1.947(3), Co1−N2 1.941(3), N1−C1 1.335(5), N2−C2 1.334(5), C1−C2 1.416(6), P1-P2-P3 98.76(6), P1-P5-P4 100.07(6), P2-P3-P4 104.21(6), P3-P4-P5 103.00(6), N1-Co1-N2 84.07(1), N1-C1-C2 116.4(3), N2-C2-C1 116.4(3).

References

[1] J. J. Weigand, N. Burford, in *Compr. Inorg. Chem. II Second Ed.* (Eds.: J. Reedijk, K. Poeppelmeier), Elsevier, Amsterdam, **2013**, pp. 119–149.

[2] A. F. Holleman, E. Wiberg, N. Wiberg, *Lehrbuch der anorganischen Chemie*, De Gruyter, Berlin, **2017**.

[3] M. Peruzzini, L. Gonsalvi, A. Romerosa, *Chem. Soc. Rev.* **2005**, *34*, 1038–1047.

[4] B. M. Cossairt, N. A. Piro, C. C. Cummins, *Chem. Rev.* **2010**, *110*, 4164–4177.

[5] M. Scheer, G. Balázs, A. Seitz, *Chem. Rev.* **2010**, *110*, 4236–4256.

[6] M. Caporali, L. Gonsalvi, A. Rossin, M. Peruzzini, *Chem. Rev.* **2010**, *110*, 4178–4235.

[7] C. M. Hoidn, D. J. Scott, R. Wolf, *Chem. – Eur. J.* **2021**, 1886–1902.

[8] L. Giusti, V. R. Landaeta, M. Vanni, J. A. Kelly, R. Wolf, M. Caporali, *Coord. Chem. Rev.* **2021**, *441*, 213927.

[9] C. M. Hoidn, K. Trabitsch, K. Schwedtmann, C. Taube, J. J. Weigand, R. Wolf, *Chem. – Eur. J.* **2023**, e202301930.

[10] C. G. P. Ziegler, T. M. Maier, S. Pelties, C. Taube, F. Hennersdorf, A. W. Ehlers, J. J. Weigand, R. Wolf, *Chem. Sci.* **2019**, *10*, 1302–1308.

[11] C. M. Hoidn, T. M. Maier, K. Trabitsch, J. J. Weigand, R. Wolf, *Angew. Chem. Int. Ed.* **2019**, *58*, 18931–18936.

[12] A. K. Adhikari, C. G. P. Ziegler, K. Schwedtmann, C. Taube, Jan. J. Weigand, R. Wolf, *Angew. Chem.* **2019**, *131*, 18757–18763.

[13] I. Krossing, I. Raabe, *Angew. Chem. Int. Ed.* **2001**, *40*, 4406–4409.

[14] M. H. Holthausen, S. K. Surmiak, P. Jerabek, G. Frenking, J. J. Weigand, *Angew. Chem. Int. Ed.* **2013**, *52*, 11078–11082.

[15] M. H. Holthausen, A. Hepp, J. J. Weigand, *Chem. – Eur. J.* **2013**, *19*, 9895–9907.

[16] M. H. Holthausen, K.-O. Feldmann, S. Schulz, A. Hepp, J. J. Weigand, *Inorg. Chem.* **2012**, *51*, 3374–3387.

[17] C. Riesinger, L. Dütsch, G. Balázs, M. Bodensteiner, M. Scheer, *Chem. – Eur. J.* **2020**, *26*, 17165–17170.

[18] M. Piesch, M. Seidl, M. Stubenhofer, M. Scheer, *Chem. – Eur. J.* **2019**, *25*, 6311–6316.

[19] M. Weber, G. Balázs, A. V. Virovets, E. Peresypkina, M. Scheer, *Molecules* **2021**, *26*, 3920.

[20] C. Riesinger, A. Erhard, M. Scheer, *Chem. Commun.* **2023**, *59*, 10117–10120.

[21] M. Piesch, S. Reichl, M. Seidl, G. Balázs, M. Scheer, *Angew. Chem. Int. Ed.* **2021**, *60*, 15101–15108.

[22] K. Trabitsch, *Reactivity Studies of an Anionic Cyclotriphosphido Cobalt Complex*, Masterarbeit, Universität Regensburg, **2020**.

[23] A. H. Cowley, R. A. Kemp, *Chem. Rev.* **1985**, *85*, 367–382.

[24] J. J. Weigand, K.-O. Feldmann, F. D. Henne, *J. Am. Chem. Soc.* **2010**, *132*, 16321–16323.

[25] F. D. Henne, A. T. Dickschat, F. Hennersdorf, K.-O. Feldmann, J. J. Weigand, *Inorg. Chem.* **2015**, *54*, 6849–6861.

[26] C. Taube, K. Schwedtmann, M. Noikham, E. Somsook, F. Hennersdorf, R. Wolf, J. J. Weigand, *Angew. Chem. Int. Ed.* **2020**, *59*, 3585–3591.

[27] K. Schwedtmann, J. Haberstroh, S. Roediger, A. Bauzá, A. Frontera, F. Hennersdorf, J. J. Weigand, *Chem. Sci.* **2019**, *10*, 6868–6875.

[28] P. Royla, K. Schwedtmann, Z. Han, J. Fidelius, D. P. Gates, R. M. Gomila, A. Frontera, J. J. Weigand, *J. Am. Chem. Soc.* **2023**, *145*, 10364–10375.

[29] S. Hauer, T. M. H. Downie, G. Balázs, K. Schwedtmann, J. J. Weigand, R. Wolf, *Angew. Chem. Int. Ed.* **2023**, e202317170.

[30] M. M. Khusniyarov, K. Harms, O. Burghaus, J. Sundermeyer, *Eur. J. Inorg. Chem.* **2006**, *2006*, 2985–2996.
[31] P. Rigo, A. Turco, *Coord. Chem. Rev.* **1974**, *13*, 133–172.
[32] G. Socrates, *Infrared and Raman Characteristic Group Frequencies: Tables and Charts*, Wiley, Chichester, **2004**.
[33] *A Search of the Cambridge Crystal Structure Database (CCSD), Version 5.44, 04/2023, Revealed 120 Cobalt Complexes Bearing Only One Terminal Cyanide Ligand with a Mean Co−C Distance of 1.899 Å (Median 1.888 Å) and a Mean C≡N Distance of 1.137 Å (Median 1.144 Å)*, **2023**.
[34] P. Pyykkö, M. Atsumi, *Chem. – Eur. J.* **2009**, *15*, 186–197.
[35] P. Pyykkö, M. Atsumi, *Chem. – Eur. J.* **2009**, *15*, 12770–12779.
[36] K. Trabitsch, *Unpublished Results*, Universität Regensburg, **2024**.
[37] E.-M. Schnöckelborg, J. J. Weigand, R. Wolf, *Angew. Chem. Int. Ed.* **2011**, *50*, 6657–6660.
[38] C. M. Knapp, J. S. Large, N. H. Rees, J. M. Goicoechea, *Chem. Commun.* **2011**, *47*, 4111–4113.
[39] S. Charles, B. W. Eichhorn, A. L. Rheingold, S. G. Bott, *J. Am. Chem. Soc.* **1994**, *116*, 8077–8086.
[40] S. Charles, J. C. Fettinger, S. G. Bott, B. W. Eichhorn, *J. Am. Chem. Soc.* **1996**, *118*, 4713–4714.
[41] E. Mädl, M. V. Butovskii, G. Balázs, E. V. Peresypkina, A. V. Virovets, M. Seidl, M. Scheer, *Angew. Chem. Int. Ed.* **2014**, *53*, 7643–7646.
[42] F. Riedlberger, S. Todisco, P. Mastrorilli, A. Y. Timoshkin, M. Seidl, M. Scheer, *Chem. – Eur. J.* **2020**, *26*, 16251–16255.
[43] S. Pelties, T. Maier, D. Herrmann, B. de Bruin, C. Rebreyend, S. Gärtner, I. G. Shenderovich, R. Wolf, *Chem. - Eur. J.* **2017**, *23*, 6094–6102.
[44] P. H. M. Budzelaar, in IvorySoft: gNMR for Windows, NMR Simulation Program, **2006**.
[45] E. G. Finer, R. K. Harris, *Mol. Phys.* **1967**, *13*, 65–75.
[46] S. Aime, R. K. Harris, E. M. McVicker, M. Fild, *J. Chem. Soc. Dalton Trans.* **1976**, 2144–2153.
[47] J. P. Albrand, H. Faucher, D. Gagnaire, J. B. Robert, *Chem. Phys. Lett.* **1976**, *38*, 521–523.
[48] H. C. E. McFarlane, W. McFarlane, J. A. Nash, *J. Chem. Soc. Dalton Trans.* **1980**, 240–244.
[49] M. A. M. Forgeron, M. Gee, R. E. Wasylishen, *J. Phys. Chem. A* **2004**, *108*, 4895–4908.
[50] J. E. Del Bene, J. Elguero, I. Alkorta, *J. Phys. Chem. A* **2004**, *108*, 3662–3667.
[51] G. M. Sheldrick, SADABS, Bruker AXS, Madison, USA, **2007**.
[52] CrysAlisPro, Scale3 Abspack, Rigaku Oxford Diffraction, **2019**.
[53] R. C. Clark, J. S. Reid, *Acta Crystallogr. Sect. A* **1995**, *51*, 887–897.
[54] G. M. Sheldrick, *Acta Crystallogr. Sect. Found. Adv.* **2015**, *71*, 3–8.
[55] O. V. Dolomanov, L. J. Bourhis, R. J. Gildea, J. a. K. Howard, H. Puschmann, *J. Appl. Crystallogr.* **2009**, *42*, 339–341.
[56] G. M. Sheldrick, *Acta Crystallogr. Sect. C Struct. Chem.* **2015**, *71*, 3–8.
[57] G. M. Sheldrick, *Acta Crystallogr. A* **2008**, *64*, 112–122.

5 Reactivity of Cyclotetraphosphido and Cyclotriphosphido Cobalt Complexes toward Group 14 Ambiphiles[a,b]

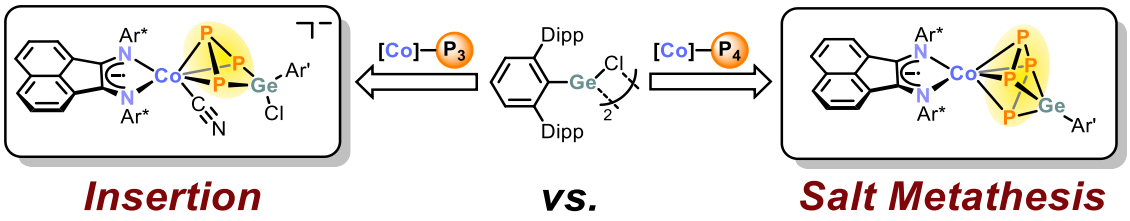

[a] S. Hauer, K. Trabitsch, R. Wolf, unpublished results.

[b] S. Hauer performed the synthetic investigations and the characterization of the reported compounds. K. Trabitsch performed the reactions with the related PHDI cobalt complexes that are discussed for comparison. S. Hauer wrote the chapter. R. Wolf supervised the project.

5.1 Introduction

Tetrahedranes (tricyclo[1.1.0.$0^{2,4}$]butanes) have attracted considerable attention due to their highly strained molecule structure and the ensuing high reactivity. However, synthetic access to these species remains challenging.[1] In particular, neutral heteroatomic tetrahedranes are extremely scarce. Transition metal polyphosphido complexes emerged as promising vehicles to such unique phosphorus-containing compounds, inaccessible by other synthetic pathways.[2–8] Two remarkable examples are the mixed binary group 15 tetrahedranes EP_3 (E = As, Sb).[9,10] The syntheses of these interpnictogen compounds proceed *via* salt metathesis of the niobate complex $[(\eta^3\text{-}P_3)Nb(ODipp)_3]^-$ with ECl_3 (Dipp = 2,6-*i*$Pr_2C_6H_3$). Furthermore, the first tetrahedranes comprised of carbon and phosphorus have become accessible in recent years: (*t*BuCP)$_2$, (*t*BuC)$_3$P and HCP_3.[11–13] Replacing the CR fragment by heavier homologues within the series of tetrels could give rise to further heteroatomic species. Thus, mixed group 14/15 ligands are of particular interest, for the synthesis of heavier homologues of the well-known tetrahedrane.

To the best of our knowledge, Figure 1 summarizes all reported complexes bearing such a functionalized and P_4-derived polyphosphido ligand in a chronological order. In the period 2004–2008, Cummins and co-workers reported a series of niobium complexes **A**-**D** which are products of salt metathesis of anionic niobium P_1 or P_3 complexes, with group 14 halides.[14–17] Specifically, the silylation and stannylation at the nucleophilic phosphorus atom in $[P{\equiv}Nb\{N(Np)Ar\}_3]^-$ (Np = CH_2*t*Bu, Ar = 3,5-$Me_2C_6H_3$) was achieved by treatment with Me_3ECl (E = Si, Sn), affording complexes **A**. The reaction of the same P_1 niobate with divalent group 14 element salts EX_2 (E = Ge, Sn Pb; X = Cl, $SO_3CF_3^-$) leads to dinuclear compounds **B** containing a bridging $\mu,\eta^3{:}\eta^3$-*cyclo*-EP_2 ligand. Moreover, the stannylation of *cyclo*-P_3 complexes $[\{(OC)_5W\}(\eta^3\text{-}P_3)Nb\{N(Np)Ar\}_3]^-$ and $[(\eta^3\text{-}P_3)Nb(ODipp)_3]^-$ afforded **C** and **D**, respectively. More recently, Ruiz and co-workers reported the functionalization of anionic molybdenum P_2 complex with $ClER_3$ (E = Ge, Sn, Pb; R = Ph, Me) , yielding tetryldiphosphenyl bridged species **E**.[18,19] In 2020, Roesky and Scheer reported the synthesis of complexes **F** and **G** involving the reaction of $[Cp^*Fe(\eta^5\text{-}P_5)]$ (Cp^* = η^5-C_5Me_5) with a silylene, or bisgermylene, respectively.[20,21] In the same work the authors also reported a to **F** structurally related complex which was afforded from the insertion of two Si moieties. A year later, Scheer and co-workers reported **H**, also from the reaction of $[Cp^*Fe(\eta^5\text{-}P_5)]$ with a silylene.[22] Interestingly, en route to FeP_4 complex **F**, the formation of a neutral

complex related to **H** is initially observed, which undergoes simultaneous P atom extrusion and insertion of LSi (L = [PhC(N*t*Bu)$_2$]), affording silaphosphaferrocene **F**. The analogous reaction employing [Cp'''Co(η^3-P$_3$)] (Cp''' = C$_5$H$_2$*t*Bu$_3$) affords **I**, bearing a P$_3$SiL heterocycle.[23] Very recently, Scheer, Roesky and co-workers reported the synthesis of **J**, from the reaction of [Cp*Fe(η^5-P$_5$)] with a gallasilylene, as end-product of a sequence of isomerization reactions.[24]

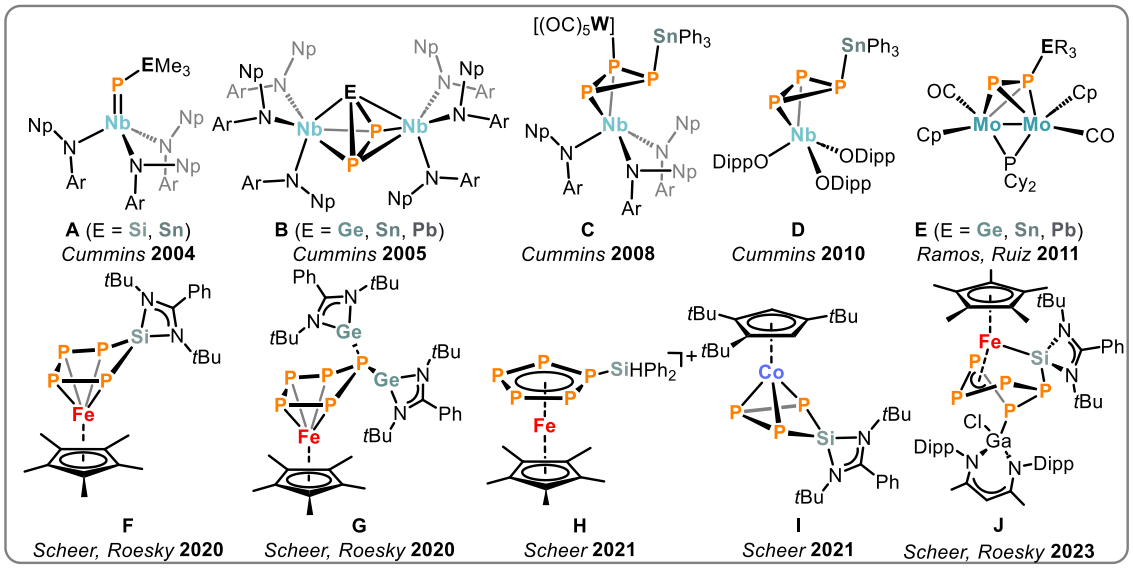

Figure 1. Functionalized polyphosphido ligands accessible *via* derivatization with group 14 electrophiles; Np = CH$_2$*t*Bu, Ar = 3,5-Me$_2$C$_6$H$_3$, Dipp = 2,6-*i*Pr$_2$C$_6$H$_3$; Cp* = η^5-C$_5$Me$_5$; Cp = η^5-C$_5$H$_5$; R = Ph, Me.

As highlighted by this overview, complexes of the TM-P$_n$ type are suitable precursors for the synthesis of mixed group 14/15 ligands. However, only selected examples have been reported so far (*vide supra*) and their subsequent chemistry remains underdeveloped. In particular, germylated P$_n$ ligands remain scarce and only complexes **B**, **E** and **G** have been reported so far, further limiting further studies into their chemistry. By subsequent and targeted release of these functionalized P$_n$ ligands new (poly-)phosphorus compounds become accessible. This might ultimately pave the way to remarkable tetrahedrenes, in which one or more of the CR fragments are substituted by heavier homologues within the series of tetrels. Thus, the reactivity of *cyclo*-P$_3$ complex **1** and its *cyclo*-P$_4$ counterpart **3** toward group 14 halides will be investigated in the following.

5.2 Results and Discussion

Initially, the cyclotriphosphido cobaltate [K(18c-6)][(Ar*BIAN)Co(CN)(η^3-P$_3$)] (**1**, 18c-6 = 18-crown-6, Ar* = 2,6-dibenzhydryl-4-isopropylphenyl; BIAN = 1,2-bis(arylimino)acenaphthene diamine) was treated with 0.5 equivalents of the terphenyl-supported tetrylene halide complexes [Ar'E(μ-X)]$_2$ (Ar' = 2,6-Dipp$_2$C$_6$H$_3$; E = Ge, Sn: X = Cl; E = Pb: X = Br). For E = Sn, a highly broadened signal at δ = −195 ppm was

observed in the $^{31}P\{^{1}H\}$ NMR spectrum of the reaction mixture, which was shifted slightly downfield with respect to the signal of the starting material (see the Supporting Information (SI), Figure S8). This was taken to indicate the stannylene acts as a Lewis acid, forming an adduct with **1** *via* the coordination of the cyanide ligand.[25] For E = Pb, no reaction was observed by ^{1}H and $^{31}P\{^{1}H\}$ NMR spectroscopy. In contrast, the $^{31}P\{^{1}H\}$ NMR spectrum after four days of the reaction mixture involving a slight excess (0.66 equiv.) of $[Ar'Ge(\mu\text{-}Cl)]_2$ and **1** displays the emergence of an A_2X spin system (Scheme 1).

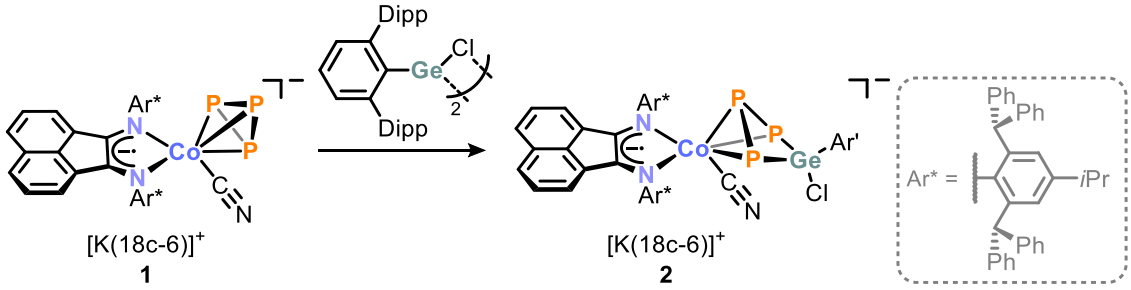

Scheme 1. Insertion of $[Ar'Ge(\mu\text{-}Cl)]_2$ into *cyclo*-P_3 moiety in **1**, yielding anionic *cyclo*-$P_3GeAr'Cl$ complex **2**; reagents and conditions: +0.5 $[Ar'Ge(\mu\text{-}Cl)]_2$; toluene, r.t., 4 d; isolated yield: 65%; Dipp = 2,6-*i*$Pr_2C_6H_3$.

After work-up dark purple crystals were obtained in 65% isolated yield. X-ray diffraction analysis (XRD) of these crystals revealed the nucleophilic insertion of the germanium moiety into the triphosphido ligand, yielding [K(18c-6)][(Ar*BIAN)Co(CN)(η^3-$P_3GeAr'Cl$)] (**2**). The reactions of the related complex $[(PHDI)Co(CN)(\eta^3\text{-}P_3)]^-$ with $[Ar'Ge(\mu\text{-}Cl)]_2$ yielded the analogous compound to **2**.[26] Complex **2** features a η^3-coordinating *cyclo*-$P_3GeAr'Cl$ ligand in a puckered conformation (Figure 2a) with P–P bond lengths of 2.1787(6) Å and 2.1882(6) Å within the P_3 moiety. They thus lie between typical P–P single and P=P double bonds ($\Sigma_{r\mathrm{PP}}$ 2.22 Å vs. 2.04 Å), indicating a delocalized system.[27,28] In comparison, the Ge–P bond lengths (2.2996(5) Å and 2.3114(5) Å) are well within the typical range for calculated Ge–P single bonds ($\Sigma_{r\mathrm{GeP}}$ 2.32 Å).[27,28] Additionally, the IR spectrum of **2** exhibits a characteristic stretching vibration at $\tilde{\nu}_{CN}$ = 2076 cm^{-1}, within the typical range for cobalt cyanide complexes, as are the Co–C (1.931(9) Å) and C–N (1.158(4) Å) bond lengths.[29–31] Germanium-substituted polyphosphido ligands are very scarce (*vide supra*). So far, only two binuclear examples have been reported, bearing bridging P_2-ligands. These niobium (**B**) and molybdenum (**E**) complexes are synthesized from germanium halides and their anionic precursors $[P{\equiv}Nb\{N(Np)Ar\}_3]^-$, or $[Mo_2Cp_2(\mu\text{-}PCy_2)(CO)_2(\mu\text{-}\kappa^2\text{:}\kappa^2\text{-}P_2)]^-$, respectively (*vide supra*, Figure 1).[15,19] Thus, **2** represents the first mononuclear complex bearing such germanium-functionalized polyphosphido ligand.

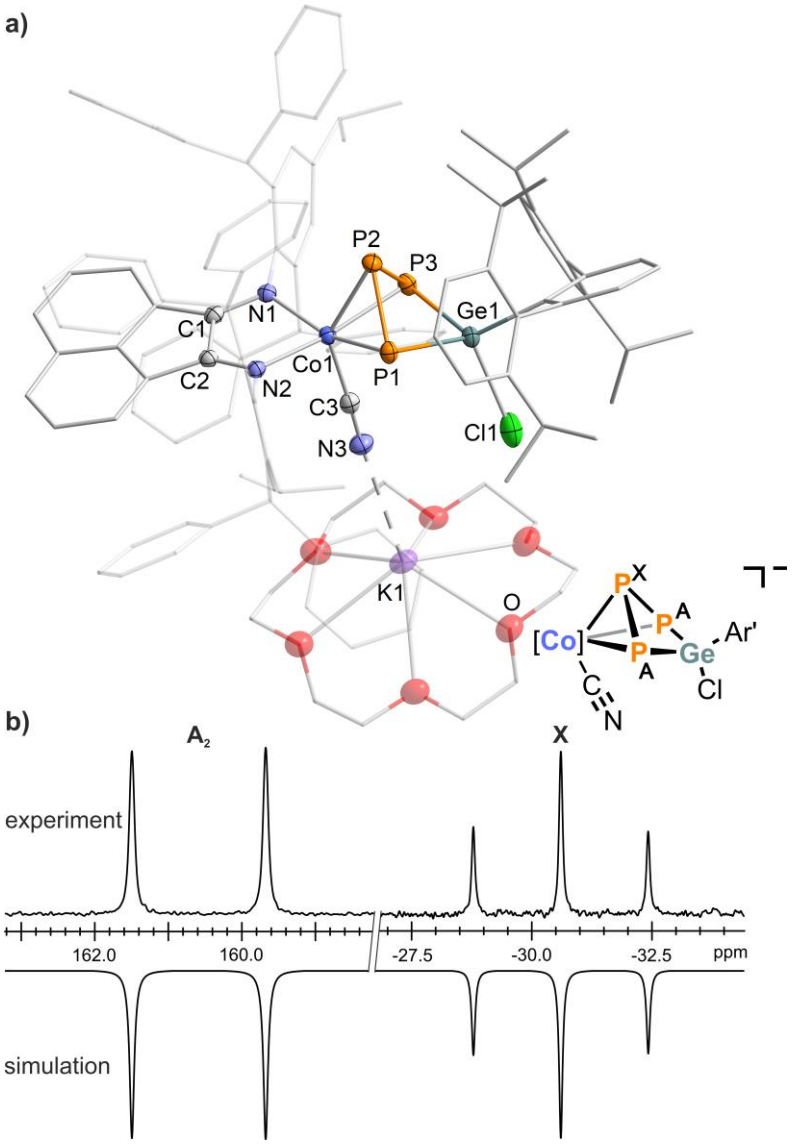

Figure 2. a) Solid-state molecular structure of [K(18c-6)][(Ar*BIAN)Co(CN)(η^3-P_3GeAr'Cl)] (**2**); thermal ellipsoids are shown at the 50% probability level; hydrogen atoms, disorder and non coordinating solvent molecules omitted for clarity. The halogen at Ge1 was refined with a split model as a Cl atom with a chemical occupancy of 0.8 and an I atom with the occupancy of 0.2. Residual iodide was attributed to insufficient washing during synthesis of the starting material. Selected bond lengths [Å] and angles [°]: P1−P2 2.1787(6), P2−P3 2.1882(6), Ge1−P1 2.2996(5), Ge1−P3 2.3114(5), Ge1−Cl1 2.4564(4), Ge1−I1 2.45637(2), Co1−P1 2.3295(5), Co1−P2 2.2545(5), Co1−P3 2.3064(5), Co1−C3 1.9241(2), C3−N3 1.159(3), Co1−N1 2.0254(1), Co1−N2 1.9794(1), C1−N1 1.316(2), C2−N2 1.315(2), C1−C2 1.459(2), N3−K1 2.9038(2), P1-P2-P3 90.38(3), P2-P3-Ge1 79.437(2), P3-Ge1-P1 84.84, P1-Ge1-Cl1 111.349(2), Co1-C3-N3 177.94(2), N1-Co1-N2 81.90(6), N1-C1-C2 116.58(2), Co1-N2-C2 112.58(1); b) experimental (upward) and simulated (downward) $^{31}P\{^1H\}$ NMR spectra of **2**, with nuclei assigned to an A_2X spin system: $\delta(P_A)$ = 160.6 ppm, $\delta(P_X)$ = −30.6 ppm, $^1J_{AX}$ = −295 Hz; [Co] = (Ar*BIAN)Co.

Compound **2** exhibits an A_2X spin system in the $^{31}P\{^1H\}$ NMR spectrum, which readily lent itself to iterative simulation (Figure 2b), identifying a $^1J_{PP}$ coupling constant of −295 Hz (*c.f.* the PHDI analogue: $^1J_{PP}$ = −303 Hz).[26] However, a second set of signals composed of a doublet and a triplet (ca. 15%) was observed, which could not be removed by repeated recrystallization of the isolated material (Figure S3, see SI). This second compound was also observed in the ^1H NMR spectrum as an Ar*BIAN containing species

with very similar chemical shifts to **2** (Figure S1, see SI). Nevertheless, C,H,N analysis on an isolated sample is in excellent agreement with the elemental composition of **2** (see also SI for details). These observations suggest that the second set of signals observed in the NMR spectra can be attributed to a configurational isomer of **2** (*c.f.* the *exo*-/*endo*-isomers of compound **6** in Chapter 2). Note that a closely related PHDI analogue of **2** features a similar, second set of signals in the $^{31}P\{^{1}H\}$ NMR spectrum.[26] Moreover, in the ^{1}H NMR spectrum of compound **2** a downfield shifted singlet was detected at δ = 8.83 ppm for the dibenzyhdryl protons. This observed deshielding is in contrast to all other Ar*BIAN containing compounds within this thesis and the free Ar*BIAN ligand, which features a resonance at δ = 8.83 ppm

An attempt to abstract the chloride anion from **2** using $NaBAr^{F}_{4}$ ($Bar^{F}_{4}^{-}$ = $[\{3,5\text{-}(CF_3)_2C_6H_3\}_4B]^-$) yielded dark blue crystals upon work-up, from a saturated diethyl ether fraction. XRD analysis revealed the neutral complex [(Ar*BIAN)Co(CN)(η^3-P_3GeAr'Cl)] (Figure S12, see SI), presumably resulting from the oxidation of **2**. During the reaction, the radical anionic Ar*BIAN$^{\bullet-}$ ligand is retained, suggesting that oxidation occurs at the metal center.[32] Nonetheless, this neutral species features very similar structural parameters to **2**. This compound was not reliably obtained in a meaningful yield, precluding further characterization.

Next, the reactivity of *cyclo*-P_4 complex [K(18c-6)][(Ar*BIAN)Co(η^4-P_4)] (**3**) toward $[Ar'Ge(\mu\text{-}Cl)]_2$ was also examined (Scheme 2). From the reaction of half an equivalent of $[Ar'Ge(\mu\text{-}Cl)]_2$ with **3** in toluene a dark green reaction mixture was obtained, from which large crystals of [(Ar*BIAN)Co(μ-η^4:η^3-P_4)GeAr')] (**4**) were isolated in 35% yield (Scheme 5). XRD analysis revealed the formation of the salt metathesis product **4** (Figure 3), featuring a chain of four P atoms sandwiched between cobalt and germanium in a μ-η^4:η^3 coordination mode. To the best of our knowledge, only a single related tetraphosphido complex, **F**, has been reported (see Figure 1).[20]

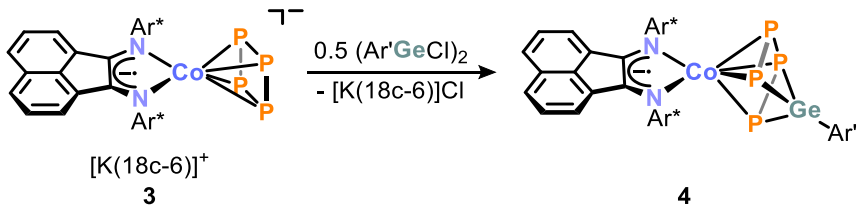

Scheme 2. Reaction of **3** with $[Ar'Ge(\mu\text{-}Cl)]_2$ *via* salt metathesis affording complex **4**; reagents/by-products and conditions: +0.5 $[Ar'Ge(\mu\text{-}Cl)]_2$/−[K(18c-6)]Cl; toluene, r.t., 1 d; isolated yield: 35%.

In contrast to the former planar *cyclo*-P_4 ligand, the now bridging P_4 chain is slightly bent, exhibiting a dihedral angle of 12°. The Ge–P bond lengths to the terminal phosphorus

atoms P1 and P4 are significantly shorter (2.2561(1) Å and 2.2610(1) Å) than the remote Ge−P bond (2.6128(1) Å) to P3. The terminal P−P bonds (P1–P2 2.1131(2) and P3–P4 2.1485(2) Å) exhibit shorter bond lengths compared to the internal P2−P3 bond (2.2952(2) Å). Additionally, there is a significant distance between the terminal phosphorus atoms P1 and P4 of 3.4008(2) Å, suggesting no significant interaction (*c.f.* Σr_{PP} 2.22 Å for a single bond).[27,28] Similar discrepancies have been reported for the related complex [(Cp'''Co)$_2$(μ_3,η^2:η^2-P$_4$)SmCp*$_2$], accessible *via* an intramolecular P−P coupling process, though the P$_4$-chain is significantly more bent (63°).[33] Further dinuclear and structurally related complexes have been reported, including [Cp'Rh(μ,η^4:η^2-P$_4$){Rh(CO)Cp'}] (Cp' = η^5-C$_5$Me$_4$Et), [{Cp'''Fe}$_2$(μ,η^4:η^4-P$_4$)], [LSi(μ,η^2:η^2-P$_4$)-NiL'] (L = CH[(C=CH$_2$)Cme][N(Dipp)]$_2$; L' = CH[CmeN(Dipp)]$_2$), [{Cp^{R}Fe}$_2$(μ,η^4:η^4-P$_4$)] (Cp^R = 1,3-(Me$_3$Si)$_2$C$_5$H or 1,3,4-(Me$_3$Si)$_3$C$_5$H$_3$), [{(P$_2$N$_2$)Zr}$_2$(μ,η^4:η^4-P$_4$)] (P$_2$N$_2$ = PhP(CH$_2$SiMe$_2$NsiMe$_2$CH$_2$)$_2$PPh) and more recently a heterobimetallic cobalt gallium complex from our group, [(^{Mes}BIAN)Co(μ,η^4:η^2-P$_4$)GaL'].[34–40]

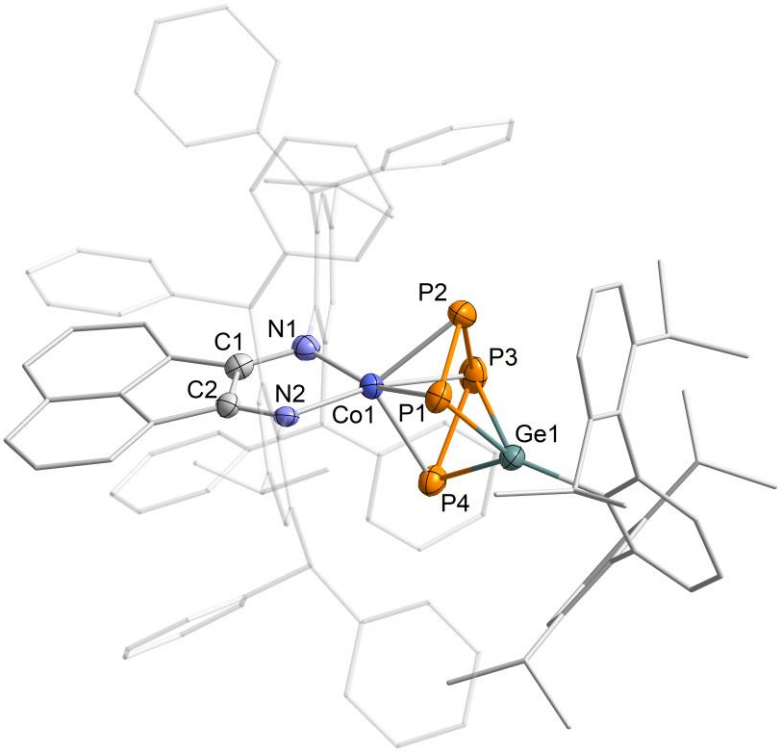

Figure 3. Solid-state molecular structure of [(Ar*BIAN)Co(μ-η^4:η^3-P$_4$)GeAr')] (**4**); thermal ellipsoids are shown at the 50% probability level; hydrogen atoms and non coordinating solvent molecules omitted for clarity. Selected bond lengths [Å] and angles [°]: P1−P2 2.1131(2), P2−P3 2.2952(2), P3−P4 2.1485(2), P1−P4 3.4008(2), Co1−P1 2.3623(1), Co1−P2 2.2622(1), Co1−P3 2.3494(1), Co1−P4 2.3453(1), Ge1−P1 2.2561(1), Ge1−P3 2.6128(1), Ge1−P4 2.2610(1), Co1−N1 1.953(4), Co1−N2 1.915(3), N1−C1 1.327(5), N2−C2 1.327(5), C1−C2 1.442(6), P1-P2-P3 102.24(7), P2-P3-P4 107.04(6), P1-Ge1-P3 89.38(4), P3-Ge1-P4 51.70(4), N1-Co1-N2 83.75(1), N1-C1-C2 115.6(4), N2-C2-C1 115.2(3).

In sharp contrast to the solid-state structure, compound **4** gives rise to a single, slightly broadened ($\Delta\nu_{½}$ = 380 Hz) signal at δ = 75.7 ppm, in the $^{31}P\{^{1}H\}$ NMR spectrum, suggesting circumambulation of the Ar'Ge substituent around the P_4 moiety on the NMR time scale. Similar behavior was reported for stannylated *cyclo*-P_3 complex **D**, which gives rise to a sharp singlet at δ = −235 ppm, even at −90 °C.[17] In comparison, variable temperature (VT) $^{31}P\{^{1}H\}$ NMR spectroscopy of compound **4** revealed that the single resonance splits into four distinct, albeit broad signals at −80 °C, in good agreement with the asymmetric *catena*-P_4 unit observed in the solid state (Figure 4). Additionally, an increase in temperature up to 60 °C leads to sharper resolution of the signal, suggesting a faster dynamic process in solution. This movement of the Ar'Ge substituent is also reflected in the ^{1}H and $^{13}C\{^{1}H\}$ NMR spectra, where **4** gives rise to symmetric Ar*BIAN and Ar' groups.

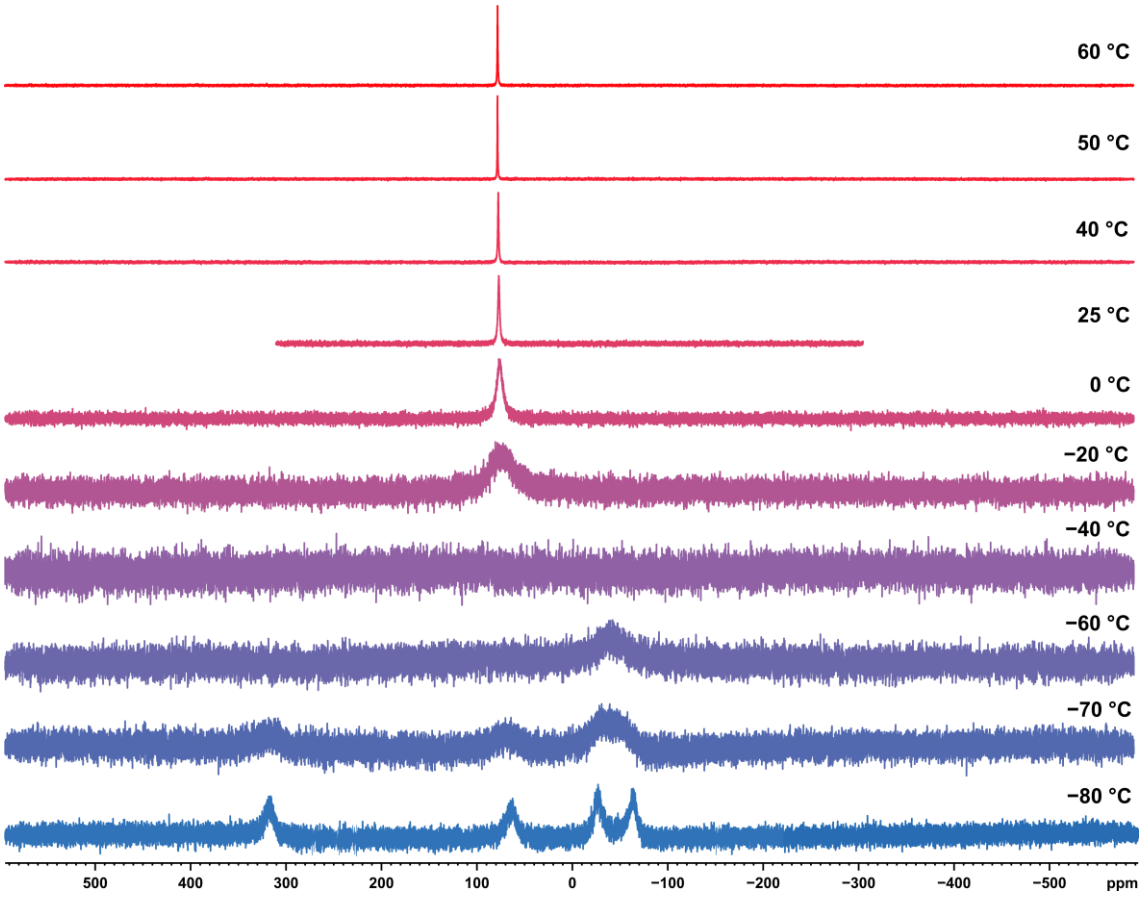

Figure 4. Variable temperature $^{31}P\{^{1}H\}$ NMR spectra of **4** in toluene-d_8.

5.3 Conclusion

The first mononuclear example of a germanium functionalized polyphosphido complex is accessible *via* insertion of $[Ar'Ge(\mu\text{-}Cl)]_2$ into the *cyclo*-P_3 ligand of **1**. The resulting anionic complex, **2**, features a puckered *cyclo*-$P_3GeAr'Cl$ ligand and can be isolated in high yield (65%). Upon employing *cyclo*-P_4 complex **3** as the reactant, salt metathesis was facilitated, yielding complex **4**, with a distinct $Co(\mu\text{-}\eta^4\text{:}\eta^3\text{-}P_4)GeAr'$ core. In solution, the Ar'Ge moiety exhibits circumambulatory behavior around the *catena*-P_4 unit at room temperature, while variable temperature $^{31}P\{^1H\}$ NMR spectroscopy revealed the chemical inequivalence of the phosphorus atoms at low temperature. The novel complexes **2** and **4** were characterized using single-crystal X-ray diffraction analysis and spectroscopic methods.

Overall, these findings highlight the potential of P_4-derived polyphosphido complexes for targeted functionalization with group 14 halides. In particular, P−Ge bond formation was achieved, resulting in mixed group 14/15 ligands. Ongoing investigation in this field plays a crucial role in enhancing our understanding of reactivity patterns and mechanisms, establishing the necessary groundwork for developing systems capable of achieving the release of the functionalized polyphosphido moiety, including mixed binary group 14/15 tetrahedranes, e.g. $Ar'GeP_3$.

5.4 Experimental Details

General Synthetic Methods

All reactions and product manipulations were carried out in flame-dried glassware under an inert atmosphere of argon using standard Schlenk-line or glovebox techniques (maintained at <0.1 ppm H_2O and <0.1 ppm O_2). S. Hauer prepared [K(18c-6)][(Ar*BIAN)Co(η^4-P_4)], as well as [K(18c-6)][(Ar*BIAN)Co(CN)(η^3-P_3)], according to procedures previously reported within this thesis (Chapter 2).[41] {[Ar'Ge(μ-Cl)]$_2$,[42] [Ar'Sn(μ-Cl)]$_2$[42] and [Ar'Pb(μ-Br)]$_2$[43] were prepared according to literature procedures. All other chemicals were purchased from commercial suppliers and used without further purification.

Solvents were dried and degassed with a Mbraun SPS800 solvent purification system. All dry solvents except *n*-hexane were stored under argon over activated 3 Å molecular sieves. *n*-Hexane was instead stored over a potassium mirror.

General Analytical Techniques

NMR spectra were recorded on Bruker Avance 400 spectrometers at 300 K and were internally referenced to residual solvent resonances (^{1}H NMR: C_6D_6: 7.15 ppm; ^{13}C{^{1}H} C_6D_6: 128.06 ppm). ^{31}P{^{1}H} spectra were referenced externally to 85% $H_3PO_{4(aq.)}$. Chemical shifts, δ, are given in ppm referring to external standards of tetramethylsilane (^{1}H, ^{13}C{^{1}H}). ^{1}H, ^{13}C and ^{31}P NMR signals were assigned based on 2D NMR spectra (COSY, HSQC, HMBC, NOESY and ROESY).

UV/Vis spectra were recorded on an Ocean Optics Flame Spectrometer with a DH-2000-BAL light source. Elemental analysis were performed by the Central Analytics Department of the University of Regensburg using a Vario micro cube. IR spectra were recorded with a Bruker ALPHA spectrometer equipped with a diamond ATR unit.

NMR Simulations

For compounds which give rise to a higher order spin system in the ^{31}P{^{1}H} NMR spectrum, the resolution enhanced ^{31}P{^{1}H} NMR spectrum was transferred to the software gNMR, version 5.0.6, by Cherwell Scientific.[44] The full line shape iteration procedure of gNMR was applied to obtain the best match of the fitted to the experimental spectrum. ^1J(^{31}P^{31}P) coupling constants were set to negative values and all other signs of the coupling constants were obtained accordingly.[45–50]

5.4.1 Synthesis of Compounds

[K(18c-6)][(Ar*BIAN)Co(CN)(η³-P₃GeAr'Cl)] (2):

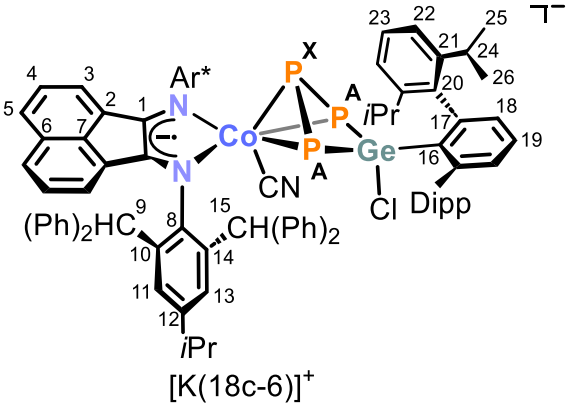

Solid [Ar'Ge(μ-Cl)]$_2$ (20.5 mg, 0.020 mmol, 0.66 equiv.) was added to a purple solution of [K(18c-6)][(Ar*BIAN)Co(CN)(η^3-P$_3$)] (50 mg, 0.031 mmol, 1.0 equiv.) in toluene (3 mL). The reaction mixture was stirred for four days. The color changed to dark purple during that period. The suspension was filtered, and the filtrate was concentrated to approximately 4 mL. Slow vapor diffusion of *n*-hexane into this solution for one day at room temperature and one week at −35 °C afforded dark purple crystals of **2** suitable for single-crystal X-ray diffraction. The crystals were isolated by filtration, washed with *n*-hexane (4 × 1 mL) and dried *in vacuo*. The crystalline solid contains 0.7 molecules of *n*-hexane and 0.5 molecules of toluene per molecule of compound after drying as indicated by the ^{1}H/^{13}C{^{1}H} NMR spectra and elemental analysis.

Yield: 41 mg (65%, based on **1**).

^{1}H NMR (400.13 MHz, 300 K, C_6D_6): δ/ppm = 1.19-1.24 (m, 24H, −CH(C*H*$_3$)$_2$ of *i*Pr overlapping with −CH(C$^{25/26}$*H*$_3$)$_2$), 1.59-1.66 (br m, 12H, −CH(C$^{25/26}$*H*$_3$)$_2$), 2.71 (sept, $^3J_{HH}$ = 6.9 Hz, 2H, −C*H*(CH$_3$)$_2$ of *i*Pr), 2.83 (s, 24H, 18c-6), 3.42 (br sept, 4H, −C^{24}*H*(CH$_3$)$_2$), 5.38 (s, 2H, −C^9*H*(Ph)$_2$), 5.72 (d, $^3J_{HH}$ = 6.9 Hz, 2H, C^3−*H* of BIAN), 6.19-6.23 (m, 2H, C^4−*H* of BIAN), 6.51-6.57 (m, 8H, C−*H*$_{Ar}$ of Ph overlapping with C−*H* of Ar'), 6.74-6.85 (m, 8H, C−*H*$_{Ar}$ of Ph overlapping with C−*H* of Ar'), 7.00-7.18 (m, 15H, C−*H*$_{Ar}$ of Ph overlapping with C−*H* of Ar' overlapping with C_6D_6 solvent signal), 7.24-7.43 (m, 16H, C−*H*$_{Ar}$ of Ph overlapping with C−*H* of Ar'), 7.87-8.04 (m, 8H, C−*H*$_{Ar}$ of Ph), 8.83 (s, 2H, −C^{15}*H*(Ph)$_2$).

^{13}C{^{1}H} NMR (100.61 MHz, 300 K, C_6D_6): δ/ppm = 24.8 (s, −CH(*C*H$_3$)$_2$ of *i*Pr), 24.8 (s, −CH(*C*$^{25/26}$H$_3$)$_2$), 25.3 (s, −CH(*C*$^{25/26}$H$_3$)$_2$), 31.9 (br s, −*C*^{24}H(CH$_3$)$_2$), 34.6 (s, −*C*H(CH$_3$)$_2$ of *i*Pr), 51.1 (s, −*C*^{15}H(Ph)$_2$), 51.7 (s, −*C*^{9}H(Ph)$_2$), 69.9 (s, 18c-6), 124.0 (s, *C*^{5}−H of BIAN), 125.9 (s), 126.2 (s), 126.3 (s), 126.3 (s), 126.5 (s), 127.0 (s), 127.1 (s), 129.9 (s), 130.4 (s, *C*^{6} of BIAN), 131.2 (s), 131.5 (s), 131.5 (s), 132.0 (s, *C*$_{Ar}$−H of Ph), 132.3 (s, *C*$_{Ar}$−H of Ph), 132.7 (s, *C*^{2} of BIAN), 134.5 (s), 134.6 (s), 140.0 (s), 141.4 (s), 144.5 (s), 145.6 (s), 145.8 (s), 146.1 (s), 146.1 (s), 147.3 (s), 149.2 (s, *C*^{8}−N), 165.5 (s, *C*^{1}=N of

BIAN); *C*≡N of coordinated cyanide not detected; not all signals could be assigned unambiguously.

$^{31}P\{^{1}H\}$ NMR (162.04 MHz, 300 K, C_6D_6): (A_2X) spin system δ/ppm = −30.6 (t, 1P, P_X), 160.6 (d, 2P, P_A); $^{1}J_{AX}$ = −294.8 Hz see also Figure S4 and Table S1.

UV/Vis (THF, λ_{max} / nm, ε_{max} / L·mol^{-1}·cm^{-1}): 320 (16000), 460sh (4000), 550 (7000), 710 (1000).

IR (solid state): ν/ cm^{-1} = 3057w (C−H), 3028w (C−H), 2954m (C−H), 2919m (C−H), 2861w (C−H), 2076m (C≡N), 1598w, 1532m, 1489s, 1435m, 1380m, 1354m, 1290m, 1251m, 1189m, 1110s, 1035m, 1004w, 952m, 890w, 842m, 818m, 744s, 700vs, 633m, 605m.

Elemental Analysis calcd. for $(C_{125}H_{129}ClCoGeKN_3O_6P_3)\cdot(n\text{-hexane})_{0.7}\cdot(\text{toluene})_{0.5}$ (Mw = 2068.41 g·mol^{-1}): C 73.29, H 6.62, N 1.93; found C 73.30, H 6.55, N 1.84; compare this with the calculated elemental analysis for: $(C_{125}H_{129}ICoGeKN_3O_6P_3)_{0.2}(C_{125}H_{129}ClCoGeKN_3O_6P_3)_{0.8}\cdot(n\text{-hexane})_{0.7}\cdot(\text{toluene})_{0.5}$ (Mw = 2193.14 g·mol^{-1}): C 72.67, H 6.56, N 1.95.

[(Ar*BIAN)Co(μ-η^4:η^3-P$_4$)GeAr')] (4):

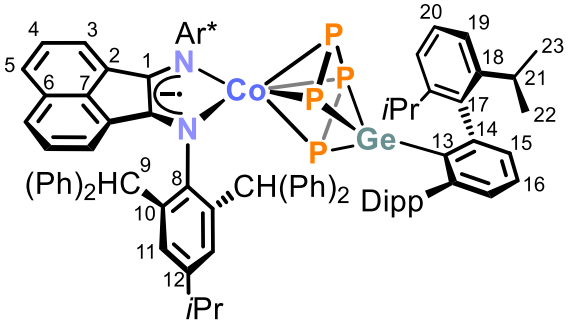

Solid [K(18c-6)][(Ar*BIAN)Co(η^4-P$_4$)] (50 mg, 0.032 mmol, 1.0 equiv.) and [Ar'Ge(μ-Cl)]$_2$ (21 mg, 0.021 mmol, 0.65 equiv.) were dissolved in toluene (3 mL). The resulting purple reaction mixture was stirred for one day while the color gradually changed to dark green. The suspension was filtered over a pad of silica (1 × 0.5 cm) and the solid residues were washed with toluene (4 × 1 mL). Volatiles were removed from combined filtrates *in vacuo*. The resulting dark solid was extracted with Et_2O (2 × 1 mL). Concentration by slow evaporation of the solvent over the course of three days afforded large, dark green crystals of **4**, which were isolated by decantation of the mother liquor and dried *in vacuo*. Slow evaporation of a saturated *n*-hexane solution containing **4** yielded crystals suitable for single-crystal X-ray diffraction.

Yield: 19 mg (35%).

^{1}H NMR (400.13 MHz, 300 K, C_6D_6) δ/ppm = 0.99 (d, $^{3}J_{HH}$ = 6.8 Hz, 12H −CH(C$^{22/23}H_3$)$_2$), 1.09 (d, $^{3}J_{HH}$ = 6.9 Hz, −CH(CH_3)$_2$ of *i*Pr), 1.41 (d, $^{3}J_{HH}$ = 6.8 Hz, 12H −CH(C$^{22/23}H_3$)$_2$), 2.50 (sept, $^{3}J_{HH}$ = 6.8 Hz, 4H, −C^{21}H(CH$_3$)$_2$), 2.65 (sept, $^{3}J_{HH}$ = 6.9 Hz,

2H, −C*H*$(CH_3)_2$ of *i*Pr), 5.51 (d, $^3J_{HH}$ = 7.1 Hz, 2H, C^3–*H* of BIAN), 6.17 (s, 4H, −C^9*H*$(Ph)_2$), 6.22-6.26 (m, 2H, C^4–*H* of BIAN), 6.53-6.62 (m, 8H, C−H_{Ar} of Ph), 6.82-6.90 (m, 3H, $C^{15/16}$–*H*), 6.96 (d, $^3J_{HH}$ = 8.2 Hz, 2H, C^5–*H* of BIAN), 7.01-7.03 (m, 8H, C−H_{Ar} of Ph), 7.14-7.17 (m, 6H, $C^{12/20}$–*H* overlapping with C_6D_6 solvent signal), 7.22-7.31 (m, 16H, C^{11}–*H* overlapping with C−H_{Ar} of Ph), 7.49-7.51 (m, C−H_{Ar} of Ph).

^{13}C{^{1}H} NMR (100.61 MHz, 300 K, C_6D_6) δ/ppm = 23.7 (s, −CH($C^{22/23}H_3)_2$), 24.6 (s, −CH($CH_3)_2$ of *i*Pr), 26.7 (s, −CH($C^{22/23}H_3)_2$), 31.9 (s, −C^{21}H$(CH_3)_2$), 34.4 (s, −C*H*$(CH_3)_2$ of *i*Pr), 52.4 (s, −C^9H$(Ph)_2$), 121.7 (s, C^3–H of BIAN), 124.1 (s, C^{19}–H), 125.4 (s, C^5–H of BIAN), 126.5 (s, C_{Ar}–H of Ph), 127.0 (s, C_{Ar}–H of Ph), 127.6 (s, C^4–H of BIAN), 128.9 (s, C^{11}–H overlapping with C_6D_6 solvent signal), 128.9 (s, C_{Ar}–H of Ph overlapping with C_6D_6 solvent signal), 129.1 (s, C_{Ar}–H of Ph), 129.7 (s, C^{16}–H), 130.2 (s, C^6 of BIAN), 130.3 (s, C^{20}–H), 130.9 (s, C_{Ar}–H of Ph), 131.5 (s, C_{Ar}–H of Ph), 132.0 (s, C^{15}–H), 132.2 (s, C^2 of BIAN), 136.4 (s, C^{17}), 137.5 (s, C^{10}), 138.3 (s, C^7 of BIAN), 140.3 (s, C^{13}), 143.7 (s, C_{Ar} of Ph), 145.9 (s, C^{12} overlapping with C^{14}), 147.1 (s, C_{Ar} of Ph), 147.3 (s, C^{18}), 154.4 (s, C^8–N), 156.0 (s, C^1=N of BIAN).

^{31}P{^{1}H} NMR (162.04 MHz, 300 K, C_6D_6): δ/ppm = 75.7 (br s, $\Delta\nu_{½}$ = 380 Hz); (161.98 MHz, toluene-d_8, 193 K): δ/ppm = −63.6 (br s, $\Delta\nu_{½}$ = 1500 Hz, 1 P), −26.9 (br s, $\Delta\nu_{½}$ = 1500 Hz, 1 P), 63.8 (br s, $\Delta\nu_{½}$ = 1800 Hz, 1 P), 137.1 (br s, $\Delta\nu_{½}$ = 1800 Hz, 1 P).

UV/Vis (THF, λ_{max} / nm, ε_{max} / L·mol^{-1}·cm^{-1}): 340sh (7000), 490 (4000), 630 (6000).

Elemental Analysis calcd. For ($C_{112}H_{105}CoGeN_2P_4$) (Mw = 1734.50 g·mol^{-1}):
C 77.56, H 6.10, N 1.62; found C 77.94, H 6.56, N 1.44.

5.4.2 NMR Spectra

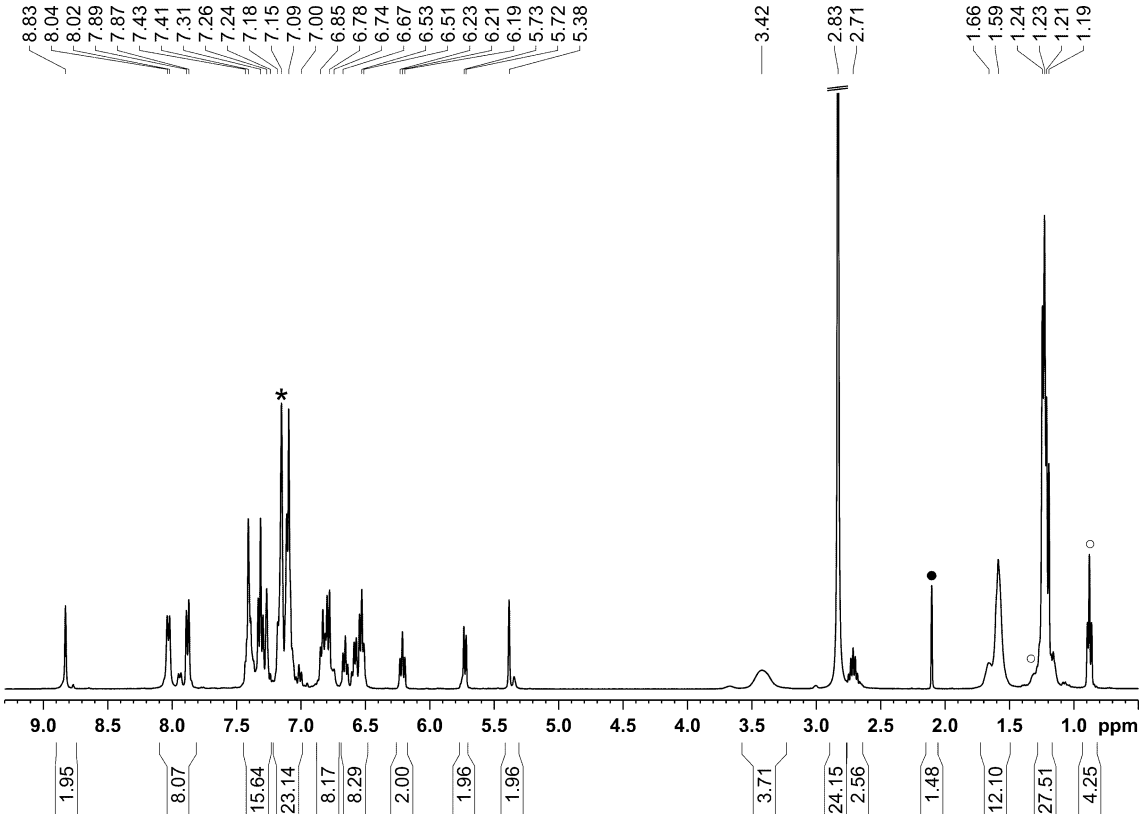

Figure S1. ^{1}H NMR spectrum (400.13 MHz, 300 K, C_6D_6,) of [K(18c-6)][(Ar*BIAN)Co(CN)(η^3-P_3GeAr'Cl)] (**2**); * C_6D_6.

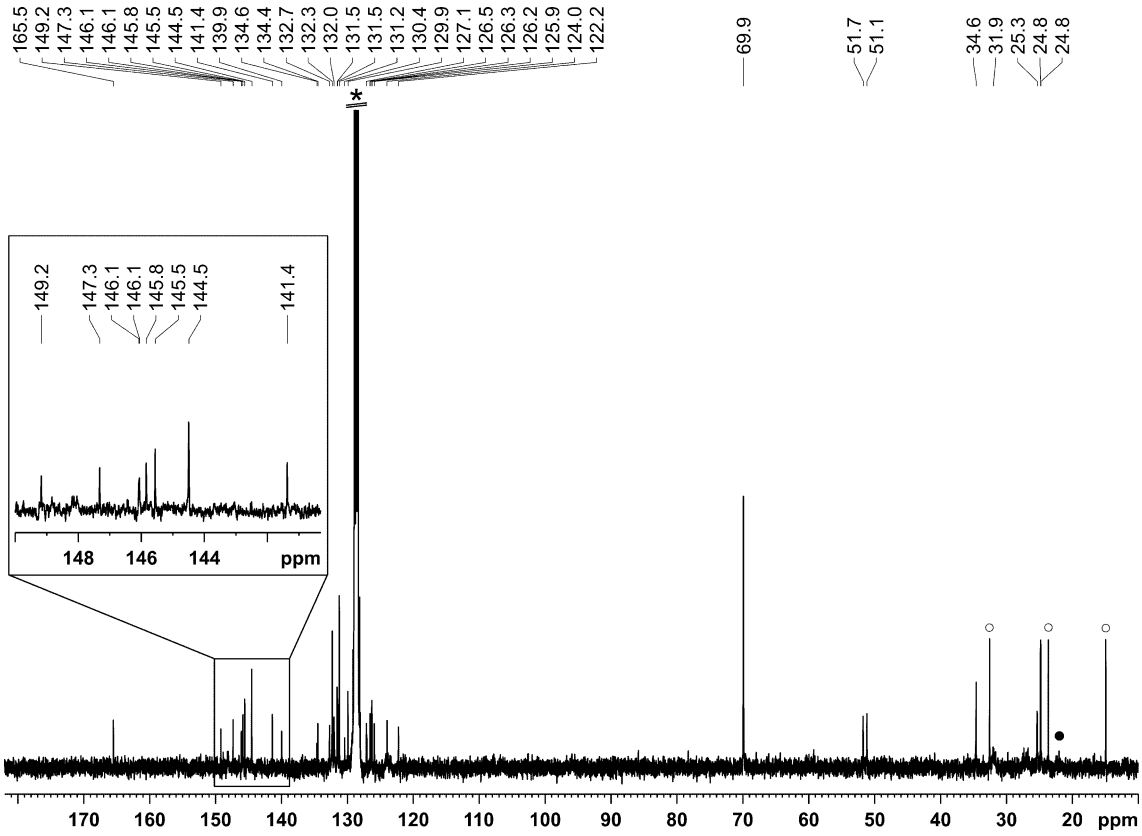

Figure S2. ^{13}C{^{1}H} NMR spectrum (100.66 MHz, 300 K, C_6D_6) of [K(18c-6)][(Ar*BIAN)Co(CN)(η^3-P_3GeAr'Cl)] (**2**); ○ *n*-hexane; • toluene; * C_6D_6.

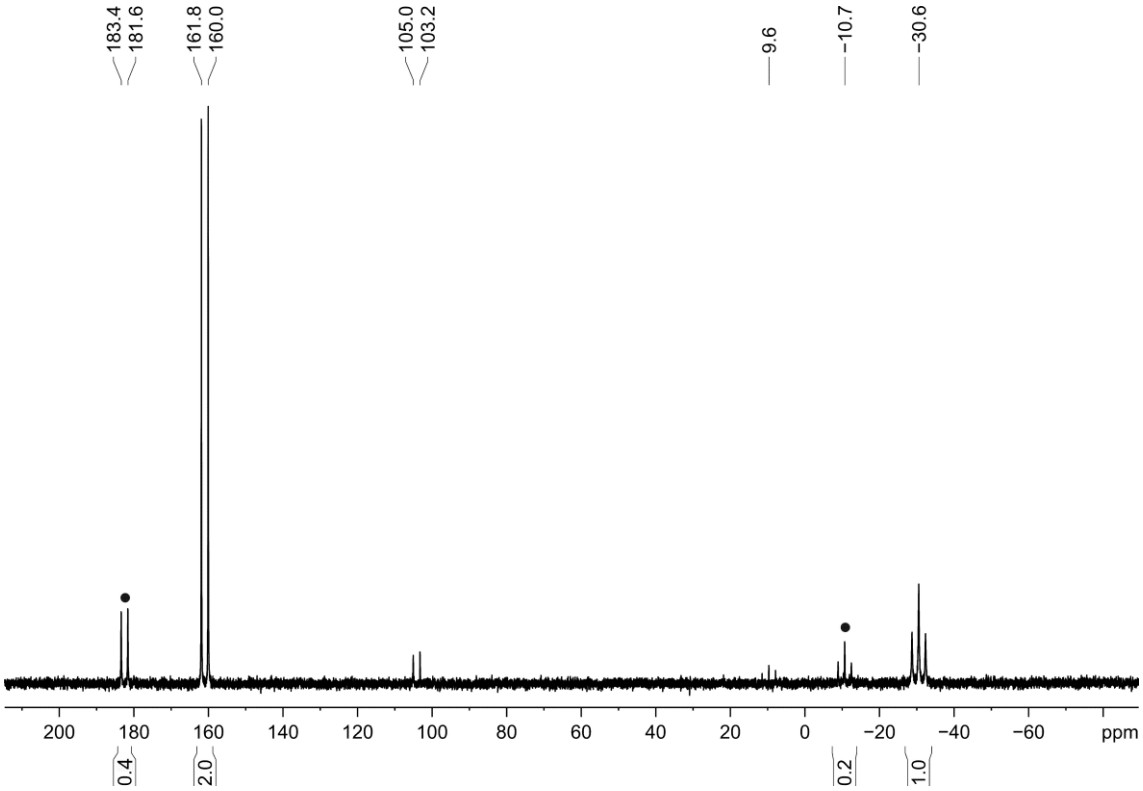

Figure S3. $^{31}P\{^{1}H\}$ NMR spectrum (162.04 MHz, 300 K, C_6D_6) of [K(18c-6)][(Ar*BIAN)Co(CN)(η^3-P_3GeAr'Cl)] (**2**); • unknown phosphorus containing compound attributed to an isomer of **2**, or the iodide-substituted derivative of **2**.

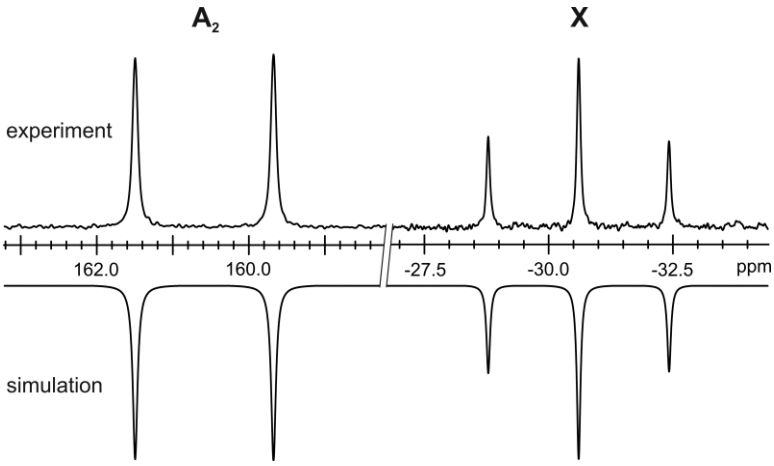

Figure S4. Section of the $^{31}P\{^{1}H\}$ NMR (162.04 MHz, 300 K, C_6D_6) spectra of [K(18c-6)][(Ar*BIAN)Co(CN)(η^3-P_3GeAr'Cl)] (**2**); experimental (upwards) and simulation (downwards).

Table S1. Chemical shifts and coupling constants from the iterative fit of the A_2X spin system and schematic representation of the CoP_3GeAr' core of [K(18c-6)][(Ar*BIAN)Co(CN)(η^3-P_3GeAr'Cl)] (**2**).

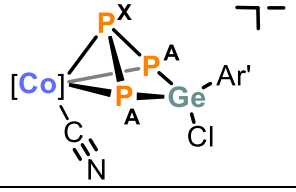	$\delta(A) = 160.6$ ppm	$^{1}J_{AX} = -294.8$ Hz
	$\delta(X) = -30.6$ ppm	

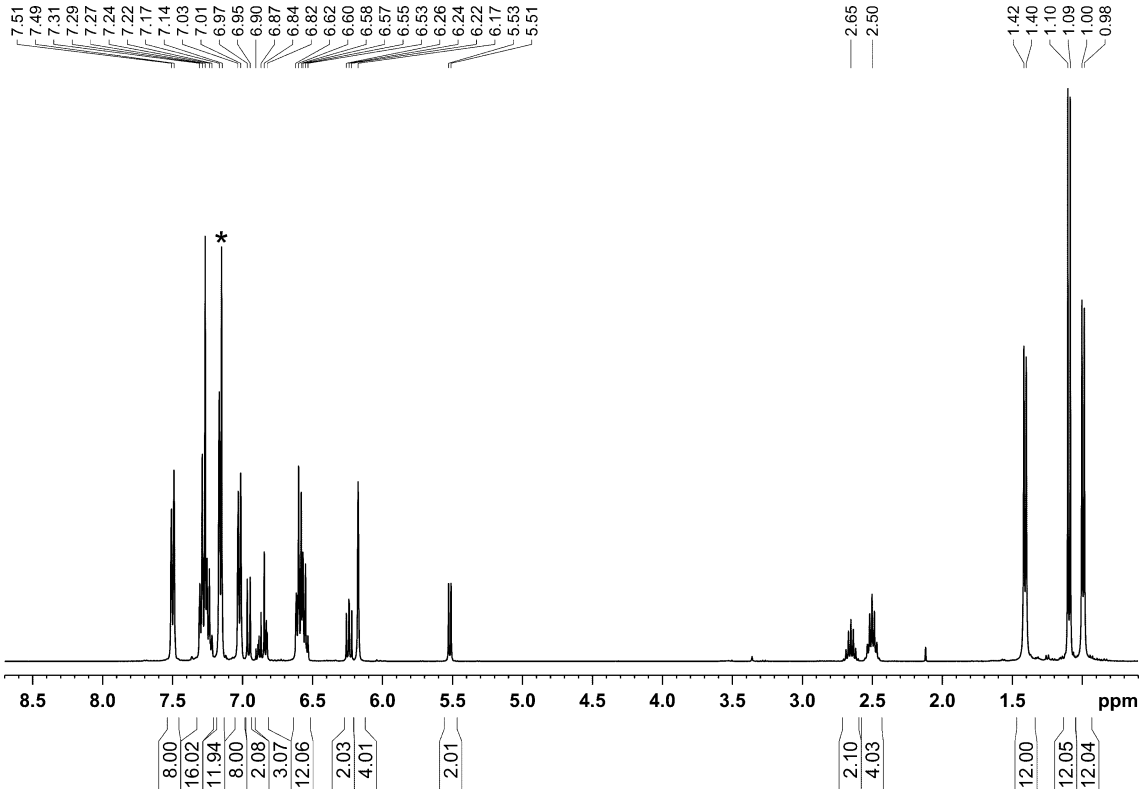

Figure S5. ^{1}H NMR spectrum (400.13 MHz, 300 K, C_6D_6,) of [(Ar*BIAN)Co(μ-η^4:η^3-P_4)GeAr')] (**4**); * C_6D_6.

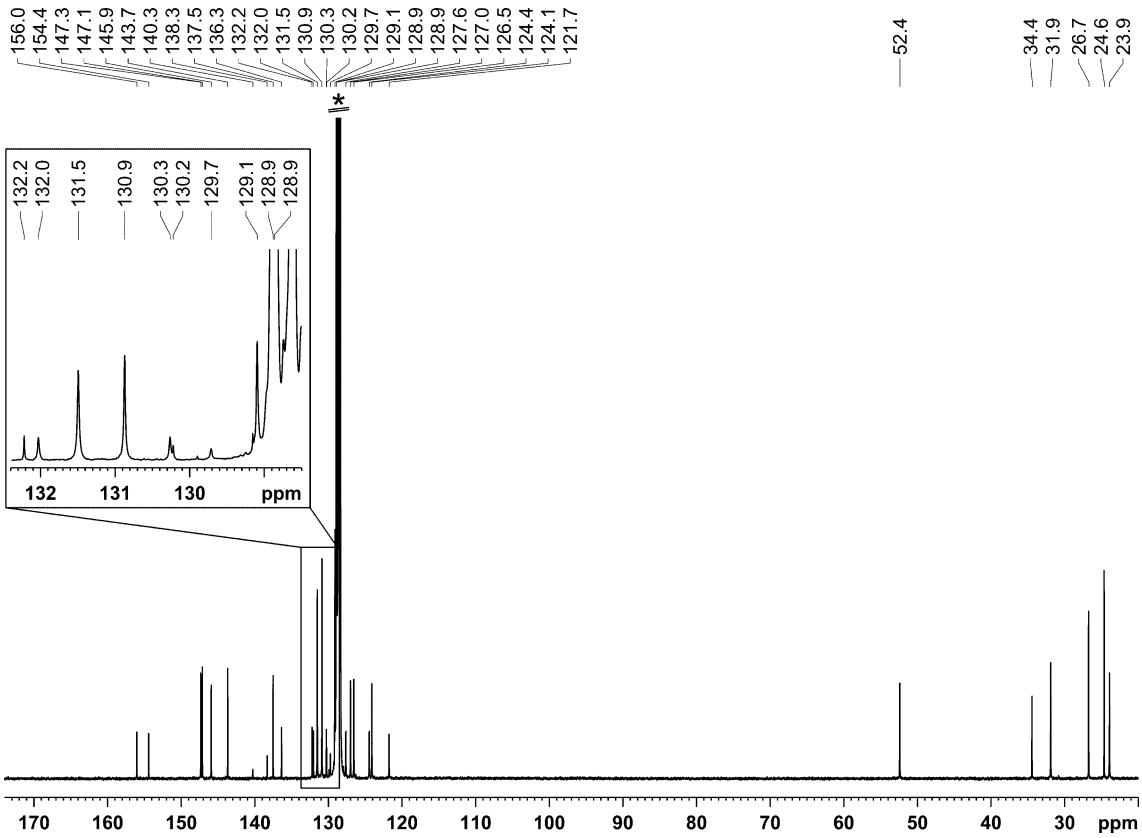

Figure S6. $^{13}C\{^{1}H\}$ NMR spectrum (100.61 MHz, 300 K, C_6D_6) of [(Ar*BIAN)Co(μ-η^4:η^3-P_4)GeAr')] (**4**); * C_6D_6.

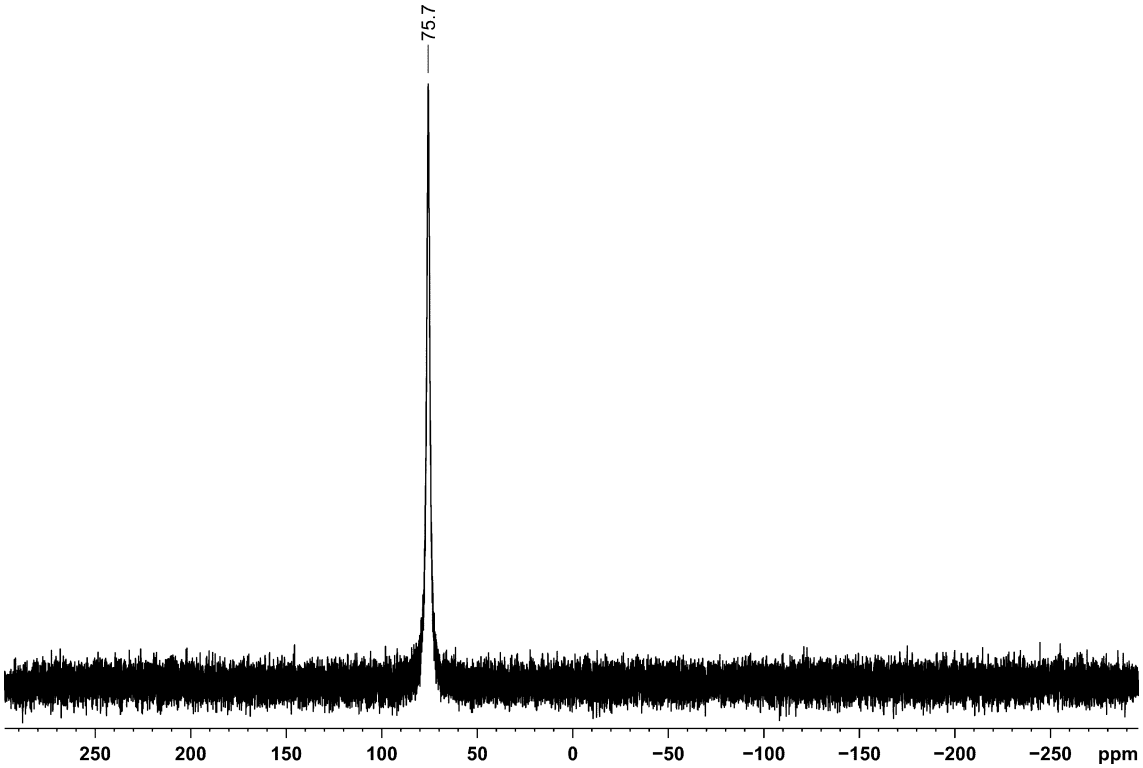

Figure S7. $^{31}P\{^{1}H\}$ NMR spectrum (162.04 MHz, 300 K, C_6D_6) of [(Ar*BIAN)Co(μ-η^4:η^3-P_4)GeAr')] (**4**).

5.4.3 Additional Experiments

Reactions of [K(18c-6)][(Ar*BIAN)Co(CN)(η^3-P_3)] (1) with [Ar'Sn(μ-Cl)]$_2$, or [Ar'Pb(μ-Br)]$_2$:

Solid [Ar'Sn(μ-Cl)]$_2$ (5.0 mg, 0.00453 mmol, 0.50 equiv.) was added to a purple solution of [K(18c-6)][(Ar*BIAN)Co(CN)(η^3-P_3)] (15 mg, 0.0092 mmol, 1.0 equiv.) in C_6D_6 (0.5 mL) and a $^{31}P\{^{1}H\}$ NMR was recorded (Figure S8, *vide infra*). The reaction between [Ar'Pb(μ-Br)]$_2$ (8.4 mg, 0.0061 mmol, 1.00 equiv.) and [K(18c-6)][(Ar*BIAN)Co(CN)(η^3-P_3)] (10 mg, 0.0092 mmol, 1.0 equiv.) was performed in an analogous fashion. The $^{31}P\{^{1}H\}$ NMR and ^{1}H NMR spectra of the reaction mixture revealed only unreacted starting material.

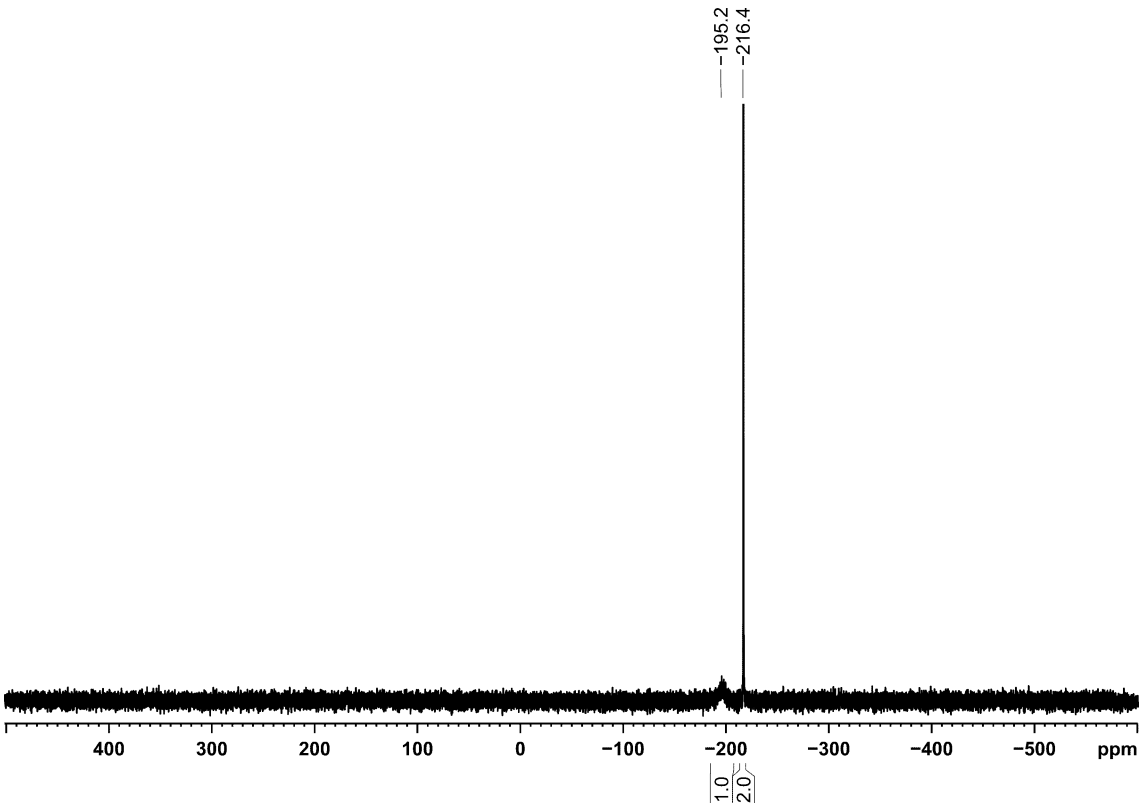

Figure S8. $^{31}P\{^{1}H\}$ NMR (162.04 Mz, 300 K, C_6D_6) of the reaction between [K(18c-6)][(Ar*BIAN)Co(CN)(η^3-P_3)] (**1**) and [Ar'Sn(μ-Cl)]$_2$.

Reaction of [K(18c-6)][(Ar*BIAN)Co(CN)(η^3-P_3GeAr'Cl)] (2) with NaBAr$^F_4$:

Solid [Ar'Ge(μ-Cl)]$_2$ (13.9 mg, 0.0137 mmol, 1.50 equiv.) was added to a purple solution of [K(18c-6)][(Ar*BIAN)Co(CN)(η^3-P_3)] (15 mg, 0.0092 mmol, 1.0 equiv.) in C_6D_6 (0.5 mL) to generate **2** *in situ*. NaBAr$^F_4$ (8.1 mg, 0.0092 mmol, 1.0 equiv.) was added and the reaction mixture was stirred for three days. Volatiles were removed *in vacuo*. The resulting dark solid was extracted with *n*-hexane (2 × 125 μL) and subsequently with Et_2O (2 × 200 μL). The extracts were filtered and concentrated to half of their original volume. After four days, dark blue crystals of [(Ar*BIAN)Co(CN)(η^3-P_3GeAr'Cl)] of sufficient quality for XRD analysis were obtained from the Et_2O fraction.

5.4.4 UV/Vis Spectra

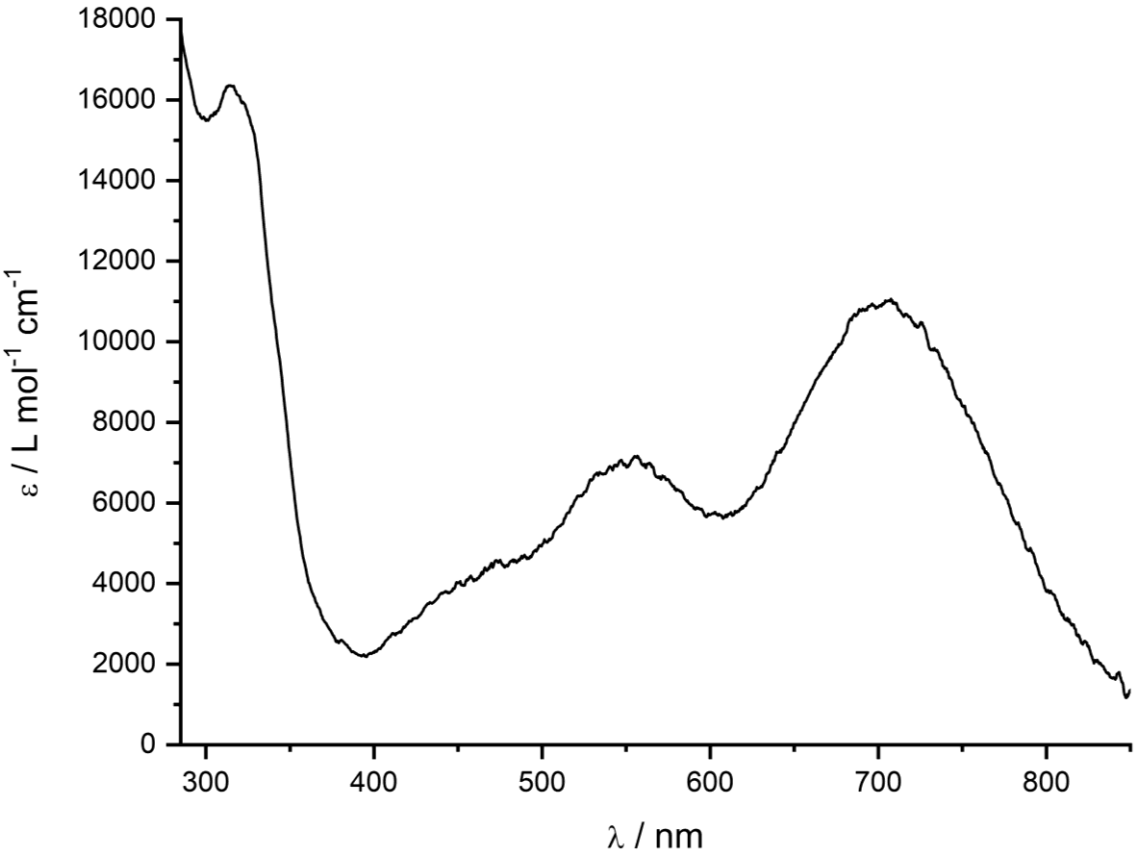

Figure S9. UV/Vis spectrum of [K(18c-6)][(Ar*BIAN)Co(CN)(η^3-P_3GeAr'Cl)] (**2**) recorded in THF.

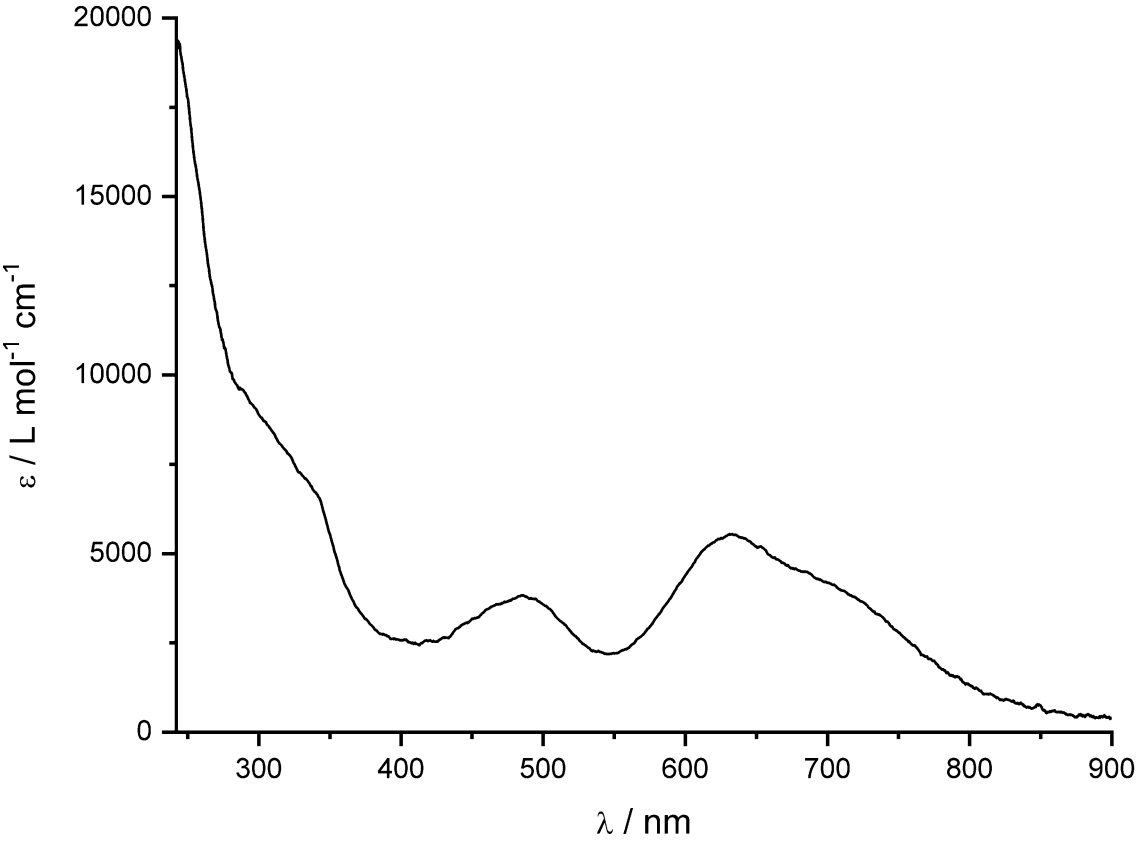

Figure S10. UV/Vis spectrum of [(Ar*BIAN)Co(μ-η^4:η^3-P_4)GeAr')] (**4**) recorded in THF.

5.4.5 IR Spectra

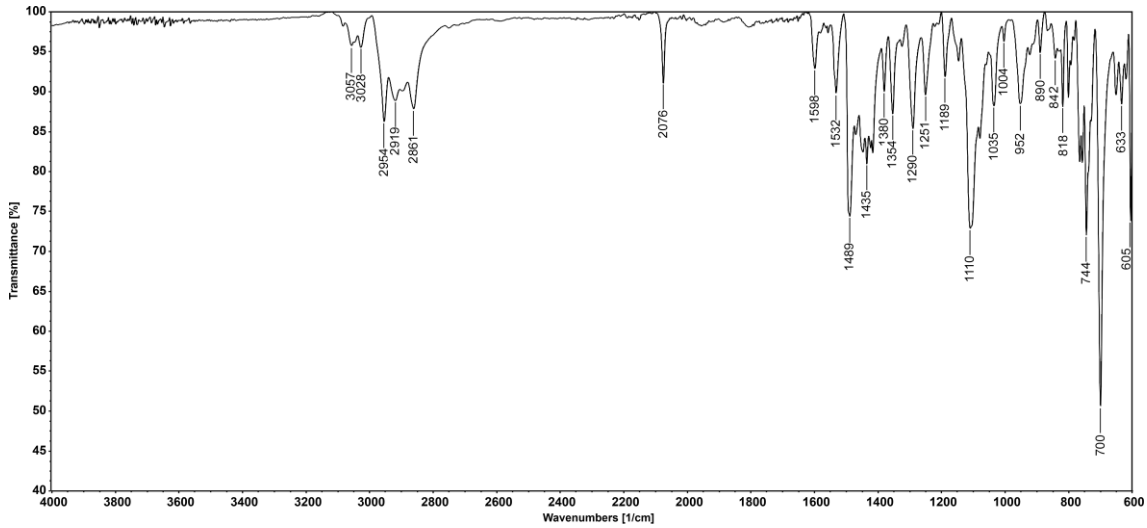

Figure S11. Solid state IR spectrum of [K(18c-6)][(Ar*BIAN)Co(CN)(η^3-P_3GeAr'Cl)] (**2**).

5.4.6 Single Crystal X-Ray Diffraction Data

Single-crystal X-ray diffraction data were recorded on Rigaku Oxford Diffraction XtaLAB Synergy R (DW system, Hypix-Arc 150) device with Cu-K_α radiation (λ = 1.54184 Å). Crystals were selected under mineral oil, mounted on micromount loops and quench-cooled using an Oxford Cryosystems open flow N_2 cooling device. Either semi-empirical multi-scan absorption corrections[51,52] or analytical ones[53] were applied to the data. The structures were solved with SHELXT[54] solution program using dual methods and by using Olex2 as the graphical interface.[55] The models were refined with ShelXL[56] using full matrix least squares minimization on F^2.[57] The hydrogen atoms were located in idealized positions and refined isotropically with a riding model.

[(Ar*BIAN)Co(CN)(η^3-P_3GeAr'Cl)] (**2**): The crystal contained two severely disordered Et_2O molecules per asymmetric unit, which were refined using the solvent mask command: A solvent mask was calculated and 330 electrons were found in a volume of 2816 $Å^3$ in one void per unit cell. This is consistent with the presence of 2 Et_2O molecules per Formula Unit which account for 336 electrons per unit cell.

The single crystal XRD data of **2** could only be refined satisfactorily, if the halogen substituent at Ge1 was refined using a split model as a Cl atom with a chemical occupancy of 0.8 and an I atom with the occupancy of 0.2 (Figure 2a). The origin of the iodine atom for this partial occupancy was attributed to the synthetic route, where the terphenyl iodide Ar'−I is utilized.[42] The insufficient purity of the starting material and thus the presence of residual iodide might have caused the observed halogen exchange. For the PHDI analogue of **2** no such halogen substitution was observed, and the corresponding Ge−Cl bond length is 2.239(4) Å.[26] This discrepancy strongly suggests that the observed, seemingly long Ge−Cl bond distance in **2** (2.4564(4) Å) can be attributed to the mixed chlorine/iodine position.

[(Ar*BIAN)Co(μ-η^4:η^3-P_4)GeAr')] (**4**)**:** The crystal of **4** contained 1.5 severely disordered *n*-hexane molecules per asymmetric unit. The *n*-hexane molecules were refined by using the solvent mask command: A solvent mask was calculated, and 666 electrons were found in a volume of 3320 $Å^3$ in one void per unit cell. This is consistent with the presence of 1.5 *n*-hexane per Formula Unit which account for 600 electrons per unit cell.

The following section provides figures of the molecular structures with selected bond lengths and angles, which were not given in section 5.2 itself.

Table S2. Crystallographic data and structure refinement for compounds **2**-**4**.

Compound	**2**	**[(Ar*BIAN)Co(CN)(η^3-P_3GeAr'Cl)]**	**4**
Empirical formula	$C_{132}H_{137}Cl_{0.77}CoGeI_{0.23}KN_3O_6P$	$C_{113}H_{105}ClCoGeN_3P_3$	$C_{121}H_{126}CoGeN_2P_4$
Formula weight	2181.22	1764.87	1863.63
Temperature/K	123(1)	123(1)	123(1)
Crystal system	monoclinic	monoclinic	tetragonal
Space group	$P2_1/c$	$P2_1/c$	I-4
a/Å	16.52889(4)	17.6442(3)	37.02870(10)
b/Å	19.96040(5)	18.8082(3)	37.02870(10)
c/Å	34.29681(10)	33.8758(4)	15.04040(10)
α/°	90	90	90
β/°	94.6780(3)	96.5420(10)	90
γ/°	90	90	90
Volume/Å^3	11277.62(5)	11168.7(3)	20622.26(18)
Z	4	4	8
ρ_{calc}g/cm^3	1.285	1.050	1.201
μ/mm^{-1}	3.318	2.443	2.576
F(000)	4585.0	3700.0	7880.0
Crystal size/mm^3	0.262 × 0.201 × 0.125	0.035 × 0.090 ×0.142	0.523 × 0.051 × 0.048
Diffractometer	XtaLAB Synergy R, DW system, HyPix-Arc 150	XtaLAB Synergy R, DW system, HyPix-Arc 150	XtaLAB Synergy R, DW system, HyPix-Arc 150
Radiation	CuKα (λ = 1.54184)	CuKα (λ = 1.54184)	CuKα (λ = 1.54184)
2Θ range for data collection/°	5.126 to 148.94	5.042 to 134.152	4.772 to 150.188
Index ranges	−19 ≤ h ≤ 20, −24 ≤ k ≤ 24, −42 ≤ l ≤ 42	−21 ≤ h ≤ 21, −22 ≤ k ≤ 22, −34 ≤ l ≤ 40	−46 ≤ h ≤ 45, −45 ≤ k ≤ 45, −18 ≤ l ≤ 17
Reflections collected	251730	253730	74548
Independent reflections	22884 [R_{int} = 0.0225, R_{sigma} = 0.0110]	19940 [R_{int} = 0.1515, R_{sigma} = 0.0564]	20178 [R_{int} = 0.0297, R_{sigma} = 0.0291]
Data/restraints/ parameters	22884/717/1521	19940/405/1194	20178/12/1093
Goodness-of-fit on F^2	1.011	1.100	1.065
Final R indexes [I>=2σ (I)]	R_1 = 0.0375, wR_2 = 0.1086	R_1 = 0.0855, wR_2 = 0.2588	R_1 = 0.0458, wR_2 = 0.1175
Final R indexes [all data]	R_1 = 0.0399, wR_2 = 0.1104	R_1 = 0.1003, wR_2 = 0.2761	R_1 = 0.0512, wR_2 = 0.1205
Largest diff. peak/hole / e Å^{-3}	1.01/−0.86	1.29/−0.74	0.54/−0.33
Flack parameter	/	/	−0.0263(15)

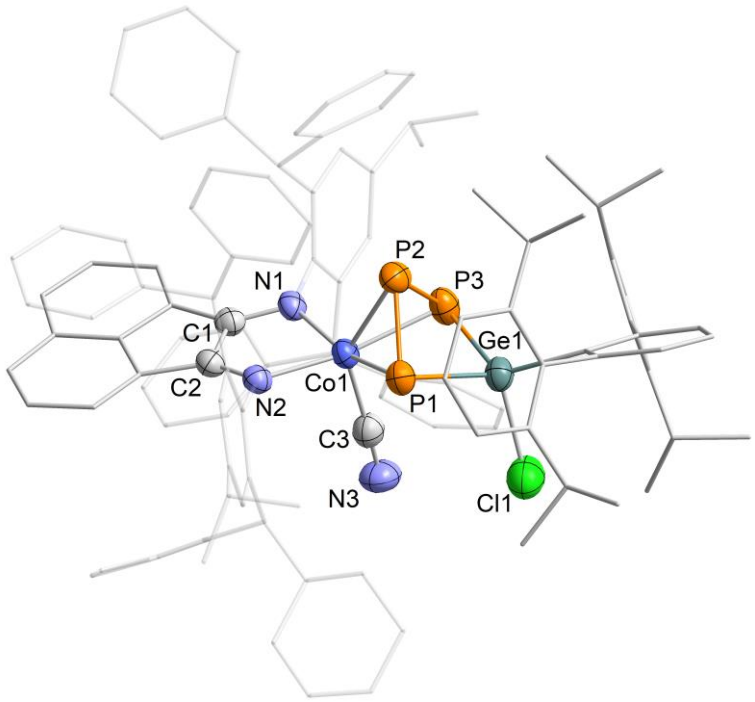

Figure S12. Solid-state structure of [(Ar*BIAN)Co(CN)(η^3-P_3GeAr'Cl)]; thermal ellipsoids are shown at the 50% probability level; hydrogen atoms, non coordinating solvent molecules and disorder in der Ar*BIAN ligand are omitted for clarity. Selected bond lengths [Å] and angles [°]: P1−P2 2.1771(2), P2−P3 2.1921(2), Ge1−P1 2.2987(1), Ge1−P3 2.3124(1), Ge1−Cl1 2.2791(2), Co1−P1 2.3461(1), Co1−P2 2.2641(1), Co1−P3 2.3201(1), Co1−C3 1.908(5), C3−N3 1.160(6), Co1−N1 1.995(3), Co1−N2 1.991(3), C1−N1 1.323(4), C2−N2 1.310(5), C1−C2 1.449(5), P1-P2-P3 89.85(6), P2-P3-Ge1 81.34(5), P3-Ge1-P1 84.00(4), P1-Ge1-Cl1 108.41(5), Co1-C3-N3 176.6(4), N1-Co1-N2 81.39(1), N1-C1-C2 115.8(3), Co1-N2-C2 113.0(3).

References

[1] G. Maier, *Angew. Chem. Int. Ed. Engl.* **1988**, *27*, 309–332.
[2] M. Peruzzini, L. Gonsalvi, A. Romerosa, *Chem. Soc. Rev.* **2005**, *34*, 1038–1047.
[3] B. M. Cossairt, N. A. Piro, C. C. Cummins, *Chem. Rev.* **2010**, *110*, 4164–4177.
[4] M. Scheer, G. Balázs, A. Seitz, *Chem. Rev.* **2010**, *110*, 4236–4256.
[5] M. Caporali, L. Gonsalvi, A. Rossin, M. Peruzzini, *Chem. Rev.* **2010**, *110*, 4178–4235.
[6] F. Scalambra, M. Peruzzini, A. Romerosa, in *Adv. Organomet. Chem.* (Ed.: P.J. Pérez), Academic Press, **2019**, pp. 173–222.
[7] C. M. Hoidn, D. J. Scott, R. Wolf, *Chem. – Eur. J.* **2021**, 1886–1902.
[8] L. Giusti, V. R. Landaeta, M. Vanni, J. A. Kelly, R. Wolf, M. Caporali, *Coord. Chem. Rev.* **2021**, *441*, 213927.
[9] B. M. Cossairt, M.-C. Diawara, C. C. Cummins, *Science* **2009**, *323*, 602–602.
[10] B. M. Cossairt, C. C. Cummins, *J. Am. Chem. Soc.* **2009**, *131*, 15501–15511.
[11] G. Hierlmeier, P. Coburger, M. Bodensteiner, R. Wolf, *Angew. Chem. Int. Ed.* **2019**, *58*, 16918–16922.
[12] M.-L. Y. Riu, R. L. Jones, W. J. Transue, P. Müller, C. C. Cummins, *Sci. Adv.* **2020**, *6*, eaaz3168.
[13] M.-L. Y. Riu, M. Ye, C. C. Cummins, *J. Am. Chem. Soc.* **2021**, *143*, 16354–16357.
[14] J. S. Figueroa, C. C. Cummins, *Angew. Chem. Int. Ed.* **2004**, *43*, 984–988.
[15] J. S. Figueroa, C. C. Cummins, *Angew. Chem. Int. Ed.* **2005**, *44*, 4592–4596.
[16] N. A. Piro, C. C. Cummins, *J. Am. Chem. Soc.* **2008**, *130*, 9524–9535.
[17] B. M. Cossairt, C. C. Cummins, *Angew. Chem. Int. Ed.* **2010**, *49*, 1595–1598.
[18] M. A. Alvarez, M. E. García, D. García-Vivó, A. Ramos, M. A. Ruiz, *Inorg. Chem.* **2011**, *50*, 2064–2066.
[19] M. A. Alvarez, M. E. García, D. García-Vivó, A. Ramos, M. A. Ruiz, *Inorg. Chem.* **2012**, *51*, 11061–11075.
[20] R. Yadav, T. Simler, S. Reichl, B. Goswami, C. Schoo, R. Köppe, M. Scheer, P. W. Roesky, *J. Am. Chem. Soc.* **2020**, *142*, 1190–1195.
[21] R. Yadav, B. Goswami, T. Simler, C. Schoo, S. Reichl, M. Scheer, P. W. Roesky, *Chem. Commun.* **2020**, *56*, 10207–10210.
[22] C. Riesinger, G. Balázs, M. Seidl, M. Scheer, *Chem. Sci.* **2021**, *12*, 13037–13044.
[23] M. Piesch, S. Reichl, M. Seidl, G. Balázs, M. Scheer, *Angew. Chem. Int. Ed.* **2021**, *60*, 15101–15108.
[24] X. Sun, A. Hinz, S. Schulz, L. Zimmermann, M. Scheer, P. W. Roesky, *Chem. Sci.* **2023**, *14*, 4769–4776.
[25] K. Trabitsch, *Reactivity Studies of an Anionic Cyclotriphosphido Cobalt Complex*, Masterarbeit, Universität Regensburg, **2020**.
[26] K. Trabitsch, *Unpublished Results*, Universität Regensburg, **2024**.
[27] P. Pyykkö, M. Atsumi, *Chem. – Eur. J.* **2009**, *15*, 186–197.
[28] P. Pyykkö, M. Atsumi, *Chem. – Eur. J.* **2009**, *15*, 12770–12779.
[29] G. Socrates, *Infrared and Raman Characteristic Group Frequencies: Tables and Charts*, Wiley, Chichester, **2004**.
[30] P. Rigo, A. Turco, *Coord. Chem. Rev.* **1974**, *13*, 133–172.
[31] *A Search of the Cambridge Crystal Structure Database (CCSD), Version 5.44, 04/2023, Revealed 120 Cobalt Complexes Bearing Only One Terminal Cyanide Ligand with a Mean Co−C Distance of 1.899 Å (Median 1.888 Å) and a Mean C≡N Distance of 1.137 Å (Median 1.144 Å)*, **2023**.
[32] M. M. Khusniyarov, K. Harms, O. Burghaus, J. Sundermeyer, *Eur. J. Inorg. Chem.* **2006**, *2006*, 2985–2996.

[33] T. Li, N. Arleth, M. T. Gamer, R. Köppe, T. Augenstein, F. Dielmann, M. Scheer, S. N. Konchenko, P. W. Roesky, *Inorg. Chem.* **2013**, *52*, 14231–14236.
[34] Y. Xiong, S. Yao, E. Bill, M. Driess, *Inorg. Chem.* **2009**, *48*, 7522–7524.
[35] C. G. P. Ziegler, T. M. Maier, S. Pelties, C. Taube, F. Hennersdorf, A. W. Ehlers, J. J. Weigand, R. Wolf, *Chem. Sci.* **2019**, *10*, 1302–1308.
[36] W. W. Seidel, O. T. Summerscales, B. O. Patrick, M. D. Fryzuk, *Angew. Chem. Int. Ed.* **2009**, *48*, 115–117.
[37] V. A. Miluykov, O. G. Sinyashin, P. Lönnecke, E. Hey-Hawkins, *Mendeleev Commun.* **2003**, *13*, 212–213.
[38] M. D. Walter, J. Grunenberg, P. S. White, *Chem. Sci.* **2011**, *2*, 2120–2130.
[39] O. J. Scherer, M. Swarowsky, H. Swarowsky, G. Wolmershäuser, *Angew. Chem. Int. Ed. Engl.* **1988**, *27*, 694–695.
[40] O. J. Scherer, T. Hilt, G. Wolmershäuser, *Organometallics* **1998**, *17*, 4110–4112.
[41] S. Hauer, T. M. H. Downie, G. Balázs, K. Schwedtmann, J. J. Weigand, R. Wolf, *Angew. Chem. Int. Ed.* **2023**, e202317170.
[42] L. Pu, A. D. Phillips, A. F. Richards, M. Stender, R. S. Simons, M. M. Olmstead, P. P. Power, *J. Am. Chem. Soc.* **2003**, *125*, 11626–11636.
[43] S. Hino, M. Olmstead, A. D. Phillips, R. J. Wright, P. P. Power, *Inorg. Chem.* **2004**, *43*, 7346–7352.
[44] P. H. M. Budzelaar, in IvorySoft: gNMR for Windows, NMR Simulation Program, **2006**.
[45] E. G. Finer, R. K. Harris, *Mol. Phys.* **1967**, *13*, 65–75.
[46] S. Aime, R. K. Harris, E. M. McVicker, M. Fild, *J. Chem. Soc. Dalton Trans.* **1976**, 2144–2153.
[47] J. P. Albrand, H. Faucher, D. Gagnaire, J. B. Robert, *Chem. Phys. Lett.* **1976**, *38*, 521–523.
[48] H. C. E. McFarlane, W. McFarlane, J. A. Nash, *J. Chem. Soc. Dalton Trans.* **1980**, 240–244.
[49] M. A. M. Forgeron, M. Gee, R. E. Wasylishen, *J. Phys. Chem. A* **2004**, *108*, 4895–4908.
[50] J. E. Del Bene, J. Elguero, I. Alkorta, *J. Phys. Chem. A* **2004**, *108*, 3662–3667.
[51] G. M. Sheldrick, SADABS, Bruker AXS, Madison, USA, **2007**.
[52] CrysAlisPro, Scale3 Abspack, Rigaku Oxford Diffraction, **2019**.
[53] R. C. Clark, J. S. Reid, *Acta Crystallogr. Sect. A* **1995**, *51*, 887–897.
[54] G. M. Sheldrick, *Acta Crystallogr. Sect. Found. Adv.* **2015**, *71*, 3–8.
[55] O. V. Dolomanov, L. J. Bourhis, R. J. Gildea, J. a. K. Howard, H. Puschmann, *J. Appl. Crystallogr.* **2009**, *42*, 339–341.
[56] G. M. Sheldrick, *Acta Crystallogr. Sect. C Struct. Chem.* **2015**, *71*, 3–8.
[57] G. M. Sheldrick, *Acta Crystallogr. A* **2008**, *64*, 112–122.

6 1,2,4-Diazamonophospholes and 1,2,3,4-Diazadiphospholes Derived from Diazoalkenes: Synthesis and Coordination Chemistry[a,b]

Abstract: Reactions of a novel 1,2,3-triazole-based diazoalkene with *tert*-butylphosphaalkyne and white phosphorus afford a rare 3*H*-1,2,4-diazamonophosphole **2** and a 1,2,3,4-diazadiphosphole **3**, respectively. Both phospholes are versatile ligands toward main group compounds (BPh_3, $AlEt_3$) and transition metal (Co, Ni, Ru, Rh W, Au) complexes. These compounds are characterized by multinuclear NMR studies, single crystal X-ray diffraction and further analytical methods. Their molecular structures show that **2** and **3** can adopt various coordination modes, such as coordination *via* N and P atoms as well as π-coordination. Additionally, C−C and C−N bond activation was observed with cobalt(0) and nickel(0) N-heterocyclic carbene complexes, demonstrating that the ligand framework itself is accessible for further reactivity with highly electron-rich first-row transition-metal centers.

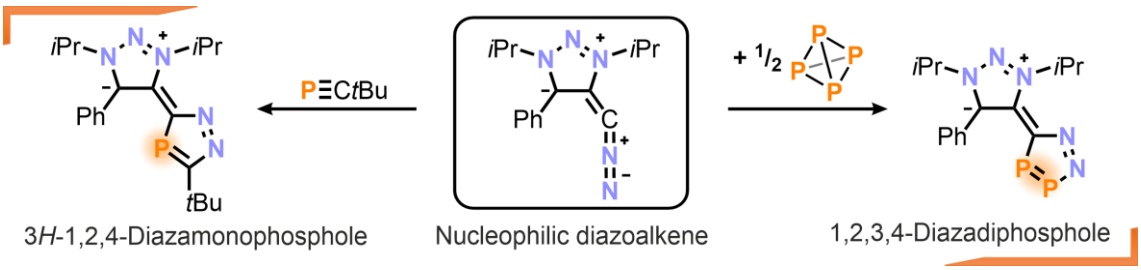

3*H*-1,2,4-Diazamonophosphole

[a] Reproduced from S. Hauer, J. Reitz, T. Koike, M. M. Hansmann, R. Wolf, *Angew. Chem. Int. Ed.* **2024**, e202410107.

[b] S. Hauer performed the synthetic investigations and the characterization of the reported compounds. J. Reitz synthesized the diazoalkene **1**. T. Kaiki carried out the DFT calculations. S. Hauer wrote the chapter, which was reviewed and edited by R. Wolf and M. M. Hansmann. R. Wolf and M. M. Hansmann supervised the project.

6.1 Introduction

(Hetero-)phospholes have found a broad variety of applications ranging from ligands in metal complexes, as polymers in materials science, and are of fundamental importance in theoretical and experimental research.[1–10] 1*H*-1,2,4-diazamonophospholes constitute a well-investigated and thus important subclass, of which selected examples **A** and **B** are shown in Figure 1a.[11–15] They can be seen as hybrids of phospholes and pyrazoles, exhibiting characteristic properties of both: hard nitrogen and soft phosphorus donor atoms, which makes them promising ligands with varying coordination modes.[16,17] Almost four decades ago, the groups of Märkl, Regitz and Schmidpeter almost simultaneously reported different methods for the synthesis of 1*H*-1,2,4-diazaphospholes, including cyclocondensation, [3+2]-cycloaddition, and O/P-exchange reactions.[18–27] More recently, Zheng and co-workers reported an improved condensation protocol, and the group of Grützmacher reported the reaction of a $NaPH_2/(NaO\mathit{t}Bu)_x$ mixture toward chlorinated diazabutadiene to give functionalized neutral and anionic 1*H*-1,2,4- and 1,3,4-azadiphospholes.[28,29]

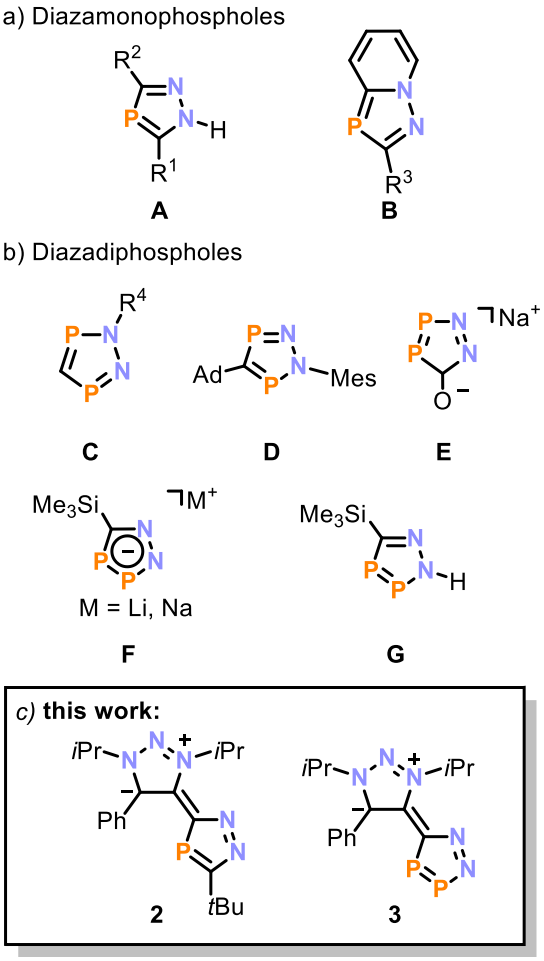

Figure 1. Selected examples for 1*H*-1,2,4-diazamonophospholes (**A**, **B**) and all reported examples of 1,2,3,5- (**C**, **D**), 1,2,3,4-diazadiphospholes and -phospholides (**E**, **F**, **G**); R^1 = H, Me, CO_2Me; R^2 = *i*Pr, *t*Bu, $CH_2\mathit{t}Bu$; R^3 = Me, *i*Pr, *t*Bu, Ph; R^4 = Me, Ph.

Very recently the synthesis of related 1,3-azaphospholes through a [3+2]-cycloaddition between 1,3-dipolar triflatophosphanes and alkynes has been reported by Weigand and co-workers.[30]

Considering only the relative positions of the three heteroatoms in diazamonophospholes, six regioisomers are feasible and all of them have been synthesized.[14] However, the 3*H*-1,2,4-diazamonophospholes, which feature no substituent at the nitrogen atom, remain elusive. It has been suggested that this isomer is formed initially during cycloadditions of phosphaalkynes and diazoalkanes. However, a rapid [1,5]-shift results in aromatization and the formation of 1*H*-1,2,4-diazaphospholes.[21,24,31]

Crucially, related diazadiphospholes have only been explored to a limited extent.[32] Examples of only two out of six possible regioisomers have been reported, namely the 1,2,3,5- and 1,2,3,4-diazadiphospholes (**C**-**G**, Figure 1b).[32–35] Selected examples of their corresponding 1,2,3,4-phospholides were included in a computational study.[36] The synthesis of **C** was reported by Schmidpeter, *via* the dehydrohalogenation of $CH_2(PCl_2)_2$ with substituted hydrazines.[33] More recently, Cummins and co-workers utilized the diazene $MesN_2PA$ (Mes = 2,4,6-$Me_3C_6H_2$; A = anthracene) as a phosphorus transfer reagent in reactions with OCP^- and AdCP (Ad = 1-adamantyl) for the preparation of **D** and **E**.[35] Furthermore, in a report that is highly relevant to the present work, Mathey and co-workers demonstrated that the diazomethyl anion reacts with white phosphorus (P_4) to afford diazadiphospholide Li[**F**].[34] However, this species was not structurally characterized, and its subsequent chemistry has remained rather limited. Protonation of this lithium salt with HOTf resulted in the protonated phosphole **G**. Subsequent deprotonation with NaH gave the sodium salt of Na[**F**]. These pioneering works have demonstrated the accessibility of certain diazadiphospholes and phospholides. However, the reported synthetic procedures often suffer from poor yield, or the compounds exhibit thermal instability, limiting investigations into their reactivity.[32–35]

Recently, Hansmann and co-workers reported the synthesis and characterization of room-temperature stable, though highly reactive diazoalkenes.[37–39] Reactions with main group compounds CS_2, CO and isocyanide show their potential for the synthesis of unique organic compounds. This chapter reports the preparation of 3*H*-1,2,4-diazamono- and 1,2,3,4-diazadiphospholes by cycloadditions of *t*BuCP and P_4 with a new nucleophilic diazoalkene, which represents one of the strongest carbon nucleophiles known to date.[40] Their electronic structures have been elucidated by quantum chemical calculations and

their coordination behavior toward a variety of main group and transition metal salts and complexes has been investigated.

6.2 Results and Discussion

This study utilizes the highly nucleophilic diazoalkene **1** prepared by Justus Reitz in the group of Prof. M. M. Hansmann at TU Dortmund.[37,38,41] Inspired by the known propensity of phosphaalkynes to undergo [2+3] cycloaddition reactions, **1** was treated with one equivalent of *t*BuCP in THF (Scheme 1a).[11–15] The reaction was monitored by $^{31}P\{^{1}H\}$ and NMR spectroscopy, confirming the quantitative conversion into a single new phosphorus species **2**.

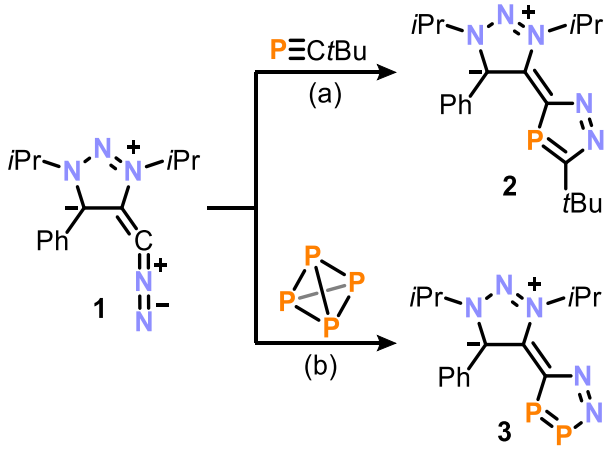

Scheme 1. [3+2] Cycloaddition reactions of the nucleophilic diazoalkene **1** with PC*t*Bu and P_4 affording 3*H*-1,2,4-diazamonophosphole **2** and 1,2,3,4-diazadiphosphole **3**; reagents/by-products and conditions: a) +1.0 eq. PC*t*Bu; THF, r.t., 6 h; b) +0.5 eq. P_4, THF, r.t., 5 h; yields: **2**: 70%, **3**: 54%.

Compound **2** crystallized as light yellow needles in an isolated yield of 70%, providing an accessible precursor for subsequent investigations of reactivity. Analysis of these crystals by X-ray diffraction (XRD) revealed the formation of 3*H*-1,2,4-diazamonophosphole **2**, featuring a nearly planar C_2N_2P (diazamonophosphole) unit connected *via* a C−C bond to a C_2N_3 (triazaphosphole) backbone (Figure 2 left). Both units are nearly coplanar, with a torsion angle of 17°. The P−C bond lengths in **2** are very similar (P1−C3 1.759(6) Å and P1−C4 (1.754(2) Å) and lie between typical P−C single and P=C double bond lengths ($\sum r_{PC}$ 1.86 Å vs. 1.69 Å), indicating significant π-delocalization.[42,43] Similar structural features have been reported for the related class of 1*H*-1,2,4-diazaphospholes.[13,31] In comparison to the precursor diazoalkene **1**, the C2−C3 bond bridging the two heterocycles is elongated (**1**: 1.407(1) Å vs. **2**: 1.455(9) Å). This indicates a higher single bond character in **2**, which is also reflected in the calculated Wiberg Bond Index (WBI) of 1.12 for **2**.

The $^{31}P\{^{1}H\}$ NMR spectrum of **2** features a sharp singlet at δ = 79.6 ppm, which falls within the more upfield range of typical values reported for related 1*H*-derivatives of 1,2,4-diazaphospholes (δ = 65−178 ppm).[44] In the ^{1}H NMR spectrum of **2** the expected signals were observed. This class of heterocycle was postulated decades ago as intermediates in cycloaddition reactions between phosphaalkynes and diazomethanes, but eluded isolation.[21,24,31] The reaction mechanism most likely represents a [3+2] cycloaddition reaction, selectively forming only one of the two possible regioisomers.[45,46]

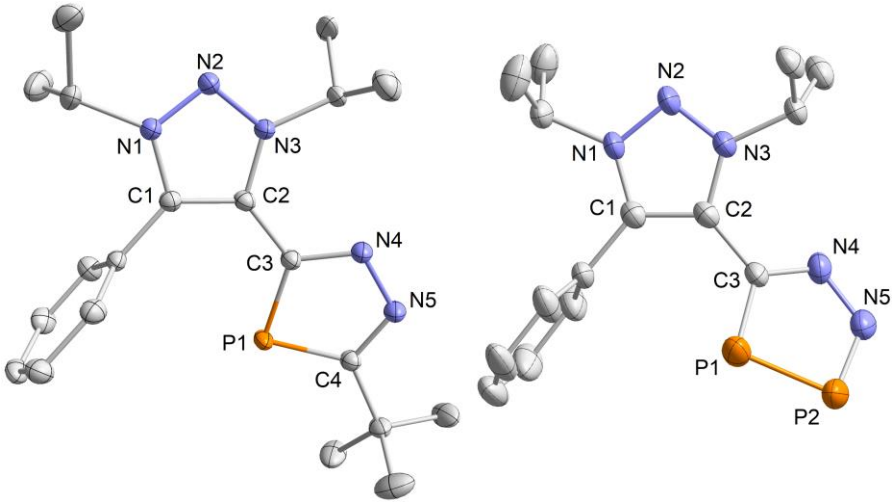

Figure 2. Solid-state molecular structures of **2** (left) and **3** (right). Hydrogen atoms and disorder are omitted for clarity and thermal ellipsoids are drawn at the 50% probability level. Selected bond lengths [Å] and angles [°]: **2**: P1−C4 1.7542(1), P1−C3 1.7596(1), C4−N5 1.3393(1), N4−N5 1.3495(1), N4−C3 1.3478(1), C2−C3 1.4559(2), C1−C2 1.3879(2), N1−N2 1.3207(1), N2−N3 1.3301(1), C3 P1 C4 84.97(5), P1 C4 N5 115.01(8); **3**: P1−P2 2.0877(1), P2−N5 1.669(4), P1−C3 1.752(4), N4−N5 1.336(4), N4−C3 1.347(5), C2−C3 1.466(5), C1−C2 1.383(5), C1−N1 1.339(5), N1−N2 1.340(4), N2−N3 1.329(4), C3 P1 P2 88.58(1), P1 P2 N5 97.64(1), P2 N5 N4 117.2(3).

Having established the ability of the diazoalkene to act as precursor for new heterocycles, **1** was reacted with 0.5 equiv. of white phosphorus, yielding the 1,2,3,4-diazadiphosphole **3** (Scheme 1b). Compound **3** was isolated as an orange solid in 54% yield, and represents a rare example of a 5*H*-1,2,3,4-diazadiphosphole.[34,35]

Crystals of **3** suitable for single crystal X-ray diffraction (SCXRD) were grown from a MeCN/*n*-hexane mixture. The solid-state structure of **3** is shown in Figure 2 and reveals a CN_2P_2 diazadiphosphole linked to the triazolium moiety through a C−C bond. In contrast to coplanar **2**, the CN_2P_2 group in **3** is tilted at an angle of 43° with respect to the triazolium heterocycle. The P1−P2 bond length of 2.087(7) Å is between those reported for anionic **F** (2.102(8) Å) and protonated **G** (2.070(6) Å) diazadiphospholes.[34,35] This indicates a fairly localized P=P double bond, which is consistent with DFT calculations and the calculated WBI of 1.46.

The reaction most likely necessitates an initial nucleophilic attack of the diazoalkane carbon atom on P_4, yielding a **1**-P_4 adduct. This adduct is subject to a second nucleophilic attack and thus two molecules of **1** are thus involved at the point of the breakdown of the tetrahedron. The reaction can be described as a formal [3+2] cycloaddition reaction, where P_4 reacts as a convenient source of [P≡P].

The $^{31}P\{^{1}H\}$ NMR spectrum of isolated **3** features two doublets at δ = 364.2 ppm (P2) and δ = 217.5 ppm (P1) with a large coupling constant of $^{1}J_{PP}$ = 444 Hz), characteristic of 1,2,3,4-diazadiphospholes.[32–35] These resonances are in good agreement with those reported for anionic **F** (δ = 353 and 231 ppm), suggesting a high contribution for a resonance structure of **2**, with a negative charge residing within the phosphole ring.[34] In comparison, the signal observed for the carbon-bound phosphorus atom P1 at δ = 217.5 ppm is significantly shifted downfield compared to related anionic Na[**E**] (δ = 97 ppm), where the negative charge is mainly localized on the exocyclic oxygen atom.[34,35]

To get a deeper insight into the electronic structures, **2** and **3** were both studied computationally (Figure 3), revealing a high contribution of the diazamonophosphole and diazadiphosphole units to the HOMO in both cases, explaining the observed coordination behavior (*vide infra*). Moreover, the HOMO and HOMO-1 feature a similar energy in both cases, suggesting comparable reactivity. However, the HOMO-LUMO gap is slightly higher for the diphosphole **3** (5.78 vs. 5.63 eV), indicating increased stability.

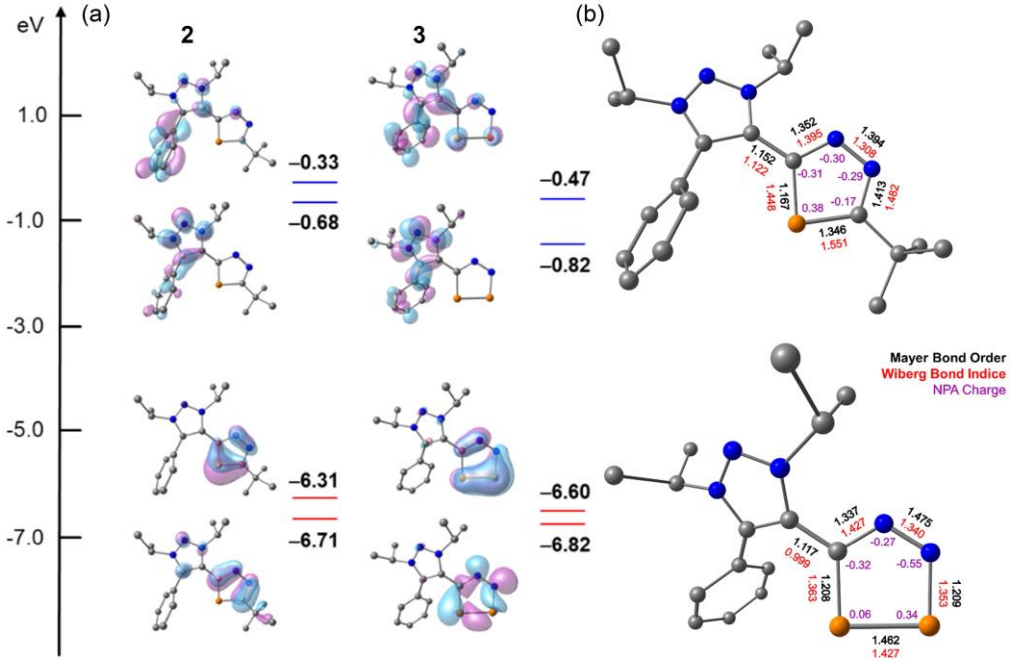

Figure 3. (a) Kohn-Sham HOMO-1 to LUMO+1 of **2** and **3** calculated at the M06-2X/def2-TZVP [P, N,C] & def2-SVP [H]//B3PW91-D3(BJ)/def2-TZVP level of theory (isosurface value: 0.05); (b) NPA charge, Mayer bond order (MBO) and Wiberg bond indice (WBI) of **2** (top) and (**3**) (bottom).

While the LUMO is centered on the 1,2,3-triazole framework in both cases, the LUMO+1 in diphosphole **3** is centered on the CN_2P_2 ring, in contrast to monophosphole **2**. It is noteworthy that a theoretical study on various azaphospholes, including the parent 1*H*-1,2,4-diazaphosphole and 1*H*-1,2,3,4-diazadiphosphole alongside the corresponding anions, has been reported in the literature, revealing similar optimized geometries.[36]

To gain insight into the donor capabilities of **2** and **3**, their reactions with first-row transition metals and main group Lewis acids were studied. Complexes of 1*H*-1,2,4-diazadiphospholes with metal carbonyls of Cr, Mo and W have been reported.[47,48] In these compounds, the diazadiphosphole ligands exhibit a variety of different binding modes. Thus, **2** was initially treated with varying equivalents of $[W(CO)_5(thf)]$, ranging from a 1:1 up to a 1:3 stoichiometry (Scheme 2).

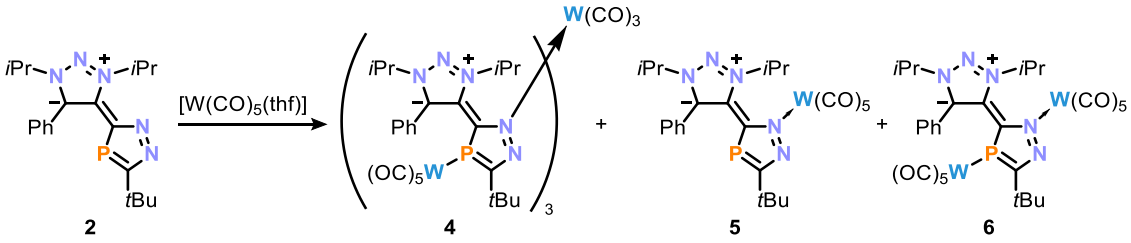

Scheme 2. Reaction of monophosphole **2** toward $[W(CO)_5(thf)]$ affording complexes **4**-**6**; reagents and conditions: + 1.0 up to 3.0 eq. $[W(CO)_5(thf)]$; THF, r.t., 1 d; yields: **4** and **5**: not isolated, **6**: 80%.

After crystallization, a total of three complexes were identified by SCXRD, namely $[W(CO)_3\{W(CO)_5(\mathbf{2})\}_3]$ (**4**), $[W(CO)_5(\mathbf{2})]$ (**5**) and $[\{W(CO)_5\}_2(\mathbf{2})]$ (**6**) (Figure S61−63, see Supporting Information (SI)). In these complexes, **2** coordinates either *via* the nitrogen only in **5** or *via* both the N and P atoms, thereby acting as a bridging ligand in the multinuclear complexes **4** and **6**. Compounds **4**-**6** are always formed as a mixture in reactions with 1.0 to 1.3 equivalents of $[W(CO)_5(thf)]$ and crystallize as such from saturated solutions of THF. However, from a targeted synthesis, using an excess of $[W(CO)_5(thf)]$ to saturate the coordination sphere of **2**, complex **6** was isolated in a good yield of 80%.

In the $^{31}P\{^1H\}$ NMR spectrum, **6** gives rise to a sharp singlet at δ = 52.3 ppm with characteristic tungsten satellites and a coupling constant of $^1J_{PW}$ = 234 Hz. In the IR spectrum, **6** exhibits a total of six intense bands in the region of $\tilde{\nu}_{CO}$ = 1855 to 2068 cm^{-1}, corresponding to the two $W(CO)_5$ fragments.[49] As highlighted by the tungsten complexes **4**-**6**, the ligand **2** is capable of adopting different coordination modes, making it a promising candidate for use in coordination chemistry.

In this study, the aim was to study the donor strengths and various accessible coordination modes for diazamonophosphole **2** toward various Lewis acids. Pleasingly,

in agreement with the calculated charges and frontier molecular orbitals (Figure 3), the inner and "harder" nitrogen atom coordinates to the Lewis acids $[Rh(cod)Cl]_2$ (cod = 1,5-cyclooctadiene) and $AlEt_3$ (Scheme 3a). The resulting products, [Rh(**2**)(cod)Cl] (**7**) and [$AlEt_3$(**2**)] (**8**), were isolated in good yields of 81% and 55%, respectively.

SCXRD analysis of both compounds revealed that the C_2N_2P unit is no longer coplanar with the 1,2,3-triazolium ring, exhibiting twist angles of 56° and 74° in **7** and **8**, respectively (Figure 4, top). This observed twist can be attributed to the steric demand of the metal centres and, interestingly, is in opposite directions in both complexes.

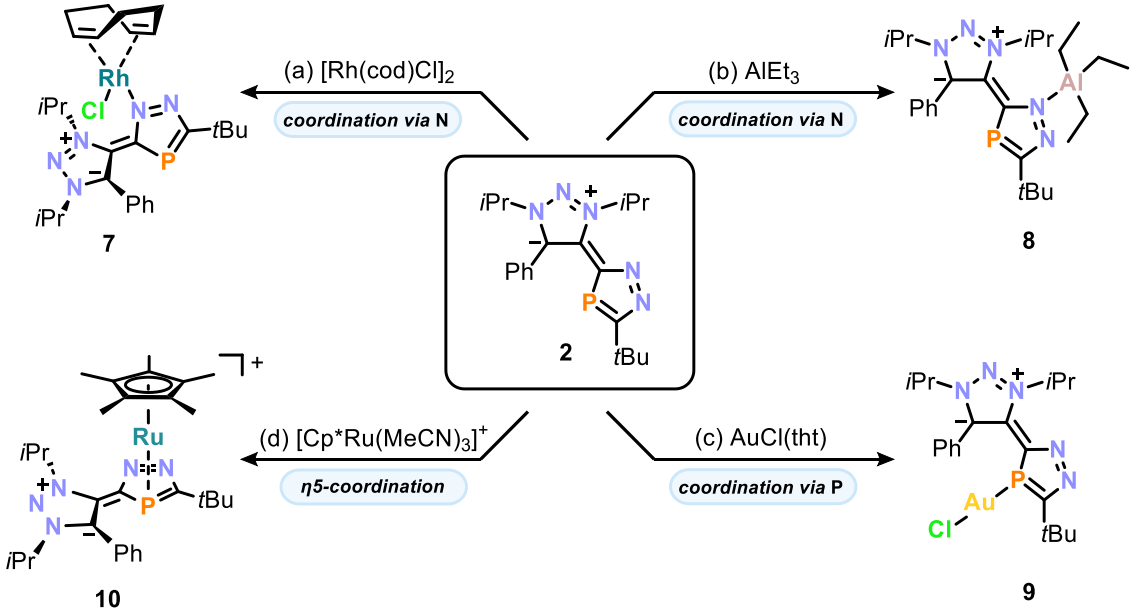

Scheme 3. Reactivity of **2** toward different Lewis acids. Depending on the metal source, different coordination modes can be achieved; reagents/by-products and conditions: a) +0.5 eq. $[Rh(cod)Cl]_2$; toluene, r.t., 6 h; b) +1.0 eq. $AlEt_3$; THF, −35 °C to r.t., 2 h; c) +1.0 eq. [AuCl(tht)]/−tht; toluene, r.t., 7 h; d) +1.0 eq. $[Cp^*Ru(MeCN)_3]$/−3 MeCN; THF, 65 °C, 1 d; yields: **7**: 81%, **8**: 55%, **9**: 96%, **10**: 60%; cod = 1,5-cyclooctadiene, tht = tetrahydrothiophene, Cp* = η^5-C_5Me_5.

Furthermore, the signals corresponding to the *i*Pr groups and the cod ligand in the ^{1}H NMR spectrum of complex **7** are significantly broadened (Figure S10, SI). This may be attributed to the partial double bond character along the C2−C3 axis (1.474(4) Å), in combination with a square planar rhodium center, resulting in hindered rotation of the two units. By gradually decreasing the temperature in a variable temperature (VT) ^{1}H NMR monitoring experiment, these broadened signals sharpen into well-resolved multiplets (Figure S11, SI). The $^{31}P\{^1H\}$ NMR spectra of **7** and **8** reveal sharp singlets at $\delta = 86.7$ ppm and $\delta = 90.3$ ppm, respectively. These signals are slightly shifted downfield compared to the uncoordinated monophosphole **2**, which resonates at $\delta = 79.6$ ppm.

1*H*-diazaphospholes prefer coordination *via* the nitrogen atom(s), or complexes with higher hapticity.[48] Only two examples for 1*H*-diazaphospholes are known involving a

dative phosphorus-metal bond in complexes of palladium or tungsten.[48,50] To achieve targeted coordination solely *via* phosphorus, the 3*H*-diazaphosphole **2** was treated with softer Lewis acids. Satisfyingly, addition of [AuCl(tht)] to a solution of **2** in toluene yields complex [AuCl(**2**)] (**9**) in an almost quantitative isolated yield of 96% (Scheme 3c).

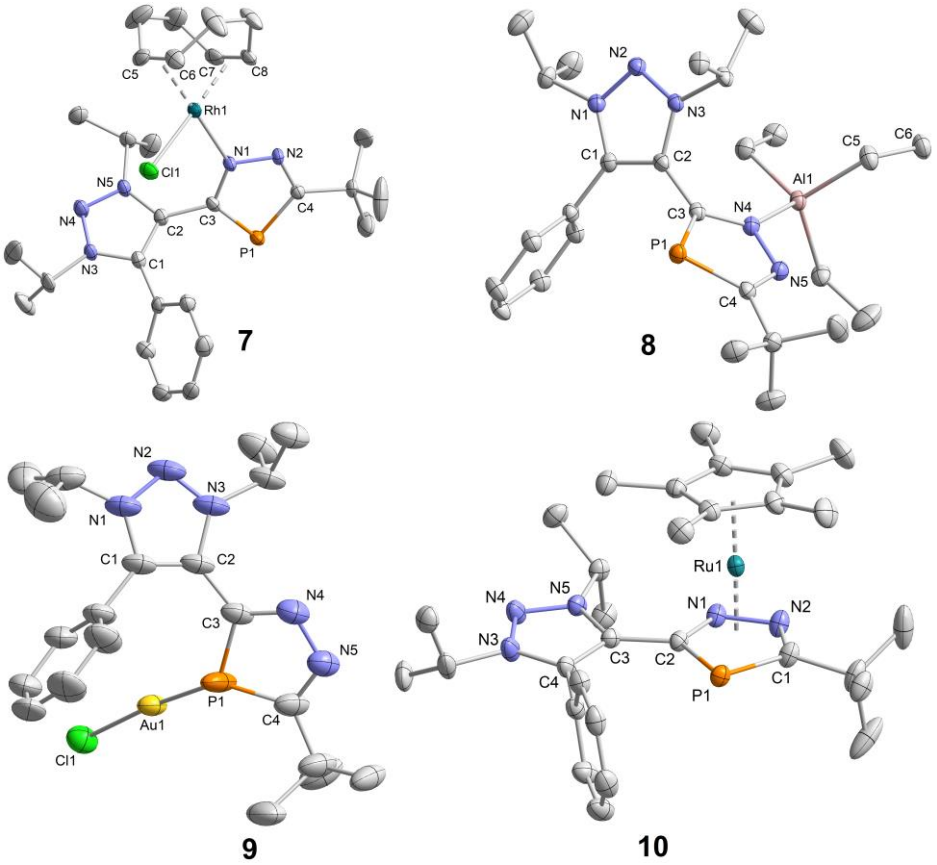

Figure 4. Solid-state molecular structures of **7**-**10**. Hydrogen atoms, PF_6^- (**10**) and disorder are omitted for clarity and thermal ellipsoids are drawn at the 50% probability level. Selected bond lengths [Å] and angles [°]: **7**: Rh1−Cl1 2.3827(7), Rh1−N1 2.116(2), Rh1−$C_{56}^{centr.}$ 2.014(2), P1−C4 1.755(3), N1−N2 1.359(3), C2−C3 1.474(4), C1−C2 1.387(4), N3−N4 1.327(3), Cl1-Rh-N1 91.30(6); **8**: Al1−N4 1.9926(1), Al1−C5 1.9972(2), P1−C4 1.7608(2), N4−N5 1.3599(2), C2−C3 1.468(2), N1−N2 1.3217(2), Al1-N4-C3 136.12(1); **9**: Au1−P1 2.2232(1), Au1−Cl1 2.2841(9), P1−C3 1.735(3), P1−C4 1.739(4), N4−N5 1.370(5), C2−C3 1.449(5), C1−C2 1.368(6), N1−N2 1.316(4), N2−N3 1.307(5), P1-Au1-Cl1 173.18(5); **10**: Ru1−Cp*$^{centr.}$ 1.8189(1), Ru1−$C_2N_2P^{centr.}$ 1.8219(8), P1−C1 1.779(2), N1−N2 1.383(2), C2−C3 1.464(3), N3−N4 1.321(3), N4−N5 1.315(3), C1-P1-C2 85.11(1)

Structural analysis of **9** by XRD revealed the coordination of **2** to AuCl *via* the P atom (Figure 4). In the solid-state, two complexes are connected *via* aurophilic interactions, featuring an Au–Au distance of 3.0705(4) Å, which is in the typical range for such interactions (3.05 Å).[51] The asymmetric unit contains one molecule of **9**, while the second half is related by a glide plane.

Coordination of the phosphole ligand **2** *via* one P atom is corroborated by $^{31}P\{^1H\}$ NMR spectroscopy, as evidenced by broadening of the singlet at $\delta = 58.5$ ppm ($\Delta\nu_{1/2} = 136$ Hz). This signal is shifted upfield with respect to uncoordinated **2** and the

related complex [W(CO)$_5$(bdap)] (bdap = bis(1*H*-1,2,4-diazaphosphol-1-yl)methane), which exhibit resonances at δ = 79.6 ppm and δ = 80.7 ppm, respectively.[48]

Since **2** contains a delocalized π system that might be accessible for coordination, **2** was next treated with complexes bearing multiple open coordination sites. To this end, [Cp*Ru(MeCN)$_3$]PF$_6$ (Cp* = η^5-C$_5$Me$_5$) was added to a solution containing **2** in C$_6$D$_6$, yielding the ruthenocene derivative [Cp*Ru(**2**)]PF$_6$ (**10**) (Scheme 3d). ^{31}P{^{1}H} NMR spectroscopic monitoring of the reaction progress revealed the appearance of a singlet at δ = 87.7 ppm at room temperature (Figure S45, SI). Based on the very similar ^{31}P{^{1}H} NMR chemical shifts observed for complexes **7** and **8** (δ = 86.7 ppm and δ = 90.3 ppm, respectively), this resonance can be attributed to an intermediate in which **2** coordinates *via* one, or two N atoms to Ru. By heating the reaction solution to 65 °C for one day, the signal at 87.7 ppm disappears while a new signal at δ = −48.9 ppm emerges. The upfield-shifted signal was assigned to the sandwich complex **10**, which was isolated in 60% yield. To the best of our knowledge, only two related neutral diazamonophosphole complexes [Cp*M(η^5-3,5-R$_2$C$_2$N$_2$P)] have been reported for M = Fe and Ru, starting from their corresponding 1*H*-diazaphospholide anions (R = *t*Bu or Ph).[52–54]

Structural analysis of **10** by SCXRD confirmed its sandwich structure with two coplanar π-ligands featuring a dihedral angle of 1° in an eclipsed conformation and a PF_6^- anion (Figure 4). The bond lengths within the C$_2$N$_2$P moiety are elongated compared to uncoordinated **2**.

In summary, a wide range of coordination compounds have been synthesized by reacting the new 3*H*-monophosphole **2** with various Lewis acids. Depending on the metal center, **2** adopts different coordination modes ranging from η^1 *via* the N or P atoms to η^5 *via* the π-system of the phosphole unit.

Strikingly, an entirely different outcome was observed when **2** was treated with low-valent transition metal complexes. Upon heating a solution of **2** and [Ni(cod)$_2$] to 60 °C for 5 h, the formation of C−C bond activation product **11** was observed (Scheme 4a). Monitoring of the reaction by ^{1}H and ^{31}P{^{1}H} NMR spectroscopy revealed that the reaction reaches a maximum conversion of ~70%, although unreacted [Ni(cod)$_2$] and **2** remain present in the reaction solution (Figure S46, SI). Despite the incomplete reaction and the light sensitivity of complex **11**, it was isolated in a 9% yield by crystallization from *n*-hexane.

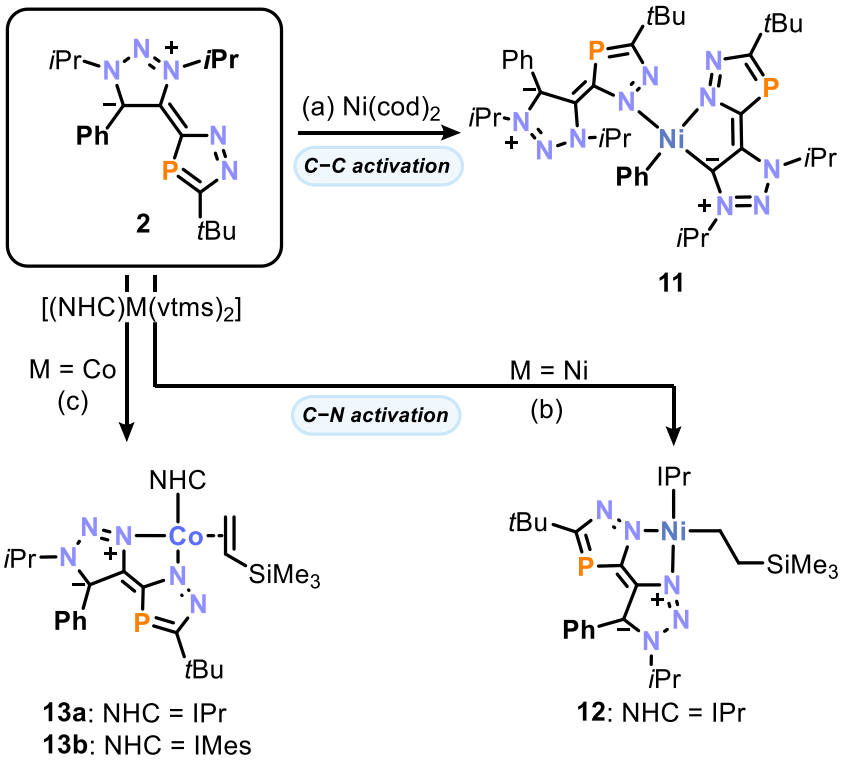

Scheme 4. Reactivity of **2** towards low-valent complexes of Ni and Co, affording complexes **11**-**13**; reagents/by-products and conditions: a) + 1.3 eq. $Ni(cod)_2$/−2 cod; toluene, 60 °C, 5 h; b) +1.4 eq. $[(IPr)Ni(vtms)_2]$/−vtms; toluene, 65 °C, 11 d; c) **13a**: + 1.1 eq. $[(IPr)Co(vtms)_2]$/−vtms; toluene, 60 °C, 16 h; **13b**: + 1.1 eq. $[(IMes)Co(vtms)_2]$/−vtms; C_6H_6, 60 °C, 1 d; yields: **11**: 9%, **12**: 56%, **13a**: 52%, **13b**: 50%; vtms = vinyltrimethylsilane, IPr = 1,3-bis(2,6-diisopropylphenyl)imidazolin-2-ylidene, IMes = 1,3-bis(2,4,6-trimethylphenyl)imidazolin-2-ylidene.

SCXRD analysis of **11** confirmed, that at least two molecules of **2** are involved in the reaction. One molecule of **2** engages η^1-N coordination *via* the inner nitrogen which is consistent with the higher calculated negative natural charge of −0.3 (*vide supra, c.f.* compounds **7** and **8**), whereas the second unit undergoes oxidative addition and C−C bond activation mediated by the nickel(0) center (see Figure 5). The resulting complex features a formal nickel(II) center with four ligands in a square planar geometry, an η^1-N **2** ligand, a phenyl ligand, and the residual η^2-N,C fragment of **2** undergoing the C−Ph activation at the 1,2,3-triazolium ring. This η^2-N,C coordination forces the two ring systems into an orientation that is opposite to all other compounds within this chapter, presumably because of the preferential coordination *via* the N atom over the P atom, due to natural charges and the HSAB theory. The C4−Ni1 (1.905(2) Å) and C5−Ni1 (1.892(2) Å) bond lengths are well within the typical range for Ni−C single bonds in nickel aryl complexes.[55,56] Moreover, the bond lengths within the monophosphole ligands are similar to those in **2**.

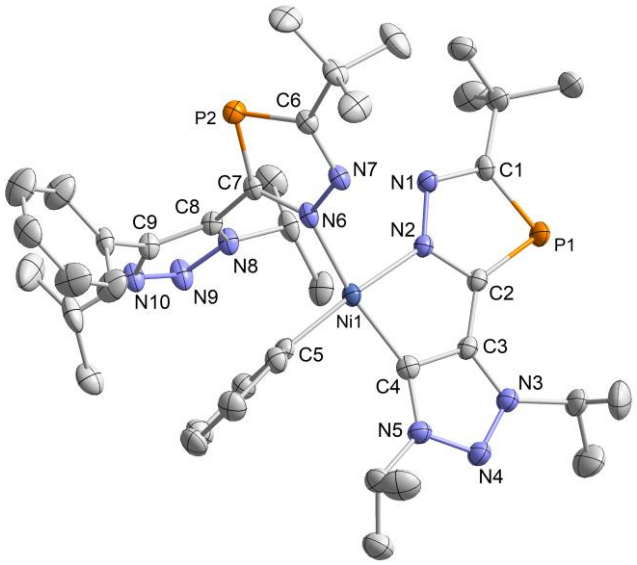

Figure 5. Solid-state molecular structure of **11**. Hydrogen atoms and non-coordinating solvent molecules are omitted for clarity and thermal ellipsoids are drawn at the 50% probability level. Selected bond lengths [Å] and angles [°]: Ni1−N2 1.9894(2), Ni1−C4 1.905(2), Ni1−C5 1.892(2), Ni1−N6 1.918(2), N1−N2 1.355(3), N6−N7 1.356(3), C2−C3 1.438(3), N2-Ni1-C5 173.02(9), N6-Ni1-C4 169.27(9), N6-Ni1-N2 91.42(8), N2-Ni1-C4 82.65(9).

The above-mentioned C−C bond activation is also reflected in the $^{31}P\{^{1}H\}$ NMR spectrum of **11**, which exhibits two singlets, one at $\delta = 87.5$ ppm and a more upfield shifted signal at $\delta = 54.7$ ppm (*c.f.* **2** resonates at $\delta = 79.6$ ppm). The more downfield shifted signal was assigned to the monophosphole, which coordinates only *via* nitrogen, due to the similar chemical shifts of η^1-N complexes **7** and **8** of $\delta = 86.7$ ppm and $\delta = 90.3$ ppm, respectively. The upfield shifted signal was assigned to the more shielded phosphorus atom P1 of the monophosphole, which underwent oxidative addition.

In order to further investigate the reactivity of the ligand framework, reactions of **2** with highly electron-rich first-row transition-metal centers, such as nickel(0) and cobalt(0) N-heterocyclic carbene complexes, were examined. Upon treatment of **2** with [(IPr)Ni(vtms)$_2$] (IPr = 1,3-bis(2,6-diisopropylphenyl)imidazolin-2-ylidene, vtms = $H_2CCH(SiMe_3)$), the C−N bond activation product **12** was cleanly formed (Scheme 4b).[57,58] The reaction mechanism for the formation of **12** is proposed to involve an initial substitution of a labile olefin ligand by one equivalent of **2**, forming a nickel(II) species structurally related to **7** and **8** (*vide supra*, see also the SI, Scheme S1). *β*-H elimination from this N-coordinated intermediate then results in a nickel(II) hydride complex, with concomitant release of propene. Evidence for this is provided by the visible evolution of gas during the reaction. The olefin vinyltrimethylsilane (vtms), still present in the reaction mixture, then undergoes migratory insertion into the hydride, resulting in the final product, **12**.[59,60]

In comparison, upon treatment of **2** with the related bis(alkene) complexes [(NHC)Co(vtms)$_2$], the formation of product **13** was observed (NHC = IPr (**13a**), IMes (**13b**), Scheme 4c), featuring the olefin vtms instead of the alkyl ligand in **12**. The proposed reaction sequence for the formation of **13** is similar to that of **12** (Scheme S1, SI). However, for the cobalt(0) complexes, elimination of a H• radical and coordination of vtms is favored over insertion of the hydrogen.

Although related C−C and C−N bond activation reactions have been reported for NHCs and the imidazole (= 1,3-diazole) framework, these reactions mostly involve ring opening and insertion, as well as coordination *via* exocyclic moieties.[61–70] Thus, the selective C−N and C−C bond activation reactions, as shown in Scheme 4, are unprecedented for the 1,2,3-triazolium scaffold.

Compounds **12** and **13a** were isolated by crystallization from saturated Et_2O solutions in 56% and 52% yields, respectively. The solid-state structures of both compounds are depicted in Figure 6. Complex **12** features a nearly square planar nickel center, exhibiting a typical single Ni−C6 bond of 1.940(2) Å.[55,71] In contrast, complex **13a** exhibits a tetrahedral geometry around the Co core. In **13a**, the Co−C7 carbene distance of 2.035(3) Å is elongated compared to the corresponding distance in [(IPr)Co(vtms)$_2$] (1.9519(2) Å), suggesting a weaker interaction between the NHC and the metal center.[72] Moreover, the C6−C7 distance in alkyl complex **12 (**1.532(3) Å), is significantly longer than the C5=C6 bond length in the olefin complex **13a** (1.351(7) Å), reflecting the single, respectively double bond nature of the corresponding C−C bonds, thus corroborating the insertion and eliminiation reactions, respectively. In comparison, the calculated C=C bond length in the free vinylsilane is 1.322 Å.[73] Additional single-crystal XRD data sets were acquired for the isostructural complex **13b**, both with and without Et_2O incorporated into the crystal lattice (see Figure S65-66).

The $^{31}P\{^1H\}$ NMR spectrum of **12** in C_6D_6 exhibits a sharp singlet at δ = 60.7 ppm, which is very similar to the observed value of δ = 54.7 ppm for **2**. Additionally, the $^{29}Si\{^1H\}$ NMR spectrum reveals a singlet at δ = −4.1 ppm for the coordinating alkyl group, consistent with the typical range for $-SiMe_3$ groups.[74] In agreement with the paramagnetic nature of **13a**, the ^1H NMR spectrum in C_6D_6 exhibits broad paramagnetically shifted signals spanning a wide frequency range from δ = 96 to −26 ppm. The solution magnetic moment (3.49 μB) aligns well with the spin-only value (3.87 μB) for high-spin d^7 ions (S=3/2), suggesting the presence of three unpaired electrons.

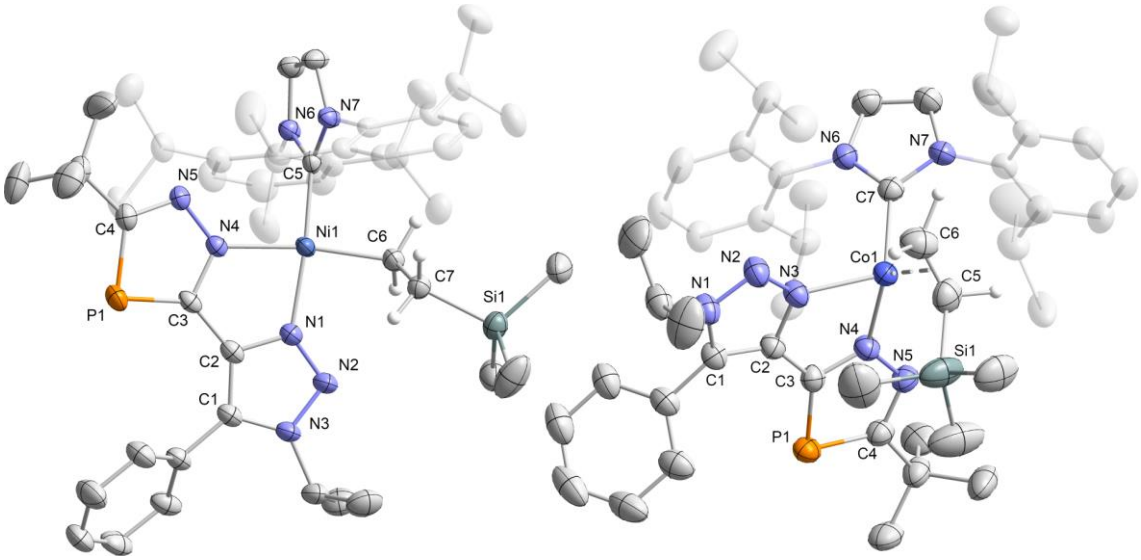

Figure 6. Solid-state molecular structure of **12** (left) and **13a** (right). Hydrogen atoms, except $C_2H_4SiMe_3$ and $C_2H_3SiMe_3$ moiety (positions refined), and disorder are omitted for clarity. Thermal ellipsoids are drawn at the 50% probability level. Selected bond lengths [Å] and angles [°]: **12**: Ni1−N1 1.9313(2), Ni1−N4 1.9825(2), Ni1−C5 1.8593(2), Ni1−C6 1.940(2), N6−C5 1.369(3), C6−C7 1.532(3), Si1−C7 1.877(2), N1−N2 1.322(2), C2−C3 1.452(3), N4−N5 1.355(2), C5-Ni1-N1 172.36(8), N4-Ni1-C6 168.35(8), N6-C5-N7 103.62(2), Si1-C7-C6 112.85(1); **13a**: Co1−N3 2.078(3), Co1−N4 2.006(3), Co1−C7 2.035(3), Co1−$C_{56}^{centr.}$ 1.937(3), P1−C3 1.742(4), C2−C3 1.454(5), N2−N3 1.313(4), N6−C7 1.359(4), C5−C6 1.351(7), Si1−C5 1.850(5), C7-Co1-N4 118.31(1), N3-Co1-C5 110.01(2), N3-Co1-C6 96.59(2), C6-C5-Si1 126.0(4), N6-C7-N7 102.8(3).

In summary, the new class of 3*H*-diazamonophosphole also exhibit unexpected bond activation reactivity within the 1,2,3-triazolium framework.

To investigate the potential donor capabilities of the rare 5*H*-1,2,3,4-diazadiphosphole, compound **3** was treated with various Lewis acids. Initial attempts with e.g. $[Rh(cod)Cl]_2$, [AuCl(tht)], $[Cp^*Ru(MeCN)_3]PF_6$ resulted primarily in the formation of suspensions which exhibited no observable signals in the $^{31}P\{^1H\}$ NMR spectra.

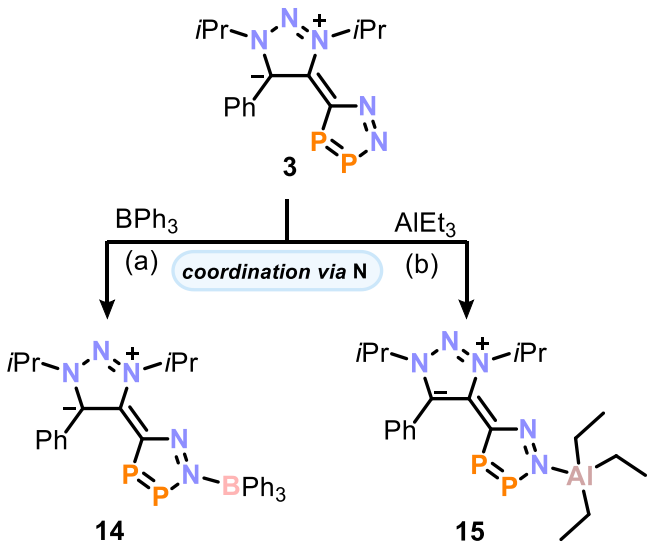

Scheme 5. Coordination of diphosphole **3** affording compounds **14** and **15**; reagents and conditions: a) +1.0 eq. BPh_3; THF, −35 °C to r.t., 1 h; b) +1.0 eq. $AlEt_3$; toluene, −35 °C to r.t., 2 h; yields: **14**: 69%, **15**: 85%.

Pleasingly, a selective reaction when BPh_3 or $AlEt_3$ was added to a solution containing **3** (Scheme 5). Analysis of the $^{31}P\{^1H\}$ NMR spectra of the reaction mixtures revealed the complete consumption of **3**, with the concomitant formation of new species, **14** and **15**, which each exhibit two distinct resonances in a 1:1 ratio. Complex **14** features two characteristic doublets at δ = 216.4 ppm and δ = 380.9 ppm, with $^1J_{PP}$ coupling of 453 Hz, while the two doublets for **15** exhibit chemical shifts of δ = 217.5 ppm and δ = 364.2 ppm ($^1J_{PP}$ = of 444 Hz). In the $^{11}B\{^1H\}$ NMR spectrum of **14**, the resonance corresponding to the boron coordinating to the nitrogen is detected at δ = 2.8 ppm.

Both compounds **14** and **15** crystallize from a THF/toluene mixture in good isolated yields of 69% and 85%, respectively. XRD analysis revealed the presence of a CN_2P_2 unit, with BPh_3, or $AlEt_3$ bonded to the outer nitrogen in compounds **14** and **15**, respectively. Both compounds are isostructural and their crystal structures are depicted in Figure 7. The coordination of the diphosphole **3** *via* the outer nitrogen atom, N4, is in line with the DFT calculations, which show a higher negative natural charge of −0.56 localized on N4 compared to −0.28 on the inner nitrogen, N5. This finding contrasts with the observed coordination behavior of **2**, where coordination *via* the inner nitrogen was typically observed (*vide supra*). This discrepancy is most likely due to the diminished steric shielding of the outer nitrogen atom in **3** compared to **2** (P vs. C*t*Bu). In **14**, the diphosphole and 1,2,3-triazolium planes are twisted by 43° with respect to each other. The twist angle is identical to that observed in the starting material **3** (43°). The heterocyclic moieties exhibit greater co-planarity in **15**, with a dihedral angle of 28°.

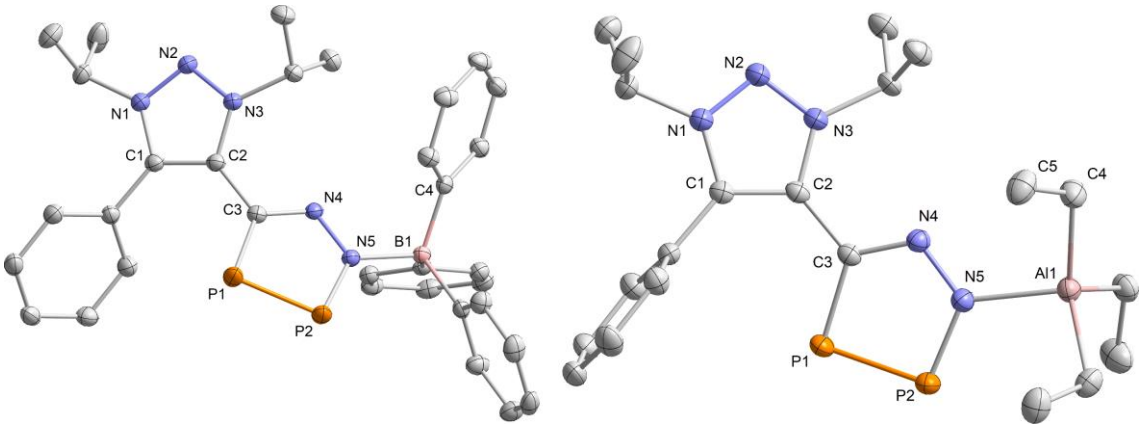

Figure 7. Solid-state molecular structures of **14** (left) and **15** (right). Hydrogen atoms omitted for clarity and thermal ellipsoids are drawn at the 50% probability level. Selected bond lengths [Å] and angles [°]: **14**: B1−N5 1.6191(2), B1−C4 1.6360(2), P1−P2 2.0809(5), P2−N5 1.6885(1), N4−N5 1.3406(1), B1-N5-N4 115.70(9), C3-P1-P2 89.64(4), P1-P2-N5 95.78(4); **15**: Al1−N5 1.9990(1), Al1−C4 1.9923(2), C5−C4 1.538(2), P1−P2 2.0739(6), P2−N5 1.6864(1), N4−N5 1.3395(2), Al1-N5-N4 120.17(9), C3-P1-P2 89.56(5), P1-P2-N5 96.44(5).

Furthermore, the B1−N5 bond length of 1.619(1) Å in **14** is notably shorter than the sum of the van der Waals radii ($\sum r_{BN}$ 3.47 Å) but is in the typical range for four-coordinate boron centers engaging Lewis adduct formation involving a nitrogen donor atom (1.656 Å).[75] In contrast, the Al1−N5 bond length (1.999(1) Å) in **15** closely resembles that calculated for a Al−N single bond ($\sum r_{AlN}$ 1.97 Å).[42,43]

6.3 Conclusion

In this study, a facile one-step synthesis of elusive 3*H*-1,2,4-diazamonophospholes, and 1,2,3,4-diazadiphospholes starting from recently reported diazoalkenes is reported. The ligand frameworks **2** and **3** are accessible in high yield *via* [3+2] cycloaddition reactions with PC*t*Bu and P_4, respectively. Thus, the electronic and structural features were elucidated by quantum chemical calculations and XRD. The donor capabilities of **2** and **3** were studied through the synthesis of a series of coordination complexes, featuring main group (B, Al) and transition metal (Co, Ni, Ru, Rh W, Au) centers. Herein, different Lewis acids gave rise to various coordination modes, as featured in complexes **4**-**10**, **14** and **15**, including mononuclear η^1-N- and η^1-P-complexes, as well as compounds featuring a higher hapticity by η^5-coordination *via* the aromatic π-system. Remarkably, in the presence of highly electron-rich first-row transition-metal centers such as nickel and cobalt, the 1,2,3-triazole ring of **2** undergoes C−C or C−N bond activation to give complexes **11**-**13**. In summary, these results demonstrate the potential of diazoalkenes for the synthesis of novel types of heterocycles, which serve as versatile ligands in coordination chemistry. Considering the increasing accessibility of diazoalkenes, bearing e.g. pyridine or related NHC frameworks, it is anticipated that the simple synthetic

approach should allow facile tuning of their electronic and steric properties, and should grant access to further classes of heterocycles. Future investigations should focus on further exploring these avenues along with coordination chemistry of the resulting species.

6.4 Experimental Details

General Synthetic Methods

All reactions and product manipulations were carried out in flame-dried glassware under an inert atmosphere of argon using standard Schlenk-line or glovebox techniques (maintained at <0.1 ppm H_2O and <0.1 ppm O_2). J. Reitz prepared the precursor *i*Pr-Diazoalkene **1** from recently reported N-heterocyclic olefin R=CH_2.[41,40] The starting materials PC*t*Bu,[76] AuCl(tht),[77] [(IPr)Ni(H_2CCH($SiMe_3$))$_2$],[57,58] [(IMes)Co(H_2CCH($SiMe_3$)$_2$] and [(IPr)Co(H_2CCH($SiMe_3$)$_2$][72] were prepared according to previously reported procedures. All other chemicals were purchased from commercial suppliers and used without further purification.

Solvents were dried and degassed with a MBraun SPS800 solvent purification system. All dry solvents except *n*-hexane and *n*-pentane were stored under argon over activated 3 Å molecular sieves in gas-tight ampules. *n*-Hexane and *n*-pentane were instead stored over a potassium mirror.

General Analytical Techniques

NMR spectra were recorded on Bruker Avance 400 spectrometers at 300 K and were internally referenced to residual solvent resonances (^{1}H NMR: C_6D_6: 7.15 ppm, THF-d_8: 1.72 ppm; ^{13}C{^{1}H} C_6D_6: 128.06 ppm, THF-d_8: 25.31 ppm). ^{31}P{^{1}H} spectra were referenced externally to 85% $H_3PO_{4(aq.)}$. Chemical shifts, δ, are given in ppm referring to external standards of tetramethylsilane (^{1}H, ^{13}C{^{1}H}). ^{1}H, ^{13}C and ^{31}P NMR signals were assigned based on 2D NMR spectra (COSY, HSQC, HMBC, NOESY and ROESY). The solution magnetic moment was determined using the Evans Method.[78–80]

UV/Vis spectra were recorded on an Ocean Optics Flame Spectrometer with a DH-2000-BAL light source. Mass spectra of compounds **2** and **11** were recorded on a Jeol AccuTOF GCX device by the by the analytical department of the University of Regensburg and compound **10** on a Finnigan MAT 95 device. Elemental analysis were performed by the Central Analytics Department of the University of Regensburg using a Vario micro cube. IR spectra were recorded with a Bruker ALPHA spectrometer equipped with a germanium ATR unit.

6.4.1 Synthesis of Compounds

Synthesis of 2:

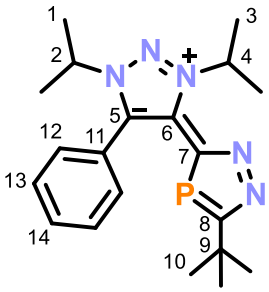

While stirring, to a light yellow solution of **1** (150 mg, 0.56 mmol, 1.0 equiv.) in THF (3 mL) was added dropwise a stock solution of PC*t*Bu (134.5 µL, c = 4.1 M in hexamethyldisiolaxane (HMDSO), 0.56 mmol, 1.0 eq.). After 6 h, the reaction mixture was filtered and layered with *n*-hexane (7 mL). After one week, pale yellow crystals of **2**, of sufficient quality for analysis by XRD, were obtained, which were decanted, washed with *n*-hexane (2 × 5 mL) and dried *in vacuo*. The solid contains 0.1 molecules of THF per molecule of compound after drying as indicated by ^{1}H/^{13}C{^{1}H} NMR spectra and elemental analysis.

Yield: 144 mg (70%).

^{1}H NMR (400.13 MHz, 300 K, THF-d_8): δ/ppm = 1.30 (d, $^{4}J_{PH}$ = 0.8 Hz, 9H, C^{10}H of *t*Bu), 1.59 (d, $^{3}J_{HH}$ = 6.6 Hz, 6H, C^{1}H of *i*Pr), 1.65 (d, $^{3}J_{HH}$ = 6.6 Hz, 6H, C^{3}H of *i*Pr), 4.76 (sept, $^{3}J_{HH}$ = 6.6 Hz, 1H, C^{2}H of *i*Pr), 6.42 (sept, $^{3}J_{HH}$ = 6.6 Hz, C^{4}H of *i*Pr), 7.43-7.53 (m, 5H, C$^{12/13/14}H$ of Ph).

^{13}C{^{1}H} NMR (100.66 MHz, 300 K, THF-d_8): δ/ppm = 22.2 (s, C^{1}H of *i*Pr), 22.4 (s, C^{3}H of *i*Pr), 33.2 (d, $^{3}J_{PC}$ = 7.2 Hz, $C^{10}H$ of *t*Bu), 36.1 (d, $^{2}J_{PC}$ = 20.1 Hz, C^{9} of *t*Bu), 55.5 (s, C^{2}H of *i*Pr), 56.5 (s, C^{4}H of *i*Pr), 125.8 (d, $^{4}J_{PC}$ = 2.0 Hz, C^{11} of Ph), 129.6 (s, C^{13}H of Ph), 131.3 (s, C^{14}H of Ph), 132.0 (d, J_{PC} = 3.3 Hz, C^{12}H of Ph), 136.6 (s, C^{5}), 143.0 (d, $^{2}J_{PC}$ = 29.7 Hz, C^{6}), 154.5 (d, $^{1}J_{PC}$ = 46.0 Hz, C^{7}) 193.0 (d, $^{1}J_{PC}$ = 52.6 Hz, C^{8}).

^{31}P{^{1}H} NMR (162.04 MHz 300 K, THF-d_8): δ/ppm = 79.6 (s).

UV/Vis (THF, λ_{max} / nm, ε_{max} / L·mol^{-1}·cm^{-1}): 310 (14000).

LIFDI-MS (QTOF, toluene): m/z(%) calcd. for $C_{20}H_{28}N_5P$: 369.21; found: 369.19.

Elemental Analysis calcd. for $(C_{20}H_{28}N_5P)$•$(THF)_{0.1}$ (Mw = 369.45 g·mol^{-1}):
C 65.05, H 7.71, N 18.59; found C 65.44, H 7.98, N 18.91.

Synthesis of 3:

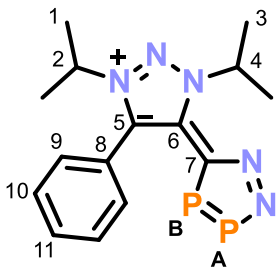

THF (9 mL) was added to a mixture of solids **1** (116 mg, 0.43 mmol, 1.0 equiv.) and P_4 (27 mg, 0.22 mmol, 0.5 equiv.) The resulting orange suspension was stirred for 5 h and filtered. Pale orange crystals of **3** were grown by addition of *n*-hexane (5 mL) to the filtrate and storing the solution at −35 °C for two days. The supernatant was decanted. The crystals were washed

with *n*-hexane (2 × 1 mL) and dried *in vacuo*. Slow diffusion of Et_2O into a saturated acetonitrile solution of **3** yielded crystals suitable for single-crystal X-ray diffraction.

Yield: 77 mg (54%).

^{1}H NMR (400.13 MHz, 300 K, THF-d_8): δ/ppm = 1.49 (d, $^3J_{HH}$ = 6.7 Hz, 6H, C^3*H* of *i*Pr), 1.68 (d, $^3J_{HH}$ = 6.6 Hz, 6H, C^1*H* of *i*Pr), 4.89 (sept, $^3J_{HH}$ = 6.6 Hz, 1H, C^2*H* of *i*Pr), 5.70 (sept, $^3J_{HH}$ = 6.7 Hz, 1H, C^4*H* of *i*Pr), 7.43-7.57 (m, 5H, C$^{9/10/11}$*H* of Ph).

^{13}C{^{1}H} NMR (100.61 MHz, 300 K, THF-d_8): δ/ppm = 22.2 (s, *C*^{3}H of *i*Pr), 22.3 (s, *C*^{1}H of *i*Pr), 55.9 (s, *C*^{2}H of *i*Pr), 56.3 (s, *C*^{4}H of *i*Pr), 125.5 (s, *C*^{8} of Ph), 129.6 (s, *C*^{10}H of Ph), 131.3 (s, *C*^{11}H of Ph), 132.0 (d, J_{PC} = 2.5 Hz, *C*^{9}H of Ph), 138.7 (s, *C*^{5}), 143.2 (s, $^2J_{PC}$ = 29.8 Hz, *C*^{6}), 160.7 (dd, $^1J_{PC}$ = 75.8 Hz, $^2J_{PC}$ = 14.7 Hz, *C*^{7}).

^{31}P{^{1}H} NMR (161.98 MHz, 300 K, THF-d_8): δ/ppm = 217.5 (d, $^1J_{PP}$ = 444.0 Hz, 1P, P_B), 364.2 (d, $^1J_{PP}$ = 444.0 Hz, 1P, P_A).

UV/Vis (THF, λ_{max} / nm, ε_{max} / L·mol^{-1}·cm^{-1}): 340sh (7000), 490 (4000), 630 (6000).

Elemental Analysis calcd. for ($C_{15}H_{19}N_5P_2$) (Mw = 331.30 g·mol^{-1}):
C 54.38, H 5.78, N 21.14; found C 55.16, H 5.41, N 20.45.

[{W(CO)$_5$}$_2$(2)] (6):

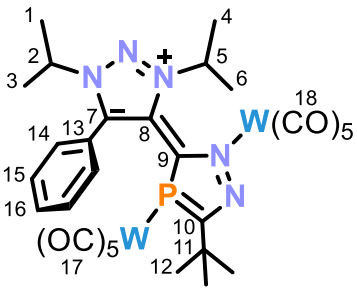

A stirring, colorless solution of [W(CO)$_6$] (171 mg, 0.1487 mmol, 3.0 equiv.) in THF (2 mL) was irradiated with UV-light (365 nm, 10 W) for 45 min. The solution turned deep yellow, was added to solid **2** (60 mg, 0.162 mmol, 1.0 equiv.) and stirred for 1 d. The yellow solution was cooled to –80 °C and the inert gas was exchanged for 1 atm. CO, by evacuating the schlenk flask until gas evolution from the solution ceased and repressurizing it with CO. The flask was closed and warmed up to room temperature (Caution: the pressure in the flask increases by approximately 2-3 bar upon warming to room temperature; use pressure-resistant glassware). The reaction was stirred for 4 d and filtered. All volatiles were removed *in vacuo* and excess [W(CO)$_6$] was sublimed off under reduced pressure (32 °C, 1 × 10^{-3} mbar, 6 h). The product was obtained as a light yellow solid. Slow diffusion of *n*-hexane into a saturated THF solution of **6** yielded crystals suitable for single-crystal X-ray diffraction.

Yield: 132 mg (80%).

^{1}H NMR (400.13 MHz, 300 K, THF-d_8): δ/ppm =1.73 (s, 9H, C^{12}*H* of *t*Bu), 1.89 (d, $^3J_{HH}$ = 2.7 Hz, C$^{1/3}$*H* of *i*Pr), 1.90 (d, $^3J_{HH}$ = 2.7 Hz, C$^{1/3}$*H* of *i*Pr), 1.92 (d, $^3J_{HH}$ = 6.5 Hz,

6H, C$^{4/6}$*H* of *i*Pr), 2.15 (d, $^{3}J_{HH}$ = 6.5 Hz, 6H, C$^{4/6}$*H* of *i*Pr), 5.12 (sept $^{3}J_{HH}$ = 6.6 Hz, 1H, C^{5}*H* of *i*Pr), 5.42 (sept, $^{3}J_{HH}$ = 6.6 Hz, 1H, C^{2}*H* of *i*Pr), 7.78-7.93 (m, 5H, C$^{12/13/14}$*H* of Ph).

^{13}C{^{1}H} NMR (100.61 MHz, 300 K, THF-d_8): δ/ppm = 21.9 (s, *C*$^{1/3}$H of *i*Pr), 22.6 (s, *C*$^{4/6}$H of iPr), 22.6 (s, *C*$^{4/6}$H of iPr), 24.0 (s, *C*$^{1/3}$H of *i*Pr), 32.7 (d, $^{3}J_{PC}$ = 4.9 Hz, *C*^{12}H of *t*Bu), 37.7 (d, $^{2}J_{PC}$ = 18.9 Hz, *C*^{11} of *t*Bu), 57.5 (s, *C*^{2}H of *i*Pr), 57.5 (s, *C*^{5}H of *i*Pr), 123.0 (s, *C*^{13} of Ph), 130.7 (s, *C*$^{14/15}$H of Ph), 130.7 (s, *C*$^{14/15}$H of Ph), 132.9 (s, *C*^{16}H of Ph), 138.2 (d, $^{2}J_{PC}$ = 27.3 Hz, *C*^{8}), 142.7 (d, $^{3}J_{PC}$ = 4.0 Hz, *C*^{7}), 157.2 (d, $^{1}J_{PC}$ = 34.2 Hz, *C*^{9}), 185.4 (d, $^{1}J_{PC}$ = 6.6 Hz, *C*^{10}), 196.6 (d, $^{2}J_{PC}$ = 7.7 Hz, $^{1}J_{WC}$ = 117.7 Hz, *C*^{17}O), 199.8 (s, $^{1}J_{WC}$ = 130.8 Hz, *C*$_{cis}$^{18}O), 202.7 (s, $^{1}J_{WC}$ = 145.6 Hz, *C*$_{trans}$^{18}O).

^{31}P{^{1}H} NMR (161.98 MHz 300 K, THF-d_8): δ/ppm = 52.3 (t, $^{1}J_{PW}$ = 233.9 Hz).

UV/Vis (THF, λ_{max} / nm, ε_{max} / L·mol^{-1}·cm^{-1}): 240 (90000), 290sh (21000), 300sh (18000), 350 (15000).

IR (solid state): ν/ cm^{-1} = 2068w (C=O), 1944w (C=O), 1931s (C=O), 1915s (C=O), 1890s (C=O), 1855s (C=O).

Elemental analysis calcd. for ($C_{30}H_{28}N_5PO_{10}W_2$) (Mw = 1017.23 g·mol^{-1}):
C 35.42, H 2.77, N 6.88; found C 35.75, H 2.96, N 6.89.

[Rh(2)(cod)Cl] (7):

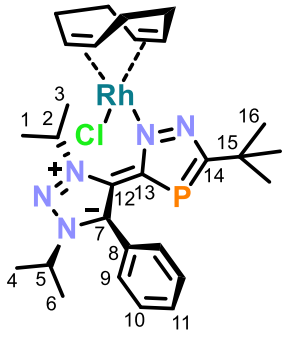

To a mixture of solids **2** (35 mg, 0.095 mmol, 1.0 equiv.) and [Rh(cod)Cl]$_2$ (23 mg, 0.074 mmol, 0.5 equiv.) toluene (2 mL) was added. The resulting suspension was stirred for 6 h and subsequently filtered. Yellow crystals of **7**, of sufficient quality for XRD analysis, were grown by slow vapor diffusion of *n*-hexane into this filtrate over five days. The crystals were decanted off, washed with *n*-hexane (2 × 0.5 mL) and dried *in vacuo*. The solid contains 0.1 molecules of toluene per molecule of compound after drying as indicated by ^{1}H/^{13}C{^{1}H} NMR spectra and elemental analysis.

Yield: 47 mg (81%).

^{1}H NMR (400.13 MHz, 193 K, THF-d_8): δ/ppm =1.24 (s, 9H, C^{16}*H* of *t*Bu), 1.41 (d, $^{3}J_{HH}$ = 6.5 Hz, C$^{4/6}$*H* of *i*Pr), 1.45-1.65 (m, 5H, d ($^{3}J_{HH}$ = 6.2 Hz) of C$^{1/3}$*H* of *i*Pr overlapping with C*H*$_2$ of cod), 1.78 (d, $^{3}J_{HH}$ = 6.4 Hz, 3H, C$^{4/6}$*H* of *i*Pr), 1.89-2.02 (m, 2H, C*H*$_2$ of cod), 2.06-2.24 (m, 5H, d ($^{3}J_{HH}$ = 6.2 Hz) of C$^{1/3}$*H* of *i*Pr overlapping with C*H*$_2$ of cod), 2.50-2.69 (m, 2H, C*H*$_2$ of cod), 3.89-3.92 (m, 1H, C*H* of cod), 4.04-4.09 (m,

1H, C*H* of cod), 4.18-4.22 (m, 1H, C*H* of cod), 4.93 (sept, $^{3}J_{HH}$ = 6.5 Hz, C^{5}*H* of *i*Pr), 5.00-5.05 (m, 1H, C*H* of cod), 6.49 (sept, $^{3}J_{HH}$ = 6.6 Hz, C^{2}*H* of *i*Pr) 7.45-7.49 (m, 3H, C$^{10/11}$*H* of Ph), 7.67-7.69 (m, 2H, C^{9}*H* of Ph).

^{13}C{^{1}H} NMR (100.61 MHz, 193 K, THF-d_8): δ/ppm = 21.3 (s, *C*$^{1/3}$H of *i*Pr), 21.6 (s, *C*$^{4/6}$H of *i*Pr), 23.3 (s, *C*$^{1/3}$H of *i*Pr overlapping with *C*$^{4/6}$H of *i*Pr), 29.8 (s, *C*H$_2$ of cod), 30.0 (s, *C*H$_2$ of cod), 32.7 (d, $^{2}J_{PC}$ = 6.2 Hz, *C*^{16}H of *t*Bu), 32.8 (s, *C*H$_2$ of cod), 33.6 (s, *C*H$_2$ of cod), 36.5 ($^{2}J_{PC}$ = 18.4 Hz, *C*^{15} of *t*Bu), 55.5 (s, *C*^{5}H of *i*Pr), 56.1 (s, *C*^{2}H of *i*Pr), 78.4 (s, $^{1}J_{RhC}$ = 10.9 Hz, *C*H of cod), 80.0-80.3 (m, *C*H of cod overlapping with *C*H of cod), 81.8 (d $^{1}J_{RhC}$ = 9.4 Hz, *C*H of cod), 125.2 (s, *C*^{8} of Ph), 129.5 (s, *C*^{10}H of Ph), 131.3 (s, *C*^{11}H of Ph), 131.8 (s, *C*^{9}H of Ph), 139.9 (d, $^{3}J_{PC}$ = 1.2 Hz, *C*^{7}), 140.3 (d, $^{2}J_{PC}$ = 27.9 Hz, *C*^{12}), 157.3 (d, $^{1}J_{PC}$ = 40.2 Hz, *C*^{13}), 191.2 (d, $^{1}J_{PC}$ = 55.2 Hz, *C*^{14}).

^{31}P{^{1}H} NMR (161.98 MHz, 193 K, THF-d_8): δ/ppm = 86.7 (s).

UV/Vis (THF, λ_{max} / nm, ε_{max} / L·mol^{-1}·cm^{-1}) 270sh (16000), 380 (2000).

Elemental analysis calcd. for (C$_{28}$H$_{40}$N$_5$ClPRh)•(toluene)$_{0.1}$ (Mw = 615.99 g·mol^{-1}): C 55.14, H 6.58, N 11.20; found C 55.06, H 6.49, N 11.05.

[AlEt$_3$(2)] (8):

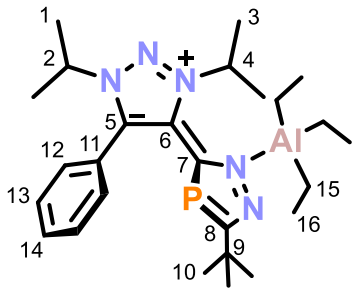

A solution of **2** (50 mg, 0.14 mmol, 1.0 equiv.) in THF (4 mL) was cooled to −35 °C. While stirring, a stock solution of triethylaluminium (72.9 µL, c = 25% by weight in toluene, 0.14 mmol, 1.0 eq.) was added dropwise. The resulting light yellow reaction mixture was stirred for 2 h and thawed. Volatiles were removed *in vacuo* and the resulting pale yellow residue was extracted with toluene (1 mL), and subsequently with THF (1 mL). The extracts were filtered and combined. Pale yellow crystals of **8**, of sufficient quality for XRD analysis, were grown by slow vapor diffusion of *n*-hexane into this extract over five days at r.t. and another day at −35 °C. The crystals were isolated by filtration, washed with *n*-hexane (3 × 1 mL), and dried *in vacuo*.

Yield: 30 mg (46%); including a second crop: 36 mg (55%).

^{1}H NMR (400.13 MHz, 300 K, THF-d_8): δ/ppm = −0.46 (q, $^{3}J_{HH}$ = 8.1 Hz, 6H, C^{15}*H* of AlEt$_3$), 0.89 (t, $^{3}J_{HH}$ = 8.1 Hz, 9H, C^{16}*H* of AlEt$_3$), 1.37 (s, 9H, C^{10}*H* of *t*Bu), 1.63 (d, $^{3}J_{HH}$ = 6.6 Hz, 6H, C^{1}*H* of *i*Pr), 1.69 (d, $^{3}J_{HH}$ = 6.6 Hz, 6H, C^{3}*H* of *i*Pr), 4.83 (br sept, 1H, C^{2}*H* of *i*Pr), 5.11 (br sept, 1H, C^{4}*H* of *i*Pr), 7.44-7.59 (m, 5H, C$^{12/13/14}$*H* of Ph).

$^{13}C\{^1H\}$ NMR (100.61 MHz, 300 K, THF-d_8): δ/ppm = 1.7 (br s, C^{15}H of $AlEt_3$), 10.9 (s, C^{16}H of $AlEt_3$), 22.4 (s, C^1H of *i*Pr), 22.6 (s, C^3H of *i*Pr), 32.8 (d, $^3J_{PC}$ = 6.4 Hz, C^{10}H of *t*Bu), 36.7 (d, $^2J_{PC}$ = 18.1 Hz, C^9 of *t*Bu), 56.5 (s, C^2H of *i*Pr), 56.7 (s, C^4H of *i*Pr), 123.9 (s, C^{11} of Ph), 129.9 (s, C^{13}H of Ph), 131.1 (s, C^{12}H of Ph), 132.0 (s, C^{14}H of Ph), 139.6 (d, $^2J_{PC}$ = 24.9 Hz, C^6), 140.9 (s, C^5), 155.1 (d, $^1J_{PC}$ = 41.2 Hz, C^7), 193.5 (d, $^1J_{PC}$ = 58.9 Hz, C^8).

$^{31}P\{^1H\}$ NMR (162.04 MHz, 300 K, THF-d_8): δ/ppm = 90.3 (s).

$^{27}Al\{^1H\}$ NMR (104.26 MHz, 300 K, THF-d_8): δ/ppm = 170.2 (s, *Al*Et_3).

UV/Vis (THF, λ_{max} / nm, ε_{max} / L·mol^{-1}·cm^{-1}): 290sh (2000).

Elemental analysis calcd. for ($C_{26}H_{43}AlN_5P$) (Mw = 483.62 g·mol^{-1}):
C 64.57, H 8.96, N 14.48; found C 64.56, H 9.12, N 14.20.

[AuCl(2)] (9):

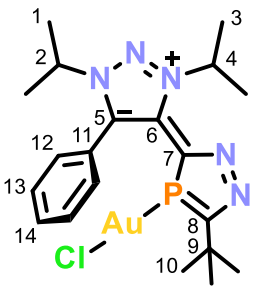

To a mixture of solids **2** (32 mg, 0.087 mmol, 1.0 equiv.) and AuCl(tht) (27.8 mg, 0.087 mmol, 1.0 equiv.) toluene (2 mL) was added. The resulting pale yellow suspension was stirred for 7 h. The solvent was removed *in vacuo*, and the off-white solid was extracted with THF (2 mL) and filtered. Pale yellow crystals of **9**, of sufficient quality for XRD analysis, were grown by slow vapor diffusion of *n*-hexane into this extract over four days. The crystals were washed with *n*-hexane (2 × 0.5 mL) and dried *in vacuo*. The solid contains 0.5 molecules of THF per molecule of compound after drying as indicated by $^1H/^{13}C\{^1H\}$ NMR spectra and elemental analysis.

Yield: 50 mg (96%).

^1H NMR (400.13 MHz, 300 K, THF-d_8): δ/ppm = 1.33 (s, 9H, C^{10}H of *t*Bu), 1.62 (d, $^3J_{HH}$ = 6.6 Hz, C^1H of *i*Pr), 1.72 (d, $^3J_{HH}$ = 6.6 Hz, 6H, C^3H of *i*Pr overlapping with THF-d_8 signal), 4.84 (sept, $^3J_{HH}$ = 6.6 Hz, 1H, C^2H of *i*Pr), 5.94 (br sept, $^3J_{HH}$ = 6.6 Hz, 1H, C^4H of *i*Pr), 7.53-7.62 (m, 5H, C$^{12/13/14}H$ of Ph).

$^{13}C\{^1H\}$ NMR (100.61 MHz, 300 K, THF-d_8): δ/ppm = 22.2 (s, C^1H of *i*Pr), 22.5 (s, C^3H of iPr), 32.7 (d, $^3J_{PC}$ = 6.6 Hz, C^{10}H of *t*Bu), 36.5 (d, $^2J_{PC}$ = 20.3 Hz, C^9 of *t*Bu), 56.3 (s, C^2H of *i*Pr), 57.5 (s, C^4H of *i*Pr), 124.1 (d, $^4J_{PC}$ = 0.8 Hz, C^{11} of Ph), 130.7 (s, C^{13}H of Ph), 131.9 (d, J_{PC} = 1.5 Hz, C^{12}H of Ph). 132.2 (s, C^{14}H of Ph), 138.5 (d, $^2J_{PC}$ = 31.9 Hz, C^6), 139.2 (s, C^5), 153.2 (br d, $^1J_{PC}$ = 25.0 Hz, C^7), 187.6 (br s, C^8).

$^{31}P\{^1H\}$ NMR (161.98 MHz, 300 K, THF-d_8): δ/ppm = 58.5 (br s, $\Delta\nu_{1/2}$ = 136 Hz).

UV/Vis (THF, λ_{max} / nm, ε_{max} /L·mol^{-1}·cm^{-1}): 260sh (10000), 290sh (9000).

Elemental analysis calcd. for $(C_{20}H_{28}N_5PAuCl)\bullet(THF)_{0.5}$ (Mw = 601.87 g·mol^{-1}): C 41.42, H 5.06, N 10.98; found C 41.73, H 5.22, N 10.96.

[Cp*Ru(2)]PF$_6$ (10):

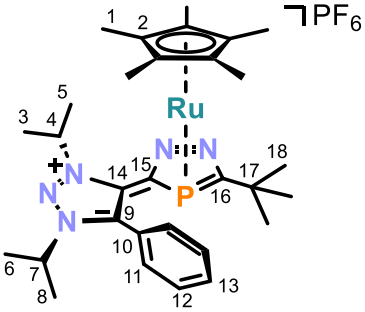

To a mixture of solids **2** (31 mg, 0.061 mmol, 1.0 equiv.) and [Cp*Ru(MeCN)$_3$]PF$_6$ (23 mg, 0.061 mmol, 1.0 equiv.) THF (2 mL) was added and the resulting yellow suspension was heated to 65 °C for one day and filtered. Yellow crystals of **10**, of sufficient quality for XRD analysis, were grown by slow vapor diffusion of *n*-hexane into this filtrate over one week. The crystals were decanted off, washed with *n*-hexane (2 × 0.5 mL) and dried *in vacuo*.

Yield: 27.4 mg (60%).

^{1}H NMR (400.13 MHz, 300 K, THF-d_8): δ/ppm = 1.16 (s, 9H, C^{18}*H* of *t*Bu), 1.49 (d, $^3J_{HH}$ = 6.6 Hz, 3H, C$^{6/8}$*H* of *i*Pr), 1.65 (d, $^3J_{HH}$ = 6.6 Hz, 3H, C$^{6/8}$*H* of *i*Pr), 1.76 (d, $^3J_{HH}$ = 6.4 Hz, 3H, C$^{3/5}$*H* of *i*Pr), 1.78 (s, 15H, C^1*H* of Cp*), 1.92 (d, $^3J_{HH}$ = 6.6 Hz, 3H, C$^{3/5}$*H* of *i*Pr), 4.76 (sept, $^3J_{HH}$ = 6.6 Hz, 1H, C^7*H* of *i*Pr), 6.20 (sept $^3J_{HH}$ = 6.6 Hz, 1H, C^4*H* of *i*Pr), 7.69-7.73 (br m, 5H, C$^{11/12/13}$*H* of Ph).

^{13}C{^{1}H} NMR (161.98 MHz, 300 K, THF-d_8): δ/ppm = 11.2 (s, *C*^{1}H of Cp*), 21.6 (s, *C*$^{3/5}$H of *i*Pr), 21.8 (s, *C*$^{6/8}$H of *i*Pr), 22.1 (s, *C*$^{6/8}$H of *i*Pr), 23.6 (s, *C*$^{3/5}$H of *i*Pr), 31.5 (d, $^3J_{PC}$ = 5.9 Hz, *C*^{18}H of *t*Bu), 35.1 (d, $^2J_{PC}$ = 14.0 Hz, *C*^{17} of *t*Bu), 57.4 (s, *C*^{7}H of *i*Pr), 60.1 (s, *C*^{4}H of *i*Pr), 92.7 (s, *C*^{2} of Cp*), 111.1 (d, $^1J_{PC}$ = 79.1 Hz, *C*^{15}), 123.7 (d, $^4J_{PC}$ = 4.2 Hz, *C*^{10} of Ph), 130.7 (s, *C*$^{11/12}$H of Ph), 131.8 (br s, *C*$^{11/12}$H of Ph), 132.9 (s, *C*^{13}H of Ph), 137.8 (d, $^2J_{PC}$ = 19.4 Hz, *C*^{14}), 139.7 (s, *C*^{9}), 151.8 (d, $^1J_{PC}$ = 79.1 Hz, *C*^{16}).

^{31}P{^{1}H} NMR (161.98 MHz, 300 K, THF-d_8): δ/ppm = −143.5 (sept, $^1J_{PF}$ = 710.6 Hz, 1P, *P*F$_6^-$), −48.6 (s, 1P, N$_2$C$_2$*P*).

^{19}F{^{1}H} NMR (376.50 MHz, 300 K, THF-d_8): δ/ppm = −72.5 (d, $^1J_{PF}$ = 711.6 Hz, P*F*$_6^-$).

UV/Vis (THF, λ_{max} / nm, ε_{max} /L·mol^{-1}·cm^{-1}): 290 (9000), 330sh (5000).

TOF-MS (ESI, MeCN): m/z(%) calcd. for $C_{30}H_{43}N_5PRu^+$ [M$^+$]: 606.2308; found: 606.1675.

Elemental analysis calcd. for $(C_{30}H_{43}N_5F_6P_2Ru)$ (Mw = 750.71 g·mol^{-1}): C 48.00, H 5.77, N 9.33; found C 48.92, H 5.87, N 9.14.

[Ni(C$_{14}$H$_{23}$N$_5$P)(Ph)(2)] (11):

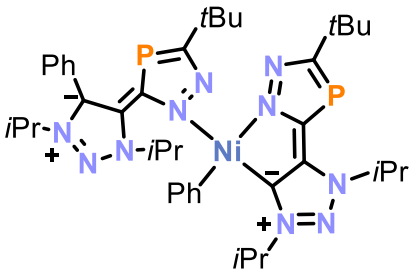

To a mixture of solids **2** (52 mg, 0.141 mmol, 1.0 equiv.) and [Ni(cod)$_2$] (50 mg, 0.183 mmol, 1.3 equiv.) toluene (2 mL) was added. The resulting dark brown suspension was heated to 60 °C for 5 h and filtered over a pad of celite (1 × 0.5 cm). Volatiles were removed *in vacuo* and the resulting dark brown residue was extracted with *n*-hexane (8 × 1.0 mL). The combined extracts were exposed to daylight for one week to decompose excess [Ni(cod)$_2$] and filtered. Concentration to one third of the original volume and standing for one week at room temperature afforded pale yellow crystals of **11**, of sufficient quality for XRD analysis. The supernatant was decanted, and the crystals were dried *in vacuo*. Elemental analysis, 2D-spectra, and ^{13}C{^{1}H} NMR were not recorded due to the high sensitivity and low amount of the isolated solid.

Yield: 5 mg (9%).

^{1}H NMR (400.30 MHz, 300 K, C_6D_6): δ/ppm = 0.82-0.96 (m, 12H, C*H* of *i*Pr), 1.05-1.14 (m, 12H, C*H* of *i*Pr), 1.71 (s, 9H, C*H* of *t*Bu), 1.81 (s, 9H, C*H* of *t*Bu), 3.08 (br sept, 1H, C*H* of *i*Pr), 3.08 (br sept, 1H, C*H* of *i*Pr), 3.83 (br sept, 1H, C*H* of *i*Pr), 4.02 (sept, $^3J_{HH}$ = 6.7 Hz, 1H, C*H* of *i*Pr), 4.97 (sept, $^3J_{HH}$ = 6.6 Hz, 1H, C*H* of *i*Pr), 5.98-5.99 (br m, 2H, C*H* of Ph), 6.51-7.08 (m, 7H, C*H* of Ph), 8.21-8.23 (m, 1H, C*H* of Ph).

^{31}P{^{1}H} NMR (162.04 MHz, 300 K, C_6D_6): δ/ppm = 54.7 (s, 1P, $C_{14}H_{23}N_5P$), 87.5 (s, 1P, **2**).

UV/Vis (THF, λ_{max} / nm, ε_{max} / L·mol^{-1}·cm^{-1}): 250 (37000), 310 (10000), 330sh (10000).

LIFDI-MS (LC-QTOF, toluene): m/z(%) calcd. for $C_{40}H_{56}N_{10}NiP_2$:
796.35; found: 796.30.

[(IPr)Ni($C_2H_4SiMe_3$)($C_{17}H_{21}N_5P$)] (12):

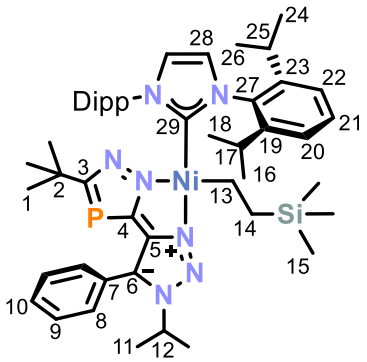

To a mixture of solids **2** (18 mg, 0.049 mmol, 1.0 equiv.) and [(IPr)Ni(vtms)$_2$] (44 mg, 0.068 mmol, 1.4 equiv.) toluene (4 mL) was added. The resulting suspension was stirred at 65 °C for 11 d. Volatiles were removed *in vacuo*, and the resulting yellow residue was extracted with Et_2O (3 × 1 mL) and filtered. Pale yellow crystals of **12**, of sufficient quality for XRD analysis, were grown by storing this extract for one day at −35 °C. The supernatant was decanted, and the crystals were dried *in vacuo*.

Yield: 24 mg (56%).

^{1}H NMR (400.13 MHz, 300 K, C_6D_6): δ/ppm = 0.09-0.13 (m, 2H, C^{14}*H*), 0.17 (s, 9H, C^{15}*H* of $SiMe_3$), 0.83 (d, $^3J_{HH}$ = 6.6 Hz, 1H, C^{11}*H* of *i*Pr), 0.98-1.08 (m, 14H, d ($^3J_{HH}$ = 6.8 Hz) of C^{24}*H* from *i*Pr overlapping with m of C^{13}*H* overlapping with d ($^3J_{HH}$ = 6.6 Hz) of C^{16}*H* from *i*Pr), 1.28 (d, $^3J_{HH}$ = 6.8 Hz, 6H, C^{18}*H* of *i*Pr), 1.44 (d, $^3J_{HH}$ = 6.7 Hz, 6H, C^{26}*H* of *i*Pr), 1.72 (s, 9H, C^{1}*H* of *t*Bu), 2.61 (sept, $^3J_{HH}$ = 6.8 Hz, 2H, C^{25}*H* of *i*Pr), 3.79 (sept, $^3J_{HH}$ = 6.6 Hz, 1H, C^{12}*H* of *i*Pr), 4.29 (sept, $^3J_{HH}$ = 6.7 Hz, 2H, C^{13}*H* of *i*Pr), 6.69 (s, 2H, C^{28}*H* of IPr), 7.02-7.13 (m, 11H, C$^{8/9/10}$*H* of Ph overlapping with C$^{20/21/22}$*H* of IPr).

^{13}C{^{1}H} NMR (100.61 MHz, 300 K, C_6D_6): δ/ppm = –0.3 (s, *C*^{15}H of $SiMe_3$), 0.8 (s, *C*^{13}H), 17.1 (s, *C*^{14}H), 22.3 (s, *C*^{11}H of *i*Pr), 23.3 (s, *C*^{26}H of *i*Pr), 23.4 (s, *C*^{16}H of *i*Pr), 26.5 (s, *C*^{18}H of *i*Pr), 26.8 (s, *C*^{24}H of iPr), 28.3 (s, *C*^{17}H of *i*Pr), 28.7 (s, C^{25}H of *i*Pr), 33.6 (d, $^3J_{PC}$ = 6.4 Hz, *C*^{1}H of *t*Bu), 36.4 (d, $^2J_{PC}$ = 20.2 Hz, *C*^{2} of *t*Bu), 51.3 (s, *C*^{12}H of *i*Pr), 123.6 (s, *C*^{22}H), 124.5 (s, *C*^{28}), 125.5 (s, *C*^{20}H), 126.9 (s, *C*^{7} of Ph), 128.9 (s, *C*$^{8/9}$H of Ph), 129.6 (s, *C*^{10}H of Ph), 129.8 (s, *C*^{21}H), 130.2 (s, *C*$^{8/9}$H of Ph), 130.2 (s, *C*$^{8/9}$H of Ph), 130.6 (s, *C*^{6}), 136.9 (s, *C*^{27}), 146.6 (s, *C*^{23}), 147.7 (d, $^2J_{PC}$ = 24.4 Hz, *C*^{5}), 148.0 (s, *C*^{19}), 164.4 (d, $^1J_{PC}$ = 42.9 Hz, *C*^{4}), 189.6 (s, *C*^{29}), 191.7 (d, $^1J_{PC}$ = 56.3 Hz, *C*^{3}).

^{31}P{^{1}H} NMR (161.98 MHz, 300 K, C_6D_6): δ/ppm = 60.7 (s).

^{29}Si{^{1}H} NMR (79.49 MHz, 300 K**,** C_6D_6): δ/ppm = −4.1 (*Si*Me_3).

UV/Vis (THF, λ_{max} / nm, ε_{max} / L·mol^{-1}·cm^{-1}): 310 (7000).

Elemental analysis calcd. for ($C_{49}H_{70}N_7NiPSi$) (Mw = 874.91 g·mol^{-1}):

C 67.27, H 8.06, N 11.21; found C 67.76, H 8.34, N 11.29.

[(IPr)Co(vtms)($C_{17}H_{21}N_5P$)] (13a):

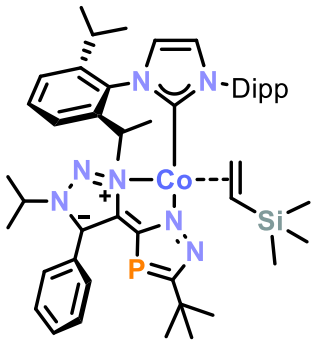

To a mixture of solids **2** (65 mg, 0.176 mmol, 1.0 equiv.) and [(IPr)Co(vtms)$_2$] (125 mg, 0.194 mmol, 1.1 equiv.) toluene (1.5 mL) was added. The light green suspension was stirred at 60 °C for 16 h, resulting in a color change to dark green. Volatiles were removed *in vacuo* and the residue was extracted with Et_2O (3 × 1 mL). The combined extracts were filtered over a plug of celite (1 × 0.5 cm) and concentrated to half of the original volume. Slow evaporation of the resulting light green solution over the course of five days afforded large green crystals, of sufficient quality for analysis by XRD. The supernatant was decanted, and the crystals were dried *in vacuo*.

Yield: 80 mg (52%).

^{1}H NMR (400.13 MHz, 300 K, C_6D_6): δ/ppm = −26.08 (br), −21.09 (br), −8.30 (br), −5.31 (br), −2.05 (br), −1.68 (br), 1.84 (br), 2.28 (br), 2.71 (br), 2.92 (br), 4.03 (br), 4.44 (br), 5.23 (br), 5.49 (br), 5.76 (br), 5.87 (br), 5.92 (br), 6.30 (br), 6.55 (br), 16.88 (br), 21.41 (br), 30.57 (br), 49.28 (br), 96.1 (br).

Evans NMR (400.13 MHz, 300 K, C_6D_6): μ_{eff} = 3.49 μB.

^{31}P{^{1}H} NMR (162.04 MHz, 300 K, C_6D_6): δ/ppm = 462.3 (br s), 490.5 (br s); the latter signal is attributed to a second isomer with a different orientation of the $SiMe_3$ substituent.

^{29}Si{^{1}H} NMR (79.49 MHz, 300 K**,** C_6D_6): No signal was observed in the range −500 - 250 ppm.

UV/Vis (THF, λ_{max} / nm, ε_{max} / L·mol^{-1}·cm^{-1}): 290 (10000), 300 (9000).

Elemental analysis calcd. for ($C_{49}H_{69}CoN_7PSi$) (Mw = 874.13 g·mol^{-1}):
C 67.33, H 7.96, N 11.22; found C 67.57, H 8.22, N 11.09.

[(IMes)Co(vtms)($C_{17}H_{21}N_5P$)] (13b):

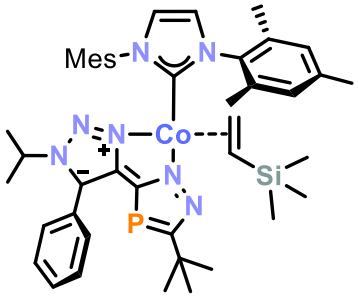

To a mixture of solids **2** (61 mg, 0.165 mmol, 1.0 equiv.) and [(IMes)Co(vtms)$_2$] (100 mg, 0.177 mmol, 1.1 equiv.) benzene (3 mL) was added. The light green suspension was stirred at 60 °C for 1 d, resulting in a color change to dark green. Volatiles were removed *in vacuo* and the resulting yellow residue was washed with *n*-pentane (3 × 1 mL). The residue was extracted with Et_2O (4 × 1 mL) and the combined extracts were filtered over a pad of celite (1 × 0.5 cm). Light green crystals of **13b** were grown by storing the filtrate for four days at room temperature. The supernatant was decanted, and the crystals were dried *in vacuo*. The compound contained fine particles of Co, which could not be removed by recrystallization which is also reflected in the C,H,N analysis.

Yield: 65 mg (50%).

^{1}H NMR (400.13 MHz, 300 K, C_6D_6): δ/ppm = −11.59 (br), −5.75 (br), −1.41 (br), −0.95 (br), 0.04 (br), 0.43 (br), 1.28 (br), 1.74 (br), 2.53 (br), 5.06 (br), 6.00 (br), 6.62 (br), 8.09 (br), 8.27 (br), 9.08 (br), 11.33 (br), 19.29 (br), 32.75 (br), 107.18 (br).

Evans NMR (400.13 MHz, 300 K, C_6D_6): μ_{eff} = 3.5(10) μB.

^{31}P{^{1}H} NMR (162.04 MHz, 300 K, C_6D_6): δ/ppm = 456.3 (br s), 515.5 (br. s); the latter signal is attributed to a second isomer with a different orientation of the $SiMe_3$ substituent.

^{29}Si{^{1}H} NMR (79.49 MHz, 300 K**,** C_6D_6): δ/ppm = No signal was observed in the range −500 - 250 ppm.

UV/Vis (THF, λ_{max} / nm, ε_{max} / L·mol^{-1}·cm^{-1}): 250 (16000), 270 (10000), 290 (10000), 440 (1000).

Elemental analysis calcd. for ($C_{43}H_{57}N_7CoPSi$)(Co) (Mw = 789.97 g·mol^{-1}):
C 60.84, H 6.77, N 11.55; found C 61.38, H 6.63, N 11.85.

[BPh_3(3)] (14):

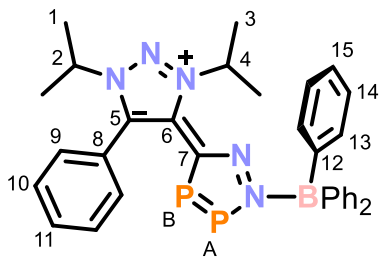

A solution of **3** (40 mg, 0.12 mmol, 1.0 equiv.) in THF (4 mL) was cooled to −35 °C. While stirring, solid BPh_3 (29 mg, 0.12 mmol, 1.0 eq.) was added. The resulting light orange reaction mixture was stirred for 1 h and thawed. Volatiles were removed *in vacuo* and the resulting orange residue was extracted with a toluene/THF mixture (3:1 *v/v*, 4 × 1 mL) and filtered. Pale yellow crystals of **14** of

sufficient quality for XRD analysis were grown by slow vapor diffusion of *n*-hexane into this extract over three days at r.t. and another four days at −35 °C. The crystals were washed with *n*-hexane (3 × 1 mL) and dried *in vacuo*.

Yield: 48 mg (69%).

^{1}H NMR (400.13 MHz, 300 K, THF-d_8): δ/ppm = 1.22 (d, $^{3}J_{HH}$ = 6.6 Hz, 6H, C^{3}H of *i*Pr), 1.59 (d, $^{3}J_{HH}$ = 6.6 Hz, 6H, C^{1}H of *i*Pr), 4.83 (sept, $^{3}J_{HH}$ = 6.6 Hz, 1H, C^{2}H of *i*Pr), 4.96 (sept, $^{3}J_{HH}$ = 6.6 Hz, 1H, C^{4}H of *i*Pr), 6.91-6.94 (m, 3H, C^{15}H of BPh_3), 6.98-7.01 (m, 6H, C^{14}H of BPh_3), 7.20-7.21 (m, 6H, C^{13}H of BPh_3), 7.53-7.54 (m, C^{9}H of Ph), 7.58-7.66 (m, C$^{10/11}H$ of Ph).

^{13}C{^{1}H} NMR (100.61 MHz, 300 K, THF-d_8): δ/ppm = 22.2 (s, C^{3}H of *i*Pr), 22.3 (s, C^{1}H of *i*Pr), 56.4 (s, C^{2}H of *i*Pr), 57.8 (s, C^{4}H of *i*Pr), 124.2 (s, C^{15}H of BPh_3), 124.4 (d, $^{4}J_{PC}$ = 1.8 Hz, C^{8} of Ph), 126.4 (s, C^{14}H of BPh_3), 130.4 (s, C^{10}H of Ph), 131.7 (d, $^{5}J_{PC}$ = 2.3 Hz, C^{9}H of Ph), 132.4 (s, C^{11}H of Ph), 136.0 (s, C^{13}H of BPh_3), 139.7-140.0 (m, d ($^{2}J_{PC}$ = 27.1 Hz) of C^{6} overlapping with s of C^{5}), 158.0 (br s, C^{12} of BPh_3), 160.7 (dd, $^{1}J_{PC}$ = 83.6 Hz, $^{2}J_{PC}$ = 5.0 HZ, C^{7}).

^{31}P{^{1}H} NMR (162.04 MHz, 300 K, THF-d_8): δ/ppm = 216.4 (d, $^{1}J_{PP}$ = 452.7 Hz. 1P, P_B), 380.9 (d, $^{1}J_{PP}$ = 452.7 Hz, 1P, P_A).

^{11}B{^{1}H} NMR (128.43 MHz, 300 K, THF-d_8): δ/ppm = 2.8 (s, BPh_3).

UV/Vis (THF, λ_{max} / nm, ε_{max} / L·mol^{-1}·cm^{-1}): 260 (28000), 300sh (11000).

Elemental analysis calcd. for ($C_{33}H_{34}BN_5P_2$) (Mw = 573.42 g·mol^{-1}):
C 69.12, H 5.98, N 12.21; found C 69.32, H 6.35, N 11.74.

[AlEt$_3$(3)] (15):

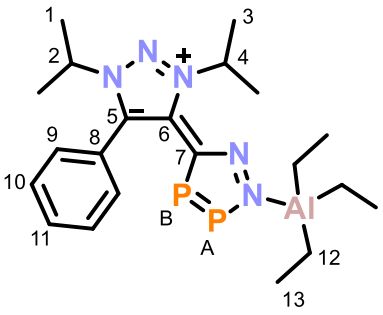

A solution of **3** (35 mg, 0.11 mmol, 1.0 equiv.) in THF (4 mL) was cooled to −35 °C. While stirring, a stock solution of triethylaluminium (56.9 µL, c = 25% by weight in toluene, 0.11 mmol, 1.0 eq.) was added dropwise. The resulting light orange reaction mixture was stirred for 2 h and thawed. Volatiles were removed *in vacuo* and the resulting orange residue was extracted with a toluene/THF mixture (4:1 *v/v*, 2 × 1.25 mL) and filtered. Pale yellow crystals of **15** were grown by slow vapor diffusion of *n*-hexane into this extract over four days at r.t. and another two days at −35 °C. The crystals were of sufficient quality for XRD analysis and were washed with *n*-hexane (2 × 1 mL) and dried *in vacuo*.

Yield: 40 mg (85%).

^{1}H NMR (400.30 MHz, 300 K, THF-d_8): δ/ppm = 0.00 (q, $^{3}J_{HH}$ = 8.1 Hz, C^{12}*H* of $AlEt_3$), 1.05 (t, $^{3}J_{HH}$ = 8.1 Hz, 9H, C^{13}*H* of $AlEt_3$), 1.73-1.77 (m, 12H, d of C^{1}*H* of *i*Pr overlapping with d of C^{3}*H* of *i*Pr), 4.99 (sept, $^{3}J_{HH}$ = 6.7 Hz, C^{2}*H* of *i*Pr), 5.88 (sept, $^{3}J_{HH}$ = 6.6 Hz, C^{4}*H* of *i*Pr), 7.58-7.69 (m, 5H, C$^{9/10/11}$*H* of Ph).

^{13}C{^{1}H} NMR (100.61 MHz, 300 K, THF-d_8): δ/ppm = 2.2 (br s, *C*^{12}H of $AlEt_3$), 11.0 (s, *C*^{13}H of $AlEt_3$), 22.4 (s, *C*^{1}H of *i*Pr), 22.5 (s, *C*^{3}H of *i*Pr), 56.7 (s, *C*^{2}H of *i*Pr), 57.7 (s, *C*^{4}H of *i*Pr), 124.6 (s, *C*^{8} of Ph), 130.4 (s, *C*^{10}H of Ph), 131.8 (s, *C*^{9}H of Ph), 132.3 (s, *C*^{11}H of Ph), 140.3-140.6 (m, d of *C*^{6} overlapping with s of *C*^{5}), 162.8 (d, $^{1}J_{PC}$ = 82.8 Hz, *C*^{7}).

^{31}P{^{1}H} NMR (162.04 MHz, 300 K, THF-d_8): δ/ppm = 217.5 (d, $^{1}J_{PP}$ = 444.0 Hz. 1P, P_B), 364.2 (d, $^{1}J_{PP}$ = 444.0 Hz, 1P, P_A).

UV/Vis (THF, λ_{max} / nm, ε_{max} / L·mol^{-1}·cm^{-1}): 310sh (4000).

Elemental analysis calcd. for ($C_{21}H_{34}AlN_5P_2$) (Mw = 445.46 g·mol^{-1}):
C 56.62, H 7.69, N 15.72; found C 57.05, H 8.07, N 15.58.

6.4.2 NMR Spectra

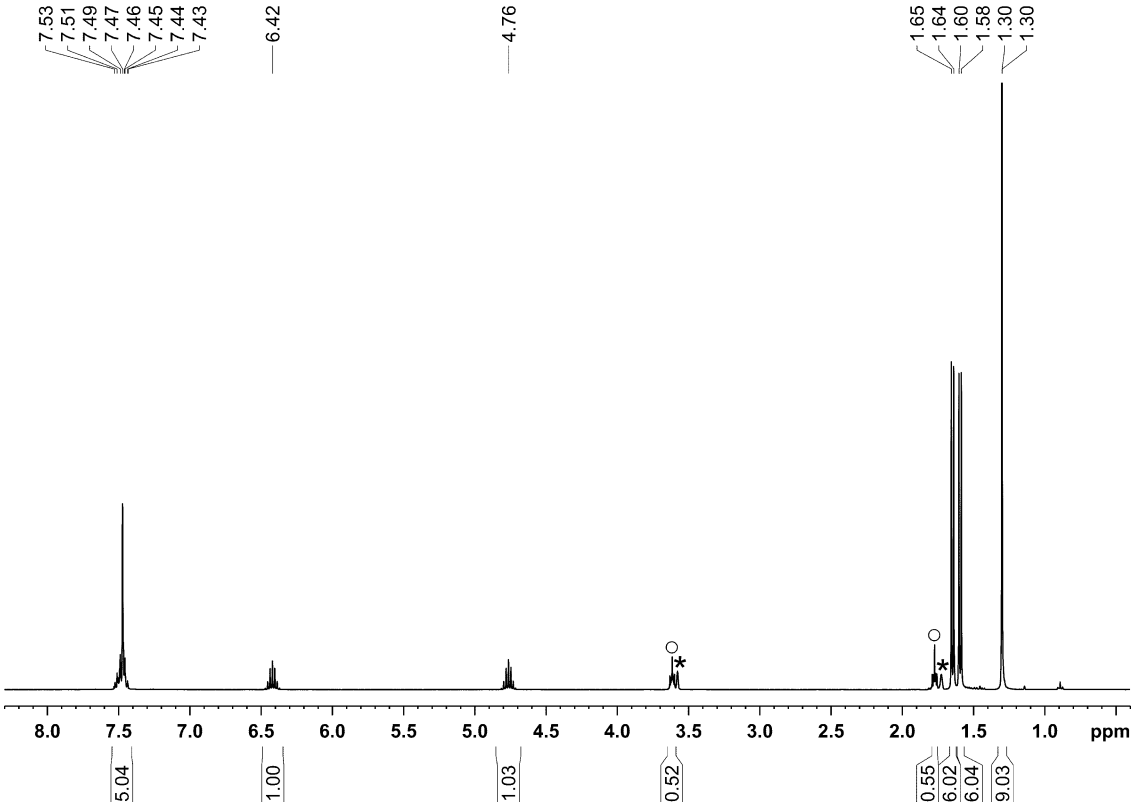

Figure S1. ^{1}H NMR spectrum (400.13 MHz, 300 K, THF-d_8) of **2**; ○ THF, * THF-d_8.

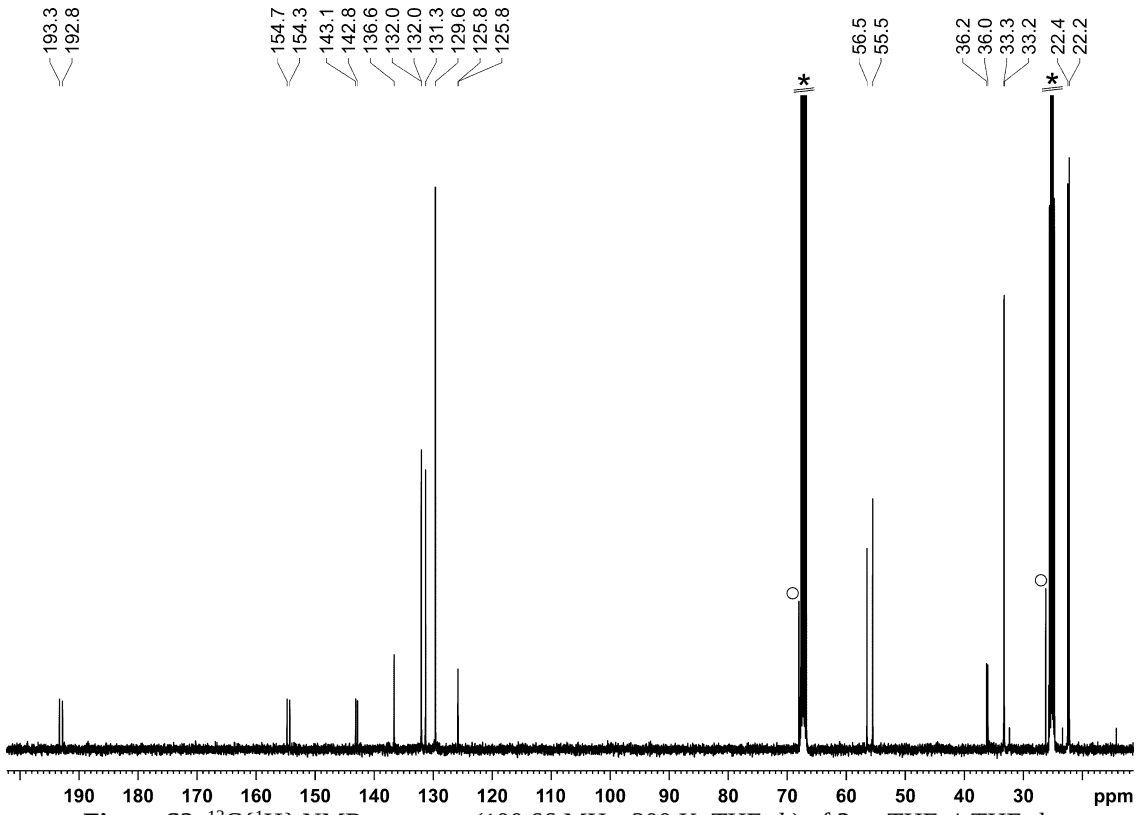

Figure S2. ^{13}C{^{1}H} NMR spectrum (100.66 MHz, 300 K, THF-d_8) of **2**; ○ THF, * THF-d_8.

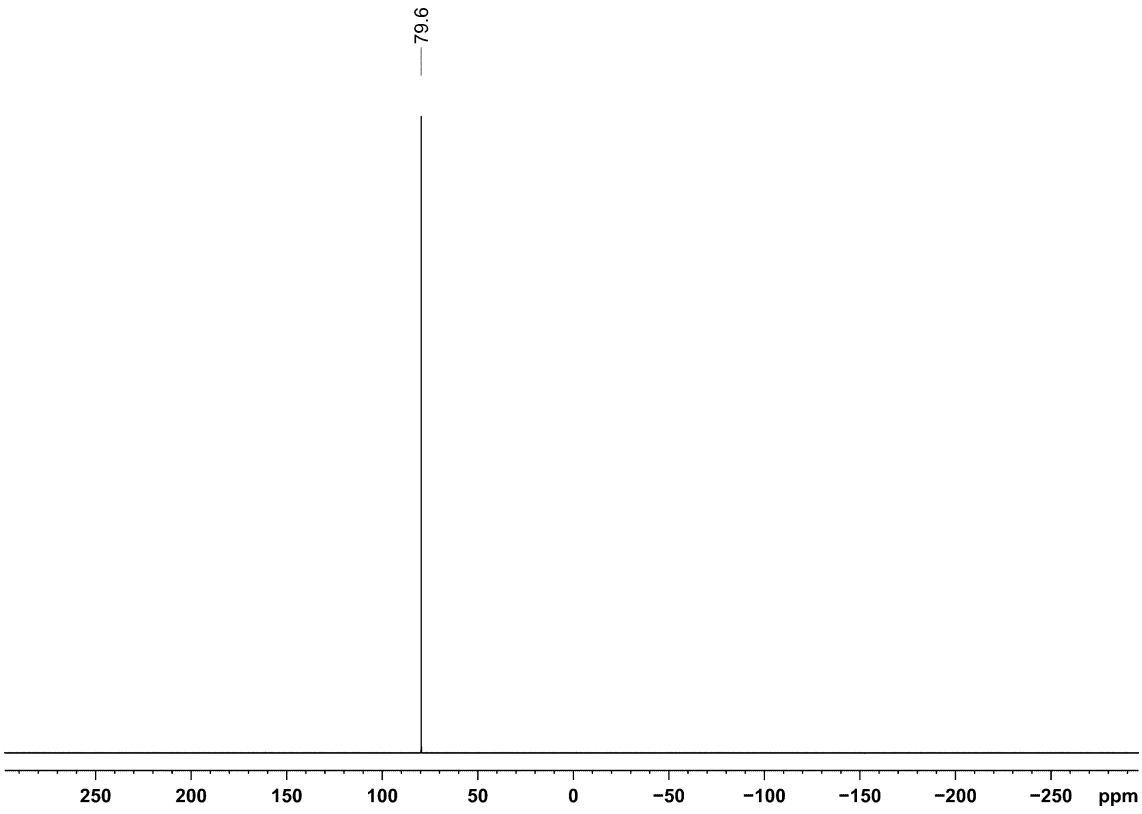

Figure S3. $^{31}P\{^{1}H\}$ NMR spectrum (162.04 MHz, 300 K, THF-d_8) of **2**.

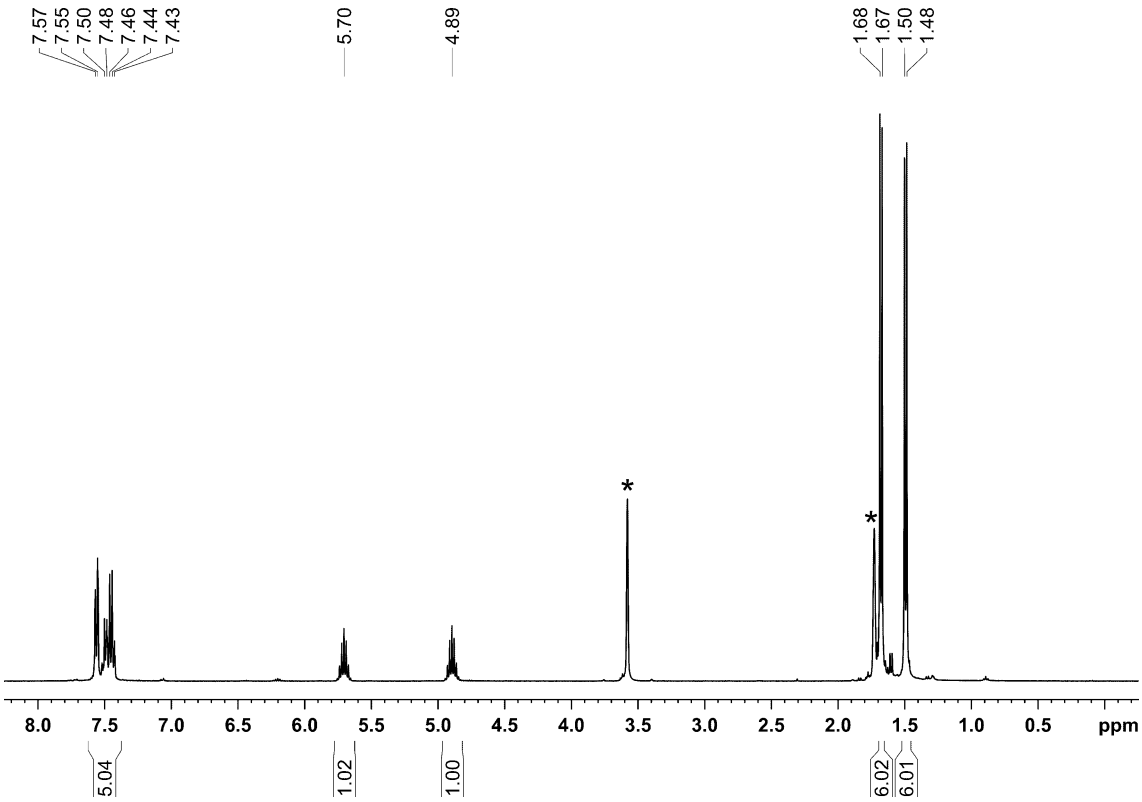

Figure S4. ^{1}H NMR spectrum (400.13 MHz, 300 K, THF-d_8) of **3**; * THF-d_8.

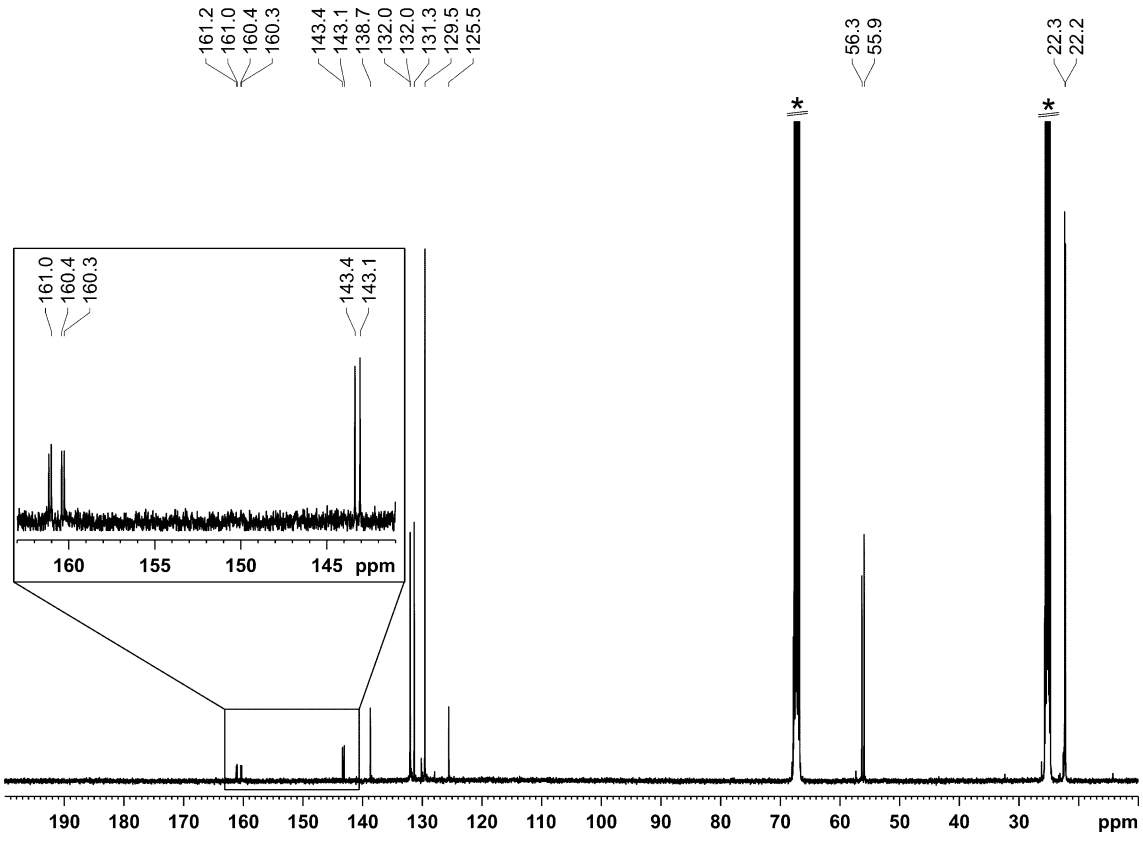

Figure S5. $^{13}C\{^{1}H\}$ NMR spectrum (100.61 MHz, 300 K, THF-d_8) of **3**; * THF-d_8.

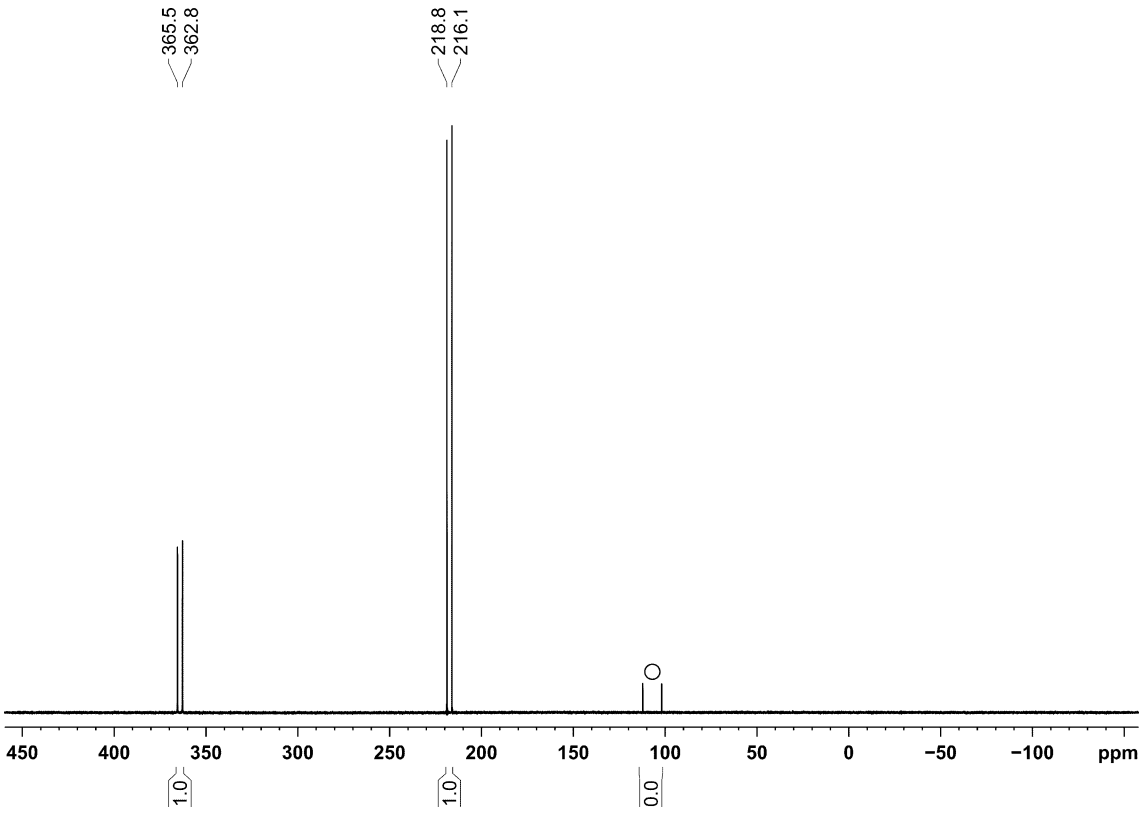

Figure S6. $^{31}P\{^{1}H\}$ NMR spectrum (161.98 MHz, 300 K, THF-d_8) of **3**; ○ minor unknown impurity.

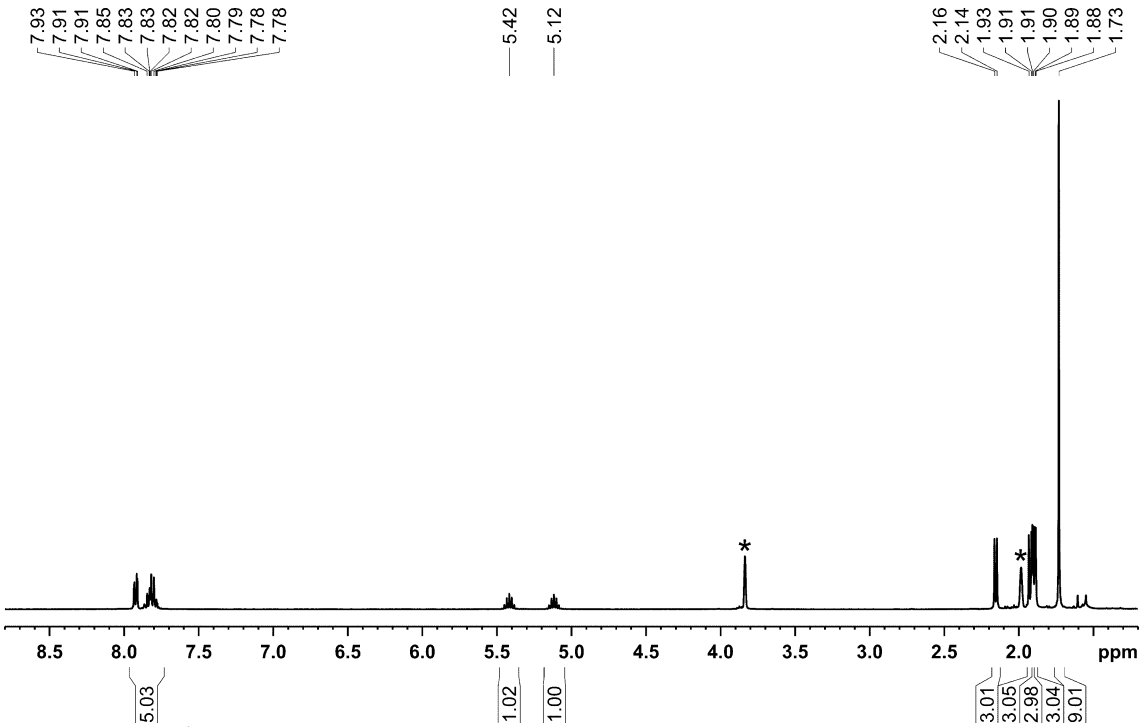

Figure S7. ^{1}H NMR spectrum (400.30 MHz, 300 K, THF-d_8) of [{W(CO)$_5$}$_2$(**2**)] (**6**); * THF-d_8.

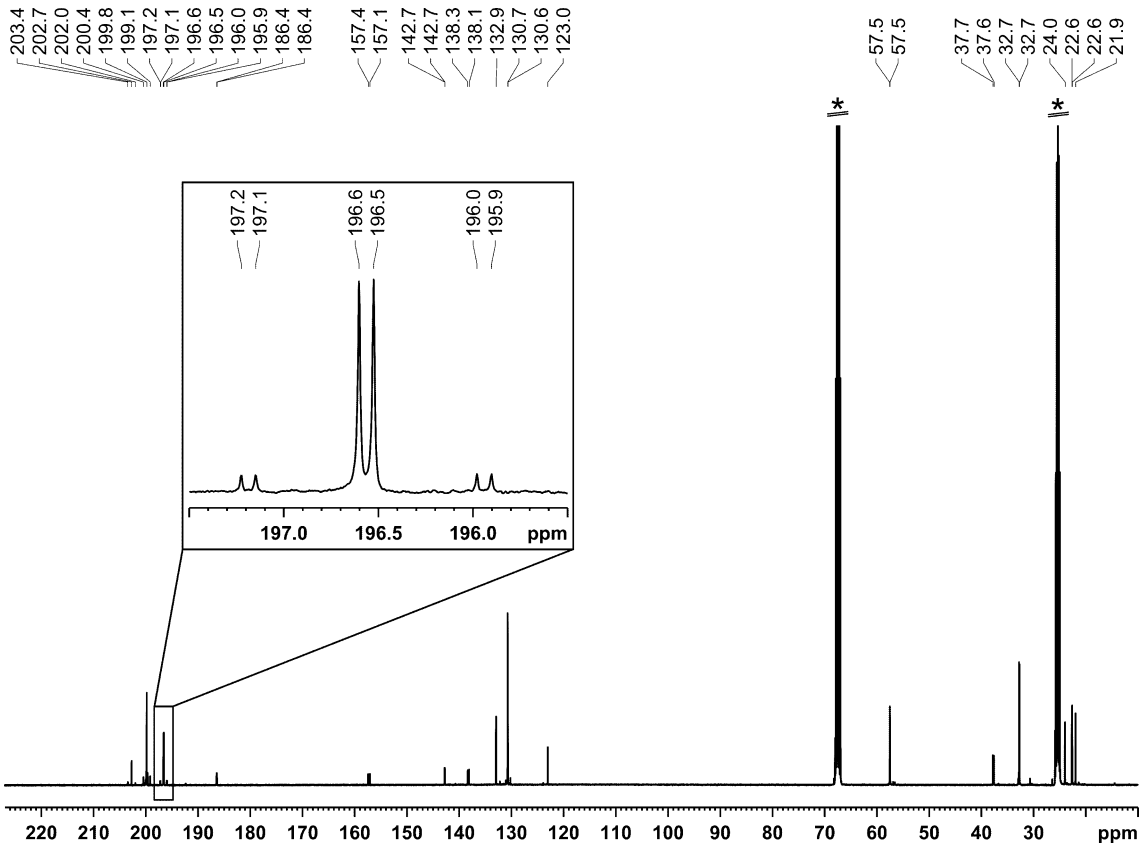

Figure S8. ^{13}C{^{1}H} NMR spectrum (100.61 MHz, 300 K, THF-d_8) of [{W(CO)$_5$}$_2$(**2**)] (**6**); * THF-d_8.

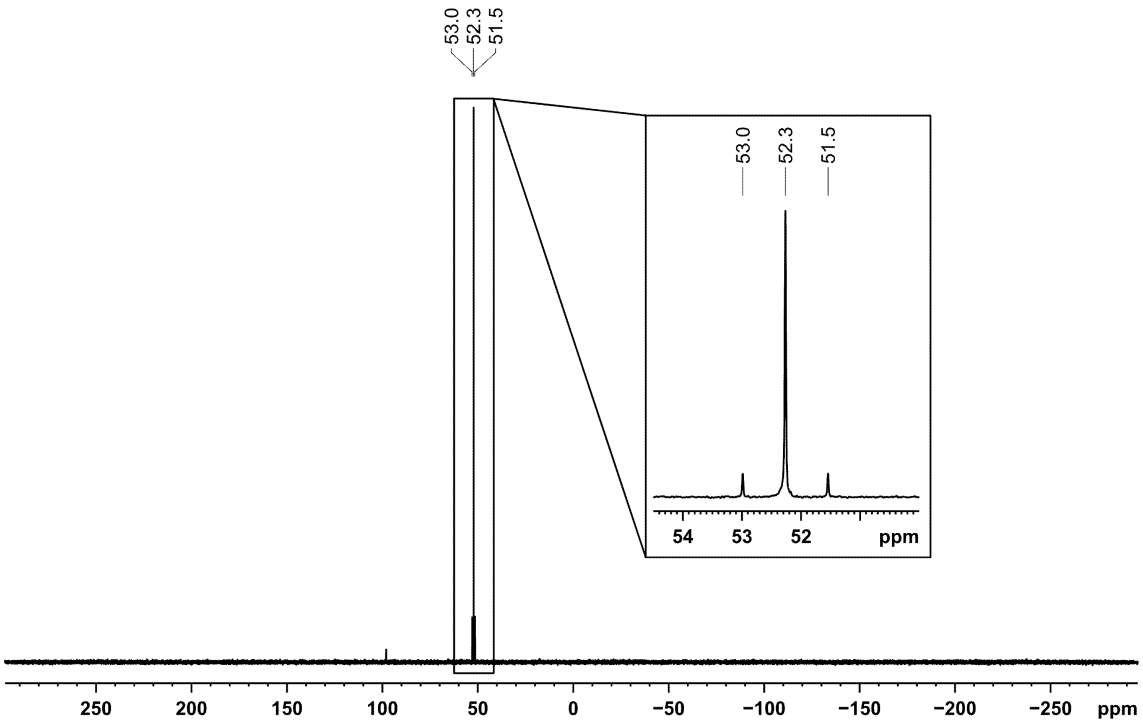

Figure S9. $^{31}P\{^{1}H\}$ NMR spectrum (162.04 MHz, 300 K, THF-d_8) of [{$W(CO)_5$}$_2$(**2**)] (**6**).

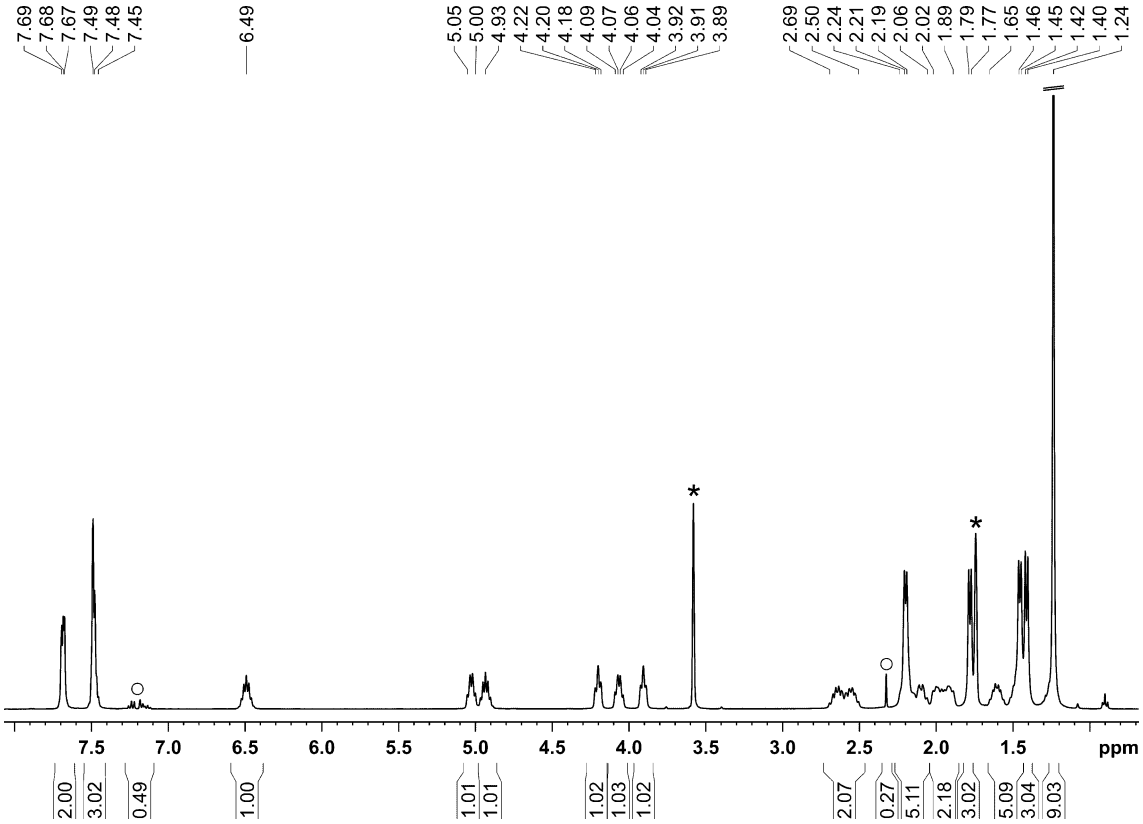

Figure S10. ^{1}H NMR spectrum (400.13 MHz, 193 K, THF-d_8) of [Rh(**2**)(cod)Cl] (**7**); ○ toluene, * THF-d_8.

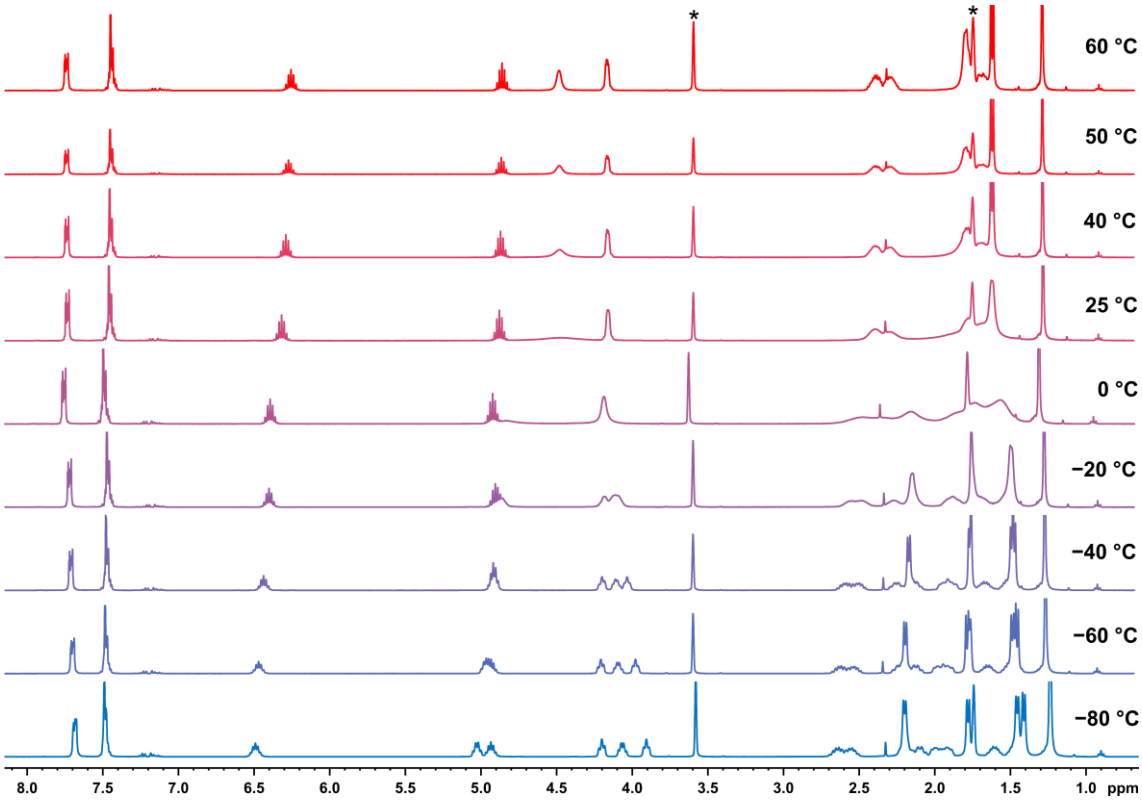

Figure S11. ^{1}H NMR monitoring (400.13 MHz, THF-d_8) of [Rh(**2**)(cod)Cl] (**7**); * THF-d_8.

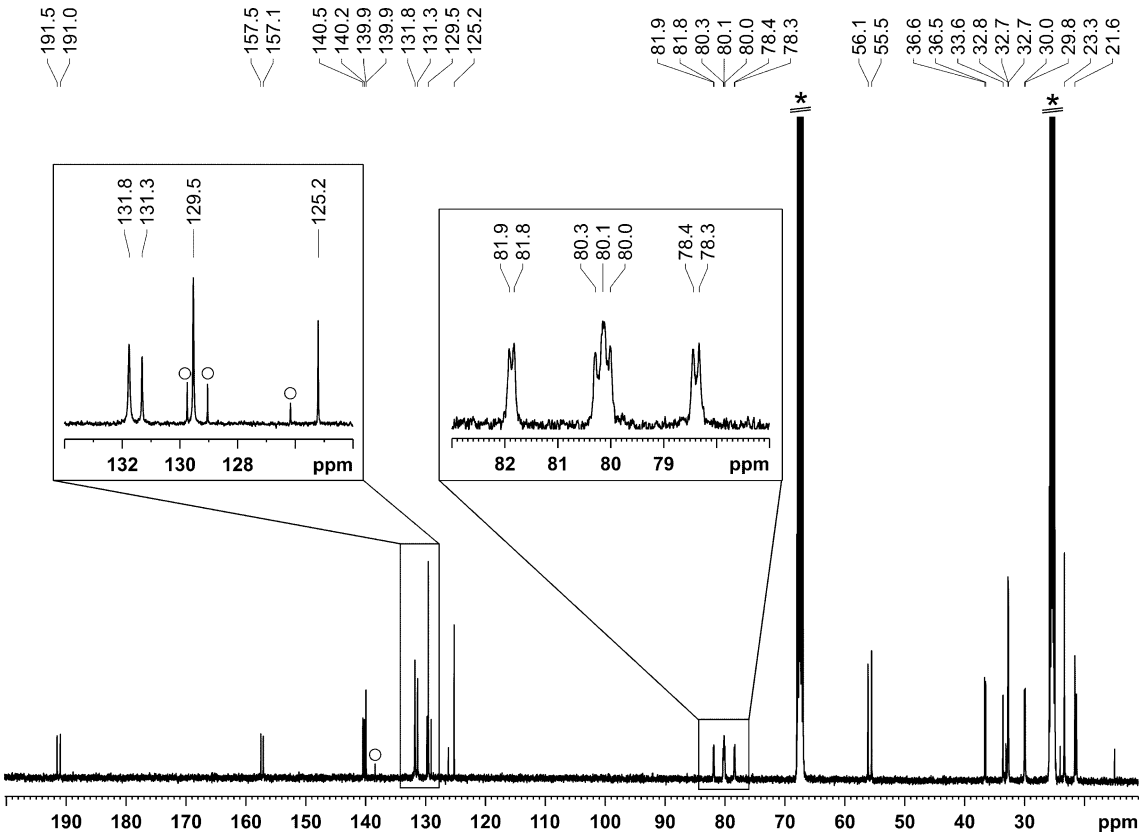

Figure S12. ^{13}C{^{1}H} NMR spectrum (100.61 MHz, 193 K, THF-d_8) of [Rh(**2**)(cod)Cl] (**7**); ○ toluene, * THF-d_8.

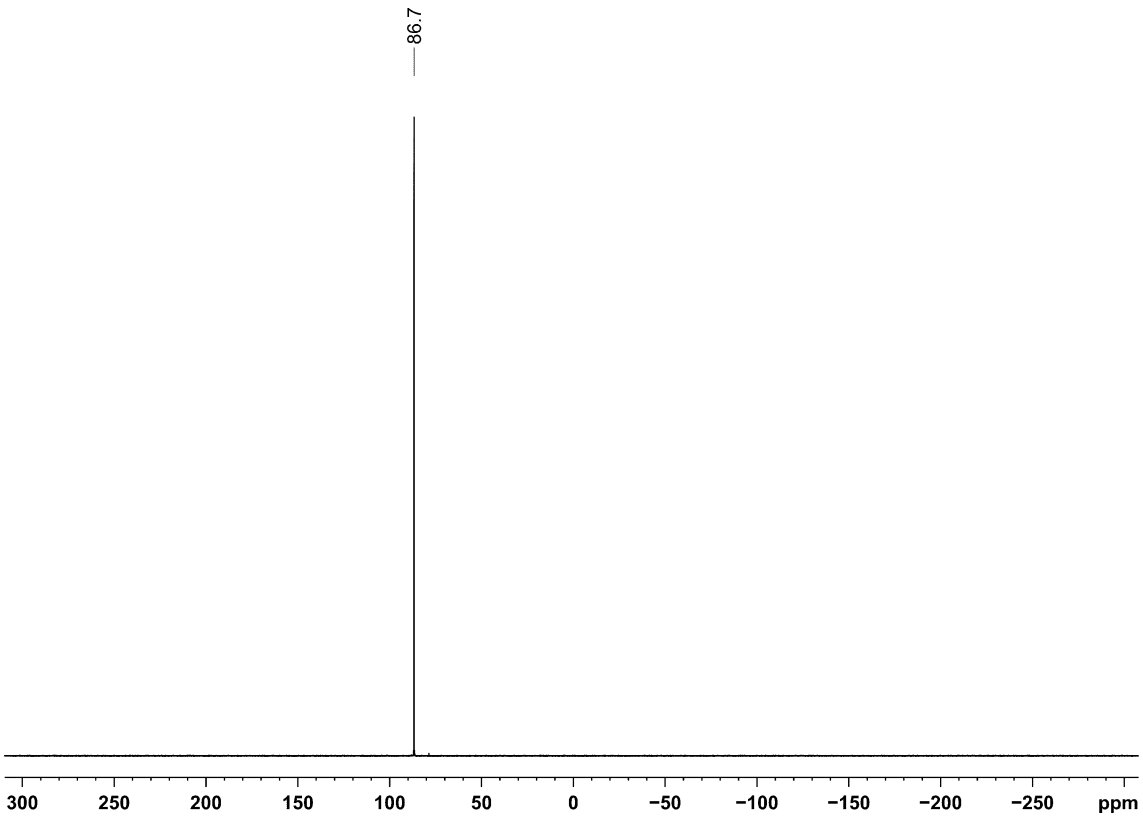

Figure S13. $^{31}P\{^{1}H\}$ NMR spectrum (161.98 MHz, 193 K, THF-d_8) of [Rh(**2**)(cod)Cl] (**7**).

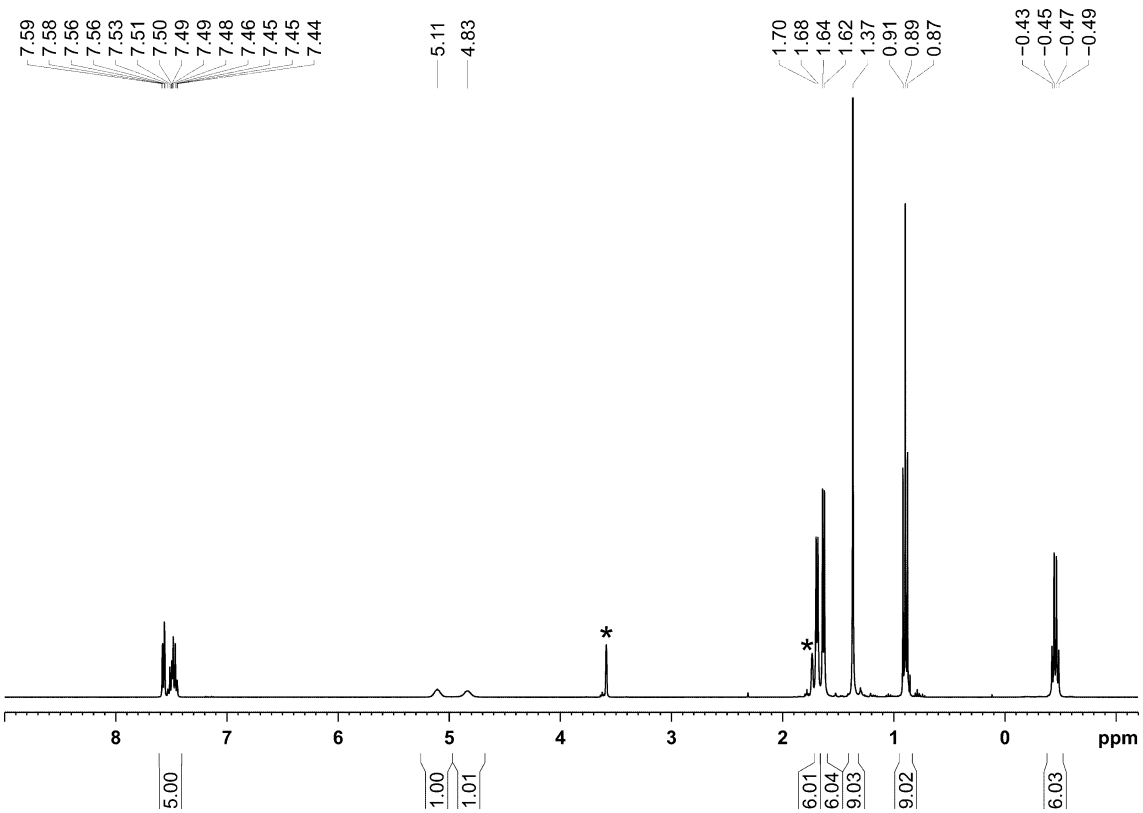

Figure S14. ^{1}H NMR spectrum (400.13 MHz, 300 K, THF-d_8) of [$AlEt_3$(**2**)] (**8**); * THF-d_8.

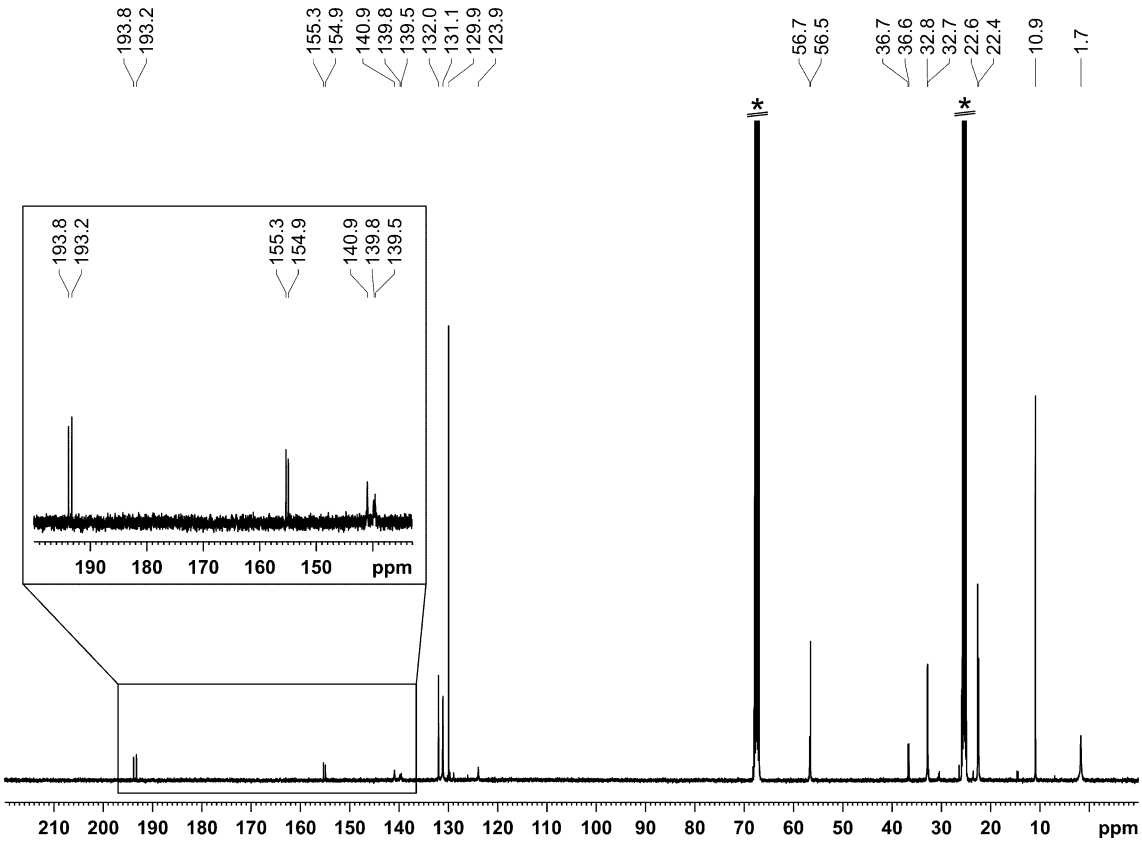

Figure S15. $^{13}C\{^{1}H\}$ NMR spectrum (100.61 MHz, 300 K, THF-d_8) of [$AlEt_3$(**2**)] (**8**); * THF-d_8.

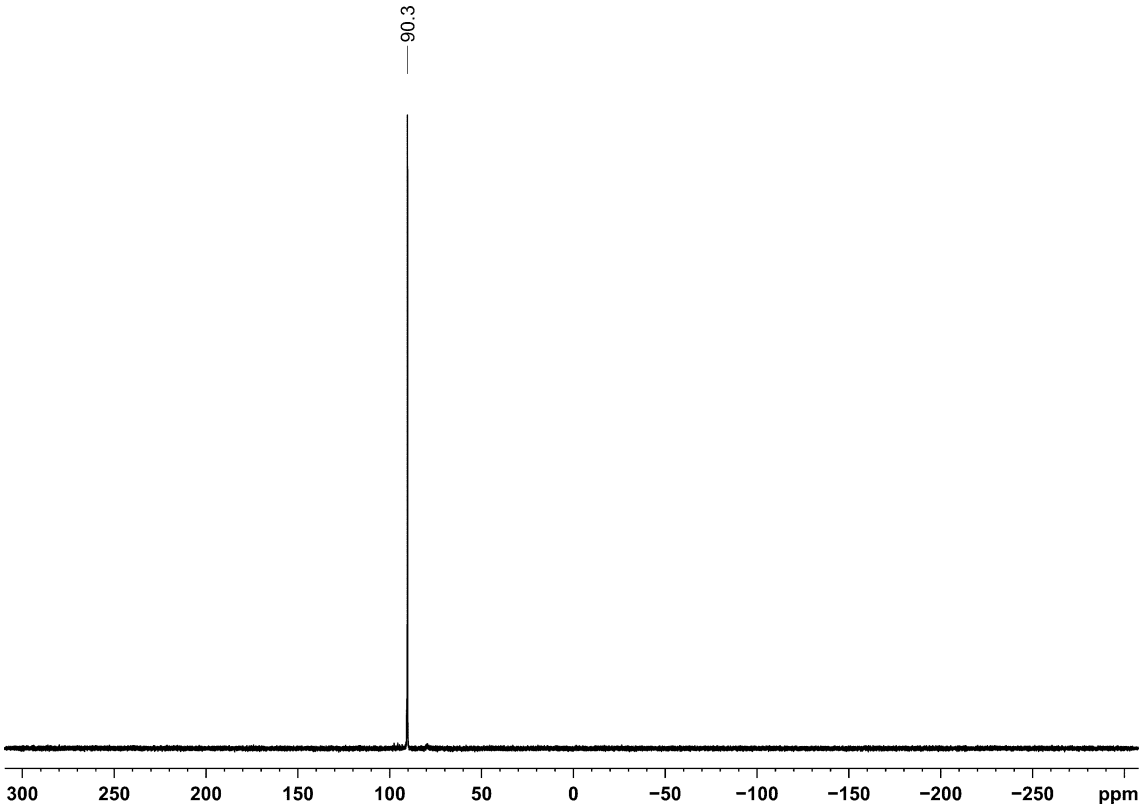

Figure S16. $^{31}P\{^{1}H\}$ NMR spectrum (162.04 MHz, 300 K, THF-d_8) of [$AlEt_3$(**2**)] (**8**).

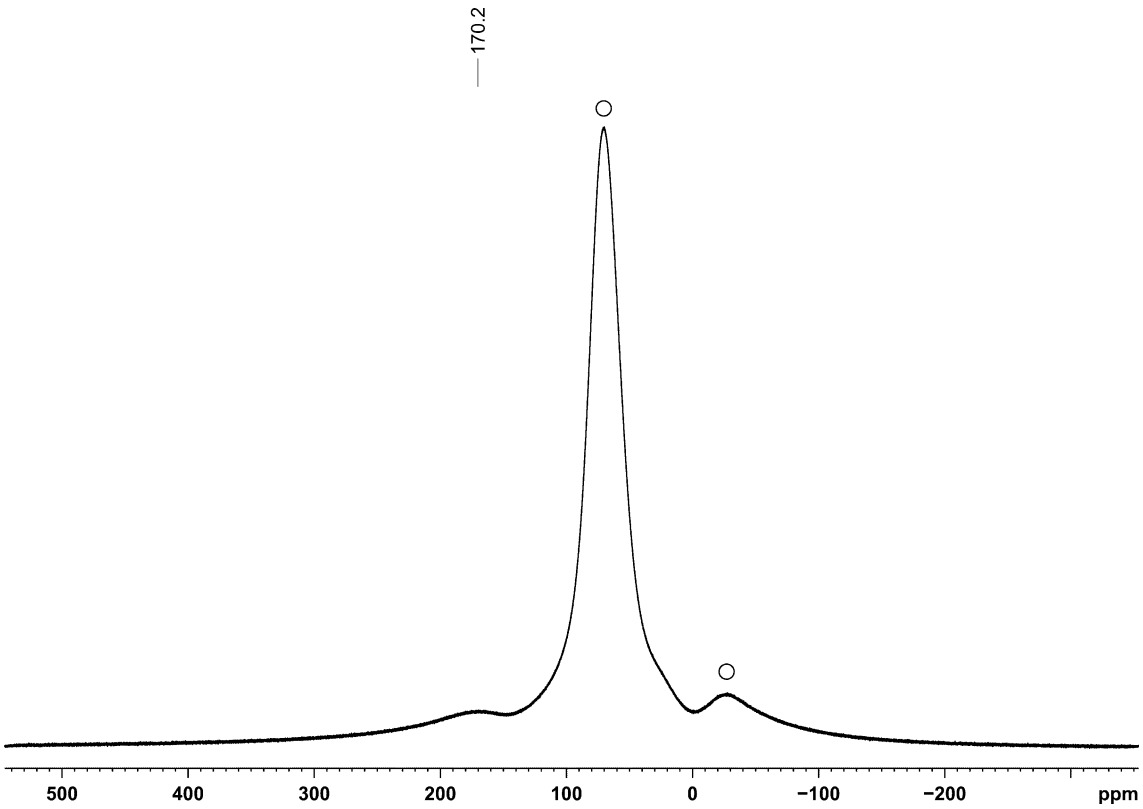

Figure S17. $^{27}Al\{^{1}H\}$ NMR spectrum (104.26 MHz, 300 K, THF-d_8) of [$AlEt_3$(**2**)] (**8**); ○ signal of probe head.

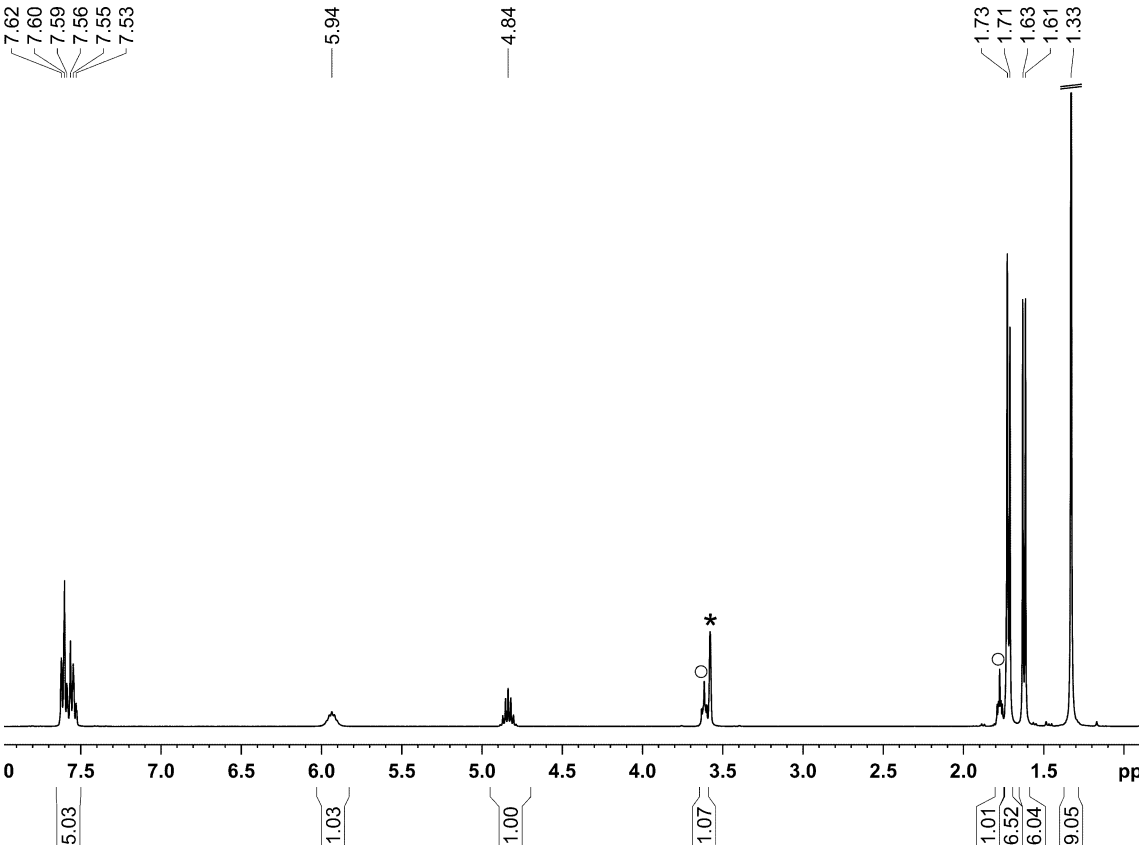

Figure S18. ^{1}H NMR spectrum (400.13 MHz, 300 K, THF-d_8) of [AuCl(**2**)] (**9**); ○ THF, * THF-d_8.

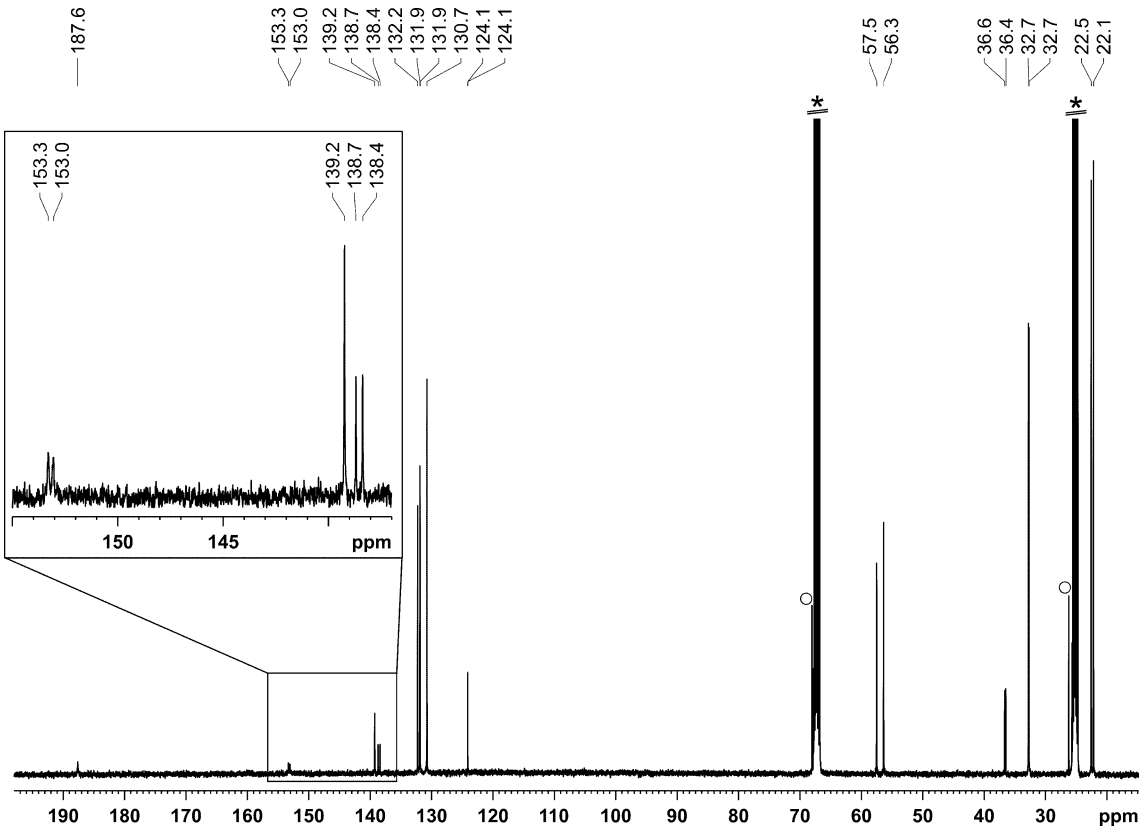

Figure S19. $^{13}C\{^{1}H\}$ NMR spectrum (100.61 MHz, 300 K, THF-d_8) of [AuCl(**2**)] (**9**); ○ THF, * THF-d_8.

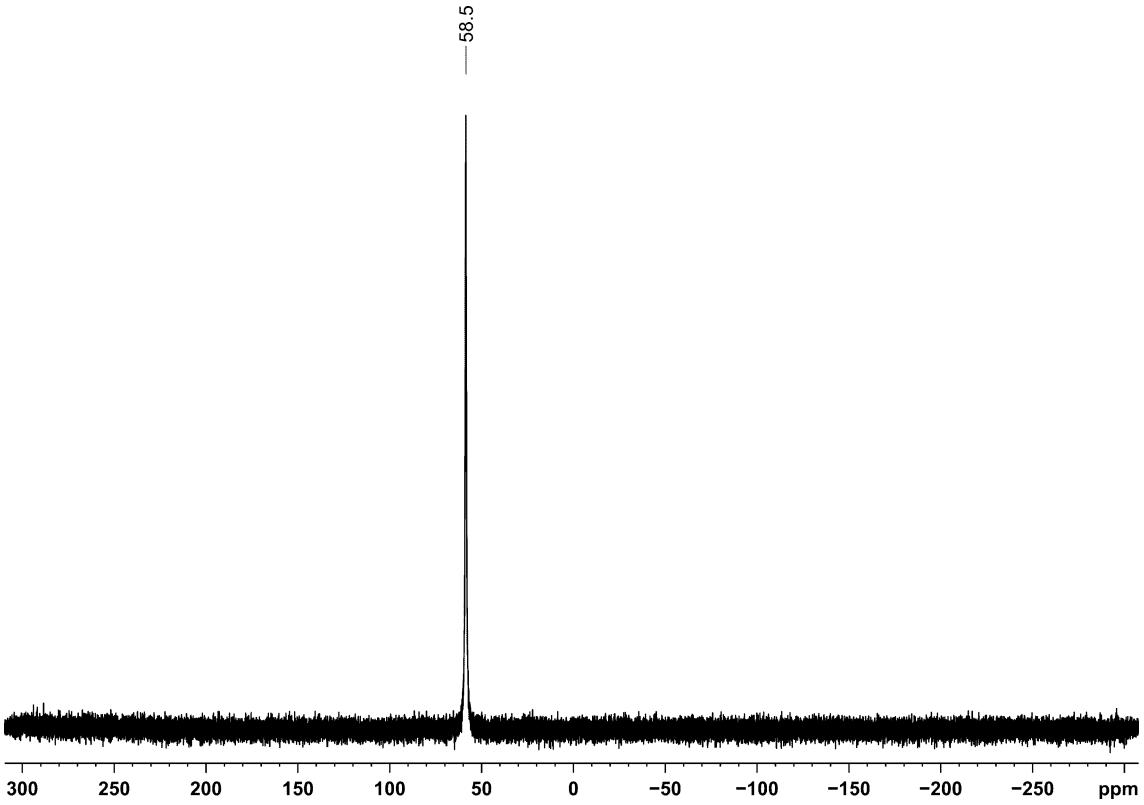

Figure S20. $^{31}P\{^{1}H\}$ NMR spectrum (161.98 MHz, 300 K, THF-d_8) of [AuCl(**2**)] (**9**).

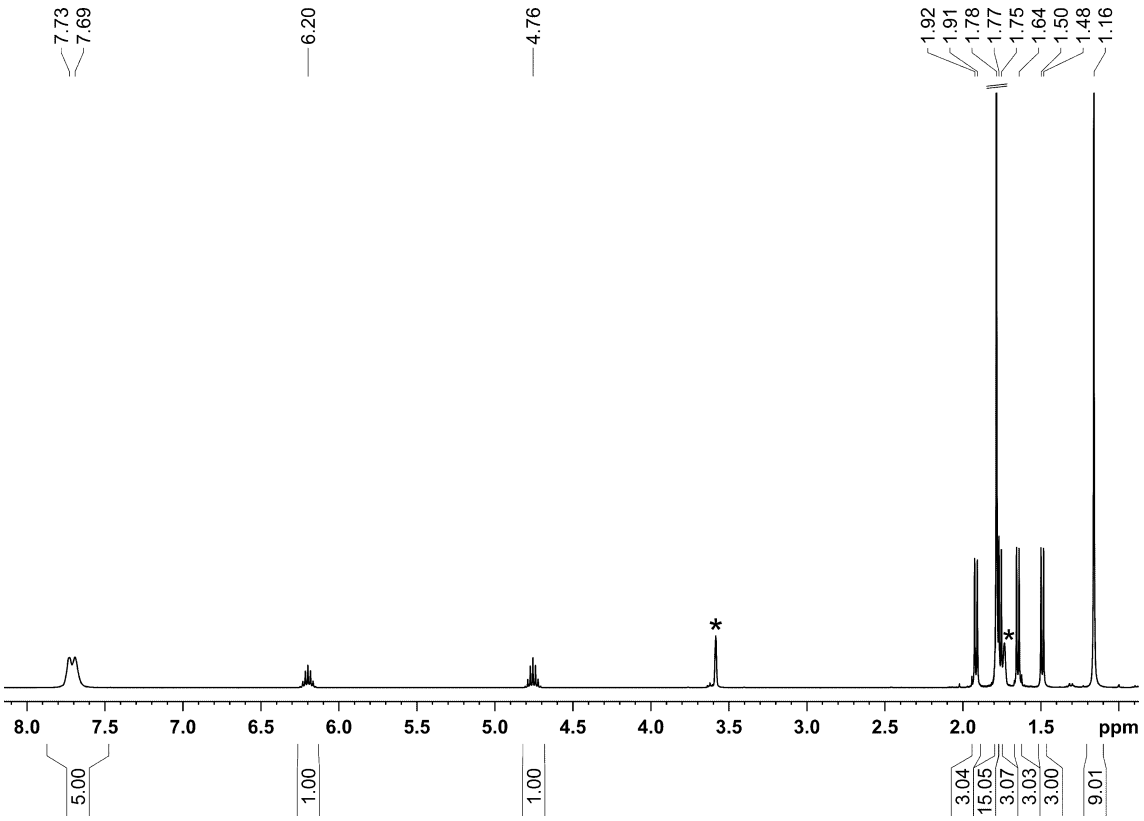

Figure S21. ^{1}H NMR spectrum (400.13 MHz, 300 K, THF-d_8) of [Cp*Ru(**2**)]PF_6 (**10**); * THF-d_8.

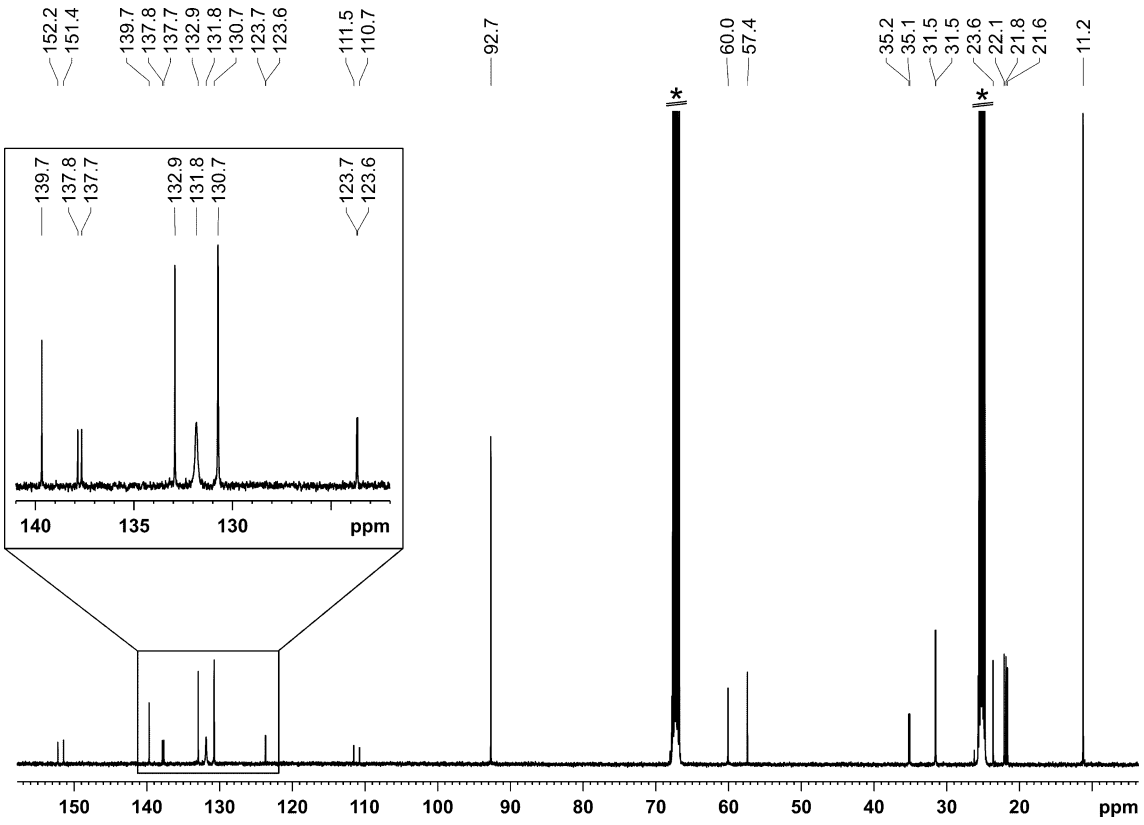

Figure S22. ^{13}C{^{1}H} NMR spectrum (100.61 MHz, 300 K, THF-d_8) of [Cp*Ru(**2**)]PF_6 (**10**); * THF-d_8.

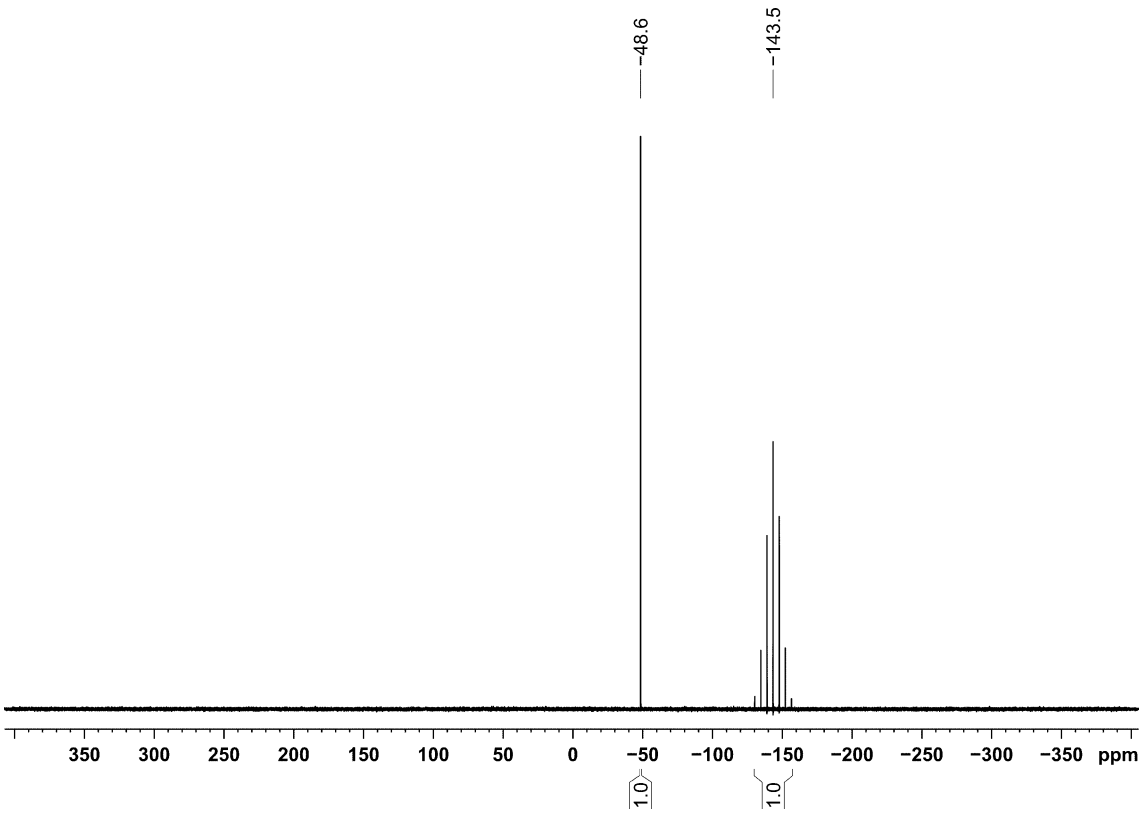

Figure S23. $^{31}P\{^{1}H\}$ NMR spectrum (161.98 MHz, 300 K, THF-d_8) of [Cp*Ru(**2**)]PF_6 (**10**).

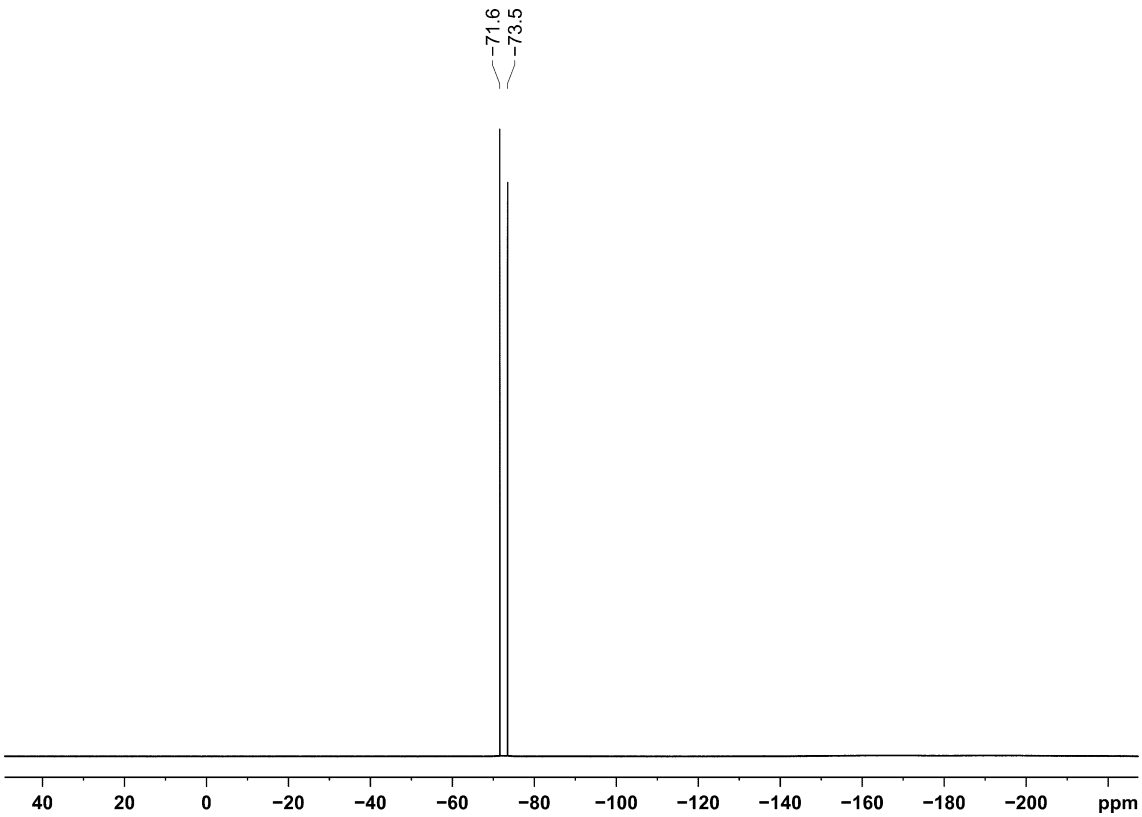

Figure S24. $^{19}F\{^{1}H\}$ NMR spectrum (376.50 MHz, 300 K, THF-d_8) of [Cp*Ru(**2**)]PF_6 (**10**).

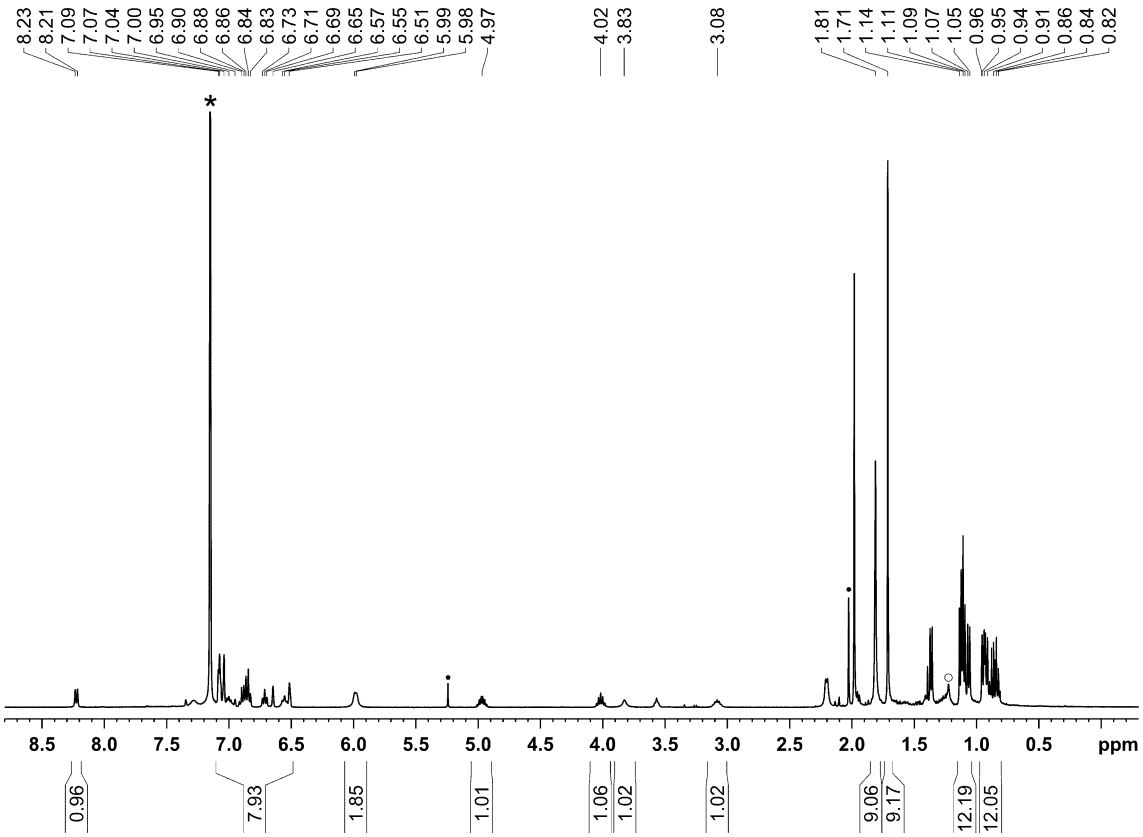

Figure S25. ^{1}H NMR spectrum (400.30 MHz, 300 K, C_6D_6) of [Ni($C_{14}H_{23}N_5P$)(Ph)(**2**)] (**11**); • minor unknown impurity, ○ *n*-hexane, * C_6D_6.

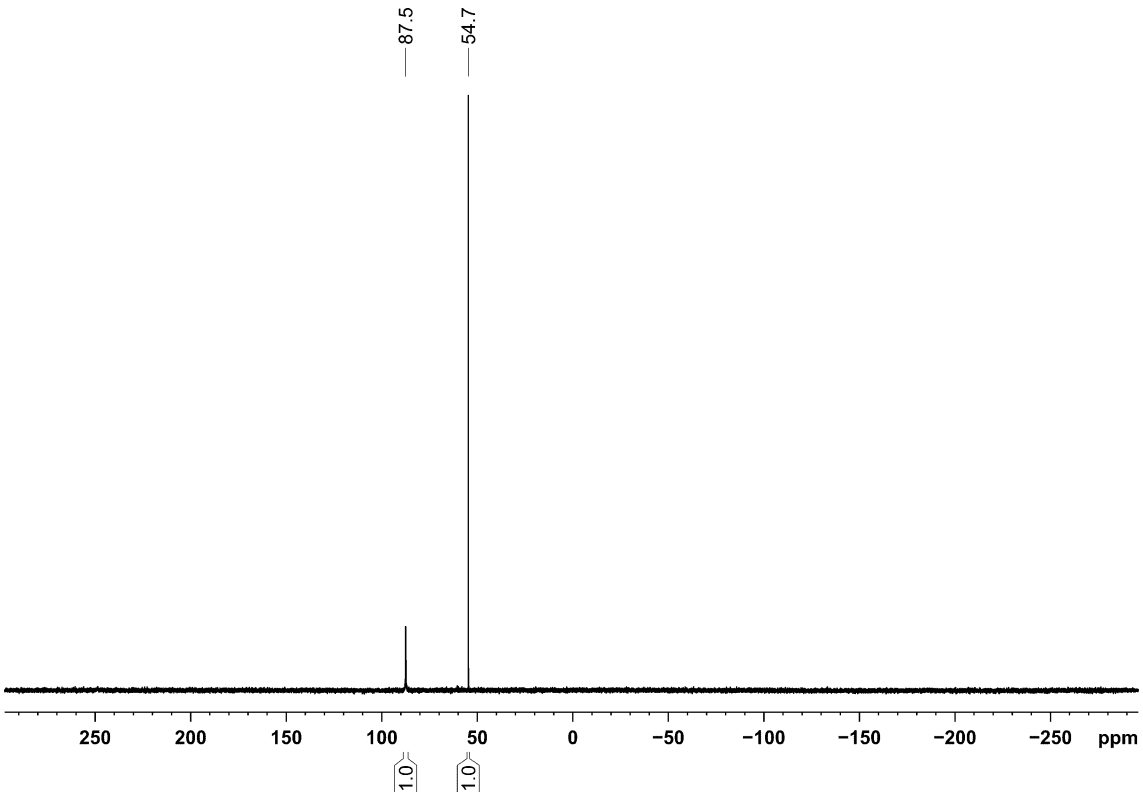

Figure S26. $^{31}P\{^{1}H\}$ NMR spectrum (162.04 MHz, 300 K, C_6D_6) of [Ni($C_{14}H_{23}N_5P$)(Ph)(**2**)], (**11**).

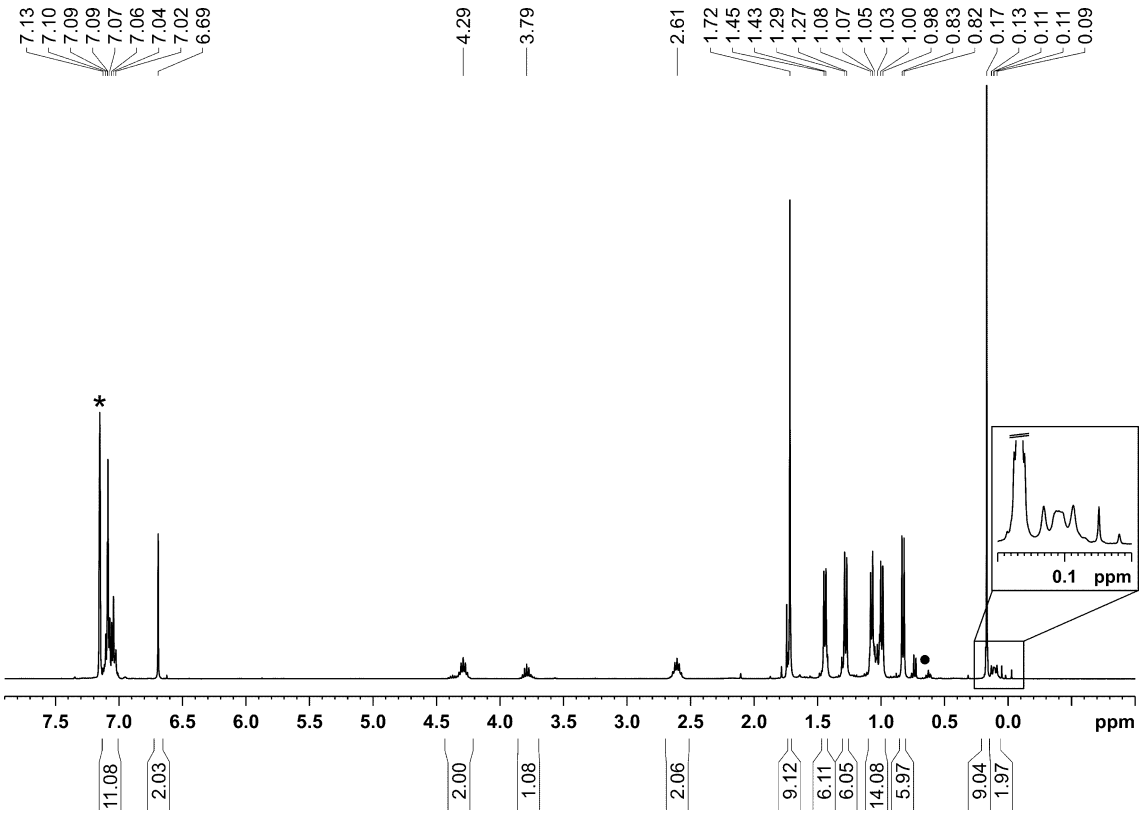

Figure S27. ^{1}H NMR spectrum (400.13 MHz, 300 K, C_6D_6) of [(IPr)Ni($C_2H_4SiMe_3$)($C_{17}H_{21}N_5P$)] (**12**); • minor unknown impurity, * C_6D_6.

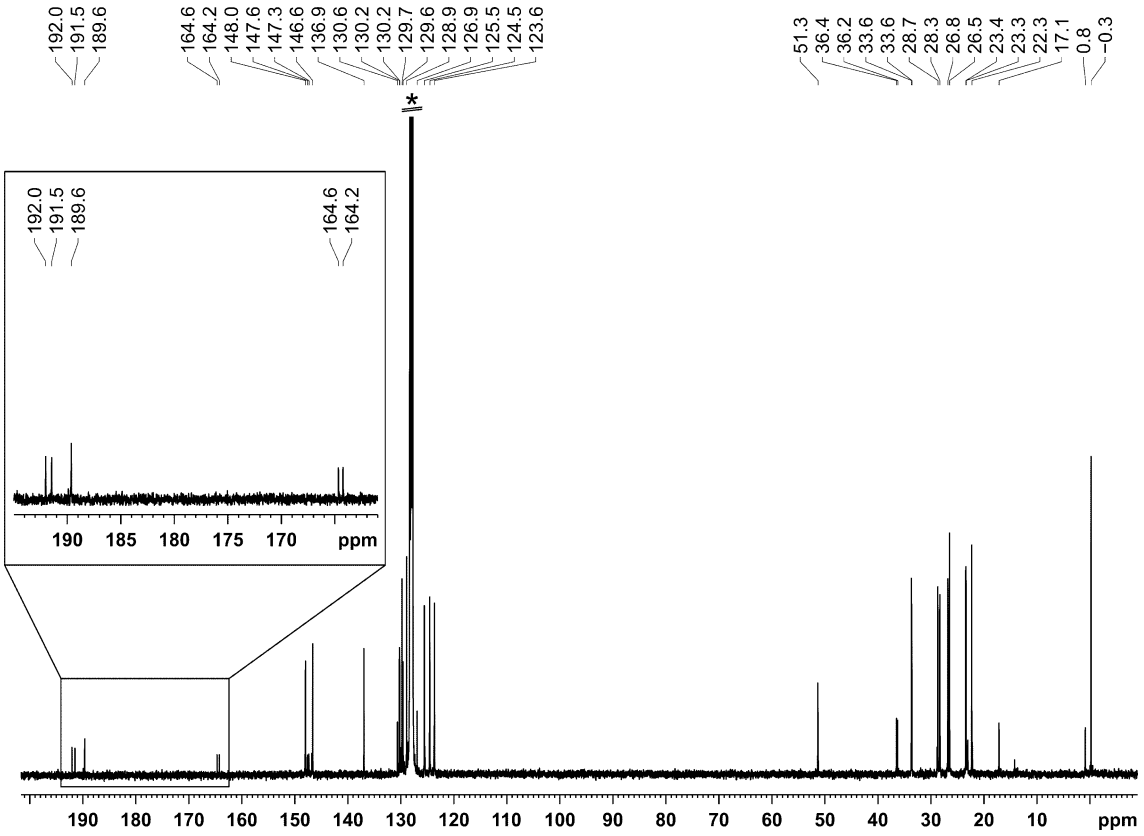

Figure S28. $^{13}C\{^{1}H\}$ NMR spectrum (100.61 MHz, 300 K, C_6D_6) of [(IPr)Ni($C_2H_4SiMe_3$)($C_{17}H_{21}N_5P$)] (**12**); * C_6D_6.

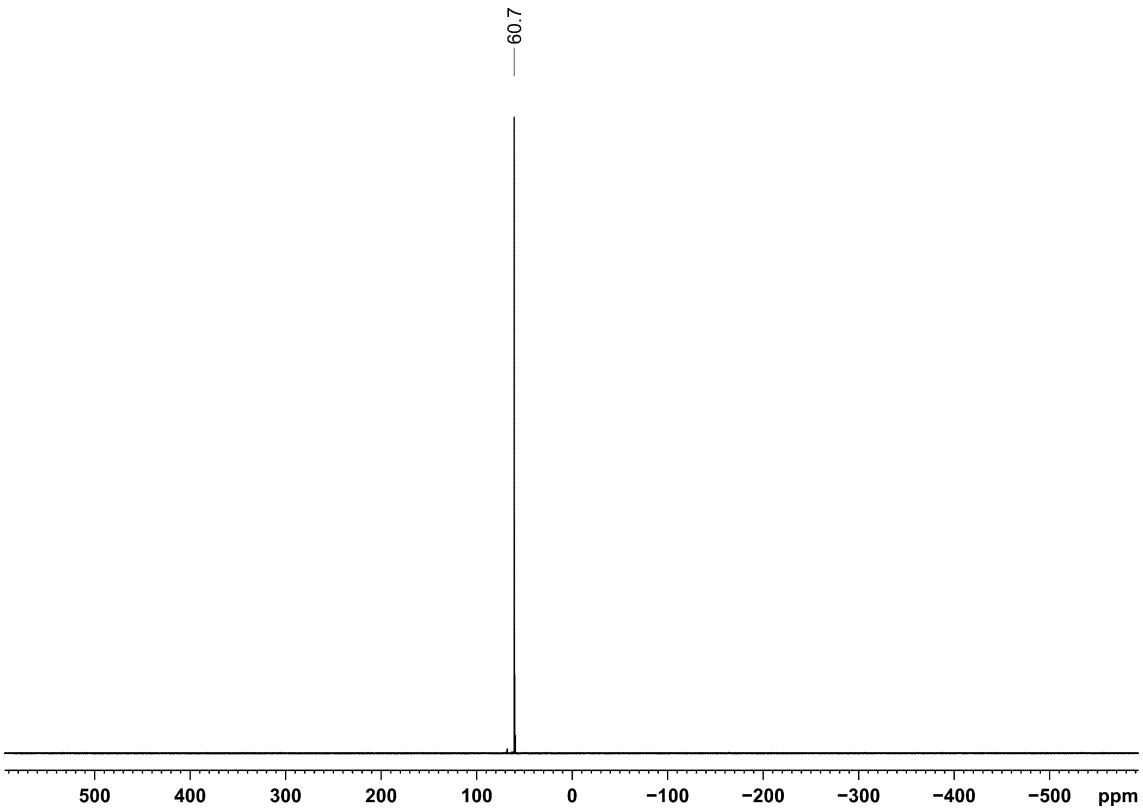

Figure S29. $^{31}P\{^{1}H\}$ NMR spectrum (161.98 MHz, 300 K, C_6D_6) of [(IPr)Ni($C_2H_4SiMe_3$)($C_{17}H_{21}N_5P$)] (**12**).

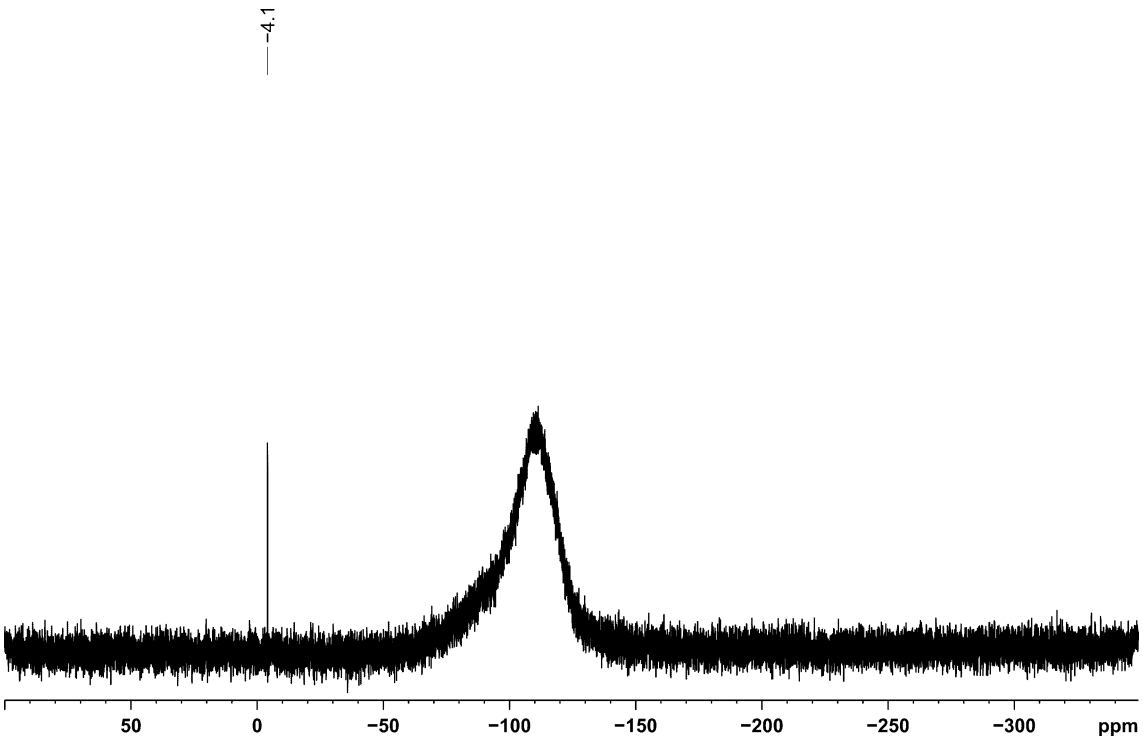

Figure S30. $^{29}Si\{^{1}H\}$ NMR spectrum (79.49 MHz, 300 K, C_6D_6) of [(IPr)Ni($C_2H_4SiMe_3$)($C_{17}H_{21}N_5P$)] (**12**).

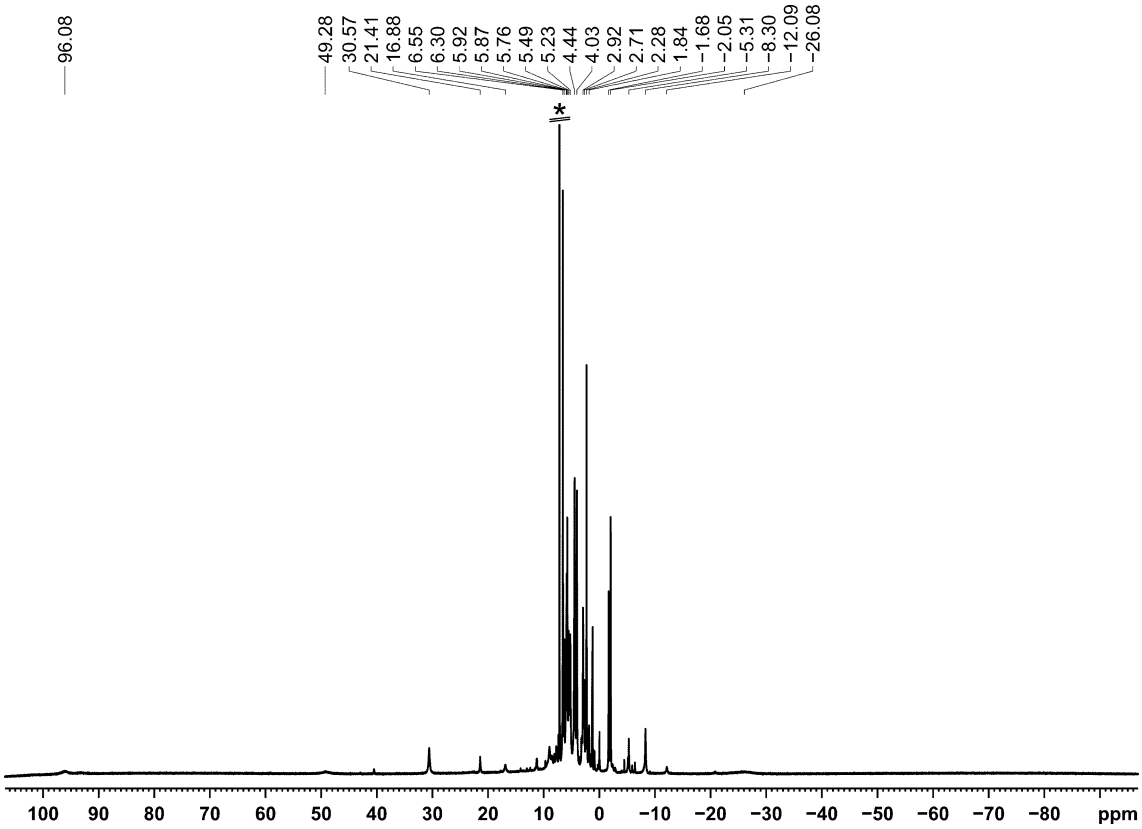

Figure S31. ^{1}H NMR spectrum (400.13 MHz, 300 K, C_6D_6) of [(IPr)Co(vtms)($C_{17}H_{21}N_5P$)] (**13a**); * C_6D_6.

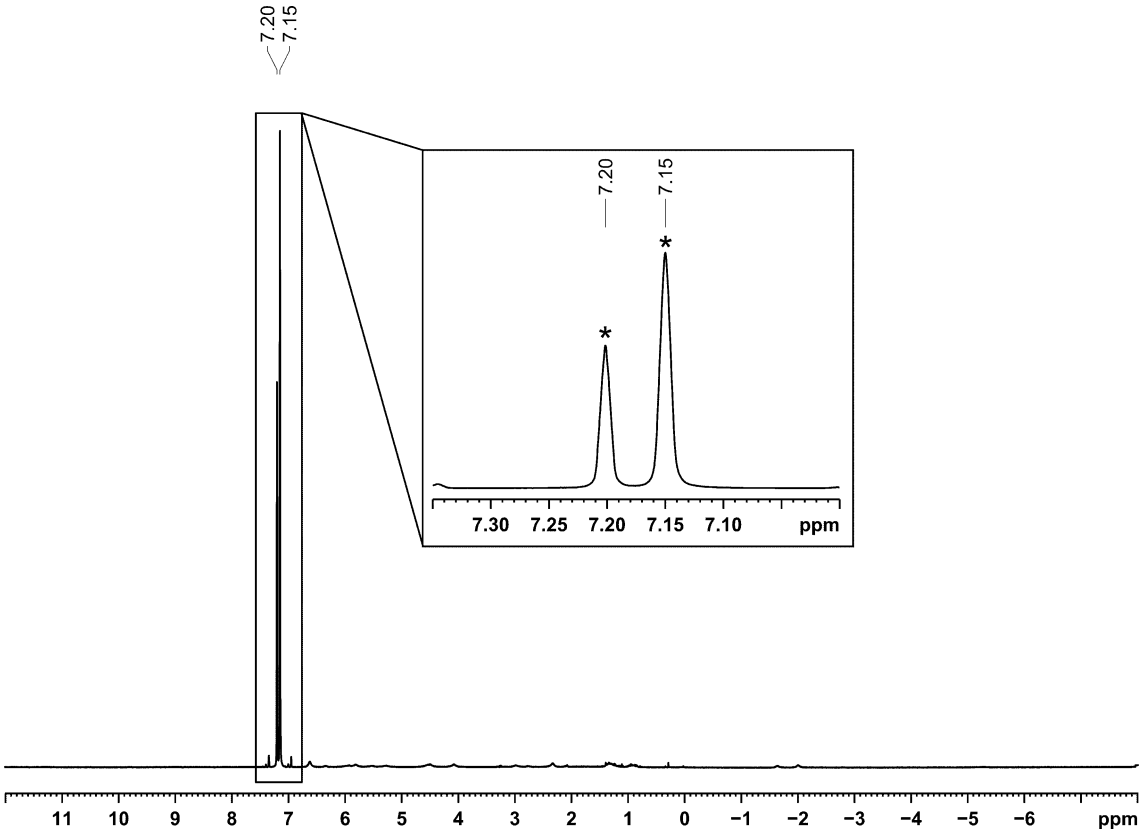

Figure S32. ^{1}H NMR spectrum (400.13 MHz, 300 K, C_6D_6) of [(IPr)Co(vtms)($C_{17}H_{21}N_5P$)] (**13a**) for the determination of the magnetic moment according to the Evans method;[78–80] * C_6D_6.

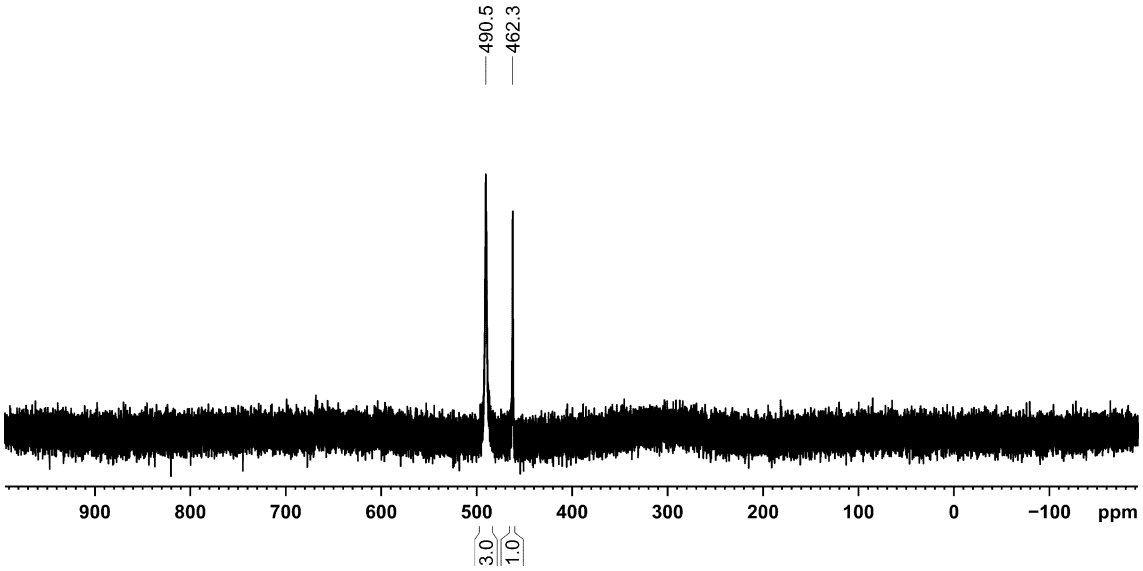

Figure S33. $^{31}P\{^{1}H\}$ NMR spectrum (162.04 MHz, 300 K, C_6D_6) of [(IPr)Co(vtms)($C_{17}H_{21}N_5P$)] (**13a**).

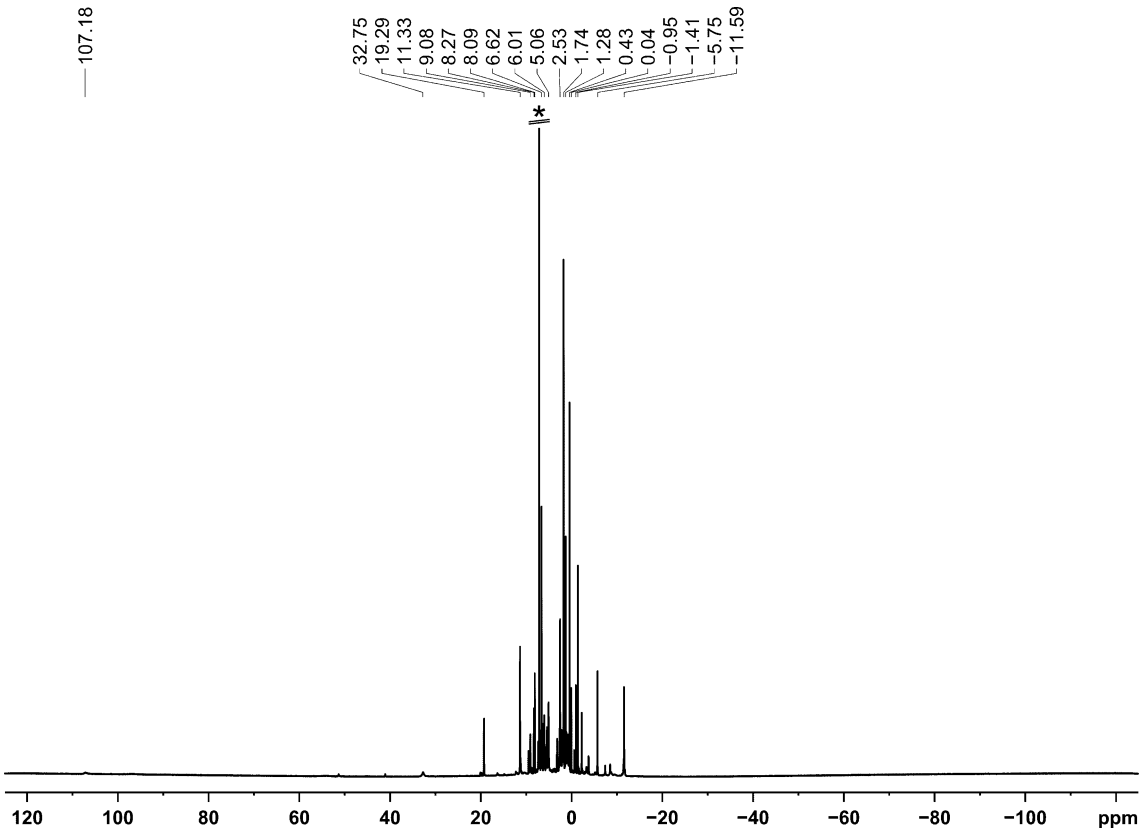

Figure S34. ^{1}H NMR spectrum (400.13 MHz, 300 K, C_6D_6) of [(IMes)Co(vtms)($C_{17}H_{21}N_5P$)] (**13b**); * C_6D_6.

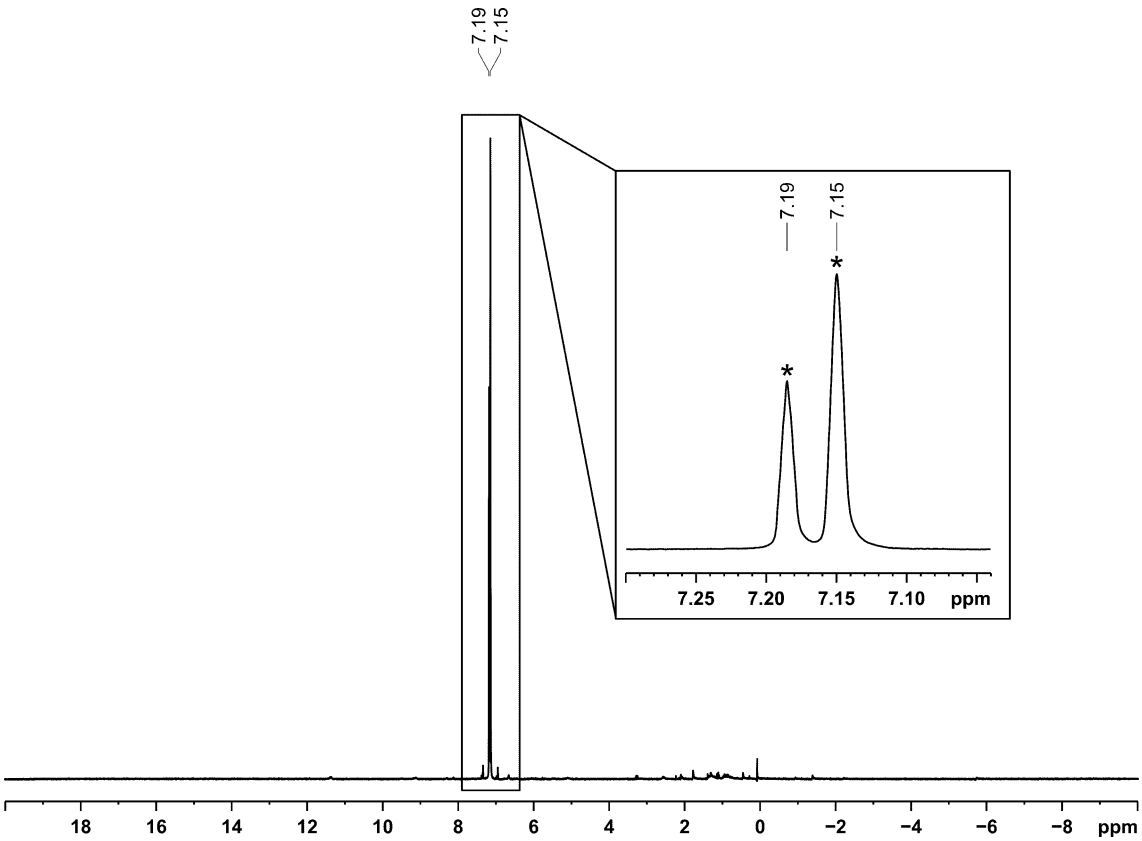

Figure S35. ^{1}H NMR spectrum (400.13 MHz, 300 K, C_6D_6) of [(IMes)Co(vtms)($C_{17}H_{21}N_5P$)] (**13b**) for the determination of the magnetic moment according to the Evans method;[78–80] ∗ C_6D_6.

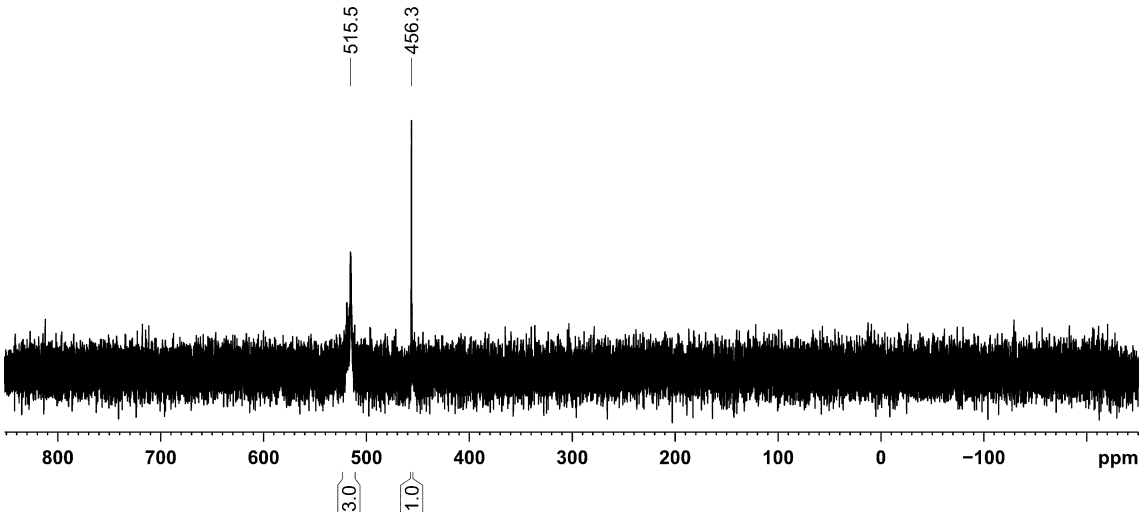

Figure S36. ^{31}P{^{1}H} NMR spectrum (162.04 MHz, 300 K, C_6D_6) of [(IMes)Co(vtms)($C_{17}H_{21}N_5P$)] (**13b**).

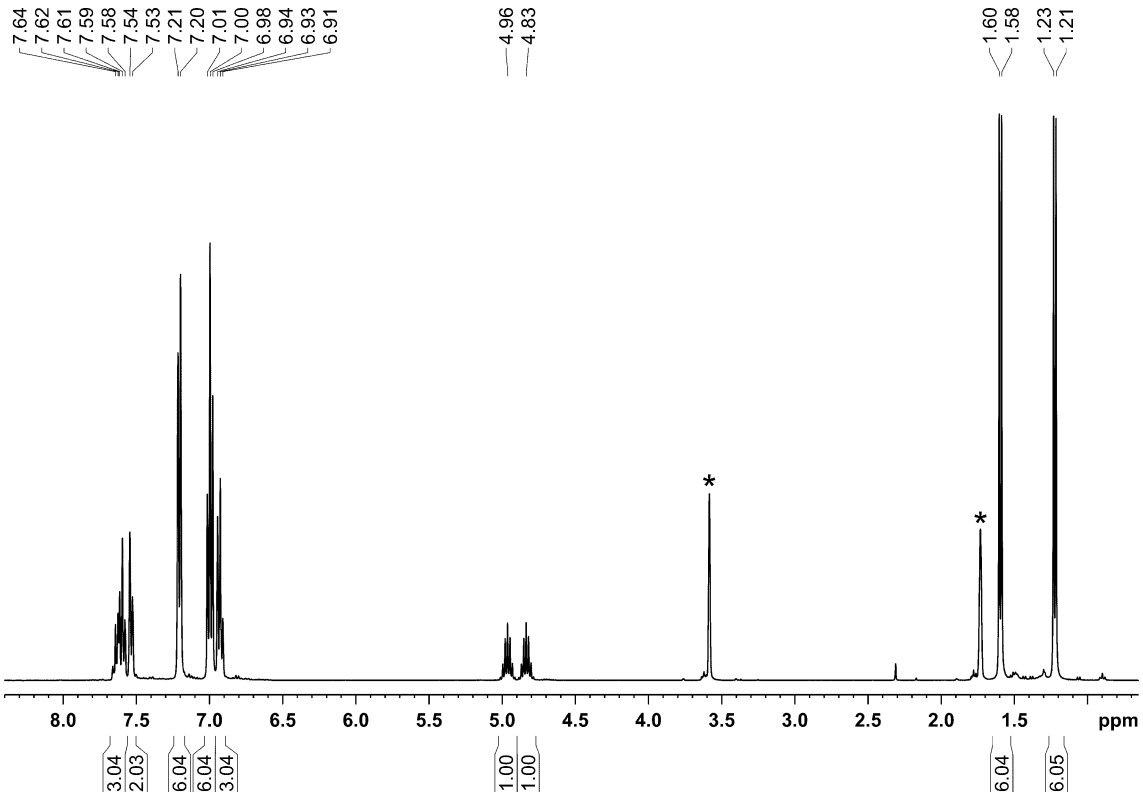

Figure S37. ^{1}H NMR spectrum (400.13 MHz, 300 K, THF-d_8) of [BPh_3(**3**)] (**14**); * THF-d_8.

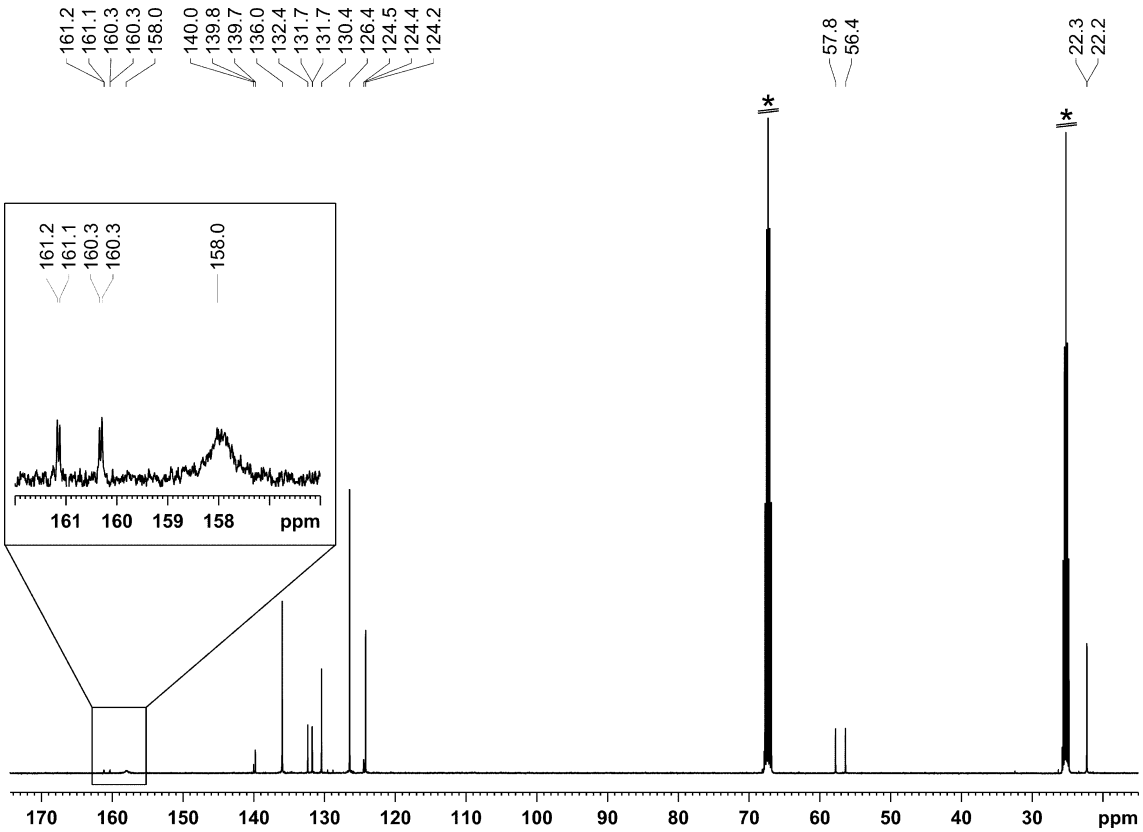

Figure S38. ^{13}C{^{1}H} NMR spectrum (100.61 MHz, 300 K, THF-d_8) of [BPh_3(**3**)] (**14**); * THF-d_8.

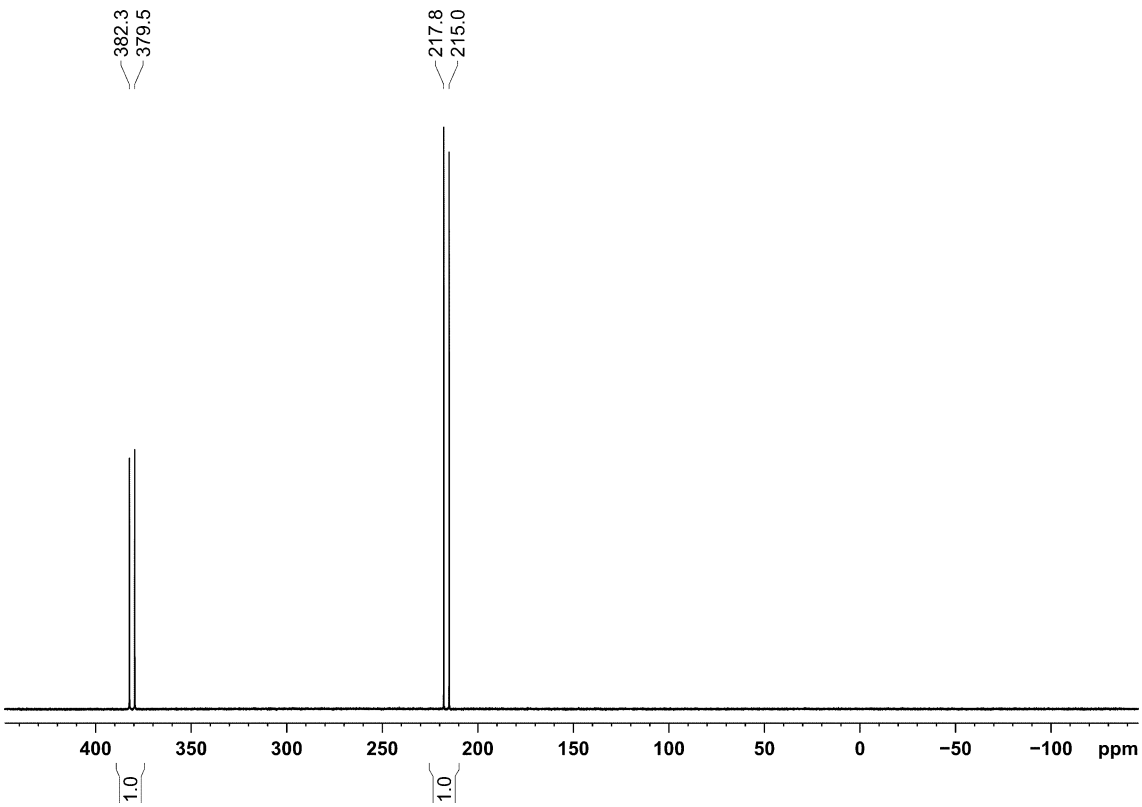

Figure S39. $^{31}P\{^{1}H\}$ NMR spectrum (162.04 MHz, 300 K, THF-d_8) of [BPh_3(**3**)] (**14**).

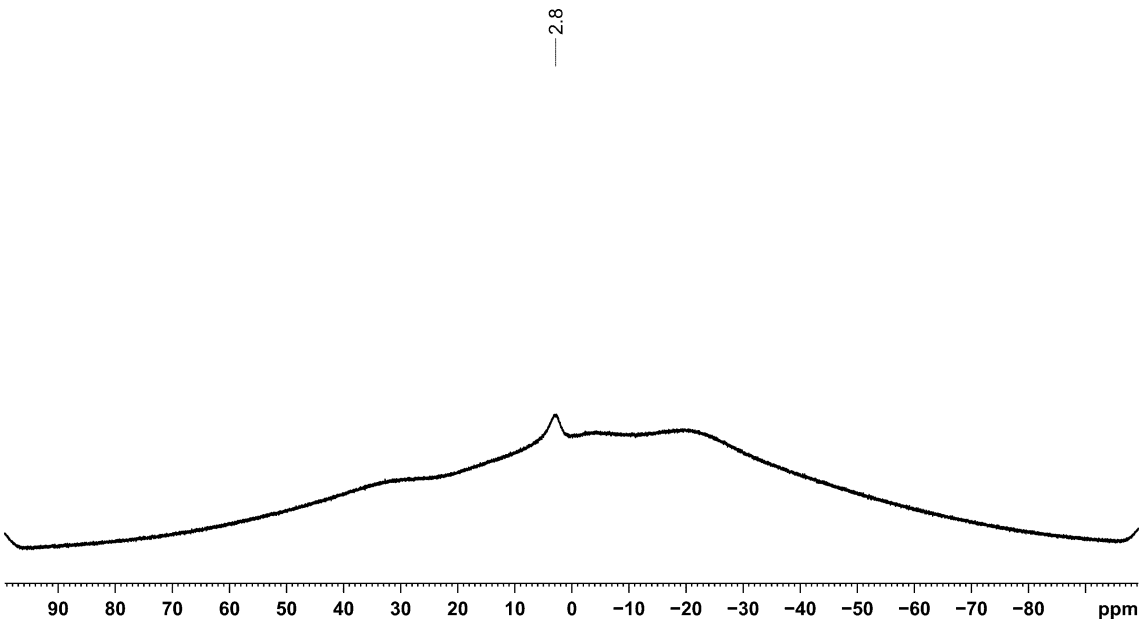

Figure S40. $^{11}B\{^{1}H\}$ NMR spectrum (128.43 MHz, 300 K, THF-d_8) of [BPh_3(**3**)] (**14**).

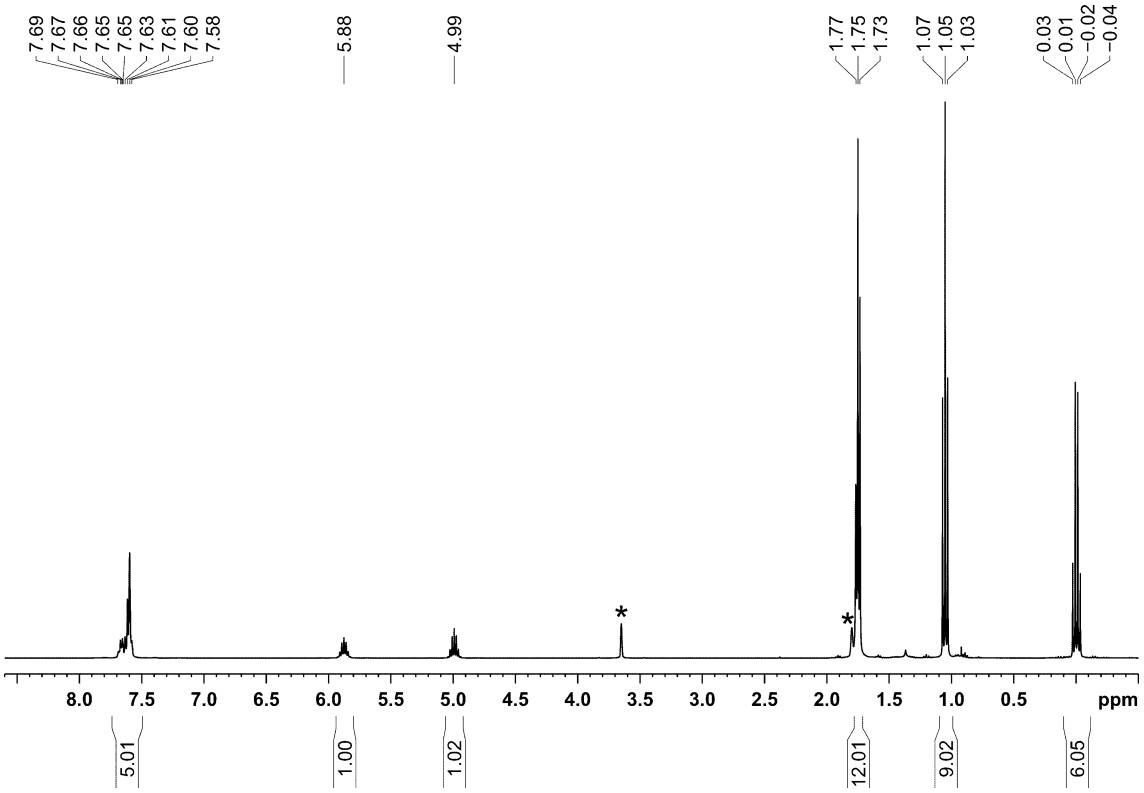

Figure S41. ^{1}H NMR spectrum (400.30 MHz, 300 K, THF-d_8) of [AlEt$_3$(**3**)] (**15**); * residual ^{1}H NMR signals of THF-d_8.

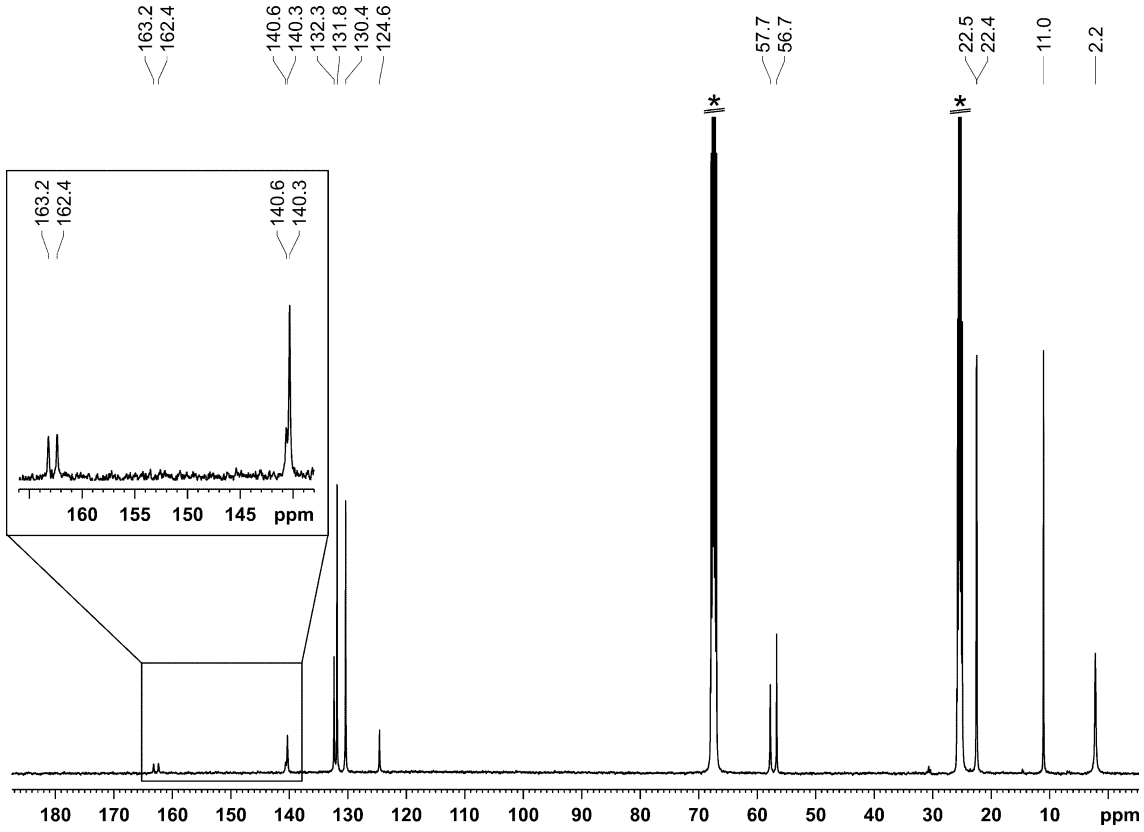

Figure S42. ^{13}C{^{1}H} NMR spectrum (100.61 MHz, 300 K, THF-d_8) of [AlEt$_3$(**3**)] (**15**); * THF-d_8.

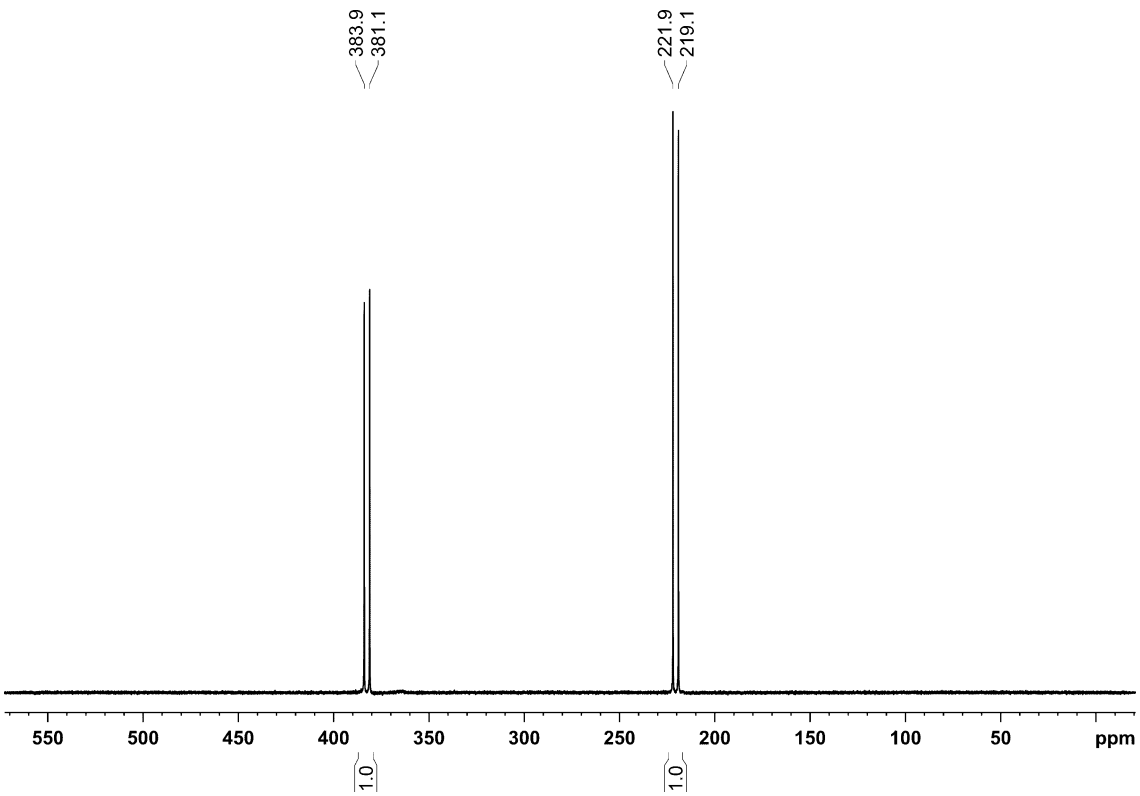

Figure S43. $^{31}P\{^{1}H\}$ NMR spectrum (162.04 MHz, 300 K, THF-d_8) of [$AlEt_3$(**3**)] (**15**).

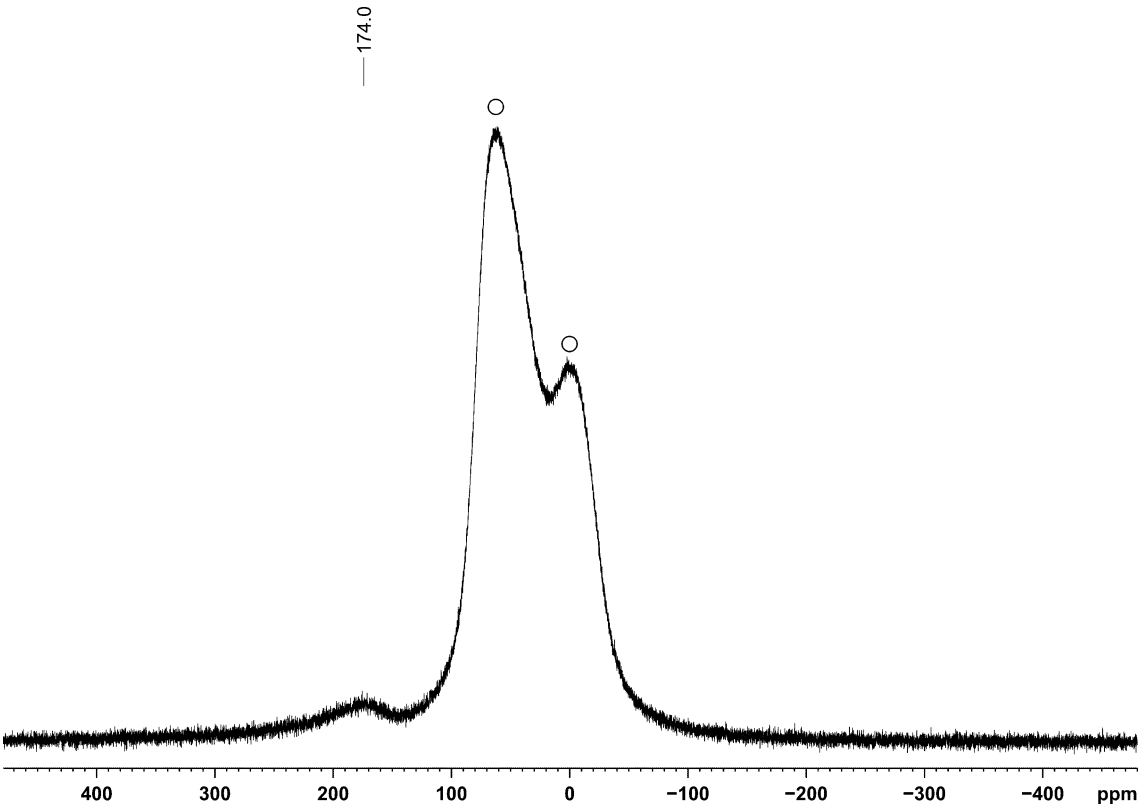

Figure S44. $^{27}Al\{^{1}H\}$ NMR spectrum (104.26 MHz, 300 K, THF-d_8) of [$AlEt_3$(**3**)] (**15**); ○ signal of probe head.

6.4.3 Additional Experiments

Reactions of *i*Pr-Diazamonophosphole (2) toward [W(CO)$_5$(thf)]:

[W(CO)$_3${W(CO)$_5$(2)}$_3$] (4):

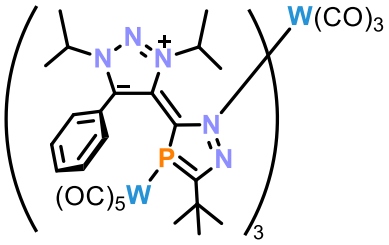

A colorless solution of [W(CO)$_6$] (6 mg, 0.0.017 mmol, 1.0 equiv.) in THF (1.5 mL) was irradiated with UV-light (365 nm, 10 W) for 2 h while stirring. The solution turned deep yellow, was added to a solution of **2** (6 mg, 0.017 mmol, 1.0 equiv.) in THF (0.5 mL) and stirred for 1 d. The yellow suspension was filtered. Crystals of [W(CO)$_3${W(CO)$_5$(**2**)}$_3$] (**4**) were grown by slow vapor diffusion of *n*-hexane into this filtrate. The crystals were of sufficient quality for analysis by XRD and transferred into mineral oil.

[W(CO)$_5$(2)] (5):

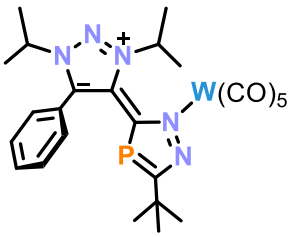

A stirring, colorless solution of [W(CO)$_6$] (6.4 mg, 0.0.018 mmol, 1.33 equiv.) in THF (2.0 mL) was irradiated with UV-light (365 nm, 10 W) for 30 min. The solution turned deep yellow, was added to solid **2** (5 mg, 0.014 mmol, 1.0 equiv.) and stirred for 1 d. The yellow suspension was filtered. Crystals of [W(CO)$_5$(**2**)] (**5**) were grown by slow vapor diffusion of *n*-hexane into this filtrate. The crystals were of sufficient quality for analysis by XRD and transferred into mineral oil.

6.4.4 Reaction Monitoring

In a glovebox, a mixture of solids diazamonophosphole **2** (5 mg, 0.014 mmol, 1.0 equiv.) and $[Cp^*Ru(MeCN)_3]PF_6$ (7 mg, 0.014 mmol, 1.0 equiv.) were suspended in 0.6 mL of C_6D_6 in a J. Young valve NMR tube. The NMR tube was closed and after 1 hour analyzed by $^{31}P\{^1H\}$ NMR spectroscopy (Figure S45; *vide infra*). The spectrum revealed one signal at δ = 87.7 ppm, which was attributed to an intermediate coordinating *via* a single nitrogen atom.

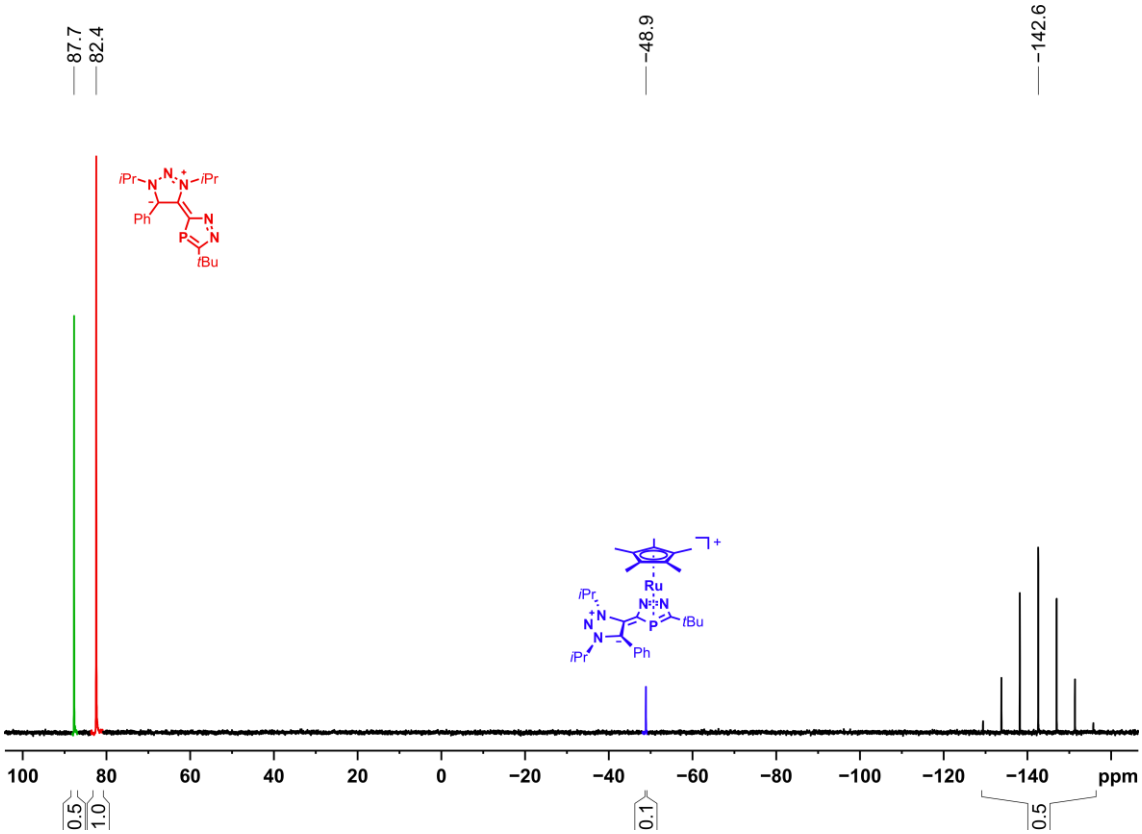

Figure S45. $^{31}P\{^1H\}$ NMR spectrum (162.04 MHz, 300 K, C_6D_6) of the reaction between *i*Pr-Diazamonophosphole (**2**, *red*) toward $[Cp^*Ru(MeCN)_3]PF_6$ resulting in the formation of $[Cp^*Ru(\mathbf{2})]PF_6$ (**10**, *blue*); *green*: δ/ppm = 87.7 attributed to an η^1-coordinating intermediate.

In a glovebox, to a mixture of solids diazamonophosphole **2** (15 mg, 0.041 mmol, 1.0 equiv.) and [Ni(cod)$_2$] (15 mg, 0.053 mmol, 1.3 equiv) in a J. Young valve NMR tube 0.6 mL of C_6D_6 was added. $^{31}P\{^1H\}$ measurements were performed every 15 min from 10 minutes after reaction onset until a total reaction time of 5 hours. NMR measurements were performed at a temperature of 333 K (60 °C). Figure S46 (*vide infra*) shows the yield in % of [Ni($C_{14}H_{23}N_5P$)(Ph)(**2**)] (**11**) as determined by integration of the $^{31}P\{^1H\}$ NMR spectra.

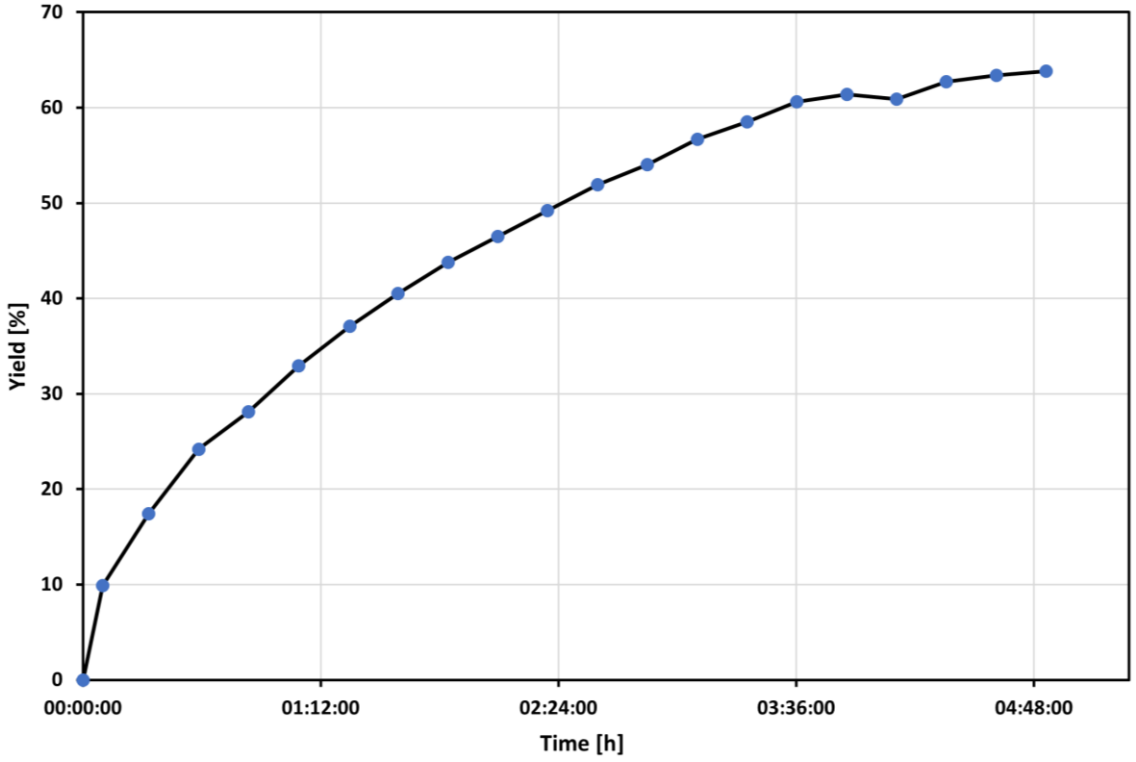

Figure S46. Yield of [Ni($C_{14}H_{23}N_5P$)(Ph)(**2**)] (**11**) as determined by integration of the $^{31}P\{^1H\}$ NMR spectra against reaction time.

6.4.5 Proposed Reaction Sequence

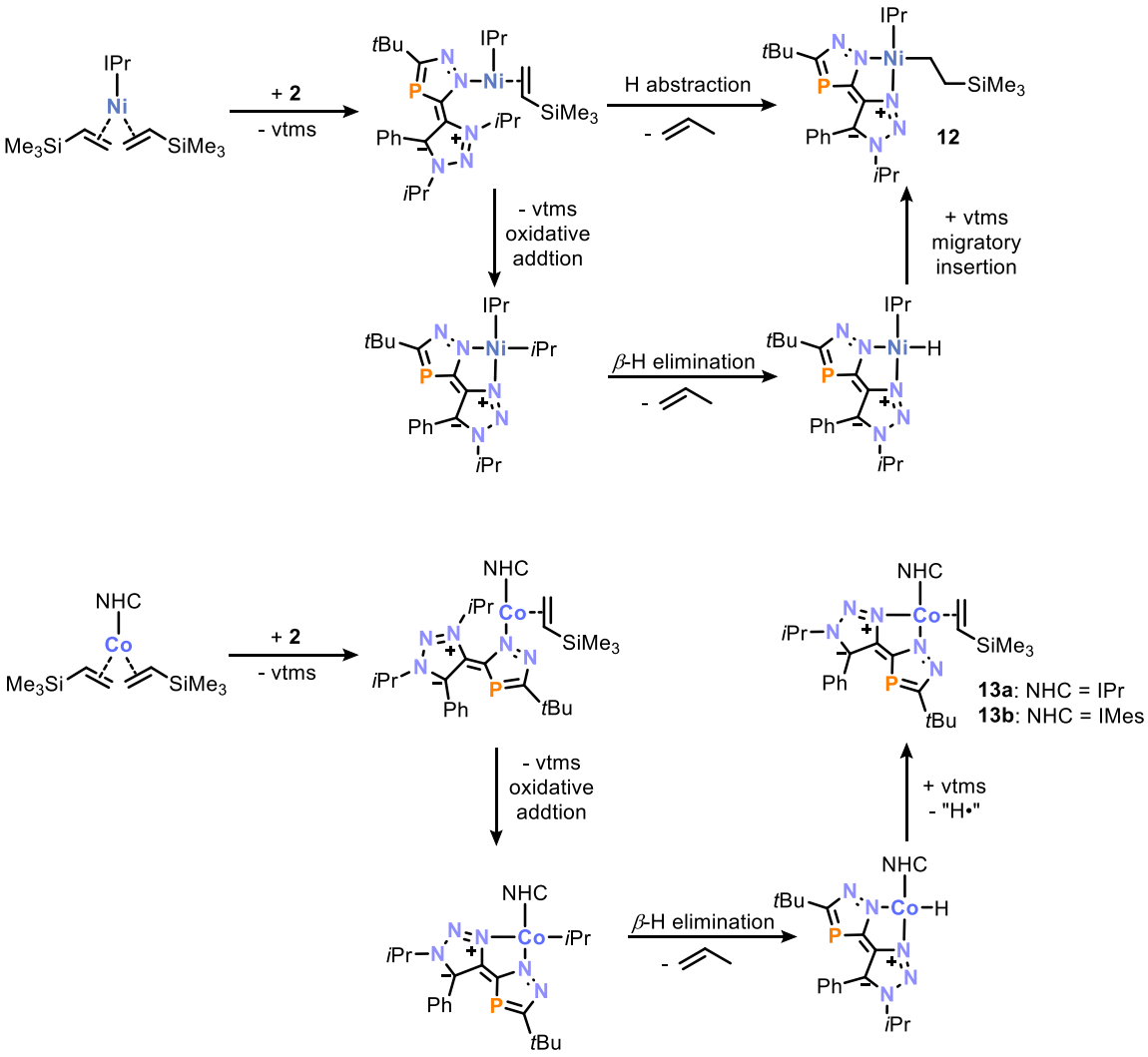

Scheme S1. Proposed reaction sequence for the formation of **12** and **13**, starting from **2** and [(NHC)M(vtms)$_2$] (NHC = IPr, IMes; M = Ni, Co).

6.4.6 UV/Vis Spectra

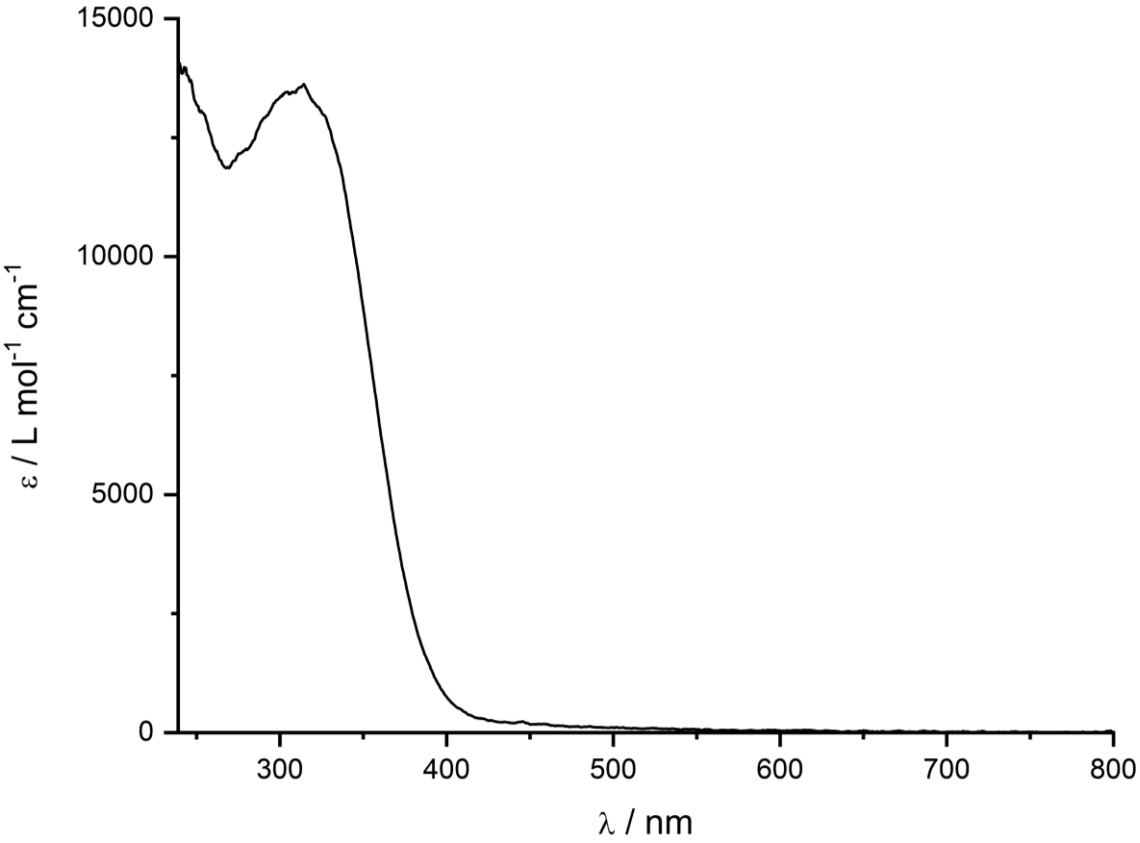

Figure S47. UV/Vis spectrum of **2** recorded in THF.

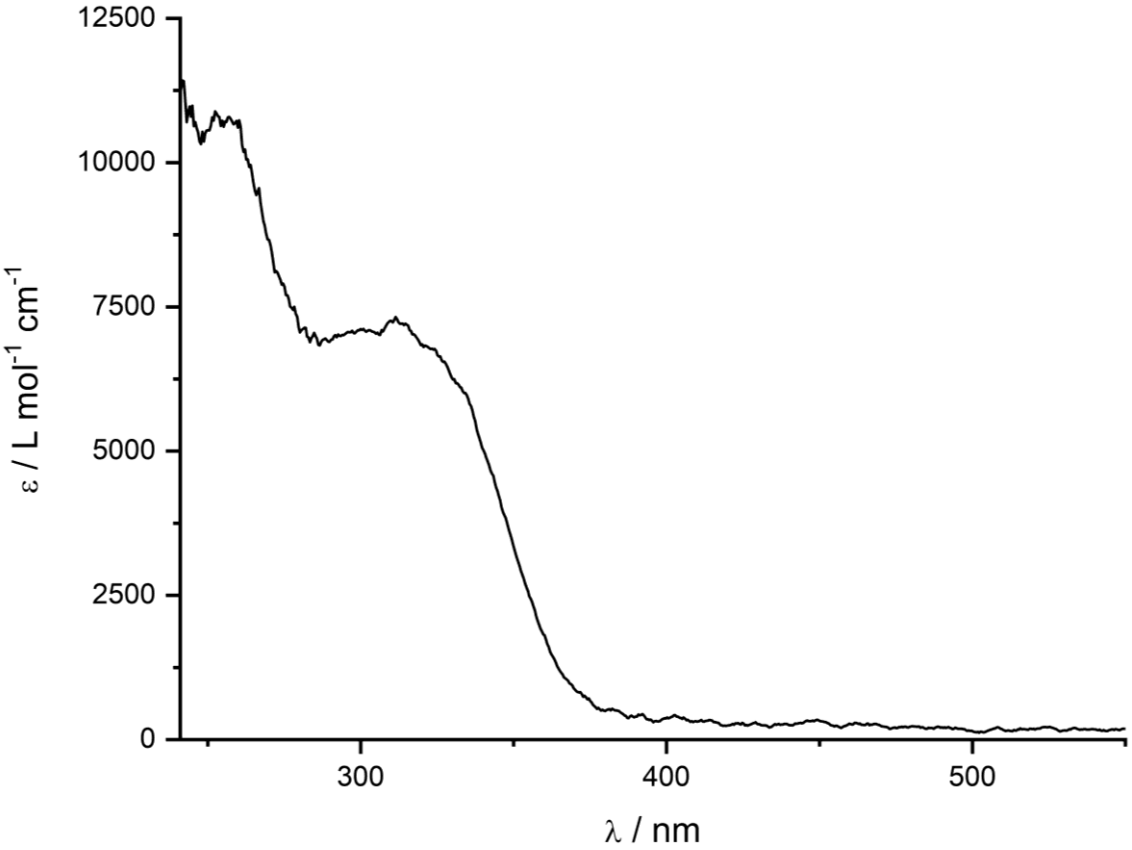

Figure S48. UV/Vis spectrum of **3** recorded in THF.

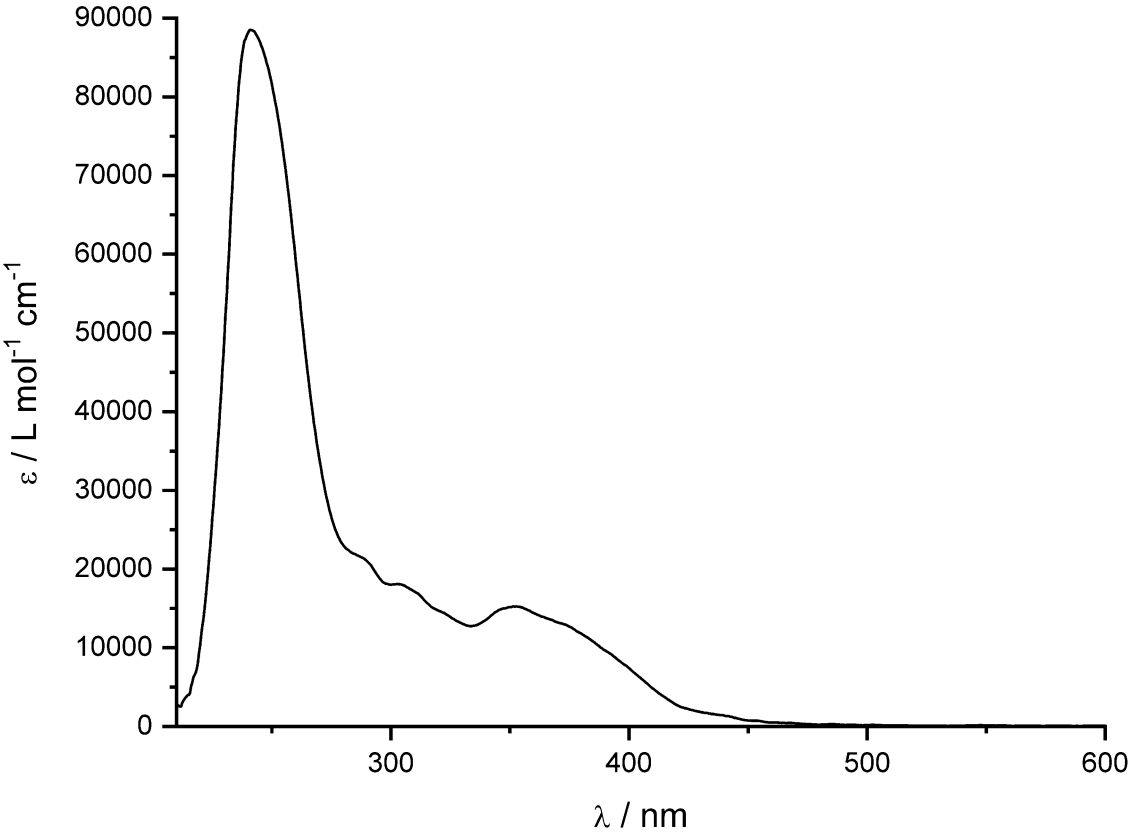

Figure S49. UV/Vis spectrum of [{W(CO)$_5$}$_2$(**2**)] (**6**) recorded in THF.

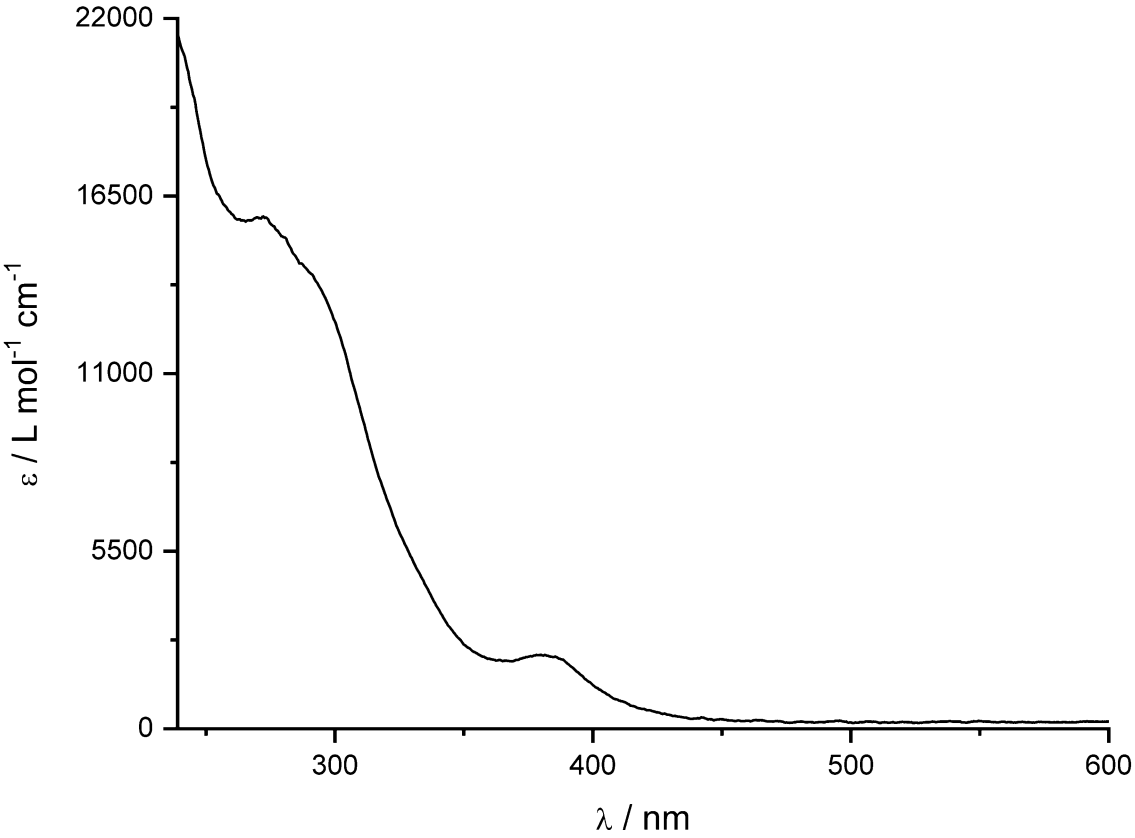

Figure S50. UV/Vis spectrum of [Rh(**2**)(cod)Cl] (**7**) recorded in THF.

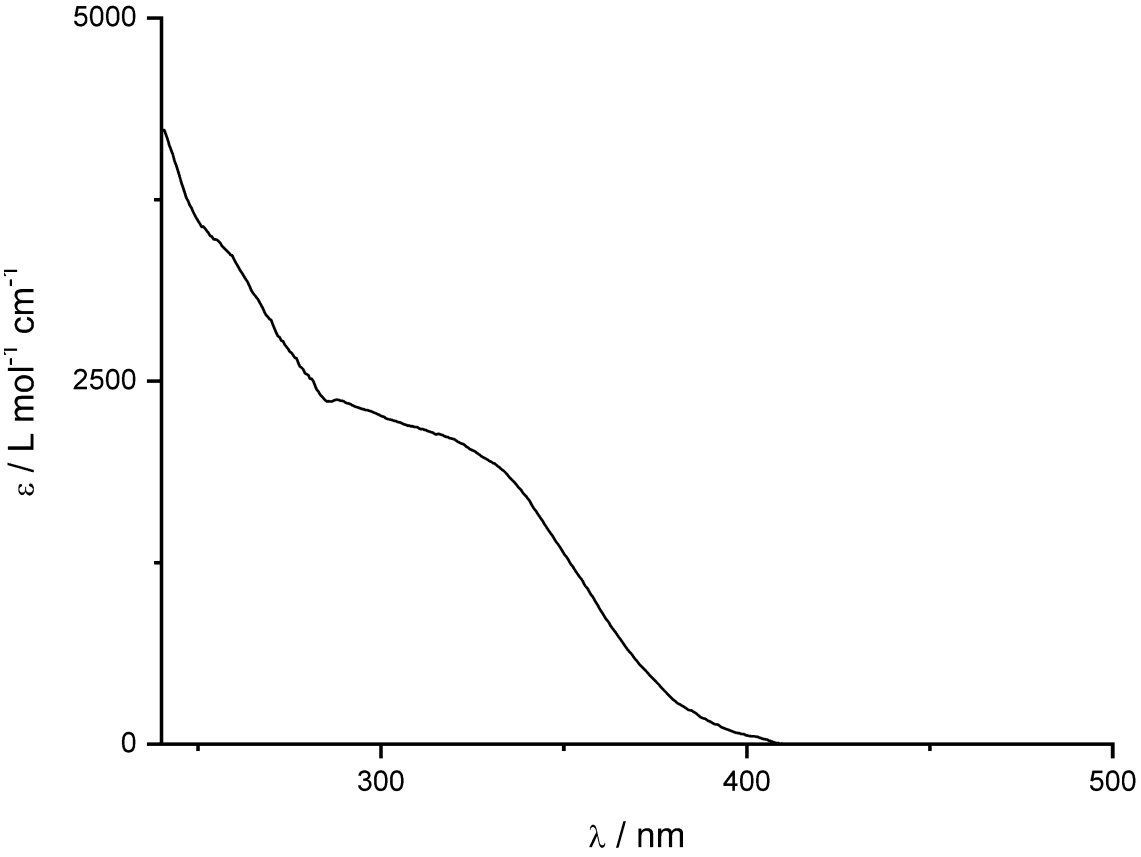

Figure S51. UV/Vis spectrum of [$AlEt_3$(**2**)] (**8**) recorded in THF.

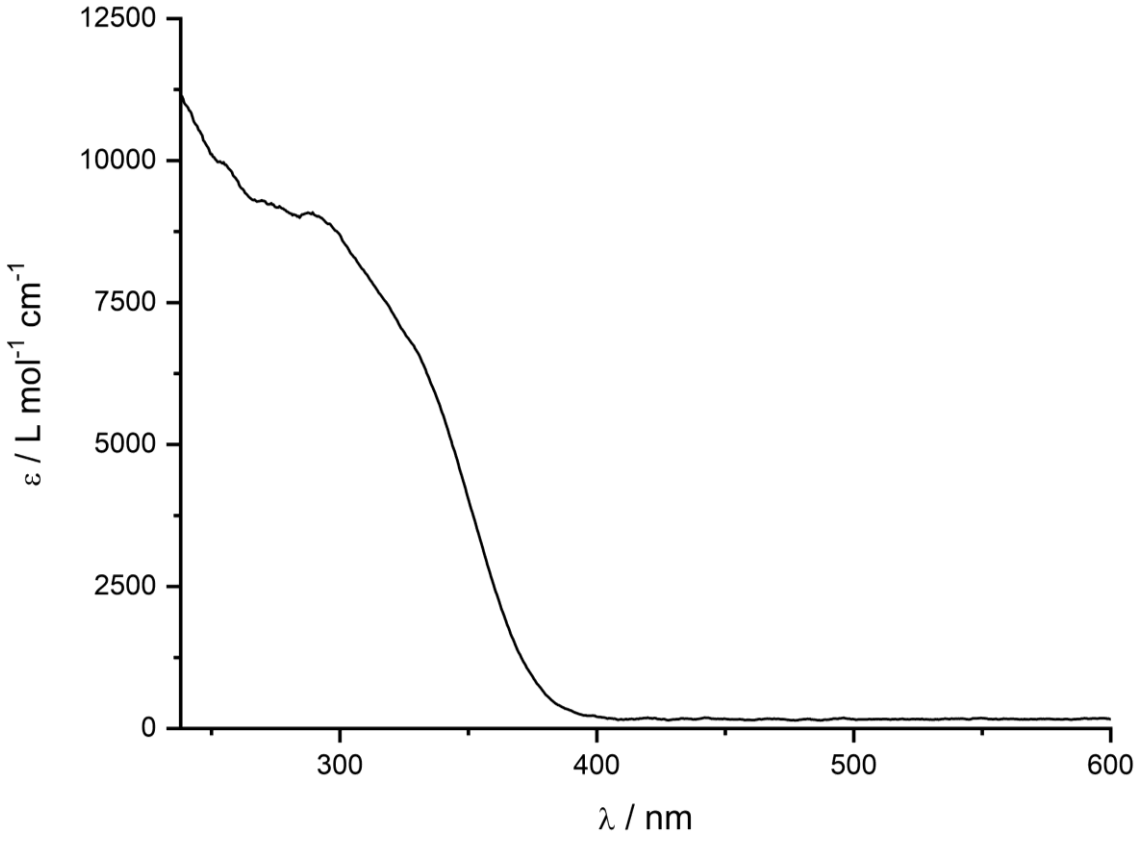

Figure S52. UV/Vis spectrum of [AuCl(**2**)] (**9**) recorded in THF.

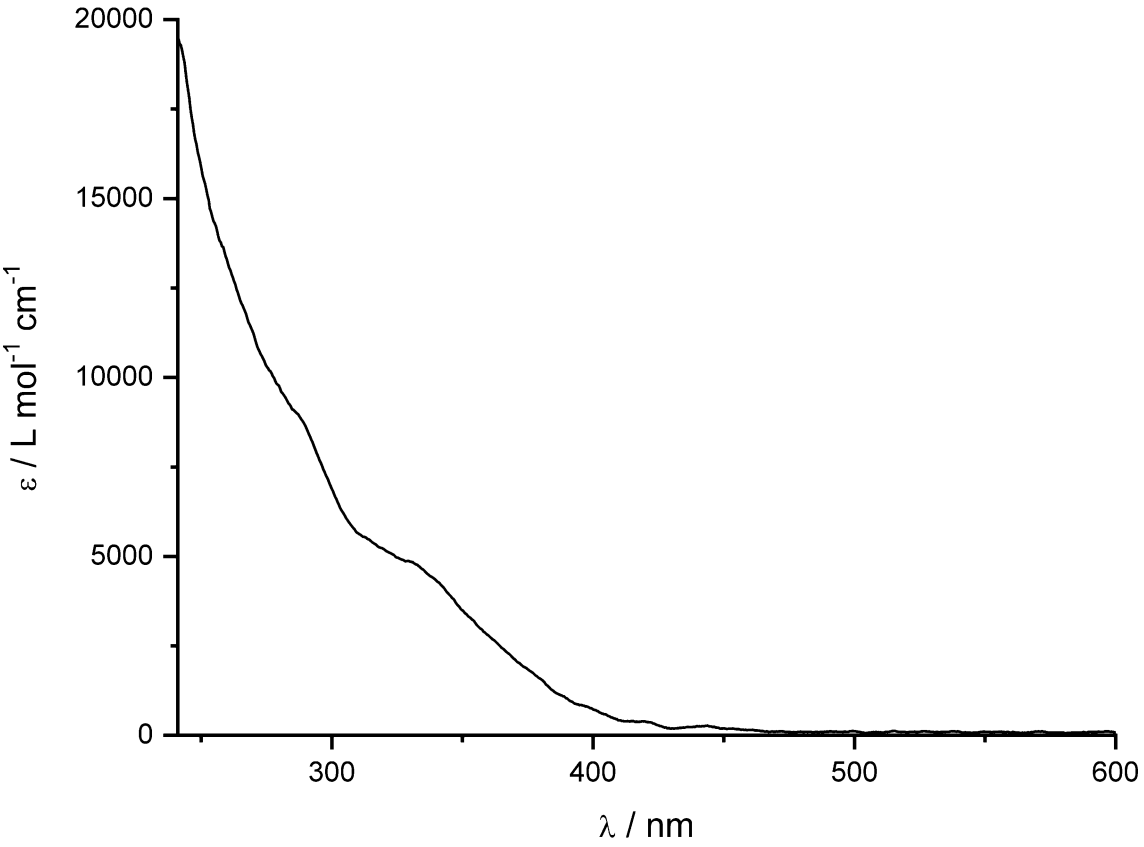

Figure S53. UV/Vis spectrum of [Cp*Ru(**2**)]PF_6 (**10**) recorded in THF.

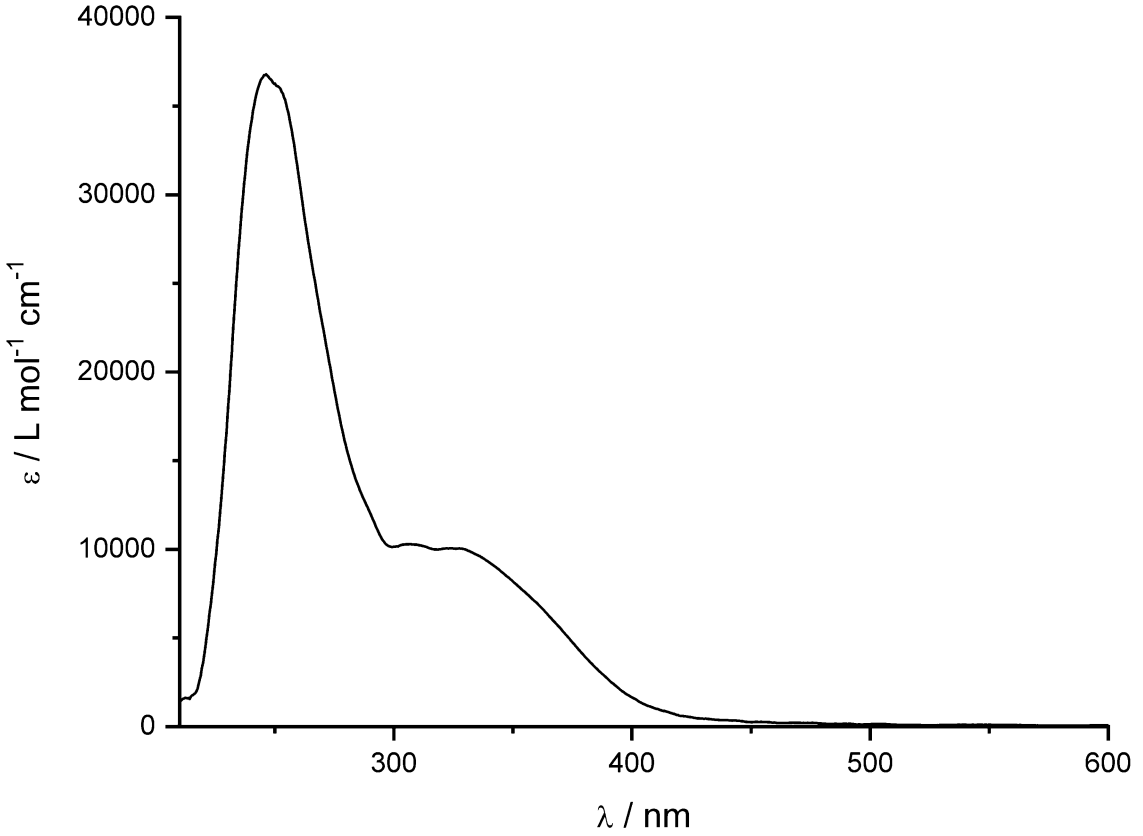

Figure S54. UV/Vis spectrum of [Ni($C_{14}H_{23}N_5P$)(Ph)(**2**)] (**11**) recorded in THF.

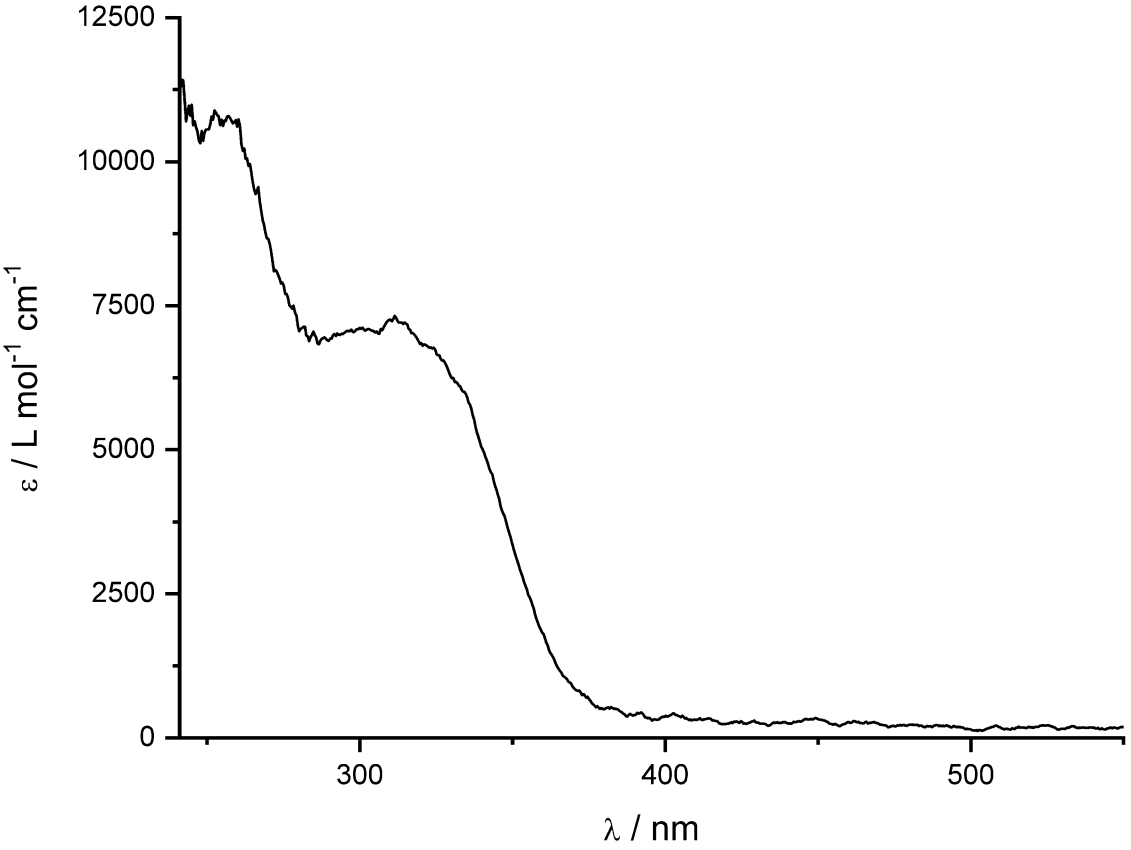

Figure S55. UV/Vis spectrum of [(IPr)Ni($C_2H_4SiMe_3$)($C_{17}H_{21}N_5P$)] (**12**) recorded in THF.

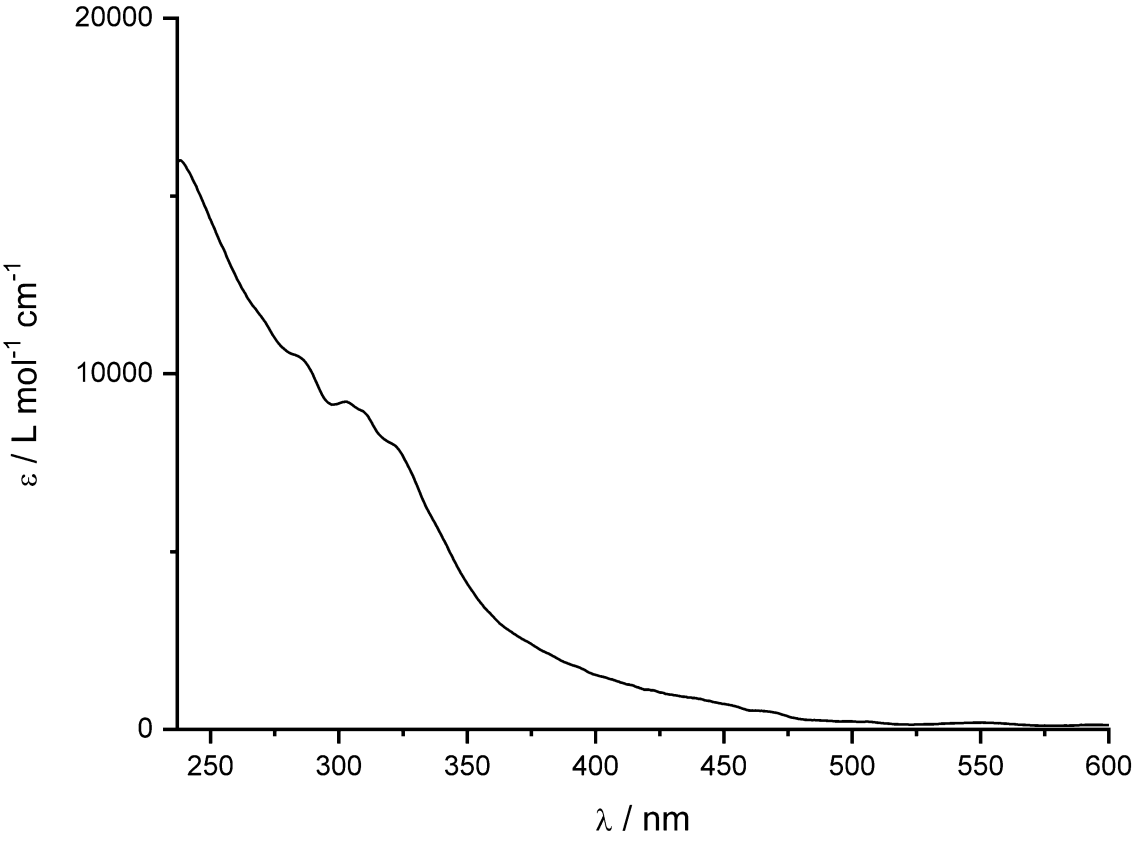

Figure S56. UV/Vis spectrum of [(IPr)Co(vtms)($C_{17}H_{21}N_5P$)] (**13a**) recorded in THF.

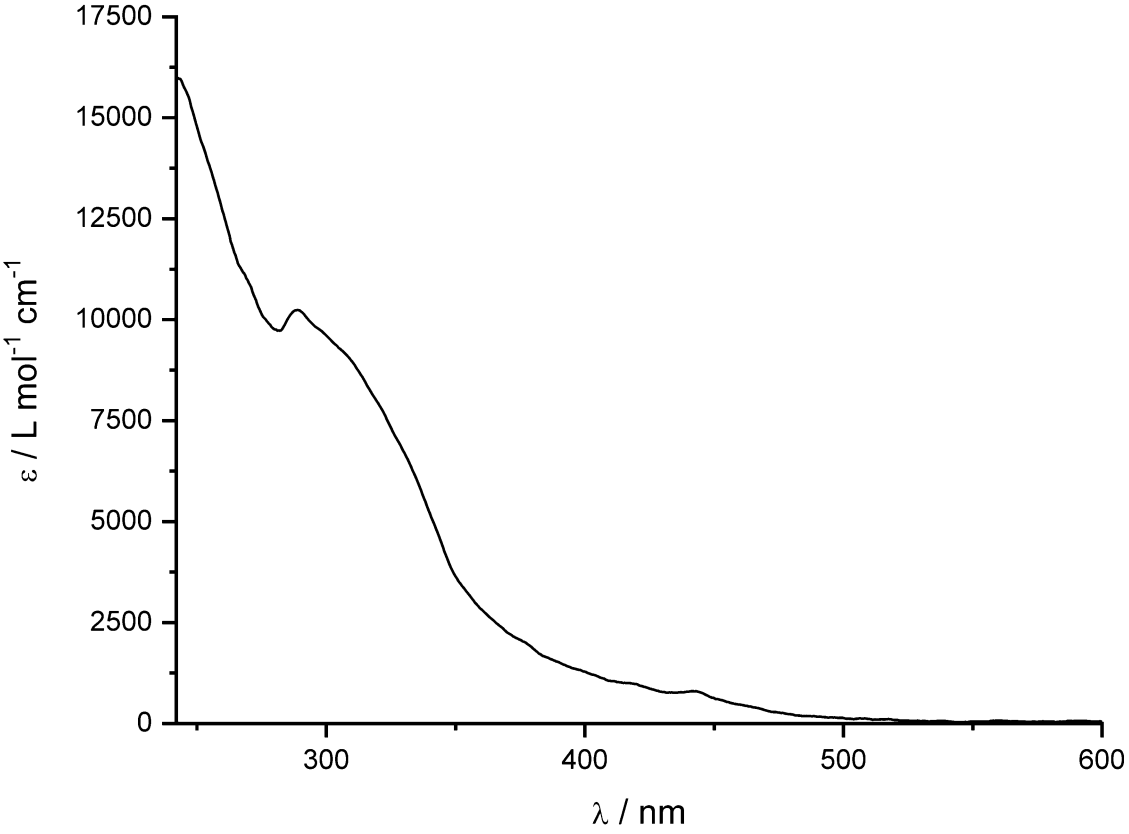

Figure S57. UV/Vis spectrum of [(IMes)Co(vtms)($C_{17}H_{21}N_5P$)] (**13b**) recorded in THF.

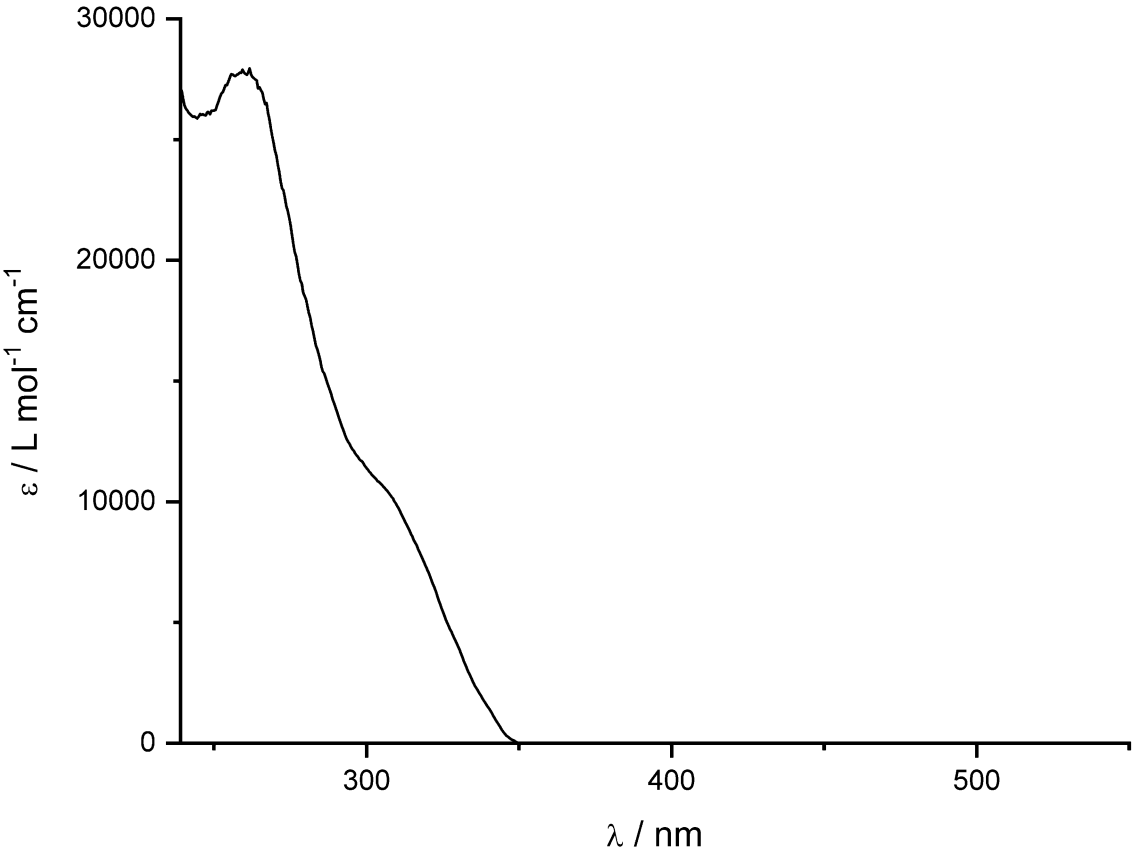

Figure S58. UV/Vis spectrum of [BPh_3(**3**)] (**14**) recorded in THF.

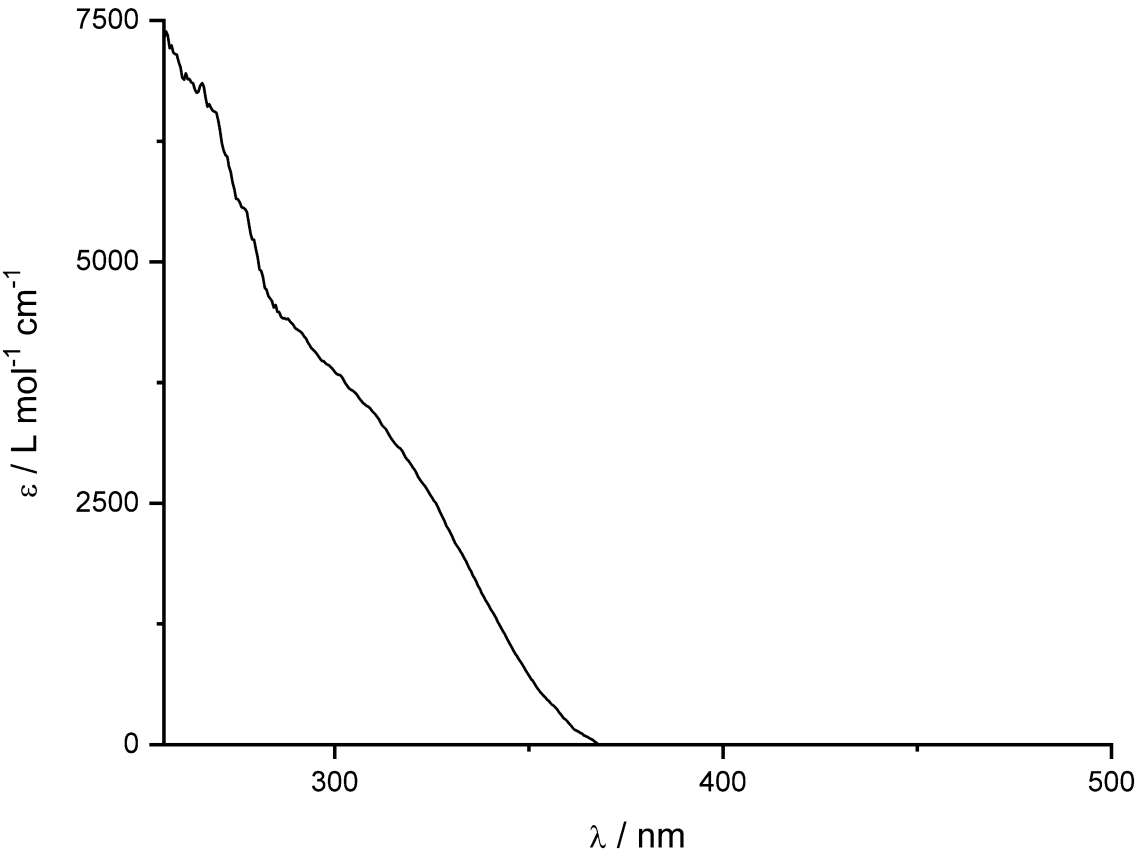

Figure S59. UV/Vis spectrum of [$AlEt_3$(**3**)] (**15**) recorded in THF.

6.4.7 IR Spectra

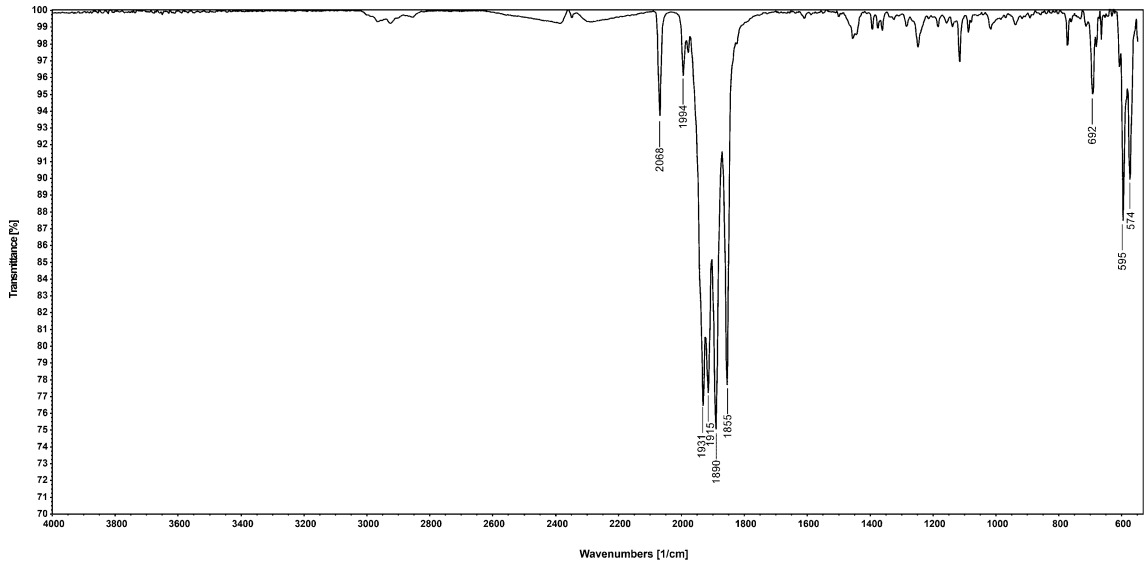

Figure S60. Solid state IR spectrum of [{$W(CO)_5$}$_2$(**2**)] (**6**).

6.4.8 Single Crystal X-Ray Diffraction Data

Single-crystal X-ray diffraction data were recorded on Rigaku Oxford Diffraction XtaLAB Synergy R (DW system, Hypix-Arc 150) or SuperNova Atlas (Titan^{S2}) diffractometers with Cu-K_α (λ = 1.54184 Å), Cu-K_β (λ = 1.39222 Å), or Mo-K_α (λ = 0.71073 Å) radiation. Crystals were selected under mineral oil, mounted on micromount loops and quench-cooled using an Oxford Cryosystems open flow N_2 cooling device. Either semi-empirical multi-scan absorption corrections[81,82] or analytical ones[83] were applied to the data. The structures were solved with SHELXT[84] solution program using dual methods and by using Olex2 as the graphical interface.[85] The models were refined with ShelXL[86] using full matrix least squares minimization on F^2.[87] The hydrogen atoms were located in idealized positions and refined isotropically with a riding model.

$[W(CO)_3\{W(CO)_5(\mathbf{2})\}_3]$ (**4**): The crystal of **4** contained three THF molecules per asymmetric unit. Two of them were modeled, while the third one was severely disordered and refined by using the solvent mask command: A solvent mask was calculated, and 74 electrons were found in a volume of 272 Å^3 in one void per unit cell. This is consistent with the presence of 1.0 THF per formula unit which account for 80 electrons per unit cell. As **4** was crystallized by slow diffusion of *n*-hexane into a saturated THF solution of **4** this serves as evidence for the presence of THF in this position.

The following section provides figures of the molecular structures with selected bond lengths and angles, which were not given in section 6.2 itself.

Table S1. Crystallographic data and structure refinement for compounds **2-5**.

Compound	**2**	**3**	**4**	**5**
CCDC	2287329	2287330	2287421	2287423
Empirical formula	$C_{20}H_{28}N_5P_2$	$C_{30}H_{38}N_{10}P_4$	$C_{86}H_{100}N_{15}O_{20}P_3W_4$	$C_{50}H_{56}N_{10}O_{10}P_2W_2$
Formula weight	369.44	662.58	2492.11	1386.68
Temperature/K	100(1)	123(1)	123(1)	123(1)
Crystal system	monoclinic	triclinic	triclinic	monoclinic
Space group	$P2_1/c$	P-1	P-1	$P2_1/n$
a/Å	15.7777(1)	9.4067(5)	14.8654(2)	18.1762(2)
b/Å	13.3846(1)	9.8993(5)	17.5148(3)	15.34710(10)
c/Å	9.9613(1)	18.8156(9)	19.5580(2)	21.9378(2)
α/°	90	80.999(4)	82.3161(12)	90
β/°	103.827(1)	88.396(4)	87.2231(13)	110.2080(10)
γ/°	90	86.508(4)	86.4994(13)	90
Volume/Å^3	2042.65(3)	1727.01(15)	5032.88(13)	5742.90(10)
Z	4	2	2	4
ρ_{calc}g/cm^3	1.201	1.274	1.644	1.604
μ/mm^{-1}	1.285	2.313	9.271	8.335
F(000)	792.0	696.0	2444.0	2736.0
Crystal size/mm^3	0.165 × 0.132 × 0.093	0.324 × 0.1 × 0.057	0.13 × 0.07 × 0.04	0.260 × 0.120× 0.09
Diffractometer	XtaLAB Synergy R, DW system, HyPix-Arc 150	XtaLAB Synergy R, DW system, HyPix-Arc 150	XtaLAB Synergy R, DW system, HyPix-Arc 150	XtaLAB Synergy R, DW system, HyPix-Arc 150
Radiation	Cu Kα (λ = 1.54184)	Cu Kα (λ = 1.54184)	Cu Kα (λ = 1.54184)	Cu Kα (λ = 1.54184)
2Θ range for data collection/°	5.768 to 149.516	9.06 to 134.54	4.562 to 150.872	7.75 to 134.088
Index ranges	−19 ≤ h ≤ 17, −16 ≤ k ≤ 16, –11 ≤ l ≤ 12	−11 ≤ h ≤ 11, −11 ≤ k ≤ 11, –14 ≤ l ≤ 22	−15 ≤ h ≤ 18, −21 ≤ k ≤ 21, −24 ≤ l ≤ 24	−21 ≤ h ≤ 20, −15 ≤ k ≤ 18, −25 ≤ l ≤ 26
Reflections collected	47880	16839	135478	54945
Independent reflections	4181 [R_{int} = 0.0190, R_{sigma} = 0.0088]	6081 [R_{int} = 0.0967, R_{sigma} = 0.0949]	20419 [R_{int} = 0.0528, R_{sigma} = 0.0391]	10172 [R_{int} = 0.0719, R_{sigma} = 0.0419]
Data/restraints/ parameters	4181/0/343	6081/0/405	20419/18/1174	10172/19/692
Goodness-of-fit on F^2	1.044	1.034	1.111	1.051
Final R indexes [I>=2σ (I)]	R_1 = 0.0301, wR_2 = 0.0795	R_1 = 0.0667, wR_2 = 0.1627	R_1 = 0.0366, wR_2 = 0.0852	R_1 = 0.0337, wR_2 = 0.0851
Final R indexes [all data]	R_1 = 0.0313, wR_2 = 0.0803	R_1 = 0.0969, wR_2 = 0.1880	R_1 = 0.0463, wR_2 = 0.0888	R_1 = 0.0378, wR_2 = 0.0887
Largest diff. peak/hole / e Å^{-3}	0.28/−0.27	0.63/−0.34	2.35/−2.05	1.22/−1.39
Flack parameter	/	/	/	/

Table S2. Crystallographic data and structure refinement for compounds **6**-**9**.

Compound	**6**	**7**	**8**	**9**
CCDC	2287425	2287432	2287433	2287437
Empirical formula	$C_{31.18}H_{31.14}N_5O_{10}PW_2$	$C_{28}H_{40}ClN_5PRh$	$C_{26}H_{43}AlN_5P$	$C_{22}H_{32}AuClN_5O_{0.5}P$
Formula weight	1034.58	615.98	483.60	637.91
Temperature/K	123(1)	123(1)	100(1)	100(1)
Crystal system	triclinic	monoclinic	monoclinic	monoclinic
Space group	*P*-1	$P2_1/n$	$P2_1/n$	$C2/c$
a/Å	11.44130(10)	10.69310(10)	11.49210(10)	19.9717(4)
b/Å	11.7869(2)	20.9320(2)	12.79310(10)	13.7499(2)
c/Å	14.4705(2)	13.9759(2)	19.5591(2)	20.7972(4)
α/°	84.4020(10)	90	90	90
β/°	87.6070(10)	110.5090(10)	100.0810(10)	120.538(3)
γ/°	71.1270(10)	90	90	90
Volume/Å^3	1837.63(4)	2929.92(6)	2831.18(4)	4918.9(2)
Z	2	4	4	8
ρ_{calc}g/cm^3	1.870	1.396	1.135	1.723
μ/mm^{-1}	12.321	6.256	1.318	6.176
F(000)	992.0	1280.0	1048.0	2512.0
Crystal size/mm^3	0.137 × 0.072 × 0.045	0.158 × 0.083 × 0.065	0.477 × 0.106 × 0.084	0.175 × 0.124 × 0.09
Diffractometer	XtaLAB Synergy R, DW system, HyPix-Arc 150	XtaLAB Synergy R, DW system, HyPix-Arc 150	XtaLAB Synergy R, DW system, HyPix-Arc 150	XtaLAB Synergy R, DW system, HyPix-Arc 150
Radiation	Cu Kα (λ = 1.54184)	Cu Kα (λ = 1.54184)	Cu Kα (λ = 1.54184)	Mo Kα (λ = 0.71073)
2Θ range for data collection/°	7.966 to 150.446	7.966 to 150.446	8.298 to 151.506	4.548 to 66.282
Index ranges	−14 ≤ h ≤ 14, −14 ≤ k ≤ 14, −18 ≤ l ≤ 17	−13 ≤ h ≤ 13, −26 ≤ k ≤ 26, −16 ≤ l ≤ 17	−14 ≤ h ≤ 14, −15 ≤ k ≤ 11, −23 ≤ l ≤ 24	−30 ≤ h ≤ 30, −21 ≤ k ≤ 19, −31 ≤ l ≤ 31
Reflections collected	92180	35698	27173	70757
Independent reflections	7443 [R_{int} = 0.0404, R_{sigma} = 0.0155]	5993 [R_{int} = 0.0344, R_{sigma} = 0.0240]	5754 [R_{int} = 0.0397, R_{sigma} = 0.0249]	9385 [R_{int} = 0.0280, R_{sigma} = 0.0200]
Data/restraints/ parameters	7443/199/572	5993/0/450	5754/0/308	9385/60/336
Goodness-of-fit on F^2	1.091	1.060	1.087	1.022
Final R indexes [I>=2σ (I)]	R_1 = 0.0306, wR_2 = 0.0725	R_1 = 0.0346, wR_2 = 0.0807	R_1 = 0.0412, wR_2 = 0.1216	R_1 = 0.0347, wR_2 0.0788
Final R indexes [all data]	R_1 = 0.0330, wR_2 = 0.0737	R_1 = 0.0384, wR_2 = 0.0824	R_1 = 0.0456, wR_2 = 0.1244	R_1 = 0.0520, wR_2 = 0.0864
Largest diff. peak/hole / e Å^{-3}	1.35/−1.65	0.76/−1.42	0.44/−0.28	2.41/−1.70
Flack parameter	/	/	/	/

Table S3. Crystallographic data and structure refinement for compounds **10**-**13a**.

Compound	**10**	**11**	**12**	**13a**
CCDC	2287439	2287447	2287449	2287452
Empirical formula	$C_{30}H_{43}F_6N_5P_2Ru$	$C_{86}H_{126}N_{20}Ni_2P_4$	$C_{49}H_{70}N_7NiPSi$	$C_{49}H_{69}CoN_7PSi$
Formula weight	750.70	1681.36	874.89	874.10
Temperature/K	123(1)	123(1)	123(1)	123(1)
Crystal system	monoclinic	triclinic	monoclinic	monoclinic
Space group	$P2_1/n$	P-1	$P2_1/n$	$P2_1/c$
a/Å	14.09840(10)	13.1335(3)	21.4772(2)	19.9005(6)
b/Å	15.6040(2)	18.3677(3)	10.28980(10)	12.7455(4)
c/Å	15.7704(2)	21.1776(3)	24.4621(2)	20.2812(5)
α/°	90	75.2186(13)	90	90
β/°	103.1590(10)	74.7461(14)	113.8830(10)	104.681(3)
γ/°	90	79.3989(16)	90	90
Volume/Å^3	3378.25(7)	4728.10(15)	4943.13(9)	4976.2(3)
Z	4	2	4	4
ρ_{calc}g/cm^3	1.476	1.181	1.176	1.167
μ/mm^{-1}	3.844	1.536	1.398	3.530
F(000)	1544.0	1796.0	1880.0	1872.0
Crystal size/mm^3	0.263 × 0.175 × 0.117	0.4 × 0.17 × 0.07	0.218 × 0.037 × 0.029	0.194 × 0.108 × 0.072
Diffractometer	SuperNova, Dualflex, TitanS2	SuperNova, Dualflex, TitanS2	XtaLAB Synergy R, DW system, HyPix-Arc 150	XtaLAB Synergy R, DW system, HyPix-Arc 150
Radiation	Cu Kβ (λ = 1.39222)	Cu Kα (λ = 1.54184)	Cu Kα (λ = 1.54184)	Cu Kα (λ = 1.54184)
2Θ range for data collection/°	7.292 to 152.734	7.384 to 133.816	4.632 to 151.536	8.272 to 147.978
Index ranges	−19 ≤ h ≤ 14, −18 ≤ k ≤ 21, −22 ≤ l ≤ 21	−15 ≤ h ≤ 15, −21 ≤ k ≤ 21, −25 ≤ l ≤ 23	−26 ≤ h ≤ 25, −9 ≤ k ≤ 12, −30 ≤ l ≤ 30	−24 ≤ h ≤ 24, −15 ≤ k ≤ 14, −25 ≤ l ≤ 18
Reflections collected	27508	87246	61155	34001
Independent reflections	9425 [R_{int} = 0.0455, R_{sigma} = 0.0328]	16655 [R_{int} = 0.0762, R_{sigma} = 0.0422]	10075 [R_{int} = 0.0284, R_{sigma} = 0.0228]	9845 [R_{int} = 0.0731, R_{sigma} = 0.0572]
Data/restraints/ parameters	9425/19/ 485	16655/12/1039	10075/0/548	9845/41/636
Goodness-of-fit on F^2	1.028	1.023	1.027	1.087
Final R indexes [I>=2σ (I)]	R_1 = 0.0420, wR_2 = 0.1134	R_1 = 0.0472, wR_2 = 0.1187	R_1 = 0.0455, wR_2 = 0.1145	R_1 = 0.0742, wR_2 = 0.2055
Final R indexes [all data]	R_1 = 0.0435, wR_2 = 0.1150	R_1 = 0.0588, wR_2 = 0.1277	R_1 = 0.0546, wR_2 = 0.1198	R_1 = 0.0928, wR_2 = 0.2178
Largest diff. peak/hole / e Å^{-3}	1.44/−0.97	0.82/−0.44	0.43/−0.61	1.30/−0.86
Flack parameter	/	/	/	/

Table S4. Crystallographic data and structure refinement for compounds **13b**-**15**.

Compound	**13b**	**13b•Et$_2$O**	**14**	**15**
CCDC	2287453	2287454	2287455	2287456
Empirical formula	$C_{43}H_{57}CoN_7PSi$	$C_{47}H_{67}CoN_7OPSi$	$C_{33}H_{34}BN_5P_2$	$C_{21}H_{34}AlN_5P_2$
Formula weight	789.94	864.06	573.40	445.45
Temperature/K	123(1)	123(1)	100(1)	123(1)
Crystal system	orthorhombic	triclinic	monoclinic	triclinic
Space group	*Pbca*	*P*-1	$P2_1/c$	*P*-1
a/Å	18.09450(10)	10.3589(2)	9.21300(10)	10.8379(2)
b/Å	20.35170(10)	11.93460(10)	17.41410(10)	11.5326(2)
c/Å	23.53500(10)	20.3206(3)	19.11760(10)	11.6533(2)
α/°	90	77.9630(10)	90	67.476(2)
β/°	90	78.3360(10)	93.0650(10)	68.607(2)
γ/°	90	76.9380(10)	90	73.5420(10)
Volume/Å^3	8666.85(7)	2361.51(6)	3062.77(4)	1235.15(4)
Z	8	2	4	2
ρ_{calc}g/cm^3	1.211	1.215	1.244	1.198
μ/mm^{-1}	4.003	3.730	1.522	2.066
F(000)	3360.0	924.0	1208.0	476.0
Crystal size/mm^3	0.079 × 0.145 × 0.206	0.344 × 0.152 × 0.041	0.208 × 0.165 × 0.125	0.217 × 0.173 × 0.143
Diffractometer	XtaLAB Synergy R, DW system, HyPix-Arc 150	XtaLAB Synergy R, DW system, HyPix-Arc 150	XtaLAB Synergy R, DW system, HyPix-Arc 150	XtaLAB Synergy R, DW system, HyPix-Arc 150
Radiation	Cu Kα (λ = 1.54184)	Cu Kα (λ = 1.54184)	Cu Kα (λ = 1.54184)	Cu Kα (λ = 1.54184)
2Θ range for data collection/°	7.512 to 151.534	7.718 to 151.156	6.87 to 151.428	8.418 to 150.854
Index ranges	−22 ≤ h ≤ 22, −24 ≤ k ≤ 18, −28 ≤ l ≤ 29	−11 ≤ h ≤ 12, −14 ≤ k ≤ 14, −25 ≤ l ≤ 25	−11 ≤ h ≤ 11, −21 ≤ k ≤ 20, –23 ≤ l ≤ 22	−13 ≤ h ≤ 10, −14 ≤ k ≤ 14, −14 ≤ l ≤ 14
Reflections collected	111365	51842	26586	24260
Independent reflections	8901 [R_{int} = 0.0288, R_{sigma} = 0.0161]	9607 [R_{int} = 0.0284, R_{sigma} = 0.0223]	6247 [R_{int} = 0.0210, R_{sigma} = 0.0172]	4987 [R_{int} = 0.0223, R_{sigma} = 0.0173]
Data/restraints/ parameters	8901/0/649	9607/0/724	6247/0/374	4987/0/269
Goodness-of-fit on F^2	1.033	1.081	1.048	1.039
Final R indexes [I>=2σ (I)]	R_1 = 0.0354, wR_2 = 0.0947	R_1 = 0.0371, wR_2 = 0.0977	R_1 = 0.0318, wR_2 = 0.0831	R_1 = 0.0340, wR_2 = 0.0899
Final R indexes [all data]	R_1 = 0.0384, wR_2 = 0.0967	R_1 = 0.0413, wR_2 = 0.0998	R_1 = 0.0339, wR_2 = 0.0845	R_1 = 0.0357, wR_2 = 0.0910
Largest diff. peak/hole / e Å^{-3}	0.83/−0.26	0.32/−0.33	0.33/−0.29	1.21/−0.40
Flack parameter	/	/	/	/

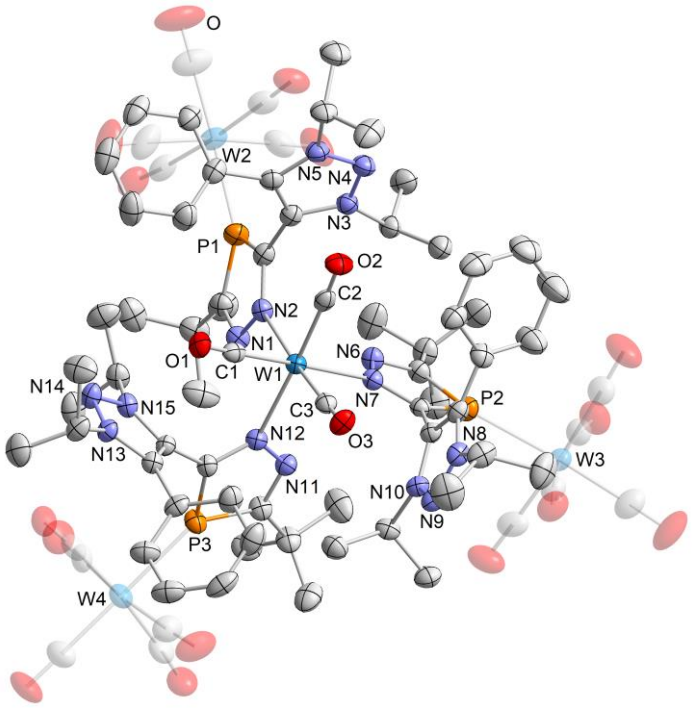

Figure S61. Solid-state molecular structure of $[W(CO)_3\{\{W(CO)_5(\mathbf{2})\}\}_3]$ (**4**): shown at the 50% probability level with hydrogen atoms and non coordinating solvent molecules omitted for clarity. Selected bond lengths [Å] and angles [°]: W1−N2 2.310(3), W1−N7 2.302(4), W1−N12 2.291(4), W1−C1 1.949(5), W1−C2 1.945(5), W1−C3 1.932(5), C1−O1 1.169(6), C2−O2 1.172(6), C3−O3 1.184, N1−N2 1.353(5), N6−N7 1.357(5), N11−N12 1.366(5), P1−W2 2.5084(1), P2−W3 2.5138(1), P3−W4 2.5221(1), N4−N5 1.321(5), N3−N4 1.321(5), N2-W1-C3 175.28(2), N7-W1-C1 175.61(2), N12-W1-C2 177.09(2), N2-W1-C2 97.38(2), N3-N4-N5 104.2(4).

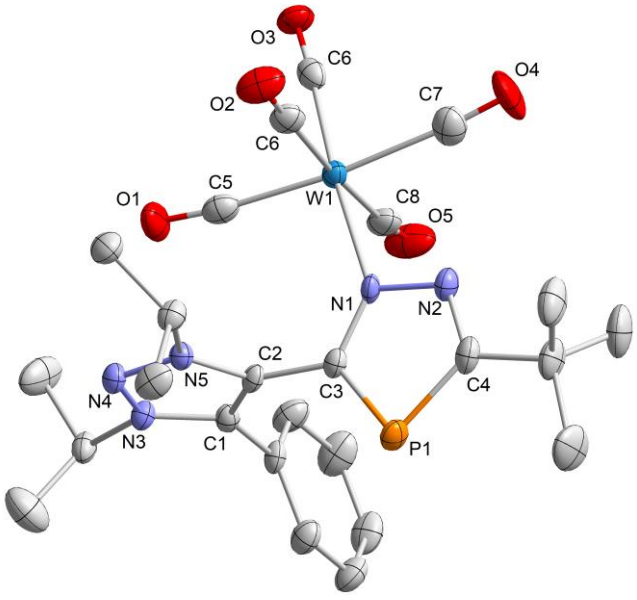

Figure S62. Solid-state molecular structure of $[W(CO)_5(\mathbf{2})]$ (**5**) shown at the 50% probability with hydrogen atoms omitted for clarity. The asymmetric unit cell contained a second crystallographically independent molecule with very similar structural parameters; only one of these molecules is shown. Selected bond lengths [Å] and angles [°]: N1−W1 2.252(3), W1−C5 2.012(4), C5−O1 1.152(5), P1−C4 1.757(5), P1−C3 1.743(4), C4−N2 1.322(6), N1−N2 1.361(5), N1−C3 1.345(5), C2−C3 1.455(5), C1−C2 1.385(5), N3−N4 1.325(5), N4−N5 1.318(5), W1-C5-O1 173.6(4), C3-P1-C4 85.37(2), P1-C4-N2 115.6(3), C4-N2-N1 111.8(3), N2-N1-C3 112.8(3), N1-C3-P1 114.5(3), N3-N4-N5 104.3(3), N4-N5-C2 112.8(3), N5-C2-C1 105.3(3), C2-C1-N3 104.4(3), N1-C3-C2-N5 81.2(4).

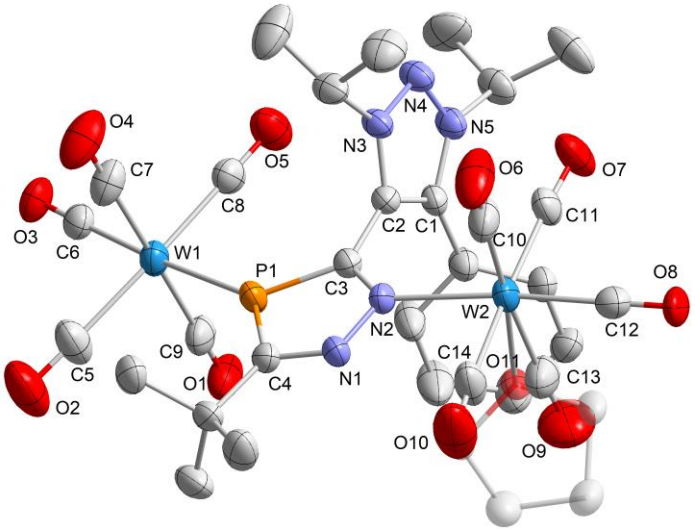

Figure S63. Solid-state molecular structure of [{W(CO)$_5$}$_2$(**2**)] (**6**) shown at the 50% probability with hydrogen atoms and disorder omitted for clarity. The C13−O9 unit, coordinating to W2, is partially occupied by a THF molecule (refined occupancy: 0.39). Selected bond lengths [Å] and angles [°]: P1−W1 2.5091(1), N2−W2 2.268(3), W1−C5 2.050(5), W2−C13 2.096(2), W2−O11 2.208(1), C5−O2 1.149(6), C13−O9 1.15(2), P1−C4 1.748(4), P1−C3 1.734(4), C4−N1 1.319(5), N1−N2 1.354(5), N2−C3 1.344(5), C2−C3 1.468(5), C1−C2 1.380(6), N3−N4 1.319(5), N4−N5 1.320(5), P1-W1-C6 176.63(1), P1-W1-C8 88.94(1), N2-W2-C12 174.53(2), N2-W2-C11 98.59(2), C3-P1-C4 87.96(2), P1-C4-N1 112.8(3), C4-N1-N2 113.5(3), N1-N2-C3 113.6(3), N2-C3-P1 112.1(3), N3-N4-N5 104.5(3), N4-N5-C1 112.7(3), N5-C1-C2 104.8(4), C1-C2-N3 105.3(3).

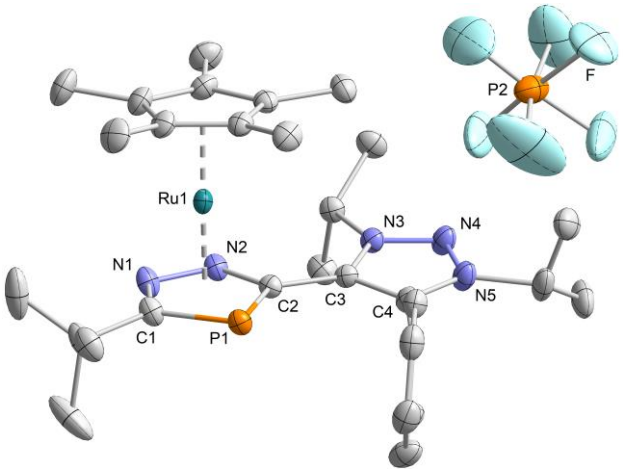

Figure S64. Solid-state molecular structure of [Cp*Ru(**2**)]PF$_6$ (**10**) shown at the 50% probability level with hydrogen atoms and disorder in one of the *i*Pr groups omitted for clarity. Selected bond lengths [Å] and angles [°]: Ru1−Cp*$^{centr.}$ 1.8189(1), Ru1−C$_2$N$_2$P$^{centr.}$ 1.8219(8), P1−C1 1.779(2), P1−C2 1.7865(2), N1−N2 1.383(2), N1−C1 1.372(3), N2−C2 1.389(3), C2−C3 1.464(3), C3−C4 1.381(3), C3−N3 1.366(2), N3−N4 1.321(3), N4−N5 1.315(3), C1-P1-C2 85.11(1), P1-C2-N2 115.39(1), C2-N2-N1 111.32(2), N2-N1-C1 112.40(2), C3-N3-N4 112.29(2), N3-N4-N5 104.82(2), N4-N5-C4 112.74(2), N5-C4-C3 105.30(2), C2-N2-C3-N3 9.5(2).

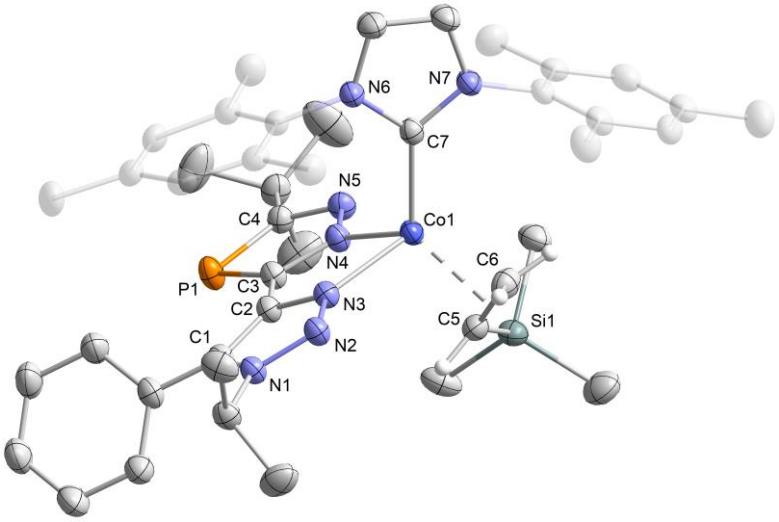

Figure S65. Solid-state molecular structure of [(IMes)Co(vtms)($C_{17}H_{21}N_5P$)] (**13b**) shown at the 50% probability level with hydrogen atoms except $C_2H_3SiMe_3$ (positions refined) moiety omitted for clarity. Selected bond lengths [Å] and angles [°]: Co1−N3 2.0989(1), Co1−N4 2.0082(2), Co1−C7 2.0371(2), Co1−$C_{56}^{centr.}$ 1.9409(1), P1−C3 1.7442(2), P1−C4 1.7682(2), C4−N5 1.330(2), N4−N5 1.3590(2), C3−N4 1.350(2), C2−C3 1.459(2), C1−C2 1.381(2), C1−N1 1.367(2), N1−N2 1.3454(2), N2−N3 1.3081(2), N6−C7 1.366(2), N7−C7 1.364(2), C5−C6 1.406(2), Si1−C5 1.8528(2), C7-Co1-N4 112.61(6), N3-Co1-C5 91.68(6), N3-Co1-C6 102.11(7), C6-C5-Si1 124.85(1), N6-C7-N7 102.75(1), C3-P1-C4 85.52(8), P1-C4-N5 115.40(1), C4-N5-N4 111.38(1), N5-N4-C3 113.60(1), N4-C3-P1 114.09(1), C1-N1-N2 111.68(1), N1-N2-N3 106.34(1), N2-N3-C2 110.41(1), N3-C2-C1 107.66(1).

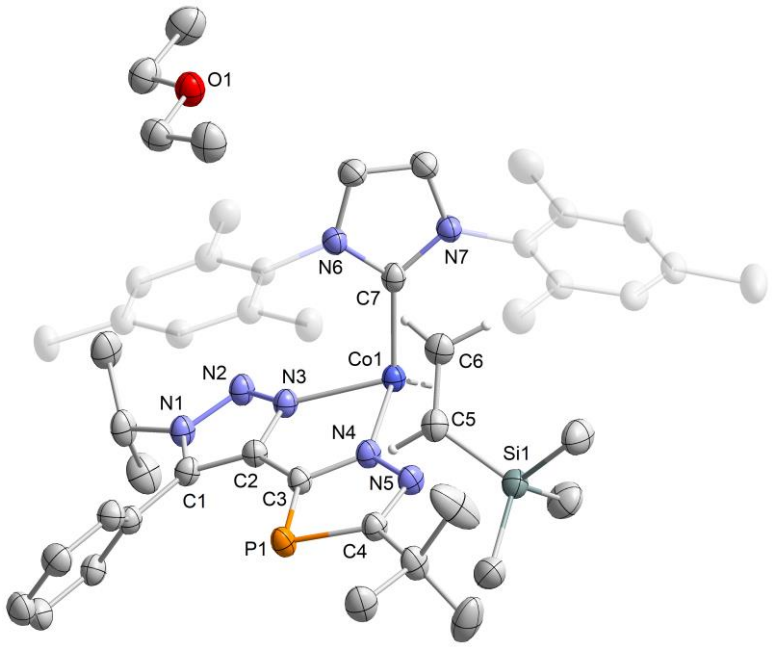

Figure S66. Solid-state molecular structure of [(IMes)Co(vtms)($C_{17}H_{21}N_5P$)]•Et_2O (**13b**) shown at the 50% probability level with hydrogen atoms except $C_2H_3SiMe_3$ (positions refined) moiety omitted for clarity. Selected bond lengths [Å] and angles [°]: Co1−N3 2.1222(1), Co1−N4 1.9882(1), Co1−C7 2.0316(2), Co1−$C_{56}^{centr.}$ 1.9286(1), P1−C3 1.7413(2), P1−C4 1.7650(2), C4−N5 1.329(2), N4−N5 1.3619(2), C3−N4 1.355(2), C2−C3 1.460(2), C1−C2 1.386(2), C1−N1 1.363(2), N1−N2 1.345(2), N2−N3 1.3174(2), N6−C7 1.367(2), N7−C7 1.374(2), C5−C6 1.406(3), Si1−C5 1.8524(2), C7-Co1-N4 111.34(6), N3-Co1-C5 91.97(7), N3-Co1-C6 102.23(7), C6-C5-Si1 122.65(1), N6-C7-N7 102.37(1), C3-P1-C4 85.63(8), P1-C4-N5 115.60(1), C4-N5-N4 111.27(1), N5-N4-C3 113.43(1), N4-C3-P1 114.06(1), C1-N1-N2 111.79(1), N1-N2-N3 106.48(1), N2-N3-C2 109.93(1), N3-C2-C1 108.02(1).

References

[1] L. Nyulaszi, T. Veszpremi, J. Reffy, B. Burkhardt, M. Regitz, *J. Am. Chem. Soc.* **1992**, *114*, 9080–9084.
[2] L. Weber, *Angew. Chem. Int. Ed.* **2002**, *41*, 563–572.
[3] F. Mathey, *Angew. Chem. Int. Ed.* **2003**, *42*, 1578–1604.
[4] H. Tsuji, K. Sato, Y. Sato, E. Nakamura, *J. Mater. Chem.* **2009**, *19*, 3364–3366.
[5] S. Graule, M. Rudolph, W. Shen, J. A. G. Williams, C. Lescop, J. Autschbach, J. Crassous, R. Réau, *Chem. – Eur. J.* **2010**, *16*, 5976–6005.
[6] M. P. Washington, V. B. Gudimetla, F. L. Laughlin, N. Deligonul, S. He, J. L. Payton, M. C. Simpson, J. D. Protasiewicz, *J. Am. Chem. Soc.* **2010**, *132*, 4566–4567.
[7] Y. Matano, A. Saito, T. Fukushima, Y. Tokudome, F. Suzuki, D. Sakamaki, H. Kaji, A. Ito, K. Tanaka, H. Imahori, *Angew. Chem. Int. Ed.* **2011**, *50*, 8016–8020.
[8] Y. Matano, H. Ohkubo, T. Miyata, Y. Watanabe, Y. Hayashi, T. Umeyama, H. Imahori, *Eur. J. Inorg. Chem.* **2014**, *2014*, 1620–1624.
[9] M. P. Duffy, W. Delaunay, P.-A. Bouit, M. Hissler, *Chem. Soc. Rev.* **2016**, *45*, 5296–5310.
[10] M. Stępień, E. Gońka, M. Żyła, N. Sprutta, *Chem. Rev.* **2017**, *117*, 3479–3716.
[11] A. Schmidpeter, in *Compr. Heterocycl. Chem. II* (Eds.: A.R. Katritzky, C.W. Rees, E.F.V. Scriven), Pergamon, Oxford, **1996**, pp. 771–818.
[12] A. Schmidpeter, in *Phosphorus-Carbon Heterocycl. Chem.* (Ed.: F. Mathey), Elsevier Science Ltd, Oxford, **2001**, pp. 363–461.
[13] V. V. Zhdankin, in *Compr. Heterocycl. Chem. III* (Eds.: A.R. Katritzky, C.A. Ramsden, E.F.V. Scriven, R.J.K. Taylor), Elsevier, Oxford, **2008**, pp. 583–601.
[14] N. Gupta, in *Phosphorus Heterocycles II* (Ed.: R.K. Bansal), Springer, Berlin, Heidelberg, **2010**, pp. 175–206.
[15] A. B. Gamble, in *Compr. Heterocycl. Chem. IV* (Eds.: D.S. Black, J. Cossy, C.V. Stevens), Elsevier, Oxford, **2022**, pp. 410–432.
[16] J. Elguero, in *Compr. Heterocycl. Chem.* (Eds.: A.R. Katritzky, C.W. Rees), Pergamon, Oxford, **1984**, pp. 167–303.
[17] F. Mathey, *Chem. Rev.* **1988**, *88*, 429–453.
[18] G. Märkl, S. Pflaum, *Tetrahedron Lett.* **1986**, *27*, 4415–4418.
[19] G. Märkl, S. Pflaum, *Tetrahedron Lett.* **1987**, *28*, 1511–1514.
[20] G. Märkl, I. Trötsch, *Angew. Chem.* **1984**, *96*, 899–901.
[21] W. Rösch, M. Regitz, *Angew. Chem. Int. Ed. Engl.* **1984**, *23*, 900–901.
[22] A. Schmidpeter, A. Willhalm, *Angew. Chem. Int. Ed. Engl.* **1984**, *23*, 903–904.
[23] K. Karaghiosoff, C. Cleve, A. Schmidpeter, *Phosphorus Sulfur Relat. Elem.* **1986**, *28*, 289–296.
[24] W. Rösch, U. Vogelbacher, T. Allspach, M. Regitz, *J. Organomet. Chem.* **1986**, *306*, 39–53.
[25] W. Rösch, H. Richter, M. Regitz, *Chem. Ber.* **1987**, *120*, 1809–1813.
[26] E. P. O. Fuchs, M. Hermesdorf, W. Schnurr, W. Rösch, H. Heydt, M. Regitz, P. Binger, *J. Organomet. Chem.* **1988**, *338*, 329–340.
[27] J. Grobe, D. L. Van, M. Hegemann, B. Krebs, M. Läge, *Chem. Ber.* **1992**, *125*, 411–414.
[28] R. Suter, Z. Benkő, H. Grützmacher, *Chem. – Eur. J.* **2016**, *22*, 14979–14987.
[29] L. Wan, I. Alkorta, J. Elguero, J. Sun, W. Zheng, *Tetrahedron* **2007**, *63*, 9129–9133.
[30] J. Fidelius, K. Schwedtmann, S. Schellhammer, J. Haberstroh, S. Schulz, R. Huang, M. C. Klotzsche, A. Bauzá, A. Frontera, S. Reineke, J. J. Weigand, *Chem* **2023**, *0*, DOI 10.1016/j.chempr.2023.10.016.
[31] R. K. Bansal, G. Neelima, in *Sci. Synth.*, Thieme Group, **2004**, p. 689.

[32] *Product Class 23: Diazadiphospholes*, Thieme Verlag, **2004**.
[33] A. Schmidpeter, C. Leyh, K. Karaghiosoff, *Angew. Chem. Int. Ed. Engl.* **1985**, *24*, 124–125.
[34] C. Charrier, N. Maigrot, L. Ricard, P. L. Floch, F. Mathey, *Angew Chem Int Ed Engl* **1996**, *35*, 2133–2134.
[35] M.-L. Y. Riu, W. J. Transue, J. M. Rall, C. C. Cummins, *J. Am. Chem. Soc.* **2021**, *143*, 7635–7640.
[36] I. Alkorta, J. Elguero, *Struct. Chem.* **2016**, *27*, 1531–1542.
[37] P. W. Antoni, C. Golz, J. J. Holstein, D. A. Pantazis, M. M. Hansmann, *Nat. Chem.* **2021**, *13*, 587–593.
[38] P. W. Antoni, J. Reitz, M. M. Hansmann, *J. Am. Chem. Soc.* **2021**, *143*, 12878–12885.
[39] J. Reitz, P. W. Antoni, J. J. Holstein, M. M. Hansmann, *Angew. Chem. Int. Ed.* **2023**, *62*, e202301486.
[40] A. Eitzinger, J. Reitz, P. W. Antoni, H. Mayr, A. R. Ofial, M. M. Hansmann, *Angew. Chem. Int. Ed.* **2023**, *n/a*, e202309790.
[41] J. Reitz, *Details of the Synthesis and Characterization of 1 Are Reported in Justus Reitz's PhD Thesis*, PhD Dissertation, Universität Dortmund, **2024**.
[42] P. Pyykkö, M. Atsumi, *Chem. – Eur. J.* **2009**, *15*, 186–197.
[43] P. Pyykkö, M. Atsumi, *Chem. – Eur. J.* **2009**, *15*, 12770–12779.
[44] K. Karaghiosoff, A. Schmidpeter, *Phosphorus Sulfur Relat. Elem.* **1988**, *36*, 217–259.
[45] L. Nyulászi, P. Várnai, W. Eisfeld, M. Regitz, *J. Comput. Chem.* **1997**, *18*, 609–616.
[46] L. Nyulászi, *J. Organomet. Chem.* **2005**, *690*, 2597–2602.
[47] L. Szarvas, Z. Bajko, S. Fusz, S. Burck, J. Daniels, M. Nieger, D. Gudat, *Z. Für Anorg. Allg. Chem.* **2002**, *628*, 2303–2310.
[48] M. Mlateček, L. Dostál, Z. Růžičková, M. Erben, *Polyhedron* **2016**, *119*, 325–334.
[49] G. Socrates, *Infrared and Raman Characteristic Group Frequencies: Tables and Charts*, Wiley, Chichester, **2004**.
[50] X. Jia, F. Zhao, *Inorganica Chim. Acta* **2017**, *461*, 145–149.
[51] H. Schmidbaur, *Chem. Soc. Rev.* **1995**, *24*, 391–400.
[52] W. Zheng, G. Zhang, K. Fan, *Organometallics* **2006**, *25*, 1548–1550.
[53] J. Yorke, L. Wan, A. Xia, W. Zheng, *Tetrahedron Lett.* **2007**, *48*, 8843–8845.
[54] L. Duan, X. Zhang, W. Zheng, *Dalton Trans.* **2017**, *46*, 8354–8358.
[55] P. W. Jolly, in *Compr. Organomet. Chem.* (Eds.: G. Wilkinson, F.G.A. Stone, E.W. Abel), Pergamon, Oxford, **1982**, pp. 37–100.
[56] C.-Y. Lin, P. P. Power, *Chem. Soc. Rev.* **2017**, *46*, 5347–5399.
[57] M. R. Elsby, S. A. Johnson, *J. Am. Chem. Soc.* **2017**, *139*, 9401–9407.
[58] M. R. Elsby, J. Liu, S. Zhu, L. Hu, G. Huang, S. A. Johnson, *Organometallics* **2019**, *38*, 436–450.
[59] C. P. Lenges, P. S. White, M. Brookhart, *J. Am. Chem. Soc.* **1998**, *120*, 6965–6979.
[60] D. Wang, Q. Chen, X. Leng, L. Deng, *Inorg. Chem.* **2018**, *57*, 15600–15609.
[61] L. J. L. Häller, M. J. Page, S. Erhardt, S. A. Macgregor, M. F. Mahon, M. A. Naser, A. Vélez, M. K. Whittlesey, *J. Am. Chem. Soc.* **2010**, *132*, 18408–18416.
[62] D. Schmidt, J. H. J. Berthel, S. Pietsch, U. Radius, *Angew. Chem. Int. Ed.* **2012**, *51*, 8881–8885.
[63] K. J. Iversen, D. J. D. Wilson, J. L. Dutton, *Dalton Trans.* **2014**, *43*, 12820–12823.
[64] R. H. Crabtree, *Chem. Rev.* **2015**, *115*, 127–150.

[65] S. Würtemberger-Pietsch, U. Radius, T. B. Marder, *Dalton Trans.* **2016**, *45*, 5880–5895.
[66] A. Hernán-Gómez, A. R. Kennedy, E. Hevia, *Angew. Chem. Int. Ed.* **2017**, *56*, 6632–6635.
[67] Y. Wang, H. P. Hickox, Y. Xie, P. Wei, H. F. I. Schaefer, G. H. Robinson, *J. Am. Chem. Soc.* **2017**, *139*, 16109–16112.
[68] A. A. Danopoulos, A. Massard, G. Frison, P. Braunstein, *Angew. Chem. Int. Ed.* **2018**, *57*, 14550–14554.
[69] P. Wang, J. Cheng, D. Wang, C. Yang, X. Leng, L. Deng, *Organometallics* **2020**, *39*, 2871–2877.
[70] A. Merschel, T. Glodde, B. Neumann, H.-G. Stammler, R. S. Ghadwal, *Angew. Chem. Int. Ed.* **2021**, *60*, 2969–2973.
[71] M. Bochmann, I. Hawkins, M. B. Hursthouse, R. L. Short, *J. Chem. Soc. Dalton Trans.* **1990**, 1213–1219.
[72] J. Du, L. Wang, M. Xie, L. Deng, *Angew. Chem. Int. Ed.* **2015**, *54*, 12640–12644.
[73] J. S. Francisco, *J. Am. Chem. Soc.* **1989**, *111*, 7353–7361.
[74] H. Marsmann, in *Oxyg.-17 Silicon-29* (Eds.: J.-P. Kintzinger, H. Marsmann), Springer, Berlin, Heidelberg, **1981**, pp. 65–235.
[75] C. Lepetit, V. Maraval, Y. Canac, R. Chauvin, *Coord. Chem. Rev.* **2016**, *308*, 59–75.
[76] G. Becker, G. Gresser, W. Uhl, *Z. Naturforschung B* **1981**, *36*, 16–19.
[77] R. Uson, A. Laguna, M. Laguna, D. A. Briggs, H. H. Murray, J. P. Fackler Jr., in *Inorg. Synth.*, John Wiley & Sons, Ltd, **1989**, pp. 85–91.
[78] D. F. Evans, *J. Chem. Soc.* **1959**, 2003–2005.
[79] S. K. Sur, *J. Magn. Reson. 1969* **1989**, *82*, 169–173.
[80] H. Lueken, C. Elschenbroich, F. Hensel, H. Hopf, *Magnetochemie*, Vieweg+Teubner Verlag, Wiesbaden, **1999**.
[81] G. M. Sheldrick, SADABS, Bruker AXS, Madison, USA, **2007**.
[82] CrysAlisPro, Scale3 Abspack, Rigaku Oxford Diffraction, **2019**.
[83] R. C. Clark, J. S. Reid, *Acta Crystallogr. Sect. A* **1995**, *51*, 887–897.
[84] G. M. Sheldrick, *Acta Crystallogr. Sect. Found. Adv.* **2015**, *71*, 3–8.
[85] O. V. Dolomanov, L. J. Bourhis, R. J. Gildea, J. a. K. Howard, H. Puschmann, *J. Appl. Crystallogr.* **2009**, *42*, 339–341.
[86] G. M. Sheldrick, *Acta Crystallogr. Sect. C Struct. Chem.* **2015**, *71*, 3–8.
[87] G. M. Sheldrick, *Acta Crystallogr. A* **2008**, *64*, 112–122.

7 Summary and Conclusion

Chapter 1. *Functionalization of Polyphosphido Ligands Derived from White Phosphorus*

This introductory chapter provides a systematic overview of the diverse chemistry of transition-metal-mediated P_4 functionalization (Scheme 1), with particular emphasis on recent developments and works relevant to this thesis. The chapter begins with a brief introduction on the relevance of P_4 transformations and categorizes the current state of this research field into systematic subunits. "One-step activation and functionalization" of P_4 mediated by transition metals is highlighted, followed by the functionalization of P_n ligands within sub-sections based on the number of phosphorus atoms within the ligand: P_1, P_2, P_3, P_4, and $P_n \geq 5$.

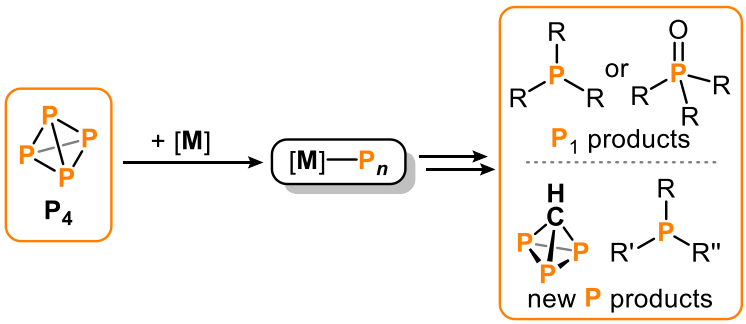

Scheme 1. Transition-metal-mediated P_4 functionalization; [M] = transition metal complex.

Chapter 2. *Cobalt-Mediated [3+1] Fragmentation of White Phosphorus: Access to Acylcyanophosphanides*

Chapter 2 describes the cobaltate complex [K(18c-6)][(Ar*BIAN)Co(cod)] ([K(18c-6)]**2-1**, 18c-6 = [18]crown-6, Ar* = 2,6-dibenzhydryl-4-isopropylphenyl, BIAN = 1,2-bis(arylimino)acenaphthene diamine, cod = 1,5-cyclooctadiene), which is kinetically stabilized by the sterically encumbering Ar*BIAN ligand. It is shown that this complex enables the selective activation of P_4 by ligand exchange of cod, yielding *cyclo*-P_4 complex [K(18c-6)]**2-2** (Scheme 2). Treatment of anionic **2-2**$^-$ with acyl chlorides afforded acylated tetraphosphido complexes **2-3-R** in high yields, bearing a range of alkyl and aryl substituents.

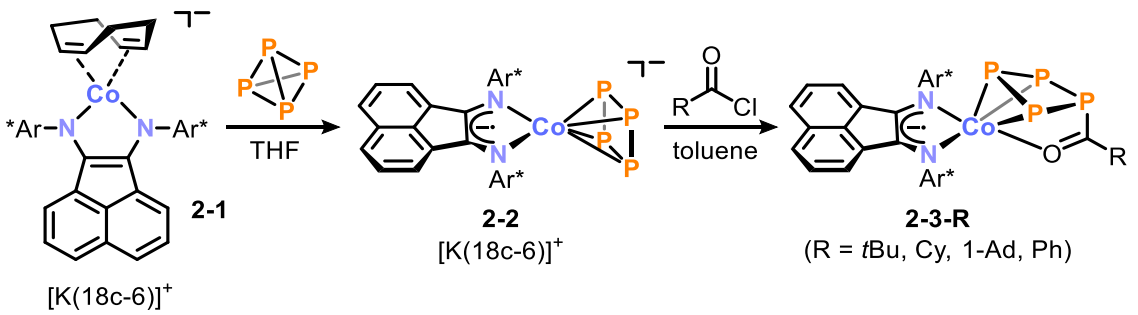

Scheme 2. Activation of P_4 and onward functionalization of [K(18c-6)]**1-2** with RC(O)Cl.

The reaction of Me_3SiCN or isocyanides with **2-3-R** led to partial release of the $P_4C(O)R$ ligand from the coordination sphere of the cobalt center and the formation of the prismane-like complex **2-4-R'**, as well as *endo*- and *exo*-isomers of η^3-coordinating tetraphosphido ligands in **2-5-R'** (Scheme 3). Treatment of **2-3-R** with two equivalents of the cyanide anion facilitated the release of acylcyanophosphanides [K(18c-6)]**2-6-R** through a [3+1] fragmentation process and concomitant release of cyclotriphosphido cobalt complex [K(18c-6)]**2-7**. Insight into the fragmentation reaction was provided through NMR spectroscopic monitoring, which suggested that complexes similar to **2-4-R'** and **2-5-R'** are key intermediates *en route* to anions **2-6-R**$^-$ and **2-7**$^-$. Additionally, a second acyl substituent was introduced to **2-6-R** (R = Cy) yielding the first bis(acyl)cyanophosphine $(CyC(O))_2PCN$ (**2-8**), highlighting the useful reactivity of these anions.

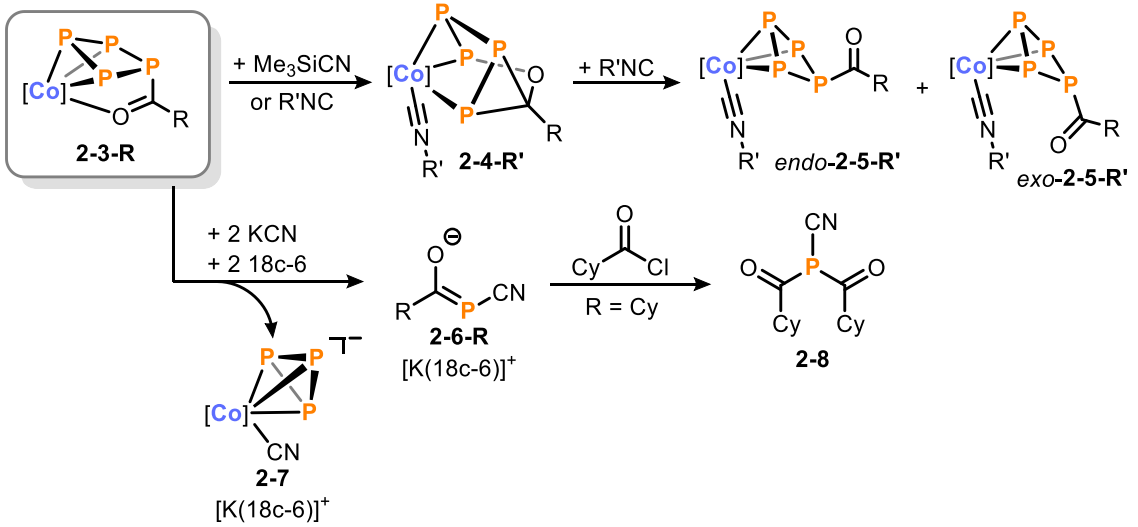

Scheme 3. Rearrangement and [3+1] fragmentation reactions of acylated tetraphosphido complexes; R' = $SiMe_3$, Cy, *t*Bu, Mes, Ph; [Co] = [(Ar*BIAN)Co].

Overall, the results of this work demonstrate that diimine cobalt complexes are an excellent platform for the functionalization of P_4 and accessing new (poly-)phosphorus species. Building on this approach, by exploring reactivity between a wider range of polyphosphides and nucleophiles, should open up avenues for the synthesis of unique

phosphorus compounds. Furthermore, reactions of anions **2-6**$^{-}$**, 2-6-R**$^{-}$ and **2-7**$^{-}$, as well as neutral **2-3-R** with electrophiles give rise to new phosphorus containing compounds, as illustrated by results reported in the following Chapters 3-5.

Chapter 3. *Functionalization of Tetraphosphido Ligands by Heterocumulenes*

The transition-metal-mediated activation and functionalization of white phosphorus allows the synthesis of distinctive phosphorus-based compounds. However, the selective and effective functionalization of the polyphosphorus ligands in the coordination sphere of transition metals remains underdeveloped. In an extension to the previous chapter, the reactivity of tetraphosphido complexes with a range of electrophilic heterocumulenes was investigated. The first part of Chapter 3 presents the reactivity of anion **2-2**$^{-}$ with sulfur diimide $S(NSiMe_3)_2$ and CS_2, which yielded compounds [K(18c-6)]**3-1** and [K(18c-6)]**3-2**, respectively (Scheme 4). In these reactions, distinct reactivity − electrophilic addition vs. P−P bond insertion − was observed, dependent on the substrate. Anion **3-2**$^{-}$ features a puckered η^3:η^1-P_4CS_2 ligand and initial reactivity studies with electrophiles indicated it readily undergoes salt metathesis reactions. In addition, the reaction of **3-1**$^{-}$ with Me_3SiCl gave rise to the azatetraphosphole complex **3-3**. The addition of the $-SiMe_3$ group was found to be a reversible process, as treatment of **3-3** with either cyanide or alkoxide salts regenerated anion **3-1**$^{-}$. All of the compounds presented within Chapter 3 were characterized using state-of-the-art analytical methods, including single crystal X-ray structural analysis at synchrotron facilities and computational chemistry studies.

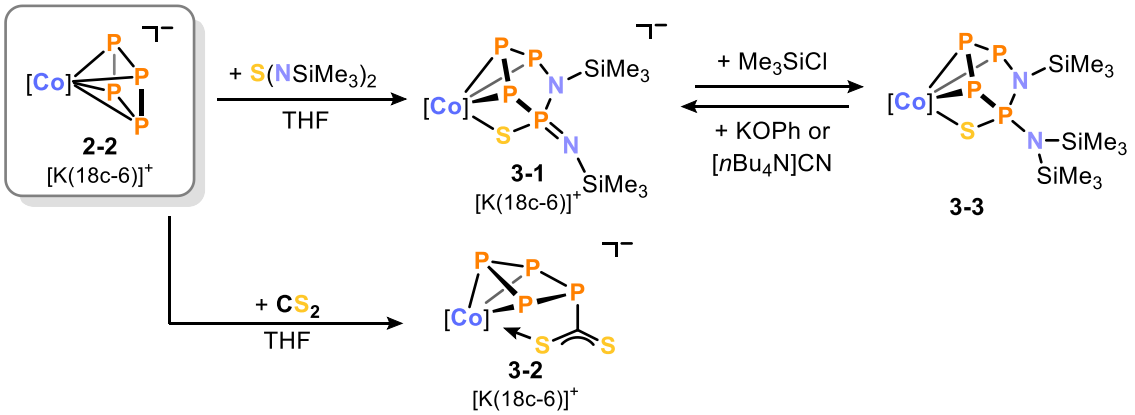

Scheme 4. Reactivity of tetraphosphido cobaltate [K(18c-6)]**2-2** with heterocumulenes.

In the second part of Chapter 3 the reactivity of the neutral complex **2-3-*t*Bu** (see Chapter 2) with related heterocumulenes was investigated. Surprisingly, complex **2-3-*t*Bu** exhibited discrepant reactivity with isothiocyanates, undergoing insertion into

the P–C bond of the acylated tetraphosphido ligand, yielding the highly derivatized complexes **3-4-R** (Scheme 5).

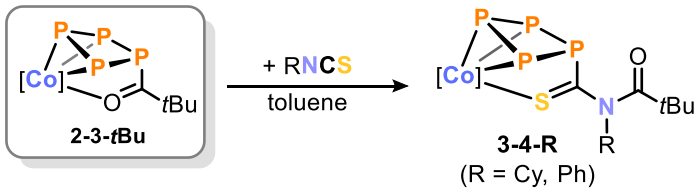

Scheme 5. Insertion of isothiocyanates into the P–C bond of **2-3-*t*Bu**.

These results are clear examples of the versatility and potential of low-valent polyphosphido complexes to achieve facile and diverse transformations of P_4. Considering the increased availability of various *cyclo*-P_4 complexes (Chapter 1), this should pave the way to unique phosphorus compounds and lay the essential groundwork for efficient transition-metal-mediated functionalization of P_4.

Chapter 4. *Synthesis of Polyphosphido Cobalt Complexes through P–P Bond Condensation*

The targeted synthesis of extended polyphosphorus frameworks through P–P condensation reactions of suitable cationic and anionic building blocks remains an attractive, yet challenging goal. In extension to the previous Chapters 2 and 3, the reactivity of the tri- and tetraphosphido cobalt complexes [K(18c-6)]**2-7** and [K(18c-6)]**2-2** with diorganochlorophosphines and cationic phosphorus species was investigated in Chapter 4. The reactivity study commenced with treatment of K(18c-6)]**2-2** and [K(18c-6)]**2-7** with R_2PCl to investigate the accessibility of these *cyclo*-P_n ligands for the synthesis of extended phosphorus frameworks. Thus, the products **4-1-R** and **4-2-R** were obtained through ring-expansion of the P_3 ligand by an R_2P^+ unit (Scheme 6).

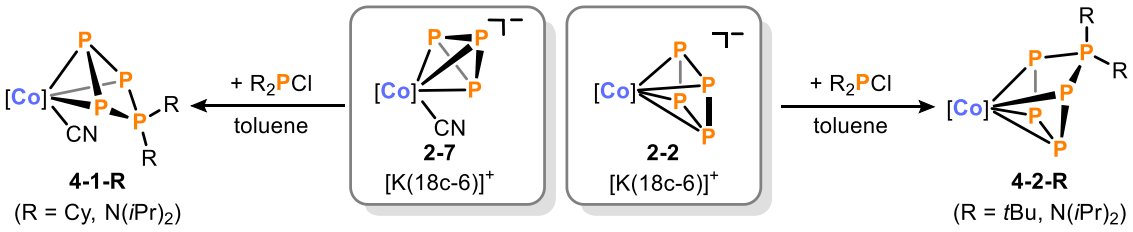

Scheme 6. Salt metathesis reactions of *cyclo*-P_3 and *cyclo*-P_4 cobaltates with diorganochlorophosphines.

Using this approach, the reactivity of anions **2-2**$^-$ and **2-7**$^-$ with tetracationic *cyclo*-tetraphosphane $[(L_C{-}P)_4][OTf]_4$ (**4-3**, L_C = 4,5-dimethyl-1,3-diisopropyl-imidazol-2-yl), an $[L_C{-}P]^+$ transfer reagent, was also investigated. NMR monitoring of the reaction between K(18c-6)]**2-2** and **4-3** revealed the selective formation of cyclotetraphosphido

complex **4-4** and cationic $CoP_5L_{C2}^+$ complex **4-5** as a side product (Scheme 6). Chapter 4 concludes with the synthesis and isolation of the neutral heptaphosphido complex **4-6**, obtained from the 1:2 reaction of **4-3** with K(18c-6)]**2-2**. The reaction most likely involves initial 1,1-insertion of a $[L_C{-}P]_2^{2+}$ fragment into the *cyclo*-P_4 ring, forming a cationic CoP_6 intermediate **4-7**$^+$, as evidenced by ESI-MS analysis.

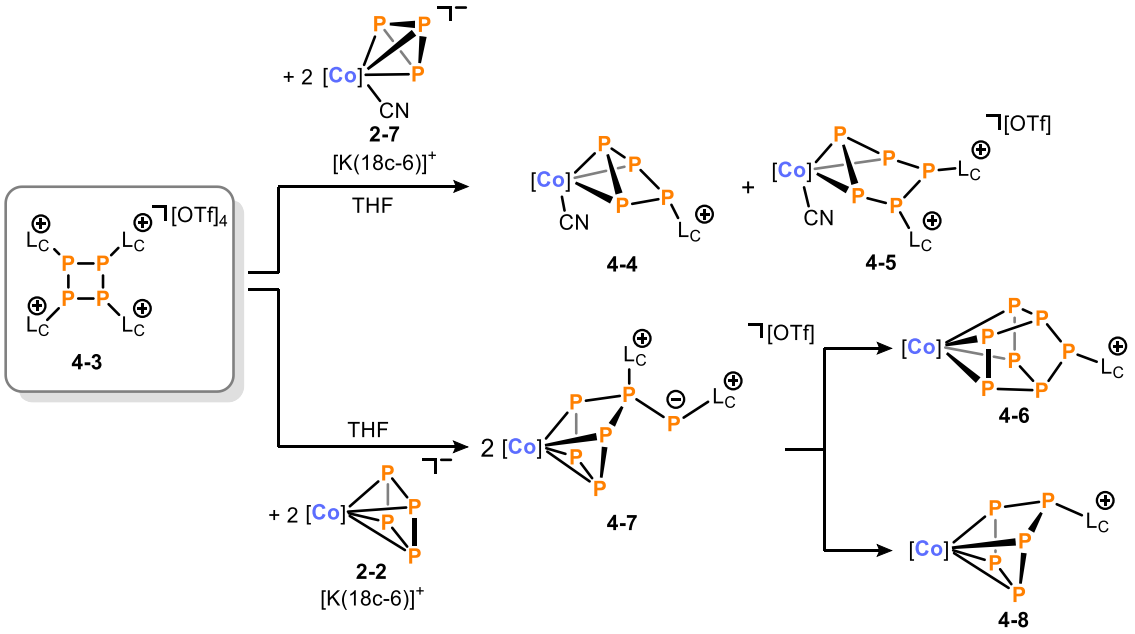

Scheme 7. Synthesis of the oligophosphido cobalt complexes.

4-7[OTf] (OTF^- = $CF_3SO_3^-$) disproportionates and gives rise to polyphosphido complexes **4-6** and **4-8**, highlighting the synthetic strategy of combining cationic P_n^+ and anionic transition metal polyphosphides TM-P_n^- for the synthesis of new oligophosphorus compounds.

Future studies should focus on performing experiments with a range of different anionic and cationic condensation partners to gain access to even larger extended polycyclophosphane scaffolds, as well as gaining further insight into the underlying reaction mechanisms.

Chapter 5. *Reactivity of Cyclotetraphosphido and Cyclotriphosphido Cobalt Complexes toward Group 14 Ambiphiles*

Heteroatomic tetrahedra (tricyclo[1.1.0.0^{2,4}]butane) composed of phosphorus and other p-block elements are very scarce, but represent an attractive synthetic goal due to their strained molecular structure and ensuing high reactivity. A transition-metal-mediated approach is promising, involving functionalization of a TM-P_n complex with heavier group 14 elements and subsequent release of these functionalized P_n ligands. Thus, in

Chapter 5 the reactivity of tri- und tetraphosphido complexes K(18c-6)]**2-2** and K(18c-6)]**2-7** with group 14 ambiphiles was investigated, the results of which are summarized in Scheme 8. The 2:1 reaction of anion **2-7**$^-$ with [Ar'Ge(μ-Cl)]$_2$ (Ar' = 2,6-Dipp$_2$C$_6$H$_3$) led to nucleophilic insertion of the germanium moiety and yielded the first mononuclear example of a germanium functionalized polyphosphido complex in K(18c-6)]**5-1**. Initial attempts to abstract the chlorine atom from the puckered *cyclo*-P$_3$GeAr'Cl ligand are also presented. In contrast, upon reaction with *cyclo*-P$_4$ complex **2-2**$^-$ [Ar'Ge(μ-Cl)]$_2$ acts as an electrophile, undergoing salt metathesis to give **5-2** in high yield, highlighting the ampibhilic character of [Ar'Ge(μ-Cl)]$_2$. ^{31}P{^{1}H} NMR studies revealed a circumambulatory behavior of the Ar'Ge moiety around the *catena*-P$_4$ ligand, which was inhibited upon cooling of the solution containing **5-2**, as evidenced by four distinct signals in the ^{31}P{^{1}H} NMR spectrum.

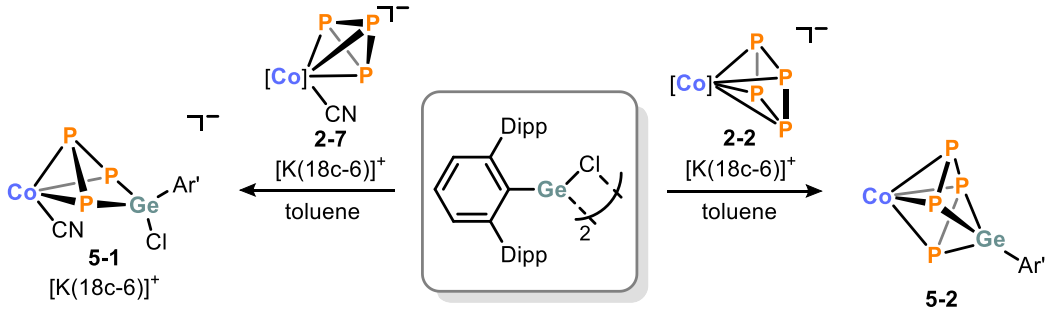

Scheme 8. Reaction of [Ar'Ge(μ-Cl)]$_2$ with polyphosphido cobaltates.

Overall, the synthesis of compounds **5-1** and **5-2** demonstrates a promising avenue to new complexes featuring mixed group 14/15 ligands by P–Ge bond formation. Future investigations will focus on the release of the functionalized polyphosphido moiety to give mixed binary group 14/15 tetrahedranes (e.g. Ar'GeP$_3$) or the development of systems capable of achieving this ligand release.

Chapter 6. *1,2,4-Diazamonophospholes and 1,2,3,4-Diazadiphospholes Derived from Diazoalkenes: Synthesis and Coordination Chemistry*

Chapter 6 of this thesis covers the synthesis of elusive 3*H*-1,2,4-diazamonophospholes, and 1,2,3,4-diazadiphospholes derived from the recently reported diazoalkene **6-1** (see Scheme 9), and their coordination chemistry. The new heterocycles **6-2** and **6-3** were synthesized *via* [3+2] cycloaddition reactions between diazoalkene **6-1** and either *tert*-butylphosphaalkyne or white phosphorus, respectively. Compounds of the type **6-2** are thought to be intermediates in cycloaddition *en route* to related 1*H*-1,2,4-

diazamonophospholes but eluded isolation until now. **6-1** and **6-2** were characterized using state-of the art analytical methods including quantum chemical calculations.

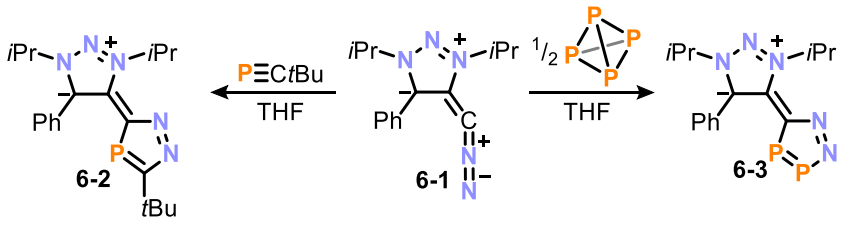

Scheme 9. [3+2] Cycloaddition reactions of the nucleophilic diazoalkene **6-1** with PC*t*Bu and P_4.

The coordination behavior of **6-1** and **6-2** was examined toward main group compounds (BPh_3, $AlEt_3$) and transition metal (Co, Ni, Ru, Rh W, Au) complexes, as (hetero-)phospholes are important ligands. From initial reactivity studies of **6-2** with varying equivalents of $[W(CO)_5(thf)]$, the three complexes **6-4**, **6-5** and **6-6** were identified (Figure 1, top). From reactions with other metal compounds, further metal complexes of **6-2** were isolated, including mononuclear η^1-N- and η^1-P-complexes **6-7**, **6-8** and **6-9**, as well as compounds featuring a higher hapticity by η^5-coordination *via* the aromatic π-system, **6-10** (Figure 1, middle). Furthermore, upon reaction of **6-1** with electron-rich first-row transition-metal complexes of nickel and cobalt, the 1,2,3-triazole ring of **6-1** underwent C–C or C–N bond activation to give compounds **6-11, 6-12** and **6-13** (Figure 1, bottom).

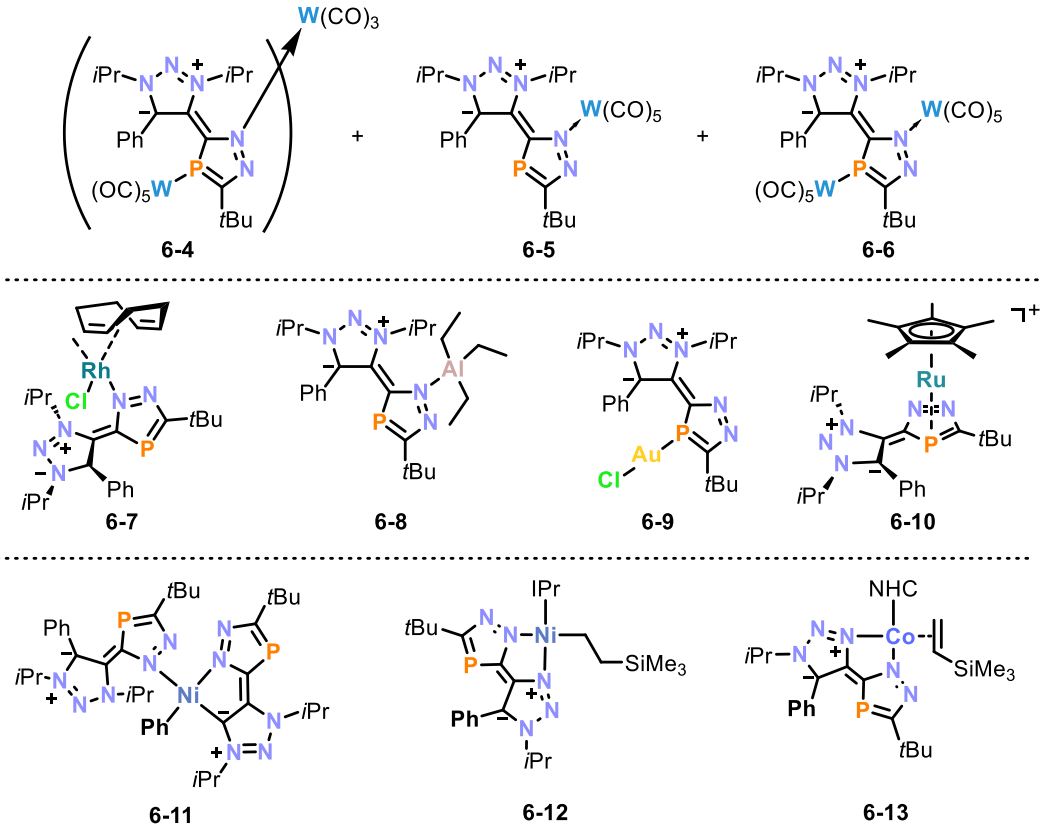

Figure 1. Various coordination modes of 3*H*-1,2,4-diazamonophosphole **6-2**.

The diazadiphosphole **6-2** reacted unproductively with the majority of the aforementioned metal complex precursors. Nevertheless, the first complexes of the 1,2,3,4-diazadiphosphole class, **6-14** and **6-15**, were prepared from reactions with BPh_3 and $AlEt_3$ in high yield, respectively (Scheme 10).

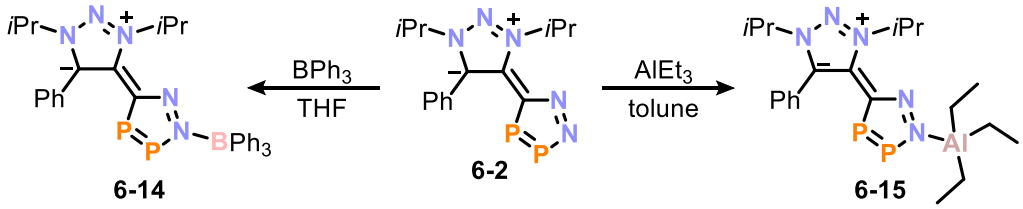

Scheme 10. Coordination of diphosphole **6-2**.

In summary, Chapter 6 demonstrates the potential of the new diazoalkene class in accessing new heterocycles through reactions with main group compounds. Taking the increasing accessibility of diazoalkenes into consideration, further tuning of this simple synthetic approach should allow facile access to additional new heterocycles and phosphorus containing compounds with distinct electronic and steric properties.

Conclusion

In summary, this thesis highlights the potential of low-valent cobalt complexes for the functionalization of white phosphorus. Although the coordination chemistry of P_4 has been studied for decades, targeted and diverse functionalization methods have been added to the underexplored "toolbox" of functionalizing *cyclo*-P_4 complexes. Future studies will further investigate the readily accessible cobalt complexes described in this thesis as attractive precursors for the synthesis of novel phosphorus compounds. A particular highlight described herein are the reactions of the anionic cobalt complex (**2-2**$^-$) to afford new monophosphorus compounds by fragmentation of the ligand to liberate P_1 species from the metal center. The acylated tetraphosphido complexes (**2-3-R**), as well as the reaction products of the involved [3+1] fragmentation procedure, opened new avenues in phosphorus chemistry. This potential was exemplified by the preparation of highly derivatized tetraphosphido complexes (**3-4-R**), polyphosphido complexes (**4-1** to **4-8**), as well as mixed group 14/15 ligands (**5-1**, **5-2**). These results illustrate the versatility of a low-valent transition metal supported by a redox-active ligand for the synthesis of previously inaccessible phosphorus compounds. Thus, it can be confidently predicted that many more exciting aspects and applications of this combination of electron-rich metal and ligand are yet to be discovered. In addition to the aforementioned results, this work has established a foundation for the future synthesis of numerous other compounds derived from P_4, including organophosphorus species and transition metal polyphosphido complexes, which are important in both fundamental and applied research.

8 Acknowledgements

Abschließend möchte ich mich bei zahlreichen Leuten für deren Unterstützung bedanken. Zuerst und ganz besonders möchte ich mich bei Prof. Dr. Robert Wolf für die Betreuung in den letzten Jahren bedanken. Danke für die exzellenten Arbeitsbedingungen, die große Freiheit bei meiner Forschung, die Unterstützung bei sämtlichen Belangen und die interessante Aufgabenstellung. Ein großes Dankeschön an unseren Kooperationspartner Prof. Dr. Jan J. Weigand, für das Anfertigen des Zweitgutachtens, die anregenden Diskussionen und den herzlichen Empfang in Dresden. Prof. Dr. Frank-Michael Matysik möchte ich für die Übernahme des Drittprüfers danken. Prof. Dr. Marcel Schorpp danke ich für die Bereitschaft, den Vorsitz zu übernehmen. Vielen Dank an Gabor Balázs, für die anregenden Diskussion, lustigen Kaffeepausen und das Korrekturlesen dieser Arbeit. Weiter möchte ich mich bei den Mitarbeitern der zentralen Analytik und Werkstätten bedanken, insbesondere bei Dr. Michael Bodensteiner, Dr. Stefanie Gärtner, Sabine Stempfhuber, Birgit Hischa und Florian Meurer (Röntgenstrukturanalyse), Georgine Stühler, Fritz Kastner, Veronika Scheidler, Annette Schramm, Tuan Anh Ngyuen und Dr. Ilya Shenderovich (NMR-Abteilung), Barbara Baumann und Helmut Schüller (Elementaranalyse), Markus Lindner (Glasbläserei), Peter Fuchs (Elektronikwerkstatt) und Andreas Graf (Feinmechanik).

Außerdem möchte ich mich bei meinen Kooperationspartnern für die gute Zusammenarbeit und wertvollen Beiträge bedanken. Danke an Prof. Dr. Jan J. Weigand, Dr. Kai Schwedtmann, Clemens Taube, Philipp Royla und Jannis Fidelius (TU Dresden), Prof. Dr. Max M. Hansmann, Dr. Taichi Koike und Justus Reitz (TU Dortmund), sowie Dr. Verena Streitferdt (Universität Regensburg). Für Unterstützung im Labor bedanke ich mich bei Fabian Gliese und Lukas Schober (Bacheloranden), Michael Witzmann und Florian Meurer (Forschungspraktikanten) für ihre Mitwirkung an den Projekten.

Ein großes Dankeschön an alle aktuellen und ehemaligen Arbeitskreismitglieder für die einmalige Stimmung, die schönen Kaffeepausen, lustigen Abende und AK Ausflüge: Christoph Ziegler, Daniel Scott, Julia Leitl, Julia Märsch, John Kelly, Marion Till, Peter Coburger, Thomas Maier, Ulrich Lennert, Alexander Erhard, Benjamin Falge, David Preitschaft, Felix Seeberger, Jannes Rückel, Jose Cammarata, Luis Coelho, Maria Uttendorfer, Martin Gawron, Michael Mende, Riccardo Grande, Sophia Vogler und Yang Liu. Insbesondere den ehemaligen Lab-22 Kollegen, Christian Hoidn, Gabriele Hierlmeier, Marco Fritz; und Karolina Trabitsch für die schöne Zeit an und außerhalb der Uni. Thank you, Thomas Horsley Downie, for proofreading almost every page of this

thesis. Vielen Dank auch an meine Studienkollegen. Ich hoffe der Kontakt bleibt weiterhin so gut. Ein ganz großes Dankeschön auch an meine Freunde aus der Heimat und der Umgebung für die ganz persönliche Unterstützung in vielfältiger und unterschiedlicher Form.

Abschließend möchte ich mich ausdrücklich bei meinen Geschwistern Simon und Samuel, sowie meinen Eltern Gerald und Kunigunde für ihr großes Verständnis und die Unterstützung in vielerlei Hinsicht bedanken. Danke für die Ermutigung in schwierigen Phasen während des Studiums und der Promotion.

9 Curriculum Vitae

Education

Since 12/2019	**Ph.D.** in the group of Prof. Dr. R. Wolf (Institute of Inorganic Chemistry), University of Regensburg, theme: "*Transformations of White Phosphorus Mediated by Low Valent Cobalt Complexes"*
10/2017 – 09/2019	**Master of Science** in **Chemistry** at the University of Regensburg with focus on Inorganic, Organic and Sustainable Chemistry and Biochemistry **Master's Thesis** in the group of Prof. Dr. R. Wolf (Institute of Inorganic Chemistry), theme: "*3d-Metallkomplexe mit sterisch anspruchsvollen Liganden"*
10/2014 – 09/2017	**Bachelor of Science** in **Chemistry** at the University of Regensburg **Bachelor's Thesis** in the group of Prof. Dr. R. Wolf (Institute of Inorganic Chemistry), theme: "*Synthese von sterisch anspruchsvollen redoxaktiven Iminliganden und deren Umsetzung mit einer niedervalenten Cobaltverbindung"*
09/2006 – 07/2014	**Abitur** (high school diploma) at the Goethe-Gymnasium in Regensburg; Abitur Subjects: German, English, Mathematics, Chemistry and Religion

Conference Contributions

03/2023	Oral presentation – 19th *European Workshop in Phosphorus Chemistry (EWPC) & 3rd Spanish Workshop on Phosphorus Chemistry (SWPC),* St. Sebastián, Spain
12/2022	Oral presentation – *Christmas Colloquium,* Regensburg, Germany
09/2022	Poster presentation – *21st Conference on Inorganic Chemistry (Wöhler Tagung),* Marburg, Germany

07/2022	Poster presentation – *16th International Symposium on Inorganic Ring Systems (IRIS)*, Graz, Austria
03/2021	Poster presentation – *Online Workshop on Phosphorus Chemistry (OWPC)*, Online, Germany
09/2020	Poster presentation – *Vortragstagung für Anorganische Chemie der Fachgruppen Wöhler-Vereinigung und Festkörperchemie & Materialforschung*, Online, Germany
02/2020	Poster presentation – 17th *European Workshop in Phosphorus Chemistry (EWPC)*, Rennes, France
08/2019	Oral presentation – *Wissenschaftliches Kolloquium von Arbeitsgruppen der Anorganische Chemie*, Hirschegg, Austria

Awards

07/2022	Best poster presentation award at *6th International Symposium on Inorganic Ring Systems (IRIS)*
06/2014	Dr. Hans Riegel-Fachpreis for W-Seminararbeit in Chemistry

10 List of Publications

1) S. Hauer, T. M. Horsley Downie, G. Balázs, K. Schwedtmann, J. J. Weigand, R. Wolf, "Cobalt-Mediated [3+1] Fragmentation of White Phosphorus: Access to Acylcyanophosphanides", *Angew. Chem. Int. Ed.* **2024**, e202317170; *Angew. Chem.* **2024**, *136*, e202317170.

2) S. Hauer, G. Balázs, F. Gliese, F. Meurer, T. M. Horsley Downie, C. Hennig, J. J. Weigand, and R. Wolf, "Functionalization of Tetraphosphido Ligands by Heterocumulenes", *Inorg. Chem.* **2024**, 10.1021/acs.inorgchem.4c00808 (Special Issue: "A Dialogue on Zintl Chemistry")

3) S. Hauer, J. Reitz, T. Koike, M. M. Hansmann, R. Wolf, "Cycloadditions of Diazoalkenes with P_4 and *t*BuCP: Access to Diazaphospholes", *Angew. Chem. Int. Ed.* **2024**, e202410107; *Angew. Chem.* **2024**, e202410107.

Eidesstattliche Erklärung

Ich erkläre hiermit an Eides statt, dass ich die vorliegende Arbeit ohne unzulässige Hilfe Dritter und ohne Benutzung anderer als der angegebenen Hilfsmittel angefertigt habe; die aus anderen Quellen direkt oder indirekt übernommenen Daten und Konzepte sind unter Angabe des Literaturzitats gekennzeichnet. Die Arbeit wurde bisher weder im In- noch im Ausland in gleicher oder ähnlicher Form einer anderen Prüfungsbehörde vorgelegt.

_____

Sebastian Hauer